Sponsored by:

PT. ARFINDO BERSINAR

PERUM PERHUTANI

HOTEL TUGU MALANG

Supported by:

PT OTSUKA INDONESIA
FACTORY LAWANG

KRISTALINDO BIOLAB

CV. MAKMUR SEJATI

PT AMERTA INDAH OTSUKA
PASURUAN

PEMERINTAH KOTA MALANG

RADIO ELFARA FM

Organizing Committee Office:
Graha Sainta, 2nd floor
Faculty of Science University of Brawijaya
Malang,Indonesia
http://icbs2011.com - icbs.mipa.ub@gmail.com

ISBN:
ISBN 978-602-97628-5-3

THE INTERNATIONAL CONFERENCE ON BASIC SCIENCE 2011 PROCEEDINGS BOOK - UNIVERSITY OF BRAWIJAYA

ISBN: 978-602-97628-5-3

PROCEEDINGS BOOK

THE INTERNATIONAL CONFERENCE ON BASIC SCIENCE 2011

Theory and Application of Mathematics, Biology, Chemistry, and Physics in Health, Environment, and Advance Technology

Widyaloka Convention Hall
University of Brawijaya
Malang,Indonesia
February 17-18th 2011

Proceedings of International Conference on Basic Science (ICBS)

"The Role of Basic Science in Health, Environment, and Advance Technology"

Faculty of Science, University of Brawijaya, Malang, Indonesia

Widyaloka Convention Hall, February, 17 – 18th 2011

Keynote Speakers

1. Assoc. Prof. Spas D. Kolev – University of Melbourne (Australia)
2. Dr. Edgar Paski – British Columbia Institute of Technology (Canada)
3. Prof. Dr. Lukman Hakim – Indonesian Institute of Science (Indonesia)
4. Prof Dr. Ir. Chandrawati Cahyani, MS – University of Brawijaya (Indonesia)

Board of Advisors

Prof. Dr. Ir. Yogi Sugito (UB – Indonesia)
Prof. Dr. Marjono, MPhil (UB – Indonesia)
Prof. Dr. Ir. Chandrawati Cahyani, MS (UB – Indonesia)
Prof. Dr. drh. Aulanniam, DES (UB – Indonesia)
Prof. Dr. Loekito Soehono, M.Agr (UB – Indonesia)
Prof. Petr Solich (Charles University – Rep. of Czech)
Assoc. Prof. Stuart R. Batten (Monash University – Australia)
Dr. Masayuki Sano (AIST – Japan)
Dr. Edgar Paski (British Columbia Institute of Technology – Canada)

Board of Editors

Dr. Hermin Sulistyarti (UB – Indonesia) – *Editor in chief*
Prof. Mick O'Neill (Advisory and Training Service Pty, Ltd – Australia)
Prof. Petr Solich (Charles University – Rep. of Czech)
Dr. Edgar Paski (British Columbia Institute of Technology – Canada)
Dr. Francois Malherbe (Swinburne University of Technology - Australia)
Dr. Lilibeth dlC. Coo (University of the Philiphine - Philiphine)
Dr. Verasak (King Mongkut's University of Technology - Thailand)
Zubaidah Ningsih, M. Phil (UB – Indonesia)
Irfan Mustafa, MSi (UB – Indonesia)
Yuniar Ponco Prananto, MSc (UB – Indonesia)

Design and Layout

Hary Agustiawan
Armeida Dwi Ridhowati Madjid

Publisher:

Galaxy Science Publisher, Malang, Indonesia

ISBN: 978-602-97628-5-3

PREFACE

Proceeding of the International Conference on Basic Science 2011 is a book containing several papers that have been presented in the seminar, either oral or in poster. The objective of this proceeding is to collect and to share any useful information that had been gathered recently in area of Mathematics, Biology, Chemistry and Physics, which is generally known as the basic science. Hence, through this book the readers are expected to gain new knowledge or information, especially in health, environment and advance technology.

In general, the papers are presented in order of health (part A), environment (part B) and advance technology (part C) in which in each part the papers are divided into two sections, the oral and poster papers. Many papers in this proceeding discuss the exploration and the development of natural resources as the medicine based compound source. Furthermore, the modification of analyzing method and modeling in health and environmental science, whether it is based on nuclear technology or advance biotechnology, has also been compiled in this proceeding. In addition, several interesting topics which present the latest information in environmental field add the usefulness of information gathered in this proceeding.

Additional information of the first author is also given at the end of this book. Hence further contact to the author is possible via the email address available at the affiliation section. Should the readers have further questions, comments or need more information, please directly contact the authors of the papers.

The editorial board has made some editing correction needed in some cases. Most of the editing correction are conducted and concentrated in the organization of the paper based on the guideline and the language, i.e. some figures or tables were corrected, or maybe printed in grayscale, and placed in the last part of the article (appendix). In addition, the language is the most time-consuming work; hence we apologize for the late publishing of this book and for any inconvenience as a result of the delay.

Lastly, on behalf of the committee, we would like to say thank you to all the participants for their kindness to be part of this conference. We also would like to acknowledge each partnerships and sponsorships that involved during this event. We believe that this proceeding still has some weaknesses; therefore any constructive comments are welcome. Once again, thank you to all, have a nice academic life and see you in the next ICBS.

Malang, May 2011

Message from President of ICBS 2011

Praise to Allah SWT, as only of his love and blessing, **our 1stth International conference on Basic Science (ICBS 2011)** was successfully held on February 17-18th, 2011 in Widyaloka Building University of Brawijaya Malang Indonesia, as one of celebration for the 48thAnniversary University of Brawijaya and the International Year of Chemistry 2011. The conference was projected to facilitate the discussion of the truth and beauty of science and its application to impact positive improvement in health, environment and advance technology for prosperity to the local society and worldwide.

We would like to thank and give highest appreciation to Rector University of Brawijaya and Dean Faculty of Science for their fully support and to **Our honourable and generous keynote and invited speakers:** Dr. Edgar Paski from BCIT & Analytical Innovation Canada; Assoc. Prof. Spas Dimitrov Kolev, from The University of Melbourne, Australia, Prof. Lukman Hakim, Head of Indonesian Institute of Science, Prof. Chandrawati Cahyani from Chemistry Department University of Brawijaya Malang Indonesia, Prof. Brenny van Groesen from University of Twente, Netherlands and LabMath-Indonesia, Bandung Indonesia; Prof. Motoki Kubo and Prof Mamoru Wakayama from Department of Biotechnology, Ritsumeikan University, Japan; Dr. Francois Malherbe from Swinburne University of Technology, Australia. **Another great appreciation goes to the board of editors:** Assoc Prof. Lilibeth Coo from University of Philippines Manila, Prof. Mick O'Neill, the Director Statistical Advisory & Training Services Australia, and Prof. Petr Solich from Charles University Republic of Czech. Many thanks go as well to **all national & international participants** for their contributions to the conference program and to this proceeding. It is our pleasant duty to also acknowledge our sponsors: PT Arfindo Bersinar, CV Makmur Sejati, Indonesian Forestry Department East Java Division, the Local Government of Malang City, Indonesian Chemistry Society, PT. Otsuka Lawang, PT. Amerta Indah Otsuka - Pasuruan, Kristalindo, Trans Zahwaa Travel, Elfara FM and Tugu Hotel **as your strong support and active participation** have made the **1st ICBS becomes a reality.**

The material in this proceeding is divided into three parts: (1) Health, (2) Environment, and (3) Advance Technology. We hope that the papers contained in this proceeding will prove helpful toward improving international collaboration research to solve the problems related to heath, environment, and advance technology.

As this conference is held annually, we are looking forward to the 2nd International Conference on Basic Science that will be held on February, 2012 at the same location. We hope that it will be a more interesting and enjoying conference.

President
Dr. Hermin Sulistyarti

Message from Dean of Faculty of Science – UB

On behalf of the faculty of Science we are very happy to complete the **1stth International conference on Basic Science (ICBS 2011)** by this proceeding. Our appreciation to Prof. Dr. Ir. Yogi Sugito, rector of the University of Brawijaya for his support and all of the keynote and invited speakers who made this conference succeeds.

This proceeding contains as the following. Part A: Health, Part B: Environment, and Part C: Advanced Technology. Oral papers are followed by posters at each part. Finally, we would like to thank all of the steering and organizing committee for their efforts in succeeding this conference, especially to Dr. Hermin Sulistyarti as the chair of the organizing committee.

Last but not least for all of the participants, we are thankful for your cooperation, contribution and very valuable support for this event.

Thank you,
Prof. Dr. Marjono, MPhil.

Table of Content

Part A. Health Section

A.1. Oral Presentation 1 – 106

ERRATUM

$CD8^+CD122^+$ Regulatory T Cells is a New Therapy for Inflammatory Bowel Disease

Agustina T Endharti [1,5,6], Nobuaki Misawa [2], Masafumi Ito [3], Haruhiko Suzuki [4]

[(1,4)] Department of Immunology, Nagoya University Graduate School of Medicine, Nagoya, Japan
[(2)]Department of Pathology, Nagoya University Graduate School of Medicine, Nagoya, Japan
[(3)]Department of Pathology, Japanese Red Cross, Nagoya Daiichi Hospital, Nagoya, Japan
[(5)]Faculty of Medicine, Brawijaya University, East-Java, Indonesia (tinapermana@yahoo.com)
[(6)]Japanese Society for Promotion of Science, Tokyo, Japan

Abstract

We identified $CD8^+CD122^+$ regulatory T cells and demonstrated their importance in the maintenance of immune homeostasis and in the recovery from experimental autoimmune encephalomyelitis (EAE). However, the role of $CD8^+CD122^+$ regulatory T cells in other diseases is unknown. Here we show that $CD8^+CD122^+$ regulatory T cells effectively prevent and cure inflammatory bowel disease (IBD) in a mouse model. In our experiments, IBD was induced in lymphocyte-deficient RAG-$2^{-/-}$ mice by transferring $CD4^+CD45RB^{high}$ cells that were excluded with $CD4^+$ Treg. $CD8^+CD122^+$ cells showed a suppressive effect when they were transferred 4 weeks after transfer of $CD4^+CD45RB^{high}$ cells. At that moment, symptoms of IBD had already appeared. Co-transfer of $CD8^+CD122^+$ cells clearly suppressed the development of IBD and this suppressive effect of $CD8^+CD122^+$ cells was similar to that of $CD4^+CD45RB^{low}$ cells that mostly contained $CD4^+$ Treg. The suppressive mechanism of $CD8^+CD122^+$ cells did not induce $CD4^+Foxp3^+$ iTreg (induced-type Treg) but directly suppressed $CD4^+CD45RB^{high}$ cells. $CD8^+CD122^+$ cells obtained from IL-$10^{-/-}$ mice showed insufficient suppressive activity for IBD, indicating IL-10 as an important effect-transmitting factor in the suppression of the development of IBD indicating the therapeutic potential of $CD8^+CD122^+$ cells. These overall findings demonstrate the potential role of $CD8^+$ regulatory T cells, in the new therapy of IBD patients.

Keywords: *Inflammatory Bowel Disease; Regulatory T cells; $CD8^+CD122^+$.*

Cytotoxic, antioxidant and antibacterial activity of methanol extract of *Xylocarpus moluccensis* fruit husk

Asep Awaludin Prihanto

Department of Fishery Product Technology, Faculty of Fisheries and Marine Science, Brawijaya University, Malang, Indonesia (asep_awa@yahoo.com)

Abstract

The aims of this study were to examine toxicity, antioxidant and antibacterial activity of methanol extract of fruit husk (Xylocarpus moluccensis). Toxicity assay was undertaken by brine shrimp lethal toxicity test, antioxidant activity was done by Diphenyl picryl hydrazil (DPPH) scavenging, and inhibition growth to Staphylococcus aureus and Escherichia coli used as antimicrobial test. The results showed that methanol extract of fruit husk was not toxic, antiradical efficiency was 0.000154, and broad spectrum antibacterial with inhibition zone to Staphylococcus aureus and Escherichia coli was 12.7±1.2 and 11.9±0.9 mm, respectively in 630000 ppm concentration.

Keywords *: Cytotoxicity, antioxidant, antibacterial, methanol extract, fruit husk, Xylocarpus moluccensis.*

1. Introduction

The *Xylocarpus moluccensis* belongs to the order Geraniales of the family meliaceae Genus Xylocarpus is distributed in the coastal regions of India, Ceylon, Burma and Malaya [1] and Indonesia. The fruit of *Xylocarpus moluccensis* is a green color, lemon fruit sized, hard and heavy, leading to the common name ‗cannon ball tree'.

This mangrove provides a several phytochemical compounds. It can be used for health therapy. Several biological properties have been attributed to *Xylocarpus moluccensis*: aphrodisiac, fever, malaria, hair preservatives, astringent, antidiarrhoea, antiemetic and haemostatic properties [2,3]. In Indonesia, the use of medicinal plants such as mangrove to cure several illnesses has been use routinely by coastal native. Furthermore, Porong estuary is rich in various mangrove species with diverse biological and pharmacological properties.

The objectives of this work were to proceed to the preliminary cytotoxic, antioxidant and antibacterial assessment of *Xylocarpus moluccensis* fruit husk.

2. Experimental Details

Plant material

The fruit of mangrove *Xylocarpus moluccensis* was collected from Porong's river estuary. The fruits of *Xylocarpus moluccensis* then were packed in Poly ethylene plastic and eventually brought to laboratory. The fruit was pelled to obtain the husk. Afterward, the husk was dried until ± 15% water content in a husk.

Extraction

The *Xylocarpus moluccensis* fruit husk was extracted by maceration method. The 25 g dried fruit husk was soaked in 75 ml methanol in an erlenmeyer for 24 hour. The extract was then separated from the debris by filtration with a Whatman no. 1, afterward the extract was concentrated using rotary vacuum evaporator. The extract then diluted to obtain several concentration of crude methanol extract. The methanol extract were subjected for bioactivity studies.

Antibacterial assay

The antibacterial activity test was done by paper disc diffusion method [4]. The microorganisms used in this study were *Staphylococcus aureus* and *Eschericia coli*. The 10^8 cfu/ml each inoculums were seeded in Mueller Hinton Agar (MHA, Oxoid) using sterile cotton swab. Sterile 6 mm paper blank discs were impregnated with different concentration of crude extract and plated onto seeded Petri disc. The plates then were incubated in 35^0C for 24 hour. The inhibition zone around each disc was measured in millimeter.

Antioxidant assay

The antioxidant was assayed using DPPH radical-scavenging activity method following [5], 1 ml Different concentrations of crude methanol extract was added to 3 ml 0.5 mM DPPH solution (0.2 mM in methanol) as free radical source. The

Scavenging activity was measured spectrophotometrically. The absorbances were recorded after 20 min at room temperature.The disappearance of DPPH was read spectrophotometrically at 515 nm. Radical Scavenging Activity (RSA) was calculated. From the obtained RSA values, the EC_{50} were calculated, which represents the concentration of the scavenging compound that caused 50% neutralization.

$$RSA\ (\%) = \frac{A_0 - A_{30}}{A_0} \times 100$$

RSA = Radical Scavenging activity
A_0 = the absorbance at 0 min test
A_{30} = the absorbance at 30 min test

Antiradical Efficiency

Antiradical efficiency (AE) is a new concept of antiradical efficiency which combines the factors EC_{50} and T_{EC50} was defined as AE. It was calculated following [6] method:

$$AE = \frac{1}{EC_{50} \times T_{EC50}}$$

AE = Antiradical efficiency
EC_{50} = Effectives concentration
T_{EC50} = the time needed to reach the steady state to EC_{50}

Cytotoxic assay

The cytotoxic of methanol extract of fruit husk was assayed using brine shrimp lethally test (BSLT), The *Artemia salina* was prepared in which hatched eggs (obtained from Laboratory of Fish Breeding, Faculty of fisheries and marine science) in 2 day lighted sea water . The assay was prepared with 3 ml of filtered sea water containing 10 free swimming nauplii of *Artemia salina* in cavity bottle. 1 ml of variably crude extract concentration was plugged in cavity bottle for 24 hour. The percentage of mortality was determined by comparing the mean surviving *Artemia salina*. IC_{50} was determined using probit analysis [7]. Extracts giving LC_{50} values greater than 1,000 ppm were considered to be nontoxic.

Data analysis

All data were calculated using the Microsoft Excel computer program.

3. Result and Discussion

***Xylocarpus moluccensis* fruit husk extract**

The extraction of *X. moluccensis* fruit husk resulted yield of 0.82 % from dried weight. Yellowish extract was obtained from fruit husk (Figure 1). Analysis phytochemical revealed that fruit husk contained flavonoid, and alkaloid (data not shown).

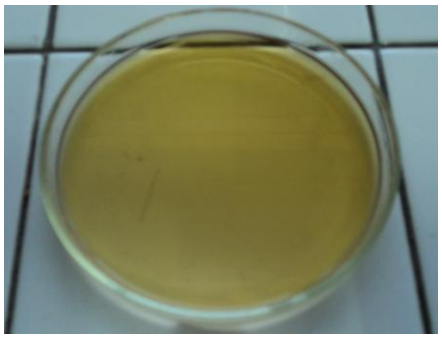

Figure 1. The extract of *X. moluccensis* fruit husk

Antibacterial assay

The antibacterial assay of methanol extract result, showed in Table 1. The extract had low in vitro potential of antimicrobial activities against *Staphylococcus aureus* and *Eschericia coli*. The maximum activity of methanol extract of *Xylocarpus moluccensis* fruit husk in S.aureus was observed against *S.aureus* (12.7±1.2 mm). Resemble result also was showed in *E. coli.* The maximum activity of methanol extract of *Xylocarpus moluccensis* fruit husk in *E. coli* is (12.7±1.2 mm) in the same concentration.

Tabel 1. Antibacterial activity of the methanolic extract of *Xylocarpus moluccensis* fruit husk in *S. aureus* against the test organisms.

Concentration (ppm)	zone inhibition (mm)	
	S.aureus	*E. coli*
630,000	12.7±1.2	11.9±0.9
63,000	8.4±0.4	7.1±0.9
6,300	8.1±0.3	6.9±0.6
630	7.6±0.3	6.6±0.9
63	7.5±0.3	6.6±0.4
6.3	7.4±0	-

Based on the color of and phytochemical screening, another antibacterial compounds that might be exist in fruit husk of *X. moluccensis* are flavonoid and alkaloid and this is probably the natural defense against microorganism contamination in *Xylocarpus* sp. seed. [8] found that *Xylocarpus* sp. contained N-Methylflindersine that was known as antibacterial compound. Catechin, The bioactive compound that can inhibit the growth of lactic acid bacteria also was found by [9].

Antioxidant assay

The Radical scavenging activity of fruit husk methanol extract show in Figure 2.

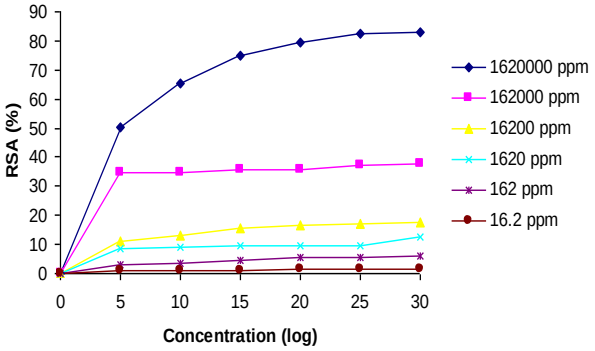

Figure 2. Radical Scavenging Activity of the methanol extract of *Xylocarpus moluccensis* fruit husk

The EC_{50} value of methanol extract of *X. moluccensis* fruit husk is 217000 ppm. This result agrees with previous result on the low antioxidant activity of *X. moluccensis* fruit peel. Considering it is still a crude extract. Therefore, *X. moluccensis* fruit husk components may be used as potential natural antioxidants in foods as well as health-promoting substances.

Antiradical efficiency

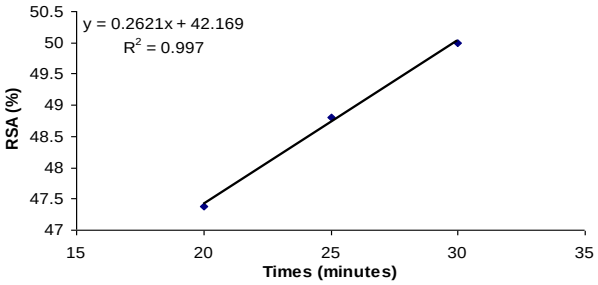

Figure 3. Regression of Antiradical efficiency of *X. moluccensis* fruit husk methanolic extract.

The antiradical efficiency was used to calculate the effectives scavenging of atiradical. In this calculation, we consider the time to reach until steady state. Based on the regression value (Figure 3), the AE of the crude methanolic extract of *X. moluccensis* of fruit husk is 0.000154.

According the classification of AE by [6], the crude methanolic extract of *X. moluccensis* of fruit husk has a low level antiradical efficiency. We proposed because the fruit husk of *X. moluccensis* is not designed to muffle radical.

Cytotoxic assay

The results of the cytotoxicity assay against brine shrimp of the methanol extract of *Xylocarpus moluccensis* fruit husk are shown in Figures 3. The methanol extract of *Xylocarpus moluccensis* fruit husk has no significant cytotoxicity activity against brine shrimp with an LC_{50} value of 2.0 x 10^5 ppm. Based on [10], the result exposed that the methanol extract of *Xylocarpus moluccensis* fruit husk might be has no potency to be used in cancer cell line therapy but this signified that it might not be toxic to human. The same result was exposed by [11] that *Xylocarpus* sp. did not show cytotoxic activity when it is extracted using polar solvent.

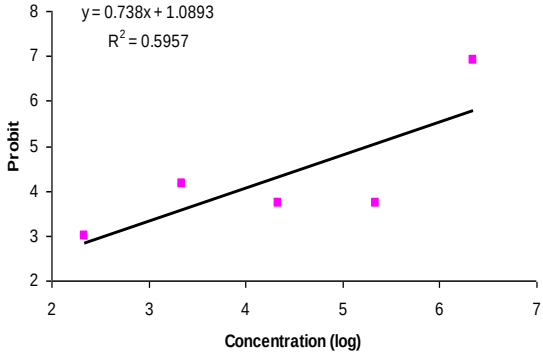

Figure 4. The toxicity effects of the methanol extract of *Xylocarpus moluccensis* fruit husk using brine shrimp lethality assay

4. Conclusion

The result of this research indicates that methanol extract of of *Xylocarpus moluccensis* fruit husk showed a broad spectrum against gram positif and gram negative bacteria, low antioxidant activity and also showed non toxic activity.

5. Acknowledgements

This research was partially funded by Indonesia's Directorate of Higher Degree.

6. References

[1]. Lakshmi, V., and Gupta, P. (2008), An Overview of the Genus Xylocarpus. *Natural Product Research*. 22 (14): 1197-1224

[2]. Bandaranayake, W.M. (1998), Traditonal and medicinal uses of mangroves. *Mangroves and Salt Marshes*. 2: 133–148

[3]. Kokpol, U., Chavasiri, W., Chittawong, V.and Miles, D.H. (1990), Taraxeryl cis-p-hydroxycinnamate,a novel taraxeryl from

Rhizophora apiculata. *Journal of Natural Products*. 53: 953–955

[4]. Sagdic, O, and Ozcan, M. (2003), Antibacterial activity of Turkish spices hydrosol. *Food Cont*. 14: 141-143

[5]. Kirby, A.J. and Schmidt, R.J.T. (1997), The antioxidant activity of Chinese herbs for eczema and of placebo herbs. *J. Ethnopharmacol*. 56: 103–8.

[6]. Sanchez-Moreno, C., Larrauri, J.A., Calixto, F.S. (1998), A procedure to measure the Antiradical Efficiency of polyphenols. *J Sci Food Agric*. 76: 270-276

[7]. Wardlaw, A.C. (1985), Practical statistics for experimental biologists, John Wiley and Sons, Chichester

[8]. Singh R.P, Murthy K.N.C, Jayaprakash G.K. (2002), Studies on the Antioxidant Activity of Pomegranate (*Punica granatum*) Peel and Seed Extracts Using in Vitro Models. *J Agric. Food Chem.* 50: 81-86.

[9]. Liu, C.R., and Chen Y. (2004), Advance of chemistry and bioactivities of catechin and its analogues. *China J. Chin. Mater.Med*. 29,1017

[10]. Simionatto E, Porto C, da Silva UF, Squizani AMC, Dalcol II, Morel AF. (2005), Composition and Antimicrobial Activity of the Essential Oil from *Aloysia sellowii*. *J Braz Chem Soc*. 16:1458–1462

[11]. Dai, H.F., Mei, W.L., Hong, K., Zeng, Y.B., Zhuang, L. (2005), Screening of the tumor cytotoxic activity of sixteen species of mangrove plants in Hainan. *Chin.J. Mar. Drugs*. 24,44.

Research-based on Herbs Exploration and Use of Animal Models: Nature Materials towards Supporting Evidence Based Medicine

Aulanni'am [1,2]

[(1)] Biochemistry Laboratory, Chemistry Department, Faculty of Sciences, University of Brawijaya, Malang, East Java, Indonesia (aulanibiochem@yahoo.com)
[(2)] Veterinary Medical School, University of Brawijaya, Malang, East Java, Indonesia (aulani@ub.ac.id)

Abstract

Evidence based medicine (EBM) can be defined as clinical expertise informed by the best available evidence obtained from systematic research. However, definitions of both clinical expertise and best evidence remain a problem. The use of herbal-based traditional medicine is a legacy handed down from our ancestors and existed related to the culture of Indonesia. Some drugs which are now being used as herbal-based is derived from plants obtained either by extraction or synthesis. Medicinal plant-based research in our laboratory indicates a pharmacological effect against some diseases, such as diabetes mellitus, hipercholesterolemia, rhematoidarthritis, cancer and also anti fertility. The results are still encouraging our team to continue to conduct exploration of bioactive substances from Indonesia's native medicinal plants. Some bio-molecular analysis techniques have been conducted in our laboratory even in Brawijaya University which already has equipment that capable for analyzing the molecular expression of proteins, enzymes and cytokines that were released and synthesized during the disease progresses. To support the development of natural ingredients and herbal medicine toward evidence-based medicine (EBM), the research using experimental animals or cell cultures become necessary. This paper will explain briefly the results of plant-based traditional medicine research which empirically has proven have capability of treating some diseases but need to be studied to answer the "why can heal and how it works at the cellular and molecular level?" question. The results of this research open a wider opportunity to develop further research.

Keywords: *Evidence Base Medicine (EBM), herbal medicine, bioactive.*

1. Introduction

The use of traditional medicine is a legacy handed down from our ancestors, and its presence is related to the Indonesia culture. Some drugs which now are being used were based on herb either single or in ingredient which is derived from plants obtained by extraction or synthesis process. Indonesia is one of ~~"m~~ega diversity" country which is rich in biodiversity. Each species of plants, animals and micro-organisms have chemical values in producing a wide variety of chemical compounds.

In the history of drug development, Indonesian nation have a lot of concocting potions and performs traditional treatment, which is also an important part of the discovery of several types of drugs. But on the other hand, it is often become a concern for history that many data are not well documented. Moreover, many findings that even already become an international patent are not named after the Indonesian people.

According to the definition of the Ministry of Health of the Republic of Indonesia, traditional medicine is defined as drugs or natural ingredients derived from plants, animals, minerals, and mixtures of these materials which have traditionally been used for treatment based on experience. But the reality of traditional medicines derived from plant portion is larger than that derived from animals or minerals, so the term for traditional medicine is almost always synonymous with medicinal plants.

The development of science-based treatment plant origin bioactive

The development of medical science-based bioactive has increased rapidly. More and more researches are being carried out to explore the bioactive medicinal plants and to try to determine the content and the benefits for improving the quality of human life. Until now, empirically proven medicinal plants in treating illness are increasing in number. The discovery of many medicinal plants showed a pharmacological effect on some diseases, such as diabetes mellitus, hipercholesterolemia, rhematoidarthritis, liver dysfunction, cancer and antifertility also encouraged some researchers to explore the

bioactive from medicinal plants. For the purposes, many pre-screening test to invitro and invivo tests are conducted to determine the role of bioactive they contain. However, few studies that have been done are not clear. In addition, the mechanisms of drug action are related to a very complex mechanism. The use of macro level methods instead of the micro level methods urges the biomolecular analysis technique te be an option to support the traditional medicine becomes evidence-based medicine (EBM). EBM aims to apply the best available evidence gained from the scientific method to clinical decision making. So the use of research models invitro, cell culture or experimental animals is one option before being applied to humans.

Several biomolecular analyses have been conducted in several research centers and universities, even in a complex R&D Health Laboratory. This research center has been equipped with advanced equipment that capable of analyzing the molecular expression. The molecular expression of proteins, enzymes and cytokine released and synthesized during the disease process enable us to determine the character of a specific disease and its progress.

This paper will briefly describe the testing of plant-based traditional medicine which empirically has proven capable of treating some diseases but need to be studied to answer the "why can heal and how it works at the cellular and molecular level?" question. The results of this research opens a wider opportunity to develop further research is original.

Our results explain how the content of the plant that serves as an antioxidant capable of improving the degree of type 1 diabetic rats insulitisis prepared by providing exposure to Multi Low Dosestreptozotocin (MLD-STZ) at a dose of 20mg/KgBW. Streptozotocin (STZ) or trivial name 2-deoxy-2-(3-(methyl-3-nitroureido)-D-glucopyranose) was synthesized by Streptomycetesa chromogenes and used to induce diabetes mellitus type 1 and type 2 [1,2].

According to its group of origin, Streptozotocinis anitrosourea serves as an alkilation agent. STZ spontaneously decomposed to produce carbon ions of high reactivity with alkaline cellular components, including DNA and proteins. STZ damage the pancreatic betacellsin in two ways: 1) alkylation of DNA through alkilnyagroup, and 2) as a NO that will increase the amount of NO in the pancreas. This excess of NO reacts with superoxide to form peroxynitrite, which is very toxic to pancreatic beta cells [2].

The mechanisms of diseases and bioactive action can be confirmed using immune histochemical techniques, such as pancreatic beta cell apoptosis, as in Figure 1 (Appendixes). Using the TUNEL method, it can be definitely confirmed that a pancreatic beta cells had apoptotic nucleus since it has a visible color. Cells which undergo an apoptosis essentially will look brown and fragmented DNA, by looking at differences in the core color with a small magnification, it can be distinguished and known to cells undergo apoptosis. TUNEL method is specific for detecting apoptosis in each cell in the network with a label immune histochemistry principle of DNA strand interruption.

During apoptosis of double-stranded, DNA will be fragmented into single-stranded or oligo nucleosome mononucleosom (nicks). This single strand can be identified using the label 3'OH terminal that has been modified nucleotide in enzymatic reactions [3].

The study of benefit of other bioactive can also be learned through exposure to cell cultures that received antioxidants as a cancer prevention and therapy based on enzyme function of protein kinase C-α (PKC) (Figure 2 – Appendixes). PKC enzyme involved in the process of proliferation and differentiation of smooth muscle cells [4,5]. This event is controlled by a genetic mechanism as stimulation of extracellular signal-specific, ie, growth factor or mitogen. The path of the signal transduction for cell proliferation is through the activation of therace → raf-1 → MEK → ERK → transcription alfactor in the cell nucleus.

PKC enzyme activity and the expression used to observe the occurrence of proliferation and smooth muscle differentiation due to infectious agents as well as its treatment by the bioactive is contained in medicinal plants (Figure 3).

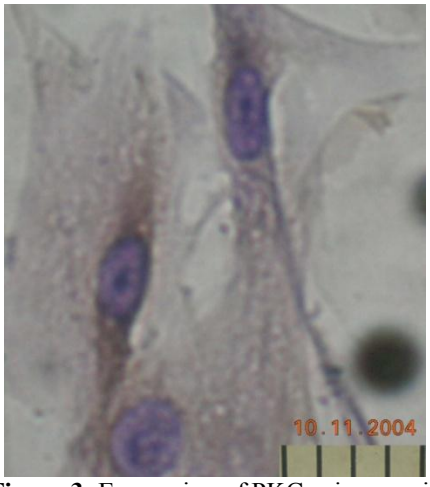

Figure 3: Expression of PKC-α isozymein prostate smooth muscle cellstengan immuno histo chemical techniques [6] (brown color, indicated

by blue arrows show expression of PKC-αsozyme present in the cytosol and perinuklear. 1 bar=0.01mm)

.

The role of plant-based traditional medicine for treatment can be studied as well as through the expression of protein from cell culture or experimental animals even at the level of use in humans by using electrophoresis (SDS-PAGE) (fig. 4). In addition to IHC (Immunohistochemistry) technique and SDS-PAGE, still there are several ways that can be used such as, iedot blot, Western blot and ELISA.

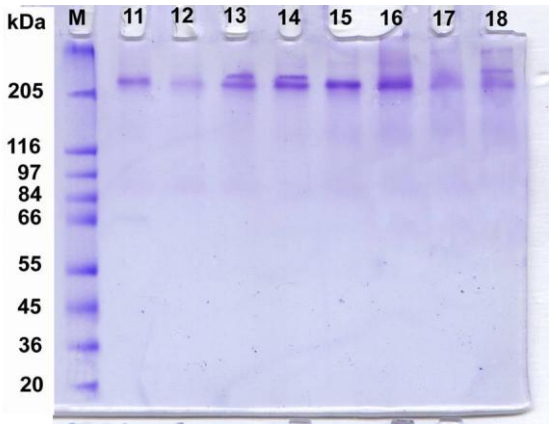

Figure 4. Erythrocyte Spectra in Membrane Protein Profiles of TF Patients who received Fe therapy

2. Conclusion

From the above description it can be concluded that Indonesia has biodiversity of tropical plants which is a promising potency to be developed as a potential source of traditional medicine. But further studies on cellular and molecular level to explain the mechanism of action in inhibiting the occurrence of disease are still need to be conducted. Moreover, it can be used as the basis for the development of treatment efforts using the active ingredients of medicinal plants.

3. References

[1]. Pechhold K., Noelle B. Patterson, Carmen Blum, Christine L. Fleischacker, Bernhard O. Boehm and David M. Harlan (2001), Low Dose Streptozotocin-Induced Diabetes in Rat Insulin Promoter-mCD80-Transgenic Mice Is T Cell Autoantigen-Specific and CD28 Dependent. *The Journal of Immunology*, 2001, 166: 2531-2539.

[2]. Szkudelski T., (2001), The Mechanism of Alloxan and Streptozotocin Action in B Cells of the Rat Pancreas.Departement of Animal Physiology and Biochemistry. University of Agriculture. Poland

[3]. Roche (2004), ……

[4]. Itoh, *et.al*, (2001), ……

[5]. Skaletz-Rorowski, *et.al*, (1999), ……

[6]. Purnomo (2006), ……

[7]. Bloodswort, A., Odonnel, V.B.V., Freeman, B.A., (2000), Nitric Oxide regulation of free radical and enzyme mediated lipid and lipoprotein oxidation. Arterioscler thromb vasc. Biol. 20: 1707-1715.

[8]. Dasagayam, T.P.A., Tilac, J.C., Bolor, K.K., Sone, K.S., Ghoshodfi, S., and Dile, R.D., (2004), Free radical and antioxidant in human health. Current status and future prospect. Radiation biology and health science division. JAPI. Vol 52: 2-7

[9]. Lodish, H., A. Berk., S.I. Zipersky., P. Matsudara., D. Baltimore., and J. Darnell (2000), Mollecular Cell Biology. W.H Freeman Company. New York

[10]. Unsal, N.C., Buyuktuncer, E.D., and Mehmet, A.T., (2005), Programmed cell death in plants. *Journal of cell and molecular biology* 4: 9-23

[11]. Valko, M. C. J. Rhodes, J. Moncol, M. Izakovic, and M.Mazur. (2006), Free Radicals, Metals and Antioxidants in Oxidative Stress-Induced Cancer. Chemical Biology Interactive

[12]. Yong, X., and Yai, L.Z., (2001), Nitric Oxide and inflamation.Superoxide anion release from inducible nitric oxide. Birkhauserverlagbasel. Switzerland. P. 9-17

Appendixes

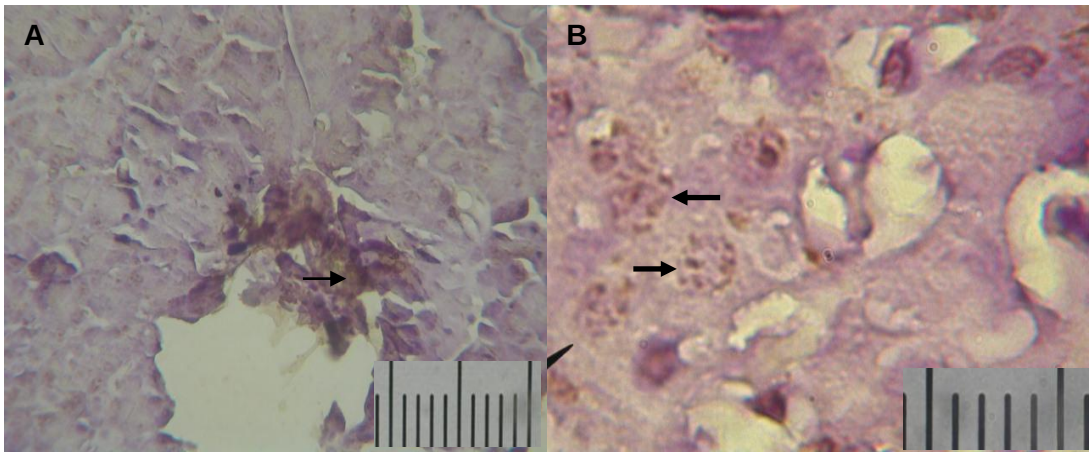

Figure 1. Apoptosis of pancreatic beta cells
(A: Apoptosis of pancreatic beta cells, B: Apoptosis of beta cells).
Black arrows indicate that apoptosis of pancreatic beta cells, 1scale= 0.01µm

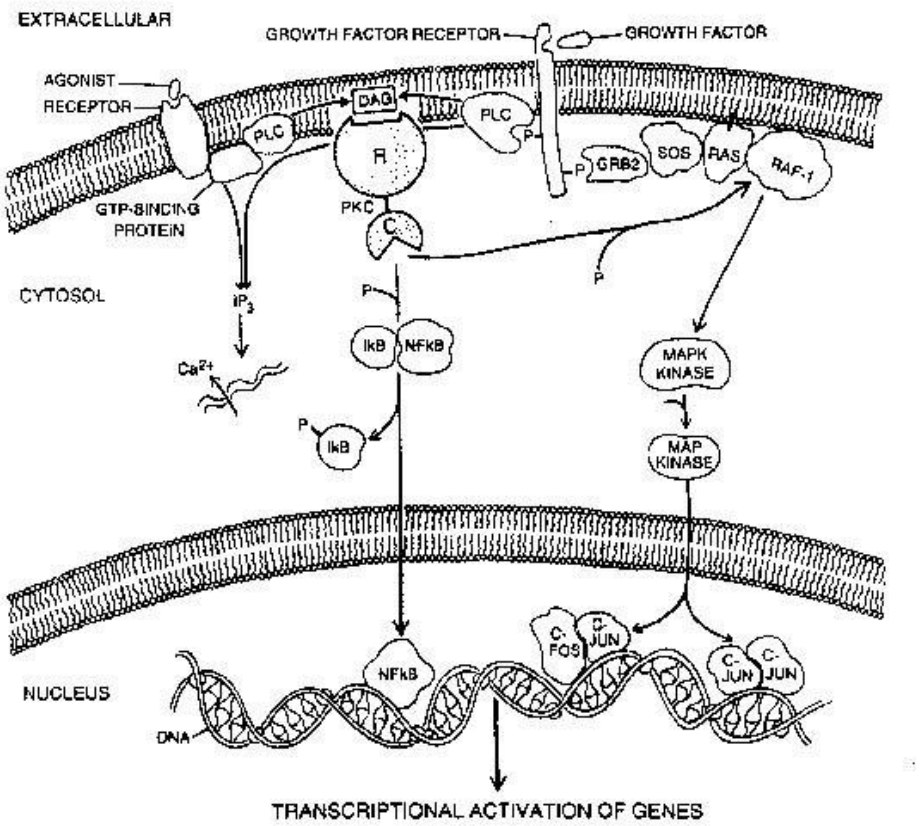

Figure 2.: The role of PKC enzyme in signal transduction in cell proliferation.

The Effect of Red Guajava (*Psidium guajava*) Fruit Extract on Tyrosinase (EC 1.14.18.1) Activity by Spectrophotometry

Ayik Rosita Puspaningtyas

Faculty of Pharmacy, University of Jember, East Java, Indonesia (aixrose_pee@yahoo.co.id)

Abstract

Tyrosinase is one of the most important key enzymes in the melanin biosynthesis. Inhibition of tyrosinase activity will cause a decrease in melanin production.Tyrosinase inhibitory activity by ascorbic acid has been studied before. Based on reported experiments, ascorbic acid can inhibit tyrosinase activity in enzymatic reaction competitively. As the effort to find an effective, safe and minimum adverse effect of skin whitening agent, we planned to study the inhibitory activities of Psidium guajava extract on tyrosinase activity. Psidium guajava is one of the fruit that contained the highest of ascorbic acid. To determine the efficacy of tyrosinase inhibition, we were using L-tyrosine as the substrate, Psidium guajava extract as inhibitor, and ascorbic acid as positive control that was measured by spectrophotometry. The optimization of method was develop too. The inhibitory kinetic were determined by measured the absorbance of dopachrome as the end product of the tyrosinase reaction. Michaelis-Menten constant (Km) and maximum velocity (Vmax) of the tyrosinase were determined by Lineweaver-Burk"s plots. The Km and Vmax without Psidium guajava fruit extract were 0.315 mM and 0.0265 µmol/min. The Km value with Psidium guajava fruit extract 1%; 2%; 3% w/v were 0.4824; 0.698; 0.543 mM, while the V_{max} value were 0.0269; 0.0283; 0.0255 µmol/min. Lineweaver-Burk"s plots of the presence Psidium guajava fruit extract showed that Psidium guajava fruit extract inhibited competitively. From Lineweaver-Burk"splots, the IC_{50} Psidium guajava extract was 0.26 mM while the control in 0.26 mM inhibited 56.523 %. Finally, Psidium guajava fruit extract showed much higher effect than ascorbic acid on Tyrosinase activity.

***Keywords**: Inhibitory kinetics, Psidium guajava fruit extract, Tyrosinase, L-tyrosine.*

1. Introduction

Indonesia is tropical country with abudant sunlight exposure. Sunlight had important use for living creature on the Earth. For human, sunlight was used to change pro vitamin D_3 (7-dehydrocolesterol) on epidermis become vitamin D on fracture formed. [1]. In contrast, sunlight can be caused negative effect on human skin such as skin cancer and hyperpigmentation [4].

Hyperpigmentation caused by increasing melanin production become local pigmentation or skin spot. Hyperpimentation were figured blacker than normally skin colour [4]. Melanin formed was important for protection efforts against negative effects from ultraviolet radiation. In addition, high melanin concentration and melanin accumulation was caused hyperpigmentation and esthetic problems.

Now, many skin lightening product on market with various active compounds to reduce hyperpigmentation and mechanism for skin light. Principal mechanism of skin lightening product were inhibition melanin (melanogenesis) so skin become more bright and white. Melanin formed can be inhibited with various mechanism such as tyrosinase activity inhibition, decrease tyrosinase synthesis and transfer and melanosit sitotoxic inhibition [3].

Tyrosinase is one of the most important enzymes in the melanin biosynthesis. It is responsible catalisis reaction from L-tyrosine on melanosit cells [6]. L-tyrosine or 4-hydroxysiphenylalanin is precursor of melanin formed. Active compounds in skin lightening product usually inhibit tyrosinase activity such as kojic acid, hydroquinone, arbutin, aloesin, ascorbic acid, cinnamic acid, and salisilic acid [3]. But not all of this was safe. For example hydroquinone, mercury, azelaic acid, kojic acid, and *Alpha Hydroxy Acids* (AHAs) can caused irritation, skin burn, acute allergy, skin inflammation, skin damaged, and skin cancer [7,8,9,11,13]. It is challange research for skin lightening agent with minimum adverse effect for example using natural product [8,9,13].

One of the fruit that contained the highest of ascorbic acid is red guajava (*Psidium guajava*). 100 g fruits of *Psidium guajava* equal to 100 mg ascorbic acid [10]. Tyrosinase inhibitory activity of ascorbic acid has been studied before. Ascorbic acid based on reported experiments, can inhibit tyrosinase activity in enzymatic reaction competitively [3]. Based on this, we research about *Psidium guajava* extracts effects on tyrosinase activity by determined inhibitory kinetic and kinetic plots.

2. Experimental Details

Materials

Mushroom tyrosinase (Sigma Aldirch), L-tyrosine (Merck), 0.4 N HCl, Mops buffer, 1N NaOH , ascorbic acid *coated* CVC tipe A dari BASF, *Psidium guajava* fruit extract, 0.01 N iodin standard, amilum indicator and aquadest.

Instruments

UV-Vis Spektrophotometer Hitachi U-1800, micropipet Soccorex 100-1,000 µL, thermometer, pH meter, *freeze dryer*, analitic Sartorius balance, volumetric flask**,** beaker glass.

Preparations

a. *Preparation of tyrosinase solutions*
Mushroom tyrosinase 4.7 mg (5370 unit) was diluted in 0.1M Mops buffer-NaOH (pH 6.5) ad 100 ml. The solutions separate in vials and save in freezer.
b. *Preparation of L-tyrosine solutions*
45.5 mg L-tyrosine were diluted in 0.1M Mops buffer-NaOH ad 25 ml (10 mM).
c. *Preparation of* Psidium guajava *fruits extract*
Psidium guajava fruit extract were collected from *Psidium guajava* fruit and homogenized with *homogenizer*, filtered and then dried with *freeze dryer*. *Psidium guajava* concentration 2.5%; 5%; and 10% w/v were diluted in 0.1M Mops –NaOH.
d. Preparation of Ascorbic Acid solutions
18.49 mg Ascorbic Acid were diluted in 0.1M Mops buffer-NaOH ad 25 ml (4.20 mM).

Determination of Ascorbic Acid Concentration

0.5 ml *Psidium guajava* fruits extract diluted in aquades ad 50 ml and titrated with 0.01 N iodin standard contains 16 g KI/L with amilum indicator ad blue solution. For compared was used aquadest as blanko [15].

Maximum Wavelenght Dopachrome Optimization

This study used Rodriquez and Flurkey method [12]. 0.5 ml tyrosinase solutions (252.39 unit/ml) and 1 ml 0.1M Mops buffer-NaOH (pH 6.5) were preincubated 25°C for 5 minute. After that added 1 ml L-tyrosine solution and scanned dopachrome absorbance by UV-Vis spectrophotometry 600-400 nm. Maximum wavelength dopachrome were determined where the highest of dopachrome absorbantion over the range of 600 to 400 nm.

Incubation Time Optimization

Incubation time with dopachrome absorbantion every 5 minute ad 25 minutes [2].

Determination of Kinetic Parameters of Tyrosinase Activity

This study used Boyer and Calzyme Lab Modification Method. 0.5 ml tyrosinase solutions (252.39 unit/ml) and 1.5 ml 0,1M Mops-NaOH (pH 6.5) were preincubated 25°C for 5 minute. Added L-tyrosine in various concentrations was measured dopachrome absorbance by spectrophotometry UV-Vis. 0.1M Mops buffer and NaOH pH 6.5 as blanko. L-tyrosine concentration were 0.5; 0.75; 1.0; and 2.0 mM. Reagent composition for determined kinetics parameter is showed in Table 1.

Table 1. Reagent composition for determined kinetics parameter on tyrosinase activity

Reagent	L-tirosine concentrations(mM)			
	0.5	**0.75**	**1**	**2**
L-tyrosine	1	1	1	1
Tyrosinase	0.5	0.5	0.5	0.5
Mops buffer	1.5	1.5	1.5	1.5

Notes: all units in mililiters.

Determination of Kinetics and Plots Effects of Psidium guajava extract

0.5 ml Tyrosinase solutions (252.39 unit/ml), 0.1 ml *Psidium guajava* extract solutions and 1.4 ml 0.1M Mops-NaOH (pH 6.5) buffer were preincubated 25°C for 5 minute. *Psidium guajava* extract concentrations were 1%; 2%; and 3% w/v and contains 0.1 ml equal to 0.029, 0.06, 0.08 mM each other. Finally added 1 ml L-tyrosine in various concentrations and measured absorbance dopachrome by UV-Vis Spectrophotometry in 10 and 20 minute. 0.1M Mops buffer-NaOH as blank. Reagent composition for determined kinetic *Psidium guajava* extract is showed in Table 2.

Table 2. Reagent composition for determined kinetic and plots of *Psidium guajava* extract inhibition

Reagent	L-tirosine concentration (mM)			
	0.5	**0.75**	**1**	**2**
L-tyrosine	1	1	1	1
Tyrosinase	0.5	0.5	0.5	0.5
Mops buffer	1.4	1.4	1.4	1.4
Sample	0.1	0.1	0.1	0.1

Note: all unit in mililiters

Determination of Inhibition Value Percentage of Ascorbic Acid

Research procedure for determined percentage inhibition value of ascorbic acid on tyrosinase activity was the same *Psidium guajava* extract but used ascorbic acid and one concentration of L-tyrosine.

Data Analysis

Determination of Ascorbic Acid Concentration

1 ml of 0.01 N iodin standard equal to 0.88 mg ascorbic acid in *Psidium guajava* extract [15].

Determination of Kinetics and Plots Effects of Psidium guajava extract

This study were taken Lineweaver-Burk curve [2]. Lineweaver-Burk curve was formed by enzymes activity plots (µmol/minute) *versus* substrate concentration ([S]). Calculation of ΔA/min value becomes µmol/menit used Lambert Beer formula:

$$c = \frac{\Delta A / \min}{E l}$$

c = dopachrome concentration had been formed (µmol/ minute)
$\Delta A/min$= changed absorbance every minute (minute^{-1})
l = thickness of kuvet from light (1 cm)
E = absorbance of molar concentrations of dopachrome (3600/M.cm)

Determined of inhibition of *Psidium guajava* extract and ascorbic acid were showed with % inhibition from ΔA/min value according to formula [2]:

$$\% \text{ inhibition} = \frac{(B - A) \times 100}{B}$$

Note A = rate of change absorbance value (ΔA/min) with sample
B = rate of change absorbance value (ΔA/min) without sample

3. Results and Discussion

Ascorbic Acid Concentrations in Psidium guajava extract

From 1500 ml *Psidium guajava* fruits were taken 105.72 gram *Psidium guajava* fruits extract equal to 1.65 g ascorbic acid. *Psidium guajava* extract concentrations were 1%; 2%; and 3% w/v and equal to 1.56 g, 3.12 g and 4.68 g each other.

Maximum Wavelength Dopachrome Optimizations

Based on literature, maximum wavelength of dopachrome is 475 nm [2]. In this research maximum wavelength of dopachrome was 477 nm (Figure 1).

Incubation Time Optimations

Incubation time of tyrosinase concentration 252.39 unit/ml and L-tyrosine concentrations 0.5; 0.75; 1.0; 2.0 mM was 20 minutes.

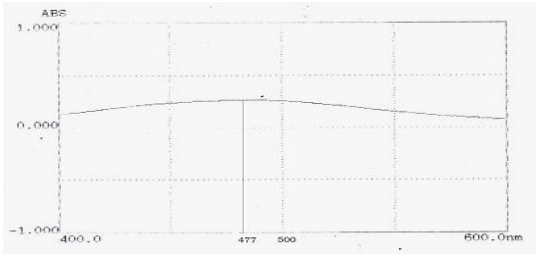

Figure 1 Result Optimization maximum wavelength of dopachrome

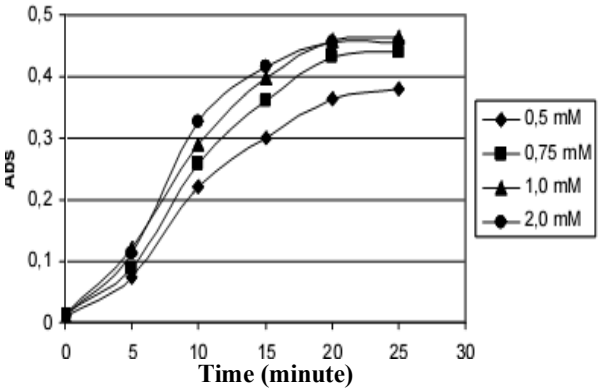

Figure 2 Result of Incubation Time Optimization

Tyrosinase Activity

This study used Michaelis menten and Lineweaver-Burk curve to get Km dan Vmax. Lineweaver-Burk curve was tyrosinase activity reciprocal *versus* with L-tyrosine concentrations. From curve Km value and Vmax were 0.315 mM and 0.0265 µmol / minute. Enzymatic reaction activity result showed in Table 3. Michaelis-Menten curve showed in Figure 3, while Lineweaver-Burk curve showed in Figure 4.

Table 3. Result of tyrosinase activity parameters

[L-tirosine] (mM)	1/[L-tirosine] (mM^{-1})	V (µmol / min)	V average (µmol / min)	1/V (µmol / min^{-1})	1/V average (µmol / min^{-1})
0.5	2	0.017	0.016	60.453	62.057
		0.016		63.660	
0.75	1.33	0.019	0.019	53.691	53.190
		0.019		52.689	
1	1	0.021	0.021	48.048	48.145
		0.021		48.241	
2	0.5	0.022	0.022	44.734	44.672
		0.022		44.610	

Michaelis-Menten Curve

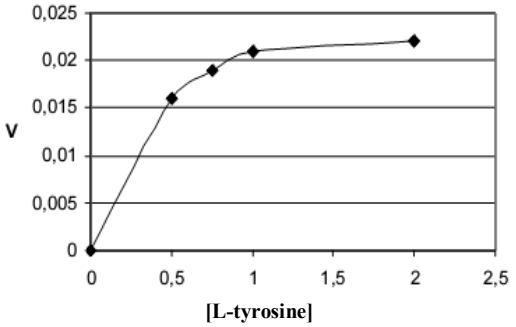

Figure 3. Relationship of tyrosinase activity *versus* L-tyrosine concentrations by Michaelis Menten curve

Lineweaver-Burk curve

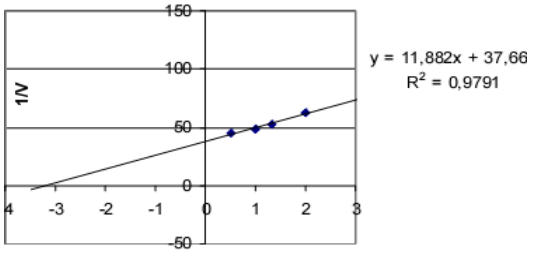

Figure 4. Relationship of tyrosinase activity *versus* L-tyrosine concentrations by Lineweaver-Burk curve

Samples Inhibition Plots

The Km and Vmax obtained in the absence and presence of *Psidium guajava* fruit extract as inhibitor in various L-tyrosine concentrations can be seem in Table 4 and Figure 5.

Table 4 Kinetic parameter of tyrosinase activity value with and without *Psidium guajava* fruit extract

Enzimatic reaction	Km (mM)	Vmax (µmol/minute)
Without inhibitor	0.315	0.0265
With inhibitor 1%	0.4824	0.0269
With inhibitor 2%	0.698	0.0283
With inhibitor 3%	0.543	0.0255

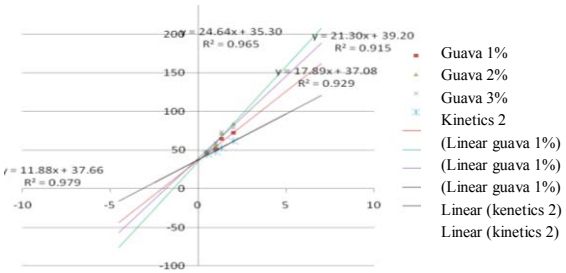

Figure 5. Relationship between enzymes kinetics with and without inhibitor

This curve showed that cross 2 cutting on y axis. The inhibitor changed Km value but not changed Vmax value. Inhibition type of *Psidium guajava* fruit extract on tyrosinase activity was competitively inhibition and showed in Figure 5.

Determined % Inhibition from product Formed

Table 5 Comparation of inhibition percentage of *Psidium guajava* fruit extract as inhibitor and ascorbic acid as control

No	Inhibitor	vit C Concentration (mM)	% inhibition
1	sample 1%	0.029	17.391
2	sample 2%	0.06	26.087
3	sample 3%	0.08	30.435
4	sample IC_{50}	0.26	50
5	control	0.26	56.523

Psidium guajava is one of the most contained of ascorbic acid. Tyrosinase is one of the most important key enzymes in the melanin biosynthesis. Inhibition of tyrosinase activity will cause a decrease in melanin production. Tyrosinase can use in two catalysis reaction for melanin production (melanogenesis), are L-tyrosine hydroxylation become dihydroxyphenilalanin (DOPA), and DOPA oxidation become dopaquinone.

Kinetic and type of inhibition were determined by invitro method with dopachrome absorbance value as tyrosinase activity parameter. *Psidium guajava* extract 1%; 2% and 3% w/v contains 0.029, 0.06, and 0.08 mM ascorbic acid. The IC_{50} of ascorbic acid on tyrosinase was 0.284 mM [14].

Determined Kinetic Parameters of Tyrosinase Activity method used Boyer and Calzyme Lab Modification Method. The condition in rooms temperature (25°C ± 2°C) and spectrophotometer in 30°C. According the literature was given temperature 25°C-30°C. pH solution buffer was used 6.5±0.05. Optimum pH for tyrosinase catalysis reaction in the literature 6.5–7.

The literature showed that maximum wavelength of dopachrome was 475 nm [2], but after optimization using spectrophotometry UV-Vis Hitachi U-1800 maximum wavelength of dopachrome was 477 nm. Dopachrome have chromophore groups such as double bonds C-O in benzena rings that can absorb light. Double bonds conjugation can decrease electron transition energy and increasing wavelength.

Incubation time optimization was 20 minute. We used this time because after 20 minute, the Michaelis-Menten curve is still proportional and differencess of absorbance value was insignificant. Enzymes concentration used was 252.39 unit/ml with 0.5 ml every procedure. According the literature tyrosinase concentration was 100-200 unit and absorbance value was 0.2 – 0.8 because it is free from *noise.*

Determined kinetics of tyrosinase activity were 10 minute and 20 minute. And then it was calculated rate of absorbance per minute (ΔA/min). ΔA/min value showed that changed dopachrome per minute (µmol/minute) using Lambert Beer formula. Inactivation of reaction such as added methanol, TCA (=*trichloroacetic acid*), extreme temperature was not done because it can dopachrome damage and made incative tyrosinase enzymes. Dopachrome was formed in µmol/minute showed tyrosinase activity in various L-tyrosine concentration.

Regression formula from Lineweaver-Burk curve in figure 10 used to determined Km and Vmax value were 0.315 mM and 0.027 µmol/minute each other. The effects of *Psidium guajava* extract on tyrosinase activity was determined Lineweaver-Burk curve showed with cutting kinetic regression in y

axis. *Psidium guajava* extract can give effects on tyrosinase activity competitively showed in Figure 5. The figure showed that Km value changed and V max value constant.

Table 5 showed that % inhibition value of *Psidium guajava* extract decrease when L-tyrosine concentration was increased. So the mechanism of enzymatic reaction was competitive [2]. Competitive inhibition of *Psidium guajava* extract was caused ascorbic acid contained.

Ascorbic acid based reported can inhibits tyrosinase enzymes competitively. Ascorbic acid can inhibit tyrosinase activity with cuprum (Cu^{+}) ion interaction in active site of tyrosinase. Ascorbic acid as antioxidant that was oxidied faster than L-DOPA in oxidation cycle and then influenced dopaquinon (product) decreasing [3]. In opposite to prove the inhibition mecanism of *Psidium guajava* extract on tyrosinase activity, we need L-DOPA as substrate to know inhibition mechanism of tyrosinase in cresolase activity or catecolase activity on the next study.

Inhibition of 0.26 mM ascorbic acid on tyrosinase activity and 1 mM L-tyrosine concentration was 56.523%. According the literature IC50 of ascorbic acid was 0.284 mM [14]. Differencess of this value was caused different of substrate using.

To know how another component in *Psidium guajava* extract can influence increasing effect on tyrosinase inhibitory activity, we need furthermore study.

4. Conclusion

Psidium guajava extract can give inhibition effects on tyrosinase activity with changed of Km value and constant in Vmax value. Km value of 1%; 2%; 3% w/v *Psidium guajava* extract concentration were 0.4824; 0.698; and 0.543 each other. V_{max} value were 0.0269; 0.0283; and 0.0255 μmol/min each other.

5. Acknowledgments

---

6. References

[1]. Anderson, A.K. (1953), Essential of Physiological Chemistry, 4th ed., John Wiley & Sons, London.

[2]. Boyer, R.F (1993), Modern Experimental Biochemistry, 2nd ed., California: The Benjamin/ Cumming Publishing Co. pp. 299-320.

[3]. Briganti, S., Camera, E., and Picardo, M. (2003), Chemistry and Instrumental Approaches to Treat Hyperpigmentation. *J. Pigment Cell. Res,* 16: 101-110

[4]. Brown, R.G. and Burns, T.(2002), Lecture Notes on Dermatology, Adapted by Zakaria. Lecture Notes on Dermatology. Erlangga, Jakarta.

[5]. Curto, E.V., Kwong, C., Hermersdorfer, H., Glatt, H., Santis, C., Virador, V.,Hearing, V. J., and Dooley, T. P. (1999), *Biochem. Pharmacol*., 57: 663-672.

[6]. Elsner, P., Maibach H. (2000), Cosmeceuticals: Drug vs Cosmetics, New York: Marcel Dekker, Inc, pp. 123-143

[7]. Lynde CB, Kraft JN (2008), Topikal treatment for melasma and postinflammatory hyperpigmentation. *Skin therapy letter*. [Serial online] vol 11. Available from: http://www.skintherapyletter.com/download/stl_11¬9.pdf, Accessed 3 June 2008

[8]. Maeda, K.,and Fukuda, M. (1991), *J. Soc. Cosmet. Chem.* 42: 361-368.

[9]. Mishima, Y., Hatta, S., Ohyama, Y., and Inazu, M. (1988), *Pigment. Cell Res*., 1: 367-374.

[10]. Morton, J. Guava. In: J.F. Morton (1987), Fruits of warm climates. Julia F. Morton, Maimi, FL. P.356-363.

[11]. Nadesul, H. (2004), *Awas!Pemutih kulit mengandung merkuri* Available from: URL : http://www.kompas.com/kcm/gprs.htm, Accessed 10 Ausgust 2004

[12]. Rodriquez, M. O. and Flurkey, W. H. A. (1992), Biochemistry Project to Study Mushroom T. *J. Chem. Ed.*, 69(9): 767-769.

[13]. Smith, C. J., Ohare, K. B.,and Allen, J. C. (1998), *Pigment. Cell Res.*1: 386-389.

[14]. Schurink, M (2007), Peptides as inhibitors of lipoxygenase and tyrosinase. *J. Biochem*, 199: 259-262.

[15]. Sudarmaji, S. (1996), Prosedur Analisa untuk Bahan Makanan dan Pertanian. Liberty, Yogyakarta, pp.26-27.

Study of Toxicity Effect of Formalin on Antioxidant Enzymatic Activities and Oxidative Damages of Rats Hepar Tissue

Chanif Mahdi [1], Aulanni'am [2]

[1,2] Biochemistry Laboratory of Chemistry Departement, Faculty of Mathematics and Natural Science, Brawijaya University, Indonesia (chanifmahdi@gmail.com)

Abstract

Using formalin or formaldehyde as an illegal preservative on food and ingredient is very danger for body health because formalin is a toxic and carcinogenic substance that potential as a sources of reactive oxygen species (ROS) and free radical exogeneous. The aim of this research was to investigate the effect of formalin toxicities that exposured through rats feeding diet on antioxidant enzymatic activity and oxidative damages of rat's hepar tissues. The research can be summarized that formalin exposure through the feeding diet of rats (Rattus novegicus) affect highly significantly on decreasing of antioxidant enzymatic and oxidative damage of hepar tissue of rat (Rattus norvegicus).

***Keywords**: Formalin, formaldehyde, ROS, oxidative damage, Rattus norvegicus.*

1. Introduction

Using formalin or formaldehyde as a illegal food preservative is very danger for the body health, because formalin is a toxic and carcinogenic substance and as source of Reactive Oxygen Species and free radical subatances.

Formaldehyde is a reactive compound, its easely reaction to nucleofilic groups, especially to NH_2 group of protein (enzyme system), that can affect on decreasing specific activity of enzyme, especially of oxidative phosphorilation system of cytochrom P450 disturbed. Overall of these will affect to acidosis condition of the cells and tissues, and tendency to over production of reactive oxygen species (ROS) and free radical substance, as a result of disturbed of Beta oxidation cycles, will affect to decrease ATP production and tendency to dead cell (*necrosis*).

Over production of reactive oxygen reactive (ROS) and free radical substances will affect both to cell membrane damages and mitochondria and canal ion damages. Ions Ca^{++} accumulated in cytosol, and stimulated NF-κB were active. These condition stimulated inflammation of the cells and tissue of hepar that charactered generation of radical notrooxide (NO.), and if it reacted to radicals superoxide (O_2.) to form radical peroxinitrit that have more toxic potent [1,2].

The danger of formalin toxicity in the body (hepar) affects to decreased antioxidant enzymatic superoxid dismutase (SOD) and reduced glutathione (GSH) of hepar. The danger of formalin toxicity affect to increase malonyldialdehide (MDA), nitrooxede (NO) and iNOS, as parameters and indicators decreasing of antioxidant enzymatic activities and increasing membrane cell damage and pathologies and inflamation of the cells and hepar tissue.

2. Experimental Details

Materials

Chemicals and Instrumentation

All of chemicals used in this research were analytical grade with the highest purity, i.e. formaldehyde, NaCl, KCl, Na_3PO_4, KH_2PO_4, TCA, TBA, HCl, Kit GSH, and KIT MDA.

Animal Experiment

Twinty five of 8- 10 week old male Rats (*Rattus norvegicus*), with the body weight 100 – 120 g, were divided into 5 groups, each group contain 5 rats. Group I was the control grop, treated with a standart pellet diet without formalin adding. Group II, III, IV and V were administrated with treatment feeding diet with formalin content of each were 25 ppm; 50 ppm 75 ppm and 100 ppm.

Methods

Measurement superoxide dismutase (SOD)

Superoxide dismutase was measured by Spectrophotometry methods at λ 580 nm. Result of measurement was be interpolarized by standart curve

Measurement of Glutathion (GSH)

Tissue glutathione content were measured colorimetrically at 412 nm according to Elman method. Homogenate were precipated with trichloro acetic acid, and after centrigution, supernatant were used for estimation of GSH level. The concentration was expressed as µmol g^{-} tissue [3]

Measurement of Malondialdehye (MDA)

Malondialdehyde (MDA) concentration was measured by spectrophotometri method at λ531 nm. Result of datas measurement was interpolarized by standart curve [4].

Measurement of hepar tissue iNOS

iNOS be measured by immunohistokimia method. Used primer antibody and secunder antibody anti rabbit IgG biotin. The substrat are used ISSAHRD and be obserbered by microscopis method [5].

Histopathologies Observaion

Histopathogy of hepar tissues was observed by hematoxylene – eosin and microscopy method [5].

3. Result and Discussion

Effect formaldehyde exposure on antioxidant activities of hepar Rats tissue

Under normal condition the cells has ability of degrade free radical. The enzyme superoxide dismutase (SOD) transforms activated Oxygen or radical superoxide into hydrogen peroxide (H_2O_2) that could be converted by enzyme catalase to harmless water (H_2O and Oxygen) [1,6].

Free radical detoxication involved the enzyme glutathione peroxidation (GPx), which converted hydrogen peroxide to water using coenzyme glutathione (GSH).

Result of study showed that formalin exposure through the feeding diet of rats effected on decresing highly significantly on antioxidant enzymatic activities in this case both are superoxide dismutase (SOD) and Reduced glutathione (GSH). Effect of formaldehyde exposure on decreasing SOD and GSH activities are presented in Table 1 and Table 2 (Appendixes).

Data from Table 1 and 2 showed that formaldehyde or formalin showed and proved that formaldehyde exposure and contamination through the feeding diet with high dosis is very danger for the body. This is because formaldehyde is a toxic and carcogenic compound. Formaldehyde has high potency as source of ROS and free radical substances that affected decreasing antioxidant enzymatic that very danger for the body health.

Effect of formaldehyde exposure through the rats feeding diet on oxidative damage

A Mismatch between the production of prooxidant and antioxidant in the cells and tissue of organs might lead to a state called oxidative stress. This lead to a elevated production of free radicals like hydroxyl radicals (OH.) and nitroxide radicals (NO.) , and mixture between NO and radical superoxide resulted radical peroxynitrite (ONOO.), which could lead to serious sellular and tissue damage (Figure 1 and 2).

Result of the study showed that formaldehyde exposure through the rats feeding died could lead to increase malonyldialdehyde production substance, as parameters membrane cells damage that affected by radical hydroxyl and iNOS by NO radicals (Table 3 and 4 – Appendixes).

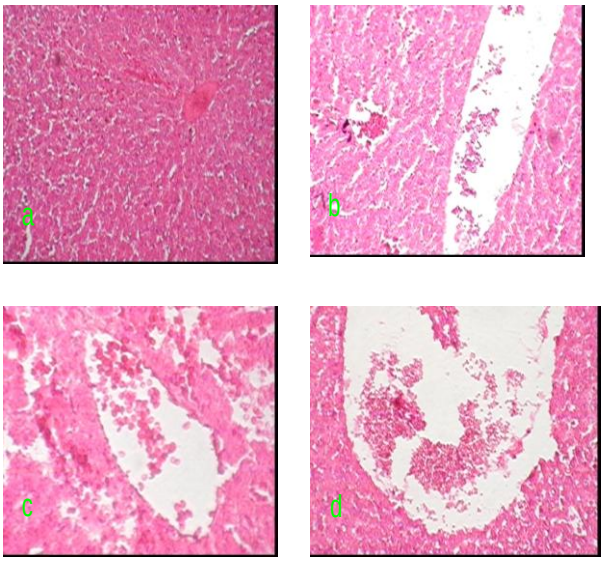

Figure 1 Effect of formaldehyde exposured on histopatologi rats hepar tissue (top left = control, top right. = 25 ppm formalin treatment, bottom left = 50 ppm formalin treatment, bottom right =75 ppm formalin treatment)

Presenting iNOS expression showed that there were pathologis a inflammation indication on cells and rats hepar tiseue [7]. The datas showed that increasing formalin concentration could lead increasing iNOS expression. More detail information is given inFigure 2.

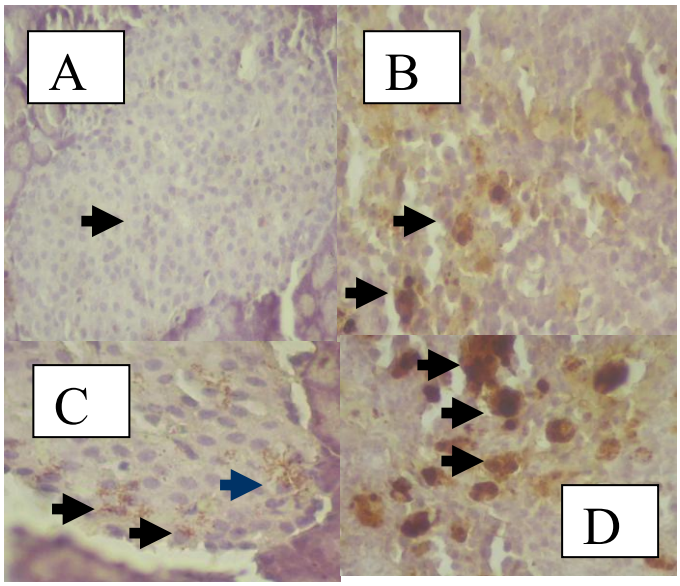

Figure 2. iNOS expression of hepar tissue that effected by formaldehyde exposure through the rats feeding diet (A. = Control, B = 25 ppm formalin treatment, C. = 50 ppm formalin treatment, D. = 75 ppm formalin treatment, E = 100 ppm formalin treatment)

4. Conclusion

1. Formaldehyde as potent a source of ROS and free radicals
2. ROS and free radicals from formaldehyde exposure could lead decreasing antioxidant enzimatis (SOD) and GSH
3. Decreasing of antioxidant enzimatis could lead cells and tissue damages and pathologies effects on Rats hepar tissue.

5. Acknowledgments

---

6. References

[1]. Muller, WE. Eckert, GP, and Schilling, SS, (2006), EU project. Local food nutraceutical. Dept. Pharmacology University of Frankfurt. Pages 1-8.

[2]. Halliwel, B. and Gutteridge, JMC. (1999), Free radical in biological medicine. Third edition. Oxford. Oxford University Press. Pages 1-35; 246- 350.

[3]. Bioxytech (2008), GSH / GSSG – 412. Colorimetric determination of reduced and oxidixed glutathione for research use only. Not for use in diagnostic procedures. Catalog number 2140.

[4]. Laboratorium Farmakologi (2007), Intro of oxidant – antioxidant measurement. Fakultas Kedokteran Universitas Brawijaya.

[5]. Laboratorium Biomedik (2004), Protokol pemeriksaan metode histokimia. Fakultas Kedoteran Universitas Brawijaya.

[6]. Bray, TM. (2006), The role of free radical in nutrition and prevention of chronic desease. College of health and human science. Origon state university, USA. Pages 1-37.

[7]. Bloodwort, A., Odonnel, VBV, Freeman, BA. (2000), Nitroc oxide regulation of free radical and enzyme mediated lipid and lipoprotein oxidation. Artioscler thromb vasc. Biol, 20: 1173- 1178.

[8]. Central laboratory of life sciences (2007), Lokakraya pengembangan riset kemitraan. Program hibah kompetisi A-2 jurusan kimia Fakultas MIPA Universitas Brawijaya.

[9]. Gulec, M., Gurel, A. and Amutcu, F. (2006), Vitamin E protect again oxidative damage, caused by formaldehyde in the liver and plasma rats. http:www.sprinklink.com/q/. pages 1-3.

Appendixes

Table 1. Effect of variety formaldehyde concentration exposures on Superoxide Dismutase activities

Formaldehyde treatment	SOD Activities (Unit)					Mean Value
	1	2	3	4	5	
Control (0 ppm)	70.66	73.05	70.47	72.55	70.93	71.53[e]
25 ppm	28.59	29.27	29.70	29.23	28.87	29.13[d]
50 ppm	24.56	26.25	27.39	26.57	25.25	26.00[c]
75 ppm	20.15	21.05	21.05	19.78	19.89	20.38[b]
100 ppm	17.21	16.89	17.11	16.91	17.17	17.06[a]

Table 2. Effect variety formaldehyde concentration exposure through rats feeding diet on hepar tissue GSH content

Formaldehyde treatment	GSH (µg / ml)					Mean Value
	1	2	3	4	5	
Control (0 ppm)	50.23	50.41	50.11	51.13	50.43	50.26[e]
25 ppm	25.07	25.21	25.21	25.33	25.41	25.25[d]
50 ppm	21.11	21.25	21.13	21.27	21.33	21.20[c]
75 ppm	17.27	17.33	17.19	17.17	17.29	17.23[b]
100 ppm	13.67	13.71	13.63	13.57	14.07	13.73[a]

Table 3. Effect of Formaldehyde exposure through the rats feeding diet on MDA production of hepar tissue

Formaldehyde treatment	MDA (µg/ml)					Mean Value
	1	2	3	4	5	
Control (0 ppm)	5.31	5.47	5.41	5.29	5.30	5.36[a]
25 ppm	18.61	19.05	18.59	18.42	18.76	18.67[b]
50 ppm	29.59	29.29	29.25	29.70	29.60	29.49[c]
75 ppm	35.26	35.43	35.26	35.27	35.41	35.33[d]
100 ppm	39.63	39.43	39.29	39.51	39.46	39.46[e]

Table 4. Effect formaldehyde exposure through the rats feeding diet on

Formaldehyde Treatment	iNOS expression of hepar tissue			Mean value
	1	2	3	
Control (0 ppm)	2	1	3	2[a]
25 ppm	19	19	16	18[b]
50 ppm	21	27	29	25.67[c]
75 ppm	21	31	29	27[d]
100 ppm	33	36	39	36[e]

Monoclonal Antibodies to Bovine Zonna Pellucida 3 (*Mab-b*ZP3) for Woman Immunocontraceptive Vaccine

Dedy Kurniawan [1], Sutiman B Sumitro [1], Aulanni'am [2]

[1,2] Department of Biology, Faculty of Mathematics and Sciences, Brawijaya University, Indonesia
(rudededy@gmail.com)
[3] Department of Chemistry, Faculty of Mathematics and Sciences, Brawijaya University

Abstract

Immunocontraception has received increased interest in last decades as a potential way of controlling the rapid growth of Indonesian population. Development of vaccine based on zona pellucida antigens represents a promising approach to potential contraception.. Recent advances in monoclonal antibody technology are enabling the development of new methods for producing specifif antibody for immunocontraception. Seven research stages were conducted to construct monoclonal antibodies to Bovine Zonna Pellucida 3 (Mab-bZP3). Stage 1, collection Bovine Zonna Pellucida 3 (bZP3), stage II, Immunisized mouse Balb/c by Bovine Zonna Pellucida 3 (bZP3), stage III, Collecting spleen cells from a mouse that has been immunized with the desired antigen, stage IV Fussion spleen cells with myeloma cells, stage V, Hybridoma screening , stage VI, single cell cloning and Monoclonal antibody production and characterization. The Result showed that Mab-bZP3 were produced both hybridoma cell and ascites fluid positively and more specific reacted with antigen Bovine Zonna Pellucida 3 (bZP3) by immunoblotting technique. Mab-bZP3 should prove useful for candidate immunocontraceptive vaccine.

***Keywords**: Bovine Zonna Pellucida 3 (bZP3), immunocontraception, monoclonal antibody.*

1. Introduction

The development of immunocontraception in women has been developed using antibodies against proteins such as bZP3 pellusida zone. Pellusida Zone (ZP) is an extracellular matrix that plays an important role in the interaction of sperm and egg cells to start the process of fertilization. These interactions involve receptors on the surface of the zone pellusida. Bovine ZP could be separated into 4 glycoproteins spots, namely *b*ZP1, *b*ZP2, *b*ZP3, and *b*ZP4, with different molecular masses and isoelectrical points [1,2].

ZP3 is selected as the focus because this is the major receptor protein in the fertilization process. Antibodies against pellusida zone to suppress the effectiveness of self-fertilization because in addition to the reactive nature of the individuals who are immunized are also able to recognize other species [3].

ZP3 is one of the main glycoproteinom pellusida zones, which acts as the sperm receptor and important role in the process of fertilization. Antibodies to sperm ZP3 inhibit interaction spermatozoa and eggs, as this will prevent the ZP3 function as sperm receptor. Polyclonal antibodies from *b*ZP3 proven inhibit in vivo fertilization, in this study becomes very important to improve the quality antibodies through biosynthesis monoclonal antibody to *b*ZP3 (*Mab-b*ZP3).

2. Experimental Detail

In order to get better quality of *b*ZP3, we disrupt the membrane of ZP by means of mechanical method. High resolution 2-dimensional polyacrylamide gel electrophoresis under reducing conditions and electroelution were used to separate the *b*ZP glycoproteins. The Zonna Pellucida 3 (*b*ZP3) as antigen was injected intraperitoneally into two female BALB/c mice. After 3 weeks the animals received booster' doses twice with bZP3 (at 1-week intervals), after which the spleen cells were prepared and fused with an exponentially growing NS0 myeloma cell line using polyethylene glycol. After 2 weeks in selection medium and isolation of positive cells, and were cloned to select hybridomas with a high mAb production. The purified mAb was used in different technique (Dot blotting and Western Blotting) after establishing the appropriate dilution.

Dot Blotting

Dot blots were carried out as described by Aulanni'am [4]; 3 cm^2 Nitrocelllulose membranes (NC) were cut and activated in PBS and 10 µL

of bZP3 (10 µL/dot) was coated in NC and allowed to bind. The papers were incubated 2 hours in blocking buffer containing 5% (w/v) milk powder in PBS. They were washed three times in PBS-T and incubated with primary antibody for 1 h. After three washes in PBS-T with and without 0.05% Tween-20 the membranes were incubated with 1/750 dilution rabbit antimouse alkalin phosphatase conjugate (Sigma) for 1 h. After further washes, they were exposed to alkalin phosphatase substrate consisting of 0.21 mg/mL Nitro Blue Tetrazolium and 0.42 mg/mL Bromo- 4-chloro-3-indoxyl-phosphate in Tris buffer. The reaction was terminated by rinsing with fresh water.

SDS-PAGE and Western blotting

Standard methods of SDS-PAGE and Western blotting were used [1,2]. The resolving gel was set at 12% (v/v) concentration, and isolate *b*ZP volume 35 µL/lane was loaded and run at a constant current of 10 mA. The transfer was attained at a constant current of 150 mA for overnight to NC membrane. After transfer the membrane was washed in PBS + NaN3 and immersed in 5-bromo-4-chloro-3-indolylphosphate / nitroblue tetrazolium (BCIP/NBT) substrate buffer to develop the band patterns.

3. Result and Discussion

Lymphocytes cell were collected form mice that induced by Bovine Zonna Pellucida 3 (*b*ZP3). For preparing fusion with myeloma cell to make hybridoma cells that produce Mab-bZP3d, we used Myeloma cell NS0.

Figure 1. Lymphocytes cells collection from Mice balb/c induced by (bZP3)

Subsequent hybridoma cells were grown in HT medium and screened for antibodies using ELISA technique. Hybridoma cells that produce antibodies against *b*ZP3 then rose back to *Mab-b*ZP3 production.

Figure 2. Hybridoma cell

The specificity of *Mab-b*ZP3 that confirmed by *Dot blot* technique is given in Figure 3

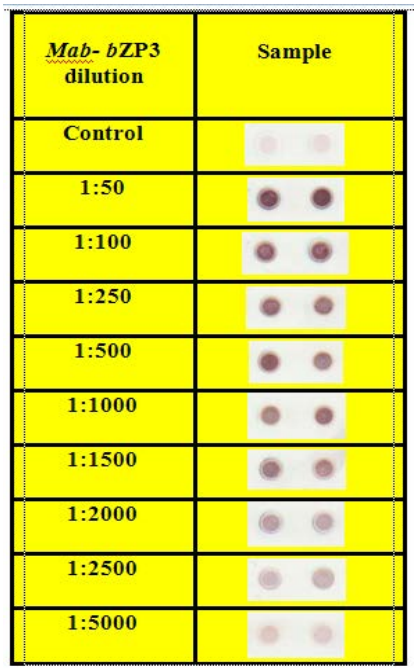

Figure 3. Specificity of monoclonal antibodies against *b*ZP3 by Dot Blot Technique

Dot blot results showed that *Mab-b*ZP3 produced by hybridoma cells capable of recognizing bZP3. Gradations of color stains formed as a result of reaction between *Mab-b*ZP3 with bZP3, which *Mab-b*ZP3 can identify up to 1:2500 dilutions. *Dot blot* technique only provides information about the presence or absence of proteins and does not provide information on concentrations and molecular weight of these

proteins, so further testing should be more specific, using *Western Blot* [5].

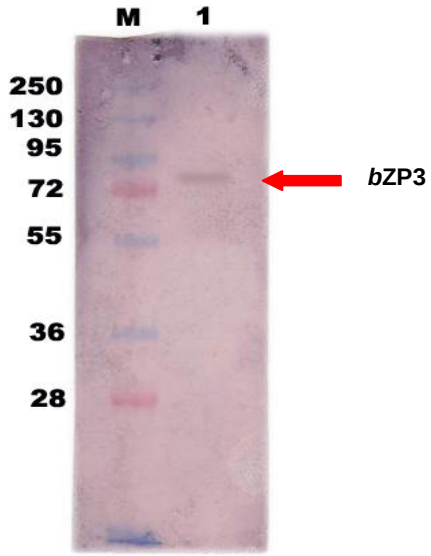

Figure 4. Positive *Mab-b*ZP3 against to *b*ZP3 by Western Blot Technique (M= Protein Marker 1.= *b*ZP3)

Test results of western blot analysis showed that the *Mab-b*ZP3 produced in this study is specific because they only recognize *b*ZP3 molecules. Antibody specificity is determined based on the ability of antibodies to recognize specific protein epitopes of other protein epitopes [6].

4. Conclusion

Monoclonal antibodies against bZP3 (*Mab-b*ZP3) have high specifity and possibility to develop of woman immunocontraceptive vacine.

5. Acknowledgements

This Study was supported by Hibah Kompetensi DIKTI. We also thank to Wibi Riawan, S.Si for skillful technical assistance of hybridoma cell culture.

6. References

[1]. Sumitro S.B. and Aulanni'am (2001), Antibodies to Bovine Zonna Pellucida-3 (anti-bZP3) Induced Reversible Immunocontraception in Local Rabbit and Wistar Rat : A Candidate For Immunocontraception Vaccine The 11th ASEAN Federation of Endocrine Societies Congress, November 7-11, 2001, Denpasar Bali (Poster)

[2]. Sumitro, S.B. and Aulanni'am (2001), Zona Pellucida 3 (ZP3) has Proper Biochemical Properties to be considered as Candidate Antigen for Immunocontraceptive Vaccine. Reprotech. *The Indonesian Journal of Reproductive Science and Technology*. 1(1) : 51–53

[3]. Peterson TE, SM Petrounkina and GM Hundrise. (2000), Oocyte-Sperm Interaction. *Anim Reprod Sci*, June, 2: 60-61, 653-62.

[4]. Aulanni'am , Sumitro S.B., Djati M.S. , Sutiyoso and Ciptadi G. (2001), Characterization of Bovine Zona Pellucida. Annual Report of Hibah Bersaing Research. IX/1. FMIPA- Unibraw, Malang.

[5]. Takagi J., (2000), Semi-Quantitative Measurement of Proteins by Dot Blotting. http://labs.idi.harvard.edu/springer/protocols/jun_dotblot.html

[6]. Kuby, J., (2004), The Anatomy of The Immune System.http://www.micro.msb.le.ac.uk/index.html: Infection and immunity.

[7]. Aulanni'am, Sumitro S.B., Sutiyoso S., Susilawati T., Djati M.S., Ciptadi G. and Roosdiana A. (2001) b. The Bovine Zonna Pellucida: The Ratio of Protein and Carbohydrate The 11th ASEAN Federation of Endocrine Societies Congress, November 7-11, 2001, Denpasar Bali (Poster) .

[8]. Sumitro, S.B, Aulanni'am and Sutiyoso S, (2002), Bovine Zona Pellucida (bZP3): A Candidate for Immunocontraceptive Vaccine. *Journal of the ASEAN Federation of Endocriine Societies (JAFES)*. Vol 20 No.1 (Supplement), January, p: 145.

[9]. Tulsiani DR. (2000), Structural analysis of asparagine-linked glycan units of ZP2 and ZP3 glyciproteins from mouse zona pellucida. *Arch Biochem Biophys* Oct 15 ; 382(2): 275-83

Monitoring and Capability Analysis of Hemoglobin Level in Pregnant Women

(Case Study of Hemoglobin Data of Pregnant Women in a Maternity Clinic in Banjarmasin)

Dewi Anggraini

Department of Mathematics, Mathematics and Natural Sciences Faculty, Lambung Mangkurat University, Banjarbaru, Indonesia (de28383wi@yahoo.com)

Abstract

This paper deploys Statistical Quality Control (SQC) to analyze and monitor quality characteristic measurements of hemoglobin level of pregnant women in a maternity clinic in Banjarmasin. The objective of this study is to assist medical practitioners in observing the hemoglobin level of pregnant women during their pregnancy period. This is a significant factor in delivering their baby with normal hemoglobin level consequently reducing the incidence of hemorhagia post partum. It is also assumed that pregnant women who deliver their baby in the clinic have been monitored during their nine-month pregnancy and each consumed 90 tablets of Vitamin C 100 mg and Sulfas Ferroses (SF) 350 mg after their third semester of pregnancy (after six month period of pregnancy). Thus, they can manage their own pregnancy to normally deliver their baby with normal hemoglobin level. The use of Statistical Process Control (SPC) tools such as; frequency histogram, probability plot, and the implementation of Shewhart, R, and S control charts as primary techniques, are presented to display the monitoring aspects of the process. In addition, Process Capability Analysis (PCA) is performed to ensure that the mother's hemoglobin level meet certain requirements or specifications limits. The Process Capability Ratio (PCR) for the hemoglobin level is also presented. This analysis is an essential part of an overall quality improvement program in a medical area.

Keywords: *Process Capability Analysis, Shewhart, R, and S control charts, Hemoglobin Level.*

1. Introduction

Background

Statistical process control (SPC) is a branch of statistics used for systematically monitoring a production process/service to achieve stability, and quality improvement in the process by reducing variability. This method combines time series analysis methods with graphical presentation of data to provide insights and better understanding about data for medical researchers and practitioners consequently improving the quality of healthcare process/service [2].

The implementation of SPC has been widely used in the medical area. Goldenberg, *et all* (2002) described an early statistical detection of anthrax outbreaks by tracking Out-The-Counter (OTC) medication sales. They used a statistical framework for monitoring grocery data to detect a large-scale but localized bioterrorism attack. They designed an early detection statistical system for bio surveillance to improve clinical preparedness for bioterrorism. Stevens (2007) has investigated SPC with its core tool, the control chart. His study can facilitate medical practitioners in managing the change of healthcare systems and improving patients' health. He also explained that SPC helped patients with chronic conditions, such as asthma and diabetes, to manage their own health and therefore, improve therapeutic qualities.

Statistical process control (SPC) has been applied to healthcare improvement in a wide range of settings and specialties. It has been noted that SPC can indeed be a powerful and versatile tool for managing changes in healthcare through Quality Improvement (QI). Besides helping diverse stakeholders manage and improve healthcare processes, SPC can also help clinicians and patients understand and improve patients' health when applied directly to health indicators such as blood sugar concentrations in diabetes. In healthcare, the ~~"s~~study subject" can also be an active agent in the process, as when patients apply SPC to their own health. Several studies indicated the empowering effects this may have on patients. SPC application thus has therapeutic potential as it can help patients manage their own health [7].

Maternal Mortality Rate (MMR) is still high and this is one example of significant health problem in Indonesia. This fact can be shown from the result of Indonesian Health Demography 2002 – 2003 that MMR in Indonesia is 307/100,000 live births. This value is still high compared to the World Health Organization (WHO) target that is 102/100,000 live births.

Based on Household Health Survey 2001, the direct causes of maternal mortality are hemorrhage post partum (28%), eclamsia or hypertension during pregnancy (24%), infection (11%), late delivery

(5%) and abortion (5%). In 2003, MMR in Banjarmasin was reported 20 people with hemorrhage post partum (3 cases), eclamsia (3 cases) and other factors (14 cases). Anemia is one significant cause of hemorrhage post partum in pregnant woman when delivering their baby. If the hemoglobin level < 11.5 gr% in a woman she will be classified as anemia while, if her hemoglobin level ≥ 11.5 gr% she will be classified as normal.

This study aims to evaluate the service characterization of a maternity clinic in monitoring pregnant women to have a normal hemoglobin level when delivering their baby. This quality of service can be investigated by first using histogram, probability plot, and the implementations of Shewhart, R, and S control charts as a primary technique for summarizing the performance of the process. In addition, this study will display the potential capability of the clinical process. We will use Process Capability Ratio (PCR) to show how capable the clinic is in helping pregnant women to have a normal hemoglobin level when delivering their baby.

This study uses a secondary data of 125 hemoglobin level samples collected between January 2005 and December 2010. We use samples of size five. All patients have delivered their baby in the maternity clinic in Banjarmasin.

Statistical Quality Control (SQC)

Statistical Quality Control (SQC) is a statistical method that requires a quality characteristic measurement of manufacturing data in order to analyze and maintain the quality of manufactured product [4]. The SQC methodologies use descriptive statistics tools to describe quantitatively variation in quality characteristics by drawing a sample from its related population and use population probability distributions for modeling or describing the quality characteristic of a process [5].

Normal Distribution

Normal (Gaussian) distribution is probably the most important distribution in both the theory and application of statistics with the probability density function:

$$f(x)=\frac{1}{\sqrt{2\pi}\sigma}e^{-\frac{1}{2}\left(\frac{x-\mu}{\sigma}\right)^2},\quad -\infty<x<\infty$$

where $\mu\ (-\infty<\mu<\infty)$ and $\sigma\ (\sigma^2>0)$ are the mean and the variance of the normal distribution, respectively.

If X is a random variable that is normally distributed with mean μ and standard deviation σ, then it is presented by:

$$X\sim N(\mu,\sigma^2)$$

In a normal distribution, there is a simple interpretation of σ. This standard deviation measures the distance on the horizontal scale associated with the limits defined by $\mu\pm\sigma$ (68.26% of the population values fall between the limits), $\mu\pm 2\sigma$ (95. 46% of the population values fall between the limits), and $\mu\pm 3\sigma$ (99.73% of the population values fall between the limits) [4].

Statistical Process Control (SPC)

Statistical Process Control (SPC) is one of techniques used to monitor manufacturing processes and provide immediate feedback control. The feedback control is used to maintain and improve the capability of the process that result in product conformance to meet customer satisfactions.

Some techniques associated with SPC include histograms, and control charts. A histogram is a visual display of frequency distribution to show shape, location, and spread of data. While, a control chart is a statistical tool used to monitor the variation and trends occurring in a process and ensure that the process is in a state of control. A control chart has its limits: Upper Control Limit (UCL), Central Limit (CL), and Lower Control Limit (LCL) measured from the dispersion happened in the process. These limits can be set as $\mu\pm\sigma$, $\mu\pm 2\sigma$, or $\mu\pm 3\sigma$, where μ is the process mean and σ is the process standard deviation [4].

A manufacturing process or service is well-controlled if the quality characteristic measurements of the process lie between the control limits. Generally, the statistical limits used in SPC are $\mu\pm 3\sigma$ which also refer to as "three sigma control limits". In a normal distribution, these limits imply that 99.73% of the samples mean lie in the interval of width 6σ. Note that σ here refers to the standard deviation of the statistics plotted on the chart (i.e. $\sigma_{\bar{x}}$) not the standard deviation of the quality characteristic [5].

Process Capability Analysis (PCA)

Process capability analysis is used to ensure that the outcomes of a process are capable to fulfill certain requirements or specifications. Application of process capability analysis is an essential part of an overall quality improvement program in any industry today. It provides guidance to how to produce products that meet required specification limits.

Process capability analysis can produce valid and accurate report if the observed process is in-control. The concept of process capability was introduced by Juran et al. (1974). The two most popular indices used in manufacturing industry are *Cp* and *Cpk* defined as follows.

$$C_p = \frac{USL - LSL}{6\sigma} \quad (1)$$

$$C_{pk} = \min\left(\frac{\mu - LSL}{3\sigma}, \frac{USL - \mu}{3\sigma}\right) \quad (2)$$

$$C_{pk} = \min\left(C_{pl}, C_{pu}\right) \quad (3)$$

Cp and *Cpk* are process capability indices which assess the ability of process products in meeting their respective specification limits. In the analysis of these measures, there are mainly two characteristics of importance, the process location in relation to its target value and the process spread. The closer the process output is to the target value or the smaller that the process spread is, the more capable is the process. The process capability indices combine the above characteristics of a capable process and transform them into a single number that reflects the capability of the process. The larger the value of a process capability index, the more capable is the process [4].

LSL and USL are the lower and upper specification limits, μ and σ are the process mean and standard deviation, respectively. Since the process mean μ and process variance σ^2 are unknown, they are often estimated using collected quality characteristics data [5].

Both of the above mentioned capability indices were designed to be used with the normally distributed data. However, these basic assumptions of normality are not usually fulfilled in practice. Most of the processes in the real world produce non-normal quality characteristics data and the quality practitioners need to consider the basic assumptions before deploying any conventional process capability technique [1].

Maternal Mortality Rate (MMR) and Anemia

As mentioned earlier, the Maternal Mortality Rate (MMR) is still high in Indonesia and anemia is one significant cause of hemorrhage post partum in pregnant women when delivering their baby.

According to WHO (1972), specification limits used to determine the anemic status of a pregnant woman is categorized as: normal (≥11 gr%), mild anemia (8-11 g%), and severe anemia (less than 8 g%). The result of blood testing show that the average hemoglobin level of pregnant women is 11.28 mg%, the lowest is 7.63 mg% and the highest is 14.00 gr%. Other anemia classification is [9]:

a. hb 11 gr% : normal
b. hb 9-10 gr% : mild anemia
c. hb 7 – 8 gr%: medium anemia
d. hb < 7 gr% : severe anemia.

2. Results and Discussion

This study has used 125 samples of size five, which are taken from a maternity clinic in Banjarmasin between January 2005 and Desember 2010. The Shewhart $\bar{x}$, R , and S charts have been designed to monitor the process average or mean quality level, variability, and standard deviation, respectively.

In constructing control charts, it is suggested to plot R , and S chart first because the control limits on $\bar{x}$ chart depend on the process variability and standard deviation that are:

$$UCL = \bar{\bar{x}} + A_2\bar{R}$$
$$CL = \bar{\bar{x}}$$
$$LCL = \bar{\bar{x}} - A_2\bar{R}$$

and

$$UCL = \bar{\bar{x}} + A_3\bar{S}$$
$$CL = \bar{\bar{x}}$$
$$LCL = \bar{\bar{x}} - A_3\bar{S}$$

where $\bar{\bar{x}}$ is the average of the samples averages (the grand average), $\bar{R}$ and $\bar{S}$ are the average of samples ranges and standard deviations, and A_2 and A_3 are constants defined by:

$A_2 = \frac{3}{d_2.\sqrt{n}}$ and $A_3 = \frac{3}{c_4.\sqrt{n}}$.

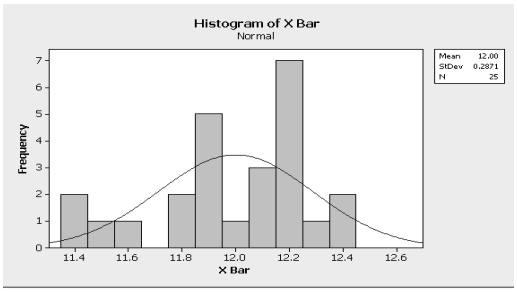

Figure 1a. Histogram of Hemoglobin Level

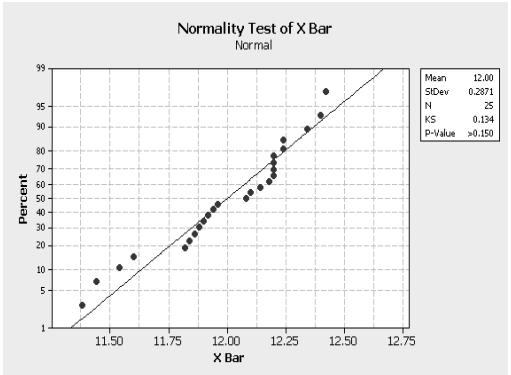

Figure 1b. Normal Probability Plot of Hemoglobin Level

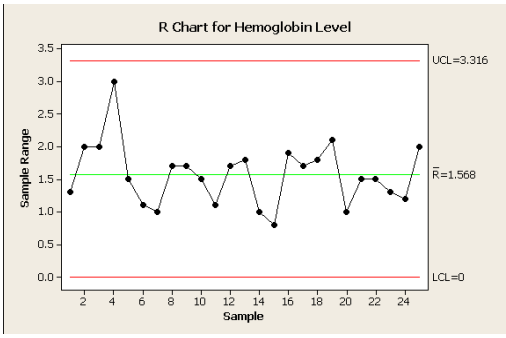

Figure 1c. R Chart for Hemoglobin Level

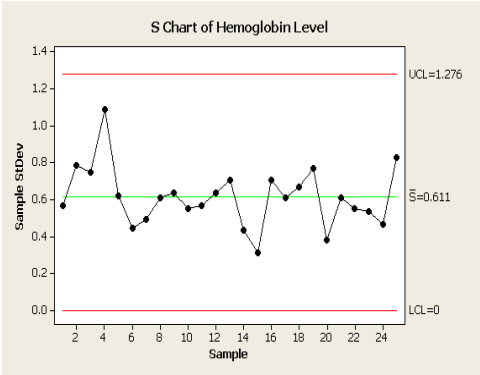

Figure 1d. S Chart for Hemoglobin Level

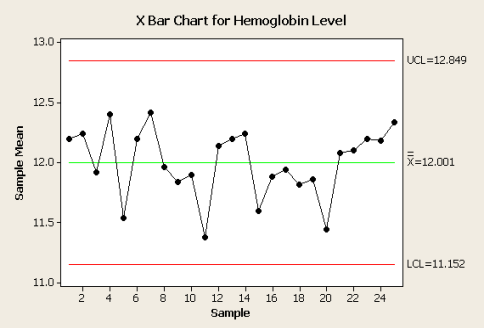

Figure 1e. $\bar{x}$ Chart for Hemoglobin Level

Figure 1a, and 1b show that the hemoglobin data are normally distributed. Figure 1c, R Chart describes that there is no out of control observations, so that the range of samples are in control. This is also justified by looking at Figure 1d, S chart where there is also no out of the control signals. Since R and S Charts both are in control we can now produce the $\bar{x}$ chart (Figure 1e).

As mentioned earlier one can assess the capability of the process only when process is in control. Using the statistical package Minitab we have provided the result of the capability analysis in Figure 2 below.

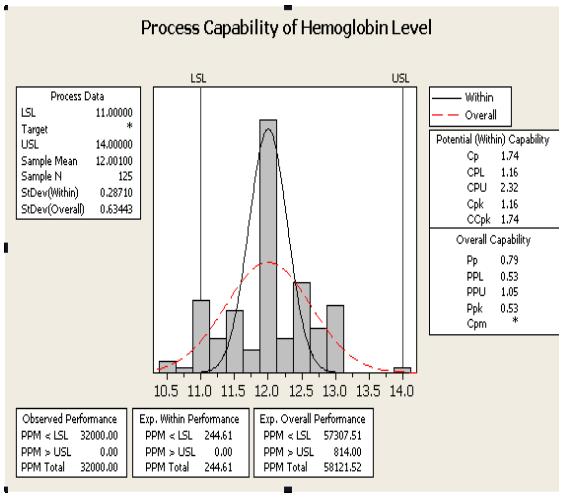

Figure 2. Process Capability Analysis for Hemoglobin Level of Pregnant Women

It can be seen from Figure 2 that the value of $C_p = 1.74$ and $C_{pk} = 1.16$. The value of C_p indicates that the potential capability of having pregnant women with normal hemoglobin level in the clinic is very good. According to our analysis, the chance of having anemic pregnant women is approximately 0.34 women per million (ppm) live births. In other words the chance/proportion of having anemic pregnant women in the clinic is very small. While, the value of $C_{pk} = 1.16$ describes that the actual capability of having pregnant women with normal hemoglobin level in the clinic is also very high. However, the fact that C_p is not equal C_{pk} means that the actual mean of having pregnant women with normal hemoglobin level is different to the nominal mean of having pregnant women with normal hemoglobin level. The nominal mean is the average of the upper and lower specifications.

3. Conclusion

In this paper we have shown that Statistical Process Control (SPC) and Process Capability Analysis (PCA) can be applied effectively in health care service. Using real data based on the hemoglobin level of pregnant women in a maternity clinic in Banjarmasin, we have first monitored the hemoglobin level using control charts. This is then followed by capability analysis to estimate the proportion of anemic pregnant women. The significant assumption used in this study is the fact that the pregnant women who have delivered their baby in the clinic have been monitored during their nine month pregnancy and treated with 90 Vitamin C 100 mg tablets and 90 Sulfas Ferroses (SF) 350 mg tablets in their second three semester pregnancy.

The study was based on 125 samples of size five. The data was normally distributed with mean

$\mu = 12.001$ gr%, and standard deviation $\sigma_{\bar{X}} = 0.2871$ gr%. The results indicated that women who have been monitored in the clinic through out their pregnancy period are certainly capable of having a normal hemoglobin level when delivering their baby at the maturity of their pregnancy period.

In conclusion, one can say that the process of observed maternity clinic in Banjarmasin is a capable process and can significantly reduce the maternal mortality rate in Indonesia and should be implemented nation wide in the country. During this study, it was also observed that the medical practitioners who run the clinic are highly qualified and provide an excellent service of care and monitoring for the pregnant women who attend the clinic.

4. Acknowledgment

I would like to thank to Dr. Mali Abdollahian (Senior Lecturer, Program Leader of Master and Graduate Diploma of Statistics and Operations Research, and Program Leader of Master and Graduate Diploma of Business Statistics of RMIT University, Melbourne, Australia) for her useful advice, discussion, and proof reading that were significantly contributed to the completion of this paper. I also would like to thank Supri Nuryani, SKM, SST, MKes, the owner of maternity clinic, for providing the hemoglobin level data of pregnant women.

5. References

[1]. Ahmad, S., Abdollahian, M., and Zeephongsekul, P. (2007), Non-normal process capability evaluation, *IKE"07 (The 2007 International Conference on Information and Knowledge Engineering),* June 25 – 28, pp. 321 – 326, Las Vegas, U.S.A.

[2]. Benneyan, J.C., Lloyd, R.C., and Plsek, P.E. (2003), Statistical process control as a tool for research and healthcare improvement, *British Medical Journal: Quality and Safety in Health Care*, Vol. 12 Issue. 6, December. pp. 458 – 464.

[3]. Goldenberg, A., *et al*. (2002), Early statistical detection of anthrax outbreaks by tracking over-the-counter medication sales, *Proceedings of the National Academy of Sciences (PMNAS),* April 16, vol. 99, no. 8, pp. 5237 – 5240, USA.

[4]. Hanna, S.M, *et al* (2003), Application of statistical process control (SPC) in the manufacturing of medical accelerators, *Proceedings of the 2003 Particle Accelerator Conference*. May 12 - 16, vol. 2, no. 8, pp. 1077 – 1079. Siemens Medical Solutions USA, Inc., Concord, CA, USA.

[5]. Montgomery, D.C. (2001), Introduction to statistical quality control, 4th edition, John Wiley and Sons Inc., USA.

[6]. Stevens, D.P. (2007), Quality lines, Quality and Safe in Health Care, October, vol. 16, no. 5, p. 322, USA.

[7]. Thor, J., *et al*. (2007), Application of statistical process control in healthcare imperovement: systematic review, *British Medical Journal: Quality and Safety in Health Care*, Vol. 16 Issue. 5, October, pp. 387 – 399.

[8]. Wijaya, A.M. (2007), Kondisi Angka Kematian Neonatal (AKN), Angka Kematian Bayi (AKB), Angka Kematian Balita (AKBAL), Angka Kematian Ibu (AKI), dan penyebabnya di Indonesia.

[9]. _____ (2007). Menkes Canangkan Stiker Perencanaan Persalinan dan Pencegahan Komplikasi, Pusat Komunikasi Publik, Sekretariat Jendral Departemen Kesehatan,http://www.depkes.go.id/index.php?option=news&task=viewarticle&sid=2707&Itemid=2, viewed 5 February 2011.

Anti-Inflammatory of Methanolic Fraction from 96% Ethanolic Extract of Honey Bee Propolis on White Male Rats Wistar Strain

Dwi Ningsih [1], Agustina Wulandari [2], Gunawan Pamudji Widodo [3]

(1, 2, 3) Faculty of Pharmacy, Setia Budi University, Surakarta, Indonesia

Abstract

Propolis is natural substance produced by honey bee. Flavonoid and CAPE (caffeic acid phenilethyl ester) are propolis components that have anti-inflammatory activity. The aim of this research is to know the anti-inflammatory activity of methanolic fraction of propolis on white male rats that is inflamed by carragenin. Propolis was extracted by maceration method with 96% ethanol. The ethanolic extract was fractionated until yielded methanolic fractions. The methanolic fraction was tested at group of the rats with dose 1.89; 2.84; and 3.78 mg/200 g bw. The positive control was given sodium diclofenac (0.9 mg/200g bw) and negative control was given 0.5% CMC solution. The test material were given orally one hour before the rat''spaw was injected by intraplantar with 1% carragenin to make edema. Anti-inflammatory activity was observed from the ability to reduce edema volume at one hour interval for five hours. The data was analyzed using two way anava followed Dunnett test.The result of this study showed that propolis methanolic fraction had an anti-inflamatory activity. The methanolic fraction of 1.89 mg/200g wb had 47.23%, dose of 2.84 mg/200g wb had 58.89%, and dose of 3.78 mg/200g wb had 58.39% anti-inflammatory activity that were not significantly different compared with positive control (48.95%). It was indicated that methanolic fraction of propolis at dose 1.89 mg/200 g wb had equal anti-inflammatory activity with positive control. The result of gastric mucous observation showed there was no ulcer as side effect from methanolic fraction of propolis.

Keywords: *propolis, anti-inflammatory, methanolic fraction.*

1. Introduction

Inflammation is a protective response to tissue injury caused by physical trauma, chemicals damage, or microbiology substances. Inflammation is the body's attempt to inactivation or destroy the organisms that attack, eliminating irritant substances, and regulate tissue repair [1].

Treatment of inflammation in general use chemical drugs such as steroids or nonsteroidal anti-inflammatory drug (NSAID). Inflammatory therapy using steroids require high doses that can cause various side effects such as moon face, fluid retention, hypokalemia, hyperglycemia (diabetes), the occurrence of adrenal suppression, increased susceptibility to infection and hypertension. Using of NSAID in inflammatory drugs often cause side effects such as gastrointestinal bleeding and ulceration and nephrotoxicity [2].

The occurrence of various side effects in the treatment of inflammation using chemical drugs such as steroids or NSAID drugs, peoples try to look for other drugs as an alternative in overcoming inflammation. Research on natural medicine clinic until the testing process has even reached the clinical trials to increase the use of natural ingredients as an alternative in the treatment [3]. One of the natural ingredients as an alternative to a known safe and effective option is propolis [4].

Propolis is the sticky dark-colored material collected by bees from plants and then mixed with wax (wax) for use in building construction and protection of the hive [5]. One of the component contained in propolis is flavonoids that may regulate immune response, reduce the release free radicals, inhibiting the growth of bacteria and fungi as well as functioning as anti-inflammatory and immunomodulatory [6].

Flavonoids may also increase several biological functions including protein synthesis, cell differentiation and proliferation, and angiogenesis, in that addition flavonoids also have very low toxicity. Flavonoids in the medical field among others, used in the treatment of diabetes mellitus, inflammatory diseases, allergic diseases, cancer, viral infections, osteoporosis, peptic ulcers, and cardiovascular [7]. In addition to flavonoids, propolis also contains CAPE (Caffeic Acid Phenethyl Ester) some form of esters of caffeic acid which proved to be effective as an antitumor and anti-inflammatory [4].

2. Experimental Details

Materials

Bee propolis honey brown taken from beekeeping in Batu, Malang, East Java. Ethanol 96%, petroleum ether, and methanol. Karagenin type I (Sigma Chemical Co.), physiological solution

(NaCl 0.9%), diclofenac sodium, CMC, distilled water. Qualitative test material sulfuric acid, acetic acid, Mg powder, concentrated HCl, 96% ethanol, amyl alcohol, Fehling A and B. Thin layer chromatography materials is CH_3COOH, distilled water, n-butanol, slabs cellulose, ammonia vapor, sitroborat reagent.

Anti-inflammatory test methods

The method used to testing the inflammation is a method of chemical stimulation. White rat test animals in this method are given tested materials orally 1 hour before giving karagenin 1% by intraplantar as inflammatory stimulus. Inflammatory response of rat foot swelling will be given within a maximum of 1 hour. Similarly, edema attributable to the large size of the foot pletismometer mice by using pletismometer. Inhibition of the inflammatory response can be calculated as a percentage of anti-inflammatory.

Preparation of ethanol extract of bee propolis

The process to making a bee propolis extract is done by maceration technique. Propolis is cut into pieces, then dried in an oven at 37°C for 3 days. Propolis then macerated using 96% ethanol (1:5) [8,9]. Mixed materials stored for 7 days in a room that is not exposed to strong sunlight with whipped several times each day [10]. The next stage is filtered with Buchner funnel and filter paper to separate the filtrate from the pulp into a glass beaker. Results filtration (filtering) is obtained is evaporated by an oven at 45°C in order to obtain propolis extract a thick consistency [8,9].

Preparation of the methanol fraction of propolis

Viscous extract obtained as much as 10 grams dissolved in 60 ml of methanol then fractionated with 60 ml PE three times in a separating funnel. Fractions obtained were evaporated in an oven and then weighed.

Identification of methanol fraction compound

Identification of chemical constituents of metanolik fractions of propolis conducted to determine the presence of flavonoids and other phenolic compounds namely esters of caffeic acid in propolis is efficacious as anti-inflammatory.

Fraction obtained was dissolved in solvent and then tested qualitatively flavonoids by means of 1 ml solution was added Mg powder, 2 ml of alcohol solution and HCl solution (1:1) and solvent amyl alcohol, the mixture shaken vigorously and allowed to separate. Positive reaction indicated by red or yellow-orange color of the lining of amyl alcohol. The presence of phenol compounds tested with the test power reduction that is 0.5 grams of methanol extract is added 0.5 ml 0.5 ml Fehling Fehling A and B are heated. The presence of phenol compounds is shown by the formation of red sediment brick.

Identification of flavonoids by Thin Layer Chromatography (TLC)

Chemical analysis of flavonoid compounds was done by using thin layer chromatography using cellulose plates stationary phase and mobile phase n-Butanol: acetic acid: water = 4:1:5 (v/v).

Treatment of test animals

Twenty-five male rats that were eligible were randomly divided into 5 equal groups are many. All animals are maintained under the same conditions, before being used in advance of rats adapted to environmental research, and kept from food eaten for 18-24 hours and fixed the drinking water provided. The treatment given to each - each group are as follows: Before giving the intraplantar karagenin 1% of each group were treated orally, Group I male rats given the negative control of 0.5% CMC solution of 0.5 ml / 200 g BW mice orally 1 hour. Group II was given propolis methanol fraction equivalent to 18 mg / 200 g BW propolis, 1 hour. Group III was given propolis methanol fraction equivalent to 27 mg / 200 g body weight of propolis. Group IV was given propolis methanol fraction equivalent to 36 mg / 200 g body weight of propolis. Group V were given diclofenac sodium 0.9 mg / 200 g BW. Similarly, edema volume of the excess volume of foot mice after injected with karagenin 1% with the previous volume was measured by dipping a foot into the appliance pletismometer rats. Measurements were taken in 1 hour intervals for 5 hours after injection karagenin solution.

Anti-inflammatory power was assessed by calculating the percentage inhibition of edema according to the formula:

$$\% \text{ inhibition of edema} = \frac{a-b}{a} \times 100\% \quad (1)$$

a = volume of control group rats

b = treatment group.

Value of the percentage inhibition of inflammation showed the ability of the test materials suppress inflammation (inflammatory activity).

Analysis results

Quantitative data percentage inhibitors and edema volume between the treatment groups of

animals were analyzed by statistical analysis of variance test followed two paths Dunnet test at level of 95%.

3. Result and Discussion

The result of ethanol extract of propolis

A total of 279.972 grams of dried propolis macerated with ethanol 96% with a ratio (1:5) in order to get as many as 78.684 grams of viscous extract with percentage yield of condensed ethanol extract of 28.10%.

Results of fractionation of propolis

The separation of chemical constituents in the ethanol extract of propolis made by fractionation using a solvent of methanol and PE.Polar compounds such as flavonoids in the form of glycosides and phenolic compounds dissolved in polar solvents namely methanol, while the compounds in the form of resins, fatty acids, waxes, and essential oils dissolved in nonpolar solvents.

The results from fractionation with methanol and PE in a row is 4.925 g and 4.003 g with a percentage yield of 48.81% and 39.67%. The result of the test dose calculation PE fraction and the methanol fraction was 2.33 mg/200 g BW and 1.89 mg/200 g BW.

Identification of the chemical content of the methanolic fraction from Table 1, can be concluded that methanol fraction contain flavonoids and phenolic compounds CAPE.

Table 1. Results of identification of the chemical content of the methanol fraction

No	Procedure	Result	References	Conclusion
1	1 g extract powder of Mg + 2ml + alcohol + HCl (1:1) + amyl alcohol	Orange	Red / yellow / orange in a layer of amyl alcohol [11]	Flavonoid (+)
2	0.5 ml extract + 0.5 ml of Fehling A + 0.5 ml of Fehling B	Brick red precipitate	Brick red precipitate [11]	Polifenol (+)

The result of thin layer chromatography (TLC) fractions of methanol

TLC fractions of methanol test using cellulose stationary phase and mobile phase n-butanol: acetic acid: water (4:1:5) with elution 8 cm long. Spots detected by UV ¬ 365, ammonia vapor and sitroborat give a positive result of flavonoid compounds in the methanol fraction (Figure 1)

Figure 1. Results chromatogram of methanol fraction

The spots obtained steamed with yellow ammonia, under UV light yellow 365 and reagent sitroborat an orange tint. Testing with ammonia vapor as he examined under ultraviolet light showed yellow flouresense flavonol type flavonoids in crude drugs. The emergence of this color is caused by salt formation and the formation of structure in ring B kuinoid because the influence of ammonia base [12].

Table 2. Type of flavonoids on TLC profils

UV rays Without NH3	With NH_3	Possible types of flavonoids [13]
Yellow dim	yellow	Flavonol-containing 3-OH-free and have or not have a free 5-OH (sometimes derived from dihidroflavonol)

Anti-inflamatory of petrolium eter and metanol fractions

Table 3. The measurement results edema volume fraction of PE and the methanol fraction

Treatment Group	Volume of edema (ml) mean ± SD				
	1	2	3	4	5
I	0.050 ±0.010	0.053 ±0.006	0.053 ±0.006	0.056 ±0.006	0.063 ±0.011
II	0.030 ±0.000	0.043 ±0.006	0.040 ±0.010	0.027 ±0.006	0.027 ±0.006
III	0.036 ±0.011	0.030 ±0.010	0.027 ±0.006	0.027 ±0.006	0.023 ±0.011
IV	0.036 ±0.006	0.033 ±0.006	0.027 ±0,006	0.017 ±0.006	0.010 ±0.000

Results reagent spray with sitroborat indicates the type of flavonoid 3', 4'-dihydroxy flavonol which appear as orange spots. Based on test results allegedly flavonoid flavonoids type is

3', 4'-dihydroxy flavonol and flavonol-containing 3-OH-free with or without 5-OH-free.

Table 4. Antiinflammatory PE fraction and the methanolic fraction

Treatment	% inhibition of edema (± SD)				
	1	2	3	4	5
I	-	-	-	-	-
II	40.00 ±0.00	18.24 ±10.8	24.53 ±18.8	53.22 ±10.1	57.67 ±9.16
III	26.67 ±23.09	43.40 ±18.8	49.69 ±10.8	53.22 ±10.1	62.96 ±18.33
IV	26.67 ±11.55	37.11 ±10.89	49.69 ±10.89	70.76 ±10.13	84,13 ±0.00

Description:
Group I : Negative control (CMC solution)
Group II : Petroleum Ether fraction
Group III : Methanolic fraction
Group IV: Positive control (Diclofenac sodium)

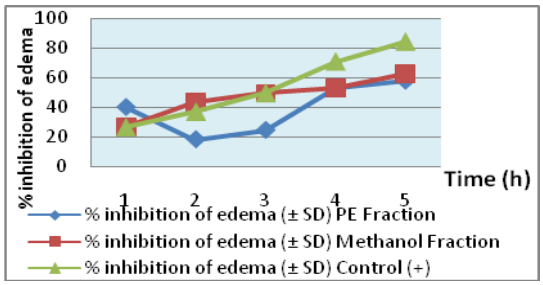

Figure 2. Graph of percentage inhibition of edema PE and methanol fractions

Edema volume measurement and anti-inflammatory of the methanol fraction

Table 5. The measurement results edema volume methanol fraction

Treatment	Volume of edema (ml) mean ± SD				
	1	2	3	4	5
I	0.050± 0.007	0.050± 0.007	0.054± 0.005	0.058± 0.004	0.066± 0.009
II	0.038± 0.008	0.034± 0.009	0.026± 0.005	0.024± 0.005	0.020± 0.007
III	0.030± 0.007	0.028± 0.008	0.022± 0.004	0.016± 0.005	0.014± 0.005
IV	0.034± 0.005	0.030± 0.000	0.022± 0.004	0.014± 0.005	0.010± 0.000
V	0.038± 0.008	0.034± 0.011	0.030± 0.012	0.020± 0.007	0.014± 0.009

Inflammatory properties of flavonoids proved both in vitro and in vivo. The mechanism of flavonoids in inhibiting the inflamation is through inhibition of the release of arachidonic acid and enzyme secretion from cells of neutrophil lysosomes. Flavonoids also inhibit the proliferation phase and the phase of exudation of the inflammatory process. High concentrations of some flavonoids can inhibit the release of arachidonic acid and enzyme secretion of lysosomes from the membrane by blocking cyclooxygenase path, the path lipoksigenase, and phospholipase A2, while at low concentrations only block the path lipoksigenase. Inhibition of arachidonic acid release from inflammatory cells would lead to less availability of arachidonic substrate for cyclooxygenase path and lipoksigenase path that ultimately suppress the amount of chemical mediators in inflammatory processes such as prostaglandins, prostasikiln, endoperoksida, thromboxane, acid hydroperoxide, and leukotrienes [7]. CAPE contained in propolis may inhibit lipoksigenase path so that played a role in inhibiting inflammation [14].

Tabel 7. Antiinflatory of methanol fraction

Treatment	% inhibition of edema (± SD)				
	1	2	3	4	5
I	-	-	-	-	-
II	24.00 ±16.73	32.00 ±17.89	51.85 ±10.14	58.62 ±9.44	69.70 ±10.71
III	40.00 ±14.14	44.00 ±16.73	59.26 ±8.28	72.42 ±9.44	78.79 ±8.30
IV	32.00 ±10.95	40.00 ±0.00	59.26 ±8.28	75.86 ±9.44	84.85 ±0.00
V	24.00 ±16.73	32.00 ±22.80	44.44 ±22.68	65.52 ±12.19	78.79 ±13.55

Description:
Group I : Negative control (CMC solution)
Group II : Methanolic fraction 1.89 mg/200 g BW
Group III : Methanolic fraction 2.84 mg/200 g BW
Group IV : Methanolic fraction 3.78 mg/200 g BW
Group V : Positive control (Diclofenac sodium)

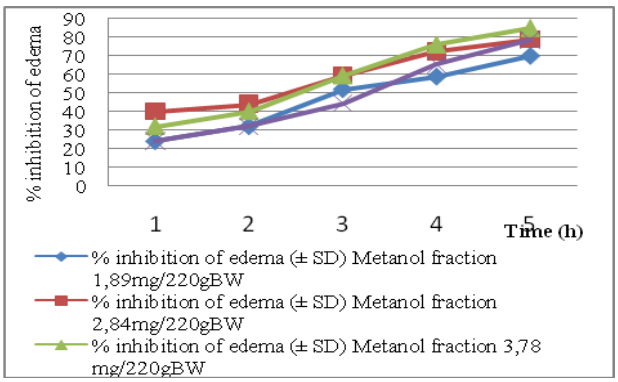

Figure 3. Graph of percentage inhibition of edema methanol fraction

Tests carried out with anti-inflammatory karagenin induce as much as 0.05 ml by

intraplantar on the soles of the feet of mice. Use of caragenin as irritant compounds provides many benefits. Karagenin not cause tissue damage, do not cause scars, and to respond more sensitive to anti-inflammatory drugs. Inflammation that occurs as a protective response to tissue injury characterizes which include swelling (tumor), redness (rubor), and thermal (heat) due to vascular changes. As a result of other inflammatory namely pain (dolor) and dysfunction (functio laesa) caused by the expansion of mediators and leukocyte-mediated damage [15].

Two-way analysis of variance results from the data obtained indicate the significance value of 0.000 on the treatment factor, this value is less than 0.05 so it can be concluded there is a difference between the percentage inhibition of edema negative control, Methano1ic fraction 1.89 mg/200g BW, Methano1ic fraction 2.84 mg/200g BW, Methano1ic fraction 3.78 mg/200 g BW, and the positive control. The factors were shown at the significance value of 0.000. This value is smaller than 0.05 so it can be concluded there are differences in the percentage inhibition of edema at the 1, 2, 3, 4, and 5. On the interaction between treatment with the clock, the value of the statistical analysis of significance of 0.000 so that concluded there is significant effect between all treatments with hours of observation.

The test results in common variant with Levene test significance value 0.000 so that the variant is not the same conclusion. Testing continued on the treatment factor and hours performed by Dunnet test. In the treatment factor looks significantly different negative control with Methano1ic fraction 1.89 mg/200g BW, Methano1ic fraction 2.84 mg/200g BW, Methano1ic fraction 3.78 mg/200 g BW, and positive control with significance value of 0.000. Fraction of methanol 2.84 mg/200g BW and 3.78 mg/200 g BW showed higher edema inhibition curve than positive controls, but statistical tests showed no significant differences so that a dose 2.84 mg/200g BW is considered as the effective dose because it is the lowest dose with activity equivalent to the dose of 2.84 mg/200g BW and 3.78 mg/200 g BW and a positive control.

In rats fed the positive control of sodium diclofenac and rats fed the methanol fraction of the test preparation performed surgery to determine the side effects of each treatment. In mice given diclofenac sodium peptic ulcers occur due to the work that is not selectively inhibit both COX1 and COX2. In observation of the gastric rats fed the methanol fraction no visible ulcers (Figure 4).

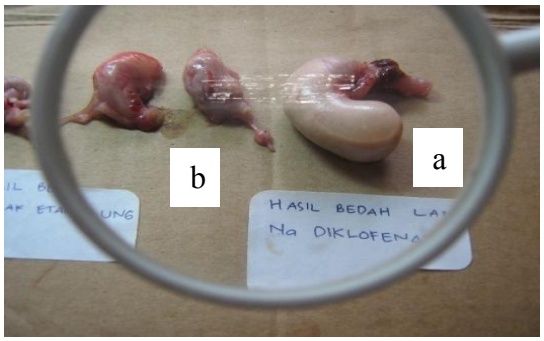

Figure 4. Profile of rat stomach after treatment. (a) rat stomach with diclofenac sodium. (b) rat stomach with methanolic fraction of propolis.

This is presumably because anti-ulcer effects of flavonoids contained in propolis work selectively against COX2.

4. Conclusion

Based on the research can be concluded that the methanolic fraction and petroleum ether fraction of honeybee propolis has an anti-inflammatory, the data showed that anti-inflammatory effects of methanolic fraction better. Honey bee propolis methanolic fraction dose 1.89 mg/200g body weight has an effective anti-inflammatory effect and does not cause adverse effects on gastric ulcers.

5. References

[1]. Mycek, J.M, Harvey RA, Champe P.C, Fisher B.D. (1997), *Farmakologi Ulasan Bergambar*, 2nd ed, Widya Medika, Jakarta p 404.

[2]. Neal, M.J, Amalia, S. (2006), *Farmakologi Medis At a Glance*, 5th ed., Erlangga, Jakarta, p 70-71.

[3]. Age (2008) ???

[4]. Galvao, *et al*. (2007), Biological Therapy Using Propolis as Nutritional Supplement in Cancer Treatment, *Int, J, Cancer Res,* 3 (1): 43-53.

[5]. Bankova, V.S, de Castro, S.L, and Marcucci, M.C. (2000), Propolis: Recent Advance in Chemistry and Plant Origin, *Apidologie* 3:3-15.

[6]. Sabir, A. (2005), Aktivitas Antibakteri Flavonoid Propolis Trigona sp terhadap Bakteri Streptococcus mutans (in vitro), *Maj Ked Gigi (Dent J)*. 38 (3): 135-141.

[7]. Sabir, A. (2003), Pemanfaatan Flavonoid di Bidang Kedokteran Gigi, Maj. Ked Gigi (Dent J), *Edisi Khusus Temu Ilmiah Nasional III*: 81-87.

[8]. Mawardi, *et al*. (2002), Pengaruh Pemberian Ekstrak Propolis Secara Aplikasi Lokal pada Proses Pembentukan Serabut Kolagen Pasca pencabutan Gigi Marmot (*Cavia Cobaya*), *Sains Kesehatan,*15(2): 173.
[9]. Sabir, A. (2005), Respon Inflamasi pada Pulpa Gigi Tikus setelah Aplikasi Ekstrak Etanol Propolis (EEP), *Maj Ked Gigi (Dent J)*, 38 (2): 77-83.
[10]. Susilo, B. (2007), Aktivitas Antimikroba Propolis dari Malang Jawa Timur terhadap Staphylococcus aureus, *Majalah Kedokteran Tropis Indonesia*, 18 (1):72-77.
[11]. Anonymous (1995), *Materia Medika Indonesia*, Departemen Kesehatan Repubik Indonesia, Jakarta 336-337.
[12]. Kosasih P. (1995), *Kandungan Organik Tumbuhan Tingkat Tinggi*, 5th ed., ITB, Bandung, 157-158, 281-286.
[13]. Kosasih P. (1998), *Cara Mengidentifikasi Flavonoid*, ITB, Bandung.
[14]. Houghton, P.J. (1998), Propolis as a medicine, in Pamela Munn, editor, *Beeswax & Propolis for Pleasure and Profit,* UK, p: 10-14.
[15]. Cotran and Mitchell (2007), Inflamasi Akut dan Kronik. in: Robbins and Contran: *Pathologic Basis of Disease*. 7th Ed.. Elsevier Saunders Inc., Philadephia, p: 37, 63.

.

Evaluation on the Phytoestrogenic Effect of Legumes Extract in Binding Competition on Estrogen Receptor

Edi Priyo Utomo

Departement of Chemistry, University of Brawijaya, Malang (edipu2000@yahoo.com)

Abstract

Phytoestrogen is belongs to plant-derived organic molecule that posses natural estrogen-like activity. The molecules occur naturally and abundantly in Leguminosae such as soybean (Glycine max), cowpea (Vigna unguiculata), green bean (Phaseolus radiatus), long bean (Vigna sinensis) and string bean (Phaseolus vulgaris). The phytoestrogen content of the methanolic extract was determined by thin layer chromatography and using genistein, daidzein and coumestrol as reference compounds. The competition binding assay was performed by fluorometry in which fluorescent-labeled estradiol (ES2) react with estrogen receptor (ER) to form ER-ES2 complex. The legume extracts as ligand displayed ES2 in the ER-ES2 complex in test tubes containing a buffer solution and changing of fluorescence of the complex was measured by using a 590 nm emission filter. Phytoestrogen extracts compete with ES2 for binding ER in the following order: estradiol (RBA = 100) > daidzein > geinstein > string bean > cowpea > soybean > long bean = green bean.

Keywords: *phytoestrogen, legumes, binding competition.*

Preparation of Constructs Gene sY86 as the Basis of Antibody Formation for Determination Method of Male Infertility

Evi Hanizar [1], Miswar [2]

[(1)] Department of Biology Education, Faculty of Mathematics and Science Education, IKIP PGRI Jember, Indonesia (ev_ha@yahoo.co.id)
[(2)] Department of Agronomy, Faculty of Agriculture, Jember University, Indonesia

Abstract

SY86 gene is one of the genes contained in the AZF region in the long arm of the Y chromosome that control male spermatogenesis. Previous research proved that this gene frequent deleted in infertile men. The objective of this research is to make a construct sY 86 gene, which will be used to make antibodies to detect infertility in men. The material used cDNA fragment sY86 with molecular weight 326 bp derived from the blood of man with normal sperm category. This fragment was ligated in PET TOPO vector, and the ligation product was transformed to E.coli TOP 10. Selection of transformants using the ampicillin because PET TOPO vector containing a gene that resistant to ampicillin. Plasmids then were isolated and the success of isolation showed by the result of electrophoresis. To ensure the size of the plasmid, the DNA fragment was performed by PCR method and PCR results were then followed elektrophoresis.The result shows that sY86 gene was ligated with pGEM-T easy vector successfully transformed into E. coli TOP 10 and the size of plasmid DNA in accordance with the target DNA. As conclusion, constructs gene SY86 was ready to be expressed in expression vector.

***Keywords**: cDNA, sY86, ligation, transformation, vector*

1. Introduction

The genes that control the process of spermatogenesis in men located in the AZF region (Azoospermic Factor) on the long arm of Y chromosome. AZF Region consists of three subregions namely AZFa, AZFb and AZFc. Various studies have reported the existence of gene deletions in this subregion in infertile men with impaired sperm category like azoospermia, severe oligozoospermia and oligozoospermia. The deletion can happen in one until three subregions along with the quantity and quality of sperm abnormalities are different also [1-5].

Genetic analysis was conducted in infertile men at one of the infertility clinic in Indonesia showed that an average 90% of infertile men have sperm with categories azoospermia, severe oligozoospermia and oligozoospermia [6]. They're trying to get children, and should have the quantity and quality of normal sperm. To determine the possibility of getting a normal sperm, it‘s necessary to have the data about the presence or absence of genes that control spermatogenesis process. AZF gene deletion analysis in infertile men that carried out so far used PCR (Polymerase Chain Reaction) method which requires a lot of reagents, cost and time. Consequently, if this is done on patients would burden the patient in terms of financing and take a long time to find out the results. Thus it‘s needed an other method of deletion analysis that is quick, easy, accurate and relatively reduce the financing.

One method that can be developed is the creation of antibody that can recognize the antigen. The gene which will be made the antibody is sY86 that contained in the AZFa subregion, and often deleted in infertile men obtained from the results of previous studies [7]. SY86 cDNA fragment was successfully cloned in pGEM-T easy vector and subsequently will be expressed to obtain recombinant proteins [7]. This study aim to obtain sY86 plasmid that will be expressed in an expression vector. Therefore each of AZF subregion consists of various genes, the results of this study is expected to proceed with the other genes. Certainty of deletions in infertile men will help patients and doctors to make a right decision and prevent the inheritance of the gene deletion from a father to his son.

2. Experimental Details

a. Preparation of DNA Plasmid

SY86 cDNA was amplificated by PCR (Polymerse Chain Reaction) method and purified using the PCR purification kit, subsequently ligated into vector pGEM-T easy. The mixture was incubated at 4°C overnight.

b. Transformation of DNA plasmid into E. Coli

One vial of *E. coli* TOP 10 was thawed on ice and added 3 mL of DNA ligation. The mixture was incubated on ice for 15 minutes, *heat shock* for 30 seconds at temperature 42 ^{o}C without shaked and transferred immediately to ice. Then the reaction was added 250 mL of SOC medium and incubated with shaked (200 rpm) at 37ºC for 1 hour. All of the reaction mixture was transformed to solid LB medium containing ampicillin, and cultured overnight at 37ºC.

.

c. Plasmid Isolation

Single colony of each transformant colony was grown in 3 ml liquid LB medium containing ampicillin 6 mL, then shaked at 37ºC overnigt. The cultures were then transferred to 1.5 ml tube, centrifuged in 12,000 rpm for 10 minutes at 4ºC. Pellet was suspended in 100 mL of solution I (150 mM glucose, 25 mM Tris HCl pH 8.0, 10 mM EDTA, pH 8.0), carried out on ice and added 200 mL of solution II (0.2 NaOH, 1% SDS; H_2O). This mixture was inverted and incubated on ice until appear transparent, then added a solution III (60 ml 5M potassium acetate, 11.5 ml glacial acetic acid, 28.5 ml H2O), inverted again and left on ice for 10 minutes. The Solution centrifuged in 12000 rpm for 10 minutes at 4ºC. Supernatant was transferred to the tubes of 1.5 ml and added PCI with the same volume, and then centrifuged in 12,000 rpm for 10 minutes at 4ºC. Supernatant was transferred to another tube, added 2.5 volumes of ethanol and 0.1 volume of sodium acetat. The mixture was precipitated at 20ºC for 1 hour, and then centrifuged in 12,000 rpm for 10 minutes at 4ºC. Pellet was washed with 1 ml of alcohol 70%, centrifuged in 12000 rpm for 10 min at 4ºC and dried up until dry. Pellet was dissolved with 20 mL TE buffer and stored at -20ºC to be used.

The success of plasmids isolation can be seen from electrophoresis. If it performed band DNA, further step was amplification with PCR method with the composition of 12.5 mL PCR master mix, primers T7 (F), primers SP6 (R) each 2 mL, 1 mL plasmid DNA, 7.5 mL mL water. The PCR condition was predenaturation 95ºC, 5 min, the cycle of denaturation 94ºC, 50 seconds; Annealing 50ºC, 1 min, extension 72ºC, 50 seconds as many as 30 cycles and final extension 72ºC, 7 minutes. PCR results were further electrophoresis and if it performed the appropriate size band DNA, it was sequenced. It‘s made 50 mL. PCR results for sequencing.

3. Result and Discussion

Plasmid sY86 that was generated from previous study was amplified by PCR method and purified with PCR purification kit. Plasmid then was conducted by electorphoresis (Figure 1) and isolated from agarose gel.

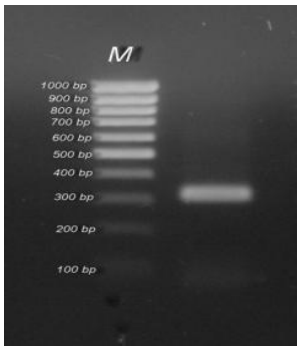

Figure 1. PCR results of sY86 gene

Figure 1 showed the results of elektrophoresis sY86 gene that has been amplified by PCR under UV illuminator and performed band in accordance with the size of the gene sY86 with molecular weight of 326 bp. After ligation with pGEM-T easy vector and transformed into Top 10 *E. coli*, it appeared colonies look like Figure 2.

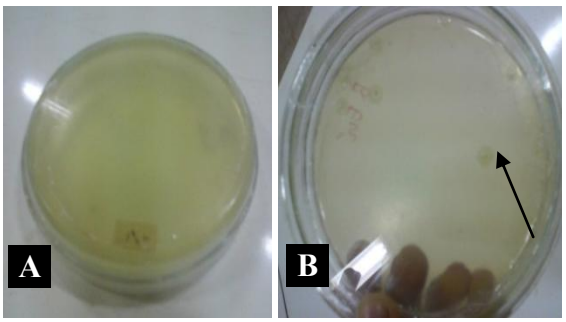

Figure 2. Results of sY86 gene transformation into *E.coli* cells, (A) Control (B) Transformant colonies

Figure 2.A showed the media that was not covered with colonies of *E. coli* TOP 10 competent cells; it‘s not transformed with pGEM-T Easy vector. This is because the media containing amphicillin and E. coli were not able to degrade amphicilin. Figure B. contained several transformant colonies (*E.coli* which were tranformed pGEM-T Easy vector and DNA sY86) becaused pGEM-T Easy vector carried the amphicillin resistance gene. The gene encoded an enzyme that can degrade amphicillin. The transformation produced six colonies and after the band was isolated and conducted electrophoresis, it appeared band look like Figure 3.

To prove the isolated plasmid containing the ligated DNA, It's amplificated by PCR method using primers T7 and SP6. PCR results from 6 colonies showed that colony number 5 appeared to band as seen in figure 4, ie ± 500 bp becused of molecular weight SY 86 genes was 326 bp, and each of the end of plasmid has a molecular weight 52 bp for T7 and 141 bp for SP6.

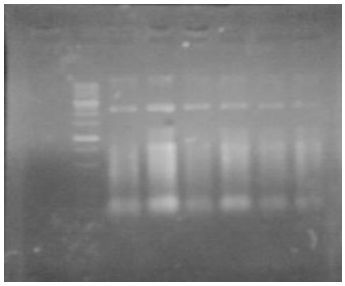

Figure 3. Electrophoresis of the isolated plasmid colony

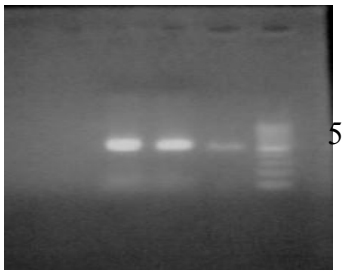

Figure 4. PCR results for colony number 5

PCR products were purified, then sequenced to prove whether the DNA sequence in accordance with the sequence of DNA target. The results of DNA sequencing were as follows:

GTGACACACA GACTATGCTT CAGCAGGTCT GTCTGGGCCC AAGACACATT GTTTCTCATC AGCTCCCAGG GGATGTCAAG GCTGCAGATC CATGGATCTC ACTTTGCAGG ACAGAGACTT GGTAATGGCT TCCCAGAGTT GTTACAAAGA AATCCCAAAG ACTGGGCCCC TTAAACAACA ACCTTGATTC TCACAGTCCT TGAGGCTAGA AGTCTGAGAT CAAGCTATGG CCAGGGCTGG TTCCTCCTGA GGCCTCTCTC CTTGGGTTGT AGATGCTGTC TTCTCCCTGT GTCCTCACAG GGTTGTCCCT CTGTGTGT

If the sequence of plasmid DNA accordance with the target DNA, the plasmid DNA was ready to ligated in expression vector and cultured to obtain recombinant protein.

4. Conclusion

The results of this study indicate that constructs pET SY86 was ready to be expressed in expression vector.

5. Acknowledgement

This research was funded by the research project of Competitive Grant-DIKTI DP2M 2007, 2009 and 2010.

6. References

[1]. Seifer, I. Amat, S. Delgado-Viscogliosi, P. Boucher, D. Bignon, Y.J. (1999). Screening for Microdeletions on The Long Arm of Chromosome Y in 53 Infertile Men. *International Journal of Andrology*. 22 (3), 148-154.

[2]. CMGS. (2000). *Y Chromosome Deletion and male Infertility*. http://www.ich.ucl.ac.uh/cmgs/ydels99.htm

[3]. Naysmith, T, Wendy S, Cynthia van Ee, Guy G. (2000). Identification of Y-Chromosome Deletion in Men with Subfertility. *Departemen of Obsetrics and Gynaecology*. Auckland University.

[4]. Friel, A. J.A. Houghton, M. Mahrer. T. Smith. S. Noel. A. Nolan. D. Egan & M. ???

[5]. Glennon (2001). Molecular Deletion of Y Chromosome Microdeletions : An Irish Study. *International Journal of Andrology*. 24 (1), 31-36.

[6]. Ferlin, A. E.Moro, A. Rossi, B.Dallapiccola, C.Foresta (2003). The Human Y Chromosome's Azoospermia Factor b (AZFb) Region: Sequence, Structure and Deletion Analysis in Infertile Men. *Journal of Medical Genetics*. 40. 18-24.

[7]. Evi Hanizar (2007). Pola Penentuan Delesi Gen Penyandi Spermatogenesis pada Pria Indonesia Sebagai Dasar Diagnosis Infertilitas Pria. Hibah Bersaing XIII – DP2M Dikti.

[8]. Evi Hanizar (2009).Produksi protein AZF untuk Pengembangan Metode Penentuan Infertilitas Pria. Hibah Bersaing XV– DP2M Dikti

Function of hINSR Mutant Againts Tyrosine Kinase Precede Abnormally on Onset Diabetes Mellitus: *In Silico* Study

Fatchiyah [1,2], NMA. Putri [3], D. W. Soeamadji [4]

[1,3] Dept of Biology, Faculty of Science, Brawijaya University, Malang (fatchiya@gmail.com)
[2] Central Lab. of Life Sciences (LSIH), Brawijaya University, Malang
[4] Medical Faculty, Brawijaya University, Malang

Abstract

The pathogenesis of NIDDM has been studied in various ethnic groups. It appears that insulin resistance can precede the clinical onset of NIDDM. Mutation of the human insulin receptor gene have been identified in patients with severe insulin resistence, and studies of these naturally occuring mutants may provide important insights into the relationship between structure and function of receptor (hINSR) of Indonesian diabetes mellitus patients. The bloods were collected from normal and DM patients from some public clinics and Saiful Anwar Hospital, Malang. DNA and RNA were isolated from blood, and then sequenced by ABIPrims Sequencer. To find out the genomic hINSR, DNA sequences were analyzed and characterized by in silicoanalysis, such as alignment by BioEdit & BLAST program from NCBI, and superimposed by Strap JAVA program, 2D- and 3D-structure analysis Swiss Model program. To examine the cytoplasm pathway tyrosine kinase, using docking hINSR-Tyrosine Kinase domain & IRS-1 (PTB domain) analyzed by Hex 5.1. We found specific of DM protein from 2D-protein profile and some type mutation of hINSR and can change the INSR 3D-protein structure and the 3D ligand structure of hINSR and insulin completely changed on DM patient. According to our result, we suggested that the hINSR protein mutation of DM patient precede abnormally hINSR function against tyrosine kinase and perhaps correlated with genetic syndrome of insulin resistance. The change function is presumed to inhibit the interaction between hINSR and IRS, makes transduction signal disturbance in the process of absorption of glucose leads to insulin resistance of diabetes mellitus.

Keywords: *insulin receptor, diabetes mellitus, genetic syndrome, in sillico, tyrinose kinase.*

The Analysis of Ca^{2+} Intensity Profile of M-II Oocyte Natural Activated by Crude Sperm Extract

Gatot Ciptadi

Faculty of Animal Husbandry, Brawijaya University, Malang, Indonesia

Abstract

Sperm factors or cytoplasmic factor in the spermatozoa have been used to activate mammalian M-II oocytes artificially. Several chemicals activator have been reported for their capability in parthenogenetic activation of M-II oocyte, but still resulted in improper, lower and partially achievement, especially for reconstructed oocytes.The aims of these research are to study the potential natural activator Crude Sperm Extract (CSE) for improving activation of the M-II oocytes. The isolate of CSE and the 100 kD protein of CSE were supplemented to culture medium of TCM 199. The intentity of calsium during activation was observed by flou-3 stainning with Concocal Laser Scanning Microscope (CLSM). Result showed image analysis of Calcium intensity, demonstrate the variations among activated M-II oocyte. Profile of Ca^{2+} intensity of M-II oocyte diffrent compare to M-II oocyte non activated. Result from In vitro culture of these oocyte observed that activation using CSE of 2.5 ug/ml resulted in about 36.33 % oocyte was cleavaged compare to activation using 100 kDa protein of CSE of 2.00 % of M-II oocyte was cleavaged. The CSE is relatively better than spesific protein of GSE of 100 kDa for their role as natural agen of activation to oocytes. It was suggested to additional researh in both the intracelluler calcium concentration and identification of spesific protein or sperm factors of CSE.

Keywords: *calcium intensity, crude sperm extract, activation, oocyte.*

1. Introduction

Two theories have been proposed to explain the induction of Ca^{2+} releases in fertilizes M-II oocyte following fertilization by sperms: (1) the sperm receptor theory and (2) the sperms factor theory. Sperm factor, postulated as cytoplasmic factor in the spermatozoa, has been used to partenogenetically activate mammalian oocytes. Spermatozoa release cytosolic substances into oocyte at fertilization and is induces Ca^{2+} oscillations [1-3]. The parthenogenetic activation of oocytes is an interesting and valid tool to investigate the comparative roles of paternal and maternal genomes in controlling early embryo development.

Repetitive Ca^{2+} rises at fertilization are necessary to accomplish degradation of MPF. Calcium oscillation in oocytes is responsible for pronuclear formation. Egg activation is caused by dramatic increase in intracellular Ca^{2+} concentrations common to every animal species including mammalian [4]. Mammalian oocytes at the time of fertilization occurred exhibit a series of transient increase in intracellular calcium ion (Ca^{2+}) concentration which are prerequisite and sufficient for oocyte activation. Immediately after the sperm attaches to the oocyte, increased in intracellular Ca^{2+} in the oocytes are firstly seen near the site of sperm-oocyte fusion.

Parthenogenetic activation of mammalian oocytes was commonly artificially induced by chemical agents, but these agents did not effectively activate pig oocyte [5] or reconstructed goat oocytes [6]. Crude Sperm Extract (CSE) that was injected into egg showed the repetitive Ca^{2+} *oscillation* as well as like normal fertilization by sperm [7]. This research was focused on study of the effect of supplementation of CSE transfected in the conventional chemical medium activation. On activation rate base on both parameters of Ca^{2+} intensity and the cleavage rate of M-II oocyte,

2. Experimental Details

In vitro Maturation (IVM) of Oocyte

The oocytes-cumulus cell complexes were isolated from goat anthral follicles of 2 – 6 mm, cultured in bicarbonate buffered medium 199 supplemented with 10% FBS, 0.1 mg sodium pyruvate [8]. The culture was carried out in 5% CO_2 in humidified air at 38ºC for 48 hours. Oocytes were completely denuded by pipetting after treated with 0.01% hyaluronidase (Sigma). Only those with a compact, non-atretic cumulus and a homogeneous cytoplasm which were

previously classified as Grades A and B [8,9], were selected. Oocytes emitting the 1st polar body were selected in this experiment.

Preparation of CSE

The CSE was prepared from local goat sperm as describe by Okada et al [5] and Swan [10]. Briefly, the sperms were distrupted by ultra sonification and fractionated by ultracentrifugation. The sperm suspension containing approximately 10 x 10^8 cells/ml was sonificated for 15 minute at 4ºC. Homogenated sperm suspension was centrifuged twice at 10.000 g for 45 minute at 4ºC and the supernatant was collected as the crude sperm extract (CSE), and then stored at –80ºC before used.

The Experiments

Treatment of this experiment were different CSE supplementation of protein concentration based on the early concentration of sperm 10x10^8 spermatozoa/ml isolation medium. GCSE was supplemented into chemical activation medium, with the experiment treatments of M-II oocyte parthenogenecally refer to Ciptadi [6] and Ongeri et al [11] are: (1) Control (M-II) oocyte, (2). 7% ethanol + CSE 2.5 ug/ml, and (3). 7% ethanol + CSE of 100 kDa. In this research, the selected M-II oocytes were exposed in this medium activation treatment after a slit of zona pellucida was performed (transfection) by micromanipulator.

3. Result and Discussion

Calsium (Ca^{2+}) Intensity Profile

The CSE used in this research was characterised for their protein profile and its indicate the 11 kinds of protein weight molecular included the 100 kD [12]. The protein of 100 kDa in this extract sperm might be potential as activation agent. Matsuura et al [13] showed that sprem extract with molecular weight 100 kDa contain effective materials for porcine oocyte activation. In this research, the intensity of Ca^{2+} showed different profile of each treatment. M-II oocyte with no treatment showed strong enough intensity on the area of pellucid zone. Meanwhile, the oocyte exposed with CSE, Ca^{2+} is well expressed spread out on cytoplasm. However, the responses on CSE supplementation are varied after 24 to 48 hour of culture (Figure 1).

It was assumed that if Ca^{2+} was expressed in the cytoplasm, it mean that its exhibits increase in Calcium intracellular. Oda [2] and Miyazaki and Ito [4] mentioned that egg exhibits increase in Ca^{2+} is indications of egg activation. Several recent research results suggest that mammalian sperm factor would be introduced in to the oocyte cytoplasm through sperm-egg cytoplasmic connection, initially distributing evenly throughout the cytoplasm [14].

Some experiments have attempted to study the molecular identity of sperm factor protein. Phospholipase C (PLC) zeta was identified as a strong candidate for the mammalian sperm factor [2]. The molecular weight of PLC zeta is approximately 74 kDa [15]. Fujinomoto et al [16] confirmed that the most convincing evidence that PLC(z) is the mammalian sperm factor. Further work is required to clarify the component of sperm factor in this goat CSE.

Oocytes activation

Activation of mammalian oocytes could be induced by a wide variety of chemical [17] and physical [18] stimuli that mimic the fertilization process by providing calcium signals to the MII arrested eggs by different mechanisms. The transfection method used in this research might be cause the lower result because of improper method of activation Result of cleavage rate especially using GCSE alone (2 %) was lower than achieved by Okada et al [5] which resulted in approximately 30 % of oocyte cleaved using microinjection method of CSE (Table 1.). CSE may be representation of the sperm factor complex that having better influence in activation compare to CSE with 100 kD proteins specific. It is necessary that a complex of unknown composition of the active factor in CSE to be determine in next research. The confirmation of Ca^{2+} intensity using fluo-3 through Confocal Laser Scann Microscope showed the different profile of M-II oocyte activated using GCSE. After 48 hours activation of the oocyte, it was observed an increase in Ca^{2+} intensity only in outer region of M-II activated by CSE alone) in contrary the increase of Ca^{2+} intracellular intensity of the oocytes was observed at all sites of M-II activated using chemical agent and CSE. The increase of Ca^{2+} intensity that equal to Ca^{2+} concentration, might lead to egg activation.

Oocytes activation was induced by chemical agent supplemented with CSE, with the evidence of rise Ca^{2+} intensity. This was considered to be sufficient factor for activation. Matsura and Maeda [15] suggested that if a large quantity of protein with high ability for oocyte activation was extracted from spermatozoa, it might improve the rate of oocyte activation. A qualitative image analysis of Ca^{2+} intensity done by histogram and line series was presented in Fig. 1 B.

4. Conclusion

The increase of Ca^{2+} intensity was considered to be sufficient indicator that showed activation of M-II oocyt is occurred.The CSE effecct on culture medium is relatively better than spesific protein of GSE of 100 kDa for their role as activation effect to goat oocytes. The supplementation of CSE in conventional chemical medium activation could improve the induction of M-II oocyte activation. It was suggested to additional research in both intracellular calcium concentration and identification of specific protein or sperm factor component of CSE.

5. Acknowledgements

This research was supported by Grant from Directorat General of High Education (DIKTI), Ministry of Education Republic of Indonesia . Especially thanks to Dr. Tanaka Hozumi, (Jichi Medical School, Japan) for the helpful assistance of cell cultured and micromanipulation and CSE teamwork: Eva Ari Wahyuni, Sri Rahayu, Aulanni'am and Budi Siswanto for very good support and collaboration.

6. References

[1]. Fissore R.E., Gordo A.C., Wu H. (1998), Activation of development in mammals: is there a role for sperm cytosolic factor?. *Theriogenology* 49: 43-52.

[2]. Oda.S. (2006), Mammalian Sperm Factor and Phospholipase C Zeta. *J. Mamm. Ova Res*. 23: 2 – 9.

[3]. Wu, H., C.L. He and R.A. Fissore (1987), Injection of a porcine triggers calcium oscilations in mouse oocytes and bovine eggs. *Mol. Reprod. Dev*, 46: 176 – 189.

[4]. Miyazaki, S. and M. Ito (2006), Calcium Signals for egg activation in mammals. *J. Pharmacol. Sci*. 100 : 545 – 552.

[5]. Okada, K., T. Miyano and M. Miyake. (2004), Activation and development of pig oocytes after microinjection of Ceude Sperm Extract. *J. Mammal Ova Research*. 21: 134 – 140.

[6]. Ciptadi, G., S.B, Sumitro, A. Boediono and T. Susilawati (2005), The improvement method of activation of reconstructed oocyte using intra cytoplasmic injection for cloning embryo production. Research Report (Desertation) Brawijaya University, Malang. Indonesia.

[7]. Han, Y.M., Y.K. Kang, D.B. Koo and K.K. Lee (2003), Nuclear reprogramming of cloned embryos produced in vitro. *Theriogenology* 59: 33-44.

[8]. Tanaka, H. (2001), Reproductive biology and biotechnology. JICA, Japan International Cooperation Agency, Indonesia.

[9]. Neglia G, Gasparrini B, Caracciolo di Brienza V, Di Palo R, Campanile G. and G.A. Presicce (2003), Bovine and buffalo in vitro embryo production using oocytes derived from abattoir ovaries or collected by transvaginal follicle aspiration. *Theriogenology*. 59. 1123–30.

[10]. Swan, K. (1990), A cytosolic sperm factor stimulates repetitive calcium increases ang mimics fertilization in hamster eggs. *J. Development*, 110 : 1295 – 1302.

[11]. Ongeri, E.M., C.L. Bormann, R.E. Butler, D. Melican, W.G. Gavin, Y. Echelard, R.L. Krisher and E. Betboodi (2001), Development of goat embryos after in vitro fertilization and parthenogenetic activation by different method. *Theriogenology* 55 (9): 1933 – 1945.

[12]. Wahyuni E. A., G. Ciptadi, Aulanni'am, B. Siwanto (2009), The Isolation and characterization of protein of the crude sperm extract of goat and bovive: potential CSE 100 kDa on oocyte activation. Thesis Report. Brawijaya University.

[13]. Matsuura, D., W., Heifeng and T. Terada. (2006), The effect of miniature pig sperm extract (CSE) and their treatment on porcine or bovine oocyte activation. *J. Mamm. Ova Research.* 23: 52 – 57.

[14]. Ogonuki., N. Sankai T, Yagami,K., Shikano, T. Oda , S., Miyazaki , S., and Ogura A. (2001), Activity of a sperm-borne oocyte activating factor in spermatozoa and spermatogenetic cells from cynomolgus monkey and its localization after activation. *J. Biol. Repro.*, 65: 351-357.

[15]. Matsura D and T Maeda (2006), Effect of sperm extract and its molecular weight fraction on oocyte activation in miniature pig spermatozoa. *J. mamm Ova Research*. 23: 122 – 127.

[16]. Fujinomoto, S, Yoshida N, Fukui T, Amanai M, Isobe T, Itagaki C., Izumi T and Perry AC. (2004), Mammalian phospolipase Czeta induce oocyte activation from the sperm perinuclear matrix. *J. Dev. Biol*, 274: 370 – 383.

[17]. Kline, D., Kline J.T. (1992), Repetitive calcium transients and the role of calcium in exocytosis and cell cycle activation in the mouse egg. *Dev Biol* 149. 80–9.

[18]. Ozil J. P. (1990), The parthenogenetic development of rabbit oocytes after

repetitive pulsatile electrical stimulation. *Development* 109. 117–27.

Appendixes

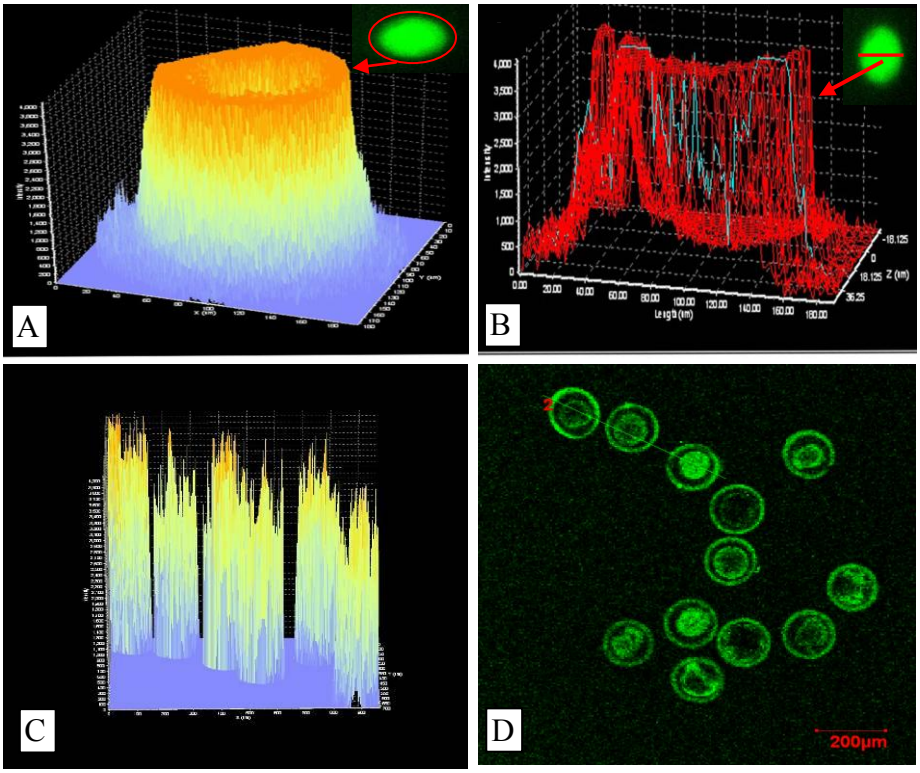

Figure.1. (A). Histogram profile of oocyte non activated (control), 48 hour of culture. Calsium intensity expressed mainly zona pellucida. (B). Calcium intensity profile of oocyte activated by CSE, intensity calsium is well expressed spread out in cytoplasm. (C,D). Variation of oocyte respons on different oocyte treated with CSE, 48 hour after treatment and cultured. Analysis was done by CLSM-fluo-3.

Table 1. Cleavage rate of different treatments of parthenogenetic using GCSE supplementation**.**

Activation method	Selected M-II Oocytes	Cleavage rate (%)
(1). Control (M-II) oocyte	40	(0.00)
(2). CSE 2.5 ug/ml	251	(36. 33)
(3). CSE of 100 kDa protein	240	(2.00)

The Effect of Prostaglandin $F_{2\alpha}$ Addition on Sperm Quality in Goat Semen Diluted with Various Solutions

Herawati

Veterinary Medicine School, University of Brawijaya, Malang, Indonesia (herawati58@ub.ac.id)

Abstract

The study was conducted to study the effect of prostaglandin $F_{2\alpha}$ (PG $F_{2\alpha}$) addition on sperm motility and sperm livability in Ettawah cross breed goat semen diluted with citrate yolk, skim milk or glycerol skim milk. The study was conducted with two experiments. The experiment I was conducted to clarify the effect of $PGF_{2\alpha}$ placebo addition in goat semen. The result of semen collection every goat was added with 0.0 mg $PGF_{2\alpha}$ (placebo) and diluted with citrate yolk, skim milk or glycerol skim milk. The sperm then were stored (5°C) for four days and evaluated everyday. The experiment 2 was conducted to clarify the effect of 2.0 mg $PGF_{2\alpha}$ addition in goat semen which diluted with citrate yolk, skim milk, or glycerol skim milk, the sperm then was stored (5°C) and was evaluated everyday. The result showed that $PgF_{2\alpha}$ addition to goat semen diluted with citrate yolk, skim milk or glycerol skim milk could increase sperm motility and sperm livability ($P<0.05$). The effect of 2.0 mg $PGF_{2\alpha}$ addition was better than the effect 0.0 mg $PGF_{2\alpha}$ addition on both sperm motility and sperm livability. Among the various solution, citrate yolk and skim milk were still in range for requirements of artificial insemination.

***Keywords**: PGF2α, sperm motility, livability, goat semen.*

1. Introduction

Until now the success of artificial insemination program in ruminants is not optimal and still allows to be improved. Based on reports from the field indicate that conception rates were still relatively low, so did the number of services per conception is still high and long lambing intervals. One cause of failure in improving the production efficiency of the above is the low quality of spermatozoa used in artificial insemination programs.

Addition of prostaglandin F_{2a} (PGF_{2a}) in vitro against the cement can increase the quality of spermatozoa. Some researchers reported that administration of prostaglandin F, providing very real benefits to the motility (viability sperm tail. Additions of prostaglandin F cement sheep, after the observable fact also can improve the fertility rate [3].

Addition of $PGF_{2\alpha}$ increased LH concentrations, testosterone, and prolactine in circulation at the bull [5-7]. Next with increased LH or testosterone increases the secretion and spermatogenesis and accessorial gland. The administration of $PGF_{2\alpha}$ before semen collection increased trajectory of spermatozoa in the male genital tract secretions of glands and accessories.

Motility of spermatozoa is an indicator and the simplest way in the assessment of semen for artificial insemination. Assessment of sperm motility was carried out under a microscope and are subjective, the movement of spermatozoa with progressive forward in unison. Wave-motion which occurs later forwarded to all parts of the tail, resulting in a tail like a whip motion trigger that drives sperm to move in the liquid [11]. The motility Goat sperm good Ettawah hybrid is 55-80% [12]. The percentage of spermatozoa that living and dying really need to know if only in motility examination show the actual number of live sperm [9]. The living and the dead of goat's spermatozoa can be distinguished from its reaction to certain dyes. Spermatozoa that are not motile and considered dead will absorb the color, while motile spermatozoa and life does not absorb color [11].

This study aims to determine the effect of (injection or addition) $PGF_{2\alpha}$ on the properties of goat semen Ettawah Hybrid (PE).

2. Experimental Details

The materials used for this study include tools and materials. The instrument used consisted of an artificial vagina, hemocytometer, microscope, refrigerator / freezer, tube cement reservoir. Materials needed include: cement Ettawah goat breed, $PGF_{2\alpha}$ egg yolk citrate diluents, dilution of skim milk, skim milk diluents of glycerol, sodium nitrate, hematocyline, eosin, nigrosin. methylene blue, giemza.

The study consisted of two experiments. The first experiment aimed to examine the effect

of adding 0.0 mg of $PGF_{2\alpha}$ (placebo) on the properties of the diluted semen. Semen obtained by the placebo plus 0.0 ml of $PGF_{2\alpha}$/ nil cement. Each goat's cement diluted with egg yolk citrate, skim milk and skim milk glycerol and cooled 5°C for 4 days. Evaluation carried out on sperm motility and percentages live every day. Experiment 2nd aims to examine the effect of adding 2.0 mg $PGF_{2\alpha}$ on the properties of the diluted semen. Semen collection basil plus 2.0 mg $PGF_{2\alpha}$ then diluted with egg yolk citrate, skim milk and skim milk glycerol. Evaluation of spermatozoa motility and percentage live every day for 4 days. All data collected were analyzed by analysis of variance on the motility and percentage live spermatozoa.

3. Results and Discussions

Assessment results motility of spermatozoa with semen diluted with egg yolk citrate, skim milk or skim milk glycerol showed that the addition of 0.0 mg of $PGF_{2\alpha}$ (placebo) did not significantly influence ($P>0.05$). However, with increasing storage duration in the temperature 5°C, motility of the less well on the addition of 0.0 mg and 2.0 mg $PGF_{2\alpha}$ ($P <0.01$). Motility of spermatozoa on the first, second, third and fourth day after the addition of 0.0 mg PGF (Placebo) are respectively 73.50%, 63.92%, 59.08% and 49.75%.

Addition of 2.0 mg, $PGF_{2\alpha}$ did not appear to affect the motility of spermatozoa in semen diluted with egg yolk citrate, skim milk or skim milk glycerol ($P>0.05$). But with increasing length of storage, motility in the diluents is further reduced ($P<0.01$). On the first day after addition of 2.0 mg PGF 80.75% sperm motility and on the fourth day is 64.33%.

The result of evaluation of the percentage of live spermatozoa in semen plus 2.0 mg PGF diluted with egg yolk citrate diluents, skim milk or skim milk glycerol showed a significant difference ($P<0.01$). Differences occur between the percentage of live spermatozoa in egg yolk citrate diluents or skim milk and glycerol between egg yolk citrate and skim milk, respectively 95.50% and 71.94% and 93.38%, and 7 1.04%.

This shows that a higher percentage of live spermatozoa in egg yolk citrate diluents and skim milk. The percentage of live spermatozoa in egg yolk citrate diluents higher is because of the high content of glucose, lecithin and lipoproteins as an energy source of spermatozoa. Similarly, the dilution of skim milk, because it is associated with the content of glucose as an energy source of spermatozoa. The reduced percentage of live spermatozoa in the skim milk diluents of glycerol may be caused by interaction between $PGF_{2\alpha}$ and glycerol.

A highly significant difference was also found on the percentage of live sperm in the diluents is stored in long periods of time ($P<0.01$). On the first day after addition of 2.0 mg PGF percentage of live spermatozoa were 93.92% to 63.17% on the fourth day. Under these conditions, the sperm can still be used for artificial insemination, because on the percentage of live cattle spermatozoa as 70% still can be used for artificial insemination.

Based on analysis of motility and percentage live spermatozoa in the semen prior to dilution indicates that there is a very significant difference between the addition of 0.00 mg $PGF_{2\alpha}$ (placebo) and 2.0 mg of $PGF_{2\alpha}$.

If the addition of 2.0 mg and 0.0 mg $PGF_{2\alpha}$, compared, it found the existence of significant differences both of motility on day 1 (80.75 vs. 73.50), on day 2 (72.08 vs. 63.92), on day 3 (74.50 vs. 59.08) and on day 4 (64.33 vs. 49.75). Similarly the percentage of live spermatozoa between the addition of 2.0 mg to 0.0 mg $PGF_{2\alpha}$ on the first day 1 is (93.92 vs75, 92), on the second day is (93.25 vs. 76.83), on the third day is (84.42 vs. 50.83) and on the fourth day is (76.17 vs. 52.75). According to Sharma and Hays (1976) that prostaglandins can activate smooth muscle. Contradictory element of spermatozoa is a layer of fibers that surround the central acronem from the main part of the tail of spermatozoa. Thus the addition of 2.0 mg $PGF_{2\alpha}$ can improve the motility of spermatozoa in a way to activate the contractile elements and be able to maintain the percentage of spermatozoa live. The percentage of live sperm can be increased or held because adding 2.0 mg of $PGF_{2\alpha}$ will further stimulate the concentrations of LH and testosterone which will increase the secretion of glands and prostate Accessories like vesicular [13].

4. Conclusion

From the day it can be concluded that the addition of $PGF_{2\alpha}$ to increase the motility and the percentage of live spermatozoa in egg yolk citrate diluents, skim milk or skim milk glycerol. Adding 2.0 mg PGF have better results than the addition of 0.0 mg PGF both motility and the percentage live spermatozoa. From the three-thinning can be inferred thinning egg yolk citrate and skim milk can maintain sperm motility and percentage live better than skim milk diluents glycerol. For further investigation, cement that will be used for

artificial insemination in goats Ettawah hybrid should get the addition of PGF and diluted with egg yolk citrate or skim milk.

5. Acknowledgments

---

6. References

[1]. Bearden, H. J. and Fuquay, J. (1984), Applied Animal Reproduction. Reston Publishing Company, Inc. Reston, Virginia.

[2]. Cole, H. H. and P. T. Cupps. (1977), Reproduction in Domestic Animal. Academic Press, New York.

[3]. Dimov, V., and G.S Georgies. (1977), Ram Semen Prostaglandin Concentration and Its Effect of Fertility. *J. Anim. Sci.* 44: 1050 – 1054

[4]. Hafez. E.S.E., (1987), Semen Evaliation. In: Hafez. E. S. E. (ed.). Reproduction in Farm Animal. 5th edition. Lea & Ferbiger. Philadelphia.

[5]. Hafz, H. D. (1975), Prostaglandin and the Control of Anterior Pituitary Hormoe Secretion. In: ―Hipothalamic Hormone". M. Motta, P.G. Corosigani, and L Martini (ed.). Academic Press. New York.

[6]. Haynes, N. R., Hafs, N.D., Water, R.J., Manns, J.C., and Railey, A. (1975), Stimulatory Effect of Prostaglandin $F_{2\alpha}$ on the Plasma Concentration. Bull. *J. Endocr.* 66:329-338.

[7]. Kisser, N. R., Hafs, N. D.,and Oxender, W.D. (1976), Increased Blood LH and Testosteron after Administration $PGF_{2\alpha}$. *Bull. Prostaglandin* II: 543-553.

[8]. Nalbandov, A. V., (1976), Fisiologi Reproduksi pada Mamalia dan Unggas. University of Indonesia Press. Jakarta.

[9]. Partodihardjo (1982), Ilmu Reproduksi Hewan. Mutiara Sumber Widya. Jakarta.

[10]. Picket, B.W., and W.E. Berndtson. (1974), Preservation of Bovine Spermatozoa by Freezing Straws. A Review *J. Dairy Sci*. 57: 1287 -1301.

[11]. Salisbury, G.W., and N.L. Van Demark (1978), Phsychology of Reproduction and Artificial Insemination of Cattle. W.H. Freeman and Company, San Francisco and London.

[12]. Sunardi (1989), Karakteristik Semen Kambing Peranakan Ettawah dan Lama Daya Tahan Hidup Spermatozoa Dalam Pengencer Kuning Telur Sitrat. Bulletin Peternakan th XIII No. 1.

[13]. Toelihere, M.R. (1985), Fisiologi Reproduksi pada Ternak. Angkasa Publisher. Bandung.

[14]. White, I.G. (1980), Secretion of the Reproductive Trant and Seminal Plasma, In: Hafez E.S.E. (Editor). Reproduction in Farm Animals. 4th edition. Lea & Febriger. Philadelphia.

Correlation Between AgNOR, MIB-1 and Radiotherapy Response in Lung Cancer

Iin Kurnia [1], Heriawati [2], Juniarti [3], Ruth ES [2], Zubaidah Alatas [1], Elisna Syahruddin [4], Made Widhyasmara [4]

[(1)] Department of Biomedical, Center for Technology of Radiation Safety and Metrology, National Nuclear Energy Agency, Jakarta, Indonesia
[(2)] Department of Pathology Anatomy, Jakarta, Indonesia
[(3)] Department of Radiotherapy, Jakarta, Indonesia
[(4)] Department of Lung, Persahabatan Hospital, Jakarta, Indonesia
[(5)] Study program of Pharmacy, Faculty of Mathematical and Natural Science, ISTN, Jakarta, Indonesia.

Abstract

Level radiosensitivity is highly correlated with the level of cell division that can be predicted by neither detection of NOR (Nucleolar Organizer Region), Ki-67 index and others. NOR is a segment of DNA (nucleic acid) associated with nucleus that contain genes encode ribosomal. From a number of papers found in the NOR positively correlated with Ki-67 index. The different of sensitivity of cancer cells to radiation will affect the success of radiotherapy in cancer control. The aim of the research is detection of NOR and MIB-1 (Ki-67) index as a marker tumor cell radiosensitivity in order to optimize the lung cancer patients treatment with radiotherapy or chemoradiotherapy. AgNOR staining has been performed and MIB-1 by double staining of 20 lung cancer cell smear results of fine needle biopsy from Department of Pathology Anatomy of Persahabatan Hospital, Jakarta before treated and observed the radiation response after 2 weeks of radiation. Radiotherapy response was classified by the good and poor response. Tend of a weak correlation between MIB-1 and AgNOR (r = 0.23) in the smear cells of lung cancer before treatment, there were no statistically significant difference in AgNOR value between good response and poor response after 2 weeks of radiation, the value of MIB-1 index poor response after 2 weeks of action more than the value of MIB-1 in good response (p = 0.12). Although statistically there is no difference, the higher value of MIB-1 before treatment is tend give poor response than in good response after 2 weeks irradiation.

Keywords: *AgNOR, MIB-1, Lung Cancer, Radiotherapy.*

1. Introduction

Non-small-cell lung cancer (NSCLC) accounts for 75–80% of primary lung cancer. Tumour node metastasis (TNM) factors are generally used in the evaluation of tumour progression, and nodal involvement (N-factor) as well as distant metastasis (M-factor) is the critical factor to determine the prognosis of NSCLC [1]. Lung cancer represents a great challenge for the oncologist because only one third of cases can be treated with surgery. In cases not eligible for surgery, chemotherapy or radiotherapy is commonly used. Despite these treatments, it gives local recurrence or distant metastases in most cases [2].

Nucleolar organizer regions (NORs) are chromosomal loops of DNA involved in ribosomal synthesis [3]. The silver staining technique can easily detect NORs in formalin fixed, paraffin embedded tissues and NORs can be identified as black dots in the nucleolus (AgNOR) [4]. This method permits the rapid evaluation of morphology and tumor cell kinetics even using small biopsies. Evaluation of AgNORs parameters (number, size, and distribution) has been applied in tumor pathology both for diagnostic and prognostic purposes [5]. Their size and number have been reported to reflect the proliferative activity of tumor cells [6].

The malignant grades of tumor cell and proliferative activity have been assessed using immunohisto-chemical staining with several cell cycle related parameters [7,8]. MIB-1, also known as Ki-67, is expressed in all cell cycle stages except for G0 and early G1 phase. This antigen is thought to be associated with a nuclear antigen protein- DNA replicase complex, similar to DNA topoisomerase II [9].

Generally, a higher MIB-1 labeling index (LI) correlates with worse prognosis; however,

tumors with higher MIB-1 LI are often radiosensitive.

Although many investigators have demonstrated a relationship between the number or mean area of AgNORs and MIB-1 expression in solid tumors [10-14], we have not known previous studies have simultaneously assessed AgNOR staining and Ki-67 expression in smear of lung cancer from fine needle biopsy tissue before treatment and observed radiotherapy response after 2 weeks irradiation.

This research propose detection of NOR and MIB-1 (Ki-67) index with double staining method as a marker tumor cell radiosensitivity and their correlate with response of radiotherapy behalf on to optimize treatment of lung cancer patients with radiotherapy or chemoradiotherapy.

2. Experimental Detail

Patient Characteristic

A total 20 cell smear from 20 patients with non small cell carcinoma of the lung from fine needle biopsy specimens taken before treatment with radiotherapy alone or combined with chemotherapy at Department of Pathology Anatomy, Persahabatan Hospital (Jakarta, Indonesia) from 2007-2009. The response of radiotherapy was observed two weeks after the initiation of radiotherapy. Their ages ranged from 28-73 years old (mean and median: 56.1 and 57.5 years old, respectively).

Destained, MIB-1, AgNOR Staining

Some modification method from originally method [15,16] was made. First the cover glass from stained slide was removed by incubation in warm xylene with temperature about 60ºC 18–24 hours. Then the slides were processed through xylene and rehydration with grades of alcohol. Before incubation with Antigen Retrieval in Mircowave 2 x 10 minute in temperature 94ºC, they were incubation in PBS 2 x 5 minutes on room temperature, then staining with MIB-1 followed with AgNOR staining as in incubated with 1 part 2% gelatin in 1% aqueous formic acid with 2 parts 50% aqueous silver nitrate at room temperature for exactly 30 min. The slides were then rinsed with distilled, de-ionized water, taken through alcohols to xylene, and mounted with an entellan. No counter staining was performed. This process was done on Department Biomedical, The Center for Technology of Radiation Safety and Metrology National Nuclear Energy, Jakarta

Assesment AgNOR, MIB-1, Radiotherapy Response

AgNOR score (the number of NORs in a tumor cell nucleoli) were counting in cell nuclei using a light microscope (magnification ×400) with the immersion oil method of Crocker *et al* [16] MIB-1 are the percentages of MIB-1 positive tumor cells in colored print photograph, (original magnification ×400) to minimize variations originating from within sections. One of the authors (MW) blindly performed cell counting [16]. We use Correlation Regression to correlate between AgNOR value and MIB-1 index, Student T test to analyze the different between AgNOR and MIB-1 among good and poor response after 2 weeks irradiation with *Medcalc* Software Program. Radiotherapy response is observed by senior Radiotherapist (YN) in Department of Radiotherapy Persahabatan Hospital, Jakarta.

3. Result and Discussion

Expression double staining AgNOR and MIB-1 in smear of lung cancer cell taken before treatment by radiotherapy or chemoradiotherapy and correlate between AgNOR value and MIB-1 index can be seen in (Figure 1 and 2). Average of AgNOR and MIB-1 index in different response after 2 weeks irradiation are given in Figure 3a and Figure 3b, respectively.

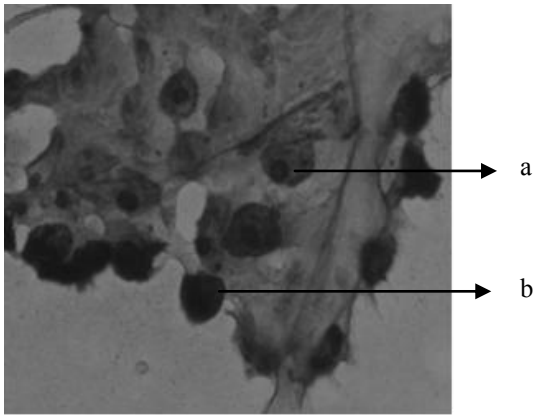

Figure 1. Double staining AgNOR dan MIB-1 from destained smear cell from fine needle biopsy lung cancer before treatment, negative MIB-1 (a) dan positive MIB-1 (b)

Cancer cell with positive MIB-1 (Ki-67) can be seen in cell nucleus with dark brown color, contrast in negative the color is light brown. The number of AgNOR in MIB-1 positive cell is higher than negative cell. It means that the positive correlation between AgNOR and MIB-1 index. In this study we found only weak

correlation between AgNOR and MIB-1 (r = 0.23) (Figure 2).

This result is the similar with previous report, with double staining in biopsy of breast cancer. In a study using double staining with AgNOR and MIB-1 (the latter being a marker for the number of cells in the cycle) demonstrated that the number of AgNORs were ranged from 2–12 in the MIB-1 positive cells and 1–3 in negative cells [17].

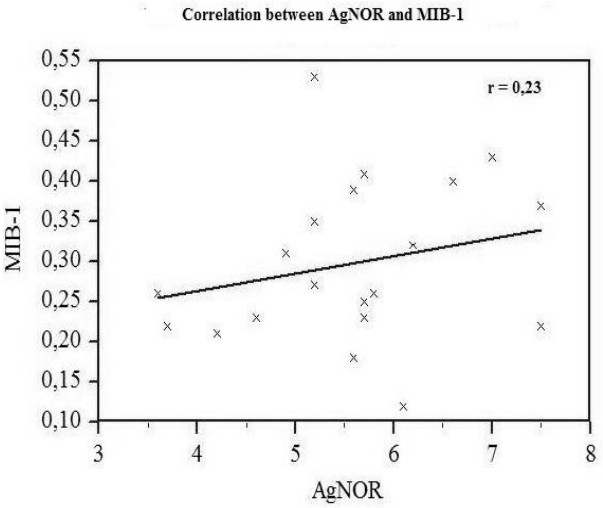

Figure 2. Weak correlation (r = 0.23) between AgNOR and MIB-1 from destained smear cell from fine needle biopsy lung cancer before treatment.

In our previous report [16] we found the strong positive correlation between AgNOR and MIB-1 in cervical cancer biopsy before treatment with chemoradiotherapy, but in this study the tissue was taken from biopsy and staining separated. Staining tissue from biopsy specimen may make more cell could be stained compare the cell from fine needle biopsy that only can get a little cancer. Another report found strong correlation between AgNOR and MIB-1 in vulva epithel [18], gastric cancer [19], oral lesion [20], and cervical epidermoid carcinoma cell line [21].

In this present study there is no statistically significant difference in AgNOR value between good response and poor response after 2 weeks of radiation. The value of MIB-1 index poor response after 2 weeks of action more than the value of MIB-1 in good response, almost border line with statistically significant (p = 0.12).

NOR that observed by AgNOR staining can be detected in phase in G1, S and G2. MIB-1 can be detected in all mitotic cells. Some report said expression of MIB-1 in was related with growth fraction of cancer cell [7,8,16]. Higher of growth fraction of lung cancer maybe also related with the resistant to radiation treatment after 2 weeks irradiation or maybe the radiation is not enough to stop of growth or proliferation of the cancer cell in the lung. High proliferation also related with angiogenesis of the lung cancer. Increased tumor cell proliferation is a contributing factor to tumor size and metabolic burden, and might be expected to be associated with angiogenesis [22]. Proliferation also essential to cancer cell invade and disseminate [23].

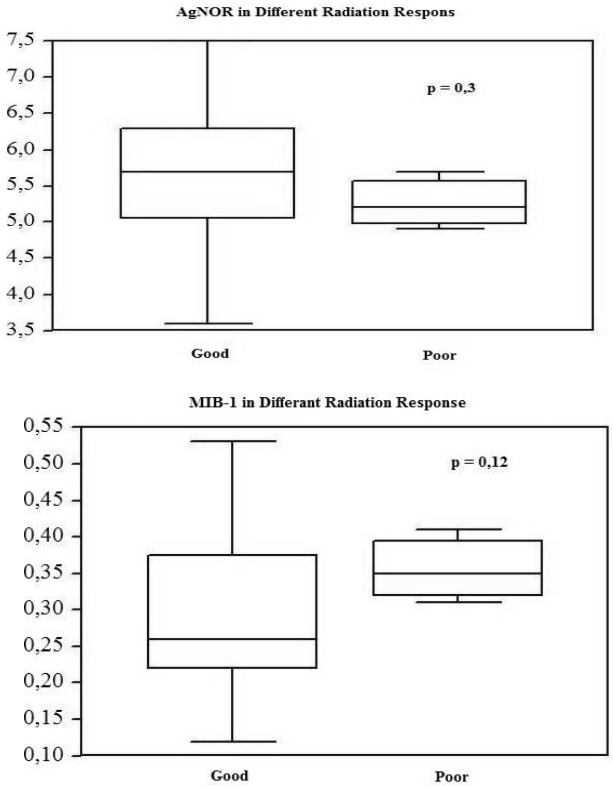

Figure 3. AgNOR (a) dan MIB-1 (b) in good and poor response, p = 0.3 (b) p = 0.12 respectively from destained smear cell from fine needle biopsy lung cancer before treatment

The number and size of NORs are highly variable within the nucleolus according to rRNA transcriptional activity. Sirri et al [24], reported that the accumulation of nucleolin and B23 (two major NOR protein) in G2 was larger than in G1 in the cell cycle. Hence, the numbers of NORs are larger in the phases of the cell cycle from S to G2[25] MIB-1 was present in all cell cycle stages except for G0 and early G1.36, [26] Dong et al[.27] reported that the AgNOR score in human cervical squamous cell carcinoma cell line showed a strong correlation with MIB-1-LI.

They also reported that both AgNOR score and MIB-1-LI showed inverse correlations with potential doubling time and the length of S phase.

Different of statistical significant between MIB-1 and AgNOR in different a response after 2 weeks irradiation proved that MIB-1 MIB-1 also showed of growth fraction of lung cancer and AgNOR showed of condition of cell cycle as a part of cell mitotic or as one of parameter related to cell proliferative activity. Even though the sample of patient is include of this research was small, we think MIB-1 index is more realize than AgNOR used as prediction of radiation response of lung cancer treated with radiotherapy or chemoradiotherapy.

4. Conclusion

Although statistically there is no difference, the higher value of MIB-1 before treatment is tend give poor response than in good response after 2 weeks irradiation.

5. Acknowledgements

This research was supported by a Research Grant from Center for Technology of Radiation Safety and Metrology, National Nuclear Energy Agency in Indonesia FY 2009. This research was approved by the Committee for Medical Research Ethics, Hospital of Persahabatan, Jakarta. The authors thank to Dr. Susilo Widodo, Head of The Center for Technology Radiation Safety and Metrology, National Nuclear Energy Agency, Jakarta and all of technician with their assistance of this research both in Department of Biomedical, The Center for Technology Radiation Safety and Metrology, National Nuclear Energy Agency, and Persahabatan Hospital, Jakarta.

6. References

[1]. Mountain C.F. (1997), Revisions in the international system for lung cancer, *Chest*; 111: 1710–1717

[2]. Viberti L, Papotti M, Abbona GC, Celano, A, Filosso PL, Bussoliti, G. (1997), Value of Ki-67 Immunostaining in Preoperative Biopsies of Carcinomas of the Lung, *Human Pathology*; 28.2:189-192

[3]. Gall J. G, Pardue M. L. (1969), Molecular hybridization of radioactive DNA to the DNA of cytological preparation, *Proc Natl Acad Sci* 64:600-604.

[4]. Derenzini M, Ploton D. (1991), Interphase nucleolar organizer regions in cancer cell, *Int Rev Exp Pathol.* 32:150-192.

[5]. Trere D. (2000), AgNOR. Staining and Quantification, *Micron.* 31:127–131.

[6]. Derenzini M, Pession A, Trere D. (1990), The quantity of nucleolar silver-stained protein is related to proliferating activity in cancer cell, *Lab Invest* ;63:137-140.

[7]. Nakano T, Oka K. (1991), Transition of Ki-67 index of uterine cervical tumors during radiation therapy.,*Cancer*; 68:517-523.

[8]. Nakano T, Oka K. (1993), Differential values of Ki-67 index and mitotic index of proliferating cell population, *Cancer*; 72:2401-8.

[9]. Gerdes J, Schwab U, Lemke H, Stein H (1983), Production of a mousemonoclonal antibody reactive with a human nuclear antigen associated with cell proliferation, *Int. J Cancer* ;31:13-20.

[10]. Kakeji Y,Korenaga D, Tsujitani S, Haraguchi, Maehara Y, Sugimachi. (1991), Predictive value of Ki-67 and argyrophilic nucleolar organizer region staining for lymph node metastasis in gastric cancer. *Cancer Res*. 51:3503

[11]. Kuratsu S, Aozasa K, Tsujimoto M, Ueda T, Uchida A, Hamada H, Ono K, Matsumoto K. (1991), Prognostic significance of argyrophilic nucleolar organizer staining in soft-tissue sarcomas. *Int J. Cancer.* 48:211

[12]. Plate KH, Riischoff J. Behnke J, Mennel HD. (1990), Proliferative potential of human brain tumours as assessed by nucleolar organizer regions (Ag-NORs) and Ki-67-immunoreactivity, *Acta Neurochir Wien* .104:103

[13]. Raymond WA, Leong ASY. (1989), Nucleolar organizer regions relate to growth fractions in human breast carcinoma, *Hum Pathol*. 20:741

[14]. Trere D, Farabegoli F, Cancellieri A, Ceccarelli C, Eusebi V, Derenzini M. (1991), AgNOR area in interphase nuclei of human tumours correlates with the proliferative activity evaluated by bromodeoxyuridine labeling and Ki-67 immunostaining. *J Pathol.* 165:53

[15]. Munakata S,Hendricks JB. (1994), A Multilabeling Technique for Simultaneous Demonstration and Quantitation of Ki-67 and Nucleolar Organizer Regions (AgNORs) in Paraffin-embedded Tissue, *Journal of Histochemistry and Cytochemistry*. 42;6:789-793

[16]. Kurnia I, Yoshiyuki S, Budiningsih S,Andri A,Irwan R, Cholid B,,Yukari Y Takashi N (2009), Nucleolar Organizer Regions in Squamous Cell Carcinomas of the Uterine Cervix Treated with Chemoradiotherapy.

Austral - *Asian Journal of Cancer* ISSN-0972-2556, Vol. 8, No. 2, April :93-102

[17]. Mourad WA, Sneige N, Katz RL, Ordonez NG (1994), Correlation of two AgNOR counts with Ki-67 labelling index: a study in fine- needle aspirates of lymphoproliferative disorders and breast carcinoma. *Diagn Cytopathol.* 10: 113–9.

[18]. Hermann B, Susanna N (2002), Expression of Topoisomerase II, Ki-67, Proliferating Cell Nuclear Antigen, p53, and Argyrophilic Nucleolar Organizer Regions in Vulvar Squamous Lesions, *Gynecol Oncology*, 86, 192–199.

[19]. Kakeji Y, Daisuke K, Shunichi T, Musarti H, Yoshihiko M, and Keizo S. (1991), Predictive Value of Ki-67 and Argyrophilic Nucleolar Organizer Region Staining for Lymph Node Metastasis in Gastric Cancer, *Cancer Research*; 51:3503-3506.

[20]. Teresa DB, Karina AN, Carlos B N,Paula AGF, Maria RBO, Jose´ Antonio S. Z. (2007), Computer-assisted analysis of cell proliferation markers in oral lesions, *Acta Histochemica* 109 :377—387.

[21]. Dong H, Carey B, Eric S, and Mark A.R. (1997), Assessment of Cell Proliferation by AgNOR Scores and Ki-67 Labeling Indices and a Comparison With Potential Doubling Times, *Cytometry*. 28:280-288.

[22]. Brockenbrough, JS, Janice KM, Stephen EH, Joshua ES, Janet SR (2009), Thymidine Kinase 1 and Thymidine Phosphorylase Expression n Non–Small-cell Lung Carcinoma in Relation to Angiogenesis and Proliferation, *Journal of Histochemistry & Cytochemistry*, Volume 57(11): 1087–1097.

[23]. Yamazaki D, Kurisu S, Takenawa T. (2005), Regulation of cancer cell motility through actin reorganization, *Cancer Sci*, 96:379-386.

[24]. Derenzini M. (2000), The AgNORs. *Micron* 31:117–120.

[25]. Sirri V, Pascal R, Marie C G, and Hernandez VD. (1997), Amount of the Two Major Ag-NOR Proteins, Nucleolin, and Protein B23Is Cell-Cycle Dependent. *Cytometry* 28:147-56.

[26]. Kidogawa, H, Nanashima A, Yano, H, Matsumoto, M. Yasutake,T. Nagayasu T. (2005), Clinical Significance, double staining MIB-1and AgNORs in primary breast carcinoma. *Anticancer Res*. 25:3957-62.

[27]. Dong AT, Shuqing L, Dan H. Moore II, and Edgerton SM. (1999), Comparison of Mitotic Index, In Vitro Bromodeoxyuridine Labeling, and MIB-1 Assays to Quantitate Proliferation in Breast Cancer. *J Clin Oncol*. 17:470-476.

Tyrosinase Activity of *Piper betle* and *Piper crocatum* Essential Oil

Irmanida Batubara[1,2], Min Rahminiwati[2,3],Latifah K. Darusman[1,2], Tohru Mitsunaga[4].

(1) Department of Chemistry, Faculty of Mathematic and Natural Sciences, Bogor Agricultural University, Bogor, Indonesia (ime@ipb.ac.id)
(2) Biopharmaca Research Center, Bogor Agricultural University, Bogor, Indonesia (bfarmaka@gmail,com)
(3) Department Physiologi and Pharmacology, Faculty of Veterinary, Bogor Agricultural Univeristy, Bogor, Indonesia (minraminiwati@yahoo,com)
(4) Faculty of Applied Biological Sciences, Gifu University, Gifu, Japan (mitunaga@gifu-u.ac.jp)

Abstract

Piper betle (Local name Sirih Hijau) and Piper crocatum (local name Sirih Merah) are two type of Piper genus which famous in Indonesia. This research is related to application of chemistry in health. The aims of this research were to find the essential oil component in Sirih Hijau and Sirih Merah and to find the potency of the essential oil against tyrosinase. The essential oils were obtained from leaves of Sirih Hijau and Sirih Merah by steam distillation. The components in the essential oils were analyzed by GC-MS. The activities of essential oils against tyrosinase were analyzed with spectrophotometry methods. The results showed that sirih hijau and sirih merah essential oils consisted of alpha thujene, alpha pinene, (+)-sabinene, beta-myrcene, alpha terpinene, beta terpinene, beta phellandrene, gamma terpinene, caryophyllene, alpha caryophyllene, and garmacrene. Camphene, chavicol and eugenol only existed in Sirih Hijau essential oil and not existed in Sirih Merah essential oil. The tyrosinase activities of these essential oils were also different. Sirih Hijau essential oil was an inhibitor for tyrosinase for monophenolase and diphenolase (inhibit about 50% activity compared to control at concentration 7mg/ml), while sirih merah essential oil was an activator for tyrosinase for monophenolase (16x more active compared to control at 7mg/ml) and diphenolase (2.5 x more active compared to control at 7mg/ml). In conclusion, camphene, beta phelandrene, chavicol and eugenol from sirih hijau essential oil can be used for whitening agent due to its inhibitory activity for tyrosinase.

***Keywords**: Piper bettle, Piper crocatum, essential oil, tyrosinase activity*

1. Introduction

Tyrosinase (EC1.14.18.1) is a multicopper monooxygenese enzyme with wide distrubution including in humans [1]. In humans, tyrosinase is responsible for melanogenesis or hyperpigmentation [2]. Tyrosinase also has been reported might contribute to the dopamine neurotoxicity and neurodegeneration associated with Parkinson‘s disease and Alzeimer diseases [3].

Indonesia has many traditional medicines. One of the famous genus is *Piper* genus. Many species belong to this genus, for instance *P. betle,* local name in Indonesia sirih hijau and *P. crocatum,* local name in Indonesia is sirih merah. *P. betle* and *P. crocatum* have essential oils which have many activities, such as anti-microbe [4]. To give added value to the two species of *Piper*, the research aims to find potency of essential oil from *P. betle* and *P. crocatum* agains tyrosinase and to find the chemical constituent in *P. betle* and *P, crocatum*.

2. Experimental Details

Samples material and preparation

P. betle and *P. crocatum* leaves was collected from Biopharmaca Research Center Field Station, Darmaga, Bogor, Indonesia in 2010. Essential oil of *P. betle* and *P. crocatum* were separated with steam distillation. The chemical component consists in the essential oils were separated and analyzed with GC-MS.

GC-MS condition

Essential oils were separated with column DB-5 MS (0.25 mm x 30 m) with helium gas (flow rate 42 ml/min). The injector temperature was 80ºC and detector temperature was 250ºC. Components separation was performed with condition temperature programme started in 80ºC for 5 minutes and increasing the temperature with

rate 5 C/min until 250ºC, the temperature then constant for 45 minutes. The MS analyses were performed in 70 eV, EI, and split ratio 25.0. MS data was collected in ranged 40 – 500 m/z. The MS spectrum then compared with the data at library.

Tyrosinase activity test

This assay was performed using methods as described earlier [5,6,7]. Essential oils were dissolved in DMSO (dimethyl sulphoxide) to a final concentration of 20 mg/ml.

The essential oils were tested at the concentrations ranged from 0.11 to 7.00 mg/ml (dissolved in 50 mM potassium phosphate buffer (pH 6.5)). In 96-well plate, 70 µl of each extract dilution was combined with 30 µl of tyrosinase (333 Units/ml in phosphate buffer) in triplicate. After incubation at room temperature for 5 min, 110 µl of substrates (2 mM L-tyrosine or 12 mM L-DOPA) was added to each well. Incubation commenced for 30 min at room temperature. Optical densities of the wells were then determined at 510 nm with multi-well plate reader. The tyrosinase activities (monophenolase and diphenolase activities) were analyzed in the present essential oils compared to control.

3. Result and Discussion

The essential oils of sirih merah and sirih hijau were obtained by steam distillation method (yielded 0.21% v/w and 0.14% v/w, respectively). The essential oils of sirih merah and sirih hijau gave different smell and different color. The different between the two essential oils for *Piper* genus were analyzed with GC-MS. The chromatograms of sirih merah essential oil and sirih hijau essential oil are shown in Fig 1a and b.

The component analyzes of each peak from chromatograms were shown in Table 1. The components in essential oils classified into two major groups, monoterpene and sesquiterpene. Monoterpene appeared first before sesquiterpene (retention time before 14 minutes for monoterpene). Major components in sirih hijau and sirih merah essential oils were the same. Some structures of essential oils consists in the two essential oils were shown in Fig 2. Sirih hijau and sirih merah essential oils were different in peak with retention time 3.3, 12.4 and 13.1 minutes, the component which only belong to sirih hijau essential oil were shown in Fig 3.

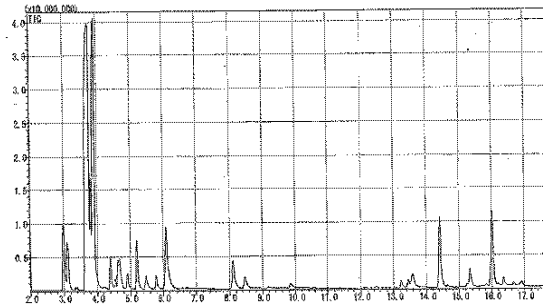

(a)

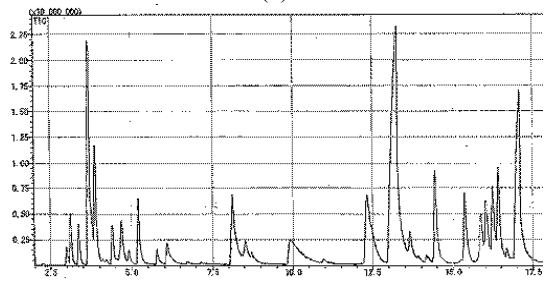

(b)

Fig 1. Chromatogram of sirih merah (a) and sirih hijau (b) essential oils separated with GC-MS.

Some reports about essential oils activities from sirih merah and sirih hijau had been published. Ngaisah (2009) reported that essential oil of sirih merah had antibacterial activity against *Bacillus cereus, Staphylococcus aureus, Escheria coli,* and *Pseudomonas aeruginosa* [8]. The other report said that essential oil from sirih hijau had antioxidant activity [9].

In this research, we search the activity of essential oil from sirih merah and sirih hijau against tyrosinase, monophenolase and diphenolase activities. The results showed that sirih merah and sirih hijau gave different activity. The activity of sirih merah and sirih hijau essential oils against tyrosinase in monophenolase and diphenolase were shown in Fig 4 and 5, respectively.

Table 1. Components of Sirih Merah and Sirih Hijau Essential oils

Retention time (min)	Major Components	
	Sirih Merah	Sirih Hijau
2.9	Alpha thujene	Alpha thujene
3.1	Alpha pinene	Alpha pinene
3.3		Camphene
3.7	Sabinene	Sabinene
3.9	Beta myrcene	Beta myrcene
4.4	Alpha terpinene	Alpha terpinene
4.7	Beta phellandrene	Beta phellandrene
5.2	Gamma terpinene	Gamma terpinene
5.4	Beta terpineol	Beta terpineol

5.8	Terpinolen	Terpinolen
8.5	Alpha terpineol	Alpha terpineol
12.4		Chavicol
13.1		Eugenol
13.2	Copaene	
14.4	Caryophyllene	Caryophyllene
15.3	Alpha Caryophyllene	Alpha Caryophyllene
16.0	Germacrene D	Germacrene D

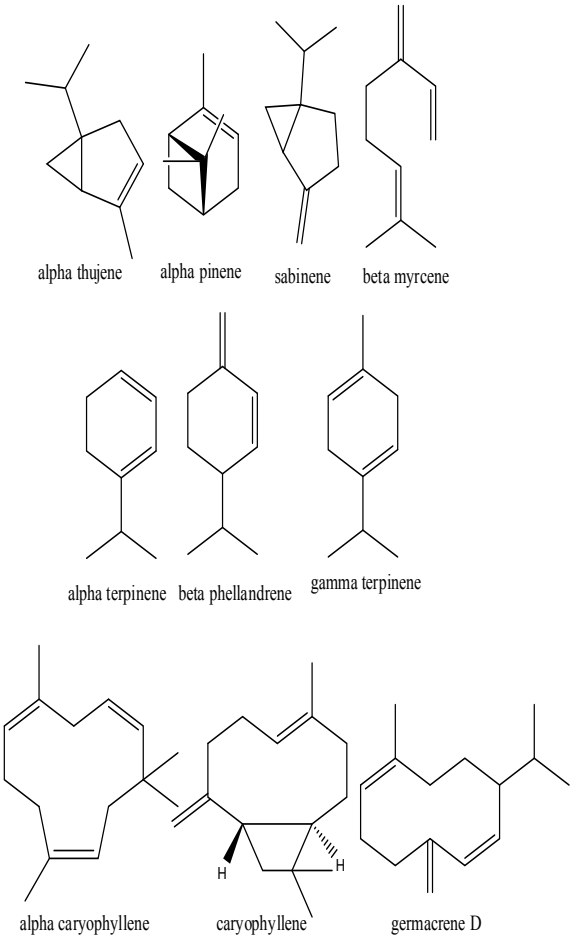

Fig 2. Major component found in *P. crocatum* and *P. bettle.*

On monophenolase activity (Fig 4), sirih merah increased the activity of monophenolase of tyrosinase. By increasing the concentration of sirih merah essential oil, the activity of monophenolase was increasing too. The increasing monophenolase activity in the present of sirih merah essential oil was up to 16 times (at concentration 7.00mg/ml) compared to control (normal activity). Different with sirih merah, sirih hijau essential oil inhibited the activity of monophenolase. The inhibition of sirih hijau essential oil was increasing by increasing the concentration (almost 50% inhibition at concentration 7.00 mg/ml).

The same tendency was found on diphenolase activity. Sirih merah essential oil had activity to increase diphenolase activity up to 2.5 times at concentration 7 mg/ml, while sirih hijau inhibited diphenolase activities of tyrosinase.

The differences between sirih merah and sirih hijau essential oils were only on phenylpropanoid (such as chavicol and eugenol) which found on sirih hijau and not found in sirih merah. It concluded that prenulated phenol can inhibit the tyrosinase activity while monoterpene and sesquiterpene can accelerated the tyrosinase activity.

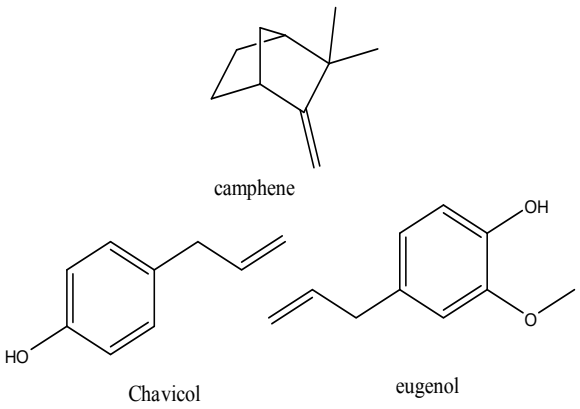

Fig 3. Major component which only found in *P. bettle*

Tyrosinase activity is important because it synthesized tyrosine by oxidation of phenol became melanin. Melanin is a pigment widely distributed in body surface, retina, nigra of brain, adrenal medullae, and so on. Moreover, it is thought to play an important role in skin cancer prevention by protection of cells from ultraviolent rays. While, it is said that melanin is a reason of sunburn and mottle. Therefore, compounds inhibiting melanin are expected to application of cosmetic as whitening agent.

On the other hand, tyrosinase produces DOPA. Martorana et al (2008) reported that L-DOPA modulates motor cortex excitability in Alzheimer‘s diseases patients [10]. In addition, L-DOPA might represent a reliable tool to study new therapeutic perspective and strategies of Alzheimer‘s diseases.

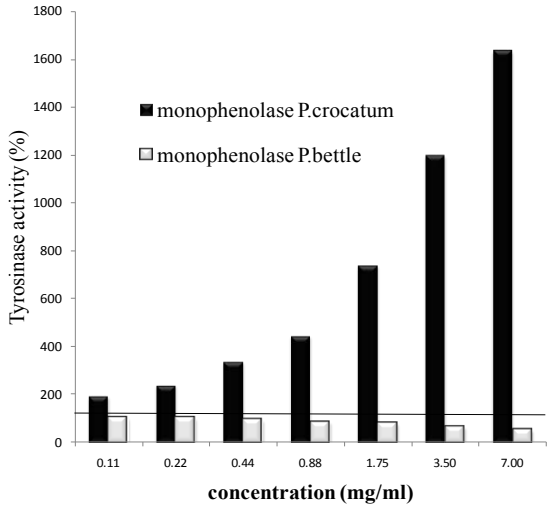

Fig 4. Monophenolase activity in the present of *P. crocatum* and *P. betle* essential oil

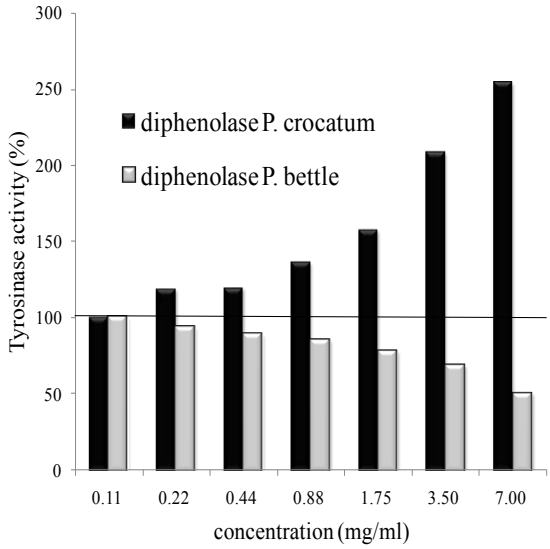

Fig 5. Monophenolase activity in the present of *P. crocatum* and *P. betle* essential oil

Based on our results, phenylpropanoid from sirih hijau essential oil can be used as whitening agent. Monoterpene and sesquiterpene from sirih merah and sirih hijau can be used for Alzheimer diseases.

4. Conclusion

Sirih merah essential oils consisted of monoterpene and sesquiterpene compounds, while sirih hijau essential oils consisted of monoterpene, sesquiterpene, and phenylpropanoid compounds. Monoterpene and sesquiterpene from sirih merah and sirih hijau essential oils can be used for Alzheimer diseases, while phenylpropanoid from sirih hijau can be used in cosmetics for whitening agents.

5. Acknowledgements

We express our gratitude to the Chemistry of Natural Products Laboratory, Gifu University, Japan for GC-MS analyses and Biopharmaca Research Center, Bogor Agricultural University for research funding.

6. References

[1]. Lithiwitayawuid, K. (2008), Stilbenes with tyrosinase inhibitory activity, *Curr. Sci.,* 94: 44-52.

[2]. Chang Te-Sheng (2009), An updated review of tyrosinase inhibitor, *International Journal of Molecular Sciences*. 10: 2440-2475.

[3]. Zheng, S.P., K. W Cheng, J. Chao, J. Wu, M. Wang (2008), Tyrosinase inhibitors from paper mulberry (*Broussonetia papyrifera*), *J Food Chem* 106: 529-535.

[4]. Nanik S. (2008), Daya Antibakteri Ekstrak Daun Sirih terhadap Bakteri Vibrio kaveyi secara in vitro, Minor Thesis, Airlangga University, Surabaya.

[5]. Curto, E.V., C. Kwong, H. Hermerdorfer, H. Glatt, C. Santis (1999), Inhibitors of mammalian melanocyte tyrosinase; in vitro comparisons of alkyl ester of gentisic acid with other putative inhibitors, *Biochem. Pharmacol*, 57:663-672

[6]. O. Nerya, R. Musa, S. Khatib, S. Tamir, J. Vaya (2004), Chalcones as potent tyrosinase inhibitors: the effect of hydroxyl positions and numbers, *Phytochemistry*, No.10 (65), 1389-1395.

[7]. Batubara I, Darusman L.K, Mitsunaga T, Rahminiwati M, and Djauhari E. (2010), Potency of Indonesian medicinal plants as tyrosinase inhibitor and antioxidant agent. *Journal of Biological Sciences,* 10 (2): 138-144.

[8]. Ngaisah, S. (2009), Identifikasi dan uji aktivitas antibakteri minyak Atsiri daun sirih merah (*piper crocatum ruiz & pav*.) Magelang, Abstract, UNS, Solo.

[9]. Parwata, IMOA, W.S Rita, R Yoga (2009), Isolasi dan Uji Antiradikal Bebas Minyak Atsiri pada Daun Sirih secara Spektroskopi Ultra Violet Sinar Tampak, *Jurnal Kimia* 3(1):7-13.

Immune System Impairment in CD122-Deficient Mice is Caused by Abnormality of Activated T Cells

Muhaimin Rifa'i

Biology Department, Faculty of Sciences, Brawijaya University. Malang Indonesia (rifa123@ub.ac.id)

Abstract

Regulation of immune system is a pivotal to prevent immune attacks against self-components. Mice deficient in the IL-2/IL-15 receptor β chain, CD122 are model animals of such immune attacks and characteristically have a high number of abnormally activated T cells. Here we show that CD122-deficient mice dominated by the development of abnormal T cells. In this study we found that CD4 and CD8 T cells express high level of CD69 and CD44 molecules. Furthermore, the expression of CD62L molecule becomes low and the number of granulocytes cell increased dramatically. This result indicating that normal cells become dangerously activated T cells in the absence of CD122 endogenous molecule.

***Key words**: regulatory T cells • CD8$^+$ T cells • CD122 • activated T cells*

1. Introduction

Immune tolerance to self and innocuous foreign antigens is a basic process to prevent non-essential and self-destructive immune responses. The process of T cell receptor (TCR) generation, based on random rearrangements and promiscuity of the resulting receptors, inevitably bears the risk for the development of autoreactive T cells. Immune reaction against virulent foreign objects could be harmful for self-organism. Therefore, a strict regulatory mechanism must exist in the immune system (1-6). Regulatory T cells are key subpopulation of T cells that control immune activity. CD4$^+$CD25 (interleukin [IL]-2 receptor β chain)$^+$ regulatory T cells are well-documented subpopulation of T cells (1,2,7-9). The importance of CD4$^+$CD25$^+$ regulatory T cells has been confirmed in many types of autoimmune diseases. However, other cells, especially those of CD8$^+$ T cell lineage, have also been suggested as regulatory T cells (5,10,11).

CD122 (IL-2/IL-15 receptor β chain)-deficient mice exhibit severe hyper-immunity (12), with augmented granulopoiesis and suppressed erythropoiesis. Severe anemia progresses and the mice die within 3-4 months after birth. We found that expansion of abnormally activated T cells is the underlying cause of all phenotypes (13). The mechanism of generation of activated memory-type T cells in CD122-deficient mice is controversial. In the initial investigations by Abbas and others (14-16), the defect of programmed cell death (apoptosis) in IL-2 or IL-2R□-deficient T cells could be applied to the mechanism for survival of activated CD122-deficient T cells, and such possibility has not been excluded. Based on our previous experimental results, we proposed that the lack of certain regulatory cells was responsible for the abnormal phenotypes and that a subpopulation of CD8$^+$ T cells could be involved in the control of CD122-deficient abnormal T cells (11). In our previous study, however, direct evidence of the responsible subpopulation in CD8$^+$ cells was not provided, and it was still unclear whether the lack of regulatory system is sufficient to cause T cell abnormalities in CD122-deficient mice, or intrinsic defect of CD122 molecules in T cells is required.

Here, we report a novel observation that CD122-deficient mice are dominated by activated T cells in the peripheral lymphoid tissue. This result indicates that normal T cells become dangerously activated T cells in the absence of intrinsic CD122 molecules.

2. Experimental Details

Mice

CD122-deficient mice were originally established by Suzuki et al. (12) and maintained in pathogen free facility. Breeding pairs of C57BL/6$^{CD45.1/CD45.1}$ congenic strain were obtained from Taconic (Germantown, NY) and maintained in pathogen free facility. RAG-2 $^{-/-}$ mice. The experimental protocol was approved by the Ethics Review Committee for Animal Experimentation of Nagoya University Graduate School of Medicine.

Antibodies

Fluorescein isothiocyanate (FITC) – conjugated anti-mouse CD8α (clone 53-6.7), phycoerythrin (PE)- or allophycocyanin (APCn)-conjugated anti-mouse CD4 (clone GK1.5), biotin-conjugated anti-mouse CD122 (clone 5H4), FITC-

conjugated anti-mouse CD25 (clone PC61.5), FITC- or biotin-conjugated anti-mouse CD45.1 (clone A20), and biotin-conjugated anti-mouse TER-119 (clone TER-119) antibodies were purchased from *e*Bioscience Inc. (San Diego, CA). FITC-conjugated anti-mouse CD69 (clone H1.2F3), FITC-conjugated anti-mouse CD44 (clone IM7), PE-conjugated anti-mouse CD62L (clone MEL-14), FITC-conjugated anti-mouse Gr-1 (clone RB6-8C5), and PE-conjugated anti-mouse VLA-4 (clone 9C10) antibodies were purchased from BD-Biosciences Pharmingen (San Diego, CA). Biotin-conjugated antibodies were visualized by streptavidin-PE-Cy5 (*e*Bioscience, San Diego, CA)

Bone marrow transplantation

Bone marrow cells from CD122-deficient and normal mice are mixed in ratio 1:1 (normal:CD122$^{-/-}$). Mixed cell then intravenously injected to recipient (RAG2$^{-/-}$). Observation was done 7 weeks after bone marrow transplantation.

3. Results and Discussion

Expansion of activated T cells occur in CD122 knockout mice

CD122-deficient mice without any treatment had high percentage of activated memory-type T cells with markers of CD69^{+}, CD44^{+}, and CD62L^{-}. In contrast to CD122 knockout mice, normal mice showed no such increased of activated CD69^{+} T cells (Figure 1) and CD44^{+}CD62L^{-} activated memory-type T cells (Figure 2). In CD122-deficient mice did not have any mechanism to prevent the development of activated CD69^{+} T cells and CD44^{+}CD62L^{-} memory-type T cells. We analyzed CD4^{+} T cells and CD8^{+} T cells separately and show representative results of CD122-deficient CD4^{+} T cells. Activation and memory-status of CD122-deficient CD8^{+} T cells analyzed by expression of CD69, CD44 and CD62L were not different from those of CD4^{+} T cells (data not shown).

CD122 knockout mice have an abnormality of B cells, granulocytes, and erythrocytes development

Examination of erythroid-lineage cells by expression of TER-119 antigen, an erythroid specific marker, showed marked reduction in the number of TER-119^{+} cells in the bone marrow of CD122-deficient mice (Figure 3). Analysis of hematocrit in peripheral blood also confirmed that CD122-deficient mice undergo severe anemia. The number of B220^{+} cells, representing all developing B cells, was also impairing in CD122-deficient mice. As a conclusive result, CD122-deficient mice have a defect in hemotopoiesis in many aspects. Examination of granulopoiesis showed that the number of Gr-1^{+} cells in the bone marrow was markedly increased in CD122-deficient mice (Figure 4). This increase was occur when the mice in the age of 4 weeks. Changes in the number of Gr-1^{+} cells in the bone marrow matched those of leukocyte numbers in peripheral blood. Increased leukocyte number in peripheral blood of CD122-deficient mice was caused by abnormality in homeostasis. Severe anemia caused by a combination of autoimmune hemolysis and suppression of erythropoiesis is another striking feature of CD122-deficient mice (12).

Hematopoietic disorders in CD122-deficient mice

The percentage of granulocytic Gr-1^{+} cells was increased to over 90% in the bone marrow of CD122-deficient mice compared with about 60% in total normal mice. On the other hand, cells in erythroid lineage that expressed TER-119 almost disappeared in CD122-deficient mice. Most of the TER-119^{+} cells in the bone marrow were VLA4^{+} erythroblasts. These bone marrow changes matched changes in the numbers of red and white blood cells in peripheral blood. The number of leukocytes was markedly increased and hematocrit was significantly reduced in CD122-deficient mice, indicating progression of anemia in these mice.

Regulatory T cells are classified into two groups, i.e., naturally occurring regulatory cells and regulatory cells induced during immune responses (5). A representative example of the former type is that in CD4^{+}CD25^{+} population. In this study, we indirectly demonstrated that regulatory T cells reminiscent of naturally occurring type, and that such regulatory cells can develop from normal mice in RAG2$^{-/-}$. In recent studies by Malek et al. (21, 22), the defect of CD4^{+}CD25^{+} regulatory T cells was proposed to be responsible for the increase of deregulated T cells in CD122-deficient mice. Based on the fact of presence of very few CD4^{+}CD25^{+} T cells in CD122-deficient mice, this idea might well explain the development of abnormalities in CD122-deficient mice. In the present study, bone marrow transplantation from mixed normal and CD122-deficient type mice can develop becomes chimera with normal phenotype.

In our experiment, the ratio between normal and CD122-deficient mice bone marrow cell is not important factor. The ratio 1:1 to 1:5 (normal: CD122-deficient mice) bone marrow cell is still effective to prevent the mice from auto-reactive diseases. Thus, the regulatory activity from normal cell occurs in this chimeric mice system since in the transfer of bone marrow cell from CD122-deficient mice only develop to memory type and activated cells. Effective normalization of the cell from CD122-deficient mice by the mixture with normal bone marrow cells allows us to make a definite

conclusion that normal cells contain stronger regulatory T cells that can control CD122-deficient T cells. $CD4^+CD25^+$ regulatory cells seem to control the development of the cell from CD122-deficient mice, because transfer of bone marrow alone in the absence of $CD4^+CD25^+$ in the endogenous gen, the cells arise from bone marrow develop to activated cells. We noted extreme activation of T cells in CD122-deficient mice. How such activated T cells are generated and which antigen(s) they are responding to remain unclear at present. The profile of TCR Vβ usage of activated $CD8^+$ T cells in CD122-deficient bone marrow cell-transferred mice was not significantly different from that of mixture of normal and CD122-deficient bone marrow (data not shown), suggesting that the activated T cells were polyclonal cells responding to multiple antigens. Whatever the antigens are, activated T cells may disappear in a usual condition with coexist of normal T cells. In this study, we propose that normal T cells include regulatory T cells that effectively regulate other T cells.

4. Conclusion

---

5. Acknowledgments

We thank T. Kato and K. Kuribayashi for providing T cell clones, M. Murakami and T. Haruhiko, Z, for providing knockout mice, M. Ito for histology, and K. Takeda, T. Shi, K. Watanabe, Y. Yi for experimental help. This work was supported by grants from the Ministry of Science, Education, Sports and Culture of Japan.

6. References

[1]. Sakaguchi, S. (2004), Naturally arising $CD4^+$ regulatory T cells for immunologic self-tolerance and negative control of immune responses. *Annu. Rev. Immunol.* 22:531-562.

[2]. Shevach, E.M. (2000) Regulatory T cells in autoimmunity. *Annu. Rev. Immunol.* 18:423-449.

[3]. Chatenoud, L., B. Salomon, and J.A. Bluestone (2001). Suppressor T cells--they're back and critical for regulation of autoimmunity. *Immunol. Rev.* 182:149-163.

[4]. von Herrath, M.G., and L.C. Harrison (2003). Antigen-induced regulatory T cells in autoimmunity. *Nat. Rev. Immunol*. 3:223-232.

[5]. Suciu-Foca, N., J.S. Manavalan, and R. Cortesini (2003), Generation and function of antigen-specific suppressor and regulatory T cells. *Transpl. Immunol.* 11:235-244.

[6]. Bach, J.F. (2003), Regulatory T cells under scrutiny. *Nat. Rev. Immunol.* 3:189-198.

[7]. Sakaguchi, S., N. Sakaguchi, M. Asano, M. Itoh, and M. Toda (1995), Immunologic self-tolerance maintained by activated T cells expressing IL-2 receptor β-chain (CD25). *J. Immunol.* 155:1151-1164.

[8]. Sakaguchi, S. (2000). Regulatory T cells: Key controllers of immunologic self-tolerance. *Cell.* 101:455-458.

[9]. Sakaguchi, S., N. Sakaguchi, J. Shimizu, S. Yamazaki, T. Sakihama, M. Itoh, Y. Kuniyasu, T. Nomura, M. Toda, and T. Takahashi (…..), Immunologic tolerance maintained by $CD25^+$ $CD4^+$ regulatory T cells: their common role in controlling autoimmunity, tumor immunity, and transplantation tolerance. *Immunol. Rev.* 182:18-32.

[10]. Najafian, N., T. Chitnis, A.D. Salama, B. Zhu, C. Benou, X. Yuan, M.R. Clarkson, Sayegh, and S.J. Khoury (2003), Regulatory functions of $CD8^+CD28^-$ T cells in an autoimmune disease model. *J. Clin. Invest.* 112:1037-1048.

[11]. Suzuki, H., Y.W. Zhou, M. Kato, T.W. Mak, and I. Nakashima (1999), Normal regulatory α/β T cells effectively eliminate abnormally activated T cells lacking the interleukin 2 receptor β *in vivo*. *J. Exp. Med.* 190:1561-1572.

[12]. Suzuki, H., T.M. Kundig, C. Furlonger, A. Wakeham, E. Timms, T. Matsuyama, R. Schmits, J.J.L. Simard, P.S. Ohashi, H. Griesser, T. Taniguchi, C.J. Paige, and T.W. Mak (1995), Deregulated T cell activation and autoimmunity in mice lacking interleukin-2 receptor β. *Science.* 268:1472-1476.

[13]. Suzuki, H., A. Hayakawa, D. Bouchard, I. Nakashima, and T.W Mak (1997), Normal thymic selection, superantigen-induced deletion and Fas-mediated apoptosis of T cells in IL-2 receptor β chain-deficient mice. *Int. Immunol.* 9:1367-1374.

[14]. Refaeli, Y., L. Van Parijs, C.A. London, J. Tschopp, and A.K. Abbas (1998), Biochemical mechanisms of IL-2-regulated Fas-mediated T cell apoptosis. *Immunity.* 8:615-623.

[15]. Van Parijs, L., A. Biuckians, A. Ibraghimov, F.W. Alt, Willerford, and A.K. Abbas (1997), Functional responses and apoptosis in CD25 (IL-2Rα)-deficient lymphocytes expressing a transgenic antigen receptor. *J. Immunol.* 158:3738-3745.

[16]. Kneitz, B., T. Herman, S. Yonehara, and A. Schimpl (1995), Normal clonal expansion but impaired Fas-mediated cell death and anergy in IL-2 deficient mice. *Eur. J. Immunol.* 25:2572-2577.

[17]. Malek, T.R., A. Yu, V. Vincek, P. Scibelli, L. Kong (2002), CD4 regulatory T cells prevent lethal autoimmunity in IL-2Rβ -deficient mice. Implications for the nonredundant function of IL-2. *Immunity.* 17:167-178.

[18]. Malek, T.R., B.O. Porter, E.K. Codias, P. Scibelli, and A. Yu (2000), Normal lymphoid homeostasis and lack of lethal autoimmunity in mice containing mature T cells with severely impaired IL-2 receptors. *J. Immunol.* 164:2905-2914.

Appendixes

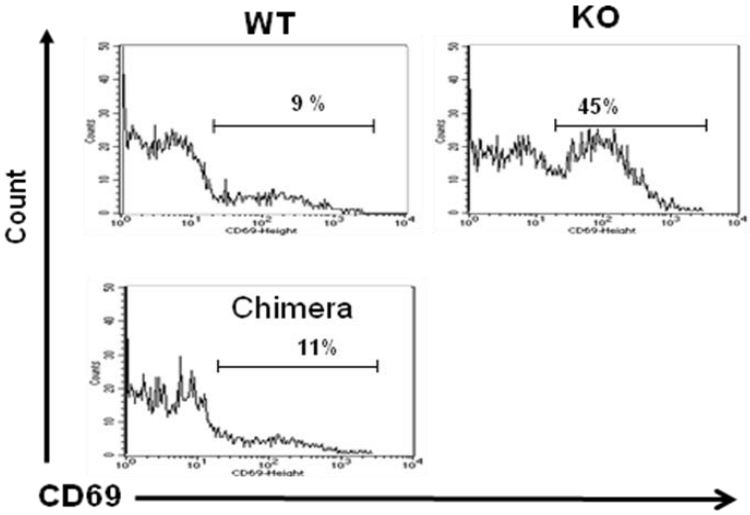

Figure 1. Activated memory-type T cells do not develop in chimera mice.
After 7 weeks from the transfer of mixture bone marrow, spleen cells obtained from the mice were stained with anti-CD69, anti-CD4 and anti-CD45.1 antibodies, and analyzed by flow cytometry. Expression levels of CD69 are shown as histograms for cells gated to $CD4^+CD45.1^-$ population. Numbers in each panel are percentages of $CD69^+$ cells in gated $CD4^+$ cells. Data obtained from a 7-week-old wild-type (WT) mouse and a 7-week-old CD122-deficient mouse (KO) are also shown as controls. Data are mean ± SD values of 3 mice in each group.

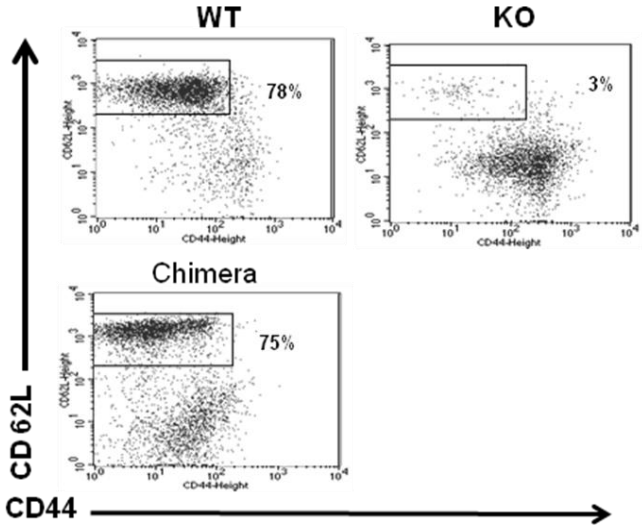

Figure 2. Most T cells in chimera mice develop in naïve type.
After 7 weeks from the transfer mixture bone marrow, spleen cells were stained with anti-CD44, anti-CD62L, anti-CD45.1 and anti-CD4 antibodies, and analyzed by flow cytometry. Data are shown as dot-plot analysis for cells gated to $CD4^+CD45.1^-$ population. Numbers in each panel are percentages of naïve type $CD44^-CD62L^+$ cells in gated $CD4^+$ cells. Data obtained from a 7-week-old wild-type (WT) mouse and a 7-week-old CD122-deficient mouse (KO) are also shown as controls. Data are mean ± SD values of 3 mice in each group.

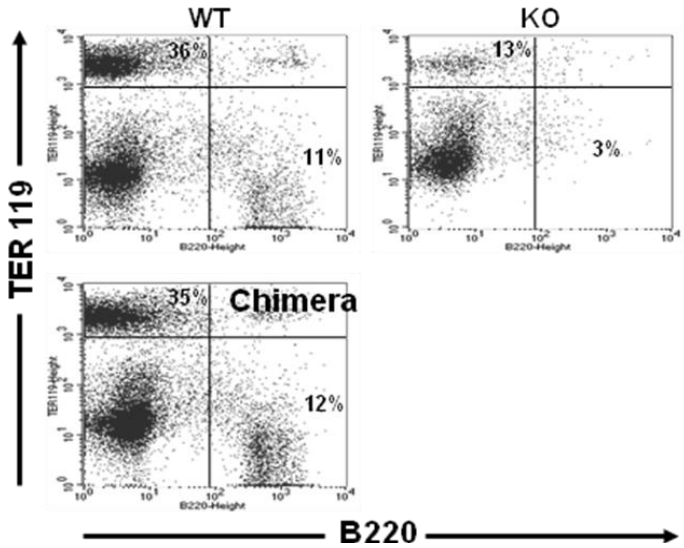

Figure 3. Erythrocytes and B cells from CD122-deficient mice can be normalized in chimeric mice.
After 7 weeks from the transfer mixture bone marrow, bone marrow cells obtained from the chimera mice were stained with anti-CD45.1 antibodies, and analyzed by flow cytometry. Percentages of B cells (B220) and erythrocytes lineage (TER119) are shown for cells gated to $CD45.1^-$ population. Data obtained from a 7-week-old wild-type mouse (WT) and 7-week-old CD122-deficient mice (KO) are also shown as controls. Data are mean ± SD values of 3 or 4 mice in each group.

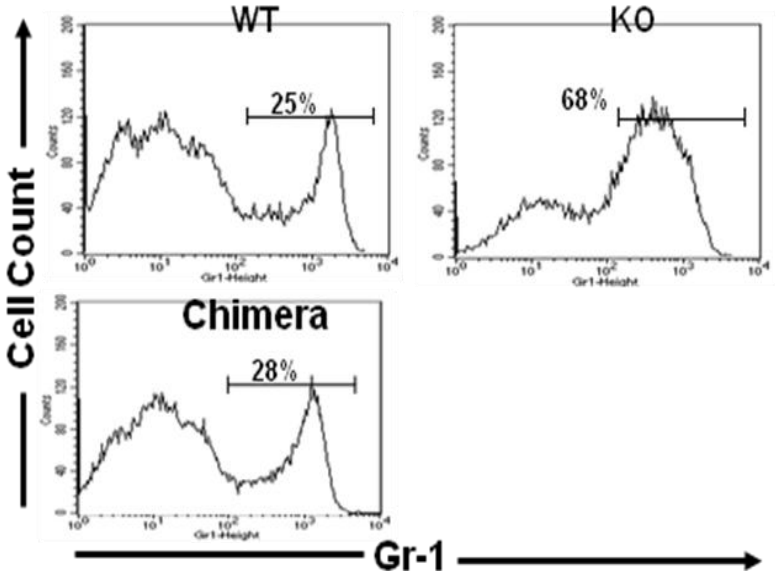

Figure 4. Granulocytes cells from CD122-deficient mice can be normalized in chimeric mice.
After 7 weeks from the transfer mixture bone marrow, bone marrow cells obtained from the chimeric mice were stained with anti-CD45.1 antibodies, and analyzed by flow cytometry. Percentages of $Gr\text{-}1^+$ cells are shown for cells gated to $CD45.1^-$ population. Data obtained from a 7-week-old wild-type mouse (WT) and 7-week-old CD122-deficient mice (KO) are also shown as controls. Data are mean ± SD values of 3 or 4 mice in each group. CD122-deficient mice that received $1x10^4$ $CD8^+CD122^+$ cells obtained from 2-week-old mice or 2-year-old mice are also shown.

The Simple Anti-oxidant Compound in Anti-cancer Potential Fraction of Kesum Leaves Extract

Muhamad Agus Wibowo [1], Lucy Ariani [2], Aulanni'am [3], M. Aris Widodo [4], Basuki B. Purnomo [5]

[(1,2)] Chemistry Department, Science Faculty, Tanjungpura University, Pontianak (Aguso2@yahoo.com)
[(3)] Chemistry Department, Science Faculty, Brawijaya University, Malang
[(4,5)] Department of Medicine, Faculty of Medicine, Brawijaya University, Malang

Abstract

Kesum (Polygonum minus L) is a plant that potentially be used in the treatment of cancer. Some researchers claim that the extract of this plant is capable of killing cancer cells and act as antioxidants. Recent research shows that n-hexane fraction of Kesum leaves have anti-cancer activity. This fraction demonstrates a proliferation activity inhibition of lung cells that exposed by benzapyrene. In this study, isolation of potential compound as anticancer that contained in the n-hexane fraction of Kesum leaves extract has been carried out. The analysis of isolated compound was carried out by using GC-MS spectroscopy. The results showed that 2-hydroxy-2-methyl-4-pentanone is a dominant compound that contained in the fraction of n-hexane and it has antioxidants activity in the DPPH test. Based on these result, 2-hydroxy-2-methyl-4-pentanone is assumed to be the compound that has potency as an anti-cancer.

***Keywords**: kesum, anti-oxidant, 2-hydroxy-2-methyl-4-pentanone.*

1. Introduction

Kesum (Polygonum minus L) is one of the typical and popular plants in West Kalimantan, which are used as additives in various typical foods [1]. This plant is potentially be used to treat cancer. The anti-oxidant test of the aqueous extract of Kesum by using the method of potassium ferricyanide, FTC (ferric thiocyanate), and TBA (thiobarbituric acid) showed that water extract of Kesum are powerful antioxidants [2]. Vimala (2008) in his research stated that the methanol and water extracts of the Kesum leaves are powerful antioxidants [3]. The anti-cancer activity is owned by Kesum leaves, too. Mackeen *et al.* (1997) in his research stated that the ethanol extract of Kesum leaves are cytotoxic to HeLa cells, with LC50 (lethal concentration 50) is 30µg/ml [4].

The n-hexane fraction of Kesum leave is a potential fraction to inhibited cancer growth [5]. Wibowo et al. (2010) in his study states that this fraction is able to increase p53 gene expression, decreased the levels of MDA (malondialdehyde), and reduce the proliferation activity of the lung cells in the animals model that exposed by benzopyrene [5].

Given that the *n*-hexane fraction of Kesum leaves is potential as a lung cancer drug, it is necessary to isolate the anti-cancer potential compound in the *n*-hexane fraction.

2. Experimental Details

Materials

Kesum (Polygonum minus L) used in this study were collected from Kota Baru, Pontianak. This species is determined in the "Laboratory of Plant Taxonomy and Structure Development, Department of Biology, Brawijaya University" and the specimen stored there. The parts of plants that used in this study are its leaves. The *n*-hexane fraction (the fraction of potential anti-cancer) is obtained by using the method Wibowo *et al*. (2010) [5].

*Determination of Anti-**oxidant** compounds by Thin Layer Chromatography method (TLC)*

The *n*-hexane fraction was developed by using methylene chloride. Test of anti-oxidant compounds made with spray reagent DPPH (2,2-diphenyl-1-picrylhydra-zyl) by using thin layer chromatography method. Antioxidants potential stain was marked with pale yellow spots are left in place for 10 hours. Determination of phenolic compound group was used the spray reagent of FeCl3 1%. Determination of terpenoid compound group was used the spray reagent of vanillin 1% in sulfuric acid.

*Isolation and analysis of antioxidant compounds from n-**hexane***

Isolation of potential anticancer stains performed gravity column chromatography (KKG) using a solvent gradient from non-polar to polar, to obtain relatively pure compound. Against the pure compounds obtained and then analyzed by using gas chromatography-mass spectroscopy (GC-MS).

3. Result and Discussion

This study begins with the determination of the dominant spots that are anti-oxidants by using the method of TLC (thin layer chromatography). Determination of antioxidant stain performed using DPPH spray reagent 0.2%. In addition, also tests the classification of compounds by TLC method. Determination of phenolic compound group was used the spray reagent of FeCl3 (1%) while the terpenoids was used the spray reagent of vanillin (1% in sulfuric acid). The results of this experiment are presented in Figure 2 and Table 1.

The results showed that the first spot (Rf 0.95) is a anticancer potencial. It is shown by the formation of yellow-pale color when tested with DPPH spray reagent. The first spot is a terpenoid compound that shown by the formation violet color when tested by vanillin spray reagent. In addition of terpenoids, the phenolic compounds are also found (spots 9, 10, and 11) that is potential as anticancer compounds.

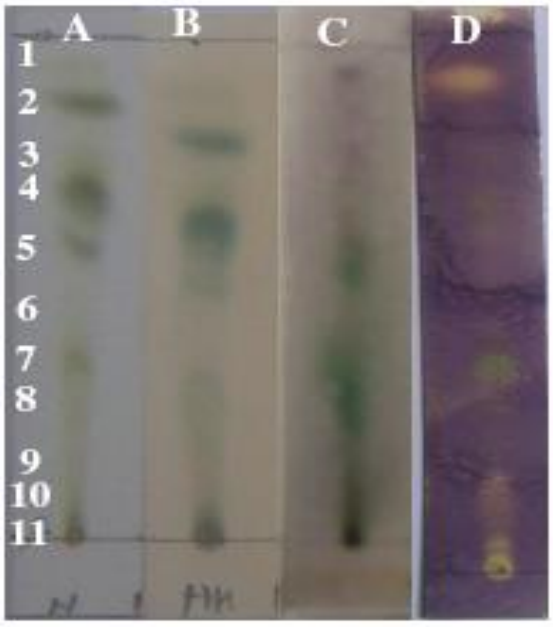

Figure 1. TLC determination of antioxidant spots. (A) visible light; (B) 1% $FeCl_3$; (C) vanillin in H_2SO_4; (D) 0.2% DPPH in methanol (developed n-hexane fraction by using MTC solvent).

Isolation of the dominant spot of anti-oxidants (first spot; Rf 0.95) is done by using the column of chromatography and the gradations of solvent from a non-polar to polar. Isolates were then analyzed by GC-MS instrument. The structure of compounds in each peak was confirmed by an internal standard.. The result of analysis is given in Figure 2 and Table 2.

Table 1. The Rf of chromatogram as a results of elution by using methanol.

No	light	$FeCl_3$	Vaniline	DPPH	Rf	Comp.
1	yellow	-	crimson	Yellow pale	0,95	terpenoid
2	green	green	green	Green base yellow	0,87	Phenolic
3	brown	-	crimson	-	0,76	terpenoid
4	green	green	green	green	0,68	Phenolic
5	green	grey	green	-	0,59	Phenolic
6	brown	blue	green	-	0,43	Phenolic
7	brown	blue	green	-	0,35	Phenolic
8	brown	blue	green	-	0,30	Phenolic
9	brown	blue	dark	Yellow pale	0,19	Phenolic
10	brown	blue	dark	Yellow pale	0,05	Phenolic
11	brown	blue	dark	Yellow pale	0	Phenolic

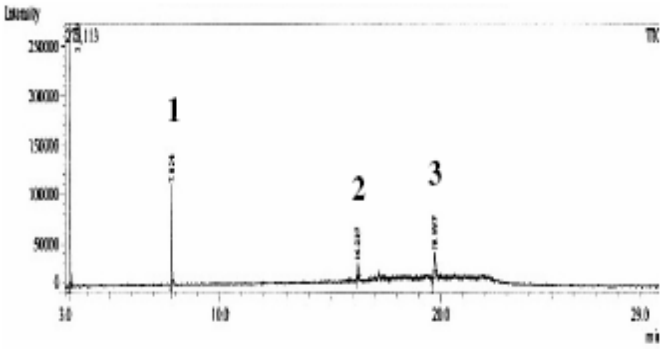

Figure 2. Chromatogram analysis of isolates by using GC-MS

Table 2. R time of the peak chromatogram on the GC-MS analysis

Peak	R Time	Concentration (%)
1	7.824	72
2	16.227	10
3	19.697	18

Analysis by MS at the first peak of the chromatogram gives the spectra as in the figure 3. The Analysis of compounds by using an internal standard has showed that the target compound is 2-hydroxy-2-methyl-4-pentanone

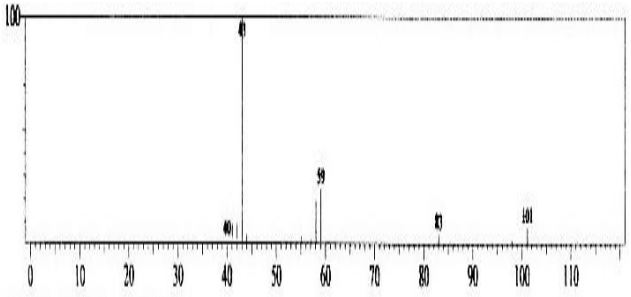

Figure 3. The spectral of the first peak (tr 7.824) from the chromatogram

From the analysis above, the compound of 2-hydroxy-2-methyl-4-pentanone is the dominant compound in the fraction of *n*-hexane that is as anti-oxidants. The ability of compound 2-hydroxy-2-methyl-4-pentanone as anti-oxidants because of these compounds are capable to d*elocalizations* of electron. The existence of the 2-hydroxy-2-methyl-4-pentanone and the several of phenolic compounds in the n-hexane fraction are allowing this fraction can reduce the levels of MDA and increased the expression of p53 gene in the lung tissue of the animal model in the research of Wibowo et al. (2010).

4. Conclusion

From the results of research, it can be concluded that the compound of 2-hydroxy-2-methyl-4-pentanone that contained in the fraction of n-hexane are dominant compounds that has anti-oxidants activities and potential to be used as an anti-cancer.

5. Acknowledgements

Our thanks are to convey to the Directorate General of Higher Education (DIKTI) that has funded this research through research grants PHB in 2010 with a contract number: **3158/H22.13/PL/2010 (21 April 2010).**

6. References

[1]. Wibowo, M.A., R. Wulandari (2007), *Isolasi dan uji Aktivitas Antimikroba Minyak Atsiri Daun Tanaman Kesum (Polygonum cf minus* Huds), Proceeding of Basic Science Seminar, University of Brawijaya, Malang

[2]. Huda-Faujan, N., Noriham, A., Norrakiah, A.S. and Babji, A.S. (2007), Antioxidative Activities of Water Extracts of Some Malaysian Herbs, *ASEAN Food Journal,* 14 (1): 61-68

[3]. Vimala, S., M. A. Ilham, A. A. Rashih, S. Rohana & M. Juliza (2008), *Antioxidant and Skin Whitening Standardized Extraxts: Cosmeceutical and Neutraceutical Products Development and Commercialization in Firm*, Forest Research Institute Malaysia FRIM), Selangor Darul Ehsan, 224-230.

[4]. Mackeen M.M., Ali A.M., El-Sharkawy S.H., Manap M.Y., Salleh K.M.; Lajis N.H., & Kawazu K. (1997), Antimicrobial and Cytotoxic Properties of Some Malaysian Traditional Vegetables (Ulam), *Pharmaceutical Biology*, 35 (3), 174-178

[5]. Wibowo, M.A., S. Anwari, F. Rahman, Aulanni'am (2010), Efek Antiproliferasi Ekstrak n-Heksan Daun Kesum (*Polygonum minus*) Pada Sel Kanker Paru Tikus: Upaya Pemanfaatan Kesum Sebagai Obat KankerParu, *Media Kedokteran Hewan*, 26(1), 15-18

Cytotoxicity, Antioxidant and Antimicrobial Activity of Methanol Extract of Bark (*Xylocarpus Granatum*)

Muhamad Firdaus

Fisheries Technology, Faculty of Fisheries and Marine Science, Brawijaya University, Malang, Indonesia (muhamadfir@yahoo.com).

Abstract

Mangrove traditionally was used by South, East and South-East Asia people for care and therapy of their health. Xylocarpus granatum is one of mangrove tree have been utilized for medicinal. The bark of Xylocarpus granatum has been used for cholera, fever and malaria. The aims of this preliminary study was to examine cytotoxic, antioxidant and antibacterial activity of bark (Xylocarpus granatum) methanol extract. Cytotoxic assay was undertaken by brine shrimp lethal toxicity test, antioxidant activity was done by Diphenyl picryl hydrazil (DPPH) scavenging, and inhibition growth to Staphylococcus aureus and Escherichia coli used as antimicrobial test. The results showed lethal concentration (LC_{50}) of the bark methanol extract was 26860 µg/mL, antiradical efficiency (AE) was 1.22 and zone of growth inhibition to Staphylococcus aureus was 13.75 – 20 mm and Escherichia coli was 15.675 – 19.275 mm for 1.13 10^5 - 1.13 10^6 µg/mL, respectively. The methanol extract of Xylocarpus granatum bark is potential as antioxidant substances but not as cytotoxic and antibacterial compounds. These difference activities may be due to the solubility of active compounds in polarity.

***Keywords**: cytotoxic, antioxidant, antibacterial, Xylocarpus granatum, methanol extract.*

1. Introduction

The extensive use of natural plants, such as mangroves, as health remedies due to their pharmacological properties is quite common. The investigation of the efficacy of plant-based drugs has been paid great attention because of their few side effects, cheap and easy availability. According to the World Health Organization (WHO) around 80 % of the world people still rely mainly on plant drugs [1,2].

Xylocarpus granatum KOENIG is one species of the Meliaceae family have been traditionally used for medicine by South East Asia shoreline inhabitants [3]. It have been used a cure for fever, cholera and malaria [4]. Bioactive compounds of *X. granatum* have been known i.e. triterpenoids, alkaloids, phenolic acids, flavanol, steroids and monoterpenoids [3]. The bark extract of this plant is considered to have astringent, antidiarrhoea, antiemetic and haemostatic properties [2]. This part contained xyloccensin O, xyloccensin P, N-methylflindersine, Chelerythrine, Dihydro-chelerythrine and Acetonyldihydrochelerythrine [3].

The utilization of *X. granatum* barks as cytotoxic, antioxidant and antibacterial substances have not been explored. The purpose of this study was to examine the cytotoxicity, antioxidant and antibacterial activity of methanol extract bark (*X. granatum*).

2. Experimental Details

The *Xylocarpus granatum* KŐENIG barks were collected in Nopember 2010 from Tegalsari village in Sidoarjo District of East Java, Indonesia and authenticated by the botanist in Department of Botany, Brawijaya University.

The bark extract of *X. granatum* was prepared by soaking ± 100 g of fresh flower samples in 300 mL of methanol three times for 24 hours. The extract filtered by using Whatman filter paper. The filtrate was vacuum evaporated, lyophilized and then used for cytotoxicity, antioxidant and antibacterial assay.

The cytotoxicity was done by brine shrimp lethality [5]. The brine shrimp capsule placed in sea water through 48 hours, 37ºC for decapsulation and obtained nauplii. Ten of brine shrimp nauplii sank in sea water, and then added with extract that diluted by sea water serially. The lethality of brine shrimp was observed after 24 hours of treatment was given. Probit analysis was used to determine lethal concentration (LC_{50}) of bark methanol extract on brine shrimp.

The antioxidant activity of bark methanol extract was examed *on diphenyl picril hydrazil* (DPPH) radical [6]. The 0.5 mM DPPH was obtained by solution with methanol. The one mL of serial concentration of extract diluted in methanol was mixed in 3 mL of DPPH solution and then read

their absorbance on spectrophotometer at 515 nm. The antiradical efficiency was determined by formula:

$$AE = \frac{1}{EC_{50} \text{ x } T_{EC50}},$$

where:

- EC_{50} : concentration to reduction 50 percent of free radical
- T_{EC50} : time needed to reach the EC_{50}

The capacity of bark methanol extract on inhibition growth of *Eschericia coli* and *Staphylococcus aureus* in Mueller-Hinton Agar were used as antibacterial assay [7]. The blank disk sank in the serial dilution of extract in dimethyl sulfoxide (DMSO), and then the blank disk placed on Mueller-Hinton Agar that contained pathogen bacteria. The zone of growth inhibition on *E. coli* and *S. aureus* was observed after incubation for 24 hours at 37ºC.

3. Result and Discussion

Cytotoxic, antioxidant and antibacterial of bark (*Xylocarpus granatum*) methanol extract are showed in Table 1.

Table 1. Cytotoxic, antioxidant and antibacterial of bark (*Xylocarpus granatum*) methanol extract

Sample	LC_{50} (µg/mL)	Antiradical efficiency	Inhibition zone (mm)
Bark methanol extract	26860	1.22	*E. coli* = 15.68 – 19.28 *S. aureus* = 13.75 – 20

Table 1 show the cytotoxic activity of bark (*X. granatum*) methanol extract to brine shrimp was weak. The LC_{50} of extract or pure compounds on brine shrimp or cell line less of the 100 ppm was categorized non potential cytotoxic and non toxic substances [8, 9]. The ethyl acetate extract of *X. granatum* showed growth-inhibitory activity on HeLa cells (IC_{50} = 23.0 µg/mL), while the H_2O extracts did not [3]. It indicates that the compounds of *X. granatum* bark as cytotoxicity obtained in semi-polar solvent. Xylogranatin A, B, C and D, respectively, were isolated from the seeds of *X. granatum*, had shown cytotocix activities against cell line of murine leukemia and human lung carcinoma. Among of them, xylogranatin B, C and D, respectively, showed moderate cytotoxicity against murine leukemia cell line, whereas xylogranatin A and B exhibited cytotoxicity against the human lung carcinoma cell line. All of these compounds were grouped of mexicanolides and it was easy soluble in semi polar solvent [4].

The EC_{50} and T_{EC50} of bark (*X. granatum*) methanol extract were determined by graph method and obtained the EC_{50} was 450 µg/mL and T_{EC50} was 1.82 minutes, respectively (Figure 1 and 2).

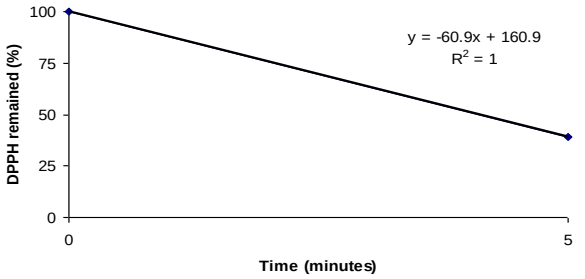

Figure 1. The EC_{50} of bark methanol extract

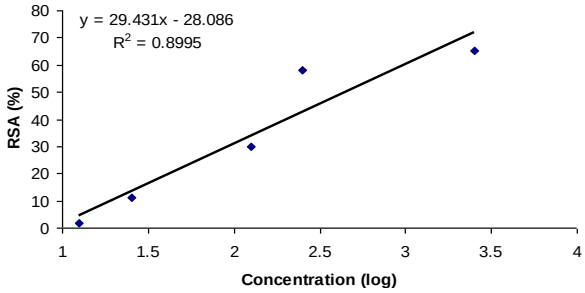

Figure 2. The T_{EC50} of bark methanol extract

Table 1 exhibit the antiradical efficiency of bark (*X. granatum*) methanol extract, which was medium. *X. granatum* was contained phenolic compounds and flavanoids [3]. The extract of bark in methanol consists of simple polyphenols and their glycosides, and tannins [10]. These substances were clustered as antioxidant compounds [4]. It was caused their capability for radical scavenging by proton transfer to free radical. Their antioxidant capacity was weaker than ascorbic acid [6]. As an extract or not pure compound, however, it was categorized as a good and potential antioxidant compounds.

Table 1 also reveal that the bark (*X. granatum*) methanol extract as anti *E. coli* and *S. aureus* were weak. The bioactive compounds of bark were extracted in methanol consists of polyphenols, glycosides and tannins. These compounds inhibit the bacterial growth by interfering of membrane cell function [8]. Whereas this capability is weak, due to the activity was succeeded on high concentration of bark methanol extract.

Mean while, Figure 3 show *S. aureus* was more sensitive than *E. coli* against the bark methanol extract. It has been caused the outer cell membrane of gram-negative bacteria has several lipid compounds that protect the cells from the antibacterial agents [11].

Figure 3. Zone of inhibition on *E. coli* and *S. aureus* growth by the bark methanol extract

4. Conclusion

The methanol extract of *Xylocarpus granatum* bark is potential to be used as antioxidant substances rather than as cytotoxic and antibacterial compounds.

5. Acknowledgment

This work was supported by Directorate of Higher Education, Ministry of Education, Indonesia.

6. References

[1] World Health Organization (1987), *The promotion and development of traditional medicine*. Technical report series 622. Geneva.

[2] Bandaranayake W.M. (1998), Traditional and medicinal uses of mangroves. *Mangroves and Salt Marshes*, 2, 133-148.

[3] Shen L.R., D Guo, Y.M. Yu, B.W. Yin, L. Zhao, Q.W. Shi, Y.L. Wang, and C.H. Huo (2009), Chemical constituents of plants from the genus *Xylocarpus*. *Chemistry & Biodiversity*, 6, 1293-1308

[4] Alvi K.A., P. Crews, B. Aalsbersberg and R. Prasad (1994), Limonoids from the Fijian medicinal plant Dabi (*Xylocarpus*). *Tetrahedron letters*, 47, 8943-8948.

[5] Yin S., C.Q. Fan, X.N. Wang, L.P. Lin. J. Ding and J.M. Yue (2006), Isolation and *in vitro* cytotoxic activity of *Xylocarpus granatum* seeds *Organic Letter*, 8. 4935-4939.

[6] Sanchez-Moreno C., J.A. Larrauri and F. Saura-Calixto (1998), A procedure to measure the antiradical efficiency of polyphenols., *J. Science of Food and Agriculture*. 76, 270-276.

[7] Jana S and G.S. Shekhawat (2010), Phytochemical analysis and antibacterial screening of in vivo and in vitro extracts of Indian Medicinal Herbs: *Anethum graveolens*. *Research Journal of Medicinal Plant*, 4, 206-210.

[8] Ara J., V. Sultana, S. Ehteshamul-Haque, R Qasim and V Uddin (1999), Cytotoxic activity of marine macro-algae on *Artemia salina* (Brine shrimp), *Phytotherapy Research*., 13, 304-307.

[9] Spavieri J., A. Allmendinger, M. Kaiser, R. Casey, S. Hingley-Wilson, A. Lalvani, M. D. Guiry, G. Blunden and D. Tasdemir (2010), Antimycobacterial, Antiprotozoal and Cytotoxic Potential of Twenty-one Brown Algae (Phaeophyceae) from British and Irish Waters, *Phytotherapy Research.,* 24, 1724–1729.

[10] Harkin J.M. and J.W. Rowe (1971), *Bark and its possible uses*. USDA Forest Service. Madison.

[11] Ceylan E. and D.Y.C. Fung (2004), Antimicrobial activity of spices. *Journal of Rapid Methods and Automation in Microbiology*, 12, 1-55.

Developing Malaria Vaccine Candidate with Gamma Rays: Alteration of Heat Shock Protein Profiles Post Irradiation

Mukh Syaifudin [1], Devita Tetriana [2], Siti Nurhayati [3], Darlina [4], Tur Rahardjo [5]
Irawan Sugoro [6]

[(1,2,3,4,5)] Center for Technology of Radiation Safety and Metrology, National Nuclear Energy Agency (BATAN), Jakarta, Indonesia (mukh_syaifudin@batan.go.id)
[(6)] Center for Technology of Isotope and Radiation Application, National Nuclear Energy Agency (BATAN), Jakarta, Indonesia

Abstract

Malaria is a major public heath problem in Indonesia. An effective immunity against malaria infection can be induced through vaccination. Because of genetic and polymorphic specifications that related to the disease predisposition, creating a typical vaccine for Indonesian population is urgently needed. Vaccine created by irradiation was proven to result in a stronger and broader immune response. The aim of this research was to get knowledge on the profile of protein that has an important role in vaccine development. Plasmodium berghei infected and non infected bloods of mice were irradiated with gamma rays at doses of 150 and 175 Gy (dose rate of 380 Gy/hour) and the profile of heat shock protein (HSP) was analyzed with Western blot methods. Results showed that HSP20 profiles of non infected and infected blood were not altered due to irradiation. HSP90 was only seen in infected blood but its profile was also not altered due to irradiation. HSP70 was seen in both infected and non infected blood and only seen at lower dose (0 and 150 Gy). The number of protein bands of infected blood seen in the 10% SDS-PAGE gel was decreased with the increasing of irradiation dose. No good results were obtained for mosquito samples due to some factors. Protein concentration was decreased in accordance with the increasing of dose of irradiation. Based on these findings, it is concluded that 150 Gy is the most effective dose to attenuate parasite and therefore this exact dose of irradiation is selected to be used in developing malaria vaccine candidate.

Keywords: *Malaria*, *Plasmodium sp., vaccine, heat shock protein, profile, gamma rays*

1. Introduction

Malaria infection remains a major global health problem in the world with high mortality and morbidity [1]. Malaria in Indonesia is still major problem and mostly concentrated on the islands of Papua, Maluku, Nusa Tenggara, Sulawesi, Kalimantan, and Sumatra. It occurs with low frequency or is absent in the islands of Java and Bali where approximately 70% of the population live. All species of human malaria were found in Indonesia [2]. Malaria is entrenched in 80 percent of the country's 500 districts, in which almost half of the population resides. According to Ministry of Health Reports, the percentage of malaria-free family in 2007 was 98.1% and it was decreased significantly to 71.3% in 2010 [3]. Attempts to control the spread of malaria have been severely impeded by the emergence of drug-resistant parasites as well as insecticide-resistant mosquitoes and by inadequate health-care infrastructures in countries that are the hardest hit by the disease.

Among the potential control measures that have been given high priority by national and international health organizations, the development of a vaccine against malaria is recognized as one of the most promising and cost-effective addition to the arsenal of current malaria-control measures [4,5]. Research on malaria vaccine showed that immunization of mice with irradiated sporozoites of *P. berghei* results in protection of more than 90% of these animals against an otherwise lethal challenge with viable sporozoites [6]. Effective immunization has also been observed in a small number of human volunteers inoculated with irradiated sporozoites of both *P. falciparum* [7,8] and *P. vivax* [9].

Heat-shock proteins (Hsp) are ubiquitously expressed, highly conserved proteins among the eukaryotes and are involved in the folding of newly synthesized proteins and their refolding under conditions of denaturing stress. Although many of the specific functions of Hsps and their cochaperones in these processes remain largely unknown, their chaperoning function appears essential for the prevention of protein misfolding and aggregation [10]. When a cell is exposed to increased temperatures or other stresses, Hsp expression increases through enhancement of transcription. This is known as the heat shock response and is thought to be caused by heat shock factor. Hsps are named based upon their molecular weight. For example, the commonly studied Hsp60, Hsp70 and Hsp90 refer to Hsps of size 60, 70, and 90 kilodaltons. Anoxia, heat, ethanol, oxygen peroxide, heavy metals, arsenicals, UV radiation, low frequency electromagnetic fields and intensive gamma-ray radiation fields are known as cell stressors that promote Hsp expression [11-14]. Recently, Hsps have been proposed to play a significant role in DNA repair after UV or gamma-ray irradiation.

Hsp90 is abundant in the cytosols of eukaryotes and prokaryotes and in contrast to other chaperones, a number of substrates are known to contain Hsp90 [15]. Studies of eukaryotes have revealed that these Hsp90 client proteins include a variety of transcription factors, protein kinases, and cellular enzymes [16]. Beside that,

it has been shown that Hsp70 plays a central role in stress preconditioning, where Hsp induction correlates with protection from subsequent injury [17]. In most organisms, Hsp70 are among prominent proteins induced by heat [18].

Ionizing radiation produces denatured proteins via direct ionization as well as by reaction with radiolysis products, enhancing Hsp 70 synthesis in Chinese hamster ovary cells exposed to 400 or 1000 Gy [19]. However there is an interest to determine cell response at low doses of gamma rays [20], and to search for a cellular indicator of ionizing radiation exposure [21, 22]. A number of strategies have been adopted in the pursuit of making a successful malaria vaccine including the use of gamma rays to attenuate parasite. The aim of this research was to determine Hsp expression in mouse blood and mosquito irradiated with high gamma-ray dose and we found that this protein profile was affected by gamma rays.

2. Experimental Details

Plasmodium berghei (ANKA strain) and *P. yoelii* were obtained from The Eijkman Institute for Molecular Biology Jakarta. *Anopheles sp.* mosquitoes were reared in the Center for Application of Isotope and Radiation Technology BATAN in controlled environments (25±1ºC and 70±5%) and only female mosquitoes were used in all experiments. Mosquitoes were fed on hamster regularly for nutrition of egg production. Swiss Webster mice of about 2 months old were obtained from National Institute of Research and Development Ministry of Health and housed for 1-2 weeks for adaptation at the Center for Technology of Radiation Safety and Metrology BATAN animal care unit before use under veterinary supervision. Research was conducted under Ethical Approval from Ethical Commission for Health Research, Ministry of Health.

Parasite infected blood of mice was injected intraperitoneally (IP) into 3-4 healthy mice. Thin blood smears were performed 7 to 12 days after infection. Parasitized red blood cells were identified by Giemsa stain. Mouse with 2-5% parasitemia was used for mosquito infection by biting. Five-day-old female *Anopheles sp.* mosquitoes were allowed for biting to *P. berghei* infected mouse for 2 hours. Infected mosquitoes were removed into new paper cup and keep in the room of 21^{o}C temperature for 2 weeks for protein analysis. Infected and non infected mosquitoes kept in paper container and infected and non infected mouse blood in sterile 1.5 ml micro-centrifuge tube were exposed to various radiation doses from a Co-60 source (150, 175, 200 Gy) at dose rate of 800 Gy/hour. The time of exposure of samples to achieve each of the target radiation doses was based on the calibration of the irradiator by dosimetry and the half life of Co-60.

For Western blotting, both infected and uninfected bloods and mosquitoes were used. Procedure was performed essentially as described [23]. Briefly, samples were added with acetone and sonicated for 15 minutes, added with Laemli buffer, warmed in boiled water for 15 minutes, centrifuged at 8000 rpm for 5 minutes, and electrophoreted onto 10-12% sodium dodecyl sulphate (SDS)-polyacrylamide gel at 200 V for 90 minutes. After stained with Commassie R-250 for 1 hour, gel was destained for 24 hours, and the number of bands on gel was analyzed. As a molecular weight marker, SeeBluePlus (Invitrogen) was used. Quantification of protein bands was performed using Gel-Pro Analyzer Software 3.1 (Media Cybernetics). Samples were centrifuged at 12,000 *g* at 4ºC, for 20 min. The supernatants were analyzed for total protein content using bovine serum albumin as standard. Into culture solution, acetone at the same proportion (1:1) was added and then it was sonicated for 15 minutes, followed by additional of Lowry I solution (1:5), and stand for 10 minutes, added with Lowry II solution (0,5:1), stand for 30 minutes and read with spectrometer at wave length of 700 nm.

3. Results and Discussion

Malaria disease remains highly endemic in most countries mainly in the developing world [24]. In Indonesia, vaccination has been one of the great success stories in health care. By integrating prevention, diagnosis and treatment with antenatal care and child immunisation, the number of malaria deaths in South Halmahera plummeted from 226 in 2003 to four in 2008, and the incidence of malaria dropped by 50 percent, according to the district health office. For prophylactic drugs to be effective they must be taken regularly according to the recommended schedule but this medication does not offer absolute protection [4]. Therefore an effective vaccine remains the most promising approach to controlling this disease but is still not available. Individual susceptibility to malaria infection is influenced by host genotype and immunity that are determined by a combination of host genes and environmental effects. The extent to which host genotype limits the spectrum of possible immune responses may influence the outcome of infection and has consequences for vaccine design [5]. Therefore vaccine development that typical or specific for Indonesian people is necessary. The aim of this research was to determine Hsp profile irradiated by high doses of gamma-rays, and to observe if there was a difference in response between infected and non infected samples. The results of the determination of molecular weight of protein bands observed in SDS-PAGE gels from both non infected and infected samples are presented in Figure 1 (Appendix) and Table 1.

In this experiment we examined the profile of a general protein (Hsp) that was expressed in a cell due to outer stimulator. We found that there was no alteration of protein profile in control (uninfected with parasite) blood of mouse caused by gamma rays for all doses where the numbers of protein bands for 0, 150 and 175 Gy were 15 each. Opposite results were found in infected blood where 25 bands of protein were seen in SDS-PAGE gels. It was suggested that this higher number of protein bands was come from *Plasmodium sp.* or an antibody that elicited by infected cell. The molecular weights of these bands were 26, 27, 30, 34, 36, 40, 44, 48, 52, 57, 94, 150 (IgG), 159, 177, 188 and 193 kDa (Table 1). The number of protein profile of *Plasmodium sp.* infected mouse blood was decreased as the increasing of irradiation dose. These numbers were 22 bands and 16 bands for 150 and 175 Gy,

respectively. The bands that were disappeared at dose of 150 Gy were 150, 159, 170, 177 kDa and a new band was seen (131 kDa), whereas at dose of 175 Gy the disappeared bands were 26, 27, 30, 34, 70, 188 and 193 kDa. Taken together, we have known that the most effective dose was 150 Gy. No good results were obtained for mosquito samples (3 most right bands of Figure 1) due to some technical factors such as the number of mosquito cell extracts needed for electrophoration.

Some interested facts were found in this simple experiment. Hsp90 was only seen in infected blood indicating that this protein was only expressed by eukaryotic cells as described by previous report [25]. It believed that although the exact role of Hsp in immunity to microbial infection is incompletely understood, Hsp apparently serve as important antigens in defence against infectious agents. Some Hsp with lower molecular weights (Hsp60, Hsp50, Hsp40 and Hsp30) were also seen in SDS-PAGE. Some proteins seen in this experiment were predicted as proteins of erythrocytic form of parasite i.e. merozoite surface protein (MSP) [26] as we used parasite infected blood where merozoite proteins that could be expressed but it should be confirmed further.

Table 1. The molecular weight of protein bands observed in SDS-PAGE gels. C-0, C-150 and C-175 are non infected blood irradiated with 0, 150, 175 Gy, respectively. I-0, I-150 and I-175 are infected blood irradiated with 0, 150, 175 Gy, respectively.

Non infected bloods			***Infected bloods***		
C-0	**C-150**	**C-175**	**I-0**	**I-150**	**I-175**
205	205	205	205	205	205
			193	193	
			188	188	
181	181	181			
			177		
170	170	170	170		
			159		159
			150		
					146
				131	
123	123	123	123	123	123
113	113	113	113	113	113
			94	**94**	**94**
79	79	79	79	79	79
70	70		**70**	**70**	
65	65	65			
60	60	60			
			57	57	57
			52	52	52
50	50	50			
			48	48	48
			44	44	44
42	42	42			
			40	**40**	**40**
			36	36	36
			34	34	
			30	30	
29	29	29			
			27	27	
			26	26	
24	24	24	24	24	24
23	23	23	23	23	23
21	21	21	**21**	**21**	**21**
Total number of bands					
15	**15**	**14**	**25**	**22**	**16**

From this research, it was reveals that irradiation at different doses subjected to *P. berghei* of erythrocytic stadium showed an alteration of total protein content (data not shown). Protein concentration was decreased in accordance with the increasing of dose of irradiation. For dose of 150 Gy the protein concentration was 435 mg/ml and for 200 Gy it was 315 mg/ml. It was predicted this is caused by the fact that irradiation cleaved the protein chain. Statistical results also showed the influence of dose of irradiation to the protein contents.

Here we described the profile of Hsp as the first step of protein analysis in which they have an important role in developing malaria vaccine. Hsps are molecular chaperones, directing protein folding and assisting in protein trafficking. Hsps are also known as stress proteins and they are considered an important part of the cellular stress response. It is thought that an increase in protein damage can trigger this response. Hsps are important in protein folding and ensuring the proper protein conformation. They play an important role in the prevention of protein aggregation. By stabilizing partially unfolded proteins, they help in the transport of proteins across various intracellular membranes. This essential role means that some Hsps are ubiquitous in all cells. Indeed, Hsps are present during non-stressful conditions, playing a house-keeping role. Some of these housekeeping tasks include transporting old proteins to proteasomes for recycling and the assistance of folding of nascent protein chains [27]. Hsps also have other roles such as the presentation of antigens to the immune system. For this reason, they can be used as a vaccine adjuvant to boost the body's response to a vaccine, including cancer vaccines. Hsps may also be important in binding protein fragments from dead malignant cells and presenting them to the immune system to further increase the effectiveness of cancer vaccines. Hsps are also present in malignant cells and they may be important in tumor survival. Small molecule Hsp inhibitors such as the Hsp90 inhibitor, 17-AAG may act as a potent anti-cancer agent. While Hsp70 and Hsp90 participate in the defense response, the role of these small Hsps remains elusive [28].

Some researchers had described the expression of Hsp induced by ionizing radiation. Calini et al. [28] demonstrated that Hsp70 over-expression acts as a radioprotective mechanism towards the first event of DNA damage and increases long term viability. A preliminary investigation on the cell cycle does not evidence a significant protective action of inducible Hsp70 on it. By using western blotting method for profiling the protein of mouse lung cells, Melkonyan HS et al. [29] revealed a higher level of Hsp70 protein although the amount of protein increased to a lesser degree than that of mRNA. Kang CM et al. [30] showed that Hsp70 was involved in the radioadaptive response based on results from mouse splenocytes irradiated with low dose of gamma rays.

Irradiation is a technically simple process that retains structural features of the bacterial pathogen without destroying the natural antigens or the intrinsic adjuvants. Therefore, a strong immune response is induced in the vaccinated host. Ideally, vaccines should stimulate a strong response not only from both arms of the adaptive immune system (antibodies and T cells),

but also the body's innate immune system. However, traditional ways of making vaccines, either by killing disease-causing agents with heat, chemicals or by weakening (attenuating) live pathogens, have characteristic shortcomings. For example, heat- and chemical-killed vaccines, while safe and relatively easy to produce, generally produce a less broad immune response than live, attenuated vaccines. Conversely, it can be difficult to create live, attenuated vaccines that safely preserve the pathogen's ability to trigger strong innate and adaptive immune responses [31,32].

It has been impossible in the past to reproduce this immunity using artificially prepared vaccines, the striking exception being the radiation attenuated vaccines. The successful use of irradiated malaria parasite as a vaccine depends on finding a radiation dose which will significantly reduce the pathogenic effect of the larvae without seriously impairing their immunogenic power. Beside the determination of optimal dose of irradiation for attenuating parasite, subjects recommended for research using a more empirical approach are: further immunization trials with radiation attenuated vaccines on various host-parasite systems with both homologous and heterologous combinations of immunizing and challenging antigenic variants; determination of optimum dosage of irradiated parasites, number of boosters, spacing of vaccination; character, duration and species specificity of the protection; occurance of undesired side effects following vaccination; radiosensitivity of the parasites at their different stages of development; and optimum range of radiation doses to be applied for attenuation [33].

4. Conclusion

Results showed that protein profiles were different between infected and non infected blood and were not altered due to irradiation. HSP20 profiles of non infected and infected blood were not altered due to irradiation. HSP90 was only seen in infected blood but its profile was also not altered due to irradiation. HSP70 was seen in both infected and non infected blood and only seen at lower dose (0 and 150 Gy). The number of protein bands of infected blood seen in the 10% SDS-PAGE gel was decreased with the increasing of irradiation dose. Based on these findings, it was concluded that 150 Gy is the most effective dose to attenuate/inactivate parasite. Protein concentration was decreased in accordance with the increasing of dose of irradiation.

5. Acknowledgements

The authors are grateful and thank to Teja Kisnanto, Harry Nugroho, Prayitno and Armanu in BATAN for their excellence technical assistance.

6. References

[1] Good, M.F. (2009), The hope but challenge for developing a vaccine that might control malaria, *Eur. J. Immunol.*, 39, 939-943.

[2] World Health Organization, Situation in South East Asia Region (SEAR) Countries : Indonesia, http://www.searo.who.int/en/Section10/Section21/Section340_4022.htm

[3] Anonim, Malaria Cases Spreading, Kompas Newspaper, Monday, December 27, 2010, http://www.flutrackers.com/forum/showthread.php?t=157205.

[4] Anonim, Malaria Update - May 2001 - includes information on Cerebral Malaria (http://www.expat.or.id/medical/malaria.html)

[5] Riley, M. (1996), The role of MHC- and non-MHC-associated genes in determining the human immune response to malaria antigens, *Parasitology*, 112, S39-51.

[6] Nussenzweig, R.S. (1977), Immunoprophylaxis of malaria: sporozoite-induced immunity. In: Immunity to blood parasites of animals and man, New York, Plenum Publishing Corp., 75-87.

[7] Clyde, DF. *et al.* (1973), Immunization of man against sporozoite-induced falciparum malaria, *American Journal of Medical Science*, 266, 169-177.

[8] Rieckmann, K. *et al.* (1974), *Transactions of the Royal Society of Tropical Medicine and Hygiene*, 68, 258-259.

[9] Clyde, D.F., V.C. McCarthy, R.M. Miller and W.E. Woodward (1975), Immunization of man against falciparum and vivax malaria by use of attenuated sporozoites, *American Journal of Tropical Medicine and Hygiene*, 24, 397-401.

[10] Kim, T.S., C.Y. Jang, H.D. Kim, J.Y. Lee, B.Y. Ahn and J. Kim (2006), Interaction of Hsp90 with ribosomal proteins protects from ubiquitination and proteasome-dependent degradation, *Molecular Biology of the Cell*, 17, 824–833.

[11] Goodman, R. and M. Blank (1988), Magnetic field stress induces expression of hsp 70*, Cell Stress Chap*., 3, 79-88.

[12] Szumiel, I. (1998), Monitoring and signaling of radiation-induced damage in Mammalian cells, *Radiation Research*, 150, S92-S101.

[13] Wolff, S. (1998), The adaptative response in radiobiology. Evolving insights and implications, *Environ. Health Perspect*, 106, 277-283.

[14] Feder, M.E. and G.E. Hoffman (1999), Heat shock proteins, molecular chaperones and the stress response: Evolutionary and ecological physiology, *Anal. Rev. Phys*., 61, 243-282.

[15] Richter, K., and J. Buchner, J. (2001), Hsp90, chaperoning signal transduction, *J. Cell. Physiol.*, 188*,* 281-290.

[16] Schulte, T. W., M.V. Blagosklonny, C. Ingui and L. Neckers, L. (1995), Disruption of the Raf-1-Hsp90 molecular complex results in destabilization of Raf-1 and loss of Raf-1-Ras association, *J. Biol. Chem.* 270*,* 24585-24588.

[17] Turman, M.A., D.A. Kahn, S.L. Rosenfel, C.A. Apple and C.M. Bates (1997), Characterization of human proximal tubular cells after hypoxic preconditioninng: Constitutive and hypoxia-induced expression of heat shock proteins Hsp70 (A, B and C), Hsc70, and Hsp90, *Biochem. Mol. Med*., 60, 49-58.

[18] Lindquist, S. (1981), Regulation of protein synthesis during heat shock, *Nature*, 294, 311-314.

[19] Sierra-Rivera E, G.J. Voorhees and M.L. Freeman (1993), Gamma irradiation increases hsp-70 in Chinese Hamster ovary cells, *Rad. Res.*, 135, 40-45.
[20] Amundson, S.A., K.T. Do and A.J., Fornace (1999), Induction of strees genes by low doses of gamma rays, *Rad. Res*., 152, 225-231.
[21] Doltchinkova, V., S. Stoilova and M. Baldjiiska (1998), Effects of gamma-irradiation of the electrokinetic properties of purple membranes, *Radiat. Environ. Biophys*. 37, 41-45.
[22] Benderitter, M., L. Vincent-Genod, S. Berroud S, Muller, M. Donner, and P. Voisin (1999), Radio-induced structural membrane modifications: a potential bioindicador of ionizing exposure?. *Intl. J. Radiat. Biol.,* 75, 1043-1054.
[23] Daubenberger, C.A., F. Poltl-Frank, G. Jiang, J. Lipp, U. Certa, and G. Pluschke (2003), Identification and recombinant expression of glyceraldehyde-3-phosphate dehydrogenase of *Plasmodium falciparum*, *Gene* 246, 255-264.
[24] Greenwood, B. and T. Mutabingwa (2002), Malaria in 2002, *Nature,* 415, 670–672.
[25] Kaufmann, S. H. E. (1990), Heat shock proteins and the immune response, *Immunol. Today*, 11, 129-136.
[26] Kauth, C.W., C. Epp, H. Bujard, and R. Lutz, R. (2003), The merozoite surface protein 1 complex of human malaria parasite *Plasmodium falciparum*, *The Journal of Biological Chemistry*, 278(25), 22257–22264.
[27] Tsuji, M., D. Mattei, R.S. Nussenzweig, D. Eichinger and F. Zavala (1994), Demonstration of S heat-shock protein 70 in the sporozoite stage of malaria parasites, *Parasitology Research*, 80(1), 16-21.
[28] Calini, V., C. Urani, M. Camatini (2003), Overexpression of HSP70 is induced by ionizing radiation in C3H 10T1/2 cells and protects from DNA damage, *Toxicol. In Vitro*, 17 (5-6), 561-566.
[29] Melkonyan, H.S., T.E. Ushakova, and S.R. Umansky (1995), Hsp70 gene expression in mouse lung cells upon chronic gamma-irradiation, *International Journal of Radiation Biology*, 68(3), 277-280.
[30] Kang, C.M., K.P. Park, C.K. Cho, J.S. Seo, W.Y. Park, S.J. Lee, and Y.S. Lee (2002), Hspa4 (HSP70) is involved in the radioadaptive response: results from mouse splenocytes, *Radiation Research*, 157(6), 650-655.
[31] Rachmilewitz, D. K. Katakura, F. Karmeli, T. Hayashi, C. Reinus, B. Rudensky, S. Akira, K. Takeda, J. Lee, K. Takabayashi, and E. Raz (2004), Toll-like receptor 9 signaling mediates the anti-inflammatory effects of probiotics in murine experimental colitis, *Gastroenterology*, 126, 520-528.
[32] Datta S.K., S. Okamoto, T. Hayashi T, S.S. Shin, I. Mihajlov, A. Fermin, D.G. Guiney, J. Fierer and E. Raz (2006), Vaccination with irradiated *Listeria* induced protective T cell immunity, *Immunity*, 25(1), 143-152.
[33] Biello, D. (2006), Irradiated pathogens used to create potent vaccine, Science News, July 26.

Appendixes

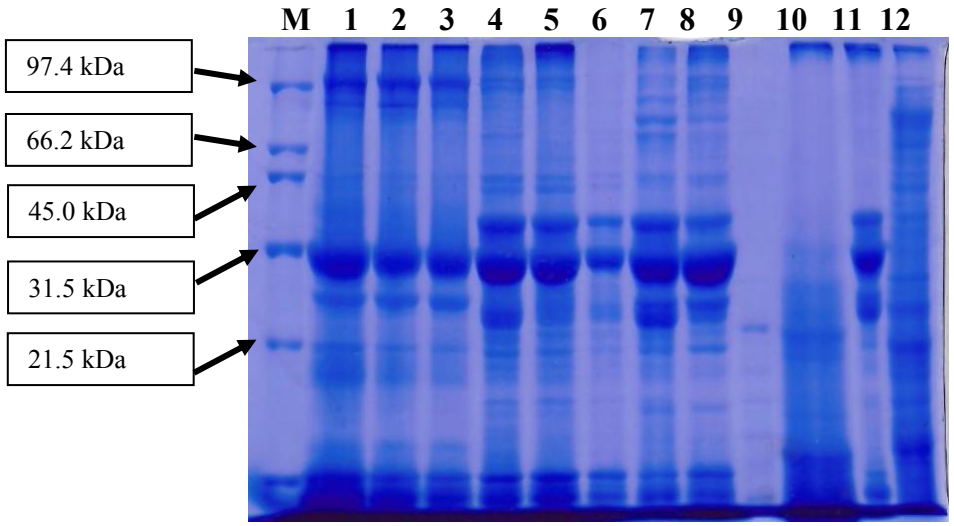

Figure 1. Profile of proteins in 10% SDS-PAGE gel.

Note:
M is protein marker, line 1 is non infected non irradiated blood, line 2 is non infected blood irradiated to 150 Gy, line 3 is non infected blood irradiated to 200 Gy, line 4 is infected non irradiated blood, line 5 is infected blood irradiated to 150 Gy, line 6 is infected blood irradiated to 200 Gy, line 7 is infected blood irradiated to 150 Gy at higher concentration, line 8 is infected blood irradiated to 200 Gy at higher concentration, and line 9-12 are mosquito samples.

Polyphenol Extract of Brown Seaweed (*Sargassum duplicatum* Bory): Phytopharmaco Exploration for Inflammatory Bowel Disease Theraphy

Nur Lailatul Rahmah [1], Aulanni'am [2], Anna Roosdiana [3]

[(1,2,3)] Department of Chemistry, Faculty of Sciences, Brawijaya University, Malang, Indonesia
(cahya_leyla@yahoo.com, aulani@ub.ac.id, aroos@ub.ac.id)

Abstract

Indomethacin as non-steroidal anti-inflammatory drug for rheumatoid arthritis theraphy was reported caused Inflammatory Bowel Disease (IBD) side effect. Exploration herbal material as phytopharmaco was developed countinously on medicinal treatment of IBD (specific on small intestine inflammation), include brown seaweed (Sargassum duplicatum Bory) polyphenol extract. Indomethacin was used to induce small intestine inflammation with 15 mg/kg body weight orally once time and continued by theraphy brown seaweed (Sargassum duplicatum Bory) polyphenol extract 100 mg/kg body weight seven times for seven days respectively. Level of malondialdehyde (MDA), protease activity and histological picture of small intestine (jejunum) was used as parameter from effect of brown seaweed polyphenol extract present to the small intestine inflammation. The MDA level is measured by TBA assay, protease activity is measured according tyrosine product formation and histological picture is observed by hematoxylen eosin staining. The result of this research showed that there was descent of MDA level and protease activity 54.20% and 44.09%, respectively. The histology observation also showed that there was repaired on jejunum small intestine tissue. These result showed that brown seaweed polyphenol extract might be improved as alternatve theraphy on IBD medical treatment, especially small intestine inflammation.

Keywords: *brown seaweed polyphenol extract, indomethacin, IBD, Sargassum duplicatum* Bory.

1. Introduction

IBD is a chronic inflammatory disease that attacks the digestive tract. The common symptoms of IBD are diarrhea, abdominal pain and bleeding in the digestive tract (including the small intestine) [16]. If not handled carefully, IBD can be at high risk of damage to the digestive tract [7]. The use of indomethacin as non-steroidal anti-inflammatory drugs (NSAIDs) at the dose of therapy in the treatment of rheumatoid arthritis disease can cause side effects such as Inflammatory Bowel Disease (IBD). This is caused by indomethacin could inhibit sikooksigenase enzyme (COX) 1 that functions on PGE_2 synthesis and production of mucus to protect the small intestinal mucosa [12].

Indomethacin proved to increase the production of reactive oxygen species (ROS), such as radical $O_2^{\bullet -}$, OH• and H_2O_2 derived from the leakage of electrons from the electron transport chain specific side and also from the activation of macrophages (the process of phagocytosis) [6,11]. It can increase level of malondialdehyde (MDA) and reduce the enzyme activity of superoxide (SOD), glutathione (GSH) peroxidase and glutathione reductase which is a parameter of oxidative stress [2]. In addition, in patients with IBD, there is increased activity of proteases [1,9,13].

Conventional treatment of IBD is done by giving of drugs such as cortisone (steroids), anti-inflammatory, immune system suppression and antibiotics. In addition, there are potential herbal therapies that using plants as medicine (phytopharmaco) [14,15]. Herbal therapy is usually safer than conventional treatment.

Brown seaweed (*Sargassum sp.*) is a type of algae that contain a protein, fat, carbohydrate, alginate, vitamins, minerals, and iodine. In addition, there are antioxidants in the form fukosantin and polyphenol compounds (flavonoids and florotanin) [5,8,10,17]. Compounds from the class of polyphenols, fucosantin, α-tocopherol and carotenoids have antioxidant activity that is useful to scavenge off free radicals [3,5]. Seaweed has also been reported to have biological activity such as antibacterial, antifungal, antitumor, and antiproliferatif [3].

This research will study the polyphenol extract potency of brown seaweed as an alternative therapy of IBD. Parameters to be studied are the level of malondialdehyde (MDA), protease activity and histological small intestinal jejunum. The purpose of this study to determine the effect of polyphenol extract of brown seaweed (*Sargassum Duplicatum* Bory) toward decreased levels of MDA, activity of protease and histological picture of small intestine jejunum that induced by indomethacin (IBD attacked), which is expected to be used as an alternative therapy in IBD.

2. Experimental Details

The tools used in this study are animal keeping box, gavage, a set of surgical tools, a set of glass equipment, centrifuges (Denley BR type 401), sonikator (Branson 200), vortex (Guo-Huq), an incubator/oven (Memmert), shaker (VRN-200), light microscope (Nicon) and UV-Vis spectrophotometer (Shimadzu).

Materials used in this study are white rat (*Rattus norvegicus*) wistar strain male aged 3 months, weight 125-175 g, *Sargassum duplicatum* Bory, indomethacin (Sigma-Aldrich), L-Tyrosin (Merck), Casein (Fluka BioChemika), MDA standards (Sigma-

Aldrich), distilled water, ethanol, PBS, PFA, phosphate buffer, hematoxylin, eosin and xilol.

This research is divided into two steps:

a. Extraction of polyphenol compounds of brown seaweed (Sargassum duplicatum Bory)

Brown seaweed is cleaned and cut into small size then wind dried untill contain between 20-30% of moisture content. Brown seaweed is weighed as much as 116 g and extracted by maceration using 1.5 L 85% of ethanol. Maceration performed for two days. The extract was then filtered and the filtrate was concentrated by rotary vacuum evaporator at 40ºC (± 2 hours). Extract was concentrated and then washed with each 100 ml of chloroform three times and the upper layer (non-lipid fraction) was extracted with 250 ml of ethyl acetate. Ethyl acetate fraction (bottom layer) was taken and dried with N_2 gas to obtain extracts with a constant weight.

Phytochemical tests of polyphenol extract are used to determine flavonoid, florotanin, alkaloid and terpenoid. Flavonoid test is done by adding of 10% NaOH to solution extracts and positive results is shown by the yellow color and become translucent or turbid colorless after the addition of dilute HCl. Florotanin test performed with the addition of $FeCl_3$ and into the extract solution. Positive results are indicated by a blue-black color. Alkaloid test is done by adding 10 ml of NH_3 (ammonia) 0.05 M and chloroform ($CHCl_3$) into 4 g of extract solution. Solution was then mixed with 1 ml, 2 M H_2SO_4, shaken until formed two layers. Sulfuric acid layer was taken and added Wagner reagents. Positive alkaloid results if brown precipitate formed in solution. Terpenoids test performed using Salkowski test: as much as 0.5 g of extract plus 2 ml of $CHCl_3$, then add 2 ml of concentrated H_2SO_4. Positive results terpenoids, if red-brown color formed at the interface of two layers of solution.

b. Testing of brown seaweed extract polyphenols (Sargassum duplicatum Bory) IBD in rat.

- Preparation of experimental animals

This research use Wistar strain, male, 3 months years old and weighed 125-175 g of rats. It were divided into 3 groups: group C: group of negative control (healthy); group S: IBD (exposed to indomethacin) and T groups: therapy.

Experimental animals were adapted for a week in animal box keeping. Group C: given no treatment. Group S: exposed to indomethacin orally at a dose of 15 mg / kg one time for 24 hours then incubated for 7 days. Group T: exposed to oral indomethacin 15 mg / kg one time for 24 hours and then treated with the extract of polyphenols brown seaweed 100 mg / kg for 7 days. On 9th day, jejunum small intestine rat is dissected and retrieved.

- Determination of malondialdehyde (MDA)

The first step is the determination of MDA level by determining the maximum wavelength of MDA and MDA standard curve using the maximum wavelength obtained. Then a linear regression equation determined MDA standard curve.

Determination of MDA is done by TBA test. Jejunum supernatant of 100 mL inserted in eppendorf, add 550 mL of distilled water, 100 mL of TCA 10%, 250 mL 1 N HCl and 100 mL of Na-thio. After that, homogenized and centrifuged at 500 rpm for 10 minutes. Supernatant is taken and incubated in a water bath 100ºC for 30 minutes. Supernatant left in room temperature and then measured the wavelength of maximum absorbance at 532 nm. Absorbance was then plotted to linear regression equation so that we will obatain the level of MDA.

- Protease isolation of jejunum small intestine

One g of organ jejunum is cut using surgical scissors, add a PBS-Tween solution: PMSF (9:1) 1 ml, add a little quartz sand and crushed using a cold mortar placed on blocks of ice. Next, the homogenate added by PBS-Tween solution: PMSF (9:1) 2 ml and transferred into a polypropylene tube that had been sterilized by autoclave, continued by homogenized with a vortex for 10 minutes, sonicated with sonikator for 10 minutes and centrifuged for 15 minutes at 6,000 rpm. Then the supernatant was taken and added with cold absolute ethanol with a ratio of 1:1 and left for overnight at 4ºC and to form precipitate. Then centrifuged for 15 minutes at 10,000 rpm, pellets were taken and dried to ethanol odor disappears. Then pellets added with a solution of 20 mM Tris-HCl pH 6.8 chilled with the volume ratio of 1:1 and homogenated.

- Determination of protease activity

The first step of determination protease activity is determination of the maximum wavelength of tyrosine and tyrosine standard curve using the maximum wavelength obtained. Then it must be determined a linear regression equation of tyrosine standard curve.

A total of 200 mL casein 500 µg/ml included in ependorf tube, add 300 mL phosphate buffer solution pH 7 and 100 mL protease isolated, then allowed to incubation for 60 minutes at 37°C in an incubator. Then add 400 mL solution of 4% TCA (w/v) and allowed to stand for 30 minutes at a temperature of 27ºC, and then centrifuged at 4,000 rpm for 10 minutes. 200 mL supernatant was taken and diluted 5 times the volume of the sample with phosphate buffer and measured absorbance of sample at maximum wave length of tyrosine at 280 nm. Blank that is used in the determination of the activity is the same with the procedure, but a solution of casein was replaced with the addition of distilled water. Protease activity was then measured by using the following formula:

$$\textbf{Protease activity} = \frac{[\text{Tyrosine}]}{\text{Mr Tyrosine}} \times \frac{v}{p \times q} \times df$$

Note:

v	=	total volume of sample (ml)
p	=	amount of enzim (ml)
q	=	incubation time (menit)
df	=	dilution factor
Mr tyrosine	=	181 µg/µmol

- Hematoxylin-Eosin (HE) staining on small intestine jejunum preparate

Hematoxylin-eosin was staining first by entering preparate in xilol absolute for 5 minutes 2 times. Then do the steps deparafinasi, where preparate

are entered in xilol graded 1-3 [xilol: absolute ethanol (3:1, 1:1, 1:3)] respectively for 5 minutes. Next on rehydration, preparate entered into graded ethanol that starts from absolute ethanol, ethanol 95, 90, 80 and 70% respectively for 5 minutes, then soaked in distilled water for 5 minutes. Further preparate stained was add with haematoxylin dye for 10 minutes to obtain the best results, washed with running water for 30 minutes, rinsed with distilled water, and inserted in the dye eosin for 5 minutes. Preparate soaked in distilled water to remove excess eosin. Then do the stages of dehydration, preparations included in graded ethanol from 80%, 90%, and 95% to absolute ethanol. Further clearing was done by entering preparate in xilol for 5 minutes, dried-aired and mounted with entellan, and then closed with a cover glass. Level of MDA and protease activity was analyzed using One Way Anova - Kruskal Wallis.

3. Result and Discussion

Phytochemical test of polyphenols extract of brown seaweed (Sargassum duplicatum Bory)

Phytochemical tests were done to determine compounds in the extract qualitatively. The results showed that the extract contained flavonoid, florotanin and alkaloid, but there is no terpenoid (Table 1).

Tabel 1 The result of phytochemistry test of brown seaweed extract

Compound in brown seaweed extract	Result of phytochemistry test
Flavonoids	+
Florotanins	+
Alkaloids	+
Terpenoids	-

Testing of brown seaweed extract polyphenols (Sargassum duplicatum Bory) in IBD rats

In this study, negative control rat compared with rat that were exposed to indomethacin and then left for 7 days and also compared with rat that were exposed to indomethacin and then treated with brown seaweed extract polyphenols for 7 days.

- Levels of malondialdehyde (MDA)

MDA is the end product of peroxidation lipid membrane by ROS, so that measurement of MDA levels indirectly reflect levels of free radicals. The results showed that the average MDA level of jejunum small intestine exposed to indomethacin groups of rat is 4.596 ± 0.429 (g/ml). This value is much higher if compared with negative control rat, 1.839 ± 0.067 (g/ml) (Figure 1). Statistical results by One Way Anova – Kruskal Wallis test showed significant differences ($p<0.05$) between sick rat (exposed to indomethacin) against the control rat.

Indomethacin can inhibit the enzyme activity of cyclooxygenase (COX) 1 and 2. Inhibition of COX-2 will work towards the reduction of pain with rheumatoid arthritis. However, inhibition of COX-1 would inhibit the synthesis of PGE_2 on mucus secretion that serves to protect the intestinal mucosa [12]. It causes weakness of the defense system in mucosa small intestine that may cause invasion of pathogenic bacteria in the intestinal wall, causing infection. The presence of infection can cause the activation of macrophages, the formation of ROS and RNS, which triggers activation of NF-kB and release of pro-inflammatory cytokines (IL-1, TNF-α, and IFN-γ) resulting in local inflammation in the small intestine tissue.

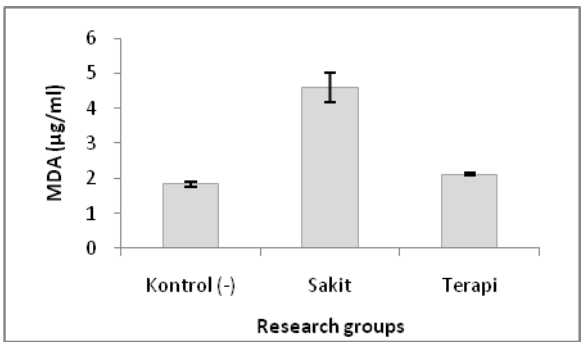

Figure 1. Average ratio of MDA level of small intestine jejunum

Brown seaweed polyphenols extract can reduce level of MDA in rat therapy group. The average level of MDA in therapy group was 2.105 ± 0.035 (g/ml) (Figure 1). Statistical analysis showed that the brown seaweed polyphenol extracts (*Sargassum duplicatum* Bory) give a highly significant effect ($p <0.05$) toward decreased levels of MDA.

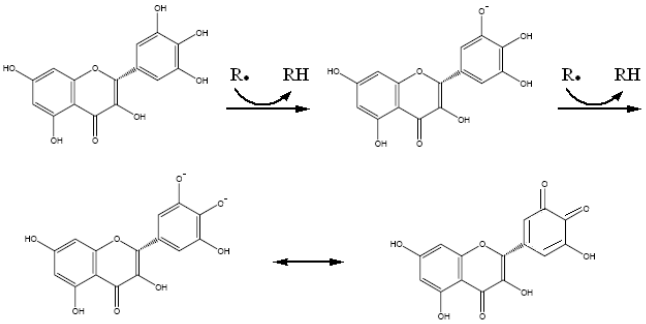

Figure 2 Scavenging free radical reactions by flavonoid

Decreased level of MDA by brown seaweed polyphenols extract caused by the antioxidant content of flavonoids and florotanin as a scavenger of ROS (R•) that can inhibit lipid peroxidation. Inhibition of lipid peroxidation is caused by flavonoid and florotanin structure that have more than one phenol group, the aromatic and conjugated double bonds that can conduct electrons delocalization and resonance to stabilize its structure after hydrogen atom abstraction process by ROS (OH•) (Figure 2).

- Protease Activity

The concentration of protease was measured as protease activity based on results of the formation of tyrosine products from the casein substrate using isolated crude protease of small intestine jejunum. The result showed that the average activity of protease in rat small intestine jejunum induced by indomethacin 1.268 ± 0.014 units. This value is higher than the negative control, 0.507 ± 0.011 units (Figure 3.3). One Way

Anova - Kruskal Wallis statistical results test showed significant differences ($p<0.05$) between sick (exposed to indomethacin) against the control.

Increased protease activity in rat IBD group (exposed to indomethacin), possibly related to leakage electron of transport electrone system and activation of macrophages which increase the production of ROS in cells resulting in activation of NF-kB. In eukaryotic cells, NF-kB (RelA and P50) is in an inactive form and form complex with kB inhibitor (IκB) located in the cytoplasm which is also called IκB kinase protein group.When getting a stimulus such as ROS, the IκB kinase protein activated, leading to IκB phosphorylated and degraded by the ubiquitin / proteasome.

Since there is no IκB, the NF-kB (P50 complex and RelA) move toward the nucleus and perform a series of transcription process to regulate gene expression dependent on NF-kB which genes coding for cytokines and chemokines including pro-inflammatory cytokines such as IL-1 and TNFα. TNF-α expression may activate neutrophils to the site of inflammation and actively release the serine protease (elastase) into the cells and tissues in the small intestine. These proteases are involved in cell and tissue damage due to proteases in active form will hydrolyze proteins including cells protein constituent.

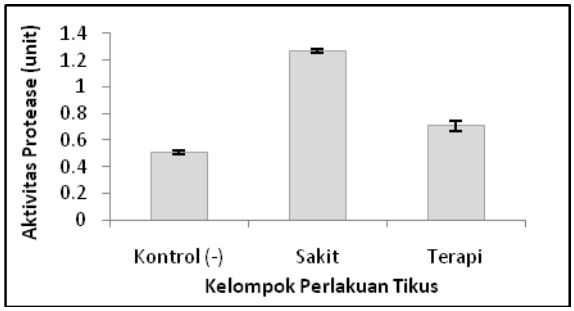

Figure 3. Average ratio of protease activity of jejunum small intestine

Brown seaweed polyphenol extract can reduce protease activity in therapy group. The protease activity average in the therapy group was 0.709 ± 0.037 units (Figure 3.3). Statistical analysis showed that the polyphenol extracts brown seaweed (*Sargassum duplicatum* Bory) give a highly significant effect ($p<0.05$) toward decreased activity protease.

The decrease of protease activity by brown seaweed polyphenols extract caused by the antioxidant content of flavonoids and florotanin as a scavenger of ROS that inhibits a stimulus to the activation of NF-kB, which indirectly inhibits the release of pro-inflammatory cytokines TNF-α thereby preventing the activation of neutrophils and release of serine proteases to the cytoplasm.

- Histological picture

Histological picture is used to determine the level of damage and repair on tissue. Figure 3.4 present the small intestine jejunum picture from negative control, sick (exposed to indomethacin at 1 time and then incubated for 7 days) and therapy (indomethacin exposed 1 time and then treated with polyphenol extracts of brown seaweed). Based on Figure 3, the mucosal jejunum of negative control group is still good. It has long and compact villi structure. But in sick rat, there is damage to the mucosa, the villi become shorter, broken and there is hollow space.

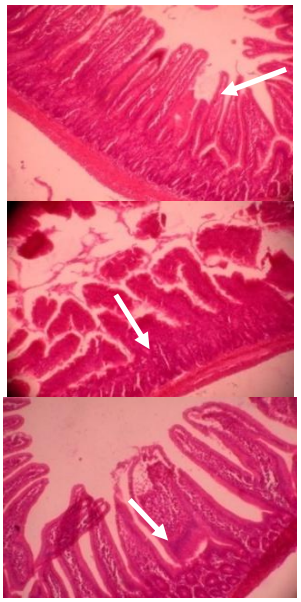

Figure 4 Histological picture of small intestine jejunum. Note: (top) negative control; (middle) sick; (bottom) therapy; white arrows: villi

Small intestine jejunum tissue damage is caused by exposure to indomethacin which trigger the production of ROS that activate NF-kB transcription factor and express proinflammatory cytokines (IL-1 and TNFα) that trigger the activation of neutrophils and release of protease. The occurrence of inflammation and the release of this protease then cause tissue damage.

After given of brown seaweed polyphenol extract in therapy group, there are improvements in the jejunum mucosa, the villi become length and compact (Figure 4). It is probably due to the antioxidant activity of flavonoid compound and florotanin as a scavenger of free radicals so that it can inhibit free radicals causing tissue damage.

4. Conclusion

Based on phytochemical test, brown seaweed polyphenol extract (*Sargassum duplicatum* Bory) contain polyphenols compounds (flavonoid and florotanin) and alkaloid.

Brown seaweed polyphenol extract can reduce MDA level and protease activity of small intestine jejunum, 54.20% and 44.09%, respectively and showed histological picture improvement of jejunum tissue in the small intestine.

5. Acknowledgements

The author would like to thank for Prof. Dr. drh. Aulanni'am, DES and Dra. Anna Roosdiana, M.App.Sc. (Laboratory of Biochemistry UB), which provides all facilities of research. Roodiyati A., MSc,

PhD (Laboratory of Plant Taxonomy and Structure, UB) for the identification of brown seaweed.

6. References

[1]. Hugli, D.J. Anjaria, D.A. Frankel and R. Coimbra (2006), Intraluminal Pancreatic Serine Protease Activity, Mucosal Permeability, and Shock, *Review,* 26, 3–9.

[2]. Basivirreddy, J., M. Jacob, and K.A. Balasubramanian (2004), Oral Glutamine Attenuates Indometachin-Induced Small Intestinal Damage, *Biochem. Clinical Science*, 107, 281-289.

[3]. Demirel, Z., F.F. Yilmaz-Koz, U.N. Karabay-Yavasoglu, G. Ozdemir, and A. Sukatar (2009), Antimicrobial and Antioxidant Activity of Brown Algae from the Aegean Sea, *J. Serb. Chem. Soc.* 74 (6), 619–628.

[4]. Halliwell and Susanna Chirico (1993), Lipid Peroxidation: its Mechanism, Measurement, and Significance, *American Journal Clinical Nutrition,* 57, 715S-25S.

[5]. Lim, S.N., P.C.K. Cheung, V.E.C. Ooi and P.O. Ang (2002), Evaluation of Antioxidative of Extracts from a Brown Seaweed, Sargassum siliquastrum, *J. Agric. Food Chem*, 50, 3862-3866.

[6]. Maity, P., S. Bindu, S. Dey, M. Goyal, A. Alam., Chinmay Pal., K. Mitra and U. Bandyopadhyay (2008), Indomethacin, a Non-steroidal Anti-inflammatory Drug, Develops Gastropathy by Inducing Reactive Oxygen Species-mediated Mitochondrial Pathology and Associated Apoptosis in Gastric Mucosa, *The Journal Of Biological Chemistry*, 284 (5), 3058–3068.

[7]. McFarland, L.V. (2008), State-of-the Art of Irritable Bowel Syndrome and Inflammatory Bowel Disease Reasearch in 2008, *World Journal of Gastroenterology.* 14 (17), 2625-2629.

[8]. Meenakshi, S., D.Manicka Gnanambigai, S. Tamil Mozhi, M. Arumugam and T. Balasubramanian (2009), Total Flavonoid and in vitro Antioxidant Activity of Two Seaweed of Rameshwaram Coast, *Global Journal of Pharmacology*, 3 (2), 59-62.

[9]. Qin, X. (2007), Inactivation of Digestive Proteases: another Aspect of Gut Bacteria that should be taken into more Consideration. *World J Gastroenterol*. 13, 2390–2391.

[10]. Samee, H., Zhen-xing Li, Hong Lin, Jamil Khalid and Yong-chao Guo (2009), Anti-Allergic Effects of Etanol Extract from Brown Seaweeds. *Journal of Zheijiang University Science B.*, 10 (2), 147-153

[11]. Takeuchi, K., A. Tanaka, R. Ohno and A. Yokota (2003), Role of COX Inhibition in Pathogenesis of NSAID-Iinduced Small Intestinal Damage. Research article. Kyoto Pharmaceutical University. Kyoto.

[12]. Tanaka, A., M. Matsumoto, A. Nakagiri, S. Kato and K. Takeuchi (2002), NSAID-induced Small Intestinal Damage: Role of COX Inhibition, *Inflammopharmacology*, 10 (4-6), 313-325.

[13]. Tarlton, J.F., C.V. Whiting, D. Tuanmore, S. Bregenholt, J. Reimann, M.H. Claesson and P.W. Bland (2000), The Role of Up-Regulated Serine Protease and Matrix Metalloproteases in the Pathogenesis of a Murine Model of Colitis, *The American Journal of Phatology*, 157, 1927-1935.

[14]. *Wu, L., (2007), Effect of Chlorogenic Acid on Antioxidant Activity of Flos lonicerae Extracts, J Zhejiang Univ Sci B*, 8 (9), 673–679.

[15]. *Wu, T.Y., Chien-Chih Chen and Horng-Liang Lay (2010), Study on the Components and Antioxidant Activity of the Bletilla Plant in Taiwan. Journal of Food and Drug Analysis, 18 (4), 279-289.*

[16]. Xavier, R.J. and D.K. Podolsky (2007), Unravelling the Pathogenesis of Inflammatory Bowel Disease, *Nature*, 448(7152), 427-434.

[17]. Zahra, R. Mehranian Mehrnaz., Vahabzadeh Farzaneh and Sartavi Kohzad (2007), Antioxidant Activity of Extract from Brown Alga, *Sargassum boveanum*, *African Journal of Biotechnology*, 6 (24), 2740-2745.

Agrobacterium Mediated Transformation of Tomato and Production of Transgenic Plants Containing Gene Increased Sucrose Transport *SoSUT1*

Parawita Dewanti [1], Bernet Agung Saputra [2], Tatik Wardiyati [3], Arifin Nur Sugiarto [4], Bambang Sugiharto [5]

[1,2] Faculty of Agriculture, University of Jember, East Java, Indonesia (parawita@yahoo.co.id)
[3,4] Faculty of Agriculture, University of Brawijaya, Malang, Indonesia
[5] Science and Technology, University of Jember, East Java, Indonesia

Abstract

The development of transgenic tomato to increase of sucrose translocation can be done through transformation by genetic engineering techniques. The process of sucrose transport from leaves to the stem/fruit is facilitated by transport proteins (sucrose transporter/SUT). In the year 2008 has been isolated SoSUT1 gene to increase of the rate of sucrose transport, so the accumulation of sucrose in storage organs (stems/fruit/sinks) increases. Cotyledon and axillary bud from L. esculentum cv. Zamrud were co-cultivated with Agrobacterium strain GV3010 that harbored a pAct binary vectors carrying genes for both Hygromycin phosphotransferase (HPTII) and S. officinarum SPS (SoSUT1). This study aims to determine transformation and obtain transgenic tomato plants transformed with the SoSUT1 gene using Agrobacterium tumefaciens. Transformation efficiency was obtained at 10 mg/L hygromisin antibiotic as a selection agent with the percentage of explants forming shoots 6.2%. PCR results showed that the plasmid pKYS: SoSUT1 already integrated in the explants and has obtained five clones of transgenic tomato plants.

Keywords: *Tomato (Lycopersicon esculentum), SoSUT1 gene, Transformation, Agrobacterium tumefaciens.*

1. Introduction

Tomato (*Lycopersicon esculentum* Mill.) is one of the most important vegetable crops and a genetic model for improving other dicotyledonous plants [1,2]. The development of transgenic tomatoes can be done by genetic engineering through recombinant DNA methods of gene transformation techniques using *Agrobacterium tumefaciens*. Tomato transformation using *Agrobacterium tumefaciens*, has developed very rapidly since 1986 [2]. Factors such as plant variety [1,3,4], explants material [2], plant growth regulators [5], bacterial concentration [6], binary vector [7], Agrobacterium strains [8] and concentration antibiotics [9,10], have a influence on transformation efficiency.

Based on assimilation of carbon (C), tomato plants were classified as C3 plants. In the Calvin cycle of CO_2 reacted with ribulose bisphosphate (RuBP) to form compound 3-phospho glyceric acid (3-PGA) catalyzed by ribulose bisphosphate carboxylase oxygenase (rubisco), the Calvin cycle occurs in mesophyll cells. The end product of carbon assimilation in the process of photosynthesis is sucrose and starch [11].

Sucrose is the largest part of the final product of photosynthesis in the leaf vascular tissue [12]. Sucrose was translocated in plant leaves (source) to the organ (sinks) such as stems, fruits, roots and flowers [13]. Isolation of DNA SUT has successfully conducted from spinach [14], tobacco [15], Arabidopsis, potato and tomato [16], citrus [1] and sugar cane [15].

The development of biotechnology by using cDNA SUT transformed the plant is expected to increase the translocation of sucrose to sink organs. The researchers suspect that by doing the over-expression of genes coding for sucrose transporters can increase the rate of sucrose transport, thus increasing its ability to accumulate sucrose in the sink [15]. Hackle [17], showed that LeSUT1 and antisense LeSUT2 on tomato plant able to produce normal tomato fruit. This study aims to determine transformation efficiency and obtain transgenic tomato plants transformed with *SoSUT1* gene using *Agrobacterium tumefaciens*.

2. Experimental Details

Plant Material

Seed of tomato var. Zamrud were obtained from Research Institute for Vegetables (Balitsa) Lembang. The Seeds were soaked in warm water for 5 minutes, and surface-sterilized with 5% hypochlorites solution for 30 seconds and rinsed 3 times with sterile distilled water. Then, seeds were implanted planted on germination medium (G): (MS + 30 g/L sucrose + 3 g/L phytagel, pH

5.8 before autoclaving) at 25ºC under 16-h and 8-h cycle with a light intensity of 1,600 lux illumination. Both axillary bud and cotyledons segment from 14 d-old in vitro plants were used as explants sources.

Effect of hygromycin on regeneration frequency from axillary shoot, cotyledon and hypocotyls explants

To determine optimal hygromycin concentration for callus induction, the axillary shoot, cotyledon and hypocotyls explants excised from non-transformed 14-d-old seedling were cut into 0.5 cm, 1x0.5 cm and 0.5 cm segments, respectively. Explants segments were cultured on callus induction medium (H): (MS + 30 g / l sucrose + 0.2 mgl^{-1} IAA + 2 mg/L BAP + 3 g / l phytagel, pH 5.8 before autoclaving) supplemented various concentrations of hygromycin (0, 10, 20 and 30 mg/L). Each experiment was repeated three times. Observations were carried out by observing the percentage of dead explants for 28 days and 7 days intervals.

Agrobacterium strain and plasmid vector

Agrobacterium tumefaciens strain LBA4404, harbouring plasmid pAct, which contained hptII asa plant selectable marker, and *SoSUT1* gene construct, was utilized for *Agrobacterium*-mediated transformation. In this construct, the expression of hptII gene was under the control of the nopaline synthase (NOS) promoter and NOS terminator and *SoSUT1* gene was driven by Rice-actin (Figure 1).

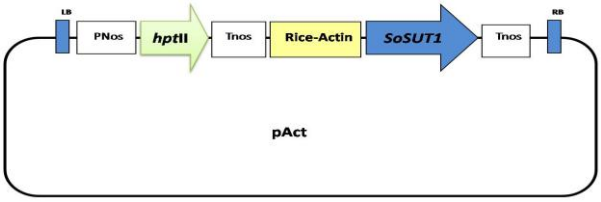

Figure 1. Map of pAct: *SoSUT1* construct. cDNA-SoSUT1 under the control of Rice-actin promoter and resistance gene (*hptII*) for hygromycin.

Transformation mediated by Agrobacterium tumefaciens

Single colonies of *Agrobacterium tumefaciens* LBA4404, harbouring plasmid pAct on Luria Betani (LB) medium plate (10 gl^{-1} pepton, 10 gl^{-1} yeast extract, 5 gl^{-1} NaCl, 14 gl^{-1} agar, pH 7.0) were inoculated in 2 ml liquid Yeast Extract Peptone (YEP) medium supplemented with 50mgl^{-1} kanamycin, 30 mgl^{-1} Streptomicyin and 50 mgl^{-1} refamicyin and incubated overnight at 28ºC with continuous shaking at 150 rpm. *Agrobacterium* resubcultured into 50 ml liquid YEP medium containing 50 mgl^{-1} kanamycin, 30 mg/L Streptomicyin and 50 mgl^{-1}refamicyin and incubated 4-h at 28ºC to a final density of 0.3-0.4 OD_{600}. *Agrobacterium* cells were harvested by centrifugation at 5,000 rpm for 10 min and resuspended in liquid MS medium.

The explants were infected by immersing in *Agrobacterium* suspension for 30 min with gentle shaking three to five times during the infection process. Subsequently, the infected explants were dried on a steril filter paper and transferred onto (C) medium (MS salts + 30 gl^{-1} sucrose + 0.2 mgl^{-1} IAA + 2 mgl^{-1} BAP + 3 gl^{-1} phytagel + 50 mgl^{-1} acetosyringone, pH 5.8 before autoclaving) for 2-d for cocultivation in dark at 25ºC. Following cocultivation, the infected explants were washed with 50 ml of liquid MS containing cefotaxime 500 mgl^{-1}, drained on steril filter paper and transferred onto E medium (MS + 30 gl^{-1} sucrose + 0.2 mgl^{-1} IAA + 2 mgl^{-1} BAP + 3 gl^{-1} phytagel + 500 mgl^{-1} cefotaxim , pH 5.8 before autoclaving) at 25ºC under 16-h light, 8-h dark cycle for 5 days.

Axillary bud and cotyledon explants were cultured subsequently on S medium (MS + 30 g / l sucrose + 0.2 mgl^{-1} IAA + 2 mgl^{-1} BAP + 3 g / l phytagel + 500 mgl^{-1} ceffotaxim + 50 mgl^{-1} kanamycin, pH 5.8) for shoot induction, R medium MS + 30 gl^{-1} sucrose + 0.25 mgl^{-1} BAP +0.25 mgl^{-1} GA3 + 3 gl^{-1} phytagel + 500 mgl^{-1} ceffotaxim + 50 mgl^{-1} kanamycin, pH 5.8) for shoot enlargement and R medium (MS + 30 gl^{-1} sucrose + 0.15 mgl^{-1} NAA + 3 gl^{-1} phytagel + 500 mgl^{-1} ceffotaxim -1 + 50 mgl^{-1} kanamycin, pH 5.8) for rooting induction.

DNA isolation and PCR analysis

Genomic DNA was isolated from nontransformed (control) and transformed leaves. PCR analysis were carried out to detect the presence of the hptII genes, using primer hpt-F/R, 480 bp. Lingkage analysis of these gene in transgenic plants was conducted using PCR amplification.

3. Results and Discussion

Effect of hygromycin on the survival from tomato explants

The sensitivity of axillary bud, cotyledon and hypocotyls to hygromycin was tested according to the survival and regeneration frequency of explans on H medium with various concentrations of hygromycin. Hygromycin is an

antibiotic that is used as a selection agent. Explants grown on media containing hygromycin, because the target gene construct contained the gene for resistance to hygromycin (hpt). For Axillary bud explants, cotyledon and hypocotyls after 28-h of cultur were not death on H medium without hygromycin. Regeneration frequency drastically declined as the hygromycin concentration increase from 10, 20 and 30 mgl^{-1}. The results showed that hygromycin concentration, 10, 20, 30 mg/L for 14-h was death at 100% on all explants. After 14-h, all explants turned brown and became completely necrotic on media with 10, 20 and 30 mgl^{-1}, respectively. No callus and shoot was produced from all explan at 10 mg/L. Thus the concentration of hygromycin 10 mgl^{-1} is effective for selection in all explants (Table 1).

Hygromycin phosphotransferase (hpt) for resistance to hygromycin is aminoglycoside antibiotic resistance marker gene in plan transformation. Hygromycin inhibits protein synthesis by causing mistranslation and interferes with protein translocation [18]. Hygromycin are poison to kill non-transformed cells, but the transformed cells are able to grow normally because the regeneration of plants are not disturbed [19]. Meng *et al*. [20] reported that concentrations of 7.5 and 20 inhibit the initiation of callus on the cotyledons and hypocotyl explants of cotton. Explants are not transformed at concentrations higro 10 and died on 15 mgl^{-1} hygromycin, the seed concentration 20 inhibits elongation of roots and shoots.

Table 1. Percentage mortality axillary bud explants, cotyledon and hypocotyl of tomato grown on MS medium containing hygromycin

Eksplant Type	**Concentration Hygromysin (*mgl*$^{-i}$)**	Percentage mortality explants on the day of			
		7	**14**	**21**	**28**
Axillary bud	0	0	0	0	0
	10	40	60	100	-
	20	60	100	-	-
	30	60	100	-	-
Cotyledon	0	0	0	0	0
	10	50	100	-	-
	20	50	100	-	-
	30	70	100	-	-
Hypocotil	0	0	0	0	0
	10	50	100	-	-
	20	70	100	-	-
	30	80	100	-	-

Transformation Efficiency

That the cotyledon explants produced shoots and putative transformant plant by 6.1% and 6.2%, respectively (Table 2). Explants that survive on S media are assumed that the target gene has been transformed. Observations on explants not infected with Agrobacterium, then grown in medium containing no hygromycin (control -) and containing hygromycin (control +) showed that explants grown on negative control to 85%, whereas explants in positive control media showed that all explants was death until the third selection. Transformed explants with *Agrobacterium* showed that the explants are able to grow on selection media until 5 cycles 13.2% (Table 3). Frary [6], showed that the transformation efficiency of 10.6% in tomato cultivar Moneymaker. Cortina [5] also reported that the transformation efficiency reached 12.5% on tomatoes.

Table 2. Percentage Plantlet Putative Transformants

Explant Type	Number of Explant	Percentage Plantlet putative transformants (%)
Axyllary bud	100	6.1
cotyledon	100	6.2

Table 3. Percentage survival of shoots explants on selection media

Treatment	Co-cultivation (%)	Elimination (%)	S1 (%)	S2 (%)	S3 (%)	S4 (%)	S5 (%)
GV-pAct	100.0	100.0	100.0	81.4	47.3	25.6	13.2
Control (+)	100.0	85.0	60.0	25.0	0	0	0
Control (-)	100.0	100	100	95.0	95.0	85.0	85.0

PCR amplification and linkage of hpt gene with SoSUT1 in T-DAN region

Five putative transgenic tomato plants were analyzed by PCR amplification to detect the presence of hpt gene (Figure 2). The result showed that a 480-bp fragment of hpt gene was amplified in the entire sample except in the nontransformed.

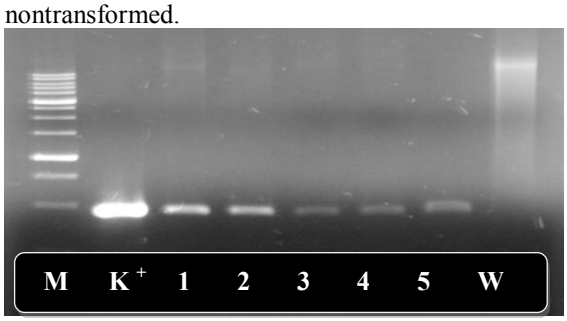

Figure 2. Result of PCR with primer F/R HPTII. (M): Marker 1 kb DNA Ladder (intron), (K+): control positive (pAct), (1,2,3,4,5): transgenic tomato plants and (W): control negative (*wild type*)

4. Conclusion

Transformation efficiency was obtained at 10 mgl^{-1} hygromisin antibiotic as an selection agent with the percentage of explants forming shoots 6.2%. PCR results showed that the plasmid pKYS: SoSUT1 already integrated in the explant and has obtained five clones of transgenic tomato plants.

5. Acknowledgements

We are thankful to Prof. Dr. Ir. Bambang Sugiharto, M.Sc., Research Center for Molecular Biology University of Jember and research grant from ‗Hibah Kompetensi Kemdiknas' for providing the necessary facilities.

6. References

[1]. Ling H.Q., Kriseleit D., Ganal, M.W. (1998), Effect of Ticarcillin/Potassium Clavulante on Callus Growth and Shoot Regeneration in *Agrobacterium*- mediated Transformation of Tomato (lycopersicon esculentum Mill.). *Plant Cell Reports* 17 : 843 -847,

[2]. McCormick S., J. Niedermeyer, J. Fry, A. Barnason, R. Horsch, and R. Fraley (1986), Leaf disc transformation of cultivated tomato *(L. esculentum)* using *A. grobacterium tumefaciens*. *Plant Cell Reports*, 5:81-84.

[3]. Santoso T.J., A. Sisharmini dan M. Herman (2009), Respon Regenerasi Beberapa Genotipe Dan Studi Transformasi Genetik Tomat (*Lycopersicon esculentum* Mill.) Melalui Vektor *Agrobacterium tumefaciens*, Balai Besar Penelitian dan Pengembangan Bioteknologi dan Sumberdaya Genetik Pertanian.

[4]. Ellul P, Garcia-Sogo B, Pineda B, Rios G, Roig LA & Moreno V. (2003), The ploidy level of transgenic plants in *Agrobacteriu-m*mediated transformation of tomato cotyledons (*Lycopersicon esculentum* L. Mill.) is genotype and procedure dependent, *Theor. Appl. Gen*., 106 (2): 231–238.

[5]. Cortina C. & F. A. Culi´añez-Maci` (2004),. Tomato transformation and transgenic plant production, *Plant Cell, Tissue and Organ Culture* 76: 269–275.

[6]. Frary, A. and E. D. Earle (1996), An examination of factors affecting the efficiency of *Agrobacterium-mediated* transformation of tomato, *Plant Cell Reports*, 16:235-240.

[7]. An, G. (1985), High efficiency transformation of cultured tobacco cells, *Plant Physiol*, 79:568-570.

[8]. Roekel J. S. C. van, B. Damm, L. S. Melchers, and A. Hoekema (1993), Factors influencing transformation frequency of tomato *(Lycopersicon esculentum), Plant Cell Reports* 12: 644-647.

[9]. Hu W. and G. C. Phillips (2001), A combination of overgrowth-control antibiotics improves Agrobacterium tumefaciens-mediated transformation efficiency for cultiveted tomato (L. esculentum), *Invitro Cell. Dev. Biol. Plant*, 37:12-18.

[10]. Qiu D., G. Diretto, R. Tavarza, G. Giuliano. (2007), Improved protocol for Agrobacterium mediated transformation of tomato and production of transgenic plants containing carotenoid biosynthetic gene CsZCD, *Scientia Horticulturae* , 112 : 172–175.

[11]. Huber, S.C. and J.L. Huber (1996), Role and regulation of sucrose-phosphate synthase in higher plant, *Annu. Rev. Plant Physiol. Plant Mol. Biol*. 47: 431 – 444.

[12]. Barker,L., Kuhn, C., Weise, A., Schulz, A., Gebhardt, C., Himer, B., Hellmann H., Schulze, W., Ward, J.M. and Frommer, W.B. (2000), SUT2, a putative sucrose sensor in sieve elements, *Plant Cell*, 12 : 1153-1164.

[13]. Sugiharto, B., H. Sakakibara, Sumadi, T. Sugiyama (1997), Differential expression of two genes for sucrose phosphate synthase in sugar cane: Molecular cloning of the cDNAs and comparative analysis of gene expression, *Plant Cell Physiol*. 38: 961-965.

[14]. Riesmeier, J.W., Himer, B., and Frommer, W.B. (1993), Potato sucrose transporters expression in minor veins indicates a role in phloem loading. *Plant Cell* 5 : 1591 -1598.

[15]. Wang, N.F.Q. (2003), Analysis of sugar transport-related gene products expressed in developing seeds of *Vicia faba* and *Hordeum vulgare,* Dissertation of Universität Halle-Witterberg, Germany.

[16]. Weise, A., Barker, L., Kuhn, C., Lalonde, S., Buschmann, H., Frommer, W.B., and Ward, J.M. (2000), A new subfamily of sucrose transporters, SUT4, with long affinity/high capacity localized in enucleate sieve elements of plants, *Plant Cell* 12 : 1345 – 1355.

[17]. Hackel A., N. Schauer, F. Carrari, A. R. Fernie, B. Grimm and C. Kuhn (2006), Sucrose transporter LeSUT1 and LeSUT2 inhibition affects tomato fruit development in different ways, *Plant Journal*, 45 :180–192.

[18]. Gonzales, A., Jimenez, A., Vazquez, D., Davies, J.E., Schindler, D. (1978), Studies on the mode of action of hygromycin B, an inhibitor of translocation in eucariotes, *Biochim. Biophys. Acta*, 521:459-469.

[19]. Nasir, M. (2002), Bioteknologi Molekuler Teknik Rekayasa Genetik Tanaman, PT Citra Aditya Bakti. Bandung.

[20]. Meng, Z., A. Liang and W. Yang (2007), Effects of hygromycin on cotton cultures and its application in Agrobacterium-mediated cotton transformation. *Invitro, Cell.Dev.Biol*., 43:111-118.

Cytotoxicity, Antioxidant and Antibacterial Activities of Methanol Extract of *Xylocarpus Moluccensis* Lam. Fruit Peel

Rahmi Nurdiani

Faculty of Fisheries and Marine Science, Brawijaya University, Malang, Indonesia
(rahminurdiani@yahoo.com)

Abstract

Xylocarpus molluccensis fruit is used in traditional medicine to treat bacterial and fungal infections. There is a need to evaluate extracts of each part of this fruit in order to provide scientific proof for its wide application in traditional medicine system. The aims of this study were to examine cytotoxicity, antioxidant and antibacterial activities of methanol extract of Xylocarpus moluccensis fruit peel. Cytotoxicity assay was undertaken by brine shrimp lethal toxicity test, antioxidant activity was done with Diphenyl picryl hydrazil (DPPH) scavenging method, and inhibition growth to Staphylococcus aureus and Escherichia coli used as antimicrobial test. The results showed that LC50 of fruit peel methanol extract was 1.6 x 10^5 ppm, antiradical efficiency (AE) was 0.0017x10^{-3}, and inhibition zones ranged from 6.43 ± 0.60 to 11.53 ± 2.23 mm and 6.7 ± 0.28 to 10.0 ± 2.69 mm for S. aureus and E.coli, respectively. Low cytotoxic, antioxidant and antibacterial activities were established from the methanol extract of Xylocarpus moluccensis fruit peel

***Keywords**: Cytotoxicity, antioxidant, antibacterial, methanol extract, fruit peel, Xylocarpus moluccensis.*

1. Introduction

The research into biologically active compounds from natural sources has always been of great interest for scientists looking for new sources of useful drugs against infectious diseases [1]. In recent years, resistance to these drugs by pathogenic bacteria microorganisms has increased and this had caused serious clinical problems in the treatment of infectious diseases [2,3].

Medicinal plants constitute an effective source of both traditional and modern medicine. Herbal medicine has been shown to have genuine utility and about 80% of rural populations depend on it as their primary health care [4]. Recently, much attention has been paid to *Xylocarpus* species due to limonoids with unique C-skeletons and their tumor cytotoxic activities. The chemical constituents of Xylocarpus include triterpenoids, alkaloids, phenolic acids, flavanoid, steroids, monoterpenes, and some others [5].

Xylocarpus granatum and *X. moluccensis are* considered to have astringent, antidiarrhea, antiemetic and haemostatic properties [6]. The fruits of *X. moluccensis* are green in color and are used as a cure for elephantiasis and swelling of the breast. The seeds or peels of the fruits are utilized to poultice swellings [7]. The mature fruits of *X. moluccensis* are used as aphrodisiacs [8]. There is a need to evaluate extracts of each part of this fruit in order to provide scientific proof for its wide application in traditional medicine system.

The aim of this research was to examine cytotoxicity, antioxidant and antibacterial activities of methanol extract of *Xylocarpus moluccensis* fruit peel.

2. Experimental Details

Collection of Samples

Plant materials were collected from bank of Porong‘s river estuary, in fresh condition. Fruits of *Xylocarpus moluccensis* were packed in polyethylene plastic and eventually brought to laboratory. The fruit was peeled to separate the peel and other fruit parts. The peel was then dried until ± 15% water content used for dry extract preparation.

Solvents Used

Organic solvent methanol was used to prepare the extracts. The solvent used was of analytical grade.

Extraction

The *Xylocarpus moluccensis* fruit peel was extracted by maceration method. The 25 g dried fruit peel was soaked in 75 ml methanol in an Erlenmeyer for 24 hour. The extract was then separated from the debris by filtration and was concentrated under reduced pressure in a rotary vacuum evaporator.

Cytotoxix assay

Cytotoxicity of methanol extract of fruit peel was assayed using brine shrimp lethally test (BSLT). Brine shrimp eggs were hatched for 48 h in a conical flask containing 500 mL of seawater. The flasks were well aerated with the aid of an air pump and kept in a water bath at 29–30ºC. A bright light source was left on and the nauplii hatched within 48 h. An aliquot of each concentration (1mL) was transferred, and seawater (9 mL) was added. Ten shrimp nauplii were transferred to each vial. After 24 h the numbers of survivors were counted and percentage of death calculated. The concentration that killed 50% of the nauplii was determined using the statistical method of PROBIT analysis. Extracts giving LC^{50} values greater than 1000 ppm were considered to be nontoxic.

Antioxidant Assay

DPPH radical-scavenging activity method was used for antioxidant assay. A 1 ml of different concentrations of plant crude methanol extract was added to 3 ml DPPH solution (0.2 mM in methanol) as free radical source. The Scavenging activity was measured using spectrophotometer. The absorbances were recorded after from 0 to 30 min at room temperature. The disappearance of DPPH was read spectrophotometrically at 515 nm. Values the IC_{50} were calculated, which represents the concentration of the scavenging compound that caused 50% neutralization. The time needed to reach the steady state to EC concentration was 50 (TEC_{50}) calculated graphically. Antiradical efficiency (AE) [9], which combines EC_{50} and TEC_{50}, was defined:

$$AE = \frac{1}{EC_{50} \times T_{EC50}}$$

AE = Antiradical efficiency
EC_{50} = Effectives concentration
T_{EC50} = the time needed to reach the steady state to EC_{50}

Bacterial Strains Used for Assay

Microbial strains viz. *Staphylococcus aureus and Escherichia coli* were obtained from the Laboratory of Medical Microbiology (Faculty of Medical- Brawijaya University). The bacterial stock cultures were maintained on Muller Hinton Agar.

Antibacterial Assay

The antibacterial activity test was done using paper disc diffusion method [10]. The 6mm discs were impregnated crude extracts and placed in the inoculated Muller Hinton agar. The inoculated plates were incubated at 35ºC for 24-28 hours. Control was maintained with solvent alone. The inhibition zone around each disc was measured in millimeter.

3. Result and Discussion

Cytotoxic assay

The results of the cytotoxicity assay of the methanol extract of *Xylocarpus moluccensis* fruit peel using BSL method is shown in Figure 1.

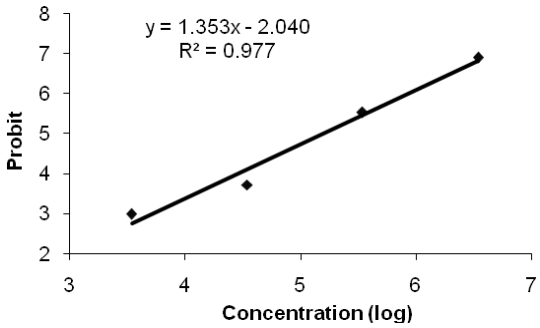

Figure 1. The toxicity effects of the methanol extract of *Xylocarpus moluccensis* fruit peel using brine shrimp lethality assay

The methanol extract of *Xylocarpus moluccensis* fruit peel has no significant cytotoxic activity against brine shrimp with an LC_{50} value of 1.6×10^5 ppm. Based on Simionatto *et al.,* [11], the result exposed that the methanol extract of *Xylocarpus moluccensis* fruit peel might be has no potency to be used in cancer cell line therapy but this signified that it might be not toxic to human.

Several studies have shown that brine shrimp assay has been an excellent method for preliminary investigations of toxicity, to screen medicinal plants popularly used for several purposes and for monitoring the isolation a great variety of biologically active compounds [12]. The technique is easily mastered, costs little, and utilizes small amount of test material. Since its introduction, this *in vivo* test has been successively employed for bioassay guide fractionation of active cytotoxic and antitumor agents [13]. Furthermore, a positive correlation between the lethality to brine shrimp and the corresponding oral lethal dose in mice of medicinal plants has been demonstrated by Parra *et al* [14].

Antioxidant assay

DPPH method has widely used to analysis antioxidant activity of natural products. The DPPH antioxidant assay is based on the ability of 1, 1-diphenyl-2-picryl-hydrazyl (DPPH), a stable free radical, to be decolorized in the presence of antioxidants [15]. The result of antioxidant assay using DPPH method is shown in Figure 2.

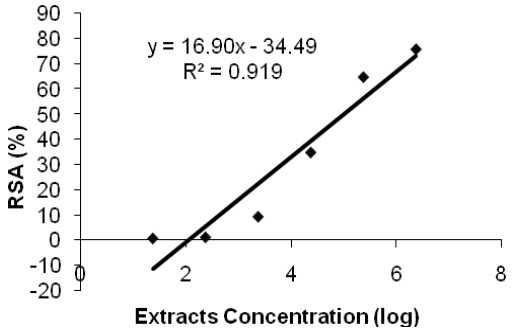

Figure 2. EC_{50} of the *Xylocarpus moluccensis* fruit peel methanol extract

The EC50 obtained was 99360 ppm while the TEC50 was 5.86 minutes. As a result, the antiradical activity of the *Xylocarpus moluccensis* fruit peel methanol extract was $0.0017x10^{-3}$. It was assumed that antiradical activity of the extract was low based on Sanchez-Moreno classification. The low antioxidant activity of the extract may be the result of extracts impurities.

Recent researches revealed that fruit peels of grape [16], banana [17], dragon fruit [18] and pomegranate [19], may potentially possess antioxidant properties. Polyphenols, as one of phenolic compounds, play the main role in contributing to the overall antioxidant activity. It has also been recognized for some time that several classes of flavonoids play a significant role in many physiological processes and show antioxidant and fungicidal activity [20] and are natural antihistamines. Flavonoid, and flavonol-lignan derivatives inhibit lipid peroxidation and are potentquenchers of triplet oxygen.

Antibacterial assay

Methanol extracts of *X. mollucensis* fruit peel were active against one or more of the tested organisms. However, as shown in Table 1, the extracts showed low in vitro potential of antimicrobial activities against *Staphylococcus aureus* and *Eschericia coli*. In general, medium inhibition zones ranged from 6.43 ± 0.60 to 11.53 ± 2.23 mm and 6.7 ± 0.28 to 10.0 ± 2.69 mm for *S. aureus* and *E.coli*, respectively.

Based on the color of and phytochemical screening, antibacterial compounds that might be exist in fruit peel of *X. moluccensis* are flavonoid and alkaloid and this is probably the natural defense against microorganism. *Xylocarpus* sp. contained N-Methylflindersine that was known as antibacterial compound. Catechin, the bioactive compound that can inhibit the growth of lactic acid bacteria also was found by [21].

Tabel 1. Antibacterial activity of the methanolic extract of *Xylocarpus moluccensis* fruit peel against tested organisms.

Concentration (ppm)	Inhibition zone (mm)	
	S.aureus	*E. coli*
840000	11.53±2.23	10.0±2.69
84000	7.45±0.07	8.43±0.74
8400	7.05±0.21	7.68±0.25
840	6.98±0.18	7.05±0.35
84	6.45±0.63	6.85±0.35
8.4	6.43±0.60	6.7±0.28

4. Conclusion

The methanol extract of *Xylocarpus moluccensis* fruit peel showed low cytotoxicity, antioxidant and antibacterial activities. Further investigation on purified extract is necessary to obtain more comprehension result.

5. Acknowledgments

This research was partially funded by Indonesia's Directorate of Higher Education.

6. References

[1] Cohen M.L., (1992), Epidemiology of drug resistance: implications for a post antimicrobial era. *Science*, 257:1050-1055.

[2] Mishra NN, Prasad T, Sharma N, Paysi A, Prasad R, Gupta DK, Singh R., (2007), Pathogenicity and drug resistance in *Candida albicans* and other yeast species. A review. *Acta Microbiol Immunol Hung*, 54:201-235.

[3] Torres JA, Villegas MV, Quinn J.P., (2007), Current concepts in antibioticresistant Gramnegative bacteria. *Expert Rev Anti Infect Ther*, 5:833-843.

[4] World Health Organization (1978), The promotion and development of traditional medicine. Geneva: World Health Organization, (Technical report series no. 622).

[5] Shen L.R., D Guo, Y.M. Yu, B.W. Yin, L. Zhao, Q.W. Shi, Y.L. Wang, and C.H. Huo (2009), Chemical constituents of plants from

the genus Xylocarpus, *Chemistry & Biodiversity*, 6, 1293-1308

[6] Kokpol, U., Miles, D.H., Payne, A.M. and Chittawong, V., (1990), Chemical constituents and bioactive compounds from mangrove plants. *In:* Atta-ur-Rahman (ed) Studies in Nat.Prod. Chemistry, Vol. 7. Elsevier Science Publishers B.V., Amsterdam, pp. 175–195

[7] Lakshmi, V., and Gupta, P., (2008), An Overview of the Genus Xylocarpus. *Natural Product Research*. 22 (14): 1197-1224

[8] Sarker, S. D., S. J. Uddin, J. A. Shilpi, R. Rouf, M. E. M. Ferdous, L. Nahar (2007), *Fitoterapia* 78, 107

[9] Sanchez-Moreno, C. S., Larrauri, J.A., Calixto, F.S., (1998), A procedure to measure the Antiradical Efficiency of polyphenols. *J Sci Food Agric*. 76: 270-276

[10] Sagdic, O, and Ozcan, M., (2003), Antibacterial activity of Turkish spice hydrosol. *Food Cont*. 14; 141-143

[11] Simionatto E, Porto C, da Silva UF, Squizani AMC, Dalcol II, Morel AF., (2005), *J Braz Chem Soc*. 16:1458–1462

[12] Quignard EL, Pohlit AM, Nunomura SM, Pinto AC, Santos EV, Morais SK, Alecrim AM, Pedroso AC, Cyrino BR, Melo CS, Finney EK, Gomes EO, Souza KS, Oliveira LC, Don LC, Silva LF, Queiroz MM, Henrique MC, Santos M, Pinto PS, Silva S.G., (2003), Screening of plants found in Amazonas state for lethality towards brine shrimp. *Acta Amazon*, 33:93-104.

[13] Pisutthanan S, Plianbangchang P, Pisutthanan N, Ruanruay S, Muanrit O., (2004), Brine shrimp lethality activity of Thai medicinal plants in the family Meliaceae. *Naresuan Univ J*, 12:13-18.

[14] Parra AL, Yhebra RS, Sardinas IG, Buela L.I., (2001), Comparative study of the assay of *Artemia salina* L. and the estimate of the medium lethal dose (LD50 value) in mice, to determine oral acute toxicity of plant extracts. *Phytomedicine*, 8:395-400

[15] Kumarasamy, Y., Byres, M., Cox, P. J., Jaspars, M.., Nahar, L., Sarker, S. D., (2007), Screening seeds of some Scottish plants for free-radical scavenging activity, *Phytotherapy Research*; 21: 615-621.

[16] Negro C, Tommasi L, Miceli A., (2003), Phenolic compounds and antioxidant activity from red grape marc extracts. *Bioresource Technol*., 87: 41-44.

[17] Mokbel M.S and F. Hashinaga (2005), Antibacterial and Antioxidant Activities of Banana (*Musa*, AAA cv. Cavendish) Fruits Peel. *American Journal of Biochemistry and Biotechnology* 1 (3): 125-131.

[18] Nurliyana, R., Syed Zahir, I., Mustapha Suleiman, K., Aisyah, M.R. and Kamarul Rahim, K., (2010), Antioxidant study of pulps and peels of dragon fruits: a comparative study. *International Food Research Journal 17: 367-375*

[19] Singh RP, Murthy KNC, Jayaprakasha G.K., (2002), Studies on the antioxidant activity of pomegranate (*Punica granatum*) peel and seed extracts using *in vitro* models. *J. Agric. Food Chem.*, 50: 81-86

[20] Larson, R.A., (1988), The antioxidants of higher plants. *Phytochemistry*. 27: 969–978.

[21] Liu , C.R., Chen Y., (2004). Advance of chemistry and bioactivities of catechin and its analogues. *China J. Chin. Mater.Med*. 29, 1017

Study of Antibacterial and Cytotoxic Activity of *Porphyra Sp* Extract

Raja B.D. Sormin [1], Sukoso [2], Happy Nursyam [3], Siti Rasminah Ch. Sy [4]

(1) Faculty of Fisheries and Marine Science, University of Pattimura, Ambon (rbd.sormin@yahoo.com)
(2,3) Faculty of Fisheries and Marine Science, University of Brawijaya, Malang
(4) Faculty of Agriculture, University of Brawijaya, Malang

Abstract

The aim of this study was to find out the antibacterial and cytotoxic activity of Porphyra sp extracted by n-hexan, ethyl acetate and methanol. For antibacterial test, disc diffusion technique was used against 3 human pathogenic bacteria those were Escherichia coli, Stapilococcus aureus and Salmonella tipy, while the Brine shrimp lethality bioassay method was used to determine the cytotoxicity activities. The range of inhibition zone of n-hexane, ethyl acetate and methanol extracts was 6.4 to 15.41 mm. The LC_{50} values of n-hexane, ethyl acetate and methanol extracts were 567.49, 108.29, and 270.46, respectively.

***Keywords**: antibacterial, cytotoxic, Porphyra sp., extract.*

1. Introduction.

Seaweed or marine macroalgae is a potential renewable resource in the marine environment. About 6,000 species of seaweed have been identified and classified as green algae (*Chlorophyta*), brown algae (*Phaeophyta*) and red algae (*Rhodophyta*). Global production of seaweed in the world in 2004 was more than 15 million metric tons which 1.3 million tons of them harvested free from the ocean and 14.8 million tons of aquacultured [1].

Seaweeds of certain species are harvested and used as a food ingredient, as a source of medicines, as a source of chemicals for industry and as agricultural fertilizer. Seaweed as raw materials of diet has been known since ancient in oriental area because it is nutritious and contain many vitamins, dietary fiber, minerals and protein that is very good for health [2,3]. Hydrocolloid products produced by seaweed has also been used as a raw material for cosmetik, pharmaceutical and food industries [4,5].

The main types of seaweed that becomes an important food ingredient in several countries like Japan, China and Korea are a genus of Undaria (commonly called wakane), Porphyra (nori) and Laminaria (kombu). Development of seaweed research as a source of bioactive components including carotenoids, fatty acids and phytosterols have become a serious concern, as have been reported that those components have a function as an antioxidant, antibacterial, anticoagulant, antitumor, and anticancer [3-6].

In Indonesia, there are several types of economically valuable seaweeds such as Eucheuma, Gracilaria, Gellidium, Sargassum and Hypnea, and some species have been cultivated like *Eucheuma cottoni*.

In addition to the type of seaweeds that have been widely recognized and valued economically in Indonesia, there are still many types of seaweeds that have been used locally by the community for generations both as vegetable and medicine. Algae of *Porphyra* species, for example, is kind of local seaweed called as runut by the people in the Wassu village, District of Haruku Island, Central Maluku regency or sea vegetables in the village Hukurila Ambon, Maluku. This Alga comes from the division Rhodophyta that grows / attached to rocks in the tidal area. Its appear when the east season began, its growth once a year between June and September. The habits of the community on consuming sea vegetable have been carried out for generations and even before a foreign from western finded that place. Written evidence left by Rumphius (1750), Dutch biologist, German-born, explains that in the 16th century when the Dutch occupied the island of Ambon, the local community were used to cook a variety of macro-algae with various spices and other ingredients to produce delicious cuisine. Traditionally, in the medical field It is believed that sea vegetable is able to facilitate digestion, lowers cholesterol and healing fever [7].

The genus Porphyra, traditionally known as *nori* in Japan, *kim* in Korea and *zicai* in China, is a popular and delicious food as well as nutritious as it contains protein, vitamins, minerals and dietary fiber [8]. This type of algae is also reported to contain iodine ranged from 2.20 to 7.32 mg / kg [9], bioactive substances, and

anti-fungal components, and other mineral components [10]. Bioactive components of seaweed are also known to show antibacterial activity [11,12]. Bansemir *et al* (2006) reported that screening on dicloromethane, methanol and water extract of various types of cultivated seaweed showed antibacterial activity [13]. This research aims to study the antibacterial and cytotoxic activity of the extract of *Porphyra sp*.

2. Experimental Details

Materials

Materials used in this research were *Porphyra sp* collected from the Hukurilla village, Ambon. Seaweed is harvested from the substrate and then dried and packaged for further analyzed.

Bacterials culture used in this research *were Escherichia coli, Stapilococcus aureus and Salmonella tipy*. Artemia salina eggs were used for Brine shrimp lethality test (BSLT).

Chemicals used in this study were: methanol, n-hexane, ethyl acetate, sea water, DMSO, and Muller Hinton Agar.

Extraction of seaweed.

Seaweed is cleaned, dried and mashed. Sequentially, 600 grams seaweed extracted with hexane, ethyl acetat and methanol in a maseration vial for 24 h. Then filtered and evaporated using a rotary vacuum evaporator to obtain viscous extract. Residues resulting from the maceration with n-hexane and then wind dried, then macerated using 600 ml ethyl acetate for 24 hours. Then filtered and evaporated using a rotary vacuum evaporator. The resulting residue and then wind dried and then macerated again with 600 ml methanol for 24 hours. Then filtered and evaporated using a rotary vacuum evaporator. All the three extracts of seaweeds were tested for their antibacterial and cytotoxic activity.

Antibacterial assay.

Antimicrobial test procedure performed by diffusion method (Bauer *et al*., 1966) as follows: Plate for Muller Hinton Agar (MHA) is marked with name, date and microorganisms to be tested. Then the sterile cotton swab dipped in a suspension culture of samples with OD: 0.1 CFU / ml. Next is the cultivation of microorganisms on the surface of the plate by wiped. Cotton swab wiped horizontally to obtain equitable growth, and then rotated the plate for 90°. The second spread with a plate rotated 45° and the third smear until all plate surfaces wiped. Plate is left to dry for approximately 5 minutes, then placed a paper disc that has been soaked with the sample tested on the surface of the plate. In 1 plate can be used for 5-6 treatment dosage, the distance between the paper disc should be large enough so that the clearl region does not coincide with each other, so that it will not difficult to measure the inhibition zone. Further, plates were incubated for 24 h at optimal growth temperature of bacterial pathogens. Finally, the clear zone can be measured by measuring the diameter.

Cytotoxicity screening.

Brine shrimp lethality bioassay (BSLT) is widely used in bioassay for bioactive compounds [14,15]. Artemia salina is used as an indicator or test animals. Artemia salina eggs hatched in a tank containing sea water and illuminated by a lamp 40 watts for 48 hours. Cytotoxicity screening performed on *Artemia salina* nauplii using the method of Meyer [14]. Samples (extracts) were prepared by dissolving it in DMSO (no more than 50 µL in 5 ml solution). Sea water is added to achieve concentrations of 50, 100, 150 and 200 ppm.

A vial containing 50µl diluted to 5ml DMSO was used as control. Then from each dilution is inserted to the bottles according to the desired screening treatment, and control is made without the extract. A total of 10 *Artemia salina* inserted into each bottle and also in the control bottles. After 24 hours, the bottle was examined using a magnifying glass and the number of survived nauplii in each vial was calculated. From this data, the percent (%) of nauplii was calculated for each concentration.

Data Analysis

Experimental design used for antibacterial test was completely randomized design with 2 factors: the type of bacteria and the type of extracting solvent. Each treatment is repeated 3 times, the significantly treatment continued by LSD Test [16]. As for toxicity tests (BSLT) performed with regression test.

3. Results and Discussion

Antibacterial assay

Based on statistical analysis of variance showed that treatments of seaweed extract *Porphyra sp* (n-hexane, ethyl acetate and methanol) and the type of bacteria (*Escherichia coli, Stapilococcus aureus and Salmonella tipy*) has a very significant effect on the inhibition zone in diffusion method. Furthermore, the results of LSD tests results are obtained as listed in Table 1. From Table 1, it can be seen that the type of the solvent of ethyl acetate has the highest ability to inhibit bacterial growth when compared with other solvents. The most inhibited bacteria growth

was *Escherichia coli,* and the inhibition zone was 15.41 mm.

Table 1. Antibacterial activity of seaweed *Porphyra sp*. extract by diffusion method

Type of Bacteria	Extractor	Diameter of zone of inhibition mm)
Escherichia coli	n-hexane	12.23 c
	Ethyl acetate	15.41 a
	Methanol	6.27 g
Stapilococcus aureus	n-hexane	7.2 f
	Ethyl acetate	10.16 e
	Methanol	6.51 g
Salmonella typi	n-hexane	11.61 d
	Ethyl acetate	14.3 b
	Methanol	6.4 g

Description:
The figures in column diameter of inhibition followed different letters (a, b, c, d, e, f, and g) showed significant differences at (p <0.05).

Cytotoxicity bioassay

According to Mc Laughlin and Rogers [17], cytoxicity based BSLT test is divided into 3 categories: LC50> 1000 ppm expressed as inactive, LC50 30-1000 ppm expressed as active and LC50 <30 ppm expressed as very active. Results from extracts BSLT.

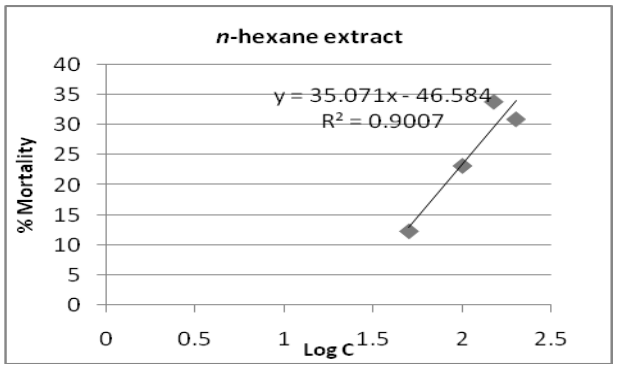

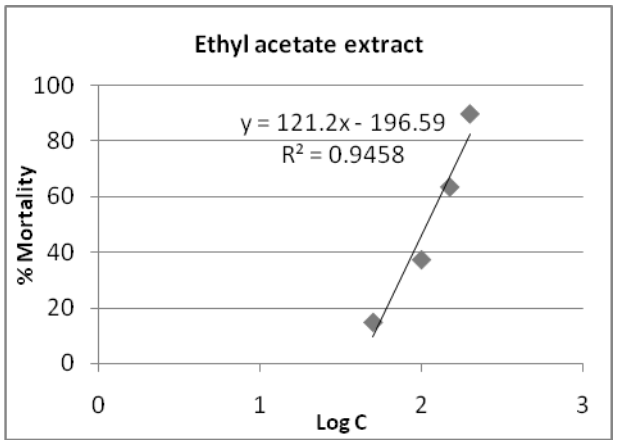

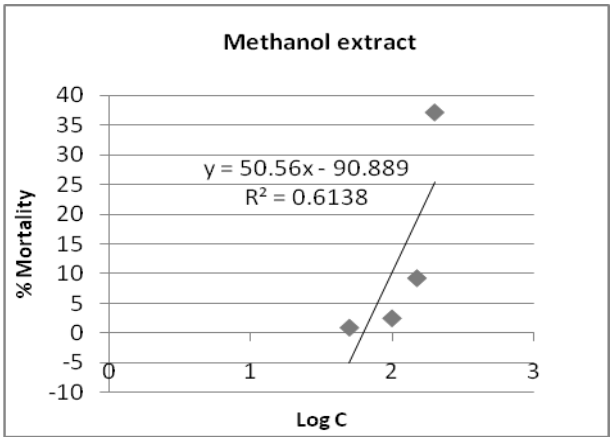

Figure 1. Correlation between the logarithmic concentration of the extract with the percent mortality of *Artemia salina* extract of *Porphyra sp*.: n-hexane extract (top), ethyl acetate extract (middle) and methanol extract (bottom).

Table 2. The Results BSLT Test (LC_{50}) of 3 extracts of seaweed *Porphyra sp*.

No.	Extracts	LC_{50} (ppm)
1	n-hexane	567.49
2	Ethyl acetate	108.29
3	Methanol	270.46

From these observations, the all three extracts of seaweed *Porphyra sp* categorized as active, according to the categories proposed by Mc Laughlin and Rogers [17], But from all extracts, the ethyl acetate extract was, arguably, the most active.

4. Conclusion.

The most active extract of seaweed *Porphyra sp*. in inhibiting the growth of *Escherichia coli*, *Stapilococcus aureus* and *Salmonella tipy* is ethyl acetate extract. The cytotoxicity tests showed that although extracts of n-hexane, ethyl acetate and methanol considered active but the ethyl acetate extract was the most active.

5. Acknowledgments

---

6. References

[1]. FAO, (2007), Year book of fishery statistics 2005 (Vol 100-1/2). Rome: Food and Agricultural Organization.

[2]. Dawczynski, C., Schubert, R., and Jahreis, G., (2007), Amino acids, fatty acids, and dietary fibre in edible seaweed products. *Food Chemistry,* 38(3); 674-677.

[3]. Lee, S.B., Lee, J.Y., Song, D.G., Pan, C.H., Nho, C.W., Kim, M.C. (2008), Cancer chemopreventive effects of Korean seaweeds extracts. *Food Science and Biotechnology,* 17(3), 613-622.

[4]. Chandini, S.K., Ganesan, P., and Bhaskar, N., (2008), Invitro antioxidant activities of three selected brown seaweeds of India. *Food Chemistry.* 107(2); 707-713.

[5]. Chandini, S.K., Ganesan, P., Suresh, P.V., and Bhaskar, N., (2008), Seaweeds as a source of nutritionally beneficial compounds-A review. *Journal of Food Science and Technology* 45(1); 1-13.

[6]. Nagai, T., and Yukimoto, T., (2003), Preparation and fungtional properties of beverages made from sea algae. *Food Chemistry,* 81(3); 327-332.

[7]. Rohmimohtarto and Sri Jualana (2005) Biologi Laut. Gadjah Mada University Press. Yogyakarta.

[8]. Sahoo, D., Tang, X., and Yarish, C., (2002), *Porphyra* – the economic seaweeds as a new experimental system. *Current Science*, 83; 1313-1316.

[9]. Sormin, R.B.D., Loppies, C.R.M dan Mamesah, J.A.B. (2007), Identifikasi dan Sifat Fisiko-Kimia Runut. Laporan Penelitian Fundamental. UPATTI. AMBON.

[10]. Rao, P.V.S., Mantri, V.A., and Ganesan, K. (2007), Mineral composition of edible seaweed *Porphyra vietnamensis*. *Food Chemistry* 102: 215-218.

[11]. Vairappan, C.S., Daitoh, M., Suzuki, M., Abe, T., Masuda, M., (2001), Antibacterial halogenated metabolites from the Malaysian Laurencia species. *Phytochemistry* 17: 291-293.

[12]. Vlachos, V., Critchley, A.T., von Holy, A., (1999), Differential antibacterial activity of extracts from selected Southern African macro alga thalli. *Bot. Mar.* 42: 165-173.

[13]. Bansemir, A., Blume, M., Schroder, S., and Lindequist U., (2006), Screening of cultivated seaweeds for antibacterial activity agaisnt fish pathogenic bacteria. *Aquaculture* 252: 79-84.

[14]. Meyer, B.N., N.R. Ferrigni, J.E. Putnam, J.B. Jacobsen, D.E. Nicholsand and J.L. Mc Laughlin (1982), Brine shrimp; a convenient general bioassay for active plant constituents, *Planta Medica* 45, pp.31-34.

[15]. Zhao, G.X., Y.-H. Hui, J.K. Rupprecht, J.L. McLaughlin, and K.V. Wood (1992), Additional bioactive compounds and trilobacin, a novel highly cytotoxic acetogenin, from the bark of *Asimina triloba*, *Journal of Natural Products*, 55, 347-356.

[16]. Sastrosupadi, A, (2000), Rancangan Percobaan Praktis Bidang Pertanian. Penerbit Kanisius, Yogyakarta.

[17]. Mc Laughlin, J.L and Rogers, L.L. (1998), The use of biological assay to evaluate botanical. *Drug Information J.* 32: 513-524.

Superoxide Dismutase (SOD) Activity and Histological Pancreas Tissue of Type 1 Diabetes Mellitus Rat Treated with Temu Giring Extract (*Curcuma heyneana)*

Rosalina A.L. [1], Aulanni'am [2], Chanif Mahdi [3]

[1,2,3] Department of Chemistry, Sciences Faculty, Brawijaya University, Malang, Indonesia
(deeochalina@yahoo.com; aulanibiochem@ub.ac.id;chanif_mahdi@yahoo.com)

Abstract

Diabetes mellitus (DM) is often known as the great imitator. The DM disease can cause organ damage in either the overall anatomy or functional. One alternative treatment of diabetes mellitus is using herbal therapy of temu giring (Curcuma heyneana) rhizome extract. This study aimed to explain the ability of rhizome extract temu giring (Curcuma heyneana) in increasing SOD activity and repair damaged pancreatic tissue of diabetic rats induced by MLD-STZ. In this study, we used animal model of type I diabetic rats by Multiple Low-Dose Streptozotocin (MLD-STZ) dose 20 mg/kgWB for 5 consecutive days. Temu giring extract as an alternative therapy was administrated to trial animals with varying doses of 1.25, 2.5 and 3.75 g/kgWB for 7 consecutive days. The results showed that temu giring rhizome extract therapy doses of 1.25, 2.5 and 3.75 g/kgWB in rats induced by MLD-STZ showed the increase of SOD activity in a consecutive at 29.42%, 52.30% and 80.16%, and repair pancreatic tissue damage. Maximum therapies in type 1 diabetic rats are shown in the temu giring extract dose of 3.75 g/kgWB.

Keywords: *DM type 1, MLD-STZ, Temu giring (Curcuma heyneana).*

1. Introduction

Diabetes Mellitus (DM) is known as the great imitator. The DM disease can cause organ damage in either the overall anatomy or functional [2]. According to WHO survey of DM cases in Indonesia in 2000 is 8.4 million people were on the fourth of the world after India (31.7 million), China (20.8 million), and the United States (17.7 million). WHO estimates that will increase in 2030, India (79.4 million), China (42.3 million), United States (30.3 million), and Indonesia (21.3 million) [9].

People with diabetes are facing danger every day because blood glucose levels are not controlled. This is due to of pancreatic cannot produce enough insulin or when the insulin produced is not be able to work effectively.

DM consisted of DM type 1 and 2. DM type 1 is characterized by selective destruction of pancreatic beta cells producing insulin via cellular mediated autoimmune mechanism. An infiltration imflamatori cells into Langerhans Island, ie insulitis, usually known to precede the destruction of beta cells in people with type 1 DM.

The damage of pancreatic ß cells through cellular mediated autoimmune mechanism caused by oxidative stress due to increased levels of free radicals leading to decreased levels of antioxidants of the body is superoxide dismutase (SOD) produced by the body cells that function inhibits superoxide radical reaction.

Free radicals produced by the body and the outside of body that is in sufficient quantity caused damage cells. Streptozotocin (STZ) is a group of N-nitroso compounds is a source of free radical NO [7]. Radical NO can trigger necrosis of pancreatic beta cells through an autoimmune reaction [5].

One alternative treatment of diabetes mellitus is using herbal therapy of temu giring *(Curcuma heyneana)* rhizome extract. Temu giring contain the essential oil that is not less than 1.5% v/w, monoterpenes, sesquiterpenes, polyphenols compounds (flavonoids, tannins and curcumin), saponins, alkaloids and piperazin citrate [8].

One of the activities compounds contained in the temu giring is catcher antioxidant activity of free radicals. Increasing of free radicals that exist in the pancreas is causing pancreatic beta cell damage that is characteristic of type 1 DM, therefore temu giring polyphenol-containing compounds (flavonoids, tannins and curcumin) and terpenoids and alkaloids are expected to reduce levels of free radicals. Kuswinarti research using water extracts of rhizome of Curcuma heyneana 2g/kgWB dose proven to reduce blood cholesterol levels of male rats [4]. In addition, Adnyana investigation using ethanol extract of noni dose of 0.5 and 1 g /kgWB and proven to reduce blood glucose levels of rats [1]. In this research, we use aqueous extract so the temu

giring extract doses will rise to 1.25, 2.5, and 3.75 g/kgWB.

Based on the description above, this research will be assessed the ability of rhizome extract temu giring (*Curcuma heyneana*) as free radical scavanger on trial animals type 1 DM that then be used as an alternative treatment of diabetes mellitus.

2. Experimental Details

Preparation of Temu Giring (Curcuma heyneana) Extract

The rhizome of temu giring cleaned with running water, dried and milled to a powder. The powder obtained roasted until free of water. Then, 25 g of powdered rhizome temu giring free water added in 100 mL aquadest. Then it is heated and filtered using a fabric. Distillate evaporated to 10 mL. Then, weighed a total weight of extract obtained. To know the weight of extract without the water of temu giring, then count the water content of the temu giring extract.

Preparation of Streptozotocin (STZ) Solution and Intraperitoneal Injection

Streptozotocin 100 mg dissolved in 3 ml citrate buffer pH 4.5 then vortex until homogeneous. STZ which will be injected was taken from the stock solution. Volume was adjusted with weight body of injected rats. Dose that used was 20 mg/kgWB 5 times in consecutive days.

Preparation of Rat Diabetes (DM) and Control

Rats were injected with STZ were incubated for 7-14 days. During 7-14 days rats monitored their blood glucose levels using a glucometer to determine the condition of diabetic rats. Mice had become diabetic if their blood glucose levels above 300 mg / dl.

Diabetes Rats Therapy with Rhizome Extract Temu Giring

DM rats treated with extracts of rhizome Intersection sleigh with doses of 1.25, 2.5, and 3.75 g / kg BW for 7 times (7 days in a row). About 25 g of powdered rhizome temu free sleigh in 100 mL water plus distilled water. After it is heated and filtered using a cloth. Distillate was evaporated to 10 mL.

Embedding Pancreas

The first step is soaking the pancreas in a solution of formalin or PFA (1-7 days). Then soaked in 70% ethanol for at least 24 hours, and continued with 80% ethanol for 2 hours. It was then soaked in ethanol 90% and 95% respectively for every 30 minutes. Continue immersed 3 times in absolute ethanol for 30 minutes. Each of the ethanol was in a different bottle. Xylol soaked in as much as 2 times for 30 minutes. The process is then performed in an incubator temperature of 56-58ºC. Soaked in xylol for 3 times, paraffin 3 times, followed by embedding with pancreatic dipped in liquid paraffin was poured in the container. After that paraffin will solidify and pancreas is in a block of paraffin (method Bancroft).

Making pancreas preparate

The pancreas in blocks of paraffin embedding results entered on the clamp (Block holder) microtome and arranged parallel to the surface of the microtome knife cuts. The cutting is set with thickness of the piece above 10 µm to accelerate the achievement of tissue slices. Pancreas sliced with size 5 µm. Good cuts will result in the form of pieces such as tape. Slices were taken with a brush and water included (room temperature) to open folds that may occur in preparate. Results slices removed with a brush into the warm water 38-40ºC to straighten the existing fine wrinkles. Sliced which runs perfectly taken with glass objects. The selected pieces are dried and placed on a hot plate 38-40ºC until dried and then preparate is stored in an incubator temperature of 38-40ºC for 24 hours.

Hematoxylin-Eosin Staining

Hematoxylin-eosin staining begins from deparafinisasi that is preparate included in xylol assessed 1-3 for 5 minutes. Next on rehydration stage, preparate included in ethanol assesed starting from absolute ethanol 1-3, ethanol 95, 90, 80 and 70% each for 5 minutes, and then soaked in aquadest for 5 minutes. The next step is the coloring. Preparate included in the dye tube hematoxylen to get the best color. Ten minutes enough to penetrate the color of the preparate. Subsequently washed with running water for 30 minutes, and then rinsed with aquadest before stained with eosin. After rinsed with aquadest, preparate including in eosin alcohol was stained for 5 minutes. The next phase is dehydration with includes the preparate in ethanol series of the rise from 80, 90 and 95% to absolute ethanol 1-3. Further clearing is done by inserting the preparate in xylol 1.2 and dried. Next step is mounting with entellan.

Superoxide Dismutase (SOD) Determination

Sampel Preparation

Pancreas homogenate sample was diluted with dilution buffer with the volume ratio 1:2 that

is by dissolving 15 µL sample solution in 30 µL dilution buffer.

SOD Measurement

Each well on the ELISA plate filled with 115 µL assay buffer. Then each well added 5 µL of assay buffer for blank or 5 µL of sample and incubated for 2 minutes. Then added 5 µL of reagent hematoxylin and measured absorbance at λ 560 nm every 3 min for 30 minutes. Between the old measurements were plotted against the measured absorbance to obtain the line equation to calculate the SOD activity.

SOD activity sample calculation was measured based on rate of hematoxylin autooxidation. The rate can be obtained from the linear regression equation curve of hematoxylin autooxidation:

$$\mathbf{Y = ax + b}$$

a=the rate of autooxidation or (ΔAbs560nm/minute)

Then, calculate the ratio of sample rate (s) and blank (b) with the formula:

$$Ratio_{s/b} = \frac{\text{the average of rate autooxidation by sample (as)}}{\text{the average of rate autooxidation by blank (ab)}}$$

Then calculate the percent inhibition SOD:

$$\% \text{ inhibition} = (1 - Rasio_{s/b}) \times 100\%$$

Finally, SOD activity obtained with the formula:

SOD (U/ml) = 1.25 x (%inhibition) x dilution factor

3. Result and Discussion

Profile Superoxide Dismutase (SOD) in Rat Pancreas Control, Rat Induced by MLD-STZ and Rat Therapy Extract Temu giring

Superoxide dismutase is an antioxidant enzyme that plays a role in catalizing free radicals superoxide onto oxygen and hydrogen peroxide. The increasing of excess ROS level may cause decrease of SOD activity. There is a link between the inactivation of SOD on oxidative stress in bronchial epithelium cells in asthma [3]. Free radicals form peroxinitrite (ONOO •) can nitrate amino acid residues of SOD, resulting in the modification and inactivation of SOD. Peroxinitrite radical is classified as *reactive nitrogen species* (RNS) that is highly reactive and is produced by the reaction between superoxide radicals with NO•.

The results in rat pancreatic tissue of type 1 diabetes mellitus MLD-STZ induction showed the decrease in SOD activity (36.996 ± 1.937 U / mL) against the control (74.956 ± 0.467 U / mL) (Table 1 and Figure 1), where the units of the SOD activity indicating micromol substrate amount that modified by an enzyme in one minute at the maximum speed of reaction and the substrate in excess.

Based on the results of the study, the present of temu giring *(Curcuma heyneana)* extracts can increase the activity of SOD on rat pancreatic tissue of type 1 DM (Table 1). From the statistical analysis showed highly significant differences between SOD activity in type 1 diabetic rat with rat that got therapeutic doses of 1.25, 2.5, and 3.75 g /kgWB, and between SOD activity of rats treated with doses of 1.25, 2.5, and 3.75 g / kg with control rats. This means that the temu giring extract can increase SOD activity of rat pancreatic tissue of type 1 DM, but this increase cannot match the activity of SOD in control rat. Based on the results of the study, rat were treated with a dose of 3.75 g/kgWB showed increased SOD activity higher than (66.652 ± 1.698 U/mL) against type 1 DM rats compared to treatment with a dose of 1.25 g/kgWB (47.880±1.429 U/mL) and 2.5 g/kgWB (56.346 ± 1.608 U/mL).

Table 1. SOD Activity Profiles of Control Rats, Type 1 DM Rats and Therapy Extract Temu Giring Rats

Treatment groups	Average SOD*	Decreasing
Control	74.956 ± 0.477	0
DM Tipe 1	36.996 ± 1.937	50.64
Therapy 1.25g/kgBB	47.880 ± 1.429	36.12
Therapy 2.5g/kgBB	56.346 ± 1.608	24.83
Therapy 3.75g/kgBB	66.652 ± 1.698	11.08

***activity in homogenate pancreas*

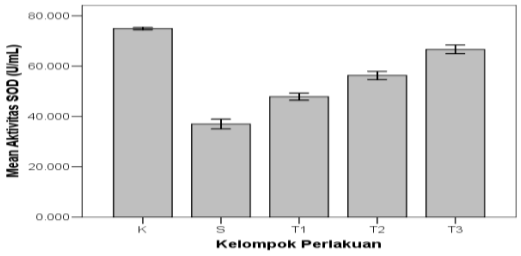

Figure 1. The Comparison of Average Value of SOD Activity in Group Treatment of Pancreatic Tissue

Increased SOD activity in rats‘ pancreatic tissue of Diabetic type 1 which got therapy of temu giring extract possibly related to the antioxidant activity of natural compounds in extracts of temu giring. Based on phytochemical tests, temu giring extract contains polyphenols (flavonoids, tannic and curcumin), alkaloids and terpenoids compounds. One of the suspects compounds that play a role in enhancing SOD activity are polyphenol compounds, particularly

flavonoids and curcumin contained in many of the most *Curcuma sp*.

Antioxidant activity of polyphenols, which serves as a scavenger (catcher) of free radicals can help to reduce the level of free radicals in the pancreas that causing damage to the cells of the pancreas beta which features of causing type 1 diabetes from streptozotocin (STZ) induced, so the effect of free radical against modification and inactivation of SOD can be overcome. Scavenging reaction of free radicals by polyphenols compounds are shown in Figure 2.

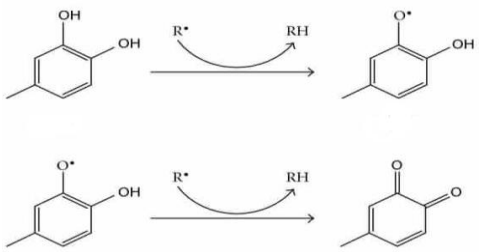

Figure 2. Scavenging reaction of free radicals (R*) by polyphenol compounds.

The ability of polyphenol compounds in warding off the free radicals caused by the structure. In the flavonoids and curcumin, hydroxyl groups on aromatic rings will donate H atoms to free radicals. Fenoxyl flavonoids or curcumin radicals formed then have the resonance stabilization by conjugated double bond system that is radicals will be less reactive.

Insulitis Degree of Rat Pancreas Tissue Control, Rat Induced by MLD-STZ, and Rat Extract Temu giring Therapy

Insulitis is intrusion or infiltration of mononuclear cells to the island of langerhans pancreatic tissue. The level of mononuclear cell infiltration into the islands of langerhans from pancreatic tissue can be determined by calculating the level of insulitis. Determination of the degree of insulitis is done through the calculation of cell damage on the island of langerhans. According to the level of insulitis score ranging 0-4. Score 0, insulitis was not found, score 1, there is less than 25% of the island of langerhans infiltrated, score 2 less than 50% insulitis, score 3 less than 75% insulitis, and score 4,> 75% had infiltration or degeneration occurs.

To determine the degree of insulitis in pancreatic tissue of trial animals, preparate of the pancreas was observed by using the method Hematoxilen and Eosin (HE) staining and the damage observed under light microscope. The result of HE staining on the island of langerhans pancreas can be seen in Figure 3.

Figure 3 shows that the control rat langerhans Island is almost fully charged with endocrine cells, particularly insulin-producing beta cells and are on a score of 1. While in rats with diabetes there are many voids (inter-cellular space) and the scores ranged between 3 and 4 on the island of Langerhans which caused a decrease in the number of insulin-producing beta cells. The condition of the island langerhans rat post-therapy temu giring extract showed decreased intracellular cavity and decrease the score to 1-3 because of repair cells for the therapy of pancreatic extract temu giring at various doses.

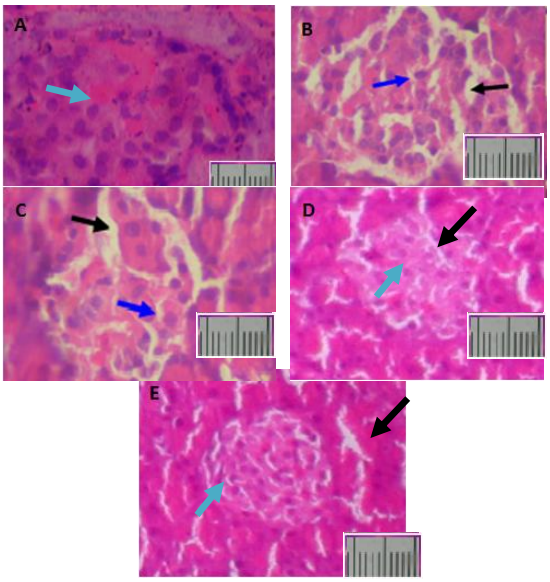

Figure 3. The result of HE staining on the island of Langerhans Pancreas; black arrows: cavity between cells; blue arrow: pancreatic beta cells.

Description: A = island of Langerhans Control Rat (score 1), B = island of Langerhans Diabetes Rat (score 4); C = Island of Langerhans Therapy Temu giring Extract Rat doses of 1.25 g/kgWB (score 3); D = Island of Langerhans Therapy Temu giring Extract Rat doses of 2.5 g/kgWB (score 2); E = Island of Langerhans Therapy Temu giring Extract Rat doses of 3.75 g/kgWB (score 2). 400 x magnifications.

The data showed the best improvement in the island of langerhans by present therapy temu giring extract dose 3.75 g/kgWB. This is in line with the results of statistical analysis that the therapy dose 3.75 g/kgWB differed significantly ($p < 0.01$) with therapy given with another dose of 1.25 and 2.5 g/kgWB. Therapy in type 1 diabetic rats with a dose of 3.75 g/kgWB showed maximum results to improve pancreatic cells. Insulitis score for each treatment can be seen in Figure 4.

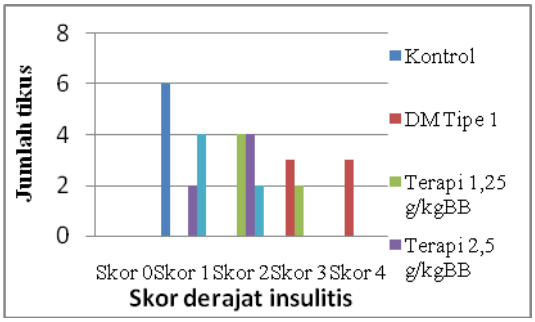

Figure 4. Score insulitis degree for each treatment

The increasing dose of temu giring extraxt therapy showed the reduce insulitis score that indicates the level of histological improvement of pancreatic tissue. This is due to temu giring extracts contain several compounds of natural materials are polyfenol (flavonoid, tannin, curcumin), terpenoids and alkaloid compounds especially polyfenol that have antioxidant activity. In addition, temu giring extract have proven inhibit the activity of NO production and anti-inflammatory activity [6]. Antioxidant activity of extracts temu giring capable of capturing free radicals that caused damage to pancreatic beta cells in type 1 diabetes. Thus, the risk of inflammation can be reduced. This situation causes the activation of immune effector cells is blocked, and due to migration of cells into pancreatic tissue is reduced. Reduce the level of free radicals such as NO radicals reduce macrophage activity triggers. Therefore, the risk of beta cells has phagocytosis by macrophages cell can reduce.

4. Conclusion

Therapy of temu giring extract doses of 1.25, 2.5 and 3.75 g/kgWB in rat induced by MLD-STZ showed the increase of SOD activity in succession at 29.42%, 52.30% and 80.16% and repair pancreatic tissue damage. Maximum dose of therapy temu giring extract is 3.75 g/kgWB that showed the best increase of SOD activity and repair pancreatic tissue damage compared with other dose 1.25 and 3.75 g/kgWB.

5. Acknowledgements

The author would like to thank to Prof. Dr. drh. Aulanni'am, DES, Prof. Dr. Ir. Chanif Mahdi, MS (Laboratory of Biochemistry UB) and Bety S that provides all facilities of research.

6. References

[1]. Adnyana I.K., Elin Yulinah, Andreanus A. Soemardji, Endang Kumolosasi, Maria Immaculata Iwo, Joseph Iskendiarso Sigit, Suwendar (2004), Uji Aktivitas Antidiabetes Ekstrak Etanol Buah Mengkudu (*Morinda citrifolia* L.), *Acta Pharmaceutica Indonesia*, 22(2) 43-49

[2]. Cockram C.S (2006), The epidemiology of diabetes mellitus in the Asia-Pacific region. HKMJ 2000;6:43-52.

[3]. Comhair, S.A.A., W. Xu, S. Ghosh, F.B.J.M.Thunnissen, A. Almasan, W.J. Calhoun, A.J. Janocha, L.Zheng, S.L. Hazen, and S.C. Erzurum (2005), Superoxide Dismutase Inactivation in Pathophysiology of Asthmatic Airway Remodeling and Reactivity, *American Journal of Pathology,* Vol. 166, No. 3.

[4]. Kuswinarti, Soegiarso N.C. (2001), Efek Ekstrak Temu Giring (*Curcuma heyneana* Val & v. Zijp) terhadap Kadar Kolesterol Darah Tikus Jantan, Penelitian Obat Bahan Alam. Sekolah Farmasi ITB.

[5]. Mahdi, A. A., A. Chandra., R. K. Singh., S. Shukla., L. C. Mishra., dan S. Ahmad (2003), Effect of herbal Hypogycemic Agents on Oxidative Stress and Antioxidant Status in Diabetic Rats, *Indian Journal of Clinical Biochemistry*, 18(2):8-15

[6]. Matsuda, H.; Morikawa, T.; Ninomiya, K.; Yoshikawa, M (2001), *Bioorg. Med. Chem*. 9, 909-916.

[7]. Orzechowski, A (2003), Justification for Antioxidant Preconditioning (or How to Protect Insulin mediated Action Under Oxidative Stress), *J.Bioscience*. 28:39-49

[8]. Rashid, Nur Yuhasliza Abd (2004), Chemical Constituents and Biological Activities of *Curcuma xanthorriza* and *Curcuma heynean,*. Thesis submitted to the school of Graduate studies, Universiti Putra Malaysia.

[9]. Tisch, Roland and Hugh McDevitt (1996), Insulin-Dependent Diabetes Mellitus, *Cell*, Vol. 85, 291–297.

[10]. Delves, P., Roit, I., (1998), Encyclopedia of Immunology. 2nd Ed. Academic Press. San Diego.

Characterization of Allergen Proteins and Alergenicity of Porang tubers (*Amorphophallus muelleri* Blume.) by using IgE-Immunoblotting

Sofy Permana [1], Sri Widyarti [2], Luccy Mutia Lingga Dewi [3], Indrian Rizka Amalia [4]

[1,2,3,4] Biology Department, Faculty of Mathematics and Natural Sciences, Brawijaya University, Malang, Indonesia (sofybraw@yahoo.com)

Abstract

The aims of this research were characterizing the allergen proteins and comparing the allergenicity between the raw and steamed-porang tubers by using IgE-Immunoblotting. Three variants of Porang: Klangon-Madiun, Sumber Baru-Jember and Sumber Bendo-Madiun were observed. Protein preparation was done according to Li et al. (2003) method, separated using SDS-PAGE electrophoresis, stained by silver and blotted with semi-dry transfer. Mouse serum with highest titer of IgE from ELISA was used as primary antibody, and Goat anti-Rat IgE Biotin Conjugated was used as secondary antibody. The density of protein bands were analyzed by Chemidoc Gel Imaging and Quantity One 4.6.8 software. The result of IgE-Immunoblotting of those three raw and steamed-porang tuber variants showed that the allergen protein bands profile were similar in each variant, with the appearance of molecular weight 26, 32 and 43 kDa. The density of a 26 kDa allergen was the highest protein in raw-porang. In the other hand, a 32 kDa allergen was the highest protein density in steamed-porang from Sumber Bendo, and a 43 and a 32 kDa allergens were in steamed-porang from Sumber Baru. The density of allergen in steamed-porang from of Klangon was in 26 kDa, but it was lower than that of raw-porang one. These suggest that both raw and steamed-porang had potency to induce allergy.

Keywords: *Allergen, protein Porang, ELISA, IgE-Immunoblotting.*

Growth Differentiation Factor-9 Gene Expression of Mice Oocytes in Vitro

Sri Rahayu [1], Manami Nishio [2], Yumi Hoshino [3], Eimei Sato [4]

[(1)] Departement of Biology, Faculty of Mathematics and Natural Sciences, Brawijaya University, Indonesia
[(2,3,4)] Graduate School of Agricultural Sciences, Laboratory of Animal Reproduction , Tohoku University, Japan

Abstract

Growth differentiation factor-9 (GDF-9) is a growth factor secreted by oocytes in growing ovarian follicles. In mice, the use of „knock-out" models has shown that GDF9 is essential for normal follicular development with BMP15 regulating the fertilization potential of oocytes. The aim of this research was to find out the influenced volume of IVM oocyte media to GDF-9 gene expression. Oocytes were collected by puncturing the surface of the mice ovaries with sterile needles 27G. Furthermore oocytes were matured within Hx medium during 22 hours at 38.5ºC temperature in the incubator with 5% CO_2 to achive metaphase II (M II) oocytes. Oocytes were cultured in 3 variations media droplet volume of 50 ul / droplet, 100 ul / droplet and 200 ul / droplet. After RT-PCR and agarose gel electrophoresis, relative mRNA abundance of GDF-9 was analyze in each group of oocytes. The GDF-9 gene expressions of oocytes were obtained when oocytes were cultured in 200 ul / droplet media.

***Keywords**: GDF-9 gene, Metaphase II (M II), mice oocyte.*

1. Introduction

Primordial follicles are the stock from which all growing follicles are derived. Initiation of ovarian follicular (follicle activation) growth is characterized by morphological changes in primordial follicles. Only about 0.1% of primordial follicles that initiate growth will ever proceed to ovulation, the vast majority of growing follicles undergoing atresia [1]. The development of ovarian follicles is a complex process dependent upon endocrine regulation involving hypophyseal gonadotropins, and regulated locally by ovarian factors. Initiation of follicular growth involves the transformation of primordial follicles from a quiescent, growth arrested state to a growth-committed state. This process is characterized by differentiation and proliferation of granulose cells and by enlargement of the oocyte [2], and is regulated by several growth factors [3,4]. Growth Differentiation Factor - 9 (GDF-9) was a member of the TGF-B super family known to regulated ovarian functions in mammals. GDF-9 belongs to the transforming growth factor B (TGF-B) super family and is secreted by the oocytes [5]. In most mammalian species, GDF-9 transcripts and protein are expressed specifically in the growing oocytes from the primary follicle stage onwards until fertilization [6]. GDF-9 has been shown to induce HAS2, COX-2 as well as StAR mRNA expression and to suppress uPa and LHR mRNA expression in cultured mouse granulosa cells [7].

GDF-9 mRNA and GDF-9 protein are not only expressed at the primary follicle stage but are also present in oocytes throughout growth to the ovulatory phase [7,8]. In GDF-9 knockout mice [6], the absence of GDF-9 resulted in a block in folliculogenesis at the type 3b stage (late, onelayer primary follicle stage), indicating that GDF-9 is associated with early folliculogenesis. The expression of GDF-9 mRNA and protein was confined to oocytes of primary and large follicles in rats [9,10], mice [6] and humans [11]. Palmer et al [12], reported that GDF9 gene contribute in mothers of DZ twins Growth differentiation factor-9 (GDF9) and bone morphogenetic protein 15 (BMP15) is oocyte-specific proteins secreted by growing oocytes in rodents, sheep, and humans [4, 11,13-15]. They are known to control folliculogenesis by acting on GC in developing follicles. Studies in genetic mutations have elucidated the role of these proteins in regulating the primary to secondary follicle transition. Mutations in GDF9 [6] and BMP15 [16,17] result in growth arrest at the primary stage.

2. Experimental Details

Animals

Mice used in this study were maintained at the Tohoku University animal house. Twenty-one-d-old mice were injected with 5 IU PMSG,

and ovaries were collected 46 h later. All animals were housed under controlled humidity, with a 12-hrs light and a 2-hrs dark phase, temperature, and fed *ad libitum.*

Oocytes collecting

Mice were killed by the cervical dislocation. Ovaries were cleaned free of adherent adipose and connective tissues and placed in HEPES-buffered tissue cultured medium-199 (H-TCM-199; ICN Biomedicals Inc., Costa Mesa, CA) supplemented with 0.1% (wt/vol) BSA (H-TCM-199/BSA). COCs were isolated by puncturing antral follicles with 27-gauge needles and collected in L-15-Meiumd/BSA. Only COCs with a uniform covering of compacted cumulus cells were used in this study. Furthermore oocytes were matured within Hx medium during 22 hours at 38.5ºC in the incubator with 5% CO_2 to achive metaphase II (M II) oocytes. Oocytes were cultured in 3 variations media droplet volume of 50ul/droplet, 100ul/droplet and 200ul/droplet, under parafin oil.

Reverse Transcription PCR

To confirm the expression of *GDF-9* mRNA MII RT-PCR analysis was performed on the isolated oocytes. Total RNA from the three oocyte groups was isolated in parallel following the manufacturer's instructions. To avoid contamination with genomic DNA, total RNA preparations were treated with DNase. Total RNA extraction and DNA synthesis was performed using Cell-to-cDNATMII. PCR was performed using Ex Taq polymerase. The sequence for primer pair was GDF-9 sense, 5-AGCAACCAGGTGACAGGA-3, and antisense primer, 5-CCTCCTTTACCAGGTCA-3

3. Result and Discussion

Morphological change was observed before and after in vitro culturing of oocytes (Figure 1). Obtainig mature oocytes after in vitro culturing of pre-antral follicles has been successful in many laboratories. We also obtained M II oocytes after 22 h in vitro oocytes culturing (Figure 1). Morphological of cumulus oocyte complexes will be change during oocytes maturation [18]. The mammalian ovary has very complex machinery, in which many factors play an important role for the maturation and growth oocytes during folliculogenesis [19].

After RT-PCR and agarose gel electrophoresis, relative mRNA abundance of GDF-9 was analyze in each group of oocytes. The GDF-9 gene expression of oocytes were obtained when oocytes were cultured in 200ul/droplet media, but not expression when oocytes were cultured in 50 and 100 ul / droplet media (Figure 2).

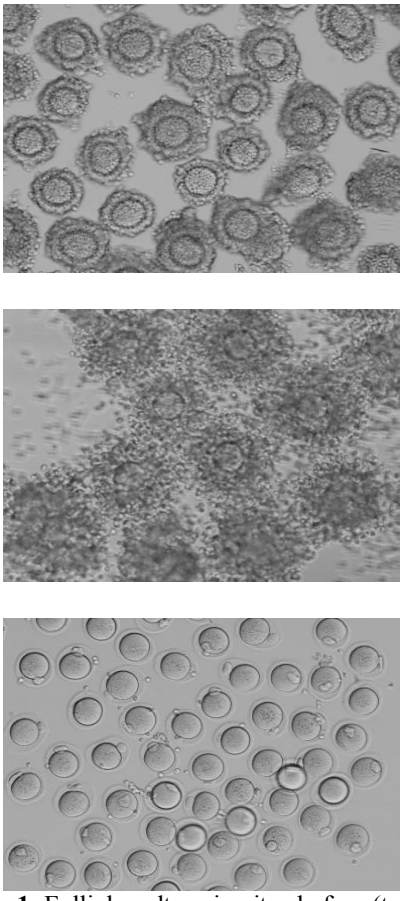

Figure 1. Follicle culture in vitro before (top) and after (middle) culturing oocytes, MII Oocytes obtained from in vitro culture (bottom).

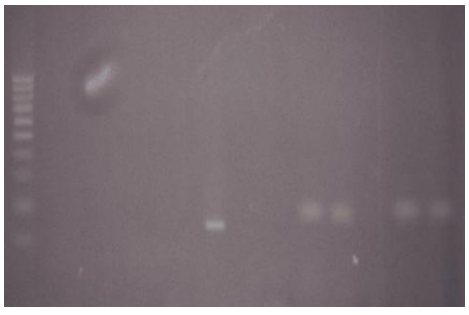

Figure 2. RT-PCR analysis of GDF-9 expression of oocytes grown in vitro. M : Marker DNA: oocytes were cultured in 50 ul / droplet media (Lane 1-2); 100 ul / droplet media (lane 3-4); 200 ul / droplet media (Lane 5-6). Control of PCR (mG3PDH) (Lane 7-12).

The paracrine factor GDF-9 secreted by oocytes plays important roles in the intercommunication between oocytes and follicle cell. Althought, Kim *et al* (2004) had worked on oocytes maturated in vitro and in vivo and foun no difference of the GDF-9 gene expression between them [20]. Shimizu *et al* (2004) found that the injection of porcine GDF-9 gene fragments resulted in an increase in the number of primary, secondary and tertiary follicles, concomitant with a decrease in the number of primordial follicles [21]. These results indicated that exogenous GDF-9 can promote early folliculogenesis in the porcine ovary, and that a technique for direct ovarian injection of GFD-9 gene fragments may contribute to a novel therapy for prevention and treatment of infertility associated with ovarian dysfunction. GDF-9 and BMP15 appear to be key regulators of normal follicular development and ovulation rate in cattle [3].

4. Conclusion

The GDF-9 gene expression of oocytes in vitro maturation depends on volume of media culture droplet. The GDF-9 gene expressions of oocytes were obtained when oocytes were cultured in 200 ul / droplet media.

5. Acknowledgements

This research was supported by the IMHERE Project, Biology Departemnet, Faculty of Mathematics and Natural Sciences, Brawijaya University, Malang.

6. References

[1]. Hsueh AJ, Billig H & Tsafriri A 1994 Ovarian follicle atresia: a hormonally controlled apoptotic process. Endocrine Reviews 15 707–724.

[2]. Braw-Tel R & Yossefi S 1997 Studies in vivo and in vitro on the initiation of follicle growth in the bovine ovary. Journal of Reproduction and Fertility 109 165–171.

[3]. Juengel,JL., Norma L H., Martin B., Keith H., Peter S., Stephen B L., Lynda W. and Kenneth P McN. 2009. Effects of active immunization against growth differentiation factor 9 and/or bone morphogenetic protein 15 on ovarian function in cattle. Reproduction 138 : 107–114

[4]. Otsuka F, Yao Z, Lee T, Yamamoto S, Erickson GF & Shimasaki S 2000 Bone morphogenetic protein-15. Identification of target cells and biological functions. Journal of Biological Chemistry 275 39523 39528.

[5]. Erickson GF & Shimasaki S 2000 The role of the oocyte in folliculogenesis. Trends in Endocrinology and Metabolism 11 193–198.

[6]. Dong J, Albertini DF, Nishimori K, Kumar TR, Lu N & Matzuk MM 1996 Growth differentiation factor-9 is required during early ovarian folliculogenesis. Nature 383 531–535.

[7]. Elvin JA, Clark AT, Wang P, Wolfman NM & Matzuk MM 1999 Paracrine actions of growth differentiation factor-9 in the mammalian ovary. Molecular Endocrinology 13 1035–1048.

[8]. Elvin JA, Yan C & Matzuk MM 2000 Oocyte-expressed TGF-b superfamily members in female fertility. Molecular and Cellular Endocrinology 159 1–5.

[9]. Hayashi M, McGee EA, Min G, Klein C, Rose UM, van Duin M & Hsueh AJ 1999 Recombinant growth differentiation factor-9 (GDF-9) enhances growth and differentiation of cultured early ovarian follicles. Endocrinology 140 1236–1244.

[10]. Picton HM & Gosden RG 2000 In vitro growth of human primordial follicles from frozen-banked ovarian tissues. Molecular and Cellular Endocrinology 166 27–35.

[11]. Aaltonen J, Laitinen MP, Vuojolainen K, Jaatinen R, Horelli-Kuitunen N, Seppa¨ L, Louhio H, Tuuri T, Sjo¨berg J, Bu¨tzowR et al. 1999 Human growth differentiation factor 9 (GDF9) and its novel homolog GDF9B are expressed in oocytes during early folliculogenesis. Journal of Clinical Endocrinology and Metabolism 84 2744–2750.

[12]. Palmer James S, Zhen Zhen Zhao, Chantal Hoekstra, Nicholas K. Hayward, Penelope M. Webb, David C. Whiteman, Nicholas G. Martin, Dorret I. Boomsma, David L. Duffy, and Grant W. Montgomery. 2006. Novel Variants in Growth Differentiation Factor 9 in Mothers of Dizygotic Twins. *J Clin Endocrinol Metab* 91: 4713–4716.

[13]. Bodensteiner KJ, Clay CM, Moeller CL & Sawyer HR 1999 Molecularcloning of the ovine growth/differentiation factor-9 gene and expression of growth/differentiation factor-9 in ovine and bovine ovaries. Biology of Reproduction 60 381–386.

[14]. Dube JL, Wang P, Elvin J, Lyons KM, Celeste AJ & Matzuk MM 1998 The bone morphogenetic protein 15 gene is X-linked and expressed in oocytes. Molecular Endocrinology 12 1809–1817.

[15]. Fitzpatrick SL, Sindoni DM, Shughrue PJ, Lane MV, Merchenthaler IJ & Frail DE

1998 Expression of growth differentiation factor-9 messenger ribonucleic acid in ovarian and nonovarian rodent and human tissues. Endocrinology 139 2571–2578.

[16]. Galloway SM, McNatty KP, Cambridge LM, Laitinen MPE, Juengel JL, Jokiranta TS, McLaren RJ, Luiro K, Dodds KG, Montgomery GW et al. 2000 Mutations in an oocyte-derived growth factor gene (BMP15) cause increased ovulation rate and infertility in a dosage-sensitive manner. Nature Genetics 25 279–283.

[17]. Hanrahan JP, Gregan SM, Mulsant P, Mullen M, Davis GH, Powell R & Galloway SM 2004 Mutations in the genes for oocyte-derived growth factors gdf9 and bmp15 are associated with both increased ovulation rate and sterility in cambridge and belclare sheep (ovis aries). Biology of Reproduction 70 900–909.

[18]. Yokoo Masaki and Eimei Sato. 200. Cumulus-Oocyte Complex Interaction during Oocyte Maturation. International Review of Cytology.235:251-291

[19]. McLaughlin EA., Mclver SC. 2009. Awakening the oocytes: Controling primordial follicle development. Reproduction 137 : 1-11

[20]. Kim DH., Ko DS., Lee HC., Lee HJ., Park WI., Kim SS. 2004. Comparassion of maturation, fertilization, development and gene expression of mouse oocytes grown in vitro and in vivo. J. Assist Reprod Genet 21 (7) : 233-240

[21]. Shimizu T., Yasunori M., Masaki Y., Yumi H., Hiroshi S. and Eimei S. 2004. Molecular cloning of porcine growth differentiation factor 9 (GDF-9) cDNA and its role in early folliculogenesis: direct ovarian injection of GDF-9 gene fragments promotes early folliculogenesis. Reproduction. 128: 537–543

[22]. Jaatinen R, Laitinen MP, Vuojolainen K, Aaltonen J, Louhio H, Heikinheimo K, Lehtonen E & Ritvos O 1999 Localization of growth differentiation factor-9 (GDF-9) mRNA and protein in rat ovaries and cDNA cloning of rat GDF-9 and its novel homolog GDF-9B. Molecular and Cellular Endocrinology 156 189–193.

[23]. Elvin JA, Yan C & Matzuk MM 2000 Oocyte-expressed TGF-b superfamily members in female fertility. Molecular and Cellular Endocrinology 159 1–5.

In Vitro Anti-Malarial Activity of Alkaloids from *Erythrina Variegata* against *Plasmodium Falciparum*

Tati Herlina [1], Unang Supratman [2], Syafruddin [3], Hideo Hayashi [4]

[1,2] Department of Chemistry, Faculty of Mathematics and Natural Sciences, Padjadjaran University, Jatinangor Sumedang, Indonesia (tatat_04her@yahoo.com)
[3] Eijkman Institute for Moleculer Biology, Jakarta, Indonesia
[4] Laboratory of Natural Products Chemistry, Division of Applied Biological Chemistry, Graduated School of Agriculture and Life Sciences,Osaka Prefecture University, 1-1 Gakuen-cho, Sakai, Osaka 599-8531, Japan

Abstract

*An Erythrina plant locally known as "dadap" is higher plant and has been used as a folk medicine for treatment of malaria. As part of our continuing search for novel anti-malarial compounds from Indonesian Erythrina plants, we found that the methanol extract of the leaves and stem bark of E. variegata showed significant anti-malarial activity in vitro against Plasmodium falciparum using the lactate dehydrogenase (LDH) method. Anti-malarial guided fractionation of the methanol extract yielded two active compounds identified as 10,11-dioxoerythratidine (**1**) and erythratidine (**2**). Compounds (**1** and **2**) showed anti-malarial activity against both 3D7 and K1 strains of the parasite used with IC_{50} of 0.01, 3.0 µg/mL against 3D7 and 1.0, 9.3 µg/mL against K1, respectively. This result strongly suggested that E. variegata is a promising source of anti-malarial agents.*

Keywords: *Anti-malarial, Erythrina variegata, Plasmodium falciparum.*

1. Introduction

Malaria is an endemic disease in many parts of Asia, Africa, Central and South America. World Health Organization (WHO) estimates that each year 200-300 million people suffer from the case of malaria, resulting in up to 2.7 million deaths. The appearance of drug-resistance *Plasmodium falciparum* since 1960 has made the treatment of malaria increasingly problematic, and apparently the battle has not been successful [1]. This could be attributed in part to the widespear problem of parasite drug-resistance [2]. Recently, attention was focused on medicinal plants to provide new and novel anti-malarial agents.

Erythrina variegata (Leguminosae) is a famous medicinal plant widely distributed in tropical and subtropical region of the world. This plant is locally known as ~~"d~~dadap ayam" in Indonesia and the *E. variegata* is used as an anti-malarial agent [3-5]. Previous studies of the leaves of *E. variegata* have shown significant anti-malarial against on *P. berghei in vivo* and *P. falciparum in vitro* [6]. Pharmacological report shows that flavonoid and triterpenoid derivate from the ethyl acetate fraction of the stem bark and the leaves of *E. variegata* showed an anti-malarial against on *P. falciparum in vitro* [7-11].

As part of our continuing search for novel anti-malarial compound from Indonesian *Erythrina* plants, we report isolation, structure elucidation and its anti-malarial activity from the stem bark and the leaves of *E. variegata*.

2. Experimental Details

General Experimental Procedure

Melting points (mp) were uncorrected. The IR spectra were recorded with a Perkin-Elmer 1760 X FT-IR spectrophotometer, and the UV spectra were recorded with a Hitachi model U-3210. Mass spectra were recorded with JEOL JMS-DX300 instrument. The ^{1}H- and ^{13}C-NMR spectra were obtained with JEOL JNM GX 270 and JNM A-500 spectrometer. Chemical shifts are given on a δ (ppm) scale with TMS as an internal standard. Column chromatography was carried out using Merck Kieselgel 60 (70-200 mesh), and thin layer chromatography (TLC) analysis was performed on precoated Si Gel plates (Merck Kieselgel GF_{254}, 0.25 mm x 20 x 20 cm).

Plant material

Samples of the stem bark and the leaves of *E. variegata* were collected on June 2008, in Bandung, West Java, Indonesia. The plant was identified by a staff at the Laboratory of Plant

Taxonomy, Department of Biology, Bandung Institute of Technology, Bandung, Indonesia, and a voucher specimen has been deposited at the herbarium.

Parasite strain

In this study two strains of *P. falciparum* were used, culture of 3D7 (chloroquine sensitive and K1 (chloroquine resistant).

Drug dilution

The lactate dehydrogenase (LDH) method was performed using 96-well microtitreplates (flat bottom). The initial concentration of the extract, chloroquine (Sigma Chemical, USA) and artemisinine (Sigma Chemicals, USA) were 1000 µg/ml and 1 µg/ml, respectively. The samples were then serially diluted in culture medium supplemented with 10% human serum 19 times.

Extraction and isolation

The dried leaves (2 kg) of *E. variegata* were soaked in MeOH. Evaporation of the MeOH gave an aqueous concentrate, wich was extracted with CH_2Cl_2. The resulting CH_2Cl_2 extract was partitioned between *n*-hexane and MeOH containing 10% water, and then the lower layer was concentrated and extracted with EtOAc to efford residue (36.31 g). The methanol layer was partitioned between *n*-butanol-water (3:1). The *n*-butanol layer was subsequently dried over anhydrous sodium sulfate, filtered, evaporated to dryness, and assayed for anti-malarial activity. The *n*-butanol fraction (4 g) was chromatographed on Kieselgel 60 (70-230 mesh) by eluting with chloroform-ethyl acetate in an increasing ratio (1:1-1:5) to yield 3 fractions (BA, BB, and BC). The BC fraction (1.5 g) was eluted with chloroform and 5% acetic acid were further flash-chromatographed on Kieselgel 60 to yield an isolate**1** (53 mg).

The dried seeds (2.5 kg) of *E. variegata* were exhaustively extracted with MeOH at room temperature. The MeOH extract was evaporated in vacuo to yield a dark brown residue that was acidified with 10% acetic acid to pH 2-3 and extracted with CH_2Cl_2 to afford a positive aqueous extract. Furthermore the aqueous extract was basic with ammonium hydroxide to pH 9-10 and then extracted with CH_2Cl_2 to yield positive CH_2Cl_2 extract (5.3 g). This CH_2Cl_2 extract was subjected to column chromatography on silica gel G 60 with eluent $CHCl_3$-EtOAc (7:3) to obtain the active fractions (B) and (C). The active fraction (B) was column chromatographed on silica gel G 60 successively with $CHCl_3$ – hexane – MeOH (6:1.8:0.2), to yield a positive fraction BB (195 mg). The positive fraction BB was further subjected to column chromatographed on silica gel G 60 successively with EtOAc-C_2H_5OH-hexane (7:2:1), to yield an isolate **2** (11.5 mg).

Anti-malarial activity

In vitro testing of the anti-malarial activity was carried by measuring the LDH activity of the parasite. Briefly, continuous culture of the 3D7 sensitive chloroquine and K1 resistant chloroquine, were maintained in a suspension consisting of RPMI 1640 culture medium supplemented with HEPES, *N*-2-hydroxyethylpiperazine-*N*'-2-ethane-sulfonic acid (25 mM), sodium bicarbonate (0.2%) and gentamycin (40 µg/ml) at pH 7.4, and O type red blood cell. For each LDH test, a blood suspension of 1% parasitemia and 2% haematocrit were prepared. Control reading of parasitised red blood cells devoid of plant extracts or drugs and non-parasitised red blood cells were done simultaneously.

After the plate has been prepared, it was placed in a candle jar and incubated for 48 h at 37ºC. After 48 h, 100 µl of Malstat (Flow Inc., Portland, OR), was dispensed into a new micro-titreplate. Next, it was added 25 µl of NBT-PES (Sigma Chemicals, USA) mixture. Twenty micro-liters of blood suspension were transferred into the plate containing the Malstat and NBT-PES. Any air bubbles were eliminated as it could interfere with the absorbance reading. Absorbance was read at 630 nm using an ELISA plate reader (MRX Micro-plate Reader, Dynex Technologies, USA). Chloroquine and artemisinin functioned well as positive controls [12].

Analysis of results

Percentage inhibition of parasite viability was determined and the mean of least IC_{50} values was calculated using the curve fitting analysis in Grafit (Grafit v.4.09, Erithacus Sofware Limited).

3. Result and Discussion

The methanol extract of dried leaves and stem bark of *E. variegata* exhibited an anti-malarial activity in vitro against *Plasmodium falciparum.* The active methanol extract was partitioned between *n*-hexane, ethyl acetate and *n*-butanol to afford *n*-butanol fraction. By using the bioassay to follow the separations, the *n*-butanol fraction was separated by combination of column chromatography on Kieselgel 60 to afford an active isolates (**1** and **2**).

The isolate (**1**) was obtained as yellow pale needless crystals, m p 72-74ºC. The molecule formula was established to be $C_{19}H_{21}NO_6$, m/z

359 by EIMS spectral data, thus requiring ten degrees of unsaturation. Its UV spectrum of isolate showed aryl and carbonyl absorption at 288 and 350 nm, respectively. The IR spectrum of compound isolate displayed some characteristic absorption for an aromatic ring, hydroxyl and carbonyl group. The ^{1}H-NMR and ^{13}C-NMR spectra of isolate showed signals assignable to a 1,2,4,5-tetrasubtituted benzene ring [δ_H 7.02 (1H,*s*) and 7.47 (1H,*s*)] and [δ_C 107.8; 110. 4; 124. 3; 139. 2; 149.3; and 153.1] and two carbonyl groups [δ_C 160.0 and 180.4] ppm, indicating isolate to be a tetracyclyc structure. Three methoxyls were also observed in the ^{1}H-NMR and ^{13}C-NMR spectra [δ_H 3.16 (3H, *s*); 3.95 (3H, *s*) and 3.98 (3H, *s*)] and [δ_C 57.2; 56.3 and 56.5]. To determine the connectivity of the partial structure, ^{1}H-^{1}H COSY, HMBC, and NOESY experiment for isolate was carried out, and the results are shown in Figure 1. The NOESY spectra showed signals assignable to α-configurated equatorial of H-1, H-2, H-3, H-4, H-7, and H-8, while of 2-OH, 3-OCH_3, H-4, H-7, H-8, H-14, 15- OCH_3, 16- OCH_3, and H-17 are β-configurated axial. The based on the spectral spectroscopic evidence, comparison with the previously reported and biogenetic point of view, the genus *Erythrina* seems to lack biogenetic ability to produce alkaloids [13,14] identified as 10,11-dioxoerythratidine.

The isolate (**2**) was shown to have the molecular formula of $C_{19}H_{25}NO_4$ by ^{1}H- and ^{13}C-NMR spectral data, indicating that **2** has eight double bond equivalents. Its UV spectrum showed aryl absorptions at 233 and 284 nm, respectively. IR absorption bands due to a hydroxyl and an aromatic ring were observed at 3381, 1512, and 781 cm^{-1}, respectively. The by ^{1}H- and ^{13}C-NMR spectra of **2** were quite similar to those of **1**, except the absence of carbonyl signal at δ_C 3.69 (1H, dd, J=3.4, 7.0 Hz) and δ_C 72.9, suggesting that **2** to be a reduction analogue of **2**. To determine the location of hydroxyl, HMBC experiment was carried out. The signal of H-1 (δ_H 5.93) was correlated with C-2 (δ_C 65.4), and H-3 (was correlated with C-2 (δ_C 65.4) and C-1 (δ_C 122.2), indicating that **2** was 2-hydroxyl analogue of **1,** as same as erythrina alkaloids. Consequently, the structure of **2** was identified as erythratidine [14].

Inhibition of the methanol extract towards sensitive strain (3D7) was also much better compared to its inhibition towards the resistant strain (K1) of the parasite (Table 1). The methanol extract (IC_{50} 6.8 µg/mL) showed good anti-plasmodial activity against K1 strain of the parasite based on the tresholds for *in vitro* anti-plasmodial activity of anti-malarial extracts [15]. The potency of methanol extract indicated that the leaves of *E. variegata* were potential candidate for anti-malarial agent. The leaves of *E. variegata* were widely used in traditional medicine [3] and it was boiled in water and used for malaria treatment [4].

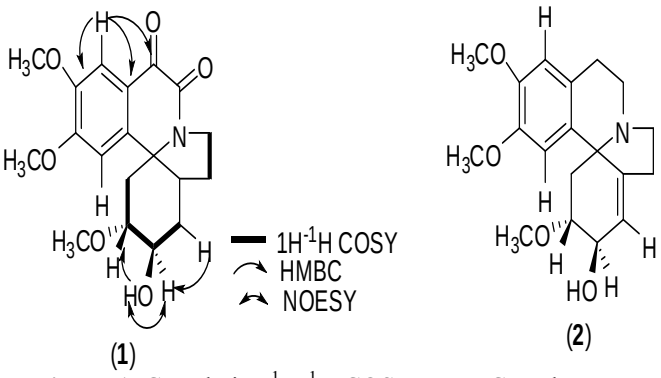

Figure 1. Correlation ^{1}H-^{1}H COSY, HMBC, and NOESY (**1**) and Structure (**2**)

Table 2. The IC_{50} of methanol extract, ethylacetate fraction, *n*-buthanol fraction and 10,11-dioxoerythratidine against *P. falciparum* K1 and 3D7 strains

Sample	IC_{50} (µg/mL)	
	K1	3D7
Methanol extract	6.8	>60
Ethyl acetate fraction	26.5	16.7
n- butanol fraction	5.1	13.2
10,11-dioxoerythratidine	0.01	1.0
erythratidine	9.3	3.0
Chloroquine	0.04	0.04
Artemisinin	0.01	0.01

The ethyl acetate fraction showed weak anti-plasmodial activity against both strains of the parasite with IC_{50} of 26.5 µg/mL and 16.7 µg/mL against K1 and 3D7 respectively. Previously, anti-malarial triterpenoid pentacyclic isolated from ethyl acetate fraction of the leaves of *E. variegata* toward *P. falciparum* FCR-3/A (chloroquine resistant) [9]. The *n*-butanol fraction and 10,11-dioxoerythratidine showed good anti-plasmodial activity against both strain of the parasite. The erythratidine (IC_{50} 3.2 µg/mL) from *n*-butanol fraction showed good anti-plasmodial activity against K1 strain of the parasite, but it showed weak anti-plasmodial activity against the 3D7 strain (IC_{50} 9.3 µg/mL).

Result from this *in vitro* anti-malarial study showed that the activity of ethyl acetate fraction (IC_{50} 26.5 µg/mL), *n*-butanol fraction (IC_{50} 5.1 µg/mL), and isolate (IC_{50} 3.2 µg/mL)

against chloroquine resistant *P. falciparum* K1 strain can be described in the following order; 10,11-dioxoerythratidine > erythratidine > *n*-butanol fraction > ethyl acetate fraction. The 10,11-dioxoerythratidine was the most potent fraction towards the target *P. falciparum* K1 strain compared to those of *n*-butanol fraction, methanol extract, and ethyl acetate fraction.

It might be an indication that 10,11-dioxoerythratidine was potential candidate for anti-malarial agents. The results obtained from this study also indicated that a variety of secondary plant metabolites displayed anti-malarial activity against *P. falciparum* in vitro. The 10,11-dioxoerythratidine is the first report on anti-malarial alkaloid.

4. Conclusion

The 10,11-dioxoerythratidine has been isolated from the leaves *E. variegata* and an erythratidine has been isolated from the stem bark of *E. variegata.* Our results strongly suggested that has been isolated from the leaves and stem bark of *E. variegata* is promising as anti-malarial agent.

5. Acknowledgement

We are grateful to Indonesian Managing Higher Education Relevance and Efficiency Project (2009) for financial support.

6. References

[1]. Tyagi, A.K., Agarwal, C., Chan, D.C.F., and Agarwal, K., (2004), *Oncology Reports,* 11, 493-499.
[2]. Lima, M.R.F., Luna, J.S., Santos, A.F., and Andrade, M.C.C., (2006), *Journal of Ethnopharmacology* 105, 137-147.
[3]. Heyne, K., (1987), The Useful Indonesian Plants. Research and development agency, Ministry of forestry, Jakarta, Indonesia, 1029-1031.
[4]. Mursito, B., (2002), Traditional Ingredients for Malaria Disease. 1st ed, Jakarta, Indonesia, 40-41.
[5]. Herlina, T., Supratman, U., Subarnas, A., and Sutardjo, S., (2007), *Bandung of Medical Journal* 1, 9-14.
[6]. Herlina, T., Supratman, U., Subarnas, A., Sutardjo, S., and Abdullah, N.R. (2007), *YARSI of Medical Journal* 15, 87-89.
[7]. Herlina, T., Supratman, U., Subarnas, A., Sutardjo, S., and Abdullah, N. R., (2007), *Indonesian of Nature Journal* 15, 2, 87-92.
[8]. Herlina, T., Supratman, U., Soedjanaatmadja, MS U., Subarnas, A., Sutardjo, S., Abdullah, N. R., and Hayashi, H., (2009), *Indonesian Journal of Chemistry*, 9, 2, 308-311.
[9]. Herlina, T., Muis, A., Supratman, U., Syafruddin, Subarnas, A., Soetardjo, S., and Hayashi, H., (2005), *Journal of Mathematics and Natural Science*, 15, 3, 21-26.
[10]. Herlina, T., Julaeha, E., Supratman, U., Subarnas, A., and Sutardjo, S., (2006), *Bionatura*, 8, 3 : 215-223.
[11]. Herlina, T., (2009), *Indonesian Journal of Cancer* ,3, 4, 151-154.
[12]. Najila, M.J.S., Rain, A.N., Kamel, A.G.M., Zahir, S.I.S., Khozirah, S., Hakim, S.L., Zakiah, I., and Azizol, A.K., (2002), *J. Ethnopharmacol.,* 82, 239-242.
[13]. Chawla, A.S., Sood, A., Kumar, M., and Jackson, A.H., (1998), *J. Planta Medica*, 16, 526-528.
[14]. Supratman, U., Fujita, T., and Hayashi, H., (2000), *Applied Biological Science*. 6 : 7-16.
[15]. Rasoanaivo, P., Deharo,Ratsimamanga-Urverg, E., and Frappier, F., (2004), Guidelines for the nonclinical evaluation of the efficacy of traditional antimalarials. in Traditional Medicinal Plants and Antimalaria. CRC Press, USA, 256-268.

Recognition Antigen and Antibody Specific Protein 24 and Protein 40 Borna Virus in Serum Patients Psychiatric Disorders

Tri Maharani

Student of Biomedical Doctoral Program of Brawijaya University (hanarani_71@yahoo.com)

Abstract

Borna Disease Virus (BDV), infects a wide variety of vertebrates and belongs to the family Bornaviridae, part of the order Mononegativirales. Borna Disease Virus (BDV) naturally infects horses and sheep. The study suggested that BDV agent can be associated with schizophrenia and affective illness in humans. BDV infection is a zoonotic illness which can be transmitted in individuals occupationally exposed to dosmetic animals, such as farmer. Subsequent serological and molecular studies have provided inconsistent evidence of an association between BDV infection and neuropsychiatric disorder. This research is the first in Indonesia. Sera were collected from patients with psychiatric disorder in two health centers in Nganjuk. The sera from patients were examined for antigen and antibodies against Borna Disease virus were measured by Enzym-linked Immunosorbent Assay. Indirect Immunofluoresence Assay (IFA) is a recently develop, highly specific method of detecting antibodies, and directed toward two BDV proteins: protein 24 kDa and 40 kDa. The result of the study showed that 17 samples or 34 % patient with psychiatric disorder were positive antibodies against BDV by IFA (p24 and p40). Quantitative by ELISA measured antigen against BDV with cut off 0.038 (result Optical density antigen and control negatif). Cut off antibodies result Optical density control positive and control negative antibody is 0.0398. The conclusion IFA and ELISA were detection antibodies spesific protein 24 and protein 40 kDa Borna virus in sera patients with psychiatric disorder. The graphic immuns respons give information state disease the patient, relationship antibodies against BDV with individual occupationally and variety psychiatric disorder.

Keywords: *Borna virus, IFA and ELISA, psychiatric disorder*

Lactobacillus Plantarum S1.30 Isolated from Dadih has Antagonistic Properties and Harbours Gene Encoding the Production of Bacteriocin

Yoga Dwi Jatmiko[1], Miguel De Barros Lopes [2], Mary Barton [3]

[(1)] Laboratory of Microbiology, Department of Biology, Faculty of Sciences, University of Brawijaya, Malang, Indonesia (jatmiko_yd@ub.ac.id)
[(2,3)] School of Pharmacy and Medical Sciences, University of South Australia, Adelaide, Australia (mary.barton@unisa.edu.au).

Abstract

Dadih is considered an important traditional fermented milk product with potential health benefits to local Indonesian communities. In addition, dadih lactic acid bacteria have antimicrobial activity believed to be important in increasing the safety and extending the shelf-life of the fermentation products. In this study, Lb. plantarum S1.30 isolated from dadih was assayed for its antagonistic activity and the presence of gene encoding bacteriocin production. Antibacterial activity of Lb. plantarum S1.30 against multidrug-resistant Gram negative pathogens (Salmonella spp. and Escherichia coli) and Gram positive pathogens was tested in vitro using well diffusion agar assay. The presence of bacteriocin activity was tested both conventional method and PCR-based method using specific primers targeting a bacteriocin regulation gene, plantaricin A. Furthermore, the antimicrobial production kinetic of Lb. plantarum S1.30 was also conducted against Listeria monocytogenes and Lactobacillus sakei ATCC 15521 in a liquid medium. The antimicrobial substances produced by Lb. plantarum S1.30 inhibited all the indicator bacterial pathogens, with the Gram positive pathogens were more sensitive than Gram negative pathogens. The bacteriocin detection was failure to be demonstrated using a conventional method. While, the PCR amplification resulted a-450 bp-DNA fragment, which indicated that plantaricin A was present in Lb. plantarum S1.30. The results obtained from kinetic studies of antimicrobial production showed that the organic acids produced by Lb. plantarum S1.30 played an essential role in inhibiting the growth of target bacteria. These result suggested that bacteriocin produced by Lb. plantarum S1.30, called plantaricin, could be regulated by a quorum sensing mechanism.

Keywords: *Lactobacillus plantarum S1.30, antimicrobial activity, bacteriocin, dadih.*

1. Introduction

Dadih is considered an important traditional fermented milk product with potential health benefits to local Indonesian communities. LAB which isolated from dadih has been shown to have probiotic properties such as anti-mutagenic and cholesterol binding activities that are stable in bile and acid conditions [1-3]. In addition, dadih LAB have antimicrobial activity. The consumption of dadih is safe, even though the sanitary conditions during manufacturing are poor. The capability of the LAB to produce bacteriocins is believed to be important in increasing the safety and extending the shelf-life of the fermentation products [4]. Bacteriocin-producing LAB has been isolated from variety of naturally fermented milk (NFM) products, such as airag, amasi, dahi, raib and gioddu.

A study by Collado et al [1] demonstrated that *Lb. plantarum* IS-10506 was the LAB in dadih that performthe most active inhibitory activity to intestinal adhesion of pathogenic bacteria. In a previous study, bacteriocin-like inhibitory substances (BLIS) active against indicator bacteria were detected in dadih LAB [3]. However, whether the antimicrobial activity was mediated by antimicrobial peptides has not been confirmed. Bacteriocins are characterized as proteinaceous compounds which can be inactivated by protease enzymes [5].

In recent study, four lactic acid bacteria strains were identified from dadih: *Lactococcus lactis* subsp. *lactis, Lb. plantarum* S1.30, *Lb. paracasei* and *Leuconostoc pseudomesenteroides* [6]. Only *Lb. plantarum* S1.30 demonstrated greater antimicrobial activity than other strains, with inhibitory activity against all bacterial indicator strains tested. In this current investigation, *Lb. plantarum* S1.30 was selected as a potential antimicrobial producer; hence the antagonistic activity against pathogenic bacteria was assayed and the presence of bacteriocins was detected using both conventional methods and a PCR-based method.

2. Experimental Details

Bacterial strains and medium

Bacterial strains used in this study were *Lb. plantarum* S1.30 and *Lactococcus lactis* S1.06 [6], *Lactococcus lactis* subsp. *lactis* ATCC 11454 as a nisin producer (positive control). Bacterial indicator used was *Lb. sakei* ATCC 15521, and a range of Gram positive of pathogenic bacteria: *Bacillus cereus*, *Enterococcus faecalis* ATCC 29212, *Listeria monocytogenes*, *Staphylococcus aureus* ATCC 25923 and *Streptococcus pyogenes* ATCC 10389. Multidrug-resistant Gram negative pathogens were five *Salmonella* spp. and *Eschericia coli* strains provided by the University of South Australia. Lactobacilli strains were maintained using de Man, Rogosa and Sharpe (MRS) medium (Oxoid Ltd, Basingstoke, UK), while lactococci was cultivated in M17 medium (Oxoid Ltd, Basingstoke, UK). All pathogenic bacteria were cultivated using Tryptone Soya Agar (TSA) medium (Oxoid Ltd, Basingstoke, UK). MRS broth and Tryptone Soya Broth with 20% of glycerol were used for the maintenance of LAB and non-LAB, respectively, at -80ºC as stocks.

Antagonistic activity assay

The well-diffusion assay method was performed according to Schillinger & Lucke [7] with a slight modification. *Lb. plantarum* S1.30 culture was prepared as follows: *Lb. plantarum* S1.30 isolate from frozen stocks were subcultured into 15 ml of MRS broth and incubated at 37 ^{o}C in 5% CO_2. After an overnight incubation, 10% (v/v) of the cultures were transferred into 15 ml of fresh MRS broth and incubated with similar condition for 24 hours.

At the same time, the indicator bacteria (Gram-positive and Gram-negative of pathogenic bacteria) were also prepared in the same way, except for the incubation conditions, which was under aerobic condition (without 5% CO_2). 100-µl of the indicator bacteria was added to 20 ml of semi solid TSA (1%, w/v) at about 45ºC and mixed gently. Subsequently, the semi solid suspensions containing the indicator bacteria were poured into sterile Petri dishes. After solidification, wells (6 mm in diameter) were made in the lawn of the hardened agar using a sterile metal cork borer.

Aliquots of the overnight test bacteria (80 µl) were dispensed into the wells. The culture suspensions in the well were allowed to diffuse into the agar for 24 hours at -4ºC. Afterward, the plates were incubated at the optimum temperature of growth of the indicator bacteria. A clear inhibition zone resulted if the cultures produced antimicrobial substances. The diameter of clear zones was measured including the diameter of the wells. This experiment was conducted in duplicate.

Conventional detection of bacteriocins

The detection of bacteriocins was performed using the well-diffusion assay as described previously. Instead of using the culture suspensions directly, a cell-free supernatant (CFS) was used. The CFS was obtained by centrifuging (5.444 x g for 20 minutes at 4ºC, Sigma 3-16K) the overnight cultures (15 ml) of *Lb. plantarum* S1.30, followed by adjusting of the supernatant to pH 6.5 to exclude the organic acid activity. Next, the neutralized-CFS (NCFS) was filtrated through a 0.2 µm membrane filter (PES membrane, Millex® GP, Millipore, Carrigtwohill Co, Cork, Ireland). This sterile neutralized supernatant (80 µl) was dispensed into the wells which had been prepared as described previously. The presence of a clear zone of inhibition indicated the result of bacteriocin-like inhibitory substance (BLIS) activity.

A protease test was used in an attempt to confirm the proteinaceous nature of the antimicrobial product from the dadih LAB. The method used in this study was described by van Belkum et al [8] with a minor modification. A 4-mm well was made next to the well (6 mm in diameter) containing the putative-bacteriocin producer cultures. Subsequently, 50 µl of proteinase-K (in Tris HCl buffer (pH 7.5) at a concentration of 1 mg/ml) was dispensed into the small wells. After incubation at 37ºC in 5% CO_2 for 24 hours, the inhibition of antimicrobial activity of the producers was observed. Nisin (0.2 mg/ml, Nisaplin – Sigma Aldrich: CAS number 1414-45-5) was used as a positive control. In this *Lb. sakei* ATCC 15521 strains were used as the indicator bacteria.

Production kinetics of Lb. plantarum S1.30

The growth and antimicrobial activity of *Lb. plantarum* S1.30 strain was assessed *in vitro*. An overnight broth culture (10 %, v/v) was inoculated into fresh MRS broth (200 ml). The culture was incubated at 37ºC in 5% CO_2 for 24 hours, and every two hours 15 ml of culture was removed to determine the cell count, pH, and antimicrobial activity. After 12 hours incubation, the sample was removed in every three hours. The total number of bacterial cells was determined using the spread plate method by serial dilution (10^{-1} – 10^{-7}). The acidity level of sample was examined using digital pH meter (Hanna Instruments). The inhibitory activity in both the cell suspensions and the NCFS was evaluated using the well-diffusion assay as described previously with *L. monocytogenes* and *Lb. sakei* ATCC 15521 as the indicator bacteria. The antimicrobial activity was indicated by the

diameter of clear zones of inhibition growth surrounding the producer colonies. The evaluation of each parameter was conducted in duplicate.

Molecular detection of bacteriocins

A PCR-based method was used to detect plantaricin A (*pln*A), a gene associated with bacteriocin activity using specific primers: *pln*A-F GTACAGTACTAATGGGAG and *pln*A-R CTTACGCCATCTATACG with the length of nucleotide is 450 bp [9]. The PCR reactions were carried out using a Mycycler thermal cycle (Bio-Rad Laboratories, Hercules, CA, USA). The master mix was prepared in 25 µl of final volume containing 5 µl of 5x PCR buffer, 2.5 µl of 25 mM MgCl2, 2.5 µl of 2.5 mM dNTPs (2 mM each dATP, dCTP, dGTP and dTTP), 0.25 µl of Taq polymerase(5 U/µl) and 3.75 µl of 2 µM each primer. The volume of DNA template was 2.5 µl. The PCR amplification was conducted for 35 cycles with conditions were 94^{o}C- 1 min, 53ºC- 1 min, 72ºC- 1 min [9]. PCR products obtained were separated using electrophoresis at room temperature on horizontal 1.5% (w/v) agarose gels. Gels containing 5% (v/v) of ethidium bromide (EtBr) were run in a tank with 1 × TAE buffer as the running buffer for at least an hour at 100 V.

3. Result and Discussion

Antagonistic activity assay

The antimicrobial activity of *Lb. plantarum* S1.30 against Gram-negative and Gram-positive of pathogenic bacteria by the agar well-diffusion assay was shown in Figure 1. Gram positive of pathogenic bacteria were more sensitive than Gram negatives. *Lb. plantarum* S1.30 showed the greatest activity against *S. pyogenes* ATCC 10389, followed by *L. monocytogenes*.

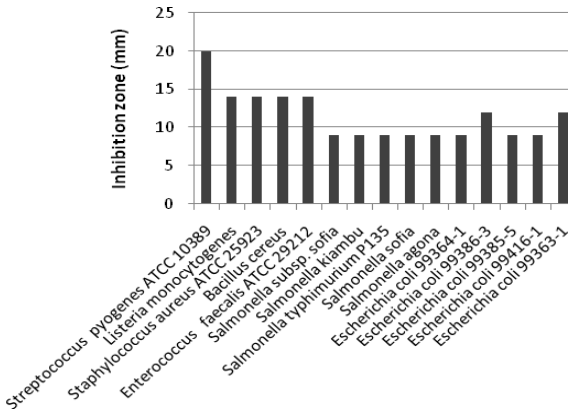

Figure 1. Antimicrobial activity of *Lb. plantarum* S1.30

Conventional detection of bacteriocins

The antimicrobial activity of dadih LAB (*Lb. plantarum* S1.30, *Lc. lactis* S1.06, and *Lc. lactis* ATCC 11454) was assessed using the agar well-diffusion method. The neutralized-cell free supernatant of these antimicrobial producers was tested against *Lb. sakei* ATCC 15521 (Figure 2) and *L. monocytogenes* (data not shown), but no bacteriocin activity was detected. A further test was applied to investigate the nature of the inhibitory activity of the producer strains. The effect of proteinase-K on the inhibition zones produced by *Lb. plantarum* S1.30 and *Lc. lactis* subsp *lactis* S1.06 was assessed but there was no effect. This suggested that the antimicrobial activity of the producers was not mediated by proteins, raising the possibility that bacteriocins were not the active agents in the antimicrobial activity.

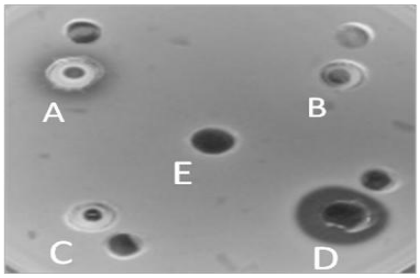

Figure 2. The nature of inhibitory substances towards proteinase-K (Indicator:*Lb. sakei* ATCC 15521; Producers: A: *Lb. plantarum* S1.30, B: *Lc. lactis* S1.06, C: *Lc. lactis* ATCC 11454, D:Nisin, E: MRS broth

Many factors can influence the production of bacteriocins. Belgacem et al [10] pointed out that the likelihood of obtaining bacteriocin-producing LAB from fermented products was variable and affected by many aspects. These include intrinsic factors associated with the products, variation in nutrients in the growth medium, variation in methodology used, and the selection of indicator bacteria. Moreover, the failure to detect bacteriocins using conventional methods may have been caused by the growth condition (pH and temperature), the composition of the media used [11], or the complex regulatory system of bacteriocin biosynthesis [5].

Production kinetics of Lb. plantarum S1.30

Lactobacillus plantarum S1.30 was utilized for further study, as this strain exhibited the greatest antimicrobial activity, especially against *Lb. sakei* ATCC 15521 and *L. monocytogenes*. A study of the inhibitory activity of this potential antimicrobial producer was performed in a static

broth culture with unregulated pH. As can be seen in Figure 3, the pH of the culture decreased from 6 to 3.54 during an overnight incubation at 37ºC in 5% CO_2 as the bacterial cell count increased. Exponential growth of *Lb. plantarum* S1.30 occurred between two and 18 hours of incubation, and early stationary phase started at 18 hours of incubation. The production of antimicrobial substances from *Lb. plantarum* S1.30 against *Lb. sakei* ATCC 15521 began after 2 hours of incubation and gradually increased, reaching maximum activity (20 mm in diameter) after 15-24 hours of incubation. When *Lb. plantarum* S1.30 was tested against *L. monocytogenes,* the antagonistic activity was detected after 8 hours of incubation and steadily increased until the end of incubation.

The maximum activity (12 mm in diameter) occurred at 21-24 hours of incubation. The increase in antimicrobial activity was positively correlated with the increasing acidity level. The antimicrobial activity of *Lb. plantarum* S1.30 commenced during the exponential phase and the maximum activity was reached in early stationary phase. However, longer incubation times should be assessed to further understand the dynamics of antimicrobial activity demonstrated by the dadih LAB. The culture supernatants were also tested (with and without neutralization to assess the effect of acid conditions on the target organisms) but no inhibition zones were observed (data not shown).

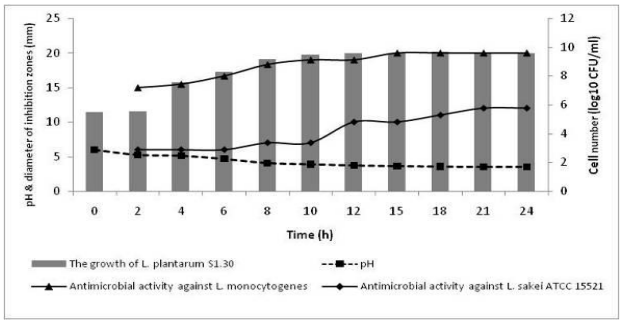

Figure 3. Effect of growth phase on antimicrobial production from *Lb. plantarum* S1.30 against *L. monocytogenes* and *Lb. sakei* ATCC 15521

The results obtained from kinetic studies of antimicrobial production showed that the organic acids produced by *Lb. plantarum* S1.30 played an essential role in inhibiting the growth of target bacteria. The beneficial activities of *Lb. plantarum* isolated from dadih have been demonstrated in the previous research [12]. A cell suspension of this bacterium actively removed the toxin, microcystin-LR, in the presence of 1% glucose [12]. Furthermore, in an *in vitro* study, this highly adhesive bacterium was able to compete with the pathogen which was trying to colonize the mucus layer of the intestinal epithelium [1].

Molecular detection of bacteriocins

Due to the failure to detect bacteriocins through an agar diffusion based method, a PCR-based method was carried out by using specific primers targeting a bacteriocin regulation gene, *pln*A. A pair of *pln*A primers targeting the plantaricin A gene was selected for this study, because plantaricin A has frequently been found in a variety of *Lb. plantarum* isolates from a wide range of environments. *Pln*A is an induction factor that can induce the production of bacteriocin in *Lb. plantarum* [13-14]. The PCR amplification resulted a-450 bp-DNA fragment (Figure 4), which indicated that plantaricin A was present in *Lb. plantarum* S1.30.

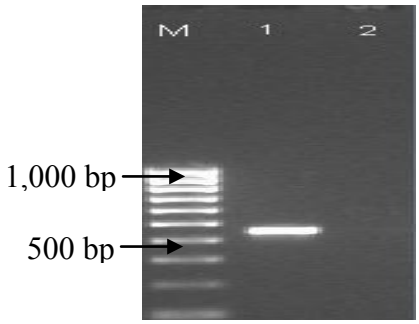

Figure 4. Amplification product of plantaricin A (450 bp); Lane M: 100 bp DNA marker; lane 1: *Lb. plantarum* S1.30 (plantaricin A); lane 2: sterile milliQ H_2O

Investigation of the regulatory mechanism for bacteriocin biosynthesis is a plausible avenue to explore as regulation is triggered by a quorum sensing mechanism. In support of this, plantaricin was detected in *Lb. plantarum* S1.30 using PCR. However, the *pln*A gene is not directly responsible for plantaricin biosynthesis. Diep et al. [13] argued that plantaricin A is a bacteriocin-like peptide which triggers bacteriocin biosynthesis when it is present in the growth media. Some *Lb. plantarum* strains containing *pln*A in their genome exhibited bacteriocin activity, such as strains C11, WCFS1 (type strain), J51 and V90 [14]. In case of *Lb. plantarum* S1.30 was required to evaluate *pln*A or related genes in inducing bacteriocin production.

The failure to detect bacteriocin production by *Lb. plantarum* S1.30 might be related to the composition of the growth medium, especially the lack of milk protein fragments, as recently proposed by Georrgalaki *et al* [15]. This group reported that the bacteriocin (macedocin) could not

be detected if either MRS or M17 media were use, leading them to cultivate the macedocin producers (*Streptococcus macedonicus* ACA-DC 198) in milk media. They concluded that the production of macedocin was not directly affected by the presence of lactose or galactose, but that the organisms produced a heat-stable protein when cultured on milk media and that this protein induced macedocin production. These findings suggest an approach that could be investigated for detection of bacteriocin production by dadih bacteria.

4. Conclusion

The failure to detect antimicrobial activity in *Lb. plantarum* S1.30 with the conventional methods warrants further investigation to see if milk media would be more suitable for culture of *Lb. plantarum* S1.30. In addition, a study of quorum sensing and investigations of *pln*A and similar genes could help determine why antimicrobial activity was demonstrated by cultures of *Lb. plantarum* S1.30 but no bacteriocin could be detected.

5. Acknowledgments

We thank to Dr. Inggrid Surono for her assistance during collecting dadih samples and the isolation of dadih micro-flora. This work was supported by AusAID / ADS 2008-2010.

6. References

[1] Collado, M.C., I. Surono, J. Meriluoto, and S. Salminen (2007), Potential probiotic characteristics of *Lactobacillus* and *Enterococcus* strains isolated from traditional Dadih fermented milk against pathogen intestinal colonization. *Journal of Food Protection*, 70, 700-705.

[2] Collado, M.C., I. Surono, J. Meriluoto, and S. Salminen (2007), Indigenous Dadih lactic acid bacteria: cell-surface properties and interactions with pathogens *Journal of Food Science*, 72, 89-93.

[3] Surono, I.S., (2003), *In vitro* probiotic properties of indigenous dadih lactic acid bacteria. *Asian - Australasian Journal of Animal Sciences*, 16, 726-731.

[4] Talon, R., S. Leroy, and I. Lebert (2007), Microbial ecosystem of traditional fermented meat products: the importance of indigenous starters. *Meat Science*, 77, 55-62.

[5] Heng, N.C.K., P.A. Wescombe, J.P. Burton, R.W. Jack, and J.R. Tagg (2007), The diversity of bacteriocins in gram-positive bacteria, in Bacteriocins: Ecology and Evolution, Editor: M.A. Riley and M.A. Chavan, Springer, Verlag Berlin Heidelberg.

[6] Jatmiko, Y.D., M. De Barros Lopes, and M.D. Barton (2010), Isolation and antimicrobial potency of indigenous lactic acid bacteria isolated from dadih, a traditional fermented buffalo milk from Indonesia. *School of Pharmacy and Medical Sciences*, Master.

[7] Schillinger, U. and F.K. Lucke (1989), Antibacterial activity of *Lactobacillus sake* isolated from meat. *Applied and Environmental Microbiology*, 55, 1901-1906.

[8] van Belkum, M.J., B.J. Hayema, A. Geis, J. Kok, and G. Venema (1989), Cloning of two bacteriocin genes from a lactococcal bacteriocin plasmid. *Appl. Environ. Microbiol.*, 55, 1187-1191.

[9] Remiger, A., M.A. Ehrmann, and R.F. Vogel (1996), Identification of bacteriocin-encoding genes in lactobacilli by polymerase chain reaction (PCR). *Systematic and Applied Microbiology*, 19, 28-34.

[10] Belgacem, Z.B., M. Ferchichi, H. Prevost, X. Dousset, and M. Mannai (2008), Screening for anti-listerial bacteriocin-producing lactic acid bacteria from ‗‗Gueddid'' a traditionally Tunisian fermented meat. *Meat Science*, 78, 513-521.

[11] Rojo-Bezares, B., Y. Saenz, L. Navarro, M. Zarazaga, F. Ruiz-Larrea, and C. Torres (2007), Coculture-inducible bacteriocin activity of *Lactobacillus plantarum* strain J23 isolated from grape must. *Food Microbiology*, 24, 482-491.

[12] Surono, I.S., M.C. Collado, S. Salminen, and J. Meriluoto (2008), Effect of glucose and incubation temperature on metabolically active *Lactobacillus plantarum* from Dadih in removing microcystin-LR. *Food and Chemical Toxicology*, 46, 502-507.

[13] Diep, D.B., L.S. Håvarstein, and I.F. Nes (1995), A Bacteriocin-like peptide induces bacteriocin synthesis in *Lactobacillus plantarum* C11. *Molecular Microbiology*, 18, 631-639.

[14] Diep, D.B., D. Straume, M. Kjos, C. Torres, and I.F. Nes (2009), An overview of the mosaic bacteriocin pln loci from *Lactobacillus plantarum*. *Peptides*, 30, 1562-1574.

[15] Georgalaki, M., M. Papadelli, E. Chassioti, R. Anastasiou, A. Aktypis, L. De Vuyst, G. Van Driessche, B. Devreese, and E. Tsakalidou (2010), Milk protein fragments induce the biosynthesis of the macedocin, the lantibiotic produced by *Streptococcus macedonicus* ACA-DC 198. *Applied and Environmental Microbiology*, 76, 1143-1151.

Aloe Gel Herbal Therapy on Diabetic Ulcer Healing

Adeodatus Yuda Handaya [1], Djanggan Sargowo [2], M. Aris Widodo [3], Diana Lyrawati [4], Askandar Tjokroprawiro [5]

[(1)] Dept. of Surgery, Kanjuruhan Hospital / Biomedic, Medical Faculty, Brawijaya University, Malang, Indonesia (yudahandaya@yahoo.com)
[(2)] Dept. of Cardiology, Medical Faculty, Brawijaya University, Malang, Indonesia (djanggan@yahoo.com)
[(3)] Dept. of Pharmacology, Medical Faculty, Brawijaya University, Malang, Indonesia (marswidodo1948@yahoo.com)
[(4)] Dept. of Pharmacology, Medical Faculty, Brawijaya University, Malang, Indonesia (eldi_7_98@yahoo.com)
[(5)] Dept. of Internal Medicine, Airlangga University, Surabaya, Indonesia (diabetes@rad.net.id)

Abstract

The increasing of Diabetes Mellitus prevalention in the world and also in Indonesia has a great impact to the number of morbidity and mortalitiy. Further Diabetes Mellitus will be progesssion to the diabetic foot ulcer formation that followed amputation of lower extremity. Delaying of diabetic wound healing process will be addition of suffering and cost therapy for diabetic patient. In the wound healing process angiogenesis is essential stage to increase the wound healing rate. The solution to stimulate of wound healing can be done by herbal treatment like Aloe vera plant that has potention to stimulate wound healing. Aloe vera is teresterial sukulen plant that cosmopolite and can be obtained from everywhere with active ingredient that knowed involve in a various herbal therapy for many disease especially wound healing. From this fact Aloe vera able to be a new natural candidate for combine therapy to diabetic ulcer patient. Aloe vera has capability as immune modulator and nutritional sources that can be stimulate wound healing rate by controlling inflammation duration on early wound healing stage and expected giving nutritional supply on the wound site to finishing wound healing process. Aloe gel with capability as immune modulator and growth factor stimulator is expected able to support in clinical combine therapy. Aloe gel is focused to balancing inflammation phase and preventing hypoxia in wound site by stimulate angiogenesis process and proteolitic activity on collagen deposition.

Keywords: *Aloe gel, wound healing, diabetic ulcer.*

1. Introduction

Diabetes Mellitus is a widespread disease and affects all nationalities and ages. The number of patients in 2003 has reached an epidemic proportion totalling a whopping 194 million with patients of 20 to 79 years of age affected (5.1 % of the population in this age group). A rise to 50% more is expected in 2010, mainly from new cases in Africa, Asia and South America. A projection of this figure shows that in 2025 diabetes patients will be 333 million or 6.3% of the total population on Earth [1,2].

According to the American Diabetes Association, 7% of the general population and 21% of people over the age of 60 are afflicted with diabetes in the United States. One of the most outward and debilitating complications of diabetes is the development of chronic non-healing foot ulcerations, occurring in 15% of diabetics. In its most unfavorable course, diabetic foot ulceration leads to amputation in 14-24% of afflicted individuals and is the leading cause of nontraumatic lower extremity amputation in the U.S. The national economic burden of diabetic foot ulceration and amputation is correspondingly staggering, estimated near 11 billion dollars in the year 2001 [2,3].

Wound healing in diabetes is crippled by aberrant cellular phenotypes of essentially all participating cells and abnormalities in the expression and activity of cytokines and growth factors required for coordinating the healing process. The pathogenic forces implicated are numerous, and include hyperglycemia, generalized chronic inflammation, impaired neuropeptide signaling, hypoxia, and altered microcirculatory structure and reactivity. As a result, whereas acute wounds progress linearly through the phases of wound healing, chronic non-healing ulcers are unable to progress in

synchrony and become stalled predominantly in the inflammatory phase [3,5].

Management of diabetic ulcer should be focused on to minimized the comorbid disease, reducing off loading, wound care and maintenance the wound moist, infection management, debridement, revascularization and electical surgery, prophylactick, kurative or energency, enhance the wound healing, and also by topical application with herbal and autolog growth factor. The management of diabetic foot ulcers is mostly development. This technology including growth factors, living skin equivalents, electrical stmulationk, cold laser and heating, Becaplermin (recombinant platelet-derived growth factor) for topical treatment diabetic foot ulcer, wound dressing (e.g, hydrocolloids dressing, alginate dressing, hydrogel dressing, iodine dressing serta promogran), biological skin substitute / living skin equivalents (LSEs) [6,7].

Mean while, *Aloe vera* is general plant that growth fastly in tropical climate and easy acquired from everywhere. This plant has most active chemical compound that correlated with a various disease, especially wound healing. This fact are proving that *Aloe vera* has probabilty as a new natural herbal therapy combination on clinic. *Aloe vera* gel has acapability as immune modulator and nutritional resource that possibly able to stimulate wound healing process by controlling inflammation phase in early healing stage.

2. Discussion

Aloe gel providing a nutritonal supply for wound site and suggested enhancing the wound healing process [8]. The result research showed that one of many pollisaccharide of aloe gel acemannan on 20 µg/mL dose able to stimulate the wound healing rate [9]. Acemannan has strong potention to stmulate cellular proliferation and migration and also cytokine production. Acemannan on Aloe gel play a pivotal role on oral wound healing by induction fibroblast proliferation and stimulate VEGF and KGF expression [10]. Acemannan has potention to enhancing haematopoietic process and a potent antioxidant. Acemannan can also reducing inflammation through prostaglandin synthesis and increasing leukocyte infiltration [11].

On the other hands, a new research is proved that new herbal extract Semelil (ANGIPARS) is very potential and effective to ulcer treatment. Semelil (ANGIPARS) has potential target on angiogenesis and making this process fasted significantly [12]. From this fact there are needed further a new research to improve the effect of Aloe vera gel in angiogenesis wound healing stimulation and the role on every stage of diabetic wound healing process.

Aloe vera plant is source of two herbal substances, there are aloe gel (AG) and aloe latex. Aloe gel contain 99% water as major ingredients and or mono/polisaccharide (25% from wet gross of gel). The major monosccharide on AG is mannose-6-phosphate, and on the other hands, the major polisaccharide is gluco-mannans (beta-(1,4) acetylated mannan). Both of this subtances is long-chain sugars that containing glucose and mannose. Aloe gel is also containing lignan, sallicilic acid, saponin, sterol, and triterpenoids. The fresh gel containing proteolitic enzyme carboxypeptidase (that breakdown bradikinin), glutation peroksidase and other isozyme from superoxide dismutase. Aloe gel has vitamin compounds like vitamin A, C, E, B12, thiamin, niasin, and folic acid. The mineral contain within aloe gel such as sodium, potassium, calcium, magnesium, mangan, cuprum, zinc, chromium, phospor and ferrum [8].

Aloe gel has five different enzymes (lipase and protease), amino acids (22 amino acie are founded within aloe gel), plant sterol (as potent antiinflammatory agent), Giberelin (stimulate growth factor that help healing process), polisaccharide lignin and also including B1-3 and B1-4 glucomannan with immunostimulant effect [13]. Aloemannan and acemannan showing anti tumor activity, anti inflammation and immunosupression. Its different with glycoprotein fraction that has a capability to bradikinin degradation and stmulate cells proliferation [14].

Aloe gel has become immunostimulant through stimulate macrophage. Aloe gel is able to increase immune cells production dan begins leucocyte activity. Aloe gel or breakdown providing many nutritional support to optimized the role of immune system [13]. Aloe gel inhibit the inflammation process by supressing prostaglandin formation, cholesterol synthesis or bradikinin enzyme activity. Acemannan has direct effect to immune system, activate and stimulate macrophage, T cells and antibody [15].

Aloe gel showing the anti inflammatory effect, analgesic, wound healing, modulate the immune system, anti tumor, anti viral, anti bacterial, anti fungal. Aloe gel on diabetic wound rat maybe stimulate wound healing process by influence the phase within wound healing stage like inflammation, fibroplasia, collagen synthesis and maturation and also wound contraction [16]. Polisaccharide of aloe that action as

iimunostimulant is also increasing macrophage and monoscyte circulation significantly [8,17].

Antraquinon as derivate of *Aloe vera* gel palting important role in the tumor treatment, diabetes, ulcers and cancer. *Aloe vera* gel has effect to progress healing in the epithelial damage tissue by providing essential micronutrient, supress the inflammation through skin fibroblast stimulation [18]. *Aloe vera* gel is reported able to stimulate the increasing of arteriolar diameter in wound site and followed by enhance re-epitelialization that related with keratinocyte proliferation and migration. But its remain fully unclear how the effect aloe gel to the stimulation of wound healing through cytokine and growth factor spesific in the wound site. *Aloe vera* has a potency to enhance the angiogenesis wound healing, because re-vascularization process are playing a pivotal role in the wound healing. Based on the result research before, it is found that beta-sitosterol component showing angiogenic activity on the CAM (*chorioallantoic membrane*) by *in vitro*. Heparin and beta-sitosterol collaborate to stimulate neovascularization in mouse Matrigel plug assay and HUVECs motility on wound migration test *in vitro* [19].

Angiogenic activity of *Aloe vera* gel is founded by *in vitro* study from *Aloe vera* extract fraxination. This fraction increase the proliferation of calf pulmonary artery endothelial cells (CPAE). F3 fraction induction the CPAE cells to invate collagen gel type I and making capilar tube through angiogenesis test [15]. Active component of *Aloe vera* able to stimulate fagocytosis activity and induce NO production, enhance angiogenic activity, increasing collagen synthesis, crosslinking and maturation, stimulate fibroblast proliferation and maturation, inhibit elevation of TNF-α level and act as antioxidant [20]. Beta sitosterol within *Aloe vera* gel stimulate formation of new blood vessel in Mongolian gerbil. Beta-Sitosterol also enhance protein expression that related with angiogenesis programme such as von Willebrand factors, vascular endothelial growth factor (VEGF), VEGF receptor Flk-1, and blood vessel matrix laminin. From this fact is suggested that beta-sitosterol has therapeutic angiogenic effects on blood vessel damage, but its needed further investigation how the aloe gel stimulate angiogenesis programme via molecular mediator that contribute in molecular signaling in vascular cells [21].

Aloe vera increase the expression of EGF and fibroblast function (for collagen formation). The enhancing of fibroblast migration on cells culture maybe has good effect to protect skin damage when the skin in healing process [13]. Glycoprotein Aloectin A is also reported has antit ulcers effect and increase the human dermal cells proliferation [22]. *Aloe vera* reported able to stimulate ability of GJIC and skin fibroblast proliferation on DM patient. *Aloe vera* has chemical component that binding with FGF-2 receptor or change the signaling pathways of FGF-2. The effect on GJIC and fibroblast proliferation is improved that *Aloe vera* has positive effect on diabetic wound healing process in patient [23].

In the aloe gel, acemannan is founded as carbohydrate complex isolated from gel on *Aloe vera* leaf consist of beta-(1-4)-linked acetylmannose polymer with molecular weight 10-1000 kDa with average weight 200 kDa. On the cellular level acemannan able to stimulate cellular proliferation, migration, and cytokine production. Glucan application on wound are showing increasing of angiogenesis rate and re-epitelialization. Generally ole gel polisaccharide enhance healing process on wound site, but is this subtances induce wound healing rate through angiogenesis molecular program that related with VEGF, eNOS, ERK1/2 pathways is not fully understood. Aloe gel extract stimulate oxygen consumption, increase collagen and angiogenic activity in wound area [15]. From the result study before are showing that acemannan able to enhancing wound healing rate on 20 µg/mL dose by solution [9]. Acemannan is polydispersed beta-(1,4)-linked acetylated mannan that playing important role as anti viral, immunomodulator, and activate macrophage. Acemannan is also increase NO synthesis in RAW 264.7 cells by inducing the expression of NOS mRNA from macrophage. Acemannan on aloe gel playing important role in oral wound healing case by induce fibroblast proliferation and stimulate KGF-1 and VEGF expression [10].

3. Conclusion

Aloe vera gel especially acemannan molecule as the major component of aloe gel has great potention as herbal clinical combine therapy candidate on diabetic ulcer wound healing. *Aloe vera* gel able to stimulate diabetic wound healing by maintenance the all phase in wound healing process and has probability as nutrient sources to growth factor stimulation within the angiogenesis process. *Aloe vera* gel suggested playing important role in the revascularization process and inflammation controling.

4. Ackwowledgements

The first author is thanking very much to Prof. Dr. Djanggan Sargowo, Prof. M. Aris Widodo, PhD., Mrs Diana Lyrawati, PhD and Prof Dr. Askandar Tjokroprawiro, Medical Faculty of Brawijaya University and Airlangga University, for their support and for helpful comments.

5. References

[1]. Goycheva, P., Gadjeva.V and Popov, B., (2006), Oxidatif Stress and Its Complication in Diabetes Mellitus.*Trakia Journal of Sciences*, Vol. 4, No.1.

[2]. Lauderdale (2006), Current Concepts in the Diagnosis and treatment of diabetic Retinophaty,Including Diabetic Molecular Udema. *Carring For Diabetes*, *E*-Newsletter.

[3]. Pradhan. L., Nicholas D. Andersen, Frank W. LoGerfo and Aristidis V., (2007), Molecular Targets for Promoting Wound Healing in Diabetes. Recent Patents on Endocrine, *Metabolic & Immune Drug Discovery*, 1: 1-13.

[4]. Ralf L., Gregory S. and Hendrik L., (2005). Proteases and the Diabetic Foot Syndrome: Mechanisms and Therapeutic Implications. *Diabetes Care*, Vol. 28 No. 2: 461-471.

[5]. Li, W. W., Dimiris T., Vincent W.LI, (2003), Angiogenesis: A Control Point for Normal and Delayed Wound Healing. *Suplement to Contemporary Surgery*, pp 5-10.

[6]. Dinh, T., Hau Pham and Aristidis V., (2008), Feature: Emerging Treatments in Diabetic Wound Care.

[7]. Suharjo, B.C., (2007), Manajemen Uklus Kaki Diabetik. *Dexa Media*, Vol. 20, No. 3.

[8]. Wendell L. Combest (2000), Aloe vera. Department of Biopharmaceutical Sciences, Shenandoah University School of Pharmacy, Winchester, VA.

[9]. Laura K.S. Parnell, Anthony D. Chinnah, Ian R. Tizard, BV., (2002), Use of Mouse Footpad Model to Test Effectiveness of Wound Dressings. *Wound Care*, Vol: 14, Issue: 5.

[10]. Ramamoorthy, L., MC Kemp and IR Tizard (1996), Acemannan, a beta-(1,4)-acetylated mannan,induces nitric oxide production in macrophage cell line RAW 264.7. *American Society for Pharmacology and Experimental Therapeutics*, Vol 50, Issue 4, pp: 878-884.

[11]. Hamman, J. H., (2008), Composition and Applications of *Aloe vera* Leaf Gel. *Molecules, 13,* 1599-1616.

[12]. Larijani, B and Hasani Ranjbar, S. (2008), Overview of diabetic foot; novel treatments in diabetic foot ulcer. *DARU, 16 (Suppl. 1) 1-6.*

[13]. Timothy R. Fray, Adrian L. Watson, Julie M. Croft, Claire D. Baker, Julie Bailey, Nicola Sirel, Amanda Tobias, and Peter J. Markwell (2004), A Combination of Aloe Vera, Curcumin, Vitamin C, and Taurine Increases Canine Fibroblast Migration and Decreases Tritiated Water Diffusion across Canine Keratinocytes in Vitro. *J. Nutr*. 134: 2117–2119.

[14]. Yagi A. and Takeo S., (2003), Anti-inflammatory constituents, aloesin and aloemannan in Aloe species and effects of tanshinon VI in Salvia miltiorrhiza on heart .*Yakugaku Zasshi*. 123 (7):51732.

[15]. Lawrence Plaskett (2005), The Healing Properti of Aloe vera.

[16]. Gallagher J, and Gray M., (2003), Is aloe vera effective for healing chronic wounds?. *J Wound Ostomy Continence Nurs*. 30(2):6871.

[17]. Barrantes E, and Guinea M. (2003), Inhibition of collagenase and metalloproteinases by aloins and aloe gel. *Life Sci*. 72 (7):84350.

[18]. Lee MJ, Lee OH, Yoon SH, Lee SK, Chung MH, Park YI, Sung CK, Choi JS, Kim KW., (1998), In vitro angiogenic activity of Aloe vera gel on calf pulmonary artery endothelial (CPAE) cells. *Arch Pharm Res*, 21(3):260-265.

[19]. Moon EJ, Lee YM, Lee OH, Lee MJ, Lee SK, Chung MH, Park YI, Sung CK, Choi JS, Kim KW., (1999), A novel angiogenic factor derived from Aloe vera gel: beta-sitosterol, a plant sterol. *Angiogenesis*. 3(2):117-23.

[20]. Aydın İ., Meral Ş., Cemile K., Metin E. and Cenap D. (2007), Effects of Aloe vera on colonic anastomoses of rats. *Journal compilation*, College of Surgeons of Hong Kong.

[21]. Choi, Seongwon.,Kim, Kyu Won., Choi, Jae Sue., Han, Sang Taek., Park, Young In., Lee, Seung Ki., Kim, Jeong Soon., and Chung, Myung Hee. (2002), Angiogenic activity of beta-sitosterol in the ischaemia/reperfusion-damaged brain of Mongolian gerbil. *Planta-Med*, 68(4): 330-5.

[22]. Miyuki, T., Eriko M., Yousuke I., Noriko H., Kouji N., Muneo Y., Tomohiro T., Hirotoshi H., Mitunori T., Masanori I., and Ryuuichi H., (2006), Identification of Five Phytosterols from Aloe Vera Gel as Anti-

diabetic Compounds. *Biol. Pharm. Bull.* 29(7) 1418—1422.

[23]. Kay M. A., Ahmed A., Mary L. J., Jerzy J. B., Kimberly P., Dale A. R., Lawrence P. R., and Anna T. G-Bilska., (2003), Effects of *Aloe vera* on Gap Junctional Intercellular Communication and Proliferation of Human Diabetic and Nondiabetic Skin Fibroblasts. *The Journal of Alternative and Complementary Medicine*, 9(5): 711-718.

[24]. Arjan W. G. and Grietje M., (2007), Angiogenesis: Potentials for Pharmacologic Intervention in the Treatment of Cancer, Cardiovascular Diseases, and Chronic Inflammation. *Pharmacological Review,* Vol. 52, Issue 2, 237-268.

[25]. Rajendran, A, V. Narayanan and I. Gnanavel. (2007), Evaluation of Therapeutic Efficacy of *Aloe vera* Sap in Diabetes and Treating Wounds and Inflammation in Animals. *Journal of Applied Sciences Research*, 3 (11): 1434-1436.

[26]. Sidartawan, S. (2007), Diabetes, The Silent Killer.http://www.medicastore.com/med/index.php.

The Effect of Teaching of Vitamin C using Problem Based Learning and Laboratory Works on Students Achievement

Afnidar [1], Sri Hamda [2], Erdawati [3]

(1) Department of Chemistry, Open University of Jakarta, Indonesia
(2) Department of Chemistry, Open University of Banjarmasin, Indonesia
(3) Department of Chemistry, State Univercity of Jakarta, Indonesia

Abstract

The aim of this study is to determine the effects of problem based learning and laboratory works on students" academic achievements, conceptual developments and scientific process skills about vitamin comparison with traditional instruction. In this research, the pre/post test control group design was applied and the research was conducted with 9th and 10th grade students from two classes at a high school in Jakarta. The classes were randomly determined as two experimental groups with problem based learning (NP =90) and the other group with laboratory (NL= 30), and one control group (NC=30). Before the instruction, the pretest (KR-20 = 0.81) was given to all the students to identify their prior knowledge about the basic subjects of „vitamin C". No significant differences were found between the groups and and control groups in each class (p>0.05). The subject of "vitamin C" was taught supported with problem based learning and laboratory experiments in the experimental groups while traditional approach was used in the control groups. The results of the post-test (KR-20 = 0.77), applied after the instruction, indicated that students who performed experiments was significantly reached higher mean scores than those of control groups (p<0.05). Students"pre and post attitudes towards problem based learning and chemistry experiment were assessed by using quistionarie. It is found that the mean scores of the experimental groups significantly increased from 68.60 to 86.50 (p<0.05).

***Keywords**: academic achievements, vitamin C, problem based learning, laboratory works.*

1. Introduction

Laboratory work as an active learning method which requires students to involve in observing or manipulating real objects and materials, have a distinctive and central role for development of students' understanding of scientific concepts, improving cognitive skills as well as developing positive attitudes[1].

Hofstein, Shore and Kipnis [2] reported that by providing students with opportunities to engage in appropriate inquiry-type experiments in the chemistry laboratory, their cognitive abilities would be improved. In the other study, Hofstein *et.al* [3] investigated the ability of high-school chemistry students who perform chemistry experiments related to acids–bases, stoichiometry, oxidation and reduction, bonding, energy, chemical equilibrium, and the rate of reactions. The students were asked to ask meaningful and scientifically questions related to their observations and findings in an inquiry-type experiment. They found that students who perform inquiry-type experiment asked questions in the chemistry laboratory outperformed the control group in their ability to ask more and better questions.

Hofstein and Walberg [4] suggest that inquiry-type laboratories are the central to learning chemistry since students are involved in the process of conceiving problems and scientific questions, formulating hypotheses, designing experimenting, gathering and analyzing data, and drawing conclusion about scientific problems or phenomena.

Problem-based learning (PBL), always starts with a problem. This problem refers to an academically or professionally relevant issue of which students are supposed to learn more [5]. Problem based learning is informed in sessions within which there are small collaborative groups comprised of 6 or 8 students with guidance from a tutor .They deal with scenarios involving several problems in above mentioned sessions and try to find appropriate answers to these problems. These sessions constitute the foundation of problem based learning model. In these sessions, it is aimed to enable the student to learn by setting off the problems that explain the subject matter in best way, the integration of school learning and

real life. This curriculum approach also addresses state and national standards and integrates disciplines. It has been supported in the literature that PBL positively influence the creative thinking, problem solving, academic achievement, attitude and scientific process. For instance, Yuzhi [6], investigated the effects of PBL group having higher scores in creative thinking measures in comparison to control group. Moreover, both Polanco [7] and Torp [8] investigated the effects of PBL on academic achievements, scientific process skills and attitudes towards lesson of students through a pretest-posttest control group design, and they revealed that the PBL group had higher scores in academic achievement, attitude towards lesson and scientific process skill measured in comparison to the control group. Similar to the above studies, several researchers claimed that PBL had a positive influence on academic achievement [9].

The aim of this study is to determine the effects of problem based learning, laboaratory works and traditional teaching methods (TTM) on students‘ academic achievements, conceptual developments and scientific process skills.

2. Method

Specifically, this study was focusing on the effects of instruction supported with problem based learning and laboratory works related to the ―vitamin C" over teacher centred traditional approach on high school students‘ achievements and attitudes toward laboratory.

This study was conducted with participation of 90 high school students (17 years of aged) from three classes in one high schools in Jakarta, Indonesia. These schools has three classes which were randomly assigned to experimental (NE-LW=30, NE-PBL=30) and control groups (NC-1=30) in each. The students in the experimental groups were taught about vitamin C and supported with laboratory works and problem based learning while the control group was instructed in a traditional teacher-centred manner.

Treatments in the PBL and Control Groups

At the beginning of implementation, the achievement pretest and scientific process skills pretest of Vitamin C were applied to both experiment and control groups. Firstly, the concepts and learning aims of the vitamin C were set. Then, scenarios were prepared in accordance with learning aims of the vitamin C. Pilot application of these scenarios was applied before PBL implementation in order to determine whether students reached learning aims or not, and finally some required corrections about scenarios were done by researcher. Sixty students in the xperiment group were divided into three groups of which consisted of 30 students.

In the first session, a presentation was made to inform students about what PBL is and how the PBL lessons proceeds. Then, three tutors, one of whom was researcher, were assigned to each group. Later, tutors presented problem scenarios to their group members. The experiment group was exposed to PBL activities involving ill-structured problem scenarios developed through the following steps:

1. Introduction of the problem situation: Ill-structured problem were introduced.
2. Expectations from the group members: Group members were introduced to each other followed by the introduction of expectations from each group member leading to an acceptable solution of the problem.
3. Opinions about the problem: Each group member delivered their ideas about the problem and reflected on their peers‘ opinions through chat or discussion forum facilities.
4. Prior knowledge about the problem: Group members shared their prior knowledge on the problem.
5. Required information to solve the problem: Group members determined and discussed the type and extent of information necessary to solve the problem.
6. Determining plans: Each group member determined an individual study plan addressing the problem situation and reflected on their peers‘ plans.
7. Solution process: Using their own and peers‘ resources and discussing with group members and the tutor, each member created their own action plan leading to a potential solution for the problem.
8. Evaluation: Each group member reflected on their and their peers‘ action plans. In addition, they assessed the contribution of each group member to the solution.

However, control group was taught the vitamin C by using traditional teaching methods. Therefore, the lessons were based on teachers‘ explanations, textbooks, questioning and discussions. Students were passively participated during the lessons. Instruction to each group of vitamin C unit took 2 class hours (2x45 minutes) in total. Then, students in experiment group carried out experiments about vitamin C topics with helping from their tutors, whereas these experiments were presented with demonstration

method to students in control group by researcher. This application about experiments took 2 class hours. Following the application, achievement posttest and scientific process skills posttest were applied to experiment and control groups again.

Treatments in the Laboratory Groups

In this study, while the subject of *"vitamin C"* was taught in the experimental groups supported with laboratory experiments. The laboratory experiments related to *indicators,* titrations*, and spectrophotometer* were developed based on constructivism by considering students' learning difficulties and misconception determined in the literature. The laboratory worksheets were prepared including -*Aims of the experiments*, -*Equipments and chemicals*, -*The warnings*, *Experimental procedures*, and *Leading questions*.

The leading questions in the experiments' worksheets were constructed critically to encourage students to do some research, connect their existing knowledge to the new ones, discuss and share their knowledge in the groups. Before begin the experimental session, the group students were informed about using laboratory worksheets, laboratory equipments and materials, laboratory rules, data evaluation, report writing techniques and laboratory safety via a preparatory lesson. All the experiments were done by students under the guidance of the teacher just after the lesson of related subject had been delivered. While students were working, teacher observed all the groups and assessed their performance by asking some guiding questions about the experiments.

Student groups were also encouraged to prepare laboratory reports for each experiment including the aim of the experiment, short explanation of the experimental procedure, results, evaluation and discussion of the results by associated with various sample, response to the questions in the laboratory worksheet, and conclusion.

The vitamin C Achievement Test

The test which consisted of 10 multiple-choice and 5 open-ended items was developed to identify students' knowledge about vitamin C. A pilot study was conducted with 90 students of different branches (mathematics, chemistry, physics, biology and science teachings) to establish the reliability of the test. Three items having low validity and reliability levels were excluded from the multiple-choice test, and total multiple choices item were reduced to 2.

Moreover, the open-ended items were evaluated two times by researcher and Pearson correlation coefficient of each item was calculated. It was found that Pearson correlation coefficient of the items was not low. Thus, the vitamin C achievement test was formed 9 multiple-choice and 4 open-ended items.

Concept Test on vitamin C, semi-structured interview and unstructured observation were used as data gathering instruments. The test consists of 13 two tier questions. Concept Test on vitamin C was applied as pre-test and post-test. The answers of students to the Concept Test on vitamin C were compared between the groups with Statistical Package for the Social Sciences (SPSS 16.0).

The comparions between the groups were analyzed using Kruskall Wallis and Man Whitney U tests. The semi-structure interviews were conducted with three students of the each experiment groups. Three questions were asked to the students and the answers of the students were recorded. The mutual interactions between student-student and student- teacher were observed with unstructured observations. The data which gained form interviews and observations were analyzed by descriptive methods.

3. Results and Discussion

The results gained from Vitamin C Concept Test

The comparisons between groups' pre and post tests' results were given in this section with Tables 1, 2, 3, 4 and 5. Note: PBL is Problem Based Learning, LW is Laboratory Work and C is Control.

Table 1. The results gained from Kruskal Wallis Test on the pre-tests

Groups	n	Mean	sd	K^2	p
PBL	30	31.92	2	0.44	0.76
LW	30	34.05			
C	30	34.65			

Table 2. The results gained from Kruskal Wallis Test on the post-tests

Groups	n	Mean	sd	K^2	p
PBL	30	35.26	2.15	15.66	0
LW	30	40.54			
C	30	34.18			

The results of the analysis in Table 1 shows that there was no significant difference among the pre-test scores of the three groups ($K2(2)= 0.46$, $p>.05$). When the mean ranks of the groups were considered, there were no significant differences among the groups as well. The analysis results in Table 2 shows that there was a significant difference among the average

post test scores of the groups ($K^2(2)= 15.66$, $p<.05$). The results of t test, conducted to detect what is the source of this difference, are presented below in Table 3 and 4.

Table 3. The results gained from t test on the post tests of the PBL and LW groups

Groups	n	t table	tSum
PBL	30	1.96	1.14
LW	30		

Table 4. The results gained from Mann Whitney _U' test on the post tests of the PBL and C groups

Groups	n	t table	tSum
PBL	30	1.96	1.68
C	30		

Table 5 The results gained from Mann Whitney _U' test on the post tests of the LW and C groups

Groups	n	t table	tSum
LW	30	1.96	2.06
C	30		

Concerning the analysis results in Table 3, there was no significant difference between the final test scores of the PBL and LW groups ($t=1.14$; $p>.05$). When the analysis results in Table 4 are examined, there was no significant difference between the post test scores of ABGM and control groups ($U=1.68$; $p>.05$). Considering the results in Table 5, it can be said that there is a significant difference between the post test scores of the LW and control group students ($7=2.06$; $p<.05$), favoring LW group.

The findings obtained by the semi-structured interviews carried out with the students in PBL and LW groups

In the interview, first the students were given the information of vitamin C sources and function. Then the students were asked to draw the structure of vitamin C molecule.

In the second question of the interview, the reaction; vitamin C + NaOH; was given to the students and they were asked to draw concentration versus time graphs during the process until the equilibrium is reached. NaOH was added to the vitamin C solution in three set of experiments which were an experiment in a constant temperature and volume, an experiment with increasing the temperature in constant volume and an experiment with decreasing the volume in constant temperature.

With the framework of the present study, the vitamin C concept was applied on experimental and control group students on pre and post test basis. Kruskal Wallis Test made to evaluate the pre-test scores of the groups showed that there was no significant differences among the pre-test scores of the three groups ($(2)= 0.46$, $p>.05$). This shows that prior to the application of the teaching strategies, the students in experimental and control groups were equivalent in terms of achievement on vitamin C concepts. Again, t test showed that there was significant differences among the post-test scores of the groups ($K2(2)= 16.56$, $p<.05$). t test results, which were applied on pairs to detect what was the source of the differences, showed that there was no significant differences between PBL-LW and PBL-Control groups ($t=1.67$, $t=,0$; $p<0.05$).

However between LW-Control groups there was a significant difference favoring the students in LW group (t, $test=2.06$; $p<.05$). This situation shows that the students in LW group had a higher achievement level towards vitamin C concepts than the students in control group. Based on this finding, it can be said that the instruction based on laboratories and animations is more effective than traditional and problem based teacher and students are passive listeners in traditional instructional process. However in learning environments based on problem learning and laboratory, students actively participate in instructional process. During this process, students maximize the learning process. They observe record data and conclude.

These deeds of students are important in terms of converting abstract knowledge into concrete knowledge and learning. Previous studies have also underlined that such activities support meaningful learning and facilitate the instruction of issues, which are referred as difficult topic and includes abstract concepts like vitamin C.

4. Conclusion

As the result of the conducted study, it was determined that Laboratory Works increased student achievement better than the students in the group instructed with problem solving based traditional education. This result refreshes the importance of laboratory based activities for chemistry course. Therefore, laboratory based activities for the other concepts in chemistry curriculum should be emphasized.

However, considering that it is not possible to find laboratory based activities for all chemistry concepts, the activities based on problem solving could also be used. Actually, the observations and interviews showed that problem solving based activities have some positive effects over students' learning related concepts, even

though they are not as effective as laboratory based instruction.

5. Acknowledgements

---

6. References

[1]. Hofstein, A. and Lunetta, V.N., (1982), The role of the laboratory in science teaching: Neglected aspects of research. Review of Educational Research, 52: 201–217.

[2]. Hofstein, A., Shore, R., and Kipnis, M., (2004), Providing high school chemistry students with opportunities to develop learning skills in an inquiry-type laboratory: A case study. International Journal of Science Education, 26: 47–62

[3]. Hofstein, A., Navon, O., Kipnis, M., and Mamlok-Naaman, R., (2005), Developing students' ability to ask more and better questions resulting from inquiry-type chemistry laboratories. Journal of Research in Science Teaching, 42(7): 791-806.

[4]. Hofstein, A. and Walberg, H.J., (1995), Instructional strategies. In B.J. Fraser & H.J. Walberg (Eds.), Improving science education (pp. 1-20). Chicago, IL: National Society for the Study of Education

[5]. Yew, E. H. J. and Schmidt, H. G., (2009), Evidence for Constructive, Self-Regulatory, and Collaborative Process in Problem-Based Learning. Adv in Health Sci Educ., 14: 251-273.

[6]. Yuzhi, W. (2003), Using Problem-Based Learning and Teaching Analytical Chemistry, The China Papers, July, 28–33.

[7]. Polanco, R., Patrica, C. & Francisco, D., (2004), Effects of a Problem-Based Learning Program on Engineering Students'Academic Achievements in a Mexican University 1. Innovations in Education and Teaching International, 41 : 145–155

[8]. Torp, L. and Sage, S., (2002), Problem as Possibilities: Problem-Based Learning for K–16 Education (2nd ed.) .Alexandria, USA: Association for Supervision and Curriculum Development, (Chapter 2)

[9]. Stattenfield, R. and Evans, R. (Ed: Mccoy, L.P.) (1996), Problem Based Learning and Student Ability Level, Studies in Teaching Research.

Isomerization and Toxicity Test of Methyl Linolenic Ester of α-Linolenic Acid Isolated from *Ocimum Basilicum* Seeds

A. Ghanaim Fasya [1,2], Rurini Retnowati [3], Moh. Farid Rahman [3]

(1) Chemistry Master Student, Faculty of Science, Brawijaya University, Malang
(2) Department of Chemistry, Faculty of Science and Technology, Maulana Malik Ibrahim State Islamic University, Malang (fasya_46@yahoo.co.id)
(3) Department of Chemistry, Faculty of Science, Brawijaya University, Malang

Abstract

Conjugated double bond increases bioactivity of fatty acid and their derivation. This reseach aim was to investigate the effect of conjugated double bonds in methyl linolenate esterificated from α-linolenic acid of O.basilicum seeds. Conjugated methyl linolenic prepared from methyl linolenate (methyl 9,12,15-octadecatrienoate) by alkaline treatment with KOH 21 % in ethylene glycol at 180 ^{0}C for about 25 minutes. The major component of the result was conjugated methyl linolenate with percentage of 82.39 % and identified as methyl-10,12,14-octadecatrienoate. The present of conjugated double bond in methyl linolenate increases its toxicity, identified by decreased of its LC_{50} value. The LC_{50} value was decreased from 117.3820 ppm before isomerization to 91.3365 ppm after isomerization.

Keywords: *Conjugated double bond, methyl linolenate, O.basilicum seeds, toxicity*,

1. Introduction

Conjugated fatty acid can be prepared from nonconjugated fatty acid, such as eicosepentaenoic acid (EPA), docosahexaenoic acid (DHA) and linolenic acid (LnA). Methyl linolenic ester (methyl 9,11,15-octadecatrienoate) treated with KOH 21 % in ethylene glycol at temperature 180ºC for about 25 minutes produces a mixture of conjugated dienes and trienes termed conjugated methyl linolenate [1]. Alkaline treatment yields a mixture of positional and geometrical isomers.

Position of conjugated double bond in fatty acids and its derivations have some effect in their bioactivity. Al-Madaney *et al*. [2]) suggest that 9E,11E-CLA increase the formation of thromboxane B_2 compared with other CLA isomers.10E,12Z-conjugated linoleic acid (CLA) is the active cytotoxic compound in CLA prepared by alkaline treatment, not 9Z,11E-CLA [3-5]. Igarashi and Miyazawa [6] reported that all-*trans* trieonoic linolenic acid have the strongest-inhibitory affact on human tumor cell lines among the conjugated trienoic acids and conjugated dienoic acids produced by alkaline treatment of α-linolenic acid.

In this study, we conjugated methyl linolenate that prepared from α-linolenic acid of *Ocimum basilicum* seeds by alkaline treatment and investigated the effect of conjugated double bonds in their toxicity againts *Arthemia salina* Leach.

2. Experimental Detail

This research was done using α-linolenic acid isolated from *Ocimum basilicum* seeds as starting material. The α-linolenic acid was isolated from other *O. basilcum* fatty acids by urea inclusion. The α-linolenic acid was esterificated by acid treatment and purified with column chromatography. The results, methyl linolenate, was isomerized (conjugated) by alkaline treatment (21 % KOH in ethylene glycol).

A porstion (1g) of methyl linolenate was added to 100 mL of 21 % potassium hydroxide/ ethylene glycol (KOH/EG, wt/vol) solution in a flask (250 mL volume). After bubbled with nitrogen gases, the mixture was refluxed at 180^{0}C for 25 minutes. Then, the reaction mixture was cooled, and 100 mL of methanol and 200 mL of 6 N HCl were added. After diluted with 200 mL of distilled water, the conjugated methyl linolenate was extracted with hexane. The hexane extract was washed with 300 mL of 30 % methanol and 300 mL of distilled water. After being separated, the hexane extract was dried under a nitrogen gas stream. The results was stored at -20ºC after being purged with nitrogen gases.

The conjugated methyl linolenate was analyzed using UV/Vis Spectrofotometer and Gas Chromathography-Mass Spectrometer, while its toxicity was determined by *Brine Shrimp Test* (BST). A series of methyl linolenate and conjugated methyl linolenate concentrations was

prepared in 25, 50, 75, 100, 125, 150, 175 and 200 ppm. A portion (250, 500, 750, 1000, 1250, 1500, 1750 and 2000 µL) of methyl linolenate and conjugated methyl linolenate was placed in test tube, then the solvent was evaporated. a volume of 2 mL of sea water and 100 µL DMSO was added to the tube and the mixture was shaked to get a solution of samples. Ten *Arthemia salina* larva's was added into each tube then destilled water was added untill 10 mL of total volume. The solution was aerated for 24 hours and the mortality of *Arthemia salina* larva's was determined.

3. Results and Discussion

Methyl linolenate double bond conjugation by alkaline tretament mechanism was started with abstraction of a proton (a hidrogen atom) from carbon wedged two carbon with double bond by hydroxide ion (OH^-) from KOH that ionized at ethylene glycol. The product of this nucleofilic abstraction is a carbanion and water. The carbanion then stabilized and resonanced and the double bond was conjugated (Figure 1), while, the analysis of conjugated methyl linolenate from the isomerization using UV/Vis spectrofotometer shows the maximum absorbance at 230, 250, 259 and 275 nm (Figure 2).

The maximum absorbance at 250, 259 and 275 nm confirm the present of conjugated triene. This result was supported by Gas Chromatography-Mass Spestroscophy analylis. CG cromatogram shows that the result of isomerization have tree peaks at retention time of 19.152 minutes with 1.24% area; 19.766 minutes with 16.37% area and 20.349 minutes with 82.39% area. From mass spectra, peak I was correspond to methyl linolenate that unreacted, peak II was methyl linolenate that conjugated only one double bond and peak III was methyl linolenate which was conjugated twice (conjugated triene).

Tabel 1. Mortality of *Arthemia salina*

Concentration (ppm)	Total mortality of *A. Salina*					
	Methyl linolenate			Conjugated methyl linolenate		
	I	II	II	I	II	III
25	1	2	2	2	2	3
50	4	3	3	5	4	5
75	4	5	4	6	4	5
100	5	5	6	6	6	6
125	5	6	6	7	8	7
150	6	6	5	7	7	6
175	6	7	7	7	8	8
200	8	7	7	9	8	8
Control	1			0		

Some research suggested that the present of conjugated double bond in fatty acids and its derivatives increases their bioctivity. Brine Shrimp Test of methyl linolenate and conjugated methyl linolenated was given at Tabel 1.

Probit analysis of *A. salina* mortality showed that LC_{50} value of methyl linolenate was 117.3820 ppm and LC_{50} value of conjugated methyl linolenate was 913365 ppm. The LC_{50} value was reverse of toxicity. The lower LC_{50} value, the higher toxicity. The LC_{50} value was decreased after isomerization, the conjugated double bond was increased the toxicity of methyl linolenate.

4. Conclusion

1. Isomerization of methyl linolenat forms conjugated trienoic methyl linolenate with percentage of 82.39% and maximum absorbance at 275 nm, conjugated dienoic methyl linolenate percentage of 16.37 % and maximum absorbance at 230 nm and only 1.24% of methyl linolenate are unconjugated.
2. The present of conjugated double bonds increases the toxicity of methyl linolenate againts *Arthemia salina* L. The LC_{50} value was decreased from 117.3820 ppm before isomerization to 91.3365 ppm after isomerization.

5. Acknowledgments

Thank to Department of Chemistry, Faculty of Science, Brawijaya University and also Mr. Warsito that has been facilitated this reseach.

6. References

[1]. Fasya, A.G., Retnowati,R. and Rahman, M.F. (2011), Bioaktivitas Metil Linolenat Hasil Isolasi, Metilasi dan Isomerisai Asam α-linolenat biji selasih (*Ocimum basilicum*). University of Brawijaya. Malang

[2]. Al-Madaney, M.M., Kramer, J.K.G., Deng, Z. And Vanderhoek, J.Y. (2003), Effects of Lipid-Conjugated Linoleic Acid Isomers on Platelet Function: Evidence for Stimulation of Platelet Phospholipase Activity, *Biochim. Biophy. Acta 635*, 75-82

[3]. Kang, K., Liu,W., Albrigh, K.J., Park,Y., and Pariza, M.W. (2003), *Trans*-10,*cis*-12 CLA Inhibits Differentiation of 3T3-L1 Adopocytes and Decreases PPARγ Expression. *Biochem. Biophys. Res. Commun. 303*, 795-799

[4]. Yamasaki, M. Chujo, H., Koga, Y., Oishi, A., Rikimaru, T., Shimada, M., Sugimachi,

K., Tachibana, H., and Yamada, K. (2002), Potent Citotoxic Effect of the *trans*10, *cis*12 Isomer of Conjugated Linolenic Acid on Rat Hepatoma dRLH-84 Cells, *Cancer Lett. 188*. 171-180

[5]. Choi, Y., Park, Y., Pariza, M.W., and Ntambi, J.M. (2001), Regulation of Stearoyl-CoA Desaturase Activity by the *trans*10, *cis*12 Isomer of Conjugated Linolenic Acid in HepG2 Cells, *Biochem. Biophys. Res. Commun. 284*. 289-293

[6]. Igarashi, M. and Miyazawa, T. (2005), Preparation and Fractionation of Conjugated Trienes from α-Linolenic Acid and Their Growth-Inhibitory Effects on Human Tumor Cells and Fibroblasts, *Lipids*. 40 (1): 109-113

Appendixes

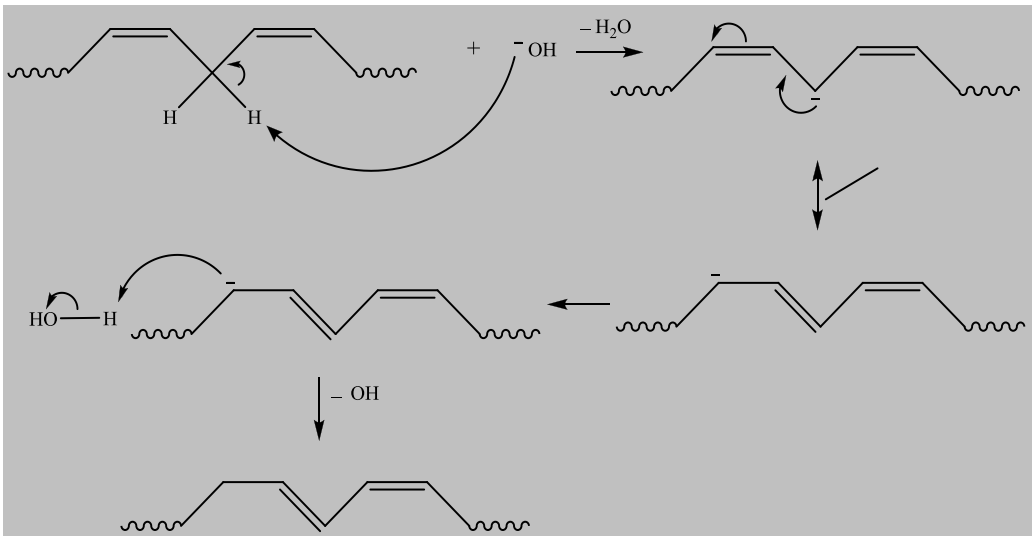

Figure 1. Mecanism of Conjugation

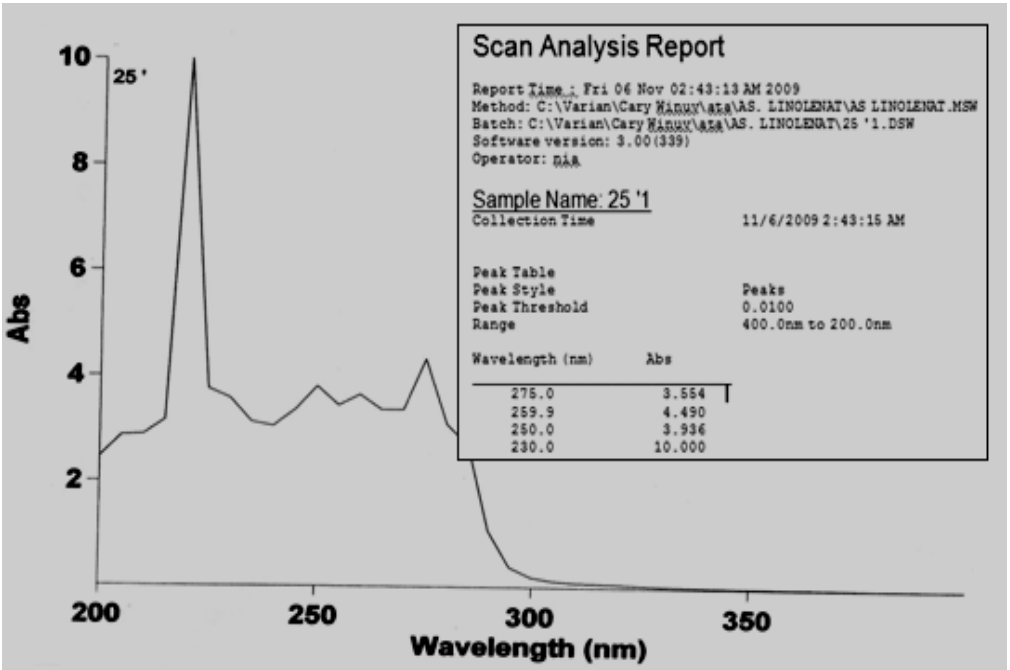

Figure 2. UV/Vis Spectrum of Isomerization Result

Biodegradable Composite Polymer for Medical Application: A Review

Agus Haryono [1], Sri Budi Harmami [2]

[1,2] Polymer Chemistry Group, Research Center for Chemistry, Indonesian Institute of Sciences (LIPI)
Puspiptek Serpong, Tangerang, Indonesia (haryonolipi@yahoo.com)

Abstract

Sustainability, industrial ecology, eco-efficiency, and green chemistry are guiding the development of the next generation of materials, products, and processes. Biodegradable plastics and bio-based polymer products based on annually renewable agricultural and biomass feedstock can form the basis for a portfolio of sustainable, eco-efficient products that can compete and capture markets currently dominated by products based exclusively on petroleum feedstock. Bio-composite product derived from renewable resources having recycling capability and triggered biodegradability with commercial viability and environmental acceptability is defined as a bio-based product. They consist of biofiber and bioplastic from renewable resources and thus are expected to be biodegradable. The combination of bio-composite such as wood flour, cellulose, starch, lignin, straw, hemp, flax, and leaf fiber with polymer matrices from both nonrenewable and renewable resources to produce composite materials that are competitive with synthetic composites. Using natural fibers with polymers based on renewable resources will allow many environmental issues to be solved. By embedding biofibers with renewable resource–based biopolymers such as cellulosic plastics; polylactides; starch plastics; polyhydroxyalkanoates (bacterial polyesters); and soy-based plastics, the so-called green bio-composites are continuously being developed. This review also examines the scientific issues that require for their application in the medical industries.

Keywords*: bio-composite, biodegradable polymer, biopolymer, medical application.*

1. Introduction

There is a growing attention to develop novel bio-based products and other innovative technologies that can decrease dependence on fossil fuel. Bio-based materials include industrial products, made from renewable agricultural and forestry feed stocks, including wood, wood wastes and residues, grasses, crops by-products. Bio-composite from plant derived fiber (natural/ bio-fiber) and crop-derived plastics (bio-plastic) are novel materials of the twenty-first century. They would be of great importance to the materials world, not only as a solution to growing environmental threat but also as a solution to the uncertainty of petroleum supply [1,2]. The growth sales of biopolymers are more than 20-30% per year [3]. Therefore the renewable biopolymer may soon be competing with commodity plastics, as a result of the sales growth, include microbial polymers and those extracted from starch. It is possible to reinforce such materials with natural fibers, from plants such as flax, jute, hemp, and other cellulose sources [4].

Biodegradable polymers begin their lifecycle as renewable resources, usually in the form of starch or cellulose. Innovative polymer research and development leads to large scale production by plastic converters. The biopolymers are formed into the specific end products and used by a consumer. Ideally, the biopolymer will be disposed in a bio waste collection, and later composted. This process will ultimately leave behind carbon dioxide and water, which are environmentally friendly byproducts [5].

One example of biopolymer for medical application is artificial bone material which adheres and integrates onto bone in the human body. The most commonly employed substance in this area is called Bio-glass [6]. Another application for biopolymers is in controlled release delivery of medications. The bioactive material releases medication by its enzymatic degradation [7]. PLA was developed for medical devices such as resorbable screws, sutures, and pins [9]. These materials reduce the risk of tissue reactions to devices, shorten recovery times, and decrease the number of doctor visits needed by patients.

Polymers have long been used in biomedical applications – for prosthetic implants, contact lenses and stents among other uses. Advances in polymer research over the past decade mean these tools are now being applied to advanced biomedical applications. A variety of polymers have been used for medical care including preventive medicine, clinical inspections, and surgical treatments of diseases [10-14]. Among the polymers employed for such medical purposes, a specified group of polymers are called polymeric biomaterials when they are used in direct contact with living cells of our body. Typical applications of biomaterials in medicine are for disposable products (e.g. syringe, blood bag, and catheter), materials supporting surgical operation (e.g. suture, adhesive, and sealant), prostheses for tissue replacements (e. g. intraocular lens, dental implant, and breast implant), and artificial organs for temporary or permanent assist (e.g. artificial kidney, artificial heart, and vascular graft). These biomaterials are quite different from other nonmedical, commercial products in

many aspects. The minimum requirements of biomaterials include non-toxicity, sterilizability, and effectiveness, as shown in Table 2 (Appendixes). The biopolymers used in medical applications must be compatible with the tissue they are found in, and may or may not be expected to break down after a given time period.

2. Recent Studies

Previous studies reported by Armentano, et al [15] showed that degradation properties are of crucial importance in biomaterial selection and design in tissue engineering [16-19]. The biomaterial should not only stimulate and support tissue growth, but it may also degrade with the same rate at which new tissue forms, and importantly, it has to possess the additional ability to withstand the loading conditions experienced in situ. The mechanical support is continuously needed as the material degrades, until the new tissue can take up the load [20-24]. Since the tissue engineering aims at the regeneration of new tissues, hence biomaterials are expected to be degradable and absorbable with a proper rate to match the speed of new tissue formation. Polymer matrix composites have the advantage of being very versatile, allowing for the tailoring of their final properties. Bionanocomposites can be designed and produced with specific requirements, using a wide range of polymeric matrices, reinforcements and processing routes. The mentioned studies suggest that the combination of biodegradable polymer and nanostructures opens new perspective in the nano-devices for biomedical applications with tunable mechanical, thermal, morphological and electrical properties.

Application of biodegradable polymers to medicine did not start recently and has already a long history. Representative synthetic biodegradable polymers currently used or under investigation for medical application are shown in Table 3 (Appendixes). Actual and possible applications of biodegradable polymers in medicine are shown in Table 4 (Appendixes). The largest and longest use of biodegradable polymes is for suturing. Collagen fibers obtained from animal intestines have been long used as absorbable suture after chromium treatment [25]. Commercial polymers used for this purpose include polyglycolide, which is still the largest in volume production, together with a glycol-lide-L-lactide (90:10) copolymer [29-31]. Extensive literature on biodegradation of polymer materials reveals the complexity of the hydrolysis mechanism, in which it is important in relation to the chemical composition of the samples, the pH of the medium, temperature, surface treatments, sample size and shape, reinforcing particles and particle functionalization [26-28].

Tissue Engineering

The biodegradable polymers of the next largest consumption in surgery are for hemostasis, sealing, and adhesion to tissues [32]. Liquid-type products are mostly used for these purposes. Immediately after application of a liquid to a defective tissue where hemostasis, sealing, or adhesion is needed, the liquid sets to a gel and covers the defect to stop bleeding, seal a hole, or adhere two separated tissues. As the gelled material is no longer necessary after healing of the treated tissue, it should be biodegradable and finally absorbed into the body. The biomaterials used to prepare such liquid products include fibrinogen (a serum protein), 2-cyanoacrylates, and a gelatin/resorcinol/formaldehyde mixture.

2-Cyanoacrylates solidity upon contact with tissues as a result of polymerization to polymers that is hydrolysable at room temperature and neutral pH, but yield formaldehyde as a hydrolysis by-product [33]. Regenerated collagen is also used as a hemostatic agent in forms of fiber, powder, and assemblies.

Mukhopadhyay (2002) [34] reported that researchers working in tissue engineering are attempting to develop organs from polymeric materials, which are fit for transplantation into humans. The plastics would require injections with growth factors in order to encourage cell and blood vessel growth in the new organ. Work completed in this area includes the development of biopolymers with adhesion sites that act as cell hosts in giving shapes that mimic different organs.

Bone Tissue Materials

Another possible application of biodegradable polymers is the fixation of fractured bones. Currently, metals are widely used for this purpose in orthopaedic and oral surgeries in the form of plates, pins, screws, and wires, but they need removal after re-union of fractured bones by further surgery. It would be very beneficial to patients if these fixation devices can be fabricated using biodegradable polymers because there would be no need for a re-operation. Attempts to replace the metals with biodegradable devices have already started, as will be described later.

Biopolymer composite can be utilized either as bone tissue replacement or bone tissue regeneration. Generally, the composite would be consisted of polymer/ biopolymer and hydroxyapatite [35]. Biopolymer was chosen for bone tissue material because it‘s biodegradable and biocompatible properties. Biocompatibility is needed for bone material to perform with appropriate response and do not trigger harmful (toxicity) response from surrounding implant environment [30]. On the other hand, biodegradable property is needed for material used as mechanical support for bone regeneration. In such application, skeletal tissue is needed for mechanical support. When applied in damaged tissue, this material would support as scaffold for bone cell growth. When the healing is completed, it is more desirable if this scaffold could be biodegraded.

Biopolymer composite is potentially used for desired biodegradable property, or as polymer matrix for hydroxyapatite bone tissue component. Introducing biopolymer would introduce ease of processibility and dispersability of hidroxyapatite as inorganic component of hard tissue. Hydroxyapatite had been studied for composite with polysaccharide and polypeptide matrixes such as chitosan, alginate, and gelatin [37]. Poly L-lactic acid (PLLA) is utilized as scaffold, graft,

bone screw, plates, and pins because it's good mechanical properties and it is readily degraded into nontoxic products. PLA also excel because it had already approved by FDA.

Augustine *et al* (2008) [36] described the bio-compatibility study of hydroxyapatite-chitosan composite for medical applications at microwave frequencies. Hydroxyapatite (HAp) was prepared using different drying techniques. The dielectric properties of HAp-chitosan composites are similar to that of fat, collagen, bone marrow, and these composites are biodegradable, nontoxic and biocompatible. These composites can be easily prepared and used as phantom materials for microwave medical tomographic applications.

Shinn-Jyh DING (2006) [29] described the preparation and properties of chitosan/calcium phosphate composites for bone repair by using a simple mixing and heating method. The maximum mechanical strength was achieved at 5 mass/vol%. Stability of the organic-inorganic hybrid composites was also found to be affected by the simulated physiological environment more apparently than by cyclic loading stress. By combining the advantageous properties of bioactive ceramic and resorbable polymer, this type of chitosan / calcium phosphate composites appeared to be acceptable for use in bone repair [8].

Biopolymer for Pharmaceutical

Polymers are very powerful for this new pharmaceutical technology. If a drug is administered through a parenteral route like injection, the polymer used as a drug carrier should be preferably absorbable, because the polymer is no longer required when the drug delivery has been accomplished. Therefore, biodegradable polymers are widely used, especially for the sustained release of drugs through administration by injection or implantation into the body.

Khunawattanakul *et al*. studied novel chitosan (CS)-magnesium aluminum silicate (MAS) nanocomposite film coatings for modified-release tablets [16]. The CS and CS-MAS dispersions resulted in continuous coated film on tablets, but the CS-MAS coated tablets provided better visual appearance and fewer film defects than CS coated tablets. The greater MAS ratio of the CS-MAS coated tablets provided lower water uptake and slower drug release when compared with the CS coated tablets. Moreover, the CS-MAS film coated on the tablets presented good stability towards enzymatic degradation in simulated intestinal fluid. The findings indicated that the CS-MAS nanocomposite films can be used as a tablet coating material for modifying drug release tablets.

Vaccine Adjuvant

Rice-Ficht, *et al* [38] studied polymeric particles in vaccine delivery. Particulate vaccine delivery is a growing technology elevated by the successful application and commercialization of particle-based vaccines. An immunologic adjuvant is defined as any substance that acts to accelerate, prolong, or enhance antigen-specific immune responses [39]; a particle may therefore exhibit adjuvant properties on a number of different levels (Table 6). First, it is clear that the uptake of antigen by APCs is favored in particulate form rather than soluble [40]; particles may therefore improve the immune response through stimulating antigen uptake. Secondly, an antigen-loaded erodible particle may also act as an antigen depot, slowly releasing antigen in either an intra or extracellular manner to prolong antigen availability.

The very recent work of Cohen *et al*. [41] showed that antigen-loaded Polyacrylamide (PA) hydrogel particles of 3.5 mm and 35 nm both act directly as an antigenspecific cytotoxic T cell response of similar magnitude. These reports suggest that the size, chemical composition, charge, and surface properties are all important for induction of antigen-specific cytotoxic T cell responses (Table 5).

3. Conclusion

Polymer composite for medical applications generally require the material to be biodegradable and biocompatible. Biodegradability is needed for material application such as support/scaffold for tissue regeneration. Meanwhile, biocompatibility is generally required for material that is applied by contact to living cell/tissue so it would not trigger harmful/toxic effect. These properties could be achieved by using biopolymer based composite. Biopolymer would introduce biodegradability to the composite and usually also biocompatible. Bio-composite polymer can be designed and produced with specific requirements, using a wide range of polymeric matrices, reinforcements and processing routes.

4. Abbreviations

APCs	:	Antigen-presenting cells
CS	:	Chitosan
CS-MAS	:	Chitosan-magnesium aluminum silicate
HAp	:	Hydroxyapatite
PA	:	Polyacrylamide
PLA	:	Poly(Lactic acid)
PLLA	:	Poly(L-lactic acid)
PLGA	:	Poly($_L$-lactide co-glycolide)
FDA	:	Food and Drug Administration
PPN	:	Propanolol HCl

5. References

[1]. A. K. Mohanty, M. Misra and G. Hinrichsen (2000), *Macromol Mater. Sci. Eng*. 267/277, 1-24.
[2]. A. K. Mohanty, M. Misra and L. T. Drzal (2001), *Compos. Interf.* 8, 313-343.
[3]. A. Scott (2000), *Chem. Week*. Sept 13, 73.
[4]. Bismarck, A., Aranberri-Askargorta, I., Springer, J., Lampke, T., Wielage, B., Samboulis, A., Shenderovick, I., Limbach, H. (2002), Surface characterization of flax, hemp, and cellulose fibers; Surface properties and the water uptake behavior. *Polymer Composites*. 23(5): 872-894.
[5]. Lorcks, J. (1998), Properties and applications of mater-bi starch-based materials. *Polymer Degradation and Stability.* 59 (1-3): 245-249.

[6]. Kokubo, T., Kim, H., Kawashita, M. (2003), Novel bioactive materials with different mechanical properties. *Biomaterials*. 24: 2161-2175.
[7]. Sakiyama-Elbert, S., Hubbell, J. (2001), Functional biomaterials: Design of novel biomaterials. *Annual Review of Materials Research*. 31: 183-201.
[8]. Y. Ikada, H. Tsuji (2000), *Macromol. Rapid Commun*. 21, 117-132.
[9]. Y. Ikada (1996), "Tissue Adhesives", in: *Wound Close Biomaterials and Devices*, C. C. Chu, L. A. von Fraunhofer, H. P. Greisler, Eds., CRC Press, New York pp. 317–346.
[10]. M. Szycher, Ed., (1991), "*High performance Biomaterials*", Technomic, Lancaster .
[11]. S. W. Shalaby, Y. Ikada, R. Lander, J. Williams, Eds., (1994), "Polymers of Biological and Biomedical Significance", ACS Symp. *Ser*. 540.
[12]. C. C. Chu, L. A. von Fraunhofer, H. P. Greisler, Eds., (1996), "*Wound Close Biomaterials and Devices*", CRC Press, New York.
[13]. A. Atala, D. Mooney, J. P. Vacanti, R. Langer, Eds., (1997), "Synthetic Biodegradable Polymer Scaffolds", Birkhauser, Boston.
[14]. Y. Ikada, (…..), "Tissue Engineering Research Trends at Kyoto University, *In Tissue Engineering for Therapeutic Use 1*"
[15]. I. Armentano, *et. al*. (2010), Biodegradable polymer matrix nanocomposites for tissue engineering: A review. *Polymer Degradation and Stability* 95, 2126-2146.
[16]. W. Khunawattanakul *et. al*, (2011), Novel chitosan-magnesium aluminum silicate nanocomposite film coatings for modified-release tablets. *Inter. J. of Pharmaceutics*….
[17]. Maquet V, *et. al*. (2004), Porous poly(a-hydroxyacid)/Bioglass composite scaffolds for bone tissue engineering. I: preparation and in vitro characterization. *Biomaterial* 25(18):4185-94.
[18]. Yang YY, *et. al.* (2003), POE/PLGA composite microspheres: formation and in vitro behavior of double walled microsphere. *J Control Release* 88(2): 201-13.
[19]. Loo SCJ, *et. al.* (2004), Radiation effects on poly(lactide-co-glycolide) (PLGA) and poly(l-lactide) (PLLA). *Polym Degrad Stab*. 83(2): 259-65.
[20]. Hurrell S, *et. al.* (2001), Polyglycolide: Degradation. *J Mater Sci Mater Med* 2001; 12(9): 811-6.
[21]. Zhang R, Ma PX. (2001), Processing of polymer scaffolds: phase separation. In: Atala A, Lanza R, editors. Methods of tissue engineering. San Diego: Academic Press. 715.
[22]. Ma PX, Langer R. (1995), Degradation, structure and properties of fibrous poly(glycolic acid) scaffolds for tissue engineering. In: Mikos AG, Leong KW, Radomsky ML, Tamada JA, Yaszemski MJ, editors. Polymers in medicine and pharmacy. PA: Materials Research Society p. 99.
[23]. Zhang R, Ma PX. (200), Degradation behaviour of porous poly(a-hydroxyl acids) / hydroxyapatite composite scaffolds. *Polym Preprint* 41: 1618e9.
[24]. Ma PX. (2004), Scaffold for tissue engineering. Mater Today 7(5): 30e40.
[25]. Smart SK, Cassady AI, Lu GQ, Martin DJ. (2006), The biocompatibility of carbon nanotubes. *Carbon* 44: 1034e47.
[26]. Wen X, Tresco PA. (2006), Fabrication and characterization of permeable degradable poly (DL-lactide-co-glycolide) (PLGA) hollow fiber phase inversion membranes for use as nerve tract guidance channels. *Biomaterials* 27: 3800e9.
[27]. Hurrell S, Cameron RE. (2001) Polyglycolide: degradation and drug release. Part I: changes in morphology during degradation. *J Mater Sci Mater Med* 12 (9): 811e6.
[28]. Dunn AS, Campbell PG, Marra KG. (2001), The influence of polymer blend composition on the degradation of polymer / hydroxyapatite biomaterials. *J Mater Sci Mater Med* 12(8): 673e7.
[29]. Shinn-Jyh DING (2006), Preparation and Properties of Chitosa/Calcium Phospate Composites for Bone Repair. *Dental Materials Journal*. 25(4) : 706-712.
[30]. D. K. Gilding (1981), in: "*Biocompatiblity of Clinical Omplant Materials*", D. F. Williams, Ed., CRC Press, Boca Raton pp. 209–232
[31]. R.A. Hule and D.J. Pochan. (2007), Polymer Nanocomposite for Biomedical Applications. *MRS Buletin*, Vol. 32. April.
[32]. R.J. Kroeza, M.N. Helder, L.E. Govaert and T.H. Smit (2009), Biodegradable Polymers in Bone Tissue Engineering. *J. Materials*. …
[33]. Sain, M., (2002), Process to Improve Thermal Properties of Natural Fiber Composites. Canadian Patent No. 2350112.
[34]. Mukhopadhyay, P., (2002), Emerging trends in plastic technology. *Plastics Engineering*. 58(9): 28-35.
[35]. L. G. Privalova, G. E. Zaikov (1990), *Polym. Plast. Technol. Eng*. 29, 445.
[36]. R. Augustine *et al*, (2008), Biocompatibility Study of Hydroxyapatite - Chitosan Composite for Medical Application at Microwave Frequencies. *Microwave and Optical Technology Letters*. Vol. 50. 2931/2934.
[37]. B. C. Benicewicz, P. K. Hopper, (1990), *J. Bioactive Compatible Polym.* 5, 453 and 6, 64 (1991).
[38]. Allison C Rice-Ficht. Polymeric particles in vaccine delivery (2010), *Current Opinion in Microbiology* 13:106-112.
[39]. Sasaki S, Okuda K (2000), In The Use of Conventional Immunologic Adjuvants in DNA Vaccine Preparations, vol 29. Edited by Lowrie DB, Whalen RG. Humana Press.
[40]. Storni T, Kondig TM, Senti G, Johansen P (2005), Immunity in response to particulate antigen delivery systems. Adv Drug Deliv Rev 57: 333-355.

[41]. Cohen JA, Beaudette TT, Tseng WW, Bachelder EM, Mende I, Engleman EG, Frechet JM., (2009), T-cell activation by antigen-loaded pH-sensitive hydrogel particles in vivo: the effect of particle size. *Bioconjug Chem* 20: 111-119.

Appendixes

Table 1. Classification of biodegradable polymers [8]

Natural Polymers		**Synthetic Polymers**	
Sub-classification	**Examples**	**Sub-classification**	**Examples**
1. Plant original - Polysaccharides 2. Animal origin - Polysaccharide - Proteins 3. Microbe origin - Polyesters - Polysaccharides	Cellulose, Starch, Alginate Chitin (Chitosan), Hyaluronate Collagen (Gelatin), Albumin Poly(3-hydroxyalkanoate) Hyaluronate	1. Aliphatic polyesters - Glycol / dicarbonic acid polycondensate - Polylactides - Polylactones - Miscellaneous 2. Polyols 3. Polycarbonates 4. Miscellaneous	Poly(ethylene succinate) Poly(butylenes terephthalate) Polyglycolide, Polylactides Poly(ε-carpolactone) Poly(butylenes terephthalate) Poly(vinyl alcohol) Poly(ester carbonate) Polyanhydrides, Poly(α-cyanoacrylate)s, Polyphosphazenes, Poly(orthoesters)

Table 2. Minimal requirements of biomaterials [8]

1. Non-toxic (biosafe)
   Non-pyrogenic, Non-hemolytic, Chronically, Non-inflammative, Non-allergenic, Non-carcinogenic, Non-teratogenic, etc.
2. Effective
   Functionality, Performance, Durability, etc.
3. Sterilizable
   Ethylene oxide, c-Irradiation, Electron beams, Autoclave, Dry heating, etc.
4. Biocompatible
   Interfacially, Mechanically, and Biologically.

Table 3. Representative synthetic biodegradable polymers for medical application [8]

Polymer	**Structure**	**Degradation rate**	**Medical application**
Poly(glycolide)	Crystalline	100% in 2 -3 months	Suture, Soft issue anaplerosis
Poly(glycolic acid-*co*-L-lactic acid)	Amorphous	100% in 50-100 days	Suture, Fracture fixation, Oral implant, Drug delivery microsphere
Poly(L-lactide)	Semicrystalline	50% in 1-2 years	Fracture fixation, Ligament augmentation
Poly(L-lactic acid-*co*-ε-caprolactone)	Amorphous	100% in 3-12 months	Suture, Dural substitute
Poly(ε-caprolactone)	Semicrystalline	50% in 4 years	Contraceptive delivery implant
Poly(*p*-dioxanone)	Semicrystalline	100% in 30 weeks	Suture, Fracture fixation
Poly(orthoester)	Amorphous	60% in 50 weeks (saline, 37^{o}C)	Contraceptive delivery implant

Table 4. Medical application of bioabsorbable polymers [8]

Function	Purpose	Examples
Bonding	Suturing	Vascular and intestinal anastomosisation
	Fixation	Fractured bone fixation
	Adhesion	Surgical adhesion
Closure	Covering	Wound cover, local hemostatis
	Occlusion	Vascular embolization
Separation	Isolation	Organ protection
	Contact inhibition	Adhesion prevention
Scaffold	Cellular proliferation	Skin reconstruction, Blood vessel reconstruction
	Tissue guide	Nurve reunion
Capsulation	Controlled drug delivery	Sustained drug release

Table 5. Chemical compositions of particles and the type of immune response engendered

Particle chemistry	Size	Surface properties	Immunity stimulated
hPGA ($_L$-phenylalanine ethylester) poly(gamma-glumatic acid)	150-200 nm	Amphiphilic	Cellular, humoral
Acid-labile polyacrylamide hydrogel	200-500 nm	Hydrophilic	Cytotoxic T lymphocyte
Acid-labile polyacrylamide hydrogel	35 nm-3.5µm	Hydrophilic	Cytotoxic T cell
Alginate-coated chitosan	300-600 nm	Hydrophilic	Th 1 biased antigen-specific antibody
Polystryrene	40-49 nm	Hydrophilic	CD8 T cell response, lgGI
Polystryrene	93-123 nm	Hydrophilic	CD4 T cell respone, IL4, lgGI
PLGA	3.4-4.3 µm	Hydrophilic	MHC II, extended epitope presentation
PLA	1 µm	Hydrophilic	MHC II, prolonged antigen presentatio
Acetalated dextran	115-270 nm	Hydrophilic	MHC I, MHC II

Table 6. Adjuvant properties of particulate vaccine delivery system [39]

Particle effect	Specific outcome
Modulate innate immune response	• Polystryrene, PLGA and alum particles stimulate release of IL 1ß and IL 18 in vitro when presented in concert with toll like receptor ligand
Modulate quality and quantity of antigen presentation: depot effect	• Enhanced antigen-specific Th1 specific cytokine profile • Antigen-specific cytotoxic T cell respone • Choice of MHC pathway controlled through particle dissolution rate • Extended antigen presentation
Targeting dendritic cells and cell compartments	• Use of amphipathic polymer to target dendritic cells • Use of surface charge to target intracellular compartments
Enhance uptake of antigen	• Use of positive surface charge to increase uptake of particles by APC • Increase antigen uptake by dendritic cells through particles entrapment

AdhF-36kDa Protein Expression Pattern of *Salmonella typhi* on Different Environmental Conditions in Vitro

[As a Study of Molecular-Based Vaccine Candidates Adhesin on Typhoid Fever]

I Nengah Kundera [1], Sanarto Santoso [2], Aulanni'am[3], Sri Winarsih [4]

[(1)] Biology, PMIPA, Tadulako University, Palu - Sulawesi Tengah, Indonesia
[(2,4)] Medical Faculty, Brawijaya University, Malang, Indonesia
[(3)] Chemistry Department, Faculty of Science, Brawijaya University, Malang, Indonesia.

Abstract

Salmonella typhi has a remarkable adaptability to the environmental changes, hence this bacteria still cause health problems in the world. The outbreak infection deseases to spread is very related to virulence factor, pathogensis and ability adaptation of Salmonella typhi and live at animal, human bodys and environmental. The adhF-36kDa protein is subunits fimbriae which is considered responsible for the adhesion and colonization factors of Salmonella typhi. This study aims to find out, adhF-36kDa protein expression pattern of Salmonella typhi in different environmental conditions in vitro, as the study of molecular-based vaccine candidate adhesion on typhoid fever. Research sample sourced from Hasan Sadikin Hospital, Labkes Palu in Central Sulawesi, Denpasar Udayana Hospital and strains from Saiful Anwar Hospital in Malang. The results showed that all strains of Salmonella typhi expressed adhF-36kDa protein. This proves that the protein is owned by the fimbriae of Salmonella typhi strains, although originated from different regions. This results also shows the differences of adhF-36kDa protein expression patterns in osmolarity conditions compared to thoses grown at different pH in vitro. In treatment of osmolarity accurred stability adhF-36kDa protein expression, compared with the treatment pH 4.5 to 6.0. This study proves the theory that changes in environmental signals affect the virulence factor of Salmonella typhi.

Keywords: *AdhF-36kDa Protein, Salmonella typhi.*

1. Introduction

Salmonella typhi is a facultative intracellular pathogen virulence factors that need to able to cell and replicate to successfully colonization into the tissue [1-3,13]. The ability of *Salmonella* Typhi through the transition to host such dynamic response, due to osmolarity, low pH (acidic stress), bile salts and other immune responses, is a form of bacterial strategies to survive in different host environments [1,4,6,7]. Increased virulence of *Salmonella* Typhi will happen when positioned on the environmental conditions of low oxygen, high osmolarity and low pH, although the mechanism is not clear [3,8,11].

AdhF-36 kDa protein is constituent protein subunits fimbria which is considered responsible for the adhesion and colonization factors of *Salmonella* Typhi. This study aims to find out, the pattern of protein expression adhF-36kDa *Salmonella* Typhi in different environmental conditions in vitro, as the study of molecular-based vaccine candidate adhesion on typhoid fever.

2. Experimental Details

The method used is experimental laboratory an explorative and carried out by two steps:thefirst stage identification *Salmonella* typhi in accordance with standard procedures for bacterial indentification, treatement with osmolarity different concentrations and pH of the environment in vivo for *Salmonella* typhi. Then fimbriae isolation, profileling adhesin fimbriae protein, SDS-PAGE and Western Blot.

3. Result and Discussion

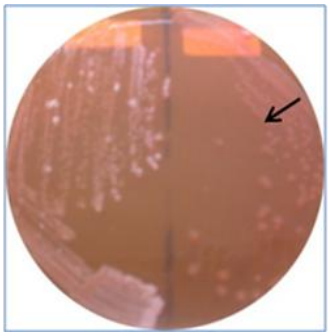

Figure 1. *Salmonella* Typhi colonies in MacConkey Agar media

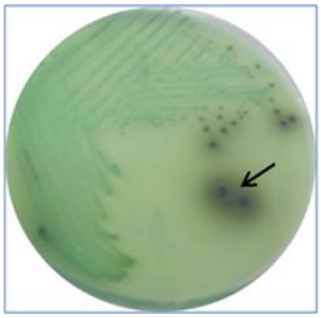

Figure. 2 *Salmonella* Typhi colonies in BSA media

Figure 1. Result on isolation and identification of *Salmonella* Typhi in selective media.

Figure 2. Visualization results TSIA test of *Salmonella t*Typhi

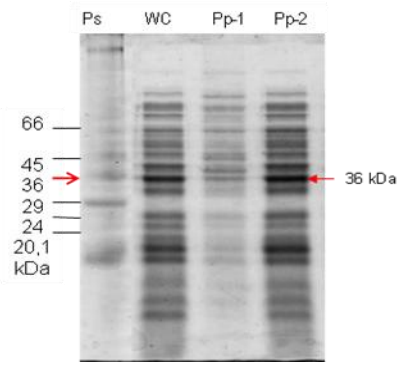

Figure 3. Profile of adhesion fimbriae protein 36kDa *Salmonella* typhi str.8873 Malang by SDS-PAGE

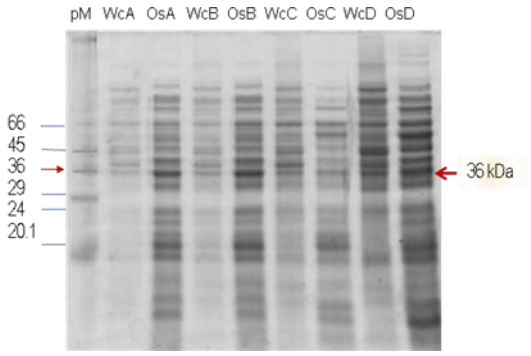

Figure 5. Results SDS-PAGE protein expression piece adhF-36 kDa *Salmonella* Typhi with differents osmolarity [Commasie blue dye]

Notes: M = marker protein, WcA = wole cell treat [50 mM], Os-A:= pili proteins-A [50 mM], WcB = wole cell treat [150 mM], Os-B = pili proteins-B [150 mM], WcC = wole cell treat [250 mM], Os-C= pili proteins-C [250 mM], WcD= wole cell treat [350 mM] and Os-D=pili proteins-D [350 mM]

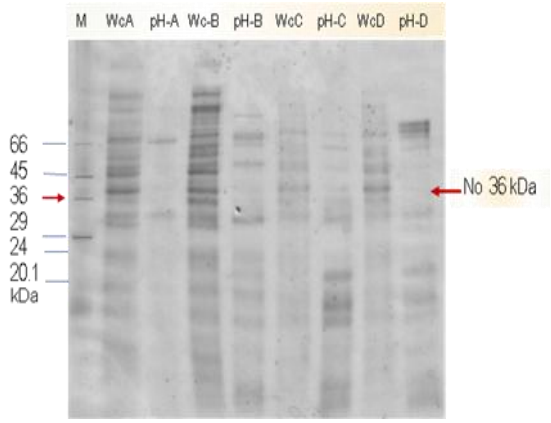

Figure 6. Results SDS-PAGE protein expression piece adhF-36 kDa *Salmonella* Typhi with different pH treatments [Commasie blue dye]

Notes: M = marker protein, WcA = wole cell treat [pH 4,5], pH-A =pili proteins-A [pH 4,5], WcB = wole cell treat [pH 5,0], pH-B = pili proteins-B [pH 5,0], WcC= wole cell treat [pH 5,5], pH-C = pili proteins-C [pH 5,5], WcD = wole cell treat [pH 6,0], pH-D =pili proteins-D [pH 6,0]

Based on the results of this research showed that all strains of *Salmonella* Typhi from various region in Indonesia have and expression fimbriae adhesion 36kDa protein. This proves that naturally was there no difference in protein expression fimbriae of *Salmonella* typhi, although located in different environmental condition. Through di study adhesion protein is expected to provide new data for the search of vaccine candidate adhesion protein molecules to prevent the initial infection by *Salmonella* typhi.

Based on the results of this study that fimbriae adhesin protein [AdhF-36kDa] proved possessed by strains of *Salmonella* typhi, from various regions in Indonesia. This proves the theory that most groups of Enterobacteriaceae have fimbria adhesin protein, as a virulence factor [13,14]. For treatments of environmental stress in vitro that there is a difference of expression AdhF-36kDa protein patterns of exposure a osmolarity, and tends to increase in treatment of 150mM NaCl to 350mM concentration.Unlike the case at pH treatment, a decline in protein expression patterns AdhF-36kDa from the treatments pH 4.5 to 6.0, which looks at the profile of the bend is the result of SDS-PAGE

protein increasingly thin on the increased concentration of pH. In the Western Blot test with Ab-36kDa showed a positive reaction and response in molecules weight 36kDa. Therefore, this protein is an important moleculer as a typhoid vaccine candicate on adhesin molecules in the future.

4. Conclusion

Fimbria adhesin protein [AdhF-36kDa] proved possessed bystrains of *Salmonella* typhi, from various regions in Indonesia, as one of the virulence factor. There is a difference of protein expression patterns of AdhF-36kDa *Salmonella* typhi in osmolarity treatment with different pH in vitro. Changes in protein expression pattens can be a clue changes fimbriae virulence of bacterial and as a consideration to be a typhoid vaccine candidate based on adhesin molecules in the future.

5. Acknowledgments

Thank you to Directorate General of Higher Republic of Indonesia, which has helped funding this research using Doctoral Grant Program DP2M in 2009.

6. References

[1] Bader, M. W., W.W. Navarre., W.Shiau., H.Nikaido., J.G. Frye., M.McClelland., F.C. Fang., and S.I.Miller (2003), Regulation of *Salmonella* Typhimurium virulence Gene expression by cationic antimicrobial peptides. *Mol.Microbiol*, 50 : 219-230.

[2] Baker, S., K.Holt., S. Whitehead., I. Goodhead., T. Perkins., B. Stocker., J.Hardy., and G. Dougan (2007), A Linear plasmid trucation Induces unidirectional flagellar Phase Change in H: z66 Positve *Salmonella typhi*. *Mol. Microbiol.* 66: 1207-1218.

[3] Bucarey, S. A., N.A. Villagra., M.P. Martinic., A. N.Trombert., C.A. Santiviago., N. P. Maule´n., P.Youderian., and G.C. Mora (2005), The *Salmonella enterica* Serovar Typhi *tsx* Gene, Encoding a Nucleoside-Specific Porin, Is Essential for Prototrophic Growth in the Absence of Nucleosides. *Infect. Immun*. 73(10): 6210-6219.

[4] Baker,S.,K.Holt.,E.Vosse., P. Roumagnac (2008), High-Throughput Genotyping of *Salmonella enterica* Serovar Typhi Allowing Geographical Assignment of Haplotypes and Pathotypes Within an Urban District of Jakarta, Indonesia. *J.Clin.Microbiol.* 46(5): 1741-1746.

[5] Cheminay, C., A. Mohlenbrink., and M. Hansel (2005), Intracellular Salmonella Inhibit Antigen Presentation by Dendritic Cells, *J.Immunol.*174 : 2892-2899.

[6] Clarke, M., and V. Sperandio (2005), Even at the Host-Microbial Interface of the Gastointestinal Tract III. Cell-to-Cell signaling among Microbial flora, Host, and Pathogens there is a whole lot of talking going on. *AJP-Gastrointes Liver Physiol*. 288:G11050-G1109.

[7] Darwin, K.H., and V.L. Miller (1999), Molecular Basis of the Interaction of Salmonella with the Intestinal Mucosa. *Clin. Microbiol. Rev.* 12(3): 405-428.

[8] Faucher, S.P., R. Curtiss III., and F. Daigle (2005), Selective capture of Salmonella enterica serovar Typhi genes expressed in Macrophages that are absent from the *Salmonella enterica* serovar Typhimurium genome. *Infect Immun*.73 : 5217-5221.

[9] Forest, C., S.P.Faucher., K.Poirier., S.Houle., C.M.Dozois., and F.Daigle (2007), Contribution of the stg Fimbrial Operon of *Salmonella enteric* Serovar Typhi during Interaction with Human Cells. *Infect.Immun*, 75(11) : 5264-5271.

[10] Gerlach, R.G., D. Jackel., N. Geymeier, and M. Hansel (2007), *Salmonella* Pathogenicity Island 4-Mediated Adhesion is Coregulated With Invasion Genes in *Salmonella enterica. Infect.Immun.* 75(10): 4697-4709.

[11] Hoare, A., M. Bittner., J. Carter., S. Alvarez., M. Zaldivar., D. Bravo., M.A. Valvano., and I.Contreras (2006), The Outer Core Lipopolysaccharide of *Salmonella enterica* Serovar Typhi Is Required for Bacterial Entry into Epithelial Cells. *Infect.Immun.* 74(3):1555-1564.

[12] Martinez, J.L., and F.Baquero (2002), Interactions among Strategies Associated with Bacterial Infection : Pathogenicity, Epidemicity, and Antibiotic Resistance, *Clin.Microbiol.Rev*. 15(4):647- 679.

[13] Pizarro-Cerda´.J., and P.Cossart (2006), Bacterial Adhesion and Entry into Host Cells. *Cell .Elsevier Inc*.124 : 715–727.

[14] Raffatellu, M., R.I. Santos., D.Chessa., R.P.Wilson., S.E.Winter., C.A. Rossetti., S.D. Lawhon., H.Chu., T.Lau., C.L. Bevins., L.G. Adams., and A.J. Baumler (2007), The Capsule Encoding the viaB Locus Reduces Interleukin-17 Expression and Mucosal Innate Responses in the Bovin Intestinal Mucosal during Infection with *Salmonella enterica* Serotype Typhi. *Infect.Immun.* 75 (9): 4342-4350.

Appendixes

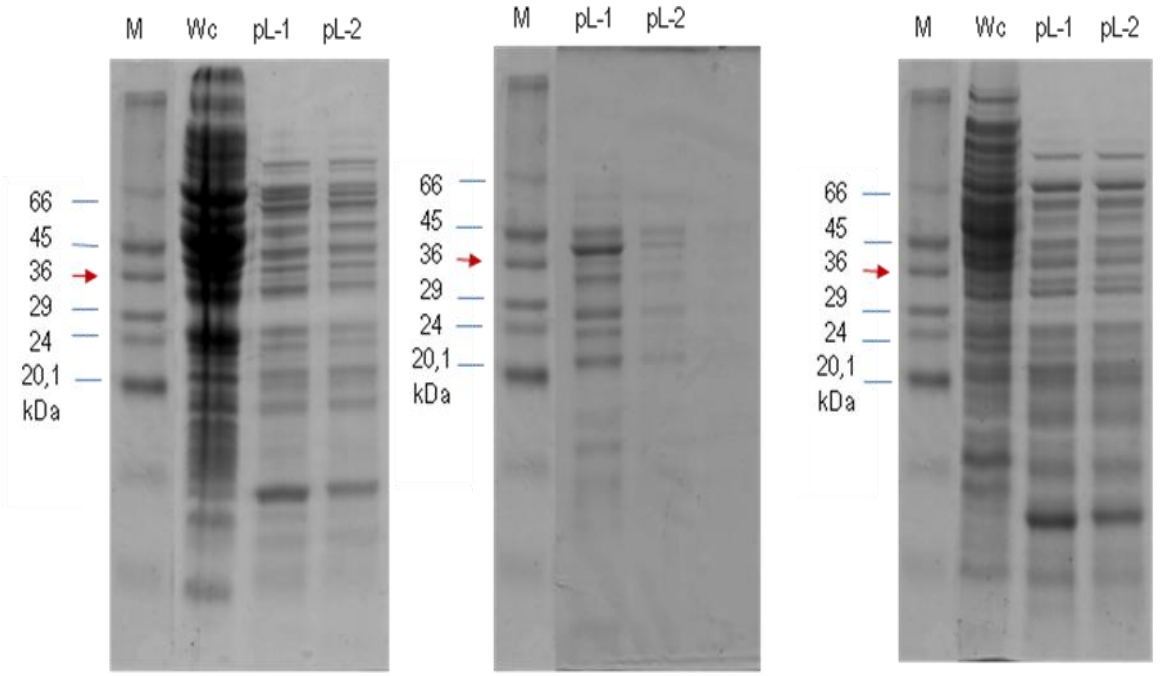

Figure 4. Adhesin fimbriae protein profiles of *Salmonella* typhi strain from several regions in Indonesia, by SDS-PAGE

Evaluation on Antioxidative Activity of Pollard Protein Hydrolysates

Khothibul Umam Al Awwaly[1], Muhammad Halim Natsir [2], Abdul Manab [3], Aris Sri Widati [4]

[(1,3,4)] Animal Product Technology Department, Faculty of Animal Husbandry, University of Brawijaya, Malang, Indonesia (aak_umam@ub.ac.id)
[(2)] Animal Feed and Nutrition Dept., Faculty of Animal Husbandry, University of Brawijaya, Malang

Abstract

The objective of this research was to prepare pollard protein hydrolysates with different enzymes and to measure their antioxidative activity. Materials used in this research were pollard, pepsin, papain, tripsin and commercial papain. Pollard protein hydrolysates were produced by enzymatic hydrolysis. The research was conducted using Nested Block Randomized Design with 3 factors and 3 replications. The fist factor was with or without preheating (90ºC, 5 min), the second factor was the enzyme type (pepsin, papain, trypsin and commercial papain). The third factor was the hydrolysis time (0.5, 1 and 6 h). Antioxidant activity assay of pollard protein hydrolysates was conducted using TBA tests. The result obtained was pollard used has 16.26% protein, 16.27% crude fiber and 4.54% crude fat. Pollard protein concentrate has 79.04% crude protein, 11.2% moisture, 0.14% crude fiber, 1.27% crude fat and 0.299% ash content. Soluble protein in the protein concentrate was 18.413%. Pollard protein concentrate has a water binding activity as 227.015%, oil absorption 139.04%, foam capacity 35% with foam stability 92.86%. Antioxidant activity of pollard protein hydrolysates with TBA method ranged from 19.1-63.186 µmol/kg. It could be concluded that hydrolysis with trypsin for 6 hours was the best treatment for producing pollard protein hydrolysates with the highest antioxidant activity.

Keywords: *protein hydrolysates, pollard, antioxidant, lipid oxidation.*

1. Introduction

The role of protein as physiologically active components in the diet is being increasingly acknowledged. Many of the proteins that occur naturally in raw food materials exert their physiological action either directly or upon enzymatic hydrolysis in vitro or in vivo. In recent years it has been recognized that dietary proteins provide a rich source of biologically active peptides. Such peptides are inactive within the sequence of the parent protein and can be released in three ways: (a) through hydrolysis by digestive enzymes, (b) through hydrolysis by proteolytic microorganisms and (c) through the action of proteolytic enzymes derived from microorganisms of plants. It is now well established that physiologically active peptides are produced from several food proteins during gastrointestinal digestion and fermentation of food materials with lactic acid bacteria.

Bioactive peptides have been defined as specific protein fragments that have a positive impact on body functions or conditions and may ultimately influence health. Basically, biologically active peptides can be produced from precursor food/nonfood proteins in the following ways: (a) enzymatic hydrolysis by digestive enzymes, (b) fermentation of food/nonfood protein with proteolytic starter cultures, (c) proteolysis by enzymes derived from microorganisms or plants. In many studies, combination of (a) and (b) or (a) and (c), has proven effective in generation of short functional peptides.

Lipid (oil and fat) oxidation is the biggest source of food quality deterioration. One of the effective way to prevent oxidative damage is antioxidant utilisation. Recent studies have shown that upon hydrolysis with certain enzymes or acids, some food proteins can act as antioxidants in model systems [1-3]. The ability of peptides to inhibit deleterious changes caused by lipid oxidation appears to be related to certain amino acids residues in the peptides, which are capable of chelating prooxidative metal ions [4]. Amino acid composition, sequence and configuration of peptides also affect their antioxidant activity. The properties of the hydrolysates are dependent on

the type of enzyme used, the degree of hydrolysis, the environmental conditions and the substrate pretreatment [5]. Utilisation of pollard protein hydrolysates as natural antioxidant can protect food from deleterious changes that caused by lipid oxidation. Research is needed to determine the possible antioxidant effect of enzyme-hydrolyzed pollard proteins on lipid oxidation.

The objective of this research was to prepare pollard protein hydrolysates with different enzymes and to measure their antioxidative activity.

2. Experimental Details

Materials used in this research were pollard, pepsin, papain, tripsin and commercial papain. Pollard protein concentrate was extracted by alkali method. Pollard protein hydrolysates were produced by enzymatic hydrolysis. The research was conducted using Nested Block Randomized Design with 3 factors and 3 replications. The fist factor was with or without preheating (90ºC, 5 min), while the second factor was the enzyme type (pepsin, papain, trypsin and commercial papain). The third factor was the hydrolysis time (0.5, 1 and 6 h). Antioxidant activity assay of pollard protein hydrolysates was conducted using TBA tests. Data were analyzed using analysis of variance (ANOVA) and the means separated by Duncan's multiple range tests.

Preparation of Pollard Protein Hydrolysates

Enzymatic hydrolysis of pollard protein was conducted according to method described by Pena-Ramos [5]. A 2% protein solution of pollard protein concentrate, with or without preheating (90ºC, 5 min), was hydrolyzed for 0; 0.5; 1 and 6 hours with four different enzymes (pepsin, papain, trypsin and commercial papain). The hydrolysis temperature was 37ºC and the enzyme-pollard protein concentrate substrate ratio was 1/100. Pepsin hydrolysis was done in 0.01 M tris-HCl buffer (pH 2.0), and hydrolysis was stopped by increasing the pH to 7.0. Papain, trypsin and commercial papain hydrolysis was carried out in 0.01 M phosphate buffer (pH 8.0) and inactivation was achieved by heating the samples in boiling water for 3 min.

Antioxidant Activity Assay

Antioxidant activity assay of pollard protein hydrolysates was conducted using thiobarbituric acid (TBA) test. The TBA test was conducted according to the combined method of [6-7]. A 1 ml of the sample from pollard protein hydrolysates were added 2 ml of trichloroacetic acid and 2 ml of thiobarbituric acid solution. This mixture was then placed in a boiling water bath at 100ºC for 10 min. After cooling, it was centrifuged at 3,000 rpm for 20 min and absorbance of the supernatant was then measured at 532 nm using UV-VIS spectrophotometer.

3. Result and Discussion

The result obtained was pollard used has 16.26% protein, 16.27% crude fiber and 4.54% crude fat. Pollard protein concentrate has 79.04% crude protein, 11.2% moisture, 0.14% crude fiber, 1.27% crude fat and 0.299% ash content. Soluble protein in the protein concentrate was 18.413%. Pollard protein concentrate has a water binding activity as 227.015%, oil absorption 139.04%, foam capacity 35% with foam stability 92.86%. Data of antioxidant activity of pollard protein hydrolysates using TBA test are shown in Table 1.

Table 1. Antioxidant activity (µmol/kg) of pollard protein hydrolysates

Substrate	Enzyme	Hydrolysis Time (h)	Means
With Preheating	Papain	0.5	63.090±4.265
		1	60.951±4.171
		6	61.312±0.273
	Tripsin	0.5	63.186±0.613
		1	62.369±0.410
		6	60.207±0.273
	Pepsin	0,5	62.946±0.291
		1	61.888±0.341
		6	59.558±0.356
	Commercial Papain	0.5	63.018±0.670
		1	61.720±1.158
		6	60.663±0.750
Without Preheating	Papain	0.5	33.203±0.110
		1	29.383±0.541
		6	22.584±0.550
	Tripsin	0.5	29.479±0.330
		1	23.617±0.463
		6	**19.100±0.661**
	Pepsin	0.5	34.596±0.544
		1	28.758±0.438
		6	25.442±1.771
	Commercial Papain	0.5	33.491±0.480
		1	28.830±0.375
		6	24.866±0.375

Table 1 shows the value of antioxidant activity of pollard protein hydrolysates using the TBA test. It shows that the antioxidant activity of pollard protein hydrolysates with TBA test ranged from 19.1-63.186 µmol/kg. Tripsin hydrolysis for 6 hours was the lowest (19.1 µmol/kg) value. It indicates that the pollard protein hydrolysates has the highest antioxidant activity and can inhibit the secondary product of oxidation such as aldehyde and ketone [8]. To date, only a few antioxidant peptides have been identified in fermented food products especially dairy products. For instance, a κ-casein-derived peptide with 2,2-diphenyl-1-picrylhidrazyl (DPPH) radical-scavenging activity was recently found in a milk fermented with *Lb delbrueckii* ssp *bulgaricus* [9].

4. Conclusion

It could be concluded that hydrolysates of pollard protein produced by enzymatic hydrolysis using 4 different enzymes have an antioxidant activity. Hydrolysis with trypsin for 6 hours was the best treatment for produce pollard protein hydrolysates with highest antioxidant activity.

5. Acknowledgments

The authors are grateful for the financial support of DP2M Ditjen DIKTI, Department of National Education (National Strategic Research Grant 2009).

6. References

[1]. Chan, W.K.M., E.A. Decker, J.B. Lee, and D.A. Butterfield (1994), EPR spin-trapping studies of the hydroxyl radical scavenging activity of carnosine and related dipeptides. *J. Agric. Food. Chem*. 42:1407-1410.

[2]. Chen, H.M., K. Muramoto and F. Yamauchi (1995), Structural analysis of antioxidative peptides from soybean β-conglycinin. *J. Agric. Food Chem*. 43:574-578.

[3]. Hattori, M., K. Yamaji-Tsukamoto, H. Kumagai, Y. Feng and K. Takahashi (1998), Antioxidative activity of soluble elastin peptides. *J. Agric. Food Chem*. 46: 2167-2170.

[4]. Karel, M., S. R. Tannenbaum, D. H. Wallace, and H. Maloney (1966), Antioxidation of methyl linoleate in freeze dried model systems. III. Effects of added amino acids. *J. Food Sci.* 31: 892-896.

[5]. Pena-Ramos, E.A., and Y.L. Xiong (2001), Antioxidative Activity of Whey Protein Hydrolysates in a Liposomal System. *J. Dairy Sci*. 84: 2577-2583.

[6]. Kukizaki, H. and Nakatani, N., (1993), Antioxidant effect of some ginger constituents. *J. Food. Sci.* 578 (6):1407-1410.

[7]. Ottolenghi, A., (1959). Interaction of ascorbic acid and mitochondrial lipids. *Archives of Biochemistry and Biophysics*. 79:355-358.

[8]. Farag, R.S., Badei, A.Z.M.A., Hawed, F.M. and El-Baroty, G.S.A. (1989), Antioxidant activity of some spice essential oils on linoleic acid oxidation in aqueous media. *J. American Oil Chemist Society*, 66 (6): 793-799.

[9]. Hernandez-Ledesma, B., Miralles, B., Amigo, L., Ramos, M. and Recio, I., (2005), Identification of antioxidant and ACE-inhibitory peptides in fermented milk. *J. Sci. Food. Agric.* 85: 1041-1048.

Exogenous IL-2 Promote T Cells Proliferation Under Anti – CD3/CD28 Combination

Muhaimin Rifa'i

Biology Department, Faculty of Sciences, Brawijaya University.
Email: rifa123@ub.ac.id

Abstract

Strategy of both activation and proliferation of the cell interest in vitro plays a very important role for clinical purpose. In this experiment we observed that exogenous IL-2 is required to maintain the survival of activated T cell in vitro. Here we also demonstrated that T cell expansion derived from lymph node activated with anti-CD3/anti-CD28 combination was greatly enhanced in the presence of exogenous IL-2. In the absence of exogenous IL-2 the cell become more susceptible to apoptosis and or necrosis. In the stimulation of anti-CD3/anti-CD28 combination, $CD8^+$ T cells were preferentially stimulated. T-cell activation which plays a central role in the regulation of immune responses, involves multiple intracellular signaling events originating from the cell surface TCR/CD3 complex. Cross-linking of the TCR/CD3 complex by anti-CD3 antibody induces T cell activation, leading to the production of cytokines. We found evidence that stimulated $CD8^+$ T cells particularly $CD8^+CD122^+$ subpopulation express high level of IFNγ, while $CD4^+$ particularly $CD4^+CD25^-$ express high level of IL-2. Interestingly $CD8^+$ T cells when stimulated with combination of anti-CD3/anti-CD28 could mimic the cell surfice molecules to double positive $CD8^+CD4^{Low}$ T cells.

Keywords : *PLN, anti-CD3/anti-CD28, IL-2.*

Potency of Inhibin B As Male Hormonal Contraception Candidates Based on Sperm Viability and LH Serum Level of *Rattus norvegicus*

Muhammad Hilman F. Amin [1], Aulanni'am [2], Agung P.W.Marhendra [3], Muslim Akmal [4]

[1,3] Department of Biology, Faculty of Sciences, Brawijaya University, Malang
[2] Department of Chemistry, Faculty of Sciences, Brawijaya University, Malang
[4] Faculty of Veterinary Medicine, University of Syiah Kuala, Aceh
(muhammadhilman87@gmail.com)

Abstract

Large population, in addition to being capital for country's development is also contrary be problem and burden for the country. One of effort to control increasing population is contraception. Men should also have same burden in family planning, so it is extremely urgent to develop new, safe, effective, and reversible male contraceptive methods. Among all male contraceptive methods, hormonal approach is the closest to clinical application. One of requirements of an ideal male contraceptive is not affected masculinity and libido, which regulated by testosterone-LH. Inhibin B is hormone which controls FSH secretion, whereas FSH is central hormone of mammalian reproduction,necessary for gonadal development and maturation at puberty and for gamete production during the fertile phase of life. The purposes of this study were to determine role of inhibin B from primary culture of testicular to sperm viability and serum LH levels of rats (Rattus norvegicus) Wistar strain. This study used four groups of treatment, ie K0, K1, K2 and K3 are each injected with inhibin B in PBS with a dose of 0, 25, 50, and 100 pg per 200 g body weight (BW) rats. Sperm viability was tested by eosin-nigrosin dye and was examined under light microscopy in 400x magnification, and measurement of serum LH levels through ELISA method. The results showed that administration of inhibin B can reduce viability of spermatozoa significantly, but did not reduce levels of LH in serum. This indicates that inhibin B has potential to be developed as a male hormonal contraceptive.

***Keywords**: contraception, inhibin B, LH, sperm viability.*

1. Introduction

World population reached 3 billion in 1960 and increased dramatically in 2000 to 6 billion [1]. Large population of a country, in addition to capital for development of country and can be a problem and burden for the country. Increase levels of unemployment, poverty and crime, and decrease environmental support capability is negative side of blast population [2]. One effort to control increasing population is contraception. According to Handelsman (2003), responsibility for family planning over last few decades in care of women, but men should have same burden in family planning, so male contraceptive method that is reliable and reversible should be developed [3].

Anderson and Baird (2002) explained that male reproductive system is a potential target for development of new contraceptives [4]. One of the targets in male contraception is to disrupt sperm quality. One of requirements of male contraception by Pasqualotto *et al*., (2003) is not affect masculinity and libido [5]. Despopoulos and Silbernagl (2003) said that libido in men was regulated by testosterone. Testosterone also regulates secondary sex characteristics, such as hair distribution, physical form, and voice change in males is regulated by Luitenizing Hormone (LH) produced by the pituitary gland, so that contraception for male should not interfere production of LH or testosterone [6].

Spermatogenesis is a process to form spematozoa [7]. Spermatogenesis in primates is primarily driven by the gonadotropic hormones luteinizing hormone (LH) and follicle-stimulating hormone (FSH) [8]. FSH is central hormone in mammalian reproduction was required for development and gonad maturation during puberty and production of gametes in fertile phase of life [9]. Microarray analysis showed that more than 300 genes in Sertoli cells are regulated by FSH [10]. Spermatogenesis is a process that occurs in the formation of spermatozoa in seminiferous tubules [7]. Microarray analysis showed that more than 300 genes in Sertoli cells are regulated by FSH [10].

Secretion and production of FSH by pituitary gland in males is regulated by inhibin B [11]. Inhibin B is produced by Sertoli cells in testis [12,13] and is a major form of inhibin in adult men [14]. Inhibin B is a gonadal polypeptide hormone that selectively potentially inhibits secretion of FSH through a negative feedback mechanism [15]. This study aims to determine potency of inhibin B in reducing viability of spermatozoa and evaluated impact of inhibin B on LH.

2. Experimental Detail

Animals and inhibin B administration

24 male rats (*Rattus norvegicus*) male strain Wistar, aged 3 months with body weight 200-250 g obtained from Laboratory of Animal Physiology-UB and randomly divided into 4 groups. KO group was injected with sterile PBS as control group. K I, K II and K III was injected with inhibin B from Sertoli cell culture with doses of 25, 50 and 100 pg per 200 g body weight (BW), respectively. Inhibin B was given intraperitoneally 5 times every 12 days [16]. On day 50, rats were sacrificed by cervical dislocatio. Cauda epididymal spermatozoa were used for the examination of sperm viability. Blood samples were taken for examination of serum LH levels by ELISA method.

Examination of Sperm Viability

10 µl suspension of semen was dropped on glass object, and eosin-nigrosin dye was dropped and mixed until homogen. Calculations performed using a light microscope 400x magnification. Spermatozoa with uncolored head are living spermatozoa, while pink colored is dead spermatozoa [17].

Examination of Serum LH

Serum LH levels examined using ELISA method by LH ELISA Test Kit (080 410 Rodent Test LH).

Analisis Data

Data of sperm viability and serum LH levels were analyzed using ANOVA test.

3. Result and Discussion

Effect of inhibin B on viability of rat's sperm

All treatment groups are given inhibin B showed a significant decrease in sperm viability ($P < 0.05$) compared with the control group (Table 1 – Appendix). Sperm viability was decline by 34.28%, 42.08% and 62.18% respectively in KI, KII and KIII. Decrease in sperm viability was negatively correlated with inhibin B dose ($r < 0.01$).

Inhibin B administration induced a decrease of FSH (data not shown) so that sperm viability decreases. FSH regulates several genes in Sertoli cells that plays a role in spermatogenesis, include lactate dehydrogenase A (LDH-A). LDH-A controls synthesis of lactate as a primary energy source for germ cells [10]. Some studies indicate that germ cells, especially post-meiotic phase, utilize lactate produced by Sertoli cells as anenergy source [18]. Several biochemical steps occurs in the production of lactate are glucose utilization, glycolysis, and inter-conversion of lactate and pyruvate. Lactate dehydrogenase (LDH) is an enzyme that acts to catalyze the inter-conversion using nicotinamide adenine dinucleotide (NAD+) as co-enzymes.

Effect of inhibin B on serum LH

Serum LH levels in rats after inhibin B administration from testicular primary culture showed no significant differences ($P < 0.05$) between control group and treated group (Table 1 – Appendix). Correlation test also showed no significant correlation ($r < 0.05$) between increasing doses of inhibin B and serum LH levels.

Increasing doses of inhibin B does not affect LH serum level. This result is consistent with opinion of [19] which explained that there is no significant correlation between inhibin B concentrations in plasma and concentrations of LH. It caused by inhibin B only inhibits FSH synthesis without inhibit synthesis of LH. Luteinizing hormone (LH) is a hormone secreted by the pituitary. LH stimulates synthesis and secretion of testosterone by Leydig cells (interstitial cells). Testosterone has an important role in male reproduction, include role in male sex differentiation, induce secondary sex characteristics, normal sex drive (libido) and coitus capacity (potentia coeundi) in male [6,20]. This makes LH and testosterone should be maintained in male hormonal contraception [5].

4. Conclusion

Based on the results of this study, inhibin B administration caused decrease in sperm viability, but the injection of inhibin B does not cause the disruption of LH secretion. This suggested that inhibin B has potential as male hormonal contraception.

5. Acknowledgements

This work was financially supported by DIKTI, in PHP program 2010.

6. References

[1]. Crosignani, P.G., (2002), Hormonal Contraception: What is New?. *Human Reproduction Update*, 8(4) : 359-371.
[2]. United Nations (2001), World Population Monitoring 2001: Population, Environment and Development. United Nations Publication. New York.
[3]. Handelsman, D.J., (2003). Hormonal Male Contraception—Lessons from the East When the Western Market Fails. *J. Clin. Endocrinol. Metab*., 88: 559-561.
[4]. Anderson, R. A. and D. T. Baird. (2002), Male Contraception. *Endocr. Rev*. 23: 735-762.
[5]. Pasqualotto, F.F., A.M. Lucon, E.B. Pasqualotto and S. Arap. (2003), Trends in Male Contraception. *Rev. Hosp. Clín. Fac. Med. S. Paulo,* 58(5):275-283.
[6]. Despopoulos, A. and S. Silbernagl. (2003), Color Atlas of Physiology. Thieme. New York.
[7]. Vander, A.J., J.H. Sherman, and D.S. Luciano (2001), Human Physiology: The Mechanism of Body Function, Eighth Edition. The McGraw Hill Companies.
[8]. Weinbauer, G.F., S. Schlatt, V. Walter and E. Nieschlag (2001), Testosterone-Induced Inhibition of Spermatogenesis is More Closely Related to Suppression of FSH than to Testicular Androgen Levels in the Cynomolgus Monkey Model (*Macaca fascicularis*). *Journal of Endocrinology,* 168: 25-38.
[9]. Simoni, M. J. Gromoli and E. Nieschlag (1997), The Follicle-Stimulating Hormone Receptor: Biochemistry, Molecular Biology, Physiology, and Patophysiology. *Endocrine Reviews*,18(6): 739-773.
[10]. Walker, W.H. dan J. Cheng (2005), FSH and Testosterone Signaling in Sertoli Cells. *Reproduction,* 130 : 15–28.
[11]. Boepple, P.A., F.J. Hayes, A.A. Dwye., T. Raivio, H. Lee, W.F. Crowley Jr and N. Pitteloud (2008), Relative Roles of Inhibin B and Sex Steroid in the Negative Feedback Regulation of Follicle-Stimualting Hormone in Men Across the Full Spectrum of Seminiferous Epithelium Function. *J. Clin Endocrin Metab,* 93(5) :1809–1814
[12]. Luisi, S., P. Florio, F.M. Reis and F. Petraglia (2005), Inhibins in Female and Male Reproductive Physiology: Role in Gametogenesis, Conception, Implantation and Early Pregnancy. *Human Reproduction Update* 11(2):123-135.
[13]. Winters, S.J., C. Wang, E. Abdelrahaman, V. Hadeed, M. A. Dyky and A. Brufsky. (2006), Inhibin B Levels in Healthy Young Adult Men and Prepubertal Boys: Is Obesity the Cause for the Contemporary Decline in Sperm Count Because of Fever Sertoli Cells?. *Journal of Andrology*, 27 (4): 560-564.
[14]. Mc Neilly *et al*., (2002), ……
[15]. Chada, M., R. Průša, J. Bronskỳ, K. Kotaška, K. Šídlová, M. Pechová and L. Lisá (2003), Inhibin B, Follicle Stimulating Hormone, Luteinizing Hormone and Testosterone During Childhood and Puberty in Males: Changes in Serum Concentration in Relation to Age and Stage of Puberty. *Physiol Res*, 52:45-51.
[16]. Johnson, M. H. and B. J. Everitt (2000), Essential Reproduction. 5th ed. Blackweel Science Ltd.
[17]. Partodihardjo (1992), Ilmu Reproduksi Hewan. Cetakan ketiga. Mutiara Sumber Widya. Jakarta. Hal. 522-556.
[18]. Boussouar, F., R. Grataroli, J. Ji and M. Benahmed (1999), Tumor Necrosis Factor-{alpha} Stimulates Lactate Dehydrogenase A Expression in Porcine Cultured Sertoli Cells: Mechanisms of Action. *Endocrinology* 140: 3054-3062.
[19]. Anderson, R.A., D.S. Irvine, C. Balfour, N.P. Groome and S.C. Riley (1998), Inhibin B in Seminal Plasma Testicular Origin and Relationship to Spermatogenesis. *Hum Reprod*, 13(4):920-926.
[20]. Mader, S.S. (2004), Understanding Human Anatomy & Physiology, Fifth Edition. McGraw-Hill Science. New York.

Appendix

Tabel 1. Effect of inhibin B administration on sperm quality and serum LH level

	K 0	K I	KII	KIII
Sperm Viability	70.50 ± 7.47^{a}	46.33 ± 2.80^{b}	40.83 ± 3.86^{b}	26.67 ± 3.26^{c}
LH Serum (pg/mL)	3.74 ± 0.61^{a}	2.74 ± 0.12^{a}	2.447 ± 0.50^{a}	2.613 ± 0.28^{a}

^{a,b,c} different notation means there is a significant difference at $P < 0,05$

Potency of Silicon Dioxide (SiO_2) as Denaturator Media of Rabies Virus

M. Misbah Khunur [1], Rizky Arief Shobirin [2], Muchid Abdul Aziz [3]

[1,2,3] Departement of Chemistry, Faculty of Mathematics and Natural Science, University of Brawijaya, Malang, Indonesia (mmisbahkhunur@yahoo.com; elite_ikhwan@yahoo.com; muchie_1@yahoo.com)

Abstract

The rabies virus is the prototype of the genus Lysa-virus from the Rhabdoviridae family, and a group of RNA viruses that are closed by the protein. The virus is mostly found in the saliva of dogs. By using the principle of cleaning "unclean" in Islamic Shari'a, the sand can be used to eliminate "viruses" from dog saliva. Silica sand has chemical constituents as much as 98% SiO_2. Silicon dioxide is formed by strong covalent bonds, and has a tetrahedral structure. Thus, it can be expected that this compound can denaturate rabies virus. Structural proteins of rabies virus are maintained by the two strong bond (peptide and sulfide) and three weak bonds (hydrogen, hydrophobic and electrostatic). In this case, SiO_2 can function as a cautropic agent, where the interaction with macromolecules such as DNA, RNA and protein can be happen via hydrogen bonds, van der Waals force and hydrophobic effect. Through these three interactions, the compounds such as RNA and proteins will be denaturated. Due to the acidic nature of hardware owned by SiO_2, H^+ ions originally bound to the RNA will be separated from RNA and bound to the SiO_2. Bonds in the SiO_2 structure have properties of 50% covalent ions. The nature of SiO_2 when interacting with RNA and viral proteins can potentially eliminate the hydrophobic effect of proteins and the virus itself. Thus, RNA or protein stability will be disrupted and cause RNA or protein undergoes denaturation.

***Keywords**: SiO_2, rabies virus, denaturation, RNA.*

1. Introduction

Bali Island has been declared a rabies outbreak status. The statement was contained in the Minister of Agriculture No. 1637/2008. This is because in the three villages, a number of people suffering from rabies from dog bite. Data from Health Department of Pekanbaru showed that during January, the number of residents who receive care due to rabies has reached 13 people. In Ambon region, since early September until this paper is derived, at least 700 people bitten by rabid dogs and 13 of them died. In Padang also there were 10 residents who died of rabies. This figure is feared to continue to soar and during 2008 alone there were seven victims died. Meanwhile, victims of dog bites to reach 1879 people. This suggests that victims of rabies are very large [1].

Determination of a rabies outbreak was issued after a through study of clinical symptoms, which looks at dog as an animal of transmitting rabies (HPR), or human beings as victims of a bite. Data World Health Organization (WHO) shows that 10 million people infected with rabies and 40 thousand of them died due to rabies on every year around the world, especially in developing countries [2].

Classified as highly dreaded rabies disease worldwide, the victim suffered extraordinary rabies before death. The disease can be transmitted acute nervous system and attacks all warm-blooded animals, especially dogs, cats and monkeys. The uniqueness of rabies is a disease incubation period is quite long, from several weeks to several months. As a result, someone could have thought to bring dogs that are healthy but there is a rabies virus in their bodies. This is how rabies spreads to various places [3].

Symptoms of these viruses usually begin to occur within 30-50 days after infection, but the incubation period varies from 10 days to more than 1 year. The incubation period is usually the shortest in people bitten on the head or the shorts that are closed or when there is bite in many places [3].

Of the 20% of patients obtained information that rabies begins with paralysis in lower limbs that spread throughout the body. But the disease usually starts with short periods of mental depression, anxiety, malaise and fever. Unrest will rise to uncontrolled excitement and the patient will spend excessive saliva [3]. A picture of patient with rabies is shown in Figure 1.

Figure 1. Patient with Rabies

Muscle spasms of the throat and vocal cords can generate incredible pain. Seizures are caused by a disturbance of the brain areas that regulate the process of swallowing and breathing. Breezes and try drinking water can cause these spasms. Therefore rabies patients are unable to drink. Because of this, then this disease is sometimes also called hydrophobia (fear of water). If immediate action is taken the proper precautions, then someone is bitten by a rabid animal patients will not suffer the possibility of rabies. People who are bitten by rabbits and rodents (including squirrels, mice) do not require further treatment because the animals are rarely infected with rabies. But when bitten by wild animals (skunks, raccoons, foxes and bats) required further treatment because the animals may be infected with rabies [3].

Generally, efforts to prevent rabies by vaccination using the rabies virus have been attenuated. Breeding of viruses for vaccines is done by injecting the virus in the brains of sheep or mice. The rabies virus is difficult artificially grown or bred for the benefit of the vaccine, so the production cost is very expensive; leading most people can not buy the vaccines which also resulted in the death of patients with rabies. In addition, the use of this vaccine can cause levels antibody decreased. It is necessary to find new solutions in preventing the development of this rabies virus [4].

In the Islamic Shari'a, if they are bitten or exposed to dog‘s saliva, then they should wash the affected area with (silica) sand, followed by water. This is done to eliminate "impurity" or diseases that may be carried by the dog. This is done as a response to transmission of disease-laden saliva found on dogs [5].

The largest component in soil or sand is silicon dioxide (SiO_2). In the silica sand, silicon dioxide (SiO_2) content can reach up to 98%. Silicon dioxide is formed by strong covalent bonds, and has a clear local structure: four oxygen atoms attached to the position of the tetrahedral angles around the central atom of silicon atoms. Silicon bonded to four atoms called orthosilicate. The structure of silicon dioxide and orthosilicate are given in Figure 2 [6,7].

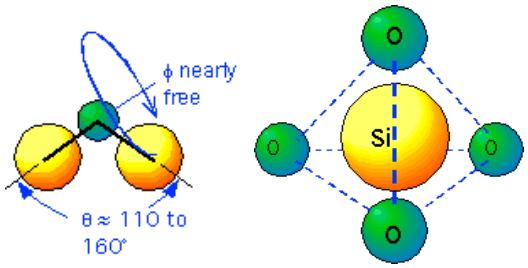

Figure 2. Silicon Dioxide (left) and Ortosilicate (right).

The purpose of this article is to discuss the possible mechanism of silicon dioxide (SiO_2) in rabies virus denaturation. Hopefully, it can provide a new understanding on rabies treatment.

2. Experimental Details

Since this work is not a laboratory experiment, the analysis was done in two approaches, which are collecting data and analyzing the data descriptively.

3. Discussion

The rabies virus is the prototype of the genus Lysa-virus from the Rhabdoviridae family. The rabies virus in shown in Figure 3 [8].

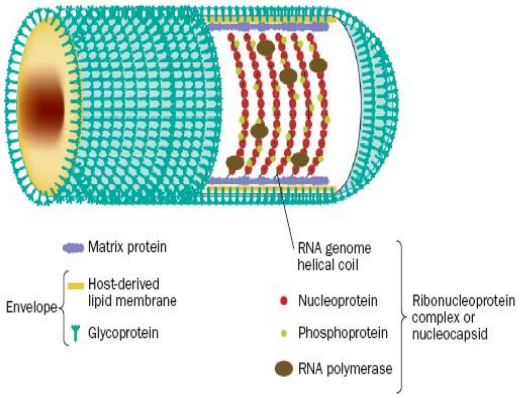

Figure 3. Rabies Virus

In general, the entire virus consists of two major parts, namely nucleic acid core and outer skin proteins. Nucleic acids that can be either RNA or DNA, carry characteristic code for a particular virus. In rabies virus, skin protein serves as a lid that protects the RNA from the nucleus and can act to help the core penetrates the cell wall. If the rabies virus is in the cell, the RNA

will reorganize the functions of the cell to make a complete virus particle. When numbers of virus particles have been quite formed, the cell will rupture, spreading the virus particles to invade other cells [9].

Protein structures are generally held by one strong bond (peptide) and three weak bonds (hydrogen, hydrophobic and electrostatic). Peptide bond is a bond that connects the alpha carboxyl bond with the alpha nitrogen atom. Hydrogen bonds are bonds that are used as the binder contained in the side chain bond peptide. Hydrophobic interactions that occur in the protein that is non-polar side chain neutral amino acids in the protein tend to align. The binding stoichiometry was not directly connected so that it can be said there is no genuine bond. Electrostatic interactions that occur are the salt bond between the charged groups opposite to the side chain of amino acids. The same also applies to RNA. However, the difference is a strong bond that the RNA structure maintained by nucleotide binding. On the denaturation of proteins and RNA, ties that were damaged were three weak bonds (hydrogen, hydrophobic, and electrostatic). Basically, the RNA is said to have been damaged if separated from the group hydrogen atom amine base [10].

Ribonucleic acid (RNA) is a molecule that consists of long chains of nucleotides consisting of an amine base, the sugar ribose, and phosphate [11]. Below is a picture of the structure of proteins and RNA [7]:

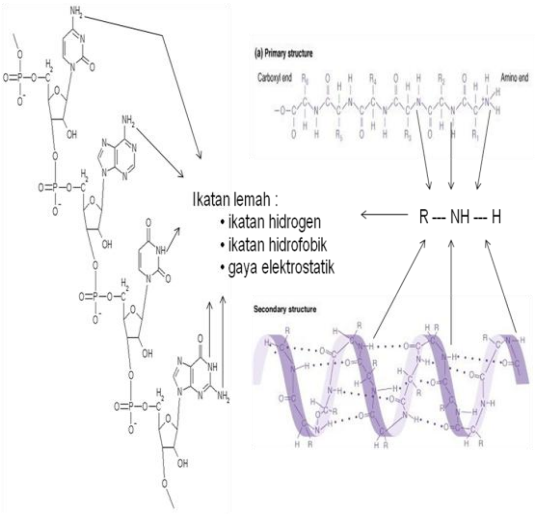

Figure 4. RNA and Protein's Structure

In the Hadiths of Muhammad the Prophet SAW, explained that in order to purify the former lick or bite the dog, it should done seven times in which the first time flushing was using water mixed with soil [12]. Land has many benefits as has been described by Allah SWT in the Qur'an. Land, where the largest chemical compound is silicon dioxide, can function as a cautropict agent where if interacting with macromolecules such as DNA, RNA and protein occurred at the same time, three chemical interactions (hydrogen bonding, van der Waals force and hydrophobic effect) will be occurred. Through these three interactions, the compounds are macromolecules (DNA, RNA and proteins) will experience a denaturation [11]. Thus, rabies virus will not infect humans.

Hydrogen Bonds of Virus becomes Damaged

Hydrogen bonding that occurs in RNA virus that causes connected of polynucleotide strands with each other, namely between the bases of certain heterocyclic amines from a single strand with certain heterocyclic amine base of the other strand. These amine bases carry a certain code in the virus. As a result of hydrogen bonding, the double helix is formed [13]. Therefore, virus code turns into inactive, as a result of the hydrogen bonds that exist in the amine group.

If we review the rules of Pearson, where there is the classification of hard and soft acid base, RNA virus can be classified as a soft acid, while silicon dioxide (SiO_2) can be classified as hard acids [14]. Because of the nature of hard acid which is owned by SiO_2, H^+ ions which was originally bound to the RNA will be separated from RNA and bound to the SiO_2. The equation is illustrated as follows:

$$\mathbf{(RNA)^- H^+ + H_4SiO_4 \rightarrow H_3SiO_3(RNA) + H_2O}$$

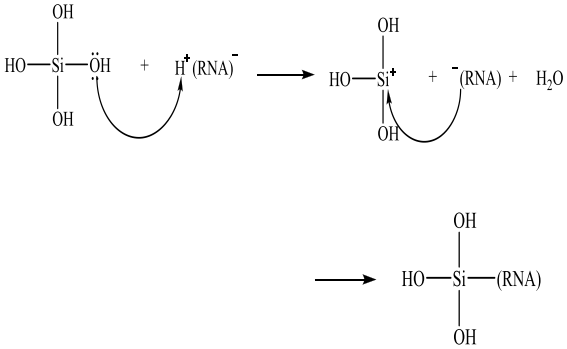

From the above equation, it can be seen that the RNA became-inactive because the H group is leaving from RNA (H group attached to the base amines).

Hydrophobic Interaction becomes Unstable

Hydrophobic interactions in the protein causes the non-polar compounds regulate protein and RNA are so minimal contact with water or amphipatict compounds such as soaps and detergents, forming structures such as micele in the water. Because proteins form a kind of micele where most of the side chain of a non polar avoid contact with water, the hydrophobic interaction is an important force in supporting the stability of a protein.

SiO_2 structure, according to Lee [15], has the properties of 50% and 50% covalent ions. In addition, the chain structure of Si - O - Si - O - Si has a very high binding energy, about 502 kJ/ mol. When interacting with RNA and viral proteins, SiO_2 can eliminate the hydrophobic effect of proteins and the virus itself. So the virus that originally could not blend with the water becomes unstable and can be carried away by water.

Van der Waals Force causes The Electrostatic Interactions Unstable

Electrostatic interactions occur between the dipole-dipole, i.e. non-covalent association between neutral molecules. It often referred to van der Waals bonding because of electrostatic interactions between dipole-dipole. This force is responsible for the various interactions between adjacent atoms. Interaction between a permanent dipole, between carboxyl groups and amide groups in the framework of the protein is an important bond. Van der Waals force is a weak bond, but because they occurred in large numbers then this bond has an important role in determining the stability of proteins.

If silicon dioxide interacts with RNA, there is a dipole-dipole force between silicon dioxide with these RNA. Thus, the stability of RNA will be interrupted and cause denaturation of RNA.

4. Conclusion

The silicon dioxide (SiO_2) in the soil or sand is potential to be used as denaturator media of rabies virus. This is due to chemical properties such as hydrogen bonding, van der Waals force and hydrophobic interaction that created in a virus core protein and RNA. As a result, the virus became unstable and then denaturated.

5. Acknowledgement

Our thanks to ICBS committee for the support grant

6. References

[1]. Anonim (2008), Bali Wabah Rabies, www.kompas.com [23 March 2009].
[2]. Chamim, Mardiyah, S. Wahyuni. (2008), Anjing Edan Menebar Maut. www.tempointeraktif.com [23 March 2009].
[3]. Easmon, C. (2005), Rabies. http://www.netdoctor.co.uk/travel/diseases/rabies.htm [23 March 2009].
[4]. Sajuthi, C. (2009), Pedoman Vaksinasi Anjing http://jakartapets.com/content/view/75/28/ [23 March 2009].
[5]. Alif, U. (2009), Membersihkan Bekas Liur Anjing, http://alifmagz.com/wp/?p=2587 [23 March 2009].
[6]. Dobkin, D.M. (2009). Silicon Dioxide: Properties and Applications. http://www.enigmatic-consulting.com/semiconductor_processing/CVD_Fundamentals/films/SiO2_properties.html [23 Macrh 2009].
[7]. Anonymous[2] (2009), Secondary Structure RNA.http://www.steve.gb.com/images/molecules/nucleotides/ssRNA.png [23 March 2009].
[8]. Kightley, R. (2009), Rabies Virion. rkm.com.au [23 March 2009].
[9]. Keenan, Kleinfelter, Wood. (1993), Kimia untuk Universitas Jilid 2. Erlangga. Jakarta.
[10]. Martin, D.W. Jr., P.A. Mayes, dan V.W. Rodwell. (1984), Biokimia. CV. EGC Jakarta.
[11]. Anonymous[3] (2009), Silica. http://en.wikipedia.org/wiki/Silica [23 March 2009].
[12]. Rasjid, S. (1976), Fiqh Islam. Penerbit Attahiriyah. Jakarta.
[13]. Effendy, (2006). Teori VSEPR: Kepolaran dan Gaya Antarmolekul Edisi 2. Bayumedia. Malang.
[14]. Saito, T. (1996), Kimia Anorganik. Iwanami Shoten Publisher. Tokyo.
[15]. Lee, J.D. (1991), Concise Inorganic Chemistry, 4th Ed. Champman & Hall. London.
[16]. Sunarya, R.R. (2008), Silikon Dioksida. http://risars.wordpress.com/2008/11/21/struktur-padatan-silika/ [23 March 2009].

Decreases of Ethanol Content in Urine Wistar Rats after Giving Acute Alcohol

Ni Made Suaniti

Chemistry Department, Faculty Mathematic and Natural Science, Udayana University, Bali, Indonesia
(suanitisr@yahoo.com)

Abstract

Alcohol is widely available in liquor, which if taken can undergo metabolism in the body through the reaction of phase I and phase II. Phase I reactions are the same alcohol with drugs can undergo oxidation, reduction, and hydrolysis. Likewise, phase II reactions can undergo conjugation reactions of ethanol which react with endogenous compounds in the body. Alcohol (ethanol) that can also be analyzed as drunken ethanol compound itself, but this lasted only within a certain time. This study aims to determine the reduction in ethanol content in urine of Wistar rats after acute alcohol administration. Gas chromatography used was Agilent Technologies GC-6890-N, carrier gas helium and nitrogen, DB-Wax capillary column (30 mx 0.25 µm x 250 m) with polyethylene glycol stationary phase, and a flame ionization detector (FID). Conditions of gas chromatography injector temperature set at 200ºC, detector temperature 300ºC, column temperature programmed at 50ºC held for 2 minutes at that temperature, then increased by the 10ºC/minute up to 200ºC and the split ratio is 20. The results showed that the ethanol content in the urine of Wistar rats was decreased after 24 hours of acute alcohol administration.

Keywords*: ethanol, urine Wistar rat, acute alcohol.*

1. Introduction

Alcohol is an organic compound consisting of alkyl groups R and hydroxyl (OH), so these types of alcohol in accordance with homologues are methanol, ethanol, propanol [1]. But the alcohol present in alcoholic beverages is allowed only in certain concentration of ethanol and excessive alcohol use is known as alcohol abuse who drink alcohol can inhibit the full composition of the center, so that alcohol is one of the substances most frequently abused addictive and cause dependency or called by alcoholism [2,3].

Alcohol has the properties of soluble in water and has a relatively small molecular size so easy to go through the cell membrane by diffusion. Alcohol is absorbed through the gastrointestinal wall, complete absorption occurs for 1-2 hours when stomach empty. After experiencing absorption, the alcohol will be distributed into the tissues and tissue fluids. Distribution of alcohol in the body quickly, its distribution volume reached 0.7 L / kg. Consumed alcohol will be oxidized in the liver up to 90%, the excretion through the lungs and urine without any change compound [2,4].

One way of proving whether a person drinks alcohol or not is by ethanol determination in biological fluids such as urine and blood. This is useful for purposes of forensic medicine to find out how much ethanol can be detected in biological fluids. In addition, the determination of ethanol metabolites useful in clinical medicine because drinking alcohol in a long time will cause health problems and chronic disease [5].

Based on literature study, drinking alcohol or ethanol oxidation into acetaldehyde will experience (toxic compounds) and subsequent oxidation to acetic acid (not toxic). Ethanol as a compound that does not change can be found in the urine as a result of excretion within a certain time by 10%. Most of the alcohol (90%) had a metabolism in the body, through the reaction of phase I and phase II, which usually can be determined in the blood. Phase I reactions are oxidation reactions that have reaction, reduction, and hydrolysis. While the phase II reactions are conjugation reactions, in which ethanol reacts with endogenous compounds in the body to form a specific metabolite. To prove ethanol can still be detected in urine it is necessary to study the decrease in alcohol content in the urine within a certain time after drinking alcohol because

alcohol is a volatile compound, the appropriate analytical method used was gas chromatography. Similarly, gas chromatography can be used for alcohol analysis, both qualitative and quantitative [6]. Qualitative analysis of alcohol is to prove whether or not alcohol based on the retention time of ethanol standard solution, while the quantitative determination is to determine the amount of ethanol content in urine samples after drinking alcohol.

This paper aims to determine the reduction in alcohol content in the urine of Wistar rats given alcohol acutely.

2. Experimental Details

Laboratory wares used were Beaker glass, 10 mL measuring flask, measuring pipette, and analytical scales. Chemicals used were ethanol and propanol (pa). Method used to determine the concentration of ethanol is gas chromatography Agilent GC-6890-N using a DB-Wax column (30 m x 250 µm x 0.25 m) with polyethylene glycol stationary phase. To detect the presence of ethanol, a flame ionization detector (Flame Ionization detector / FID) was used. Mobile phase was helium (He) is mixed with nitrogen gas. Urine samples were used Wistar rats after 6 and 24 hours exposed to alcohol.

Ethanol and propanol solution is made 1000 ppm respectively. Single solution and mixture solution were injected into the gas chromatography column to obtain the optimum conditions with the chosen system. Wistar rat urine samples 6 and 24 hours after alcohol exposure each diluted and then injected into the gas chromatography column in the system and the conditions selected above. Ethanol content was calculated based on the standard curve the ratio of standard compounds ethanol and propanol.

3. Results and Discussion

Calibration line equation ethanol using an internal standard propanol is y = 0.062 x with correlation coefficient (R^2) is 0.994 (Figure 1). Resolution or the separation between ethanol and propanol obtained ≥ 1.5. This calibration results obtained by theory, has been feasible to use gas chromatography to measure alcohol exposure urine samples [7,8]. The purpose of the use of internal standards is to reduce the fault injection into the gas chromatography column.

Next step is to determine the concentration of ethanol in urine alcohol-exposed by gas chromatography calibrated. Ethanol content in the urine of 20% alcohol exposure acutely decreases after 24 hours and obtained 7.46 ppm, as shown in Figure 2. This shows a decline in ethanol concentration in the urine of Wistar rats between 6 hours and 24 hours at 4.74 ppm.

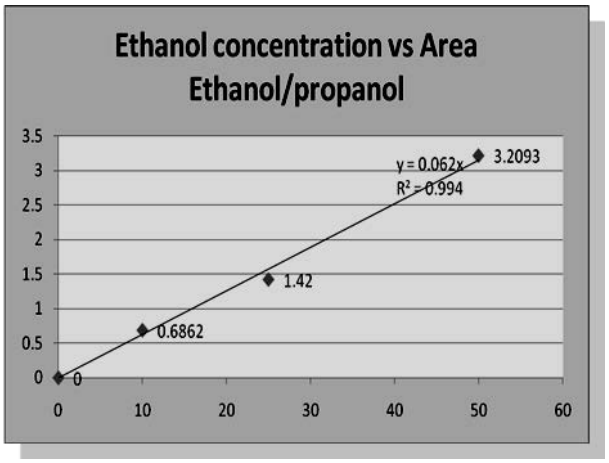

Figure 1. Calibration Curve of Ethanol

Decreasing concentration of ethanol in Wistar rat urine indicates that proof ethanol in alcohol abuse cases only with the determination of ethanol should be considered further. This research needs to be developed against other chemical biomarkers in addition to ethanol as well as on samples of other biological fluids such as blood [9]. Chemical biomarkers, such as acetaldehyde (phase I) as the metabolites and enzymes that oxidize ethanol to acetaldehyde and acetic acid [10]. Wurst et al., 2004 stated that in phase II metabolites of fatty acid ethyl esters / FAEE are toxic metabolites are new markers that are sensitive and specific to identify alcohol abuse compared with other alcohol metabolites [11].

4. Conclusion

The concentration of ethanol in urine decreased by 4.74 ppm after 24 hours exposure to alcohol than Wistar rat urine after 6 hours of alcohol exposure.

5. Acknowledgements

Thanks to Dean of Mathematics and Science Faculty and Chairman of Chemistry Department Udayana University, Bukit Jimbaran, Badung, Bali and the support of friends to the realization of this paper.

6. References

[1]. Fessenden RJ, and Fessenden JS. (1994), Organic Chemistry. 3rd ed. Gramedia. Jakarta.

[2]. Katzung BG. (2002), Basic and Clinical of Pharmacology. 8th ed., McGraw-Hill. New York.
[3]. Darmono. (2005), Toksikologi Narkoba dan Alkohol. UI Press. Jakarta.
[4]. Goldfrank, Flomenbaun, Lewin, Howland, Hoffman, Nelson. (2002), Toxicologic Emergencies. 7th ed. Mc Graw-Hill. New York.
[5]. Shepherd R. (2003), Simpson's Forensic Medicine. 12th ed Arnold. Publisher. London.
[6]. Moffat AC. (2004), Clarke's Isolation and Identification of Drugs. The Pharmaceuticals Press. London.
[7]. Mc Nair and Bonelli EJ. (1998), Dasar Kromatografi Gas. ITB. Bandung.
[8]. Mulja M, Suharman (1995), Analisis Instrumental. Airlangga University Press. Surabaya.
[9]. Sutter K. (2002), Determination of Ethanol in Blood: Analytical Aspects, Quality Control, and theoretical calculation for Forensic Applications. *Ingentaconect Chimia Chemistry*. 56: 59-62.
[10]. Deitrich R, Zimatkin S, Pronko S. (2006), Oxidation of Ethanol in the Brain and its Consequences. *J. Alcohol Reaserch and Health*. 29:4.
[11]. Wurst FM, Alexson S, Wolfersdorf M, Bechtel G, Forster S, Alling C, Aradottir S, Jachau K, Huber P, Allen JP, Auwärter V, Pragst F. (2004), Concentration of Fatty Acid Ethyl Esters in Hair of Alcoholics: Comparison to other Biological State Markers and Self Reported Ethanol Intake. *J Alcohol and Alcoholism*. 39: 33-38.

Appendix

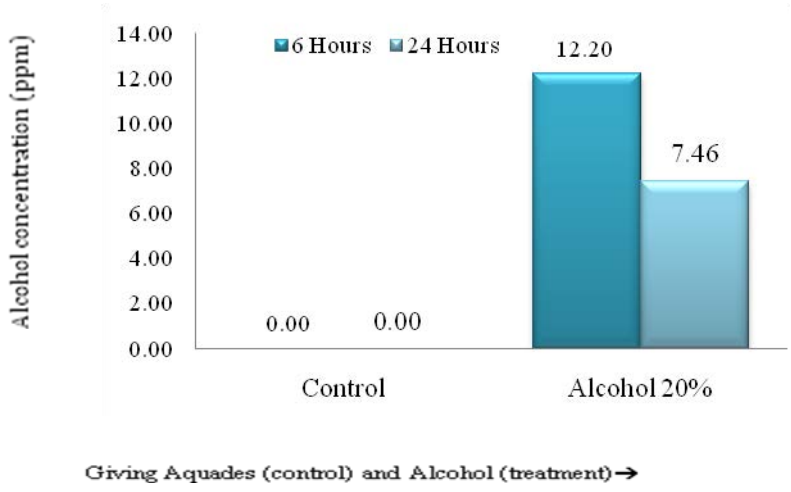

Figure 2. Decrease in concentration of ethanol in Wistar rat urine after 24 hours exposure of 20% in acute alcohol

Response of *Rhizopus Sp* in Ration to the Food Consumption, Body Weight and Feed Conversion of Chickens Layer Grower Period of I

Nur Alim Natsir

State Islamic Institute of Ambon, Indonesia (allif_af@yahoo.com)

Abstract

This study was aimed to know the response of Rhizopus sp in ration to feed consumption, body weight and feed conversion of layer grower I period of Isa Brown. The material used in this study was 64 layer grower I period strain Isa Brown age 12 weeks, with average live weight of 1121.25 ± 76.26g. The method that used was completely randomized design experiment with 4 treatments and 4 replications, each replication consisting of 4 hens. Four treatments of diet with the addition of Rhizopus sp level (T0) 0 percent, (T1), 0.2 percent, (T2), 0.4 percent, (T3), 0.6 percent. The variables measured were feed consumption, body weight, and feed conversion. Data were analyzed with analysis of variance with a level of 95%. If the results showed a difference, then it will continue with Duncan Test (BJND) at the level of 95%. The results of this research showed that feed consumption treatment not significantly (P> 0.05) and significantly (P <0.05) to the feed conversion and body weight. Average feed consumption of each treatment as chickens are as follows: T0 = 1592.75 g, T1 = 1531.81 g, T2 = 1603.00 g, T3 = 1509.06 g. The average weights were: T0 = 147.19 g, T1 = 141.81 g, T2 = 191.25 g, T3 = 138.75 g. While the average for the feed conversions were: T0 = 10.89, T1 = 10.33, T2 = 8.42 and T3 = 10.99.

Keywords: *Rhizopus sp, feed consumption, body weight, feed conversion.*

1. Introduction

Ration is a factor important in effort of livestock compared to seed and management, because the feed is one factor to be considered because their expenditure ranges from 60-70 percent of production costs [1].

Ration that nutrient for optimal growth and livestock products, need followed by the value of benefits and high efficiency of ration and economical. An effort to increase the value of the benefits and using efficiency of feed is additional material, feed additive. *Rhizopus sp* is a feed additive that helps produce digestive enzymes in the tracktus digestivus of poultry such as *protease, amylase, lipase, glucoamylase* and *phytase*. In addition, *Rhizopus sp* was able to suppress pathogenic microorganisms in the intestine (*Escherichia coli* and *Salmonella sp)* so there is not competition the use of substances of feed between the chicken and pathogenic microorganisms [2].

Yeast in the digestive will stimulate the growth of bacteria that produce of lactic acid. The culture of this yeast in the tracktus digestivus will be able to produce enzymes that help the digestive process, as well as an effort to improve feed efficiency of poultry [3]. Consideration will be a function of *Rhizopus sp* then conducted research that aims to study the response of *Rhizopus sp* to feed consumption, body weight and feed conversion.

2. Experimental Detail

Chikens layer used in this study were female strains of *Isa Brown* as many as 64 individual aged 12 weeks. Cages were battery cages as many as 16 plots measure 40x20x35cm. Feed used consisted of corn, bran and concentrates and *Rhizopus sp*. Rations containing 14.2% protein and 2531 kcal EM/kg. Rations were mixed with premix way a small percentage of mixed first with 5 percent of the total ration [4].

The method used in this research is completely randomized design with 4 treatments, 4 replications, and each replication consists of 4 chikens layer grower I [5]. The treatment in this study are T0: rations without *Rhizopus sp*, T1: + 0.2% rations with *Rhizopus sp,* T2: + 0.2% rations with *Rhizopus sp*, T3: + 0.4% rations with *Rhizopus sp.* Data analysis using analysis of variance RAL pattern and if there are significant differences followed by Duncan's test (BJND). Measurement of body weight was done by

reducing the last body weight by early body weight. Feed conversion was determined by comparing the amount of feed consumed with body weight during 3 weeks.

3. Result and Discussion

Feed consumption

From the analysis of variance is known that the addition of *Rhizopus sp* in rations of chickens layer do not showed significant differences (P>0.05) to the feed consumption. The average of feed consumption of chickens' layer grower period I of each treatment during the study is given in Table 1.

Table 1. The average of feed consumption of chickens' layer

Treatment	X Feed consumption (grams)
T0	1592.75
T1	1531.81
T2	1603.00
T3	1509.06

Body Weight

From the analysis of variance, the addition of *Rhizopus sp* in rations of chickens layer are significantly different (P <0.05) to body weight. The average of body weight of chickens' layer grower period I of each treatment during the study is shown in Table 2.

Table 2. The average of body weight of chickens' layer

Treatment	X PBB (g)	Duncan Test 5%
T3	138.75	a
T0	147.19	a
T1	149.81	a
T2	191.25	b

Feed conversion

From the analysis of variance, it is known that the addition of *Rhizopus sp* in rations of chickens layer are significant differences (P <0.05) to feed conversion. The average of feed conversion of chickens' layer grower period I of each treatment during the study contained in Table 3.

Table 3. The average of feed conversion of chickens' layer

Treatment	X Body weight (g)	Duncan test 5%
T3	10.99	a
T0	10.89	a
T1	10.33	a
T2	8.42	b

Response addition of *Rhizopus sp* in ration to feed consumption

The analysis of variance showed that the addition of *Rhizopus sp* levels into the diets did not result in significant differences (P> 0.05) on feed consumption of chickens' layer grower period I (Table 1).

Feed consumption did not differ among treatments, probably because the concentration of enzymes produced by *Rhizopus sp* in the tractus digestivus has not reached yet the optimum to react with the substrate so that not the maximum increase the digestibility of feed. Ration containing the same energy level will cause the same feed consumption. The treatment T2 showed significantly different with treatment T1, T0, T3. This condition is suspected because of the concentration of enzymes produced by *Rhizopus sp* reached the optimum point to produce enzymes such as *amylase, protease, and lipase* in the tractus digestivus. *Rhizopus sp* will be active again in the tractus digestivus of poultry when the conditions are suitable for its life so that in the active condition *Rhizopus sp* will produce enzymes like *protease, lipase* and *pitase* so that will help digestion of food substances [6].

Response addition of *Rhizopus sp* in the ration to body weight

The analysis of variance showed that the addition of *Rhizopus sp* levels into the diets showed significant differences (P> 0.05) to body weight of layer hens' grower period I (Table 2). This condition was caused by the fluctuations of feed consumption. Different treatment T2 (Table 2) caused by the activities of the enzymes in the tractus digestivus of poultry has entered the optimal stage. With this optimum enzyme, feed consumption will increase so that the body weight will also increase. The ability of *Rhizopus sp* in the production of digestive enzymes has an impact on increasing the digestibility of feed by poultry.

The value of use of feed that increase by the presence of *Rhizopus sp* in the ration can be used for the growth of the better organs. The difference of body weight in treatment T2 indicates that the absorption of protein is more active with the addition of *Rhizopus sp* so that poultry will be able to fulfill the needs for growth.

Response addition of *Rhizopus sp* in ration to feed conversion

The analysis of variance showed that the addition of *Rhizopus sp* levels into the diets showed significant differences (P> 0.05) on feed

conversion of layer hens' grower period I (Table 3). Differences in feed conversion value T2 treatment was caused by the increase amount of consumption, so significantly different and relatively the same of body weight. Both these factors influence each other in determining feed conversion. As mentioned in the literature, one affect factor of feed conversion is the growth rates [7]. In treatment, the growth rates are the same with the needs of the nutrients from the feed consumption of layer hens' grower period I. From the results of Duncan test (5%) that T0, T1, T3 there were not significant differences. This is caused from each treatment to give the amount of same consumption and body weight.

In treatment T2 showed significant response to the T0, T1, T3. This is due to increased feed intake resulting in imbalance of substances - food substances in it that gives a limitation in the digestive process. These conditions determine the different feed efficiency of production achieved. Different feed conversion ratios on T2 treatment indicates that with the addition of 0.4% *Rhizopus sp* as the optimum level, which *Rhizopus sp* able to produce digestive enzymes that improve digestibility of feed so that the substances are absorbed by the body more complete.

4. References

[1]. Anonymous (1994), *Meningkatkan Efisiensi Melalui Makanan.* Majalah Poultry Indonesia No. 176 : 62

[2]. Shin, H.T. (1988) *The Effect of Yeast Culture In Swine and Poultry Ration College of Agriculture.* Sung Kyun Kwan. University Suwon. Korea.

[3]. Fardiaz, S. (1994), *Mikrobiologi Pangan.* Penerbit Gramedia Pustaka Utama. Jakarta.

[4]. Rasyaf (1994), *Beternak Ayam Petelur.* Cetakan IV. PT Penebar Swadaya. Jakarta

[5]. Gaspersz, V. (1994), *Metode Perancangan Percobaan.* Penerbit Armico. Bandung.

[6]. Sardjoko (1992), *Bioteknologi Latar Belakang dan Penerapannya.* Penerbit Gramedia Pustaka Utama. Jakarta.

[7]. Anggorodi (1985), *Kemajuan Mutakhir Dalam Ilmu Makanan Ternak Unggas*. Penerbit UI Press. Jakarta.

Controlling *Aedes Aegypti* Mosquito Population as DHF Vector with Sterile Insect Technique in Pasar Jumat – Nuclear Research Center

Siti Nurhayati [1], Budi Santoso [2]

(1) Center for Technology of Radaition Safety and Metrology, National Nuclear Energy Agency (BATAN), Jakarta, Indonesia (nurhayati_s@batan.go.id)
(2) Center for Application of Isotope and Radiation Technology, National Nuclear Energy Agency (BATAN), Jakarta, Indonesia

Abstract

The control program of DHF in Indonesia is still problematic due to incomplete approach. The diseases are caused by Dengue virus infection through biting of the Aedes aegypti. One way to overcome this problem is Sterile Insect Technique (SIT) and assumed as the exact and potent strategy for contributing in the DHF control. The technique was done by sterilizing the male pupae or adult Aedes aegypti mosquito with various doses of gamma radiation. Sterile male mosquitoes were released continuously to a located area with aim to gain a condition where the population of mosquito in that area is reduced due to mating between sterile insect and wild type insect so that the diseases transmission can be stopped. From the experiment of the results, it was known that the dose of 70 Gy of gamma rays caused the sterility up to 100% with mating competition of 0.31 and dose of 65 Gy sterilized 98.53 % with mating competition of 0.45. Experiment on the releasing into restricted area of Pasar Jumat – Nuclear Research Center showed that the first release could reduce natural population of mosquitoes up to 35% and second release reduced population up to 68-80%.

Keywords: *DHF, Aedes aegypti, SIT, mating competitiveness.*

1. Introduction

Vector borne diseases such as Dengue Haemorrhagic Fever (DHF) is still a health problem in Indonesia because it has not been handled completely, even in some areas there were some outbreaks. This is caused by a fairly rapid development and resulting in massive urbanization to the city and create a dense settlements with poor sanitation. This will cause a very fertile area for mosquitoes as vectors of disease that could interfere with public health [1].

Dengue fever is an endemic disease both in Java and outside Java that is transmitted from sick to healthy people through mosquito bites transmitters (vectors) of *Aedes aegypti* that carries Dengue virus. Although eradication of *Aedes aegypti* as vectors of disease have been often done, but the results are not maximized because it has not supported the awareness of population to environmental hygiene, vector resistance to pesticides and there are no effective drugs or vaccines, so that dengue remains a very urgent health problems to be addressed urgently [2].

In Indonesia, there are three species of Aedes mosquitoes which have a potent to transmit dengue; these are *Aedes aegypti*, *Aedes albopictus* and *Aedes scutelaris*. Aedes aegypti is the mosquito that highly responsible for transmission of DHF disease [3]. Because the conventional vector control is less successful, the Sterile Insect Technique (SIT) is an alternative vector that can be implemented. SIT is a biological vector control technique that is specific and affects only the targeted species. This technique is reducing the number of population in the field but not destroy it. Mosquito population can be reduced by sterile insect that released gradually and continuously so that at the 5^{th} generation mosquito populations will be depleted [4,5].

SIT is a relatively new technique and reported as a potential vector control measures, effective, species-specific and compatible with other control measures. Basic principle of SIT is very simple: kill insects with the insect itself (autocidal technique). SIT is an array of activities that are intertwined with each other, ranging from maintenance of insects in the laboratory, irradiation for sterilization, and population dynamics of its release in the field [6,7]. In practice SIT will be better when combined with other vector control in an integrated manner, such as the use of insecticides, environmental sanitation, good water settings, use of predators and installation of mosquito nets and netting at

home.

SIT is a technique to eradicate the insect by sterilizing male insects. Sterile male insects are released in the field with the hope they are compete with normal males in mating with a female insect. Female insects that have been mated with sterile males will spawn, but eggs do not hatch or even not spawn at all. If the release of sterile male insects is done continuously, then the population of insects at the release site will be lower [8].

In this paper we presented the results of population control mosquito of *Aedes aegypti* as the vector of Dengue through SIT performed at Pasar Jumat – Nuclear Research Center, South Jakarta, with the aim to break the cycle of the spread of dengue disease [9,10]. This paper explain an effective dose of gamma irradiation for sterilizing mosquito and its mating competitiveness.

2. Experimental Details

Research activities included mass rearing, the determination of gamma irradiation dose for sterilization, population dynamics of mosquito, determination of mating competitiveness, and eggs bank. Maintenance of mosquitoes for the stock should be done continuously for the continuity of SIT activities. The most important part of the methodology was rearing.

Production of sterile male mosquitoes

Colonies of *Aedes aegypti* eggs attached on filter paper was soaked in plastic tray with the size of 32cm x 27cm and 7cm. After hatched into larvae, they were fed with dog/cat food pellet. After pupae stage was obtained, they were separated according to the size as small and large by using a filter (small pupae 90-95% are male). Male and female adult mosquitoes emerged from pupae were separated using the aspirator (vacuum). Male mosquitoes were kept in the 100 cc-sized plastic vials, and then was irradiated using Gamma Cell Irradiators at dose of 50, 55, 60, 65, 70 Gy and certain dose rate (Figure 1). After irradiation, mosquitoes were fed with a solution of honey/sugar at concentration of 10%. Sterilized male mosquitoes were ready for release to the restricted location.

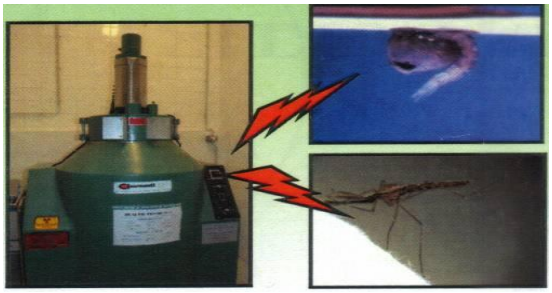

Figure 1. Sterilization can be done for pupae and adult stages using Gamma Cell Irradiator 220.

Study on the vector population dynamics on the location of SIT application

Survey was done to determine area of breeding places of *Aedes aegypti* that were endophilic at the location points. An ovitrap was placed in some locations for 1 month and observed every 1 week. Observations were done on the number of mosquitoes that emerged from eggs and they were captured in each ovitrap. From this it can be estimated the initial mosquito population so that we could determine the points of release of sterile male mosquitoes, the number of male sterilized mosquitoes that must be released and the level of success of SIT at the end of the program.

Figure 2. A. Ovitrap installation in the area to be controlled; B. Selection of male pupae for irradiation and C. Male mosquitoes are ready to be released to the location.

The release of sterile male mosquitoes

Sterile male mosquitoes were released at points/locations that have been determined and this was conducted every week with a fixed amount of mosquito based on the analysis of population dynamics study at locations that will be controlled. The mosquito release was done in the building/house/place as target of control. The number of released sterile male mosquito was 3-times of the amount of natural populations based on the analysis of population dynamics of natural populations (the application of study on the mating competitiveness of irradiated mosquitoes).

Analysis of SIT

Ovitrap was placed on the release area and observed and analyzed every week. From analysis of results it can be known the success rate of SIT, which was marked by the decline of populations of *Aedes aegypti* trapped in ovitrap. Egg banks should be performed continuously for stock and continuity of the research. *Aedes aegypti* eggs on filter paper were stored in dry condition, so that it was easily collected and used as stock.

Observation of Mating Competitiveness

To get the value of mating competitiveness post-sterilization, irradiated males mosquitoes were mated with control (non-irradiated) female mosquitoes, irradiated male mosquitoes was mated with irradiated female mosquitoes and control males was mated with control female mosquitoes. Evaluation on the offspring either at the egg, larvae and pupae stages was done for both quantity and quality.

3. Result and Discussion

From the research that has been done to the vector of *Aedes aegypti*, it was known that gamma ray dose of 70 Gy resulted in 100% sterility and mating competitiveness value of 0.31. Dose of 65 Gy sterilized 98.53% with mating competitiveness of 0.45, and dose of 60Gy sterilized 71.92% with mating competitiveness of 0.46, whereas dose of 55 Gy sterilized 69.25% with mating competitiveness of 0.47 and dose of 50 Gy sterilized 67.15% with mating competitiveness of 0.51. The release of sterilized male of *Aedes aegypti* mosquitoes was done in a restricted area in Pasar Jumat – Nuclear Research Center, South Jakarta and the results were presented in Table 2 (Appendixes).

Table 1. The experimental results of SIT for Dengue vector mosquitoes.

Dose (Gy)	Sterility (%)	Mating competitiveness
50	67,15	0,51
55	69,25	0,47
60	71,92	0,46
65	**98,53**	**0,45**
70	**100**	**0,31**

Based on Table 1, it was known that at first release was only able to reduce the population of ± 35%, this was due to the low competitiveness of *Aedes aegypti* released and the high initial population (from 101 mosquitoes to 76 mosquitoes, from 147 mosquitoes became 68). This can be overcome by increasing the number of mosquitoes that are released, especially in early release of SIT program.

In the second release there was reduction of the mosquito *Aedes aegypti* of 65-80% (from 76 became 25 and from 68 reduced to12). This is because the amount of sterile male mosquitoes released was same, as many as 180 mosquitoes at each release point, while the population at the point was decreased as a result of the first release, so that released sterile male mosquitoes have a greater mating opportunities than that of the first release.

Moreover, *Aedes aegypti* mosquitoes were able to move between indoor locations within one building, this was shown from a point of A3 (initial population was 0) but there were 10 *Aedes aegypti* found after the first release.

To be sustainable, the SIT need several conditions such as that mass production of insect, capability in sterilization, capability in mating competitiveness and isolated locations.

4. Conclusion

From the research, it can be concluded that the dose of gamma radiation given to the vector of *Aedes aegypti*, dose of irradaition of 70 Gy resulted in 100% sterility with mating competitiveness value of 0.31; dose of 65 Gy

sterilized 98.53% with mating competitiveness of 0.45, and dose of 60 Gy sterilized 71.92% with mating competitiveness of 0.46, whereas dose of 55 Gy sterilized 69.25% with mating competitiveness of 0.47 and dose of 50 Gy sterilized 67.15% with mating competitiveness of 0.51.

Experiment on the release of sterile male mosquitoes of *Aedes aegypti* in a restricted area it was known that the first release could reduce the natural population by 35% and the second release reduced the population by 65-80%. *Aedes aegypti* mosquitoes can live together with *Aedes albopictus* in one location.

5. Acknowledgements

---

6. References

[1] Directorate General of Communicable Diseases Eradication and Environmental Health (1992), Eradication of mosquitoes transmitting instructions Dengue Hemorrhagic Fever Ministry of Health-RI. Jakarta

[2] World Health Organization (1976), Resistance of vectors and reservoirs of disease to pesticides, *WHO Tech. Rep.Ser.* 585

[3] Directorate General of Communicable Diseases Eradication and Environmental Health (1986), Conduct Guidelines Types of Entomology Test Necessary to Support Operational Program Insect borne Disease Eradication. DEPKES RI. Jakarta

[4] Henneberry, T.J. (1979), Developments in Sterile Insect Release Research for the Control of InsectPopulations, Proc. of FAO/IAEA Training Course on the Use of Radioisotopes and Radiation in Entomology, Univ. of Florida, 213 – 223.

[5] Klassen, W. (1977), Strategies for Managing Pest Problems, Proc. of FAO/IAEA Training Course on the Use of Radioisotopes and Radiation in Entomology, University of Florida, 248 – 283.

[6] Hendrichs, J., M.J.B. Eysen, W.R. Enkerlin, and J.P. Cayol (2005), Strategic Option Using Sterile Insects for Area – Wide Integrated Pest Management, *In* V.A. Dyck, J.Hendrichs and A.S Robinson (eds.), Sterile Insect Technique Principles and Practice in Area-Wide Integrated Pest Management, Springer, P.O.Box 17,3300 A.A.Dordrecht, The Netherland, pp.564-567.

[7] Director General PPM and PLP. (2001), Guidelines for Vector Ecology and Behavioral Aspects. Jakarta. Ministry of Health - RI.

[8] Sutrisno, S. *et al.* (2003), Integrated Control of Malaria Vector Mosquito (Anopheles sp) and Dengue fever (Aedes aegypti) by Using the Sterile Insect Technique (TSM) and Other Control Techniques Compatible. Jakarta. BATAN-Ministry of Health , Jakarta

[9] Nurhayati, S. (2008), Prospect of Application of Nuclear Techniques in Disease Vector Control of Dengue Haemorrhagic Fever (DHF), Aedes aegypti. Presentation of Scientific Research Associate BATAN

[10] Nurhayati, S., B. Santoso, A. Rahayu and D. Tetriana (2009), Effect of Gamma Irradiation on Competitiveness Married Aedes aegypti as a vector of Dengue Hemorrhagic Fever (DHF). SNKKL V. UI-Depok.

Appendixes

Figure 3. Rearing process of Aedes aegypti, including mosquito feeding, collecting eggs, hatching into larvae, pupae and adult mosquitoes.

Table 2. Reduction of population due to the release of sterile males of Aedes aegypti in a restricted area of Pasar Jumat – Nuclear Research Center, Jakarta (ratio 3:1).

Release point	Initial population				First release				Second release			
	∑eggs	∑larvae	∑A. aegypti	∑A. albopic	∑eggs	∑larvae	∑A. aegypti	∑A albopic	∑eggs	∑larva	∑A. aegypti	∑A. albopic
A1	36	20	19	1	241	188	14	124	141	65	8	49
A2	165	144	82	36	77	62	42	11	1	0	0	0
A3	0	0	0	0	224	125	20	87	114	87	17	61
Total	201	164	101	37	542	375	76	222	256	157	25	110
B1	49	36	26	8	76	75	23	50	76	28	4	22
B2	86	78	77	1	68	65	45	17	40	16	8	8
B3	157	85	44	27	22	22	0	22	0	0	0	0
Total	292	199	147	36	166	162	68	89	116			30

Radiation Induced Micronuclei in Lymphocyte Cell of Radiation Workers

Sofiati Purnami [1], Yanti Lusiyanti [2], Masnelli Lubis [3], Dwi Ramadhani [4], Devita Tetriana [5], Siti Nurhayati [6], Mukh Syaifudin [7]

[1,2,3,4,5,6,7] Center for Technology of Radiation Safety and Metrology, National Nuclear Energy Agency (BATAN), Jakarta, Indonesia (k_lusiyanti@batan.go.id).

Abstract

Micronuclei (MN) is an indication of chromosomal damage caused by ionizing radiation which could be observed in cells with two nuclei (binucleated) that prevented to split into daughter cells using cytochalasin B. MN can be induced by ionizing radiation exposures and used to predict the occupational doses of radiation. In this research frequencies of MN were observed in blood lymphocyte samples obtained from radiation workers. Thirty radiation workers (23 males and 7 females) and 5 non radiation workers as control were involved in this research. Two milliliters of peripheral blood samples of each individual were cultured in RPMI medium with phytohaemagglutinin stimulation for 72 hours at 37°C. With the standard technique, cell proliferation was terminated with cytochalasin-B and MN was harvested and stained with Giemsa. The frequency of MN in 100-533 binucleated cells (BNC) counted was ranged between 0.00 and 0.05 MN/cell. Frequency of MN in blood of one worker was relatively higher than those of others and controls (non radiation workers). These results showed that frequencies of MN in lymphocyte cells were in normal range, indicating that monitoring of safety program was good.

Keywords: *micronuclei, lymphocyte, ionizing radiation, radiation worker, biological dosimetry.*

1. Introduction

Radiation exposure to the body will result in interaction of radiation with biological materials and will be followed by several ooutcomes such as chromosome aberrations and micronuclei. Analysis of chromosome aberrations have been used extensively as a biomarker of workers and of general public members exposed to ionizing radiation. This method is used to detect chromosome aberrations in peripheral blood lymphocytes as the most sensitive cell to radiation [1].

Cell nucleus contains chromosomes that consist of long series of deoxyribonucleic acid (DNA), which play a role as a carrier of the nature of an individual. Radiation can change both the number and structure of chromosomes, called chromosome aberrations. Damage to the structure of chromosomes are shown as chromosome with broken arm that may lead to chromosome aberrations including deletions of chromosome fragments that do not contain centromere (acentric fragment), ring chromosomes, and chromosomes with two centromeres (dicentric) [2].

Micronuclei (MN) is intermediate products (byproduct) of chromosome aberrations that is seen as a small circle in the cytoplasm outside the main nucleus and contains the fused chromosomes or its fragments, and/or chromosomes intact and appears with the same structure with the main nuclei. MN formation is strongly influenced by radiation dose and dose rate and also depends on the capacity of DNA and cellular repair [3]. MN has been used by some researchers to determine the radiation dose during radiotherapy or accidental radiation protection to ensure the program runs well.

Micronuclei are fragments of chromosomes without centromer (clastogenic effect) or a chromosome with the centromer (aneugenic effect) that do not split into two nuclei sets of the daughter during mitosis. This damage can be induced by radiation and can be observed in peripheral blood lymphocytes. Micronuclei observed as cells with two nuclei (binucleat) that failed to divide into two daughter cells with cytochalasin B. Thus micronuclei examinations consist of cell culture in the laboratory and its calculation is much faster and easier than those dicentric chromosomes.

Blocking technique that aims to obtain MN was first introduced in 1975 [4]. *In vitro* MN test with blocking cytokinesis of human peripheral blood lymphocytes has been used extensively to study chromosomal damage induced by ionizing radiation or chemicals [1]. Because radiation-induced MN showed a radiation dose and quality dependence, MN can be used as a biological dosimeter for radiation protection purposes [5] and has been recommended by the International Atomic

Energy Agency (IAEA) [6]. Rapid calculation of MN compared with dicentric chromosome and the possibility to calculate automatically and very easy to performed makes this biomarker is chosen when a large number of cells must be calculated for routine screening of workers exposed to low doses occupationally or in the case of radiation accidents [7]. MN has been used by some researchers to determine the radiation dose due to an accident during radiotherapy or radiotherapy treatment [8], assessment of the radiation effects for workers in Nuclear Power Plant [9] or to ensure the radiation protection program running well [10].

Many studies on micronuclei used as an indicator of damage to the body due to radiation. Micronucleus is a small nucleus which is the nucleus material (DNA) seen as a small body in the cytoplasm outside the nucleus, with the structure and intensity of color similar to the nucleus. Acentric MN is formed from fragments that failed to join the daughter cells during cell division process. It can also be formed from a chromosome that are left behind, or not carried away in the mitotic process, or result from a complex chromosome configuration, during the process of anaphase. Nevertheless there is strong evidence to suggest that radiation can induce the formation of micronuclei mainly derived from asentric fragments [11].

Examination by scoring MN can be used as a realistic and alternative method to determine quantitatively the existence of chromosomal damage from radiation, in addition to chromosome counting disentrik [12]. The technique is relatively easier and faster because the cells can be observed more numerous, especially when using automated computer image system. So MN technique allows ti use as a routine procedure, and can be observed at low doses of 0.05 to 1 Gy, which is the range limit of the lowest dose for induction of chromosome aberrations [1,4].

Some data shows a more complex relationship between micronuclei with chromosome aberrations. On the formation of micronuclei needed one cell division, and to test micronuclei induction occurred from one cell division, it is necessary to identify cells that have undergone one division. Method of blocking cells in the process of cytokinesis will be formed of cells with two nuclei (binucleat) from cleavage only once and only one cell. Micronuclei observed only in cells with two nuclei [6].

The criteria for MN is that diameter is less than one-fifth of that of the nucleus (10 μm), located in the cytoplasm and outside the nucleus, and no contact with the nucleus [5]. Another description states that the size of radiation-induced MN is between 6-12 μm. Approximately 80% of MN induced by gamma rays containing DNA of about 6% or less of the interphase nucleus, indicating origin derived from fragments asentrik micronuclei. In normal individual frequency of MN in 500 cells counted was 4.4 ± 2.6 [4,6].

Micronuclei are formed due to damage to the structure of chromosomes that occurs in G0-G1 phase of the cell cycle, so micronuclei appeared after cell nucleus division. Method In cell culture cytocalasin-B functions to block the process of cytokinesis so that the cell is at the level of cell division binucleat (cells with two nuclei), and micronuclei formed binucleat be observed in these cells [4,6].

The purpose of this study was to determine the frequency of MN as chromosome damage in blood cells induced by occupational exposure to radiation in order to monitor the implementation of safety regulations to radiation.

2. Experimental Details

Research subjects

Blood samples were obtained from 30 radiation workers in National Nuclear Energy Agency of Indonesia (BATAN) located in Jakarta and Tangerang, with an age range of 28-63 years old (mean 40.7 years old) and 5 people are non radiation workers aged between 25 and 43 years old (mean 39.7 years old). Every worker was given the informed consent form (willingness to provide blood samples) and biographical data include history of illness and a history of working with radiation to determine the history of work related to receipt of radiation dose as shown in Table 1.

Table 1. Informations of all radiation workers enrolled in the study.

		Subject for MN examination	
		Radiation workers	Control workers
No. subject	33	30	5
Working time (year)	1 - 10	4	4
	11 - 25	19	1
	>26	7	-
Accumulated dose (mSv)	0 - 5	13	-
	6 - 10	10	-
	11 - 30	5	-
	>50	2	-
Sex	Male	23	5
	Female	7	-
Age (year)	21 - 40	6	4
	41 - 60	23	1
	>60	1	-
Smoking habit	No	24	5
	Yes	6	-

Blood sampling and culturing for lymphocytes

About 2 milliliters of peripheral blood was taken from each subject by using a syringe and immediately added with 0.03 mL of heparin as an anti-coagulant. Culture and harvesting procedures were conducted according to the instructions in the IAEA Manual [6] with minor modifications. Briefly two milliliters of peripheral blood were cultured in 8 ml of RPMI 1640 medium (Gibco BRL) enriched L-glutamine and HEPES, 10% fetal bovine serum (FBS), 1% penstrep (Gibco) and stimulated with 2-3 % phytohemagglutinin (PHA) (Gibco BRL) in 37°C incubation for 72 hours. In the 44 hours since the start cultured, into a culture was added with 15 µL sitokhalasin B (3 mg/ml) (Sigma) and harvested at 72 hours after the beginning of culture.

Preparation of lymphocytes for MN

Samples were centrifuged at 1500 rpm for 10 minutes and the upper layer (supernatant) was removed, and then 8 ml of cold hypotonic solution (0.075 M KCl) was added, left at room temperature for 3 minutes, and then added with 3-4 drops of formaldehyde solution and cold fixative solution (methanol: glacial acetic acid = 3: 1). After mixed well the homogenous solution was placed in refrigerator (4ºC) for 10 minutes, and then centrifuged at 1000 rpm for 10 minutes. Supernatant was removed and add 6 ml cold fixative solution, centrifuged at 1000 rpm for 10 minutes. After fixation for 3 times then it will be obtained binucleated cells which may contain MN. After one night stored in the freezer, MN preparation was made by dropping 3-4 drops of cells containing MN on the glass slide and allowed to dry in air. After stained with 4% Giemsa and covered with coverglass slide was observed under microscope with a magnification of 1000 times.

3. Result and Discussion

Observation of MN, which is a by-product of chromosome aberrations, has been carried out on a number of blood samples obtained from radiation workers. MN frequencies were within normal limit and ranged from 0.00 to 0.05. One sample showed higher MN frequency than that of others. The frequency of MN in the blood of this worker was 0.05; this was confirmed by the observation of dicentric. It is known well that MN can be induced not only by irradiation but also by other stimulators such as cigarettes and other chemical compounds. It has been established that the MN frequency is 0.030 (30 per 1000 BNCs) and as the limit to find out that the radiation exposure received by a person is still in allowable limits based on the number of MN in the blood.

In Table 1 it was shown that radiation workers enrolled in this study had working time of 1 year to 41 years with individual dosimeters of <50 mSv/year, except for two donors who received the radiation exposure of >50 mSv. For each sample, the number of MN in each cell was counted according to criteria that are determined by IAEA Protocol [6]. It was known that the number of cells containing one nucleus was much higher than the cell containing two nuclei. This may be influenced by concentration sitochalasin B as blocking cell or culture period. The success in maintain the cytoplasm by adding formaldehyde BNC was also influenced the speed of calculation.

The results showed that the average number of one MN/cell for 30 radiation workers was between 0.0114 and 11.4 MN per 1000 binucleic cells (Figure 1). Blood sample with number 11 contained 11 MN in its 500 cells counted, all had one MN per cell. Sample number 9, 10 and 12 contained 8 MN in 500 cells counted (6 MN1 and 1 MN2). The number of MN per cell in radiation worker group was relatively higher than that of non-radiation worker group, but this difference was statistically not significant. There was no influence of duration of work to MN frequency, although allegedly MN tended to increased along with the accumulated radiation dose and or duration of work [13].

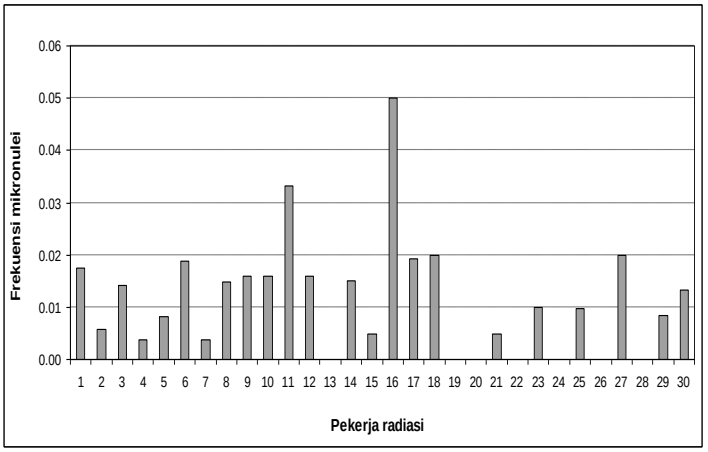

Figure 1. Frequency of MN in blood of 30 radiation workers.

In non-radiation worker group, the average of MN frequency was 0.0085 (8.5 per 1000 BNC). Sample number 4 contained MN in much higher than others. In this sample 1 MN3 (3 MN in one cell) and 4 MN1 (1 MN in one cell) was observed. One sample showed a high frequency of MN (0.028), even though this was higher than those of radiation worker group. This may be caused by the existence of a factor other than radiation exposure

such as exposure to chemical compounds, because the exposure dose data for this individual was still in normal range (Figure 2). In this study MN was varied among samples that may induced by radiation, and showed no significant difference between one donor to others, and this result is consistent with other studies that there is individual variation in MN and closely associated with age and gender [13].

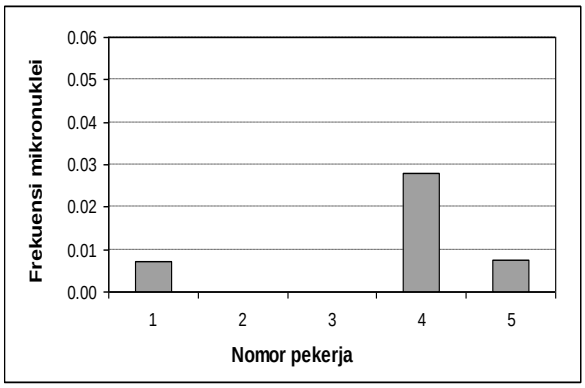

Figure 2. Frequency of MN in control blood (non radiation workers)

Data of age for 30 radiation workers was ranged between 28 and 63 years, this clearly showed that there was a link between the frequencies of background MN with age. There was no significant difference between age and the frequency of MN, however, a great variation was found between individuals [1]. Example of MN observed under microscope was presented in Figure 3 (Appendix).

Compared to classical methods of cytogenetics dose studies with CA, MN method in lymphocytes is relatively simple. This is because it can be performed in much faster and less influenced by variation between scorers. One weakness is that the high frequency of micronuclei for background, both in number and individual variation.

Micronuclei detection technique does not require cytoplasmic division after cell nucleus division and only cells with two nuclei are counted. But the background counting micronuclei in lymphocytes will increase 10 times for 20-85 years old human. This makes the technique less desirable MN test as well as the spontaneously occurred micronuclei that ranged between 3 and 30 per 1000 BNC [4]. Research by Heddle and Krepinsky [11,12] stated that the sensitivity of lymphocytes to the formation of low-dose micronuclei result is a fast and inexpensive method to determine the relative sensitivity among patients with cancer and radiotherapy dose adjustment.

Micronuclei determination in the blood of patients exposed to radiation is also very useful in assessing the possibility of acute effects. Micronuclei formation is strongly influenced by radiation dose rate and also depends on the capacity improvement of DNA mobile.

4. Conclusion

Micronuclei can be induced by exposure to radiation and micronuclei has used in the assessment of radiation effects on workers and by some researchers to determine the dose of radiation during radiotherapy or radiotherapy accident. One of the shortcomings is in terms of basic data / background of micronuclei frequency, both in terms of number, as well as individual variation. Micronuclei test using the CB technique on lymphocytes is a relevant radiobiology method when used to evaluate the effects of radiation exposure to workers. Micronuclei frequency in radiation workers who have observed is still within the normal range, indicating that the radiation protection program running well.

5. Acknowledgements

The authors are grateful to The Ministry of Education (DIKTI) that provided Block Grant Fund, Head of the Center (PTKMR) for permission to conduct this research all participants for blood sample collection.

6. References

[1] Mill, A.J., Wells, J., Hall, S.C., *et. al*, (1996), A. Micronucleus Induction in Human Lympho-cytes: Comparative Effects of X Rays, Alpha Particles, Beta Particles and Neutrons and Implications for Biological Dosimetry, *Radiation Research*, 145, 575-585.

[2] Sastrodihardjo. S. (1979), Radiation Cell and Genetics Aplication. Center of Pusat Reaktor Bandung, BATAN, 7-10.

[3] Boreham, D.R., Dolling, J.A, Maves, S.R, et. al. (2000), Dose Rate Effect for Apoptosis and Mikronucleus Formation in Gamma Irradiated Human Lymphocytes, *Radiation Research* 153, 579-586.

[4] Vral, A., Verhaegen, H. Thierens, H., *et.al*. (1994), The *In Vitro* Cytokinesis-block Micronucleus Assay: Detailed Description of an Improved Slide Preparation Tehnique for The Automated Detection of Micronuclei in Human Lymphocytes, *Mutagenesis* 9, 439-443.

[5] Hall, E.J. (1993), Radiobiology for Radiologist, 4th ed. J.B. Lippincot Company, Philadelphia, Baltimore New York, London, 161-165.

[6] International Atomic Energy Agency (2001), Biological Dosimetry Chromosomal Aberration Analysis for Dose Assessments, *Technical Reports Series No. 260*, IAEA, Vienna, 25-31.
[7] Koksal, G., Dalci, D.O., and Pala, F.S. (1996), Micronuclei in Human Lymphocytes: The Co-60 Gamma Rays Dose Response, *Mutation Research*, 161, 193-195.
[8] Hande, Mp, Boei JJ. W.A,. Natarajan AT. (1996), Induction and Persistence of Cytogenetic Damage in Mouse Splenocytes Following Whole Body X-Irradiation Analysed by Fluorescence in Situ Hybridization II. Mikronuklei *International Journal of Radiation Bioogy*, 70 (4), 375-383.
[9] Little, J.B. (1997), What are the Risks of Low Level Exposure to α Radiation from Radon. *Proc. Natl. Acad. Sci USA,* 94, 5996-5997.
[10] Vral, A., Ferhagen, F., Thierens, H., *et. al.* (1994), Micronuclei Induced by Fast Neutron Versus Co-60 Gamma Rays in Human peripheral Blood Lymphocytes, *Int. J. Radiat. Biol.,* 65(3), 321-328.
[11] Heddle, J.B. and Carrano (1977), The DNA Content of Micronuclei Induced in Bone Marrow by Gamma Irradiation: in Evident that micronuclei arise from acentric Chromosomal Fragments. *Mutation Research*, 44, 63-70.
[12] Almassy, Z., Krepinsky. A.B., Bianco. *et. al.* (1987), The Present State and Perspectives of Micronucleus Essay in Radiation Protection. In A Review, *Appl Radiat Isotop*, 38, 241-249.
[13] Fenech, M and Marley, A.A. (1985), Measurement of Micronuklei in Limphocytes. *Mutation Research*, 147, 29-36
[14] Huber, R., Schraube, H., Nahrstedt, U., *et. al.* (1994), Dose Response Relationship of Micronuclei in Human Lymphocytes Induced by Fission Neutrons and by Low LET Radiations, *Mutation Research*, 306, 135-141.

Appendix

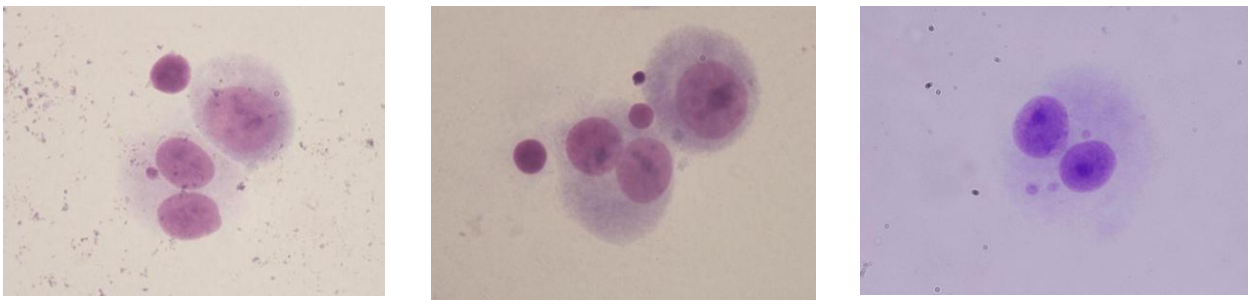

A **B** **C**

Figure 3. The BNC with one MN in blood of radiation workers (A and B), and BNC with 3 MN (C).

The Antioxidant Activity of Purple Star Apple (*Chrysophyllum cainito* L.)

Tagor M. Siregar [1], Herry Cahyana [2], Ika Narishantika [3]

[(1,3)] Food Technology Department, Pelita Harapan University, Tangerang, Indonesia (tagor_siregar@uph.edu)
[(2)] Chemistry Department, Faculty of Science, University of Indonesia, Depok, Indonesia

Abstract

The purpose of this study was to evaluate the antioxidant activity of purple star apple (Chrysophyllum cainito L.). In this study, fresh fruit were separated into three anatomically distinct parts of fruit: rind, pulp, and seed. The antioxidant compounds from each fruit parts were extracted using two different solvent: ethanol and water. Antioxidant compounds that assayed in this study were total phenolics, total flavonoid, total monomeric anthocyanin, and vitamin C. The antioxidant activity was evaluated using 2,2-diphenyl-1-picrylhydrazyl (DPPH) radical-scavenging assay. Ethanol extract of the rind had the highest total phenolics content, followed by total flavonoid content, total monomeric anthocyanin content, and antioxidant activity, while water extract of the pulp had the highest vitamin C level. Phenolics were the main phytochemical compound that play role in antioxidant activity of purple star apple extract.

Keywords: *antioxidant activity, DPPH, purple star apple, total phenolic, total flavonoid.*

1. Introduction

Several studies have reported that high consumption of fruits and vegetables are associated with reduced risks of cancer and cardiovascular disease [1]. This protective effect is related to the plant antioxidant microconstituents contained in the plant parts. Different fruits exhibit different antioxidant capacities according to their polyphenol content, vitamin C, E, carotenoids and flavonoids.

Natural phenolic phytochemicals in fruits and vegetables have been receiving increased interest from consumers and researcher for the beneficial health effects on coronary heart disease and cancer mainly due to their antioxidant activities. A number of phenolic compounds mainly flavonoid and phenolic acids are among the antioxidant compound which present in fruits and vegetables [1,10].

Star apple is the fruit that well known as a tropical fruit and planted in several places in Indonesia. There is no reports are available on the antioxidant activity of these parts of fruit.

The main objective of this research were to determine the antioxidant activity of parts of fruit (rind, pulp and seed) extract from purple star apple and to study the effect of solvent used for extraction towards the antioxidant activity of each parts of fruit extract.

2. Experimental Details

Materials

Fresh purple star apple, ethanol, methanol,1,1-diphenyl-2-picrylhydrazil (DPPH), Folin-Ciocalteau reagent, sodium carbonate, aluminium chloride, potassium acetate, Gallic acid standard, quercetin standard, ascorbic acid standard, buffer KCl 0.025 M pH 1, buffer sodium acetate 0.4 M pH 4.5, dye solution, HPO_3-CH_3COOH solution, and aquabidest.

Extraction of phenolic compounds

Fresh fruit samples were washed and separated into three anatomically distinct parts of fruit: rind, pulp and seed. The whole fruit and each fruit parts were extracted using two different solvent: ethanol and water. The extraction process was carried out for 3 hours with magnetic stirring on a hot plate (the ratio between sample and solvent was 1:4). Then, each fruit extracts were filtered using a vacuum filtration (Whatman paper no.2). After that, the supernatant was concentrated using rotary evaporator. The crude extracts were collected and stored.

Analysis of total phenolic content

Total phenolic content of the sample was measured using Folin-Ciocalteau reagent [18]. 20 µl of fruit extract solution were mixed with 1.58 ml distilled water and 100 µl of Folin-Ciocalteau reagent. After standing for 5 minutes at room temperature, 300 µl of (20% w/v) sodium carbonate solution were added. The solution were mixed and allowed for 2 hours at room temperature. Then, the absorbance was measured at 765 nm, using a spectrophotometer. A calibration curve was prepared, using a standard solution of gallic acid (20, 50, 100,250, 500, 750, 1000, 1500, 2000, 4000 mg/l, $r^2 = 0.998$). Results were expressed on fresh

weight basis as mg gallic acid equivalents/100 g of sample.

Analysis of total flavonoid content

Total flavonoid contents of the fruit extracts were determined according to the colorimetric assay [5]. 0.5 ml of properly diluted fruit extract was mixed with 1.5 ml of ethanol 95%, 0.1 ml of aluminium chloride 10%, 0.1 ml of potassium acetate 1M and 2.8 ml of distilled water. The mixture was incubated at room temperature for 30 minutes. After that, the absorbance was read at 415 nm. A calibration curve was prepared using a standard solution of quercetin (5, 10, 25, 50, 100, 200, and 300 mg/l, $r^2 = 1.000$). The results were also expressed on a fresh weight basis as mg quercetin equivalent/100 g of sample.

Analysis of total monomeric anthocyanins

Total anthocyanin analysis was performed using a spectrophotometric differential pH method [15]. Two samples of 0.1 ml were treated with 4.9 ml of buffer solution pH 1.0 (potassium chloride 0.025 M) and 4.9 ml of buffer solution pH 4.5 (sodium acetate 0.04 M). The absorbance of each mixture was read at 520 and 700 nm using a spectrophotometer. The absorbance of extracts was calculated according to the following equation:

$$A = \left[(A_{520} - A_{700})_{pH\,1} - (A_{520} - A_{700})_{pH\,4.5}\right]$$

Total anthocyanin was based on cyanidin-3-glucoside, molar extinction coefficient of 26,900, DF: diluted factor (5 ml/0.1 ml) and molecular weight 449.2. The results were expressed in terms of mg *cy-3-glu equivalent* //100g of samples.

$$Total\ anthocyanin\left(^{mg}/_{l}\right) = \frac{(A \times BM \times DF \times 1000)}{(\varepsilon \times 1)}$$

Determination of antioxidant activity

The antioxidant activity of fruit extracts was determined by using DPPH (1,1-diphenyl-2-picrylhydrazyl) method [4]. A 0.1 ml of fruit extract was mixed with 2.9 ml of 0.1 mM DPPH ethanolic solution. The mixture was thoroughly vortex-mixed and kept for 30 minutes. The absorbance was measured later, at 517 nm, against a blank of ethanol without DPPH. Results were expressed as percentage of inhibition of the DPPH radical. Percentage of inhibition of the DPPH radical was calculated according to the following equation:

$$\%\ inhibition = \frac{(Abs\ control - Abs\ sample)}{Abs\ control}\ x\ 100$$

Where Abs control is the absorbance of DPPH solution without extract.

Determination of vitamin C content

Vitamin C content was analysed using 2,6-dikloroindophenol titrimetric method [3]. First, a dye solution was standardized by ascorbic acid standard solution. Then, a 2 ml of fruit extract sample was mixed with 5 ml HPO_3-CH_3COOH in the erlenmeyer flask. The mixture was titrated slowly by the dye solution until reddish pink color formed. Vitamin C contents of fruit extract were calculated according to the following equation:

$$Titer\,(F) = \frac{\left(^{mg\ of\ ascorbic\ acid}/_{100\ ml}\right) \times 2\ ml}{(vol.of\ standard\ titration) - (vol.of\ blank\ titration)}$$

$$vit\,C\ contents\left(^{mg\ of\ ascorbic\ acid}/_{ml}\right) = (X - B) \times \left(\frac{F}{E}\right) \times \left(\frac{V}{Y}\right)$$

X = average volume of sample titration
B = average volume of blank titration
F = titer of dye (mg of ascorbic acid/ml of indophenols solution)
E = ml samples (2 ml)
V = volume of the mixture of standard solutions (7 ml)
Y = volume of the mixture of samples solutions (7 ml)

3. Result and Discussion

The antioxidant components from each part of fruit were extracted using two different solvent: ethanol and water. Antioxidant components that assayed in this study were total phenolics, total flavonoid, total monomeric anthocyanin, antioxidant activity and vitamin C.

Total Phenolic content

Total phenolic contents of the fruit extracts were determined using Folin-Ciocalteau's colorimetric method. In this method, gallic acid was used as a standard, therefore total phenolic contents were expressed in mg GAE (Gallic Acid Equivalent) per 100 g of samples. Table 1 shows the total phenolic content of part of fruit extracts.

Table 1. Total phenolic contents from each parts of fruit obtained from different solvent extraction

Part of fruit	Solvent	Total Phenolics (mg GAE/ 100 g of samples)
rind	ethanol	3265.97 ± 9.03^{cp}
	water	449.38 ± 0.95^{cq}
pulp	ethanol	39.98 ± 1.40^{ap}
	water	76.75 ± 1.74^{aq}
seed	ethanol	79.26 ± 0.73^{bp}
	water	363.46 ± 0.24^{bq}

Note :
^{a,b,c} values with different superscript letter are significantly different for solvent used ($\alpha = 0.05$)
^{p,q} values with different superscript letter are significantly different for part of fruit ($\alpha = 0.05$)

According to statistical analysis, there was significant difference between total phenolic contents of each parts of fruit ($\alpha = 0.05$). Data in Table 1 also shows that the rinds fruit extract had the highest total phenolic contents and pulp. There was significant difference between ethanol extract and water extract ($\alpha = 0.05$) in each parts of fruit. The phenolic compound that contained in purple star apple was (-)-epikatekin that more soluble in water [12]. Total phenolic contents of ethanol extract of the rinds were higher than its water extract. This fact is due to the total monomeric anthocyanin of ethanol extract was higher than its water extract.

Total Flavonoid content

Total flavonoid content was measured by using $AlCl_3$ reagent, buffer CH_3COOK 1 M and quercetin as a standard so that total flavonoid contents was express by mg quercetin equivalen per 100 g of samples. Total flavonoid contents of each parts of fruit is shown in Table 2.

Table 2. Total flavonoid content from each part of fruit obtained from different solvent extraction

Part of fruit	Solvent	Total Flavonoid (mg Quercetin eq/ 100 g of samples)
rind	ethanol	52.76 ± 0.11^{cp}
	water	23.39 ± 0.03^{cp}
pulp	ethanol	4.78 ± 0.10^{ap}
	water	5.33 ± 0.02^{ap}
seed	ethanol	29.64 ± 0.21^{bp}
	water	44.69 ± 0.05^{bp}

Note:
^{a,b,c} values with different superscript letter are significantly different for solvent used ($\alpha = 0.05$)
^{p,q} values with different superscript letter are significantly different for part of fruit ($\alpha = 0.05$)

Statistical analysis showed that there was interaction between parts of fruit extract and solvents used against the total flavonoid contents ($\alpha = 0.05$). Continued test with one-way ANOVA indicated that there was significant different between total flavonoid contents of the pulp and the seed for each solvent used ($\alpha = 0.05$).

Table 2 showed that water extract of the pulp had higher total flavonoid than its ethanol extract although the results indicated that there was no significant different between total phenolic contents of ethanol and water extract for each parts of fruit. The phenolic compound that contained in purple star apple was (-)-epikatekin that classifyied as flavanol and more soluble in water [12]. Data in Table 2 also showed that the rind of purple star apple contained flavonoid compounds that more soluble in polar organic solvent such as ethanol. The high contents of total flavonoid in extract of the rinds due to the presence of anthocyanin compounds that gave violet color on the rinds of fruit.

Total monomeric anthocyanin

Determination of total monomeric anthocyanin was performed by using pH differential method. Table 3 shows total monomeric anthocyanin of each parts of fruit extract obtained from different solvent used.

Table 3a. Total monomeric anthocyanin of fruit extract obtained from different solvent extraction

Parts of fruit	Total Monomeric Anthocyanin (mg Cy-3-glu eq./ 100 g of samples)
rind	30.80^{c}
pulp	2.45^{a}
seed	4.63^{b}

Note: values in a column with different superscript letter are significantly different ($\alpha = 0.05$)

Table 3b. Total monomeric anthocyanin of fruit extract obtained from different solvent extraction

Solvent	Total Monomeric Anthocyanin (mg Cy-3-glu eq./ 100 g of samples)
ethanol	15.40^{b}
water	9.85^{a}

Note: values in a column with different superscript letter are significantly different ($\alpha = 0.05$)

Statistical analysis showed that parts of fruit and type of solvent affected total monomeric anthocyanin of extract but there was no interaction between parts of fruit and type of solvent ($\alpha = 0.05$). Continued test with one-way ANOVA indicated there was significant different between each parts of fruit. According to table 3 total monomeric anthocyanin of extract of the rind was higher than extract of the seed and the pulp for each solvent used.

Vitamin C contents

In this study, analysis of vitamin C contents was performed by using 2,6-dikloroindophenol volumetric method. Vitamin C content was calculated as mg ascorbic acid per 100 g of fresh samples. The fresh star apple fruit contained 3.0-15.0 mg ascorbic acid/100 g of parts of edible fruit but information about vitamin C contents of the other parts of star apple fruit especially in rind and seed did not known. Vitamin C contents of each parts of fruit extract is shown in table 4.

Table 4. Vitamin C contents from each part of fruit obtained from different solvent extraction

Part of fruit	Solvent	Vitamin C content (mg ascorbic acid / 100 g of samples)
rind	ethanol	1.71 ± 0.26^{bp}
	water	3.03 ± 0.18^{bq}
pulp	ethanol	19.20 ± 0.41^{cp}
	water	21.67 ± 0.83^{cq}
seed	ethanol	0.00 ± 0.00^{ap}
	water	0.00 ± 0.00^{ap}

Note:
[a,b,c] values with different superscript letter are significantly different for solvent used (α = 0.05)
[p,q] values with different superscript letter are significantly different for part of fruit (α = 0.05)

Statistical results showed that there was an interaction between parts of fruit and solvent used for extraction towards vitamin C contents (α= 0.05). Continued test with one-way ANOVA indicated that there was significant different between vitamin C contents of extract of the rind, pulp and seed for each solvent used (α= 0.05). Extract of the pulp of fruit had the highest vitamin C contents than extract of the rind and the pulp.

Antioxidant Activity

Antioxidant activity of each parts of fruit was determined by using DPPH (2,2-diphenyl-1-picrylhydrazyl) method. DPPH method was used to measure the ability of antioxidant for scavenging DPPH radical. Antioxidant activity was evaluated with EC_{50} values (efficient concentration) or IC_{50} (inhibitory concentration), the concentration at which radical scavenging activity is 50% [2]. Table 5 showed antioxidant activity of each part of fruit that obtained from different solvent extraction

Table 5. Antioxidant activity from each part of fruit obtained from different solvent extraction

Part of fruit	solvent	Antioxidant activity (IC_{50}) (mg/ml)
rind	ethanol	0.94 ± 0.01^{cp}
	water	15.91 ± 0.04^{cq}
pulp	ethanol	15.10 ± 0.05^{ap}
	water	5.59 ± 0.05^{aq}
seed	ethanol	8.52 ± 0.05^{bp}
	water	9.57 ± 0.03^{bq}

Note:
[a,b,c] values with different superscript letter are significantly different for solvent used (α = 0.05)
[p,q] values with different superscript letter are significantly different for part of fruit (α = 0.05)

Statistical results showed that there was an interaction between parts of fruit and solvent used for extraction towards IC_{50} values (α= 0.05). Continued test with one-way ANOVA indicated that there was significant different between IC_{50} values of extract of the rind, pulp and seed for each solvent used (α= 0.05). This fact indicated that each parts of fruit contained different antioxidant components. Table 5 also showed that extract of the rind had the highest potential antioxidant. Water extract of the pulp was higher antioxidant activity than ethanol extract of the pulp due to antioxidant components in the pulp of purple star apple is polar characteristic so these components were more soluble in water than ethanol.

Correlation between antioxidant components and antioxidant activity of purple star apple

Antioxidant components such as phenolics, flavonoids, anthocyanin and vitamin C have antioxidant activity [7]. Correlation between antioxidant components and antioxidant activity is shown in figure 1, 2, 3 and 4. Correlation values (R^2) were 0.9588, 0.3916, 0.6382, and 0.0631 for total phenolics, total flavonoid, total monomeric anthocyanin and vitamin C.

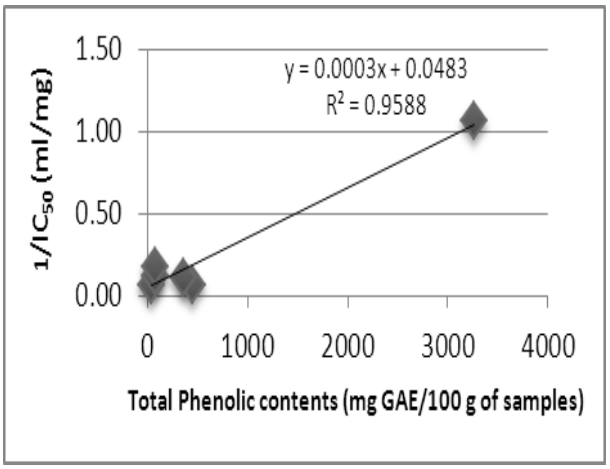

Figure 1. Correlation between total phenolic contents and antioxidant activity

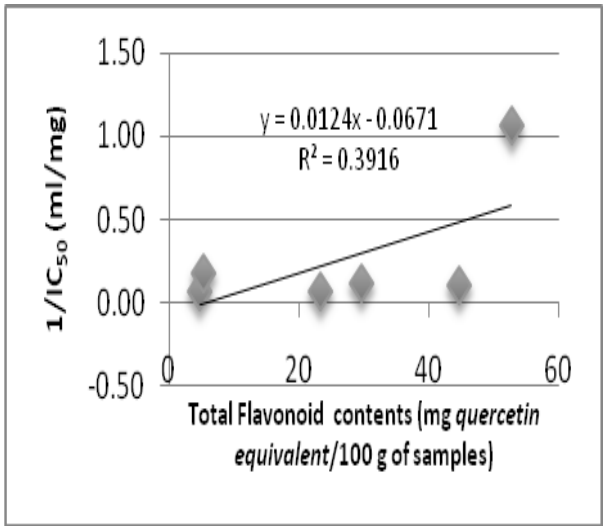

Figure 2. Correlation between total flavonoid contents and antioxidant activity

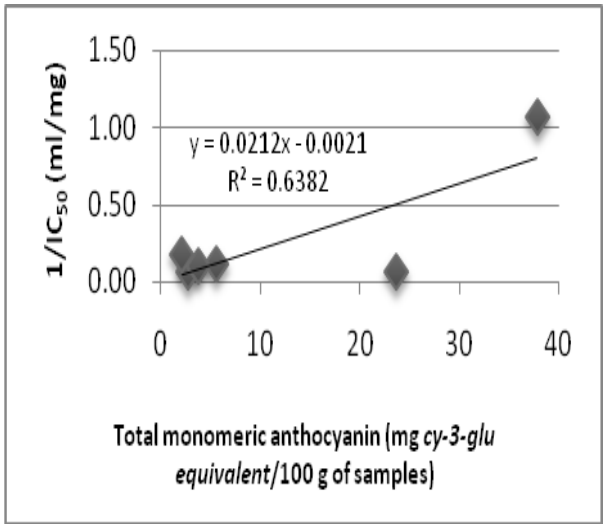

Figure 3. Correlation between total monomeric anthocyanin contents and antioxidant activity

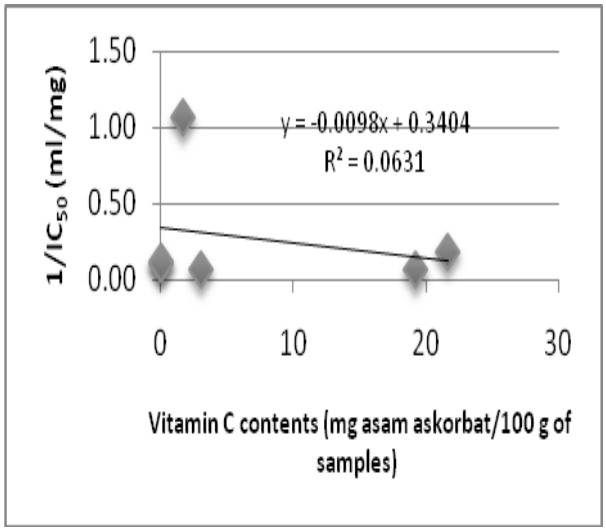

Figure 4. Correlation between vitamin C contents and antioxidant activity

The higher R^2 values indicated that there was positive correlation between antioxidant components and antioxidant activity. These correlations confirm that the phenolic compounds are the main microconstituents contributing to the antioxidant activities of purple star apple.

4. Conclusion

The antioxidant compound contents of ethanol extract for each parts of fruit was higher than its water extract except for the vitamin C content, water extract was higher than ethanol extract. For each part of fruit extract had variative antioxidant compound contents and antioxidant activity. Ethanol extract from the rinds of fruit had the highest total phenolic content, total flavonoid content, total monomeric anthocyanin, and antioxidant activity. Extract from the pulps of fruit had the highest vitamin C contents compared to those of the rinds and seeds of fruit. The phenolic compounds are the main microconstituents contributing to the antioxidant activity of purple star apple.

5. Acknowledgements

---

6. References

[1]. Alothman, M., Rajeev Bhat, and A. A. Karim. (2009), Antioxidant Capacity and Phenolic Content of Selected Tropical Fruits from Malaysia, Extracted with Different Solvents. *Food Chemistry* 115. 785-788.

[2]. Antolovich, Michael, Paul D. Prenzler, Emillios Patsalides, Suzanne McDonald, and Kevin Robards (2002), Methods for Testing Antioxidant Activity. *The Analyst* 127. 183-198.

[3]. AOAC (Association of Official Analytical Chemists) (2005), *Official Methods of Analysis of AOAC International.* 18th Edition. Edited by William Horwitz and George Latimer. Gaithersburg: AOAC International.

[4]. Benherlal, Palayyan Saraswathy, and Chami Arumughan (2007), Chemical Composition and In Vitro Antioxidant Studies on *Syzygium cumini* Fruit. *Journal of the Science of Food and Agriculture* 87. 2560–2569.

[5]. Chang, Chia-Chi, Ming-Hua Yang, Hwei-Mei Wen, and Jiing-Chuan Chern. (2002), Estimation of Total Flavonoid Content in Propolis by Two Complementary Colorimetric Methods. *Journal of Food and Drug Analysis* 10. 178-182.

[6]. Einbond, Linda S., Kurt A. Reynertson, Xiao-Dong Luo, Margaret J. Basile, and Edward J. Kennelly (2004), Anthocyanin Antioxidants from Edible Fruits. *Food Chemistry* 84. 23-28.

[7]. El Gharras, Hasna (2009),. Polyphenols: Food Sources, Properties and Applications-A Review." *International Journal of Food Science and Technology* 44. 2512-2518.

[8]. Giusti, M. Monica, and Ronald E. Wrolstad. "Characterization and Measurement of Anthocyanins by UV-Visible Spectroscopy (2001), In *Current Protocols in Food Analytical Chemistry*, edited by Ronald E. Wrolstad. New York: John Wiley and Sons, Inc.

[9]. Ikram, Emmy Hainida Khairul, *et al.* (2009), Antioxidant Capacity and Total Phenolic Content of Malaysian Underutilized Fruits. *Journal of Food Composition and Analysis*, doi:10.1016/j.jfca.2009.04.001.

[10]. Jaganath, Indu B. (2008), Overview of Health-Promoting Compounds in Fruit and Vegetables. In Improving the Health-Promoting Properties of Fruit and Vegetable

Products, edited by Francisco A. Tomás-Barberán and María Isabel Gil. Cambridge: Woodhead Publishing Limited.

[11]. Kim, Dae-Ok, and Chang Y. Lee (2002), Extraction and Isolation of Polyphenolics. In Current Protocols in Food Analytical Chemistry, edited by Ronald E. Wrolstad. New York: John Wiley and Sons, Inc.

[12]. Luo, Xiao-Dong, Margaret J. Basile, and Edward J. Kennely (2002), Polyphenolic Antioxidant from the Fruits of *Chrysophyllum cainito* L. (Star Apple)." *Journal of Agricultural and Food Chemistry* 50. 1379-1382.

[13]. Morton, J. (1987), Star Apple. In Fruits of Warm Climates, edited by Julia F. Morton, 408–410. Miami: Florida Flair Books.

[14]. Padayatty, Sebastian J., *et al*. (2003), Vitamin C as an Antioxidant: Evaluation of Its Role in Disease Prevention. *Journal of the American College of Nutrition* 22 . 18-35.

[15]. Prior, Ronald L., *et al*. (1998), Antioxidant Capacity As Influenced by Total Phenolic and Anthocyanin Content, Maturity, and Variety of *Vaccinium* Species. *Journal of Agricultural and Food Chemistry* 46. 2686-2693.

[16]. Rodriguez-Saona, Luis E., and Ronald E. Wrolstad (2001), Extraction, Isolation, and Purification of Anthocyanins. In *Current Protocols in Food Analytical Chemistry*, edited by Ronald E. Wrolstad. New York: John Wiley and Sons, Inc.

[17]. Schirmer, Roger E., (1991), Modern Methods of Pharmaceutical Analysis. 2nd Edition. Vol. 2. Boca Raton: CRC Press.

[18]. Waterhouse, Andrew L., (2002), Determination of Total Phenolics. In Current Protocols in Food Analytical Chemistry, edited by Ronald E. Wrolstad. New York: John Wiley and Sons, Inc.

The Influence of Status and The Patterns of Driving License Ownership toward The Gradation of Head Injury Suffered By Motorcycles Accident Patients in Emergency Department of Saiful Anwar General Hospital

Tri Maharani

Student of Biomedical Doctoral Program, Brawijaya University
Email: hanarani_71@yahoo.com

Abstract

Many head injuries occur in a motorcycle accident. Traffic accidents are caused by several factors, human behavior, environment and vehicle type. Knowledge and filtering capabilities of this motorhome can actually be obtained at the time to get driving license in the police. In Indonesia, Driving License is a proof of registration and identification of competencies provided by the police to someone who has met the administrative requirements, physically and mentally healthy, understand traffic rules and unskilled driving a motor vehicle. Traffic accidents take with both loss of life, material or disability. The problems that occur if there is a relationship between driving license ownership with adherence to traffic regulations in Indonesia that has been set law is the use of helmets with the level of severity of patients due to head injury motorcycle accident. Cross sectional observational study to determine the relationship driving license ownership with traffic regulation in patients head injury due to traffic accidents treated in hospital. Statistical analysis by regression and correlation suggest a link between the driving license ownership, the level of compliance with head injuries but was not significant. Driving license ownership is a letter which shows the driving competence of drivers affecting adherence to traffic regulations as well as the incidence of head injury due to traffic accident on motorcycle riders.

Keywords: *Driving license ownership, compliance, head injury*

Isolation of Active Extract of Tengkawang Seed Oil (*Shorea sumatrana* Sym.) as Antibacterial

Valentina Adimurti Kusumaningtyas [1], Ahmad Sulaeman [2], Yusnelti [3], Dewi Meliati Agustini [4]

[1,4] Department of Chemistry, Faculty of Mathematics and Natural Sciences, University of General Achmad Yani, Cimahi, Indonesia (valentina_adimurti@yahoo.com)
[2] Department of Community Nutrition, Faculty of Human Ecology, Bogor Agricultural Institute, Bogor, Indonesia (asulaema@yahoo.com)
[3] Department of Chemistry, Faculty of Mathematics and Natural Sciences, University of Jambi, Jambi, Indonesia (nelti_irsan@rocketmail.com)

Abstract

In this study, the separation of active extracts from Tengkawang seed oil (Shorea sumatrana Sym.) has successfully carried out. The extract was obtained by fractionation of the most toxic fraction of Artemia salina Leach. with LC_{50} 2.55 x 10^{-32} ppm, using Brine Shrimp Lethality Test (BSLT), and is antibacterial against Staphylococcus aureus with the value of Maximum Inhibition Concentration (MIC) is 5%, and 14.41 mm diameter of inhibition with Method Wells Plate.

Keywords: *Shorea sumatrana Sym, A. salina Leach., Staphylococcus aureus.*

1. Introduction

The genus *Shorea* comprises some 150 species trees and is distributed mainly in Asia (Malaysia and Indonesia), this plant in Indonesia is known as Meranti, Merawan or Tengkawang or Damar Mata Kucing, and Keruing. The phytochemistry of this genus has received cosiderable attention, which has resulted in a number of new natural products with intriguing structures as well as useful bio-activities [1]. For instance, we recently reported the extract of methanol from the seed oil of *Shorea sumatrana* Sym., from Jambi, Indonesia, which has been found to be a potent antibacterial.

2. Experimental Details

General Experimental Procedures

In this research consisted of five stages of the experiment including: steaming, pulverization, pressing, extraction and isolation, and antibacterial bioactivity test.

Plant Material

The plant material was collected on 10 October 2010, at Jambi, Indonesia. Herbarium voucer specimens are deposited at the Herbarium Andalas University, Padang, West Sumatera, Indonesia.

Extraction and Isolation

Tengkawang seed oil of *S. sumatrana* (1000 g) were extracted with MeOH to give (21 g) of residue. The methanolic extract (20g) were isolated by vacuum liquid chromatography on Si gel Merck 60 GF_{254} using *n*-hexane with increasing proportions of MTC followed by rechromatography of appropriate partially resolved fractions using vacuum liquid chromatography. Solvent systems used for chromatography was *n*-hexane : MTC (6.5:3.5). The yield of fractionation can be seen in Figure 1and Figure 2.

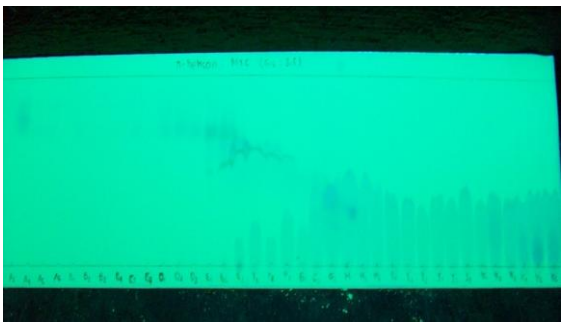

Figure 1. Thin Layer Chromatography of *S. sumatrana*

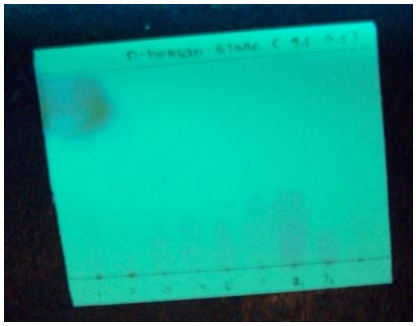

Figure 2. Thin Layer Chromatography Fractions combined of *S. sumatrana*

Antibacterial Assay

Antibacterial bioactivity was done using Wells Plate method. Microorganisms that will be used as the sample are *Staphylococcus aureus* (bacteria representing Positive Gram), *Escherichia coli* (bacteria representing Negative Gram), and *Pseudomonas aeruginosa* (microbes that are not allowed to exist in foodstuffs).

Tests by Wells Plate Method

In this methods, made emulsion Tengkawang seed oil with consentrations: 5%, 10%, 15%, 20%, 25%, and 50%. A 1 mL bacterial suspension was pipette into the petri dish test, added 15 mL NA medium, homogenized and frozen at room temperature (about 30-45 minutes). Media plates which had been perforated by the perforator solid perfect. Into each hole put a price test material concentration (emulsion Tengkawang seed oil) of 50 mL by using micropipette. All the hole in petri dish are filled, pre-incubation at room temperature for 30 minutes, then incubated with the following provisions: 35-37ºC for 24 hours for bacteria *S.aureus*. Observation well, and then measured the diameter of inhibition zone that occurs using the shove. Each zone of inhibition was measured 3 times with different directions and used mean values. Applied activity test by the addition of Tengkawang seed oil into the dough noodles and meatballs, then observations of noodles and meatballs are within a certain time until it changes color, odor and taste as the sign began to decline in food quality. The quantity of antibacterial activity was evaluated by minimum inhibitory concentration (MIC) of % [2].

Brine shrimp lethality test

Dried cysts were performed as indicated above, and incubated (1 g cyst per liter) in a hatcher at 28–30°C with strong aeration, under a continuous light regime. Approximately 12 h after hatching the phototropic nauplii were collected with a pipette from the lighter side and concentrated in a small vial. Ten brine shrimp were transferred to each well using adequate pipette. Each test consisted of exposing groups of 10 Artemia aged 12 h to various concentrations of the toxic compound. The toxicity was determined after 12 h (mainly nauplii in instar I/II), 24 h (nauplii in instar II/III) and 48 h (mainly nauplii in instar III/IV) of exposure.

The numbers of survivors were counted and percentage of deaths was calculated. Larvae were considered dead if they did not exhibit any internal or external movement during several seconds of observation. The larvae did not receive food. To ensure that the mortality observed in the bioassay could be attributed to bioactive compounds and not to starvation; we compared the dead larvae in each treatment to the dead larvae in the control. In any case, hatched brine shrimp nauplii can survive for up to 48 h without food [3] because they still feed on their yolk-sac [4]. However, in cases where control deaths were detected, the percentage of mortality (% M) was calculated as: % M = percentage of survival in the control - percentage of survival in the treatment. The percentage lethality was calculated from the mean survival larvae of extracts treated tubes and control. LC50 values were obtained by best-fit line method.

3. Results and Discussion

In this research, the antibacterial activity test of the Tengkawang seed oil (*S. sumatrana*) was using Wells Plate method. Test method Tengkawang seed oil is a form of wax that is lipophilic and can be easily tested; it needs to be formed into a preparation that is more compatible to the atmosphere of lipophilic and hydrophilic. Emulsion is the most appropriate composition for these preparations formed by the combination of hydrophilic and lipophilic substances by the addition of Tween 80 and Span 80 so as to lower the surface tension. Tengkawang contain derivatives polyphenol compounds showed bioactivity stilben a lot of useful, such as anti-inflammatory, antimitotic, cytotoxic and antibacterial. In Tengkawang seed oil found dimer stilben Diptoindonesin A, together with the already known dimeric (-) ampelopsin A, and Laevifonol, as well as α-viniferin trimer and tetramer hopeaphenol. Stilben a phenol derivative groups which can work as an antibacterial [5,6].

Phenolic compounds can inhibit bacterial growth due to phenol derivatives interaction with bacterial cells through a process involving adsorption of hydrogen bonding. At low levels of phenol will form a protein complex with a weak bond and immediately experienced dissociation,

followed by the penetration of phenol into the cell and cause the precipitation and denaturation of proteins. At high levels of phenol causes coagulation of proteins and cell membranes is experiencing lysis. As with other antibacterial compounds, the mechanism of phenol is inhibited bacterial growth and metabolism by damaging the cytoplasmic membrane and cell proteins denaturation. Thus, these compounds can be role as bactericidal or bakteriostatic, depend on doses used.

In the method of Wells, the antibacterial bioactivity of a substance can be seen from the inhibition diameter sample preparation work on the diffusion of culture medium containing the test microbe. The optimum diameter of inhibition is at the interval 14-16 mm. Thus, *Shorea sumatrana* can be said to have antibacterial activity as the inhibition diameter located within this interval.

Table 1 Experimental Results of Well Testing Methods

Bacteria	MIC (%)	Inhibition Diameter (mm)
S. aureus	5	14.41

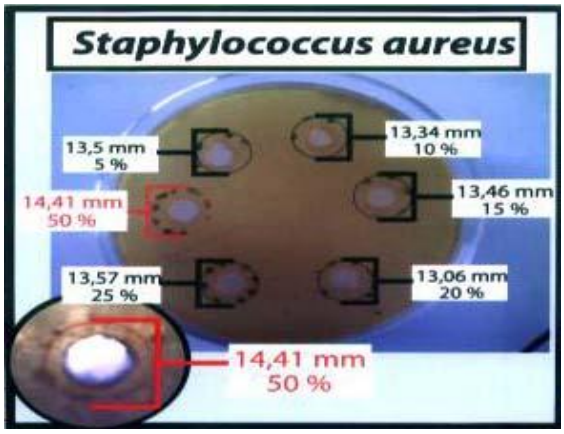

Figure 3. Results of antibacterial test against *S. aureus*

S.aureus bacterial had very clear minimum inhibitory concentration and obtained at rates of 5%. From the separation of active extracts from Tengkawang seed oil (*Shorea sumatrana* Sym.) results obtained by fractionation of the most toxic fraction of *Artemia salina* Leach. with LC_{50} 2.55 x 10^{-32} ppm, using Brine Shrimp Lethality Test (BSLT)

4. Conclusion

From the research that has been done can be concluded that the Tengkawang seed oil has antibacterial activity against S.aureus. It shows good inhibition value with the Minimum Inhibition Concentration (MIC) of (5%) and diameter of inhibition 14.41 mm and also had LC_{50} 2.55 x 10^{-32} ppm as cytotoxicity against A salina *Leach.*

5. Acknowledgments.

We thank Directorate General of Higher Education Ministry of National Education for financial support.

6. References

[1]. Cronquist, A. (1981), An Integrated System of Classification of Flowering Plants, Columbia University Press, New York, 316-318.

[2]. Chang lu, L.; Wen cheng, Y.; and Chunchou, C. (2003), Antibacterial and DPPH Free Radical Scavenging Activities of the Ethanol Extract of Propolis Collected in Taiwan, *J. Food and Drug Analysis*, 2(*4*), 277-282.

[3]. Lewis G.E., (1995), Testing the toxicity of extracts of African plants using brine shrimp (*A. salina*). *S Afr J Sci.*, 91, 382.

[4]. Pelka M, Danzl C, Distler W, Petschelt A., (2000), A new screening test toxicity testing of dental materials. *J Dent,* 28, 341-345.

[5]. Hakim, E.H., (2002), Oligostilbenoid dari Tumbuhan Dipterocarpaceae. *Buletin of The Indonesian Society of Natural Product Chemistry*, 2, 1-19.

[6]. Aminah, N.S., Ahmad, S.A., Hakim, E.H.,Syah, Y.M., Juliawati, L.D dan Ghisalberti, E.L., (2003), Laevifonol, Diptoindonesin A dan Ampelopsin A, Tiga Dimer Stilbenoid dari Kulit Batang *Shorea seminis* V. Sl (Dipterocarpaceae), *Jurnal Matematika dan Sains*, 8 (1), 31 – 34.

The Influence of *Citrus nobilis* Lour Aqueous Fraction on Mice Fertilization Rate by i*n Vitro* Fertilization Method

Widjiati [1], Raden Roro Wulan Oktavia Aryaguna Putri [2], Diah Kusumawati [3]

[1,2] Department of Veterinary Anatomy, Faculty of Veterinary Medicine, Airlangga University, Surabaya, Indonesia (widjiati@yahoo.com)
[3]Animal Teaching Hospital, Faculty of Veterinary Medicine, Airlangga University, Surabaya, Indonesia

Abstract

Hesperidin, limonene, citral, and methyl antranilate are the components of Citrus nobilis Lour rinds. Based on the previous researches, Citrus nobilis Lour aqueous fraction contains anti-fertility component. This component has inhibitory effect of hyaluronidase enzyme produced by the acrosomal cap of spermatozoa. In this study, Citrus nobilis Lour aqueous fraction was administered orally at doses of 40 mg/kg bw; 60 mg/kg bw and 80mg/kg bw daily to the male mice for one spermatogenesis cycle (35 days). The effect of Citrus nobilis Lour aqueous fraction on fertilization rate was observed by IVF (In Vitro Fertilization) method after 24-hour incubation. The fertilization happened when the ovum transformed into zygote, and if the fertilization did not happen, this transformation would not occured and the granulose cells layer will remain intact. The result from IVF method after 24-hour incubation showed that granulose cells layer were still intact and the ovum were not transformed into zygote. Conclusion: the Citrus nobilis Lour aqueous fraction at doses of 40 mg/kg BW; 60 mg/kg BW and 80 mg/kg BW could decrease fertilization rate by IVF method with percentage of 58, 25, and 0%, respectively. It means that Citrus nobilis Lour could also inhibit the penetration of mice spermatozoa. But only the highest dose (80 mg/kg BW) could show the absolute result or 100% ova remained intact.

***Keywords**: Citrus nobilis Lour, hesperidin, in vitro fertilization, fertilization rate*

1. Introduction

The involvement of contraception in male animals refers to the development of research on male contraception and family planning program for male in human at this time. In the world of veterinary medicine, the use of contraception in animals is more often intended to make the animals become sterile. Sterilization of pets such as dogs and cats are intended to control the animal population growth in an environment [1].

One of the plants commonly found in Indonesia is the citrus crop. Citrus species which is widely cultivated and commonly consumed in Indonesia is the *Citrus nobilis* Lour or tangerine [2]. According to Li (2002) as quoted by Setiawan (2006), the high rates of consumption of tangerine or *Citrus nobilis* Lour in Indonesia bring about wastes that are not used in the form of fruit rinds [3]. The citrus rinds are increasingly accumulated and disposed in vain because they are not useful. In fact, *Citrus nobilis* Lour rind contains various components, namely vitamin A, vitamin B, vitamin C, hesperidin, limonene, citral, and methyl antranilate. Hesperidin represents a flavonoid glycoside and polyphenol compound, which is an inhibitor of hyaluronidase [4].

To reach the ovum nucleus in fertilization the sperm cells must be able to penetrate several layers such as *cumulus oophorus*; *zone pellucida*, and *vitellin membrane* [5]. Hyaluronidase enzyme found in acrosomal cap of spermatozoa has a function to penetrate the cumulus oophorus and acrosin enzyme penetrates the zone pellucida. Each of these enzymes works individually; they must be specific and sequential [6].

From some previous studies we still do not know whether administration of aqueous fraction of *Citrus nobilis* Lour rind can reduce the rate of fertilization *in vitro*. Study by Setiawan (2006) investigates a function of penetration with a five-hour incubation period [3] in which this study does not determine definitely whether fertilization will not happen after such incubation period because the fertilization age of ovum and sperm cells according Partodihardjo (1992) and Ismudiono et al. (2007) is approximately 12-24 hours [5,6]. Thus, there is still the possibility of sperm cells to penetrate the cumulus oophorus after five-hour incubation.

Based on the above background it is necessary to do further research to investigate the effect of *Citrus nobilis* Lour aqueous fraction exposure on fertilization rate of mice in *in vitro* fertilization with 24-hour incubation period.

2. Experimental Details

Preparation of Citrus nobilis Lour Aqueous Fraction

Citrus nobilis Lour rinds were dried in the sunlight to dry then crushed using a blender until it becomes powder. The powder was soaked with distilled water and then filtered with flannel cloth repeatedly to obtain a clear filtrate. Afterwards the residues were added with distilled water 1.5 times the weight of residues, and wetted using NaOH 2N solution until pH of 11 - 11.5 was reached and allowed to stand at room temperature for one hour. Residue bath was filtered using a flannel cloth. The filtrates were acidified with HCl 2N to reach pH 4.2 - 4.5 and then put into the oven at a temperature between 40-45ºC for 12-24 hours. Aqueous fraction obtained in this stage took the solid form that must be dissolved first into solution before administered to the experimental animals. Solution was prepared by weighing the aqueous fraction of *Citrus nobilis* Lour according to the dosage required and then crushed to fine particles using hammer and add distilled water [3].

Treatment of Experimental Animals

Experimental animals treated in this experiment were only male mice that have been previously divided into four groups as follows:

P0: 10 male mice in this group would serve as control. They were only treated with distilled water.

P1: 10 male mice were treated with *Citrus nobilis* Lour aqueous fraction per oral with dose of 40 mg/kg bw.

P2: 10 male mice were treated with *Citrus nobilis* Lour aqueous fraction per oral with dose of 60 mg/kg bw.

P3: 10 male mice were treated orally with *Citrus nobilis* Lour aqueous fraction with dose of 80 mg/kg bw.

Citrus nobilis Lour aqueous fraction was administered orally using *gavage tube* during one spermatogenesis cycle (35 days). Every day the animals were gavaged once time with 1 ml/mouse. On day 36 all of the male mice were dissected to obtain their sperms in caudal epididymis, which will then be used for *in vitro* fertilization (IVF).

Collection of Ova (Egg Cells)

Female mice were superovulated first to collect the ova. Mice were subcutaneously injected with *Pregnant Mare Serum hormone Gonodotropin* (PMSG) hormone at dose of 5 IU. By 48 hours later, the mice were subcutaneously injected with the human chorionic gonadotropin (hCG) hormone at a dose of 5 IU and then immediately mated with male mice that have been castrated by monogamy way. After 17 hours later, the female mice were dissected and their fallopian tubes were removed. Fallopian tubes were washed with Phosphate Buffer Saline solution, then transferred to petridish and flushed under *inverted microscope* by tearing the fertilization sacs [7].

Observation of Fertilization Rate with In Vitro Fertilization Method

Ova harvested were washed in PBS media three times and then proceed with M16 media three times. The washed egg cells were then transferred to fertilization medium of M16 culture medium. Spermatozoa were collected from caudal epididymis of the male mice that have been treated orally with *Citrus nobilis* Lour aqueous fraction, and then put into the fertilization media. Egg cells mixed with spermatozoa were incubated within CO_2 5% incubator at 37ºC for 24 hours. Fertilization rate was observed by viewing a formation of zygotes using inverted microscope.

3. Results and Discussion

Results of Citrus nobilis Lour Aqueous Fraction Preparation

The research used *Citrus nobilis* Lour rinds that are dried and blended to fine powder. Aqueous fraction prepared from 600 g powder of the fruit rinds produces dry extract of 40 gram.

Observation Results of Fertilization Rate In Vitro Fertilization Method

After the drop medium was incubated for 24 hours and examined under an inverted microscope, many egg cells were fertilized into zygotes and some egg cells remain intact. In the control group (P0) treated with distilled water only, all egg cells have been fertilized and developed to zygotes (100%) while in the test group, P1 dose of 40 mg/kg bw; P2 60 mg / kg; P3 80 mg/kg, the percentages of the fertilized egg cells are 58, 25 and 0%, respectively. In the group P3 administered with *Citrus nobilis* Lour aqueous fraction at the highest dose of 80 mg/kg, all egg cells remained intact or not fertilized. This suggests that sperm cell cannot fertilize an egg cell because of the decreased activity of the enzyme hyaluronidase as a consequence of administration of the aqueous fraction. In the test

group the doses of 40 and 60 mg/kg bw still allow egg cell fertilization as the aqueous fraction cannot reduce the activity of hyluronidase enzyme totally.

Table 1. Percentage of zygotes formed after fertilization *in vitro*

Treatment	Number of Mice♂ (as source of spermatozoa)	Number of egg cells fertilized	Percentage of zygotes formed
P0	6	42	(42) 100%
P1	6	95	(55) 58%
P2	6	131	(34) 25%
P3	6	18	(0) 0%

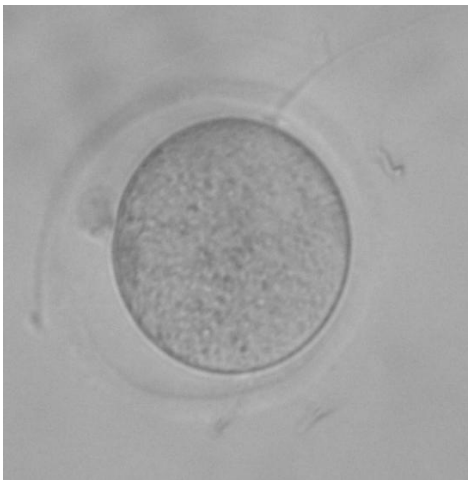

Figure 1. Egg cells fertilized and developed to zygotes

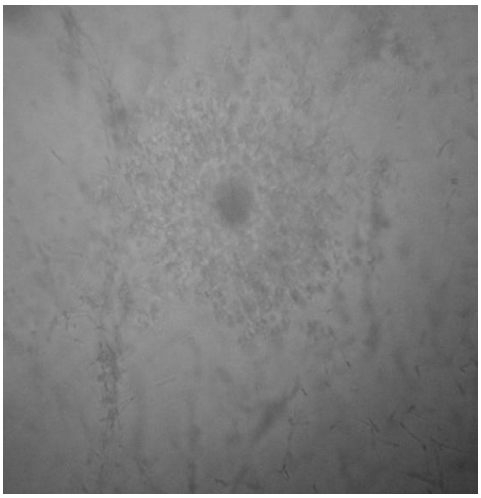

Figure 2. Egg cells remained intact or not fertilized (magnification 100x)

Microscopic examination after 24-hour incubation in the control group showed that all egg cells were fertilized and developed to zygotes. However, at the highest dose in the test groups, all egg cells remained intact or not fertilized.

4. Conclusion

From results of the current research, we can conclude that exposure to *Citrus nobilis* Lour aqueous fraction administered orally at a dose of 80 mg/kg in male mice can reduce the fertilization rate in *in vitro* fertilization process.

5. Acknowledgments

---

6. References

[1]. Amanda, R. (2009), Kontrol Populasi Pada Anjing. http://vet02ugm.wordpress.com/ [1 September 2009].
[2]. Ashari, S. (1995), Hortikultura Aspek Budidaya. UI-Press. Jakarta. Hal. 310-312.
[3]. Setiawan D.A. (2006), Efek Fraksi Air Kulit Buah *Citrus nobilis* Lour Terhadap Fungsi Penetrasi Spermatozoa Mencit Dengan Metode Fertilisasi *In Vitro*. Minor Thesis. Fakulty of Pharmacy, University of Airlangga.
[4]. Prajogo, B.E.W., Widjiati, Hamdani and Aucky, H. (1997), Hambatan Hesperidin Terhadap Penetrasi Spermatozoa Mencit Dalam Proses Fertilisasi *In Vitro*, Simposium Penelitian Bahan Obat Alami IX, Yogyakarta.
[5]. Partodihardjo, S. (1992), Ilmu Reproduksi Ternak. Fakultas Kedokteran Hewan. Jurusan Reproduksi. Institut Pertanian Bogor. Mutiara Sumber Widya. Jakarta. Pg. 202-223.
[6]. Ismudiono, H. Anwar, P. Srianto, S. P. Madyawati, A. Samik and E. Safitri (2007), Fisiologi Reproduksi Pada Ternak. Surabaya. Pg. 79-82.
[7]. Widjiati**,** M. Mafruchati, B. Purnomo, E. Luqman, H.A. Hermadi (2002), Penggunaan sel-sel granulosa pada kultur *in vitro* embrio mencit tahap satu sel. *Media Kedokteran Hewan*. Vol. 14 No. 1. Pg. 1 – 7.

Acoustic Performance Study of Human Hearing System Due To Noise Potential Damages

Wike Herawaty [1], Nurida Finahari [2]

(1) Student of Biomedic Doctoral Program of Brawijaya University, Malang, Indonesia
(drg_wike@yahoo.co.id)
(2) Student of Medical Eng. Doctoral Program of Brawijaya Univ., Malang, Indonesia
(nfinahari@yahoo.com)

Abstract

Negative impact of sound is the medical consequences that will be faced when the loudness level increases. This article explores medical consequences and prevention mechanism that is done by human hearing system. The results will be used as basic consideration on the design of sound based complementary and alternative medicine (CAM) or treatment. This research was conducted by literatures (journals and handbook) study on the field of human physioanatomy and sound mechanics. It also shows the multidisciplinary application of basic science (physics), engineering and medical that fit with theme of the seminar. The results show that negative impact of sound include hearing loss, high blood pressure, ischemic heart disease, discomfort, premature ejaculation, difficulty moving, sleep disturbances, decreased sexual function and even death. Changes in the immune system and birth defects are said to include but the evidence does not exist yet or not significant. The human auditory system has been structured in such a way so as to select the sounds received, mainly in the form of frequency selection, called the band pass filter. This mechanism is carried by cochlea in the form of dynamic interaction between basilar membrane, inner hair cells and auditory nerve cells. Performance of these organs determines the type of signal to be transmitted to the brain nerve cells. These signals will then form perceptions about sound characteristics. The selection process can be shifted to follow environmental conditions. This shift requires time for adjustment. The auditory system failures to adapt will result in the negative impacts emergence above.

Keywords: *noise, cochlea, band pass filter, the sound characteristic, the perception of sound.*

1. Introduction

The main purpose of the human auditory system is as a burglar alarm and warning [1]. The sound has a direct impact on human emotions and actions. From a psychological view as well as pathological, the sound can bring negative impact. In general, the sound that brings a negative impact on human health referred noise. Noise is unwanted sound that raise from some kinds activity within a certain time level and that may cause human health and environment discomfort [2] or any unwanted sound that comes from the means of production processes and/or work tools at certain levels that can cause hearing loss [3].

From the review of the mechanics of sound, noise is a physical quantity obtained from the superposition of the movement of some sound wave vibration, unperiodical with varying frequency. These types of noise appear in most social and environmental activities, resulting in unpleasant sensations provocation on listeners [4]. This sound is a source of danger if its intensity has exceeded 80 dB depending on the duration and systematic presentation. Noise that results in loss of hearing has the following characteristics: always be neurosensorial as a result of lesions affecting the cochlear hair cells, irreversible and bilateral (affect both of ears). At the beginning, hearing loss occurs in areas of 6.4 or 3 kHz which continues progressively in the area of 8.2 and 1 kHz and 250 Hz [5]. Noise can also cause trauma to the ear. This is called acoustic trauma. Acoustic trauma mechanism involves mechanical damage, ischemia, excitotoxin damage, metabolic exhaustion and ionic imbalance [6]. Acoustic trauma can cause temporary and permanent hearing threshold shift. Temporary threshold shift can be cured again [7].

Noise not only come from the environment or working equipment, medical devices used to aid diagnosis and therapy tool can also generate noise. In this case the patients and medical personnels who operate it are objected of high risk for negative consequences. One example is MRI (magnetic resonance imaging). The sound generated at the time of producing MRI images,

beside disrupt the communication process between patients and medical personnel, also affect their physiological condition. The bad effects can be temporary hearing threshold shift, discomfort, anxiety, mental fatigue and fear, even permanent hearing loss [8]. Under the provisions of the FDA (Food and Drug Administration / USA), MRI noise threshold is set at 90 dBA (for boosted sound) for exposure of 8 hours per day, where both patients and medical personnel who operate them must use hearing protective devices [9].

This article explores medical consequences and prevention mechanism that is done by human hearing system. The purpose of this study is to get references about human hearing response mechanism due to sound exposure. This information will be used as basic consideration on the design of sound based complementary and alternative medicine (CAM) or treatment, e.g. musical based CAM.

2. Experimental Detail

This article was conducted by literatures study on the field of human physioanatomy and sound mechanics. Journals and handbook are choosen as primary resources and it is attempted to use ones under 10 years old publication, as far as possibles. However, it is not avoidable that some basic information only be found in older publication.

3. Results and Discussion

Effects of noise on health are the medical consequences that must be faced when the loudness level of sound increases. Medical consequences include hearing loss, high blood pressure, ischemic heart disease, discomfort, premature ejaculation, difficulty moving, sleep disturbances, decreased sexual function and even death. Changes in the immune system and birth defects are said to include but the evidence does not yet exist, or not significant [10]. In brief some of the medical consequences of sound exposure can be explained as follows.

Mechanism of Hearing Loss

The mechanism of hearing loss due to noise exposure comes from the trauma that occurs in stereosilia cochlear organ. Stereosilia expose noise can induce apoptosis and necrosis of hair cells [11] so that it triggers an increase in reactive oxygen species (ROS, reactive oxygen species). Increasing ROS in the cochlea would induce inflammation that leads to organ damage.

Age Effect

Young people are more able to deal with noise exposure without losing his hearing ability when compared with the older one. Age consumpt the ability and the loss process done rapidly if noise exposure does not handled sooner. However, the women do not experience these differences. At the same age their ability to deal with noise better than the opposite sex.

Effect on Cardiovascular System

It has been proven that noise exposure increases the risk of high blood pressure attack. The ascension of blood pressure is caused by vasoconstriction of blood vessel during and post-exposure. Vasoconstriction in blood vessels occurs due to the increment on production and releasing adrenal hormones. Another mechanism is believed occur through the psychological stress pathway. Noise exposure that reaches 50 dB if heard at night may increase the risk of myocardial infarction due to increment production of the hormone cortisol. Noise exposure also resulted in the raising of headache frequency, fatigue, abdominal injuries and vertigo.

Congenital Defects

Noise exposure is also associated with the incidence of congenital defects in infant which often appears in the form of lip and spinal nerves defects. These congenital defects allegedly caused by the mother who was pregnant with impaired blood flow during noise exposure. This decreases the supply of food and oxygen to the fetus thereby inhibiting growth. Another effect that possibly occurs on the fetus is the ability to respond the sounds that came down to the uterus. This might be happens if the pregnancy had reached 15 - 60 days. Decrease in maternal hormone levels due to noise exposure is also considered as another cause.

The selection process of the sound that enters the human auditory system is carried out by the basilar membrane, hair cells and nerve fibers [12] in the inner ear (cochlea). These components form combination action to determine the frequencies that will be responded. The mechanism of that action is still unclear. However, the results of that action are known as form of boundary lines series of the filter frequency (bandpass filters) called critical limits bands. The selection process in the human auditory system occurs because of the limitation of human hearing anatomy. Those limitations include:

a. Limitation of high frequency

Technically, the listening area of human auditory system has limitations, which is associate with physical hearing limitation criteria and feelings limitation. That is, the voices on the area boundary have a characteristic frequency and pressure as the softest sounds that can be received by the auditory system. Increasing frequency and/or pressure will increase the sense of tickle in the ear. If the sound that expose the ears reach or cross the line feeling, the ear will be sore.

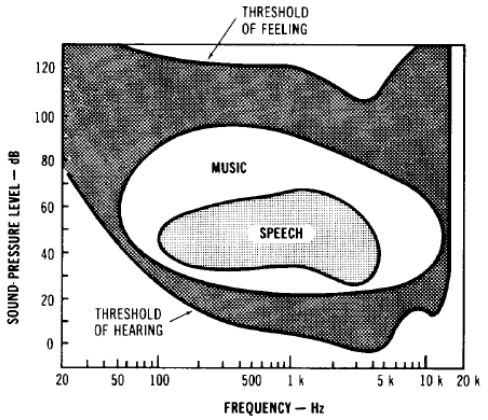

Figure 1. The boundaries of human hearing area [12]

b. Voice loudness

Loudness level is based on 1 kHz sound frequency. Analysis of auditory contour curve presents the fact that the ear is much reduced sensitivity to frequencies below 1 Hz. At high frequency, response of the ear shows the characteristics that tend to flat or the same.

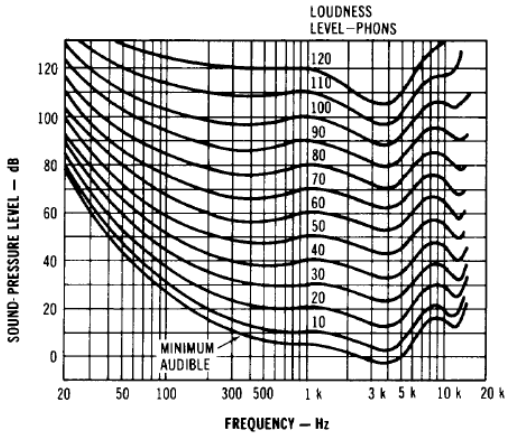

Figure 2. The loudness contour [12]

c. Ambiguity between pitch and frequency

Pitch is a subjective sensation to explain the perception of a high and low voice. So far, high and low sounds are always expressed as a frequency. Pitch differs with frequency because the frequency is a physical quantity that measured objectively.

d. Confusion of timbre and spectrum definition

Spectrum is a visualization of the sound wave bands obtained from instrument based analyzing. Visualization was obtained by comparison with a predetermined constant reference first. On the other hand, the timbre (the sound color) is affected by perception, listener position and environment of the sound source, a lot. Timbre is often expressed subjectively as smooth, rough, clear and so forth. Connecting the timbre with the spectra is not easily done because the variables that affect pretty much, making the difficulty of setting the level of consistency. So far the timbre is characterized by standard characteristics of objective illustration such as amplitude, frequency and intensity. Later contour graph of the spectrum is also used as a means of marking the character of timbre.

e. Delay time reception

A pair of human ears anatomically located on different sides of the head. The distance between them average on 8-9 inches. This position differences cause of delay time of same sound wave reception at each ear. The delay time will vary for each individual in a particular situation. Normally the lag time is valued at 10-300 μs. Delay time acceptance affect the sound characteristics that are processed in each ear. The amplitude and wave spectrum from the same source will be received differently in each ear. This difference information is the basis of brain analysis to determine the location of the sound source. The analysis process occurs automatically without the need to realize.

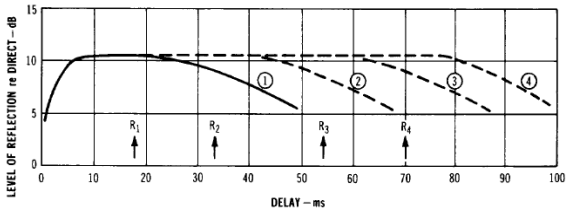

Figure 3. Fusion zone shifting due wave sound reflection when hit auricle [12]

Sound source direction determination has been widely studied to arrive at the question of whether it takes 2 pieces of ears for it? At the beginning it is known that the contour of the grooved surface of the ear leaf has an important role in the manipulation of the wave. Ear contour cause a wave reflection, so that the same wave

will be received in the form of wave fractions. There is a fraction that enter directly into the auditory canal, some are first bounced in the ear leaf and then enter into the hearing canal. Loss of ear contour for various reasons could eliminate the ability of humans to determine the sound source location. Determining the location of sound sources will be accurate if the two sides of ear function properly. However, this is more due to the habit. Determining the location of the sound source by using one ear may be done through habituation.

Delay time in the number of micro seconds is useful in determining the location of the sound source. Different conditions will arise if the delay time interval reaches miliseconds. Response formed by the arrival of the first sound wave becomes the standard reference. Delays in the arrival of the next reflection waves that reached milliseconds from the same source will be ignored. Subsequent reflection waves will only respond if the loudness reaches at least 10 dB higher than the first wave. Wave reflections are only considered as an echo. This effect is called locking effect (clamping effect) or better known as the Haas effect.

Limitations of the human auditory system are a proof of the existence of non-linearity function. Sound that hear by ears not always come from external sources. At the moment when 2 sound with different characteristics expose the auditory system, it would appear sound integration (interference), which follow the auditory response processes. This combination sound, although generally not audible but affect the process of sound propagation in the auditory system.

An effect that appear from interference sound is the emergence of the monoaural phase effect phenomenon, which seems to be evidence that the human auditory system is insensitive to the phase difference, though it is not. Sensitivity to the phase difference allows the phase distortion that can change the sound of conversation becomes noisy. It seemed obvious to someone who is near a lot of people who talk together, for example in the market, the mall or just a crowd of several people. Non-linearity of the auditory system also applies to low intensity. Non-linearity sources are not certain but believed to relate to metabolic processes. When the blood flow to the ear is interrupted, the non-linearity effect will change.

The system consists of 3 bones in the middle ear cavity build a reflex against loud noise that exposes the ear drum. Protective reflex occurs when the anvil and stirrup fastener muscles lower ossicular response level to the voice. This action caused the suitability of the impedance between the outer and inner ear, so avoid the damage.

The importance of balance impedance between the outer and inner ear can be understood when referring to the concept of impedance. The very high pressure sound waves that are not balanced by decreasing the rate reaction of medium particles will cause an increase in impedance values extremely. If related to the fact that the impedance value is directly related to density and speed of sound wave propagation, the extreme incremental of impedance values in the same medium, lead to the raising of wave sound speed propagation extremely in areas that will be passed. This chain effects if applied to the human auditory system which contains components with a very big differences will end in a fatal error that leads to membrane perforation.

On the other hand, as an illustration, the failure of the ossicular middle ear mechanism function can reduce the ability of sound wave propagation up to 0.1%. This happens due to medium differences that passed by sound waves in the outer ear area (the air majority) and the inner ear (the liquid majority). Differences of medium characteristics, which supported by organs size differences, are causing high loss of energy.

Propagation analysis n the inner ear focused on the vibration of basilar fibers. Sound resonance that occurs in basilar fibers showed free vibration behavior, where the basilar fibers can be modeled as a reed. Reed only vibrate at certain frequencies so that the unique basilar fibers dimension values, it can be determined the characteristic frequency of the basilar fibers transmitted sound.

Referring to the characteristic frequency of free vibration reed which is only affected by the mass and stiffness constant, basilar fibers vary in length. Near the stapes, basilar fiber length is only 0:04 mm. The farther from the stapes, the longer the basilar fibers until it reach 0.5 mm. In line with the increase in length, stiffness basilar fibers decreased to 100 times than fibers near the stapes. This affects fibers stiffness to mass ratio, which in turn affects the frequency of resonant voice.

Sound frequencies that resonate in basilar fibers determine the depth of the achievement of propagation in the cochlea. High frequency waves are absorbed faster by stiff short fibers near the stapes while the low frequency waves can travel further, so absorbed by the length fibers. Sound frequency is closely related to the brain's perception about acoustic wave‘s characteristics.

High-frequency waves cause the perception of high voice ranges (pitch/tone), and vice versa for low-frequency waves.

Basilar fibers also allow the detection of loudness. High amplitude sound waves cause high vibrations. Neuronal response becomes faster so that the brain detects it as a loud voice. Conversely, low amplitude wave will eventually be detected as a weak voice.

The mechanism of the auditory system that works in the inner ear also has the ability to select input frequency range. Sound wave frequencies are not entirely that reach the inner ear will responded and forwarded in the form of electrical signals to the brain. The selection process involves metabolic activity. The ability of sound selecting fades a few minutes after the metabolic process stalled. There are many methods of selection are performed by the auditory system of the middle ear.

4. Conclusion

Potential of the auditory system organ damage due to noise covers a broad area of health. This potencies raise from the human auditory system limitation, eventhough some limitation have special usage in completing the performances. In this case sound frequency is the characteristic that is used to measure the performance of auditory system defense. The first defense performed by middle ear organs which maintain the stability of impedance medium. The next defense shaped by the basilar fibers frequency selection in the cochlea. The selection process occurs because of basilar fibres length and stiffness differences, which affects the ability of sound waves absorption waves.

5. Acknowledgement

-----

6. References

[1]. Westman J.C. and Walters J.R. (1981), Noise and Stress: A comprehensive approach, *Environmental Health Perspectives,* **41,** 291-309

[2]. SK Menteri Lingkungan Hidup RI No.48 Tahun 1996

[3]. SK Menteri Tenaga Kerja RI No.51 Tahun 1999

[4]. De Almeida S.I.C., Albernaz P.L.M., Zaia P.A., Xavier O.G., Karazawa E.H.I. (2000), História natural da perda auditiva ocupacional provocada por ruído. *Rev Ass Med Brasil*, **46**, 143-58

[5]. Guida H.L., Morini R.G., Cardoso A.C.V. (2009), Audiologic and Otoacoustic Emission Evaluation in Individuals Exposed to Noise and Plaguecides, *Intl. Arch. Otorhinolaryngol*, **13(3)**, 264-269

[6]. Borg E., Canlon B., Engstrom B. (1995), Noise-induced hearing loss. Literature review and experiments in rabbits. Morphological and electrophysiological features, exposure parameters and temporal factors, variability and interactions. *Scand. Audiol., Suppl*., **40,** 1–147

[7]. Halsey K., Fegelman K., Raphael Y., Grosh K., Dolan D.F. (2005), Long-Term Effects of Acoustic Trauma on Electrically Evoked Otoacoustic Emission, *JARO*, **6,** 324–340

[8]. McJury M. and Shellock F. (2000), Auditory noise associated with MR procedures: A review, *Journal of Magnetic Resonance Imaging*, **12**, 37–45

[9]. Li M., Lim T.C., Lee J.H. (2008), Simulation Study on Active Noise Control for a 4 Tesla MRI Scanner, *Magn Reson Imaging*., **26(3),** 393–400

[10]. Passchier-Vermeer W., Passchier W.F. (2000), Noise exposure and public health, *Environ Health Perspect,* **108** (Suppl 1), 123–31

[11]. Henderson, D., Bielefeld, E.C., Harris, K.C., Hu, B.H. (2006), The role of oxidative stress in noise-induced hearing loss. *Ear Hear.,* **27**(1), 1-19.

[12]. Everest F.A. (1987), *Fundamentals of sound*, in Handbook for Sound Engineers: The new audio cyclopedia, 3rd edition, Howards W. Sams & Co, Indiana, USA.

Isolation and Characterization of A Gene Involved in DNA Repair of the Extremely Radioresistant Bacterium *Deinococcus Radiodurans*

Zubaidah Alatas

Center for Technology of Radiation Safety and Metrology, National Nuclear Energy Agency (BATAN), Jakarta, Indonesia (zalatas@batan.go.id).

Abstract

Deinococcus radiodurans was discovered in meat cannery and known as a bacterium that possesses extraordinary ability to withstand the lethal and mutagenic effects of DNA damaging agents especially ionizing radiation. D. radiodurans is attributed by its efficient capacity to repair DNA damages. In order to identify the gene responsible for DNA repair, a mutation site in the gene of the DNA damage repair deficient-mutant strain KH3111 of Deinococcus radiodurans was investigated. DNA damage resistance was restored in KH3111 by transforming with DNA of a cosmid clone pDC144 from the genomic DNA library of D. radiodurans KH8301. The cosmid clone was digested with different restriction enzymes. The generated DNA fragments were separated using agarose gel electrophoresis, cloned and transformed into host cells, Escherichia coli JM109. The high transformation efficiency of KH3111 with DNAs of pDC144 derivates indicates that the mutant is proficient in natural transformation competence, suggesting that recombination repair is undefective in the mutant. Gene affected by a mutation in the mutant was identified and its nucleotide sequence was determined. A complete open reading frame (ORF) which encompassed the KH3111 mutation region was found and designated orf144b that consists of 284 amino acids. The KH3111 mutation site was identified by sequencing DNA fragments amplified from genomic DNA of the mutant. G at nucleotide position 1384 was altered to A in the sequence of orf144b in the mutant and causes the substitution of Gly for Glu at amino acid position 149. It seems that the Gly substituted by this mutation would be one of the critical roles involved in DNA repair. The results demonstrate that the characteristic sensitive phenotype of KH3111 can be accounted for by the point mutation in unique radiation-inducible gene. Therefore, the orf144b gene in a 2.9-kb SalI-BlnI fragment from pDC144 would be one of the responsible genes for the radioresistance of Deinoccocus radiodurans.

Keywords*: Deinococcus radiodurans, radioresistance, and DNA repair*.

1. Introduction

Among the many characteristics of *Deinococcus radiodurans*, a few of the most noteworthy include an extreme resistance to extreme environments such as genotoxic chemicals, oxidative damage, high levels of ionizing and ultraviolet radiation. It is known that heat, dehydration and radiation causes double-strand breaks in chromosomal DNA, a hallmark of radiation damage. *Deinococcus radiodurans* is characterized by its unusual capability to repair damaged chromosomes DNA induced by mitomycin C (MC), ultraviolet (UV), and ionizing radiation [1-3]. *D. radiodurans* is best known for its ability to survive extremely high doses of 10,000 Gy of acute ionizing radiation that causes about 100 double strand breaks per chromosome which can be mended without lethality and mutagenesis. For comparison, 5 Gy is lethal to average human, and 2,000 Gy can sterilize a culture of *Escherichia coli* [4].

D. radiodurans designated strain R_1 was first isolated form gamma-irradiated meat in 1956. This obligate aerobic bacterium is red-pigmented, gram positive, non-sporing, non pathogenic and grows as tetracocci in the late stages of growth. The bacterium contains four chromosomes per cell during stationary phase and about ten chromosomes during exponential phase [5]. Numerous DNA repair deficient mutants of *D. radiodurans* have been isolated [6-8] and were used as materials for studying the mechanism of radioresistance of the bacterium. Three genes involved in DNA repair that have been identified and sequenced are *recA* as a gene encoding RecA which is functioning in homologous recombination and DNA damage repair [4,9], *uvrA* as a gene encoding UvrA which is involved in nucleotide

excision repair [10], and *polA* as a gene encoding DNA polymerase [11]. These genes ubiquitously distribute among bacteria and posses functions essential for DNA repair as well investigated, especially in *Escherichia coli* [12]. Since the predicted amino acid sequences of these genes do not differ greatly from their *E.coli* counterparts [3], the extraordinary radiation resistance of *D. radiodurans* cannot fully be accounted for by the functions of the genes.

A DNA repair deficient mutant *D. radiodurans* KH311 is sensitive to DNA-damaging agents including UV light, gamma radiation, MC, and 8-trimethylpsoralen [13]. However, characterization of the mutant has not enough been accomplished and remained to be analyzed. *D. radiodurans* strain KD8301 which maintains DNA damage resistance as does the wild-type, has been used in construction of cosmid and λ libraries for studies on the DNA repair mechanisms of *D. radiodurans* [13-14]. A cosmid library of *D. radiodurans* KD8301 was constructed by Kitayama and Matsuyama [7] to facilitate biochemical and genetic experiments by transforming a DNase-deficient and adenine auxotroph of strain KR_1 with DNA from a streptomycin-resistant strain of KR_1.

This paper reports the isolation and sequence of a novel *D. radiodurans* gene involved in DNA repair. After screening and analyzing a clone from the library with a mutant KH3111, a streptomycin resistant derivate of KH311, a novel *D. radiodurans* gene was found out. The KH3111 mutation site is thought to be responsible for a functional defect of the gene product. This paper shows that the resistance of KH3111 can fully be restored via transformation with DNA containing a part of the gene of KD8301. By understanding the gene responsible for a highly proficient DNA repair capacity on DNA damage induced by ionizing radiation, we could apply this knowledge for clues to why human tumors become resistant to radiation therapy. The information on the functional mechanisms of radioresistance may increase therapeutic ratio of cancer treatment in humans.

2. Experimental Details

Bacterial strains, cosmids, plasmids, and growth conditions

D. radiodurans strain KD8301, a streptomycin-resistant, DNase-defective and adenine requirement derivate of KR_1 [10], was used for the experiments. Bacterial strains, cosmids and plasmids used and constructed in this study are listed in Table 1. *D. radiodurans* was grown in TGY broth contained 0.5% Bacto Tryptone, 0.1% glucose, and 0.3% Bacto Yeast Extract or on TGY plates supplemented with 1.5% Bacto-agar at 30ºC, 2 µg of streptomycin per ml was supplemented if necessary. *Escherichia coli* JM109 used for the *D. radiodurans* plasmid construction was grown in Luria-Berini (LB)-Miller medium (1% Bacto-tryptone, 0.5% Bacto-yeast extract, and 1% NaCl) or on LB-Lenox plates (1% Bacto-tryptone, 0.5% Bacto-yeast extract, and 0.5% NaCl) supplemented with 1.5% Bacto-agar at 37ºC. If necessary, 50 µg of ampicillin per ml and 50 µg of kanamycin per ml were supplemented. A cosmid library was constructed by Narumi et al [10] using the cosmid vector SuperCos 1.

Transformation and DNA manipulations

E.coli JM109 was transformed by electroporation using Gene Pulser according to the manufacturer's instructions. *D. radiodurans* KH3111 was transformed with 500 ng of cosmid or plasmid DNA as previously described [10] except that 0.06 µg MC per ml was used for selecting MC resistance transformants of KH3111 and the supplementation of MC in agar plates was omitted when total colony numbers of samples were counted for calculating transformation efficiency. Transformation efficiency was defined as the average number of MC resistance isolates per 1×10^8 recipients per µg of DNA.

Cosmid and plasmid DNAs were isolated using Qiagen plasmid midi kit and QIAprep spin miniprep kit, respectively. DNA fragment sizing was carried out using Intellegent Quantifier electrophoresis image analysis software package with a color image scanner. DNA fragments from agarose gels were recovered by electroelution using GeneCapsule. Southern blot hybridization was carried out using digoxigenin (DIG). As a size marker for Southern analysis, 500-bp DNA ladder was labeled using DIG oligonucleotide 3'-end labeling kit to prevent the increase in size of the marker DNA fragments by labeling. Kilo-deletion kit was used to construct a series of deletion plasmids from the cloned DNA. Primers for PCR were synthesized using DNA synthesizer.

Polymerase Chain Reaction (PCR) and DNA Sequencing

A PCR test was conducted using Ampli*Taq* gold kit and DNA thermal cycler, based on the directions of the manufacturer's manual. *D. radiodurans* genomic DNA (50 ng) was used as a template DNA. PCR cycling conditions were as follows: 1 cycle of 12 min at 95ºC, 30 cycles of 1 min at 96ºC and 1 min at 60ºC, and 1 cycle of 15 min at 60ºC. After chilling the reaction mixture,

amplified PCR were purified using Microcon-100 concentrator column. Sequence analysis was performed by ABI PRISM dye terminator cycle sequencing ready reaction kit with AmpliTaq DNA polymerase FS and DNA sequence using the universal primers and the primers synthetized for PCR. The PCR product was used as template DNA for direct sequencing. Alkaline denaturation of double-stranded plasmid DNA prior to the cycle sequencing step was very extensive in order to read longer sequence of the high G+C content of *D. radiodurans* genomic DNA. One µg of alkaline denatured DNA was used for sequencing double-stranded plasmid template.

3. Result and Discussion

Subcloning of cosmid clones and localization of the KH3111 mutation

As indicated in Table 1, *D. radiodurans* KH3111 is a multiple-DNA-damaging agent sensitive mutant. In screening of cosmid clones of *D. radiodurans* KD8301 genomic DNA library, a cosmid clone pDC144 which could transform KH3111 to MC resistance was selected. For their transforming ability, several restriction fragments from pDC144 were tested. Since reproducible positive results were obtained from transformation experiment using a 17-kilo bases *Sac*I fragment from pDC144, this study was concentrated to analyze this region. Subclones having various lengths of DNA fragments the region were constructed as shown in Table 1 and Fig. 1. The transforming ability of those subclones was tested. DNAs of subclones that could transform KH3111 to MC resistance are pZA1, pZA8, pZA9 and pZA11 whereas those of subclones pZA2, pZA3, pZA5, pZA7, pZA10 and pZA12 could not transform KH3111. This result indicates that the KH3111 mutation site was located at a 2.9-kb *Sal*I-*Bln*I fragment in a subclone pZA11 that was used for further experiments.

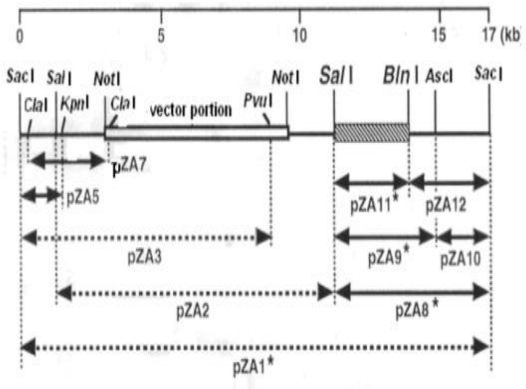

Figure 1. *D. radiodurans* KD8301 DNA fragments subcloned from pDC144.

Notes: Horizontal dotted lines represent the subclones bearing a cosmid vector portion from pDC144. Horizontal lines represent the inserted DNA of the pUC19-derived subclones. Subclones in which DNA is able to transform KH3111 to MC resistance are indicated by asterisks.

Nucleotide sequence of the 2.9-kb SalI-BlnI fragment

A series of deletion plasmids was constructed from pZA11, and used for sequencing and transformation experiment. Figure 2 showed that the nucleotide sequence of the 2.9-kb *Sal*I-*Bln*I fragment contained a complete open reading frame (ORF) of 855 nucleotide in length designated *orf144b*. Two incomplete ORFs designated *orf144a* and *orf144c* were also found in the upstream and downstream of the *orf144b*. The deduced amino acid sequence of the *orf144b* consisted of 284 amino acid. The predicted molecular weight and isoelectric point of the gene product of the *orf144b* were estimated to be 30.5 and 5.2 kD, respectively.

Although protein similarity searches were performed with the deduced amino acid sequences using the Fasta [15], and Blast [16], no significant homology with other known proteins was found in the above three gene products. Protein localization site in cells was predicted with the deduced amino acid sequence of Orf144b using the Psort [17]. It was thought that the Orf144b polypeptide was a cytoplasmic protein because of the membrane proteins. The secondary structure prediction using the method of Chou and Fasman [18] revealed that Orf144c had a helix-turn-helix structure in its N-terminal region (amino acid 2-25) (Figure 2). The N-terminal region of the Orf144c polypeptide also satisfied a stereochemical criteria proposed foe helix-turn-helix motifs in DNA-binding protein [15]: Gly was found at amino acid position 15; hydrophobic Phe was found at amino acid position 5 and 21; Pro was not found in both helices (amino acid positions 2-11 nor 16-25); and non-β-branched Ala was found at amino acid position 6.

The G+C contents of the *orf144a, orf144b* and *orf144c* coding regions were 71.9, 70.9 and 69.1% respectively, while those of two non-coding regions were low (60.4% between *orf144a* and *orf144b* and 50.6% between *orf144b* and *orf144c*) because of the relative richness of T in these regions. No typical transcriptional terminator signal was found in this non-coding region. The G+C content of whole 2922-nucleotide sequence of the *Sal*I-*Bln*I fragment was 68.1%, which was within that *D.radiodurans* total genome (62-70%) [19].

Identification of the KH3111 mutation site

A series of deletion plasmids constructed from pZA11 was examined for their transforming ability. The results showed that the KH3111 mutation was located within a 169-base pair's limited portion in the *orf144b* coding region (Fig.3). Transformation efficiency is defined as the average number of MC resistance isolates per $1x10^8$ recipients per μg of DNA. The transformation efficiency of *D. radiodurans* rec30, a *recA* mutant, with pBC2 containing the wild type *recA* gene in an 11-kb genomic DNA fragment is 1 x 10^3 MC resistance isolates per 1 x 10^8 recipients per μg of pBC2 DNA [20]. The transformation efficiency of KH3111 with the deletion plasmids having relatively large fragments is about two orders of magnitude higher than that of rec30, indicating that recombination repair is not defective in KH3111.

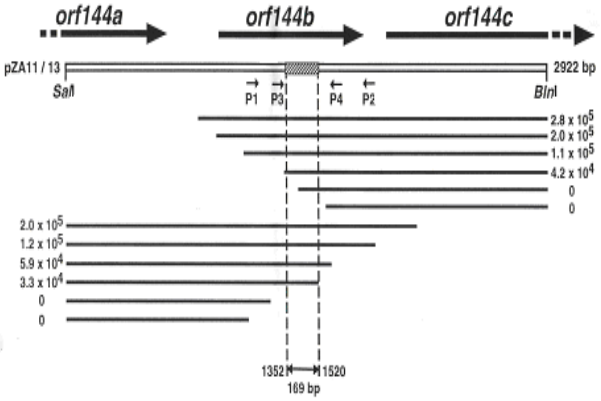

Figure 3. Localization of the KH3111 mutation site.

Notes: The open box represents the parent pZA11 DNA from nucleotide positions 1 to 2923. Thick and thin arrows represent the locations and directions of the ORFs found in the fragment and of the PCR primers, respectively. Horizontal lines represent the deletion plasmids derived from the parental plasmids. Transformation efficiency of these deletion plasmids is represented on the right or left hand. The location of the KH3111 mutation region is indicated by a thin arrow and the nucleotide positions corresponding to both ends of the region are indicated by the numbers.

A DNA region containing the 169-bp portion of interest was amplified using genomic DNA from KH3111 with a set of appropriate primers P1 and P2 in order to identify the exact mutation site (Fig. 2 and 3). The yield of PCR amplification is unique products of the approximated length 651bp. It is assumed that the KH3111 mutation is not owing to large deletions nor the intervention of insertion sequence elements, which have been found in the *D.radiodurans uvrA* gene of MC sensitive mutants 2621 and 3021 [10]. Another set of primer P3 and P4 was generated (Figure 2 and 3) and used to complete DNA sequencing of both strands. Results demonstrated that the sequence of the PCR products were consistent with that of the corresponding region of wild type DNA except that G at nucleotide position 1384 was altered to A (Fig.2). The KH3111 mutation causes the substitution of Gly for Glu at amino acid position 149 of Orf144b (Fig.2). It seems that the Gly substituted by the mutation would be one of the important residues to fulfill the function involved in DNA repair of Orf144b.

4. Conclusion

Deinococcus radiodurans has the capacity to reform its chromosome from multiple, subgenomic fragments immediately without any loss of viability or evidence of mutation. This study identified a gene affected by a mutation in *D. radiodurans* KH3111 and determined its nucleotide sequence. The KH3111 mutation was also identified as a point mutation in the gene. The orf144b gene in a 2.9-kb *Sal*I-*Bln*I DNA fragment of *Deinoccocus radiodurans* subcloned from pDC144 would be one of the responsible genes for regulating multiple DNA repair pathways in response to radiation exposure.

5. Acknowledgements

This work was supported by Ministry of Education, Culture, Sports, Science and Technology of Japan. Authors thank I. Narumi, M. Kikuchi, and H. Watanabe for their supervision and support.

6. References

[1] Moseley, B.E.B., and D.M. Evans (1983), Isolation and properties of strains of *Micrococcus* (*Deinococcus*) *radiodurans* unable to excise ultraviolet light-induced pyrimidine dimers from DNA: Evidence for two excision pathways. *J.Gen. Microbiol*., 129, 2437-2445.

[2] Minton, K.W. (1994), DNA repair in the extremely radioresistant bacterium *Deinococcus radiodurans*. *Mol. Microbiol*. 13, 9-15.

[3] Minton, K.W. (1996), Repair of ionizing radiation damage in the radiation resistant bacterium *Deinococcus radiodurans*. *Mutat. Res*. 363, 1-7.

[4] Narumi, I. (2003), Unlocking radiation resistance mechanisms: still a way to go, *TRENDS in Microbiology*, 11(9), 422-425.
[5] Anderson, A.W., H.C. Nordan, R.F. Cain, G. Parrish, and D. Duggan (1956), Studies on radio-resistant micrococcus: I. isolation, morphology, cultural characteristics, and resistance to gamma radiation. *Food Technol*. 10, 575-578.
[6] Moseley, B.E.B. (1983), Photobiology and Radiobiology of *Micrococcus* (*Deinococcus*) *radiodurans*. *Photochem. Photobiol. Rev.*7, 223-274.
[7] Kitayama, S., and A. Matsumaya (1975), Loss of characteristic radiation resistance by mutation of *Micrococcus radiodurans. Mutat. Res*. 29, 327-332.
[8] Mattimore, V., K.S. Udupa, G.A. Berne, and J.R. Battista (1995), Genetic characterization of forty ionizing radiation-sensitive strains of *Deinococcus radiodurans* : linkage information from transformation. *J. Bacteriol*. 177, 5232-5237.
[9] Gutman, P.D., J.D. Caroll, C.I. Masters, and K.W. Minton (1994), Sequencing, targeted mutagenesis and expression of a *recA* gene required for the extreme radioresistance of *Deinococcus radiodurans. Gene* 141, 31-37.
[10] Narumi, I., K. Cherdchu, S. Kitayama, and H. Watanabe (1997), The *Deinococcus radiodurans uvrA* gene: identification of two mitomycin-sensitive strains and the first discovery of insertion sequence element from Deinobacteria. *Gene* 198, 115-126.
[11] Moseley, B.E.B., and H.J.R. Copland (1978), Four mutans of *Micrococcus radiodurans* defective in the ability to repair DNA damaged by mitomycin C, two of which have wild-type resistance to ultraviolet radiation. *Mol. Gen. Genet*. 160, 331-337.
[12] Fridberg, E.C., G.C. Walker, and W. Siede (1995), *DNA Repair and Mutageneis*, American Society of Microbiology Press, Washington, DC.
[13] Kitayama, S., S. Asaka, and K. Totsuka (1983), DNA double-strand breakage and removal of cross-links in *Deinococcus radiodurans. J. Bacteriol.,* 155, 1200-1207.
[14] Kitayama, S., M. Kohoruku, A. Takagi, and H. Itoh (1997), Mutation of *D. radiodurans* in a gene homologous to *revB* of *E. coli*, Mutat. Res., 385, 151-157.
[15] Pearson, W.R., and D.J. Lipman (1988), Improved tools for biological sequence comparison. *Proc. Natl. Acad. Sci. USA,* 85, 2444-2448.
[16] Altschul, S.F., W. Gish, W. Miller, E.W. Myers, and D.J. Lipman (1990), Basic local alignment search tool. *J. Mol. Biol*. 215, 403-410.
[17] Nakai, K., and M. Kanehisa (1991), Expert system for predicting protein socalization Sites in gram-negative bacteria. *Proteins: Struct. Funct. Genet.* 11, 95-110.
[18] Chou, P.Y.S and G.D. Fasman (1978), Prediction of the secondary structure of proteins from their amino acid sequence. *Adv. Enzymol*. 47, 45-147.
[19] Murray, R.G.E., and B.W. Brooks (1986), Deinococcus. in *Bergey's Manual of Systematic Bacteriology*, Vol. 2 Editors : Sneath, P.H.A., N.S.Mair, M.E. Sharpe, and J.G. Holt, Williams & Wilkins, Baltimore, Maryland, 1035-1043.
[20] Kreszman, G. (1975), Induction of mutation to streptomycin resistance in *Micrococcus radiodurans. Mutat. Res.,* 28, 9-14.

Appendixes

Table 1. Bacterial strains, cosmids and plasmids.
(^{R},resistant;^{S},sensitive; and ::,novel junction)

Designation	Relevant description	Reference
D. radiodurans		
KR_1	wildtype; MC^R, UV^R,γ-ray^R	[7]
KN101	As KR_1 but Ade^-	[7]
KD830	As KN101 but $Dnase^-$	[7]
KD8301	As KD830 but Streptomycin^R	[10]
KH311	As KN101 but MC^S, UV^S, γ-ray^S	[13]
KH3111	As KH311 but Streptomycin^R	This study
E. coli		
XL1-Blue MR	Host for cosmid clone	Stratagene
JM109	Host for plasmid subclones	Lab. Stock
cosmid		
SuperCos 1	Cosmid vector; 7.6 kb; Ampicilin^R Kanamycin^R	Stratagene
pDC144	*Dr* KD8301 DNA in SuperCos 1; 43 kb	This study
plasmid		
pUC19	*Ec* cloning vector; 2.7 kb; Ampicilin^R	Fermentas MBI
pGEM-T	*Ec* cloning vector for PCR product; 3.0 kb; Ampicilin^R	Promega
pZA1	17.0-kb *Sac*I-*Sac*I fragment from pDC144;self-ligation	This study
pZA2	10.0-kb *Sal*I-*Sal*I fragment from pDC144;self-ligation	This study
pZA3	9.0-kb *Sac*II-*Pvu*I fragment from pDC144; in vitro blunt-ent self-ligation	This study
pZA5	pUC19 *Sac*II-*Kpn*I::1.0-kb *Sac*I-*Kpn*I fragment from pDC144	This study
pZA7	pUC19 *Sma*I::2.7-kb *Cla*I-*Cla*I fragment from pDC144; in vitro blunt-ent self-ligation	This study
pZA8	pUC19 *Sal*II-*Sac*I::6.0-kb *Sal*II-*Sac*I fragment from pDC144	This study
pZA9	6.6-kb *Asc*I-*Sal*I fragment from pZA8; in vitro blunt-ent self-ligation	This study
pZA10	4.8-kb *Sac*I-*Asc*I fragment from pZA8; in vitro blunt-ent self-ligation	This study
pZA11	2.9 -kb *Bln*I-*Sal*I fragment from pZA8; in vitro blunt-ent self-ligation	This study
pZA12	5.8-kb *Sac*I-*Bln*I fragment from pZA8; in vitro blunt-ent self-ligation	This study

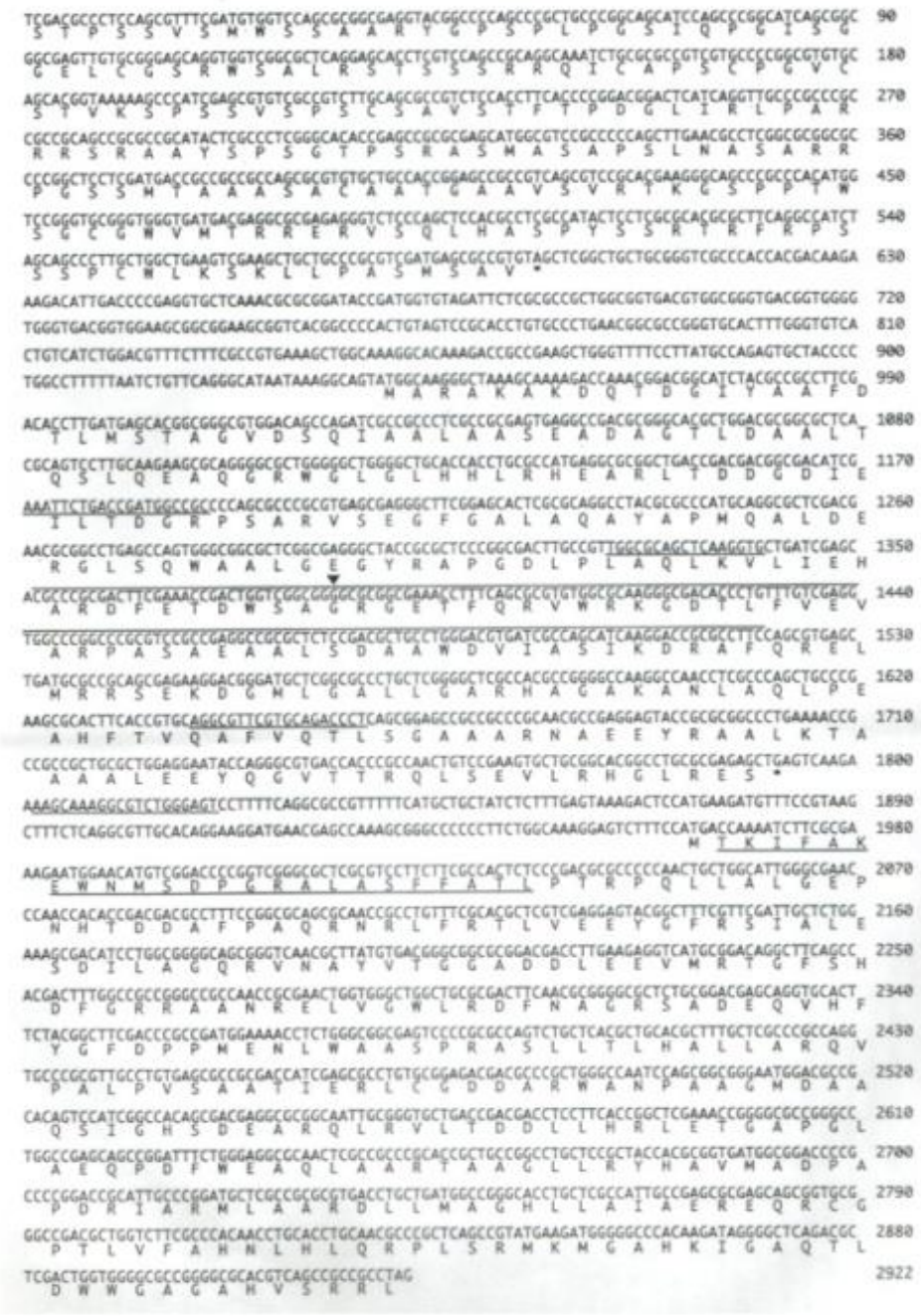

Figure 2. Nucleotide sequence of the 2.9-kb *Sal*I-*Bln*I fragment

Deduced amino acids of Orf144a, Orf144b and Orf144c (in a descending order) are represented by one letter. Asterisks represent stop codons. The location of the PCR primers used for amplifying DNA of KH3111 is marked under nucleotide sequence by underline: P1, P3, P4 and P2 in a descending order. An over line indicates a 169-bp region in which the KH3111 mutation site is expected to be located by the transformation experiments using a series of deletion plasmids from pZA11. The mutation site in orf144b of KH3111 is indicated by an arrow. The underline under amino acid sequence of Orf144c indicates the location of helix-turn-helix motif.

Utilization of Bagasse Fly Ash for Nickel and Chromium Immobilization in Cement-Solidified Metal Plating Sludge

Ahmad Husni [1], Angga Dheta Sirajuddin Aji [2], Yusi Arisandi [3]

[1,2,3] Master Program in Environmental Chemistry, Department of Chemistry, Faculty of Mathematics and Natural Sciences, Brawijaya University, Malang, Indonesia
(solonese2002@yahoo.com; anggadheta@rocketmail.com; yusi_ar@yahoo.com)

Abstract

Nickel and chromium in industrial metal plating sludge (130 ppm and 21 ppm, respectively on dry weight basis) was successfully immobilized in bagasse fly ash–cement matrix. Dried-to-constant-weight bagasse fly ash and portland-pozzolan cement were mixed according to the cement: fly ash (C:F) ratio of 1:3, 1:2, 1:1, 2:1 and 3:1. These mixtures were added to the metal plating sludge (containing 51.43 % water) which its weight was maintained constant at 76 % of the total mixture. After 28 days curing period, all samples were subjected to leaching test as directed for Toxicity Characteristic Leaching Procedure (TCLP) and Unconfined Compressive Strength (UCS) test. Both test results for all samples complied with US EPA requirement. Compressive strength showed a decreasing trend from 305.75 psi (at C:F = 3:1) to 175 psi (at C:F = 1:3) while nickel and chromium leaching reached their minimum value at C:F ratio of 3:1 (0,0005 mg Ni/g sample) and of 1:1 (0,012 mg Cr/g sample), respectively. More significant leaching of both metals at lower C:F ratios could be due to the increasing matrix porosity and disruption of calcium silicate hydrate (CSH) gel formation in the final product. In C:F = 2:1 and 3:1, immobilization of chromium was mainly achieved through adsorption while in C:F = 1:2 and 2:1, the immobilization was mostly affected by low matrix strength which facilitated chromium dissolution. Fly ash addition did not show a profound effect in nickel immobilization, indicating that nickel was mainly immobilized through physical entrapment in the matrix; therefore its leaching would rely mostly on the strength of the matrix. These findings might provide preliminary environmental feasibility information to reuse the final concrete-like products under certain safety precautions as construction materials, hence reducing waste discharge to the environment.

Keywords: *Immobilization, solidification, metal plating sludge.*

1. Introduction

Indonesian government regulates and classifies metal plating activities as one of potential source of hazardous wastes based on the fact that such activities often involve the use of concentrated acids and metal solutions of which residues may be harmful for surrounding environment. Although ideally waste should be treated to recover their reusable constituents, these efforts are costly and in some cases are difficult to perform due to the nature of the wastes which may require tedious pre-treatments such as physical and chemical separations and proper conditioning before recovery attempts take place. Therefore, a more economically feasible option for routine tasks is often carried out through immobilization of the containing pollutants before the waste is kept in a secured landfill.

This research focuses on immobilization of nickel and chromium in metal plating sludge through solidification process. This technique has been well known for its‘ effectiveness in modifying physical properties of the waste in order to either minimize pollutants solubility, and/or to improve handling of the waste form and/or to reduce its‘ surface area [1]. Moreover, on the basis of treated waste volume, these treatments are usually less expensive than conventional semisolid waste treatment methods such as incineration [1].

Solidification and therefore immobilization are typically achieved through either physical and/or chemical entrapment of pollutants in cured cementitious matrices. These matrices consist mainly of Portland cements doped in most cases with mineral materials (e.g. zeolite, fly ash) and less likely, with the synthetic ones to improve workability and sometimes also to achieve effective immobilization of the pollutants [2]. Pollutants are also immobilized by cement hydration products, presumably through the coordinative bonds [1]. This technique is therefore suitable for heavy metals which indeed have some tendencies to form complexes.

Previous researches have confirmed that fly ash can be incorporated to some extents into cementitious matrix resulting in stronger pollutants

retention inside the matrix compared to the ones occur in matrix from cement alone [3-5].

Simultaneous action of fly ash to act as filler to the porous cement matrix to increase compressive strength and as adsorbent to retain heavy metal ions contained in the matrix is advantageous for waste treatment process, including solidification [5,6]. Moreover, due to its abundance as residual materials, fly ash has become an economically interesting choice. Thus, in making of concrete-like products as is usually performed in solidification, higher fly ash to cement weight ratio in a product would reduce the production (i.e. treatment) cost. Therefore, this research were directed to obtain the highest proportion of fly ash to cement ratio while maintaining compliance of the resulting waste form with US EPA regulations in terms of maximum leaching thresholds for nickel and chromium, and minimum required compressive strengths for solidified wastes. The effective proportion of fly ash was also evaluated in order to define the limit.

2. Experimental Details

Metal plating waste was obtained in the form of sludge (51.4 % water) from a nickel and chromium plating small industry. This sludge contained (on dry weight basis) 130 ppm of chromium and 21 ppm of nickel and was employed without any pre-treatment. The cement was commercial Portland pozzolan cement and was also used without any pre-treatment. The fly ash was bagasse combustion residues (21 % water) obtained from Kebon Agung sugar mill, Malang, Indonesia. The fly ash was dried to constant weight at 110ºC. Composition of the three materials was determined using an X-ray fluorometer (MiniPal4) and shown in Table 1.

On dry weight basis, cement and fly ash were mixed according to the compositions as listed in Table 2. The sludge was actually mixed in the condition it was obtained, i.e. including the water content. Dry cement needs water to become cement paste and later to set in the final product.

In this experiment, the required water was taken solely from the sludge water content thus no extra water was added to the mixture. Prior to this experiment, our group had done a preliminary research to determine the optimum water content necessary to achieve maximum compressive strength of the final product that has been cured for 28 days. The result showed that the optimum water content was 40 % (w/w) of the final product (data not shown). Therefore, for all compositions listed in Table 2, weight of the added sludge must be kept constant in order to achieve 40 % water content in all samples. To achieve this, the dry weight of the sludge must be 1.6 times as much as the total weight of cement and fly ash. Since the sludge contained water as much as 51.4 %, the actual weighing was made 3.2 times as much of that amount, or simply 76 % of the total weight of the final mixture.

Table 1. Composition (% dry weight) of cement, fly ash and sludge used for the experiment

Element	Cement	Fly Ash	Sludge
Ag	-	-	0.38
Al	3.9	-	-
Ba	0.2	-	-
Ca	70.33	7	27
Cu	0.07	0.15	-
Fe	7.64	17.3	0.024
In	2.3	-	-
K	0.68	15.6	-
Mn	0.15	0.39	0.0009
Na	-	-	72
P	-	1.5	-
S	1.43	0.66	-
Si	12	55.6	-
Sr	0.19	-	0.07
Ti	0.53	0.953	-
Zn	0.05	0.06	0.01

Table 2. Mixture compositions (on dry weight basis) of cement and fly ash for each mixture

Mixture	Cement	Fly Ash
A	1	3
B	1	2
C	1	1
D	2	1
E	3	1

Mixture pastes of each composition were molded into three cylindrical steel molds (triplicate samples were made from each composition) of 8 cm internal diameter and 16 cm high each and cured for 28 days inside the molds under room temperature. In the 28th day, all specimens were subjected to Unconfined Compressive Strength (UCS) test (ASTM D1632-87). Results were evaluated against the minimum standard of 50 psi [9].

In the same day, samples were also subjected to Toxicity Characteristic Leaching Procedure (TCLP) test for leachable chromium and nickel [10]. For TCLP test, randomly selected portions of each specimen were extracted using acetic acid solution of pH 2.8 as the extraction solution. Extraction was performed in 100mL Erlenmeyer flasks rotated in a shaker (Edmund Buhler SM 25) set in 100 rpm for 18 hours. Both metal concentrations in the extract were determined using an atomic absorption

spectrometer (Shimadzu Type AA–6200). Results were evaluated against the maximum concentration of 0.12 mg/g and 0.2 mg/g for chromium and nickel, respectively [11]. Though not regulated as the part of TCLP test by US EPA, due to the high toxicity of chromium (VI), colorimetric determination of chromium (VI) in TCLP extracts were also performed [12]. The absorption measurement was performed using a Spectronic 20 photometer.

All volumetric glass apparatus were of Class B and had been washed thoroughly before use. All reagents were of Reagent Grade.

3. Result and Discussion

Unconfined compressive strength test results

The results of compressive strength test for each composition given in Figure 1, shows a consistent decrease in compressive strength as fly ash proportion in the mixture increases. Nevertheless, all results are still above the minimum required threshold (50 psi). This declining trend is in agreement with the previously reported ones [5,7].

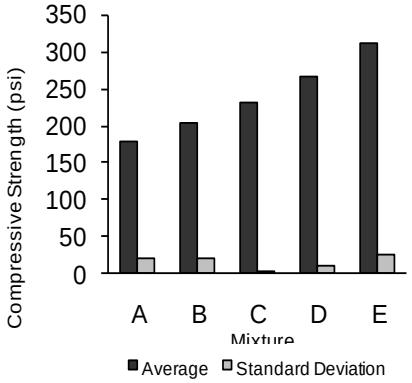

Figure 1. Average compressive strength values from each composition and their respective standard deviations

Compressive strength of cement based products mainly originates from what is called C-S-H gel. This gel is the main product of cement hydration reaction, consisting of various calcium silicate hydrate compounds which vary in stoichiometry and calcium hydroxides [8]. Therefore, a decrease in compressive strength must be the result of some disruptions in C-S-H gel formation. This might be due to occlusion of some cement particles by the fly ash because of the voluminous nature of the latter even though the mass was smaller. This caused the occluded cement particle hindered from contact with water therefore prevented the hydration reaction of the respective particle. This account is also supported by the result of determination of particle size distribution which was performed during our preliminary research. It was found that 65% of fly ash particles used in this experiment was finer than 0.075 mm while only 39% of cement particles of that was in the same size.

TCLP Test Results

Average and standard deviation of chromium and nickel concentrations showed a more irregular trend (Figure 2 and 3). However, all results were still lower than the maximum threshold for chromium and nickel (0.12 mg/g and 0.2 mg/g, respectively).

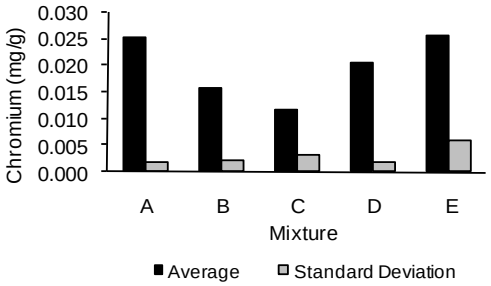

Figure 2. Average chromium concentrations in TCLP extracts from each composition and their respective standard deviations

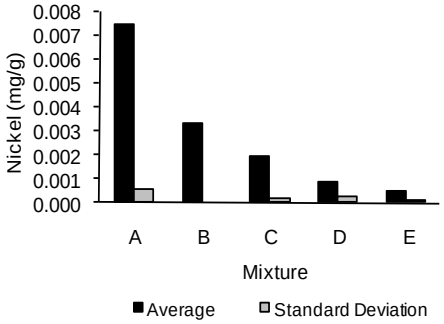

Figure 3. Average nickel concentrations in TCLP extracts from each composition and their respective standard deviations

In the case of chromium, addition of fly ash had resulted in lower leaching as observed in mixture E, D and C. This decreasing trend showed the action of fly ash as an effective immobilizer against chromium. However, this addition was also decreasing compressive strength of the final product (Figure 1). Since the immobilization takes place not only via a chemical or physical

interaction but also takes place through physical entrapment of a pollutant in an inert and durable matrix, thus the decrease in compressive strength of the final product must have also been responsible for a higher release of the pollutant from the respective matrix. However, data in Figure 2 indicated that albeit the mixture E, D and C had experienced some decrease in compressive strength, their chromium retention capability were still considerably high. It was proven by lower leaching as fly ash proportion increased. From this point, it can be concluded that the expected adsorption action of the fly ash could still prevail over the adverse action of lower compressive strength.

In contrast, in mixture A and B, chromium leaching was found to increase with fly ash proportion. In these mixtures, the compressive strength might have fallen too low to prevent the TCLP solution from seeping through the pores of the particles. Particles were then easier to crumble further into smaller ones thus increasing their effective surface area and eventually became more vulnerable to solvent actions to dissolve previously retained chromium species. Even if the adsorption action of the fly ash toward soluble chromium was supposed to increase as fly ash proportion increased, it might have not been able to counteract the increase in effective surface area of the particles due to the falling compressive strength.

Compared to chromium, nickel species in the sludge seemed to be immobilized differently. Figure 3 showed a steady increase in nickel leaching as fly ash proportion increased. This finding suggested that (1) immobilization of nickel species in the matrix was mainly the result of physical entrapment (i.e. adsorption by fly ash was a minor factor) which therefore relied upon the strength of the matrix and (2) this cement-fly ash mixture could probably had some degree of preference to adsorb chromium than nickel. The adsorption might involve the electrostatic interaction between the surface of the adsorbent and the adsorbate. The difference between chromium and nickel might be due to the difference in charges of chromium(III) and nickel(II) in water. Fly ash was known to possess negative surface charges therefore cations with more positive charges [i.e. chromium(III)] may be preferred upon those with the lesser ones [i.e. nickel(II)]. Accordingly, this postulation would not apply for chromium(VI) which exists as anions in solution.

The suggested electrostatic interaction would also suggest that the immobilization of chromium(VI) must be less likely influenced by the fly ash adsorption ability. Experimental results displayed on Figure 4 have confirmed this prediction. Although total chromium leaching varies significantly from one mixture to another (which also means vary in fly ash proportion), chromium(VI) leaching is only slightly affected. The only notable change in leaching of chromium(VI) species is observed between mixtures C and D, where the decrease in compressive strength (from D to C) could no longer protect chromium(VI) from contact with the solvent. Thus, chromium(VI) was dissolved in this way.

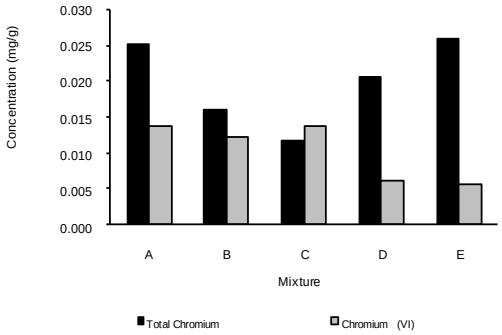

Figure 4. Average total chromium and chromium (VI) concentrations in TCLP extracts

4. Conclusion

Immobilization of nickel and chromium in metal plating sludge carried out through solidification had successfully produced concrete-like products with good compressive strength and appropriate retention properties toward soluble nickel and chromium species. Incorporation of bagasse fly ash as a partial substitution to cement up to a certain limit could improve chromium retention in the final product matrix whilst nickel retention did not seem to depend on the amount of the added fly ash. Fly ash addition resulted in more effective immobilization of chromium (III) than that of chromium (VI), indicating possible occurrence of electrostatic interactions between negatively charged fly ash surface and positively charged ions.

5. Acknowledgements

Authors would like to thank Prof. Dr. Ir. Chandrawati Cahyani and Ir. Bambang Ismuyanto M.S. for their technical advice on the experiments and reports.

6. References

[1]. R. D. Spence and C. Shi (2005), Stabilization of Hazardous and Mixed Wastes, CRC Press, Boca Raton.

[2]. K. E. Eylands (1995), Solidification and Stabilization of Wastes Using Coal Fly Ash: Current Status and Direction, American Coal Ash Association, Alexandria.

[3]. Yin, C. Y., (2008), Optimization of S/S of Nickel Hydroxide Sludge Using OPA and OPC, Proceedings of International Conference of Environmental Research and Technology.

[4]. Indrawati, L., (2009), Coal Fly Ash Activation and Its Application in Adsorption Process of Chromium in Electroplating Sludge, Department of Chemistry of Semarang State University, Semarang.

[5]. Gupta, V. K., Mohan, D., Sharma S., and K. T. Park (1999), Removal of Chromium (VI) form Electroplating Industry Wastewater Using Bagasse Fly Ash—A Sugar Industry Waste Material, *The Environmentalist*, 19, 129 – 136.

[6]. Chindraprasirt, P. Jaturapitakul C., and T. Sinsiri (2005), Effects of Fly Ash Fineness on Compressive Strangth and Pore Size of Blended Cement Paste, *Cement and Concrete Composites*, 27, 425 – 428.

[7]. Shi, C. and A. F. Jimenez (2006), Stabilization / Solidification of Hazardous and Radioactive Wastes with Alkali-Activated Cements, *Journal of Hazardous Materials*, B137, 1656 – 1663.

[8]. Mac Laren, D. C. and M. A. White (2003), Cement: Its Chemistry and Properties, *Journal of Chemical Education*, 80, 6, 623 – 634.

[9]. US EPA (1989), Stabilization / Solidification of CERCLA and RCRA Wastes, EPA/625/6-89/022, Office of Research and Development, Cincinnati.

[10]. US EPA., (1992), SW–846 Method 1311, Toxicity Characteristic Leaching Procedure, Office of Solid Waste and Emergency Response, Washington D. C.

[11]. US EPA (1990), Obtaining a Soil and Debris Treatability Variance for Various Remedial Actions in Superfund LDR Guide No. 6A-2nd Edition, Office of Solid Waste and Emergency Response, Washington D. C.

[12]. US EPA, (1992), Method 7196A, Chromium, Hexavalent (Colorimetric), Office of Solid Waste and Emergency Response, Washington D. C.

Alkaloids From Marine Sponges: Isolation of A New Aaptamine Related Compound from An Indonesian *Aaptos Aaptos*

Ajuk Sapar [1], I Wayan Mudianta [2,3], Andi H. Alimuddin [4], and Mary J. Garson [5]

[1,4] Department of Chemistry, Faculty of Mathematics and natural Sciences, Tanjungpura University, Pontianak, Indonesia
[2] Department of Analytical Chemistry, Faculty of Mathematics and Natural Sciences, Ganesha University of Education, Bali, Indonesia
[3,5] School of Chemistry and Molecular Biosciences, The University of Queensland, Brisbane Queensland, Australia (m.garson@uq.edu.au)

Abstract

Sponges continue to be an important source of novel secondary metabolites possessing a wide variety of biological properties [1]. Marine sponges of the genus Aaptos have been proven to be a rich source of a group of 1H-benzo[d,e][1,6]-naphthyridine alkaloids known collectively as the aaptamines [2]. Aaptamine and the related compounds, 9-demethylaaptamine, isoaaptamine, 9-demethyloxyaaptamine, and 4-N-methylaaptamine have been identified in Aaptos sp. Known secondary metabolites related to aaptamine have shown potent antiviral activity, α-adrenoceptor blocking activity as well as inhibition of Ehrlich tumor cell growth [3]. Recently, bisdemethylaaptamine and the first naturally occurring sulfated aaptamine have also been identified from the same sponge that was obtained from North Sulawesi, Indonesia [4]. Herein we wish to present the isolation of two new aaptamine-related compounds (1) and (2) from the sponge Aaptos aaptos harvested in Randayan Island, West Kalimantan, Indonesia. The structures of the compounds were unambiguously elucidated by extensive 1D and 2D NMR experiments and by accurate mass measurement. Compound (2) is closely related to aaptanone (3), a novel zwitterionic metabolite recently reported from a Vietnamese sample of Aaptos aaptos [5].

***Keywords**: Aaptos, aaptamine, alkaloid.*

1. Introduction

Sponges continue to be an important source of novel secondary metabolites possessing a wide variety of biological properties [2]. Marine sponges of the genus *Aaptos* have been proven to be a rich source of a group of 1H-benzo[*d,e*][1,6]-naphthyridine alkaloids known collectively as the aaptamines [3]. Aaptamine and the related compounds, 9-demethylaaptamine, isoaaptamine, 9-demethyloxyaaptamine, and 4-*N*-methylaaptamine have been identified in *Aaptos* sp. Known secondary metabolites related to aaptamine have shown potent antiviral activity, α-adrenoceptor blocking activity as well as inhibition of Ehrlich tumor cell growth [4]. Recently, bisdemethylaaptamine and the first naturally occurring sulfated aaptamine have also been identified from the same sponge that was obtained from North Sulawesi, Indonesia [5].

The parent 1*H*-benzo[*d,e*][1,6]-naphthyridine, known as aaptamine (**4**), was first isolated by Nakamura and coworkers from the Okinawan marine sponge *Aaptos aaptos* in 1982 [6]. Subsequently, it was identified from a Taiwanese *Aaptos aaptos* in 1997 [7], and an Indonesian sample of *Aaptos sp.* collected off Jakarta in 2003 [5].

Aaptamine (**4**) possesses a unique fused tricycle aromatic ring structure and is probably considered as a chemotaxonomic marker for sponges of the genus *Aaptos* (Hadromerida, Suberitidae) [8]. The isolation of aaptamine from the taxonomically unrelated species *Luffariella* [9] (Order Dictyoceratida: Family Thorectidae), *Hymeniacidon* [8] (Order Halichondrida: Family Halichondriidae), and *Xestospongia* [10] (Order Haplosclerida: Family Petrosiidae) may provide a hint that aaptamine could probably be a product of a microbial symbiont [11].

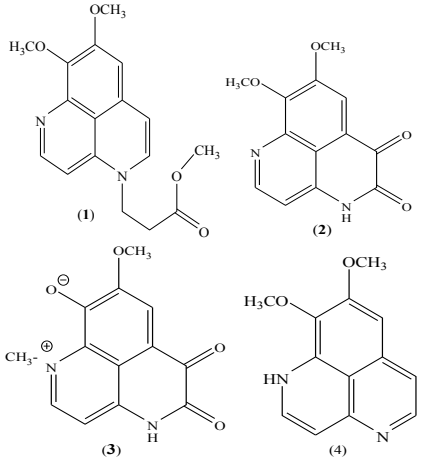

2. Experimental Details

General experimental procedures

Solvents

Analytical Reagent grade solvents were purchased from the Chemical store at The University of Queensland. They were distilled prior to use for extractions, partitions and flash column chromatography. HPLC grade solvents (LabScan) were selected for HPLC purposes. The solvents used included hexanes, dichloromethane, chloroform, ethyl acetate, methanol and acetonitrile. Ionic and basic solvent modifiers including trifluoroacetic acid (TFA) was used during the flash column chromatography and HPLC. Deuterated solvents such as $CDCl_3$, CD_3OD and d_6-DMSO were used for NMR measurements.

Thin layer chromatography

Normal phase and reversed phase thin layer chromatography were performed on Merck Art 5554 and 5559 aluminium backed plates precoated with silica gel Merk Kieselgel 60 F_{254} respectively. Plates were visualised by UV 254 and 365 nm and sprayed with stain reagents including Dragendorff's reagent followed by heating if necessary.

Normal and reverse phase flash column chromatography

Normal phase flash column chromatography was performed on Scharlau silica gel 60, 0.04-0.06 mm (230-400 mesh ASTM) while reverse phase flash column chromatography was carried out on silica gel prepared as outlined below. Gradient elutions from hexanes to methanol and from 100% H_2O to 100% methanol were employed during the normal phase and reverse phase flash chromatography respectively. Flash column chromatography was carried out under a pressure of compressed air and the resultant fractions were combined according to their TLC profile.

High performance liquid chromatography (HPLC)

Reversed-phase HPLC was carried out on an Agilent 1100 series instrument fitted with variable wavelength UV and refractive index detector, an Agilent D1311A quaternary pump and semi-preparative Waters® HPLC column (μ-Bondapak C_{18} 7.8 x 300 mm) or Phenomenex® column (Gemini 5 micron 10 x 250 mm).

Mass spectrometry

Positive or negative ion electrospray mass spectra (LRESMS) were recorded using a Bruker Esquire HCT instrument or (HRESIMS) using a MicroTof Q instrument equipped with a standard ESI source. Samples were prepared in MeOH mass spectrometry grade solvent.

1D and 2D NMR Spectroscopy

Proton nuclear magnetic resonance (^{1}H NMR) spectra were recorded on a Bruker Avance 500 MHz using a 5 mm SEI probe, or on a Bruker Avance 750 MHz with a 5 mm TXI Zgrad probe. Carbon-13 nuclear magnetic resonance (^{13}C NMR) and DEPT135 spectra were measured on a Bruker Avance 400MHz with a 5 mm bbo probe or on a 500 MHz spectrometer using an inverse probe. Spectra were measured in deuterated methanol (d_4-MeOH), deuterated chloroform ($CDCl_3$) or deuterated d_6-DMSO. Chemical shifts (δ) were recorded in parts per million (ppm), and were referenced relative to d_4-MeOH (^{1}H δ 3.30; ^{13}C δ 49.0), $CDCl_3$ (^{1}H δ 7.26; ^{13}C δ 77.0) and d_6-DMSO (^{1}H δ 2.50; ^{13}C δ 39.5). Coupling constants (*J* values) were measured in Hertz (Hz)

Two dimensional NMR (2D NMR) data were acquired from a Bruker Avance 500 MHz or a Bruker Avance 750 MHz using a 2 K x 256 or 2 K x 512 complex data matrix, which was zero filled once in each dimension, then a π/2 shifted sine-squared bell curve window function was applied in both dimensions before Fourier transformation. Gradient enhanced HMBC (geHMBC) and HSQC (geHSQC) spectra were obtained with 64 or 32 transients per increment. The evolution delay was set for $^nJ_{CH}$ of 8 Hz, 6 Hz or 4 Hz (geHMBC) and $^1J_{CH}$ of 135 Hz (geHSQC). Double Quantum Filtered COSY (DQF COSY) spectra were recorded with 64 or 32 transients per increment and a pulse delay of 2.0 seconds. NOESY spectra were obtained with 64 or 32 transients per increment, a recycle time between scans of 3.4 seconds and mixing time between 0.8 and 1.5 seconds.

Animal material

The sponge *Aaptos aaptos* was obtained by hand using SCUBA at a depth of approximately 20 meters at Randayan Island West Kalimantan Indonesia in May 2007. The sponge sample was massive, dense, and dark brown in color with a relatively smooth surface and deep yellow interior.

Extraction and isolation

The frozen sponge (48.0 g) was homogenised and then extracted three times (500 mL) with MeOH to give 24.4 g dark brown gum. The dark brown extract was partitioned between hexanes (3 x 100 mL) and water, followed by DCM (3 x 100 mL) and finally EtOAc (3 x 100 mL). The DCM fractions were combined, dried over anhydrous Na_2SO_4, filtered, and concentrated under reduced pressure to yield 218 mg brown oil. The DCM fraction was passed through a RP flash column (50.0 x 2.5 cm in diameter) eluting with 100% MeOH to give six fractions. The second fraction (fraction B) was submitted to reversed phase HPLC eluting with a gradient from 20 to 100% MeCN/H_2O plus 0.1 % TFA yielding 2.6 mg of (**1**), and (**2**). The second

attempt to reisolate compound **5** was carried out by RP-HPLC of the DCM fraction using a solvent gradient from 20 to 100% MeCN/H_2O plus 0.1 % TFA. 20.0 mg of the DCM extract was passed through the RP HPLC to give 1.7 mg pale yellow oil of **2**.

Compound 1: Methyl 3-(8,9-dimethoxy-4H-benzo[de][1,6]naphthyridin-4-yl)propanoate (1):
brownish oil; HRESIMS (positive ion mode) *m/z* 315.1327 $[M + H]^+$ (calc. for $C_{17}H_{19}N_2O_4$, 315.1345); ^1H NMR (MeOD, 500 MHz) and ^{13}C NMR (100 MHz) see Table 1.

Compound 2: 8,9-Dimethoxy-4H-benzo[de][1,6]naphthyridine-5,6-dione (2):
amber oil; HRESIMS (positive ion mode) *m/z* 259.0709 $[M + H]^+$ (calc. for $C_{13}H_{11}N_2O_4$, 259.0719); ^1H NMR (MeOD, 500 MHz) and ^{13}C NMR (100 MHz) see Table 2 and 3.

3. Results and Discussion

Structure elucidation of compound 1

Metabolite **1** was obtained as dark brown oil from RP-HPLC at a retention time of 16.6 minutes. The molecular formula of **1** was established to be $C_{17}H_{18}N_2O_4$ according to the HR-ESIMS analysis that exhibited a protonated molecular ion at *m/z* 315.1327 $[M+H]^+$, implying the presence of ten unsaturations and with a mass 87 amu more than aaptamine.

The ^1H NMR spectra of **1** (Table 1) indicated the presence of the same benzo[*de*][1.6]napthyridine core structure as in the aaptamine related compounds. Two sets of coupled protons at δ_H 7.92 (d, J = 7.3 Hz, H-2) and 6.54 (d, J = 7.4 Hz, H-3), and at δ_H 7.36 (d, J =7.5 Hz, H-5) and 6.91 (d, J = 7.5 Hz, H-6), were clearly seen together with one isolated singlet at δ_H 7.12 (s, H-7). Two distinctive methoxy signals that were attached to the aaptamine structure were observed at δ_H 4.04 and 3.94 respectively. The first methoxy signal was found to couple with a quaternary carbon at δ_C 157.1 while the second methoxy signal together with the methine signal H-7 were observed to have three-bond gHMBC correlations to a carbon at δ_C 132.5. These assignments confirmed the positions of the methoxy groups at C-8 and C-9 respectively. The most striking differences between **1** and aaptamine (**4**) were the presence of two additional coupled methylene triplets at δ_H 4.34 (J = 6.7 Hz) and 2.89 (J = 6.7 Hz), and an additional upfield methoxy at δ_H 3.67. A carbonyl signal resonating at δ_C 171.7 was also observed in the ^{13}C NMR spectrum. Inspection of the long-range gHMBC correlations of these new signals revealed that the coupled methylene triplets and the methoxy singlet coupled to the same carbonyl at δ_C 171.7. When a methyl ester substructure was proposed as in Figure 1, it was found to be consistent with the 87 mass unit differences to that of aaptamine (**4**).

Other long-range gHMBC couplings between the methylene proton at δ_H 4.34 which was later assigned to H-1‘ to the quaternary carbon at δ_C 150.2 (C-3a) and the methine carbon at δ_C 134.1 (C-5) confirmed the connection of the methyl ester side chain to the heteroatom of the naphthyridine ring as shown in Figure 2. Based on these data, the structure of metabolite **1** could be unambiguously assigned as a new methyl ester derivative of aaptamine (**4**). To the best of our knowledge compound **1** has not been reported either isolated from natural source or obtained as a synthetic product.

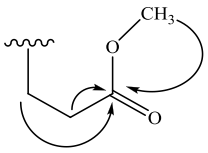

Figure 1. Methyl ester said chain of 1

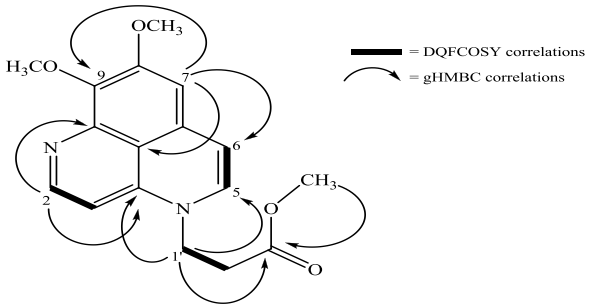

Figure 2 Selected long-range HMBC correlations of 1

Table 1. ^1H and ^{13}C NMR data of 1

C	^1H (mult, J, Hz)[a,b]	^{13}C, ppm[c]	gHMBC[d,e]	DQF COSY
2	7.92 (d, 7.3)	141.9	3, 3a, 9a	3
3	6.54 (d, 7.4)	96.1	9b	2
3a		150.2		
5	7.36 (d, 7.5)	134.1	1‘, 3a, 6, 6a	6
6	6.91 (d, 7.5)	113.5	5, 7, 9b	5
6a		131.7		
7	7.12 (s)	101.5	6, 9, 9b	
8		157.1		
9		132.5		
9a		133.7		
9b		117.5		
1‘	4.34 (t, 6.7)	48.3	3a, 5, 2‘, 3‘	2‘
2‘	2.89 (t, 6.7)	31.1	1‘, 3‘	1‘
3‘		171.7		
8-OCH_3	4.04 (s)	55.5	8	
9-OCH_3	3.94 (s)	59.6	9	
3‘-OCH_3	3.67 (s)	52.2	3‘	

[a]500 MHz, MeOH-d_4 referenced to ^{1}H at δ 3.30 ppm; [b]coupling constant in Hz; [c]100 MHz, MeOH-d_4 referenced to ^{13}C at δ 49.0 ppm [d] HMBC connectivity from H to C; [e] correlations observed for one bond $J_{C\text{-}H}$ of 145 Hz and long range $J_{C\text{-}H}$ of 8 Hz.

The simplicity of the tri-cyclic core of aaptamine has already led to a structure activity relationship study (SAR). Recently, Bowling and co-workers investigated some semisynthetic analogues of *N*-alkylated aaptamine and other derivatives in relation to their activity against microbial and AIDS related opportunistic infections.[4] Overall, the research revealed that some *N*-alkyl analogues have high potency against some bacteria and are moderately active as antifungal agents. Specifically, none of the alkylation products possessing less that five carbon units were active against the methicillin resistant strain of *Staphylococcus aureus* (MRSa). On the other hand, notable improvement of the activity against chloroquinone sensitive and resistant *Plasmodium falciparum* strains was observed for the analogs having more than five carbon units in the alkyl chain. Although several analogs have been evaluated to have significantly improved activity against HIV-1 in human peripheral blood mononuclear (PBM) cells, their cytotoxic properties were found to be too high in comparison to the standard aaptamine.[4] The new compound (**1**) is a unique analog of aaptamine having a *N*-methylester side chain, and its bioactivity is likely to be of considerable interest.

Structure elucidation of compound 2

Two samples of compound **2** were isolated. The first sample was obtained as pale yellow oil from the RP-HPLC of the fraction B yielded from RP flash column chromatography of the DCM extract. Meanwhile the second sample was isolated from the RP-HPLC of the DCM extract eluting with a gradient from 20 to 100% MeCN/H_2O plus 0.1 % TFA.

A mass spectrometric investigation of **2** of the first sample indicated an intense HRESIMS peak at 259.07 [M + H] and supported the proposed molecular formula of $C_{13}H_{10}N_2O_4$ corresponding to eight degree of unsaturation, one less than that of aaptamine (**4**).

The ^{1}H and ^{13}C spectra of the first sample of **2** (Table 2) were comparable to those of aaptamine (**4**) except for the absence of two coupled protons. Two doublet protons at δ_H 8.77 (d, J = 4.9 Hz, H-2), 7.14 (d, J = 4.9 Hz, H-3) and a singlet at δ_H 8.33 (s, H-7) were clearly observed from ^{1}H NMR together with two characteristic methoxy groups at δ_H 4.11 and 4.24. These methoxy groups were found to be attached to C-8 and C-9 of the aaptamine structure respectively according to the three-bond HMBC correlations observed for the methoxy at δ_H 4.11 to a quaternary carbon at δ_C 153.9 (C-8) and the methoxy at δ_H 4.24 together with the methine proton H-7 to a quaternary carbon at δ_C 152.4 (C-9). The expected NH broad signal did not appeared and as a consequence the NOE coupling expected between NH and the proton H-3 was not observed.

There was a signal at δ_C 176.6 that clearly established the presence of a carbonyl group in the molecule. This was assigned to C-6 rather than C-5 since there was a correlation from H-7 in the HMBC spectrum (run under conditions set for an 8 Hz long range correlation). Since the molecular formula revealed four oxygens, it was suspected that there was a second carbonyl group, as shown at C-5. However there was no evidence for the existence of such carbon in either 2D data or from a 1D carbon spectrum. Attempts to get ^{13}C data, even at 900 MHz, were hampered by the small amount of material. HMBC data sets were acquired with the long range J value set at 6 Hz, and at 2 Hz, but neither experiment revealed any evidence of correlations from any of H-3, H-5 or the NH to a second carbonyl. It should be noted that H-3 and H-7 are four bonds away from the proposed carbonyl, while the broadness of the NH proton may have prevented the observation of any correlations from it. If present, the C-5 carbon would have been expected to have a chemical shift in the range 157- 176 ppm by comparison with the literature compounds including hadranthine [12] and griffithdione [13].

In order to obtain the ^{1}H chemical shift of the NH proton of **5**, NMR data was acquired on the second sample in d_6-DMSO and the ^{1}H and partial ^{13}C NMR data presented in Table 3. A broad singlet at δ_H 12.1 was assigned to the expected NH proton and a dipolar NOE coupling was also observed between a distinctive NH broad signal at δ_H 12.1 and the proton H-3 (Figure 3). Based on the partial NMR data, and the mass spectroscopic data, the structure could be tentatively assigned as in **2**.

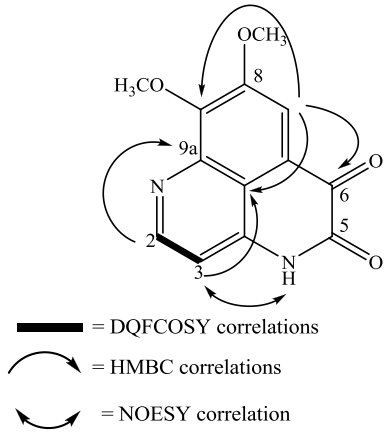

Figure 3. Selected long-range HMBC and NOESY correlations of 2

Table 2 ^{1}H and ^{13}C NMR data of the first sample of 2

C	^{1}H (mult, *J*, Hz)[a,b]	^{13}C, ppm[c]	HMBC[d,e]
2	8.77 (d, 4.9 Hz)	152.5	3a, 9b
3	7.14 (d, 4.9 Hz)	107.2	9b
3a		142.0	
5			
6		176.6	
6a		124.2	
7	8.33 (s)	117.2	6, 6a, 8, 9, 9b
8		153.9	
9		152.4	
9a			
9b		114.7	
8-OCH_3	4.11 (s)	57.7	8
9-OCH_3	4.24 (s)	62.5	9
NH			

[a]500 MHz, MeOH-d_4 referenced to ^{1}H at δ 3.30 ppm; [b]coupling constant in Hz; [c]obtained from HMBC data; MeOH-d_4 referenced to ^{13}C at δ 49.0 ppm; [d]HMBC connectivity from H to C; [e] correlations observed for one bond $J_{C\text{-}H}$ of 145 Hz and long range $J_{C\text{-}H}$ of 8 Hz.

Table 3 ^{1}H and ^{13}C NMR data of the second sample of 2

C	^{1}H (mult, *J*, Hz)[a,b]	^{13}C, ppm[c]	HMBC[d,e]
2	8.80 (d, 4.9 Hz)	-	
3	7.12 (d, 4.9 Hz)	-	
3a		-	
5		-	
6		175.8	
6a		-	
7	8.14 (s)	115.0	6, 9b
8		153.0	
9		150.8	
9a		-	
9b		113.7	
8-OCH_3	4.05 (s)	-	8
9-OCH_3	4.17 (s)	-	9
NH	12.1 (bs)		

[a]500 MHz, d_6-DMSO referenced to ^{1}H at δ 2.50 ppm; [b]coupling constant in Hz; [c]obtained from HMBC data; d_6-DMSO referenced to ^{13}C at δ 39.5 ppm [d] HMBC connectivity from H to C; [e] correlations observed for one bond $J_{C\text{-}H}$ of 145 Hz and long range $J_{C\text{-}H}$ of 8 Hz.

4. Conclusion

Marine sponges of the genus Aaptos have been proven to be a rich source of a group of 1H-benzo[d,e][1,6]-naphthyridine alkaloids known collectively as the aaptamines. Aaptamine and the related compounds, 9-demethylaaptamine, isoaaptamine, 9-demethyloxyaaptamine, and 4-N-methylaaptamine have been identified in *Aaptos* sp. The two new aaptamin-related compounds have been found from the sponge *Aaptos aaptos* from Randayan Island, West Kalimantan, Indonesia namely methyl 3-(8,9-dimethoxy-4*H*-benzo[*de*][1,6]naphthyridin-4-yl)propanoate and 8,9-Dimethoxy-4*H*-benzo[*de*][1,6]naphthyridine-5,6-dione. The structures of the compounds were unambiguously elucidated by extensive 1D and 2D NMR experiments and by accurate mass measurement.

5. Acknowledgements

We thank to Directorate of Higher Education Indonesia and AusAID for an Australian Partnership Scholarship (to IWM). The assistance of Dr Tri Le (NMR), Graham McFarlane (MS) and Rachmaniar Rachmat, Indonesian Institute for Science, Jakarta, Indonesia for taxonomic identification is gratefully acknowledged.

6. References

[1]. Utkina, N. K.; Denisenko, V. A.; Pushilin, M. A. (2009), *Tetrahedron Letters 50* 2580–2582.
[2]. Blunt, J. W.; Copp, B. R.; Hu, W.-P.; Munro, M. H. G.; Northcote, P. T.; Prinsep, M. R. (2009), *Nat. Prod. Rep. 26*, 170–244.
[3]. von Nussbaum, F.; Schumann, S.; Steglich, W. (2001), *Tetrahedron 57*, 2331-2335.
[4]. Bowling, J. J.; Pennaka, H. K.; Ivey, K.; Wahyuono, S.; Kelly, M.; Schinazi, R. F.; Valeriote, F. A.; Graves, D. E.; Hamann, M. T. (2008), *Chem Biol Drug Des 71*, 205–215.
[5]. Herlt, A.; Mander, L.; Rombang, W.; Rumampuk, R.; Soemitro, S.; Steglich, W.; Tarigan, P.; von Nussbaum, F. (2004), *Tetrahedron*, *60*, 6101–6104.
[6]. Nakamura, H.; Kobayashi, J.; Ohizumi, Y. (1982), *Tetrahedron Lett*, *23*, 5555-5558.
[7]. Shen, Y. C.; Chein, C. C.; Hsieh, P. W.; Duh, C. Y. (1997), *J. Fish. Soc. Taiwan 24*, 117-125.
[8]. Bergquist, P. R.; Cambie, R. C.; Kernan, M. R. (1991), *Biochem. System. Ecol. 19*, 289-290.
[9]. Park, S. K.; Kim, S. S.; Park, J. D.; Hong, J. S.; Kim, I. K. (1995), *J. Korean Chem. Soc.*, *39*, 559-563.
[10]. Calcul, L.; Longeon, A.; Mourabit, A. A.; Guyot, M.; Bourguet-Kondracki, M.-L. (2003), *Tetrahedron 59*, 6539–6544.
[11]. Pettit, G. R.; Hoffmann, H.; McNulty, J.; Higgs, K. C.; Murphy, A.; Molloy, D. J. (2004), *J. Nat. Prod. 67*, 506-509.
[12]. *Muhammad, I.; Dunbar, D. C.; Takamatsu, S.; Walker, L. A.; Clark, A. M. (2001), J. Nat. Prod. 64* 559-562.
[13]. Zhang, Y.-J.; Kong, M.; Chen, R.-Y.; Yu, D.-Q. (1999), *J. Nat. Prod. 62* 1050-1052.

The Effect of Refugia Blog to Spatial and Temporal Distribution of Natural Enemies in Rice Field

Asyik Nur Allifah AF [1], Bagyo Yanuwiadi [2], Zulfaidah P. Gama [2], Amin S. Leksono [2]

[(1)] Magister Program, Faculty of Sciences, Brawijaya University, Malang, Indonesia
[(2)] Department of Biology, Faculty of Sciences, Brawijaya University, Malang, Indonesia

Abstract

The aims of this research were 1) to know the effect of refugia blog to the amount and type of natural enemy visitors of refugia blog, 2) to know the effect of refugia blog to the pattern of spatial and temporal distribution of natural enemies. The study has been conducted on the farmland in Sekarpuro Pakis, Malang regency at May to October 2010. Refugia collections consist of a group of four plant species (Eupatorium odoratum, Mimosa pudica, Brachiaria mutica, Panicum repens). Refugia blog sized 1x1 m^2. Observations were done as many as 4 periods: the first period were done at 07:00 to 8:00 pm, second period at 9:00 to 10:00 pm. Third period at 12:00 to 13:00 pm and the fourth period at 3:00 pm to 16:00 pm. Observation consist of 4 observation plots with spatial 2 m. Length of observation 15 minutes. Observation method used is modification of the "visual control". Analysis was done by factorial design ANOVA. The result of this research showed that natural enemies with the mostly arrived was Coccinellidae family (71.47 ± 5.09), while the fewest was Tettigonidae family (3.53 ± 0.84). Effect of refugia blog showed significantly affect (P<0,05) to temporal distribution and not significantly affect (P>0,05) to spatial distribution of Arthropod in rice field.

Keywords: *refugia blog , spatial and temporal distribution, natural enemies*

1. Introduction

Agroecosystem or agricultural ecosystems are human-managed ecosystems, monocultures and vulnerable to pest attacks [1]. Farming systems that tend to be homogeneous causes decreased plant resistance to insect pests, mainly due to using of pesticides [2].

Intensification of agriculture by the government, consider pesticides as a right step in eradicating the pest species, meaning to kill out with the aim of prevention of pests does not arise. But the reality pesticide caused the emergence of repeatedly pests in agricultural systems, the effect pest resistance, resurgence and other impacts that affect the ecological balance. The ecological approach by exploiting the role of natural enemies is one way to overcome pest attack on the farmland. Natural enemy is one of the components of the ecosystem that determine the balance of the pest population.

Utilization of natural enemies such as predators, parasitoids and pathogens due to several factors such as not to cause pollution, in terms of ecology remain stable, relatively cheap for the long term and produce a balanced state than the state which is indicated when there are not natural enemies and do not work (De Bach, 1979; Stern et al., 1959 in Jumar) [3]. Natural enemies can function effectively if made the procurement of plants that are closely related to natural enemies of the procurement and planting of crops that are often visited and inhabited by insects [4]. Blog refugium is an area that covered several types of wild plants that can provide shelter, food resources or other resources for natural enemies such as predators and parasitoids [5].

As reported by Karindah [6], through the olfactory test percentage interest in adult insects and nympha *Metioche vittaticoles* to weeds likes *Brachiaria mutica* and *Panicum repens* planted in groups (blog) was greater than singly planted. Results of previous research by Widiastutie [7] showed that the combination of wild plants from the Family Asteraceae; *Eupatorium odoratum* and *Bidens pilosa* were preferred by the insect Family Coccinellidae. Consideration of the importance of refugia area then conducted research that aims to know the effects of refugia blog on spatial and temporal distribution patterns of natural enemies on the farmland.

2. Experimental Details

Plants used in this study were *Eupatorium odoratum, Mimosa pudica, Brachiaria mutica, Panicum repens*. Plants were planted in polybags

for the next in place on the corner of the rice fields. Dimension of refugia blog was 1x1 m^2. Observation of insects consists of 4 plots. The distance between plots was 2 m.

Length of observations on each plot was 15 minutes. The observations made were grouped in 4 periods. The period of observation I at 7:00 a.m. to 8:00 pm, period II was held at 9:00 to 10:00 pm. Period III was held at 12:00 to 13:00 pm and the fourth period at 3:00 p.m. to 16:00 pm. Observation method used is the method of "visual control" Observations were made during 15 days. Data were analysed using descriptive statistical method ANOVA with factorial design.

3. Result and Discussion

Types of natural enemies found during the observation consist of five Ordos / Classes, namely Coleoptera, Orthoptera, Hymenoptera, Odonata, and Arachnida. From the 5 Order there were 10 Families / Classes which visited the refugia blog. Family Coccinellidae of the Order Coleoptera showed a dominant number of arrivals during the study with an average of 71.47 ± 5.09 and Tettigonidae Family of the Order Orthoptera showed the number of arrivals was at least with an average of 3.53 ± 0.84 (Table.1 - Appendixes).

Natural enemies with dominant arrival shown by Coccinellidae Family with average of numbers was 71.47±5.09 and least of natural enemies was Tettigonidae Family with 3.53± 0.84 (Table 1). The ability of Coccinellidae Family in response to odors released by one or several of wild plants test suspected determinants of abundance of this Family at each plot observation beside the abundant availability of prey in alternative host. This condition is supported by research of Finlayson et al [8] that the Family Coccinellidae able to compete in the attraction of prey. The dominance of predators is related to the ability to breed rapidly, adaptation and competitiveness, suitability and breadth of prey, the ability to find prey quickly, and the ability to prey quickly. During observation of predator from Coccinellidae Family for the pest mainly from type of *Micraspis sp* and *Harmonia sp*, were found at refugia blog and crops. Coccinellidae can prey pest counted 2.83 WBC / day. Predator can prey more than one host in finishing its one life cycle so that predator can pass off its life without depended one host.

Based on statistical analysis (α = 5%) spatial and temporal distribution patterns showed that F > F table the insects showed distribution spatial or temporal patterns of variation occurred even between the spatial and temporal interactions (Table 2 - Appendixes). In this research, there are 5 types of natural enemies that show patterns of spatial and temporal patterns (F > F table) namely Coccinellidae, Libellulidae, Tetragnatidae, Tettigonidae, Formicidae.

Differences in the ability of insects to respond to the smell (odor) emitted by the test plants is predicted to affect of the average number of visits of insect visitors to the blog so that affects the pattern of distribution. In the process of habitat selection of insects always consider the availability of food, avoidance of competitors and the avoidance of predators [8]. Each type of Arthropods has characterized morphology, anatomy, behavior and resource needs in different environments. Distribution of insects closely related to the life cycle, morphological type, and climatic conditions at the time of the type chosen its habitat besides the time looking for prey, reproduction and host recognition.

Diversification of plants (refugia blog) suspected has a significant effect on temporal and spatial dispersion, in addition to alternative resources generalist predator besides density and species richness [9]. The ability of each individual insect to spread in time and space is a combination of certain physical properties, biomorphology and environmental conditions, so that in one type Arthropods can show different spatial and temporal variation.

Based on the analysis of variance, refugia blogs had no significant effect (P > 0.05) to average numbers of natural enemies that visiting to refugia blog between plots (Table 2). This condition suspected to relate to behavior of dispersal from each Arthropod which could probably exceed from furthermost plot (8m). Competition in activity and seeking process of host plants also influence distribution pattern of Arthropod each plot. There is not according to host plants also influence distribution pattern which random from insect so that showed the amount not significantly of each plot. Effect of refugia blog showed significant effect (P<0,05) at fourth period. This condition suspected to relate with activity from each insect also ability in recognizing wild plant as alternative host.

In optimum temperature, natural enemy activity is increased and at other temperature it will decrease. According to Jumar [3], the minimum temperature is 15ºC, optimum temperature is 25ºC, and maximum temperature is 45ºC. Insect perceived to have the character of diurnal. This active insect in the day time visit flower, putting down of egg or eat the parts of crop and others. Factor of microclimate in the form of light, is also influences insect activity in a

period of finding opposite gender for mating and also of the prowl activity [3].

4. Conclusion

Coccinellidae Family showed dominating amount of arrival (71.47 ± 5.09), while the fewest is Tettigonidae Family (3.53 ± 0.84). Effect of refugia blog showed significant effect ($P<0.05$) to temporal distribution and not significantly affect ($P>0.05$) to spatial distribution of Arthropods in rice field.

5. Acknowledgements

---

6. References

[1]. Tobing, M.C., D. Bakti and Lisnawita (2009), *The research of insecticide marketing for vegetable and horticultural crops in Karo District, Sumatera Utara*. Dept. Plant Pests & Diseases, Fac. Agric. Univ. Sumatera Utara, 65.

[2]. Altieri and Nicholls (2004), *Biodiversity and Pest Management in Agroecosystems*. Food Product Press. 236.

[3]. Jumar (2000), *Entomologi Pertanian*. Rineka Cipta. Jakarta.

[4]. Sharon S. White, Karen A. Renner, Fabian D. Menalled, and Douglas A. Landis (2007), Feeding Preferences of Weed Seed Predators and Effect on Weed Emergence. *Weed Science,* 55:606–612.

[5]. Nentwig (1998), *Weedy Plant Species and Their Benefecial Arthropods: Potential for Manipulation in Field Crops. In. C.H Pickett and R.L Bugg (ed) Enhancing Biological Control, Habitat Management to Promote Natural Enemies of Agricultural Pest.* University of California Press. Berkeley. Los Angles. London. 49 – 71

[6]. Karindah, S. (2006), *The Use of Weed Plant Species to Enhance The Conservation of Metioche vittaticollis (Stai) (Orthoptera: Gryllidae), Ageneralist Predator of Rice Hopper.* Dissertation. Agricultultural Science Pest and Plant Disease. Brawijaya University.

[7]. Widiastuti (2000), *Uji Preferensi Serangga Coccinelidae Pada Tanaman Familia Asteraceae.* Skripsi. FMIPA. Universitas Brawijaya. Malang

[8]. Leksono, A.S. (2007), *Ekologi Pendekatan Deskriptif dan Kuantitatif*. Penerbit Bayumedia Publishing. Malang.

[9]. Andow, D.A. (1985), Predation in diversified agroecosystems: relations between a coccinellid predator coleomegilla maculta and its food. *Journal of Applied Ecology*. 357-372.

Appendixes

Table 1. Average numbers of individual family that visiting to refugia blog

No	Order	Family	Numbers of individual	X
1	Coleoptera	Coccinellidae Staphylinidae Carabidae	1072 289 68	71.47 ± 5.09 19.27 ± 2.53 4.53 ± 0.95
2	Odonata	Libellulidae Coeagrionidae	476 125	31.73 ± 4.99 8.33 ± 1.43
3	Hymenoptera	Brachonidae Formicidae	150 240	10.00 ± 2.57 16.06 ± 2.85
4	Orthoptera	Tettigonidae	53	3.53 ± 0.84
	Class	**Family**		
5	Arachnida	Lycosidae Tetragnatidae	68 56	4.53 ± 0.95 3.73 ± 0.81

Table 2. Data of spatial and temporal distribution patterns of Arthropods

Variant sources	**$F_{count\ (Plot)}$**	**$F_{count\ (Period)}$**	**$F_{interaction\ (Plot\ *Temporal)}$**
Individual variants			
Coccinellidae	0.654^{ns}	6.054*	0.376^{ns}
Staphylinidae	0.059^{ns}	0.935^{ns}	0.267^{ns}
Carabidae	1.443^{ns}	0.605^{ns}	0.707^{ns}
Libellulidae	4.173 *	15.707*	1.371^{ns}
Coeagrionidae	0.603^{ns}	0.830^{ns}	0.442^{ns}
Brachonidae	0.361^{ns}	1.016^{ns}	0.239^{ns}
Formicidae	0.721^{ns}	4.400*	0.444^{ns}
Tettigonidae	2.763 *	8.288*	0.577^{ns}
Lycosidae	1.840^{ns}	1.469^{ns}	1.012^{ns}
Tetragnatidae	1.346^{ns}	3.694*	0.864^{ns}
Natural enemy	2.146^{ns}	5.755*	0.279^{ns}

*) significant
ns) insignificant

F table $_{(0.05)}$ = 2.90

Airborne Measurements of Particle Concentration from Biomass Burning in Northern Territory Australia

Arinto Yudi Ponco Wardoyo

Physics Deparment, Faculty of Science, Brawijaya University
Email : a.wardoyo@ub.ac.id

Abstract

Airborne measurements of particle number concentrations from biomass burning were conducted in the Northern Territory, Australia, during June and September campaigns in 2003, which is the early and the late dry season in that region. The airborne measurements were performed along horizontal light tracks, at several heights using an aircraft Beech Super King B200 in order to gain insight into the particle concentration levels and their variation with height within the lower boundary layer (LBL), upper boundary layer (UBL), and also in the free troposphere (FT). The particle measurements were conducted using a TSI Scanning Mobility Particle Sizer (SMPS) that was mounted in a single, two levels, 19-inch rack, with anti-vibration mounts, and was located on the left hand side of the aircraft. The measurements found that the concentration of particles during the early dry season was lower than those in the late dry season. For the June campaign, the concentration of particles in LBL, UBL, and FT were (685±245) particles/cm^3, (365±183) particles/cm^3, and (495±45) particles/cm^3, respectively. For the September campaign, the concentrations of particles were found to be (1233±274) particles/cm^3 in the LBL, (651±68) particles/cm^3 in the UBL, and (568±70) particles/cm^3 in the FT.

Keywords : *Airborne measurement, particle concentration, biomass burning.*

Zeolite Carbon Composite Polyvinylchloride-Coated Wire Electrode for Lead Detection as an Environmental Sensor

Atikah [1], Qonitah F [2], Chasan Bisri [3], Bagus Setiawan [4], Tyas Karya P [5]

[1,2,3,4,5] Department of Chemistry, Faculty of Science, Brawijaya University, Indonesia
(atikadhikara@yahoo.com)

Abstract

The composite carbon –polyvinyl chloride (C-PVC) with zeolite as an ionophore in a selective and sensitive coated wire electrode (CWE) for lead determination by potentiometric method is demonstrated. The membrane's sensor consist of mixture an active material of zeolite from Turen was activated by impregnated with HCl 2N, active carbon to improve conductivity, polyvinylchloride (PVC) and dioktilphtalate (DOP) as a plasticizer = 31.3:15.6:6.3:46.9 (% w/w) dissolved in tetrahydrofuran (THF) solvent (1:2 w/v). The characterization of the basic properties of sensor included: sensitivity and linearity of response (detection limit), response time, influence of pH, soaking time, selectivity against foreign ions and also life time. The sensor shows a good Nernstian slope of 29.03 ± 0.33 mV per decade in wide linear range concentration from 1.0×10^{-4} to 1.0×10^{-1} M for $Pb(NO_3)_2$.The detection limit of this electrode 4.0×10^{-5}M of $Pb(NO_3)_2$, and was found to be very selective towards Cu (II) Cd(II) and Hg(II) ions, and usable in pH range of 3.0 – 7.0, soaking time of 10 minutes, fast response time approximately 30 second. The electrode is reproducible and stable for a period of three months. This kind of CWE was successfully applied in determination of lead in industrial wastewater and river's water as real sample and their result was compare to standard Atomic Absorption spectrophotometric method. In addition, the lead CWE was simpler and faster than the spectrophotometric method.

***Keywords**: C-PVC, CWE, zeolite, lead, wastewater.*

1. Introduction

The quick determination of minute quantities of ionic species by simple methods is of special interest in analytical chemistry. Construction and application of ion selective electrode (ISE) as a potentiometric sensor offers interesting advantages such as simplicity, speed, relatively fast response, low cost, wide linier dynamic range and ease of preparation and procedures, makes it suitable for routine analysis. From the instrumentation stand point, it is possible for miniaturization and determination of sample in flow analysis [1]. These characteristics have inevitably led to the preparation of numerous sensors for several ionic species, and the list of available electrodes has grown substantially over the past decade [2].

Lead is an extremely stable element *categorized* as heavy metals. It is very toxic to human and animals, which are used in paint, electroplating and gasoline additives and chemical industries, and thus occur widely in environment, can contaminate air, food, water, or soil. Exposures to even small amounts of lead over a long time can accumulate to reach harmful levels. Lead can adversely affect the developing nervous system in children, including learning disabilities and reduced fertility in women [3]. The determination of lead(II) ion in wastewater has been carried out directly or indirectly by a variety of instrumental methods include spectrophotometry, atomic absorption spectrometry and ion chromatography. However, most of these methods are susceptible to interference from different cationic or anionic species and either time-consuming or need sophisticated instruments and cannot use in the field of trace analysis. Thus the development of convenient direct methods for the assay of lead(II) ion in wastewater samples is of urgent need, and it is for this reason that extensive effort has been made to develop highly selective lead(II) electrodes [4-8]. It is because the potentiometry with ion selective electrodes is in principle particularly well suited to speciation studies because of its selective response to free ions in aqueous solutions.

Most of the reported lead ion selective electrodes (ISE) are disc type *i.e.* PbS based solid state ISEs, has complicated construction with the inner reference electrode system, is to interfered by Hg^{2+}, Ag^{+} and Cu^{2+}. We have recently reported a number of highly selective and sensitive coated wire-PVC – membrane ion selective electrode for

lead ion using bentonite as an ionophore [7] and diamine compound [6] are innovation in the field of potentiometric sensor, was made by incorporating the membrane deposited directly onto a metal wire electronic conductor to replace the inner reference electrode system. Their characteristics of basic properties are equal to and occasionally better than the disc type conventional ones. In this paper, we wish to introduce a highly lead(II) ion selective potentiometric sensor based on activated zeolite as ion exchanger membranes to overcome interference from such common contaminants as Hg^{2+}, Ag^{+} , Cd^{2+} and Cu^{2+} ions in the wastewater samples for the direct determination of lead(II) ion without the need for prior separation steps, for monitoring lead(II) ion. However, in comparison, only a few recent report on the ion exhcange-based polymeric membrane lead(II)$^{-}$ ion selective electrodes are available.

During the last decade, a number of studies have focused on properties of functionalized natural zeolite, a relatively new class of an adsorbent, catalyst and ion exchange. The abilities of natural zeolite as ion exchanger have been assessed using different methods and techniques. It was also shown that natural zeolite (bentonite) can be used as potential ionophores for the preparation of ion selective-sensors [7].

Recently, the application of functionalized activated zeolite as ionophores in Pb^{2+} ion selective electrodes was investigated. Many ion selective electrodes (ISEs)'s membrane have been constructed employing various ion exchange as well as neutral and charged ionophores as sensing materials with excellent selectivity for cations [9]. The potentiometric selectivy coefficients of ISEs sensitive to inorganic cation have been reviewed in detail. The application of function so far, several experimental studies have demonstrated that the generation of a membrane potential of those type of ISEs could be attributed to perm selective ion transport across the liquid membrane/solution interface, *i.e.*, charge separation through a preferential uptake of a primary ion by a sensing element in the liquid membrane, leaving its hydrophilic counter ion in an aqueous sample solution and usually exhibit the Hofmeister pattern with the largest selectivity to lipophilic cations [9,10].

2. Experimental Details

Apparatus and emf measurements

All potential measurements were performed using the following assembly: Hg, Hg_2Cl_2 (Sat'd)//sample solution/PVC –C membrane/Pt electrode. A pH-meter (Fisher E 520) was used for potential measurements at 25°C ± 0.5ºC. The activities of metal ions in the aqueous phase were calculated according to the Debye–Hückel approximation.

Reagent and solution

Natural zeolite derived from Turen, Malang was activated by impregnated using HCL 2N is use as ionophore, polyvinyl chloride (PVC) of high molecular weight and dibutyl phthalate (DBP) as a plasticizer were purchased from sigma, tetrahydrofuran is products from Merck. Platinum wire (99.9% ; ∅ 0.5 mm) is products from Aldrich and RG-58 Coaxial cable as connector ISE to mV potentiometer. All other reagent used were of analytical reagent grade, and doubly distilled water was used throughout. $Pb(NO_3)_2$; NaOH; Phosphoric Acid conc.(85%); Hydrochloric acid conc. (36%); $CuSO_4$, $Hg(NO_3)_2$, $CdCO_3$.

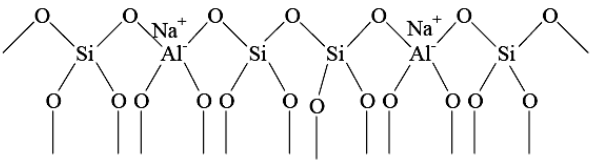

Figure 1. Structure of the zeolite ionophore.

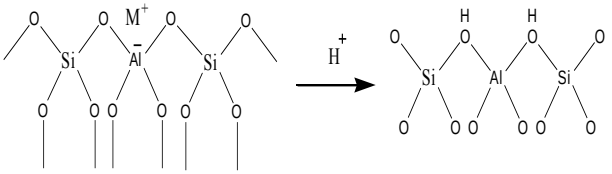

Figure 2. Structure of the activated zeolite ionophore.

Construction and calibration of the electrodes

The membranes solution was prepared by dissolving 2 g activated zeolite, 1 g PVC, 3 g DOP plasticizer and 0.4 g active carbon in THF solvent (1:2 v/w). This solution was deposited directly onto a platinum wire approximately 0.5 mm in diameter and 10 cm in length whose tip had been melted in flame to form a spherical button was soldered to a length of RG-58 coaxial cable, and the solvent was evaporated for approximately 30 minutes and then allowed to stand overnight in the oven at 50ºC. A membrane was formed on the platinum surface and the electrode was allowed to stabilize overnight. Prior to use the electrode was initially conditioned by soaking it overnight in a 0.1M solution of $Pb(NO_3)_2$ to be measured. When not use, the electrode was store in air between use and

reconditioning immediately before using by soaking for at least 1 hour in a 0.1M solution of $Pb(NO_3)_2$. The utility, composition of polymer membrane, respon characteristic, and selectivity of Pb(II) - coated wire electrode (CWE) were investigated. The electrode potential measurement was made under constant conditions by taking 25 mL of solution for each measurement in a thermostatic cell at 25 ± 0.5ºC, immersing the electrode to a constant depth in the solution, and stirring at a constant rate by means of a magnetic stirring bar. Potential measurement was carried out from low concentration to high concentration. The electrode tip was rinsed with de-ionized water and then immersed in one of the standard solution.

Procedure for the determination of lead(II) ion in waters

The well water samples taken from Klayatan (K) and Sumbersari (S) area, the electroplating industrial wastewater samples taken from Landungsari (L) and Blimbing (T) covered when taking the survey. River water samples taken from 10 points on the flow of upstream of the Brantas river basin base on width and depth of the river Brantas namely: (1) Source Brantas, (2) Coban Talun dam, (3) Bridge Brantas, (4) Bridge Pendem, (5) Bridge Dinoyo, (6) Bridge Bumiayu, (7) Bridge Kedung Pedaringan, (8) Up Stream Sengguruh dam, (9) Bridge Sengguruh and (10) Reservoir Karangkates. The water samples covered from the left side, center and right of the river flow in each sampling area at the time of survey. The results of determination of lead(II) on both the SSA and the potentiometric method using sensors Pb(II) tested for their accuracy and precision

3. Result and Discussion

Influence of membrane composition

The different aspect of membrane preparation based on the activated zeolite as ionophore containing different PVC /plasticizer/active carbon ratios were mix in THF solvent (2:1 ratio v/w) were studied and the results are summarized in Table 1.

Table 1 Optimization of membrane ingredients

No	Membran composition				Slope/mV decade^{-1}
	Zeolite	PVC	Active carbon	DOP	
1	3	1	0.4	2	27.8 ± 0.98
2	2	1	0.4	3	29.06 ± 0.3
3	1	1	0.4	4	23 ± 1.69

It is obvious from Table 1 revealed that the amount of ionophore, the nature of solvent mediator, the plasticizer/PVC ratio significantly influence the sensitivity of ion selective electrodes. It should be noted that the nature of plasticizer influences both the dielectric constant of the membrane and the mobility of ionophore and its complex with Pb(II) ion [11].Thus, based on the result obtained on the optimization of the membrane composition, the membrane 2 with the optimized composition of activated zeolite:PVC:DOP: active carbon percent ratio (w/w) of 2:1:3:0.4 was selected for preparation the polymeric membrane electrode for lead(II) ion.

Response Characteristics

The resulting five prepared lead(II) CWE are small, its construction simple. The slope and detection limit of the electrode were evaluated from repeatedly carrying out calibration graphs between 10^{-8} and 10^{-1}M. The calibration parameters thus obtained are included in Figure 3.

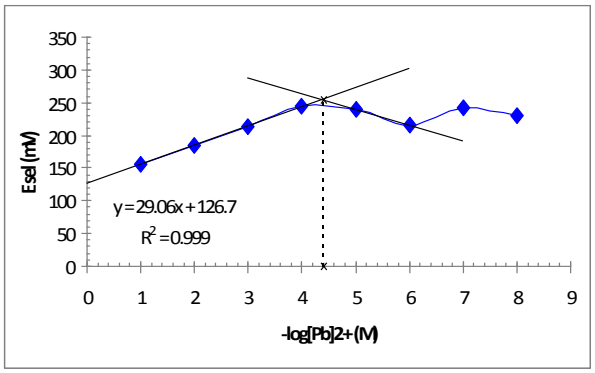

Figure 3 Potential response of the electrode prepared with composition 2 in Table 1 for Pb^{2+}-ion selective electrode.

As an example, Figure 3 shows the variation of the cell potential as a function of the logarithm of the concentration of lead ions for the lead (II) CWE prepared by composition 2. This membrane with a composition of 31.3% activated zeolite, 15.6% PVC, 46.9% DOP, 6.3% active carbon dissolve in 2:1 v/w THF solvent gives the best characteristics with a slope of 29.03 ± 0.33 mV decade^{-1} in the concentration range of 1.0×10^{-4} to 1.0×10^{-1} M for $Pb(NO_3)_2$. The detection limit of this electrode The limit of detection determine from the intersection of the two extrapolated segments of the calibration curve was found to be 4.0×10^{-5}M of $Pb(NO_3)_2$. The response time was obtained from dynamic response curves corresponding to Pb^{2+} cocentration step to obtain a 10 times more concentrated solution. An average response time of about 30 s was found in the entire examined

concentration range and also soaking time of about 10 minutes. The plateau of the variation of electrode potential *versus* log[Pb^{2+}] at higher concentration of Pb^{2+} (Figure 2) can be explained by considering the saturation of the test solution/ membrane interface by the lead complexes.

The effect of pH

The effect of the pH (in the range 2.0 – 8.0) of the test solutions on the potential response of the sensor was investigated. The results are shown in Figure 4.

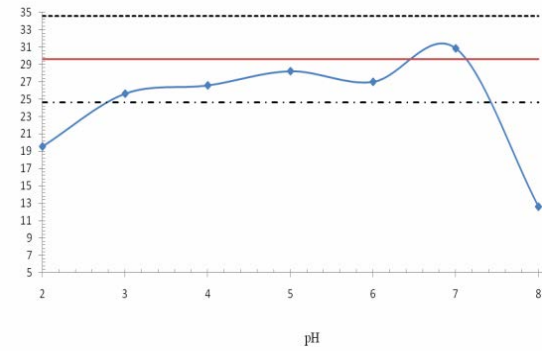

Figure 4 Electrode response of the lead-ion selective electrode to the pH of sample solutions at 10^{-4}-10^{-1} M of Pb^{2+}. The membrane conditions are the same as Figure 3.

The potential is independent of pH and remained constant in the range 3.0 – 7.0. However, drastic potential changes are observed when the pH value higher than 7 or lower than 3. This observation can be attributed to the formation of lead hydroxide in solution or when the pH is less than 3.0 is a consequence of the electrode response to the hydrogen ions.

Selectivity of the electrode

Selectivity of the electrode towards lead ions over some divalent ions was tested using the fixed interference method. The concentration of interfering anion was fixed at 10^{-3} M. Selectivity coefficient of the Pb(II) CWE were determined by fitting calibration data to the Nicolskii-Eisenman equation for mixed –ion and the results are summarized in Table 2. It is seen from that electrode is very selective to Pb^{2+} ion and the observed selectivity pattern for proposed sensor in order: Pb^{2+}> Hg^{2+}>Cu^{2+} >Cd^{2+} (i.e. selectivity based on lipophilicity and charge density of cations).This reflects the binding abilities of the activated zeolite for cations were tested

Table 2. Potentiometric selectivity coefficient

Ion	K_{Pb}^{2+}, foreign cation
Pb^{2+}	1.000
Cu^{2+}	0.222
Cd^{2+}	0.080
Hg^{2+}	0.508

Application

The new coated wire Pb(II) selective electrode was satisfactorily applied to the determination of Pb(II) as cation in wall, industrial wastewater and Brantas river water sample. The analysis was performed by direct potentiometry using the standard technique. The results compared to those of Atomic Absorption Spectrometric (AAS) analysis. The result obtained is summarized in Table 3. Good recoveries in all matrices were obtained. From this results we can conclude that the proposed sensor could be used in the environmental monitoring of lead(II) ions

Table 3. Determination of lead(II) as $PbCl_4^{2-}$ ion in water sample

Sample of water	ppm Pb found from AAS	Recovery (%)	ppm Pb found from potentiometric	Recovery (%)
Well- K	0.046	98.60	0.06	96.20
Well- S	0.219	98.60	0.23	96.20
Wastewater T	0.109	99.64	0.51	99.96
Wastewater L	0.367	99.90	0.56	99.10
River R-1	0.068	98.40	0.33	97.52
River R-2	0.773	98.64	0.47	96.20
River R-3	1.217	97.90	0.33	96.20
River R-4	0.483	98.40	0.29	97.10
River R-5	0.275	98.60	0.40	95.60
River R-6	1.005	98.60	0.35	96.50
River R-7	0.909	98.60	0.33	96.20
River R-8	1.033	98.60	0.44	96.40
River R-9	1.269	98.60	0.34	96.10
River R-10	2.227	98.60	0.37	96.20

To determine whether the SSA standard methods can be replaced by potentiometric method using Pb(II) CWE in water samples, the measurement results of Pb in the water by the SSA and potentiometric method (Table 3), their correlation performed tested using the regression equation. As the x-axis is the SSA standard method and the y-axis is the potentiometric method. Calculation results obtained by the regression equation for water samples are:

Potentiometric method = 0.1007 + 1,037 SSA (1)

Equation 1 yield curve slope (b) = 1.037; point of intersection, intercept (a) = 0.100 and regression coefficient (r) = 0.880, reveal that the potentiometric method has a good correlation with the SSA standard method. Results standard deviation calculation (S) obtained: $S_{v/x} = 3.3 \times 10^{-5}$; $S_a = 2.9.10^{-10}$ and $S_b = 0.0104$. By using the appropriate t value for the degrees of freedom (N-2) at 95% confidence limits were obtained 2.18 value of crossover point accuracy (a) and slope (b) as follow: $a = a \pm t.S_a = 0.1007 \pm 6.32.10^{-10}$; $b = b \pm t.S_b = 1.037 \pm 0.023$.

It is mean that intersection of the results are not significantly different from the ideal value of 0 (both methods have the same error) and the slope of the results are not significantly different from the ideal value of 1 (sensitivity of both methods are same). The value of a = 0.1007 was still within the limits of the interval $0 \pm aS_a$ and value of b = 1.060 was still within the limits of the interval 1. It is means that both methods are tested on Pb measurement applications in water samples did not show such differences significantly. From this results we can conclude that the prepared sensor could be used in the environmental monitoring of lead(II) ions in water samples as a alternative method replace to standard atomic absorption spectrophotometric (AAS) method.

4. Conclution

The membrane compositions influence the Nernstian character of Pb sensor. The membrane with the composition of of 31.3% activated zeolite, 15.6% PVC, 46.9% DOP, 6.3% active carbon dissolve in 2:1 v/w THF solven can be use as chemical sensor for lead(II) ion in the construction of coated wire Pb(II) ion selective electrode which has optimum characteristics for lead(II) ion analysis. This kind of CWE was successfully applied in determination of lead in well, industrial wastewater and of upstream of the Brantas water river basin analysis in concentration ranging from 0.0364 - 2.32 ppm provides accuracy of 96.3% and accuracy of 99.0%, replace to the spectrophotometric (AAS). In addition, the lead ISE was simpler and faster than the spectrophotometric method.

5. Acknowledgments

---

6. References

[1]. Wang, J., (2002), Real-time electrochemical monitoring: toward green analytical chemistry, *Acc. Chem. Res*., 35, 811-816.

[2]. Buhlmann, P., E., Pretsch, E., Bakker, (1998), Carrier-based ion selective electrodes and bulk optodes. 2. Ionophores for potentiometric and optical sensors, *Chem.Rev*., 98, 1593-1687.

[3]. Logan, T., (2006), Lead Contamination in Environmental, www.EPA/USA/Ohio Agriculture research and Development Center.

[4]. Zielinska, D., H, Radecka., and J, Radecku., (1998), Ion selective liquid membrane electrode for discrimination of alkyl lead derivatives and inorganic lead ions, *Analytical Science*, 14, 151-155.

[5]. Gholivand, M.B., and A., Mohammadi, (2003), Lead ion selective membrane electrode containing 2,2'-dithiodibenzoic acid as ionophore, *Che. Anal. (Warsaw),* 48, 305.

[6]. Ardakany, M., AA, Ensafy., H, Naeimi., A, Dastanpour and A, Shamlli, (2003), Coated wire-based, new schiff base potentiometric sensor for lead (II) ion , *Russian Journal of Electrocheimistry*, 39, 269-273.

[7]. Izadyar, A., (2004), Bentonite carbon composite polyvinyl-coated wire electrode for lead detection as an environmental sensor, *Russian Journal of Electrocheimistry*, 52, 91-96.

[8]. Yaftian, M.R., S, Rayati., D, Emadi and D, Matt, (2006), A Coated wire-type Lead(II) Ion Selective Electrode Based on a Phosphorylated Calix[4]arene Derivative, *Analytical Science*, 22, 1075-1078.

[9]. Itoh, Y., Y, Ueda., M, Sugawar, M, Katako., H, Sato dan Y, Umezawa, (2006), Nitrogenous synergist induced potentiometric response to metal ions with polymeric liquid membranes containing thenoyltrifluoroacetone as an ionophore, *Analytical Science*, 22, 219-222.

[10]. Kobayashi, F., T, Maki., Y, Nakamura and K, Ueda, (2005), Determination of Cu,Pb, Fe and Zn in plant component polymer of a Hyperaccumulation Plant, *Analytical Science*, 21, 1553-1556.

[11]. Zanjanchi, M.A., A.M. Akbari, K, Tabatabaeian, and G. Zaraei, (2006), Perchlorate-selective polymeric membrane electrode based on a cobaloxime as a suitable carrier, *Sensor and Actuator B*, 113, 304-309.

Geochemical Fractions of Heavy Metals in the Sediment of Brantas River Downstream

Barlah Rumhayati [1], Enco Sukarsa [2,3]

[1,2] Chemistry Department, Faculty of Science, Brawijaya University, Malang, Indonesia
[3] SMAN I Sanggar, Bima, NTB, Indonesia

Abstract

Studies of geochemical fraction of heavy metals in sediment are important to give information of their origin, metals bioavailability and mobility, sediment contamination, and the acting of sediment. Sequential fractionation of Pb, Cu and Zn in Brantas River Downstream has been carried out for four fractions, i.e ELFE (Easily Leachable and freely exchangeable), AR (acid reducible), OO (oxidisable-organic), and RF (resistant fraction). Six sediment samples were taken from three locations (A, B, C) by using sediment cores. The sediments were sliced up to 5 cm, homogenized, sequential extracted and analyzed using atomic absorption spectrophotometer. Results showed that Cu and Zn in the sediment dominant than Pb. Cu and Zn were found as all fractions while Pb was found as OO and resistant fractions. The Brantas River was polluted with Pb and Zn while Cu was naturally available in the sediment.

Keywords*: sequential fractionation, heavy metals, anthrophogenic source, bioavailability.*

1. Introduction

Some heavy metals are essential elements for living organism but its accumulation in the organisms could induce serious problems of health. Source of heavy metals in water system may from anthropogenic activities and industrial waste. These metals may accumulate in the suspended particulate matter and settle on the bottom sediment [1] which is affected by many factors, such as pH of sediment, organic matter content and cationic exchange capacity of sediment. In a case of low concentration of metals in water column, the metals in sediment will be diffused into water column and cause eco-toxicological problems. In sediment, heavy metals are present in different geochemical forms which determine their mobilization capacity and bioavailability [2]. Determination of total metal concentration is not sufficient to give information about their environmental behavior because only a fraction of the total metal is available for biological processes. Information of the origin of the metals will not be also provided by assessment of total heavy metals concentration [3,4].

Brantas River downstream is one of inlet river for Sutami reservoir in Karangkates. The reservoir has been used for irrigation, power plant, and fisheries for decades. Eco-toxicological problems in one of its inlet rivers will cause serious problem in reservoir. Therefore, it is needed information of geochemical fractions of heavy metals in the inlet river of Sutami reservoir.

2. Experimental Details

Samples of sediment were taken from three locations (A, B and C) of Brantas River (Figure 1) in Sumberpucung, Karangkates, East Java. The distance between two locations was 20 m. Samples were taken using a sediment core made from acrylic with length of 30 cm and 8 cm in diameter. The top of 5 cm of each sediment sample was sliced and homogenized. The samples were characterized chemically and physically. Geochemical fractions of Pb, Cu and Zn in the sediments were obtained by using the modified sequential extraction technique [5,6]. The four fractions considered, the extraction solutions and the condition employed were:

1. ELFE (Easily leachable and freely exchangeable) fraction: about 10 g of sample was shaken for 3 h with 50 ml of 1.0 M ammonium acetate (NH_4CH_4COO), pH 7.0 at room temperature;
2. AR (acid reduction) fraction: the residue of ELFE fraction was continuously shaken for 3 h with 50 ml of 0.25 M hydroxyl ammonium chloride ($NH_2OH.HCl$) acidified to pH 2 with HCl, at room temperature;
3. OO (oxidisable organic) fraction: the residue of AR fraction was oxidized with 15 ml of hydrogen peroxide in a water bath at 90ºC. After cooling, the mixture was shaken for 3 h with 1.0M NH_4CH_3COO acidified to pH 2.0 with HCl at room temperature;
4. Resistant fraction: the residue of OO fraction was digested with 40 ml of the

mixture of concentrated nitric acid and perchloric acid for 3 h.

All of the extracts then were centrifuged and the supernatants were filtered using a disposable syringe consisted of *polyethersulfon* membrane with pore size of 0.45 µm and 2.5 cm diameter. Concentration of metals were measured using AAS at their specific wavelength. The sum of ELFE, AR and OO fractions were categorized as non resistant fraction.

3. Result and Discussion

Brantas Rivers in Sumberpucung could receive heavy metals from domestic, sand mining and domestic activities as anthropogenic source besides its nature source from weathering of igneous and metamorphic rocks and decomposition of biota detritus [5]. From three locations of sampling, all sediment has been characterized as sandy clay sediment which could consist of mineral Illit and Chlorit. Cationic exchange capacity (CEC) and other chemical properties of all sediment samples were depicted in Table 1.

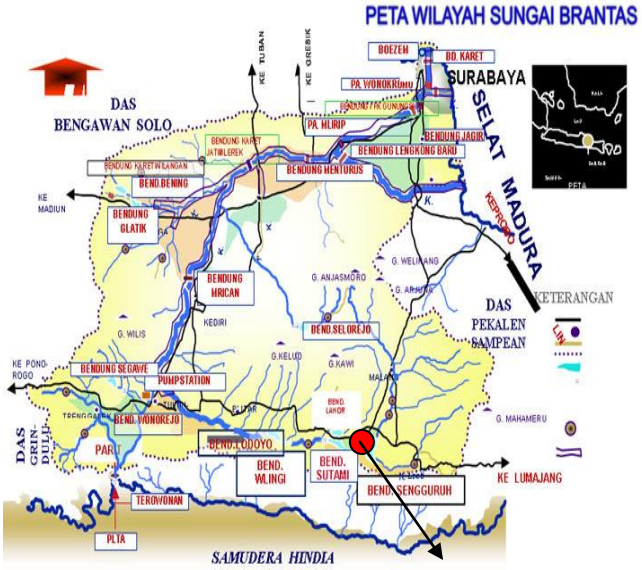

Figure 1. Sampling location in Sumberpucung

At pH from 5.8 to 6.7, all of investigated heavy metals could be as ionic species in the sediment porewater and exchanged with cationic exchanger sites of mineral. Other ―pool" of the metals in sediment were within organic matter such as humic acid and fulvic acid and in the particulate phase adsorbed to iron (III) or manganese (IV) (oxy)hydroxides and to a lesser extent to sandy clay minerals. From Fig. 2, it could be seen that Cu and Zn were more dominant than Pb in all fractions and all sampling location. It also could be seen that Pb was mostly found as OO and FR fractions while Cu and Zn were found in all fractions. Distribution of all metal fractions in all location was high for all metals with exception for AR fraction of Cu and Zn in location C. In all location, it was found that ELFE fractions were lower than other fractions. It means that only a few amounts of Pb, Cu and Zn were presented in pore water sediment. In other word, the Brantas River sediment could act as a sink for Pb, Cu and Zn where the metals were bound in organic matter or be adsorbed by iron(III) or Mn (IV) oxyhidroxides.

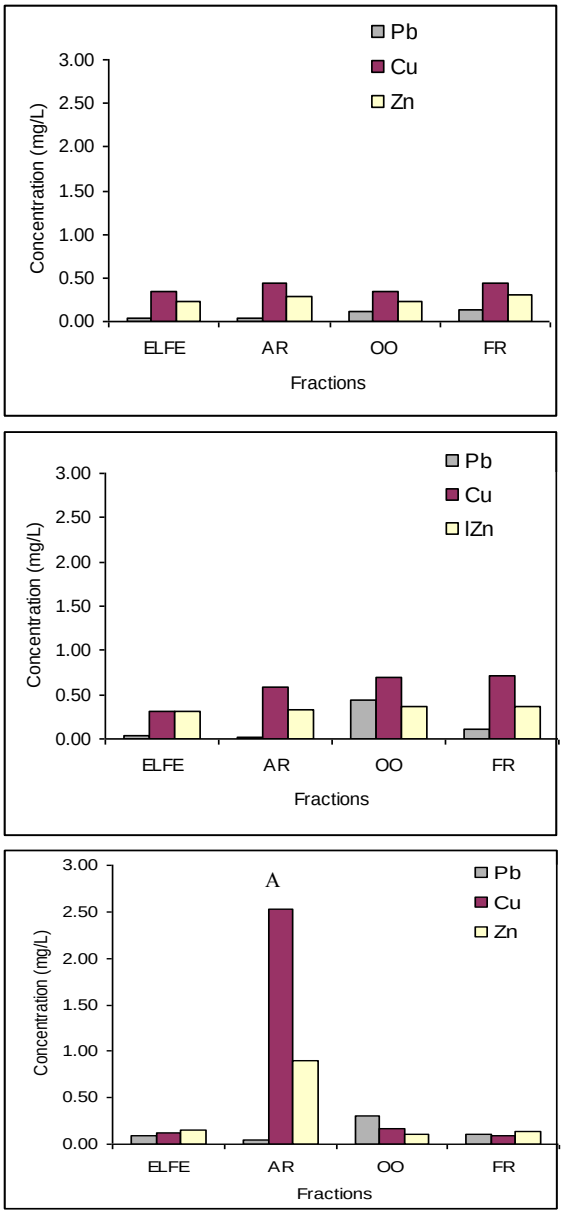

Figure 2. Metal fractions in location A, B, and C

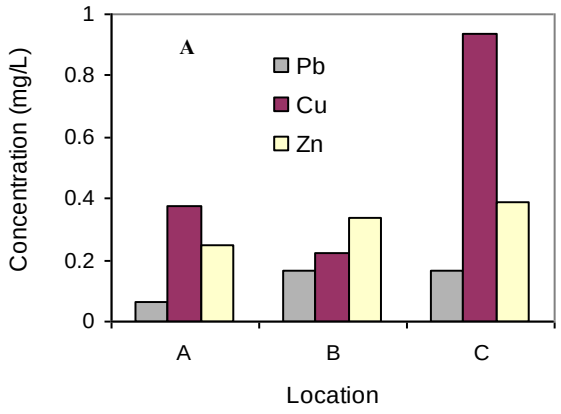

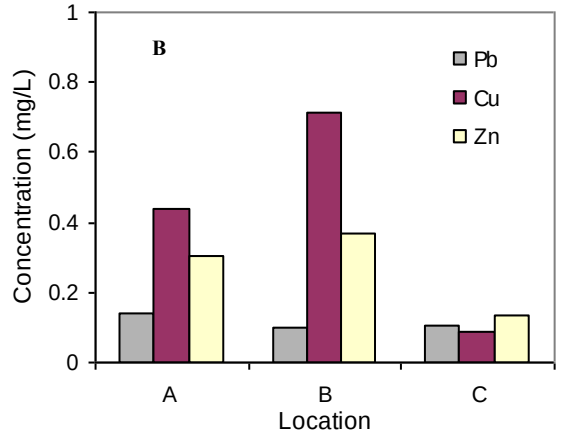

Figure 3. Non resistant (A) and resistant fraction (B) of Pb, Cu and Zn

From Figure 3, it can be seen that in location B and C, Pb was found as non resistant fraction. Cu was found as resistant fraction in location A and B. Zn was found mostly as non resistant fraction. It means that the Brantas River was polluted with Pb and Zn while Cu was naturally available in the sediment. Even though the river has been polluted by heavy metals, the metals were deposited in the sediment.

4. Conclusion

The sediment of Brantas River has been polluted by Pb and Zn but the sediment acted as a sink for these metals while Cu was originally found in the sediment.

5. Acknowledgments

Authors would like to thank you to BPPS for research funding.

6. References

[1]. Gomez-Parra, A., J.M Forja, T.A DelVall, I. Saenz and I. Riba, (2000), Early contamination by heavy metals of the Guadalquiver estuary af ter the Aznalcollar mining spill (SW Spain), *Mar. Poll. Bull.,* 40, 1115-1123.

[2]. Yu, K.C., L.J Tsai, S.H Chen and S.T ho, (2001), Correlation analyses binding behaviour of heavy metals with sediment matrices, *Wat. Res,* 35, 2417-2428.

[3]. Morillo, J., j. Usero and I. Gracia, (2004), Heavy metal distribution in marine sediments from the soutwest coast of Spain, *Chemosphere,* 55, 431-442.

[4]. Ramizes, M., S. Massolo, R. Frache and J.A Correa, (2005), Metal speciation and environmental impact on sandy beaches due to El Savador copper mine, Chile, *Mar. Poll. Bull,* 50, 62-72.

[5]. Badri, M.A and S.R Aston, (1983), Observation on heavy metal geochemical associations in polluted and nonpolluted estuarine sediments, *Environ. Poll.* Series B, 6, 181-193.

[6]. Yap, C.K., M.S Choh, F.B Edward, A. Ismail and S.G Tan (2006), Comparison of heavy metal concentrations in surface sediment of Tanjung Piai wetland with other sites receiving anthropogenic inputs along the southwestern coast of Peninsula Malaysia, *Weland Scie,* 4(1), 48-57.

Appendixes

Table 1. Chemical properties of Brantas River sediment

Location	pH 1:1		Redox potential	Organic carbon	Organic material	Humic Acid	Fulvic Acid	CEC
	H_2O	KCl 1 N				NaOH 0.1 N		NH_4OAC 1N pH 7
			mV	%				Me/100g
A	6.7	5.8	-102	0.80	1.38	0.017	0.006	24.34
B	6,7	5.8	-102	0.81	1.40	0.018	0.008	24.37
C	6.7	5.8	-102	0.82	1.42	0.019	0.009	24.39

A Preliminary Study: Towards Molecular Phylogeny of *Endiandra* (Lauraceae)

Deby Arifiani [1,2], Adi Basukriadi [1], Mien A. Rifai [2], Tatik Chikmawati [3]

(1) University of Indonesia, Jakarta
(2) Research Center for Biology-LIPI, Jakarta
(3) Bogor Agricultural University, East Java
Email: debyarifiani@yahoo.com

Abstract

Endiandra R. Br. is one of large genus of Lauraceae, consisting of more than 100 tree species. Endiandra has an Old World distribution, occurs in Asia, and Australia to Fiji with its absence in Africa. Phylogenetic relationships within Endiandra based on the molecular data is never been done before, therefore in this research we focus on reconstructing its phylogenetic relationships in order to understand species relationships and morphological variation occurred. Morphologically, it is recorded that extra-staminal glands can be presence or absence within Endiandra, so that we would like to know what molecular data will tell us about the relationships among species both with and without extra-staminal glands. Molecular data have been collected from trnL-F (cpDNA), Rpb2 and ITS regions (nuclear DNA). DNA sequences amplified from trnL-F are not variable enough to show the relationships among species of Endiandra. It is expected that molecular data from nuclear DNA will show more variability. Throughout the process of molecular data collection from Endiandra species, some problems have been encountered, from DNA extraction, amplification, purification up to sequencing. It is noted that Endiandra is not an easy plant to work with. The problems and its attempted procedures done in trying to get good result will also be discussed.

Keywords: Endiandra, phylogenetic, ITS regions, glands

The Adsorption Desorption of Ag(I), Pb(II), Cu(II), Cr(III), Ni(II) Toward Mercapto-Silica Hybrid by Coloumn System

Dwi Rasy Mujiyanti [1], Nuryono [2], Eko Sri Kunarti [3]

[(1)] Department of Chemistry, Lambung Mangkurat University, Banjarbaru, South Borneo, Indonesia, 70714
[(2,3)] Department of Chemistry, Gadjah Mada University, Sekip Utara, Yogyakarta, Indonesia, 55281

Abstract

A mercapto-silica hybrid (MSH) adsorbent has been prepared from rice hull ash (RHA) by product of brick burning process in the village of Jambidan, Banguntapan, Bantul through sol-gel process. The synthesis of mercapto-silica hybrid (MSH) was carried out by adding 3M chloride acid solution to a mixture of Na_2SiO_3 solution resulted from RHA destruction with NaOH and 3-(trimethoxysilyl)-1-propanthiol (MPTS) until pH 7 (neutral). The adsorption – desorption of multi metal Ag(I), Pb(II), Cu(II), Cr(III), Ni(II) was conducted in a column system at variation of metal ion concentration. Adsorption-desorption used cartridge solid phase extraction (SPE) with loading sample to the cartridge that contain adsorbent three times and then sample eluted by three eluent : HCl 2M, H_2O, Na_2EDTA 0.1M. Total metal adsorbed and the total metal percentage eluted was calculated based on the analysis with AAS method. The result of adsorption-desorption using silica gel and MSH by column system and desorption by loading three kind eluents respectively showed that the adsorption mechanism was tend to involve hydrogen bond formation.

***Keywords**: Adsorption, desorption, mercapto-silica hybrid (MSH), coloumn system.*

1. Introduction

Adsorption and ion exchange are the most often used processes for heavy metal removal. Adsorption is one of commonly process that always used in order to affect the mobility and fate of contaminants. However, the need for low cost, effective, and re-generable adsorbents materials, which are capable of removing metal ions from wastewater, urges the invention of new adsorbent.

Silica is a particular interest because it does not swell and has a good mechanical strength and thermal stability. Among the promising surface modified silica is the silica-attached organosilanes which are widely used in various technologies [1]. Silica gel can be synthesized through sol-gel process by the condensation of sodium silicate to an acid solution. Silica gel has silanol (Si-OH) and siloxan (≡Si-O-Si≡) that used for many adsorption processes. But on the other hand, the capability of silica gel to adsorb is limited. It is because of the active site, the both of functional groups of silica gel; have to be activated prior to the application in order to absorb the hard metal ions [2].

Hence, the modification of silica gel with organic groups is needed in order to make it capable of adsorbing metal ions even in hard and soft metals ion. By sol-gel process, Cestari *et.al* [2], Airoldi *et.al* [3], Narsito *et.al* [4] has modification silica gel with functional groups and use for adsorption study. The adsorption of the metal can be analyzed by batch and column system.

Some applications of SPE column techniques can be seen in some previous studies. Tokman *et al* [5], review the SPE of Bi(II), Pb(II) and Ni(II) using silica gel modified with 3-aminopropiletoksisilan placed on the column syringe of SPE. The adsorbent was successfully separates Bi(II), Pb(II) and Ni(II) with a recovery ranging between 95-99%. After the application to sea water that also contains metals the recovery was > 95%.

In another study conducted by Khasanah [6], Hartanto [7] and Wulandari [8], modified silica gel using the ligand 3-(trimethoxysilyl)-1-propantiol was used to assess the individual adsorption of metal ions Ag(I), Ni(II), Pb(II), Cu(II) and Cr(III) in water. The modification of silica gel with ligands 3-(trimethoxysilyl)-1-propantiol can increase the adsorption ability of metal Ag(I), Ni(II), Cu(II) and Pb(II). While the metal Cr(III) even able to increase the adsorption capacity up to three to ten times higher than silica gel (SG). While at Mujiyanti, *et.al* [9], studies of multi metals or simultaneous adsorption of Ag(I), Ni(II), Cu(II) and Pb(II) in water by MSH and SG obtained a thermodynamic of adsorption,

include the value of adsorption capacity on the SG with the order: Cu(II) > Cr(III) > Pb(II) > Ni(II) > Ag(I), while on MSH: Ag(I) > Cu(II) > Ni(II) > Pb(II) > Cr(III).

Based on the study of adsorption on the adsorbent of SG and MSH in individual by Hartanto [7], Khasanah [6] and Wulandari [8] for the metals Ag(I), Ni(II), Pb(II), Cu(II) and Cr(III) individually and Mujiyanti, *et.al* [9] in multi metals in water by batch techniques, the researchers continue the study of adsorption-desorption by individual and multi metals in water through the column technique using the adsorbent SG and MSH as charges for EFP column (sorbent).

2. Experimental Details

Chemical and Apparatus

The chemical used in this experiment were the rice hull ash as the main source of silica, 3-(trimethoxysilyl)-1-propanthiol (MPTS) (Aldrich), NaOH, 3-(trimetoksisilil)-1-propantiol, HCl 37%. The source of metal ion solution was (Merck) $Pb(NO_3)_2$, $Ni(NO_3)_2.6H_2O$, $Cr(NO_3)_3.9H_2O$, $AgNO_3$, $Cu(NO_3)_2.6H_2O$.

The absorption measurements were made with a Perkin Elmer 3110 atomic absorption spectrophotometer, equipped with hollow cathode lamps for lead, cuprum, nickel, chrome and silver as well as a deuterium lamp for background collection. The other instruments are infrared spectrophotometer Shimadzu FTIR-8201 PC, X-Ray diffractometer, pH-meter equipped with a combined electrode and the supports apparatus.

Preparation rice hull ash into sodium silicate solution

Rice hull ash was scrapped and sieved to obtain RHA with particle size of 200mesh. A 20 g RHA then cleaned with 150 ml HCl 6M and neutralized with aquadest. The washed RHA was then dried in oven. A 20 g of clean RHA enhanced by 167 ml NaOH 4M, boiled and swirled with the magnet churn. After rather dry, condensation infused by a porcelain cup and melted at 500ºC until 30 minutes. After chilled with 200 ml aquadest and left over night it was filtered with the filter paper of Whatman 42. Filtrate yielded represents the condensation of sodium silicate solution (Na_2SiO_3) that will be ready to use for substance of making adsorbent (silica gel and mercapto-silica hybrid).

Hybridization mercapto compound to the silica by sol-gel process

A 20 ml of condensation of sodium silicate from RHA was poured into plastic glass and added with 8 mL of 3-(trimetoxysilyll)-1-propanthiol (MPTS). The solution was slowly added with HCl 3M while being swirled with magnet churn until gel was formed and the pH is neutral. Gel was left over night then cleaned with aquadest until the pH was neutral. The gel was dried in oven with the pressure reduction of at 70ºC. The gel then scrapped and sieved at 200mesh. Basically, the making of silica gel is analogue with the making of mercapto-silica hybrid, except that there is no addition of MPTS during condensation of sodium silicate.

Adsorption – desorption multi metals of Ag(I), Pb(II), Cu(II), Cr(III), Ni(II)

Our initial procedure is to prepare the adsorption-solid phase extraction column (SPE) and the second filter is in the column. Columns and filters were cleaned first using distilled water and 70% alcohol solution so that it were clean and dry. After the column conditioning process, 0.5 g of mercapto-silica hybrid (MSH) was placed into a plastic bottle and was added with 5 mL 70% methanol and then homogenized for 5 minutes using an ultrasonic (Braunsonic). Once the solution was homogeneous, the adsorbent column was inserted into the EFP to occupy column under appropriate conditions.

The next process was the sample loading. Solution of 20 mg/l of multi metals Ag(I), Ni(II), Pb(II), Cu(II), Cr(III) was gradually inserted into the SPE with each addition was 10 ml. The solution passed through the column was placed in a beaker glass and analyzed further with atomic absorption spectrophotometer (AAS). The column then washed with 10mL distilled water followed by elution using three type of eluent, which are 5ml HCl 2M, 10ml H_2O and 5ml of Na_2EDTA 0.1M. The eluent was then collected and analyzed using AAS. The same procedures was done for both silica gel (SG) using a solution of the mono and multi metals.

3. Result and Discussion

Preparation of silica gel modified by mercapto group

Preparation of modified silica gel was done in two steps, first was the preparation of Na_2SiO_3 solution from RHA and second was the addition of HCl to form gel. The interaction of anion species of silicate with the MPTS compound was anticipated by the oxygen atom protonation at methoxy ($-OCH_3$) group from MPTS compound and continued with the silicate anion attack. The inorganic compound reacted

through SN_2 mechanism. The protonation of oxygen in methoxy group create cation which was attacked by the silicate anion to form siloxane, followed by methanol release. The polymerization continued due to the abundance of methoxy group and the silicate anion.

Adsorption – desorption of multi metals of Ag(I), Pb(II), Cu(II), Cr(III), Ni(II) by silica gel(SG) and mercapto-silica hybrid (MSH) by column system

The study of mono and multi metals, Ag(I), Ni(II), Pb(II), Cu(II), Cr(III), adsorption-desorption through the column toward SG and MSH was initiated by the homogenization of 0.5g adsorbent which then inserted into the column of solid phase extraction (SPE). A 10mL sample solution was passed through the adsorbent inside the column. This procedure was repeated three times; hence the total sample solution run through the column was 30mL which took approximately 30 minute per 10mL to run flow the column. A vacuum pump was used in order to accelerate the sample flow rate. However, the pressure from the vacuum pump was adjusted so that the adsorbent would not run dry due to the suction, which will affect the adsorption capacity.

The column technique by SPE is also used by Sitompul [10] in the purification of aflatoxin sample. The filtrate from each of the flow rate of 10 ml were then collected and analyzed using AAS to estimate the total metal adsorbed. Subsequently, the column was washed with distilled water EFP as much as 10 ml and followed by desorption processes using some solvent (eluent) in sequence: 5 mL of HCl 2M, 10 ml of distilled water (H_2O) and 5 mL of Na_2EDTA 0.1M. Flow rate of each eluent into the sorbent lasts about 5ml/15minutes. The obtained eluent was then analyzed using AAS method to estimate the total metal desorbed. The analysis was done for the individual metal and for the multi metals desorbed from both adsorbents.

Based on Table 1 (Appendixes), the order of adsorption of metals on SG was Cr(III) > Ni(II) > Cu(II) > Ag(I) > Pb(II), while on MSH the order was as follows: Ni(II) > Cu(II) > Cr(III) > Ag(I) > Pb(II). Cr(III) was the highest metal adsorbed by SG while Ni(II) was the highest metal adsorbed by MSH. The existence of active –OH group, which is a strong base of silica gel, is more likely to bind Cr(III) metals strongly, in which known to be one of the hard metals. Meanwhile, at MSH the group -SH which is a soft base metal, can bind Ni(II) which are secondary metal.

The total atom adsorbed become smaller with the order: Cr(III) > Cu(II) > Ni(II) > Ag(I) > Pb(II) both in SG and MSH. The smallest value is Pb(II), this is because Pb is generally tend to have a weak holding capacity both when interacting individually or simultaneously. Interactions can directly bind monometal or form a layer (multi metal). Since the metal layer forms indirect binding and it is supported, Pb(II) is less able to interact and could not compete. Hence, it forms weak layer in the outer layer. Pb(II) might be adsorbed on the outer layer when interacting with the adsorbent.

After the sample loading process, washing process was done using 5mL distilled water followed by three elution consecutively, HCl 2M, H_2O and Na_2EDTA 0.1 M. Each eluent was added with 5mL in each flow. The eluent then analyzed using AAS. The same procedure was done for both silica gel using a solution of multi metal and mono metal Ag(I), Ni(II), Pb(II), Cu(II), Cr(III).

The elution process has generated some data from which the total metal concentration eluted is obtained as shown in Table 1. Overall recovery from this study is still relatively small. Only certain metal ion has a considerable recovery value (percentage eluted) which is Pb(II) on both SG by mono metal and multi metal. In MSH, the highest percentage of eluted metal ions is given by Ni(II) to mono metal and metal ions Pb(II) for multi metal. From the four data, Pb(II) is more easily eluted. This is because the metal ion interaction with the adsorbent is weak and being bound by hydrogen bonds which cause Pb(II) easily eluted.

According to the data that Ni(II) and Pb(II) are the easiest ion to be eluted, it can be assumed that both ions interact with the adsorbent via hydrogen bond in the outer layer. This makes both ion are easily eluted compare to the ions which form coordination interaction in the inner layer.

Simultaneous adsorption causes competition among the metal ions (adsorbate) to occupy the adsorbent active sites and form the multi layers. The existence of the layers of the adsorbent and adsorbate interaction enables the binding of more ions. However, different interaction strength makes the ion eluted differently. The weak interaction between adsorbent-adsorbate will make the ion is easily eluted such as Pb(II).

Overall, the percentage of eluted ions is less than 50% due to the imperfect elution process. This is might be due to the interaction of adsorbent-adsorbate itself or due to insufficient eluent volume. The volume of the eluent can be

added with considering the volume of the eluent which will not damage the adsorbent structure

Adsorption of metal ion mechanism in both SG and MSH

In this research, desorption of metal ions Cr(III), Pb(II), Cu(II), Ni(II), Ag(I) is aimed to determine the mechanism of adsorption. Desorption process was done using sequential elution HCl 2M, H_2O and Na_2EDTA 0.1 M. From the elution of solid phase extraction which has been summed up, the trend of adsorption mechanism that occurs in both SG and MSH by mono metal and multi metals has been derived. The result of desorption on adsorbent SG and MSH are expressed as percentage of total eluted from each eluent which can be seen in Table 2 (Appendixes).

In general, this research involves the mechanism of hydrogen bond formation as the dominant adsorption mechanism. This is because the metal ions from multi metal solution in water to form each complex is $[Ag(H_2O)_6]^{+}$, $[Ni(H_2O)_6]^{2+}$, $[Cu(H_2O)_6]^{2+}$, $[Pb(H_2O)_6]^{2+}$ and $[Cr(H_2O)_6]^{3+}$. The presence of H_2O ligands bound to the metal ion in solution can be used to form hydrogen bonds with the active group of the adsorbent.

The contribution of adsorption mechanism through the formation of hydrogen bonds in the SG and MSH can be seen in Table 2. From both adsorbents, it can be seen that the percentage of eluted ions is quite varied either in solution by mono metal and multi metal. In the SG and MSH, the value of the percentage eluted ranged from 5.4 to 24.6% of the individual adsorption (mono metal) and the largest percentage is Cr(III). This is because of the strong acid nature of Cr(III) that is strong enough to interact with hard bases (-OH group) of SG which makes the ion easier to elute than the four other metals. In the simultaneous adsorption (multi metal) the percentage of eluted ions range from 1.8 to 17.6% which is smaller than the percentage of ions eluted individually. Simultaneous adsorption put metal ions to compete with each other in their interactions with the adsorbent active sites so that the desorption process becomes more difficult and produce a relatively small value.

Based on the results obtained from the adsorption mechanism, Ag(I), Ni(II), Cu(II), Pb(II) and Cr(III) tend to form hydrogen bonds during the adsorption process on silica gel and MSH. This is consistent with the data obtained on the adsorption and percentage of eluted ions from solution of mono metal and multi metal Ag(I), Ni(II), Cu(II), Pb(II) and Cr(III)) on silica gel and MSH, with largest value is Pb(II) 31%.

4. Conclusion

Based on the results of the experiment, it can be concluded that RHA as silica source applicable to make the MSH through sol-gel process. Adsorption-desorption studies using SG and MSH adsorbents through column system shows that the metal ions are adsorbed well either individually (mono metal) or simultaneously (multi metal). The desorption process with three different eluents revealed the possibility of hydrogen bond formation during the adsorption.

5. Acknowledgements

The first author is thankful to Prof. Nuryono and Dr. E.S. Kunarti from University of Gadjah Mada for their supervisions and suggestions which significantly improved the quality of the manuscript.

6. References

[1]. Scott, R.P.W., (1993), Silica Gel and Bonded Phases: Their Production, Properties and Use in LC, John Wiley & Sons, Toronto.

[2]. Cestari, A.R., Vieira, E.F.S., Simoni, J.A., and Airoldi, C., (2000), Thermochemical Investigation on the Adsorption of Some Divalent Cations on Modified Silicas obtained from Sol-Gel Process, *Thermochimica Acta*, 348, 25-31.

[3]. Airoldi, C. and Arakaki, LNH., (2001), Immobilization of ethylensulfide on silica surface through sol-gel process and some thermodynamic data of divalent cation interaction, *Polyhedron*, 20, 929-936.

[4]. Narsito, Nuryono, and Suyanta (2004), Kinetika Adsorpsi Zn(II) dan Cd(II) pada Silika Gel Termodifikasi Hasil Pengolahan Abu Sekam Padi, Laporan Penelitian Dasar, Research Institute GMU.

[5]. Tokman, N., Akman, S., dan Ozcan, M., (2003), Solid-phase Extraction of Bismuth, Lead and Nickel From Seawater Using Silica Gel Modified With 3-aminopropyltriethoxysilane in A Syringe Prior to Their Determination by Graphite Furnace Atomic Absorption Spectrometry, *Talanta*, 59, 201-205.

[6]. Khasanah, E.N., (2006), Termodinamika Adsorpsi Ag(I) dan Ni(II) pada n Hibrida Merkapto-Silika dari Abu Sekam Padi, Skripsi, FMIPA-UGM, Jogjakarta.

[7]. Hartanto, L.T., (2006), Termodinamika Adsorpsi Cu(II) dan Pb(II) pada Adsorben

Hibrida Merkapto-Silika Hasil Pengolahan dari Abu Sekam Padi, Skripsi, FMIPA-UGM, Jogyakarta.

[8]. Wulandari, W., (2006), Sintesis Hibrida Merkapto-Silika dari abu Sekam Padi untuk Adsorpsi Logam Cr(III), Skripsi, FMIPA-UGM, Jogyakarta.

[9]. Mujiyanti, D.R, Nuryono and Kuniarti, E.S., (2007), Simultaneous Adsorption of Ag(I), Pb(II), Cu(II), Cr(III), and Ni(II) on Mercapto Immobilized Rice Hull Ash Silica, *Proceeding of International Conference on Chemical Science in Yogyakarta*, 24-26 May 2007.

[10]. Sitompul, W.S., (2006), Survey Cemaran Aflatoksin dalam Sampel Daging Ayam di Yogyakarta dengan High Perfomace Liquid Cromatography (HPLC), Skripsi, FMIPA UGM, Yogyakarta.

Appendixes

Table 1. The data of adsorption – desorption by coloumn technique

Metal ions	Adsorbent	Total of adsorbed metal (µmol)		Total of eluted metal (µmol), (%)	
		Monometal	Multimetals	Monometal	Multimetals
Ni(II)	SG	9.88	9.12	1.94 (19.6)	1.04 (11.4)
	MSH	9.32	9.11	6.49 (69.7)	2.74 (30.0)
Pb(II)	SG	2.99	2.89	1.51 (50.3)	1.44 (49.8)
	MSH	2.73	3.06	0.82 (30.2)	1.25 (41.1)
Cu(II)	SG	9.09	11.10	3.52 (38.7)	0.26 (2.4)
	MSH	8.99	11.10	2.33 (25.9)	0.69 (6.3)
Ag(I)	SG	5.58	5.95	0.70 (12.6)	0.56 (9.6)
	MSH	5.48	5.96	0.88 (16.0)	1.82 (30.6)
Cr(III)	SG	10.39	14.73	3.72 (35.8)	5.13 (34.9)
	MSH	5.52	15.06	3.42 (61.9)	2.29 (15.2)

Table 2. The contribution of adsorption mechanism of metal ions in solution by individually and simultaneously toward SG and MSH through column technique

Metal ions	Adsorbent	Hydrogen Bond Formation				Complex Formation		Percentage of eluted metal (%)	
		HCl 2M (%)		H_2O (%)		Na_2EDTA (%)			
		Monometal	Multimetals	Monometal	Multimetals	Monometal	Multimetals	Monometal	Multimetals
Ni(II)	SG	16.2	9.4	3.2	1.2	0.3	0.8	19.7	11.4
	MSH	20.7	17.6	19.5	6.2	29.4	6.2	69.7	30.0
Pb(II)	SG	11.1	16.2	31.0	19.3	8.3	14.3	50.4	49.8
	MSH	22.5	9.9	3.5	24.4	4.2	6.8	30.2	41.1
Cu(II)	SG	24.6	1.8	10.6	0.3	3.5	0.3	38.7	2.4
	MSH	5.4	5.1	18.5	0.6	2.0	0.6	25.9	6.3
Ag(I)	SG	8.3	7.8	3.8	1.6	0.6	0.2	12.6	9.6
	MSH	10.9	15.1	0.8	7.7	4.4	7.7	16.0	30.6
Cr(III)	SG	12.5	17.0	18.5	10.7	4.9	7.2	35.8	34.8
	MSH	20.6	4.9	25.9	7.6	15.4	2.7	61.9	15.2

Synthesis and Ability Test of Mg/Al Hydrotalcite-like from Artificial Brine Water to Remove Eosin Yellow

Eddy Heraldy [1], Sri Juari Santosa [2], Karna Wijaya [3], Triyono [4]

[(1)] Department of Chemistry, Faculty of Mathematics and Natural Sciences, Sebelas Maret University, Surakarta, Indonesia (eheraldy@gmail.com);
[(2,3,4)] Department of Chemistry, Faculty of Mathematics and Natural Sciences, Gadjah Mada University, Yogyakarta, Indonesia (sjuari@yahoo.com; karna_ugm@yahoo.com; triyn02@yahoo.com)

Abstract

The synthesis of Mg/Al hydrotalcite-like compound (Mg/Al HTlc) from artificial brine water for the first time and its ability test as an adsorbent of eosin yellow has been conducted. Attempts to synthesis of Mg/Al HTlc's using magnesium from several raw materials are widely investigated. One of raw material would purpose as source of magnesium to synthesis of Mg/Al HTlc is brine water which is well known as the desalination process waste. Mg/Al HTlc are widely investigated for their potential applications in research and industrial processes as adsorbents. As adsorbents, Mg/Al HTlc are receiving greater interests in the environmental community due to their high anion retention capacity. However, a very few literature is available on the adsorption behavior of eosin yellow (EY) as anionic dye on Mg/Al HTlc's in aqueous system. The objective of this research is to synthesis of Mg/Al HTlc from artificial brine water (the desalination process waste model) as source of magnesium. The synthesized Mg/Al HTlc was then its ability test as an adsorbent for EY removal. The research initiated with the synthesis of Mg/Al HTlc from artificial brine water. Characterization of the Mg/Al HTlc synthesized was confirmed through X-ray Diffraction and FT-IR Spectroscopy. The determination of optimum acidity, adsorption rate, and energy and capacity adsorption were studied. The result showed that pH 4 was the optimum acidity for the adsorption of EY on Mg/Al HTlc. EY was adsorbed at first order adsorption rate of 3.83 × 10^{-4} s^{-1} on the Mg/Al HTlc, the adsorption capacity was 7.14 × 10^{-5} mol g^{-1}, and adsorption energy of eosin yellow was 26.59 kJ/mo^{1}.

Keywords: *Mg/Al hydrotalcite-like, artificial brine water, adsorption, eosin yellow.*

1. Introduction

Hydrotalcite-like compound (HTlc) also called layered double hydroxides (LDHs) or anionic clays consist of brucite-like hydroxide sheets. The general formula is $[M^{II}_{1-x}M^{III}_{x}(OH)_2](A^{n-})x/n.mH_2O$, where M^{II} is divalent cationic like Mg^{2+}, Zn^{2+}, Cu^{2+}, etc., M^{III} trivalent cationic like Al^{3+}, Cr^{3+}, Fe^{3+}, etc., and A^{n-} is anion. HTlc have a great variety of uses in many applications as an adsorbent, anionic exchange, catalyst, photocatalyst or precursor for the preparation of inorganic materials [1]. There have been numerous studies on synthesis and adsorption capacity of Mg/Al HTlc and several studies on their use for the preservation of water environment [2-4]. Previous research has shown that HTlc can uptake some organic anionic pollutants [5].

Color removal from dye effluents is one of the several major environmental concerns. Traditionally, biological, physical and chemical methods have been applied for dye removal [6]. However, many dyes are poorly biodegradable or recalcitrant to environmental conditions due to their complex structure and xenobiotic properties. Furthermore, many dyes are toxic to some microorganism and may cause direct destruction or inhibition of their catalytic capabilities [7]. Chemical and electrochemical oxidations, coagulation and reverse osmosis are generally not feasible on a large scale due to economic consideration. Adsorption, however, is an effective method for dye removal. Activated carbon is perhaps the most widely used adsorbent because of its high specific surface area, high adsorption capacity and low-selectively for both inorganic and organic pollutants [8]. Unfortunately, activated carbon adsorption is an expensive method due to its high price and the difficulties involved in its regeneration for re-use.

In recent years, many low-cost natural materials such as natural clay, materials produced from agricultural by-products and industrial solid wastes such as fly ash and coal, as dye adsorbents have attracted interests of environmental scientists [9-12]. However, these materials generally have low adsorption capacities and hence, large adsorbent dosage is required to achieve a low dye

concentration of the effluents. Difficulties involved in regeneration of these low-cost adsorbents for re-use also increase economic burdens disposing of the used adsorbents.

The applications of hydrotalcite-like as adsorbents to selectivity remove anionic pollutants from aqueous solutions have attracted considerable attention in the recent decade [13-15]. However, studies on sorption of Eosin Yellow (EY) on Mg/Al HTlc from brine water are limited. In the present study, the removal of EY on Mg/Al HTlc synthesized from artificial brine water was investigated. The performance of the Mg/Al HTlc was evaluated in term of its capacity and rate of sorption for dissolved EY. Sorption capacity is determined using the Langmuir isotherm model, while sorption rate is calculated using a kinetics model of first order sorption reaching equilibrium developed by Santosa [16].

2. Experimental Details

Materials

All reagents in analytical grade, i.e. $MgCl_2.6H_2O$, NaCl, $CaCl_2.2H_2O$, KCl, Na_2CO_3, $NaHCO_3$, (Merck Co Inc., Germany) and $AlCl_3.6H_2O$ (Aldrich, Germany) were used for the make artificial brine water, preparation of starting solution and synthesis of Mg/Al HTlc without further purification. The redistilled water was used during the synthesis. EY provided by the Merck and used as received without further purification. EY solutions were prepared by dissolving EY in redistilled water.

Preparation of Starting solution

An artificial brine water (i) was prepared from 0.710 M NaCl, 0.411 M $MgCl_2.6H_2O$, 0.056 M $CaCl_2.2H_2O$ and 0.019 M KCl. Filtrate was obtained by adding a mixed 0.1 M Na_2CO_3-0.2 M $NaHCO_3$ (ii), solution to (i) until the 1.2 equivalent of calcium ion in (i) and stirring for 1 h at 95^{o}C.

Synthesis of Mg/Al HTlc

A co-precipitation method following Kameda [2] with some modifications was used to synthesis of Mg/Al HTlc. Briefly, one thousand milliliter of 0.10 M Na_2CO_3 solution was added slowly to 50 mL of (ii) containing $AlCl_3.6H_2O$, with an initial Mg/Al molar ratio of 2.0 at constant pH 10.5 and then the solution was stirred for 1 h at 70°C. The product was centrifuged to recover the white solid at a speed of 2800 rpm for 15 min. The wet cake was washed with redistilled water until free of ion Chloride ($AgNO_3$ test) and dried overnight with oven.

Sorption of EY

Effect of medium acidity

A series of 50 mL of 5 mg L^{-1} EY solutions was prepared and their acidity was adjusted to pH 2, 4, 6, 8, 10, 12 and 13 by using either HCl or NaOH solution. Into every EY solution, 50 mg of Mg/Al HTlc was poured and then stirred for 2 h. After filtering through 0.45-μm membrane filter, the concentrations of EY in the supernatants were analyzed by using UV-vis spectrometer at wavelength 512 nm. Sample and blank solutions were analyzed under the same condition. The amount of EY sorbed was determined from the difference between the initial and remaining amounts of EY in the reacting solution each time the sample was analyzed.

Sorption rate

Experiments for the determination of sorption rate were carried out using a batch-type reactor of a 100 mL Erlenmeyer in a water bath at 25ºC. The initial volume and EY concentration were 100 mL and 5 mg L^{-1}, respectively. To each solution, 50 mg of Mg/Al HTlc was added; the medium acidity was adjusted to pH 4.0, and stirred continuously. At selected time periods, a sample is immediately filtered through 0.45-μm membrane filter.

In every selected time period, the concentration of the remaining EY in the supernatant was analyzed by using UV-vis spectrometer at wavelength 512 nm. Sample and blank solutions were analyzed under the same conditions. The amount of EY adsorbed was calculated by the difference between the initial and remaining of EY in the reacting solution.

Capacity and energy of sorption

Experiments for the determination of capacity and energy of sorption were also carried out using a batch-type reactor of a 100 mL Erlenmeyer in a water bath at 25ºC. The initial volumes of the EY solutions were 100 mL, and the concentration of EY in the solutions were varied from 0 to 120 mg L^{-1}. Into each EY solution, 50 mg of Mg/Al HTlc was added and followed by continuous stirring for 2 h. After stirring, the solutions were immediately filtered through 0.45-μm membrane filter.

The concentration of EY remaining in the supernatant was analyzed by using UV-Vis spectrophotometer at 512 nm. Sample and blank solutions were analyzed under the same conditions. The amount of EY adsorbed was calculated by the difference between the initial and the remaining of EY in the reacting solution.

3. Results and Discussion

Synthesis and Characterization of Mg/Al HTlc

Calcium ion should be removed from brine water as $CaCO_3$ since it is an impurity that co-precipitates with HTlc when Na_2CO_3 solution is added to brine water containing $AlCl_3$ (Figure 1). When a mixed Na_2CO_3-$NaHCO_3$ solution was added to (i) to prepare (ii), Ca^{2+} was selectively removed from (i). Figure 2 shows the XRD pattern of product precipitated from (ii) containing $AlCl_3$ with an initial Mg/Al molar ratio of 2.0 at 70^0 C. The XRD pattern of the HTlc (Figure 2) consists of both sharp and symmetrical peaks with some asymmetrical peaks at high angle, indicating good crystalline [17]. The three strong peaks at 2θ values of about 11.3^0 , 23.1^0 and 34.6^0 are characteristic of a layered structure and correspond to the (00*l*) reflections and the diffraction peak near 61.0^0 corresponds to the (110) crystal plane. It was thought that CO_3^{2-} was intercalated into the precipitated HTlc since (003) reflection of HTlc intercalated CO_3^{2-} is around 7.83 Å. According to Kloprogge, the value of 7.83Å is characteristic for the (003) reflection of carbonate – bearing hydrotalcite [18].

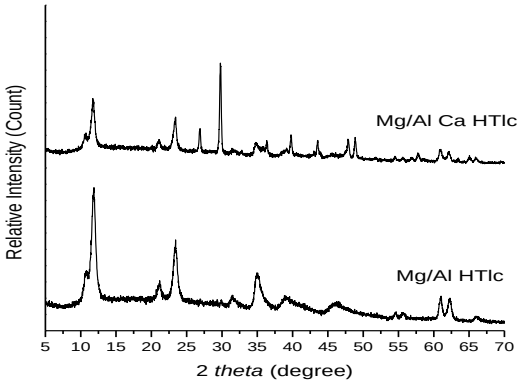

Figure 1. XRD patterns of HTlc with and no Ca^{2+} impurities

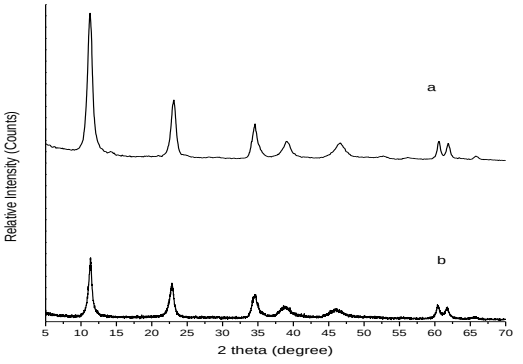

Figure 2. XRD patterns of Mg/Al HTlc (a) synthesis and (b) commercial

FT-IR spectra of the HTlc samples are shown in Fig. 3. The broad peak around 3565 cm^{-1} can be ascribed to the stretching of OH groups attached to Al and Mg in the layers. The shoulder at 3046 cm^{-1} is due to hydrogen bonding of interlayer water with interlayer CO_3^{2-} anions. The bending vibration of interlayer water is found at 1637 cm^{-1}. The anti-symmetric vibration of CO_3^{2-} appears at 1361 cm^{-1}. The peak around 644 cm^{-1} is attributed to the overlap of the anti-symmetric vibration of CO_3^{2-} and Mg-O stretching vibrations. The bands at 947, 790, and 554 cm^{-1} can be assigned to Al-O stretching modes.

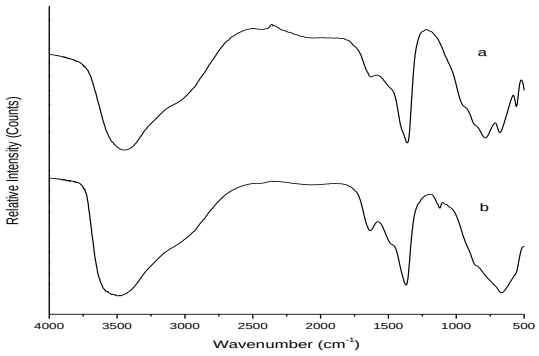

Figure 3. FT-IR spectra of Mg/Al HTlc (a) synthesis and (b) commercial

Sorption of EY

Effect of medium acidity

The sorption of EY on Mg/Al HTlc tends to increase with increasing medium acidity from pH 3 to 4 and then falls rapidly from pH 4 to 10 (Fig. 4). Since the EY have $pKa_1 = 3.7$ and $pKa_2 = 3.4$ [19], with the increasing pH from 3 to 4, more EY species are suspected negatively charged and hence the sorption of EY on the positively charged Mg/Al HTlc is enhanced. At pH > 4, however, the negatively charged EY must compete with the excess of hydroxide ion in the solution in occupying the active sites of the Mg/Al HTlc. This is why that the sorption falls at pH higher than 4.

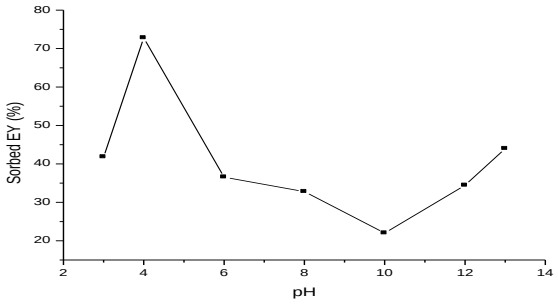

Figure 4. Effect of medium acidity on the sorption of EY on Mg/Al HTlc

Rate of sorption

The sorption profile of EY as a function of interaction time is presented in Figure 5 above. The sorption is initially rapid and then goes slower. The initial rapid sorption was observed for the first 15 min and the sorption still increased even at at the sorption time more than 180 min.

The sorption data matches well with the kinetic model of first order sorption reaching equilibrium proposed by Santosa [16] as mathematically expressed in the following equation:

$$\frac{\ln\left(\frac{C_0}{C}\right)}{C} = k_s \cdot \frac{t}{C} + Q$$

where C_0 and C are the initial and remaining concentration of EY in the solution after sorption, respectively, k_s the first order sorption rate constant, t the interaction time, and Q is the sorption-desorption constant.

Plot of $(ln(C_0/C))/C$ against t/C resulted in linear relationship with linearity (R^2) as high as 0.954 (Fig.5 below). Based on the slope of the plot, the obtained sorption rate constant (k_s) was 3.83×10^{-4} s^{-1}.

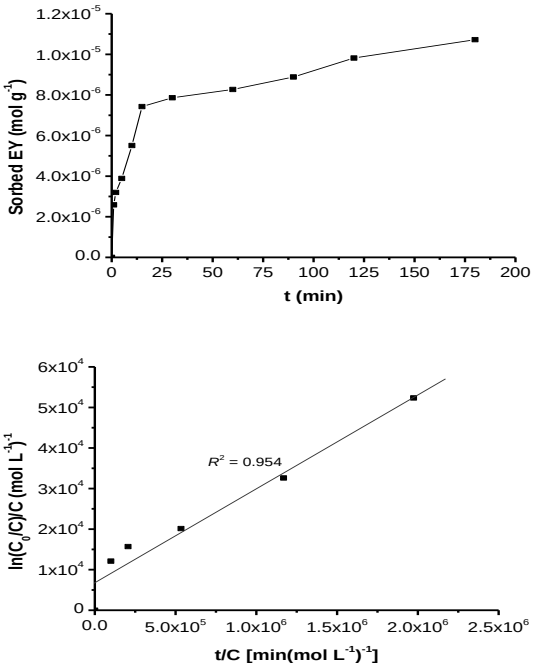

Figure 5. Sorption profile of EY on Mg/Al HTlc as a function of interaction time (above) and plot of $\{\ln(C_0/C)\}/C$ against t/C in the kinetic model of first order sorption reaching equilibrium (below)

Capacity and energy of sorption

The sorption profile of EY on Mg/Al HTlc as a function of EY concentration at equilibrium is given in Figure 6. The sorption was non-linear, abruptly increased at low level of initial concentration of EY from 0 to 8.91×10^{-5} mol L^{-1} and only slightly increased when the applied EY concentration was between 8.91×10^{-5} and 14.37×10^{-5} mol L^{-1}. As shown in Figure 6, the sorption closely follows the Langmuir model as expressed in the following equation:

$$m = \frac{b.K.C}{1+K.C} \quad \text{or} \quad \frac{C}{m} = \frac{C}{b} + \frac{1}{K.b}$$

where C is the EY concentration in the solution after sorption reaches equilibrium, m is mol of EY sorbed on 1 g Mg/Al HTlc, K the equilibrium constant, and b is the maximum amount of EY sorbed on Mg/Al HTlc (sorption capacity).

By plotting C/m against C, the values of b can be obtained from the 1/slope. From this plot of C/m against C, the obtained value of b for the sorption of EY on Mg/Al HTlc was 7.14×10^{-5} mol g^{-1}. The linearity (R^2) of the plot was 0.994 (Figure 6).

After obtaining b, the value of K is then able to be determined from the intercept of plot of C/m against C. The calculation yields K value was 3.84×10^4 (mol $L^{-1})^{-1}$. According to the equation $E_s = -\Delta G_s = RT \ln K$, the sorption energy ($E_s$) is then obtained as high as 26.59 kJ mol^{-1}.

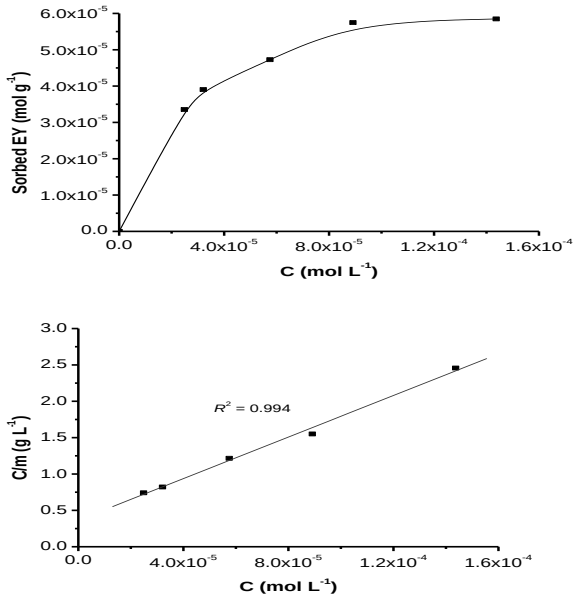

Figure 6. Sorption profile of EY on Mg/Al HTlc as a function of the remaining EY concentration at equilibrium (C) (above) and the relationship between C and C/m in the Langmuir isotherm model (below)

4. Conclusion

As prepared the other HT or HTlc, this sample result exhibit the (003) reflection around 7.83 Á, typical for Mg/Al HTlc with carbonate interlayers. It was confirmed that Mg/Al HTlc synthesized from artificial brine water was able to be use as adsorbent for EY in solution. The sorption of EY was predicted to occur mainly on the outer surface through first order sorption reaching equilibrium with relatively high sorption rate constant, i.e. 3.83×10^{-4} s^{-1}.

5. Acknowledgements

The authors are grateful to thank to Higher Education Directorate for Research Grants and Gadjah Mada University, Yogyakarta for providing the research facilities, and to Dian Prasasti, Dhanik Hermawan, R. Iwa, Gita Savitri and E.H. Suryo were contributed to support this research.

6. References

[1]. Kovanda, F., Kolousek, D., Cılova, Z. and Z. Hulınsky (2005), Crystallization of synthetic hydrotalcite under hydrothermal conditions, *Appl. Clay Sci.*, 28, 101– 109.

[2]. Kameda, T., Yoshioka, T., Uchida, M. and A. Okuwaki (2000), Synthesis of hydrotalcite using magnesium from seawater and dolomite, *Mol. Cryst. Liq. Cryst.*, 341, 407-412.

[3]. Heraldy, E., Pranoto, Wijanarko, D.M., Nugrohoningtyas, K.D., Dinala, B.B. and I. Sujarwo (2006), Studi pengaruh perbedaan rasio mol antara Mg/Al dalam sintesis Mg/Al hydrotalcite-like, *J. Alchemy*., 5 (1), 54-59.

[4]. Heraldy, E., Pranoto, Wijanarko, D.M. and I. C. Riasdianti (2007), Kajian Optimasi Jumlah Adsorben dan Waktu Kontak pada Adsorpsi Red 2B oleh Mg/Al hydrotalcite-like, *J. Alchemy*, 6 (2), 23-30.

[5]. Orthman, J., Zhu, H.Y. and G.Q. Lu (2003), Use of anion clay hydrotalcite to remove coloured organics from aqueous solutions, *Sep. Purif. Technol.*, 31, 53-59.

[6]. O'Neill, C., Hawkes, F.R., Hawkes, D.L., Lourenco, N.D., Pinheiro, H.M. and W. Delee (1999), Colour in textile effluents-sources, measurement, discharge consents and simulation: a review, *J. Chem. Technol. Biotechnol.*, 74, 1009-1018.

[7]. Zhu, M.X., Li, Y.P., Xie, M. and H.Z. Xin (2005), Sorption of an anionic dye by uncalcined and layered double hydroxides: a case study, *J. Hazard. Mater. B*, 120, 163-171.

[8]. Faria, P.C.C., Orfao, J.J.M., and M.F.R. Pereira (2004), Adsorption of anionic and cationic dyes on activated carbons with different surface chemistries, *Water Res.*, 38, 2043-2052.

[9]. Tsai, W.T., Chang, C.Y., Lin, M.C., Chien, S.F., Sun, H.F. and M.F. Hsieh (2001), Adsorption of acid dye onto activated carbons prepared from agricultural waste bagasse by $ZnCl_2$ activation, *Chemosphere*, 45, 51-58.

[10]. Wang, C.C., Juang, L.C., Hsu, T.C., Lee, C.K., Lee, J.F. and F.C. Huang (2004), Adsorption of basic dyes onto montmorillonite, *J. Colloid Interface Sci.*, 273, 80-86.

[11]. Meshko, V., Markovska, L., Mincheva, M. and A.E. Rodrigues (2001), Adsorption of basic dyes on granular activated carbon and natural zeolite, *Water Res.*, 35, 3357-3366.

[12]. Janos, P., Buchtova, H., and M. Ryznarova, (2003), Sorption of dyes from aqueous onto fly ash, *Water Res.*, 37, 4938-4944.

[13]. Ulibarri, M. A., Pavlovic, I., Hermosin, M. C. and J. Cornejo (1995), Hydrotalcite-like compounds as potential sorbents of phenol from water, *Appl. Clay Sci.*, 10, 131-145.

[14]. Crepaldi, E. L., Tronto, J., Cardoso, L. P. and J.B. Valim (2002), Sorption of terephthalate anions by calcined and uncalcined hydrotalcite-like compounds, *Colloid Surface A*, 211, 103-114.

[15]. You, Y., Vance, G.F. and H. Zhao (2001), Selenium adsorption on Mg-Al and Zn-Al layered double hydroxides, *Appl. Clay Sci.*, 20, 13-25.

[16]. Santosa, S.J., Siswanta, D., Kurniawan, A. and W.H. Rahmanto (2007), Hibrid of chitin and humic acid as high performance sorbent for Ni(II), *Surf. Sci.*, 601, 5155-5161.

[17]. Ulibarri, M. A., Pavlovic, I., Barriga, C., Hermosin, M. C. and J. Cornejo (2001), Adsorption of anionic species on hydrotalcite-like compounds: effect of interlayer anion and crystallinity, *Appl. Clay Sci.*, 18, 17-27.

[18]. Kloprogge, J.T., Wharton, D, Hickey, L. and R.L. Frost (2002), Infrared and Raman study of interlayer anions CO_3^{2-}, NO_3^-, SO_4^{2-} and ClO_4^- in Mg/Al-hydrotalcite, *American Mineralogist*, 87, 623-629.

[19]. Sabnis, R. W., 2010, Handbook of Biological Dyes and Stains: Synthesis and Industrial Applications, A John Wiley & Sons, Inc., Hoboken, New Jersey.

Optimation of Bioethanol Production from Sugar Cane Baggase using Separated Hydrolysis and Fermentation Method Based on Cellulase System of *Bacillus Circulans*

Evi Susanti [1], Neena Zakia [2], Sumari [3]

[1,2,3] Chemistry Department, Faculty of Mathematics and Science, State University of Malang, Malang, Indonesia
(esusanti.kim@gmail.com)

Abstract

Production of bioethanol consist of two reaction i.e. hydroliysis and fermentation. Hydrolysis is converted cellulose in sugar cane baggase to glucose and fermentation is converted glucose to ethanol. Hydrolisis is the rate limitting step of production bioethanol process from baggase. Cellulase system of Bacillus circulans was used it this step. The aim of this research was to determine the optimum condition of hydrolysis and fermentation steps of bioethanol production from baggase using separated hydrolysis and fermentation (SHF) method. The result are as follows: (1) hydrolysis of 10 g of pretreatment baggase optimum yield 1.321% saccharification at 45ºC, pH 5.0, for 12 hour, using 50 mL crude extract of cellulose system and stirred continously, and (2) the optimum fermentation of the hydrolysis results in the addition of 10% (v/v) Saccharomyces cereviciae culture at the end lag phase for 3 days, while the bioethanol yield was 160 mL of etanol/kg of sugar cane baggase.

***Keywords**: bioetanol, sugar cane baggase, hydrolisis, fermentati*

1. Introduction

Production of bioethanol on a large scale in Indonesia focused only of glucose containing materials such as molasses and starchy materials such as cassava and maize. The availability of molasses is limited, because only supplied from the sugar factory, while the use of starchy material constantly feared to potentially cause a decrease in biodiversity through monoculture of raw materials following agricultural practices that damage the quality of land [12]. This problem can be solved by diversification of raw material for bioethanol from non-food agricultural materials such as agricultural waste in the form of lignocellulose. This is in addition to the group dismissed concerns that counter to the production of bioethanol, also encourages the use of cheaper raw materials as well as to enhance the economic value of lignocellulosic waste. Lignocellulosic wastes can be found in straw, sawdust, oil palm empty fruit bunches, fiber or sugarcane bagasse [2].

Sugarcane agasse used as a model in this study due to abundant availability in Indonesia. According to statistical data in 2002, sugarcane planted area in Indonesia 395.399.44 ha [3]. It is estimated that each hectaproduce 100 tons of waste bagasse. So the potential of bagasse waste national reach 39.5 million tons. Of this amount only 60% of which have been used as *boiler* fuel, raw materials of paper, canvas brakes and mushroom cultivation [3]. Bagasse has a large surface area making it easier operationally than the other ligoselulosa waste and the prosentage cellulose in baggase is also quite high at around 35% [1]. However the technology for production of bioethanol from lignocellulosic bagasse in Indonesia particularly underdeveloped. This is because the structure of naturally lignocellulosic is difficult to degradated [8].

Stages production of bioethanol from lignocellulosic consist of: (i) pretreatment of raw materials into a substrate that is more easily hydrolyzed enzymatically, (ii) the enzymatic hydrolysis reaction to change the lignocellulosic material to glucose, (iii) conversion of glucose into ethanol and the separation and concentration ethanol product from the product side [8]. The chemical production of bioethanol from bagasse waste consists of two main stages i.e. hydrolysis of cellulose in the bagasse into glucose and fermentation glucose as result of hydrolysis into bioethanol.

$$\text{Step 1: } \underset{\text{cellulose}}{(C_6H_{10}O_5)_n} + H_2O \xrightarrow{\textit{cellulase}} \underset{\text{glucose}}{C_6H_{12}O_6}$$

$$\text{Step 2: } \underset{\text{glucose}}{C_6H_{10}O_5} \xrightarrow{\textit{S. cerevisiae}} \underset{\text{ethanol}}{2CH_3CH_2OH} + 2CO_2$$

Hydrolysis bagasse into glucose is a critical step in the process of bioethanol production [1,8]. Several studies have been

developed to optimize this step. Pretreatment of baggase and the use of cellulase which has a high activity is a dominant factor that determines the optimization hydrolysis in addition to the hydrolysis process itself. Appropriate pre-treatment would alter the physical properties of waste lignocellulosic bagasse thus simplifying the access cellulase system and decided binding glycosidic bonds in cellulose without producing products that act as inhibitors for the formation of bioethanol fermentation process [1,4,10,11]. Previous research has succeeded in determining the optimum pre-treatment to increase saccharification yields of baggase enzymatically and have been able to isolate the crude extract of cellulase system from *Bacillus circulans* which have high activity to degrade bagasse into glucose [11,12]. The aim of this research were to determine the optimum conditions of hydrolysis and fermentation stage in the production of bagasse into bioethanol by separated hydrolysis fermentation method (SHF).

2. Experimental Details

Isolation of cellulase from Bacillus circulans

Bacillus circulans were obtained from pure culture collection of Microbiology Laboratory of ITB. The media used was Berg's mineral salt medium, containing avicel as carbon source in aerobic conditions.

Preparation of bagasse

Materials are stored in plastic bags at a temperature of about 5ºC. First, bagasse was washed to remove soil and other dirt, squeezed to obtain dry bagasse (approximately 48% by weight).Dry bagasse received pretreatment [11]

Optimization Hydrolysis of Baggase into Glucose

a. Determination incubation time optimum

Ten grams of pretreatment bagasse added 50 mL crude extract of cellulase system and 450 mL phosphate buffer 0.1 M pH 7.0. The mixture was stirred at 45ºC. The mixture was filtered. Measurement of glucose levels at filtrate was done at 0, 4, 8.12 and 16 hours.

b. Determination amount of crude extract cellulase system optimum

Ten grams of pretreatment bagasse was added each with 25, 50 and 100 mL crude extract of cellulase system and phosphate buffer 0.1 M pH 7.0 to 500 mL.The mixture was stirred continuously at 45ºC for optimum incubation time. Measurement of glucose levels at filtrate done at each reaction.

c. Determination of pH optimum

Ten grams of pretreatment baggase was added with optimum crude extract of cellulase system and phosphate buffer 0.1 M, each with pH 5.0, 7.0 and 9.0 until the mixture volume was 500 mL. The mixture was stirred continuously at 45ºC for optimum incubation time. The mixture was filtered. Measurement of glucose levels wascdone at the filtrate obtained.

d. Determination of temperature optimum

Ten grams of pretreatment baggase was added with optimum crude extract of cellulase system and optimum pH of phosphate buffer to 500 mL. The mixture was stirred continuously at medium speed on the temperature of each room temperature, 40 and 50°C for the optimum incubation time. Measurement of glucose levels done at the filtrate obtained.

Optimization of the number of microbes and the fermentation time

Filtrate the results of hydrolysis included in fermentor, arranged around pH 5.0, respectively added each with 0, 3, 10, 20 and 30% (v / v) *Saccharomyces cereviciae* which are harvested at the end of log phase. Homogenized mixture, then sealed reactor. Fermentation carried out respectively for 1, 2, 3 and 4 days at 37°C. Purified ethanol from fermentation was done by fractional distillation. Determination of concentration of ethanol was done using alcoholmeter.

Characterization of bioethanol

Cerrium of ammonium nitrate ($NH_{4(2)}Ce(NO_3)_6$) Test

About 0.5 mL of a solution of cerium ammonium nitrate ($NH_{4(2)}Ce\ (NO_3)_6$) is inserted into the test tube, added with 3 ml dioxane (dioxane can be replaced by aquades, if the tested substances dissolve in water), shaken until homogeneous, added 1 ml of the tested solution, and then shaken.The color of the solution became red or brown color indicates the tested substances containing hydroxy group (-OH).

Iron(III) chloride ($FeCl_3$) Test

If ammonium nitrate series positive test indicates that the sample contains a hydroxy group then continued with test $FeCl_3$ to determine whether the sample is a phenolic hydroxy or not. A total of 3 ml sample solution add 1-2 drops of iron(III) chloride ($FeCl_3$)1%, the color purple indicates a phenolic hydroxyl.

Lucas Test

Theoretically bioethanol would produce ammonium nitrate test series of positive and negative test of $FeCl_3$, Then to ascertain whether the sample actually contains bioethanol third test is lucas test, carried out by 1 ml sample in a test tube plus 1 ml reagent Lucas, beaten until homogeneous, then observed the formation of a cloudy solution or a solution separation into 2 layers. Controls on this test is used ethanol (primary alcohol), 2-propanol (secondary alcohol), isopropanol (tertiary alcohol). Tertiary alcohols react with 1 minute, secondary alcohol reacts after 5 minutes and primary alcohols do not react (the solution remains clear and not separately) after 1 hour.

Flame Test

About 0.5 mL of samples tested in place on a watch glass, then burned with fire from a match directly. Negative control used distilled water.

Analysis

The optimum conditions of hydrolysis is determined based on the highest value of % saccharification (percentage of mass of glucose / mass of baggase). The optimum conditions of fermentation is determined by the highest amount of ethanol produced by the following formula: volume (mL) X concentration of ethanol (% weight per volume). Bioethanol yield was in percentage of mg ethanol/Kg baggase.

3. Result and Discussion

Bioethanol production methods developed in this research is to separate fermentation hydrolysis method (SFH) which uses a cellulase system of *Bacillus circulans* to hydrolyzed and *Saccharomyces cereviciae* to fermented as shown in the research scheme in Figure 1.

Optimization of Hydrolysis of Sugarcane Waste

Hydrolysis time is the time required of cellulase to degrade cellulose to glucose. The results showed the optimum time for the process, as shown in Figure 2.

Based on Figure 2, the optimum incubation time occurred at the 12th hour. It is characterized by the highest resultant percent saccharification i.e. 1.22%.Once the optimum time (hour-12) a decline in result. Cellulase from *Trichoderma viridie* is inhibited by glucose, δ-glukonolakton, selebiosa, and an organic solvent such as ethanol, butanol, and acetone [5]. β-glucosidase (a type of activity cellulase) from *Trichoderma reesei, Aspergillus niger,* and *Phanaerocheate chrysosporium* competitively inhibited by glucose and glukonolakton [4]. Both of the opinion.

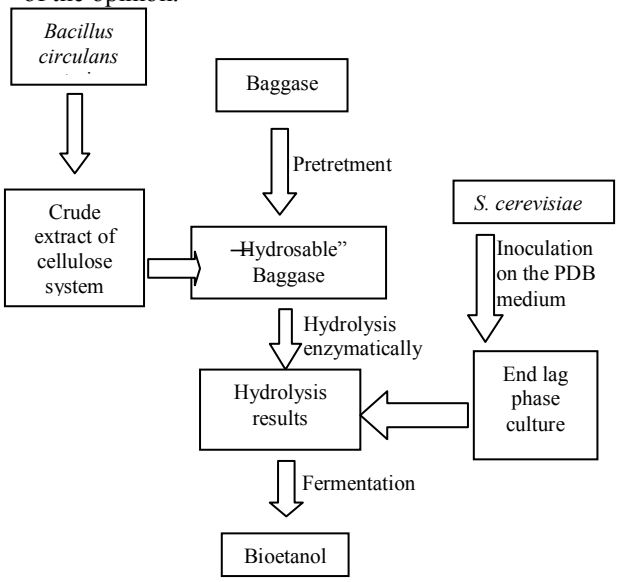

Figure 1. Research Scheme Bioethanol Production from Baggase (Sugar Cane Waste)

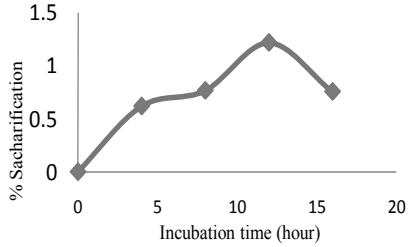

Figure 2. Percentage of Saccharification of Sugarcane Waste at Different Time Incubation

The amount of enzyme is one of the aspects that are important in enzymatic reactions. The optimum amount of enzyme is strongly influenced by the amount of substrate. In this study the amount of substrate is made permanent. Figure 3 shows the results obtained. The result shows that increase in the value was proportional to the increase in the amount of enzyme used. This is due to as more substrate can be converted into products, the amount of enzyme excess of 100 mL seen a reduction percent saccharification

Presumably this is related to the nature of the reaction products of glucose which is a competitive inhibitor of cellulase. At the same hydrolysis time, the more the number the more enzyme the amount of product formed, but the high glucose levels lead to glucose as an inhibitor that is in excess of the amount of enzyme activity decreased.

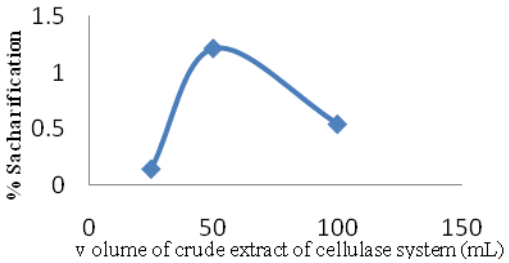

Figure 3. Percent Saccharification of Sugarcane Waste at Different Volume of The Crude extract of cellulose System.

Most of the enzymes, including cellulase used in the hydrolysis of bagasse, can work most effectively on environmental pH range is quite narrow so-called optimum pH. Outside the optimum pH, the increase or decrease in pH causes a decrease in enzyme activity rapidly. The enzyme has an active side with certain clusters which act as a catalyst in the formation of enzyme-substrate complex (ES). Changes in pH affect the ionization of functional groups, which can result in changes in cellulase enzyme conformation and catalytic properties [6]. Therefore, pH is one of the important aspects in the process of saccharification of bagasse enzymatically.The results showed that the pH affects the magnitude % saccharification obtained, as shown in Figure 4.

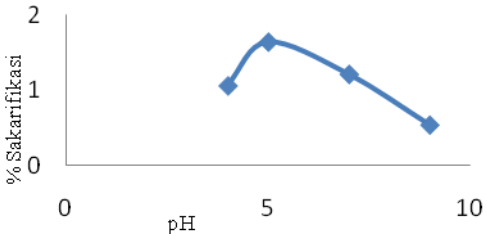

Figure 4. Saccharification of Sugarcane Waste at Different pH

In general, in a chemical reaction for each increase in temperature of 10°C, the reaction rate doubles. The heat generated due to temperature increase the movement of molecules so that the speed increases The result is a frequency and power of molecular collisions also increases. Most of the enzyme has the same optimum temperature to normal temperature cell organism. The temperature rise within reasonable limits does not result in any change of three-dimensional structure of the enzyme (denaturation). Denatured enzyme will lose the ability of the catalyst. Therefore, the temperature is one of the important aspects of enzymatic reactions that need to be determined optimum value. The results showed that the temperature greatly affect the enzymatic process, as shown in Figure 5.

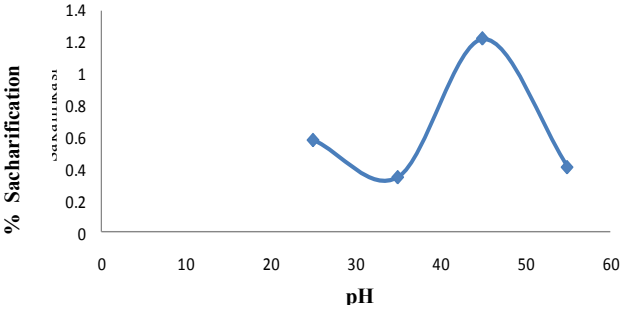

Figure 5. Percentage of Saccharification of Sugarcane Waste at Different pH.

Of the various variations of temperature examined, i.e room temperature, 35, 45 and 55°C, obtained at 45ºC is the optimum temperature of saccharification that occurs. Optimum incubation temperature produced in this study is in line with the optimum temperature generated in the other research that the optimum temperature of cellulase of *Bacilllus circulan*s occur at relatively high temperatures (above 40°C) [13].

During chemical reactions take place needs to be stirred continuously to maintain homogeneity of the reaction mixture. In this trial observed how much influence saccharification stirring than without stirring. The results are shown in Figure 6.

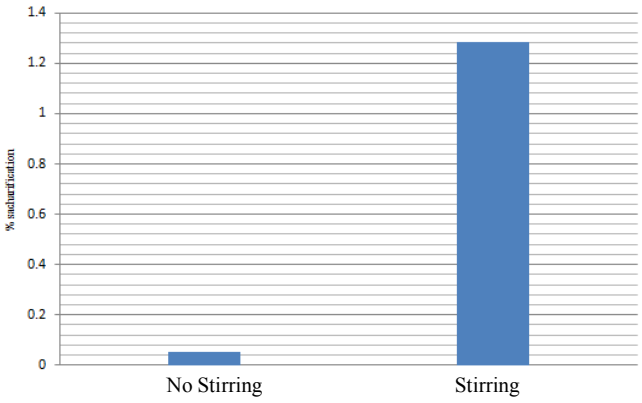

Figure 6. Percentage of Saccharification of Sugarcane Waste With and Without Stirring.

Figure 6 shows the increase generated by the use of stirring continuously for 16 times that of 0.081% produced in the process without stirring to 1.321% in the saccharification process by stirring continuously. This information is very important for designing the means of production

of bioethanol from bagasse generated from the method developed in this study.

Fermentation of glucose to ethanol can be made by certain microbes that have the metabolism of alcohol fermentation, such as *Saccharomyces cerevisiae.*

The goal is to find out the location of the phases of its growth so that we can do the harvesting at the right culture that is at the end of log phase and early stationary phase. In these conditions we can obtain a culture with many cell count and cell viability is high. The experimental results are shown in Figure 7.

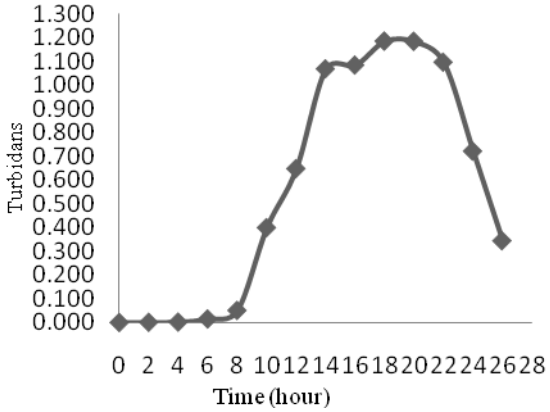

Figure 7 Growth Curve of Saccharomyces cerevisiae in PDB Medium at growth temperature 37°C and 86 rp

Based on Figure 7 can be suggested that *Saccharomyces cerevisiae* harvesting time can be done from the end log phase to early stationary phase, which began at the 16 th till the 20 th hour with absorbance values. Determination of optimum fermentation condition can be seen in Figure 8. The results showed that the highest ethanol yield on all the variations of culture occurs on the third day of fermentation.

Increased yield of alcohol seen from the slope of the fourth variation is the addition of the microbes. Although the initial yield of alcohol is different but it appears clearly that the highest increase occurred in the addition of 10% and 20% of microbes. But the different is not significant. Bioethanol yield different values of the four variations of the addition amount is anticipated by microbial fermentation stage through which the microbes in each of the different additions. The increase in yield of alcohol are caused by microbial activity in *S.cerevisiae* that has been increasing. *S.cerevisiae* role convert glucose into ethanol [7]. The longer after an increase in yield of alcohol will decrease the yield of alcohol. This decline occurred mainly due to: (1) food substances needed for fermentation is reduced, (2) the bacteria itself eskresi be buried so that disrupt breeding and growth, and (3) changes in pH and temperature [9].

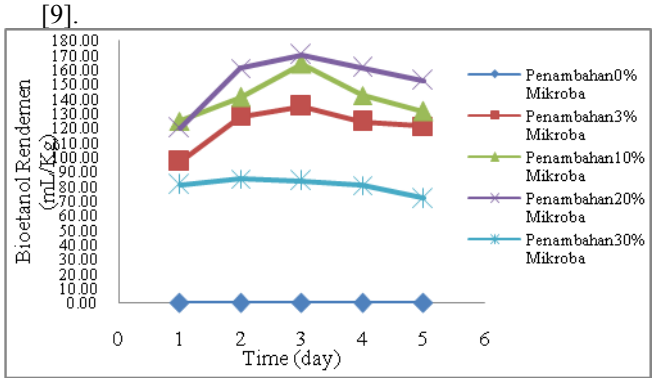

Figure 8. Bioethanol yields from Sugarcane waste

Characterization of Bioethanol from Sugarcane Waste

Summary results of identification that has been done to test whether bioethanol is produced containing ethyl alcohol is presented in Table 2.

Table 2. Identification of bio-ethanol from distillate

Sample	Type Test			
	Flame Test	**CAN Test**	**$FeCl_3$ Test**	**Lucas Test**
Fermentation's distillate	No Flame	+	-	No react >1 hour
Hydrolysis's filtrate	No Flame	-	Not Tested	Not tested
Ethanol (1°)	Flame	+	-	No react > 1 hour
2-propanol (2°)	Flame	+	-	Reacts after 5'
Isopropanol (3°)	Flame	+	-	Reacts at 1'
Aquadest	No Flame	-	-	Not react > 1 hour

Description: CAN (+) yellowish brown, brown, (-) yellow; $FeCl_3$ (-) no color

These results indicate that in the distillate of fermented contain primary alcohols such as ethanol. Fermented distillate flame test can not be flame, while the positive control (ethanol) can be lit with a blue flame color. This result is expected because the concentration of alcohol distillation results are still very low.The highest ethanol concentration only was 33.56%. Yet through a simple test on various ethanol solution with different levels indicates that the flame test in ethanol solution showed a positive result if the alcohol content above 35%. This reinforces that the process undertaken has been able to produce ethanol, but etanolnya levels are still low so it can not be tested flame.

Conclusion

1. Hydrolysis ten grams of pretreatment bagasse with cellulase system of *Bacillus circulans* optimum yield of 1.321% saccharification at 45ºC, pH 5.0, for 12 hours using crude extract

of 50 mL cellulase and stirring continuously. The optimum fermentation of the hydrolysis results in the addition of 10% (v/v) *Saccharomyces cereviciae* culture at the end lag phase for 3 days while the bioethanol rendemen was 160 mL of ethanol/kg of sugar cane baggase.

5. Acknowledgements

The researcher would like to thank very much to the DP2M who has funded this research through the Hibah Bersaing Program year 2009-2010 and 2010-2011, entitled "Optimation of Bioethanol Production from Sugarcane Waste Based On System cellulose of Bacillus circulans Local Strain", and to Mr. Ardian Trio Wicaksono and Mrs. Farina from Chemistry Department of FMIPA Malang State University for his support during this research.

6. References

[1]. Bon, Elba, PS (Scientific Coordinator), (1996), *Ethanol Production via enzymatic Hydrolysis of Sugar-Cane Baggase and Straw,* Chemistry Institute Federla University of Riode Janeiro, Brazil (online).

[2]. (http://www.fiesp.com.br/agencianoticias/2007/05/15/elba.bon.pdf, accessed January 10, 2008).

[3]. Dewi, K. H., (2002). Hidrolisis Limbah Hasil Pertanian Secara Enzimatik, *Akta Agrosia,* Vol 5 N0.2 p. 67-71.

[4]. Fauzi, A., (2005). *Pemanfaatan Ampas tebu (Baggase) Untuk Bahan Baku Pulp dan Kertas Masih Hadapi Kendala*, Pusat Informasi Kehutanan (http://www.dephut.go.id/INFORMASI/HUMAS/2005/563_05.htm, accessed on 10 January 2008.

[5]. Forgaty, William M. (Editor), (1987), *Microbial enzymes and Biotechnology,* London: Applied Science Publishers.

[6]. Holtzapple, M, Cognata, M., Shu, Y., Hendrickson, C., (1989), Inhibition of *Trichoderma reesei* Cellulase by Sugars and Solvents. *Biotechnology and Bioengineering*, Vol. 36, No.3.

[7]. Irawadi, T.T. (1991), Produksi Enzim Ekstraseluler dan Neurospora Sitophila pada Substrat Limbah Padat Kelapa Sawit. *Dissertation.* Magister Program IPB. Bogor.

[8]. Judoamidjoyo, M. Darwis, A and Sa'id, E. G. (1990), *Teknologi Fermentasi*. Bogor: PAU-Bioteknologi IPB.

[9]. Koesnandar, Helianti, Is. Dan Nurhayati N. (2008), Recent Development in the Bioconversion of Lignocelluloses into Ethanol, *Microbiology Indonesia*. Volume 2, Number 3, December 2008, p. 101-102.

[10]. Rahayu, E. S. (1987). *Teknologi Pengolahan Minuman Beralkohol*.Yogyakarta: Pusat Antar Universitas UGM Yogyakarta.

[11]. Susanti, E., Zakia N., Sumari dan Izzati, N., (2010). Pengaruh Perlakuan Awal Penguapan dan Penguapan-Impregnasi Menggunakan H_2SO_4 dan Etanol Terhadap Hasil Hidrolisis Ampas Tebu Secara Enzimatis, *Proceedings of the Seminar Nasional MIPA - Universitas Negeri Malang 13 November 2010*.

[12]. Susanti, E., Neena Z. and Sumari. (2009). Optimasi Produksi Bioetanol dari Limbah Ampas Tebu Berbasis Sistem Selulase *Bacillus circulans* strain lokal. Laporan Akhir Hibah Bersaing 2009/2010. (unpublished). State UniversityMalang.

[13]. Toharisman, Aris, (2007), *Sekali lagi: Etanol dari Tebu*, P3GI (online). (http://p3gi.net, accessed on 10 January 2008.

[14]. Waeonukul, R., Kyu K.L., and Ratanakhanokchai K., (2007), Multiple Cellulases and Xylanases from Bacillus circulans B6 During Growth on Avicel Under An Aerobic Condition, *Thai Journal of Biotechnology*, July 2007, p 27-32.

Conversion of West Kalimantan's Tropical Peat Into Bioethanol as Renewable Energy

Ferry Hadary [1], Lucy Arianie [2], Danial [3], Sri Rezeki [4]

[1,3] Department of Electrical Engineering, Faculty of Engineering, University of Tanjungpura, Pontianak, Indonesia (ferryhadary@yahoo.com; danial_mt@gmail.com)
[2] Department of Chemical, Faculty of Mathematic and Natural Science, University of Tanjungpura, Pontianak, Indonesia (lucy205@yahoo.com)
[4] Postgraduate student in Environmental Chemistry Program, Department of Chemical, Faculty of Mathematic and Natural Science, University of Gadjah Mada, Jogjakarta, Indonesia (rantisi_k1e@yahoo.co.id)

Abstract

The tropical peat is abundant of lignocellulosic materials. It means that tropical peat has big potency to be converted into bioethanol as alternative energy. This research was aimed to: (i) determine the percentage of lignin, cellulose, and hemicellulose of tropical peat, and (ii) convert the energy of tropical peat into bioethanol. Peat sample was taken in Pontianak Regency, West Kalimantan, Indonesia. The analysis of lignin, cellulose, and hemicellulose contents was carried out. It was hydrolyzed using sulfuric acid. Then, fermentation process was done by Saccharomyces cerevisiae for 5 days at 30ºC of incubation temperature. Bioethanol product was analyzed by pH, UV-Vis, and GC instruments. The result of this research showed that the concentration of bioethanol was 0.05 % with 91% of converted glucose into bioethanol.

***Keywords**: peat, hydrolysis, bioethanol, Saccharomyces cereviceae, energy.*

1. Introduction

Energy crisis is one of Indonesia national problems that must be looked for the way out. Energy is crucial for household, transportation and industry activities. Nowadays, energy necessity in Indonesia is fulfilled by exploiting the petroleum reserve (54.5%), natural gas (26.5%), coal (14.4%), and others (4.6%) [1].

The big dependency on fossil fuel energy resource causes the increase of national budgeting expense for domestic fuel price subsidy. In 2008, energy crisis which began by the rising of fossil fuel price has been causing the suffering life of poor people in Indonesia. The dependency on fossil fuel must be decreased slowly. The bad effect to the environment that caused of fossil fuel burning also becomes the urgent factor to find alternative energy non fossil fuel. One of alternative energy that is environment friendly is bioethanol.

Several research approaches are being carried out in order to assess the possibility of increasing bioethanol yields from alternative and available feed stocks. Bioethanol produced from lignocellulose and agro-industrial wastes can be seen as the most promising ones with the great advantage of a bioenergy not competing with food resources. Some of these residues such as, beet molasses, citrus waste pulp or carob pulp, represent an abundant, cheap and readily available source of raw-material to be converted into fuel [2].

Peat is one of alternatives that needs to be studied as energy resource. Peat in Indonesia has big potency, since it is reach more than 18 million hectare (ha) in wide and more than 30 cm in thickness [3]. Indonesia is the fourth of the widest peat area in the world after Canada, Russia, and USA. While West Kalimantan is the widest peat area in Indonesia [4].

Peat is composed of lignocellulosic materials from plants. Because of that, peat has potency to be converted into bioethanol through hydrolysis process of lignocelulose to simple sugar which finally fermentated becomes bioethanol. The objectives of this research were to: (i) determine the percentage of lignin, cellulose, and hemicellulose of West Kalimantan's tropical peat; and (2) convert West Kalimantan's tropical peat into bioethanol.

2. Experimental Details

Pretreatment

Peat sample was dried at 105ºC for 16 hours and placed in desicator to preserve the moisture level. Then it was cut into smaller size

(120 mesh). The analysis of lignin, cellulose, and hemicellulose contents was carried out.

Hydrolysis

Peat hydrolysis was done at 100 – 110ºC for 30 minutes with various concentration of sulfuric acid: 0.2; 0.3; 0.4; 0.5; and 0.6 M. The hydrolyzates were placed in vials to have glucose test using UV-Vis spectrophotometer. The residue was dried and measured in gravimetry. Then it was tested to identify the functional groups using IR (Infra Red) spectrophotometer.

Fermentation

Fermentation process was done using *Saccharomyces cerevisiae* at 30ºC for 24, 48, 72, 96 and 120 hours. Glucose level was measured using UV-Vis spectrophotometer. The yield of bioethanol was analyzed using GC (gas chromatography) instrument. The pH changing before and after fermentation was evaluated.

3. Result and Discussion

Peat Sampling

Sampling location was determined through preliminary investigation. Based on literature study, it was known that bioethanol can be produced from materials contain cellulose. Higher number of cellulose, much higher number of materials which can be hydrolyzed becomes glucose and then fermentated into bioethanol.

Fibric and hemic are known as kinds of peat which abundant of lignocelluloses [5]. These peat have characteristics brown color, and take place in 40-60 cm depth from the soil surface [4,6]. Peat sampling must be done in area which far enough from the water flow since it can cause cellulose decaying and form hemicellulose, lignin, and hydrogenous materials [6]. Based on above criterias, it was decided to get peat sample in Galang Village, Pontianak Regency, West Kalimantan Province, Indonesia.

Peat sample was obtained in 40-60 cm depth from the soil surface. The coordinate position was recorded using GPS (Global Positioning System) instrument. Sampling point was relatively far away from both of agricultural and plantation areas. It was expected that peat sample in its natural condition and has not contaminated by materials from human activities, such as fertilizer and others.

Peat sample was stored in plastic bag and transported to the laboratory to get identification about its physical characteristics and preparation process. Physical characteristics of peat sample were brown-blackish color, fibrous, and wet.

Analisys of Lignin, Cellulose and Hemicellulose

Lignocellulosic materials predominantly contain a mixture of carbohydrate polymers (cellulose and hemicellulose), lignin, extractives, and ashes. Lignin is a very complex molecule constructed of phenylpropane units linked in a three-dimensional structure. Generally, softwoods contain more lignin than hardwoods. Chemical bonds have been reported between lignin and hemicellulose and even cellulose. Lignin is extremely resistant to chemical and enzymatic degradation [7].

Peat is composed of organic materials such as plants residual which have not decayed completely. Because of that, peat contains amount of lignocellulosic materials. In this research, lignin, cellulose, and hemicellulose was analyzed to give information about each percentage in peat, as shown in Table 1.

Table 1. Percentage of Lignin, Cellulose and Hemicellulose in peat

Lignin	Cellulose	Hemicellulose	Others
68.0%	20.6%	6.6%	4.8%

Fourier Transform Infra Red (FTIR) of lignin compound that was isolated from peat is shown in Figure 1. Spectrum of lignin have band characteristic at 1330 cm^{-1} which indicate S and G ring; 1272 cm^{-1} for G ring and carbonyl; 1126 cm^{-1} which specific for S unit, secondary alcohol and carbonyl; and also 800 cm^{-1} which due to C-H binding at 2.5 and 6 position from G unit [8].

Peat Hydrolysis

Hydrolysis is representative of lignin, cellulose, and hemicellulose degradation. In this reseacrh, hydrolysis was done using various concentration of sulfuric acid. Concentration variation was applied to investigate the optimum condition for peat hydrolysis. The optimum concentration of peat hydrolysis was 0.3 M of sulfuric acid (Table 2).

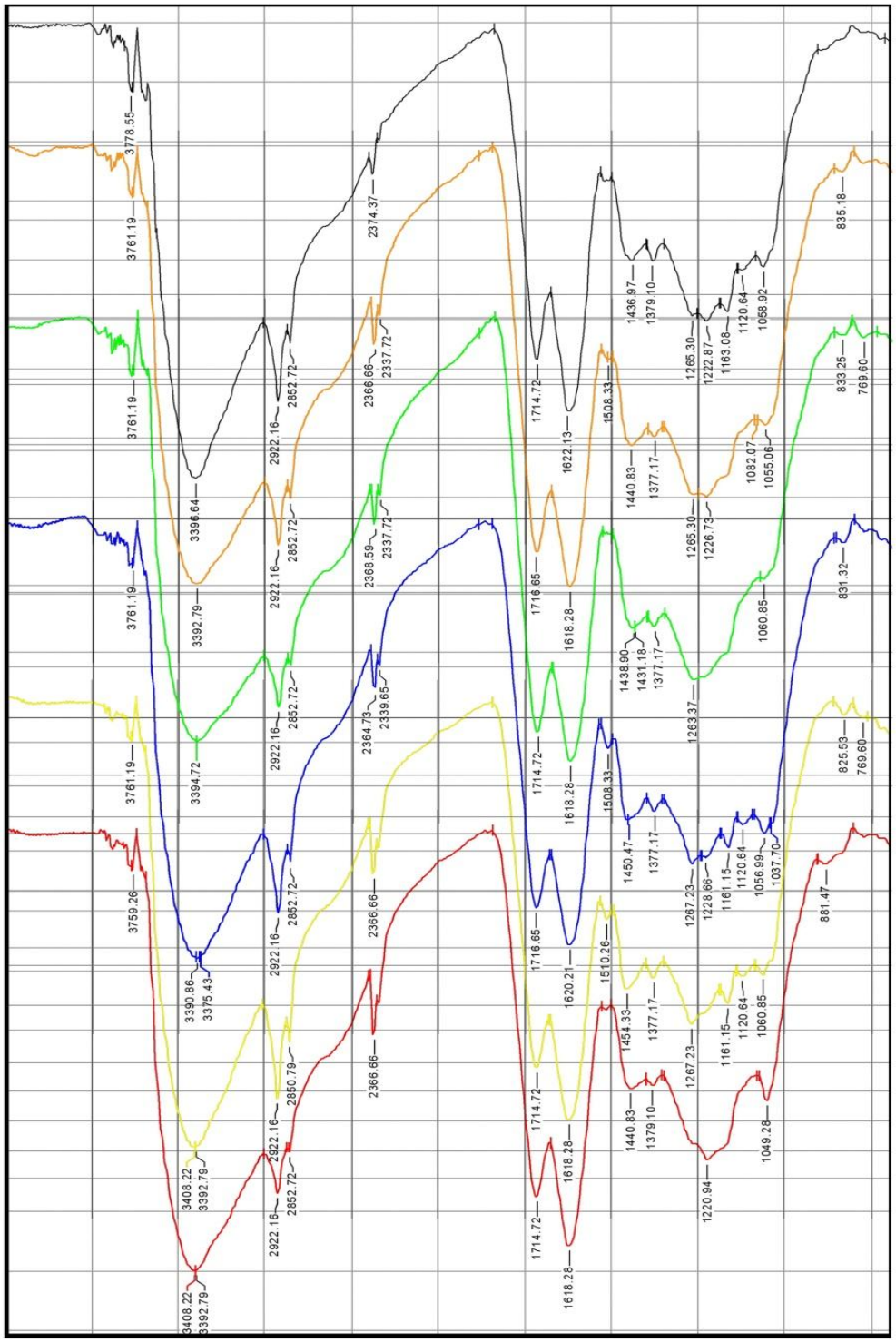

Figure 1. FTIR spectrum of lignin compounds from peat

Table 2. Correlation of various concentration of sulfuric acid to glucose yield

Concentration of H_2SO_4 (M)	Concentration of Glucose (ppm)
0.2	0.0078
0.3	0.0103
0.4	0.0077
0.5	0.0086
0.6	0.0029

Peat Fermentation

Ethanol can be derived by fermentation process from any material that contains sugar or compounds that can be converted to sugar. Cellulose must likewise be converted to sugars, generally by the action of mineral acids. Once simple sugars are formed, enzymes from yeast can readily ferment them to ethanol [9]. *Saccharomyces cereviceae* is the most commercially used microorganism in fermentation process to produce bioethanol [10,11].

In this research, concentration of glucose before and after fermentation was measured to evaluate the numbers of glucose that converted into bioethanol. The percentage of converted glucose was reach 91%. pH of hydrolyzate was changed from 5 becomes 6-7. The fermentation process took time 3–5 days.

GC Analysis

GC analysis in this research was aimed to observe the presence of ethanol that was resulted from fermentation process. Retention time (t_R) and % wide area all of ethanol standards and sample is shown in Table 3. From all of ethanol standards in Table 3, GC chromatograms of sample at t_R 2.952 (1st injection) and t_R 3.531 (2nd injection) as shown in Figure 2 was similar with GC chromatogram of ethanol standard 2 (0.05%) and have t_R that closed with t_R of ethanol standard 2 (0.05%), which have t_R 2.935 (1st injection) and t_R 3.480 (2nd injection) as shown in Figure 3.

Table 3. Chromatogram of Fermentation Result Compounds

	t_R (1)	t_R (2)	% wide area (1)	% wide area (2)
Ethanol standard 1 (0.01%)	2.920	3.491	15.719	84.280
Ethanol standard 2 (0.05%)	2.935	3.478	32.601	67.399
Ethanol standard 3 (1%)	3.025	3.500	91.495	8.505
Sampel	2.952	3.531	26.593	73.407

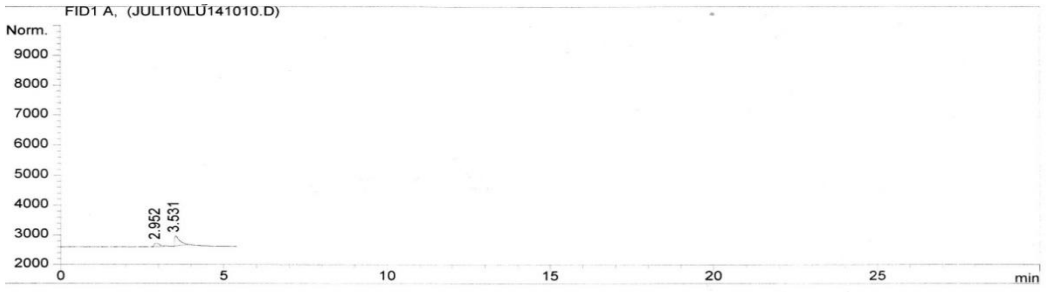

Figure 2. GC chromatogram for bioethanol of peat

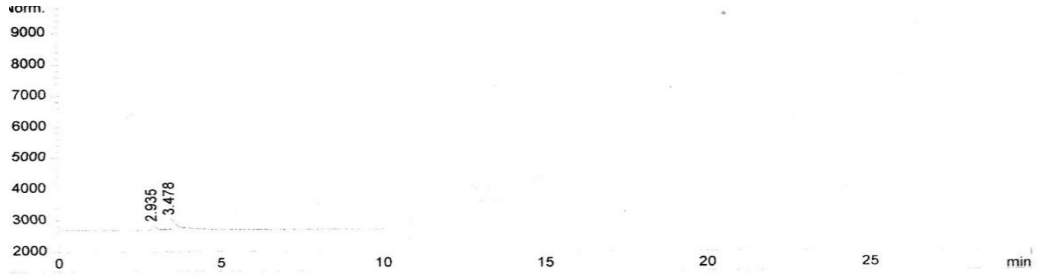

Figure 3. GC chromatogram for ethanol standard 2 (0.05%)

4. Conclusion

Peat contained 68% lignin, 20.6% cellulose, 6.6% hemicellulose and 4.8% other compounds. Peat can be hydrolyzed into bioethanol through fermentation process using *Saccharomyces cerevisiae*. The percentage that was obtained in this research at 30ºC of incubation temperature for 5 days was 0.05% with 91% of converted glucose into bioethanol.

5. Acknowledgement

Sincere thanks to Department of Research, University of Tanjungpura, for the research fund (STRANAS 2010- No: 79a/H22.10/PL/2010).

6. References

[1]. Soeparno, W., and Gunawan, B. (2007), Sumber Energi Alternatif Masa Depan, *BDB*, 3(1):1-5.

[2]. Raposo, S., Pardao, J.M., Diaz, I., and Lima-Costa, M.E. (2009), Kinetic modelling of Bioethanol Production Using Agro-Industrial By-Products, *International Journal of Energy and Environment,* 3(1):1-8.

[3]. Eka, L., and Herman (2004), Pirolisis Gambut dengan Katalis. Proceedings of National Seminar in Chemical Changes and Process, Semarang, 1-4.

[4]. Sagiman, S (2007). Pemanfaatan Lahan Gambut dengan Perspektif Pertanian Berkelanjutan. Scientific professor's speech paper. Pontianak: University of Tanjungpura, 5-27.

[5]. Tim Sintesis Kebijakan, (2008), Pemanfaatan dan Konservasi Ekosistem Lahan Rawa Gambut di Kalimantan, *Pengembangan Inovasi Pertanian,* 1(2): 149-156.

[6]. Wijaya, T. (2000), Pengkajian Endapan Gambut Bersistem di Daerah Pakiban-Beyuku Kecamatan Air Sugihan Kabupaten Ogan Komering Ilir Provinsi Sumatera Selatan. Colloquium of Outdoor Activities Result DIK-S, DSM, Ogan Komering Ilir, 1-14.

[7]. Taherzadeh, M.J., and Karimi, K. (2008), Pretreatment of Lignocellulosic Wastes to Improve Ethanol and Biogas Production: A Review. *Int. J. Mol. Sci., 9*: 1621-1651.

[8]. Pan, X-J. and Sano, Y. (1999), Atmospheric Acetic Acid Pulping of Rice Straw IV: Physico - Chemichal Characterization of Acetic Acid Lignins from Rice Straw and Woods. *Holzforschung*, 53(5): 511-518.

[9]. Bashori, M. (2008), Production of Bioethanol from Tapioca Starch Using Saccharomyces serevisiae: Effect of Inoculum Concentration and Temperature, Thesis, Pahang: University Malaysia Pahang, 7-12.

[10]. Li, B., Cheng, J., Qiao, B., and Yuan, Y. (2010), Genome-wide Transcriptional Analysis of *Saccharomyces cerevisiae* During Industrial Bioethanol Fermentation, *J. Ind. Microbiol. Biotechnol*., 37:43–55.

[11]. Gray, K.A., Zhao, L., and Emptage, M. (2006), Bioethanol, *Chemical Biology*, 10: 141–146.

Synroc Performance for Immobilization of High Level Liquid Radioactive Waste

Gunandjar

Center for Radioctive Waste Technology, National Nuclear Energy Agency of Indonesia (BATAN)
Tangerang Selatan, Banten (gunand@batan.go.id)

Abstract

The long lived of high level liquid radioactive wastes (HLLW) is generated from reprocessing of spent nuclear fuel. Moreover, the HLLW is generated also from ^{99}Mo radioisotope production using uranium target and post irradiation examination of nuclear fuel element. The HLLW has to be treated through immobilization (solidification) process to become wasteform prepared to disposal. In this paper was studied the synroc performance for immobilization of HLLW. Synroc is a crystalline wasteform comprising a stable assemblage of titanate phases chosen for their geochemical stability and collective ability to immobilize all the radioactive elements present in HLLW. Development of synroc for waste immobilization depends on the containing of radionuclides. For the HLLW containing actinides was developed zirconolite ($CaZrTi_2O_7$) rich synroc, for the waste containing uranium and plutonium was developed pyrochlore ($CaATi_2O_7$, A = Gd, Hf, U, and Pu) rich synroc with neutron absorbers (Hf and Gd) were needed to suppress criticality potential, whereas for the waste containing Tc, Cs, and Sr (from the heat producing of HLLW) was developed hollandite/perovskite [$Ba(Al,Ti)_2Ti_6O_{16}$ / $CaTiO_3$] rich synroc. All basic science studies confirm that the leach-rates and α-decay damage in synroc relatively very low and acceptable. The synroc wasteforms should succeed for HLLW and particularly very well for immobilization of the long-lived α-emitter of actinide elements. Synroc performance for immobilization of HLLW is better than borosilicate glass. In Indonesia, adaptation of HLLW immobilization technology using synroc materials will be carried out for HLLW generated from ^{99}Mo radioisotope production and post irradiation examination of nuclear fuel element.

Keywords: *synroc, waste immobilization, high level liquid radioactive waste.*

1. Introduction

Nuclear technology development and its application have been much utilized in the world for energy generation and non energy application such as in industries, nuclear medicine, etc. The radioactive wastes generated from the activities has to be managed conform to the safety standard for protect occurring the radiologic impact which hazardous to the public and environment. One of the radioactive waste type generated from nuclear application is the long lived of high level liquid radioactive wastes (HLLW).

In some countries which have closed nuclear fuel cycle strategy, the HLLW are generated from the first cycle extraction of the spent fuel reprocessing plant. Reprocessing of spent nuclear fuel is a process to recover the remaining uranium (U) and plutonium (Pu) elements in spent nuclear fuels. The HLLW contains fission product elements as major elements and transuranic elements as minor (contaminated) elements. In the second cycle extraction is generated transuranic liquid waste (TRULW) containing transuranic elements as major elements and fission product as minor elements.

In the other hand, some countries which have open fuel cycle strategy, such as Indonesia, the high level radioactive waste (HLW) means the spent fuel it self. At present in Indonesia, the HLLW are generated from Mo-99 radioisotope production (using uranium target) at Radioisotope Production Plant (RPP) and post irradiation examination of nuclear fuel at Radiometallurgy Installation (RMI). The HLLW has to be immobilized through solidification process to become wasteform readily to be stored for long-term (many million of years) in the disposal facility (Deep Geological Disposal Facility).

At present, the nuclear power industry strategy of incorporating fission product wastes (in HLLW) from nuclear fuel reprocessing in borosilicate glass (by vitrification process), followed by deep burial, was subject to little question until early 1970s. However it was then realized by geochemists that borosilicate glasses were not particularly stable when buried in the ground, because radiogenic heating (gamma

heating) within the glass and groundwater could not be guaranteed to avoid contact with the glasses, even when a series of additional barriers such as metal containers and clay overpacks were introduced into a geological repository [1].

Technology development was carried-out continuously to find faithfully the immobilization technology of HLLW. The synroc is an alternative matrix material for immobilzation of long lived radioactive waste especialy for HLLW. The immobilization technology using synroc has been developed in Australia, United State of America, and Japan**.** Synroc is a crystalline wasteform comprising a stable assemblage of titanate phases chosen for their geochemical stability and collective ability to immobilize all the radioactive elements present in HLLW [2].

In this paper, we investigate the synroc performance for immobilization of HLLW, related to the basic science studies concerning the solid-state chemistry of synroc phases and wasteform development, and basic research results for synroc performance with review some parameters especially leach-rates (aqueous durability) and α-decay damage (α-radiation durability) of the synroc. The both parameters are very importance to evaluate the immobilization technology of HLLW. The study was carried-out by assessment based on various data gathering from many references. This paper also studies the adaptation especially for immobilization of long lived HLLW types in Indonesia.

2. Experimental Detail

Based on the data related the experimental detail concerning basic research for synroc performance**,** there are three main components for basic research concerning the development of synroc as matrix material for immobilization of HLLW, namely: solid-state chemistry of synroc phases and wasteform development, aqueous durability, and studies of radiation damage phenomena.

Solid-state chemistry of synroc phases and wasteform development

The R&D was started by immobilization of Purex type HLLW into synroc-C. Further development of synroc for many other types of HLLW, which synroc variants had, is potential for immobilization, where safe containment is required over geological timescales. Development of synroc composition comprising of synroc phases depend on the content of radionuclides in the HLLW.

Aqueous durability of synroc

In the aqueous durability study, leach rate is a parameter to inform the leaching behavior of synroc wasteform. Based on IAEA procedures, whereby the wasteform of synroc is leached by a fixed volume of deionized water in a closed container for a specific period, after which the leaching solution is decanted, analysed and replaced by fresh deionized water. Leach rates are calculated according to the relationship [3]:

$$\textbf{Leach rate} = (C_l / C_s)\ \textbf{(w/t.s)} \qquad (1)$$

Where C_l = quantity of each species in solution, C_s = quantity of each species in solid sample, w = initial weight of solid test specimen, t = duration of leaching, and s = geometrical surface area of sample. The synroc performance concerning the leach-rates parameter is compared with borosilicate glass. In this study, waste loading is one of synroc performance for incorporating the waste containing fission products and associated actinides in the crystalline lattices of synroc.

Study of radiation damage phenomena

Radiation damage studies were perfomed with diffraction studies of metamict synroc analogue minerals, and electron, neutron, and heavy ion irradiated syntetic samples, including the use of incorporated actinides α-emitters such as ^{244}Cm and ^{238}Pu (half-lives of 18 and 87 years respectivelly). In this study was carried-out by experiments concerning the α-radiation effects on synroc damage and it was related to the leaching rate, swelling, and microcracking.

3. Result and Discussion

Solid-state chemistry of synroc phases and wasteform development

The synroc production method is basically to first mix the HLLW in nitric acid solution with the precursor oxides to make the synroc minerals. The standard synroc precursor has the following composition (wt% oxide): Al_2O_3 (5,4); BaO (5,6); CaO (11,0); TiO_2 (71,4); and ZrO_2 (6,6). The mixture is dried, calcined, and hot pressed under reducing condition at about 1200 ^oC to form a dense multiphase ceramic [1].

The major phases of minerals in synroc are: *hollandite* [$Ba(Al,Ti)_2Ti_6O_{16}$], *zirconolite* ($CaZrTi_2O_7$), and *perovskite* ($CaTiO_3$). In addition, titan-oxides and alloy phases occur in small amount. Table 1 shows the phase constitution of synroc-C, containing 20 wt% HLW, and radionuclides incorporated in the various mineral-analogue phases present.

The formation of major phases in synroc minerals occur at high temperature at about 1200°C by equation of reaction as follows:

$BaO + Al_2O_3 + 8\ TiO_2 \rightarrow Ba(Al,Ti)_2Ti_6O_{16} + 2\ O_2$ (*Hollandite*) (2)

$CaO + ZrO_2 + 2\ TiO_2 \rightarrow CaZrTi_2O_7$ (*Zirconolite*) (3)

$CaO + TiO_2 \rightarrow CaTiO_3$ (*Perovskite*) (4)

Tabel 1: Composition and mineralogy of *synroc-C* (*synroc* standard) containing 20 wt% HLW [1].

Phases	Wt %	Radionuclides in lattice
-Hollandite, $Ba(AlTi)_2Ti_6O_{16}$	30	- Cs and Rb.
-Zirconolite, $CaZrTi_2O_7$	30	- Rare earths (RE), Actinides (An).
-Perovskite, $CaTiO_3$	20	- Sr, RE, and Actinides (An).
-Titan Oxides	10	
-Alloy phases	5	- Tc, Pd, Rh, Ru, etc.

Since 1984 onwards, the production of synroc has been prepared by hydrolysing a slurry mixture of Al, Ti, and Zr alkoxides with aqueous slurry of Ba and Ca hydroxides (as the precursor rather than using oxides) [4]. This precursor provides better solid-state reactivity with formation of phases mentioned above. Further of the synroc development were known existing some the other phases formed from derivative of major phases caused by exchange (substitution) of elements in mineral phases with some elements contained in the waste. The derivative phases are *pyrochlore* $CaATi_2O_7$ (A= Gd, Hf, Pu, U), *brannerite* ($AnTi_2O_6$), and *freudenbergite* ($Na_2Fe_2Ti_6O_{16}$), they are derivative phases from *zirconolite*, *perovskite*, and *hollandite,* respectivelly.

Development of synroc for waste immobilization depends on the containing of radionuclides. The HLLW containing actinides was developed *zirconolite* ($CaZrTi_2O_7$) rich synroc, the waste containing U and Pu was developed pyrochlore ($CaATi_2O_7$) rich synroc with neutron absorbers (Hf and Gd) were needed to suppress criticality potential, whereas for the waste containing Tc, Cs, and Sr (from the heat producing of HLLW) was developed *hollandite* [$Ba(Al,Ti)_2Ti_6O_{16}$ / *perovskite* $CaTiO_3$] rich synroc.

Result of Studies for Aqueous Durability of Synroc

Basic research result giving detail experiment data concerning the aqueous durability of synroc performance related to the leaching behavior of synroc compared with leaching behavior of borosilicate glass are shown at Figure 1-2**.**

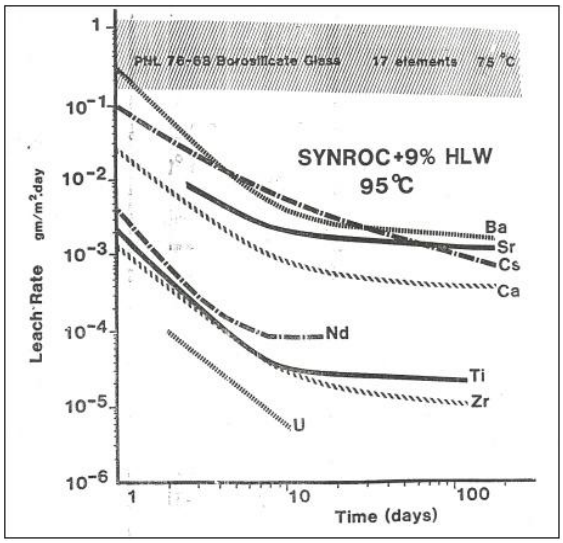

Figure 1. Comparative leaching behaviour of *synroc* + 9% HLW at 95ºC and PNL 76-68 borosilicate glass at 75ºC in pure water [5-8].

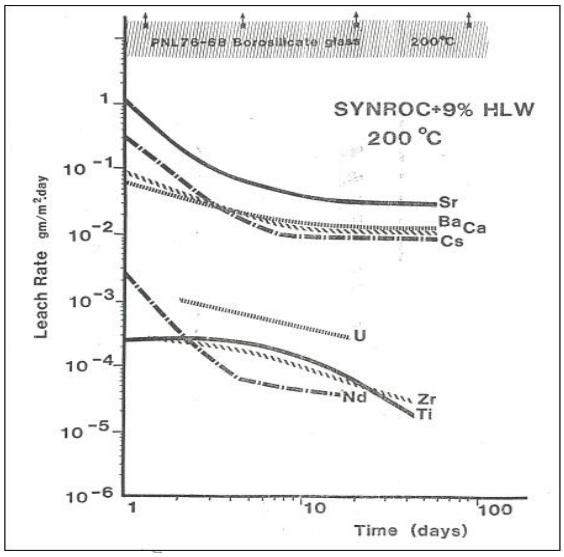

Figure 2. Comparative leaching behaviour of *synroc* + 9% HLW and PNL 76-68 borosilicate glass at 200ºC in pure water [6,8].

In Figure 1 and 2, leach rates for a typical borosilicate glass developed for radioactive waste immobilization (PNL 76-68**)** remain essentially constant over long periods as the glass dissolves in a quasi-congruent manner, with value of leach rate about 0.8 – 1.0 g/m^2.day. On the other hand, leach rates for synroc are exhibit a wide range of different elements and cannot be characterized by a single representative value at given temperature.

Moreover, the leach-rates are not constant but fall rapidly in the first 10-30 days, after which they level off. After 10-30 days in pure water at 95ºC, the leachabilities of univalent and divalent elements (Cs, Ca, Sr, and Ba) are 500 to 2000 times smaller than those of borosilicates glass. Multivalent elements display even lower leachabilities from synroc. Nd, Ti, Zr, and U are on the average about 10,000 times less leachable from synroc than from boroslicate glass. Similar behavior is displayed at 200ºC (Figure 2)**.**

It is evident that synroc is vastly more resistant to leaching by ground-waters than is borosilicate glass. The difference is most pronounced in the case of multivalent elements (modeled by U and Nd). It follows that synroc wasteforms should succeed particularly well in immobilizing the long-lived alpha-emitting actinides elements.

The leaching performance of synroc at 95ºC and 200ºC as a function of waste loading are shown in Figure 3 and 4. It is important to note that its leaching characteristics are very similar, as waste loadings increase from 9 to 16 to 20 wt %. These data provide evidence of the synroc capacity to tolerate variations in waste-stream composition. Moreover, it was shown that waste loading of 20% could be readily accepted by synroc without significantly impairing its resistance to leaching by groundwaters.

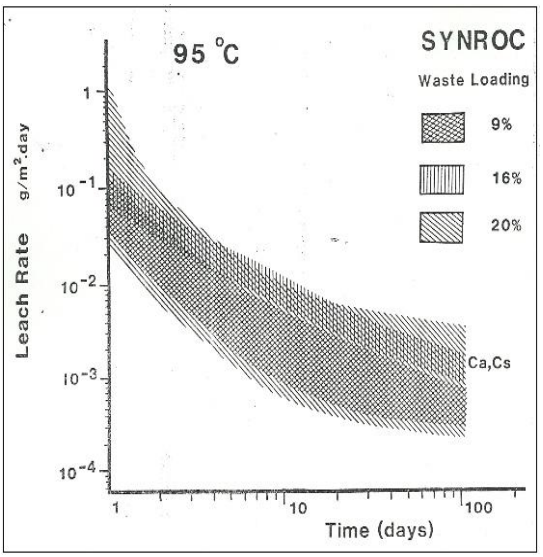

Figure 3. Ca and Cs leach-rates for Synroc with waste-loadings of 9, 16, and 20 weight % at 95 ºC [6,8].

The other experiment for transuranic wastes, the solubility of actinides in *zirconolite* and *perovskite* is quite high and the actinides partition between these two phases. The leach rates of actinides from synroc are very low and decrease in the order of Np > Pu > Am > Cm. The normalised total leach rates after 1000 days tend to approach 10^{-5} to 10^{-6} g/m^{2}day at 70 ºC [9]. For alkalis and alkaline earths showed also leaching behavior similar with the Figure 1-4, that leach rates of alkalis and alkaline earths at 90^{o}C in water are typically < 0,1 g/m^{2}day for the first few days, and they decrease asymptotically to values of ~ 10^{-5} g/m^{2}day after 2000 days. Leach rates of 10^{-5} g/m^{2}day correspond to ~ 1 nm/day [1]**.**

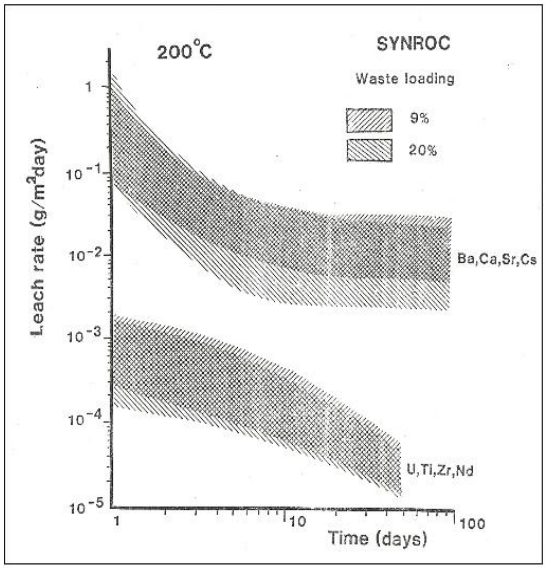

Figure 4 : Leach-rates at 200ºC for synroc with waste-loadings of 9 and 20 weight % (for HLW containing Ba, Ca, Sr, Cs , U, Ti, Zr, and Nd) [6,8].

Radiation Effects (α-radiation durability) of synroc

Radiation damage studies were perfomed with diffraction studies of metamict synroc analogue minerals, and electron, neutron, and heavy-ion irradiated syntetic samples, including the use of incoporated ^{244}Cm and ^{238}Pu α-emitters. It was shown that the only significant and permanent damage processes to solid wasteforms arise from α-decays events, with the main damage arising from the recoil atom, not the α-particle itself. Because of the short range (~20 nm) of the recoil atoms, most of the damage occurs in the phases which host the actinides. The experiments results concerning the α-radiation effects on synroc damage indicated by increasing of leaching rate, swelling, and microcracking are shown at Table 2**.**

The effects on leachability, microcracking and X-ray structure of Cm-doping (α-emitters) of synroc-type wasteforms was studied and the leach

rate increases accompanying the amorphism of Cm-doped *zirconolite* were only ~ 10 times or only a factor of 10 leach rate enhancements ($1x10^{-5}$ become $1x10^{-4}$ g/m^{2}day). The long-term research on synroc has been most fruitful in understanding the behaviour of synroc subjected to high dose rates of α-radiation; it has indicated no sign of intergranular cracking in hot pressed synroc-C [10]. The other experiment showed that ^{238}Pu doped zirconolite/pyrochlore expanded by ~ 6% when it was rendered X-ray amorphous [11].

Table 2. The effects of α-radiation on synroc damage.

Types of *synroc*	Doping of α-emitter	Effects of α-radiation on *synroc*
Synroc-C and Synroc amorf phase *zirconolite*	^{244}Cm	Leach-rates increases accompanying the amorphous of Cm-doped *zirconolite* were only ~ 10 times ($1x10^{-5}$ become $1x10^{-4}$ g/m^{2}day) [10].
Synroc *zirconolite* / pyrochlore rich	^{238}Pu	The swelling occur ~ 6 vol. % [11].
Synroc-C and single phase specimens of *zirconolite* and *perovskite*.	^{238}Pu and ^{244}Cm .	The swelling occur: 4.0–6.9 vol %. Differential swelling of the various crystaline phases did not cause micro-cracking [12].
Synroc containing *zirconolite*, pyrochlore and *brannerite*.	α-emitter Actinides	It are occured the microstructural changes (amorphise) caused from α-radiation in synroc by approximately a factor of 3 [13,14].

A principle concern with crystalline waste forms containing high actinide content is α-decay damage which may render them amorphous and could lead to significant changes in physical and chemical properties. The most extensive measurements of α-decay damage have been performed on synroc-C and single phase specimens of *zirconolite* and *perovskite*, containing up to 11.2 wt% $^{238}PuO_2$ or 4% $^{244}Cm_2O_3$ with doses up to $1.5x10^{19}$ α-decays/g. At 300K, the saturation swelling in synroc-C ranges between 4.0 and 6.9 vol%, depending on the relative amounts of *zirconolite* ($CaZrTi_2O_7$) and *perovskite* ($CaTiO_3$) [12]. Differential swelling of the various crystaline phases did not cause microcracking in synroc-C.

Naturally-occuring *zirconolites* exposed to about $3x10^{20}$ α-decays/g have been shown to have retained actinides for periods of up to $2.5x10^9$ years**.** The nature of the micro-structural changes in accelerated tests on synthetic *zirconolite*, pyrochlores, and *brannerite* are similar to those in natural *zirconolites* containing uranium and/or thorium and the onset of amorphisation occurs at similar α-doses [13]. The doses of heavy ions (simulating α-recoil nuclei) required to amorphise the different actinide-bearing phases vary by approximately a factor of 3 [14].

Based on all basic science studies mentioned above confirm that the leaching-rates and α-decay damage in synroc relatively very low and acceptable. Synroc performance for immobilization of HLLW is better than borosilicate glass.

Adaptation of HLLW Immobilization Technology Using Synroc in Indonesia

In Indonesia, The Center for Radioactive Waste Technology – BATAN will performed adaptation of immobilization technology using synroc materials. The first step, adaptation have been carried-out for immobilization of sludge waste containing uranium generated from decommisioning of phosphoric acid purification facility (Petrokimia Gresik). The sludge waste contains uranium including long-live alpha waste classification, must be immobilized by solidification process. The immobilization of radioactive sludge waste using matrix material of synroc was conducted by sintering process. Immobilization process of the waste in synroc was carried-out by mix the radioactive sludge waste with precursor oxide standard. The mixture is dried, calcined, and pressed in moulder, and then the wasteform of pressing result was prosessed by sintering at 1000 – 1200ºC form the solid multiphase ceramic. The performance of the synroc wasteform was determinated by test of density, pressing streng, and leaching-rate. The test results showed that the optimum performance of synroc wasteform was obtained at the waste loading 30% weight, sintering process at 1200ºC for 3 hours with values of density 2, 8 g/cm^3, pressing strength 10, 4 kN/cm^2, and total of leach-rate at the first day is 2,64 x 10^{-4} g/cm^2.day [15]. The performance of the synroc wasteform producted by sintering process relativelly conform to the hot pressing process. Further, the adaptation of immobilization technology using synroc materials will be carried-out for HLLW generated from ^{99}Mo radioisotope production and post irradiation examination of nuclear fuel element.

4. Conclusion

Synroc is a crystalline wasteform comprising a stable assemblage of titanate phases chosen for their geochemical stability and collective ability to immobilize all the radioactive elements present in HLLW. Development of synroc for wastes immobilization depends on the containing of radionuclides. For the HLLW containing actinides was developed zirconolite ($CaZrTi_2O_7$) rich synroc, for the waste containing uranium and plutonium was developed pyrochlore ($CaATi_2O_7$) rich synroc with neutron absorbers (Hf and Gd) were needed to suppress criticality potential, whereas for the waste containing Tc, Cs, and Sr (from the heat producing of HLLW) was developed *hollandite* [$Ba(Al,Ti)_2Ti_6O_{16}$ / *perovskite* $CaTiO_3$] rich synroc. All basic science studies confirm that the leach-rates and α-decay damage in synroc relatively very low and acceptable. The synroc wasteforms should succeed for HLLW and particularly very well for immobilization of the long-lived α-emitter of actinide elements. Synroc performance for immobilization of HLLW is better than borosilicate glass. In Indonesia, adaptation of HLLW immobilization technology using synroc materials will be carried out for HLLW generated from ^{99}Mo radioisotope production and post irradiation examination of nuclear fuel elements.

5. Acknowledgement.

---

6. References

[1]. Vance E.R. (1999), *Status of Synroc Ceramics for HLW,* Proc. of The 2nd Bianual Int. Workshop on HLRW Management, Dep. of Nuclear Eng., Faculty of Engeneering, Gadjah Mada University, Yogyakarta, 10-17.

[2]. Ringwood, A.E., Kesson, S.E and Ware, N.G. (1980), *Immobilization of US Defence Nuclear Waste Using the Synroc Process,* in Scientific Basis for Nuclear Waste Management, Vol 2, Plenum Press, New York, p 265.

[3]. Hespe, E.D. (1971), *Leach testing of immobilized waste solids*, a proposal for a standard method, Atomic Energy Review 9, 1-12.

[4]. Ringwood, A.E, Kesson, S.E, Reeve K.D., Levins, D.M and Ramm, E.J. (1988), *In Radioactive Waste Form for the Future*, Elsevier, North-Holland, p. 233-334.

[5]. Vance E.R., Day, R.A., Carter, M.L., and Jostsons, A. (1996), *A Melting Route to Synroc for Hanford HLW Immobilisation,* in Scientific Basis for Nuclear Waste Management XIX, Materials Research Society, Pittsburgh, PA, USA, p. 289-296.

[6]. Oversby, V.M. and Ringwood, A.E. (1980), "*Leach testing of Synroc and glass samples at 85 °C and 200 °C"*, Nuclear Chem. Waste Management.

[7]. Ringwood A.E., Oversby V.M., and Kesson S.E. (1982), *Synroc: Leaching Performance and Process Technology*, Research School of Earth Science, The Australian National University, Australia, p. 495-506.

[8]. Coles, D.G. and Bazan, F. (1980)," *Contiuous flow leaching studies of crushed and cored synroc"*, UCRL preprint 84679, also Jour. of Nuclear Technology.

[9]. Coles, D.G., Bazan, F., Weed, H.C., and Schweiger (1981), J.S., *Leaching behavior of Synroc,* Unpublished results.

[10]. Weber, W.J., Wald, J.W., and Matzke H.J. (1986), *"Effects of Self-Radiation Damage in Cm-Doped $Gd_2Ti_2O_7$ and $CaZrTi_2O_7$, Journal of Nuclear Materials*, 138, p.196.

[11]. Clinard, F.W.Jr., Peterson, D.E., Rohr, D.L., and Hobbs, L.W. (1984), Journal of Nuclear Materials, 126, p. 245.

[12]. Ewing, R.C., Weber W.J., and Clinard, F.W.Jr. (1995), *"Radiation Effects in Nuclear Waste Forms for High Level Radioactive Waste"*, Program in Nuclear Energy, 29, p.63.

[13]. Lumpkin, G.R., Hart, K.P., McGlinn, P.J., Payne, T.E., Giere, R., and Williams, C.T. (1994), *"Retention of Actinides in Natural Pyrochlores and Zirconolites"*, *Radiochemica Acta*, Vol. 66/67, p. 469.

[14]. Smith, K.L., Zaluzec, N.J., and Lumpkin, G.R. (1998), *"Scientific Basis for Nuclear Waste Management XXI,* Materials Research Society, Pittsburgh, PA, USA, p.931.

[15]. Endang Nuraeni and Gunandjar (2010), *Technology Development of Radioactive Waste Treatment from Industry: The Immobilization of Radioactive Sludge Waste using Matrix Material of Synroc by Sintering Process*, Research Activity Report, The Center for Radioactive Waste Technology-BATAN.

Bambara Groundnut (*Vigna subterranea (L.) Verdc*) as Sustainable Food: Strategic Consideration Future Prospect

Hayyu Febriani [1], Endah Sri Redjeki [2]

(1) Agriculture Faculty, University of Brawijaya, Malang, Indonesia (ayie.redluph@gmail.com)
(2) Agriculture Faculty, University of Muhammadiyah, Gresik (endah.sriredjeki@yahoo.co.uk)

Abstract

Bambara groundnut is an underutilized African legume which provides security for many farmers as it shows considerable drought resistance. This crop is suitable for semi arid climates and needs few input. To date, the full genetic diversity of the crop remains largely unexploited. Until recently bambara groundnut never received any appreciable research effort, especially for its genetic improvement. Research on bambara groundnut strains exist in Indonesia is rarely done in Indonesia. Screening of bambara groundnut has been held in Jatikerto-Malang, on February until September 2010. There are 44 strains of bean Bambara, i.e.: 28 lines origin Indonesia and 16 the rest, origin Swaziland, Namibia, Botswana, Ghana, Nigeria and Mali. From the results of heritability estimates, obtained high value heritability for the character Petiole length 0.57, internodes length 0.52, banner length of flower 0.68, pod length 0.69 and width of pods 0.85. The ability to form a symbiotic relationship with nitrogen fixing rhizobia is common to 88% of legume species. Legumes used as crops benefit greatly from symbiotic nitrogen fixation, with a total amount of nitrogen fixed of the order of 100-250 kg N ha. In addition, Bambara nuts have high nitrogen content; so as to reduce the use of fertilizer N. Bambara groundnut has good prospects in addressing drought, hence it is possible to be used as an alternative sustainable food.

***Keywords**: Bambara groundnut, Vigna subterranea, Heritability, sustainable food.*

Introduction

Bambara groundnut is an underutilized African legume which provides security for many farmers as it shows considerable drought resistance. This crop is suitable for semi arid climates and needs few input. bambara groundnut plays an important socio-economic role in the semi-arid regions in Africa. It is rich source of protein and along with other local source of protein could help to alleviate nutritional problem in these areas.

In Indonesia, Bambara groundnut has great potential to be cultivated. Increasing consumer demand, will improve also their economic value. This is shown by frequent in the village of Rawa and and Nagarakembang (Majalengka) which is a center of Bambara fried groundnut producers of raw material shortage, so it must be brought from outside the area gap between consumer demand with the willingness of the crop is an excellent opportunity to begin to develop the commodity [1].

Bambara groundnut seeds may be eaten raw when immature, but become too hard when mature. When roasted or boiled, even the mature seeds are sweet and pleasant tasting. The seed are often roasted and ground into nutritious flour [2]. It seeds can be use to produce vegetable milk that is comparable with soy milk. Protein functionality test on the ground seed indicate that it can be complete with or replace other conventional flours in a range of processed products [3]. Bambara groundnut is useful crop with nutrition content including 16 – 21% protein, 50 – 60% carbohydrate and only 4.5 – 6.5 % fat [4]. The seed makes a complete food, as it contains sufficient quantities of proteins, carbohydrates and lipid [3,5]. It will be support the sustainable food program that balance emerging food issues about various healths, environmental and social concerns. *Sustainable food system is defined as one in which food production; processing, distribution and consumption are integrated to enhance the environmental, economic, social and nutritional health of a particular place.*

Nowadays, the full genetic diversity of the crop remains largely unexploited. Until recently bambara groundnut never received any appreciable research effort, especially for its genetic improvement. Research on bambara groundnut strains exist in Indonesia is rarely done in Indonesia. Biochemical and molecular analyses of selected bambara groundnut landraces have also revealed great genetic diversity between and within landraces [6-9].

Plants of the introduction result can become the new varieties, either directly or indirectly, in accordance with it is ability to adapt [10]. Bambara groundnut takes about 4-5 months to mature. Farmers in Indonesia have not much reason to plant this crop with a long harvest age. With the introduction of testing of the parental strains from Africa and Indonesia, it is expected to be obtained genotypes Bambara shorter-lived, have high yield potential and can adapt well in Indonesia.

To obtain new varieties with traits offspring better than ever, need to be election lines / elders. A superior plant variety in a region, have a good combination that form a high yield character. The differences character is caused by the differences of genes and interactions. Lots of genetic types that may be formed from a single plant of a species, a type of genetic diversity were utilized by breeders by forming strains. From these strains, the superior strains can be obtained. In plant breeding, genetic diversity is absolutely necessary; because the more extensive genetic diversity of a plant, in plant breeding programs the greater the chances of getting increased genetic potential for desirable traits [11].

Genetic potential is the maximum capacity of individuals who are determined by genetics. To know the genetic potential of a crop is required knowledge of genetic diversity and heritability. Genetic potential elder-elders are needed later in the hybridization for the improvement of plant traits and in preparing the description of varieties. So the goal of sustainable food can be reach in the future.

2. Experimental Details

The research was conducted at the experimental station UB Jatikerto Village, District Kromengan, Malang. Elevation at the study site ± 330 m dpl, with a temperature range of 27-29ºC and rainfall is 1924 mm/year. Research was conducted in February to July 2010. Materials that used in this study are 44 genotypes Bambara. Planting material obtained over South cooperation Laboratory, School of Biosciences, University of Nottingham.

All strains are planted together in a population without repetition. Estimation of genetic potential among strains was based on the potential of each phenotype. The influence of genetic variants is known from the reduction phenotype with variant environment. Genetic diversity obtained from genetic differences between strains.

Estimation of genetic diversity and estimation of heritability used in this study. Quantitative characters were calculated using the formula range of environmental, phenotypic, genetic and heritability. Diversity can be caused by the environment is called environmental diversity [10]. Variety is measured from a population for a particular character is a variety of phenotypes. Variety phenotype consists of various genetic, environmental diversity and the genetic interaction and environmental diversity [12]. To calculate the range of phenotypes between lines, use the formula:

$$\sigma^2 p = \frac{\sum x^2 - (\sum x)2/n}{n-1}$$

$\sigma^2 p$ = phenotype variant
x = value
n = number of plant

Genetic variant obtained from genetic differences between strains using the formula:

$\sigma^2 g = \sigma^2 p - \sigma^2 e$
$\sigma^2 g$ = genetic variant
$\sigma^2 p$ = phenotype variant
$\sigma^2 e$ = environment variant.

Estimate of heritability value can be calculated using the formula:

$$h^2 = \frac{\sigma^2 g}{[\sigma^2 g + \sigma^2 e]}$$

Criteria of heritability value according to [16]: 0.0 < h^2 < 0.2 = low heritability; 0.2 < h^2 < 0.5 = medium heritability; h^2 > 0.5 = high heritability.

3. Result and Discussion

Heritability on the observed characters based on analysis of data (Table 2) indicates that the value of heritability has a range of low to high values of between 0 to 0.85. Results of analysis of heritability on the observation of character traits emergence rate, terminal leaflet length, number of leaves, Petiole length, internodes length, terminal leaflet width, banner length, Number of days from sowing to flowering, peduncle length, number of flowers per peduncle, plant spread, plant height, number of pods, pod length, pod width, seed length, seed width, number of stems per plant, number of branches per stem, number of nodes per stem, and mature.

Results of analysis of data obtained heritability values in Table 2, show that high heritability values was found in the character Petiole length, internodes length, banner length, mature. At length the character of the terminal leaflet length obtained heritability values of 0.45 that is show as low heritability. On the character number of leaves obtained heritability values of

0.08 which show a low heritability. Petiole length characteristic values obtained heritability of 0.57 shows a high heritability. In the internodes length character heritability values obtained at 0.52 it is including high heritability.

At the terminal leaflet width character heritability values obtained at 0.07 it is including the mid heritability. At banner length obtained heritability values of 0.68 which includes a high heritability. On the character number of days from sowing to flowering, it was obtained heritability values of 0.04 which includes a low heritability. At peduncle length obtained heritability values of 0.01 which includes a low heritability.

On the number of flowers per peduncle character obtained heritability values of 0 which includes a low heritability. In plant spread character 0.11 that is included low heritability. On plant height obtained heritability values 0.5 which is included mid heritability. At the character number of pods obtained heritability values of 0.02 which includes a low heritability. In the pod length character obtained heritability values of 0.69 which includes a high heritability. On the characters of pod width obtained heritability values of 0.02 which includes a low heritability. At seed length obtained heritability values of 0.4 which is included a mid heritability. In broad bean character heritability values obtained at 0.5 which is included mid heritability.

On the number of stems per plant character obtained heritability values of 0.26 that is include in mid heritability. At the character number of branches per stem obtained heritability values of 0.69 which includes a high heritability. On the number of nodes per stem character obtained heritability values of 0.02 which includes a low heritability. At the mature character heritability values obtained at 0.91 including high heritability.

Diversity contained within a species (species) is caused by two factors, namely diversity caused by the environment and diversity caused by inherited traits or genetic. The diversity in plants usually caused by the interaction of environmental factors and genetic factors and influences the appearance of plant phenotype [13]. Genetic diversity in a species can be known through observation of plant phenotypes, such as: high and low, color, age of the plant, high and low yield, and so forth. The nature of the phenotype is determined by specific genes found on chromosome, gene-gene interaction or gene by environment [13]. The heritability reflects the work of the core genes that lie at the core; high heritability values indicate that the involvement of genes in the cell nucleus is high enough in the appearance of a character. Thus, only families with a high heritability value opportunity for further breeding activities of selection.

Heritability values needed to find a trait (difference of character appearance) due to genetic or environmental factors. Predictive value of heritability of a character can be used as one criterion for selection of a population, where the characters with high heritability value indicate that selection is more effective than low heritability [14]. Based on the results that are categorized as high heritability value is in characters 0.57 Petiole length, internodes length 0.52, length of the flag of interest 0.68, 0.69 pod length, pod width 0.85, number of branches per stem 0.69, mature of 0.91. High heritability value in some characters in this study indicate that the diversity that arises on 44 genotypes Bambara influenced by genetic factors. High heritability value indicates that the character of genetic diversity observed had a relatively greater than the environments variant.

If the heritability of a trait is more than 50%, then the trait can be selected in a variety improvement through selection programs [15]. According to [16] adds that the high heritability close to 100% is a sign that the phenotypic trait is a good index for the characters will be improved and provide the greater genetic progress in selection. Based on the observations of high heritability value which is close to 100%, the mature character has 0.91 heritability value. This shows that character of the plant has a big genetic potential in improving results through selection. A high heritability value indicates that the selection can be done since the early generations, while the low heritability values should be the selection of characters was conducted on further generation [17].

In some characters have medium heritability values include the emergence rate, terminal leaflet length, plant height, seed length, seed width, and number of stems. While the characters who have a low heritability value includes the number of leaves, terminal leaflet width, the number of days appears flower, flower stem length, number of flowers per stem, plant area, number of pods, and the sum of books per stem. The characters that have medium and low heritability values, indicating that the greater environmental impact than genetics can be done on next-generation selection. This is consistent with the statement [18] that a low and medium heritability is showing the environment influence on appearance so that the selection is more effective if done in further generations.

4. Conclusion

There are a high heritability values in character Petiole length, internodes length, banner length, pod length, pod width, number of branches per stem, and the ripe age of plant. At the mature character has the highest heritability value so that this character has a huge genetic potential of improved results through selection. Bambara groundnut has good prospects in addressing drought, so that it can be an alternative for sustainable food

5. Acknowledgements

We are thankful to all Lecturers in South Cooperation Laboratory, School of Biosciences, University of Nottingham for the seeds and work relationship.

6. References

[1]. Rukmana, H.R. dan Y.Y Oesman (2000), Kacang Bogor. Raising and Prospect Farm. Kanisius. Yogyakarta

[2]. Stephens, J.M. (2003), Bambara groundnut-*Voandzeia subterrane (L.) Thouars*, Institute of Food and Agricultural Science, University of Florida.

[3]. Brough S.H., Taylo, A.J., Azam-Ali S.N. (1993), The potential of bambara groundnut (*Vigna subterranea*) in vegetable milk production and basic protein functionality systems. *Food Chem*. 47: 277-283.

[4]. Purseglove, J. W. (1968), *Tropical Crops*. Dicotyledons 1. Longman, Green & Co. Ltd. London.

[5]. Brough S.H., Azam-Ali S.N. (1992), The effect of soil moisture on the proximate composition of bambara groundnut (*Vigna subterranea* L. *Verdc*). *J. Sci. Food and Agric*. 60: 197-203.

[6]. Pasquet R.S., Schwedes S., Gepts P. (1999), Isozyme diversity in bambara groundnut. *Crop Sci.* 39: 1228-1236.

[7]. Amadou H.I., Bebeli P.J., Kaltsikes P.J. (2001), Genetic diversity in bambara groundnut (*Vigna subterranean* (L.) *Verdc*) germplasm revealed by RAPD markers. *Genome* 44: 995-999.

[8]. Massawe F.J., Dickinson M., Roberts J.A., Azam-Ali,S.N. (2002), Genetic diversity in bambara groundnut landraces (*Vigna subterranea* (L.) *Verdc*) revealed by AFLP markers. *Genome* 45: 1175-1180.

[9]. Massawe F.J., Roberts J.A., Azam-Ali S.N., Davey M.R. (2003), Genetic diversity in bambara groundnut (*Vigna subterranea* (L.) *Verdc*) landraces assessed by Random Amplified Polymorphic DNA (RAPD) markers. *Genet. Resour. Crop Evol*. 50: 737-741.

[10]. Poespodarsono, S. (1988), *Dasar-dasar Ilmu Pemulian Tanaman.* Faculty of Agriculture, Brawijaya. Malang.

[11]. Hermiati (1999), *Pengantar Pemuliaan I: Menyerbuk Sendiri.* Program Pengembangan Kemampuan peneliti Tingkat S1 Non Pemuliaan Dalam Ilmu dan Teknologi Pemuliaan. Kerjasama antara Departemen Pertanian dan Fakultas Pertanian Universitas Padjajaran. Bandung.

[12]. Syukur (2005), *Pendugaan Parameter Genetik. Pada Tanaman*. Makalah Individu Pengantar Falsafah Sains (PPS 702). Program S3 Sekolah Pasca Sarjana. Institut Pertanian Bogor. Bogor

[13]. Makmur (1985), *Pokok-Pokok Pengantar Pemuliaan Tanaman*. PT. Bina Aksara. Jakarta.

[14]. Zen, S. (1995), Heritabilitas, korelasi genotipik dan fenotipik karakter padi gogo. Zuriat. 6 (1): 25-31

[15]. Kuswanto, Ashari, S., M. A. Wijoyo (2000), Keragaman genotipa varietas harapan kedelai dan implikasi seleksi untuk musim penghujan. *Habitat*. 11 (111): 71-75.

[16]. Rosmini (2003), Penampilan fenotipik dan penampilan genetik galur-galur padi di Pasang Surut Sulfat Masam Danda Jaya. *Habitat* 16 (3): 162-170

[17]. Pinaria. A, et. al. (1995), Variabilitas genetik dan heritabilitas karakter-karakter biomassa 53 Genotip Kedelai. *Zuriat*. 6 (2): 88-92.

[18]. Rachmadi. M, *et. al*. (1990), Variasi genetik dan heritabilitas komponen hasil dan hasil galur harapan kedelai. *Zuriat*. Juli-Agustus. 2 (2). p.169

[19]. Stansfield, W.D. (1983), *Theory and Problem of Genetic, Second Edition (Schaum series)*. Mcgraw-Hill Inc. New York. p 248.

Appendixes

Tabel 1. Landraces as research material

Landraces	Accession	Locality	Landraces	Accession	Locality
S19-3 (22105)	P1	Namibia	GHC (37105)	P24	Gresik
S19-3 (22107)	P2	Namibia	BC (12105)	P25	Bogor
Uniswa Red (25105)	P3	Swaziland	BC (12105)	P26	Bogor
Uniswa Red (27107)	P4	Swaziland	BHC (14107)	P27	Bogor
GH (17105)	P5	Gresik	BCGC(13107)	P28	Bogor
GH (37107)	P6	Gresik	Tiga Nicuru	P29	Mali
GC (32105)	P7	Gresik	Ankpa 2	P30	Nigeria
GCL (31105)	P8	Gresik	S19-3 (21107)	P31	Namibia
GHC (36105)	P9	Gresik	DIPC (35105)	P32	Botswana
BH (17107)	P10	Bogor	Uniswa Red (26107)	P33	Swaziland
BC (14105)	P11	Bogor	NAV-4.1. C105	P34	Ghana
BCL (33107)	P12	Bogor	GH (36107)	P35	Gresik
BCGC (12107)	P13	Bogor	GC (35107)	P36	Gresik
BCGC (23107)	P14	Bogor	GCL (13105)	P37	Gresik
S19-3 (23105)	P16	Namibia	GHC (24105)	P38	Gresik
DIPC (34105)	P17	Botswana	BH (16107)	P39	Bogor
Uniswa Red (26105)	P18	Swaziland	BC (31107)	P40	Bogor
NAV-4.1. C103	P19	Ghana	BCL (32107)	P41	Bogor
GH (21105)	P20	Gresik	BHC(15107)	P42	Bogor
GC (34107)	P21	Gresik	BCGC (11107)	P43	Bogor
GCL (11105)	P22	Gresik	Tiga Nicuru	P44	Mali
GHC (16105)	P23	Gresik	Ankpa 4	P45	Nigeria

Tabel 2. Estimates of heritability in bambara groundnut

Characters	σ2 e	σ2 f	σ2 g	h^2	Criteria
Emergence rate	0.26	0.8	0.54	0.45	Medium
Terminal leaflet length	0.35	0.64	0.29	0.45	Medium
Number of leaves	67.91	73.94	6.03	0.08	Low
Petiole length	2.81	6.46	3.65	0.57	High
Internode length	0.1	0.21	0.11	0.52	High
Terminal leaflet width	0.14	0.15	0.01	0.07	Low
Banner length	0.52	1.62	1.1	0.68	High
Number of days from sowing to flowering	5.46	5.69	0.23	0.04	Low
Peduncle length	1.86	1.88	0.02	0.01	Low
Number of flowers per peduncle	0	0	0	0	Low
Plant spread	39.94	44.77	4.83	0.11	Low
Plant height	10.1	20.22	10.12	0.5	Medium
Number of pods	47.16	48.05	0.89	0.02	Low
Pod length	0.12	0.39	0.27	0.69	High
Pod width	0.03	0.2	0.17	0.85	High
Seed length	0.03	0.05	0.02	0.4	Medium
Seed width	0.02	0.04	0.02	0.5	Medium
Number of stems per plant	0.45	0.61	0.16	0.26	Medium
Number of branches per stem	0.52	1.67	1.15	0.69	High
Number of nodes per stem	8.09	8.25	0.16	0.02	Low
Mature	6.28	73.62	67.34	0.91	High

Damping Concentration Effect Simulation on the Particulate PM10 Average Dynamic Dose Rate per Year in X Region at Serpong Residency

Icuk Setiyawati [1], Abdurrouf [1], Eko Pujadi [2], P.A Saraswati [1]

[1] Department of Physics, Brawijaya University, Malang (icunk_ube@yahoo.com)
[2] National Nuclear Energy Agency (BATAN), Jakarta

Abstract

This research aims to predict the damping concentration effect on the dynamic of annually average dose of Particulate PM10 in a specific region. In this research, the damping concentration is predicted numerically by simulating Particulate PM10 average dynamic dose rate in the air. Dynamic dose rate is calculated by using numeric integration method, which is trapezoidal method of concentration rate in a defined period of time. After calculation, dynamic dose rate before and after damping concentration effort per year is obtained. From the calculation, it is concluded that before the damping concentration effect applied, dynamic dose rate in the air increases along with time increment. If damping concentration effort of 10% is applied per year, the dose rate is suppressed four times smaller than before. By applying concentration damping by 50%, one can reduce the average dose rate to constant.

Key word: *dynamic dose rate, damping concentration, trapezoidal method.*

1. Introduction

This paper is a research result about physics application in environment. Physics modeling and computation are used to estimate the effect in environment in form of average dose rate spreading around us.

Particulate dust is solid particle that has size around 100 micron to less than 1 micron. Based on the size, particulate dust can be classified as total suspended particle (TSP) which is particles that has diameter size around 0.1 to 30 micrometer. Based on the US EPA (1987), PM10 particle exposure can enter the human lung and caused health problems [5]. PM10 particle is a particulate with diameter size less than 10 micron. Particulate can spread directly in environment through air. Therefore it can enter the living organism body through a process called radiation or exposure. This process can take place in several ways: inhalation; ingestion; dermal contact.

This research will explain how the particulate enter the living organism body through the inhalation process. For radioactive contaminant or particulate, radiation can occur without direct contact with the contaminant. This is because the radioactive material can emit exposure with large range. Exposure effect receives by the environment depends on factor such as: contaminant concentration, exposure process, duration, frequency, physical appearance and contaminant chemistry. Exposure amount for radioactive material can be stated in the form of effective dose and equivalent dose. Quantitative result of the exposure estimation can be expressed generally as daily average dose. Therefore this research is done by doing numerical calculation to predict PM10 particulate dose rate average spread in the environment

In environment risk analysis caused by inhalation process of particulate exposure, measurement of contaminant that mixed in the environment is needed. Analytically, particulate concentration can be expressed from differential equation below:

$$\frac{dC}{dt} = \pm kC^n \qquad (1)$$

From the differential form above, two ways integral resulted in mathematic equation for contaminant concentration every time unit:

$$C(t) = C_0 e^{-kt} \qquad (2)$$

Particulate Inhalation Dose

Dose is the amount of contaminant concentration that enters living organism body for every unit of body weight. The amount of total inhalation dose rate in n years can be calculated with the equation below:

$$D_T = \int_{t_0}^{t_c} \frac{CR(t)C(t)dt}{BW(t)} \qquad (3)$$

Where CR shows the quantity of contaminant contact rate with living organism

body (m^3/days), C(t) contaminant concentration (mg/m^3), BW(t) body weight/time (mg/day). Which means total dose rate is determined by the contaminant concentration that goes into the environment. These incoming concentration decays exponentially in 24 hours.

2. Experimental Detail

Numerical Method

Average particulate dose rate per years calculated numerically using trapezoidal numeric integration method. Numeric equation for trapezoidal method can be seen below:

$$\int_a^b f(x)dx \approx \left(\frac{b-a}{N}\right)\left[\frac{f(a)+f(b)}{2}+\sum_{k=1}^{N-1} f\left(a+k\frac{b-a}{N}\right)\right] \quad (4)$$

Where,

$$x_k = a + k\frac{b-a}{N}$$

$$k = 0,1,\ldots,N$$

Program algorithm

Algorithm for the program can be seen below:

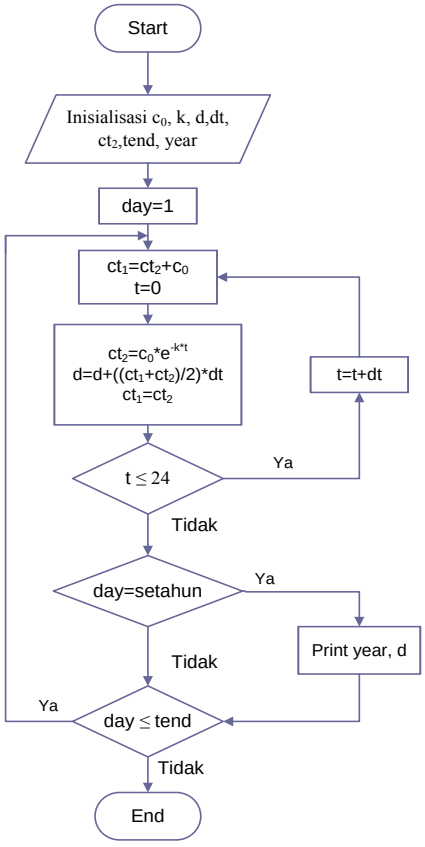

Figure 1. Flow Chart of Program Algorithm.

3. Result and Discussion

Given a graph of the approximate calculation of the average dose rate per year within 50 years in X region at Serpong residency and attenuation prediction curve of concentration against dose rate using C programming language as below:

Below are presented the results of the calculation of the particulate dose rate calculation estimates annually in X region at Serpong residency before attenuation concentration efforts. Measurements are conducted during 5 days in the X region Serpong residency area consist of cluster A, B, C, D and E. Measurement result in form of concentration data every 15 minutes for 12 hours time period. These data are averaged using Ms. Excel and average initial concentration is obtained as an input to the input concentration in the numerical calculation. Numeric calculation result using C programming language is showed in the curve below:

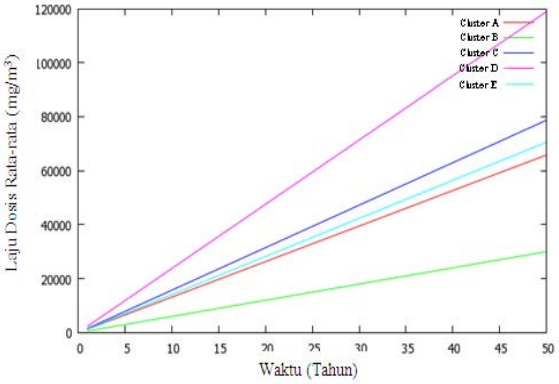

Figure 2. Prediction curve of particulate PM10 dynamic dose rate per year in X region at Serpong before damping concentration.

From the curve above, estimated that the concentration of initial particulate PM10 C_0 (mg/m^3) in the air is inhaled by population and enter the body. These concentration decays exponentially so that only a few percent of its original concentration remains within 24 hours. In second day, concentration in amount of C_0 entering the body again. Causing a total amount of C_0+C_0 exp(-kt) (mg/m^3) presented in the body. This process will repeat itself in the following days. So that the total concentration entered and accumulated in the body is increasing, as well as the annual average dose rate. It can be seen in the curve that the highest annual average dose rate occurs in cluster D, in the 50th year it reaches 120,000 mg/m^3. While the lowest annual average dose rate is in the cluster B with 30,000 mg/m^3 in the 50th year.

Increasingly higher concentrations accumulation will cause a further increment in the average dose rate per year – increasing dose inhalation per year by the community. This will have a negative impact for the X region at Serpong residency resident for years ahead. Government have to give more attention in reducing the negative effects that can occur several years into the future by reducing the percentage of particulate PM10 concentrations present in the air in each year.

After the reduction of concentration of particulates is done, calculation result of particulate dose rate obtained as follows.

In the research, the influence of percentage reduction in particulate PM10 concentration to PM10 dose rate in air variation is given. Percentage reduction variation started from 5, 10, 15, 20, 25, 30, 35, 40, 45, and 50%. From the numerical calculation results, annual average dose rate prediction curve obtained after the variation of concentration reduction as follows.

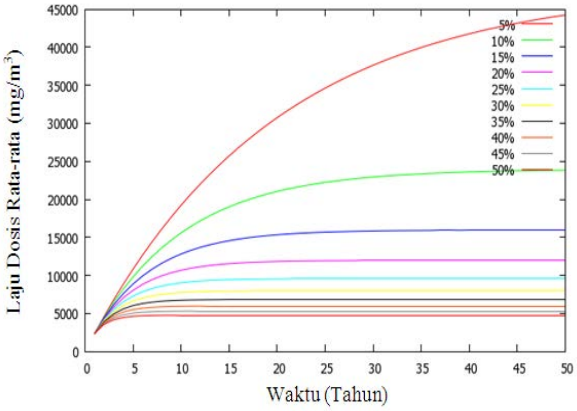

Figure 3. Prediction curve of particulate PM10 dynamic dose rate per year in X region at Serpong with variation of damping concentration.

From the above curve can be seen that as the concentration percentage reduction increasing, the average dose rate every year decreasing. Which means that by increasing the particulate concentration percentage reduction can decrease the average dose rate every year. For example in cluster D, by decreasing concentration by 10% every year will cause the initial dose rate in the 50th year to decrease from 120,000 mg/m^3 to 24,000 mg/m^3 – dose rate every year can be reduced by 4x smaller than before the reduction scheme from the government.

For more details, the comparison curve below showed the before and after of particulate PM10 concentration reduction in cluster D.

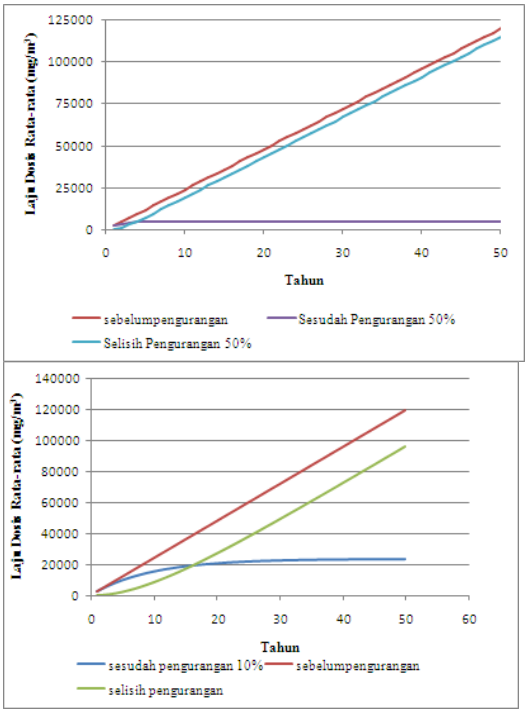

Figure 4. Comparison curve of the particulate PM10 dynamic dose rate per year before damping, after and the differences of both (top) 10%, (bottom) 50%.

From the curve above, can be seen that prior to the particulate concentration reduction, average dose rates per year increasing up to 120,000 mg/m^3 in the 50th year. By giving 10% attenuation, average dose rate can be reduced by 96,000 mg/m^3. By reducing that much, negative impact appearance can be slowed down 4x smaller than before. If the concentration reduction carried out at 50% the particulate annual average dose rate relatively constant. Which means no additional dose was able entering the body. Therefore the expected negative risks that arise could be inhibited by nearly 100%. Given is the comparison curve of the percentage difference in concentration reduction of 10% and 50%.

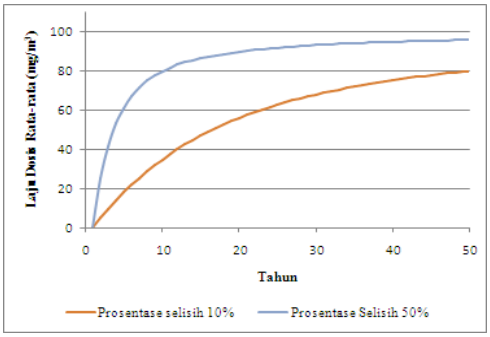

Figure 5. Curve Percentage Comparison the Difference Concentration Damping of Particulate PM10 10% and 50%.

Based on the above curve can be predicted that by making the effort to reduce particulate PM10 concentration by 10%, the dose rate average of particulate in the air can be to 80%. If concentration reduction of 50% is performed then we can reduce the average dose rate per year to constant.

4. Conclusion

Dose rate increases each year because the concentrations that enter the environment continues to grow at concentrations of initial entry plus the concentrations were already decayed and accumulated in the body. Predicted in the next 50 years the dose entering the region X continues to increase. The accumulation of more and more of this can lead to negative risks. For that we need a government effort to suppress the particulate concentration of PM10 in the air. If reducing the concentration by 10% can reduce the dose rate of 80%, a reduction of 50% can reduce the dose rate to constant.

5. Acknowledgement

---

6. References

[1]. Casas, J.S., Josè Sordo. (2006), Lead Chemistry, Analytical Aspects, Environmental Impact and Health Effects. Elsevier. United Kingdom.

[2]. Dahlquist, G, dan Åke Bjőrck (2003), Numerical Methods. Dover Publications, Inc. New York.

[3]. Kant, K, et al. (2004), Measurement of Inhalation Dose Due to radon and its Progeny in an Oil Refinery and its Dwellings.

[4]. Fjeld, R.A., N.A. Eisenbergh, K.L. Compton (2007), Quantitative Environmental Risk Analysis for Human Health. John Wiley and Sons, INC. New Jersey.

[5]. http://www.hcdoes.org/airquality/Monitoring/tsp.htm. accessed on 5 January 2011.

Determination of Optimum pH and Adsorption Time of Malachite Green on Coal Fly Ash

M. Lathifurrijal [1], Anton Prasetyo [2], Diana Candra Dewi [3]

[1,2,3] Department of Chemistry, Faculty of Science and Technology, State Islamic University of Maulana Malik Ibrahim, Malang, Indonesia (antoniaprasetyo@gmail.com)

Abstract

Coal fly ash is one of the most abundant waste materials from modern coal-burning power plant that having major compositions such as SiO_2, Al_2O_3, Fe_2O_3, and CaO, so it has potentiality for dyes removal from water or wastewater through adsorption. Malachite green, one of the dyes, is widely used in various industries for coloring their final product. Malachite green is also used as an agent for treatment in aquaculture industries, but its negative effects make it a hazard wastewater and very important to be removed. This research studied the effects of different initial pH and contact time adsorption of malachite green on coal fly ash. The experimental result showed that pH 2 was the most effective pH to remove malachite green. It was 1,824 mg/g adsorbed from initial malachite green concentration 2 ppm and 0.1g of coal fly ash. The effect of adsorption time showed that 50 minutes was the best time to adsorb malachite green. It was 1,824 mg/g adsorbed from 2 ppm of malachite green and used the optimum pH (pH 2).

Keywords: *adsorption, coal fly ash, malachite green, optimum pH, optimum adsorption time.*

1. Introduction

Malachite green that commercially called Basic Green 4, Victoria Green B, Aniline Green and Diamond Green B is a toxic chemical. The chemical name of malachite green is 4-[(4-dimethylaminophenyl)-phenyl-methyl]-N,N-dimethyl-aniline [1].

Malachite green can be found in wastewater from textile and dye industries. Malachite green has been extensively used as anti-bacterial and anti-fungal in aquaculture in order to protect fish and egg fish from bacteries, fungal infection and parasites. In the other hand, malachite green has been used as food dyeing, disinfectant, dye in silk, wool, jute, leather, cotton and paper [4].

Many methods can be used to remove malachite green from aqueous solution [1], such as precipitation, flocculation, adsorption, ion exchange and membrane separation. The simplest and the most effective method to remove malachite green from aqueous solution is adsorption.

Adsorption is one of the wastewater treatment alternatives that have been widely used for the removal of toxic compounds. The material that has been widely usually used as a good adsorbent is activated carbon, but the high cost of activated carbon made it not effective. Several researchers found the low cost adsorbent, such as zeolites, red mud, clays, and fly ash [3].

Coal fly ash is one of the most abundant materials produced from combustion of the power plant station. Generally, coal fly ash is used as basic elements in brick and concrete, but most of coal fly ash is land filling as waste materials in large number. The possibility of coal fly ash as adsorbent can be known from its composition. Composition of coal fly ash is different depending on the source of coal burned, such as SiO_2, Al_2O_3, FeO_3, CaO, MgO, SO_3, Na_2O, K_2O dan LOI, but all of coal fly ash contains SiO_2 and CaO [2]. The large number of coal fly ash and its composition make the coal fly ash as a low cost and effective adsorbent to remove malachite green from aqueous solution.

2. Experimental Details

Coal fly Ash

The coal fly ash used in this study was obtained as a result of burning coal in modern power plant station Probolinggo East Java, Indonesia. This material was treated with sufficient H_2SO_4 solution (1 mol/L) at 50°C for 24 h. The sample was then washed several times with distilled water, filtrated, dried at 105°C for 20 h, sieved to the particle size 125-250 mesh, and then stored in desiccators for further tests.

Malachite green

Prepared malachite green 0.1 g L^{-1} as a stock solution with distilled water. All working solutions used in tests were prepared by appropriately diluting the stock solution to a pre-determined concentration.

Determination of optimum pH of adsorption

2 ppm of malachite green adjusted at various pH (1-6) using NaOH/HCl and buffer solution. Add the solution into flasks containing 0.1 g of coal fly ash. The mixtures were then shaken with the agitation speed 150 rpm for 50 minutes at room temperature (27±2°C). The final action, measured the samples using spectronic-20 at 615 nm. The amount of malachite green uptake by coal fly ash was obtained as follows:

$$Q_e = \frac{(C_0 - C_e)\ V}{W}$$

Where Q_e is amount of adsorbed adsorbate (mg/g), C_0 is initial adsorbate concentration (mg L^{-1}), C_e is equilibrium concentration of adsorbate (mg L^{-1}), V is volume (L), and W is amount of adsorbent (g).

Determination of optimum time of adsorption

A 2 ppm of malachite green adjusted at the optimum pH of adsorption using NaOH/HCl and buffer solution. Add the solution into flasks containing 0.1 g of coal fly ash. The mixtures were then shaken with the agitation speed 150 rpm for various contact times 10, 20, 30, 40 and 50 minutes at room temperature (27±2°C). The final step is measured the samples using spectronic-20 at 615 nm.

3. Result and discussion

Effect of initial pH

pH is one of the aspects playing important role in the adsorption process. The amount of adsorbed malachite green can be influenced by pH. In this work, pH was varied from 1 to 6 as an initial pH of adsorption. Figure 1 shows the amount of adsorbed malachite green in various pH.

Figure 1 is likely shows that there was no important effect of different pH to the adsorption process. The trend line shows the same range in value, 1.8 mg/g of adsorbed malachite green. The trend line is linear because the point of value is in the same range. Adjustment of pH 1 to 6 was done because of the properties of malachite green to the different pH. The strong green colored of malachite green occurs at low pH (acidic), while in alkaline water it may seem that it has disappeared because it is converted to a colorless carbinol form, but it is invisible and still present.

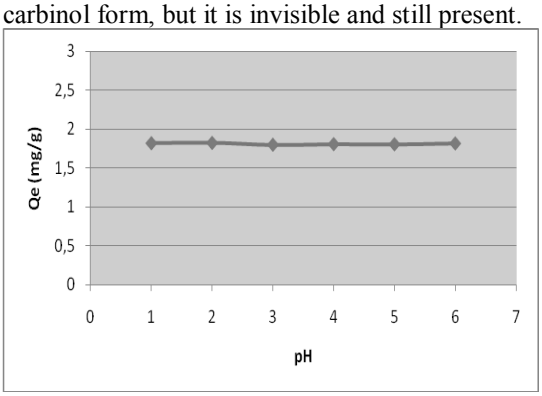

Figure 1. effect of initial pH to the amount of adsorbed malachite green.

Although the trend line is linear, it is necessary to determine the top point, where the maximum uptake of malachite green occurs in current pH. According to the figure 1 above, pH 2 is the best pH for coal fly ash to adsorb malachite green from aqueous solution with the value 1,824 mg/g.

Effect of adsorption time

Various adsorption times in this study were done to see in what time the maximum amount of adsorbed malachite green. In this study, 2 ppm of malachite green was adjusted at pH 2 as the optimum pH of adsorption. Figure 2 shows the amount of adsorbed malachite green in various contact times.

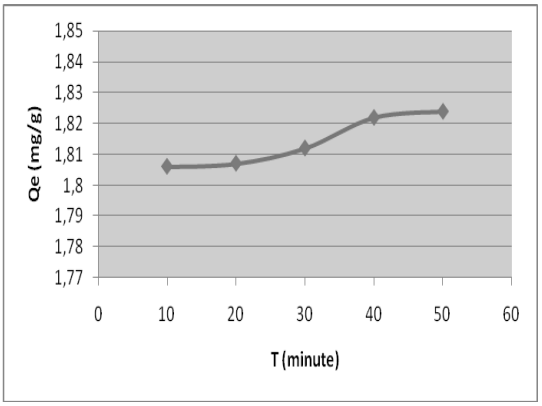

Figure 2. effect of adsorption time to the amount of adsorbed malachite green

It is a good trend line of the figure 2, the amount of adsorbed increases with the increasing of adsorption time. Although the amount of adsorbed malachite green in the same range in value (1.8mg/g), it shows the presence of significant interaction between adsorbent and

adsorbate in time. It was 1.824 mg/g of the maximum uptake of malachite green at 50 minutes.

4. Conclusion

Even though the value of maximum uptake of determining optimum pH and maximum time of adsorption is relatively the same; the top point can be obtained from the different initial pH adsorption and various adsorption times. pH 2 is the optimum pH of adsorption and 50 minutes is the optimum time of adsorption.

5. Acknowledgements

We express gratefully to chemistry laboratory for the serving and thank to Modern Power Plant Station Paiton Probolinggo-Indonesia for the providing of coal fly ash.

6. References

[1]. Ariyanto, E. (2009), Adsorption Malachite Green On Natural Zeolite. Palembang: Department of Chemical Engineering, Faculty of Technology, University of Muhammadiyah.

[2]. Loka (2009), Abu Batubara sebagai Soil Conditioner. www.tekmira.esdm.go.id.

[3]. Papandreou, A, Stournaras, C.J, dan Panias, D., (2007), Copper and Cadmium Adsorption on Pellets Made from Fired Coal Fly Ash. *Journal of Hazardous Materials* 148 538–547. Greece: ceramics and refractory technological development company.

[4]. Srivastava, S, Sinha, R, dan Roy, D., (2003), Toxicological Effect of Malachite Green. *Aquatic Toxicology* 66 319–329. India: Department of Zoology, S.M.M. Town Post-Graduate College, Ballia 277001.

Groundwater Mapping in Coastal Plain, North Kelantan – Malaysia

Nur Islami [1,2], Samsudin Hj Taib [3], Ismail Yusoff [4]

[(1,3,4)] Department of Geology, Faculty of Sciences, University of Malaya, Kuala Lumpur, Malaysia (nris@um.edu.my)
[(2)] Department of Physics, PMIPA, University of Riau, Pekanbaru, Indonesia (nris74@yahoo.com)

Abstract

The study area is located in coastal plain, North Kelantan - Malaysia. The coastal plain is covered with Quaternary sediments overlying granite bedrock. The geoelectrical resistivity profiling surveys and hydrogeocemical methods were conducted to determine the characteristics of the subsurface and the groundwater within the aquifer. They made up of thirty fife traverse lines of different site location with Wenner configuration. All the high-resolution electrical images show a remarkable resistivity contrast between relatively lower resistivity values in the shallow layers and relatively higher resistivity zones in the deeper subsurface. In particular, the electrical imaging highlights the occurrence of lower resistivity (around 15 ohm.m) in a depth ranging from 10-25 m below the surface level which distribute from the southeast to the northwest. Chemical soil analysis result shows that the low resistivity anomaly corresponds to the high Fe and Al content in the soil. Finally, the zone with high Fe concentration in groundwater aquifer can be mapped.

***Keywords**: Geoelectrical resistivity, Groundwater, Aquifer.*

1. Introduction

Groundwater is important natural resources. It sustain for human life. It provides drinking water to urban and rural communities. Good quality groundwater is one of the great natural resources. Unfortunately it might become contaminated when even seemingly harmless materials and wastes materials introduce into the ground are improperly handled. Contamination may involve different chemicals which come either from the nature or human activity. The chemical may such as, excess amounts of nitrogen, phosphorus, Fe and many else. A number of factors can affect the quality of a groundwater reservoir, such as contamination by salt-water intrusion [1,2] or by toxic industrial chemic waste [3]. These pollutants pose common environmental problems that have created the need to find suitable methods for monitoring the extent of such environmental damage [4].

Geophysical methods have been widely used in groundwater investigations. It can provide information over large areas at a relatively inexpensive cost compared to other methods (e.g. borehole drilling and trenching). Geoelectrical resistivity have already been demonstrated as useful quantitative methods for sub-surface investigation. Geoelectrical resistivity is minimally invasive and thus does not disturb ongoing hydrological processes at the site. Geoelectrical resistivity imaging surveys aim to determine the physical properties on the plane delineated by injecting current along different path and measuring the associated voltage drops [5]. The geoelectrical imaging method has been widely used in environmental and geotechnical investigation for more mapping complex geological structures as it can delineate the resistivity distribution of such structures. Geoelectrical imaging surveys aim to determine the physical properties on the plane delineated by injecting current along different path and measuring the associated voltage drops. In this paper, the efficiency of the geoelectrical imaging method for the detecting of Fe and Al contamination within aquifer and investigating subsurface profiling are examined.

Review of Geology Study Area

The study area covers approximately 150 square kilometres. It is about 35 km from the beach line. The west and east side boundaries are bounded by Kelantan River and the high hill respectively. The hill is a part of the Boundary Range Composite Batholith. It consists of two major components, the Machang Batholith which is about 100 x 20 km, with the smaller Kerai Batholith situated on is western flank. The study area is covered with Quaternary sediments overlying granite bedrock. It is drained mainly by

short rivers and streams which flow into the South China Sea. The thickness of the Quaternary deposits varies from 20 m inland to about 200 m near the coast. The loose quaternary sediments consist of alternating layers of coarse gravels to silt or mixtures of the two [6].

2. Experimental Details

2D electrical resistivity imaging surveys were performed at the selected sites. The geoelectrical resistivity surveys of nineteen traverse lines were made of different lengths. The maximum line spreading was 400 m in length, and the minimum spreading was 80 m in length, each line spreading depended on the available space in the field.

The wells W1 and W2 were installed to obtain subsurface data in the area of low resistivity anomaly and no low resistivity anomaly respectively. The drilling was stop after the drilling bit reached a compact material (pre-Quaternary basement). Gravel was found from a depth of 1.5 m before reaching the basement. PVC pipe with 3 inch of its diameter was put for the well casing. Well perforation was done at which coarse sand grain size was found.

Soil was collected in certain depth and kept in the plastic bag with temperature of 4°C. In the hydrogeochemical laboratory, the soil was divided into two containers. The first container was used to obtain soil grain size distribution, while the second container was used for soil chemical analysis. Water sample was collected one day after the drilling completion. Water in the well was pumped for 10 minutes before collecting the water sample.

A hydrogeochemical analysis was used to study the groundwater characters in this area. Samples of groundwater were collected from the wells. In-situ parameters such as well depth, water level, total dissolved solid, pH, conductivity, salinity and temperature were measured. Water samples of 500 ml were kept in plastic bottles and maintained at a temperature of 4°C. The subsequent analysis in hydrogeology lab using IC and ICP was done to determine the major anion and cation contents.

3. Results and Discussion

In this paper only the lines 21 and line 23 will be shown and discussed (Figure 1 – Appendixes). The line 21 was carried out on a site elevated at 13 m above the mean sea level. It was done in between artificial drainage system and paddy field with a southwest-northeast direction. Puddle of water was measured around 1 m below the survey plane. In the geolectrical model of line 21 (Figure 1A), average resistivity value of 200 ohm.m is observed on the surface, corresponding to clayey sand soil with moderate moisture content. Starting from a depth of around 6 m to 25 m, the possibility of an aquifer is encountered with average resistivity value of around 40 ohm.m. The nearest well WA210 shows the freshwater character existed within the aquifer. Relatively higher resistivity values of more than 400 ohm.m occur at the depth of 34 m downward corresponding to the pre-Quaternary bedrock. The granite basement is noted dipping to the northeast direction.

The survey line 23 was conducted at a site surrounded by paddy field on the eastern and rubber trees plantation on the western. The survey line was exactly between artificial drainage system and minor road which has elevation of 11 m above mean sea level. Puddle of water was around 2 m below survey plane in the drainage system. The geoelectrical model of line 23 (Figure 1B) shows a minimum resistivity value of ± 12 ohm.m in the zone of coloured light blue. The value is similar to contaminated aquifer with light brackish water content [7]. For comparison, the other lines 03, 07 and 08, which are more closed to the beach, do not show the lower anomaly as shown in line 23. That mean, the possibility of light brackish water content within the aquifer is almost impossible. Furthermore, the hydrogeocemical results do not show any salt/brackish water indication. The anomalies such as in line 23 also can be found in the lines of 01, 02, 04, 05, 06, 14, 16, 17 and 18. The highest resistivity value of more than 400 ohm.m is obtained at the northeastern from the depth of 33 m downward. The highest resistivity value correlates to the occurrence of basement within this area.

In order to find the cause of the anomaly, two new well (W1 and W2) were drilled at the position of around the survey line. The W1 was drilled at line 23 which the lower resistivity anomaly found. The W2 was drilled at line 15 where there is no lower resistivity anomaly observed. Base on the soil chemical result, relatively higher Al and Fe concentration are found in the W1, while in the W2, Al and Fe show with lower concentration (Figure 2). In the W1, water chemical result also show higher Fe concentration (12.34 mg/L), while in the W2 Fe concentration is less than 0.2 mg/L (maximum Fe concentration for human consumption, WHO 1984). Al do not soluble in water, it is reason why lower Al concentration (less than 0.2 mg/L) is found in both wells although higher Al concentration is obtained in the soil.

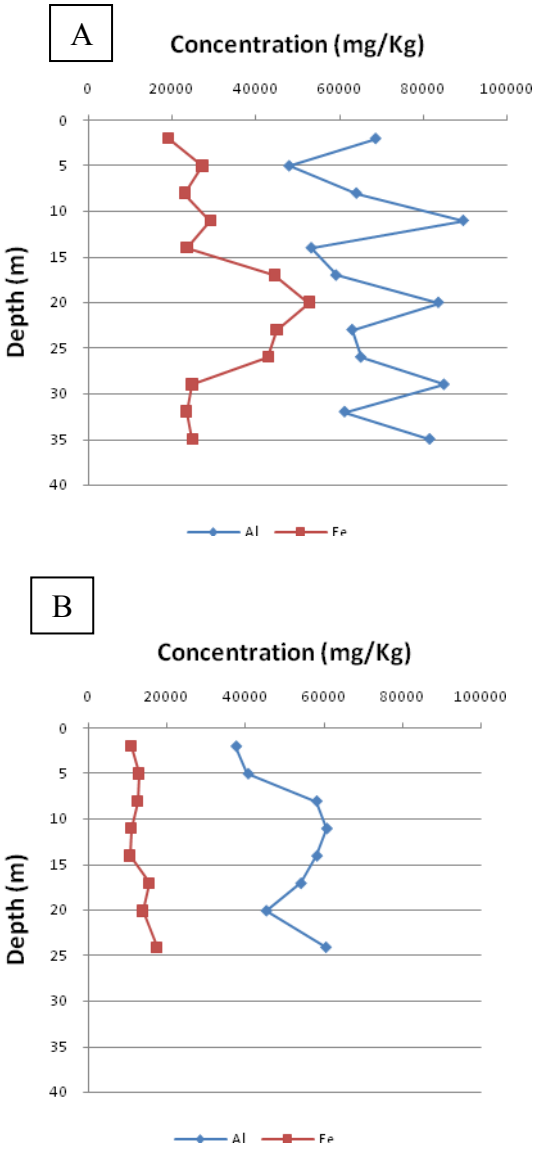

Figure 2. Al and Fe concentration in soil sample at certain depths for W1 (A) and W2 (B)

The zones of higher Fe concentration has been mapped along 3D resistivity value distribution (Figure 3). Fe concentration extends from northern side of Boundary Range to the Northwestern. High Fe concentration occurs at the depth around 0 to -20 m relative to the mean sea level at the southeast and dip to northwest direction. At the northwestern, High Fe concentration occur at -5 to -25 m above mean sea level. Within this depth interval, geoelectrical model shows lower resistivity anomaly (less than 15 ohm.m) in the zone with high Fe concentration within the soil formation which also indicates high Fe concentration in groundwater of more than 7 mg/l.

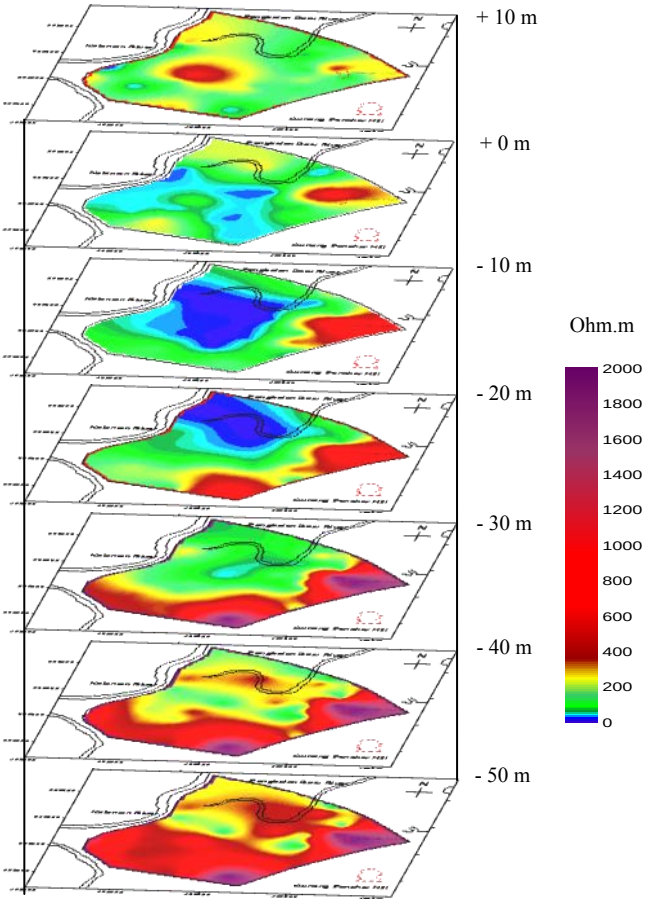

Figure 3. 3D resistivity distribution

4. Conclusion

The illustrated case studies show that electrical resistivity imaging is a valuable method for studies in the coastal environments. In this study, the geoelectrical resistivity method is successfully imaging the subsurface with relatively higher Fe concentration zone. The zone of higher Fe concentration is clearly seen along 3D resistivity distribution. Fe concentration extends from northern side of Boundary Range to the northwestern. High Fe concentration occurs at the depth around 0 to -20 m relative to the mean sea level at the southeast and dip to northwest direction. At the northwestern, high Fe concentration (more than 7 mg/l) occur at -5 to -25 m above mean sea level. Within this depth interval, geoelectrical model shows lower resistivity anomaly of less than 15 ohm.m.

5. References

[1]. Samsudin, A. R., Haryono, A., Hamzah, U., Rafek, A.G., (2007), Salinity mapping of coastal groundwater aquifers using hydrogeochemical and geophysical methods: a case study from north Kelantan, Malaysia, *Environ Geol* 10.1007/s00254-007-1124-9.

[2]. Abdul, N.S.S., Loke, M.H., Lee, C.Y., Nawawi, M.N.M. (2000), Salt-water intrusion mapping by geoelectrical imaging surveys, *Geophysical Prospecting*, V 48, 647-661.

[3]. Barker, R.D. (1996)a. The application of electrical tomography in groundwater contamination studies. 58th EAGE conference, Amsterdam, The Netherlands, Extended Abstracts, p 082.

[4]. Bernstone, C., Dahlin, T. (1996), Electromagnetic and DC resistivity mapping of waste deposits and industrial sites – experiences from southern Sweden. 58th EAGE conference, Amsterdam, The Netherlands, Extended Abstracts, M014.

[5]. Schrott, L., Sass, O., (2008), Application of field geophysics in geomorphology: Advances and limitations exemplified by case studies, *Geomorphology* 93 (2008) 55–73.

[6]. Saim, S. (1997), Groundwater protection in North Kelantan, Malaysia: An integrated mapping approach using modeling and GIS. Unpubl. PhD Thesis, Univ of Newcastle Upon Tyne.

[7]. Islami, N., Samsudin, T., Yusoff, I. (2010), High-resolution imaging of the groundwater mapping with geoelectrical resistivity tomography in coastal plain, North Kelantan – Malaysia.International Symposium on a Robust and Resilient Society against Natural Hazards & Environmental Disasters and the third AUN/Seed-Net Regional Conference on Geo-Disaster Mitigation August 24-26, 2010, Kyoto, JAPAN.

[8]. Koopmans, B.N., (1972), Sedimentation of Kelantan Delta (Malaysia). *Sedimentary Geology*, Vol.7, 65-84.

[9]. Loke, M.H. (2007), Rapid 2-D Resistivity & IP inversion using the least-squares method, Geoelectrical Imaging 2D & 3D, GEOTOMO SOFTWARE, Malaysia.

[10]. Noor, I.M. (1979), Prefeasibility study of potential groundwater development in Kelantan, Malaysia. PhD thesis, University of Birmingham, UK.

Appendixes

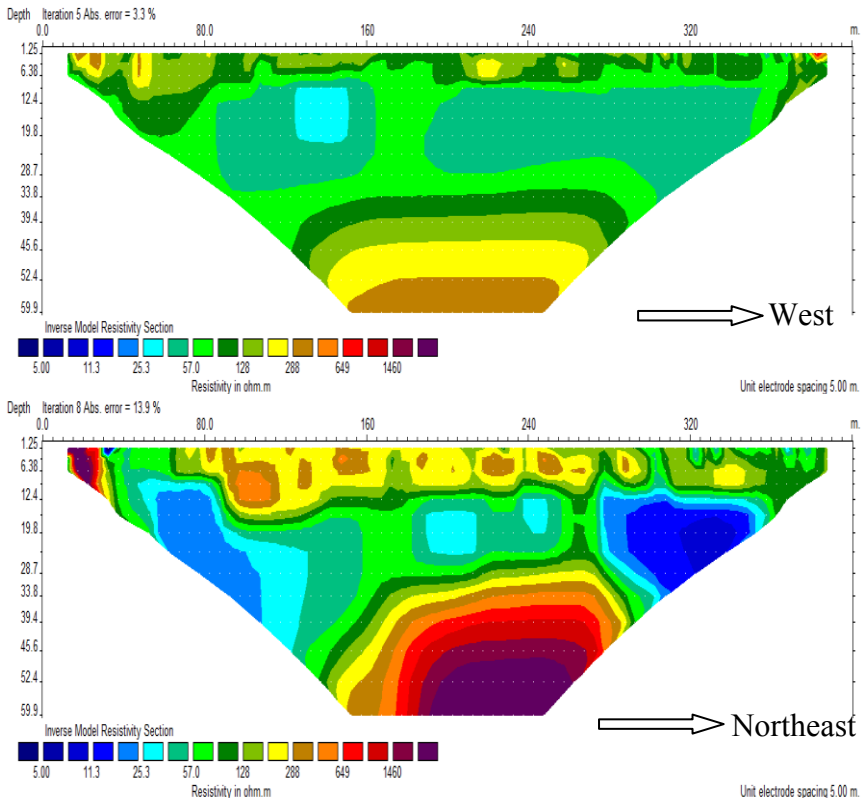

Figure 1. Geoelectrical model of line 21 and line 23

The Application of The Gompertz, Richards and Hyperbolastic Growth Models to Describe Weight Growth

NW Surya Wardhani [1], Solimun [2], Era Setiarini [3]

[(1,2,3)] Department of Mathematics, Faculty of Sciences, University of Brawijaya, Indonesia

Abstract

A new flexible growth model called Hyperbolastic (H1, H2 and H3) was developed in 2005 and assumed appropriate in describing growth pattern of broiler chicken. Compared to the classic Gompertz and Richards growth models, the conclusion are : the most suitable model in describing the body growth pattern of female Lohmann broiler chicken is Gompertz model with the predicted maximum weight of 2812,57 gram and the maximum growth rate occurs at about day 23; for the male chicken, the Hyperbolastic 1 is better, which predicts its maximum weight of 3311.71 gram and the maximum growth rate occur at day 18. The most effective growing time is around the maximum growth rate so that some efforts can be done for the best growth such as giving a proper composition of chicken consumption, vitamine and vaccine, etc.

Keywords*: Gompertz, Richards and Hyperbolastic model, Broiler Chicken.*

1. Introduction

It is known that the size, as well as the weight of individual animal changes during development, because of the different growth of the particular part. At the beginning, the growth rate is slowly and then going faster up to a certain point and then slow down to reach a constant [1,2]. The advantage of fitting mathematical model to the data of weight growth is that the model has some biological meaning, the parameters may provide useful information. The best fit parameters can be found by minimizing the sum of the squares of the residuals. The parameters will be estimated using a non linear regression technique, namely *Levenberg Marquardt* iteration [3].

The S-shaped growth pattern has long been used to describe a biological process such as an animal body weight growth, to estimate a potential evaluation. The use of growth model is emphirical and chosen by the data scatter plot; besides, the parameter of the model could be interpreted biologically. The curves are often sigmoid, but not necessarily symmetrical [4]. There was a slowing down in growth at the first period and an upswing in growth at the second period to a maximum and then slowing down to a constanta; and the relative growth rate decreases linearly. The parameters predict when the maximum growth rate is and what the potential value is. Besides, it is important to determine how fast the growth rate in a certain time is (namely AGR =Absolute Growth Rate).

In many works, the Gompertz and Richards growth curve are common to be applied for describing broiler chicken weight growth due to its simplicity [5]. Then in 2005 it was found that three types of Hyperbolastic (those are H1, H2 and H3) may describe broiler weight growth well. However, those models are not flexible enough to fit all sigmoid growth curve.

The objective of this research was fitting the broiler weight growth using Gompertz, Richards and the three hyperbolastic applied to *Lohmann* broiler as most of the Indonesian chicken farm do. It is important to know which model may fit the growth data well so that the result may be used as a farmer's guideline. The model will be explored in this experiment, by ignoring the growth factors.

2. Experimental Details

This research was conducted at farm laboratory in February and March 2010, the materials were female and male broiler chicken strain Lohmann. The observation of chicken body weight was conducted within a three-day-interval, started at day 1 of age up to day 61.

The plan of the data analysis was as follows: first, making a scatter plot to get a brief description of chicken body weight data. Especially for hyperbolastic model, only one which probably fit the data was chosen. Then a non linear least-square was used to get the parameters of the models.

The Gompertz model was $W(t)= M \exp(-A \exp(-M\beta t))$, where the inflection point was at $t= [1/(M\beta)]$ in α or about 36.8% of potential weight. The Richards model was written as $W(t) = M/(1+A\exp(-M\beta t))^{\gamma}$ with the inflection point occured at $t = -1/M\beta \ln [(1+\alpha \exp(-M\beta t))/(\alpha(\gamma+1))]$ where W(t) was the body weight at age t, M was the asymptotic growth response or potential weight and assumed to be constant, β represented the intrinsic growth rate parameter [4,6]. The mathematical models of hyperbolastic were: $W(t)=M/[1+\alpha \exp(-M\beta t-\text{arcsinh } t)]$, $W(t) = M/[1+\alpha \text{ arcsinh } \exp(-M\beta t^{\gamma}]$, and $W(t)=M - [\alpha \exp(-M\beta t^{\gamma}-\text{arcsinh } (\theta t))]$ H1, H2 and H3 respectively [7]. The inflection point could be found by finding the second derivative of the function that equals to zero. Goodness of fit was determined by R-squared value as well as mean square error. The best fit was determined by Akaike's Identification Criterion (AIC) and Bayesian Identification Criterion (BIC).

3. Results and Discussion

It is easier to choose such a growth model by looking at the scatter plot. Here is the scatter plot of the body weight data (gram) versus age (days) for female and male chicken

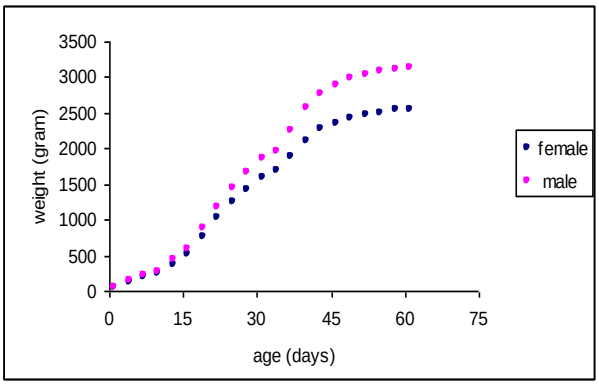

Figure 1. Scatter plot body weight versus age

Using L-M method to estimate the parameter of each model with some initial value, the results are presented in Table 1 (Appendixes). Based on the F test, we accepted the alternative hypothesis that those growth models fit the data well because we have F calculated > F table. It seems that all of those models are suitable to describe the trend of the body weight growth.

As chicken raised commercially for meat production, there must be a special treatment to reach market weight rapidly. As consequences of unnaturally rapid growth and heavy body weight, it should be found when the maximum growth rate. From the table, it is seen from the inflection point that for female and male chicken, the inflection point (the time when the maximum growth rate occurs) varies in the interval 18 to 28 days of age.

Moreover, at those days the chicken weight also varies about 678.70 to 1510.79 gram. We can also see the trend of growth rate at any point; the appearance are almost the same as seen on the picture below :

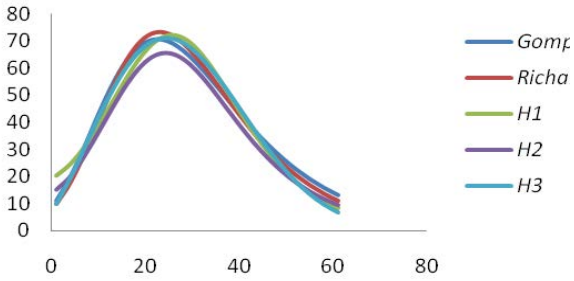

Figure 2. Body weight growth rate

It can be seen that the maximum growth rate occured at about the days explained above. Furthermore, to choose the best fit by counting the AIC_C ($AIC_C = AIC + \frac{2p(p+1)}{n-p-1}$) and BIC (BIC = -2 ln L + p ln (n)), where p is model parameters, L is maximum likelihood function, n is sample size. The smaller the AIC_C and BIC, the better the model is. The results of analysis were given in Table 2 (Appendixes).

Looking at the adjusted coefficient of determination (R^2_{adj}) for the goodness of fit, it seems that all the growth model are suitable because the accuracy is very high, which is more than 99.5%. To get a more accurate prediction and a better result, we could use another two statistic; we see that the smallest AIC_C and BIC are on Gompertz model for female chicken, and H1 for male chicken.

4. Conclusion

Recognizing the body weight growth of the chicken should be of great benefit to the farmers as well as modelers. Understanding chicken body weight growth trend is very important, especially when farmers would like to get marketable chicken to be sold in a shorter period and give good diet at the _right' time.

It is very important to look at the scatter plot before determining such a model to fit the growth data. It is almost clear that the Gompertz curves fit the data well, but in conclusion, it is reasonable to choose H1 to fit a broiler chicken growth data set as well. This model enables farmers to decide the right treatment at the right time, that is when the maximum growth rate is about to reach.

5. Acknowledgments

---

6. References

[1]. Brown, D and Rothery, P., (1993), Models in Biology: Mathematics, Statistics and Computing. England :John Wiley and Sons Ltd. Chicester, pp 13-56.

[2]. Gille, U., (2004), Analysis of Growth. http://www.UniLeipzig.de/~vetana/growthe.htm. Accessed on June 25, 2008.

[3]. Sanjoyo (2006), Non-Linear Estimation. http://mhs.blog.ui.edu/sanj55/files/2008/11/non-linear.pdf. Accessed on October 14, 2009.

[4]. O'Neill, M E., Bartimote, K., Hindmarsh, D. (2003), Biometry 1. Lecture notes. University of Sydney. Unpublished

[5]. Gille,U. and F.–V.Salomon (1995), Growth of Duck Bills. Http://elibrary.unm.edu/sora/Condor/files/issues/v101n03/p0710p0713.pdf#search=%22janoschek%20growth%20curve%22. Accessed on February 2, 2009.

[6]. Foldager, L., (2002), Growth Curve Models. Lecture Notes. Biometry Research Unit. Danish Institute of Agricultural Sciences. pp 1-45

[7]. Tabatabai, M., D.K. Williams and Z. Bursac (2005), Hyperbolastic Growth Models : Theory and Applications. Theoretical Biology and Medical Modelling 2:14. http://www.tbiomed.com/content/2/1/14. Accessed on September 15, 2009.

[8]. Fry, J.C., (1993), Biological Data Analysis. New York : Oxford University Press Inc. pp. 313-339.

[9]. Sengul, T. and S. Kiraz (2005), Non Linier Models for Growth Curve in Large White Turkeys. *J. Vet. Anim. Sci*. (29) 331 – 337

[10]. Yakupoglu, C. and H. Atil (2001), Comparison of Growth Curve Models On Broilers II: Comparison of Models. *J. Biol. Sci*. (1) 682 – 684.

Appendixes

Tabel 1. The mathematical model and the inflection point

Growth Model	**Mathematical Equation W(t)** **Inflection point**	
	Female	**Male**
Gompertz	$2812.57 \exp(-4.64 \exp(-0.07\ t)$ (22.54 , 1034.95)	$3507.25 \exp(-4.81 \exp(-0.063t)$ (22.93 , 1290.10)
Richards	$2743.67/[1+0.54 \exp(-0.08\ t)]^{10.72}$ (23.31 , 1078.91)	$3426.44/[1+0.44 \exp(-0.07)]^{12.81}$ (24.22 , 1346.63)
H1	$2664.25/[1+140.6 \exp(-0.08t-0.67\text{arcsinh } t)]$ (17.72 , 678.70)	$3311.71/[1+169.45 \exp(-0.08t-0.71\text{arcsinh } t)]$ (18.24 , 806.45)
H2	$2737.19/[1+172.14 \text{ arcsinh } \exp(-0.82t^{0.55})]$ (27.63 , 1366.67)	$3412.95/[1+208.92 \text{ arcsinh } \exp(-0.85t^{0.54})]$ (26.80 , 1434.22)
H3	$2618 - [2589.95 \exp(-0.0004t^{2.32}-\text{arcsinh } (0.006t))]$ (24.77 , 1165.28)	$3209.84 - [3190.45 \exp(-0.0001t^{2.32}-\text{arcsinh } (0.006t))]$ (26.64 , 1510.79)

Tabel 2. The results of best fit analysis

Growth Model	**Female**			**Male**		
	R^2_{adj}	**AIC_C**	**BIC**	**R^2_{adj}**	**AIC_C**	**BIC**
Gompertz	0.9968	*165.2391*	*166.6615*	0.9968	179.7737	181.1961
Richards	0.9978	165.8324	167.5542	0.9967	181.3623	183.0841
H1	0.9967	167.5493	169.2711	0.9967	*179.4460*	*181.1678*
H2	0.9978	166.1634	167.8852	0.9967	180.1962	181.9180
H3	0.9977	167.3877	169.0657	0.9965	179.9027	181.5808

Nitrogen Leaching on Coffee Based Agroforestry Systems in the Presence of Different Shade Trees

R. Priyadarshini [1], K. Hairiah [2], D. Suprayogo [3], J.B.Baon [4]

[(1)] UPN –Veteran" Surabaya, Indonesia (rssyd_priyadarshini@yahoo.com)
[(2,3)] University of Brawijaya, Malang, Indonesia
[(4)] ICCRI – Jember, , Indonesia

Abstract

Coffee based agroforestry system was characterized by diversity of shade trees. Litter quality input of shade trees has an important role on nitrogen leaching. However, little is known regarding the kind of the shade trees which could inhibit the nitrogen leach. We studied the nitrogen leach in coffee plantations on two types coffee agroforestry systems, shaded coffee and multistratra coffee. They have different shade trees, either quantity nor quality. Litter input on multistrata coffee was higher (6.55Mg ha $^{-1}$) than shaded coffee(4.68 Mg ha $^{-1}$). The contratry results was found on litter quality. Leaching loss on multistrata coffee (3.00 kg ha^{-1}) are greater than those from shaded coffee (1.87 kg ha^{-1}). It was concluded that tree species of shade trees influence the nitrogen loss.

Keywords: *Coffee ,shade trees, litter input, nitrogen leach.*

1. Introduction

Coffee *(Coffea sp*.) is one of the most economically important agricultural crops. Traditionally, coffee grown in association with a variety of shade tree species. Shade trees has an important role on coffee productivity. It was because their canopy cover and their litter quantity and quality will determined either micro climate or soil characteristics.

Coffee based agroforestry system was believed can maintain coffee productivity. It was characterized by diversity of shade trees. Shade trees will influence litter input quantity and quality. Litter characteristics will influence the decomposition rate of organic matter [1], more diverse the shade trees, the decomposition rate will increase [2].

Decomposition rate was an important processes for nutrient release, especially nitrogen. Nitrogen is the nutrient most limiting the productivity of coffee plantations [3]. In the soil, N released during soil organic matter decomposition is subject to a series of biologically mediated transformations of which NO_3^- and N_2O represent two possible end products. One study suggests that only 30% of the N added through fertilization is assimilated by coffee plants [4] , presenting the possibility for high rates of N loss from coffee agroecosystems.

Nitrogen leaching will happen if nitrogen release is not synchronize with plant demand. Nitrate leaching from coffee agroecosystems could potentially affect groundwater quality. Few studies have compared the mechanisms controlling N retention and loss in shaded or multistrata coffee agroecosystems [1]. That is why it is important to know the relationship between shade tree characteristics and nitrogen release.

Our research was conducted to understand the dynamics of N loss in different coffee agroecosystems. Our objectives were to quantify and compare N losses via leaching coffee grown in different shade trees.

2. Experimental Details

Study Sites

This study was conduct on two types of coffee agroforestry systems; shaded coffee and multistrata coffee at Sumberagung and Tulungrejo village, Ngantang District, Malang. This site geographically is located at 7°40 – LS 00 and 5°8° 30 – 5° 40 BT. The soils in all plantations were classified as Inceptisols. Soil organic matter, pH, and texture were initially quantified (Table 1 – Appendixes). The soils were moderately neutral (pH 6.0 – 7.0), organic matter ranged from 2.62 to 5.95%. Soil properties were relatively similar amongs ites.

Vegetation

Vegetation sampling transects were taken at 10 x 20 m^2. Canopy was measured with a measuring length headers on all ordinate system. All types of crops included in the plot were recorded their types and abundance.

Shannon Diversity Index (H') was used to see plant diversity, and is calculated according to the formula:

$$H' = -\sum_{i=1}^{s} pi \, pi \, 2 \, lg$$

where:

H ' = Shannon-Wiener Diversity Index

pi = proportion of i-th species abundance or the proportion between the number of individuals sspesies to-i (ni) of the total number of individual species (N) so that pi = ni / N

Nitrate Leaching

Lysimeters were located 60 cm below the soil surface in each plantation. Lysimeter consisted of a plastic tube (10 cm diam.). The open end was sealed by a plastic bottle to collect water. Two lysimeter were placed on each plantation. Soil solution was collected at weekly interval for two month to quantify leaching losses in each plantation. Soil solution was taken to the laboratory for NO_3^- determination.

Soil samples were collected from the main microenvironmental conditions in each plantation type to determine soil water content on each sampling date [4]. Nitrate-N loss was expressed on an areal basis by multiplying the soil water excess (precipitation – actual evapotranspiration) by the soil water NO_3^-N concentration for each lysimeter.

Statistical Analysis

Diversity and species richness between shade coffee and multi-*strata* coffee were calculated and compared by t-test. Significant differences in NO; leaching between plantations and sampling dates were determined using an analysis of variance (ANOVA) for a repeated-measures, randomized complete block design.

3. Results and Discussion

Tree diversity on multistrata coffee more diverse than shaded coffe. Shade trees found on shaded coffee was *Gliricidia sp* , but on multistrata coffee the shade trees was diverse. It can use timber tress, fruit trees or *Gliricidia sp* as shade trees.

Biomass reserves for multistrata coffee and shaded coffe were 38.43 Mg ha^{-1} and 29.72 Mg ha^{-1}, respectively.

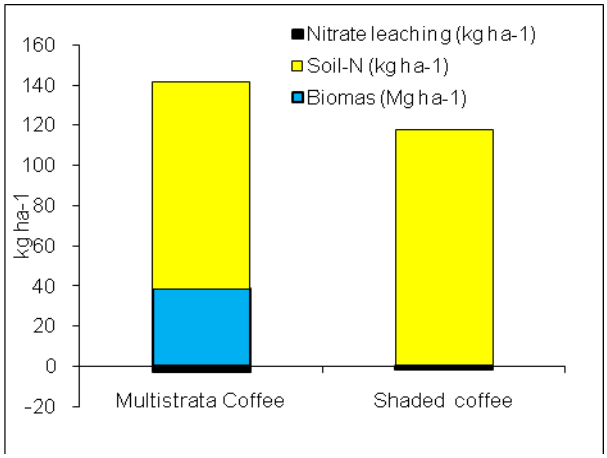

Figure 1. Biomass reserves and annual litter input for shaded coffee and multistrata coffee and Their contribution to soil N

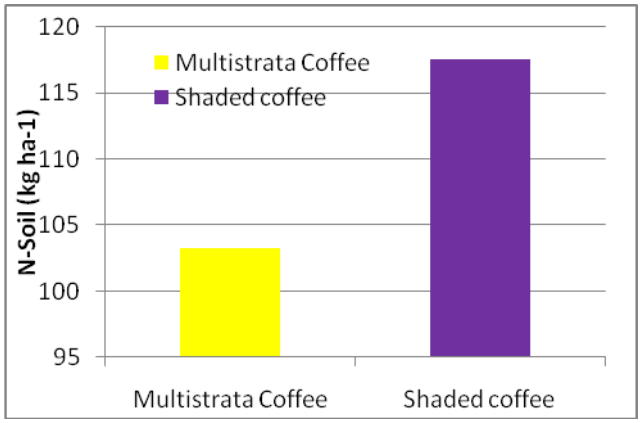

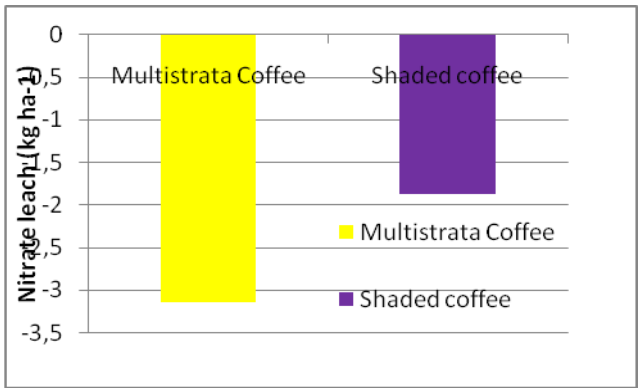

Figure 2. Soil NO_3^- concentration (A) and NO_3^- leached in Shaded Coffee and Coffee multistrata

Annual litter inputs in coffee agroforestry were 6.55 and 4.68 Mg ha1 $year^{-1}$ for multistrata coffee and shade coffee respectively. If the N concentration was 2.2% and 3.27% then the N were 0.14 Mg ha^{-1} $year^{-1}$ (shaded coffee) and 0.15 Mg $ha^{-1}year^{-1}$ (multi-*strata* coffee).

The results showed that the soil-N concentration in shaded coffee and coffee

multistrata significantly different, where soil-N content in coffee multistrata (109.2 kg ha^{-1}) lower than shade coffee (119.2 kg ha^{-1}). This condition occurs because even the annual litter input and the litter quality was larger but decomposition rate was faster; so nitrate washed away as leaching.

Some studies show that only 30% of the N that enters the soil to be assimilated by the coffee plants [1] which causes the magnitude of potential N loss [4]. In the study area 51.27% N (shade coffee) and 53.23% N (coffee multistrata) were assimilated into NO_3^- and assimilate into $NH4^+$ was 47.94%, and 46%, 63% respectively for shade coffee and coffee multi-*strata*. NO_3^- and NH_4^+ obtained from the assimilation is not all utilized by the plants; partially leached or undergo denitrification. NO_3^-leached in multistrata coffee (3.09%) was greater compared to shade coffee (1.61%).

Coffee plantation management affect the amount of nitrate leached (Figure 2.), where the nitrate leaching in coffee multistrata was higher (3,14 Mg ha^{-1}) compared to shade coffee (1,86 Mg ha^{-1}). It means that nitrate leaching in coffee multi-*strata* was 2 times greater than those observed in shade coffee (bulk soil = 0.84 multistrata coffee; 1.06 = shaded coffee).

Litter input in multistrata coffee was greater than shaded coffee. It was happened because plant diversity and density on multistrata coffee was higher too. Litter input was important factor on soil characteristics. Litter characteristics was depend on tree species. Multi-*strata* coffee with diverse tree species has higher decomposition rate compared with shaded coffee, and finally will determine N release.

Our results indicate that NO_3^- losses through leaching are higher from multistrata systems than from those containing shaded coffee. Nevertheless , NO_3^- leaching from both plantation types was lower than values reported for other tropical agroecosystems (50-100 kg NO_3^- N ha^{-1} yr^1; [3]. The higher rates of NO_3^- leaching from multistrata plantations indicates that plant N-use efficiency was relatively low in this plantation type. For example, approximately 2% of the N was lost via leaching in the multistrata plantations, whereas only 1.4% of N from organic matter moved below the rooting zone in shaded plantations. In many agricultural systems, up to 50% of N applied as fertilizer can be lost through leaching and volatilization [6], suggesting NO_3^- leaching from both plantation types was relatively small.

Organic matter inputs from the pruning and litter of different shade trees also may contribute to differences in NO_3^- leaching between coffee management practices. In multistrata plantations, higher NO_3^- concentrations could result from recent tree litter , while in shaded coffe it can be from litter or pruning. Pruning will decreases leaf area, transpiration rate, and N uptake. Decreasing of transpiration rate will reduce nitrate leaching.

Different temporal patterns of NO_3^- loss between management practices could reflect differences in temporal patterns of release of N from tree litter.

4. Conclusion

It was conclude that NO_3^- leaching on multistrata higher than shaded coffee. The NO_3^- leaching was determined with kind of litter, decomposition rate, dan other environment factors like transpiration.

5. Acknowledgments

We gratefully acknowledge support from DIKTI (–Doctor Hibah" fund) and for Technician from Soil Biology Laboratory for provided laboratory assistance.

6. References

[1]. Bardgett R.D. and Shine A., (1999), Linkages between plant litter diversity, soil microbial biomass and ecosystem function in temperate grasslands. *Soil Biol. Biogeochem.* 31, 317-321.

[2]. Hector A., Beale A.J., Minns A., Otway S.J. and Lawton J.H., (2000), Consequences of the reduction of plant diversity for litter decomposition: effects through litter quality and microenvironment. *Oikos* 90, 357-371.

[3]. Van Lauwe, B., Diels, J., Sanginga, N., Merck, R., (1997), Residue quality and decomposition: an unsteady relationship? In: Cadisch, G., Giller, K. (Eds.), Driven by Nature: Plant Litter Quality and Decomposition. CABI, Wallingford, UK, pp. 157–166.

[4]. Hooper D.U. and Vitousek P.M., (1997), The effects of plant composition and diversity on ecosystem processes. *Science* 277, 1302-1305

[5]. Babbar and Zak (1994), Nitrogen cycling in Coffee Agroecosystems: Net N mineralization in abesence and Presence of Shade Trees. *Agriculture, Ecosystems, and Environment* (48) 107-113

[6]. Jenkinson and Smith (1988), Nitrogen efficiency in agriculture systems. Elsevier.

Appendix

Table 1. Soil Characteristic at Ngantang-Malang

Land Use	Depth (cm)	Texture			C-org (%)	pH
		Sand	Silt	Clay		
Shaded Coffee	0 -10	48	41	12	0.98	6.07
Multistrata Coffee		42	46	12	2.23	6.21
Shaded Coffee	10-20	48	36	15	0.88	6.15
Multistrata Coffee		41	46	13	1.27	6.30
Shaded Coffee	20-30	45	40	15	0.74	6.24
Multistrata Coffee		41	44	15	1.24	6.54

Functional Morphology of Deposit Feeder Bivalve *Theora lata* (Bivalvia: Semelidae)

Reni Ambarwati [1], Trijoko [2]

[(1)] Department of Biology, Faculty of Mathematics and Natural Science Surabaya State University, Surabaya, Indonesia (renibio95@yahoo.co.id);
[(2)] Faculty of Biology, Gadjah Mada University, Yogyakarta, Indonesia

Abstract

Semelidae bivalves have ecologically significance in estuaries and shallow waters ecosystems. However, the functional morphology of this bivalve has not been studied. The purpose of this research was to study the morphological characters of Theora lata, one of Semelidae bivalves. Specimens collected from Sidoarjo Coastal Water, Jawa Timur. Specimens relaxed by using $MgCl_2$ 7% in sea water and fixed in 10% formalin in sea water. Finally, specimens were preserved in 70% ethanol. Observation was done on the morphology internal of all specimens. Measurements of morphometric were conducted on the length, the height, and the width of shells; on the length and width of ctenidium and labial palp. The results of this research showed that the diagnostic characters of Theora lata were exterior and interior characters of the shell, form and the type of siphon, and the form of foot. Ratio length: height of the shell=1: 0,6; ratio length= width of the shell: 1: 0.3, ratio height: width of the shell= 1: 0.6. Based on the morphometric measurements of ctenidium and labial palp, Theora lata can be categorized as deposit feeder. The ctenidium of Theora lata is smaller than its labial palp, the ratio of ctenidium: labial palp is 1: 1.2.

Keywords: *Theora lata, Semelidae, Bivalvia, morphological character of bivalve, deposit feeder.*

1. Introduction

Indonesia is an archipelago with wide sea, long shore line, and many rivers in almost all of the islands. These conditions provide an ideal habitat for many kinds of bivalves. Most of bivalves are marines, they can be found in the sea, littoral zone, and estuaries. Nybakken and Bertness [1] stated that shore and estuary are ideal habitat for bivalves.

Many bivalves are important for trading and consumed by local people. These kind of bivalves are very well-known and some of them have been studied, for example their distribution, nutrition, and also their taxonomy, including their functional morphology [2,3]. Contrary to these conditions, bivalves that do not have economic significance get less attention. The publication and shell collection of these kinds of bivalves are still limited.

Theora is one of genera of Semelidae. Shells of *Theora* are small, thin and fragile [4,5]. *Theora* are not collected well because the nature of their shell and sometimes they have been neglected because less economic significance. Actually, however, Semelid bivalves have ecological significance. *Theora lubrica* and *Theora fragillis* are important food source for estuarine and shallow-water fishes [6]. *Theora lata* is an indicator species of disharmonic environments [7]. NIMPIS [8] also state that *Theora lubrica* is an indicator species for eutrophic and anoxic areas.

Theora are very abundace in muddy bottom at littoral zone and shollow waters [4]. Kastoro *et al*. [7] reported the occurrence of *Theora lata* in the estuary of Porong River. *Theora lata* is very similar to *Theora lubrica*. Detail observations are needed to the diagnostic characters of Theora lata to avoid misidentification in the future. The purposes of this research were to study the morphological characters of *Theora lata* (Hinds, 1843) and to analysis the fuctional morphology of this bivalve.

2. Experimental Details

Bivalve samples were collected from Sidoarjo coastal water, East Java Indonesia. Specimens were collected by using scooped-nest and modification of vertical core sampler. Specimens were relaxed by using $MgCl_2.6H_2O$ 7% in sea water, and fixed by using formalin 10% in sea water. Finally, specimens fixed in Alcohol 70%. Morphometric measurements were done to 50 specimens by using caliper, including length, height, and width of the shell, and length and the width of ctenidium (gill) and labial palp. Internal morphology of the specimens was observed carefully under magnifier lamp.

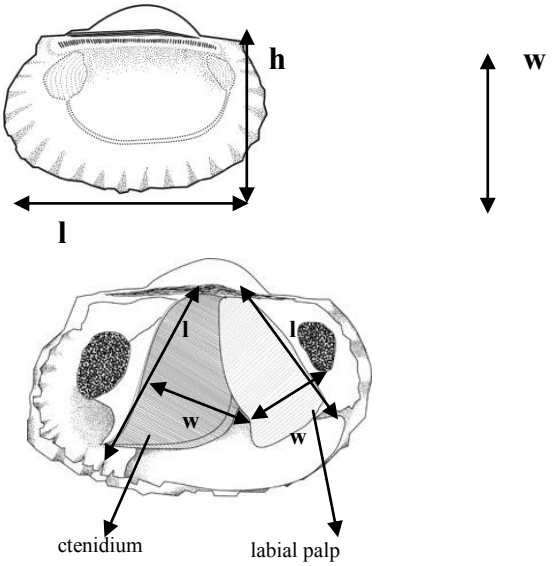

Figure 1. Morphometry of shell, ctenidium, and labial palp; l: length, h: height, w: width

3. Results and Discussion

Diagnostic characters:

Shell white, transparent, very thin, and fragile. Shell elliptical and small (average 11.25–17.25 mm). Posterio-dorsal area of the shell rather flattened. Internal surface smooth, without internal rib (Figure 2).

Description:

Shell inequilateral. Shell elliptical. Anterio-dorsal area smooth, rounded, and oriented to ventro-anterior. Posterio-dorsal area rather concave. Ventral margin straight, narrowed in the posterior area. Shell white, transparent, very thin, and fragile. Exterior surface smooth, white, and glossy, with smooth concentric line. Periostracum very thin. Umbo prosogyrate, not inflated. Umbo median. No lunule and eschuteon. Ligament external and internal , brown (Figure 3). Hinge heterodont, one cardinal teeth and anterior lateral teeth. Cardinal area very narrow. Posterior adductor scar rather larger than anterior adductor scar. Anterior adductor scar at the anterio-dorsal area of the shell. Posterior adductor scar located at the posterio-dorsal area of the shell. Anterior pedal retractor scar smaller than posterior pedal retractor scar. Anterior pedal retractor scar at the dorsal of anterior adductor scar. Posterior pedal retractor scar at the dorsal of posterior adductor scar. Palial line present. Palial sinus very deep and oriented to the anterior (Figure 3). The body yellowish-white. Mantle open, fused in the posterior region. Margin of mantle not fused, wide. Ctenidia eulamelibranchia. Outer demibranchia smaller than inner demibranchia, oriented to the dorsal are, having leaf-like appearance. Ctenidium located along the ventral of umbo until the posterior end. Labial palp located at the anterior side of the ctenidium. Labial palp very wide. Food axe-like, very big. Anterior adductor muscle oval. Posterior adductor muscle rounded and bigger. Pedal retractor anterior smaller that pedal retractor posterior. Siphon very long, retractile. Siphon tips without tentacles. Siphon exhalans smaller that siphon inhalans. Siphon slim, pointed at the tip. (Figure 4).

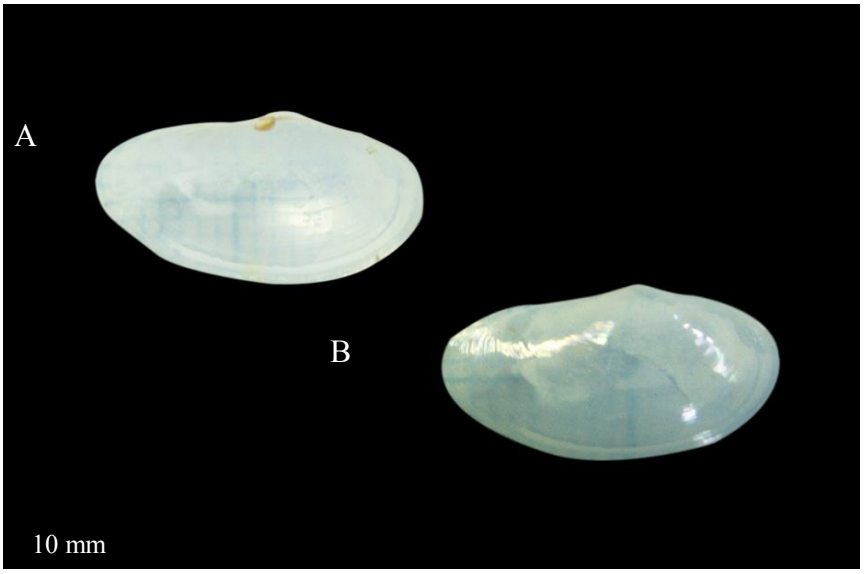

Figure 2. Morphology of *Theora lata*; A: interior of left valve; B: exterior of right valve

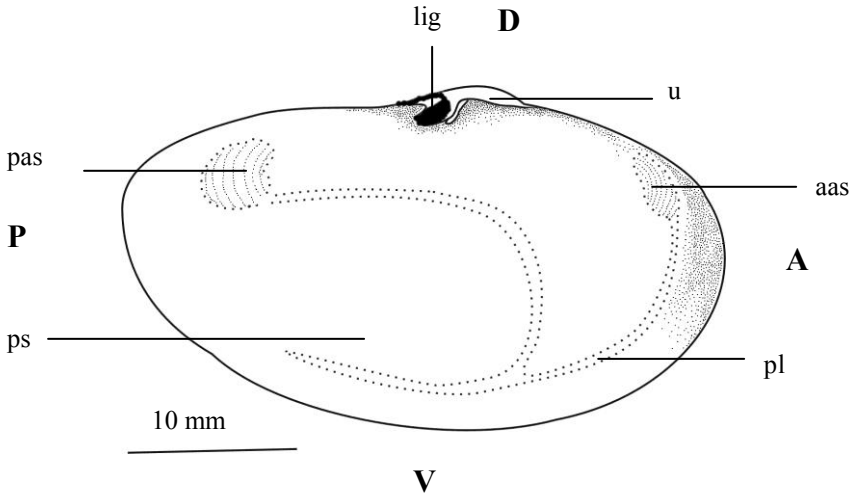

Figure 3. Interior of shell of *Theora lata;* A: anterior, P: posterior; D: dorsal; V: ventral; aas: anterior adductor scar; pas: posterior adductor scar; pl: palial line; ps: palial sinus; lig: ligament, u: umbo.

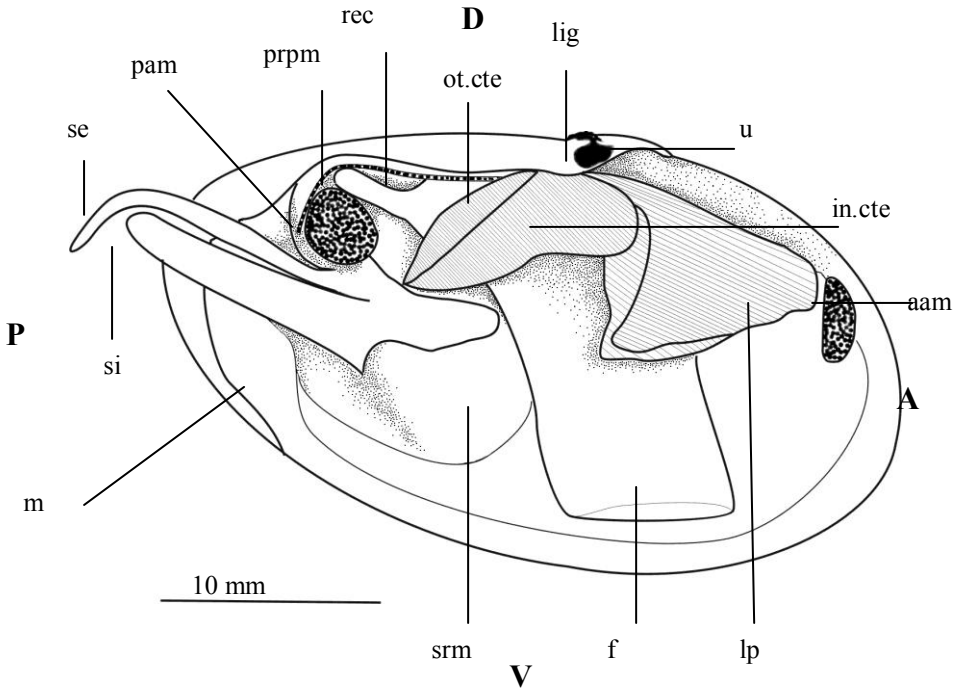

Figure 4. Internal anatomy of *Theora lata* A: anterior, P: posterior; D: dorsal; V: ventral; aam: anterior adductor muscle; pam: posterior adductor muscle; prpm: pedal retractor posterior muscle; srm: siphon retractor muscle; u: umbo; ot.cte: outer demibranchia; in.cte: inner demibranchia; cte: ctenidium; lp: labial palp; rec: rectum; si: siphon inhalans; se: siphon exhalans; m: mantle; f: foot.

Morphometric measurements of fifty specimens of *Theora lata* are given in Table 1.

Table 1. Morphometry of *Theora lata* from Sidoarjo coastal water

Morphometry *Theora lata*	
Length of shell (mm)	12.82±1.43 (11.25–17.25)
Height of shell (mm)	7.42±0.79 (6.35–9.80)
Width of shell (mm)	4.21±0.66 (3.6-6.6)
Ratio Length: Height of shell	1: 0.6
Ratio Length: Width of shell	1: 0.3
Ratio Height: Width of shell	1: 0.6
Ratio Ctenidium: Labial palp	1: 1.2

Based on above description, it can be shown *Theora lata* can be distinguished from *Theora lubrica* because the interior of shell is smooth without internal rib. In addition, the posterior area of the umbo is more concave in *Theora lata*.

The shell of *Theora lata* is elliptical, narrowed at the posterior end, and almost flattened. Ratio of length and height of shell = 1: 0.6, ratio length and width of shell = 1: 0.3, ratio height and width of shell = 1: 0.6. This condition of the shell is very ideal for burrowing. Burrowing bivalves usually have smooth and flattened shells [3,8]. During this research, *Theora lata* was found burrowing at ±10 cm. The pattern of morphometry of *Theora lata* shell can be shown as a linear curve. Pattern of length and height of the shell can be described as Y=0.668+0.528X, R^2= 0.903; Pattern of length and width of the shell can be described as Y=-1.406+0.439X, R^2= 0.890; Pattern of height and width of the shell can be described as Y=-1.272+0.739X, R^2= 0.778 (Figure 5).

Figure 5 also provide information of the growth of *Theora lata* shell. The growth of height and width of shell toward the length of the shell are negative allometric (b<1), hence the shell grow faster in the length than in height and width.

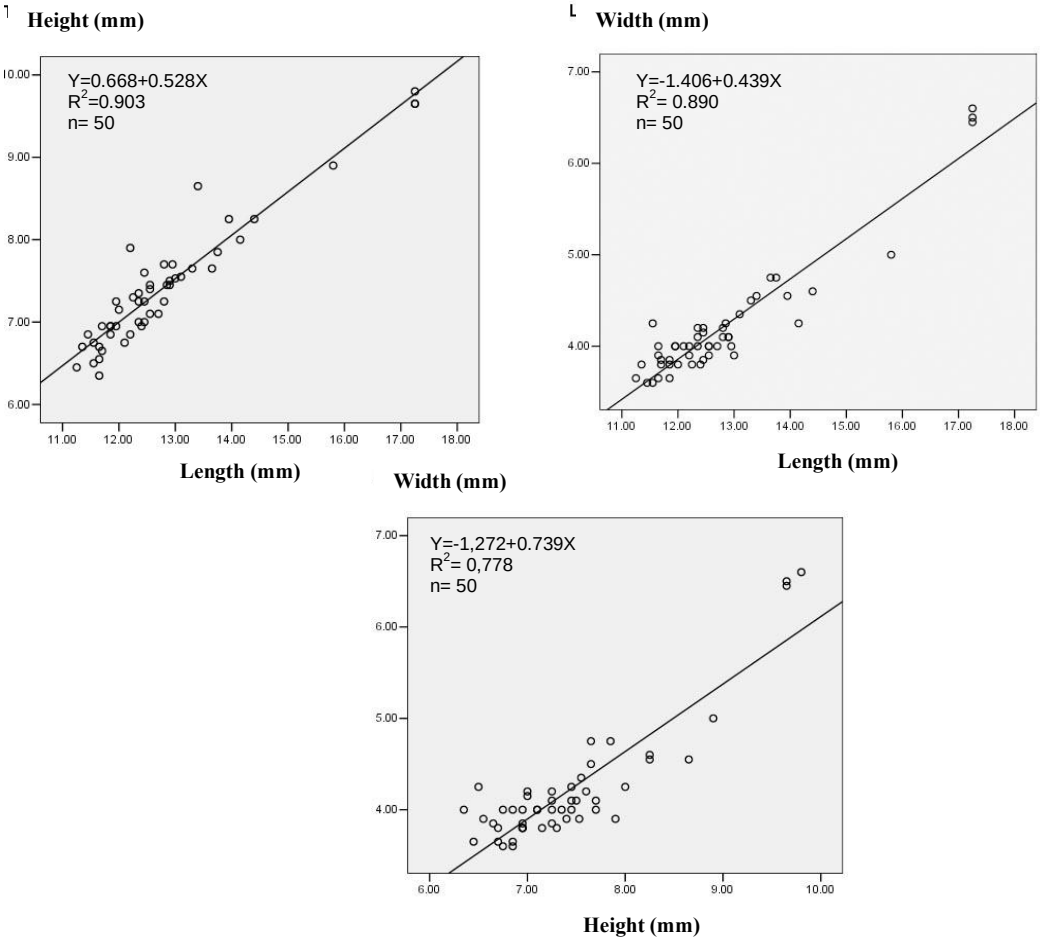

Figure 5. Pattern of morphometry of *Theora lata* shell based on linear regression.

Theora lata is small, the length of shell= 11.25–17.25 mm, height 6.35–9.80 mm, and width 3.6–6.6 mm. Most of them were 11.25–13 mm in length. *Theora lata* has separated siphon. Siphon inhalans and exhalans are slim and long. There is no tentacle at the tip of siphon. It differences from suspension feeder bivalves, for example venerid bivalve. Suspension feeder bivalves have tantacles on the tip of their siphon to sort particles dissolved in the water [3]. Labial palp of *Theora lata* is much bigger than the ctenidium, the ratio is 1: 1.2. It is different from suspension feeder bivalve. In suspension feeder bivalves, ctenidium is bigger than the labial palp because the function for pumping more develope [3,10]. In contrary, bigger labial palp is very ideal for deposit feeder bivalves. NIMPIS [8] reported that *T. lubrica*, another member of genus *Theora*, feeds on organic material on the surface of sediment by using their siphons. Hence, they are very abundance in the soft bottom with rich organic materials. *Theora lata* can be found in 0–10 cm depth under the surface of soft bottom shallow water.

4. Conclusion

Theora lata can be categorized as deposit feeder. The ctenidium of *Theora lata* is smaller than its labial palp. Morphology of *Theora lata* is suitable for burrowing and feeding in soft bottom shallow water with rich organic materials.

5. Acknowledgements

We are very grateful to Dr. Richard C. Willan, Senior Curator Museum and Art Gallery, Northern Territory, Australia for his great help on the species identification.

6. References

[1]. Nybakken, J.W. and Bertness (2005), *Marine Biology: an ecological approach, sixth edition,* Benjamin Cumig, San Franscisco.

[2]. Ambarwati, R. and Trijoko (2010), Kekayaan Jenis *Anadara* di Perairan Pantai Sidoarjo, Jawa Timur. *Berkala Penelitian Hayati*, Edisi Khusus (In Press).

[3]. Ambarwati, R. and Trijoko (2010), Morfologi Fungsional Kerang Batik *Paphia undulata* (Bivalvia: Veneridae). *Berkala Penelitian Hayati*, Edisi Khusus (In Press).

[4]. Habe, T. (1968), *Shells of The Western Pacific in Color, Volume II*, Hoikhusa Publishing Co., Ltd., Osaka.

[5]. Lamprell K., and Whitehead T. (1992), *Bivalves of Australia, Volume 1*, Bathurst, New South Wales, Crawford House Press.

[6]. Willan, R.C., (1998), Superfamily Tellinoidea, pp 342–348 in Beesley PL, Ross GJB & Wells A (eds) *Mollusca: The Southern Synthesis. Fauna of Australia. Vol. 5*. CSIRO Publishing, Melbourne, Part A xvi 563 pp

[7]. Kastoro, W., I. Aswandy, I. Al Hakim, P.A.W.J. De Wilde, dan J.M. Everarts, (1989), Soft-Bottom Benthic Community in the Estuarine Waters if East Java, Netherlands *Journal of Sea Research*; 23(4): 463–472.

[8]. NIMPIS. (2002), *Theora lubrica species summary*. National Introduced Marine Pest Information System (Eds: Hewitt C.L., Martin R.B., Sliwa C., McEnnulty F.R., Murphy N.E., Jones T., Cooper S.) Web publication http://crimp.marine.csiro.au/nimpis. Accesed on 13 April 2010.

[9]. Harte M.E., (1998), Superfamily Veneroidea. pp 355–362 in Beesley PL, Ross GJB & Wells A (eds) *Mollusca: The Southern Synthesis. Fauna of Australia. Vol. 5*. CSIRO Publishing, Melbourne, Part A xvi 563 pp.

[10]. Compton TJ, Drent J, Kentie R, Pearson GB, van deer Meer J, Piersma T. (2007). Overlap in the feeding morphology of bivalves from spesies-rich and spesies-poor intertidal flats using gill-palp ratios for comparative analyses of mollusc assemblages. *Mar Ecol Prog Ser*, 348: 213–220.

Soluble Quinone Reductase from Methanosarcina acetivorans binds a *Flavin Adenine Dinucleotide*

Suharti

Chemistry Department, Mathematic and Natural Sciences Faculty, State University of Malang, Malang, Indonesia (s.suharti@um.ac.id)

Abstract

Several species have been shown to have flavin-dependent enzymes that allow the two-electron reduction of quinones to the hydroquinone form to avoid the generation of one-electron reduced semiquinone that is known to cause oxidative stress. Methanosarcina acetivorans belongs to the Archaea domain and obtains energy for growth by converting the methyl group of acetate to methane, which accounts for at least two-thirds of the total methane produced in the Earth's biosphere. Interestingly, although quinone has never been reported present in M. acetivorans, the genome of M. acetivorans contains a gene encoding a quinone reductase. In a study of the function of the gene product of quinone reductase, the gene was over expressed in Escherichia coli as C-terminal histidine tag proteins. Chemical analysis showed that the purified protein contains one molecule FAD per molecule protein and biochemical assay showed that the enzyme is capable of using NADPH as artificial electron donor. Furthermore, sequence alignment showed a similarity between the quinone reductase of M. acetivorans and the human quinone reductase type 2, which suggests that it might play a role in the mitigation of chemically-induced skin carcinogenesis. The similarity might lead to similar function of which M. acetivorans quinone reductase might play a role in protection against environmental stress.

Keywords: *M. acetivorans, quinone reductase.*

1. Introduction

Methane-producing microbes are essential to the global carbon cycle. Methane and carbon dioxide are the final products of the microbial decomposition of organic matter in a diversity of oxygen-free (anaerobic) habitats, such as the rumen of cattle, sewage treatment plants, rice paddies, and natural wetlands. An estimated one billion metric tons of methane are produced annually and most of this methane is produced by a two-step process in which complex organic matter is decomposed to acetate by fermentative microbes. Acetate is further converted to methane and carbon dioxide by methane-producing species from the genera *Methanosarcina* and *Methanosaeta* [1].

Methanosarcina acetivorans is a marine isolate for which the genome, the largest yet among the *Archaea*, has been sequenced, suggesting extensive metabolic diversity [2]. The genome sequence of *M. acetivorans* contains a gene (MA0326) encoding quinone reductase. Interestingly, the existence of quinone in methanogens has never been reported. Furthermore the predicted secondary structure derived using HSSP version 1.1 showed a homology with the structure of human quinone reductase type 2 from a protein with menadione (vit K3) as physiological substrate. Quinone reductase type 2 (QR2) is expressed in various mammalian tissues, including heart, liver, skeletal muscle, and kidney [3]. It was first purified and characterized as a flavoprotein quinone reductase in 1961 [4]. Quinone reductase type 2 has not been investigated in the *Archaea*. In order to study the physiological role of the gene product of MA0326, the gene was cloned and over-expressed in *E. coli*. This paper reports the overexpression and initial characterization of purified quinone reductase from *M. acetivorans*.

2. Experimental details

Cloning and overexpression

The open reading frame (ORF) of the quinone reductase encoding gene was amplified by PCR from *M. acetivorans* genomic DNA. A pair of sense ($^{5'}$TTGTTGCATATGAAAGTTTTGTACATTTAC) and antisense ($^{5'}$GATGATCTCGAGTAGTTCG GAAATTCTC) primers was used to amplify the gene. Primers also were designed to introduce the *Nde*I and *Xho*I restriction sites (underlined sequences). The PCR fragments were cloned into the pET22b(+) (Novagen) vector. The

C-terminal six histidine-tagged recombinant proteins were expressed in *Escherichia coli* Rosetta pLacI cells. The transformed cells were cultured at 37°C in Luria-Bertani broth containing 100 mg ampicillin per liter. When the OD600 of the cells reached quinone reductase was overproduced by the addition of 1 mM IPTG. The culture was incubated for 16 h at 16°C. Cells were harvested and stores at -20°C.

Purification of Recombinant quinone reductase

Approximately 15g thawed cells were resuspended in 20 mM potassium phosphate buffer (pH 7.4) containing 500 mM NaCl and 20 mM imidazole. DNase and 0.25 mM phenylmethanesulfonyl fluoride were then added and the cells lysed by being passed twice through a French pressure cell at 110 MPa. Cell debris and membranes were removed by centrifugation at 100000*g* for 45 min at 4°C. The supernatant was filtered and loaded onto a Ni Sepharose high-performance column (1.6 x 13cm) (GE Healthcare) equilibrated with a phosphate buffer containing 500 mM NaCl and 20 mM imidazole.

The column was then washed with 3 column volumes of phosphate buffer containing 500 mM NaCl and 40 mM imidazole. The yellow fraction of flavodoxin was eluted with a phosphate buffer containing 500 mM NaCl and 250 mM imidazole. The eluted yellow fraction (~ 15 mL) was dialyzed at 4°C against 50 mM Tris-HCl (pH 7.5) using a 10 kDa cutoff cellulose membrane and concentrated up to a final volume of 1-2 ml using a Centricon YM-10 (Millipore) an stored at -20°C. UV-Vis spectra of partially purified quinone reductase were recorded.

Biochemical Analysis of quinone reductase.

For the analysis of noncovalently bound flavin, purified quinone reductase was denatured by either adding trichloroacetic acid to a final concentration of 5% or boiling for 5 min. The precipitated protein was removed by centrifugation and the supernatant was filtered using an Ultrafree-MC 5000 NMWL filter unit (Millipore). The filtrate was then neutralized by adding 2M K_2HPO_4. The free flavin concentration was determined spectroscopically using an extinction coefficient of 12.2 $mM^{-1}cm^{-1}$ at 452 nm (oxidized form) [5].

The flavin was released by boiling the protein solution for 5 min or by adding *trichloroacetic acid* to a final concentration of 20% (w/v). The flavin type was determined by thin layer chromatography (TLC) using a silica gel matrix (Fluka) with an *n*-butanol/acetic acid/water mixture (4:1:5) as the mobile phase. The protein concentration was quantified by the bicinchoninic assay (Pierce).

3. Results and Discussion

Characterization of quinone reductase

The histidine-tagged flavodoxins were overproduced in *E. coli* as a soluble protein and partially purified. SDS-PAGE of purified quinone reductase showed an apparent molecular mass of 24±0.5kDa in good agreement with the theoretical molecular mass of 24.15 kDa (Figure 1). The purified quinone reductase is a yellow protein and its UV-Vis spectrum exhibited an absorbance typical of a flavoprotein with two peaks at 379 and 458 nm (Figure 2). The flavin was released by boiling the protein solution for 5 min or by the addition of a 20% *trichloroacetic acid solution i*ndicating that quinone reductase contains a noncovalently bound flavin. The released flavin migrated to the same position as *flavin adenine dinucleotide* (FAD) on the thin-layer indicating that the type of flavin.

Furthermore, stoichiometric analysis showed a FAD: protein ratio of 0.92:1 suggesting that the quinone reductase bound one FAD molecule per protein molecule. The crystal structure of human quinone reductase contains one FAD molecule and one zinc ion per protein molecule. Atomic absorption spectroscopy did not reveal the presence of a zinc atom in the *M. acetivorans* quinone. Zinc might be lost during the enzyme purification.

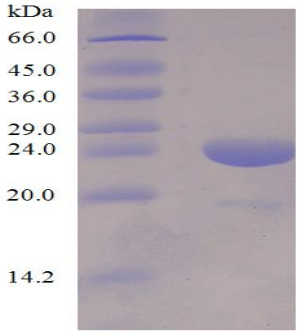

Figure 1. SDS-PAGE of purified quinone reductase. Line 1: molecular standard, line 2: purified quinone reductase.

Figure 3 shows the initial biochemical assay of the quinone reductase of *M. acetivorans* using *nicotine* adenine dinucleotide phosphate (NADPH) and 2,6-dichlorophenol-indophenol (DCPIP) as artificial electron donor and acceptor, respectively. It shows that the enzyme is capable of utilizing NADPH as an electron source. However, the existence of NADPH has not yet been reported. F_{420} is known as an electron carrier

in methanogens. Considering the midpoint potential of Factor 420 (F_{420}) which is close to the midpoint potential value of NADPH, F_{420} might serve as a physiological electron donor. Methanophenazine, a quinol analog in methanogens, might serve as an electron acceptor of *M. acetivorans* quinone reductase.

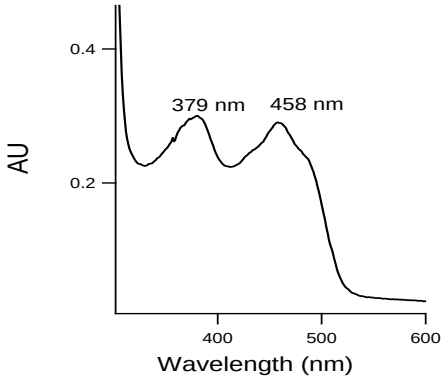

Figure 2. UV-Vis spectrum of *M. acetivorans* quinone reductase

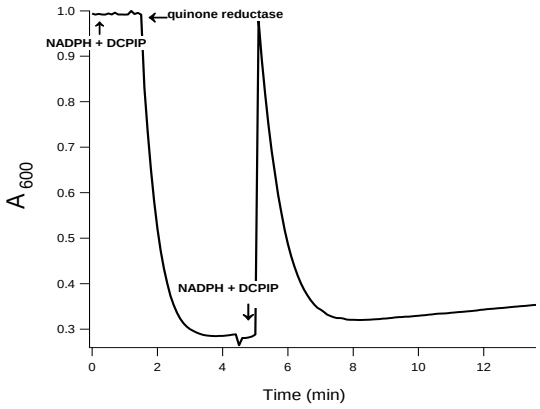

Figure 3. DCPIP reduction by *M. acetivorans* quinone reductase using NADPH followed spectroscopically at 600 nm.

Quinone reductase type 2 is a soluble protein and unable to use NADPH as a reductant. Human quinone reductase type 2 is suggested to play a role in the mitigation of chemically-induced skin carcinogenesis. This protection is due to its control of factors that mediate cell growth and differentiation, proliferation, and apoptosis [6]. It has been hypothesized that the ancestor of the eukaryotes diverged early from the *Archaea* [7,8].

Figure 4 (appendix) shows the sequence alignment of quinone reductase of *M. acetivorans* and human quinone reductase type 2, indicating a high similarity between both quinone reductases. *M. acetivorans* has not been reported to have vitamin K_3 and NADH suggesting that the quinone reductase of *M. acetivorans* has a different substrate specificity compared to human quinone reductase type 2. However, similar to human quinone reductase type 2, the quinone reductase of *M. acetivorans* might mediate the growth of *M. acetivorans* cells during stress conditions. Clearly, further study must be done to understand the physiological role of the quinone reductase of *M. acetivorans* and to broaden the fundamental knowledge of the diversity of quinone reductases among living cells

4. Conclusion

M. acetivorans quinone reductase can be overproduced in *E. coli*. The enzyme contains one molecule FAD per molecule protein, similar to the prosthetic group found in human quinone reductase type 2. However, zinc has not yet been found in *M. acetivorans* quinone reductase. In vitro reconstitution might be carried out to incorporate zinc into the protein.

5. Acknowledgements

---

6. References

[1]. Ferry, J., (2008) Acetate Based Methane Production. In Bioenergy (Wall, J., Harwood, C. S. and Demain, A., Eds.), ASM Press, Washington, 155-170.

[2]. Galagan, J. E., Nusbaum, C., Roy, A., Endrizzi, M. G., Macdonald, P., FitzHugh, W., Calvo, S., Engels, R., Smirnov, S., Atnoor, D., Brown, A., Allen, N., Naylor, J., Stange-Thomann, N., DeArellano, K., Johnson, R., Linton, L., McEwan, P., McKernan, K., Talamas, J., Tirrell, A., Ye, W., Zimmer, A., Barber, R. D., Cann, I., Graham, D. E., Grahame, D. A., Guss, A. M., Hedderich, R., Ingram-Smith, C., Kuettner, H. C., Krzycki, J. A., Leigh, J. A., Li, W., Liu, J., Mukhopadhyay, B., Reeve, J. N., Smith, K., Springer, T. A., Umayam, L. A., White, O., White, R. H., Conway de Macario, E., Ferry, J. G., Jarrell, K. F., Jing, H., Macario, A. J., Paulsen, I., Pritchett, M., Sowers, K. R., Swanson, R. V., Zinder, S. H., Lander, E., Metcalf, W. W., and Birren, B., (2002), The genome of M. acetivorans reveals extensive metabolic and physiological diversity, *Genome Res.* 12, 532-542.

[3]. Foster CE, Bianchet MA, Talalay P, Zhao Q, Amzel LM., (1999), Crystal structure of human quinone reductase type 2, a

metalloflavoprotein, *Biochemistry* 38, 9881-6.

[4]. Liao, S., and Williams-Ashman, H. G., (1961), Enzymatic oxidation of some non-phosphorylated derivatives of dihydronico-tinamide, *Biochem. Biophys. Res. Commun.* 4, 208-213.

[5]. Suharti, S., Murakami, K. S., de Vries, S., and Ferry, J. G., (2008), Structural and biochemical characterization of flavoredoxin from the archaeon Methanosarcina acetivorans, *Biochemistry* 47, 11528-11535.

[6]. Jun Shen, Roberto J. Barrios and Anil K. Jaiswal (2010), Inactivation of the Quinone Oxidoreductases NQO1 and NQO2. *Cancer Res.* 70, 1006-1014.

[7]. Yutin, N., Makarova, K. S., Mekhedov, S. L., Wolf, Y. I., Koonin, E. V., (2008), The deep archaeal roots of eukaryotes. *Mol. Biol. Evol.* 25, 1619–30.

[8]. Lake, J. A., (1988), Origin of the eukaryotic nucleus determined by rate-invariant analysis of rRNA sequences. *Nature* 331, 184–6.

Appendix

```
---MKVLYIYAHQEPKSFNAALKDTALAALKEKGHEVELSDLYAMNFNPV  M.acetivorans
MAGKKVLIVYAHQEPKSFNGSLKNVAVDELSRQGCTVTVSDLYAMNLEPR  Human

LTEKDFTDRK-KPDVFKPFLEAIQASKTGAFAPDILAEMEKVKWADFLIF  M.acetivorans
ATDKDITGTLSNPEVFNYGVETHEAYKQRSLASDITDEQKKVREADLVIF  Human

QFPIYFTSMPAILKGWIDRVLAPGFGFNPLTNSAYETGLLKGKTTMITTT  M.acetivorans
QFPLYWFSVPAILKGWMDRVLCQGFAFDIPG--FYDSGLLQGKLALLSVT  Human

TGASEEWYSEGGEHGDLNRHLESVTHCVFEYMGMKVLPSHIIYEVSSLTK M.acetivorans
TGGTAEMYTKTGVNGDSRYFLWPLQHGTLHFCGFKVLAPQISFAPEIASE

ERGAEELEKYRKRISEL----------------                   M.acetivorans
EERKGMVAAWSQRLQTIWKEEPIPCTAHWHFGQ                   Human
```

Figure 4. Sequence alignment of *M. acetivorans* quinone reductase and human quinone reductase type 2. The highlighted amino acid residues show the identity between both sequences.

Monitoring for the Effect of Chlorination in Drinking Water by Using Solid-Phase Spectrometry

Sulistyo Saputro [1], Kazuhisa Yoshimura [2], Kô Takehara [3], Shiro Matsuoka [4], Narsito [5]

[(1)] Chemistry, Department of Mathematics and Natural Science Education, Faculty of Teacher Training and Education, Sebelas Maret University, Surakarta, Indonesia (sulistyo68@yahoo.com)
[(2,3)] Department of Chemistry, Faculty of Sciences, Kyushu University, Hakozaki, Higashi, Fukuoka, Japan (kazz@chem.kyushu-univ.jp)
[(4)] Department of Environmental Science, Faculty of Science, Niigata University, Ikarashi, Niigata, Japan (matsuoka@env.sci.niigata-u.ac.jp)
[(5)] Department of Chemistry, Faculty Mathematics and Natural Sciences, Gadjah Mada University, Yogyakarta, Indonesia (narsito@yahoo.com)

Abstract

Oxidants are often added by drinking water plants as disinfectants to provide a residual that stays in the water distribution system. Sodium hypochlorite solutions were generally used for the source of free available chlorine as hypochlorous acid or hypochlorite ion equilibrates with chlorine. The disinfection ability of chlorine depends on its concentration. The WHO drinking water standard states that 2 to 3 mg Cl dm^{-3} gives satisfactory disinfection and maximum residual concentration of free chlorine allowed is 5 mg Cl dm^{-3}. If treated drinking water containing Cr(III) is exposed to a disinfectant residual in the distribution system, Cr(III) may be oxidized to the toxic Cr(VI), potentially increasing the health risk to the consumers. This paper will give the kinetic information of Cr(III) oxidation in three different pH. Cr VI) which was produced during the chlorination process was monitored by using the improved solid-phase spectrometric procedure. In order to check the free chlorine concentration in each sample solution after bubbling with N_2 gas, a differential pulse voltammetric (DPV) measurement was used. The oxidation processes were investigated at pH 5, 7 and 8. The result shows that free chlorine was oxidized Cr(III) to Cr(VI) during the chlorination process in the acidic, neutral and alkaline condition. This reaction is follows the pseudo-first order kinetic reaction, and the half life times were 3.04, 3.30 and 14.44 hours, respectively.

Keywords: *Chlorination, drinking water, chromium (VI), solid-phase spectrometry.*

1. Introduction

The role of analytical chemistry in solving the environmental problems increases continuously as fast as the development of science and technology. Chlorination is a technique widely used for disinfection of tap water. Sodium hypochlorite solutions were generally used for the source of free available chlorine as hypochlorous acid or hypochlorite ion equilibrate with chlorine [1-2]. The residual chlorine concentrations at water supply systems must be controlled within a tight range in order to ensure public health and safety. The disinfection ability of chlorine depends on its concentration. The WHO drinking water standard states that 2 to 3 mg Cl dm^{-3} gives satisfactory disinfection and maximum residual concentration of free chlorine allowed is 5 mg Cl dm^{-3} [3].

In Japan, the concentration of residual chlorine is regulated in the range of 0.1 to 1 mg Cl dm^{-3} [4], which stricter than that of WHO regulation. In addition, the residual chlorine gives the possibility of oxidizing processes of some trace metals that naturally found in natural water, such as chromium. If treated drinking water containing Cr(III) is exposed to a disinfectant residual in the distribution system, Cr(III) may be oxidized to the toxic Cr(VI), potentially increasing the health risk to the consumers [5-6].

Cr(III) is well- known as an essential trace element for humans, required for the maintenance of normal glucose, cholesterol and fatty acid metabolism. On the other hand, water-soluble Cr(VI) is highly toxic to humans and animals [7] and other studies have indicated that it is an extremely toxic carcinogen [8]. Because the health effects are determined largely by the oxidation states, different guideline values for Cr(III) and Cr(VI) should be derived. However, current analytical methods and the variable

speciation of chromium in water favor a guideline value for total chromium of 50 μg dm^{-3} [9-10].

Some works related to the characterization and oxidation of Cr(III) by sodium hypochlorite was reported. The kinetics experiments were conducted at different concentrations of NaOH and NaClO which showed the pseudo-first-order conditions with respect to Cr(III) [11]. The oxidation of Cr(III) in the de-ionized water, synthetic water and natural water also has been investigated [5]. The influence of 2.04 mg Cl dm^{-3} to 400 μg Cl dm^{-3} upon Cr(III) in the tap water was also studied [12]. The other studies related to the oxidation of Cr(III) by using other oxidant, MnO_2 have also been done [13-14]. However, it seems to be very few that the oxidation studies of Cr(III) is in the ppb or sub-ppb levels in the tap water samples, as the normally occurrence. Therefore, a study on the oxidation of Cr(III) in tap water samples by using NaClO for the monitoring of Cr(VI) in tap water during the chlorination process will be very useful for environmental and health area.

2. Experimental Details

In the study of the oxidation of Cr(III) to Cr(VI), the concentration of generated Cr(VI) is generally measured with the colorimetric method using diphenylcarbazide (DPC) as the coloring agent [15]. Absorbance measurements for Cr(VI) were made with a double-beam UV-visible spectrophotometer (Model V-630, Jasco, Tokyo, Japan), using the improved cell holder [16]. The ion exchanger was measured with an ion-exchanger aliquotting device. A PTFE tube (1.0 mm i.d. and 7 cm long) was fitted on one side with a PP resin filter tip and connected to a 10 cm^3 disposable syringe [17].

The electrochemical measurements for free chlorine were carried out using a BD-101 electrochemical analyzer (Satoda Science, Japan) with a C-1B cell stand (BAS, USA). An Au disk (1.6 mm diameter), Ag/AgCl (saturated KCl) and Pt wire were used as the working, reference and counter electrodes, respectively. For the Cr(VI) measurements, 25 cm^3 solution of water sample containing 4 mg dm^{-3} of NaClO, KCl 0.01 mol dm^{-3} was made and adjusted at pH 5.0 using acetate buffer solution or pH 7 and pH 8 using phosphate buffer solutions. A 20 cm^3 water sample was added with 0.2 cm^3 of a H_2SO_4 solution then bubbled with N_2 gas for 15 minutes. After bubbling, 0.8 cm^3 of a H_2SO_4 solution, 0.5 cm^3 of a coloring agent solution, and 0.06 cm^3 of the ion exchange were added using an aliquotting device. The mixture then stirred for 20 minutes at 20°C. After allowing the ion exchanger to settle, the supernatant solution was removed, and approximately 1 cm^3 of the mixture was transferred into a disposable PE syringe (SS-10S2, Terumo, Tokyo) connected to a flow cell. The absorbance was directly measured at 540 nm (absorption maximum wavelength) and 700 nm (non-absorption wavelength), and the difference between the two absorbance was used for Cr(VI) analyses by using solid-phase spectrometry (SPS) procedure. After the absorbance measurement, the ion-exchanger beads were removed from the cell for the next measurements.

The kinetic measurements was done by allowing the sample solution to contact with the NaClO for 0, 10, 15, 30, 45 and 60 minutes at pH 5.0; 0, 15, 35, 50, and 60 minutes at pH 7.0 and 0, 15, 30, 45, 60, 75, 90 and 105 minutes at pH 8.0 for the Cr(VI) measurements. In order to check the free chlorine concentration in each sample solution after bubbled with N_2 gas, a differential pulse voltametric (DPV) measurement was used [18]. The scan rate of the DPV was 20mV/sec. To a 20 cm^3 of water sample, potassium chloride was added until the final concentration was 0.01 mol dm^{-3} as supporting electrolyte. All measurements were carried out at room temperature thermostated at about 25°C.

3. Result and Discussion

In this Cr(VI) determination method, the residual free chlorine which existed mainly as HClO should be removed from the Cr(III) solution which reacted with chlorine. This is due to residual free chlorine which interferes in the determination of Cr(VI) with DPC method. In this measurement, aqueous solution of initial HClO concentration of 4 mg Cl dm^{-3} was bubbled by passing nitrogen gas for 15 minutes with stirring. SPS is based on the direct spectrophotometric measurement of a solid phase that has adsorbed a sample component. This method enable the determination of trace components in natural and other water samples without pre-concentration since a sensitivity enhancement was easily accomplished by increasing the sample volume [19-20]. By employing DPC as a coloring agent, selective SPS for Cr(VI) has also been developed [21]. The oxidation rate of chromium (III) during the chlorination process of tap water could be expressed as:

$$-\frac{d[Cr(III)]}{dt} = k_1[Cr(III)][HClO] \qquad (1)$$

From the ionization of hypochlorous,

$HClO = H^+ + ClO^-$ pKa = 7.5,

$$Ka = \frac{[H^+][ClO^-]}{[HClO]}$$

$$\text{or } [ClO^-] = \frac{Ka[HClO]}{[H^+]}$$

where $C_{HClO} = [HClO] + [ClO^-]$

$$= [HClO] + \frac{Ka[HClO]}{[H^+]}$$

$$= [HClO](1 + Ka/[H^+])$$

(2)

$$[HClO] = \frac{C_{HClO}}{1 + \frac{Ka}{[H^+]}}$$

Then,

$$-\frac{d[Cr(III)]}{dt} = k_1[Cr(III)][HClO]$$

$$= [Cr(III)].\ k_1/(1 + Ka/[H$$

$$= [Cr(III)].\ k_{obs} \quad (3)$$

where, k_{obs} is the observed oxidation rate constant.

Figure 1 shows that the k_{obs} value of the Cr(III) oxidation at pH 5 is similar with that of pH 7 and decrease at pH 8. The oxidation rate at pH 8 was very low and therefore the major chromium species in tap water is not Cr(VI). In addition, the pH of natural water basically is more than 7 and the treatment of chlorination using NaClO will makes tap water become alkaline.

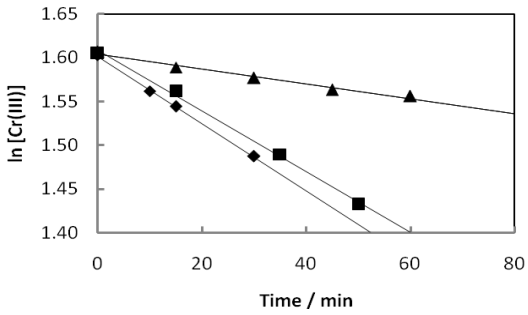

Figure 1. Plot of oxidation rate of chromium (III) at different pH (◆ = pH 5; ■ = pH 7; ▲ = pH 8).

Cr(III) in the reaction is can be found as the species of $Cr(OH)^{2+}$ and $Cr(OH)_2^+$, so the equation can also expressed as:

$$-\frac{d[Cr(III)]}{dt} = k'[Cr(OH)^{2+}][HClO] + k''[Cr(OH)_2^+][HClO] \quad (4)$$

Figure 2 shows that the value of the estimated k is similar with that of observed k, and based on Figure 2 the k^I and k^{II} value in the equation (4) is the same and the oxidation rate of Cr(III) can be expressed as equation (3). This reaction follows the pseudo-first order kinetic reaction, similar with that of previous study [11]. The half life times of the reactions are 3.04, 3.30 and 14.44 hours, respectively.

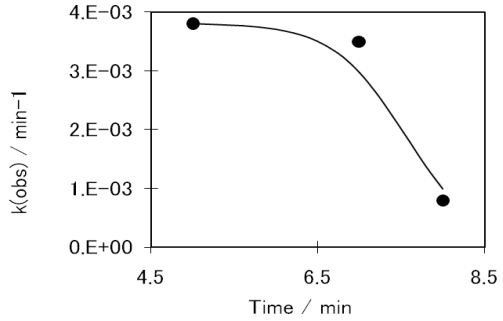

Figure 2. Simulation of the oxidation rate constant of chromium (III) at different pH. —, $k_{(est)}$; —●—, $k_{(obs)}$.

4. Conclusion

Cr(III) in tap water could be oxidized by free chlorine during the chlorination process in acidic, neutral and alkaline condition. The result shows that free chlorine oxidized chromium (III) to chromium (VI) at the pH 5.0, 7.0 and 8.0, and follows the pseudo-first order kinetic reaction with the half life times of 3.04, 3.30 and 14.44 hours respectively. In principle, the disinfection process of a tap water by using free chlorine is relatively safe if the dose of the chemical is strictly monitored.

5. Acknowledgements

This work was partially supported by the Japan Society for the Promotion of Science (JSPS) Ronpaku Program (DGHE-10715) for S. S. (2009), by Grant-in-Aids for Scientific Research (B), No. 19310011 for K. Y., from the Ministry of Education, Science, Sports and Culture, Japan, and by Takaoka Chemical Company.

6. References

[1]. Murata, T.A. Ivandini, M. Shibata, S. Nomura, A. Fujishima, and Y. Einaga, (2008), Electrochemical detection of free chlorine at highly boron-doped diamond electrodes, *J. Electroanal. Chem.*, 612, 29-36.

[2]. G.C. White (1986), Handbook of Chlorination, 2nd ed, Van Nostrand, Reinhold, New York.

[3]. Guidelines for Canadian Drinking Water Quality (2007), in Health Canada on behalf of the Federal-Provincial-Territorial Committee on Drinking Water.

[4]. Okumura, A., Hirabayashi, A., Saaki, Y., Miyake, R., (2001), Simple miniaturized amperometric flow cell for monitoring residual chlorine in tap water, *Anal. Sci.*, 17, 1113-1115.

[5]. H. Lai, L. S. McNeill (2006), Chromium redox chemistry in drinking water systems, *J. Environ. Eng.*, 132, 842-850.

[6]. D. Clifford, J. M. Chau (1988), The fate of chromium (III) in chlorinated water, *EPA Project Summary*, EPA/600/S2-87/100, 1-7.

[7]. J. Kota´s and Z. Stasicka (2000), *Environ. Pollut.*, 107, 263.

[8]. A.M. Zayed and N. Terry (2003), *Plant and Soil*, 249, 139.

[9]. WHO (2006), –Chromium in Drinking-water", World Health Organization (WHO), Geneva.

[10]. EU's Drinking Water Standards (1998), Council Directive 98/83/EC on the Quality of Water Intended for Human Consumption.

[11]. H. Jiang, L. Rao, Z. Zhang, D. Rai (2006), Characterization and oxidation of chromium (III) by sodium hypochlorite in alkaline solutions, *Inorg. Chim. Acta*, 359, 3237-3242.

[12]. N. S. Ulmer (1986), Effect of chlorine on chromium speciation in tap water, Water Engineering Research Laboratory, USEPA, EPA/600/M-86/015.
P. S. Nico, R.J. Zasoski (2000), Importance of Mn(III) availability on the rate of Cr(III) oxidation on δ-MnO_2. *Environ. Sci. Technol.* 34, 3363-3367.

[13]. R. Dai, J. Liu, C. Yu, R. Sun, Y. Lan, J.D. Mao (2009), A comparative study of oxidation of Cr(III) in aqueous ions, complex ions and insoluble compounds by manganese-bearing mineral (birnessite), *Chemosphere*, 76, 536-541.

[14]. S. Matsuoka, Y. Nakatsu, K. Takehara, S. Saputro, K. Yoshimura (2006), On-line electrochemical oxidation of Cr(III) using flow electrolysis cell for the determination of total Cr by flow injection-solid phase spectrophotometry, *Anal. Sci.*, 22, 1519-1524.

[15]. S. Saputro, K. Yoshimura, K. Takehara, S. Matsuoka, Narsito (2009), Improved solid-phase spectrophotometry for the microdetermination of chromium(VI) in natural water, *Anal. Sci.,* 25, 1445-1450.

[16]. U. Hase and K. Yoshimura (1993), Determination of silicic acid in highly purified water by improved gel phase absorptiometry, *Anal. Sci*., 9, 111-115.

[17]. S. Saputro, K. Takehara, K. Yoshimura, S. Matsuoka, Narsito (2010), Differential pulse voltametric determination of free chlorine for water disinfection process, *Electroanalysis*, 22, 2765-2768.

[18]. K. Yoshimura and H. Waki (1976), Ion exchanger colorimetry-I, *Talanta*, 23, 449-454.

[19]. K. Yoshimura and H. Waki (1985), Ion exchanger phase absorptiometry for trace analysis, *Talanta*, 32, 345-352.

[20]. K. Yoshimura and S. Ohashi (1978), *Talanta*, 25, 103.

Zoning on Vulnerability Potency of Geology Disaster Area in Malang-East Java Indonesia by Means of Geophysics Data

Sunaryo [1]

[(1)] Division of Geophysics, Physics Department of MIPA Faculty, Brawijaya University, Malang, Indonesia.
(sunaryo@ub.ac.id)

Abstract

Zoning on vulnerability potency of geology disaster area in Malang-East Java Indonesia by means of geophysics data which aims to get geology disaster safety levels in this area, i.e. floods-landslides, earthquakes, volcanic eruptions, and tsunamy has been done. Floods-landslides data obtained by using geoelectrical resistivity method with took samples at Jabung, Dampit, and Kasembon. Earthquakes data was obtained by using gravity method in almost all districts of Malang, especially in south Malang area. Volcanic eruption data was obtained by using gravity and magnetic methods. While the tsunami of data obtained from the height of topography on the path along the coast of south Malang. Besides the above mentioned geophysical data, zoning determination also was based on geological disasters that have been occurred in these areas. By means of the analysis and interpretation of these data in above, the area that have the vulnerability potency of geology disasters for floods-landslides are sub-districts of: Ampelgading, Tirtoyudo, Gedangan, Donomulyo, Sumbermanjing wetan, Kasembon, Jabung, Dau, and Dampit. Areas that have the vulnerability potency of geology disaster for volcanic eruption are the sub-districts: Kasembon, Ngantang, Pujon, Karangploso, Singosari, Lawang, Poncokusumo, Jabung, Ampelgading, Tirtoyudo, Dampit, Wajak, and Poncoksumo. Areas that have the vulnerability potency of geology disaster for earthquake are sub-districts of: Gedangan, Sumbermanjing wetan, Dampit, Tirtoyudo, and Ampelgading. While the areas that have the vulnerability potency of geology disasters for tsunami are the sub-districts of: Ampelgading, Bantur, Dampit, Donomulyo, Gedangan, Kalipare, Pagak, Pronojiwo, Sumbermanjing, Tempursari, Tirtoyudo, and Wates. Thus, sub-districts of Tirtoyudo and Ampelgading are areas that have the highest vulnerability potency of geology disasters in the district of Malang. The second level is the sub-districts of: Gedangan, Sumbermanjing Wetan, and Dampit. The third level is the sub-districts: Donomulyo, Kasembon, and Jabung. Finally, the fourth level is the sub-districts of: Dau, Ngantang, Pujon, Karangploso, Singosari, Lawang, Poncokusumo, and Wajak.

Keywords: *zoning, vulnerability, geology disaster, geophysics.*

1. Introduction

Malang has a total area of approximately 351,000 hectares (114,000 hectares (30%) is forest) with a population of 2,393,959 people in all 33 districts, 389 villages with a population density of 681 people/km^2. Malang district is surrounded by volcanic either already entered the phase of history and which is still active. Administratively, the northern district of Malang bordered by Pasuruan and Probolinggo district, in the eastern bordered by Lumajang district, in the western bordered by district of Blitar, and in the southern bordered by Indian Ocean with length of coastline reached 102,625 km. Physiographically, northern district of Malang is the path of Solo volcanic zone which is a quarter of the volcanic line. While in the south is southern mountain line.

Based on the general description above, district Malang is a very complex area that has a vulnerability to various types of geological disasters.

Disaster in Malang Regency has shown that almost every year there is flooding and landslides. All potential hazardous mentioned above also have occurred in Indonesia, but almost all of them handled sporadic, slow and not coordinated in a comprehensive, integrated, and systematic.

Based on the variety of potential disaster above, Malang district should build a comprehensive and integrated system in order to minimize the impact that caused by disasters through mitigation efforts. Zoning the area of geological disasters is also need to be done in order to realize these efforts.

.

2. Experimental Detail

Data Acquisitions

This study used secondary and primary data. Secondary data are needed in this research are the maps: Physiography [1], Geomorphology and Geology [2], Administration, Malang Regency in Figures, Digital RAB basis of GIS, GIS Digital BPN base, topography and slope . While the primary data used were 3-D position data and geophysical data (gravity, magnetic, and electrical resistivity, and resistivity).

3-D position data obtained from measurements using the GPS and Digital Elevation Model (DEM). Geophysical data obtained through measurement by using gravity, magnetic, and electrical resistivity. Data acquisitions of position, gravity, and magnetic respectively performed at the same time using the GPS, Gravitymeter La Coste & Romberg, and Proton Precision Magnetometer (PPM). Data acquisition of geoelectrical resistivity was performed by ABEM SAS 200 and OYO McOHM. Combined gravity and magnetic methods used to obtain the condition of the volcanic magma pockets and Arjuno Kelud-Welirang. Gravity method is also used to obtain the geological area prone to earthquakes. Geoelectrical resistivity method used to obtain the geometry of landslide.

Data Processing

Gravity data processing is done through corrections: tidal, drift, base station, tie, normal gravity, free air, Bouguer, and terrain to obtain the complete Bouguer anomaly. Residual gravity anomaly obtained from the differencing of regional gravity anomaly to the reduced gravity anomalies onto a even surface at the highest topographic. To get the position of the cross section is also used in consideration of the horizontal gradient of residual gravity anomaly [3].

Total magnetic field data processing is done through corrections: drift correction, and the IGRF (International geomagnetic Reference Field). Residual total magnetic anomaly obtained from the differencing of regional total magnetic anomaly obtained from upward continuation to total magnetic anomaly reduced to the even surface. To get the exact position of the cross section which is also used horizontal gradient of total magnetic anomaly [3].

Interpretation to obtain the value of 3D-volkano quantity of geothermal reservoirs in use approach of Talwani 2.5D polygon method for arbitrary shape objects [4,5] with the help of the program mag2dc and grav2dc.

The gravity method works based on the density contrast from the rock of the earth. If there is an anomaly under the surface, then the value of the gravitational field will deviate from the normal measured. If the deviation is the addition of value, called a positive anomaly. Conversely, if the deviation is reduction of the value, called a negative anomaly. Measured gravity value is influenced by the earth-moon tide, the advantages and disadvantages of mass due to topography of the earth, and reference. Therefore, the measured data must be corrected to eliminate these influences.

Magnetic method is a method that responds to contrast of susceptibility. Besides, due to the susceptibility contrast, the measured magnetic values are also influenced by external factors. So that should be corrected to eliminate the influence of these external factors.

Processing of geoelectrical resistivity was done by using Jacobi matrix method with the res2dinv software [6]. To make interpretation of the potential tsunami, digital map data of BPN was used by using the considerations of topography altitude.

3. Result and Discussion

Floods and Landslides

Based on the results of data processing by using geoelectric resistivity pseudodepthsections configuration with Jacobi matrix method, res2dinv, the modeling results of the 4 lines mentioned above were obtained, as can be seen in Figure 1, Figure 2, Figure 3, and Figure 4.

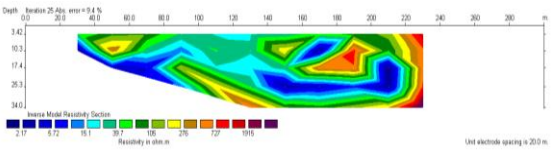

Figure 1. Pseudodepthsection geoelectric resistivity result modeling for line Barakan_01.

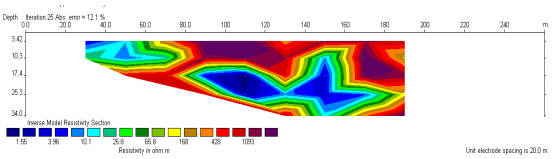

Figure 2. Pseudodepthsection geoelectric resistivity modeling result for line Kasembon_02.

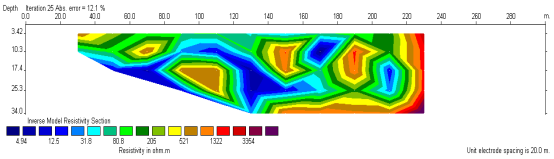

Figure 3. Pseudodepthsection geoelectric resistivity modelingresult for line Kemiri_03

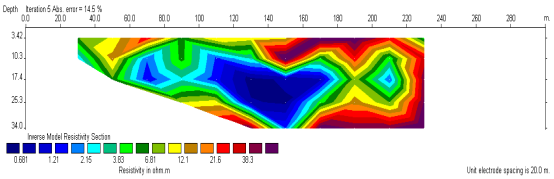

Figure 4. Pseudodepthsection geoelectric resistivity modeling result for line Srimulyo_04.

Table 1. Physical parameters of landslides vulnerability potency.

NO.	LINES	*F*		H_{rerata} stable (m) for *F*=1.2	
		MIN	MAX	MIN	MAX
1	BARAKAN_01	0.27	0.02	1.49	0.0705
2	KASEMBON_02	0.33	0.05	1.94	0.226
3	KEMIRI_03	0.30	0.05	1.74	0.193
4	SRIMULYO_04	0.99	0.36	6	1.65

Slope stability analysis is based on the concept of plastic limit equilibrium to determine the safety factor from the landslides plane. Safety factor can be expressed as the ratio between the tangential component to needed with the tangential component existing.

$$F_{\varphi} = \frac{tg\varphi}{tg\varphi_d} \qquad (1)$$

Table 2. The load stability calculation of sliding plane.

NO	LINES	TOPOGRAPHICS SLOPES (□)	SLIDING PLANE SLOPES (□)		H_{rerata} (m)
			MIN	MAX	
1	BARAKAN_01	45	40	85	12
2	KASEMBON_02	40	35	75	12
3	KEMIRI_03	40	37	77	12
4	SRIMULYO_04	20	18	38	8

Based on Figure 1 to Figure 4, obtained sliding plane to topography slope respectively were: Barakan_01 was 45º, 45º Kasembon_02 was, Kemiri_03 was 40º, and Srimulyo_04 and the local fault location was 20º.

Based on the analysis and interpretation of geoelectrical data were done at the sampling location, i.e. in Kasembon, Jabung, and Sri Mulyo zones were obtained physical parameters of potential landslide vulnerability conditions as in Table 1.

By doing the calculations for the cohesion (c) (kN/m^2) is 18.75, in angle of friction (φ) (degrees) is 13, heavy volume load (γ) (kN/m^3) is 6.19, an effective load volume weight (γ') (kN/m^3) is 9.79, and the safety factor (F) is 1.2, then it can be expected that stable conditions for the local area in accordance with sliding plane as in table 3.2.

The data and the calculation shows that in the condition of the slope that varies between 18º to 85º have average thickness/depth layer about 12m above sliding plane, except SRIMULYO_04 that has 8m thickness. Stability factor (F) after a calculated varies between 0.02 and 12.36, except SRIMULYO_04 which has magnitude 0.99. This case indicates that the weigth of material conditions is unstable, because the conditions of stable and secure are F ≥ 1.2. By conducting simulation calculations based on local plane sliding data, the loading material should be varied from 0.07m to 1.94m, except SRIMULYO_04 which can reach 6m.

Based on average rainfall data in the last 5 years, known that the high rainfall for each potential area of vulnerable flood and landslide are in the months of February, March, June, and July which is a peak of rain with a quantity is more than 30mm/hari. However, in the districts Dampit, Tirtoyudo and Ampelgading, rainfall have a relatively lower compared to the other. Therefore, because the rain is one of the main parameters for flooding and landslides natural disaster potential, in the months February, March, June, and July that more vigilance is needed in local areas.

Volcanics Eruption

The eastern part of the volcanic crater there Kelut crater wall, while in the western part of the crater tends to be flat. This shows that the movement of growing volcanic Kelut is westward as evidenced from the results of research on the structure of magma chamber of Kelud volcano [7]. This allows the discharge of lava which is destructive to the west. Therefore, bursts of lava, and other materials eruption have a tendency to impact into west direction. Nevertheless, in the eastern of crater towards Malang district boundaries need to be aware from the material eruption in the form of gas, volcanic ash, and other materials that come spit out and fly during the eruption, particularly in the Ngantang and Kasembon area.

Arjuno-Welirang volcanoes are included in the volcanic category of C to history type. Therefore, heat and pressure in the magma chamber of this volcano can already be used as a source of volcano-geothermal energy [8]. Alert area which includes administration of Malang regency that located at the floor of the Arjuno_Welirang volcanoes are Pujon, Karangploso, Singosari, and Lawang.

Bromo and Semeru volcanoes are included in the Tengger caldera has a type of eruption is typical, that is vomit material in the form of volcanic ash, pebbles, gravel, and a little bomb. This is because the Bromo and Semeru volcano lava has a relatively open pipe (open vein), so if have accumulation of pressure is not too long will be erupted. Regions involved in Malang district administration which could be affected by the eruption is Poncokusumo, Jabung, Ampelgading, Tirtoyudo, Dampit, and Wajak. Because of the height of this volcano (3678m), the impact of Semeru volcano eruptions of volcanic ash can reach the Batu city.

Until the 1990 eruption, Kelud volcano have central eruptions characteristic of St.Vincent type with erupted material in the form of bombs, gravel, volcanic ash clouds, incandescent, gas (S/SO_4, SiO_2), and pyroclastic. Material can be ejected directly up to a radius of 5km. Areas that are vulnerable from the impact of this eruption are Kasembon (Pondok Agung, Bayem, and Sukosari), and Ngantang (Pagersari, Sidodadi, Ngantru, Banturejo, and Pandansari) with the material eruption of volcanic ash material (SiO_2), and gas (S/SO_4) which can damage the health.

At the eruption of 2007, presumably because of the cracks in the pipes (veins) that connect the magma chamber and the crater lake, causing explosive eruptions do not occur. Freatic eruption was expected, but the reality is still occurring in the form of effusive lava pyroclastic which is preceded by up going of lava dome with a diameter of 250m and a height of about 190m.

Earthquake

To get the fault distribution in the district of Malang, then used the analysis of gravity data. The analysis is based on the gravity data processing results are expressed in the form of contours. Gravity anomaly contours express lanes with the same gravity value (isogravity). There is a variation of the distance between the lines to one another, giving rise to the existence of horizontal gradients. The existence of contrasting structures suddenly causing the value of the gradient will become increasingly tight. Based on the horizontal gradient and the local geological conditions, it can be interpreted that in a local fault lines of the local place. Gravity contour can be seen in Figure 5.

Based on Figure 5, the six local fault lines are located in sub-districts of Gedangan, Sumbermanjing wetan, Dampit, Tirtoyudo, and Ampelgading.

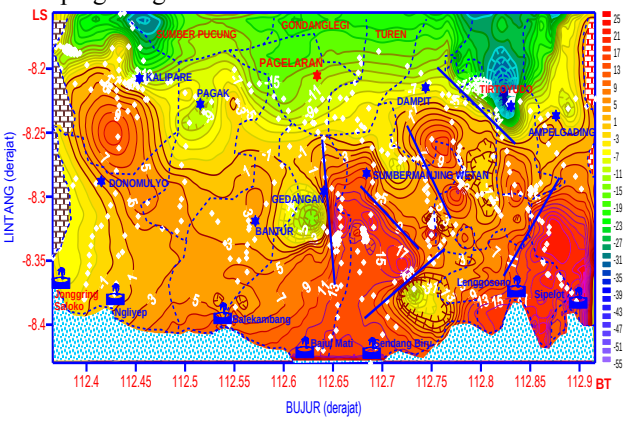

Figure 5. Local fault paths in the district of Malang by means of gravity anomaly analysis.

Earthquakes that have a high intensity usually occurs in tectonic earthquakes that could trigger to destabilize the local faults. Based on geological maps and the interpretation of gravity data, indicate the existence of the path/location of the corresponding local faults, namely: Gedangan (1), Sumbermanjing Wetan (2), Dampit (1), Tirtoyudo (1), and Ampelgading (1). Bearing capacities of rock in these pathways are relatively lower than the surrounding areas. Therefore, these pathways are volatile.

Tsunami

Tsunami data analysis was based on topography height data. Tsunami waves crashing directly will be able to arrive at a height of 25m, it can even damage of up to 75m in height. Most of the residential areas along the coast south of Malang are generally located in the lowland to the bays or beaches of Jonggring Saloko, Ngliyep, Kondangmerak. Balekambang, Bajulmati, Sendangbiru, Lenggosono, and Sipelot. By using these considerations, it is vulnerable to tsunamis zoning class as follows:

1. 1st Class Vulnerability: Red zone. Regions that have the potential to directly affected (≤ 25m).
2. 2nd Class Vulnerability: Yellow zone. Regions that could possibly hit by the tsunami if the tsunami is very large (> 25m and ≤ 75m).
3. 3rd Class Vulnerability: Green zone. Safe limit regions (border line) (> 75m and ≤ 100m).

Based on the above terminology, sub-districts that have a vulnerability to the tsunami

disaster are: Gedangan, Sumbermanjing Wetan, Tirtoyudo, Ampelgading, and Donomulyo.

Overlapping of Natural Disaster Vulnerability Zones

The various potential disasters listed in the district of Malang, can be seen as in Table 3.

Table 3. Natural potency disaster in the district of Malang

FLOODS AND LANDSLIDES	VOLCANO ERUPTIONS	EARTHQUAKES	TSUNAMI	NUM. OF POTENCY
Gedangan		Gedangan	Gedangan	3
Sumbermanjing Wetan		Sumbermanjing Wetan	Sumbermanjing Wetan	3
Dampit	Dampit	Dampit		3
Tirtoyudo	Tirtoyudo	Tirtoyudo	Tirtoyudo	4
Ampelgading	Ampelgading	Ampelgading	Ampelgading	4
Donomulyo			Donomulyo	2
Kasembon	Kasembon			2
Jabung	Jabung			2
Dau				1
	Ngantang			1
	Pujon			1
	Karangploso			1
	Singosari			1
	Lawang			1
	Poncokusumo			1
	Wajak			1
			Bantur	1

4. Conclusion

Based on the results of research that has been done, it can be concluded and recommended the following matters:

1. Vulnerable to floods and landslides natural disasters are in the district of: Gedangan, Sumbermanjing wetan, Dampit, Tirtoyudo, Ampelgading, Donomulyo, Kasembon, Jabung, and Dau.
2. Vulnerable to volcano eruptions natural disasters are in the district: Dampit Tirtoyudo, Ampelgading, Kasembon, Jabung, Ngantang, Pujon, Karangploso, Singosari, Lawang, Poncokusumo, and Wajak.
3. Vulnerable to earthquake natural disasters are in the district of: Gedangan, Sumbermanjing wetan, Dampit, Tirtoyudo, and Ampelgading.
4. Vulnerable to tsunamy natural disasters are in the district of: Gedangan, Sumbermanjing wetan, Tirtoyudo, Ampelgading, Donomulyo, and Bantur.
5. Based on overlapping for all potential hazard, then the District of Tirtoyudo and Ampelgading most potential to disasters with a total potential each 4. Gedangan, Sumbermanjing Wetan, and Dampit have a total potential each 3. Donomulyo, Kasembon, and Jabung have a total potential each 2. And Dau, Ngantang, Pujon, Karangploso, Singosari, Lawang, Poncokusumo, Wajak, and Bantur have the potential each 1.
6. From the 33 sub-districts in Malang regency, there are 17 districts that have a potential disaster-vulnerability with varying the number and types of potential natural disaster-vulnerability.

5. Acknowledgement

---

6. References

[1]. Bemmelen, R.W.V. (1949), *The Geology of Indonesia vol. 1A General Geology of Indonesia and Adjacent Archipelagos*, Government Printing Office, The Hague.

[2]. Suyanto, Hadisantono, R., Kusnama, Chaniago, R., dan Baharuddin, R. (1992), *Peta Geologi lembar Turen, Jawa skala 1:100*.000, Puslitbang Geologi, Bandung.

[3]. Blakely, R.J. (1995), Potential Theory in Gravity and Magnetic Applications, Cambridge University Press, USA.

[4]. Shuey, R.T., and Pasquale, A.S. (1973), End Corrections in Magnetic Profile Interpretation, *Geophysics*. vol.38 No. 3, 507 – 512.

[5]. Cady, J.W. (1980), Calculation of gravity and magnetic anomalies of finite-length rigth polygonal prisms, *Geophysics,* vol. 45 No. 10, 1507 – 1512.

[6]. Loke M.H. and Barker R.D. (1996), Rapid Least-squares Inversion of Apparent Resistivity Pseudosection by Quasi-Newton Method. *Geophysics Prospecting* 44,131-152.

[7]. Sunaryo, (2001), A Study on Magma Chambers of Kelut Volcano by means of Magnetic Survey, Tesis, UGM, Yogyakarta.

[8]. Sunaryo, Heru Budiono, Adi Susilo (…..), A Study on Volcano-Geothermal Energy in Arjuno-Welirang by means of Density and Susceptibility Contrast Parameters, *Research Grant Proceeding*, TPSDP Batch II.

Development of Radionuclide Monitoring Stations in Indonesia in Anticipating the Increasing of Peaceful Uses of Nuclear Energy in ASEAN Region - An Initial Assessment

Susilo Widodo [1], Syarbaini [2], Dadong Iskandar [3], Bunawas [4]

[(1,2,3,4)] Center for Technology of Radiation Safety and Metrology (PTKMR),
National Nuclear Energy Agency (BATAN), Jakarta, Indonesia

Abstract

Radioactive materials in the form of gas and particulate radionuclides potentially released to atmosphere by nuclear power plant (NPP) or by other nuclear facilities need to be monitored continuously to ensure protection against people and environment. Development of radionuclide monitoring system in Indonesia become urgent as in ASEAN like Vietnam, Thailand, Malaysia and even Singapore have recently showed their interest to "go nuclear". Regardless whether Indonesia will introduce an NPP soon or later, based on lesson learnt of the spread of smoke haze caused by land and forest fires in Sumatra and Kalimantan, any radioactive material released from a nuclear facility located anywhere in South East Asia region is potentially transported by wind to cross the islands and the borders. Although the owner of an NPP is usually required to install monitoring equipment to control the release of the radionuclides so that it will not exceed such authorized discharge limits, independent radionuclide monitoring station need to be established. For this purpose, PTKMR-BATAN will initiate the development of a national monitoring system for radionuclide. A plan has been made since the budget year 2011 and forward. Initially, assessment will be carried out to determine appropriate locations and required level of sensitivity of the stations including their infrastructure requirements. This paper describes an initial assessment of options for installation of the monitoring stations that ideally shall be capable to cover all area of Indonesia. The monitoring station(s) shall also be capable to provide early warning whenever radionuclides released from any nuclear facility in South East Asia region exceed the authorized discharge limits to environment.

Keywords: *radionuclide, monitoring station, gas and particulate, people and environment protection.*

1. Introduction

Radionuclide monitoring stations measures the abundance of radioactive materials, i.e. radionuclide, in the air. A radionuclide is an isotope with an unstable nucleus that loses its excess energy by emitting radiation in the form of particles or electromagnetic waves. This process is called radioactive decay. Radionuclides are often called radioisotopes. Radionuclides may occur naturally, but they can also be anthropogenic radionuclides artificially produced by nuclear fission or nuclear activation reactions. The nuclear fission recations can be in a controlled nuclear reactor, or, an uncontrolled nuclear weapon explotion, result radionuclides as fission products that potentially be released to the atmosphere in the form of gases and particulates. The highest yields of fission products are radionuclides with mass numbers in the range of around 90 to 100 and 130 to 140 [1]. Radioxenon noble gases (^{131m}Xe, ^{133}Xe, ^{133m}Xe, and ^{135}Xe) and particulates (^{140}Ba-^{140}La) are considered as the most interested radionuclides for the purpose of detection of such event [1].

As nuclear energy is one of the best options in reducing polution caused by fosil energy, some countries like Vietnam, Thailand, Malaysia and even Singapore have recently showed their interest to "go nuclear". Vietnam has decided to introduce the first nuclear power plant to fulfil his electricity need at central Ninh Thuan province. The first nuclear power plant in Vietnam will be commisioned around 2020 [2]. Indonesia has also long preparation history in introducing nuclear power plant (NPP). However, regardless whether Indonesia will introduce an NPP soon or later, based on lesson learnt of the spread of smoke from forest fires in Sumatra and Kalimantan islands, any radioactive materials released from a nuclear facility located anywhere in South East Asia region will potentially transported by wind to cross the islands and borders. Although the owner of an NPP is usually required to install monitoring equipment to control the release of the radioactives so that it will not exceed such authorized discharge limits, independent monitoring system needs to be established.

Currently, a global radionuclide monitoring system has been established as part of a multi-

technology verification system for the Comprehensive Nuclear Test Ban Treaty (CTBT) to monitor our planet for nuclear explosions. The system is capable to detect airborne radioactive particulates and gases that can indicate nuclear weapons test debris [3]. The backbone of the system is a network of eighty remote detection stations located at selected locations around the word. These stations enable a continuous worldwide observation of particulate samples of radionuclides. However, pursuant to the Tabel-2A of Treaty of CTBT [4], among eighty radionuclide stations, five stations are located near, but none of them inside the Indonesian teritory. They are located at Australia, Malaysia, Papua New Guinea and Thailand.

It is therefore an initial assessment is carried out to consider for developing radionuclide monitoring station(s) that will be capable to function for two aims, as the frameworks of an independent monitoring system in Indonesia for anticipating the grow of the peaceful uses of nuclear energy in Sout East Asia and to become part of the Global Monitoring Network so that it will be capable to validate the measurement and analysis undertaken by ***neighbor*** stations.

Theoretical Considerations

If a nuclear facility or a nuclear explosion release fission products of radioactive materials to the atmosphere in the form of gases or particulates, some amount of the materials would be transported by wind. Once these particles passed a radionuclide monitoring station, they would be measured and a signal identifying the origin of these radioactive particles would be traced. Compared to the particulates, the noble gases are not subject to wet deposition in the atmosphere and they have a better chance to escape from the stacks of nuclear reactors or cavity of an underground nuclear explosion. A well contained facility is not expected to release any particulates into the atmosphere. Noble gases radioxenon may easier to leak out and a noble gas detection system would be capable of warning that such event was happened. A station monitoring which has capability to detect both forms of radionuclides would therefore be needed.

Distance from the origin of the event to the monitoring station along side with meteorogical conditions would determine the probability of the event would be detected by the station. This become major challenge of the efectivity of a station. It is obviously passive, and relies on the movement of air masses to the detector site in the station. This requires the deployment of a relatively dense network of detectors in order to ensure that air masses will be carried to one or more stations from any site of the origin in a timely manner. A netwotk consists of so many stations is therefore needed for the monitoring of radionuclides. A meteorogical data would help in tracing the origin of such event. The range of fission products produced and their isotopic ratios could distict wether the event was caused by a nuclear facility or a nuclear explosion.

Leason learnt maybe adopted from trans-boundary smoke haze from agricultural and forest fires that has been a recurrent feature in the ASEAN region in the past few decades. These fires are caused mainly by land clearing and ~~"s~~lash and burn" agricultural practices during the traditional dry period between June and October in Indonesia, particularly in Sumatra and Kalimantan and during the traditional dry season between December and March in the northern ASEAN region. The smoke haze situation is usually exacerbated when it coincides with the El Niño, a climatic phenomenon that often leads to prolonged and drier weather conditions in the region. Apart from satellite imageries, various haze related information, air quality indicators and dispersion model forecasts are usually used as monitoring and assessment tools in regional fire and smoke haze surveillance [5].

An atmospheric dispersion model, e.g. HYSPLIT (HYbrid Single-Particle Lagrangian Integrated Trajectory) model developed by the Air Resource Laboratory of US NOAA is used as tools to forecast the transport and dispersion of the smoke haze particles at South East Asia region [6]. These three-dimensional models employ mathematical algorithms to estimate or predict the downwind concentration of air pollutants (haze particles) emitted from sources (fires). They require input fields which include forecasts of meteorological conditions (e.g. wind speed and direction, air temperature, atmospheric stability, presence of inversion, etc) and emission parameters (e.g. source location and height, emission rate). The model products are concentration forecasts showing the spatial diffusion of the smoke particles. It is interesting to futher study the applicability of this atmospheric dispersion model as tools to forecast the transport and dispersion of airborne radioactive materials. This might give better results because the input of locations of the radiactive sources are more certainty and the emission rates of the gases and particulates can be quantified more accurately.

2. Experimental Details

Assessment of the Available System

Two categories of radionuclide monitoring stations will be discussed here, one is the stations operated for the CTBT and the other one is the stations operated for monitoring of nuclear facilities.

Global Monitoring System for the CTBT

A global radionuclide monitoring system is established to monitor our planet for nuclear explosions. The system consists of a network of eighty remote stations those capable a continuous worldwide observation of particulate samples of radionuclides. High-volume air sampling and high-

resolution gamma spectrometry are utilized in these stations to provide in-situ assay and near-real time reporting. Forty of the eighty stations have additional noble gas detection capabilities. The noble gas detection system can provide conclusive evidence of a well-contained underground nuclear explosion where the particulate radionuclides may not be released to the atmosphere. The stations are linked to the International Data Centre (IDC), which is a central data processing hub where raw spectral data is automatically processed and analyzed. The data and products of the IDC are made available to the states parties.

The monitoring system supported by sixteen qualified laboratories capable to analyze particulate samples with minimum detectable activity (MDA) as low as 1 mBq / kg sample for ^{140}Ba. An ultra low level laboratory has been developed at the Austrian Research Centers Seibersdorf as one of the CTBT radionuclide laboratory. A high sophisticated active and passive detector shielding has been installed to the high resolution germanium detector so that the count rate as low as 0.18 counts s^{-1} kg^{-1} (Ge) over the energy interval from 40 to 2700 keV has been successfully achieved [7].

The laboratories require to be certified based on an international standard. The laboratories analyse samples suspected of containing radionuclide materials that may have been produced by a nuclear explosion. They also conduct routine analyses of regular samples to provide quality control of the particulate monitoring stations.

As required by the Treaty, the stations are expected to achieve more than 90% detection probability for a nuclear explosion of one kiloton ore above within forteen days after the detonation. This objective sets requirement for the sensitivity of airborne radionuclides detection and predetermine the selection of the location of stations in the network design phase based on modelling of atmospheric transport and mixing. To achieve the desired detection probability the minimum detectable activity of ^{140}Ba and ^{133}Xe should be around 10 – 30 µBq m^{-3} and 1 mBq m^{-3} respectively. This value is based on assumption of one kilo-ton nuclear explosion as the source term that result the short half life radionuclides of ^{140}Ba and ^{133}Xe with estimated activities about 10^{15} Bq and $10^{14} – 10^{15}$ Bq respectively [8].

The stations operate in continuous mode, collect particulates in the air filter sampler for 24 h with a minimum air flow rate of 500 m^3 h^{-1}. The filter is capable to retain more than 85% of all particles that reach it. The used filter is then stored for 24 h to reduce the background from natural radionuclides which mainly contributed by ^{7}Be, ^{40}K and radon progenies from uranium and thorium decay series, typically ^{212}Pb, ^{212}Bi, ^{208}Ti, ^{214}Pb and ^{214}Bi. The concentration of ^{212}Pb has a predominant influence on the minimum detecable concentration. As ^{212}Pb has half life of 10.64 h, during 24 h decay period its concentration in the sample decrease substantially. Finally a gamma-ray specrum is collected for 24 h with a HPGe detector. At any given time, one sample is in measurement, a second one in decay, and a third one is being collected. The gamma ray spectra data measured in the stations are sent to the IDC together with the meteorological and state-of-health information. The state-of-health provide information on the station‘s operational status and the quality of the raw monitoring data it transmit [9].

Currently, in the end of 2010, more than 70% of particulate stations has been certified, while the radionuclide noble gas monitoring system has reached a state of maturity with at least 30 units have been installed. This achievents shows that the global monitoring system is closer to be an effective tool for nuclear test monitoring, as well as other applications such as radiological emergency response, public health monitoring, and scientific research.

Monitoring System for Nuclear Facilitities

Radioactive monitoring system is commonly operated in order to ascertain conditions near perimeter of supervised area at NPPs, nuclear research reactors, and isotope production, fuel fabrication and nuclear waste facilities and other facilities those use or produce radioactive materials. The ^{137}Cs, ^{134}Cs, ^{131}I, ^{95}Zr, ^{90}Sr, ^{89}Sr, ^{65}Zn, ^{60}Co, ^{3}H and radioxenon noble gases are common radionuclides of interest to be monitored for an NPP operation. Various systems, equipment, and methods with various levels of sensitivity are required and operated by nuclear countries for monotoring of the radionuclides in order to protect public and environment against hazards caused by ionizing radiation.

In anticipating such introduction of an NPP, radionuclides monitoring programme need to be undertaken during pre-operation and operation phases as well as during nuclear emergency. The monitoring could be on continuoues or discontinuoues basis. Specific radionuclides are usually required to be monitored on continuous basis depending on the nuclear facilities. The discontinues monitoring is commonly undertaken by periodical sampling of air, water, plantation, soil and other potencial pathways of radioactive materials from the sources of release to environment to human. Periodically reporting of radionuclide specific values of activity released are required to be reported to an authorization body and must notified if limits are exceeded [10].

Fission product of ^{133}Xe has been monitored continuously for a long time in the regions where the NPP is operated like in Central Europe. A few mBq/m^3 is typical level of ^{133}Xe in that region. This level is reduced a factor of ten into mid Scandinavia

and further a factor of ten into the Arctic [9]. Sensitivity of such station is commonly lower than the stations operated for the CTBT. However, some countries operate monitoring stations with sensitity close to the CTBT requirements. In Germany, the Federal Office for Radiation Protection (BfS) performs trace analysis measurements in both the frameworks of the German Integrated Measuring and Information System as well as of the International Monitoring System for verification of the CTBT[11]. The Swiss Federal Office of Public Health (SFOPH), that responsible for the surveillance of environmental radioactivity in Switzerland and for the protection of the public from ionizing and non-ionizing radiation, uses a high volume air sampler (DIGITEL DHA-80) for aerosol radioactivity monitoring. A detection limit for artificial ^{137}Cs of 2 $\mu Bq/m^3$ has been obtained [12].

3. Result and Discussion

Station Development in Indonesia

Indonesia is a large country that may need so many radionuclide monitoring stations in covering all area in the country. It is expected that by this assessment a clearer picture will be obtained on the selection of the station locations as well as theirs need of sensitivity and capability. Leason learnt from the development of global monitoring system which require more than 12 years to achieve a maturity level, the development of monitoring stations in Indonesia need to be initiated soon. The stations will complementary the environmental sampling and analysis system developed for collecting baseline data of radiation and radioactivity in Indonesia and mobile monitoring system developed fo a nuclear and radiological emergency response.

Development Plan

A plan has been started from the budget year 2011 and forward for development of radionuclide monitoring stations in Indonesia. Initial assessment is carried out to consider potential locations and required level of capability and sensitivity of the independent monitoring stations including their infrastructure requirements.

It is planned that in the fortcoming years, the basis components of a radionuclide station include housing for detection equipment (i.e. gamma ray detector, compressed filter, decay chamber) a high volume air sampler and a satellite antenna will be provided. The sequential four-step process used for the establishment of CTBT‘s stations will also be applied. It involves site survey, installation, certification and operation. Certification, as formal end of a process, recognizes that a station meets certain requirements to become part of the CTBT‘s international monitoring network. These requirements cover technical functionality, detection sensitivity, communication and data availability.

Indonesia may take advantages of the maturity of the CTBT‘s network of global monitoring system after more than one decade of development by international scientists. Choosing the level of sensitivity in the same order as the CTBT‘s system will allow the Indonesian stations be part of the global network with some advantages of opening road to international certification, quality assurance programme, and exchange radionuclide data including data from the ASEAN region. In other hand, as the CTBT still need suplementary stations in the tropical belt, Indonesia should consider to give its contribution.

Site Survey for Stations

As Indonesia geographically located in the equator belt, a denser presence of stations are required than in higher latitudes because global wind fields in the equatorial region are virtually vertical, while in the North and South they are more lateral. This means that, in the higher latitudes, radionuclides are transported horizontally most effectively. The more stations here are, the greater the probability of detection and the shorter the probable time period of doing so.

In term of air sampling at the station site, it is advantageous to have a good mixing of surface air with upper layers of air. In principle, the site should be a windy, exposed place where the passing air really hits the sampler used to collect particulates transported by the wind. The larger the air volume, the greater is the efficiency for particulate sampling.

In the initial steps, site survey will be conducted to assess the suitability of the site to host a station and identify any specific conditions that would impact on station design. Indonesia is not bounded by the CTBT Treaty for such station location, so the main consideration of the site will be its capability to cover as large as possible, to detect all possible anomalous radionuclide release from anySouth-East Asia sources and to function as an early warning system.

4. Conclusion

An initial assessment has been made for the development of radionuclide monotoring station(s) in Indonesia. Two types of stations have been disscussed, one is the stations intended to monitor nuclear facilities at national level and the other one is CTBT‘s stations as part of the global monitoring network with higher sensitivity. The network supported by sixteen CTBT‘s laboratories is capable to analyze particulate samples with minimum detectable activity better than 1 mBq / kg sample for ^{140}Ba. Indonesia may take advantages of the maturity of the global monitoring network developed by international scientists. It come to an initial recommendation that there are options in selecting a

system for monitoring - lower sensitivity in denser locations - or - higher sensitivity in fewer locations.

However, the cost-benefit analysis for both types is not undertaken in this assesssment yet. Choosing the high sensitivity similar to the CTBT's stations will allow the Indonesian stations be part of this network.

Leason learnt from time consumed for the development of the CTBT's global monitoring network that has initiated for more than one decade ago, the development of monitoring stations in Indonesia need to be initiated soon. The aplicability of an atmospheric dispersion model commonly used as as tools to forecast the transport and dispersion of the smoke haze particles need to be further assessed. Finally, further comprehensive study on the selection of sites and equipment, as well as its infrastructure requirements are suggested.

5. Acknowledgements

This assessment is partially funded by DIPA PTKMR-BATAN 2011 and by the "Percepatan Persiapan Pembangunan PLTN di Indonesia" 2010 -2014 program.

6. References

[1]. WIKIPEDIA (2011), Fission Product Yield, http://en.wikipedia.org/wiki/Fission_product_yield.

[2]. Many news, for example Forbes (2009), http://www.forbes.com/2009/03/20/japan-vietnam-nuclear-markets-economy-agreement.html.

[3]. Anders Ringbom and Harry Miley (2009), Radionuclide Monitoring, International Scientific Studies Conference, ISS Publication 09, Science for Security, Vienna, Austria, 23 28.

[4]. United Nations (1996), Protocol to the Comprehensive Nuclear Test-Ban Treaty. Part I, Chapter C: Radionuclide monitoring.

[5]. National Environment Agency, Singapore (2011), ASEAN Specialised Meteorological Centre (ASMC), Regional Weather, http://www.weather.gov.sg/wip/web/ASMC/Regional_Weather.

[6]. National Environment Agency, Singapore (2011), ASEAN Specialised Meteorological Centre (ASMC), Haze Information, http://www.weather.gov.sg/wip/web/ASMC/Haze_Information.

[7]. M Schwaiger, F Steger, T Schroettner and C Schmitzer (2002), A Ultra Low Level Laboratory for Nuclear Test Ban Measurements, Applied Radiation and Isotopes 56, 375 – 378.

[8]. P. Karhu (2001), Radionuclide Monitoring as Part of the Verification Regime for the Comprehensive Nuclear Test Ban Treaty, Radiochemistry, Vol. 43 No.5, 455 -457.

[9]. Comprehensive Nuclear-test Ban Treaty Organization (2011), http://www.ctbto.org/verification-regime/monitoring-technologies-how-they-work/ radionuclide-monitoring.

[10]. International Atomic Energy Agency (2000), Regulatory Control of Radioactive Discharge to the Environment, Safety Standards Series No. WS-G-2.3, IAEA, Vienna.

[11]. J. Bieringer, C. Schlosser, H. Sartorius and S. Schmid (2009), Trace analysis of aerosol bound particulates and noble gases at the BfS in Germany, Applied Radiation and Isotopes, Volume 67, Issue 5, 672-677.

[12]. Thomas Flury and Hansruedi Völkle (2008), Monitoring of Air Radioactivity at the Jungfraujoch Research Station: Test of a New High Volume Aerosol Sampler , Science of The Total Environment, Vol. 391, Issues 2-3, 284-287.

Diversity, Composition, and Community Structure of the Teak Canopy Arthropods in Porang Crop Area Saradan Forest, Madiun, East Java

Syahrudin Agung Permana [1], Amin Setyo Leksono [1], Bagyo Yanuwiadi [1]

[(1)] Department of Biology, Faculty of Science, University of Brawijaya
Email: syahrudin.agung@gmail.com

Abstract

Increasing of management Porang (Amorphophallus muelleri Blumei (Schott) Engl.) productions were to developes the forest peoples with agroforestry system on the base of forest.areas. This research aimed to analyse and to compare diversity, composition, and community structure of Canopy Arthropod in the different location (Porang Crop area and Non-Porang Crop Area of agroforestry forest) and both of correlation with its abiotic factors. Sampling methods performed by adopting yellow and blue colored water pan trap hanged on the trees (5-15m). The samples were identified and analysed in the Laboratorium. Bray Curtis Index, Diversity (Shannon-Wienner), and number of important values index measured to compare of Community structure between two areas. A total of 283 specimens belong to 9 orders and 19 families of the Canopy Arthropods were collected in Porang Crop area and 560 specimens belong to 10 orders and 22 families of the Canopy Arthropods in Non-Porang Crop area. The yellow traps had better trapping efficiency than the blue traps in abundance. The result showed the significant difference in abundance among two areas (F-test, $P < 0.05$). The value of both communities was 0.788 were measured in this research, indicated that the difference of Arthropods composition had a similarity. Community Structure was dominated by Simuliidae in the both of areas with number of important species index 60.48 in the porang crop area and 73.03 in the non-porang crop area. There was significant light intensity decerasing and this fact affected on the canopy Arthropods abundances. It increases with the negative correlation of -0.582. The significant air moisture decreasing was affected on The Canopy Arthropods diversity with the negative correlation of -0.515.

Keywords: *Community structure, composition, diversity, porang, canopy arthropods*

Biology of Fungi's Pelawan Tree (*Tristaniopsis Merguensis*)

Triadiati[1], Anastastia Raditya Hidayanti[1], Nampiah Sukarno[1]

(1) Department of Biology, Faculty of Mathematics and Natural Sciences, Bogor Agricultural University, Bogor
Corresponding author: adiatiipb@gmail.com

Abstract

Tristaniopsis merguensis (pelawan tree) is a potential plant, however, it has not cultivated and conserved optimally due to slow growth and lack of information in plant cultivation. In T. merguensis forest, fungi growth periodically under the T. merguensis tree, closed to its roots. The price of T. merguensis fungi is very expensive, because they growth in forest once time in a year and can not cultivated. Information of T. merguensis fungi is very limited; therefore, research in biology of T. merguensis fungi was important. The aim of the research was to evaluate the status of the T. merguensis fungi, fungal isolation, and fungal identification. Status of T. merguensis fungi was studied by analyzing root morphology and anatomy derived from field and green house experiment, fungal isolation was carried out from colonized root and fungal fruiting body.The bioassay of fungi isolates with T. merguensis seedling was done by using isolate obtained from colonization root at a different level of phosphate fertilizer, and fungal identification was conducted using fungal fruit body harvested from field. The result showed that T. merguensis was associated with ectomycorrhizal fungi which produced fungal sheath and formed typical root branches that called heterohizy, in root obtained from field and initial colonization structures were formed in root from green house experiment of 5 months old. Fungal isolation from root produced 2 isolates and from fruit bodies were 7 isolates. Colonization of inoculation treatment formed only in the addition of P 25% (P 25% i) and this treatment showed high growth rates. In treated plants without inoculation, the addition of P 25% (P 25% k) increased number of leaves at 5 months old inoculated plant. Result of identification fungi fruit body field was Boletaceae, genus Boletus.

Key words: *Tristaniopsis merguensis, ectomycorrhizal fungi, Boletus.*

Mathematical Model of Interactions Immune System with Micobacterium Tuberculosis

Usman Pagalay [1], Marjono [2], Kusworini Handono [3], Agus Suryanto [4]

[1,3] Faculty of Medicine, Brawijaya University of Malang, Indonesia
[2,4] Faculty of Basic Science, Brawijaya University of Malang, Indonesia

Abstract

Tuberculosis (TB) remains a public health problem in the world, because of the increasing prevalence and treatment outcomes are less satisfactory. About 3 million people die each year and an estimated one third of the world's population infected with Mycobacterium Tuberculosis (M.tb) is latent. This is apparently related to incomplete understanding of the immune system in infection M.tb. When this has been known that immune responses that play a role in controlling the development of M.tb is Macrophages, T Lymphocytes and Cytokines as mediators. However, how the interaction between the two populations and a variety of cytokines in suppressing the growth of Mycobacterium tuberculosis germ is still unclear. To be able to better understand the dynamics of infection with M tuberculosis host immune response is required of a model.One interesting study on the interaction of the immune system with M.tb mulalui mathematical model approach. Mathematical model is a good tool in understanding the dynamic behavior of a system. With the mediation of mathematical models are expected to know what variables are most responsible for suppressing the growth of Mycobacterium tuberculosis germ that can be a more appropriate approach to treatment and prevention target is to develop a vaccine. This research aims to create dynamic models of interaction between macrophages (Macrophages resting, macrophages activated and macrophages infected), T lymphocytes (CD4 + T cells and T cells CD8 +) and cytokine (IL-2, IL-4, IL-10,IL-12,IFN-γ dan TNF-α) on TB infection in the lung. To see the changes in each variable used parameter values derived from experimental literature. With the understanding that the variable most responsible for defense against Mycobacterium tuberculosis germs, it can be used as the basis for the development of a vaccine or drug delivery targeted so hopefully will improve the management of patients with tuberculosis. Mathematical models used in building Ordinary Differential Equations (ODE) in the form of differential equation systems Non-linear first order, the equation contains the functions used in biological systems such as the Hill function, Monod function, Menten-Kinetic Function. To validate the system used 4th order Runge Kutta method with the help of software in making the program Matlab or Maple to view the behavior and the quantity of cells of each population.

***Keywords**: Mathematical Model, Runge Kutta, Mycobakterium Tuberculosis, macrophages, T lymphocytes, Cytokines.*

1. Introduction

Mycobacterium tuberculosis (Mtb) is a facultative intracellular pathogen that has infected almost onethird of the world population. Although the majority (about 90%) of infected individuals mounts a protective and effective cell-mediated response and do not develop active disease, tuberculosis (TB) is still one of the major causes of death by infectious disease worldwide with more than 3 million deaths per year [1]. Most individuals infected with Mtb are able to control infection (not clear it) and settle into a latent state. Others develop active disease in either short term (primary infection) or long term (reactivation). What distinguishes these different infection outcomes is unclear and it is the motivation for this work.

Mycobacterium tuberculosis is rod bacteria, approximately 2–5 μm long and 0.2–0.3 μm thick. It is non-motile gram-positive and isaeros oltransmitted. TB disease progression is relatively slow compared to many other bacterial and viral infections: Mycobacterium tuberculosis doubles approximatively every 18–48 hours [2].

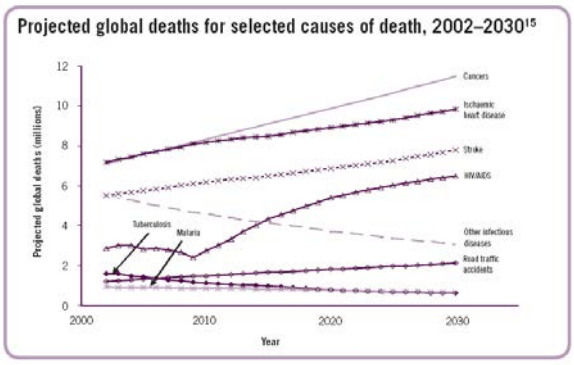

Figure. 01. Mortality estimates in the World According to Cause in the Year 2002-2030 (Source: WHO, 2007).

A cell-mediated immune response is essential for control of Mtb infection. Mtb infection initiates in the lungs, where resident macrophages take up bacteria. Mtb can effectively evade killing processes in resting macrophages, thus avoiding elimination. Clearance of bacteria by macrophages is in part dependent on macrophage activation by the cytokine IFN-γ secreted by CD4+ T cells, CD8+ T cells, and NK cells. Infected macrophages secrete other proinflammatory cytokines

such as TNF and IL-12 as well as chemokines that recruit immune cells to the site of infection [3].

Both CD4+ and CD8+ T cells participate in the immune response. Activated T cells of both types contribute to control of infection by activating macrophages (via production of cytokines such as IFN-γ) and by lysing chronically infected macrophages (via apoptosis and cytotoxic T cell action). Activated macrophages are highly efficient at phagocytosing and eliminating extracellular bacteria, while lysis of chronically infected macrophages serves to release M. tuberculosis, allowing their uptake by activated macrophages [2].

This model makes specific predictions concerning the roles of IL-10,IL-2, IL-12, TNF-α, IFN-γ, and IL-4 and describes key elements of cell-mediated immunity that lead to latency or active disease.

Cytokines

IL-10 plays a number of important roles in down-regulating an active immune response in TB, including deactivation of macrophages, inhibition of T cell proliferation, and suppression of cytokine production by T lymphocytes. IL-10 is produced primarily by macrophages in response to infection with *M. tuberculosi*.

IL-12 is a key Th1-type cytokine. Produced by activated and infected macrophages in response to Ag stimulation, IL-12 regulates the ongoing immune response, primarily by inducing differentiation of Th0 lymphocytes to Th1 lymphocytes, but also by enhancing the production of IFN-γ. Macrophage production of IL-12 is considerably enhanced when the macrophage is primed with IFN-γ.

IL-4 is considered to be the prototypical Th2 cell cytokine. It is the cytokine that governs differentiation of Th0 cells to Th2 cells. As discussed above, the role of IL-4 in the immune response to TB is controversial.

IFN-γ, a Th1-type cytokine, is a key to the development of an effective cell-mediated response to *M. tuberculosis*. IFN-γ activates resting macrophages, enhancing their ability to effectively clear pathogens and also to release cytokines. IFN-γ is also involved in the process of T cell differentiation by enhancing the rate of Th0 to Th1 differentiation and by overriding opposition by IL-4 to this process [4].

CD4+ T lymphocytes

We include in the model known interactions for CD4+ T cells. *CD*4+ T lymphocytes play two main roles in TB infection: the first is in the production of cytokines that govern the cell-mediated immune response; the second is elimination of infected macrophages via apoptosis.

CD8+ T lymphocytes

CD8+ T cells and TNF are believed to participate in the immune response to Mtb infection in humans. The role of CD8+ T cells in immunity against Mtb infection has been controversial. However, there are data supporting a role for these cells in protection against TB. It has been demonstrated repeatedly that mycobacteria-specific CD8+ T cells are induced in response to Mtb infection and that these cells can recognize Mtb infected macrophages. Cytotoxic activity of CD8+ T cells includes at least two separate mechanisms: apoptosis via the Fas-FasL pathway and killing via perforin and granulysin. In humans, CD8+ T cells can kill intracellular mycobacteria via the release of the antimicrobial peptide granulysin [3].

Model equations

We model human TB infection at the site of infection in the lung by tracking the interactions between two bacterial populations, seven cell populations, and six cytokines ((IL-2, IL-4, IL-10, IL-12, IFN-γ and TNF-α) using nonlinear, ordinary differential equations to describe rates of change. These 13 populations are placed into 4 groups: 1) macrophages; 2) CD8+ and CD4+ T lymphocytes; 3) cytokines; and 4) bacteria.

Macrophage dynamics

*T*he equations describing the rates of changes for macrophage populations during *M. tuberculosis* infection are given by Eqs. (1)-(3).

$$\frac{dM_R}{dt} = sr_M + \alpha_{4A}(M_A + w_2 M_I) + sr_{4B}\left(\frac{F_\alpha}{F_\alpha + f_8 I_{10} + s_{4b}}\right) - k_2 M_R\left(\frac{B_E}{B_E + c_9}\right) - k_3 M_R\left(\frac{I_\gamma}{I_\gamma + f_1 I_4 + s_1}\right)\left(\frac{B_T + \beta F_\alpha}{B_T + \beta F_\alpha + c_8}\right) - \mu_{MR} M_R \quad \text{.....(1)}$$

$$\frac{dM_A}{dt} = k_3 M_R\left(\frac{I_\gamma}{I_\gamma + f_1 I_4 + s_1}\right)\left(\frac{B_T + \beta F_\alpha}{B_T + \beta F_\alpha + c_8}\right) - k_4 M_A\left(\frac{I_{10}}{I_{10} + c_3 I_\gamma + c_4}\right) + k_{3A} M_I\left(\frac{I_\gamma}{I_\gamma + a_2}\right) - \mu_{MA} M_A \quad \text{...(2)}$$

$$\frac{dM_I(t)}{dt} = k_2 M_R\left(\frac{B_E}{B_E + c_9}\right) - k_{17} M_I\left(\frac{{B_I}^2}{{B_I}^2 + (N.M_I)^2}\right) - k_{14b} M_I\left(\frac{F_\alpha}{F_\alpha + f_9 I_{10} + s_{4b}}\right) + k_4 M_A\left(\frac{I_{10}}{I_{10} + c_3 I_\gamma + c_4}\right) - k_{3A} M_I\left(\frac{I_\gamma}{I_\gamma + a_2}\right) - \mu_{MI} M_I \quad \text{.....(3)}$$

2. Experimental Details

For the resting macrophage population, there is both a source of new cells coming into the site (sr_M) and death of cells that stay the remainder of their life span ($-\mu_{MR} M_R$). With no infection, the macrophage population should remain at the equilibrium value $M_R = sr_M / \mu_{MR}$. In the course of infection, additional resting macrophages are

recruited in a TNF-dependent fashion at a rate of *sr*4B, and this process is inhibited by IL-10. We also account for the recruitment of macrophages due to TNF-independent mechanisms such as chemokines secreted primarily by activated and infected macrophages (33) at rates of α_{4A}.

Cytokine dynamics

Equations describing the rate changes of the six cytokines in the model are given are as follows. Each equation is comprised of terms accounting for cytokine roduction from different cell lines as well as cytokine half-life. The equations of cytokine dynamics are given by Eqs. (4)-(9).

$$\frac{dI_{10}(t)}{dt} = \delta_7 M_A\left(\frac{s_6}{I_{10}+f_6 I_\gamma + s_6}\right) + k_{7av} M_I\left(\frac{c_{7a}}{I_{10}+c_{7a}}\right) + \alpha_{16}T_4 + \alpha_{18}T_8 - \mu_{I10}.I_{10} \ldots(4)$$

$$\frac{dF_\alpha(t)}{dt} = \alpha_{30}M_I + \alpha_{31}M_A\left(\frac{I_\gamma + \beta_2 B_T}{\beta_2 B_T + I_\gamma + f_1 I_4 + f_7 I_{10} + s_{10}}\right) + \alpha_{32}T_4 + \alpha_{33}T_8 - \mu_{F_\alpha}.F_\alpha \ldots(5)$$

$$\frac{dI_\gamma}{dt} = s_g\left(\frac{B_T}{B_T + c_{10}}\right)\left(\frac{I_{12}}{I_{12}+s_7}\right) + \left(\alpha_u T_4 + \alpha_y T_8\right)\left(\frac{I_{12}+M_A}{I_{12}+M_A+f_4 I_{10}+s_4}\right) + \alpha_{5C}M_I - \mu_{I\gamma}.I_\gamma \ldots(6)$$

$$\frac{dI_{12}(t)}{dt} = \alpha_{23}M_R\left(\frac{B_E}{B_E+c_{23}}\right) + \alpha_{81}M_A\left(\frac{c_{81}}{c_{81}+I_{10}}\right) - \mu_{I12}I_{12} \ldots(7)$$

$$\frac{dI_2(t)}{dt} = k_{10}T_4 - (k_{11}T_4 + k_{12}T_8)\left(\frac{I_2}{I_2+c_{100}}\right) - \mu_{I2}I_2 \ldots(8)$$

$$\frac{dI_4(t)}{dt} = \alpha_{112}T_4 - \mu_{I4}I_4 \ldots(9)$$

IL-10 and IL-12 are produced by infected and activated macrophages at rates of *k*7av and α_{81}, respectively, but both processes are inhibited by IL-10. In addition, IL-12 is produced by resting macrophages in response to infection at a rate of α_{23}.IL-2 is secreted by CD4+ T cells and is consumed by activated CD4+ and CD8+ T cells. IFN-γ is secreted by CD4+ and CD8+ T cells in the presence of IL-12 and activated macrophages.

T lymphocyte dynamics

CD4+ (T4) and CD8+(T8) T cells densities evolve by ,

$$\frac{dT_8(t)}{dt} = \lambda_x(M_A + w_2 M_I)I_{12} + s_r\left(\frac{F_\alpha}{F_\alpha + f_8.I_{10} + s_{4b}}\right) + k_{44}T_8\left(\frac{I_2}{I_2+c_{100}}\right) - \mu_{Tc\gamma}T_8 M_A\left(\frac{I_\gamma}{I_\gamma + c}\right) - \mu_{T8}T_8 \ldots(10)$$

$$\frac{dT_4(t)}{dt} = \lambda_z M_A I_{12} + sr_{3B2}\left(\frac{F_\alpha}{F_\alpha + f_8.I_{10} + s_{4b}}\right) + k_{13}T_4\left(\frac{I_2}{I_2+c_{110}}\right) - \mu_{Tc\gamma}T_4 M_A\left(\frac{I_\gamma}{I_\gamma + c}\right) - \mu_{T4}T_4 \ldots(11)$$

we take the rate of MHCII activation λz. Similarly, we take the rate of MHCI activation λx. IL-12 combined with antigen presented in the context of MHCII stimulates CD4+ T cells to proliferate, thereby expanding the CD4+ T cell population.

Bacterial dynamic

Equations describing the interactions and growth of *Mtb* are given by Eqs. (12)-(13).

$$\frac{dB_E}{dt} = \alpha_{20}B_E - k_5 M_A B_E - n_3.k_2 M_R\left(\frac{B_E}{B_E+c_9}\right) + k_{17}NM_I\left(\frac{B_I^2}{B_I^2+\left(NM_I\right)^2}\right) + k_{14b}.N.M_I\left(\frac{F_\alpha}{F_\alpha + f_8 I_{10} + s_{4b}}\right) + n_2\mu_{MA}B_I \ldots(12)$$

$$\frac{dB_I}{dt} = \alpha_{19}B_I\left(1 - \frac{B_I^2}{B_I^2+\left(NM_I\right)^2}\right) + n_3.k_2 M_R\left(\frac{B_E}{B_E+c_9}\right) - k_{17}NM_I\left(\frac{B_I^2}{B_I^2+\left(NM_I\right)^2}\right) - k_{14b}NM_I\left(\frac{F_\alpha}{F_\alpha + f_8.I_{10}+s_{4b}}\right) - n_2\mu_{MA}B_I \ldots(13)$$

Intracellular bacteria (Equation 13) grow at a maximal rate of α_{19} with logistic Hill kinetics accounting for a maximal carrying capacity of a macrophage. we assume that one-half of the infected macrophages burst when the intracellular bacterial load reaches *NMI*. Extracellular bacteria (Equation 12) grow at a maximal rate of α_{20} and are taken up by activated macrophages at a rate of ***k5***. A resting macrophage becomes infected at an assumed threshold of ***n3***

bacteria, Bursting of macrophages ($k17$) adds to the extracellular subpopulation.

3. Result and Discussion

Simulation Results

Table 1 lists Variables, initial values and their explanation. Table 2 lists Different parameters between young and old. Table 3 gives the parameter values of the differential equations (1)-(13). Figure 8 shows IL-12 levels, with a significant early increase in IL-12 production by old mice compared to young After 40 days, however this reverses and the IL-12 for young mice becomes larger. Both densities stabilize after 100 days of infection.

Figure 1, 3 simulates the bacterial load is larger for old mice. Figure 2 simulates the profile of Intracellular bacteria for young and old mice. Initially there are more Intracellular bacteria in the lungs of young mice in response to enhanced IFN-γ. However this later becomes reversed as antigen specific responses are generated in young mice, resulting in more Intracellular bacteria in the lungs of old mice up to day 30 of infection, both densities stabilize after 200 days of infection.

Figure 9 simulates the profile of IFN-γ is larger for old mice, both concentration stabilize after 200 days of infection. Figure 10 simulates the profile of TNF-α is larger for old mice, both concentration stabilize after 200 days of infection.

5. Acknowledgments

---

6. References

[1]. Marino S, K. D., (2004), The human immune response to Mycobacterium tuberculosis in lung and lymph node. *J Theor Biol* 227:463–486.

[2]. Jose L., (2004), Identifying control mechanisms of granuloma formation during M. tuberculosis infection using an agent-based model. *J Theor Biol* 231:357–376.

[3]. Sud D, Bigbee C, Flynn JL, Kirschner DE (2006), Contribution of CD8+ T cells to control of Mycobacterium tuberculosis infection. *J Immunol* 176:4296–4314.

[4]. Wigginton, J. E., and D. Kirschner. (2001), A model to predict cell-mediated immune regulatory mechanisms during human infection with *Mycobacterium tuberculosis*. *J. Immunol.* 166: 1951–1967.

[5]. David G., (2005), Understanding the Immune Response in Tuberculosis Using Different Mathematical Models and Biological Scales

[6]. World Health Organization (2007), Geneva: World Health Organization. 10-12. World Health Organization. 2007. Geneva: World Health Organization. 10-12.

[7]. Friedman A, Turner J, Szomolay B (2008), A model on the influence of age on immunity to infection with Mycobacterium tuberculosis. *Exp Gerontol* 43:275–285.

[8]. Judy, Day (2009), Modeling the immune rheostat of macrophages in the lung in response to infection. *J Immunol* : 11246–11251.

[9]. Kirschner, D. (1999), Dynamics of coinfection with *M. tuberculosis* and HIV-1. *Theor. Popul. Biol. 55:94.*

[10]. Magombedze. G, (2006), Modeling the human immune response mechanisms to Mycobacterium Tberculosis infection in the lung : 661-682.

Appendixes

Table I. Variables and initial values [3,7]

Symbol	Description	Young	Old	Unit
M_R	density of resting macrophages	5.10^5	5.10^5	Cell/ml
M_A	density of activated macrophages	200	1800	Cell/ml
M_I	density of infected macrophages	1800	200	Cell/ml
I_2	concentration of Interleukin-2	10	5	pgl/ml
I_4	concentration of Interleukin-4	5	5	pgl/ml
I_{12}	concentration of Interleukin-12	50	200	pgl/ml
I_{10}	concentration of Interleukin-10	100	50	pgl/ml
TNF α	concentration of TNF α	5	5	pgl/ml
IFN-γ	concentration of IFN-γ	5	5	pgl/ml
T_4	density of CD4+ T cells	2.10^5	10^5	Cell/ml
T_8	density of CD8+ T cells	8.10^4	8.10^4	Cell/ml
B_E	density of extracellular bacteria	1000	1000	Cell/ml
B_I	density of bacteria residing in infected macrophages	36000	4000	Cell/ml

Table 2. Different parameters between young and old[7]

Symbol	Description	Young	Old
λ_x	rate of MHCI activation	0.005266 ml/pg/day	0.0022854 ml/pg/ day
K_3	activation rate of infected macrophages	0.023415/ day	0.02544/day
K_4	deactivation rate of activated macrophages	0.28876/ day	0.61707/day
K_6	rate of activation of resting macrophages	0.077068/ day	0.13539/ day

K_7	IL-10 production rate by infected macrophages	0.5061/ day	0.55044/ day
K_8	IL-12 production rate by activated macrophages	0.28503/ day	0.53162/ day
K_9	IL-12 production rate by resting macrophages	5.10^{-4} pg/cell/ day	0.001 pg/ cell day
K_{10}	IL-2 production rate by CD4+	$2.1873.10^{-4}$ pg/cell/ day	$1.7301.10^{-4}$ pg/ cell day
K_{11}	loss of IL-2 due to proliferation of CD4+	$1.6383.10^{-4}$ pg/sel/ day	$1.4788.10^{-4}$ pg/ cell day
K_{12}	loss of IL-2 due to proliferation of CD8+	$1.6383.10^{-5}$ pg/cell/ day	$1.413.10^{-5}$ pg/ cell day
K_{13}	rate of proliferation of CD4+ by IL-2	0.1638 pg/cell/ day	0.14789 pg/ cell day
K_{14}	rate of proliferation of CD8+ by IL-2	0.01638 pg/cell/ day	0.01413 pg/ cell day

Table 3. Parameter values

1	Description	Range	Reference
α_8	IL-12 production by MA	$8x10^{-5}$ pg/ MA/day	Zhang, M., at.all (1994) 111
α_{30}	TNF-α production by MI	$10^{-3} – 2x10^{-2}$ ($3x10^{-3}$) pg/ml MI day	Sud D, at. all (2006)
α_{5c}	IFN-γ production by MI	0.0002-0.0006 (0.0003) pg/ml MI	Sud D, at. all (2006)
α_{4A}	TNF-independent recruitment of MR	$5x10^{-2}$/ day	Sud D, at. all (2006)
α_{23}	IL-12 production by MR	$2.75x10^{-5} – 2.75x10^{-4}$ ($2x10^{-4}$) pg/ml MR	Zhang, M., at.all (1994) 56,60,111
α_{31}	TNF-α production by MA	$0.3x10^{-4} – 1.5x10^{-4}$ ($4x10^{-3}$) pg/ml MA day	Sud D, at. all (2006)
α_{32}	TNF-α production by CD4+	$8.16x10^{-4}$ pg/ml CD4/ hari	Sud D, at. all (2006)
α_{33}	TNF-α production by CD8+	$0.6x10^{-4}$ - $1.1x10^{-4}$ ($0.5x10^{-4}$) pg/ml CD8/ day	Sud D, at. all (2006)
Sr_{3B2}	TNF-dependent recruitment of CD4	10^3/ day	Sud D, at. all (2006)
Sr_{4B}	TNF-dependent recruitment of MR	$2x10^4$ MR/ day	Sud D, at. all (2006)
f_9	Ratio adjustment, TNF/IL10	1 - 100 (50)	Wigginton, J. E., and D. Kirschner. 2001
f_7	Effect of IL-10 on IFN-γ -induced CD4	1	Wigginton, J. E., and D. Kirschner. 2001
f_8	Ratio Adjustment, IL-10/TNF on MR Recruitment	1 – 100 (1)	Wigginton, J. E., and D. Kirschner. 2001
S_{4b}	Half-sat, TNF on MR recruitment	138 – 556 (200) pg/ml/ day	Sud D, at. all (2006)
C_{23}	Half-sat, BT on IL-12 by MR	10^3 - $5x10^6$ ($5x10^5$) BT/ml	Wigginton, J. E., and D. Kirschner. 2001
w_2	Max, percentage contribution of MI-produced chemokines to MR recruitment	0.15	Sud D, at. all (2006)
μ_{Ty}	IFN-γ induced apoptosis rate of CD4	$10^{-5}– 10^{-3}$ (10^{-4}) /MA day	Sud D, at. all (2006)
μ_{BI}	BI turnover to BE due to MI death, other mechanisms	0 - 0.005 (0.004)/ day	Wigginton, J. E., and D. Kirschner. 2001
μ_{TNF}	decay rate of TNF-α	1.112/ day	Sud D, at. all (2006)
k_{14a}	Fas-FasL-induced apoptosis of MI	0.01 - 0.1 (0.1) / day	Sud D, at. all (2006)
k_{14b}	TNF induced apoptosis of MI	0.1 - 0.8 (0.1) / day	Sud D, at. all (2006)
s_{10}	Half-sat, IFN-γ on TNF production by MA	50 - 100 (80) pg/ml	Sud D, at. all (2006)
δ_7	IL-10 production by MA	0.001 - 0.01 (0.01) pg/ml MA	Westermann, M., at.all (1992)
α_{20}	BE growth rate*b*	0 - 0.26 (0.05) / day	Silver, R. F., at.all (1998)
α_{19}	BI growth rate	0.17 - 0.6 (0.4) / day	Silver, R. F., at.all (1998)
α_{16}	IL-10 production by CD4	$10^{-4}– 10^{-3}$($2x10^{-2}$) pg/CD4 day	Ladel, C. H., at.all (1997)
S_{rM}	MR recruitment rate	600 - 1000 (1000) MR/ day	Wigginton, J. E., and D. Kirschner. 2001
f_6	Penyesuaian, IFN-γ pada IL-10	0.025-0.053 (0.025)	(Chomarat, P., at.all (1999), Isler, P., at.all (1999))
f_4	Adjustment, IL-10/IL-12 on IFN-γ	0.76 - 3.2 (2)	Fishman, M. A., and A. S. Perelson. (1994)
f_1	Adjustment, IL-4/IFN-γ	3 - 410 (200)	Kirschner, D. (1999)
s_2	Half sat., IL-4	1 - 10 (5) pg/ml	Gong, J. H., at.all (1996)
s_6	Half-sat, IL-10 self-inhibition in MA	51 - 60 (60) pg/ml	Zhang, M., at.all (1998)
s_4	Half-sat, IL-12 on IFN-γ	50 - 100 (50) pg/ml	Yssel, H., at.all (1992)
s_7	Half-sat, IL-12 on IFN-γ by NK cells	5 – 100 (40) pg/ml	Wigginton, J. E., and D. Kirschner. 2001
s_1	Half-sat, IFN-γ on MR to MA	50 – 110 (70)	Wigginton, J. E., and D. Kirschner. 2001
c_9	Half-sat, BE on MR infection	10^6- 10^7 ($2x10^6$) BE	Wigginton, J. E., and D. Kirschner. 2001
c_8	Half-sat, BT on MR activation	$5x10^4 – 5x10^5$ (10^5) B_T/ml	Sadek, M. I., at.all (1998)
c_4	Half-sat, T/MI ratio for MI lysis	1 – 60 (40) T/MI	Wigginton, J. E., and D. Kirschner. 2001
c_{10}	Half-sat, bacteria on IFN by NK cells	$10^3 – 10^4$ (10^3) BT/ml	Chan, J., at.all (1992)
μ_{MR}	death rate of MR	0.0033/ day	Van Furth, R., at.all (1973)
μ_{MI}	death rate of MI	0.0011/ day	Van Furth, R., at.all (1973)
μ_{MA}	death rate of MA	0.07/ day	Van Furth, R., at.all (1973)

$\mu_{I\gamma}$	decay rate of IFN-γ	2.16 - 33.2 (2.16) / day	Zhang, M., at.all (1998)
μ_{I4}	decay rate of IL-4	2.77/ day	Sprent, J. (1993)
μ_{I10}	decay rate of IL-10	3.7 - 7.23 (5) / day	Westermann, M., at.all (1992)
μ_{I12}	decay rate of IL-12	1.188/ day	Zhang, M., at.all (1998)
k_2	MR infection rate	0.2 - 0.4 (0.4) / day	Oddo, M., at.all (1998)
k_3	MR activation rate	0.2 - 0.4 (0.1) / day	David Gammack, (2005)
k_{17}	Max. MI death due to BI	0.02 - 0.8 (0.02) / day	Rojas, M., at.all (1998)
k_4	MA deactivation by IL-10	0.01 - 0.4 (0.08) / day	Rojas, M., at.all (1999)
s_g	IFN-γ production by NK cells	0 – 1000 (100) pg/ml day	Sud D, at. all (2006)
N	Carrying capacity of infected macrophages	10 – 100 (20) BI/MI	(Hirsch, C. S., at.all (1994), Zhang, M., at.all (1998))
β	Scaling factor of TNF for MR to MA	10^2–10^5 (10^2) BT/pg	Hirsch, C. S., at.all (1994)
β_2	Scaling factor of BT for TNF production by MA	10^{-3}-10^{-4} (10^{-3})	Hirsch, C. S., at.all (1994)
λ_u	rate of IFN-γ production by CD4	1.24×10^{-4} pg/cell day	Friedman A, at. all (2008)
λ_y	rate of IFN-γ production by CD8+	1.24×10^{-5} pg/ cell day	Friedman A, at. all (2008)
λ_x	rate of MHCI activation	0.005266 pg/ cell day	Friedman A, at. all (2008)
λ_z	rate of MHCII activation	0.010532 pg/ cell day	Friedman A, at. all (2008)
α_{112}	IL-4 production by CD4+	10^{-4}–9.1×10^{-3} (10^{-4}) pg/CD4+ day	Friedman A, at. all (2008)
k_4	deactivation rate of activated macrophages	0.28876 / day	Friedman A, at. all (2008)
k_{3A}	activated M_1 by INF- γ	0.023415 / day	Friedman A, at. all (2008)
k_{7av}	IL-10 production rate by infected macrophages	0.50610 pg/ml cell	Friedman A, at. all (2008)
k_{10}	IL-2 production rate by CD4+	2.187×10^{-4}pg/ cell day	Friedman A, at. all (2008)
k_{11}	loss of IL-2 due to proliferation of *CD4+*	1.6383×10^{-4} pg/ cell day	Friedman A, at. all (2008)
c_3	IFN-γ inhibition for deactivation of activated macrophages	3	Friedman A, at. all (2008)
c_{100}	saturation for T cell proliferation by IL-2	50 pg/ml	Vesosky B, Turner J. (2005)
c_{7a}	saturation for IL-10 inhibition by IL-10	5000 pg/ml	Wigginton, J. E., and D. Kirschner. 2001
μ_{T4}	death rate of CD4+	0.33 / day	(Sornasse, T., at. all. (1996), Tough, D. F., at. all (1995))
μ_{T8}	death rate of CD8+	0.33 / day	Sprent, J. (1993)
μ_g	decay rate of IFN- γ	2.16 –33.2 (2.16) / day	Cooper AM, at. all (1995)
a_2	saturation for activation of infected macro	50 pg/m	Haynes L, at.all (1999)
c_{81}	saturation for IL-12 inhibition by IL-10	200 pg/ml	Turner J, at.all (2002)
n2	average number of *BI* in an activated macrophage	5	Friedman A, at. all (2008)
n3	threshold at which a resting macrophage becomes infected	10	Friedman A, at. all (2008)
μI2	decay rate of IL-2	1.188/ day	Friedman A, at. all (2008)
α_{18}	IL-10 production by CD8+	10^{-4}– 10^{-3}(2×10^{-2}) pg/CD8 day	Assenmacher, M., at.all (1998)

BE, extracellular bacteria; BI, intracellular bacteria; BT, total bacteria; Half-sat, half-saturation; MA, activated macrophages; MI, infected macrophages; MR, resting macrophages.

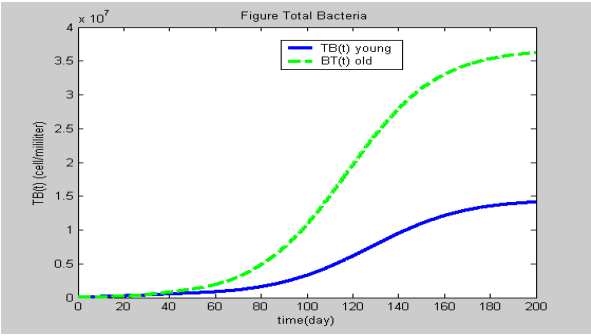

Figure 1. The bacterial load for young and old mice

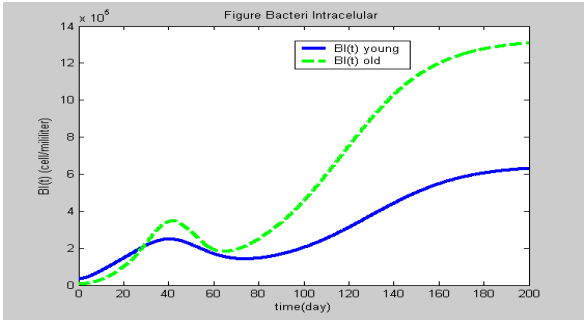

Figure 2. The Intracelular bacterial load for young and old mice

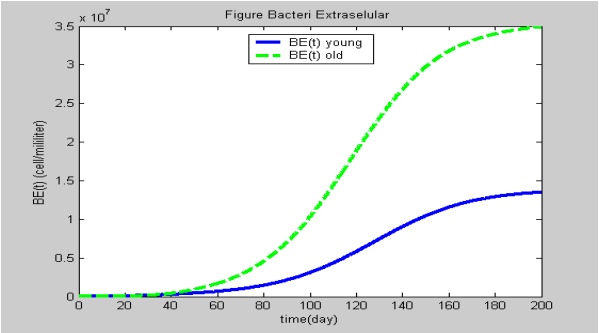

Figure 3. The Extracelular bacterial load for young and old mice

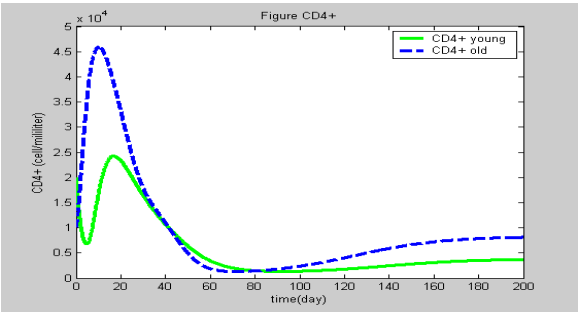

Figure 4. The densities of CD4+ T cells in young and old mice.

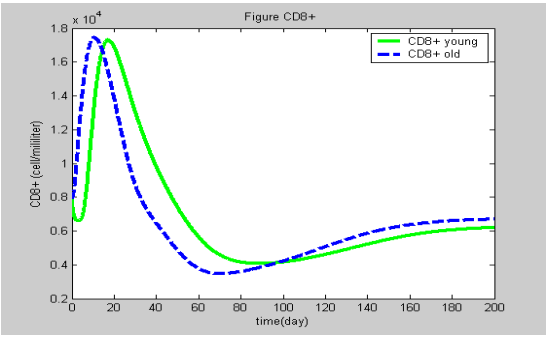

Figure 5. The densities of CD8+ T cells in young and old mice.

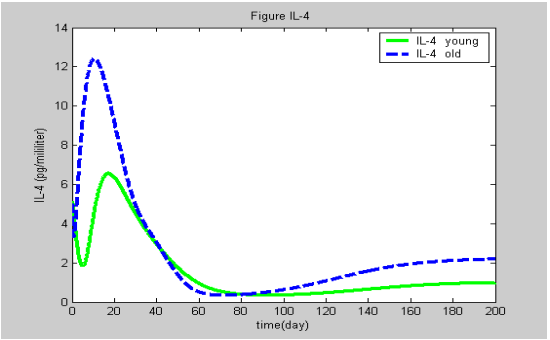

Figure 6. Concentration of IL-4 in young and old mice.

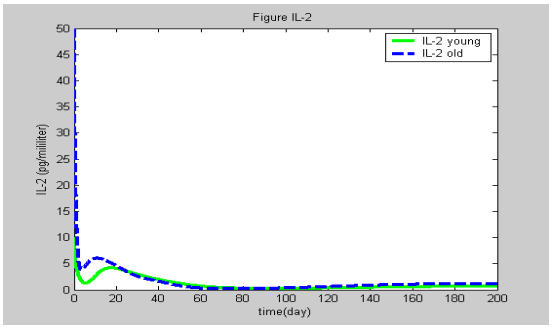

Figure 7. Concentration of IL-2 in young and old mice.

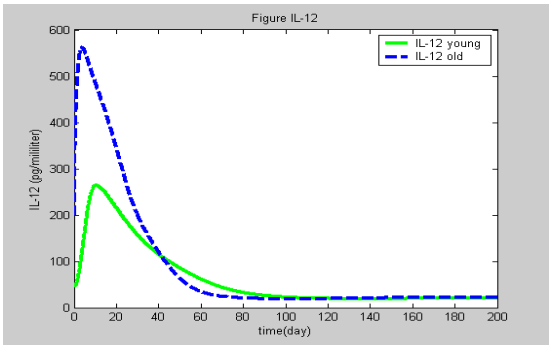

Figure 8. Concentration of IL-12 in young and old mice.

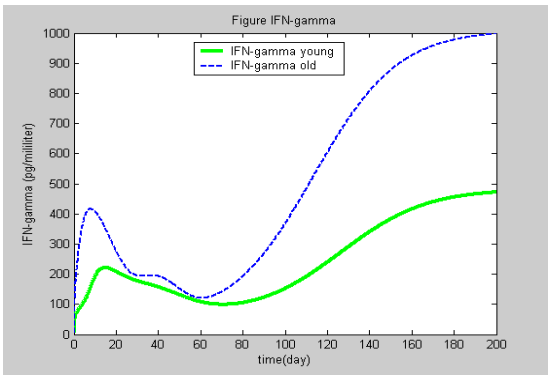

Figure 9. Concentration of IFN-γ in young and old mice.

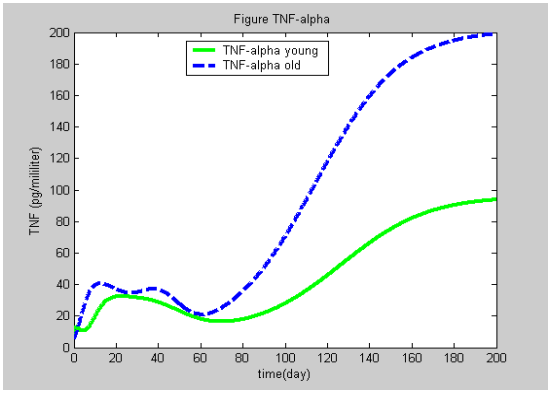

Figure 10. Concentration of TNF-α in young and old mice.

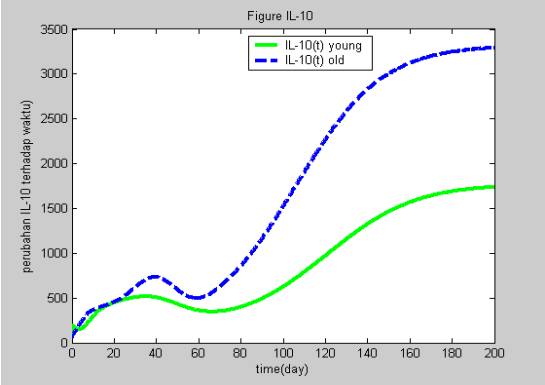

Figure 11. Concentration of IL-10 in young and old mice.

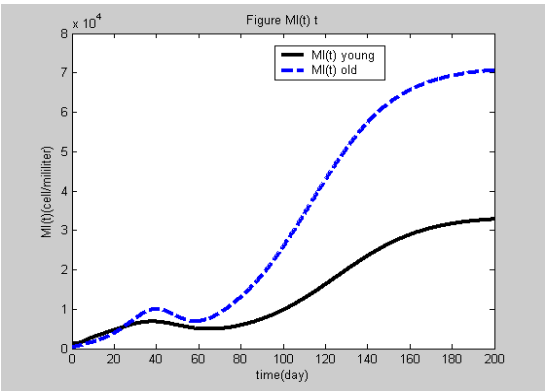

Figure 12. Simulation of infected macrophages in young and old mice.

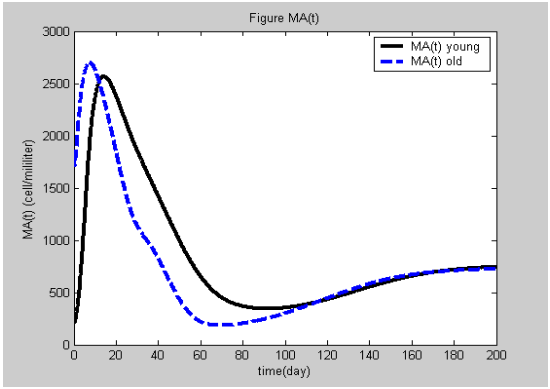

Figure 13. Simulation of activated macrophages in young and old mice.

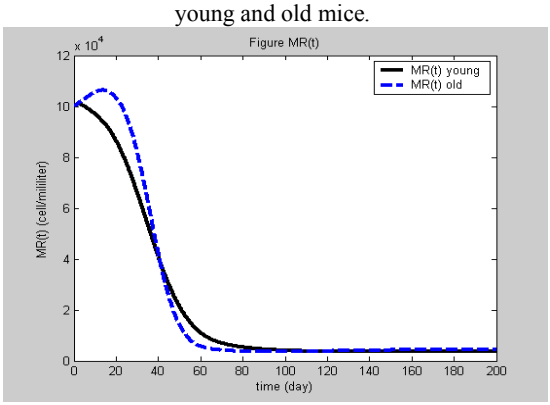

Figure 14. Simulation of resting macrophages in young and old mice.

Role of Wild Plant as Alternative Habitat for Natural Enemies in Agricultural Land

Wiwin Maisyaroh [1], Bagyo Yanuwiadi [2], Amin Setyo L. [3], Zulfaidah P.Gama [4]

[(1)] Graduate School of Mathematics and Science Brawijaya University, Malang, Indonesia (may_nis@yahoo.co.id);
[(2)] Department of Biology, Brawijaya University, Malang, Indonesia (yanuwiadi@brawijaya.ac.id)
[(3,4)] Department of Biology, Brawijaya University, Malang, Indonesia

Abstract

Use of chemicals in the agricultural industry is known to provide a considerable impact is also alarming for the health and sustainability of ecosystems. The use of improper chemicals in controlling pests such as pesticides can give side effects such as target pests becoming resistant to pesticides and the occurrence of pests resurjensi. Effort in maximizing the performance of natural enemies in agricultural land one of them is by creating habitat favored by natural enemies, habitat management is done to increase the number of natural enemy populations and maximize its role in controlling pests. The purpose of this study is to determine interest in natural enemies of insect pests of rice to some wild plants is: Mimosa pudica, Vernonia cinera, Marsilea crenata, and Pistia startiotes in rice plants. This research was conducted in March-April 2010 in Malang Sawojajar farmland. This research was done by placing a patch of weeds in rice fields located at the corner of the block, hereinafter referred to as refugia, attraction of insects were observed ranging from refugia blocks and each block distance of 2 meters away from the refugia. Observation method used is the method of "visual control" developed Freie and Manhart (1992). The results showed that the insects that visit refugia block consists of 9 orders namely: Coleoptera, Odonata, Aaraneae, Hymenoptera, Diptera, Homoptera, Orthoptera, Lepidoptera, and Hemiptera. Insect visitors refugia block consisting of 24 families and is divided into 3 roles of predators, parasites, and pests. Of the 24 families of the 15 family is the natural enemy insects and 9 family is an insect pest. In the first plot of insect natural enemies are most of the family Formicidae, whereas on the plot the second, third and fourth largest insect natural enemies is of the family Coccinellidae. The second largest number in the plot first, second, and fourth is from the family Aeshnidae, while the number of insects at least almost in each plot is the insect family Lycosidae.

Keywords: *Refugia, Natural Enemies, Visual Control.*

1. Introduction

Industrial agriculture is the human effort in increasing demand for food; various attempts were made to increase crop yields, especially in controlling pests. One is the use of chemicals that turned out to provide a worrying impact for health and also the continuity of existing ecosystems. The use of improper chemicals in controlling pests such as pesticides can give side effects such as target pests becoming resistant to pesticides and the occurrence of pests resurgence. One effort in controlling pests naturally is to maximize the role of natural enemies to control pest populations [1]. Effort in maximizing the performance of natural enemies in agricultural land can be done by creating habitat favored by natural enemies, habitat management carried out to increase the number of natural enemy populations and maximize its role in controlling pests.

Providing an alternative habitat for natural enemies can be done by using wild plants found in the vicinity of agricultural land. Weeds in rice fields are able to attract a variety of insect predators and parasitoids as well as other important arthropods [2]. Wild plants can serve as refugia for predators of insect pests, plant is a plant refugia in the surrounding rice fields that can provide shelter, supplementary food source, a place to reproduce, and a place to rest [3,4].

The purpose of this study is to determine interest in a natural enemy to block refugia (a combination of plant *Mimosa pudica* L., *Vernonia cinera* Less, *Marsilea crenata* Presl., *Pistia startiotes* L.) in rice.

2. Experimental Details

This research was conducted in March-April 2010 in Sawojajar farmland – Malang.

Materials used in this study are: Alcohol 70%, plant *Mimosa pudica* L., *Vernonia cinera* Less., *Marsilea crenata* Presl., *Pistia startiotes* L., and rice crops.

This research was done by placing a wild plant on a corner plot in the field, hereinafter referred to as block refugia. Observation method is "visual control" which was developed by the Freie and Manhart [5]. Visual control method is a method of long-distance observation by directly observing the insects that visit refugia blocks and blocks away from the clump of rice refugia, a distance of observations 2 meters and made within a certain time.

Observations of insects consists of 4 plots, the distance between plots was 2 meters, the first plot is a refugia block contained a combination of plant, while the plot of the second, third, and fourth is the plot of observation on the rice clumps blocks away from refugia. Old observations on each plot are 15 minutes and consist of 4 temporal observations, which are Temporal I 7:00 to 08:00 o'clock, temporal II at 9:00 to 10:00 a.m., 12:00 to 13:00 o'clock temporal III, and IV at 3:00 p.m. to 4:00 p.m. temporal. Observations were carried out for 15 days (15 replications).

3. Results and Discussion

Insect Visitors Refugia Block

Based on the observation of refugia blocks, namely a combination of plant *Mimosa pudica* L., *Vernonia cinera* Less, *Marsilea crenata* Presl., and *Pistia startiotes* L. contained in rice fields, showed that the insects that visit refugia block consists of 9 ordo namely: Coleoptera, Odonata, Aaraneae, Hymenoptera, Diptera, Homoptera, Orthoptera, Lepidoptera, and Hemiptera. Based on table 1 it can be seen that 9 of the ordo of insect visitors such refugia block consisting of 24 families and is divided into 3 roles of predators, parasites, and pests. Of the 24 families of the 15 family is the natural enemy insects and 9 family is an insect pest.

The existence of both natural enemies of many insects and pests is influenced by several factors including the availability of food and shelter [6]. This is in accordance with the results of studies showing that the type of insects found at the time of observation is quite varied. The diversity of both natural enemies of insect pests in the suspect and influenced by the availability of alternative food and shelter in the form of a wild plant (test plant) located in the vicinity of rice fields. In Wratten et al. [3] also mentioned that the diversification of habitats to provide nectar and pollen for parasitoids and predators and may serve as a temporary shelter.

The use of some wild plants of *Mimosa pudica* L., *Vernonia cinera* Less, *Marsilea crenata* Presl., *Pistia startiotes* L. in this study proved capable of delivering various types of insects. This is in line with the explanation Nentwig and Poehling [4] that the increased diversity of plant species correlated positively to increasing species richness of insects. The research results of Dadi [7], Fillaeli [8], Rohman [9], and Mukti [10], also concluded that the wild plants proved capable of providing support to the existence of Arthropods in the vicinity of agricultural land and also on another farm.

Table 1. Insect Visitors Block Refugia

ORDO	FAMILY / SPECIES	ROLE
Coleoptera	Coccinellidae / *Verania lineate*	Predator
	Staphylinidae / *Paederus fuscipes*	Predator
	Chrysomelidae	Pest
	Cucurlionidae	Pest
	Carabidae / *Ophionea nigrofasciata*	Predator
Odonata	Aeshnidae	Predator
	Libellulidae	Predator
	Coenagrionidae / *Agriocnemis sp.*	Predator
Araneae	Tetragnathidae / *Tetragnatha maxillosa*	Predator
	Oxyopidae / *Oxyopes sp.*	Predator
	Lycosidae / *Lycosa pseudoannulata*	Predator
Hymenoptera	Vespidae	Predator
	Ichneumonidae	Parasit
	Formicidae	Predator
Diptera	Syrpidae	Predator
	Muscidae	Pest
	Drosophillidae	Pest
Homoptera	Cicadellidae / *Nephotettix* spp.	Pest
	Delphacidae / *Nilaparvata lugens*	Pest
Orthoptera	Acrididae	Pest
	Tettigoniidae /*Conocephalus longipennis*	Predator
	Gryllidae / *Metioche vittaticollis*	Predator
Lepidoptera	Pappilionidae	Pest
Hemiptera	Reduviidae / *Leptocorisa oratorius*	Pest

Some insects found in this study proved to be the predators that potentially reduce plant hopper on rice crop pests such as family Lycosidae, Coccinellidae, and Carabids. As

reported by Santosa and Sulistyo [11] which describes the number of predators that potentially reduce planthopper pest populations such as: *Lycosa pseudoannulata* (Arachnidae; Lycosidae), *Paederus* sp. (Coleoptera: Coccinellidae), *Ophionea* sp. (Coleoptera; carabids), *Coccinella* sp. (Coleoptera: Coccinellidae) and *Cyrtorhinus lividipennis* (Hemiptera: Miridae).

Number and Type of Insect Visitors in Block Refugia

Effectiveness of natural enemies, especially predators depends on many factors including spatial and temporal [12]. Based on the results of this research is that in each plot was found differences in the type and number of natural enemies; this suggests that each family of insects have different levels of preference for some plants. Figure 1 show that in the first plot of the natural enemy of most of the family Formicidae, whereas on the plot the second, third and fourth largest natural enemies is of the family Coccinellidae. The second largest number in the plot first, second, and fourth is from the family Aeshnidae, while the number of insects at least almost in each plot is the insect family Lycosidae.

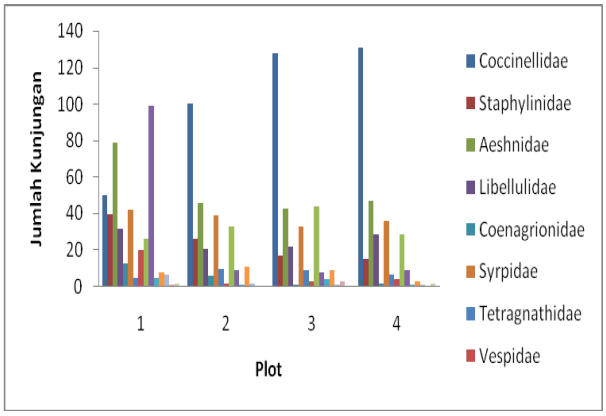

Figure 1. Graph the number of visits of natural enemies on each plot

Formicidae are ants that live in colonies, are generally carnivorous and eat other animals both living and dead. Some kinds of ants eat the plants and mushrooms, other food is honey dew or similar liquids [13]. The results showed that Formicidae is found most frequently in the first plot, so it can be concluded that the wild plants used in research trials are highly preferred by the family Formicidae and used as an alternative habitat and food providers for the family.

Coccinellidae are often found on the plot two, three and four, is one of the groups of beneficial insects, some insects of this family Coccinellidae eat aphids, scale insects, and insects that destroy others, and mites [13]. Although more dominant in the plots of two, three and four, the existence of this family are also suspected because of the presence of wild plants that exist. Coccinellidae is able to respond to odors released by these wild plants. This is consistent with the explanation from Rohman [9] that insects are able to select and respond to volatile compounds from plants.

The response of insect predators to the presence of volatile compounds released by plants is influenced by height sensitivity of olfactory receptor organs. If the source of chemical compounds from plants that received by the insects is less clear, then the insects will move with an irregular pattern and tend towards the object nearby and then moving back up to these insects find a favorite plant volatile signals.

Lycosidae that at least found in each plot, is one of predator insect pests, including moths and aphids [14]. Abundance is not too much its allegedly the plants less preferred by the Lycosidae, but it is also suspected because of insufficient food availability and competition with other insects.

4. Conclusion

Based on the results of this study concluded that block refugia (a combination of plant *Mimosa pudica* L., *Vernonia cinera* Less, *Marsilea crenata* Presl., *Pistia startiotes* L.) placed around the rice fields are able to invite the arrival of natural enemies. Natural enemies consist of 9 ordos namely: Coleoptera, Odonata, Aaraneae, Hymenoptera, Diptera, Homoptera, Orthoptera, Lepidoptera, and Hemiptera. Insect visitors refugia block consisting of 24 families and is divided into 3 roles of predators, parasites, and pests. Of the 24 families of the 15 family is the natural enemy and 9 family is an insect pest. In the first plot of insect natural enemies are most of the family Formicidae, whereas on the plot the second, third and fourth largest insect natural enemies is of the family Coccinellidae. The second largest number in the plot first, second, and fourth is from the family Aeshnidae, while the number of insects at least almost in each plot is the insect family Lycosidae.

5. Acknowledgements

---

6. References

[1]. DeBach, P. (1979), Biological Control by Natural Enemies. Cambridge University Press. London.

[4]. (ed.). Enhanching Biological Control: Habitat management to promote natural enemies of agricultural pest. University of California Press. Berkeley, Los Angeles, London.

[5]. Nentwig, W., H. M. Poehling. (1994), Insektengesllscften auf Selbstbegrünten und eingesäten Ackerbrachen. Paul Haupt Berne. Switzerland.

[6]. Frei, G. dan C. Manhart. (1992), Nützlinge und Schadlinge an Kunstlich Angelegten Ackerkraustreifen in Getreidefeldern. Agrarökologie 4.

[7]. Jumar (2000), Entomologi Pertanian. Rineka Cipta. Jakarta.

[8]. Dadi (2010), Potensi Agroforestri Pendukung Eksistensi Arthropoda Predator Wereng Padi di Ekosistem Sawah. Disertasi Program Studi Ilmu-ilmu Pertanian Pascasarjana Fakultas Pertanian Universitas Brawijaya Malang.

[9]. Fillaeli, S. N. (2009), Ketertarikan Arthropoda pada Kunyit (*Curcuma domestica* Val.) dan Bawangan (*Commelina benghalensis* L.) di Lahan Budidaya Porang Madiun. Skripsi Jurusan Biologi FMIPA Universitas Brawijaya. Malang.

[10]. Rohman, F. (2008), Struktur Komunitas Tumbuhan Liar dan Artrhopoda sebagai Komponen Evaluasi Agroekosistem di Kebun Teh Wonosari Singosari Kabupaten

[2]. Heinrich, E.A. (1994), Biology Management of Rice Insect. Willey Eastern Limited.

[3]. Wratten. S.D., H.F. Van Emden, and M.B. Thomas. (1998), Within-field and Border Refugia for the Enhancement of Natural Enemies. *In*. C.H. Pickett and R.L. Bugg Malang. Disertasi Program Doktor Ilmu Pertanian Program Pascasarjana Universitas Brawijaya Malang.

[11]. Mukti, M. (2007), Preferensi Kumbang Kubah (Coccinellidae), Belalang Sembah (Mantidae), dan Laba-laba Serigala (Lycosidae) Terhadap Tumbuhan Liar *Borreria repens* DC., *Bidens pilosa* L., dan *Centella asiatica* (L.) Urb. Skripsi Jurusan Biologi FMIPA Universitas Negeri Malang.

[12]. Santosa, S. J. and J. Sulistyo (2007), Peranan Musuh Alami Hama Utama Padi pada Ekosistem Sawah. INNOFARM : Jurnal Inovasi Pertanian Vol. 6, No. 1 (1 – 10).

[13]. Bugg, R. L., and C. H. Pickett (1998), Introduction: Enhancing Biological Control : Habitat Management to Promote natural enemies of agricultural pest. University of California Press. Berkeley, Los Angeles, London.

[14]. Borror, D.J., C.A. Triplehorn, dan N.F. Johnson (1992), Pengenalan Pelajaran Serangga. Terjemahan Soetiyono Partosoedjono. Edisi Keenam. Gadjah Mada University Press. Yogyakarta.

[15]. Shepard, B.M., Barrion, A.T., and Litsinger, J.A. (1987), Helpful Insect, Spider, and Pathogens. International Rice Research Institute. Los Banos Philippines.

Biosorption Phenomena of Heavy Metals and Radionuclides by Dispersed Bacterial Extracelular Polymeric Substances

Zainus Salimin [1], Endang Nuraeni [2]

[1,2] Radioactive Waste Technology Center, National Nuclear Energy Agency of Indonesia

Abstract

Bacteria can accumulate the heavy metals and radionuclides from its external environment by biosorption accumulation mechanisms of phyisical, chemical, and biological processes including flocculation, adsorption, coprecipitation, complex formation, and mass transfer phenomenas. The processes can occurs by functional support of bacterial extracellular polymeric substance (EPS) resulting from bacterial excretion, cell lysis or organic matter in surroundings. The EPS is composed of polysaccarides (40-95% of total EPS), protein (1-60%), nucleic acid (1-10%), lipids (1-10%), and polymers of amino acids and other compounds of microbial origin. The operation of Serpong Nuclear Facilities generates liquid waste containing detergent and various radionuclides. The simulation waste containing detergent of 0,748 g/l and the radionuclides of Co-60, Fe-55, Sr-90 and Cs-137 on the activities of $1,5x10^{10}$, $8,16x10^{9}$, $3,09x10^{9}$ and $4,8x10^{9}$ Bq/l respectively was treated by biooxidation process using mixed aerob bacterias of bacillus sp, pseudomonas sp, arthrobacter sp, and aeromonas sp. The bacteria need the period for adaptation of 4 days, indicated by generating of brown active sludge of biomass. Bacterial biomass performs the biosorption of radionuclides by sequence of its selectivity i,e $Sr^{+2}>Co^{+2}>Cs^{+2}>Fe^{+2}$. The Sr-90 having highest selectivity will be firstly absorbed by biomass then it is normally followed by absorption of Co-60, Cs-137, and Fe-55. When the influence of selectivity is not coming yet in its sequence caused of waiting time for attaching the radionuclide of high selectivity, the atom weight (a.w) takes over the loading role for flocculation and precipitation of the radionuclides. Performance unification between the roles of selectivity and atom weight gives the result of flocculation and precipitation time for each element of Cs (a.w 133), Sr (a.w 88). Co (a.w 60), and Fe (a.w 56) on the value of 5, 6, 10, and 12 days, respectively. On the processing time of 20 days, the activity of each element on supernatant result was attained the standard value of environmental radioactivity level (Decree of Chairman of National Nuclear Energy Control Agency No. 02/Ka-Bapeten/V-99) i.e $3x10^{4}$ Bq/l for Fe-55, $4x10^{3}$ Bq/l for Sr-90, $7x10^{2}$ Bq/l for Cs-137 and $2x10^{3}$ Bq/l for Co-60.

Keywords: *biosorption, extracellular polymeric substance, ion selectivity.*

1. Introduction

The nuclear industry activities generates low level radioactive organic liquid waste i.e detergent waste from nuclear laundry, spent solvent of 30% TBP (tri-n-butyl) in kerosene from uranium purification or uranium recovery from the operation failure of nuclear fuel fabrication, organic solvent as xylene, toluene, dioxin, etc. The activity of Serpong nuclear facilities as radioisotope production, nuclear fuel fabrication, reactor operation, radiometallurgy, radioactive waste treatment, etc generates low level radioactive waste water containing radionuclide elements of Co-60, Fe-55, Sr-90, Cs-137, etc. From the activity of laundry operation of the contaminated cloth performing by Radioactive Waste Technology Center at Serpong generates very low level radioactive waste water containing persil detergent (the compound of alkyl-aril sulfonat with chemical formula of CH_3-$(CH_2)_{10}$-CH_2-OSO_3Na)[1]. The detergent waste water is mixed with another radioactive waste water to become the low level radioactive liquid waste containing detergent of 0.748 g/l on the activity Co-60, Fe-55, Sr-90, Cs-137, etc of 10^9 Bq/l. At the present, that's liquid waste is treated by evaporation to concentrate its radioactivity on the concentrate. The evaporation concentrate is then solidified with cement matrix. The evaporation of liquid waste containing detergent generates the foam evoking the radioactivity contamination of distillate; in this case the failure of evaporation operation occurs. For avoiding the contamination of distillate by radionuclides elements, it is necessary to utilize antifoaming matter as silicon-oil [1]. The evaporation operation cost is enough expensive cause of the fulfillment of steam need from oil burning on the boiler, and the needs of antifoaming and descaling matters [2].

The biodegradation of organic matters and the biosorption of radionuclide and heavy metal elements by bacterial bio-oxidation are the effective processes for detoxification and decontamination of organic and radioactive liquid waste. It is necessary to study the bacterial bio-oxidation process for the assessment of alternative treatment of low level radioactive liquid waste containing detergent.

Theory

Bio-oxidizing Process

For waste water contains the organic compound, the removal of organic content from solution can be performed by sorption, stripping and biodegradation. Non degradable organic compound such as detergent or solvent having closed chair carbon compound can be removed from waste water by sorption using biological solid. The removal of volatile organic carbon is performed by stripping process using the counter-current operation process of gas-solution mass transfer. The removal of organic contents by biodegradation using bio-oxidizing process is done specifically for degradable organic having straight chain carbon compound [3].

Bio-oxidizing process of the most remaining organic matters occurs in the aeration tank, and the final clarifier removes the biological sludge, which are partially returned to mix with the incoming feed as the bacteria resources. On the biodegradation process of organic waste water using microorganism particularly the aerobic bacteria, oxygen and nutrient are consumed by bacteria for energy resources and regeneration of new cell/new bacteria. Living cells will use the organic compound as its food until that's compound changed into CO_2 and H_2O following reaction on the equation 1 and equation 2. The organic compound is toxic substances, by its degradation into CO_2 and H_2O the detoxification of solution occurs. The cells are quickly regenerated and grew and then dead. The living and dead of cells or new cells and non biodegradable cellular residue according the equation 1 and 2 respectively will form microbial biomass, which are precipitated to transform the biological sludge [3].

$$Organics + a'O_2 + N + P \rightarrow a\ new\ cells + H_2O + non\ biodegradable\ soluble\ residue \quad (1)$$

$$Cells + b'O_2 \rightarrow b\ CO_2 + H_2O + N + P + non\ biodegradable\ soluble\ residue \quad (2)$$

In equation (1), k is a rate coefficient and is a function of the biodegradability of the organic or the mixture of organics in the waste water. The coefficient a' is the fraction of the organics removed that is oxidized to end products for energy. *a* is the fraction of organics removed that is synthesized to cell mass. The coefficient b is the fraction per day of degradable biomass oxidized and b' the oxygen required for this oxidation. The need of nutrients of N and P on the treatment of industrial waste water is calculated from the ratio BOD, N, and P on the quantities of 100:5:1. Trace nutrient requirement for bio-oxidation is shown on the Table 1. When water contains the organic compound, metals and radionuclides elements (ion contaminants), and the microbial biomass will absorbs metals and radionuclides that mentioning biosorption [4].

Table 1. Trace nutrient requirements for biological oxidation [3]

Trace nutrient	mg/mg BOD
Mn	$10x10^{-5}$
Cu	$14.6x10^{-5}$
Zn	$16x10^{-5}$
Mo	$43x10^{-5}$
Se	$14x10^{-10}$
Mg	$13x10^{-5}$
Co	$62x10^{-4}$
Ca	$5x10^{-5}$
Na	$45x10^{-4}$
K	$12x10^{-3}$
Fe	$27x10^{-4}$
CO_3	$30x10^{-4}$

Source: Eckenfelder (1989)

The accumulation mechanism of radionuclide and heavy metal elements on the bacterial biomass can occurs by processes of physical, chemical, and biological including adsorption, precipitation, complex formation, and mass transfer phenomena. Living and dead cells resulting by bacterial cell as cell wall composer, pigment, polysaccharide, metal bonding protein, non biodegradable cellular residue, have the capability to remove the radionuclide and metal element. The kinds of specifics bacteria for corresponded metals and radionuclides elements removal are shown on the Table 2.

The biological sludge will be loaded by metals and radionuclides elements. Table 3 shows the bacterial cell component, each component can function to perform the sorption radionuclide and heavy metal elements [5]. It appears that the metals are largely bound by the extracellular polymeric substances (EPS), produced by bacteria. The EPS result from bacterial excretion, cell lysis or organic matters in surrounding. The EPS have a complex composition consisting polysaccharides (40-95% of total EPS), protein (1-60%), nucleic acids (1-10%), lipids (1-10%),

and polymer of amino acid and other compounds of microbial origin [6]. The EPS has to function for ion exchange due to the high amount of negatively charged functional group like carboxyl, phosphate and sulphat group in EPS. The ion exchange reaction on the EPS is similar to the organic ion exchange resin as follows:

$$M^{+}_{1} + \text{EPS.}\, M_2 \rightleftharpoons M_2 + \text{EPS.}\, M_1$$

where M_1^+ and M_2^+ are cations of difference species in which M_1^+ has the greater selectivity. The greater selectivity is the preference for the ion by the exchanger [7]. An ion exchanger tends to prefer: (1) ions of higher valence, (2) ions with a small solvated volume, (3) ions with greater ability to polarize, (4) ions that react strongly with the ion exchange sites of the exchanger solid, and (5) ions that participate least with other ions to form complexes. For the usual cation exchangers, the preference series for the most common cations is as follows [8]: $Ba^{+2} > Pb^{+2} > Sr^{+2} > Ca^{+2} > Ni^{+2} > Cd^{+2} > Cu^{+2} > Co^{+2} > Zn^{+2} > Mg^{+2} > Ag^{+1} > Cs^{+1} > K^{+1} > NH_4^{+1} > Na^{+1} > H^{+1}$.

Table 2. Some examples of bacterial heavy metal and radionuclide accumulation [4]

Organism	Element	Uptake (% dry weight)
1.Bakteria		
Streptococcus sp.	U	2-14
S. viridochro- mogenes	U	30
Thiobacillus ferrooxidans	Ag	25
Zooglea sp.	Cd	4-9
	Co	25
	Cu	34
	Ni	13
	U	44
Citrobacter sp.	Pb	34-40
	Cd	40
	U	90
Pseudomonas aeruginosa	U	15
Mixed culture	Cu	30
Mixed culture	Ag	32
Bacillus sp.	Pb	60.1
	Cu	15.2
	Zn	13.7
	Cd	21.4
	Ag	8.6

Note: U* uranium and its decay radionuclides

The overall process sequences are the adding of nutrients and aeration, then the adding of conformed bacteria, adaptation of bacteria on the organic solution milieu, bacteria eats organic compound, detoxification process from organic compound, growing-regeneration-dead of bacteria by natural cycle, formation of biomass, biosorption of metals and radionuclides elements and detoxification process from heavy metals.

Tabel 3. Description of bacteria cell components functions to support biosorption

Cell component	Function
Cell wall	Provides strength to maintain the cell shape and protects the cell membrane. Some bacteria can produce a sticky polysaccharide layer outside the cell wall, called a capsule or slime layer.
Cell membrane	Controls the passage of dissolved organics and nutrients into the cell and the waste materials and metabolic by-products out of the cell.
Ribosomes	Particles in the cytoplasm that are composed of ribonucleic acid (RNA) and protein and are the sites where proteins are produced
Flagella	Protein hair-like structures that extended from the cytoplasm membrane several bacteria lengths out from the cell and provide mobility by rotating at high speeds.
Fimbriae and pili	Short protein hair-like structures (pili is longer) that enable bacteria to stick to surfaces. Pili also enable bacteria to attach to each other.

2. Experimental Details

Material

Materials utilizing on the experiment are persil detergent, mixed mutant bacteria of *bacillus sp*, *pseudomonas sp, arthrobacter sp and aeromonas sp*, urea, tri super phosphate (TSP), potassium carbonat, sulfuric acid, silver sulfate, mercury sulfate, manganese sulfate, sodium hydroxide, potassium iodide, sodium thiosulfate, amilum indicator, cesium nitrate, strontium nitrate, cobalt nitrate, and ferrous ammonium sulfate.

Tools and instrumentations

Tools utilizing on the experiment are bio-oxidatoin process unit (see Figure 1), water checker for measuring dissolved oxygen and pH, UV-VIS spectrophotometer for measuring of chemical oxygen demand, and atomic absorption spectrophotometer for measuring of Co, Fe, Sr, and Cs contents.

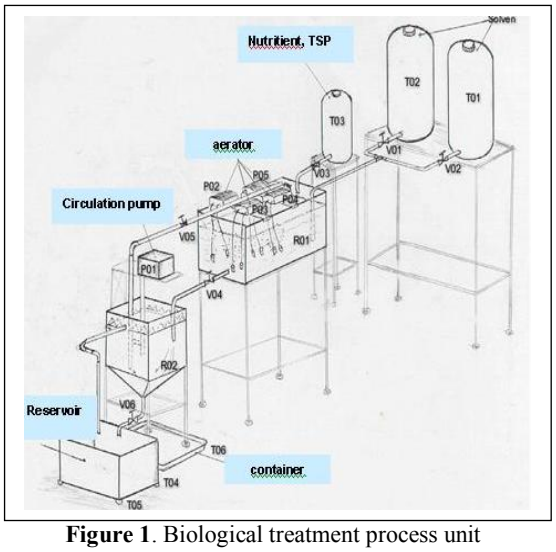

Figure 1. Biological treatment process unit

Method

Preparation of Simulation Waste

The simulation waste is prepared by weighing of $Co(NO_3)_2.6H_2O$ 2.95 g, $Fe(NH_4)_2(SO_4)_2.6H_2O$ 2.81 g, $Sr(NO_3)_2$ 0.97 g, and $CsNO_3$ 1.17 g, then those salts were dissolved into 200L of aquadest. It is obtained the solution having the activities of Co-60 1.5 x 10^{10} Bq/l, Fe-55 8.16 x 10^9 Bq/l, Sr-90 3.09 x 10^9 Bq/l and Cs-137 4.8 x 10^9 Bq/l. Percil detergent is weighted on the quantity of 37.4 g and then dissolved on the 200L of aquadest, it is obtained the solution of 0.788g/L of detergent.

Waste Treatment by Bio-oxidation

Simulation liquid waste with the persil detergent concentration of 0.748 g/L in which its BOD 68 ppm, COD 128 ppm, and the activities of Co-60, Fe-55, Sr-90 and Cs-137 on the value of 1.5x10^{10}, 8.16x10^9 and 4.8x10^9 Bq/l respectively is putted into bio-oxidation process unit, 120L into aeration vessel R-01 and 50l into sludge separation vessel R-02. The circulation pump P-01, aerators P-02, P-03 and P-04 are served in operation using the configuration of valve V-06 close, valve V-04 and V-05 open in which the liquid level in R-01 and R-02 constant. The nutrients of urea and TSP on the ratio of BOD:N:P=100:5:1 is introduced into solution. Measuring of pH and DO are performed using water checker. The mixed bacteria are putted into the solution. The solution of nutrition is prepared and putted on the nutrient tank T-03, during the process operation, valve of V-03 open so the solution of nutrient dispensing drop by drop. The solution sample is taken every 2 hours after adaptation of bacteria on the solution. The content of activity of Co-60, Fe-55, Sr-90 and Cs-137 on the solution is analyzed.

3. Result and Discussion

The initial simulation liquid waste has the parameters of COD 128 ppm and BOD 68 ppm. Water utilizing for experiment is treated water coming from Cisadane River in which trace nutrient indicating on the Table 1 is enough concentration in water, it is necessary to inject trace nutrient in the solution for experiment. The mixed bacterias utilizing on the experiment are conformed to the kinds of radionuclide on the liquid waste as shown on Table 2. The bacteria need to adapt the waste milieu during 4 days, indicated by generating of brown active sludge of biomass. Figure 2 indicates the relation between activity of Co-60 on the supernatant liquid and sludge as the function of process period. It is indicated that from the initial period until the period of less than 10 days the activity Co-60 on supernatant liquid always superior than the activity on the sludge. In that case the bacteria are still on the very small floating colony, the formation of bacterial biomass having the gravity weight forces not occurred yet. The biosorption of Co-60 be not take place yet cause of the bacterial biomass at the beginning chose to perform the biosorption of Sr-90 having the biggest selectivity. After the process period being superior to 10 days, the activity of sludge began to increase but the activity of supernatant liquid starts to decrease significantly. On the process period more than 10 days, the formation bacterial biomass occurs significantly to become the big flocculated colony in which the biosorption of Co-60 occurs, it having the weighted force for gravity precipitation.

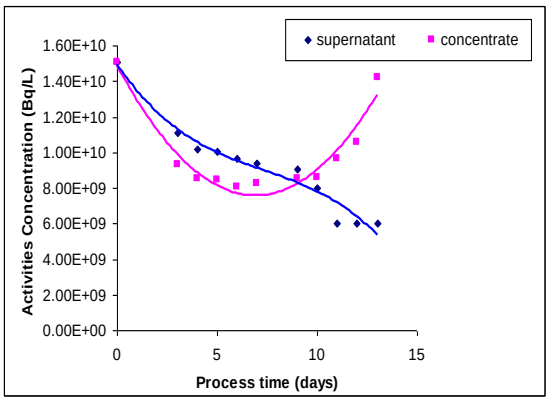

Figure 2. Relation between activity of Co-60 on the supernatant liquid and sludge as the function of process period

Figure 3 indicates the relation between activity of Fe-55 on the supernatant liquid and sludge as the function of process period. There is the same and Fe-55 indicating by Figure 2 and Figure 3; however the process period on the formation of flocculated and precipitated biomass for Fe-55 is 12 days, longer than for Co-60. Cation Fe utilized on the experiment is ferrous ion (Fe^{2+}) so on the point of view its selectivity is smaller than the selectivity of Co^{2+}. The atom weight of Co is higher than for Fe, when the element is absorbed by biomass so the loaded floc by cation Co will previously precipitated than cation Fe.

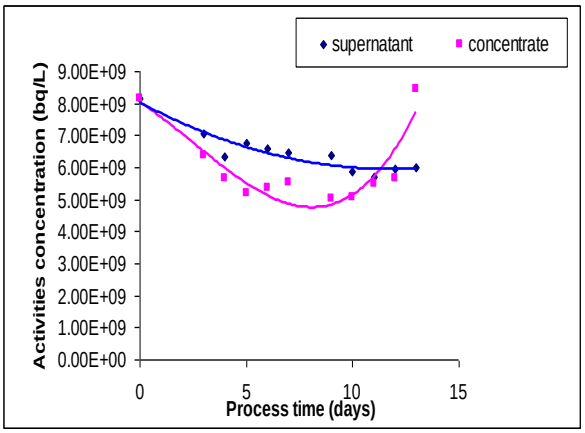

Figure 3. Relation between activity of Fe-55 on the supernatant liquid and sludge as the function of process period

Figure 4 shows the relation between activity of Sr on the supernatant liquid and sludge as the function of process period. It is indicated the difference phenomena comparing Figure 3 (For Fe) and Figure 2 (for Co), the activity of Sr-90 on the sludge is always superior to those observed on the supernatant liquid even at the beginning of the process. The difference is enable because the selectivity and atomic weight of Sr being highest than for Co and Fe. From the beginning of process the cation Sr is already absorbed by biomass and then flocculated and precipitated by gravity force.

Figure 5 shows the relation between activity of Sr on the supernatant liquid and sludge as the function of process period, there is difference phenomena comparing Figure 4 (for cation Sr). The activity of Cs on the supernatant liquid is higher than on the sludge for process period of 5 days. That's difference is enable because of the selectivity of cation Cs being smaller than for cation Sr even the atom weight of Cs being higher than for Sr. In that case the selectivity is more dominant than the atom weight on the formation of precipitated biomass floc.

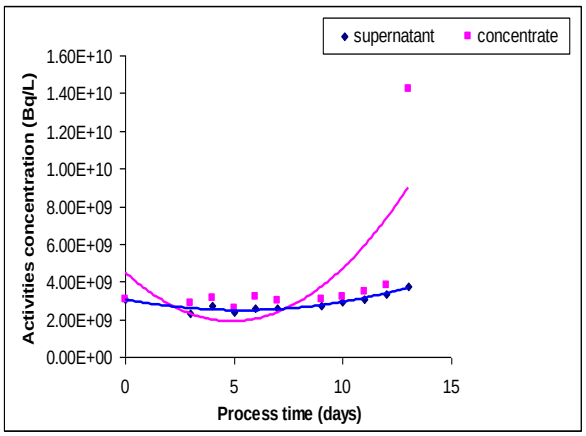

Figure 4. Relation between activity of Sr-90 on the supernatant liquid and sludge as the function of process period

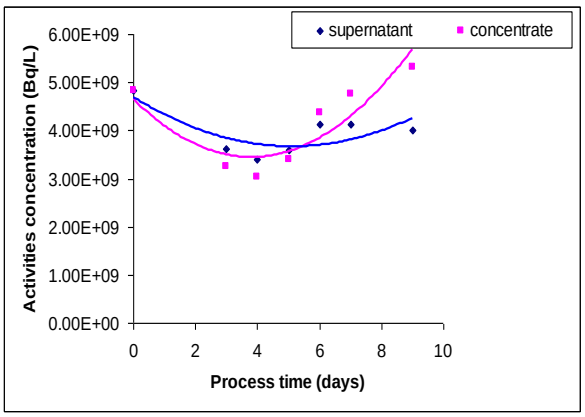

Figure 5. Relation between activity of Cs-137 on the supernatant liquid and sludge as the function of process period

Observation of Figure 2,3,4 and 5 can be concluded that the bacterial biomass performs the biosorption for radionuclide and heavy metals according the selectivity sequence of $Sr^{2+} > Co^{2+} > Cs^{2+} > Fe^{2+}$. The Sr-90 having highest the selectivity will be absorbed at first by biomass, and then it is normally followed by biosorption of Co-60, Cs-137 and Fe-55. When the influence of selectivity is not coming yet in its sequence caused of waiting time for attaching the radionuclide of high selectivity, the atom weight (a.w) takes over the loading role for flocculation and precipitation of the radionuclides. The process period of flocculation and settling for Co-60 (a.w 60) is longer than for Cs-137 (a.w 133). Also the flocculation and settling time for Fe-55 (a.w 55) is longer than for Co-60. Performance unification between the roles of selectivity and

atom weight gives the result of flocculation and precipitation time for each element of Cs, Sr, Co, and Fe on the value of 5,6,10, and 12 days respectively.

According to the Table 3, the bacteria cells component has the characteristic to support the biosorption of radionuclide and heavy metal elements. Those bacteria cells components consist of cell wall containing sticky polysaccharide layer on the outside wall so the cation elements can be easily attached, cell membrane controls the passage of any substance into and or out the cell, ribosomes and flagella composing protein that can react with metal from its surrounding to become the metal organoprotein, and fimbriae and pilli having the sticky surface for attaching the cation elements.

On the processing time of 20 days, the activity of each element on supernatant result was attained the standard value of environment radioactivity level (Decree of chairman of National Nuclear Energy Control Agency No.02/Ka-BAPETEN/V-99) i.e $3x10^4$ Bq/l for Fe-55, $4x10^3$ Bq/l for Sr-90, $7x10^2$ Bq/l for Cs-137 and $2x10^3$ Bq/l for Co-60.

4. Conclusion

The aerob bacterial biomass of *bacillus sp, pseudomonas sp, arthrobacter sp,* and *aeromonas sp*, can perform the biosorption of Co-60, Fe-55, Sr-90, and Cs-137 from its solution. The radionuclides are largely bound by EPS that can function for ion exchange due to the high amount of negatively charged functional group like carboxyl, phosphate, sulphate groups in EPS. According to the sequences of its selectivity, i.e $Sr^{2+} > Co^{2+} > Cs^{2+} > Fe^{2+}$, Sr-90 is attached at first by biosorption. For other elements, when the influence of selectivity is not coming yet in its sequences cause of waiting time for attaching high selectivity radionuclide, the atom weight takes over the loading role for flocculation and precipitation of the radionuclides. The radionuclide element having higher atomic weight gives the shorter time of flocculation and precipitation. The result of experiment indicates that the biosorption of radionuclides of Co-60, Fe-55, Sr-90, and Cs-137 from liquid waste by the bacterial biomass gives the decontamination of solution attaining the standard value of environmental radioactivity level.

5. Acknowledgements

The research data utilizing in this paper comes from the activity of Insentive Program for Increasing of Capability of Researcher and Designer Year 2009 with the title of Treatment Process of Liquid Radioactive Waste from Nuclear Industries Containing Organic by Bio-oxidation Process and Its Immobilization with Polymeric Matrix. We are thanks to the member of team of the Insentive Program for our mutual cooperation on the carrying out the jobs.

6. References

[1]. Salimin, Z (1997), Evaporasi Limbah Radioaktif Cair yang Mengandung Detergen dengan Antibuih Minyak Silikon, Prosiding Pertemuan dan Presentasi Ilmiah Teknologi Pengelolaan Limbah I, Serpong.

[2]. Salimin, Z (2000), Problem Solving of Evaporator Operation on the Treatment of Radioactive Liquid Waste in Serpong Nuclear Facilities, Presented Paper at the Symposium on Waste Management and Environmental Restoration, Tucson, Arizona.

[3]. Wasley, E (1989), Industrial Water Pollution Control (2nd edition), Mc Graw-Hill Book Company: Singapore.

[4]. Fry, J.C *et a.,l* (1992), Microbial Control of Pollution, Cambridge University Press: Cambridge, United Kingdom

[5]. Tchobanoglous, G *et al.* (2003), Wastewater Engineering, Treatment and Reuse (Fourth Edition), Mc Graw-Hill Book Company: Singapore

[6]. Yu Tian (2008), Behaviour of Bacterial Extracellular Polymeric Substance from Activated Sludge: a review, *International Journal Environment and Pollution*, Vol 32, No. 1.

[7]. Reynolds, T.D., (1982), Unit Operation and Processes in Environmental Engineering, PWS Publishing Company, Boston

[8]. Helfferich. F., (1962), ...

The Study of Phosphate Released from Aquatic Sediment and Its Effect on Algal Growth

Asep Saefumillah [1], Nining Betawati Prihantini [2], Dini Damayanti [2], Zaenab Sahamiddina [1]

(1) Deparment of Chemistry, Faculty of Science, Universitas Indonesia
(2) Department of Biology, Faculty of Science, Universitas Indonesia
Email: asep-s@ui.ac.id,

Abstract

Study on the release of phosphate from laboratory aquatic sediment incubation and its effect on algal growth has been conducted. The experiment shows interesting results in the context of climate change issue due to a steadly increase of global mean earth temperature on the internal loading of phosphate from sediment. Green algae Scenedesmus collected from Lake Agathis Universitas Indonesia (Prihantini et al, 2007) has been used to test the effect of phosphate from both synthetic nutrient medium and filtrate solution obtained from sedimen incubation. Firstly, Scenedesmus is cultured in Bold Basal Medium (BBM) with the variation of high phosphate concentration (P) around the level concentration of phosphate in BBM standard, whereas other elements compositions were maintain to be constant. The second experiment was conducted with lower phosphate concentration, less than 1 ppm to approach the level phosphate concentration in the commonly actual situation in the environment. At the third experiment, different phosphate concentration used as a medium collected from sedimen incubation and synthetic medium containing different concentration of P and N. Experiment to study the release of phosphate from sedimen incubation conducted under oxic and anoxic condition, temperature and incubation time have also succesfully been conducted. The effect of of oxygen level in sedimen suspension on the phosphate release from sedimen is shown that anoxic sedimen suspension facilitates the higher phosphate release than oxic sediment suspension. The effect of temperature is very significant on the amount of phosphate release from sedimen incubation conducted under anoxic condition. It is found that nutrient addition in synthetic medium in contrast to control, shows the growth of algae Scenedesmus. Experiment using filtrat sample containing different phosphate concentration from sedimen incubation produce a positive effect on the increase of algal Scenedesmus growth in line with the period of incubation time.

Keywords: *phosphate sedimen, algae, eutrophication.*

Normative Law Dimension Introduction of Variety Description for Pests and Plant Disease in Sustainable Food Crop Cultivation

Bambang Sudjito

Faculty of Law, Brawijaya University, Malang, Indonesia (b_jito@ub.ac.id)

Abstract

Within the framework of sustainable food crop cultivation need to be considered seed crop, crop protection, and food crop cultivation that to be good and right, as the legal provisions in the Act 12 – 1992, Government Regulation 44 - 1995, Government Regulation 6 - 1995, and Regulation of the Minister of Agriculture. 48/Permentan/140.OT/8/2006. Henceforth, within the framework of sustainable food crop cultivation has been made possible threat germ and plant diseases, that has not been early prevented through superior variety with its each descriptions and developed in the form of "bina" seed. Similarly, the existence of regulations related to sustainable food crop cultivation is possible there have been inconsistent, unclearness, and inclarity, beside vacuum of law substance. With a through normative law study was expected to be able give the inputs related with sustainable food crop cultivation to scientists or academics beside practitioner or bureaucrat.

Keywords: *Normative law, Variety description, germ and plant disease prevention, and sustainable food crop cultivation.*

1. Introduction

Within the framework of crop cultivation known various kinds of food crops, including rice or *Oryza sativa*, corn or *Zea mays*, and soybean or *Glycine max Merr*, similarly, various types of pests / diseases of plants in cultivation of food crops. Against many pests / plant diseases in the cultivation of food crops, which includes data for plant pests for food crops with the potential loss resulting from it in addition to endemic areas the main plant pests, as a description in Table 2.

Similarly, attacks a variety of pests/plant diseases in the cultivation of food crops, as contained in the following print media [1]:

a. Articles "Corn caterpillar epidemic", published in the daily Kompas, August 11, 2008;
b. Article "Soybean green caterpillar pests and locusts", as published in the daily Surya, September 28, 2008;
c. Articles "corn downy mildew threatens farmers back", published in the daily Kompas, May 18, 2009;
d. Article "Pests of paddy spread can be explosive in East Java because of changes in the weather", as published in the daily Kompas, January 17, 2011;
e. Articles "pest dominates, in some areas began to harvest rice," which appeared in Kompas daily, dated January 18, 2011
f. Articles "chocolate bar hopper, the feared pests and how to eradicate", published in Kompas daily, dated February 9, 2011.

The existence of legal substance of the laws and regulations related to the introduction of variety descriptions for the prevention of pests and plant diseases in a sustainable food crop cultivation possible inconsistent, unclearness, and inclarity, beside vacuum of law substance. Thus, the objectives to be achieved in this research are:

1. knowing and understanding the reality of inconsisten, inclearness, and inclarity beside vacuum of law and regulations substance related to the introduction of variety descriptions for the prevention of pests and plant diseases in the sustainable cultivation of food crops;
2. Knowing, understanding, and implementing various legal efforts should be made in the face of the reality of inconsistent, unclearness, and inclarity beside vacuum of law and regulations substance related to the introduction of variety descriptions for the prevention of pests and plant diseases in the sustainable cultivation of food crops.

The benefits expected from this research are:

1. Benefits for academics and researchers associated with the development of science and technology. In this sense, legal science, agricultural science, and related area, including taxonomy, morphology, and physiology of plants within the framework of sustainable crop cultivation
2. The benefits for bureaucrats within the scope of agriculture/farm outside the scope of the description associated with the introduction of varieties for the prevention of pests and plant diseases in the sustainable cultivation of food crops in addition to law enforcement.

2. Experimental Detail

This type of research within the scope of judicial normative, while the method of approach through statute approach [2]. Therefore, the type of data in this study, which includes primary legal materials, secondary, and tertiary [3], while the source of the data in this study, which covers the laws and regulations in addition to the writings of experts through results of research, journals, and articles. Henceforth, data collection techniques used through the identification and classification of legal substance of the laws and regulations related to the introduction of variety descriptions for the prevention of pests and plant diseases in the sustainable cultivation of food crops, while the data analysis techniques through

descriptive analytical through the legal principle and legal policy in the regulation the laws [4].

3. Result and Discussion

The existence of legal systems in public life [5] mechanism that functions as an integrator with adaptive systems procurement facilities instrumental to overcome obstacles be side adaptive structures, which include science and technology. In this case, science and technology, as the science of humanities, social, and natural sciences, including scientific knowledge related to pests and plant diseases and control.

Crop protection, which includes prevention of loss of crops caused by plant pests and outside plant pests [6]. Therefore, crop protection policy, in addition to do with technical policy of plant protection, which includes prevention of loss of crops caused by plant pests and outside plant pests; also performed with the policy of plant protection law, which includes preparation/renewal of law, correctional/law enforcement, and law enforcement related to crop protection, as well as pest and disease control with respect to the description of varieties of crops to prevent pests/plant diseases within the framework of sustainable cultivation.

The various steps that need to be known and understood within the framework of sustainable food crop cultivation, including cultivation of food crops is good and right, which includes the experimental stage, valuation, disposition, and the withdrawal of crop varieties, production, certification, and circulation building next to the entry of seed and expenditure of seeds, and cultivation of food crops is good and right. Furthermore, the existence of Sutau that resistance to pests/plant diseases can only be known and understood through the description of the variety in the stages of testing, evaluation, disposition, and the withdrawal of varieties of a crop. In this case, descriptions of different varieties of food crops with the advantages and disadvantages to pests/plant diseases through various decisions of the Minister of Agriculture relating to the release of varieties to be developed in plant cultivation as "bina" seed, which is certified and labeled. Therefore, within the framework of food crop is good and right, from the beginning has been known and understood the advantages and disadvantages to pests and plant diseases through the description of varieties, so that will facilitate the prevention and control of pests/plant diseases within the framework of sustainable cultivation of food crops .

Various legal provisions in the laws and regulations related to the cultivation of food crops are good and right, which includes:

1. Legal provisions in the Act 12 - 1992 on Plant Cultivation System, among others, Article 12 paragraph (1), and paragraph (2), article 13 paragraph (2) and paragraph (3), and Article 17 paragraph (2), and paragraph (3);
2. Legal provisions in the Act 16 - 1992 concerning Animal, Fish, and Plants, among others, Article 5 and Article 10;
3. Legal provisions in Government Regulation 44 - 1995 on the Seed Plants, among others, Article 18 paragraph (2) and paragraph (3), chapter 20, article 21, article 24, article 25 paragraph (2), article 32, article 33 paragraph (1), article 34 paragraph (1) and (2), and article 38;
4. Legal provisions in Government Regulation 6 - 1995 on Plant Protection, among others, Article 5 paragraph (2) and Article 6 paragraph (1);
5. Legal provisions in Government Regulation 14 - 2002 on Plant Quarantine, among others, article 2 and article 7;
6. Legal provisions in the Regulation of the Minister of Agriculture No 48/Permentan/140.OT/8/2006 on Food Crop Cultivation of Good and True, as the seed and crop protection in the annex to Regulation of Minister of Agriculture 48 / Permentan / 140.OT / 8 / 2006;
7. Legal provisions in the Regulation of the Minister of Agriculture No 37/Permentan/140.OT/8/2006 of Testing, Assessment, Disposal, and Withdrawal Variety, among others, Article 4 paragraph (1), article 10 paragraph (2), article 11 paragraph (3), and Article 19 paragraph (2);
8. Legal provisions in the Regulation of the Minister of Agriculture No 39/Permentan/140.OT/8/2006 of Production, Certification, and Distribution of Seed Development, among others, Article 5 paragraph (1) and paragraph (2), article 11 paragraph (1) and paragraph (2), article 13 paragraph (2) and paragraph (3), article 14 paragraph (2), paragraph (3), and paragraph (4), and article 24;
9. Legal provisions in the Regulation of the Minister of Agriculture No. 38 / Permentan/140.OT/8/2006 of Revenue and Expenditure Seeds, among others, Article 11, Article 16 paragraph (1), and paragraph (2), article 29 paragraph (1), and Article 30 paragraph (1);

Furthermore, the existence of legal substance in the Minister of Agriculture No. 37 / Permentan / 140.OT / 8 / 2006, which is implemented in a variety of Decree of the Minister of Agriculture relating to the release of varieties. In this case, the description of rice plants (***Oryza sativa***), maize (***Zea mays***) and soybean (***Glysine max Merr***) with various advantages and disadvantages of each, among others:

By considering the findings of the data with testing, evaluation, disposition, and the withdrawal of varieties of plants can be analyzed, that law substance related to test adaptation and / or observation to test new varieties, beside e legal provisions of article 18 paragraph (2) and (3) Government Regulation 44 - 1995 also legal provisions of Article 4 paragraph (1), article 10 paragraph (2), and article 11 (3) Regulation of the Minister of Agriculture No 37 / Permentan / 140.OT / 8 / 2006 have found any inconsistent, unclearness, and inclarity. Therefore, it can be seen and understood that the purpose of the laws and regulations to be inconsistent, unclearness, and inclarity, because only follow mere consumer tastes.

By considering the findings of the data with the production, certification, and "bina" seed distribution it can be analyzed, that substance of law related to the production, certification, and distribution of "bina" seed as the legal provisions of article 13 paragraph (2) and paragraph (3) the Act 12 - 1992, Article 33 paragraph (1) government regulation 44 - 1995, and

article 11 paragraph (2), article 13 paragraph (2), article 14 paragraph (2), and article 24 Regulation of the Minister of Agriculture No 39/Permentan/140 .OT/8/2006 in addition to income and expediture of seed, as the legal provisions of article 17 paragraph (3) the Act 12 - 1992, article 34 paragraph (1) and (2) Government Regulation 44 - 1995, and article 16 paragraph (1) and paragraph (2) Regulation of the Minister of Agriculture No. 38 / Permentan / 140.OT / 8 / 2006 have found any inconsistent, unclearness, and inclarity, so the goal rather than the laws and regulations to be inconsistent, unclearness, and inclarity beside vacuum. In this case, certification can be interpreted with certification through field inspection, laboratory testing, and installation of labels, seed certification, quality management system certification, or certification of products. In the future, "stipulation of certain seeds from the outside does not need to check the truth of the seed source ...." Therefore, it can be seen and understood the objectives of the laws and regulations are inconsistent, unclearness, and inclarity beside vacuum, especially during the process of seed health certification that the indicator only in the purity of seeds, a mixture of other varieties, growing power, and water content.

Thus, based on data findings related to cultivation of food crops is good and right can be analyzed, that linkage legal substance testing, evaluation, disposition, and the withdrawal of varieties that were followed by Ministerial Decree on the release of varieties by a description of variety, production, certification, and circulatory "bina" seed in addition to the income and expenditure of seeds, and cultivation of food crops is good and right, as the legal provisions in the Act 12 - 1992, the Act 16 - 1992, Government Regulation 44 - 1995, Government Regulation 6 - 1995, and Government Regulation 14 - 2002 in addition to the legal provisions in the Regulation of the Minister of Agriculture No. 37 / Permentan / 140.OT / 8 / 2006, Regulation of the Minister of Agriculture No. 39 / Permentan / 140.OT / 8 / 2006, Regulation of the Minister of Agriculture No 38 / Permentan / 140.OT / 8 / 2006, and Regulation of the Minister of Agriculture No 48 / Permentan / 140.OT / 8 / 2006 had found inconsistent, unclearness, and inclarity beside vacuum, in addition to descriptions of superior variety and / or weakness that has not / is not loaded in containers and / or label products, as well as certification that the term can be interpreted with certification through field inspection, laboratory testing, and installation of labels, seed certification, quality management system certification, or certification of products, so that the objectives of the legislation invitation to be inconsistent, unclearness, and inclarity beside vacuum.

4. Conclusion

The conclusions that can be obtained in the study of this law are:

1. The laws and regulations related to the introduction of the description of varieties to prevent pests / plant diseases within the framework of sustainable food crop cultivation in the implementation is still found any inconsistent, unclearness, and inclarity beside vacuum.
2. Remedies associated with the introduction of the description of varieties to prevent pests / plant diseases within the framework of sustainable cultivation of food crops through the preparation / renewal of the law based on the principle of legal principle and legal policy in the laws and regulations, especially the description of the variety of advantages and/or weaknesses that have not / not loaded in packaging and/or label products in addition to seed health indicators in the process of seed certification.

5. Acknowledgements

---

6. References

[1]. Anonymous (…..), KOMPAS, 11 August 2008; 11 September 2008; 18 Mei 2009; 17 January 2011; 18 January 2011; 9 February 2011
[2]. Marzuki and Peter Mahmud (2008), ……
[3]. Sukanto, S dan Mamudji, S, 1985, Penelitian Hukum Normatif, Rajawali Pers, Jakarta
[4]. Lembaga Administrasi Negara, 1995, Sistem Administrasi Negara Republik Indonesia, Hajimasagung, Jakarta
[5]. Vihelm, Aubert, 1973, Sociology of Law, Penguin Books – Middlesex
[6]. Untung, K, 2007, Kebijakan Perlindungan Tanaman, Gajah Mada University pers, Yogyakarta
[7]. Anonymous (1992), UU No 12, RI
[8]. Anonymous (1992), UU No 16, RI
[9]. Anonymous (1995), PP No 44, RI
[10]. Anonymous (1995), PP No 6, RI
[11]. Anonymous (1995), PP No 14, RI
[12]. Anonymous (2006), PP No 37 / Permentan / 140.OT / 8 / 2006.
[13]. Anonymous (2006), PP No 38 / Permentan / 140.OT / 8 / 2006.
[14]. Anonymous (2006), PP No 39 / Permentan / 140.OT / 8 / 2006.
[15]. Anonymous (2006), PP No 48 / Permentan / 140.OT / 8 / 2006.

Appendixes

Figure 1.Example of organism (Ind: Wereng batang coklat) that causes disease in paddy (*Oryza sativa*) crops (left: reported in 2005; right: reported in 2011)

Table 1. Potential loss result to attacks superior plants disturber organism of food crops in East Java

No	Commodity	Plant pests	Year		
			2004 (ton)	2005 (ton)	2006 (ton)
1	Paddy	1. Rat	4749.69	5721.68	4866.60
		2. Stem borer	4008.29	4775.91	6606.85
		3. Stem brown Planthopper	1289.94	1275.33	3552.19
		4. Bacterial leaf Blight	8048.74	8380.63	26811.12
		5. Tungro	1207.12	1391.11	1718.05
		6. Blas	522.47	4797.27	2243.44
2	Corn	1. Rat	321.07	207.02	382.55
		2. Stem borer	61.35	132.32	669.46
		3. Cob borers	192.72	115.53	762.90
		4. Grasshopper	521.79	272.87	2709.10
		5. Leaf rust	479.84	717.37	2093.03
		6. Albino	255.65	742.03	3422.64
3	Soybean	1. Silkworm span	73.93	126.41	23.82
		2. Armyworm	28.18	146.96	52.77
		3. Soybean beetle	22.80	72.48	23.50
		4. Pod borer	22.80	16.38	19.23
		5. Caterpillar pod	16.95	30.80	5.17
		6. Leaf rust	53.51	36.02	46.29

Data source: Department of Agriculture Province of East Java, Annual Report 2004 to 2006 (recycled).

Table 2. Regional endemic plant pests attack main food crops in East Java (Season Planting 2006)

No	Commodity	Plant pests	Regional (District)	Amount
1	Paddy	1. Rat	Tuban, Bojonegoro, Lamongan, Sidoarjo, Madiun, Malang, Lumajang, Jember, Banyuwangi	9
		2. Stem borer	Tuban, Bojonegoro, Lamongan, Ngawi, Lumajang, Jember, Bondowoso, Banyuwangi	8
		3. Stem brown	Madiun, Jember	2
		4. Planthopper	Tuban, Bojonegoro, Lamongan, Magetan, Madiun, Trenggalek, Jember	7
		5. Bacterial leaf Blight	Pasuruan, Probolinggo, Lumajang, Jember, Bondowoso, Situbondo, Banyuwangi	7
		6. Tungro	Pacitan	1
		7. Blas	Tuban, Bojonegoro, Lamongan, Malang, Lumajang, Jember	6
2	Corn	1. Rat	Probolinggo	1
		2. Stem borer	Probolinggo	1
		3. Cob borers	Bojonegoro	1
		4. Grasshopper	Tuban, Bojonegoro, Jombang, Tulungagung	4

		5. Leaf rust	Kediri	1
		6. Albino	Kediri Situbondo	2
3	Soybean	1. span caterpillar	Tulungagung, Jember	2
		2. "grayak" caterpillar	Bojonegoro, Lamongan, Pasuruan, Banyuwangi	4
		3. Soybean bumble	Ponorogo	1

Data source: Department of Agriculture Province of East Java, Annual Report 2004 to 2006 (recycled).

Table 3. Description superior varieties of rice (*Oryza sativa*) with resistance against pests / diseases

No	Variety	Variety released		Desecription pests / disease endurence	
		Kep.Mentan	Date	Superior	Weakness
1	Ciherang	60/Kpts/TP.240/2/2000	25-02-2000	Hold brown planthopper biotype 2 and 3	
2	Cibogo	393/Kpts/SR.120/8/2003	05-08-2003	Hold brown planthopper biotype 2, moderately resistant strains HDB IV, and brown planthopper biotype 3	"tungro" virus susceptible
3	Yuwono	573/Kpts/SR.120/10/2004	12-10-2004	Hold brown planthopper biotypes 1 and 2, moderately resistant biotype 3, resistant bacterial leaf blight strains III, and moderately resistant strains IV	
4	Rojolele	126/Kpts/TP.240/2/2003	14-02-2003		Brown rice pests sensitive
5	Pandanwangi	163/Kpts/LB.240/3/2004	17-03-2004		Biotype 2 and 3 brown rice pests, Rise pests susceptible, Strain 4 leaf blight bactaeria, Tungro
6	Way Apo Buru	21/Kpts/TP.240/1/98	13-01-1998	Hold brown planthopper biotype 2 and 3, leaf blight-resistant strains III and IV	Peka brown planthopper Vulnerable brown planthopper biotype 2 and 3,
7	Memberamo	584/Kpts/TP.240/9/95	04-09-1995	Blight-resistant strains III, moderately resistant " tungro"	bacterial leaf blight strains 4, tungro
8	IR 64	449/Kpts/TP.240/7/1986	17-07- 1986	Hold brown planthopper biotype 1, 2 and green leafhoppers, hold dwarf grass, moderately resistant leaf blight	
9	Intani 2	644/Kpts/TP.240/12/2001	03-12-2001		Somewhat sensitive to brown planthopper biotype SU (scale 4.3), somewhat sensitive strain BLB VIII
10	Mira 1	134/Kpts/SR.120/3/2006	06-03-2006	Moderately resistant brown planthopper biotype 3 (scale 3.67), moderately resistant strains III and IV BLB Hold brown planthopper biotype 2, moderately resistant biotype 3, resistant bacterial leaf blight strains III, and IV moderately resistant strains	

Data source: The decisions set of Agriculture Minister beside superior variety description Rice 1943 - 2009, Center for Agricultural Crops-Food Research and Development, Bogor, 2009 (recycled).

Table 4. Description superior varieties of maize (*Zea mays*) with resistance against pests / diseases

No	Variety	Variety released		Desecription pests / disease endurence	
		Kep. Mentan	Date	Superior	Weakness
1	Semar 9	172/Kpts/TP.240/6/99	22-06-1999	Hold downy mildew, leaf spot and rust	
2	Bisma	585/Kpts/TP.240/9/95	04-09-1995	Leaf spot and rust resistant	

3	Jaya 3	304/Kpts/TP.240/4/2002	25-04-2002	Downy mildew resistant	
4	SHS 11	375/Kpts/SR.120/6/2004	04-06-2004	Downy mildew resistant	
5	Bisi 2	589/Kpts/TP.240/9/95	04-09-1995		Tolerant of downy mildew and leaf rust
6	P 21	388/Kpts/SR.120/7/2003	29-07-2003	Leaf rust resistance, gray leaf spot Cercuspora zeaemaydis, moderately resistant Diplodia cob rot, viruses, and the germination of cob,	Somewhat susceptible stem rot bacteria, and downy mildew
7	NK 33	129/Kpts/TP.240/2/2003	14-02-2003	Moderately resistant downy mildew, leaf blight, and rust Stainless	
8	DK 3	162/Kpts/LB.240/3/2004	17-03-2004	Rust Tolerant	Tolerant of downy mildew

Data source: The decisions set of Agriculture Minister beside superior variety description Rice 1943 - 2009, Center for Agricultural Crops-Food Research and Development, Bogor, 2009 (recycled).

Table 5. ***Description superior soybean plant varieties (Glysine max Merr) with resistance against pests / diseases***

No	Variety	Variety released		Desecription pests / disease endurence	
		Kep. Mentan	Tanggal	Kunggulan	Kelemahan
1	Anjasmoro	537/Kpts/TP.240/10/2001	22-10- 2001	Hold split peas,	Medium leaf rust
2	Argopuro	204/Kpts/SR.120/4/2005	11-04-2005	Moderately resistant bean fly, armyworm, the suction pods	Sensitive leaf virus (CMMV
3	Baluran	275/Kpts/TP.240/4/2002	15-04-. 2002		Rust tolerant
4	Gepak Kuning	240/Kpts/SR.120/3/2008	06-03- 2008	Moderately resistant armyworm and leaf rollers	

Data source: The decisions set of Agriculture Minister beside superior variety description Rice 1943 - 2009, Center for Agricultural Crops-Food Research and Development, Bogor, 2009 (recycled).

Approach Method Self Organizing Maps (SOM) for Grouping Zone Season (ZOM) District Ngawi and Accuracy Evaluation Method ZOM with General Regression Neural Network (GRNN)

Bambang Widjanarko Otok [1], Muhammad Sjahid Akbar [2], Agnisa Bhakti Persada [3]

[(1)] Department of Statistics, ITS, Surabaya, Indonesia (bambang_wo@statistika.its.ac.id)
[(2)] Department of Statistics, ITS, Surabaya, Indonesia (m_sjahid_a@statistika.its.ac.id)
[(3)] Department of Statistics, ITS, Surabaya, Indonesia (agni_pinky@statistika.its.ac.id)

Abstract

Evaluation BMKG ZOM shows there are some locations that have poor performance. Some things that cause low accuracy, the data including the observation stations are often not homogeneous, due to the replacement of observation equipment (instrumentation); transfer the location of observation stations and the influence of urbanization. The data are not homogeneous observations will result in accuracy on the Zone Season less accurate. This study aims to help the BMKG in determining the best methods in grouping and evaluating their accuracy ZOM formed. ZOM grouping is based on rainfall intensity information at the District Ngawi Self Organizing Maps, and then the grouping was evaluated by the method of General Regression Neural Network. SOM and GRNN method is a nonparametric method based on machine learning with the main advantage is being able to represent the relationships linear and nonlinear, particularly nonlinear relationships are complex, directly from raw data. Underlying the use of machine learning based method is due to the fact that rainfall is non-linear. The results of clustering with SOM method of rainfall data has been reduced by four-factor analysis of optimum ZOM with 77.8% of classification accuracy. These results confirm the Complete Linkage clustering method that produces 100 percent classification accuracy. Clustering of SOM with rainfall data without reduction has 100 percent accuracy. GRNN method used to evaluate the classification ZOM give optimum results with a spread of 0.1 and RMSE 0.

Keywords: *Complete Linkage, GRNN, SOM, Zone Season.*

1. Introduction

Indonesia as an archipelagic state, including areas, are particularly vulnerable to climate change. Changes in rainfall patterns, temperature and the increase of extreme events are serious impacts of climate change faced by Indonesia. When viewed from the impact caused the prediction of climate elements, especially considering the much-needed rainfall in the district agriculture Ngawi is one of livelihood is one of the largest and central areas of rice in East Java [1]. Based on the evaluation BMKG on performance modeling and prediction of rainfall, there are several locations ZOM who have poor performance (low accuracy). Some things that cause low accuracy, the data including the observation stations are often not homogeneous, due to the replacement of observation equipment (instrumentation), transfer the location of observation stations and the influence of urbanization, it is expressed by Bunkers, Miller and DeGaetano (1996) in Nature (2010) [2].

Several studies on grouping ZOM, among others, research has been carried out by BMG in 2003 using the complete linkage method, and Wigena in 2006 using Ward's method and Centroid. Other research-related cases ZOM grouping has been carried out by Alam [3] by using the method of agglomerative Hierarchical Clustering. The method is applied to the grouping ZOM Ngawi district has been the parametric method, but in this study is to apply nonparametric methods for classifying and evaluating classification accuracy ZOM formed. The observed rainfall data is non linear and does not meet the assumption of multivariate normal distribution so that the data distribution is unknown, it is the underlying non-parametric methods applied in this study. SOM and GRNN method is a nonparametric method based on machine learning with the main advantage is being able to represent the relationships linear and nonlinear, particularly nonlinear relationships are complex, directly from raw data. Underlying the use of machine learning based method is due to the fact that rainfall is non-linear. This research is applying Self Organizing Maps for classifying rainfall stations in the District Ngawi and evaluation methods of grouping ZOM with General Regression Neural Network.

2. Experimental Details

Self Organizing Maps (SOM)

Self Organizing Maps (SOM) is one model of neural networks using unsupervised learning methods, meaning that network to do the learning without manual input of data and models created and arranged according to the input data (Otok, 2010). Trained SOM is iterative, for each input data point x i, where the nearest cluster determined using equation 1.

$$\|x_i - w_c\| = \min_j \{\|x_i - w_j\|\} \text{ atau } c = \arg\min_j \{\|x_i - w_j\|\} \quad (1)$$

Norm Euclidean is usually chosen to measure distance. Furthermore, w j and persekitarannya updated at each data point is entered by using the formula according to equation 2.

$$w_j(t+1) = w_j(t) + \alpha(t)h_{ij}(t)\left[x_i - w_j(t)\right] \quad (2)$$

This equation shows that each prototype is updated each time a given input x_i whose value depends on the Gaussian function as follows.

$$h_{ij}(t) = \exp\left(-\frac{\|x_i - x_j\|^2}{2\sigma^2(t)}\right) \quad (3)$$

Architecture *Self Organizing Maps*

This network consists of two layers (layer), namely the input layer and output layer. Each neuron in the input layer connects with each neuron in the output layer. Each neuron in the output layer represents a class (cluster) of the given input. Network output is the closest group or similar to the input given. There are some proximity measures that can be used. The size of the most frequently used is the minimum Euclidian distance. Johnson et al. [4] suggests that the distance euclidius originated from the distance between two objects.

$$d(x_r, x_s) = \sum_{i=1}^{p}((x_{ri} - x_{si})^2)^{\frac{1}{2}} \quad (4)$$

r, s = 1,2 … n where r ≠ s

$d(x_r, x_s)$ is the distance between two objects *r* and *s*. x_{ri} is the value *r* object in the variable *i* and x_{si} is the value *s* object in the variable *i*. Euclidius distance equation can also be transformed into a vector equation.

$$d(x_r, x_s) = \sqrt{(x_r - x_s)'(x_r - x_s)} \quad (5)$$

Where x_r and x_s is the vector *r* dan object *s*.

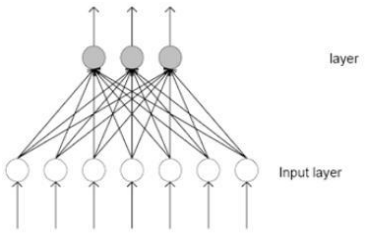

Figure1 Network *Self Organizing Maps[5]*

Validity Index

Determination of the cluster can be done by calculating the index of validity. The validity of the non-hierarchical clustering is determined by many groups through the optimum Validity Index, one of validity used was Root Mean Square Standard Deviation (RMSSD). This index measures the homogeneity of the cluster is obtained, so the value of this index should be the minimum for a cluster [6]. RMSSD calculation is as in equation 6.

$$RMSSD = \left[\frac{\sum_{i=1}^{m}\sum_{k=1}^{n}(x_{ik} - \bar{x})^2}{n-1}\right]^{\frac{1}{2}} \quad (6)$$

General Regression Neural Network (GRNN)

One form of the development of the NN model with activation function is a Gaussian kernel estimator function in the hidden layer [7]. Polat and Yildirim (2008) mention the most popular choice for the Gaussian activation function which is written in equation 3 [8]. Output of hidden layer unit is in the form according to equation 7.

$$y(x) = \sum_{i=1}^{n} b_i . \beta_{ij} . h_{ij}(t) \quad (7)$$

Coefficient b_i is the weight bias on the *i*-th observation and $(\beta_1, \beta_1, ..., \beta_n)$ are the magnitudes of weights (network weights) and the Gaussian function is $h_{ij}(t)$. GRNN network architecture generates output predictions as written in equation 8.

$$Y(x) = \frac{\sum_{i=1}^{n} Y_i \exp\left(\frac{-D_i^2}{2\sigma^2}\right)}{\sum_{i=1}^{n} \exp\left(\frac{-D_i^2}{2\sigma^2}\right)}$$

(8)

σ is the spread value that is used when the iteration and D_i is the distance between the sample observation and prediction points.

GRNN Architecture

Figure 2 is the overall network topology implementation of GRNN. GRNN consists of three layers of nodes with different roles, namely the input layer where input is applied, the hidden layer (consisting of the pattern layer and summation layer) where the nonlinear transformation applied to data from input space to hidden space in most applications the hidden space is high dimensional, linear output layer where the output is produced.

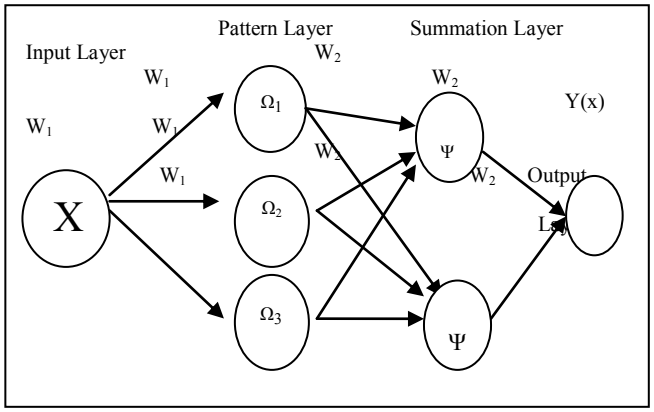

Figure 2. Architecture *General Regression Neural Network*

3. Result and Discussion

Description Ngawi District Rainfall

Initial discussion prior to further analysis is analyzing the characteristics of rainfall of each rainfall station in the District Ngawi. Average rainfall is highest in Karangjati station with an average rainfall that occurred was 205.57 mml. In Karangjati station also has the largest variant of 26133.683 mml. This shows that the rainfall variability in these stations is very high, with a minimum 22 mml rainfall and maximum rainfall of 451.64 mml. The high value of rainfall variation on Karangjati station indicates that the area around the station Karangjati has extreme rainfall, in other words the difference in the level of rainfall in the dry season and rainy season is very high. Station robber has the lowest rainfall, where the average rainfall in the area around the station robber at 126.33 mml with the most amount of rainfall and rainfall mml 293.47 at a minimum of 18.87 mml. The station has a variety of the lowest rainfall is in the station Kedung Galar, so that the area around the station Kedung Galar has no striking differences in rainfall during the rainy season and dry season. From 18 rainfall stations, area around Kedung Bendo has the lowest rainfall and the area around Karangjati has the highest rainfall.

Clustering Zone Season Using Self Organizing Maps with Reduction

SOM algorithm applied to the grouping ZOM score factor based on the results of factor analysis. SOM attempted to cluster with members as much as two to four stations in the cluster. The optimum number of groups is determined as the smallest RMSSTD. RMSSTD smallest value is the result of SOM clustering with the number of groups of four with RMSSD value of 1.2693. It can be concluded that the ideal number of groups to classify ZOM Ngawi district are four groups (ZOM) with members in each group are presented in Table 1. The criteria of each ZOM are presented in Table 2.

Table 1. Identification ZOM Results Clustering Methods SOM

Zone Season	Rainfall Station
ZOM 1	Mantingan, Ngale, Paron and Mardiasri.
ZOM 2	Kedung Urung-Urung, Jogorogo, Karangjati andGuyung.
ZOM 3	Ngawi, Ngrambe, Tretes, Kedung Galar andWalikukun.
ZOM 4	Bekoh, Kedung Bendo, Padas, Sambiroto and Begal.

Table 2. Criteria Zone Season Results Clustering Using SOM

Zone Season	Verage Rainfall	The Percentage of Rainfall	Criteria
ZOM 1	166.821	103.318	Normal
ZOM 2	189.474	117.349	Above normal
ZOM 3	151.162	93.62	Normal
ZOM 4	145.068	89.846	Normal

Rainfall criteria are categorized into 3, namely normal rainfall, above normal and below normal based on comparison of average rainfall in each of the ZOM compared with an average rainfall Ngawi district. ZOM rainfall at 1.3 and 4 tend to be normal and the rainfall in ZOM 2 above normal. ZOM maps and elevation maps of the results of SOM clustering method can be seen in Figure 3 and Figure 4.

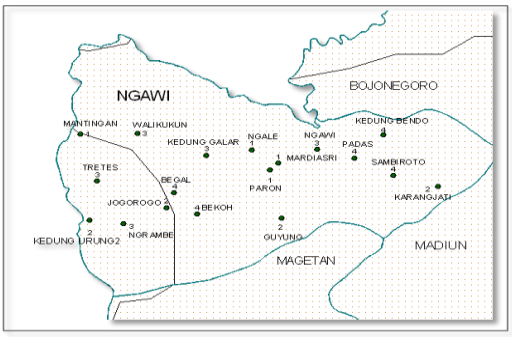

Figure 3. ZOM Map Results Clustering of SOM

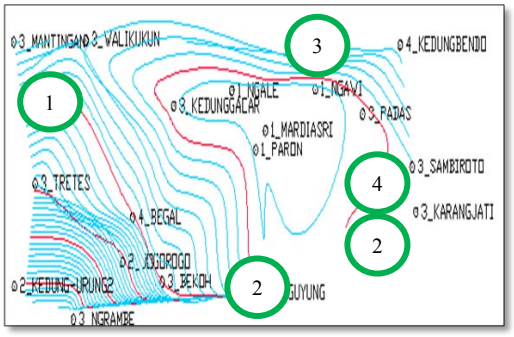

Figure 4. Reclustering Elevation Map Of SOM Result

ZOM Reclustering of SOM Result

Some stations that occupy a certain plateau comes from the ZOM is different, so needs a re-grouping for a particular terrain occupied by the same ZOM. The result of re-grouping can be seen in Table 3.

Tabel 3. Reidentification of ZOM Members Based on Elevation Map

Location	Rainfall Station
Plateau	Kedung Urung-Urung, Jogorogo, Ngrambe and Tretes.
Plain Medium	Mantingan, Walikukun, Bekoh, Kedung Bendo, Karangjati, Sambiroto, Guyung, Kedung Galar and Begal.
Lowland	Ngawi, Ngale, Paron, Padas and Mardiasri.

Plateau tends to be occupied ZOM 2 with a height above 200 meters above sea level, terrain is the location of stations on ZOM ZOM 3 and 4 with a height of 88-130 meters antaara to ZOM ZOM 4 3 and a height between 130-200 meters, while ZOM 1 with an average altitude of less than 88 meters above sea level tend to occupy the lowlands. Some stations with extreme tend criteria grouped in Zone 4, which is Kedung Bendo and spice. Bendo Kedung Station has the most minimal rainfall intensity while the robber had an average rainfall of at least among the other rainfall stations in the District Ngawi.

ZOM Cluatering Using Self Organizing Maps without Reduction

In this discussion, SOM will be used for grouping ZOM from rainfall data without reduction. Selection of the optimum number of groups based on the results of SOM clustering method RMSSD smallest value that is equal to 0. The result of clustering with SOM method of rainfall data without reduction is as follows:

ZOM 1 Mantingan, Ngawi, Ngrambe, Tretes, Kedunggalar, Walikukun, Bekoh, Kedung Bendo, Ngale, Paron, Mardiasri, Padas, Sambiroto and Begal.

ZOM 2 Kedung Urung-urung, Jogorogo, Karang-jati and Guyung.

Clustering results will be modified based on the location of contour height, in order to obtain ZOM with member stations that have been modified. Identification of which have been re-ZOM dimodefikasi based contour heights are as follows:

ZOM 1 Mantingan, Ngawi, Kedunggalar, Walikukun, Bekoh, Kedung Bendo, Ngale, Paron, Mardiasri, Padas, Karangjati, Sambiroto, Guyung and Begal.

ZOM 2 Ngrambe, Tretes, Kedung Urung-urung and Jogorogo.

Stations which clustered at ZOM 2 has a height above 200 m, while station at ZOM 1 has a height of less than 200 m, with rainfall at ZOM criteria 1 and 2 is a zone with normal rainfall season. Average rainfall in ZOM 1is 158.132 mml and average rainfall in ZOM 2 is 168.698 mml. The average value of the ZOM rainfall 1 and 2 when compared with an average rainfall Ngawi district, namely 161.463 mml then obtained the percentage ratio of average rainfall. Percentage ratio of average rainfall in ZOM 1 amounting to 97.397 percent and 104.48 percent ZOM second, so ZOM 1 and ZOM 2 has the properties of normal rainfall.

Spread Parameter Selection in General Regression Neural Network

Spread that will be used is the spread that produces the smallest RMSE, therefore GRNN algorithm will be simulated with the parameters that it tries to spread is between 0 to 1. Results of classification with the smallest RMSE will be used as a reference in evaluating the results of

classification ZOM Complete Linkage and SOM. RMSE of GRNN results are as follows.

Tabel 4. Spread Value and RMSE GRNN

Spread	RMSE
0.1	0
0.2	$1.58x10^{-09}$
0.3	$9.92x10^{-05}$
0.4	0.0047
0.5	0.0266
0.6	0.0659
0.7	0.1143
0.8	0.1679
0.9	0.2244
1.0	0.2802

Results GRNN algorithm running with a different determination of the value spread is shown in Table 4 which shows that the spread is 0.1 resulting RMSE values of 0, while the spread is a value obtained by the RMSE of 0.20802. The greater the spread is used; the higher RMSE value. Results of groups with spreads 0.1 GRNN method will be used as a reference group in the evaluation of classification that is formed based ZOM Complete Linkage method and the SOM.

ZOM Classification Accuracy Evaluation using General Regression Neural Network.

ZOM will be evaluated is the initial formation and the elevation. ZOM results of clustering with SOM method of data reduction by factor analysis have a classification accuracy of 77.8%. There are few rainfall stations are grouped in the wrong zone, namely Mantingan station that should be grouped on one but placed as ZOM 3, while the station Guyung Karangjati and placed on three ZOM when they should be grouped in 2, and the stations that should be grouped in Ngawi ZOM 3 but was placed on 1. Station robber grouped in ZOM 4, but should be robber entered the station at ZOM 3. The value of classification error of 27.8 percent, so that the obtained classification accuracy of 72.2 percent. Grouping by SOM with the data reduction method has a classification accuracy of 100 percent and after dimodidikasi provide 77.8 percent accuracy. stations are grouped in the wrong zone is Ngrambe and Tretes that should be grouped at ZOM 2 but was placed on 1, and Karangjati and Guyung that should be grouped on one but placed on ZOM 2.

4. Conclusion

1. Zone Method Season Ngawi District uses Self Organizing Maps methods produce four-season zones. The result of clustering with SOM method in ZOM 1 result grouping with SOM is Mantingan, Ngale, Paron and Mardiasri, while ZOM 2 consists of Kedung Urung-Urung, Jogorogo, Karangjati and Guyung. ZOM 3 consists of Ngawi station, Ngrambe, Tretes, Kedung Galar and Walikukun, while ZOM 4 consisted of Bekoh station, Kedung Bendo, Padas, Sambiroto and spice.
2. The best classification accuracy of the method of the General Rgression Neural Network with spread 0.1 shows that initial formation ZOM method Self Organizing Maps with data reduction, while the classification accuracy after the elevation of 72.2 percent. Classification accuracy of rainfall data with no reduction with SOM method has a precision of 100 percent, while after modification with elevation map has 77.8%accuracy.

5. Acknowledgements

---

6. References

[1]. Eksawati, R. (2009), Use of Neural Network Analysis (Neural Network Analysis) to Develop Models of Rainfall in the district of East Java Ngawi, IPB, Bogor.
[2]. Bunkers, Miller, and DeGaetano (1996),…
[3]. Alam, D.P.A. (2010), Grouping Zone Season (ZOM) with Agglomerative Hierarchical Clustering, Department of Statistics, ITS, Surabaya.
[4]. Johnson, N., and Wichern, D. (1992), Applied Multivariate Statistical Analysis, 3th ed., Prentice Hall, Englewood Chiffs, New Jersey.
[5]. Sebayang (2009), …
[6]. Puspowati, T. (2009), Algorithm Self Organizing Maps (SOM) for grouping District in Malang Based Education Equality Indicators, Thesis, Department of Statistics, ITS, Surabaya.
[7]. Kusumadewi, S. (2004), Building Artificial Neural Networks Using MATLAB and EXCEL LINK,……
[8]. Polat, O., and Yildirim, T. (2008), Hand Geometry Identification without Extraction by General Regression Neural Network: Expert System with Application 34:845-849.
[9]. Dillon, W. R., and Goldstein, M. (1984), Multivariate Analysis Methods and Applications, John Willey and Sons, New York.
[10]. Morrison and Donald F. (1990), Multivariate Statistical Methods, 3rd ed., Mc Graw Hill Inc.
[11]. Otok, B. W. (2010), Machine Learning Model Development Food Security through the Establishment of the Zone Season, ITS, Surabaya.

Biosorption of Lead(II) And Cadmium(II) by Biomass of *Azolla Microphylla*-Silica in Continuous System

Danar Purwonugroho[1], Sri Wardhani[2], Darjito[3], Deasi Ari Shandi [4],Descaniati Chan [5]

[1,2,3,4,5] Department of Chemistry Faculty of Mathematics and Natural Sciences, Brawijaya University, Malang, Indonesia (danar@ub.ac.id)

Abstract

The ability of *Azolla microphylla* biomass immobilized in polysilicate for removal of lead(II) and cadmium(II) from aqueous solution was investigated. Batch experiments were performed with oven-dried and ground (120-150 mesh) of *Azolla microphylla* biomass to evaluate optimum pH of metal ion binding. It was found that optimum conditions were pH 4 for lead(II) binding and pH 5 for cadmium(II) binding. Column experiments were performed to study the binding of lead(II) and cadmium(II) to silica-imobilized *Azolla microphylla* biomass under flow conditions. For column studies, 720 mL (120 bed volumes) of 5 mg/L metal ion solution at optimum pH were passed through *Azolla* pack columns at the flow rate of 2 mL/min. These experiments showed that 99.70 % of lead(II) and 99.53 % of cadmium(II) were bound by biomass in the column. In order to recover metal ions from the column, 15 bed volumes of 0.1 M HCl solution were passed through the column at the flow rates of 2 mL/min. and 1 mL/min. These experiments showed that 89.30 % of lead(II) and 75.83 % of cadmium(II) were recovered by the eluent at flow rate of 1 mL/min.. The results from these studies will be useful for a novel phytofiltration technology to remove and recover lead(II) and cadmium(II) from aqueous solution.

Keywords*: biosorption, column, lead(II), cadmium(II), Azolla microphylla.*

1. Introduction

The presence of heavy metals in the water environment is a major concern due to their toxic effects since they cause severe health problems to animals and human beings [1]. Lead (II) accumulates mainly in bones, brain, kidney,and muscles and may cause many serious disorders like anemia, kidney diseases, nervous disorders, and sickness even death [2]. Cadmium and cadmium compounds are especially dangerous and highly toxic. Cadmium toxicity contributes to a large number of health conditions, including the major killer diseases such as heart disease, cancer, and diabetes [1]. It is, therefore, essential to remove heavy metal ions including lead(II) and cadmium(II) from wastewater before disposal.

The different methods are used for the removal of heavy metals as important contaminants in water and wastewater. Current methodologies used in the removal of toxic contaminants found in both water and wastewater include procedures such as chemical precipitation, membrane filtration, ion exchange, carbon adsorption, and coprecipitation/adsorption [3]. However, because of the high cost of these methods, development of a less cost but effective remediation system is necessary.

Biosorption is a relatively new process that has proven very promising in the removal of contaminants from aqueous effluents [3]. Biosorbents might be classified according to the following sources: bacteria, algae, fungi, plant-derived, and animal-derived. Dead biomass offers several advantages over living organisms since the former does not need maintenance and is not affected by high concentrations of pollutants [3]. Celullar components including carboxyl, hydroxyl, sulfate, sulfhydryl, phosphate, amino, amide, imine, and imidazol moieties have metal binding properties [3].

Azolla has been shown to be able to effectively adsorb lead(II), cadmium(II), copper(II), and zinc(II) from solutions [4] and chromium(III) from aqueous solution in continuous system [5]. The objective of the research was to investigate the ability of *Azolla microphylla* biomass immobilized in polysilicate for removal of lead(II) and cadmium(II) from aqueous solution under flow conditions.

2. Materials and Methods

Preparation of Biomass

Oven-dry and ground (120-150 mesh) of *Azolla microphylla* biomass were washed twice with 0.01 M HCl to remove any debris or soluble

biomolecules that might interact with metal ions, followed by washing with deionized water to remove chloride and subsequently dried in an oven at 60ºC.

pH Profile Studies for Metal Ions Binding

Batch experiment was performed for the pH studies. Twenty five milliliter of 100 ppm metal ion at certain pH and 0.10 mg biomass were added to 100 mL conical flask and shaked for 60 minutes. The suspensions were centrifuged at 3,000 rpm for 5 minutes, and the supernatants were collected in the sample bottle. The concentration of metal ion in the supernatants was analyzed by AAS (atomic absorption spectrophotometer).

Immobilization of Azolla Biomass

A 75 mL of 5% sulfuric acid (H_2SO_4) was mixed with 6% sodium silicate (Na_2SiO_3) solution to raise the pH to 2.0. At pH 2.0, the 5 grams of biomass (120-150 mesh) was added to the silica solution and allowed to stir for 15 minutes. The pH was then raised slowly by the addiition of 6% Na_2SiO_3 to reach a final pH of 7.0. The polymer gel was washed with water enough times so that by the addition of two drops of barium chloride ($BaCl_2$), there was no white precipitate forming. $BaCl_2$ was used to indicate whether the sulfates had been removed. The polymer gel with the immobilized biomass was dried overnight at 60^{o}C and then ground by mortar and pestle and sieved to pass 20-40 mesh size.

Column Experiments

One bed volume equals the volume of immobilized biomass inside the column. A 6 ml of the immobilized alfalfa was used in the column. The column was washed with HCl solution (optimal binding pH) and the effluent pH was checked to ensure that the column was at the optimal binding pH. A flow rate of 2 ml per minute was used to pass 120 bed volumes of 5.0 ppm metal ion (Pb^{2+} or Cd^{2+}) solution in HCl solution at the optimal binding pH. Each bed volume was collected and analyzed by AAS.

Recovery of Metal Ions

To remove the bound metal ion, 15 bed volumes of 0.01 M HCl were passed through the column at a flow rate of 2 ml per minute and 1 mL per minutes. Each bed volume was collected and analyzed by AAS.

3. Results and Discussion

The pH profile studies were performed at various pH of 2-5 for lead(II) and pH of 2-6 for cadmium(II). Studies at pH higher than 6 was not conducted due to precipitation of the metals. Figure 1 shows the binding of lead(II) and cadmium(II) to *Azolla* biomass as a fuction of pH. Binding of every metal ion by *Azolla* biomass was affected by pH of solution. It can be observed that as the pH was increased, the amount of metal bound also increased until maximum binding, and remained constant or slightly decreased at pH higher than the optimum condition. Optimum pH for lead(II) binding was pH 4. On the other hand, optimum pH for cadmium(II) binding was pH 5.

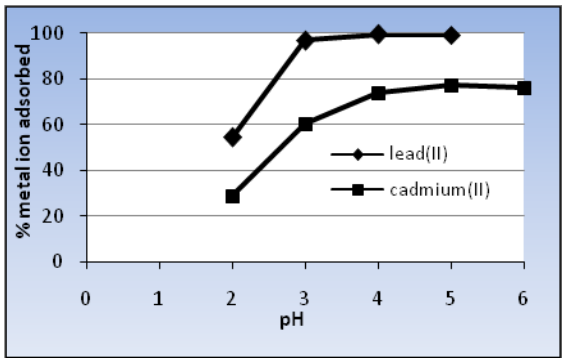

Figure 1. Effects of pH on metal ion binding

The trend in pH-dependent binding suggests that carboxyl groups may play a role in the metal ion binding by the biomass. The ionization constants (pK"s) for various carboxyl groups have been reported to be around 3-4 [6]. Free carboxyls groups are protonated at pHs lower than 3 and reduce any metal binding. At pHs higher than 4, the carboxyl groups are deprotonated and attract positively charge metal ion. Metal ions bind to the carboxyl groups through an ion exchange-type mechanism [3]. It is, therefore, if carboxyl groups do play a role in the binding of metal ion, lowering the pH would cause the metal ions to be released back into solution. It means that metal ions bound can be recovered from the biomass. This is one of the advantages of biosorption utilizing plant biomass.

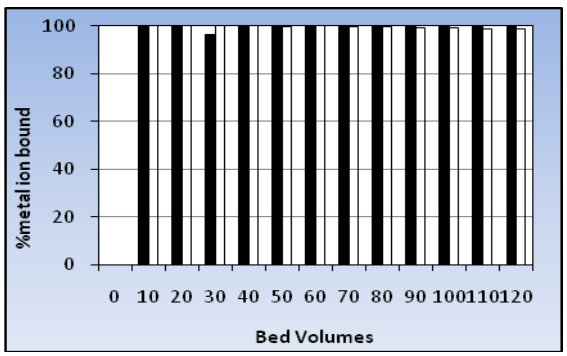

Figure 2. Metal ions absorbed by *Azolla* biomass-silica in the column (■ lead(II), □ cadmium(II))

Column experiments were performed in order to evaluate the ability of *Azolla* biomass to bind lead(II) and cadmium(II) in flow system. Before used, biomass of *Azolla* was immobilized in polysilicate matrix. One bed volume of *Azolla* biomass-silica (20-40 mesh) was packed in the column. Figure 2 shows % metal ions bound by biomass after 720 mL of 5 mg/L metal ion passed through the column at flow rate of 2 mL/min. Figure 2 also shows that 99.70 % (3.59 mg) of lead(II) were bound by biomass in the column and 99.53 % (3.57 mg) of cadmium(II) were bound by biomass in the column.

Effects of flow rate of eluent on the recovery of metal ions are presented in Figure 3 for lead(II) and Figure 4 for cadmium(II). Recovery of metal ions was significantly influenced by the flow rate of eluent. Fifteen bed volumes of 0.1 M HCl solution at flow rate of 2 mL/min recovered 41.21 % of lead(II) and 5.32 % of cadmium(II). In addition, 15 bed volumes of 0.1 M HCl at flow rate of 1 mL/min could recovered 89.30 % of lead(II) and 75.83 % of cadmium(II).

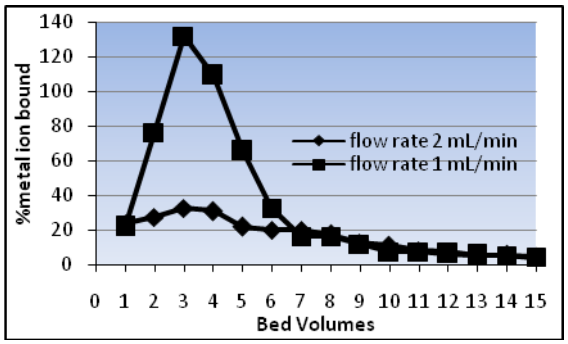

Figure 3. Effect of flow rate of eluent on lead(II) recovery

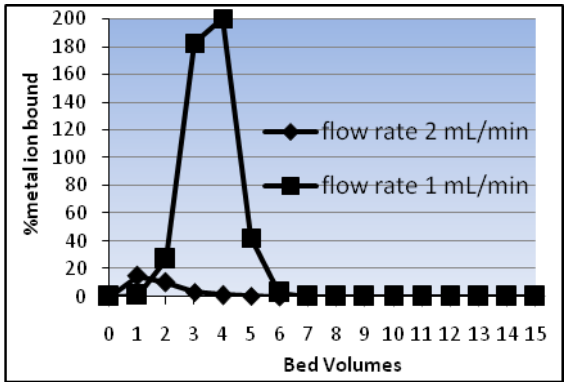

Figure 4. Effect of flow rate of eluent on cadmium(II) recovery

4. Conclusion

Batch pH profile experiments showed that the optimum pHs of metal ion binding were pH 4 for lead(II) and pH 5 for cadmium(II). Almost 100 % of metal ions in 720 mL of 5 ppm metal ions solutions were bound by biomass in the column. Solution of 0.1 M HCl at flow rate of 1 mL/min could recovered 89.30 % of lead(II) and 75.83 % of cadmium(II).

5. Acknowledgements

The authors thank to Dept. of Chemistry, Faculty of Science, University of Brawijaya for financing this paper in ICBS 2011.

6. References

[1]. El-Sayed, G.O., H.A. Dessouki, and S.S. Ibrahim (2010), Biosorption of Ni(II) and Cd(II) Ions from Aqueous Solutions onto Rice Straw, *Chemical Sciences Journal*, Volume 2010: CSJ-9, pp.1-11.

[2]. Chua, L.W.H., K.H. Lam and S.P. Bi (1999), A comparative investigation on the adsorption of lead (II) by filamentous fungal biomass. Chemosphere, 39: 2723-2736.

[3]. Gardea-Torresdey, J.L., G. de la Rosa, and J.R. Peralta-Videa (2004), Use of phytofiltration technologies in the removal of heavy metals: A review, *Pure Appl. Chem*., Vol. 76, No. 4, pp.801-813.

[4]. Ganji, M.T., M. Khosravi, and R. Rakhshaee (2005), Biosorption of Pb, Cd, Cu, and Zn from the wastewater by treated *Azolla filiculoides* with $H_2O_2/MgCl_2$, *International Journal of Environmental Science & Technology*, Vol. 1, No. 4, pp. 265-271.

[5]. Purwonugroho, D., S. Wardhani, and U. Andayani, (2007), Separation of chromium(III) from aqueous media using ion exchanger of *Azolla microphylla* immobilized in polysilicate matrix, *Natural*, Vol. 11 (3), MIPA, Brawijaya University.

[6]. Gardea-Torresdey, J.L., K.J. Tiemann, J.H. Gonzalez, J.A. Jenning, and M.S. Towsend (1997), Ability of Silica-Immobilized *Medicago sativa* (Alfalfa) to Remove Copper Ions from Solution, *J. of Hazardous Materials*, 48, pp. 181-190.

Variation Shape and Color of Gland from Genus *Orophea* (Annonaceae) in Purwodadi Botanical Garden

Dewi Ayu Lestari

Purwodadi Botanical Garden, Indonesian Institute of Sciences, Indonesia (chunyang_dee@yahoo.co.id)

Abstract

Orophea is included in groups of Miliusa, family of Annonaceae, and order of Magnoliales. The numbers of Orophea species in the world are 66 species, in which two of them are exist at the Purwodadi Botanical Garden, which are Orophea enneandra Blume and Orophea hexandra Blume. Both of species is a collection of plant exploration results from East Java and Maluku. The Orophea in Purwodadi Botanical Garden has variation of shape and color of gland. The purpose of this study was to investigate a variation shape and color of gland from genus Orophea in Purwodadi Botanical Garden. The method used was observations of the flower and fruit genus Orophea to know its distinctive variations gland. The observation result showed that the gland of Orophea enneandra Blume has varied both the shape (rounded up to the line) and colors (yellow, pink, pink to purple), while Orophea hexandra Blume has no gland. The number of Orophea species in the Purwodadi Botanical Gardens only 3.03% of the total number of Orophea species in the world.

Keywords: *Orophea, species, gland, Purwodadi Botanical Garden.*

1. Introduction

Orophea is one genus of the groups Miliusa [1], family Annonaceae are included in the order Magnoliales. Annonaceae is a large family of mainly tropical trees and shrubs, some of which are cultivated for their large and edible fruit. The tropical Annonaceae, have diverged into about 130 genera and 2.300 species [2-3]. Habits of *Orophea* have a small tree or shrub with gray blackish bark. Leaves alternate, simple, entire, without stipules and flat blade. The flowers are fragrant, in terminal or axils inflorescence. The sepals are 3, free, partially connate at the base, or wholly connate; unequal in size. The petals are usually 6 or in 2 whorls of 3, equal or variable in size. A reduction in the number of stamens in staminodia in several genus of *Orophea* to 15, as follow 3.6.9 and 12 [1,2,4]. Carpels moniliform. Single fruit, fleshy and contain 1-4 seeds. Young green beans, then turns red and becomes brown when old. Shape of like chilies [5].

The number of *Orophea* species in the world are 66 species, spread over forest areas of tropical and sub tropical [6]. There are two species of *Orophea* grown as plants collection in Purwodadi Botanical Garden, whereas one of the ex-situ conservation institute. Namely are *Orophea enneandra* Blume and *Orophea hexandra* Blume. Both species are derived from the exploration flora in East Java and Maluku; Buru Island [7]. The interesting things about these two species are morphological of *Orophea*, especially in flower. There are some differences in shape and color variations gland. Gland is an organ-like rash that appears on the petiole or the leaf blade. Another sense of the gland is an appendage, protuberance or other structure or only with secretes sticky substances [8]. Existence of glands in a plant can be used as one character of the plant identification [9]. Therefore it needs to do research on the variety of shapes and colors gland genus *Orophea* in Purwodadi Botanical Garden, for the benefit of the activities of plant identification.

1. Experimental Details

The study was conducted in June until December 2010 on the Annonaceae collection in Purwodadi Botanical Garden, especially genus *Orophea* in vak XVIII.C, XVIII.D and XVIII.E. Observations made on *Orophea* collection of flowering and fruiting.

Tools and materials used are *Orophea* collection of flowering and fruiting, ruler, stationery, magnifying glass, digital camera and literature as a supporting element.

The method used was to make observations on the flower and fruit *Orophea*. Were photographed with a digital camera, and then measured with a ruler and note the appearance of morphologic observations as

follow shape, its color and gland with magnifying glass. This is because the distinguishing morphological features are of interest to the genus *Orophea* is existence gland as well as shape and color. Results of the observations identified according to Flora of Java [10].

2. Result and Discussion

The species of *Orophea* in Purwodadi Botanical Garden are two species, as follow *Orophea enneandra* Blume and *Orophea hexandra* Blume. Full details on both these species will be described in the following Table 1.

Table 1 show that there are differences in habits between *O. enneandra* and *O. hexandra*. *O. enneandra* have habits of shrub while *O. hexandra* have habits of tree. According to [10], habits of *O. enneandra* is shrubs, while *O. hexandra* can trees or shrubs. Origin of both species *Orophea* is a region of East Java and Maluku; Buru Island. Distribution of the spread of these *Orophea* is Malesia region, but for *O. enneandra* and *O. hexandra* exist only on the island of Java [2,10]. *Orophea* morphology of both species are described in Table 2.

Based on Table 2 it can be seen that the morphology difference between *O. enneandra* and *O. hexandra* located on leaves, flowers and fruit. Leaf tip of *O. enneandra* aristulate and leaf base asymmetrical, entire; whereas leaf tip of *O. hexandra* retuse to acute, base of leaf-shaped pins and entire. In addition, the upper and lower leaf surfaces *O. hexandra* fluffy. The emergence of young leaves of *O. hexandra* simultaneously as proposed by [11] compared to young leaves of *O. enneandra* that emerged after the plants bear fruit.

Orophea flowers shaped like Chinese latterns [11], the crown or coupling. Based on observation results show that flower *O. enneandra* smelled like jasmine or ylang-ylang. So there is a possibility that interest *O. enneandra* can be used as an aromatherapy oil-producing material such as ylang-ylang essential oils that have been made [12]. But have not done further research about the content of volatile compounds in the interest. Studies on chemical constituents in *O. enneandra* have been done by [13] concerning anti-fungal compounds and anti-oxidants from leaf extracts *O. enneandra*.

Interesting distinction between *O. enneandra* and *O. hexandra* is the presence or absence of glands in the inner petal of flowers. At the inner petal of *O. enneandra* have gland, is not the case with *O. hexandra*. The variation of shape and color of the gland is of interest to be studied (Figure 1). Inner petal in *Orophea* joined, while the outer petal is free. This is an interest character of the genus *Orophea* in plant identification.

Figure 1 shows that there is a fairly interesting differences among *O. enneandra* and *O. hexandra,* both among species and intra species. It is apparent that *O. hexandra* do not the gland. While *O. enneandra* have a gland whose shape varies from round to line. The color of this gland also varied from pink (figure 1b and 1d), yellow (figure 1c) and pink to purple (figure 1a). Inner petal of *O. hexandra* flowers that joined and do not have the gland has a variety of forms. In XVIII.D.4 collection (figure 1e) have a slightly rounded shape, thick with yellow-green color. Collection of XVIII.E.8-a have inner petal shape in a longer, transparent and colored peach. There is a tendency that *O. enneandra* in XVIII.D.4 collection is another species because the color differences are quite striking. The tip of the inner petal is also more blunt. But need further research to prove the statement.

While the distinguishing characteristics of the *Orophea* fruit between species are the surface and the tip of the fruit. Fruits surface of *O. enneandra* is glabrous but has no indumentum like *O. hexandra*, although rarely. This tip of fruit also more blunt than *O. hexandra* that a larger fruit size.

The species of *Orophea* in the Purwodadi Botanical Garden distinguished by presence or absence of glands that differ in color or shape. But the diversity of *Orophea* species in the Purwodadi Botanical Garden tends to be slightly (3.03%) when compared with the number of *Orophea* species that spread in the world. Therefore it is necessary to explore the flora, especially genus *Orophea* in Indonesia. So that conservations areas can continue to be done, both in-situ and ex-situ.

3. Conclusion

Purwodadi Botanical Garden has only 2 species of *Orophea*, as follow *Orophea enneandra* Blume and *Orophea hexandra* Blume. These species is a collection of plant exploration results from East Java and Maluku. *O. enneandra* Blume has a gland which varies in shape (rounded up to the line) and color (yellow, pink, pink to purple), while *O. hexandra* Blume did not have the gland. The number of *Orophea* species in the Purwodadi Botanical Garden only 3.03% of the total number of *Orophea* species in the world.

4. Acknowledgements

We wish to acknowledge Dwi Narko and Nursali for fully assistance in this research.

5. References

[1]. Kubitzki, K., J.G. Rohwer and V. Bittrich (1993), *The Families and Genera of Vascular Plants: Flowering Plants – Dicotyledons. Magnoliid, Hamamelid and Caryophyllid Families*, Volume II, Springer, Germany.

[2]. Heywood, V.H., R.K. Brummitt, A. Culham and O. Seberg (1978), *Flowering Plant Families of The World*, Firefly Books Ltd, Ontario, Canada.

[3]. Okada, H. (1990), Reproductive Biology of Polyalthia littoralis (Annonaceae), *Pl. Syst. Evol.*, 170, 237-245.

[4]. van Balgooy, M.M.J. (1998), *Malesian Seed Plants: Portraits of Tree Families*, Rijksherbarium/ Hortus Botanicalus, Leiden.

[5]. Phylodiversity (2010), *Orophea*. http://www.phylodiversity.net, Accessed Agustus 24, 2010.

[6]. Brummitt, R.K. (1992), *Vascular Plant Families and Genera*, The Royal Botanical Gardens, Kew, http://culturesheet.org/annonaceae:orophea, Accessed Agustus 25, 2010.

[7]. Suprapto, A., D. Narko and Kiswojo (2007), *An Alphabetical List of Plant Species Cultivated in The Purwodadi Botanical Garden,* PubDoc Purwodadi Botanical Gardens – Indonesian Institute of Sciences, Pasuruan.

[8]. Harris, J.G. and M. Woolf (1980), *Plant Identification Terminology: An Illustrated Glossary*, Spring Lake Publishing, Utah.

[9]. Sutisna, U., T. Kalima and Purnadjaja (1998), *Guidelines for Introduction of Forest Trees in Indonesia*, PROSEA, Bogor.

[10]. Backer, C.A. and R.C.B. van den Brink Jr, (1963), *Flora of Java (Spermatophytes only)*, Volume I, NVP Noordhoff Groningen, The Netherlands.

[11]. van Steenis, C.G.G.J. (1972), *The Mountain Flora of Java*, E.J. Brill, Leiden, Netherlands.

[12]. Oyen, L.P.A. and N.X. Dung (1999), *Plant Resources of South-East Asia*, No.19, PROSEA Foundation, Bogor.

[13]. Cavin, A., O. Potterat, J.L. Wolfender, K. Hostettmann and W. Dyatmyko, (1998), Use of On-flow LC/H NMR for The Study of an Antioxidant Fraction from Orophea enneandra and Isolation of a Polyacetylene, Lignans, and a Tocopherol Deritative, *J. Nat. Prod.* 61 (12), 1497-1501

Appendixes:

Table 1. The species of *Orophea* in Purwodadi Botanical Garden

No	Species	Habits	Origin	Accession number	Location
1.	*O. enneandra* Blume	Shrub	Meru Betiri, Banyuwangi	P198105274/ Mar.114	XVIII.C.25-a
			Lebak Harjo, Malang	P19821169/ Fac.92	XVIII.C.26
			Tempursari, Lumajang	P19860266/ Ml.139	XVIII.E.3-a
2.	*O. hexandra* Blume	Tree	Maluku; Buru Island	P198502361/ Kis.360	XVIII.D.4
			Banyuwangi	P19860266/ Ml.139	XVIII.E.8-a

Table 2. Distinguishing morphology of *O. enneandra* and *O. hexandra*

No	Distinguishing morphology	*O. enneandra*	*O. hexandra*
1.	Root	Topsy-turvy	Topsy-turvy
2.	Stem	Cylindrical, blackish gray, smooth surface, pepagan in fibrous with fragrant scent.	Cylindrical, blackish gray, smooth surface, pepagan in fibrous with fragrant scent.
3.	Leaves	Singled, alternate, glabrous, pale brown young leaves that emerged after the formation of fruit, 5.6 to 19.5 cm long and 2.9 to 8.8 cm wide, aristulate leaf tip and leaf base asymmetrical, entire.	Singled, alternate, glabrous, young leaves pale and appeared simultaneously, from 2 to 16.5 cm long and 0.8 to 5.6 cm wide, leaf tip retuse to acute, base of leaf-shaped pins, entire. The upper and lower leaf surfaces contain rare indumentums.

4.	Flower	Complete with lids numbered 3, outer petals were 3 and inner petal were 3, joint; stamens of 9, translucent color with yellow pollen and pistil shaped head. 0.15x0.1 cm sepal size with a little yellow indumentums. Outer petal size 0.8x0.4 cm, yellowish, free. Inner petal size 1.2x0.6 cm, yellowish, joined. At the inner petal of the gland there. 0.8-1 cm long flower stalk.	Complete with lids numbered 3, outer petals were 3 and inner petal were 3, joint; stamens of 3, yellowish and capitates stigma. 0.2x0.1 cm sepal size, light green color with a little yellow indumentums. Outer petal size 0.5x0.45 cm, peach to light green, free. Inner petal size 1.2x0.4 cm, yellow, joined. At the inner petal of no gland. 0.5-0.7 cm long flower stalk.
5.	Fruit	Like the pepper fruit. When young green, towards the old red and if the old become brown, withered, wrinkled and then fall. The size of the fruit: 2 to 4.3 x 0.5 to 0.6 cm. Glabrous. The tip of the fruit is blunter than *O. hexandra.* Width is more slender fruit with seed number in 1 piece as much as 1-3 seeds.	Like the pepper fruit. When young green, towards the old red and if the old become brown, withered, wrinkled and then fall. The size of the fruit: 2.1 to 5.4 x 0.5 to 1.2 cm. Glabrous, rare indumentums. The tip of the fruit is more pointed than *O. enneandra* and its width is greater. The number of seeds in a fruit as much as 1-4 seeds.

Figure 1. (top) *O. enneandra* (a) the collection of XVIII.C.25-a, (b) collection of XVIII.C.26, (c) collection of XVIII.E.3a, (d) collection of XVIII.E.3
(bottom) *O. hexandra* (e) collection of XVIII.D.4, (f) collection of XVIII.E.8-a

Single Nucleotide Polymorphism Identification of Porang in East Java

Estri Laras Arumingtyas

Department of Biology, Faculty of Science, University of Brawijaya, Malang
E-mail: laras@ub.ac.id

Abstract

Porang (Amorphophallus muelleri Blume) belong to the genus of Amorphophallus which is is a large genus of some 170 tropical and subtropical tuberous herbaceous plants from the Arum family (Araceae). Twenty seven species of Amorphophallus are found in Indonesia. Amorphophallus species are valued for its tuber glucomanan among the species found in Indonesia; A.muelleri Blume is a species with the highest content of glucomannan. Many variants of this species were grown in different places at East Java. Based on morphological characters it is difficult to differentiate between them. To identify whether they were similar variety, a Single Nucleotide Polymorphism (SNP) of non-coding sequence, intergenic region in the chloroplast DNA, trnL-F, was studied using PCR technique.. Primers used were trnL-F r 5'-CGA AAT CGG TAG ACG CTA CG-3' and trnL-F f 5'- ATT TGA ACT GGT GAC ACG AG-3' The program used was pre heating at 96ºC for 2 minutes, followed by 36 cycles of denaturation at 96°C for 30 seconds, primer annealing at 56ºC for 30 seconds and elongation at 72ºC for 120 seconds, and the last extention at 72ºC for 7 minutes. The PCR resulted in a single band of about 500 bp. Sequencing result show that all the 14 samples from 5 places at East Java had exactly similar sequence that suggested that all sample were similar varieties. Alignment with trnL of Amorphophallus muelleri Blume from NCBI, show that the samples were similar to the species Amorphophallus muelleri Blume.

Keywords: *Amorphophallus muelleri Blume, polymorphism, SNP, glucomannan.*

Logging Impact to Diversity of Epiphytes at Malinau Research Forest (MRF)-CIFOR Malinau Regency

Ismail [1], Akas Pinaringan Sujalu [2]

[1,2] Forest Management, Faculty of Agriculture, University of 17 Agustus 1945, Samarinda, East Kalimantan, Indonesia (pinaringan_b@yahoo.co.id)

Abstract

The aim from this research is to find out impact of the 6 years after logging to the various kinds of epiphytes and its porophyte in the climax forest to the broadness of 6 hectares and the log over area to the broadness of 12 hectares at Malinau Research Forest (MRF-CIFOR) the village of Seturan – district of Long Loreh, the regency of Malinau. In the climax forest it could be found 8009 or 11.5 individual epiphytes of each porophytes, in log over area being found 4671 or 6,7 individual epiphytes of each porophytes. Bring about of degradation sum of individual 71.1% and species 18.1%. The porophyte in the climax forest to the amount of 696 trees are consisting of 179 species in 85 genera of 39 families, with 417 trees (59.9%) each of them has a diameter runs 36-67 cm, whereas in the log over area being found 610 trees consisting of 162 species in 101 genera of 42 families with 484 trees (79.9%) each of them has got a diameter runs from 20-51 cm.

***Keywords**: climax forest, log over area, microclimate, epiphyte.*

1. Introduction

Influence of plants in a community became very important with the increasingly large size of plants and increasing numbers of plants. In the early growth phase, plants, micro-climate is only influenced by it, but then gradually affected by meso-and macro-climate. Plants, either individual or in a group, are seen as something complex and sensitive to changes in climate elements [1].

Conditions and the availability of the elements of a favorable climate are very important for the regeneration and establishment of forest formations. Conversely canopy closure condition of an expanse of forest stands will affect the fluctuation of the elements of microclimate, so that every form of life in the forest ecosystem components including plants have different abilities in terms of meeting needs for environmental conditions including light, humidity, air temperature and climate elements other. Therefore, differences in the fulfillment of the necessities of life can form a community of plants that have certain characteristics [2].

Forests and climate are two components that is related both macro and especially micro. Changes in any one of these components are directly or indirectly affect the other component [2]. Vegetation that grows in rain forests to produce micro-climate which is three dimensional and very complex, in this collection significantly umbrella canopy formed naturally produces micro-climatic conditions under the canopy were significantly different compared with the micro-climate outside the forest and especially in open land. Most micro-climatic conditions are very different types of rain forests and varied vertically from the top of the canopy to the forest floor, and horizontally from one location to another in an "umbrella" of forest canopies [3].

2. Experimental Detail

Research Areas

The details are described by Machfudh and Kartawinata [4], as follows:

1. Location

The experiment was conducted at the climax forest and logged-over forest at the Forest Research Station Bulungan Research Forest (BRF) - Center for International Forestry Research (CIFOR), village-subdistrict Seturan Long Loreh in Malinau (180 km from the town of Malinau). Size total acreage of Forest Research Bulungan (BRF-CIFOR) is approximately 321 000 hectares. The observation in 1997 to use the Landsat TM-5 showed a wet tropical forest in the area of Research Station Forest-CIFOR BRF Seturan consists of climax forest (97.84%), secondary forest (2:12%) and the open land (0.04%).

2. Topography

Topographic conditions of the area of Forest Research Station BRF - CIFOR Malinau Seturan-hilly, located at an altitude between 100-300 m above sea level, with slopes varying between 10% - 70%. While 40% of the total BRF

area has slopes between 25-40% (including in Seturan), while areas with greater slope (steep to very steep) lots located on the west and southwest. Based on data obtained by using the Digital Elevation Model (DEM) from satellite Radarsat can be obtained information that the 84.24% area of BRF is hilly area with altitude of more than 300 m above sea level. An 11.43% is an area with undulating topography, with little there is a flat area.

3. Climate

Climate data have been obtained from PT Inhutani II Unit Malinau show that the forest areas managed by the BRF-CIFOR and its surroundings are included in the precipitation type A on the basis of Schmidt and Fergusson [5] with dry periods of less than two months and wet months over nine months, the average rainfall was recorded around 3790 annual mm/year.

Permanent sample plots at the Forest Research Area BRF Seturan CIFOR Malinau [4]

Dipterocarpaceae forest Lowland is a major extensive forest type contained in the BRF, very rich with trees that have a 35-40 m tall, dominated by trees with ≥ 10 cm a diameter tribes, particularly Meranti (*Shorea* sp.), Keruing (*Dipterocarpus* sp.) and Merawan (*Hopea* sp.). *Agathis borneensis*, are commonly found growing in forests with sandy soils in the BRF area, apart from that are commonly found in species of Fabaceae, especially *Koompassia excelsa*, or called "Bengeris" or "honey tree" by local residents.

Number of permanent sample plots in the plot (PSP) in the BRF-CIFOR totaling 24 plots, each measuring 100m x 100m (1 hectare), and the whole is a mixed forest Dipterocarpeceae. PSP location is located approximately 30 km east of Forest Research station BRF-CIFOR.

3. Result and Discussion

Microclimate Forest

Observations of climate elements using Data Logger that records every 5 minutes automatic, to know his condition at the climax forests and logged-over forests, in locations that are still often found epiphytic. The observation is presented in Figure 1 and 2 (Appendixes).

Condition of the elements vertically on the microclimate of forest stands or tree has been described by Sujalu (1999) who quoted from Walsh (1952) and Geiger (1959) [3,6] that the micro-climate conditions most of the rain forest type is very different and very varied vertically from the top canopy to the forest floor, and horizontally from one location to another within a forest canopy umbrella. While in the woods differs between the various sizes hiatus, between the forest growing and forest climax. In the rain forest, the intensity of light reaching the forest floor is very low compared to the peak (above) canopies. The maximum air temperature and the average is also lower in the forest floor with air humidity (RH) is always higher than in the forest canopies.

According to Daniel [7], quoting from Larcher (1975), the reduction of the number of transmissions (interception) of light through the forest canopy depends on canopy types, shapes and canopy strata, and the homogeneity of canopies. Because of the high intensity of light available at different strata within a forest stand is very influential on the size of species dominance, diversity of vegetation, canopy class differentiation, the ratio of live crown and crown overall dimensions. So, if the requirements of the lighting needs of plants will be known, then it can be controlled stand structure and productivity, regeneration type, etc.

Conditions elements in a vertical micro-climate are very determine the diversity of other life forms found on a tree. In a forest stand type formation, composition and diversity of epiphytes is different for each different height in a host tree. Composition and vertical distribution of epiphytic vegetation is primarily determined by the variability microhabitat while its characteristics are determined by the humidity and lighting under the canopy [8].

Table 2 shows the diversity of epiphytes in the forest climax and the LOA. Mean while, Table 1 shows the number of individuals and the number of epiphytic species that does not always follow the changes in the levels of micro-climatic conditions of the same. Changes in air temperature and light intensity on a daily average at each show the lower strata of the canopy to the base of the tree turned out to produce the conditions change in the number of epiphytic species from the canopy to the base of trees but is not accompanied by changes in the number of epiphyte individuals / ha. These conditions are not the same as that found in the LOA to those in Table 2. That situation has been explained that the diversity of vegetation on the vertical structure of forest stands or on a tree is formed as regulated by the availability of lighting vertically as well. That situation has been explained that the diversity of vegetation on the vertical structure of forest stands or on a tree is formed as regulated by the availability of lighting vertically as well.

Species composition and community structure of epiphytes is strongly influenced by fluctuations in environmental factors, so that environmental factors are the most important component because it affects the stability of the forest interior environment, especially the components that maintain stable levels of bark wetness and this means a relatively fixed rate sunlight penetration so that the percentage of sunlight blocked by every strata of the forest canopy is also relatively not change [9].

Logging activity can affect the presence of epiphytic through changes in canopy closure and depreciation, which would lead to the condition of the elements of interior forest microclimate changed suddenly and lasts a long time especially penetration of sunlight, temperature and humidity, which will potentially affect abundance and distribution of species [9-11].

4. Conclusion

Air temperature and average daily radiation on canopy is always higher than the other trees; on the contrary there is always the highest air humidity at the base of the tree. Air temperature and radiation conditions of daily average in the LOA is higher than in the climactic forests, instead of air humidity on the daily average is higher than the climactic forest LOA.

Logging activities have caused degradation number of individuals and number of epiphytic species.

5. Acknowledgements

---

6. References

[1]. Marjenah (2000), derived from Tjasjono (1999), …..
[2]. Sujalu, A.P. (1999), Iklim Mikro Hutan. Makalah Pendidikan dan Latihan Perlindungan & Konservasi Hutan Tropis. Kerjasama antara Dirjen PHPA dengan Fakultas Kehutanan Universitas Mulawarman.
[3]. Walsh, R.P.D. (1952), Microclimate and Hydrology. in Richards, P.W. (1952), Tropical Rain Forest an Ecological Study. Cambridge University Press. Cambridge. 187-208
[4]. Machfudh and K. Kartawinata (2001), A Guide To The Bulungan/Malinau Research Forest. Bulungan Research Forest Field Guide Series No. 3. CIFOR-Bogor. 36
[5]. Schmidt and Fergusson (1952), …..
[6]. Geiger, R. (1959), The Climate Near the Ground. Blue Hill Meteorological Observation. Harvard University Press. Cambridge – Massachusetts, 309-316.
[7]. Daniel (1992), ……
[8]. Malcolm (1995), ……
[9]. Sutton, S.L., T.C. Whitmore, and A.C. Chadwick (1983), Tropical Rain Forest: Ecological and Management. Blackwell Scientific Publishing. 11-22.
[10]. Wolf, J.H.D. (1994), Factors Controlling The Distribution of Vascular and Non-Vascular Epiphytics in The Northen Andes. Vegetation 112. 15-28.
[11]. Hazell (1998), ……
[12]. Catling, P.M. and Lefkovitch, L.P. (1989). Association of Vascular Epiphytes In A Guatemala Cloud Forest. Biotropica 21: 35-40.
[13]. Chadwick, A.C., S.L. Sutton and T.C. Whitmore (1983). Tropical Rain Forest; Ecological and Management. Blackwell Scientific Publications. Oxford University, 11–15.
[14]. Claudio, R. (1999), Reduced Impact Logging Effects On Commercial Non-Vascular Pendant Epiphyte Biomass In a Tropical Montane Forest In Costa Rica. Forest Ecology and Management 118, 117-125.
[15]. Griffiths, J. F. (1976), Climate and the Environment; The Atmospheric Impact On Man. The Camelot Press Ltd. Southampton. Great Britain. 316.
[16]. Ingram, S. and Nadkarni, N. (1993). Composition and Distribution of Epiphytic Organic Matter in a Neotropical Cloud Forest, Costarica. Biotropica 25: 370 – 383.
[17]. Mitchell, A. (1989), Between the Trees - The Canopy Community. dalam Silcock, L. 1989. The Rainforest: A celebration. The Living Earth Foundation. 153-157. Cresset Press. London.
[18]. Parker, G. G. (1995), Structure and Microclimate of Forest canopies. In M.D. Lowman and N.M. Nadkarni (Eds.). Forest Canopies. 73 -106. Academic Press. San Diego. California.
[19]. Rosenberg, N.J. (1984), Microclimate: The Ecological Environment. John Willey & Sons. New York. 2-4.
[20]. Walter, H. (1971). Vegetation of the Earth in Relation to Climate and Ecophysiological Condition. The English University Press Ltd. London. 186.

Appendixes

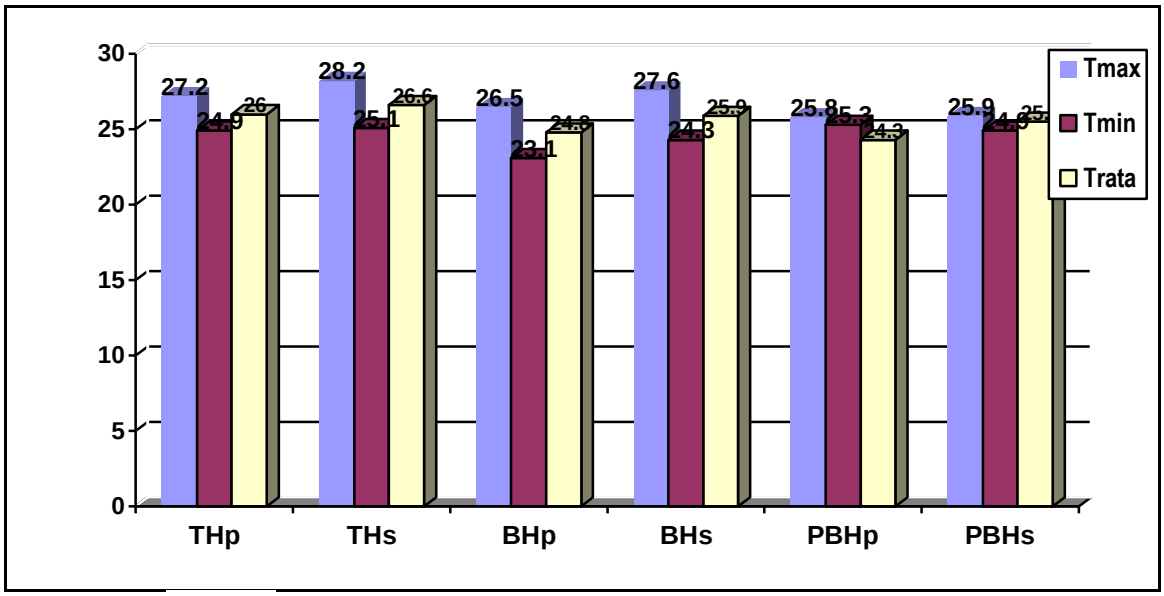

Figure 1. Conditions Temperature (C) at Climax Forest and Secondary Forest

Description: THP: Crown Climax forest; THS; Heading Secondary Forest; BHP: Trunk Climax forest, BHS: Trunk Secondary Forest; PBHs: Jetty Climax forest Trunk; PBHs: Base of Secondary Forest Trunk.

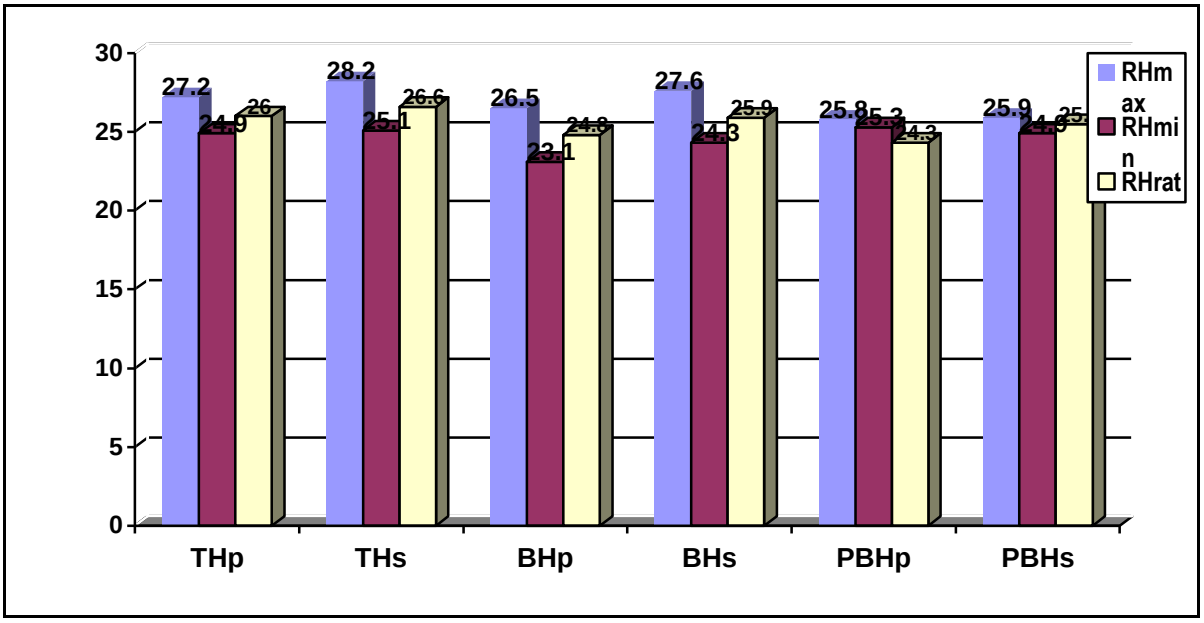

Figure 2. Conditions of Relative Humidity (%) at Primary and Secondary Forest

Description: THP: Crown Climax forest; THS; Heading Secondary Forest; BHP: Trunk Climax forest, BHS: Trunk Secondary Forest; PBHs: Jetty Climax forest Trunk; PBHs: Base of Secondary Forest Trunk

Table 1. Epiphyte Diversity in Forest Forest Climax and logged over areas

No	Vertical Stratum	Climax forest		Log over area	
		Sum of individu	Sum of species	Sum of species	Sum of species
1	Trunk	1042	101	318	93
2	Stem	118	43	17	22
3	Bole of tree	176	27	54	25

Table 2. Fifteen Epiphyte Best Many Types Found in the Subject Tree in Climax forest (CF) and Log over area (LOA)

No	**Species**	**Genera**	**Family**	**Sum Of Individual**	
				CF	**LOA**
1.	*Lycopodium* sp.	*Lycopodium*	Lycopodiaceae	204	169
2.	*Bulbophyllum binnendijkii* J.J.S.	*Bulbophyllum*	Orchidaceae	197	-
3.	*Selliguea lima (*v.A.v.R.) Holtt.	*Selliguea*	Polypodiaceae	178	161
4.	*Drynaria quercifolia* (L.) J.Sim.	*Drynaria*	Polypodiaceae	176	-
5.	*Bulbophyllum beccariu* Rchb.f.	*Bulbophyllum*	Orchidaceae	165	102
6.	*Bulbophyllum gracillum* Rolfe.	*Bulbophyllum*	Orchidaceae	143	-
7	*Pyrrosia angustata* (Sw.) Ching	*Pyrrosia*	Polypodiaceae	141	99
8.	*Bulbophyllum lepidum* (Bl.) J.J.S.	*Bulbophyllum*	Orchidaceae	132	-
9.	*Bromheadia finlaysiniana* (Lindl.) Miq.	*Bromheadia*	Orchidaceae	117	-
10.	*Bulbophyllum vaginatum* (Lindl.) Rchb.	*Bulbophyllum*	Orchidaceae	144	-
11.	*Cimbidium finlaysonium* Lindl.	*Cymbidium*	Orchidaceae	110	-
12.	*Acriopsis javanica* Reinw.	*Acriopsis*	Orchidaceae	108	102
13.	*Sarcanthus subulatus* Rchb.f.	*Sarcanthus*	Orchidaceae	107	-
14.	*Humata repens* (L..fill.) Diels.	*Humata*	Davaliaceae	106	-
15.	*Crypsinopsis wrayi (*Baker) Copel	*Crypsinopsis*	Polypodiaceae	104	88
16.	*Nephrolepis acutifolia* (Desv.) Chrst.	*Nephrolepis*	Nephrolepidaceae	-	176
17.	*Nephrolepis davaloides*	*Nephrolepis*	Nephrolepidaceae	-	169
18.	*Bulbophyllummacranthum* Lindl.	*Bulbophyllum*	Orchidaceae	-	98
19.	*Bulbophyllumpurpurescens* Ted. & B.	*Bulbophyllum*	Orchidaceae	-	89
20.	*Goniophlebium subauriculatum* (Bl.) Presl.	*Goniophlebium*	Polypodiaceae	-	89

The Comparative Air Analysis of the Institute of Chemistry, UP Diliman using Passive Sampler with Activated Charcoal and Commercially Available Adsorbent

Lilibeth dlC. Coo [1], Christian Mark G. Salvador [2], Abegail Z. Rasco [3]

[(1)] Institute of Chemistry, University of the Philippines, Diliman, Quezon City, Philippines (ldlccoo@yahoo.com)
[(2)] Institute of Chemistry, U.P., Diliman, Quezon City, Philippines (Christian_11_lr@yahoo.com)
[(3)] National Science Research Institute, U.P., Diliman, Quezon City, Philippines (azrasco@yahoo.com)

Abstract

Air sampling and analysis play a vital role in the protection of the workers, students, analysts and other people against toxic gases in the environment. This study aims to use inexpensive and locally available activated charcoal as adsorbent of Ultra II Passive Sampler (SKC. INC) and compare it with Tenax TA (SKC, INC), a commercial adsorbent in analyzing the working environment and ambient air of the Institute of Chemistry, UP. The study was divided into two analyses which include the preliminary analysis characterization of the adsorbing property of the adsorbents and the sampling and analysis of the volatile organic compounds (VOCs) present in the air environment of the institute. The target VOCs were methanol, ethanol, acetonitrile, hexane, ethyl acetate, benzene, tetrahydrofuran and toluene. The preliminary analysis was done under a desiccator, with the target VOCs solutions placed at the bottom and the samplers with adsorbents attached underneath the cover of the desiccator in an 8-hr period. The adsorbents were analyzed using Headspace-Gas Chromatography-Flame Ionization Detector (HS-GC-FID). Results showed that activated charcoal was found to be a better adsorbent in the sampling of methanol, hexane and ethanol. Furthermore, exposure study was also carried out in six indentified personnel of the institute wearing the two adsorbents at 8-hr period. Results showed that exposure of these individuals to benzene exceeded the Threshold Limit Value Time weighted average (2.5 ppm) with readings of 3.84 to 146.64 ppm and some readings for toluene (TLV-TWA=50ppm) ranging from 20.31 to 80.18 ppm.

Keywords: *Activated Charcoal, Air Analysis, Headspace-Gas Chromatography.*

1. Introduction

Knowledge of air quality is crucial in the safety and protection of the analysts, laboratory staff and even those people far from the laboratory. Different organizations and institutions such as Occupational Safety and Health Administration (OSHA) and the American Conference of Governmental industrial Hygienists, Inc (ACGIH) and Environmental Protection Agency (USEPA) issued a set of criteria for worker"s exposure to airborne hazardous gases present in the ambient or atmospheric air to prevent complications in health due to these toxic contaminants [1].

However, air sampling and analysis are very expensive due to high cost and unavailability of local suppliers of adsorbents, samplers and equipment for air sampling. Here in the Philippines, most of the equipment and necessary articles for air sampling are all imported from overseas.

Collection of gases and vapors can be done using adsorptive passive and active sampling. Active sampling employs defined air volume sucked using a pump through an adsorbent tube which contains one or more adsorbents while passive sampling uses diffusion method. Among the known adsorbents in passive sampling, activated charcoal is not commercially sold [2]. Activated charcoal, which is mainly used in passive sampling for work place monitoring, has broad pore size distribution, high specific area ($800\text{-}1500 m^2 g^{-1}$) and has a thermal stability of up to 600ºC, thus thermal desorption can be employed to remove the adsorbed gases which would be analyzed by gas chromatography. Such adsorbent is termed as the universal adsorbent due to its adsorption which is based on non-specific and specific interactions and can be used on both polar and non-polar substances [3].

Furthermore, most air analysis employ the use of purge and trap thermal desorption to retrieve the collected vapors in the adsorbents. Only a number of air analyses had used the

headspace technique due to minimal optimized procedures using such technique.

The Institute of Chemistry (IC), University of the Philippines, Diliman had its air analysis done by the Occupational Safety and Health Administration (2006) and results showed presence of negligible amounts of toxic gases in the air environment of the Institute despite evidence from the odorous surroundings. Thus, this experimentation aims to measure the harmful gases, which include methanol, ethyl acetate, ethanol, acetonitrile, tetrahydrofuran, toluene, benzene and hexane, of the different representative sampling locations in the IC using inexpensive and locally available activated charcoal as adsorbent of passive sampler and compare the results with sampling using commercially available adsorbent.

The study is divided into two analyses which include the preliminary analysis characterization of the adsorbing property of activated charcoal and Tenax TA and the sampling and analysis of the volatile organic compounds (VOCs) present in the air environment of the institute using headspace gas chromatography (HS-GC).

2. Experimental Details

Reagents, Materials and Equipments

The standard solvents used in the study were purchased from Merck (methanol, ethanol, ethyl acetate, DMF and benzene), Fischer Scientific (acetonitrile), JT Baker (Hexane) and tetrahydrofuran (EMF Science). Twelve 10 mL standard solutions for each solvent were prepared using DMF as the diluent. The activated charcoal (Fluka), Tenax TA (SKC,Inc), headspace vials and septa were preconditioned by heating at inert atmosphere inside the oven at 250°C for 16 hours before it was packed in Ultra II Passive Sampler (SKC, Inc).

Manual injection of standard solvents was employed to determine the order of elution in the column of the gas chromatograph, GC (Shimadzu, Japan GC-14 B Model Japan) equipped with flame ionization detector with equity^{TM}-5 fused silica capillary column with 0.5-µm thick film (30 m X 0.25 mm I.D). Headspace (HS) auto injector (Shimadzu, Japan AOC-5000 Auto Injector) equipped with syringe (KIT HS Syringe 2.5 mL for Combi PAL, Shimadzu) was used together with 20-mL headspace vials with silicon-teflon septum and magnetic screw cap (Shimadzu). The HS-GC parameters are given in Tables 1 and 2 (Appendixes).

Comparison of the Adsorption Property of Activated Charcoal and Tenax TA

Solutions of the eight target VOCs were placed in the bottom of a desiccator with its silica gel removed. On the other hand, samplers were clipped to each other and attached underneath the cover of the desiccator. After the 8-hour sampling, the samplers were removed from the set-up and immediately returned to the refrigerator to minimize further uptake of vapors. The adsorbents were analyzed using the HS-GC parameters in Tables 1 and 2 (Appendixes).

Air Sampling in the Institute of Chemistry

After the adsorbents were cooled and packed in the Ultra II sampler in the manner prescribed by SKC. Inc [4], the samplers were attached to six identified personnel of the IC at different dates. The sampling period for each individual was set at 8-hours, equivalent to a one working day. The temperature and relative humidity were monitored every hour using the portable electronic barometer. The adsorbents were analyzed using the HS-GC parameters in Tables 1 and 2 (Appendixes).

3. Results and Discussion

Comparison of the Adsorption of Activated Charcoal and Tenax TA

The choice of adsorbent in air sampling and analysis is critical since every adsorbent has its own property. Thus adsorption property, which largely affects air analysis, varies for different compounds. The bar graph (Figure 1) shows the average peak area of three trials of the desorbed eight target VOCs from activated charcoal and Tenax TA using HS-GC. The bar graph reveals that the activated charcoal is a better adsorbent for methanol, ethanol and hexane. Such findings can be supported by the properties of the two adsorbents.

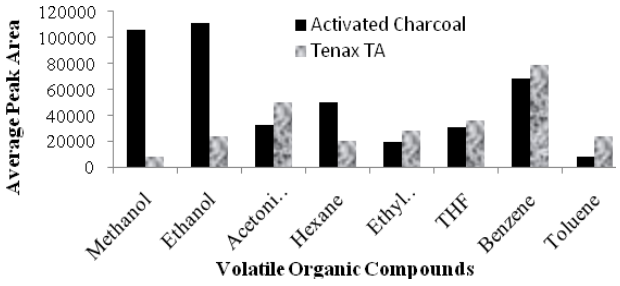

Fig 1.The adsorption effectiveness of Tenax TA and Activated Charcoal against the target VOCs

The sampling range for Tenax TA was between C_7-C_{26} and the three solvents (methanol, ethanol and hexane) were outside the said range

[2]. Only compounds with boiling point range below 60ºC were recorded to be unsuitable compounds for the sampling using Tenax TA. The low response of Tenax TA can be further explained due to its low specific surface area. It has an area of $30m^2/g$ that makes suitable only for sampling of medium to high boiling points compounds, because low boiling compounds will just breakthrough to Tenax TA without being adsorbed. The T-test analysis using Microsoft Excel 2007 Analysis ToolPak showed that there were significant differences in the peak areas obtained for methanol, ethanol, hexane and ethyl acetate in the two adsorbent at 90% significance level. This supports the initial findings that activated charcoal is a better adsorbent for sampling and analysis of methanol, ethanol and hexane.

Air Sampling in the Institute of Chemistry (IC)

Table 3 (Appendixes) shows the equation of the best fit line of the calibration curve, regression coefficient (r^2) and the general standard deviation of the signal response, $S_{y/x.}$ The standard deviation of the signal response was calculated using the LINEST function of the Microsoft Excel 2007. It can be observed that each calibration curve has high linearity coefficient and a wide concentration range suggesting an efficient calibration curve. Also, the obtained equations had a small standard deviation of the signal response suggesting a good method response.

Based from the standard deviation, the signal detection limit (y_{dl}) or the minimum detectable signal can be determined using the equation $y_{dl}=b + 3s_y$ where b is the y-intercept of the equation of the line. Table 4 shows the signal detection limit for each solvent calibration curve. In the sample analysis, no reading for the eight VOCs was obtained from the blank activated charcoal and Tenax TA, thus no correction was done in the reading from the six samples of activated charcoal and Tenax TA. Table 5 shows the data for the exposure analysis of the eight personnel.

It can be observed that among the eight VOCs, ethanol, toluene and benzene were the most prevalent VOCs. The average uptake of the ethanol, toluene and benzene among the six personnel was approximately 74, 30, and 45 ppm. Ethanol is one of the most common solvents used in the laboratory. In most organic synthesis, ethanol is used as the solvent and subsequent distillation is done to remove ethanol. In Natural Products Organic Chemistry, ethanol is used as a mobile phase in different column such as gravity column and TLC. In analytical chemistry, ethanol is commonly used as mobile phase in separation and analysis of analytes in High Performance Liquid Chromatography. It is also used as disinfectant during microbiological assay. Fortunately, the amount of ethanol in the working environment and ambient air of the institute has not yet reached the TLV-TWA (1000 ppm) despite its frequent use in the Institute.

However, the average concentration of toluene and benzene were found to exceed the TLV-TWA, 20 and 2.5 ppm respectively in the air atmosphere of the IC. Half of the personnel who took the exposure study had uptake of toluene beyond the TLV-TWA. Toluene is commonly used as reagent in the laboratory courses offered by the Institute. It was observed that most of the students using such reagent handle it outside the fume hood, thus the large amount of toluene. Among the six personnel, Research Associate 1 (RA1) had the highest uptake of toluene possibly due to diffusion of toluene from the other laboratory rooms and lack of exhaust in the laboratory room where the RA1 stayed.

Among the findings in the concentration of the VOCs, the readings from benzene should be closely noted. All the IC personnel had a benzene uptake beyond the threshold limit value which suggests that benzene is very common in the working environment and ambient air of IC and its concentration is beyond the allowed concentration for exposure of workers. The average uptake of benzene among the personnel was 18 times higher to the TLV-TWA of benzene. Even though it was already banned from its use, benzene is still used as a solvent in some of the experiments in Chemistry courses and other research projects in the laboratories of the institute.

4. Conclusion

In the characterization of the adsorbing property of Tenax TA and activated charcoal, activated charcoal is a good alternative choice as adsorbent to expensive Tenax TA in the sampling of methanol, ethanol and hexane based on the obtained percent deviations of the peak areas of the VOCs. Statistical analysis supports such findings where significant differences in the mean peak area of the three VOCs were calculated at 90% significance level.

The concentrations of the eight VOCs (methanol, ethanol, acetonitrile, benzene, hexane, ethyl acetate, tetrahydrofuran and toluene) in the air environment of the institute were determined using the optimum conditions of the HS-GC and external headspace calibration method. Results

reveal that only benzene and toluene in the exposure studies exceeded the threshold limit value. While the other VOCs are present below the threshold limit, the more toxic benzene and toluene are in higher concentrations, suggesting a poor quality and health hazard air environment inside the buildings of the Institute of Chemistry. It is therefore suggested that the use of benzene and toluene in laboratory classes be minimized or substituted with less harmful solvents.

5. Acknowledgements

We would like to express our deepest gratitude to the National Science Research Institute and Institute of Chemistry, UP Diliman for providing the funds and the necessary equipment and reagents for the completion of this study.

6. References

[1]. Himmelsbach, B. (1982), Toxic Materials in the atmosphere: Sampling and Analysis, ASTM Special Technical Publication, New York.
[2]. Dettmer, K and Engewald, W. (2003), Ambient Air Analysis of Volatile Organic Compounds Using Adsorptive Enrichment, Chromatographia, 57.
[3]. Kettrup, A. (1993), Analyses of hazardous substances in air, Wiley-VCH.
[4]. SKC, INC. SKC SHOPPING. [Online] SKC, 2010. [Cited: January 18, 2010.] http://www.skcshopping. com.

Appendixes

Table 1. Headspace Conditions and Parameters

Headspace conditions			
Cycle:	HS-INJ	Incubator Temp.:	90°C
Syringe:	2.5 mL-HS	Incubator Time:	10 minutes
Sample Volume:	500 µL	Agitation Speed:	500 rpm
Agi. on –time:	10 secs	Fill Speed:	500µL/s
Agi. off-time:	10 secs	Pull-up Delay:	1.0 sec
Syringe Temp:	90°C	Inject to:	GC INJ1
Pre inj del:	500 ms	Post inj del:	500 ms
Inject speed:	1 mL/sec	Syringe Flushing:	00:00:30
GC Runtime:	00:25:00		
Agitator conditions			
Needle Penetr:	12.0 mm	Tray type:	Agitray
Standby Temp:	85.0°C		

Injector (Syringe) conditions			
Actual ID	28	Fill strokes	0
Fill vol:	0 nL	Fill speed:	1 mL/sec
Eject Speed:	1 mL/sec	Standby Temp:	85.0°C
Plunger Pos:	36.0 mm		

Table 2. Gas Chromatography Conditions

Injector Temperature:	225°C
Detector Temperature:	250°C
Column Conditions	
Initial Temperature:	40°C
Initial Time:	6 minutes
Program Rate:	10°C per minute
Final Temperature:	120°C
Final time:	5 minutes
Flow rate:	140 mL/sec

Table 3. Figures of Merit of The Calibration Curve

Solvent	Concentration	Equation of the line	r^2	$S_{y/x}$
Methanol	6-200	y = 173.08(± 6)x + 5380.33(± 500)	0.994	980.20
Ethanol	0-300	y = 234.75(± 9)x + 2061(±1000)	0.992	2505.651
Acetonitrile	10-300	y = 230.9(±4)x + 2309(500)	0.998	1026.281
Ethyl Acetate	0-300	y = 443.6(±6)x + 1693(700)	0.998	1749.861
Hexane	10-200	y = 140.20(±1)x + 17247(±100)	0.999	135.9214
THF	4-300	y = 521.66(±20)x + 14455.39(±3000)	0.990	6323.251
Benzene	0-300	y = 1063.36(± 30)x + 306.94(±4000)	0.992	9578.553
Toluene	0-300	y = 698.01(±10)x + 1661(±1000)	0.997	3466.296

Table 4. The Minimum Detectable Signal of The External Calibration Curve of The Target VOCs

Analyte	y_{dl} (Peak area)
Methanol	6360 ± 500
Ethanol	4568 ± 1000
Acetonitrile	3336 ± 500
Hexane	17383 ±700
Ethyl Acetate	3444 ±100
THF	20779 ±3000
Benzene	9885 ±1000
Toluene	5128 ±1000

Table 5. VOC Concentration (Ppm) During the Exposure Study of the Personnel of The Institute

VOCs	Instructor		Research Associate 1		Office Staff	
	Tenax TA	AC	Tenax TA	AC	Tenax TA	AC
Methanol	**	**	**	36.2775 ± 3	**	**
Ethanol	**	16.03 ± 5	218.29 ±9	64.18 ± 5	**	78.58 ±6
Acetonitrile	5.20± 2	**	18.26± 2	15.65± 2	**	12.28± 2
Hexane	34.28± 2	**	85.54±6	**	87.35± 6	**
Ethyl Acetate	**	**	4.83± 1	**	**	**
THF	**	**	**	**	**	**
Benzene	***54.50 ± 10***	**	***146.64± 20***	**	***129.85± 20***	**
Toluene	***20.31± 1***	**	***80.18± 2***	**	***58.47±2***	**

VOCs	Lab Aide		Maintenance officer		Research Associate 2	
	Tenax TA	AC	Tenax TA	AC	Tenax TA	AC
Methanol	**	**	**	30.89 ±3	**	91.98±4
Ethanol	**	23.33 ± 5	12.15 ±5	40.52 ±5	14.76 ± 5	74.27 ± 6
Acetonitrile	**	**	**	12.22± 2	58.10± 3	11.91± 2
Hexane	**	**	**	**	**	**
Ethyl Acetate	**	**	1.79± 1.67	**	**	**
THF	**	**	**	**	**	**
Benzene	***13.76± 10***	**	***27.03 ± 10***	**	***16.23± 10***	**
Toluene	4.11± 2	**	11.31± 2	**	9.50± 2	**

***** –Not detected***
Red mark – Above TLV-TWA

Synthesis and Characterization of Nickel(II) doped Calcium Tartrate Tetrahydrate ($Ca_xNi_{(1-x)}C_4H_4O_6.4H_2O$) Single Crystals in Metasilicate Gel Using $CaCl_2$ Made of *Achatina fulica* Snail Shell Waste

Mohammad Misbah Khunur [1], Muchamat Chasan Basori [2], Yuniar Ponco Prananto [3], Rachmat Triandi Tjahjanto [4]

[1,2,3,4] Department of Chemistry, Faculty of Science, University of Brawijaya, Malang, Indonesia
(anto_inorgchem@yahoo.com)

Abstract

*Nickel(II) doped calcium tartrate tetrahydrate single crystals can been used as catalysts sources in the synthesis of carbon nanotubes. Synthesis of nickel(II) doped calcium tartrate tetrahydrate ($Ca_xNi_{(1-x)}C_4H_4O_6.4H_2O$) single crystals from snail shell waste (Achatina fulica) in metasilicate gel had been conducted at room temperature based on the optimum condition of calcium tartrate tetrahydrate (CaTT) synthesis. $CaCl_2$ as supernatant was prepared from CaO which previously made by calcinations of the snail shell waste at 1000°C, and then reacted with HCl 1.5 M. The data showed that the optimum condition of CaTT synthesis were obtained at pH of 3.5 and $CaCl_2$ concentration of 0.45 M. Single crystal of CaTT doped Ni(II) were successfully yielded at that condition with efficiency of 79.81%. Characterization of the obtained crystal by AAS showed that the mol ratio of Ca(II):Ni(II) was 0.985:0.015. Moreover, FTIR spectra show tartaric ion specific spectrum, Ca-O and Ni-O stretching at 817.47 and 634.54 cm^{-1}, respectively. Finally, the XRD suggests that the parameter cells of Ni(II) doped CaTT crystal is bigger than those observed in CaTT, which are **a** = 9.201, **b** = 9.579 and **c** = 10.614.*

Keywords: *CaTT, snail shell, silica gel, nickel(II).*

1. Introduction

The population of *Achatina fulica* snail species in Indonesia is high because Indonesia has a tropical climate that strongly supports snails. Certain snail species, i.e. *Achatina fulica*, are cultivated because it has larger size than other types of snails; hence it is very potential to be used as raw material for making kebabs or satays. During this, snail shell waste is generated from the industry and has not been used optimally but as traditional toys only. Calcium that contained in the snail shell is relatively high (around 36.1%) with only small amount of another metal in the shell [1]. Therefore, those shells are also potential to be used as raw material of supernatant in the synthesis of calcium tartrate tetrahydrate (CaTT) single crystals.

Synthesis of CaTT single crystals in metasilicate gel from other industrial waste i.e. sugar cane has also been carried out and gives optimum results at pH of 3.25. Supernatant of $CaCl_2$ were previously prepared from CaC_2O_4 or $CaCO_3$ waste. However, the yields are only around 5.45% [2].

Single crystals of CaTT are known to be piezoelectric. With the addition of another metal (doped), either primary metals or transition metals, single crystals CaTT have better electrical properties [3,4].

Study of CaTT single crystals with the addition of Ni(II) of pure material gives greenish color effects. Ni(II) doped CaTT single crystals have the nature of magnetism and electricity in particular piezoelectric, and the degree of violence are increased so that the crystals are more durable. Previously, Torres *et al*. (2002) succeeded synthesizing single crystals of Ni(II) doped CaTT using the supernatant $CaCl_2$ and $NiCl_2$ in the solution of a mixture of acetic acid and Na-silicate gel formation at pH of 4.5 and $CaCl_2$ 1M [3].

Nickel(II) doped CaTT single crystals has also been used as catalysts sources in the synthesis of carbon nanotubes [5]. Prediction of reaction in the formation of Ni(II) doped CaTT is as follows:

$$Ca^{+2}_{(aq)} + Ni^{+2}_{(aq)} + C_4H_4O_6^{-2}{}_{(aq)} \rightarrow Ca_xNi_{1-x}C_4H_4O_6.4H_2O_{(s)} \quad (1)$$

The use of gel is considered as the most promising technique for growing single crystals of metal tartrate [6] compared with solution saturation method or hydrothermal reaction. This is due to tartrate is partly dissolved in water and easily decomposes before its melting point [4].

2. Experimental Detail

Materials and Instrumentations

Laboratory reagents, which are tartaric acid ($C_4H_6O_6$), sodium metasilicate ($Na_2SiO_4.9H_2O$), HCl, $CaCl_2.2H_2O$, $NiCl_2.6H_2O$; and solvents, i.e. were used without further purification and obtained from standard commercial suppliers. Instrumentations that are used in this research were a high temperature Barnstead Thermolyne and a HERAEUS KR170E Oven, an Orion 420A pH-meter, a Shimadzu FTIR-8601PC, an AA-6200 and Perkin Elmer Analyst 100 AAS, and a Panalytical PHILIPS-XPERT XRD.

Preparation of Supernatant

Firstly, CaO was prepared by calcinating the snail shell waste at 1000°C, and then reacted with HCl 1.5M until all the precipitate was dissolved. The solution was then concentrated and after that, it was directly placed in a cold waterbath in which white solid of $CaCl_2$ was yielded. Next, the supernatant was made by combining $CaCl_2$ with $NiCl_2$ in a 20mL of mixed solution with Ca(II):M(II) mol ratio of 1:0.05; 1:0.10 and 1:0.15.

Synthesis of Ni(II) doped CaTT

Synthesis of Ni(II) doped CaTT was conducted at the optimum gel pH of CaTT synthesis, which was investigated previously in preliminary research. The gel was prepared by reacting 0.5M tartaric acid and 0.5M sodium metasilicate solution. The mixed solution was mantained at pH of 3.5 and placed in a single tube (*h = 20 cm; d = 2-3 cm*) for 10 days until the gel is formed. Next, the supernatant was added slowly via the inner wall onto the tube to avoid the damage of gel surface, then closed with alumunium foil and placed in a tube rack. The reaction was stand at room temperature for 2 and 3 weeks.

3. Result and Discussion

Preparation of Supernatant

Around 35.85 g of CaO was yielded from 70 g of dry powdery snail shell waste. Next, a 36.23 g of $CaCl_2$ hydrate was produced from 23 g of CaO with efficiency of 79.6%. Based on the AAS data, the purity of synthesized $CaCl_2$ was found 82.6%. Based on our previous research, although the impurity of the synthesized $CaCl_2$ hydrate was high, the synthesized $CaCl_2$ are still available to be used without further purification.

Synthesis of Ni(II) doped CaTT

Small crystalline solid was started to grow in 3 days on the gel surface, which is slightly faster than the growth of un-doped CaTT crystals (7 days). The concentration of ions in the supernatan was much higher due to additional ions from Ni(II) salts. Consequently, the diffusion rate was much greater, hence more nucleous formed on the gel surface (crowded) and resulting small crystals. The synthesized crystal between doped and un-doped CaTT are given in Figure 1.

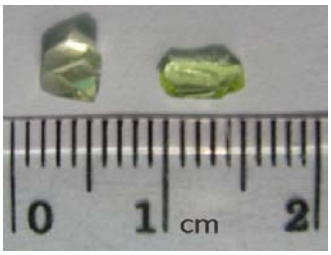

Figure 1. CaTT (left) and Ni(II) doped CaTT (right)

As reported in many journals, higher yield of single crystals was produced if more growth time was applied. The metal ions has more times to diffuse deeper into the gel and forms bigger and better-shaped crystals. More crystals were formed in 3 weeks than in 2 weeks (Table 1). Most of the bigger and better-shaped crystals grew until ±0.5 cm few cm below the gel surface.

Experimental data also shows that higher yield of single crystals was produced if less Ni(II) concentration of supernatant used in the synthesis (Table 1). High concentration of Ni(II) in the supernatant makes the competition between Ni(II) and Ca(II) to react with tartaric ions in the gel is getting higher. Hence, the gel become significantly less condusive for the growth of CaTT. The highest yield of crystals were produced from Ca(II):Ni(II) mol ratio of 1:0.05; followed by 1:0.10 and 1:0.15, respectively.

Table 1. The average yields (g) of synthesized Ni(II) doped CaTT growth in silica gel

Mol ratio of Ca(II):Ni(II)	Yields (g)	
	2 weeks	3 weeks
1:0.05	1.230	1.240
1:0.10	0.350	0.440
1:0.15	0.220	0.300

Characterization of Ni(II) doped CaTT

All synthesized crystal was characterized by FTIR, AAS, and Powder XRD. Mohs test was also conducted to investigate the effect of doped ions toward the crystal"s physical hardness.

AAS data reveales that the synthesized crystals has similar Ca(II):Ni(II) mol ratio of 0.985:0.015 in every Ca(II):Ni(II) mol ratio of supernatant (Table 2). This indicates that at pH of 3.5, the concentration of Ni(II) in the supernatant

solution does not influence the amount of Ni(II) that can doped in CaTT crystal. This ratio was also represent the optimum amount of Ni(II) that can fill the interstitial sites in the CaTT crystal lattice. In other word, the different ratio of Ca(II):Ni(II) in the supernatant only affect the crystal yield.

Table 2. Mol Ratio of Ca(II):Ni(II) in Ni(II) doped CaTT

Mol ratio of Ca(II):Ni(II) in supernatant	Ca (mg)	Ni(II) (mg)	Mol ratio of Ca(II):Ni(II) in crystal
1:0.05	1390.25	31.07	0.985:0.015
1:0.10	1216.75	28.91	0.985:0.015
1:0.15	1127.25	25.91	0.985:0.015

FTIR analysis shows several characteristic peaks of tartaric ions, as presented in Figure 2. This spectrum indicates that the synthesized crystal contains tartaric compounds. In other words, the tartaric does not decompose, as many thermal synthesized type-reaction reported for the case of tartaric compounds. Moreover, there is a change in intensity at 600-700 cm-1, which is corresponding to Ni–O (Table 3). It is likely that the more Ni(II) concentration used in the supernatant, the higher FTIR intensity of synthesized crystal occurred. However, further analysis still needs to be done to gain comprehensive conclusion.

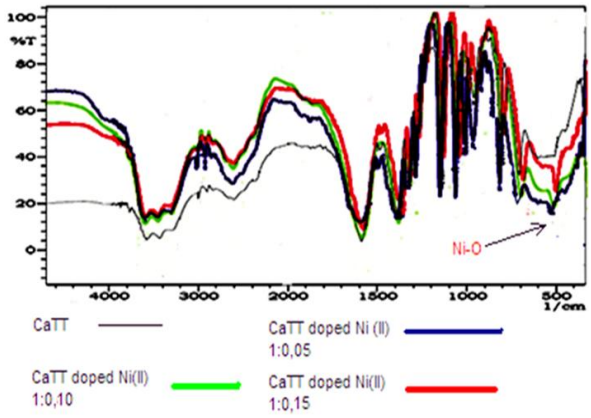

Figure 2. FT-IR of undoped CaTT and Ni(II) doped CaTT

Table 3. The FTIR Vibration of CaTT and Ni(II) doped CaTT

CaTT*	CaTT	Ni(II) doped CaTT	Vibration Type
3261 2881	3292.38 2899.17	3278.76 2896.88	O-H *stretch* C-H *stretch*
1588	1588.47	1590.2	C=O *stretch*
1382	1388.01	1385.76	C-O *symmetric*
1326	1334.04	1331.76	C-O *stretch*
1278	1280.07	1282.57	C-H *bend*
957	963.96	964.34	C-C *stretch*
813	817.47	816.8	Ca-O
-	-	634.54	Ni-O

*Note: * = Shajan and Mahadevan, 2004 [4].*

Furthermore, powder XRD data (Figure 4 and Table 4) shows that Ni(II) doped CaTT has identical crystal system to those observed in undoped CaTT single crystals. Only at this stage, we believe that the doped ions were not change the crystal system of CaTT. However, due to the presence of Ni(II) in the crystal lattice, parameter cell of doped crystal is bigger than those observed in un-doped crystal, which are ***a*** = 9.201, ***b*** = 9.579 and ***c*** = 10.614.

As many literature suggested that in the interstitial sites, Ni(II) ions were coordinated with two oxygen atoms from hydroxyl group of two tartaric ions and four oxygen of water molecule (Figure 3). As a result doped crystal has higher hardness scale (3-4) than un-doped crystal (2-3). This is might be due to more Ni(II) ions filling the interstitial sites and increase the density of the crystal. As a result, the crystal packing of Ni(II) doped CaTT leaving less space between the atoms in the crystal lattices.

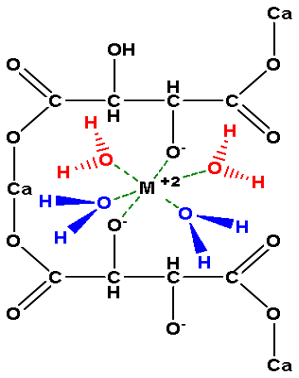

Figure 3. M(II) in the interstitial site of CaTT

4. Conclusion

Single crystal of Ni(II) doped CaTT were successfully yielded in silica gel at pH of 3.5 and $CaCl_2$ concentration of 0.45 M with efficiency of 79.81%. Characterization of the obtained crystal by AAS showed that the mol ratio of Ca(II):Ni(II) was 0.985:0.015. Moreover, FTIR spectra show tartaric ion specific spectrum, Ca-O and Ni-O stretching at 817.47 and 634.54 cm^{-1}, respectively. The XRD also suggests that the parameter cells of Ni(II) doped CaTT crystal is bigger than those observed in un-doped CaTT, which are ***a*** = 9.201, ***b*** = 9.579 and ***c*** = 10.614.

5. Acknowledgment

This research is funded by DPP/SPP 2010 scheme of Faculty of Science UB and all authors are thank to Chemistry Department of UB for facilitating this research.

6. References

[1]. Cresswell, D. C. and Kompiang, P., (2005), Studies on Snail Meal as a Protein Source for Chickens. 1. Chemical, Metabolizable Energy and Feeding Value for Broiler, *Metabolism and Nutrition* 60: 1854-1860.

[2]. Prananto, Y. P., M. M. Khunur and S. Mutrofin, (2007), Sintesis Kristal Tunggal Kalsium Tartrat Tetrahidrat dari Limbah Kalsium Oksalat Nira Tebu dengan Metode Gel Metasilikat, *Natural*, vol. 11 No. 1, October, FMIPA UB, Malang.

[3]. Torres, M. E., T. Lopez, J. Stockel, X. Solans, M. Garcia-Valles, E. Rodriguez-Castellon and C. Gonzalez-Silgo, (2002), Structural Characterization of Doped Calcium Tartrate Tetrahydrate , *J. Solid State Chem*., 491, p.163.

[4]. Shajan, X. S. and C.Mahadevan, (2004), On the Growth of Calcium Tartrate Tetrahydrate Single Crystal, *Bull. Mater. Sci*., Vol. 27, No.4, pp.327 – 331, Indian Academy of Sciences, New Delhi.

[5]. Shlyakova, E. V., Yudanov, N. F., Shubin, Y. V., Yudanova, L. I., Bulusheva, L. G., dan Okotrub, A. V., (2009), Catalytic Synthesis of Carbon Nanotubes Using Ni- and Co-doped Calcium Tartrates, *Carbon*, vol 47, p. 1701 – 1707.

[6]. Henisch, H. K., (1988), *Crystal in Gel and Liesegang Rings*, Cambrige, University Press, Australia.

Appendixes

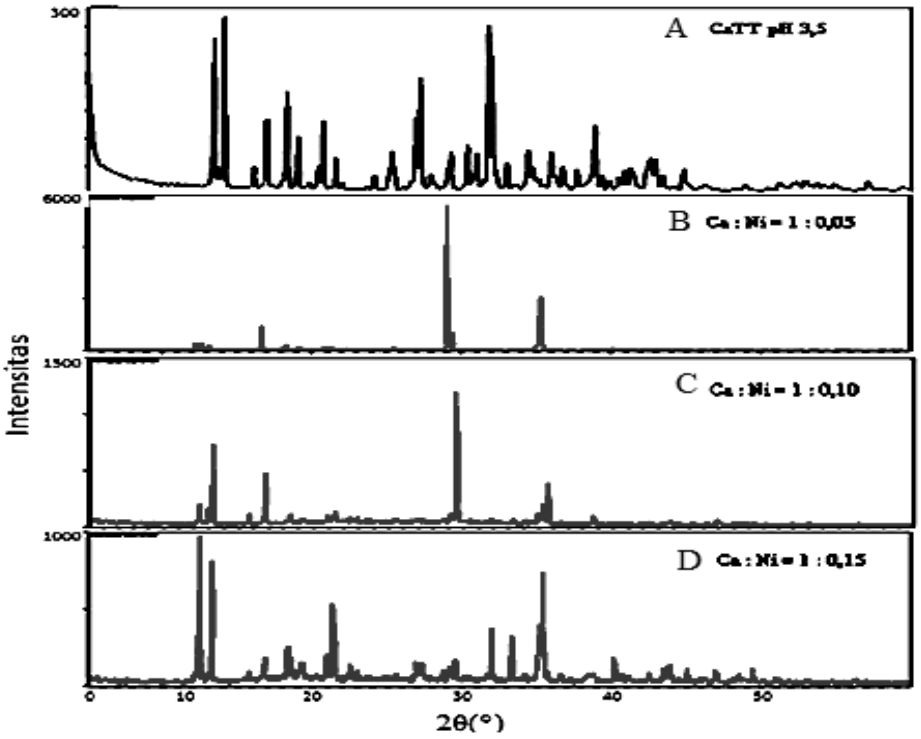

Figure 4. Powder Diffraction of CaTT and Ni(II) doped CaTT

Table 4. The XRD data of CaTT and Ni(II) doped CaTT in different supernatant ratio of Ca(II):Ni(II)

Comparison of 2θ (°) and I / Io of the synthesis and JCPDS									
CaTT (JCPDS)		CaTT		CaTT doped Ni(II) with mol rasio Ca(II):Ni(II)					
				1 : 0.05		1 : 0.10		1 : 0.15	
2θ (°)	I/Io	2θ (°)	I/Io	2θ (°)	I/Io	2θ (°)	I/Io	2θ (°)	I/Io
12.25	60	12.26	88.3	12.37	57.4	12.37	77.36	12.47	100
13.11	100	13.12	100	13.15	43.9	13.29	61.6	13.29	84.02
29.48	40	29.48	65.9	29.55	100	29.51	100	29.57	76.43
35.12	40	35.12	95.6	35.29	36.29	35.61	52.89	35.39	100
35.32	55	35.32	78.2	35.41	37.18	35.63	39.72	35.41	48.16

Synthesis and Characterization of Mangan(II) doped Calcium Tartrate Tetrahydrate ($Ca_xNi_{(1-x)}C_4H_4O_6.4H_2O$) Single Crystals from *Achatina fulica* Snail Shell Waste

Mohammad Misbah Khunur [1], Imam Sakdi [2], Yuniar Ponco Prananto [3], Rachmat Triandi Tjahjanto [4]

[1,2,3,4] Department of Chemistry, Faculty of Science, University of Brawijaya, Malang, Indonesia
(anto_inorgchem@yahoo.com)

Abstract

Snail shell (Achatina fulica) contains high calcium and can be used as supernatant in the single crystal synthesis. The purposes of this research are to synthesis and characterize mangan(II) doped calcium tartrate tetrahydrate ($Ca_xMn_{(1-x)}C_4H_4O_6.4H_2O$) single crystals from snail shell (Achatina fulica) waste in metasilicate gel, and to investigate the influence of growth time and Ca:Mn moles ratio in the supernatant solution toward Mn(II) doped CaTT single crystal properties. The $CaCl_2$ supernatant was prepared from CaO which previously made by calcinating the snail shell waste at 1000°C, and then reacted with HCl 1.5 M. The optimum growth condition of CaTT was firstly determined by varying the pH of the gel (3; 3.5; 4; 4.5 and 5) and the $CaCl_2$ concentration (0.27; 0.36; 0.45; and 0.54 M). Next, synthesis of Mn(II) doped CaTT was conducted in a 20 mL of supernatant with Ca(II):Mn(II) mol ratio of 1:0.05; 1:0.10 and 1:0.15; with growth time of 2 and 3 weeks. The data showed that the optimum conditions of CaTT synthesis were yielded at pH of 3.5 and $CaCl_2$ concentration of 0.45M. Higher yield was produced if more growth time and less Mn(II) concentration in the supernatant was applied in the synthesis. The obtained Mn(II) doped CaTT single crystal have a Ca(II):Mn(II) mol ratio of 0.997:0.003, equal hardness, and identical crystal system to those observed in undoped CaTT single crystals.

Keywords: *CaTT, snail shell, silica gel, mangan(II).*

1. Introduction

Indonesia has a tropical climate that strongly supports snail"s population. Certain snail species, i.e. *Achatina fulica*, are cultivated because it has larger size than other types of snails; hence it is very potential to be used as raw material for making kebabs or satays. As a result, snail shell waste is generated from the industry and has not been used optimally but as traditional toys only. Snail shell contains high calcium (around 36.1%) and only small amount of another metal [1]. Therefore, those shells are also potential to be used as raw material of supernatant in the synthesis of calcium tartrate tetrahidrat (CaTT) single crystals.

Synthesis of CaTT single crystals in metasilicate gel from other industrial waste i.e. sugar cane has also been carried out and gives optimum results at pH of 3.25. As reported by Prananto (2003), supernatant of $CaCl_2$ were previously prepared from CaC_2O_4 or $CaCO_3$ waste. However, the yields are only around 5.45% [2].

Single crystals of CaTT are known to be piezoelectric. With the addition of another metal (doped), either primary metals or transition metals, single crystals CaTT have better electrical properties [3,4].

Torres (2002) also explained that if a transition metal was added, it will occupy the interstitial sites. The presence of transition metals is able to shorten the distance Ca-O bond and changing the angle of torsion of tartrate ions and hydrogen bonds [3]. Satyanarayana (1983) showed that the metal ion added (doped) into the position of interstitial site with octahedral symmetry field surrounded by eight oxygen atoms originating from hydroxyl ions and water molecules tartrate [5].

The use of ion Mn (II) as the dopant is very interesting to be studied further. Suthar and Joshi (2006) reported that the presence of Mn (II), space charge polarization can increase the value of the dielectric constant without changing its nature [6]. Single crystal of Mn (II) doped CaTT is used as piezoelectric material at high-voltage energy source, sensors and piezoelectric motors.

Prediction of reaction in the formation of Mn(II) doped CaTT is as follows:

$$Ca^{+2}_{(aq)} + Mn^{+2}_{(aq)} + C_4H_4O_6^{-2}{}_{(aq)} \rightarrow Ca_xMn_{1-x}C_4H_4O_6.4H_2O_{(s)}$$

The use of gel is considered as the most promising technique for growing single crystals of metal tartrate compared with solution saturation method or hydrothermal reaction. This is due to tartrate is partly dissolved in water and easily decomposes before its melting point [4].

2. Experimental Detail

Materials

Laboratory reagents, which are tartaric acid ($C_4H_6O_6$), sodium metasilicate ($Na_2SiO_4.9H_2O$), HCl, $CaCl_2.2H_2O$, $MnCl_2.4H_2O$, and solvents, i.e. were used without further purification and obtained from standard commercial suppliers. Instrumentations that are used in this research were a high temperature Barnstead Thermolyne and a HERAEUS KR170E Oven, an Orion 420A pH-meter, a Shimadzu FTIR-8601PC, an AA-6200 and Perkin Elmer Analyst 100 AAS, and a Panalytical PHILIPS-XPERT XRD.

Preparation of Supernatant

Firstly, CaO was prepared by calcinating the snail shell waste at 1000°C, and then reacted with HCl 1.5M until all the precipitate was dissolved. The solution was then concentrated and after that, it was directly placed in a cold waterbath in which white solid of $CaCl_2$ was yielded. Next, the supernatant was made by combining $CaCl_2$ with $NiCl_2$ in a 20mL of mixed solution with Ca(II):M(II) mol ratio of 1:0.05; 1:0.10 and 1:0.15.

Synthesis of Mn(II) doped CaTT

Synthesis of Mn(II) doped CaTT was conducted at the optimum condition (pH) of CaTT synthesis, which was investigated in preliminary research. The gel was prepared by reacting 0.5M tartaric acid and 0.5M sodium metasilicate solution. The mixed solution was mantained at pH of 3.5 and placed in a single tube (*h = 20 cm; d = 2-3 cm*) for 10 days until the gel is formed. Next, the supernatant was added slowly via the inner wall onto the tube to avoid the damage of gel surface, then closed with alumunium foil and placed in a tube rack. The reaction was stand at room temperature for 2 and 3 weeks.

3. Result and Discussion

Preparation of Supernatant

For about 35.85 g of CaO was yielded from 70 g of dry powdery snail shell waste. Next, a 36.23 g of $CaCl_2$ hydrate was produced from 23 g of CaO with efficiency of 79.6%. Based on the AAS data, the purity of synthesized $CaCl_2$ was found 82.6%. Based on our previous research, although the impurity of the synthesized $CaCl_2$ hydrate was high, it was still available to be used without further purification.

Synthesis of Ni(II) doped CaTT

After the supernatant was added on the gel, small crystalline solid started to grow in 3 days on the gel surface. This is slightly faster than the growth of un-doped CaTT crystals (7 days). The concentration of ions in the supernatan was much higher due to additional ions from Ni(II) salts. Consequently, the diffusion rate was much greater, hence more nucleous formed on the gel surface (crowded) and resulting small crystals. The synthesized crystal between doped and un-doped CaTT are given in Figure 1.

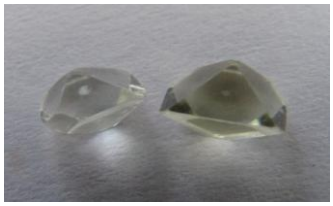

Figure 1. CaTT (left) and Mn(II) doped CaTT (right)

More and bigger crystals were formed in 3 weeks than in 2 weeks (Table 1). As reported in many journals, higher yield of single crystals was produced if more growth time was used. The metal ions has more times to diffuse deeper into the gel and forms crystals. Most of the bigger and better-shaped crystals grew until ±0.5 cm few cm below the gel surface.

Table 1. The average yields (g) of synthesized Mn(II) doped CaTT growth in silica gel

Mol ratio of Ca(II):Mn(II)	Yields (g)	
	2 weeks	3 weeks
1:0.05	1.200	1.225
1:0.10	0.725	0.725
1:0.15	0.470	0.485

Experimental data also shows that higher yield of single crystals was produced if less Mn(II) concentration incorporated in the supernatant (Table 1). The competition between Mn(II) and Ca(II) ions to react with tartaric ions in the gel is getting higher. Hence, the gel become significantly less condusive for the growth of CaTT. The highest yield of crystals were produced from supernatant with a Ca(II):Mn(II) mol ratio of 1:0.05; followed by 1:0.10 and 1:0.15, respectively.

Characterization of Mn(II) doped CaTT

All synthesized crystal was characterized by FTIR, AAS, and Powder XRD. Mohs test was also conducted to investigate the effect of doped ions toward the crystal"s physical hardness.

AAS data reveales that the synthesized crystals has similar Ca(II):Mn(II) mol ratio of 0.997:0.003 in every Ca(II):Mn(II) mol ratio of supernatant (Table 2). This indicates that at pH of 3.5, the concentration of Mn(II) in the supernatant solution does not influence the amount of Mn(II) that can doped in CaTT crystal. This ratio was also represent the optimum amount of Mn(II) that can fill the interstitial sites in the CaTT crystal lattice. In other word, the different ratio of Ca(II):Mn(II) in the supernatant only affects the yields.

Table 2. Mol Ratio of Ca(II):Mn(II) in Mn(II) doped CaTT

Mol ratio of Ca(II):Mn(II) in supernatant	Ca (mol)	Mn(II) (mol)	Mol ratio of Ca(II):Mn(II) in crystal
1:0.05	0.2417	0.0008	0.997:0.003
1:0.10	0.2361	0.0007	0.997:0.003
1:0.15	0.2331	0.0007	0.997:0.003

FTIR analysis shows several characteristic peaks of tartaric ions, as presented in Figure 2. This spectrum indicates that the synthesized crystal contains tartaric compounds (Table 3). In other words, the tartaric does not decompose, as many thermal synthesized type-reaction reported for the case of tartaric compounds. Unfortunately, there is no band that corresponds to Mn–O bond observed. It is probably because only small amount of Mn(II) observed in the crystal. However, further FTIR studies still need to be done to gain comprehensive conclusion.

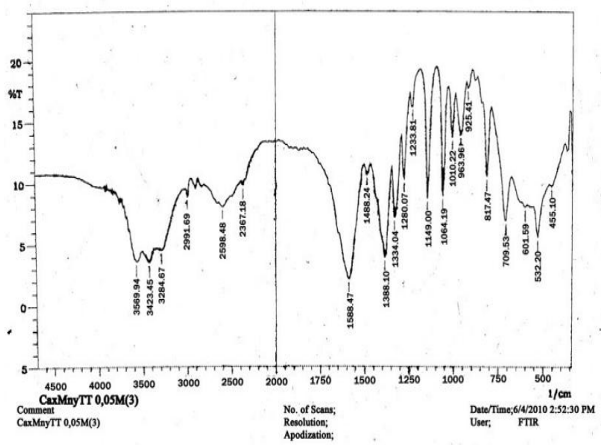

Figure 2. FT-IR of Mn(II) doped CaTT (taken from crystal made of supernatant with Ca(II):Mn(II) ratio of 1:0.05)

Table 3. The FTIR Vibration of CaTT and Mn(II) doped CaTT

CaTT*	CaTT	Mn(II) doped CaTT			Vibration Type
		1:0.05	1:0.10	1:0.15	
3392	3292.4	3284.7	3284.7	3284.7	O – H stretch
2962	2991.7	2991.7	2991.7	2991.7	C – H stretch
1731	1588.5	1588.5	1588.5	1588.5	C = O stretch
1382 1330 1282	1388.0 1334.0 1280.1	1388.0 1334.0 1280.1	1388.0 1334.0 1280.1	1388.0 1334.0 1280.1	C – O stretch
1147 1060 1012	1149.0 1064.2 1010.2	1149.0 1064.2 1010.2	1149.0 1064.2 1010.2	1149.0 1064.2 1010.2	O – H deformation C – O stretch
530	532.2	532.2	532.2	532.2	Ca – O stretch

*Note: * = Selvarajan, 1993.*

Furthermore, powder XRD data (Figure 4 and Table 4) shows that Mn(II) doped CaTT has identical crystal system to those observed in undoped CaTT single crystals. Only at this stage, we believe that the doped ions were not change the crystal system of CaTT.

As many literature suggested that in the interstitial sites, Mn(II) ions were coordinated with two oxygen atoms from hydroxyl group of two tartaric ions and four oxygen of water molecule (Figure 3). The hardness scale of doped and un-doped crystal is similar, which is in level of 2-3. This is might be due to only small amount of Mn(II) ions are filling the interstitial sites. Hence, the presence of Mn(II) does not affect significantly on the crystal density and hardness

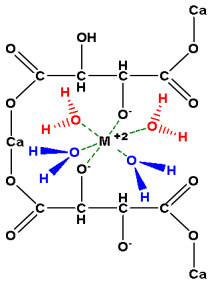

Figure 3. M(II) in the interstitial site of CaTT

4. Conclusion

The optimum conditions of CaTT synthesis in gel were pH of 3.5 and $CaCl_2$ concentration of 0.45M. Higher yield was produced if more growth time and less Mn(II) concentration in the supernatant was applied in the synthesis. The obtained Mn(II) doped CaTT single crystal have a Ca(II):Mn(II) mol ratio of 0.997:0.003, equal hardness, and identical crystal system to those observed in undoped CaTT single crystals.

5. Acknowledgment

This research is funded by DPP/SPP 2010 scheme of Faculty of Science UB and all authors

are thank to Chemistry Department of UB for facilitating this research.

6. References

[1].Cresswell, D. C. and Kompiang, P., (2005), Studies on Snail Meal as a Protein Source for Chiekens. 1. Chemical, Metabolizable Energy and Feeding Value for Broiler, *Metabolism and Nutrition* 60: 1854-1860.

[2].Prananto, Y. P., M. M. Khunur and S. Mutrofin, (2007), Sintesis Kristal Tunggal Kalsium Tartrat Tetrahidrat dari Limbah Kalsium Oksalat Nira Tebu dengan Metode Gel Metasilikat, *Natural*, vol. 11 No. 1, October, FMIPA UB, Malang.

[3].Torres, M. E., T. Lopez, J. Stockel, X. Solans, M. Garcia-Valles, E. Rodriguez-Castellon and C. Gonzalez-Silgo, (2002), Structural Characterization of Doped Calcium Tartrate Tetrahydrate , *J. Solid State Chem*., 491, p.163.

[4].Shajan, X. S. and C. Mahadevan, (2004), On the Growth of Calcium Tartrate Tetrahydrate Single Crystal, *Bull. Mater. Sci*., Vol. 27, No.4, pp.327 – 331, Indian Academy of Sciences, New Delhi.

[5].Satyanarayana, N., K., Kariharan, S., Radhakrisna, (1983), Nickel Centers In Strontium Tartrate Tetrahydrate Single Crystals, *Bull. Mater. Sci*., Vol. 27, No.4, pp.327 – 331, Indian Academy of Sciences, New Delhi.

[6].Suthar, S. R., and M. J., Joshi, (2006), Growth and Characterization of Mn^{2+} doped Calcium L-Tartrate Crystals, *Cryst. Res. Techno*., 41. No.7. Departement of Physics, Saurashtra University, India, pp., 664 – 670.

Appendixes

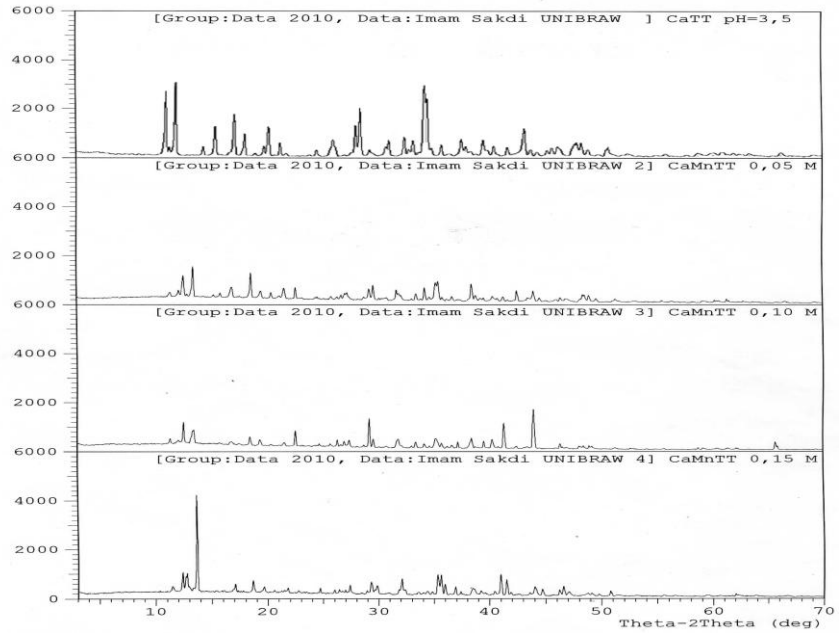

Figure 4. Powder Diffraction of CaTT and Ni(II) doped CaTT

Table 4. The XRD data of CaTT and Ni(II) doped CaTT in different supernatant ratio of Ca(II):Ni(II)

Peak	JCPDS			CaTT			1:0.05			1:0.01			1:0.15		
	2θ (°)	d(A)	I/Io	2θ (°)	d(A)	I/Io	2θ (°)	d(A)	I/Io	2θ (°)	d(A)	d(A)	2θ (°)	d(A)	I/Io
1	12,4318	7,12	60	12,46	7,0974	88	12,57	7,0370	67	12,55	7,0503	36	12,60	7,0086	13
2	13,2942	6,66	100	13,31	6,6425	100	13,46	6,5744	10	13,48	6,5633	24	-	-	-
3	29,4795	3,03	40	29,48	3,0273	65	29,62	3,0131	54	29,58	3,0180	17	29,60	3,0498	4
4	35,0582	2,56	40	35,12	2,5531	95	35,26	2,5433	61	35,32	2,5392	14	35,28	2,5418	24
5	35,3660	2,53	55	35,32	2,5391	78	35,50	2,5267	68	35,48	2,5281	7	35,59	2,5203	24

Epiphytic Orchid Diversity at Wilis Mountain, District of Ponorogo, East Java

Nina Dwi Yulia [1], Sugeng Budiharta [2]

[1,2] Purwodadi Botanic Garden-Indonesian Institute of Sciences (LIPI), Pasuruan, East Java, Indonesia.
(ndyulia@yahoo.com)

Abstract

This study aims at documenting the diversity of epiphytic orchids at forest reserve area in Wilis Mountain. This area is managed by BKPH (Sub-forest District) Wilis Barat under Perum Perhutani (State Owned Forest Company). All data on orchid species were recorded including its number, host trees and zone of the host tree where the orchid attached. The results showed that as many 36 epiphytic orchid species and total of 992 individual orchids were recorded at the study site. Three most abundant epiphytic orchids were Flickingeria angulata (278 individuals) and Eria monostachya (102 individuals). Zone three (bottom part of the branches) was revealed as the most favorable part at the host tree (371 individuals).

***Keywords**: Epiphytic orchid, Diversity, Wilis Mountain.*

1. Introduction

Wilis Mountain is a non-active volcano located at East Java Province. Mount Wilis has a height of 2552 meter and its peak located on the border between the six districts of Kediri, Tulungagung, Nganjuk, Madiun, Ponorogo and Trenggalek. Nowadays, the forest in Wilis Mountain is destroyed by various causes including forest fires, landslides and illegal logging. Inevitably, these processes have threatened biological diversity of the area, and particularly orchid species, which are further threatened by illegal harvesting (Perhutani‟s forest rangers, pers. comm.). The forest reserve in Wilis Mountain is one of orchids‟ natural habitats in Java which has not been explored so far. However, there is no accurate information on orchid diversity of the area. There are several conservation insitu areas in the region include Forest Reserve (FR) Gunung Manyutan, FR Gunung Bunder and Gunung Picis Nature Reserve. The area protection is located on the western slope of Mount Wilis.

This local situation in Wilis is in accordance with [7,8] that orchid diversity and abundance in many protected areas in Java has changed considerably. Therefore, data and information gathering on the occurrence of orchid in its natural habitat is urgently required in order to develop the potential conservation strategies. This effort is important considering the fact that in Java, large extents of natural forest areas have been converted into human settlements, agricultural lands and plantations which can lead to local population extinction of orchid. The impacts of such causes will be exaggerating if the extinction occurs before its being described and documented.

This study aims at documenting the diversity of epiphytic orchids at Forest Reserve in Wilis Mountain. This was achieved by conducting a fieldwork in order to record all data on orchid in the area. The objective measures of species diversity, such as species-area and species-abundance relationships, should receive more prominence in orchid research [3]. Local forest rangers reported that the studied area is rich in epiphytic orchid‟s species particularly from the genus Vanda (Perhutani‟s forest rangers, pers. comm.). This was used as baseline information in conducting this research.

2. Experimental Details

This study was conducted from 26 April to 3 May 2010 at Forest Reserve, Wilis Mountain (7º46.751‟ S; 111º39.637‟ E) (Figure 1). This area is administratively located at Pupus Village, Sub-district of Ngebel, District of Ponorogo, East Java and managed by Bagian Kesatuan Pemangkuan Hutan (Sub-forest District) Wilis Barat under Perum Perhutani (State Owned Forest Company).

The research method used explorative method means to do data collection orchid species follow the existing path or and to make a new path and to do observation each orchid epiphytic found attached in host tree. All epiphytic orchid species attached to trees were recorded. Various data were also collected including the species name of host tree and the zone on the tree where the orchid attached. Environmental data were

also recorded including temperature, humidity and altitude.

Epiphyte position on the host tree was divided into five zones, which are: (i) Zone 1: the bottom part (1/3) of the main stem; (ii) Zone 2: the upper part (2/3) of the main stem; (iii) Zone 3: the bottom part of the branches; (iv) Zone 4: the middle part of the branches; and (v) Zone 5: the outer part of the branches [2].

Figure 1. The situation of forest reserve at Wilis Mountain, Ngebel, Ponorogo, East Java

3. Result and Discussion

The results showed at Forest Reserve in Wilis Mountain, a total of 36 epiphytic orchids were recorded, from 18 different genera. In most epiphytic orchids species found are consistent with the environmental conditions of the mountains, because this area has altitude above 1000 m asl and the humidity this area less than 80%. These environmental conditions play a major role to form the type of wealth that can grow these orchids.

Table 1 show a summary of the number of species recorded for each genus present in the survey, *Eria* was the genus with the highest quantity of species (9 species). The high level *Eria* diversity is presumably related to relatively low temperature and middle range humidity. Most species from *Eria* genus were recorded at locations with altitude between 500 and 2500 m *asl* [4].

Table 1. Summary of genera and species of orchid epiphytic in Wilis Mountain, Pupus, Ponorogo

No	Genera	Number of species
1	*Agrosthophyllum*	2
2	*Appendicula*	1
3	*Bulbophyllum*	3
4	*Coelogyne*	2
5	*Dendrobium*	2
6	*Dendrochillum*	1
7	*Eria*	9
8	*Flickingeria*	3
9	*Liparis*	2
10	*Luisia*	1
11	*Pholidota*	1
12	*Pteroceras*	1
13	*Schoenorchis*	1
14	*Thrixspermum*	2
15	*Trichoglottis*	1
16	*Trichotosia*	1
17	*Tuberolabium*	1
18	*Vanda*	2

The three most abundant species at the area were *Flickingeria angulata* (No= 278, Figure 2), *Eria monostachya* (No = 102) and *Appendicula* sp. (No = 78) (Table 2). Number of individual *F. angulata* abundant than other orchids species, among other supported by environmental conditions still suitable for this species to breed well. The dominance of *F. angulata* over other epiphytic orchids also recorded at Penanggungan Mountain, East Java [9].

Figure 2. Flower of *Flickingeria angulata*

The result comparing of the number individual of orchid species and number of host tree that *Eria javanica* showed higher value than other epiphytic orchid species. The value of this comparison showed that certain epiphytic orchids that grows on a host tree. *Eria javanica* commonly grows epiphytic on tree trunk or covering rocks in both shady and open spots [1]. In addition, this species can grow well in the

lowlands to the highlands and at Java are found at an altitude of 900 – 1300 m asl, and able to grow in humid and less humid conditions [6].

Table 2. List of epiphytic orchid species at the study site and the value of parameters (Nt is the number of trees in the hosting a particular orchid species; No is the number of individuals of a particular orchid species)

No	Orchid Species	Nt	No	Value of Comparison No/Nt
1	*Agrosthophyllum majus*	1	1	1
2	*Agrosthophyllum sp.*	1	1	1
3	*Appendicula sp.*	20	78	3.9
4	*Bulbophyllum sp1.*	15	72	4.8
5	*Bulbophyllum sp2.*	3	16	5.3
6	*Bulbophyllum sp3.*	3	21	7
7	*Coelogyne longifolia*	2	2	1
8	*Coelogyne speciosa*	11	57	5.2
9	*Dendrobium linearifolium*	2	3	1.5
10	*Dendrobium sp.*	3	10	3.3
11	*Dendrochillum sp.*	7	16	2.3
12	*Eria flavescens*	8	16	2
13	*Eria floribunda*	1	2	2
14	*Eria hyacinthoides*	9	47	5.2
15	*Eria javanica*	6	46	7.7
16	*Eria lamonganensis*	1	1	1
17	*Eria moluccana*	6	9	1.5
18	*Eria monostachya*	24	102	4.3
19	*Eria oblitterata*	1	1	1
20	*Eria sp.*	13	37	2.8
21	*Flickingeria angulata*	47	278	5.9
22	*Flickingeria aurieloba*	4	7	1.8
23	*Flickingeria sp.*	6	34	5.7
24	*Liparis condulybulbon*	5	9	1.8
25	*Liparis sp.*	2	7	3.5
26	*Luisia zollingeri*	4	7	1.8
27	*Pholidota imbricata*	9	16	1.8
28	*Pteroceras compressus*	1	1	1
29	*Schoenorchis sp.*	1	1	1
30	*Thrixspermum sp.*	10	21	2.1
31	*Thrixspermum subulatum*	3	13	4.3
32	*Trichoglottis sp.*	3	4	1.3
33	*Trichotosia angulata*	3	7	2.3
34	*Tuberolabium odoratissimum*	1	5	5
35	*Vanda limbata*	1	1	1
36	*Vanda tricolor*	18	43	2.4
		255	992	

There are sixteen tree species into the host trees for epiphytic orchid species in this area include *Bischofia javanica, Glochidion* sp., *Schima wallichii, Lithocarpus teysmannii*, *Pinus merkusii* and *Engelhardia spicata* (Table 3). From the entire host tree is a tree species that are generally grown in mountainous regions. Entire species of trees that became the host for epiphytic orchids have a rough bark characters and easy to peel, so support for the attachment of the roots of epiphytic orchids.

Table 3 Host tree of epiphytic orchid species at Wilis Mountain

No	Host Tree
1	*Bischofia javanica*
2	*Bridelia sp.*
3	*Callophyllum* sp.
4	*Engelhardia spicata*
5	*Eudia sp.*
6	*Glochidion sp.*
7	*Lithocarpus sp.*
8	*Lithocarpus sundaicus*
9	*Lithocarpus tesymanii*
10	*Litsea sp.*
11	*Nauclea* sp.
12	*Pinus merkusii*
13	*Proteacea*
14	Proteaceae
15	*Schima wallichii*
16	Tunggak pohon

The presence of epiphytic orchids in the host tree is not found in all parts of the tree. The epiphytes on host trees divided in 5 zones [2]. The pattern of distribution of epiphytic orchids in the host tree trunks and branches adapted to the needs of light and humidity for growth. Epiphytic orchids naturally will choose certain zones on the host trees to get sunlight. From the results of this study the presence of epiphytic orchids is more often found in zone 3 (620 individual epiphytic orchids, Figure 3). In this study, zone three, which is located at the bottom part of the branches, is the most favorable zone for epiphytic orchid to grow. The distribution patterns of epiphytic orchids on the stems and branches of host tree are influenced by the needs of sunlight and humidity that make epiphytic orchids to favor specific zone on the host tree [9]. The orchids grew at zone three; four and five are those that favor plenty of sunlight [5]. However, individual state of host tree also influences the occurrence of epiphytic orchid in term of creating appropriate conditions such as light intensity, aeration and humidity [10].

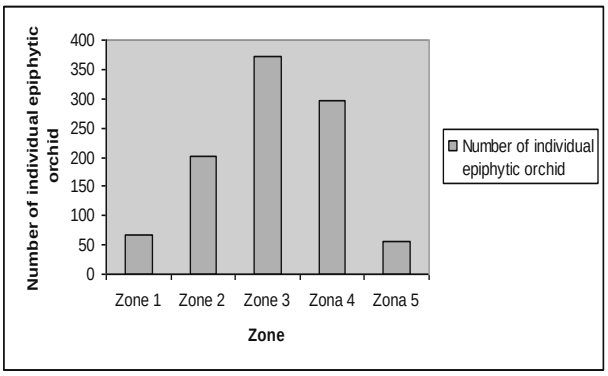

Figure 3. Number of epiphytic orchids at each zone of host tree (Zone 1: the bottom part (1/3) of the main stem; Zone 2: the upper part (2/3) of the main stem; Zone 3: the bottom part of the branches; Zone 4: the middle part of the branches; Zone 5: the outer part of the branches)

4. Conclusion

Ephypitic orchid diversity at Forest Reserve in Wilis Mountain is relatively high. There were 36 epiphytic orchid species (totally 992 individuals) recorded. The most abundant orchid species were *Flickingeria angulata*, followed by *Eria monostchya* and *Appendicula* sp. In addition, there were 16 host tree species recorded, such as *Bischofia javanica, Glochidion* sp., *Schima wallichii, Lithocarpus teysmannii*, *Pinus merkusii* and *Engelhardia spicata*. Zone 3 (bottom part of the branches) was noted as the most preferred zone on host trees to be attached by epiphytic orchid species.

5. Acknowledgments

This research is funded by „Insentif Ristek Peneliti dan Prekayasa 2010" on project entitled „Evaluation of orchid in southern part of East Java". We acknowledge the contributions of exploration team members (Pa'i, Suhadinoto and Totok Hartoyo) and Perhutani"s forest rangers (Narlan and Sukardi) during fieldwork.

6. References

[1]. Comber, J.B. (1990), *Orchids of Java*. Royal Botanic Gardens, Kew.

[2]. Dressler, R.L. (1990), *The Orchid: natural history and classification*. Harvard University Press. USA.

[3]. Kindlmann, P. & C. Vergara (2009), Objective measures of orchid species diversity. In: Pridgeon AM, Suarez JP (eds) *Proceedings of the Second Scientific Conference on Andean Orchids.* Universidad Técnica Particular de Loja, Loja, Ecuador, pp 71-83

[4]. Mahyar, U.W., & A. Sadili (2003), *Orchid of Gunung Halimun National Park*. Biodiversity Conservation Project LIPI-JICA-PHKA. Bogor.

[5]. Puspitaningtyas, D.M. & E. Fatimah (1999), Orchids inventory in Kersik Luway Wildlife Sanctuary, East Kalimantan. *Bull. Kebun Raya Indonesia* 9(1): 18-25.

[6]. Puspitaningtyas, D.M., S. Mursidawati, Sutrisno & D. Asikin (2003), *Wild orchid in conservation areas in Java Island.* Bogor Botanic Garden-LIPI. Bogor.

[7]. Puspitaningtyas, D.M. (2005), Study on orchid diversity in Gunung Simpang Wildlife Sanctuary, West Jawa. *Biodiversitas* 6 (2): 103-107.

[8]. Puspitaningtyas, D.M. (2007), Inventory of orchids and their host trees in Meru Betiri National Park, East Java. *Biodiversitas* 8 (3): 210-214.

[9]. Yulia, N.D. & R.M. Yanti (2010), Anggrek Epifit dan Pohon Inangnya di Kawasan Gunung Penanggungan, Pasuruan – Jawa Timur. *Berkala Penelitian Hayati Edisi Khusus* 4A: 37-40.

[10]. Zotz, G & P. Hietz (2001), The physiological ecology of vascular epiphytes: current knowledge, open question. *J Ex Bot* 52 (364): 2067-2078.

Study of Infrared Spectra in the Interaction of Cr(VI), Mn(II), Ni(II), Cu(II), Zn(II), Cd(II), Hg(II), and Pb(II) by Seaweed (*Gracilaria* Sp) Biomass

Noer Komari [1], Filomena Matilda [2]

[1,2] Department of Chemistry, Faculty of Mathematics and Natural Science, University of Lambung Mangkurat, Banjarbaru, South Kalimantan, Indonesia (noerkomari@yahoo.com)

Abstract

Biosorption process involves the interaction between metal ions with functional groups of biomass. This study investigates the functional groups of Gracilaria sp biomass, before and after interaction with Cr(VI), Mn(II), Ni(II), Cu(II), Zn(II), Cd(II), Hg(II), and Pb(II). Interaction is done by adding biomass of Gracilaria sp with metals in the solution to 100 ppm at pH 5. Determination of functional groups was done using Infrared Spectrophotometer. The results showed that biomass of Gracilaria sp, before and after interaction with each of Cr(VI), Mn(II), Ni(II), Cu(II), Zn(II), Cd(II), Hg(II), and Pb(II), has hydroxyl group, CH_2 chain, carboxyl group, C-O bond, and disulfide bonds. Hydroxyl groups and disulfide bonds in the biomass plays an important role in the binding of each Cr(VI), Mn(II), Ni(II), Cu(II), Zn(II), Cd(II), Hg(II), and Pb(II), whereas the carboxyl group only plays a role in binding of Cr(VI), Ni(II) and Cd(II).

Keywords: *biosorption, Gracilaria sp, metals, infrared spectra.*

1. Introduction

The presence of heavy metals, such as Cr(VI), Mn(II), Ni(II), Cu(II), Zn(II), Cd(II), Hg(II) and Pb(II) in the environment makes a serious problem. Heavy metals pollution cause harmful effects to living organisms in the water and can risks to human health [1]. Heavy metals come from the mining process, washing the ore, waste disposal, gilding metal, electrical equipment, paints, batteries, pesticides or preservatives [2]. One method to reduce heavy metal contamination was biosorption.

Biosorption process involves the interaction between metal ions with functional groups present in the cell wall of biomass. Functional groups such as carboxyl, hydroxyl, amino acids found in cell wall of biomass can play a role in binding metal ions. These functional groups can be identified using infrared spectrophotometer. Various studies show that after interaction biomass with metal ions, the absorption bands of certain functional groups can undergo a shift, or does not appear, or appears again and an absorption band of new functional groups. Based on infrared spectra it can be seen that clusters of potential to be able to bind with metal ions.

One of the aquatic plants that can be used as biomass is seaweed (algae) species *Gracilaria*. Various studies have shown that functional groups contained in the algae are able to do the binding with metal ions. Therefore, the purpose of this research is to investigate the functional groups that play a role in binding heavy metal ions such as Cr(VI), Mn(II), Ni(II), Cu(II), Zn(II), Cd(II), Hg(II) and Pb(II) by biomass of *Gracilaria sp.*

2. Experimental Details

Biomass Preparation

A total of 2.00 kg of *Gracilaria sp* washed under running water and with distilled water. After that, *Gracilaria sp* was cut up to a certain size and then dried and pulverized. Next, it was washed with 0.10M HCl twice and centrifugated at 2800 rpm. The precipitate obtained was washed with distilled water and filtered, then dried in oven at 105°C for 3 hours. Biomass was then mashed and sieved through 120 mesh, then stored in desiccators.

Metal Interaction with biomass

Preparation for the interaction of metal ions by biomass as practiced by Hashim and Chu [3] are modified. A total of 1,00 g biomass added to 50 mL solution of Cr(VI) 100 ppm which is set pH with the addition of 0.1 M HCl and 0.1 M NaOH so that the pH 5. The mixture is reacted with a shaker at 200 rpm for 2 hours and filtered using filter paper. The precipitate was washed with distilled water and dried at 60°C for 2 hours. The above procedure was repeated using a solution of Mn(II), Ni(II), Cu(II), Zn(II), Cd(II), Hg(II) and Pb(II).

Infrared Analysis

Biomass was washed with distilled water respectively and HCl, and interaction with each metal solution. The precipitate obtained is dried and made pellet by adding KBR, then analyzed using an infrared spectrophotometer.

3. Results and Discussion

Metals Interaction with biomass

Biomass was contacted with metals for interaction through the formation of chemical bonds between metals with functional groups contained cell wall biomass. Prior contacted, a solution of metal arranged in advance its pH, *i.e.* at pH 5. pH are important factors that play a role in metal ion interaction with the biomass, because of this phenomenon can explain the chemical properties of heavy metals [4] and load the active site, such as carboxyl groups found on the surface of the biomass. Interaction of metal ions by biomass is done by shaking at a speed of 200 rpm. Agitation speed is one other factor affect the interaction of metals, because increasing the speed it will also improve the diffusion of metal ions on the surface of the seaweed biomass [5]. Functional groups contained in the biomass can be ascertained from the resulting infrared spectra. Infrared spectra of biomass interaction with each metal ion will be compared with infrared spectra of the biomass of *Gracilaria sp* to determine the absorption shift is happening so that it can predict any functional groups that play a role in binding metal ions. Figure 1 and 2 show infrared spectra of the biomass.

Comparison of Metal Ion Interaction with biomass

The interaction of metal ions with the biomass can be seen from the absorption bands appearing in infrared spectra of each metal. Functional group of -COO-absorption occurring at wave numbers 1650 – 1620 cm^{-1} involves the coordination covalent bonds. Functional group absorption appearing at wave number 1635.5 cm^{-1}, 1651.0 cm^{-1}, and 1654.8 cm^{-1} as-COO- stretching vibration in infrared spectra of biomass with metal ions, indicating that the interactions that occur between the biomass with Cr(VI), Mn(II), Ni(II), Cu(II), Zn(II), Cd(II), Hg(II) and Pb(II) coordination involving covalent bonds.

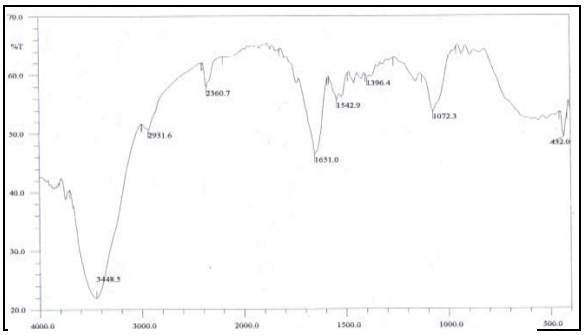

Figure 1. Infrared Spectra of Biomass with water

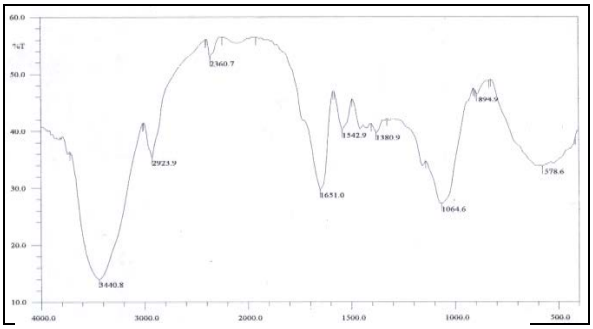

Figure 2. Infrared Spectra of Biomass with HCl

Interaction of metal ions with the biomass can be evaluated from the ratio of acid properties of metal ions. Based on the nature of acidity, chromium, manganese, nickel, copper, and zinc are borderline, who can interact well with a strong base and weak base are present in the cell wall biomass. Figure 3, 4, 5, 6 and 7 show these interactions. This is in contrast with cadmium, mercury, and lead is weakly acidic. The three metal ions will interact strongly with a weak base and the interactions that formed were more covalent [6]. Figure 8, 9 and 10 shows these interactions.

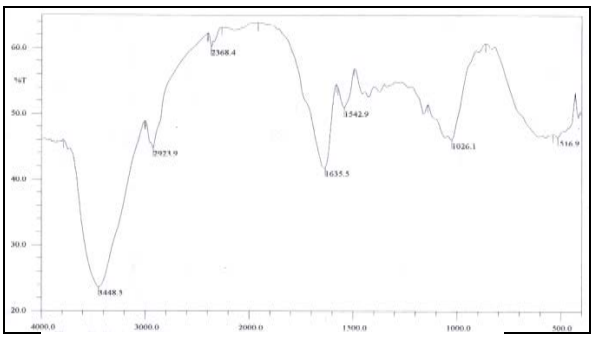

Figure 3. Infrared Spectra of Biomass with Cr(VI)

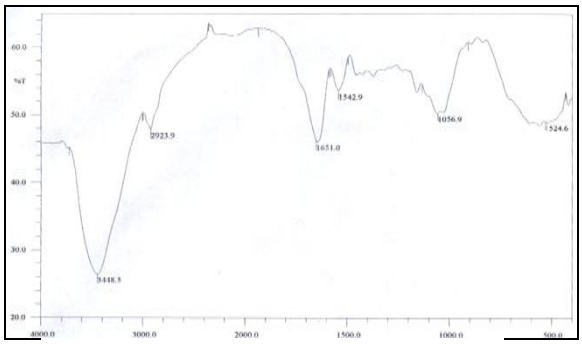

Figure 4. Infrared Spectra of Biomass with Mn(II)

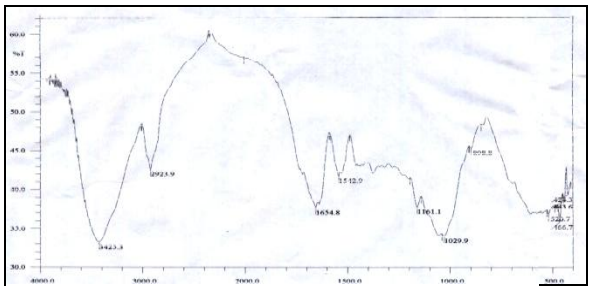

Figure 5. Infrared Spectra of Biomass with Ni(II)

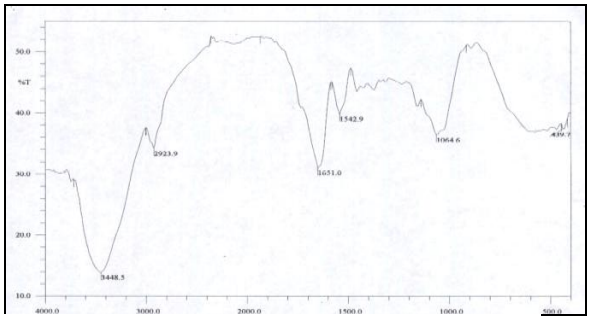

Figure 6. Infrared Spectra of Biomass with Cu(II)

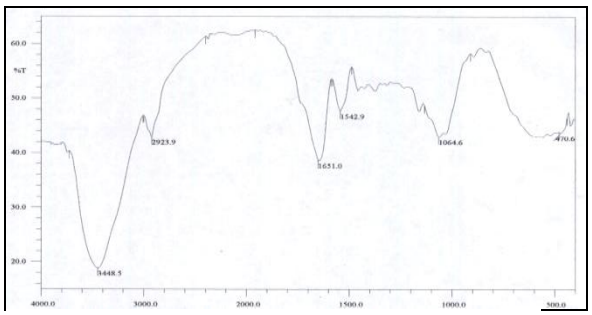

Figure 7. Infrared Spectra of Biomass with Zn(II)

Atoms with smaller ionic radii will interact strongly with the ligands contained in the biomass cell walls than atoms with larger ionic radii. Therefore, Cr(VI) with the ligand will interact more strongly than the other metal ions, because the ionic radius of Cr(VI) is smaller (0.52Å) compared with other metal ions (ion radius of Mn(II), Ni(II), Cu(II), Zn(II), Cd(II), Hg(II) and Pb(II) are 0.67, 0.69; 0.73, 0.74, 0.95, 1.02, and 1.19Å, respectively).

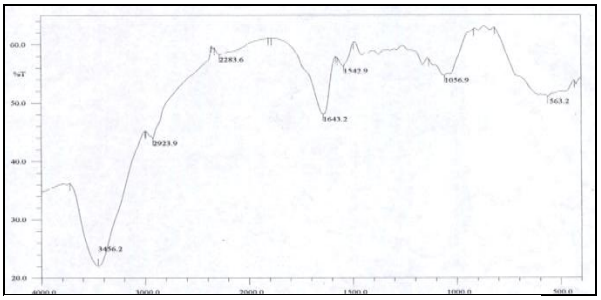

Figure 8. Infrared Spectra of Biomass with Cd(II)

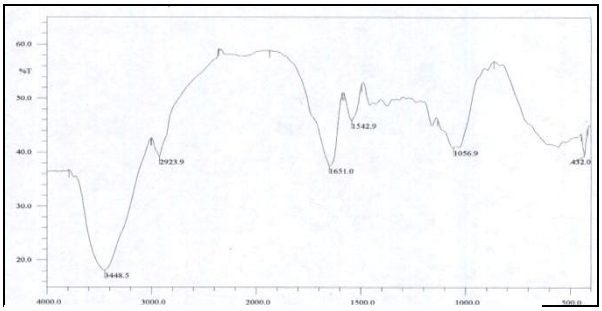

Figure 9. Infrared Spectra of Biomass with Hg(II)

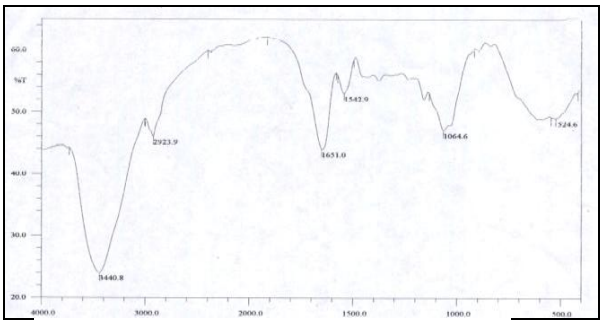

Figure 10. Infrared Spectra of Biomass with Pb(II)

4. Conclusion

Hydroxyl group,-CH2-, carboxyl group, C-O bond, and disulfide bond contained in the biomass of *Gracilaria sp*, before and after interaction with each of Cr(VI), Mn(II), Ni(II), Cu(II), Zn(II), Cd(II), Hg(II) and Pb(II). Hydroxyl groups and disulfide bonds contained in the biomass of *Gracilaria sp* plays a role in the binding of each of Cr(VI), Mn(II), Ni(II), Cu(II), Zn(II), Cd(II), Hg(II), and Pb(II), whereas the carboxyl group plays a role in binding of Cr(VI), Ni(II) and Cd(II).

5. Acknowledgements

The authors wish to thank Ms. Hasnah and Ms. Fahriza for their assistances during the analyses of samples in Chemistry Lab., Faculty of

Mathematics and Natural Science, University of Lambung Mangkurat.

6. References

[1]. Vilar, V.J.P., C.M.S. Botelho, & R.A.R. Boaventura (2006), Equilibrium and Kinetic Modelling of Cd(II) Biosorption by algae Gelidium and algal order Extraction Waste. *Water Research* 40, 291-302.

[2]. Ahalya, N., R.D. Kanamadi, & T.V. Ramachandra (2005), Biosorption of Chromium (VI) from Aqueous Solutions by The Husk of Bengal gram (Cicer arientinum). *Research Article*, vol.8 No.3: 258-264.

[3]. Hashim, M.A. & K.H. Chu (2004), Biosorption of Cadmium by Brown, Green, and Red Seaweed. *Chemical Engineering Journal*, 249-255.

[4]. Gardea-Torresday, J.L., G. De La Rosa, & J.R Peralta-Videa (2004), Use of Phytofiltration Technologies in The Removal of Heavy Metals: *A Review. Pure Appl. Chem*., 76: 801-813.

[5]. Antunes, W.M., U. S. Luna, C.A. Henriques, & A.C. Costa (2003). An Evaluation of Copper Biosorption by Brown Seaweed under Optimized Conditions. *Research Article*, vol.6 No.3: 174-184.

[6]. Duffus, J.H., (2002), Heavy Metals – a Meaningless Term?. *Pure and Applied Chemistry* 74, 793-807.

Evaluation of Accuracy Clustering Zom BMKG in Ngawi with Multivariate Adaptive Regression Spline (MARS) Approaching

Nur Faizah [1], Bambang Widjanarko Otok [2], Sutikno [3]

[(1,2,3)] Statistics, FMIPA-ITS, Surabaya, Indonesia
(nur_faizah39@yahoo.com; bambang_wo@statistika.its.ac.id; sutikno@statistika.its.ac.id)

Abstract

BMKG has made climate classification by making Zone Season (ZOM). Based on the results of an evaluation of the climate modeling (rainfall) indicates that there are several locations (ZOM) had a poor performance of the low accuracy. Some things that allegedly resulted in low accuracy, such as forecasting methods and ZOM determination is not suitable anymore. Therefore, this research aims to evaluate the classification accuracy ZOM BMKG with MARS approach. The process of grouping was using monthly rainfall data in Ngawi on original data (without reduction) and reduction data of factor analysis. Grouping method was using complete linkage and euclidean distance. Furthermore, the results of the grouping are modified through a correction elevation maps, and conducted an evaluation with MARS approach. The results showed that re-grouping ZOM obtained an optimum number of groups as much as 2 groups for the original data and 4 groups for reduction data. Evaluation of the accuracy of the classification ZOM BMKG with MARS approach in the original data and reduction data is 88.9% and 100%. This indicates that MARS is one of the best classification methods in evaluating the classification accuracy ZOM because it has a high classification accuracy.

Keywords: *Zone Season, Complete Linkage, MARS.*

1. Introduction

Climatology Meteorology and Geophysics Agency (BMKG) has carried out the grouping of climate (rainfall patterns) to create a Zone Season (ZOM) in East Java. ZOM is used as a base to see the similarity of climate (rainfall patterns) in a region. For Ngawi, it is divided over 2 ZOM. Based on the evaluation that has been done BMKG against climate modeling (rainfall patterns) shows that there are some sites that have ZOM poor performance, which has a low degree of accuracy. Some things that cause the low accuracy, such as forecasting methods used to predict still not fit and the determination of ZOM which is no longer relevant.

To solve the first problem, BMKG been using several forecasting methods to forecast and predict the climate, the ARIMA method, wavelet transform, and Adaptive Neuro-Fuzzy Inference Systems (ANFIS). However, for evaluation ZOM until now has never been done by the BMKG [2]. Thus, efforts to solve the problem one is to evaluate ZOM BMKG, where the grouping method used by BMKG is complete linkage method. ZOM evaluation is done by using MARS classification method, because Mars has a small classification error [6]. Therefore, in this study will evaluate the classification accuracy ZOM BMKG with MARS approach. The existence of this research is expected to be able to describe ZOM BMKG and able to provide recommendations to obtain the best classification method that can be used as a reference in classifying ZOM.

2. Experimental Detail

Sources of Data

Sources of data in this study are secondary data obtained from BMKG. This data is in the form of monthly rainfall data taken from each rainfall station in Ngawi began in January 1989 to September 2010.

Research Variables

Variables used in this study are the result of averaging rainfall data monthly from each station.

Data Analysis Method

The steps in analyzing the data consist of two stages, which are:

Phase 1

Perform clustering with hierarchical cluster analysis method (complete linkage) with euclidean distance measure up to modified grouping results by correction Ngawi elevation maps and contour maps of rainfall. The steps can be described as follows.

a. Describe the rainfall data which represents the average results from each station in Ngawi.
b. Perform dimensional reduction from the original data variables with factor analysis produced independently and subsequently performed classification with hierarchical cluster analysis. To clarify the relationship between variables from the main component used Varimax rotation.
c. Forming groups using hierarchical cluster analysis using complete linkage and euclidean distance measure on the original rainfall data (non-reduced) and the value of the reduction factor score.
   Euclidean distance formula is as follows.

$$d(x_i,x_j)=\sqrt{\sum_{k=1}^{p}(x_{ik}-x_{jk})^2} \text{ dengan i, j = 1, 2, 3, ..., n}$$

k = 1, 2, 3, ..., p
(1)

   Where, $d(x_i,x_j)$ is the distance between two objects i and j, x_{ik} is the value of object i on variable k, and x_{jk} is the value of object j in the variable k, while the complete linkage method can be formulated as equation (2).

$$d_{k(i,j)} = maks(d_{ki}, d_{kj}) \quad (2)$$

   with i, j = 1, 2, 3, ..., n, $d_{k(i,j)}$ is a measure different between the group-k by group (i, j), d_{ki} and d_{kj} row is the distance between the nearest neighbor to the group-k and the i-th and k th group and j th [8].
d. Using the elevation map as a reference in Ngawi Regency modify grouping results obtained.
e. Modifying the results of clustering based on the elevation map and contour Ngawi rainfall.
f. Getting a new ZOM ZOM by identifying members of the grouping results obtained.
g. To evaluate criterion standard deviation in the group and between groups.

Phase 2

From the results of grouping which has been formed, the next is to evaluate the accuracy of the results of grouping ZOM with MARS approach. Evaluation of classification accuracy ZOM performed on original data (without reduced) and factor scores of factor analysis (data reduction).

Multivariate Adaptive Regression Spline (MARS)

Multivariate Adaptive Regression Spline (MARS) is a nonparametric regression procedure that requires no assumptions about the underlying functional relationship between response and predictor variables. Instead, MARS build this relationship from a set of coefficients and the basic functions of data regression. This makes MARS is suitable for problems with higher input dimensions (ie, with more than 2 variables). MARS model is focused to overcome the problems that have a high-dimensional data. In addition, MARS is the development of Partition Regression Recursive approach (RPR), which still has a weakness where the model produced is not continuous at the knots.

MARS general model equation is formulated as follows [5].

$$\hat{f}(x)=\alpha_0+\sum_{m=1}^{M}\alpha_m\prod_{k=1}^{K_m}\{S_{km}(x_{v(k,m)}-t_{km})] \quad (4)$$

where:

α_0 = parent basis function (constant)
α_m = coefficient of basis function to-m
M = number of basis function
K_m = degree of interaction
S_{km} = value 1 or -1 if the data is on the right or the left knot
$x_{v(k,m)}$ = predictor variables
t_{km} = value of knots of predictor variables $x_{v(k,m)}$

Selection of best model based on the minimum GCV value. Minimum GCV function is:

$$GCV(M)=\frac{ASR}{\left[1-\frac{C(\hat{M})}{n}\right]^2}=\frac{\frac{1}{n}\sum_{i=1}^{n}[y_i-\hat{f}_M(x_i)]^2}{\left[1-\frac{C(\hat{M})}{n}\right]^2} \quad (5)$$

where:

y_i = response variables
$\hat{f}_M(x_i)$ = responses variables on the estimated value of M basis function
n = number of observations
$C(\hat{M})$ = C(M)+ dM

$C(M)$ = $\text{trace}\left[\mathbf{B}(\mathbf{B}^T\mathbf{B})^{-1}\mathbf{B}^T\right]+1$

d = value when each basis function reaches optimation ($2 \le d \le 4$)

Classification of MARS

In the MARS model, the classification is based on the approach of regression analysis [4].

If **Y** categorical response variable with m predictor variables, $\mathbf{x} = (x_1, \cdots, x_m)$ The MARS model can be written as follows.

$$\text{logit}\,\pi(x) = \ln\left(\frac{\pi(x)}{1-\pi(x)}\right) = \alpha_0 + \sum_{m=1}^{M}\alpha_m \prod_{k=1}^{K_m}[s_{km}.(x_{v(k,m)} - t_{km})] \quad (6)$$

Classification method is quite good when the produce fewer errors in classification or in providing opportunities for misclassification (allocation) are small [1].

APER

APER (Apparent Error Rate) is an evaluation procedure that is used to see opportunities classification error made by a classification function [7]. Determination of classification error can be known through misclassification tables as in Table 1 below.

Table 1. Table Error Classification

Actual Group	Prediction Group	
	1	**2**
1	n_{11}	n_{12}
2	n_{21}	n_{22}

Source: Rencher, 2002 [9]

Where,

n_{11} = Number of observations from group 1 were classified as group 1 right

n_{12} = Number of observations from group 1 either classified as group 2

n_{21} = Number of observations from group 2 either classified as group 1

n_{22} = Number of observations from group 2 were classified as group 2 right

The calculation of the value of APER is as equation (7).

$$\text{APER}\,(\%) = \frac{n_{12} + n_{21}}{n_{11} + n_{12} + n_{21} + n_{22}} \quad (7)$$

3. Result and Discussion

ZOM Cluster on Ngawi

Before clustering ZOM, first we described the general description of rainfall characteristics of each station in Ngawi and reduction variables with factor analysis to avoid dependences between variables.

General Description Each Rainfall Stations in Ngawi

Description or overview of the characteristics of rainfall at each station Ngawi is required as initial information about the shape and pattern data used for deeper analysis. The description states that the average rainfalls for each station in Ngawi almost the same. Karang Jati station has an average rainfall is highest at 205.571 with the highest rainfall of 451.64 mm and the lowest rainfall of 22 mm, while the station has an average rainfall was lowest for the Begal station is 126.38 mm. The lowest rainfall was 18.87 mm while the highest rainfall was 293.47 mm. When viewed from the variability of rainfall for each station, Jogorogo and Karang Jati have the highest rainfall variability compared with other stations. This indicates that the area around the station has a rainfall extremes, in other words there are different levels of high rainfall in the dry season and rainy season. While the station of Kedung Galar and Begal has the lowest rainfall variability that is equal to 89.68 and 92.04. When viewed on the basis of average rainfall by month showed that the type of rainfall in Ngawi is the monsoonal type. The rainy season in Ngawi occurred from November-April, while dry season occurs in the month of May to October.

Factor Analysis

Based on the percentage of the total diversity of factors are known that are formed from five factors, four factors which formed was able to explain the total variability more than 70%, ie 77.64%. The percentage of variability of each factor in sequence is 37.626, 16.739, 12.328, and 10.942. Thus, in this case only taken 4 factors are optimum. It is adapted also to the climatic conditions in Indonesia especially Ngawi, where there are two seasons namely dry season and rainy. Eigen value of each sequentially factor is 4.515, 2.009, 1.479, and 1.313. To clarify in describing the characteristics of the monthly rainfall in Ngawi can be seen in Table 2.

Tabel 2. Loading Factor with Varimax Rotation

Variable	F1	F2	F3	F4
January	**0,635**	0.697	0.149	-0.055
February	**0,9**	0.141	0.214	-0.097
March	**0,89**	-0.158	0.053	0.217
April	**0,607**	0.192	-0.102	0.67
May	0.424	-0.136	**0.8**	0.329
June	0.164	**0.82**	-0.047	0.219
July	-0.005	0.168	-0.004	**0.79**
August	-0.007	0.037	**0.072**	0.006
September	0.038	0.206	**092**	-0.035
October	-0.209	**0.78**	0.270	0.260
November	0.046	0.233	0.323	**0.8**
December	**0.65**	0.280	0.540	0.125

Note: Figures in bold letters is the highest value of each factor loading.

Table 2 shows the result of loading factors with Varimax rotation to explain the position of each variable into a number of factors that shape. Based on the factor loading value indicates that the months on factor 1 (F1) is the rainy season, i.e. January, February, March, April, and December. The dry season in Ngawi occurred in July and November which can be seen in factor 4 (F4). Factor 2 (F2) and 3 (F3) shown a transition season in both dry and rainy season. May-June is the dry season transition, while the month of August to October is the rainy season transition. Based on Table 2 indicates that the District Ngawi longer rainy season compared with up to 4-month dry season.

Clustering ZOM in Ngawi with Complete Linkage Method

The method is one of complete linkage clustering method that uses the farthest distance to classify objects [8]. Election ZOM based on the percentage of the value of the highest classification accuracy using discriminant analysis that shows how much the level of diversity or homogeneity ZOM formed. ZOM is formed from the original data of rainfall in Ngawi (without reduction) and have been reduced. From the results of the classification accuracy ZOM using discriminant analysis on original data and data reduction was chosen value of 100% classification accuracy. The optimum number of groups in the original data there are 2 and 4 ZOM ZOM on data reduction.

ZOM members who formed the original data (without reduction) is as follows.

ZOM 1 : Mantingan, Ngawi, Ngrambe, Tretes, Kedung Galar, Walikukun, Bekoh, Kedung Bendo, Ngale, Paron, Mardiasri, Padas, Sambiroto, and Begal.

ZOM 2 : Kedung Urung-urung, Jogorogo, Karang Jati, and Guyung.

ZOM member formed on the data reduction :

ZOM 1 :Mantingan, Ngale, Paron, and Mardiasri.

ZOM 2 : Kedung Urung-urung, Jogorogo, Karang Jati, and Guyung.

ZOM 3 : Ngawi, Ngrambe, Tretes, Kedung Galar, Walikukun, Bekoh, Padas, Sambiroto, and Begal.

ZOM 4 : Kedung Bendo.

Re-Clustering ZOM in Ngawi

The initial phase after the known members of ZOM, by using the elevation map of Ngawi as a reference to modify the grouping results obtained. Next, identify ZOM areas with contour maps. This identification process allows re-member grouping occurred ZOM which have been formed. The result of re-clustering based ZOM BMKG contour map of elevation and rainfall on the original data as given in Figure 3.

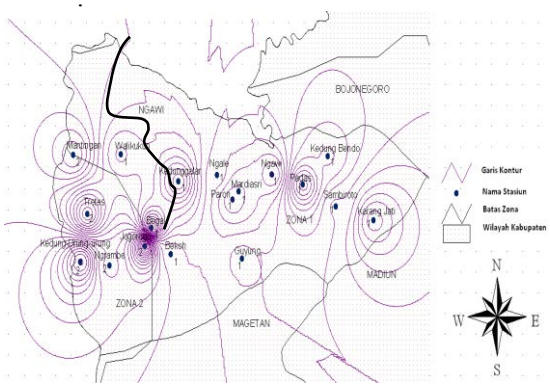

Figure 3. Re-Clustering ZOM in the Original Data (No Reduction)

Members of each group ZOM BMKG formed as shown in Figure 3 is as follows.

ZOM 1 : Walikukun, Kedung Galar, Begal, Bekoh, Ngale, Paron, Mardiasri, Ngawi, Guyung, Padas, Sambiroto, Kedung Bendo, and Karang Jati.

ZOM 2 : Mantingan, Tretes, Jogorogo, Kedung Urung-urung, and Ngrambe.

The intensity of rainfall on average in ZOM 1 amounting 158.676 mm and ZOM 2 were equal to 161.54mm. Furthermore, with the same consideration as in the original data, be re-clustering ZOM in the data reduction. Figure 4

shows the results of re-clustering ZOM for data reduction based on rainfall contour map.

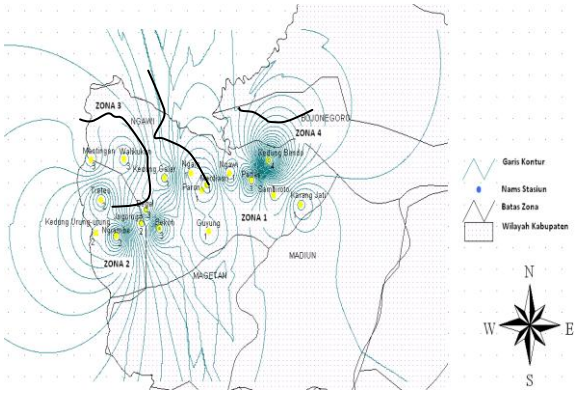

Figure 4. Re-Clustering ZOM in Reduction Data

Finally, the identification of members of ZOM results is re-clustered:

ZOM 1 : Ngawi, Kedunggalar, Ngale, Paron, Mardiasri, Padas, Karang Jati, Sambiroto, and Guyung.

ZOM 2 : Ngrambe, Tretes, Kedung Urung-urung, and Jogorogo.

ZOM 3 : Mantingan, Walikukun, Bekoh, and Begal.

ZOM 4 : Kedung Bendo.

The intensity of the average rainfall in ZOM 1, 2, 3, and 4 were 164.278 mm, 168.698 mm, 154.499 mm, and 135.037 mm, respectively.

Accuracy Evaluation of Clustering ZOM with MARS Approach

After the combination between the number of basic functions (BF), the maximum interaction (MI), and the minimum observation (MO), the MARS model in re-clustering ZOM BMKG in Ngawi without involving the interaction (MI = 1) yields the best model because it has a value of GCV smaller, that is equal to 0.1635 with R^2 equal to 57.48%. The best MARS model of clustering ZOM in Ngawi is:

$$\hat{f}(x) = 1{,}109 + 0{,}006(X_{januari} - 213{,}33)_+ - 0{,}006(X_{april} - 166{,}93)_+ \quad (9)$$

Model in equation (9) noted that there are two predictor variables that influence the response. $X_{january}$ is the value of rainfall in January and X_{April} is the value of rainfall in April. Table of classification in clustering ZOM BMKG rest can be seen in Table 3.

Table 3 shows that the MARS model without interaction produces clustering accuracy 88.9%, of which there are 2 errors identified grouping. The size classification error can be calculated using the following APER.

$$APER = \frac{(1+1)}{(14+4)} = \frac{2}{18} = 0{,}111$$

Table 3. Accuracy of Classification of ZOM BMKG in the Original Data

Classification Accuracy		Prediction		Total	% Accuracy
		Zone 1	Zone 2		
Actual	Zone 1	13	1	14	88,90%
	Zone 2	1	3	4	

Table 3 also noted that there is a station that should be included in zone 2 but is allocated to the zone 1, ie Mantingan station. In contrast, a station that should enter into the zone 1 but is allocated to the zone 2, i.e. Walikukun station. Furthermore, in the same way the original data carried out the formation of MARS in the reduction data. From all models that have been obtained, without involving interaction MARS model is selected and considered as the best model, because it has the smallest GCV value, which is 0.86012 with R^2 equal to 34.84%. MARS model of data reduction based on adjustment of map elevation without involving the interaction is as follows.

$$\hat{f}(x) = 2{,}9556 - 0{,}5815(F_4 + 1{,}93)_+ \quad (10)$$

Table 4. Accuracy of Classification of ZOM BMKG in the Reduction Data

Classification Accuracy		Prediction				Total	% Accuracy
		Zone 1	Zone 2	Zone 3	Zone 4		
Actual	Zone 1	9	0	0	0	9	100%
	Zone 2	0	4	0	0	4	
	Zone 3	0	0	4	0	4	
	Zone 4	0	0	0	1	1	

The calculation of error value grouping with APER for ZOM is as follows.

$$APER = \frac{0}{(8+4+5+1)} = \frac{0}{18} = 0$$

Based on the value generated from APER, it shows that there was no error in re-clustering ZOM in the reduction data. This means that the accuracy of grouping ZOM on data reduction with MARS approach is 100%.

4. Conclusion

Based on the results of data analysis and discussion, it was concluded as follows.

1. Clustering ZOM BMKG with complete linkage method based on the adjustment of map elevation contours Ngawi and precipitation reduction on the original data and found that the optimum number of groups of 2 and 4 groups of ZOM. The intensity of rainfall on average in ZOM 1 and 2 equal to 158.676 mm and 161.54 mm. While the data reduction, the intensity of rainfall on average in ZOM 1, 2, 3, and 4 is 164.278 mm, 168.698 mm, 154.499 mm, and 135.037 mm.
2. Evaluation of the accuracy of clustering ZOM BMKG in the original and reduction data based on adjustment of map elevation Ngawi district with MARS approach produces precision value of 88.9% and 100%. This shows that the grouping ZOM BMKG complete linkage method on the original data (without reduction) gives a value less than the maximum classification accuracy. Also note that the MARS is the best classification method in evaluating the classification accuracy ZOM because it has a high classification accuracy.

5. Acknowledgements

The first author thanks to Almighty Allah for His blessings, mercy, blessings, and His guidance so that he can finish this research. The first author also would like to thank to Dr. Bambang W. Otok, M.Si as the faculty mentor.

6. References

[1]. Agresti, A. (1990), *Categorical Data Analysis*. New York: John Willey and Sons.

[2]. Alam, D.P. (2010), Grouping Zone Season (ZOM) with A*gglomerative Hierarchical Clustering*. Surabaya: Department of Statistics, Science Faculty, Institute of Technology.

[3]. BMKG. (2009), *Evaluation and Forecast 2008/2009 Wet Season Dry Season 2009 Province of Banten and Jakarta*. Jakarta: BMKG.

[4]. Cox, D.R, Snell, E.J. (1989), *Analysis of Binary Data*. Second Edition. London: Chapman & Hall.

[5]. Friedman, J.H. (1991), *Multivariate Adaptive Regression Splines*. *The Annals of Statistics*, Vol. 19 No. 1.

[6]. Hidayat, U. (2006), *Classification Analysis of Village in East Java Using Multivariate Adaptive Regression Spline (MARS)*. Surabaya: Department of Statistics-S2, Institute of Technology.

[7]. Johnson, R.A. and Wichern, D.W. (1992), *Applied Multivariate Statistical Analysis*. New Jersey: Prentice Hall.

[8]. Anonymous (2002), *Applied Multivariate Statistical Analysis*, *5th Ed*. New Jersey: Prentice Hall, Englewood Cliffs.

[9]. Rencher, A.C (2002), *Methods of Multivariate Analysis, Second edition*. New York: John Wiley & Sons, Inc.

[10]. Tjasjono, B. (1999), *General Climatology*. Bandung: ITB.

The Effect of Cadmium as Reductor and Reduction Time in the Measurement of NO_2 Gas in Ambient Air using KI-Amylum Absorber

Qonitah Fardiyah [1], Hermin Sulistyarti [2], Nur Hayba Islamiyah [3]

[1,2,3] Chemistry Department, Faculty of Science, Brawijaya University, Malang, Indonesia, (qfardiyah@yahoo.com)

Abstract

The effect of cadmium as reductor and reduction time in the measurement of NO_2 gas in ambient air using KI-amylum absorber was studied. Nitrogen dioxide in water easily forms NO_2^- and NO_3^-. NO_3^- reduced to NO_2^- by addition of cadmium and react with KI-amylum to form blue complex of I_2-amylum which can be measured at 610 nm. The variation of cadmium mass are 0.028; 0.031; 0.034; 0.036; and 0.039 g was studied to know effect reductor of form NO_3^- to NO_2^-. The reduction time are 5, 10, 15, 20, and 20 minutes was studied to determine time of reduction. The results showed that addition of cadmium and reduction time had an effect on absorption NO_2 gas concentration. The optimum conditions were reached at cadmium mass of 0.034 gram and reduction time 15 minutes with NO_2 gas efficiency 84%. The statistic test results showed that F test ($F_{count}>F_{table\ 5\%}$) and BNT test revealed a significant different to determination of cadmium mass and reduction time.

Keyword: *cadmium, NO_2 gas, reduction time, KI-amylum.*

1. Introduction

One pollutant of air pollutants are nitrogen oxides (NOx). Nitrogen oxide is very dangerous to humans that can cause breathing problems and damage plants [1]. Nitrogen oxides (NOx) consist of NO and NO_2 gases. A second study showed that the NO_2 component four times more toxic than NO [2].

Measurement of NO_2 gas can be detected using a solution of potassium iodide-amylum absorbent. In solution, the NO_2 gas will break down to form NO_2^- which will react with potassium iodide which will produce iodine with the addition of acetic acid or dilute sulfuric acid, which can be identified from the blue that came from iodine-amylum complex [3]. In the study of Rakhwanto (2010), NO_2 gas measurement has been performed using KI-amylum absorption solution which produces a blue complex [4]. Optimization of parameters obtained in these studies is the optimum concentration of KI-amylum for $16x10^{-3}$M, with exposure time for 45 minutes and a flow rate of 400 mL / min. But in that study, the efficiency of NO_2 gas is absorbed by the KI-amylum solution only reached 70%. This is because the amount of NO_2 gas is converted to NO_2^- in the absorption solution was not optimal. In the solution, NO_2 will react with H_2O to form nitric acid (HNO_3) and nitrous acid (HNO_2) [5]. In Rakhwanto research, can be detected in solution that NO_3^- still there and cannot be absorbed by the KI-amylum solution [4]. According to Ignarro *et.al*. (1993), NO_2 gas measurement using a solution of KI absorber can only detect the presence of NO_2^-, NO_3^- while cannot be detected with KI [6]. Therefore, to maximize the absorption of NO_2^- by KI-amylum solution needs to be studied the influence of the addition of reductor. Addition of reductant aims to reduce NO_3^- to NO_2^-. NO_2 gas can all converted to NO_2^-, so that the efficiency of NO_2^- is absorbed by the KI-amylum solution increased.

According to Vogel (1985), NO_3^- can be reduced to NO_2^- by metallic zinc and detected using Griess method that forms red azo dye [3]. Meanwhile, according to Howse (1997), reducing agent that can reduces NO_3^- to NO_2^- namely cadmium metal [7]. Cadmium can reduce NO_3^- in acidic conditions and produce divalent ions (Cd^{2+}). Cadmium is also insoluble in alkaline conditions. Therefore, the use of cadmium to maximize the reduction of NO_3^- to NO_2^- in absorbent KI-amylum solution must be in acid condition [8].

In the determination of NO_2 gas, NO_2 will react with the H_2O contained in the solution that will form the $NO_3^-$and NO_2^-, as given in equation 1 [9]:

$2NO_{2(g)} + H_2O_{(l)} \rightarrow NO_2^-{}_{(aq)} + NO_3^-{}_{(aq)} + 2H^+{}_{(aq)}$ (1)

Measurement of NO_2^- can be performed using KI in glacial acetic acid solution, while $NO_3^-$was not detectable with KI because it cannot reduce the NO [6]. Similar results can be obtained from a solution containing NO_2^- and added with KI-amylum with dilute acetic acid. Then the iodine would be released and can be identified from the resulting blue color with amylum paste, as given in equations 2 and 3 [3]:

$2NO_2^-{}_{(aq)} + 2I_{aq)} + 4CH_3COOH_{(aq)} \rightarrow I_{2(aq)} + 2NO_{(g)} + 4CH_3COO^-{}_{(aq)} + 2H_2O_{(l)}$ (2)

I_2 + amylum $\rightarrow$ I_2-amylum (3)

(blue)

$NO_3^-$and NO_2^- produced from the NO_2 gas in solution such as equation 1, NO_3^-formed can be reduced to NO_2^- using cadmium as the reducing agent, cadmium metal used to analyze the presence of NO_3^- in sea water, in acidic conditions can be reduced NO_3^- such as equations 4 and 5 [7]:

$NO_3^-{}_{(aq)} + 2H^+{}_{(aq)} + 2e \rightarrow NO_2^-{}_{(aq)} + H_2O_{(l)}$ (4)

$NO_3^-{}_{(aq)} + Cd_{(s)} + 2H^+{}_{(aq)} \rightarrow NO_2^-{}_{(aq)} + Cd^{2+}{}_{(aq)} + H_2O_{(l)}$ (5)

Standard potential of the metal cadmium at 25°C is presented in equation 6 [3]:

$Cd^{2+}{}_{(aq)} + 2e^- \rightarrow Cd_{(s)}$ $E° = -0{,}40$ V (6)

Thus the standard potential, it is known that cadmium can reduce NO_3^- to NO_2^- which have Eo = +0.94 V in acidic and Eo = +0.015 V in alkaline conditions [10].

The process of oxidation reduction between NO_3^- and cadmium are influenced by a variety of measurement parameters, such as cadmium mass used and the reduction time of cadmium. Reduction time was investigated to find out the course of the reduction reaction in the absorber solution.

Based on the above background, this research study the effect of cadmium and reduction time in the measurement of NO_2 gas in the air using KI-amylum absorption solution.

2. Experimental Details

Materials

The materials used in this study is pro analysis (pa) include nitric acid 65% (v/v) (Merck, Germany), copper powder, potassium iodide, amylum, cadmium powder, glacial acetic acid, and distilled water.

Lab wares

The tools used in this research include micro-pipette digital assipette no.115, hot plate/stirrer 502 series, analytical balance (Ohaus, USA), magnetic stirrer (IKAMAG® RH) and stirer, oven (Memmert, Germany) , spectrophotometer 301-A and kuvet, suck balls, spray bottles, 20 mL impinger, glassware, stopwatch, flowmeter, and pump air.

Preparation of NO_2 Gas

Preparation of NO_2 gas is done by inserting 0.04 grams of Cu powder into the glass tube which is then dropped into the manufacture of gas in excess of concentrated HNO_3. This reaction took place in a vacuum system to produce NO gas with a concentration 1200 ug / mL. NO_2 gas manufacture 150 ug / mL performed by reacting NO gas is formed by O_2 from the air. Then the NO_2 gas will be absorbed by KI-amylum solution with a volume of 10 mL with the aid of a pump suction system and carried gas exposure for 45 minutes. The experiment design is shown in Figure 1.

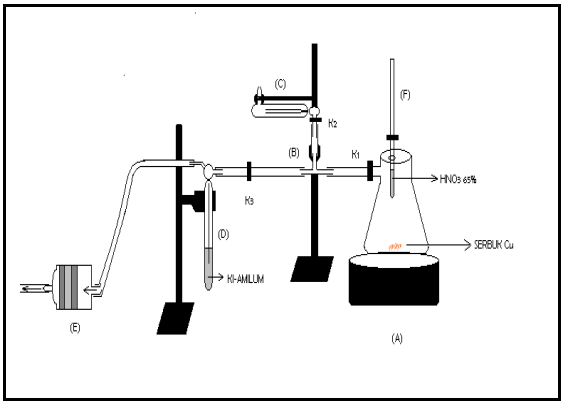

Figure 1. Experiment Design for NO_2 preparation

Determination of Optimum Mass Cadmium

Cadmium powder is 0.028 grams inserted into the beaker, then added a solution of KI-amylum after exposure to NO_2 gas 150 ug / mL for 45 min (experimental result 3.3) and added 1 mL acetic acid and shaken with a magnetic stirer for 15 minutes. Shuffle is calculated starting from the addition of absorbent into the cadmium solution. We then performed the same procedure with the mass variation of cadmium is 0.031, 0.034, 0.036, and 0.039 g. The solution was then measured with a spectrophotometer at 610 nm.

Determination of Optimum Reduction Time

Determination of optimum reduction time experiment conducted as above. but the mass of cadmium that was used is the optimum mass obtained from the experiment above. The solution was shaken with a magnetic stirer for variation reduction time of 5, 10, 15; 20; and 25 minutes.

3. Results and Discussion

In this research, the measurement of NO_2 gas in the air using absorbent KI-amylum solution. NO_2 gas dissociates easily in water to form NO_2^- and NO_3^-. KI-amylum absorption solution is specific only to NO_2^-. The measured NO_2^- , which is due to addition of cadmium, is proportional to the NO_2 gas absorber by KI-amylum solution.

Determination of cadmium mass was conducted to determine the effect of cadmium as reductor in the formation of NO_2^- reduction resulted from NO_3^- in the absorption solution after reacting with NO_2 gas.

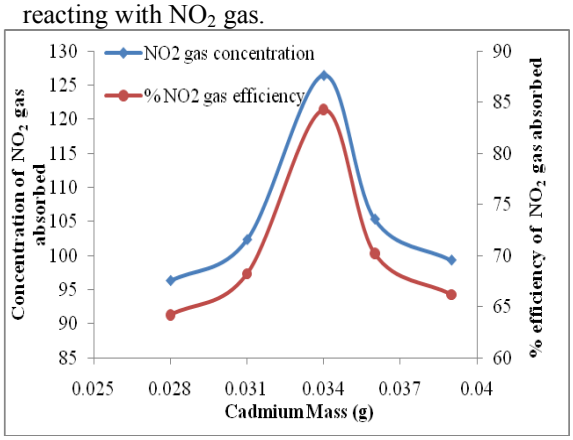

Figure 2. Graph the relationship between the mass of cadmium with concentration and % efficiency of NO_2 gas that absorbed

In Figure 1, shows the addition of 0.028 to 0.034 g of cadmium increased the concentration of NO_2 gas is absorbed, so the optimum mass of 0.034 g. NO_2 gas concentrations measured at 126.41 ug / mL with an efficiency of 84%. This suggests that cadmium has been reduced NO_3^- to NO_2^- with a maximum in the absorption solution, so that can know the greater the addition of cadmium that are used cause NO_2^- which absorbed by the absorption solution will be increased so that the concentration of NO_2 gas has increased as well. At the optimum mass showed cadmium as reductor can affect the measurement of NO_2 gas. This is because without redactor, gas concentrations of NO_2 are measured only at 84.27 ug / mL and when compared with the mass of 0.034 g cadmium, concentrations of NO_2 gas is measured 126.41 ug / mL.

At 0.036 and 0.039 g mass, decreased concentrations of NO_2 gas. This decrease was due to the reduction process continues to run, so not only the reduction to be NO_2^- from NO_3^-but NO_2^- contained in the absorption solution can also undergo reduction to form NO gas is shown in equation 7 [11].

$$M_{(s)} + 2HNO_{2(aq)} \rightarrow M^+_{(aq)} + 2NO_{(g)} + 2H^+_{(aq)} \quad (7)$$

Therefore, the absorbed of NO_2^- by KI-amylum solution will be decreased by increasing NO gas that form. As a result, measurable concentrations of NO_2 gas became lower.

Reduction time is the time required to reduce NO_3^- to NO_2^- in KI-amylum absorption solution after reacting with NO_2 gas. On the timing variation reduction of time to find out the reduction process is running optimally.

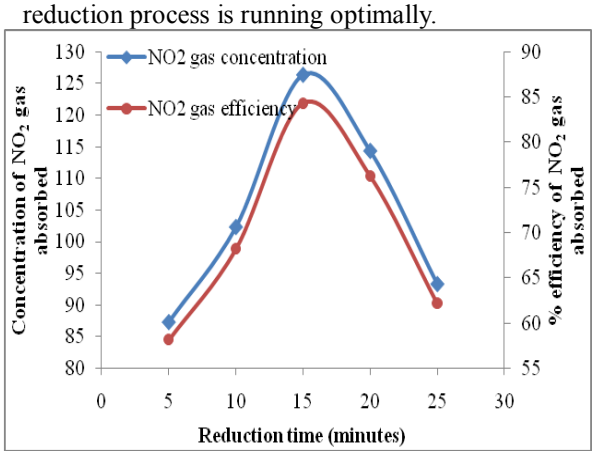

Figure 3. Graph showing the relationship between reduction time and % efficiency concentrations of NO_2 gas that absorbed

In Figure 3, shows at the time of 5-15 minutes of absorbed NO_2 gas concentrations increase. The optimum time is at 15 minutes to obtain the concentration of NO_2 gas at 126.41 ug / mL with an efficiency of 84%. At the optimum time there has been reduction of NO_3^- to NO_2^- in a solution of KI-amylum absorption maximum. While at times 20 and 25 minutes had decreased concentrations of NO_2 gas is absorbed. This is because the reduction of NO_3^- to NO_2^- has reached equilibrium that will affect the formation of NO_2^-. NO_2^- whose existence tends to be unstable, so the longer the time used will influence the form of NO_2^-which would lead to absorption by the absorption solution of KI-amylum decreased [12]. The decline was also due to optimum condition KI-amylum solution in a previous study less, with the reduction of NO_3^- to NO_2^- which yields NO_2^- the remainder so that the absorption process by KI-amylum solution was not optimal.

4. Conclusion

Addition of cadmium as reducing agent affects measurement of NO_2 gas to increase the percentage of 14%. The mass of cadmium is used at 0.034 grams and the optimum reduction time of NO_3^- to NO_2^- at 15 minutes, so concentrations of NO_2 gas at 126.41 ug / mL. In the mass and time were obtained which absorbed NO_2 gas efficiency

84%.

5. References

[1]. Peavy, H. S., Rowe, D. R., and Techobanoglous, G., (1985), Environmental Engineering, McGraw Hill Inc., Singapore.
[2]. Pohan, (2002), Pencemaran Udara dan Hujan Asam, USU digital library, Sumatera Utara.
[3]. Vogel, A. I., (1985), Buku Teks Analisis Anorganik Kualitatif Makro dan Semimakro, Edisi kelima, Alih bahasa Pudjaatmaka, PT. Kalman Media Pustaka, Jakarta, 235.
[4]. Rakhwanto, E. W., (2010), Pengaruh Konsentrasi Larutan Penyerap KI dan Waktu Pemaparan Terhadap Penentuan Gas NOx di Udara, Laboratorium Kimia Universitas Brawijaya, Malang.
[5]. Shen, C.H., and Rochelle, G.T., (1998), Nitrogen Dioxide Absorption and Sulfite Oxidation in Aqueous Sulfite, *Environmental sciences & Technology*, 32(13):1994-2003
[6]. Ignarro, L.J., Jon M.F., Jeanette M G., Norma E.R. dan Russell E.B., (1993), Oxidation of Nitric Oxide in Aqueous Solution to Nitrite but not Nitrate: Comparison with Enzymatically Formed Nitric Oxide from L-Arginine, 90:8103-8107
[7]. Howse, F., (1997), The Determination of Nitrate in The Sea Water, Bermuda Biological Station For Research, Inc., Bermuda, p. 61-62.
[8]. Cotton, F.A. and Wilkinson, (1989), Kimia Anorganik Dasar, edisi pertama, alih bahasa Suhaerto, UI press, Jakarta, 398.
[9]. Klepper, L., (1990), Comparison between NOx Evolution Mechanisms of Wild-Type and nr_1 Mutant Soybean Leaves[1], *Plant Physiol*, 93:26-32
[10]. Sun, J., Zhang, X., Broderick, M., and H. Fein, (2003), Measurement of Nitric Oxide Production in Biological Systems by Using Griess Reaction Assay, Sensors 2003, 3:276-284.
[11]. Wahyono, H., Iis H. and Sutri I., (2007), Pengaruh Hidrazin dan Nitrat dalam Proses Reoksidasi Uranium (IV) menjadi Uranium (VI), PTBN-BATAN, Serpong.
[12]. Marnis, H., (2008), Karakterisasi Molekuler dan Uji Aktivitas Bakteri Pereduksi Nitrat dari Muara Cimanderi Pelabuhan Ratu Sukabumi Jawa Barat, IPB, Bogor.

The Optimization Time of Steam Distillation of Vacuum Oven Dried Aceh Patchouli Leaves (*Pogostemon cablin* Benth) and The Characterization by TLC and GC – MS

Sentot Joko Raharjo [1]; Dr. Rurini Retnowati[2]

(1) Master Program, Chemistry Department, Mathematics and Natural Sciences Faculty, Brawijaya University
(sentotjoko@yahoo.co.id)
(2) Chemistry Department, Mathematics and Natural Sciences Faculty, Brawijaya University
(rurini_retnowati@yahoo.com)

Abstract

This research aims to determine the optimization time of steam distillation of patchouli oils by vacuum drying oven. The optimization time was determined by observing the characteristics of the patchouli oils collected by using steam distillation for 2, 4, 6, and 8 hours of the time process, compared by the oils collected every two hours in 8 hours of distillation time. The patchouli leaves were dryed by using vacuum drying oven before distilled. The characteristics of the patchouli oils observed were the yield and the composition of the oils components. The characterization of the components composition of the patchouli oils were done by thin layer chromatography (TLC) by using silica gel stationary phase F_{254} with eluent benzene-ethyl acetate (90:10) and visible stain of vanillin-sulfuric and gas chromatography-mass spectroscopy (GC-MS). The highest yield of patchouli oils was obtained in the distillate collected at 2 hours and for 8 hours. The highest patchouli oils were obtained by vaccum drying oven with distillate collected for 8 hours of distillation time (4.3019%). The characterization of patchouli oils by TLC method showed six colorful spot, the dark purple color (R_f-1 = 0.87) red hearts (R_f-2 = 0.68); color purple (R_f-3 = 0.56); pale purple color (R_f-4 = 0.47); purple-pink color (R_f-5 = 0.43) and pink (R_f-6 = 0.25). No defferent in the result of TLC analysis by collecting the distillate in every 2 hours from 2 to 8 hours of distillation and collecting the distillate in 2 hours, 4 hours, 6 hours and 8 hours of steam distillation. The Characterization of the patchouli oils of the optimization time of steam distillation by using GC-MS analysis showed a difference of components and composition of each patchouli oils of the distillate collected every 2 hours from 2 to 8 hours and steam distillation for 2 hours, 4 hours, 6 hours, and 8 hours. The highest main component of pachouli oils was patchouli alcohol (79.06%) in the distillate collecting time for 4 hours. Other components of patchouli oils were aromadendrene, seychellene, alpha-patchoulene, pogostol, alpha-gurjunene, and dehydroaromadendrene.

Keywords: *patchouli oils, patchouli leaves, vaccum drying ovens, steam distillation, distillate collecting time.*

1. Introduction

Essential oils of patchouli are known by the name of patchouli oils (patchouli oils). Patchouli oils have good prospects because the price is relatively high and it can not be made by synthesis. Indonesian patchouli oils have been known already 65 years ago and meet the needs of the world's patchouli oils with 80-90% market share. In 2004, it reached 2074 tons worth US$ 27.137 million. In the next few years the starting position will be threatened by the state of Brazil, China, India, and Vietnam. In the perfume / cosmetics industry, there are no other products whether natural or synthetic which are able to substitute the patchouli oils as a fixative material (binder fragrances) that can not be synthesized and the applications as free antiradical and antibacterial [1,2].

Patchouli plants are considered to be mature and ready to be harvested in 5-8 months. The leaves of patchouli contain more oils than the stems. According to Eni (2004), the highest percentage of the essential oils (4-5%) was found in the leaves [3]. Before the distillation, the patchouli leaves was dryed by a drying vacuum oven to decrease the water to 15%, because dry leaves produce more oils. Different modes of isolation have been done, such as solvent extraction, distillation sthal, water distillation, and water steam distillation. But the common method used is steam distillation [4]. According to Ellyta and Elmi (2005), the concentration of patchouli oils was increased by hour by using steam distillation. The highest concentration of patchouli alcohol was in the fifth hour and the lowest was in the first hour because in the first hour the light components evaporate faster than the heavy components such as sesquiterpenes compounds with high molecular weight [5].

According to Maryadhi (2005), the patchouli oils contains more than 30 kinds of chemical components, including four hydrocarbon monoterpenes, nine hydrocarbons sesquiterpenes, two oxigenated monoterpenes, four epoxy

compounds, five sesquiterpenes alcohol, one norsesquiterpene alcohol, two sesquiterpenes ketone and 3 sesquiterpenes ketoalcohol. The main components are ß-patchoulene, α-gurjunene, α-guaiene, α-bulnesenepoxide, ß-caryophyllene, α-patchoulene, seychellene, α-bulnesene, ß-guaienepoxide, norpatchoulenol, patchoulol, and pogostol [6].

Based on the research so far, the purpose of isolation were to obtain high yield of the essential oils by collecting the distillate accumulatively, without observing the component which determine the quality of the essential oils and the effectivity of the distillation time. Therefore this research was done by collecting the distillate in every 2 hours from 2 to 8 hours of distillation and collecting the distillate in 2, 4, 6, and 8 hours of steam distillation. The patchouli leaves were dried by vacuum drying oven before distilled.

2. Experimental Details

Materials and Equipment

The sample used in this study was fresh patchouli leaves from Pujiharjo, District of Tirtoyudo, Malang (Kabupaten – Ind). The sample were fresh leaves that separated from the stem with a cut on the stem of the leaf, then dried in the oven at 70ºC for 24 hours.

Chemicals in this study that had a degree of pro analysis (pa), namely n-hexane, benzene, ethyl acetate, sulfuric acid, and ethanol, while the chemicals that had technically grade were vanillin, magnesium sulfate heptahydrate, distilled water, nitrogen gas, and TLC plates silica gel 60 f_{254}.

The eqiupment used in the study include a set of steam distillation apparatus with a capacity of 5 kg, local vacuum dryer, 500 ml separating funnel, 10 ml measuring pipettes, micro pipette, pipette drops, plate evaporator, heater, desiccator, clamps, vessel developer chromatography, peck 25 ml flask, conical flask 250 ml, sprayer gun, a set of tools kg-ms-2010s Shimadzu QP type, balance Mettler PE 3600, pH meters, and sample bottles of 10 ml and 25 ml.

Patchouli oils distillation

The sample of patchouli leaves were dryed by using vacuum drying oven (weighed 0.5 kg for the steam distillation in which the distillate were collected every 2 hours from 2 to 8 hours and weighed 0.25 kg for the steam distillation for 2, 4, 6, and 8 hours) then distilled by using steam distillation. Each 250 ml distillate was extracted with 3x10 ml of n-hexane. The patchouli oils obtained was determined the yield and constituent components.

Patchouli oils profile analysis by TLC

The patchouli oils obtained from the every 2 hours distillate collection from 2 to 8 hours of steam distillation and the oils obtained by distillation for 2, 4, 6, and 8 hours were spoted using capillary tube (2 µl) at a distance of 1 cm from the bottom plate measuring 1x10 cm. The plate was eluated in the developer vessel using the eluent of benzene : ethyl acetate (90:10) and then sprayed with a spot stain solution vanillin-sulfuric acid, then performed preparative TLC of treatment and oven drying for 8 hours and analyzed by GC-MS.

Profile analysis of the patchouli oils components by total ionic chromatogram (tic) produced by GC-MS

The patchouli oils were analyzed using GC-MS Shimadzu qp-2010s. Number of peaks in the tic data was used to determine the number of components contained in the patchouli oils. The area percentage in the tic data was used to determine the composition of the patchouli oils.

Characterization of each component of patchouli oils based mass spectral analysis by GC-MS

The characterization of components of patchouli oils was based on mass spectral data in GC-MS analysis. The mass spectra data was used to analyze the structure of the component of essential oils through the analysis of fragmentation patterns. Further data analysis by GC-MS tic of each composition of patchouli oils components illustrated graph vs the percentage of the peak component of patchouli oils.

3. Result and Discussion

Patchouli oils distillation

Patchouli oils obtained had a light yellow color. Furthermore, to find out the effective time of distillation from distillate from vacuum oven drying product was collected time at 2 hours, 4 hours, 6 hours, 8 hours and for 2 hours, 4 hours, 6 hours, 8 hours was determined yield of each patchouli oils. The yield data were presented in Table 1. Based on the yield data in Table 1, it can be observed that based on the yield of the essential oils obtained by steam distillation, the effective time for steam distillation was 2 hours because it was decreasing after 2 hours of steam distillation. The decresing value of the yield value presumably was because several components had been evaporated in two hours of distillation.

Second overall on the clock so that the already exhausted after distillation for 2 hours. This shows that the effective time of the steam distillation based on the yield of the essential oils was 2 hours. But the yield of the patchouli oils obtained by steam distillation for 2 hours until 8 hours was increasing. Generally, the highest yield of patchouli oils was found in the distillate obtains by steam distillation for 8 hours (4.3019%).

Table 1. Yield of patchouli oils which dryed by vaccum drying oven

Treatment	Code	Yield (%)
Distillate collecting time in every 2 hours from 1 to 8 hours	On-s-2	2.1260
	On-s-4	0.6737
	On-s-6	0.2640
	On-s-8	0.1164
Distillate collecting time for 2 hours, 4 hours, 6 hours and 8 hours of distillation	On-l-2	1.6668
	On-l-4	2.2807
	On-l-6	3.7943
	On-l-8	4.3019

Patchouli oils analysis by TLC

The analysis of the essential oils components in TLC were presented in Figure 1. Characterization of patchouli oils by TLC method produces six spots color, the dark purple color (r_f-1 = 0.87), red hearts color (r_f-2 = 0.68), purple color (r_f-3 = 0.56), pale purple color (rf-4 = 0.47), purple-pink color (r_f-5 = 0.43), and pink color (r_f-6 = 0.25).

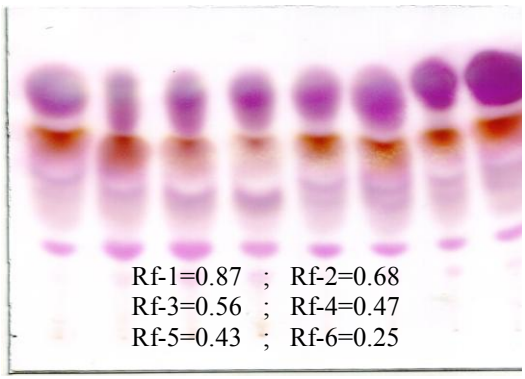

Figure 1. The result of TLC chromatograms of patchouli oils obtained by steam distillation which the distillate were collected in the second, forth, sixth and eight hours of distillation and for 2 hours, 4 hours, 6 hours and 8 hours of distillation

Note : Distilate collecting time :
1 : 2nd hour 5 : For 2 hours
2 : 4th hour 6 : For 4 hours
3 : 6th hour 7 : For 6 hours
4 : 8th hour 8 : For 8 hours

Results of analysis of each patchouli oil of the optimization time of steam distillation with thin layer chromatography method (figure 1) showed stains of rf-1 - rf-6 there was not difference of each patchouli oil of the distillate collected every 2 hours from 2 to 8 hours and steam distillation for 2 hours, 4 hours, 6 hours 8 hours.

The oils obtained from 8 hours of steam distillation was analyzed by preparative TLC followed by GC-MS. The analysis showed the components of r_f-1 were aromadendrene, 3-methylene-1.0.6-heksadiene; alpha-patchoulene, alpha-sinensal, seychellene, 6-hydroxymethyl-oxabicyclo-2-(3.3.0)-octa-6-en-3-one.

The component of r_f-2 was patchouli alcohol (100%), and the components of r_f-3-r_f-6 were undetectable. The TLC analysis information will help to isolate the main component of patchouli alcohol by using column chromatography for further analysis

Patchouli oils component characterization by using GC-MS analysis

Results of analysis of essential oils by using GC-MS resulted chromatogram called the total ion chromatogram (tic). Tic is used to determine the profile and components structure of patchouli oils obtain by steam distillation which the distillate were collected every 2 hours from 1 to 8 hours, and the distillate were collected in the distillation of 2, 4, 6, and 8 hours.

Based on the tic data, it was observed that the main component of patchouli oils was patchouli alcohol and the other components were aromadendrene, seychellene, alpha-patchoulene, pogostol, dehydroaromadendrene, and alpha-gurjunene. The structure of components of patchouli oils was presented in Figure 3. The tic of the components of the patchouli oils obtained by 4 hours of steam distillation was presented in Figure 2 which shows 7 peaks.

The order of the components in GC-MS analysis related to the polarizability. The data of polarizability in 10-24 cm^3 are alpha-gurjunene (25.66); aromadendrene (25.69); seychellene (25.71); alpha-patchoulene (25.76), patchouli alcohol (26.54); pogostol (27.13), and dehydroaromadendrene (-) [7].

Table 2. The composition of the patchouli oils obtained by 4 hours of steam distillation based on GC-MS analysis

No.	Retention time	% area relatif	Component name
1	6.600	1.59	Alpha-gurjunene
2	8.514	12.45	Aromadendrene
3	9.273	8.65	Seychellene
4	10.176	2.71	Dehidroaromadendrene
5	15.982	18.89	Alpha-patchoulene
6	16.149	52.27	Patchouli alkohol
7	18.593	3.43	Pogostol

Dehydroaromadendrene polarizibility was unknown, but presumably it had a higher value than aromadendrene. It was the third component that eluted after alpha-gurjanene and aromadendrene. The order of the compounds eluated based on the polarizability in GC-MS analysis was also supported by the order of the compounds in TLC analysis in Figure 1.

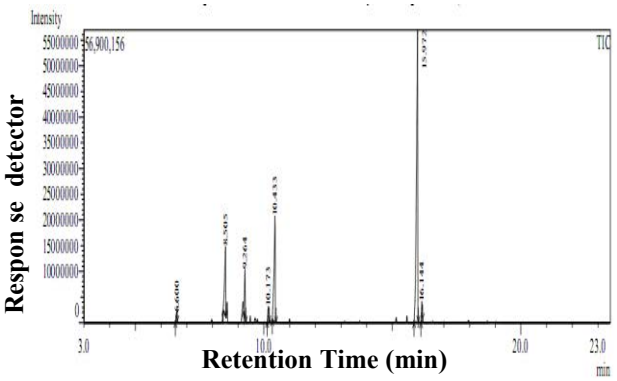

Figure 2. The tic of the patchouli oils obtained by 4 hours of steam distillation (on-l-4) were analyzed by by using GC-MS Shimadzu qp-2010s, rtx-wax column

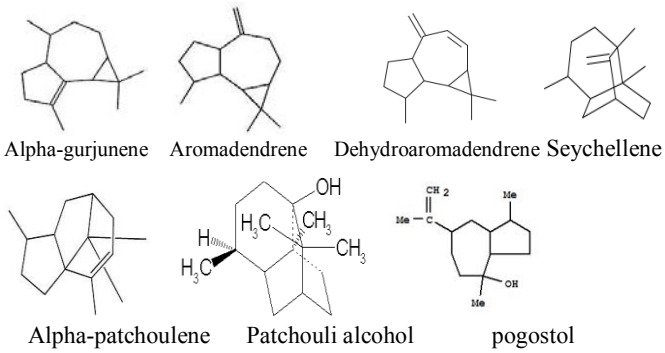

Figure 3 the structure of several components in patchouli oils

The effect of the distillate collectiong time to the profile of the patchouli oils

The effect of the distillate collection time to the patchouli oils component profiles were observed by analyzing the compositions of the components in the oils obtained by collecting the distillate every 2 hours from 2 to 8 hours (Figure 4a) and collecting the distillate for 2, 4, 6, and 8 hours of distillation (Figure 4b) based on GC-MS analysis.

The components with high vapor pressure evaporate first at the steam distillation process. The order of the components vapor pressure data in mmhg were alpha-gurjunene (0.01640), aromadendrene (0.02260), seychellene (0.034000), alpha-patchoulene (0.017700), patchouli alcohol (0.000278), pogostol (0.000083), and dehydroaromadendrene (not detected).

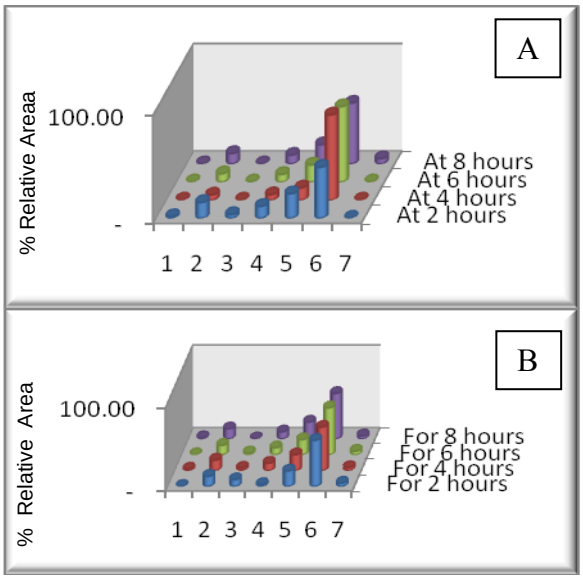

(1)alpha-gurjunene; (2)aromadendrene; (3)dehydroaromadendrene; (4)seychellene; (5)alpha-patchoulene; (6)patchouli alcohol alkohol; (7)pogostol

Figure 4. The percentage of relative areas of the components of patchouli oils obtained by collecting the distillate every 2 hours from 1 to 8 hours (a) and collecting the distillate for 2 hours, 4 hours, 6 hours, 8 hours (b)

The components with high vapor pressure evaporate first at the steam distillation process. The order of the components vapor pressure data in mmhg were alpha-gurjunene (0.01640), aromadendrene (0.02260), seychellene (0.034000), alpha-patchoulene (0.017700), patchouli alcohol (0.000278), pogostol (0.000083), and dehydroaromadendrene (not detected). Dehydroaromadendrene was reported in Figure 4 decreasing in the percentage of area but the other was relatively stable.

Composition of patchouli oil in the optimization time steam distillation showed no alpha gurjunene (at 4 hours, at 6 hours, at 8 hours, for 6 hours and for 8 hours); no dehydroaromadendrene (at 4 hours, at 8 hours and for 8 hours), and no pogostol (at 2 hours, at 4 hours, and 8 hours). The other, the patchouli oils obtained by collecting the distilate every 2 hours from 2 to 8 hours of distillation contains more components than the oils obtained by collecting

the distillate for 2 hours, 4 hours, 6 hours, and 8 hours of distillation.

Results of analysis of each patchouli oil of the optimization time of steam distillation with GC-MS showed a difference of components and composition of each patchouli oil of the distillate collected every 2 hours from 2 to 8 hours and steam distillation for 2 hours, 4 hours, 6 hours 8 hours.

Patchouli alcohol has the highest percentage. The concentration of patchouli alcohol in patchouli oils obtaind by collectiong the distillate every 2 hours from 1 to 8 hours of distillation was 47.24%, 79.06%, 69.85%, 56.33% respectively. While the concentration of patchouli alcohol in patchouli oils obtained by collecting the distillate for 2 hours to 8 hours in was 55.49%, 52.27%, 56.44%, 54.76% respectively. The increasing of the relative percentage of patchouli alcohol in patchouli oils obtained by collecting the distillate in the forth hours of steam distillation were because there were no pogostol and the increasing components, such as aromadendren, seychellen and alpha-patchoulene. It was presumably because of the lower vapor pressure of patchouli alcohol. The increasing and the decreasing of patchouli alcohol obtained by collecting the distillate for 2 hours (55.49%), 4 hours (52.27%), 6 hours (56.44%), 8 hours (54.76%) are related to the increasing and decreasing of components in patchouli oils. Patchouli alcohol was the major component of essential oils compounds and can be used as a compound to determine the time of the distillation.

4. Conclusion

The highest yield of patchouli oils were obtained in the distillate collected for 2 hours and 8 hours. The highest patchouli oils were obtained by vaccum drying oven with distillate collected for 8 hours of distillation (4.3019%).

The characterization of patchouli oils by TLC method showed six colorful spot, the dark purple color (r_f-1 = 0.87) red hearts (r_f-2 = 0.68); color purple (r_f-3 = 0.56); pale purple color (r_f-4 = 0.47); purple-pink color (r_f-5 = 0.43) and pink (r_f-6 = 0.25). No defferent in the result of TLC analysis by collecting the distillate in every 2 hours from 2 to 8 hours of distillation and collecting the distillate in 2 hours, 4 hours, 6 hours and 8 hours of steam distillation.

The characterization of the patchouli oils of the optimization time of steam distillation by using a GC-MS analysis showed difference of components and composition of each patchouli oil of the distillate collected every 2 hours from 2 to 8 hours and steam distillation for 2 hours, 4 hours, 6 hours, and 8 hours. The highest main component of pachouli oils was patchouli alcohol (79.06%) in the distillate collecting time for 4 hours. Other components of patchouli oils were aromadendrene, seychellene, alpha-patchoulene, pogostol, alpha-gurjunene, and dehydroaromadendrene.

5. Acknowledgment

Authors are very thankful to Chemistry Department, Brawijaya University and Pharmacy and Food Analysis Academic "Putra Indonesia Malang" for instrumental support and facilities during the course of work. Authors are also very thankful to Pujiharjo community and Biology Department, Brawijaya University for identification of plant material.

6. References

[1]. Harborne, J.B., (1984), Phytochemical Methods. Chapman and Hall Ltd. K. Padmawinata (translator). ITB. Bandung.

[2]. Hyung W.K., (2008), *Pogostemon Cablin* As Ros Scavenger In Oxidant-Induced Cell Death of Human Neuroglioma Cells, Department of Herbology, College of Oriental Medicine, Dongshin University

[3]. Eni H., (2005), Teknik Analisis Mutu Minyak Nilam, *Buletin Teknik Pertanian* Vol. 10, Nomor 1

[4]. Erika, (2010), Pengaruh Jenis Metode Terhadap Hasil Isolasi Patchouli Alkohol Dalam Minyak Nilam, Skripsi.

[5]. Ellyta and Elmi, (2005), Upaya Peningkatan Kualitas dan Permasalahan Perdagangan Minyak Nilam Di Sumatra Barat, Fakultas Teknologi Industri. Universitas Bung Hatta Padang

[6]. Maryadhi, A. P., (2008), Pembuatan Bahan Acuan Minyak Nilam, Pusat Penelitian Sistem Mutu Dan Teknologi Pengujian – LIPI, Indonesia

[7]. Thegoodscents, 2010. Essential Oils Information. Www.Thegoodscentscompany.Com. Accesed on 20 June 2010.

[8]. Faizal, (2009), Karakterisitk Simplisia Dan Isolasi Serta Analisis Komponen Minyak Atsiri Dari Daun Nilam (Pogostemon Cablin Benth.) Asal Aceh Tenggara, Skripsi. Fakultas Farmasi, USU, Medan.

[9]. Ngampong Kongkathip, *et.al*, (2009), Development of Patchouli With Quality Control And Isolation of Active Coumpound With Antibacterial Activity, *Kasetsart J. (Nat Sci.)* 43: 519-525.

[10]. Nguyên X.D., (1989), Chemical Composition Of Patchouli Oils from Vietnam, Department Of Technical Chemistry, University Of Hanoi, 19 Le Thanh Tong Street, Hanoi, Vietnam, Patchouli Oils, *J. Essent. Oils Res.*

Potencies of Plants around Fishes Ponds in Karang Sentul Village, Gondang Wetan District Pasuruan, East Java

Solikin

Purwodadi Botanical Garden, Pasuruan, East Java
Email: lipisolikin@gmail.com

Abstract

The land use around the fish ponds in farm garden optimally is important to fulfill needs for life sustainably such as foods, spices, medicinal plants, ornamental plants and others. Research to invent and to study the potency of the plant species around the fish ponds in the farm garden in Karang Sentul village, Gondang Wetan District, Pasuruan East Java conducted in August 2005. All the plants obtained on the locations were recorded, identified and studied their potencies. The results showed that there were 45 species, 44 genera, and 30 families of the plants planted around the fish ponds. The potencies of the plants that can be used as medicinal plants are 14 species, as food are 3 species, as fruit are 12 species, as ornamental plants are 15 species, as vegetables are 8 species and for colouring foods is 1 species.

Keywords: *pond, land use, plants, potency, Dondang wetan.*

Woody Plant Diversity and Structure of Coffee Agroforests in the Recharge Area of Some Springs in Ngantang Subs District, Malang Regency, East Java

Titut Yulistyarini [1], Zaenal Kusuma [2], Soemarno [3], Endang Arisoesilaningsih [4]

(1) Purwodadi Botanical Garden, Indonesian Institute of Sciences (LIPI), Pasuruan Regency, East Java
(2,3) Soil Department, Faculty of Agricultures, Brawijaya University, Malang, East Java, Indonesia
(4) Biology Department, Faculty of Mathematics and Natural Sciences, Brawijaya University, Malang, East Java, Indonesia

Abstract

Ngantang have potential as a regional distribution of springs, there are about 71 springs distribute in a group. More than half of them discharged in a small debit, less than 5 l/sec. Krisik, Complang and Pusung pegat springs discharged about 1 l/sec. These springs have decreasing water debit, the last two springs even produce no more discharge. The recharge areas of third springs were dominated by coffee agroforestry land cover. This study to compares woody plant diversity and structure among coffee agroforests in the recharge area of each spring. Woody vegetation was sample in plots 100x 20 m^2 to class of tree (dbh > 30 cm) and in sub plots 40x5 m^2 to class of small tree (dbh < 30 cm). Woody species diversity of Krisik was lower than diversity of Complang and Pusung pegat. Tree species of Krisik and Pusung pegat had a highest similarity index.

Keywords: *Diversity, cofee-agroforest, woody vegetation, spring.*

1. Introduction

Ngantang is one area in Malang Regency potentially spreading area springs. Ngantang located between three volcanoes namely Mount Anjasmoro, Mt. Kelud and Mt. Kawi-Butak. There are about 71 springs distributed in a group in this district. More than half of them belong to small springs that discharged in a small debit (less than 5 l/sec) as much as 37 springs. While 34 other springs have debit 5-125 l/sec., only one spring discharged 125 l / sec, i.e. Tito Ayu located in Sidodadi village [1]. The water of these springs is used to drinking water, washing, cooking and irrigation. The results of team survey of Brawijaya University stated that many springs in Ngantang dried during the dry season and the springs that have a greater flow pattern were permanent [2]. Drought is particularly problematic for upland residents who rely on natural springs for their domestic water supply.

Krisik, Complang and Pusung pegat springs were including the Ngantang springs with small discharges, they had debit less than 1 l/sec. The measurement of spring debit monthly within one year showed that Krisik spring discharged throughout the year, despite its debit decreased in the dry season. Whereas Complang and Pusung pegat springs had different water flow patterns with Krisik spring, the both of springs dried up several months [3]. Spring debit depends on the area contributing recharge to aquifer and the rate of recharge. While the rate of recharge ground water depend on geologic and hydrologic condition [4]. Based on geoelectric data, the third springs occur where surface topography causes the water table to intersect the land slope. These springs were fed from a shallow aquifer consist of sand which had more permeable layer underlain by clay (a less permeable layer). Krisik, Complang dan Pusung pegat springs can be identified as contact springs which naturally were supported by more local ground water flow [3].

The springs that affected by local flow, the ground water came from a relatively small contributing area with the recharge zone relatively near the spring [5]. In consequence, the recharge area of Krisik, Complang and Pusung pegat springs from adjacent narrow recharge areas. Based on a land use map and the result of location surveys, coffe agroforests were largely covered the recharge area of three springs up to 70-80%. While the remaining recharge area consist of ther land uses i.e. horticulture, Pine plantations and housing.

Ngantang is one of Konto watershed area, which has most important functions as a water

supplier to the lake Selorejo for irrigation and electricity generation and an agriculture production area (vegetable, fruit, dairy and timber). Forest in this area converted to other land uses since 50-60 years ago. Natural forests cut down and burned, intensively planted with seasonal crops, potentially accelerating land degradation occurring in the 1930's. In 1942, former forest land was rehabilitated by planting trees and combined with corn, dadap (*Erythrina subumbarns*), pine *(Pinus merkusii*), coffee and vanilla. Then in the early 1980s, the diversity of trees was increased by the planting of some woody species that had high economic value like sengon (*Albizia falcataria*, waru gunung (*Hibiscus macrophyllus), cempaka (Michelia champaca*) and fruit trees (*Durio sp., Persea americana, Lansium domesticum*).

Krisik, Complang and Pusung pegat springs tend to be affected by more local ground water flow systems and thus are at risk from activities that threaten the shallow water table. From the reason, debit of this spring were depended on the characteristics of recharge area. Besides geophysics and biophysical soil, the characteristics of recharge area were determined by vegetation structure. This study was aimed to compare woody plant diversity and structure among coffee agroforests in the recharge area, which supported ground water recharge in the three springs.

2. Experimental Details

Ngantang includes tropical monsoon climate, characterized by the presence of the rainy and dry season which is firm and the air temperature is always hot all year. These research areas are including wet areas with annual rainfall ranges from 2,200 mm to 3,880 mm and mean annual rainfall was 3,000 mm per annum. Mean daily temperature in this area is 23ºC.

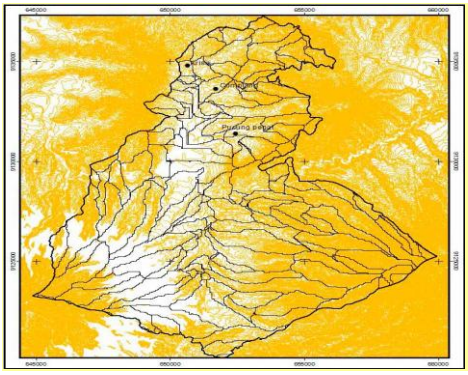

Figure 1. A countour map of Ngantang and the location of Krisik, Complang and Pusung pegat Springs

Krisik, Complang and Pusung pegat springs were selected for this study based on the same of the morphology, geology and debit magnitude. A Krisik spring located in Jombok village was occuring at the foot of the hill with a slope 8-15% and on altitude 650 m above sea level (asl.) Whereas Complang (Waturejo village) and Pusung pegat (Sumberagung village) were formed on slope 3-8% and altitude 668 and 677 m asl, respectively. Geologically, three springs were developed on old Holecene Volcanic Rocks of Mt. Anjasmara, consisting of volcanic breccias, lava, tuff and dikes [6].

Delineation recharge area for each spring were estimated using the WCA Micro maps, that were made by overlay topography (scale 1: 25.000), contour and drainage maps. Then, land use of recharge area for each springs were delineated based on the land use map and the result of location surveys. Area of each land use was determined by using the Arcview 3,2 program (Table1.).

Table 1. Land use systems in recharge area of Krisik, Complang and Pusung pegat springs

No.	Land Use Sytems (LUS)	Area (ha)		
		Krisik	Complang	Pusung pegat
1	Coffee agroforest	16,85	30,30	138,38
2	Albizia plantation	0,97	-	-
3	Pines plantation	5,82	-	27,01
4	Horticulture/ rice field	0,84	-	11,90
5	Housing	-	8,07	17,58
	Total of area	24,48	38,37	194,865

Woody vegetation in a sampling unit were classified into trees and small trees. Trees with a diameter at breast height (dbh) of more than 30 cm were registered within plots 100 m x 20 m. Whereas small trees with dbh less than 30 cm were sampled in sub plots of 40 m x 5 m [7]. Forty-five plots were sampled in cofee agroforstry in the recharge area of three springs.

For the analysis of the vegetation structure of the coffee agroforest, density and basal area were compared between three cofee agroforests in each recharge area using analysis of variances (F-test) by Minitab 14.0 programme. Important Value Index (IVI) of each species (tree, small tree and ground cover) for each plot was calculated by summing the relative frequency and relative density cover [8]. Species diversity described diversity of woody plant that included non-coffee trees per agroforest inside the spring recharge

areas. The species diversity was calculated by Shannon-Wiener diversity index (H‟). Species homogenity or distribution pattern in relation to other species in a sample unit area was calculated using Piélou equatibility index (E) [9]. H‟ was computed as $H' = \Sigma p_i . ^2 \log p_i$; $p_i = ni/N$, while E was expressed as $E = H'/ \ln S$, where ni = number of individual from species i, N = total number of individual and S = number of species. Floristic silimilarity among coffee agroforests was assessed using Jaccard‟s Similarity Index (ISj) : ISj = c/(A+B-c) x 100, where A = total number of species in site A, B = total number of species in site B, and c = number species common to site A and B [8].

3. Result and Discussion

Woody plant structure

A total of 28 tree species and 85 small trees species were found associated with coffee in the 45 plots samples inside the three spring recharge areas. Among the three agroforests in the spring catchment areas, the coffee agroforests in the Complang spring had highest number of tree species (20 species). Meanwhile the coffee agroforests in the Pusung pegat spring had highest number of small tree species (58 species).

The coffee agroforests in the Complang spring were significantly highest ($p < 0.05$) in tree density (87 individual.ha^{-1}) and basal area (10.27 m^2.ha^{-1}). Moreover Krisik spring had the same tree density and basal area with Pusung pegat spring statistically. The density of small tree was not significantly different among coffee agroforest in three spring recharge area. Similarly, the basal area of small tree in three areas was not different (Table 2.).

Table 2. Average woody plant density and basal area (± standard error) per coffee agroforests in three spring recharge areas

Springs	Density (individual.ha^{-1})		Basal Area (m^2.ha^{-1})	
	Tree	small tree	Tree	small tree
Krisik	38±28 a	3763±1100	3.83±3,3 a	20.44±7.96
Complang	87±37 b	4147±1772	10.27±4.68 b	22.43±10.69
Pusung pegat	29±26 a	3820±1841	3.66± 2.93 a	26.4±9.83

In general, three spring recharge areas were mainly dominated by tree species like *A. falcataria, Durio zibethinus and Coccos nucifera*. *A. falcataria* had highest importance value in the Krisik spring. Whereas in the Complang and Pusung pegat springs, *D. zibethinus* had highest importance value (Table 3).

The density of tree and small tree in three spring recharge area had higher density (3763 – 4147 indv..ha^{-1}) than that in Mexico (1383.75 indv.ha-1) [9]. Its density indicated the area of land cover by vegetation.

Tabel 3. Five most important tree species in each spring recharge area

Tree Species	Frequency (%)	Density (individual ha^{-1})	IVI
Krisik spring			
Albizia falcataria	16.13	40	51.53
Durio zibethinus	14.52	24	35.76
Cocos nucifera	14.52	13	26.02
Swietenia macrophylla	9.68	6	14.99
Litsea firma	8.06	6	13.37
Complang spring			
Cocos nucifera	14	16	32.32
Durio zibethinus	14	16	32.32
Albizia falcataria	12	17	31.85
Erythrina subumbarns	13	13	28.27
Parkia speciosa	9	4	13.58
Pusung pegat spring			
Durio zibethinus	19.64	8	49.40
Albizia falcataria	14.29	4	28.57
Parkia speciosa	14.29	4	28.57
Artocarpus heterophyllus	8.93	2	16.07
Aleurites moluccana	7.14	1	11.90

Different from that of tree, the small tree structure in the Krisik and Complang spring recharge areas was dominated by banana species (*Musa paradisiaca*). Some cultivar banana which planted in this area, i.e. pisang santen, pisang sembot and pisang ambon. While *A. falcataria* dominated in the Pusung pegat spring (Table 4.), its density reached 410 individual.ha^{-1}.

Tabel 4. Five most important small tree species in each spring recharge area

No.	Small tree Species	Frequency (%)	Density (indiv.ha^{-1})	IVI
Krisik spring				
1	*Musa paradisiaca*	7.45	323	16.05
2	*Albizia falcataria*	6.83	220	12.68
3	*Durio zibethinus*	8.07	130	11.53
4	*Hibiscus macrophyllus*	6.83	117	9.93
5	*Lansium domesticum*	5.59	90	7.98
Complang Spring				
1	*Musa paradisiaca*	9.80	410	35.11
2	*Hibiscus macrophyllus*	7.84	215	21.11
3	*Durio zibethinus*	8.33	120	15.74
4	*Albizia falcataria*	6.86	143	15.66
5	*Litsea firma*	4.90	173	15.55
Pusung pegat spring				
1	*Albizia falcataria*	5.61	410	35.11
2	*Musa paradisiaca*	5.10	215	21.11
3	*Durio zibethinus*	5.61	120	15.74
4	*Leucaena leucocephala*	4.08	143	15.66
5	*Gliricidia sepium*	4.08	173	15.55

The dominance of some tree species could be shown in Figure 2. *A. falcataria* tree had highest density in Krisik, but small tree of this species commonly found in Pusung pegat recharge area. Similarly *D. zibethinus* tree had highest density in Krisik recharge area. Whereas Complang recharge area dominated *E. sumbarn*s trees and *H. macrophyllus.*

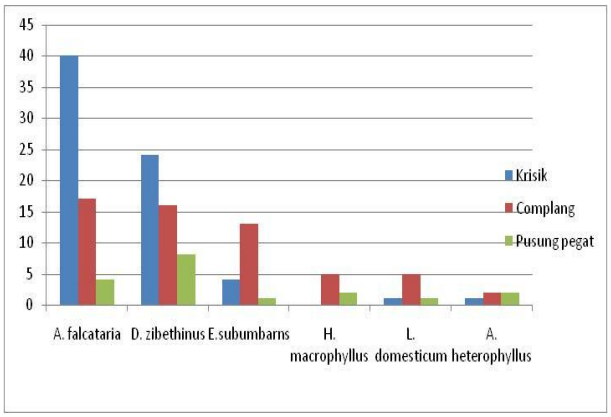

Figure 2. Density of tree species in coffee agroforest in three spring recharge area

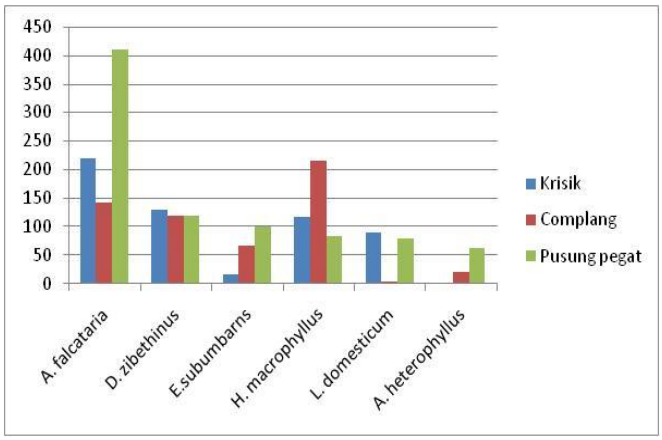

Figure 3. Density of small tree species in coffee agroforest in three spring recharge area

Species diversity

Shannon-Wiener diversity index (H") for both plant classes were categorized as high enough. In general, woody species of coffee agroforests in Pusung pegat recharge had highest H", with H" of 3.31 for tree and 2.91 for small tree. Coffee agroforest in Complang also had high H" of tree (3.25), but the H" of small tree only 2.22 (Table 5). That H" had higher value than H" of coffee agroforests in coastal Oaxaca, Mexico (1.71-1.88). The high diversity indicated that its ecosystem became stable, even though the third spring recharge areas had occured forest conversion in fifthy years ago.

In contrast, Piélou equatibility index (E) at study area were categorized very low, between 0.58-1.19 (tree and small tree) referring that species were not evenly dispersed and tended to be clumped. This clumping was probably due to the dominant species belong to cultivated plants. The E value of trees in the thrid recharge areas were higher than that in cocoa agroforests in Southern Cameroon, only 0.62 – 0.74 [10]. The low E value also was shown on sub-montane forest in Mt. Gede-Pangrango National Parks (1.95) [11].

Table 5. Tree and small tree species diversity in three spring recharge areas (see Appendix)

Spring	Krisik		Complang		Pusung pegat	
	trees	small trees	Trees	small trees	trees	small trees
Species number	14	40	20	50	16	58
Genus number	14	37	18	40	16	46
Family number	10	23	10	25	10	27
Shanon-Wiener index (H')	2,91	2,13	3,25	2,22	3,31	2,91
Piélou equitability (E)	1,1	0,58	1,08	0,57	1,19	0,72

Floristic silimilarity among coffee agroforests was assessed using Jaccard"s Similarity Index (ISj). Based on the calculation results of ISj, tree species of Krisik recharge area had medium similarity (Ijs = 57,89) with tree species of Pusung pegat recharge area. While tree species in Complang-Pusung pegat and Krisik – Complang had low similarity (ISj< 0,5) such 44 and 36, respectively. A small tree species in Krisik-Complang had highest ISj (0,50).

Most of the third coffee agroforest in spring recharge area consisted of woody plants which had economic values. *A. falcataria, Swietenia macrophylla, Erythrina subumbarns, Hibiscus macrophyllus, Toona sureni* and *Litsea firma* were widely known as timber trees. Beside that, *D. zibethinus, C. nucifera, Artocarpus heterophyllus, Lansium domesticum, Parkia speciosa* and *Artocapus heterophyllus* belong to edible fruit plants.

The majority of tree and small tree of coffee agroforets in three recharge area were exotic species *like A. falcataria, S. macrophylla, H. macrophyllus, L. firma*. Nonethelles, the native species still founded in surrounding springs i.e. *Arenga pinnata, Artocarpus elasticus, A. heterophyllus, Ficus hispida, F. capiosa, Syzigium aromaticum, Mangifera foetida and Tremna orientalis* (anggrung). Beside woody tree species, other species were founded such as pisang

(*Musa paradisiaca*) and bamboo *(Bamboo spp.)*. Bamboo species that commonly founded i.e *Gigantochloa apus* (pring apus), *G. atter* (pring jawa) and *Dendrocalamus asper* (pring petung). Pusung pegat recharge area had more native tree species out than Krisik and Complang recharge area. There were *Aleurites moluccana, T. orientalis, Parkia timoriana and Syzigium polychepallum (*gowok). The second last species was categorized as rare species.

4. Conclusions

Three spring recharge areas mainly dominated by tree species such sengon *(A. falcataria*), durian (*D. zibethinus*) dan kelapa (*C. nucifera*). Whereas pisang (*Musa paradisiaca*) and A. *falcataria* were dominant tree species.

Species diversity of trees and small trees in this area were categorized high enough, based on Shannon-Wiener diversity index. Woody species diversity of Krisik was lower than species diversity of Complang and Pusung pegat recharge areas.

5. Acknowledgements

---

6. References

[1]. Anonymous (2007), Inventory Report of Water Resources Malang. Department of Energy and Mineral Resources (EMR) Malang. (*unpublished*).

[2]. Anonymous (1984), Soil and soil conditions in Upper Konto Watershed , East Java. NUFFIC- Unibraw Soil Science Project. Soil Science Department Brawijaya University. Malang. East Java. Indonesia.

[3]. Yulistyarini T, Solikin, A.P. Fiqa and R. Irawanto (2009), Evaluation on the relationship between quality of vegetation, biogeophysical soil and debit of some topography springs in Malang Raya, East Java. Incentive Program Activity For Researcher And Engineer Indonesian Institute of Science. Final report.

[4]. Todd D.K. and L.W. Mays (2005), Groundwater Hydrology. John Willey & Son Inc, Singapore

[5]. Sada, D.W and K.F. Pohlmann (2006), Draft U.S. National Park Service Mojave Inventory and Monitoring Network Spring Survey Protocols: Level I and Level II. February I.

[6]. Santosa, S. and T. Suwarti (1992), Geology maps Malang sheet, Java. Geological Research and Development. Bandung.

[7]. Hairiah, K. and S. Rahayu (2007), Practical guidance of "Carbon-Sink Measurement" in various land Use. World Agroforestry Centre.

[8]. Ludwig J.A. and J.F. Reynolds (1988), Statistical Ecology, a primer on methods and computing. John Willey and Sons. New York.

[9]. Asteggiano, L. (2008), Woody species diversity and vegetation structure in managed and abandoned shade coffee system in Coastal Oaxaca. Mexico.

[10]. Sonwa D.J., B.A. Nkongmeneck, S.F. Weise, M. Tchatat, A. Adesina and M.J.J. Janssens (2007), Diversity of plants in cocoa agroforests in the humid forest zone of Southern Cameroon. Biodiversity Conservation 16: 2385-2400.

[11]. Arrijani, D. Setiadi, E. Guharja and I. Qayim (2006), Vegetation analysis of the upstream Cianjur watershed in Mt. Gede-Pangrango National Parks. Biodiversitas 7: 147-153.

Appendix

Table 5. Tree and small tree species diversity in three spring recharge areas

Spring	Krisik		Complang		Pusung pegat	
	trees	small trees	Trees	small trees	trees	small trees
Species number	14	40	20	50	16	58
Genus number	14	37	18	40	16	46
Family number	10	23	10	25	10	27
Shanon-Wiener index (H')	2,91	2,13	3,25	2,22	3,31	2,91
Piélou equitability (E)	1,1	0,58	1,08	0,57	1,19	0,72

Analyzing The Double Pulse Experiment by Using Fourier Transformation

Abdurrouf

Dept. of Physics, University of Brawijaya, Malang 65145, Indonesia (abdurrouf@ub.ac.id)

Abstract

In typical double pulse experiments, an ensemble of gas is first subject to a femtosecond pump pulse to set it into free rotation condition. The second more intense femtosecond probe pulse, was delayed with respect to the first by successively increasing the time intervals t_d, is given to generate the observed signals. In many cases, the observed dynamic signals are plotted as a function of delay time t_d. To obtain more succinct and clearer information concerning the interaction, I present the observed signals in frequency domain, obtained by Fourier transforming the dynamic signal. From the simulation by using N_2 , O_2, and CO_2 molecules, it is conclude that the spectrum in frequency domain provides more succinct and clearer information of the beats involved in the signal and provides a better way for understanding the interactions. In addition, the frequency spectrum is powerful for (i) determining molecular symmetry, (ii) determining the ratio of total angular momentum of molecule, (iii) estimating gas temperature, and (iv) constructing the theoretical model of the interaction.

Keywords: *double pulse experiment, Fourier transformation, angular momentum, molecular symmetry*

1. Introduction

Among the interesting research topics in atomic and molecular physics, the double pulses experiment is of particular interest, no less because of its potential applications as a source of coherent ultraviolet light and/or for generation of ultrashort attosecond laser [1]. In this experiment, an ensemble of gas is first subject to a femtosecond pumping pulse to controls its wave-function and its alignment [2]. The second more in intense femtosecond probe pulse, was delayed with respect to the first by successively increasing the time intervals t_d, is given to generate the observed signals, either in ionization, dissociation, optical Kerr effect (OKE), Raman transition, or high harmonic generation (HHG) scheme [3]. By plotting the observed signal as a function of delay time between two pulses, one obtains the dynamic signal describing the molecular behavior due to the interaction. However, the dynamic signal does not give enough information to understand the interaction and to image the molecular orbital.

As an alternative way, the data can be presented in the frequency domain, known as Fourier spectrum, obtained by Fourier transforming the dynamic signal with basis frequency Bc [5]. In this paper, I present the frequency spectrum of HHG signal of N_2, O_2, and CO_2, and directly compare them with the experimental ones [3]. The frequency is then used to analyze the molecular properties as well as its interaction with laser pulse.

2. Computational Details

In general, the observed dynamic signal of double pulse experiment revives with period [4]:

$$T = \frac{1}{2Bc} \tag{1}$$

where B is rotational molecular constant. Depends on the molecular symmetry of the HOMO (highest occupied molecular orbital), the observed signal can mimic the alignment degree $\langle\langle \cos^2\theta \rangle\rangle$ for σ-symmetry, or mimic $\langle\langle \sin^2\theta\cos^2\theta \rangle\rangle$ for π-symmetry. The $\langle\langle \cos^2\theta \rangle\rangle$ generates a transition with $\Delta J = 0,\pm 2$.

The transition with $\Delta J = 0$ creates a peak at frequency zero, whereas the transition with $\Delta J = \pm 2$ is associated with phase differences with

$$\Delta\phi(J \to J \pm 2) = 2\pi Bc(4J + 6) \tag{2}$$

with c in cm/s. According to Eq. (2), one can make a Fourier transform of the observed signal Bc as basis frequency and find a series of peaks at $4J + 6$. On the other hand, the $\langle\langle \sin^2\theta\cos^2\theta \rangle\rangle$ is associated with phase differences

$\Delta J = 0,\pm 2,\pm 4$. The transition with $\Delta J = \pm 4$ is associated with phase differences with

$$\Delta\phi(J \to J \pm 4) = 2\pi Bc(8J + 20) \qquad (3)$$

According to Eq. (3), the Fourier spectrum related to $\langle\langle \sin^2\theta\cos^2\theta \rangle\rangle$ term creates peak series of (4*J*+6)*Bc* and (8*J*+20)*Bc*. Then by analyzing the Fourier spectrum, one can determine which term, $\langle\langle \cos^2\theta \rangle\rangle$ or $\langle\langle \sin^2\theta\cos^2\theta \rangle\rangle$, contributes to the HHG signals, and therefore can deduce the symmetry of the molecule. Moreover, by comparing the strong ratio of peaks due to J_{even} to that of J_{odd}, one can deduce the nuclear statistics of the molecule.

3. Results and Discussion

The typical dynamic signal for N_2 obtained by using HHG schema is shown in Fig.1. Both experimental and calculated signal revives with *T*=8.4 ps, allows us to calculate the rotational molecular constant *B* according to Eq. 1. This revival has been observed to remain constant until 10 periods occurs [6].

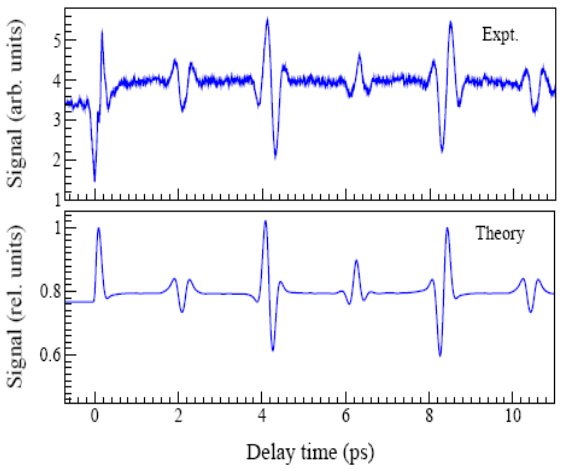

Figure 1. The experimental (upper panel) [3] and calculated (lower panel) dynamic of 19th harmonic signal of N_2.

Note: I use here the pump intensity of $I_{pump} = 0.8x10^{14}$ W/cm^2, the probe intensity of $I_{probe} = 1.7x10^{14}$ W/cm^2, duration 40 fs, wavelength 800 nm, and temperature 200 K

The spectrum in frequency domain, obtained by Fourier transforming data in Fig. 1, is shown in Fig. 2. The figure shows that both the experimental and calculated Fourier spectrum of N_2 consist of peak series located at (6,10,14,18,22,..)*Bc* or (4*J*+6)*Bc*, indicating that its HOMO has σ-symmetry. The figure also shows that the peaks of J_{even}: (6,14,22,30,38…)*Bc* (blue marked) is twice as strong as that of J_{odd}: (10,18,26,34,….)*Bc* (green marked). It implies that both even and odd *J* levels are present in N_2, in the ratio J_{even}:J_{odd} = 2:1. It could be understood, as an individual N atom has momentum *J*=1. Then the N_2 molecule could be has *J*=0,1,2. If each *J* level has degeneracy factor (2*J*+1), then there are 1 states for *J*=0, 3 states for *J*=1, and 5 states for *J*=2. Then the total J_{even} states is 6, whereas the total J_{odd} states is 3, gives us the ratio J_{even}:J_{odd} to be 2 : 1. The nuclear statistics is one of the important data needed for inverse method, a novel for constructing the molecular wave function from its harmonic signal.

It is worthwhile to note here that the nuclear statistics also can be deduced from the dynamic signals, by comparing the ratio of depth modulation at fourth revival ($A_{1/4}$) to that of half revival ($A_{1/2}$) [4]. The ratio J_{even} to J_{odd} is then equal to $(A_{1/2} - A_{1/4})/(A_{1/2} + A_{1/4})$. However, the conclusions from Fourier spectrum are clearer than analysis based on the dynamic signals.

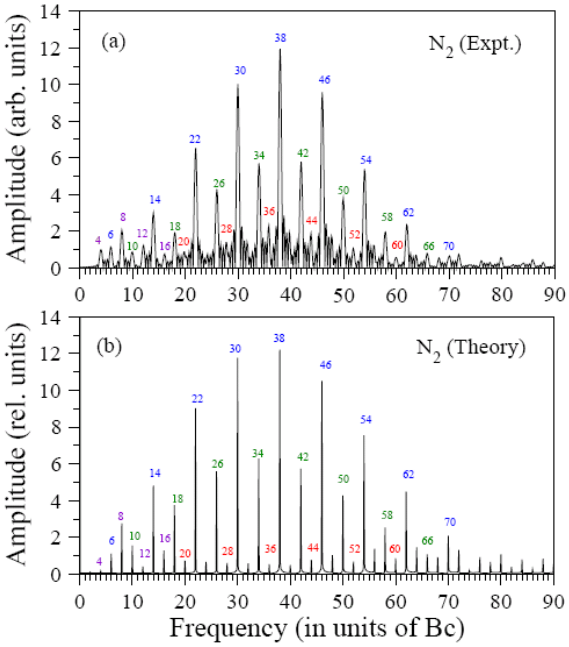

Figure 2. The experimental (upper panel) [3] and calculated (lower panel) Fourier spectrum of dynamic of 19th harmonic signal of N_2.

The Fourier spectrum of N_2 also shows another weak series (20,28,36,….)*Bc* (red marked), arises from the higher terms of the

interaction, or from the sum and difference frequencies due to the presence of the signal as a square of dipole moment. This series can not be identified from the dynamic signal. However, analyzing its existence is very important for describing the interaction between molecular gas and laser pulse, as will be discussed later.

I mention that the peak of Fourier spectrum is sensitive to the initial temperature of gas jet. In Fig. 2 (upper panel), the experimental of N_2 peaks at 38 *Bc*, corresponding to *J*=8. The similar calculated spectrum (Fig. 2, lower panel), peaked at the same position, can be obtained for *T*=200 K. Then one can deduce the initial temperature of as N_2 to be 200 K. This method is very important, because the gas jet temperature is very difficult to determine experimentally.

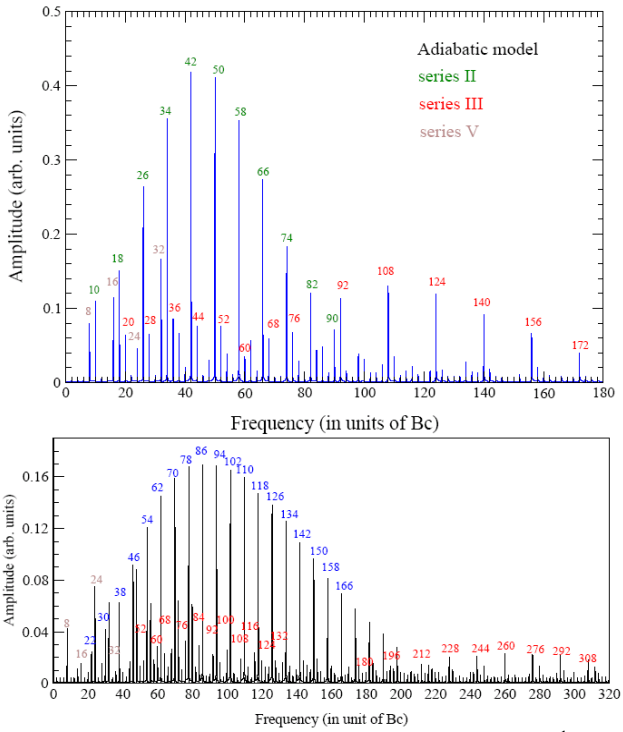

Figure 3. The theoretical Fourier spectrum of 19th harmonic signal of O_2 (upper panel) and CO_2 (lower panel).

For both molecules, pulse of duration 40 fs and wavelength 800 nm at initial temperature is 200 K. (The pulse intensities are

$I_{pump} = 0.5x10^{14}$ W/cm^2 and

$I_{probe} = 1.2x10^{14}$ W/cm^2 for O_2; as well as

$I_{pump} = 0.6x10^{14}$ W/cm^2 and

$I_{probe} = 1.3x10^{14}$ W/cm^2 for CO_2)

Figure 3 shows the calculated Fourier spectrum of O_2 (upper panel) and CO_2 (lower panel). From the figure, one can see that both spectrum consist not only (4*J*+6) *Bc* series (green and blue marked), but also (8*J*+20) *Bc* series (red marked), implies that both molecules has a π-symmetry. More specific, the spectrum of O_2 show the series peaked at (10,18,26,34,…) *Bc* corresponding to J_{odd} only, implies there are only J_{odd} for O_2. In contrast, the spectrum of CO_2 show the series peaked at (22,30,38,42,…) *Bc* corresponding to J_{even} only, implies there are only J_{even} for CO_2.

In Fig. 4, I show the Fourier spectrum of N_2 for different initial temperature. It is shown that the peaks of the spectrum is shifted to right position for higher initial temperature. It could be understood as a Boltzmann distribution, where the Boltzmann population at *J* level with energy E_J, is given by

$$P(J) = (2J+1)e^{-E_J/kT} . \qquad (4)$$

Equation above implies that molecule tends to occupy a higher energy level, as its temperature increases.

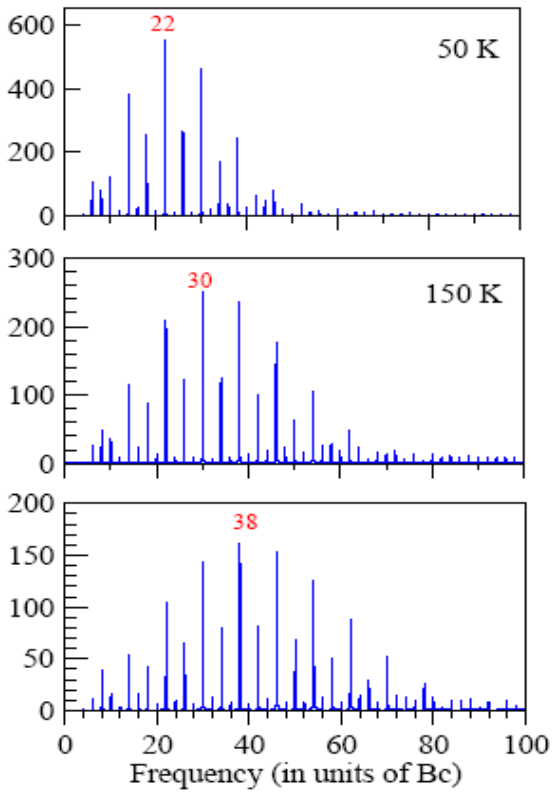

Fig. 4: The Fourier spectrum of 19th harmonic signal of N_2, for different initial temperature. The pulse parameters are similar as in Fig. 1.

At the end, I briefly discuss the Fourier spectrum as a tool for describing the interaction between molecular gas and laser pulse. I note that the present calculated signal is obtained by using adiabatic theory [4]. The theory uses quantum transition amplitudes for the coherent harmonic emission from and back to the linearly independent reference wave-packet states $|\chi_i(t)\rangle, i=(e,J_0,M_0)$, consisting of the product of the ground electronic and the coherent rotational wave-packet states, to define the independent harmonic emission probabilities corresponding to the initial occupation of the rotational states. And in accordance with the quantum statistical theory, it averages the independent probabilities to define the observable HHG signal.

The other alternative definitions of HHG signals, that have been employed earlier, are the frozen nuclei model and Madsen and Madsen's (MM) model.

It is worth noting that the quantum amplitude calculation in the intense field theory corresponds to the ~~"a~~diabatic nuclei" approximation, in which the matrix elements with respect to the rotational wave-packet states are evaluated at the level of the adiabatic amplitude-operator, and not at the level of the adiabatic probability operator, occurs in the more drastic ~~"f~~rozen nuclei" approximation. Also, in the present theory, as in the laboratory, the operational angle is the relative polarization angle α, and not the angle between the polarization direction and the molecular axis, θ. In fact, the angle is a rotational coordinate that, as required for a quantum formulation, is integrated over to obtain the quantum transition amplitudes or the expectation values of Hermitian operators.

The definitions of the HHG according to frozen nuclei model and MM model differ from each other, and they differ from the adiabatic definition. The frozen nuclei model defines the statistically averaged signal by weighting the individual amplitudes first, and then taking the absolute square of the weighted sum. This procedure runs counter to the quantum statistical theoretical method of averaging the probabilities, not amplitudes, and/or the expectation values of Hermitian observables themselves, and not their Fourier transforms that are proportional to the emission amplitudes. Furthermore, the definition of frozen nuclei causes the signal to depend on the mixed products of the statistical weights, which are in principle independent.

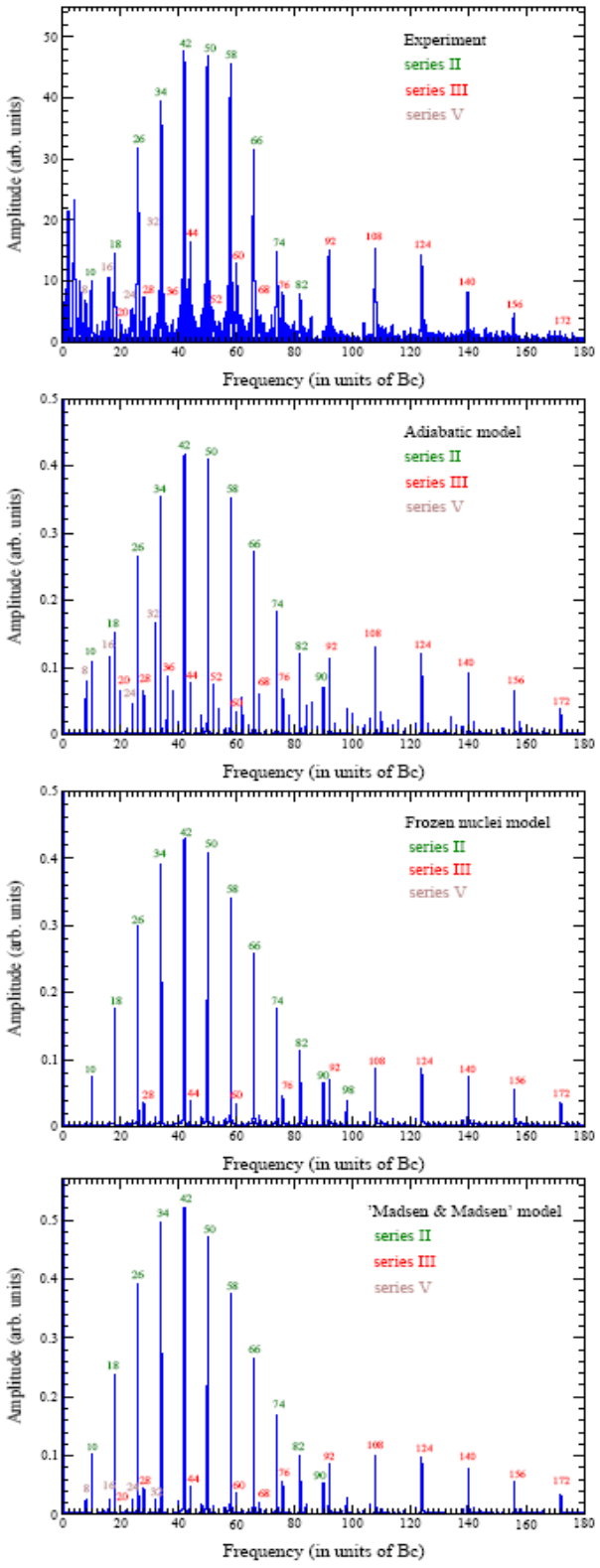

Fig.ure 5. Direct comparison between the experimental Fourier spectrum of 19th harmonic signal of O_2 [3] and that obtained theoretically by using different models.

The signal defined by MM model,is seen to depend on the weighted sum of the diagonal matrix elements between the rotational wave-packet states of the ―probability operator" —this, of course, is not equal to the weighted sum of the absolute squares of the diagonal matrix elements of the transition operator. In MM model, the above circumstance is a consequence of the more drastic ―frozen nuclei" approximation and an effective inclusion of all transitions, those between the same wave-packet states ―elastic-like" as well as those between the different wave-packet states ―inelastic-like". However, unlike in frozen nuclei model, in MM model the weighted statistical sum is taken in accordance with the quantum statistical theory, at the level of the probabilities.

In Fig. 5, I show the experimental Fourier spectrum of O_2, and directly compare it with the theoretical ones obtained by using various models. There two points to compare: (i) the strong ratio between series II (green marked) and series III (red marked), and (ii) the existence of series V: (8,16,24,….) *Bc.*

From the figure, one can see that the adiabatic model well reproduce the experimental signal. The frozen nuclei model, on the other hand, produce too weak series III, and can not produce series V. The Madsen and Madsen's models, even though well reproduce series V, but both series V and series III seems too weak compare to those of experiment.

4. Conclusion

To summarize, the Fourier spectrum due to double pulse experiment observed by using HHG schema for N_2, O_2, and CO_2 has been calculated. Comparing to dynamic signal, the spectrum in frequency domain provides more succinct and clearer information of the beats involved in the signal and provides a better way for understanding the interactions. The Fourier spectrum is also powerful for (i) determining molecular symmetry, (ii) determining the ratio of total angular momentum of molecule, (iii) estimating gas temperature, and (iv) constructing the theoretical model of the interaction

5. Acknowledgemnet

---

6. References

[1] A. H. Zewail (2000), Femtochemistry: Atomic-scale dynamics of the chemical bonds, *J. Phys. Chem.* A, **104**, 5660-5694

[2] H. Stapelfeldt and T. Seideman (2003), Colloquium: Aligning molecules with strong laser pulses**,** *Rev. Mod. Phys.*, **75**, 543-557.

[3] K. Miyazaki, M. Kaku, G. Miyaji, A. Abdurrouf, and F.H.M. Faisal (2005), Field-Free Alignment of Molecules Observed with High-Order Harmonic Generation, *Phys. Rev. Lett.*, **95**, 243903 (1-4).

[4] A. Abdurrouf dan F.H.M. Faisal (2009), Theory of intense-field dynamic alignment and high-order harmonic generation from coherently rotating molecules and interpretation of intense-field ultrafast pump-probe experiments, *Phys. Rev. A*, **79**, 023405 (1-28)

[5] F. H. M. Faisal, A. Abdurrouf, K. Miyazaki, and G. Miyaji (2007), Origin of Anomalous Spectra of Dynamic Alignments Observed in N_2 and O_2, *Phys. Rev. Lett***.,** **98**, 143001 (1-4).

[6] P.W. Doodley *et al*. (2003), Durect imaging of rotational wave-packet dynamics of diatomic molecules, *Phys. Rev. A***,** **68**, 023406 (1-11).

Dominant Frequency Analysis and Seismic Vulnerability Index in subdistrict of Klojen, Malang Regency, using "Horizontal to Vertical Spectral Ratio" for Seismic Microzonation

Adi Susilo [1], Dwi Wahyudi [2]

[(1)] Geophysics, Physics Department, University of Brawijaya, Malang, Indonesia (adisusilo@ub.ac.id)
[(2)] Meteorological, Climatological and Geophysics Agency, Tretes, East Java, Indonesia

Abstract

Microtremor measurements in the subdistrict of Klojen, Malang regency using short period seismometers TDL type-303S (three components, namely NS, EW and UD) has been carried out at 16 points. Malang regency, which is part of Malang, is a region where growth of buildings is very rapid. Because the top of Malang regency which was a fertile area and it has been a lot of standing buildings, the vulnerability to the propagation of seismic waves is assumed to be large. Microtremor data analysis were calculated using the Horizontal to Vertical Spectral Ratio (HVSR) to determine the dominant frequency (fo) and the ratio of peak value of the spectrum HVSR (amplification factor-A). Sampling rate of data acquisition is 100 Hz, distance of each measurement point is about 100 m and the length of time for each recording is 30 minutes. Analysis of the frequency spectrum and the ratio of peak value of HVSR spectrum are very useful to compile a map microzonation seismic amplification factor mapping and mapping of seismic vulnerability index. The results showed that the dominant frequency in the sub-district of Klojen, Malang regency ranges from 0.9 to 8.9 Hz with an average below 2.8 Hz. HVSR peak value (amplification factor) ranged between 1.4 and 2.8. Results of seismic vulnerability analysis of the two obtained values ranged between 0.4 and 5.9. In addition, the analysis of the three parameters is found that the highest damage potential of seismic waves will occur at about the point of KL 5 (7.95245 LS, 112.6402 E), because this region has a low dominant frequency, but amplification and seismic vulnerability index is quite high.

***Keywords**: HVSR, Dominant Frequency, Seismic Vulnerability Index, Microtremor, Seismic Microzonation.*

1. Introduction

Malang region is earthquake-prone areas. This is due in this region is geologically the area that have a relatively high seismic activity. The high seismic activity is due to the two tectonic collisions, the collision between the Eurasian Plate and Indo Australia. "If there is a collision between two tectonic plates which exceeds the limit, then the plates will be issued with vibration energy. This can cause an earthquake. This occurs not only in the area of Malang, but the area in the southern region of East Java. In most cases of earthquake shows that the level of damage inflicted an earthquake depend strongly on the surface topography and geology. One case of interest was the Yogyakarta earthquake, occurring in 2006. When it was compared with the earthquake in Padang (victims around 1000 inhabitants) which has a much greater magnitude scale, Yogyakarta earthquake caused the collapse of a larger loss of life (about 6000 inhabitants). The main reason of this difference can be found based on the research of Daryono [1] showing that the Yogyakarta earthquake caused major damage, which is caused by a site effect of Yogakarta area.

Based on the data available at the Karangkates Geophysics station, in 2009, Malang has got earthquakes 10 times. The data indicate that from January to May, the public do not feel an earthquake. Malang society could feel the earthquake in June. In that month there were two earthquakes, namely on June 9, with the strength of an earthquake 4.9 on the Richter Scale (SR) and 30 June with the strength of 4.3 on the Richter scale. In July, the earthquake was also felt by the people two times, namely July 13 with a 4.9 magnitude earthquake and 28 July with the strength of SR 5.4. Earthquake intensity felt by the public in August rose to three times, which are on August 1, an earthquake with a magnitude of 4.5, the next on August 14, magnitude of 4.8, and on August 28, with a magnitude of 6.9. Similar to August, in September was also an earthquake three times. In September, a strong earthquake is felt by the people of Malang. On September 2, an earthquake with the SR 7.3, then 7 September there was an earthquake with magnitude 6.8 forces, and on September 19, an earthquake with magnitude 6.4. Ten earthquakes can be felt in 2009 was equal to that occurred in 2008. As for the number of earthquakes in 2006 and 2007 earlier, respectively, there were 13 earthquakes felt by the people of Malang. While overall, the number of earthquakes recorded at stations Karangkates are 196 earthquakes. In January, there are 28 earthquakes, February 39, March 17, and April 16. Furthermore, in May there were 14 earthquakes, June 20, July recorded 18, August 23, and in September recorded 21 earthquakes.

Most big cities in Indonesia have a high level of earthquake vulnerability, but most planning and development of infrastructure in those areas have not considered the effect of topography and geology. The absence of detailed mapping of vulnerable areas is a problem that really needs to be solved for future development planning.

One method that is used for mapping the damage caused by earthquake-prone areas in greater detail is by utilizes a microtremor survey to see how the influence of sites effects and soft soil towards the building in an area (seismic microzonation). This method is considered cheaper and easily to be implemented, so the mapping of disaster prone areas can be quickly created. Surveys can be conducted in areas, which have not been affected yet by earthquake and in the area where the earthquake had just happened. This will be useful to look at the characteristics of the sediment layer as the dominant frequency and amplification factor so that the effects of geology and topography can be reduced when the earthquake occurred.

Surveys using microtremor have not been familiar in Indonesia, but in some countries like Japan and Germany, this survey has been carried out and provide a significant contribution to disaster mitigation. Effort ever undertaken in Indonesia is the survey after the occurrence of an earthquake in Yogyakarta. In his research, Daryono [1] states that the area worst hit by the earthquake damage, is to form a belt pattern, caused by a site effect, which is also the same pattern. Therefore, it is necessary to investigate the level of vulnerability to damage from earthquakes recorded in all regions / cities prone to direct or side effects of the earthquake.

In this occasion, the author realizes to conduct research in the part of Malang City, i.e Sub-district of Klojen. The research was conducted by using the method of Nakamura [2] to record ambient noise or vibration arising naturally from nature. By using this method, and taking into account other information available, it can be known that the potential damage in the local area of Sub-district of Klojen, if there are earthquakes.

2. Experimental Detail

Field site study

The study was conducted in the area of Klojen Sub-district, Malang, East Java. The location for data acquisition is given in Table 1. The equipment used is this research as follows:

1. A set of computer hardware
2. Operating system Windows XP SP2
3. Some supporters of Geopsy Software, Datapro and Surfer.
4. A set of portable short-period Seismometer type TDL-303S (3 components)
5. GPS (Global Positioning System), Portable

Primary data acquisition is done by recording microtremor directly in the field using portable short period seismometers equipment TDL-303S type, consisting of digitizer, sensors, laptops, accumulator and support equipment. Acquisitions carried out during three days (14-16 April 2010) with 16 points. At each point, it was measured during 30 minutes microtremor with 100 Hz sampling rate, so that for each data point, there will be 180000 data. Timing recommendations are presented in Table 2.

Elections for 100 Hz sampling rate is intended to ease the data processing, and also refers to other research studies [2,3] which mostly use 100 Hz as the sampling rate. The data collection process was carried out by recording microtremor directly. All devices are connected and controlled using a portable computer. At each data collection, data is stored directly into the computer records in hexadecimal format.

In collecting data, the laying of the sensor does not consider the location, but can be taken in place of grassy and asphalt because they do not affect the value of the ratio of H/V. The important thing to note in the laying of this sensor is that the sensor should not be placed on building such an underground pipe or an underground building.

Table 1. Location for data acquisition

No	Name	Location	Latitude	Longitude
1	KL 1	pojokan jl tumapel dekat pasar burung	7.97811	112.6329
2	KL 2	parkiran MIPA brawijaya jur. Fisika	7.95214	112.6116
3	KL 3	jl bunga matahari (depan masjid al-huda masuk lewat jl kumis kucing)	7.95396	112.6235
4	KL 4	jl melati /jl bungur (pojokan jl teratai)	7.95612	112.6317
5	KL 5	samping pos PKK/sebelah kel, depan warung baso Malang jl Ciliwung	7.95245	112.6402
6	KL 6	jl bendung riam kanan dan bendungan sutami kekiri masuk kekiri perumahan	7.96204	112.6126
7	KL 7	Komplek kesehatan jl jakarta pertigaan jl dekat taman	7.96417	112.6228
8	KL 8	pojok lapangan basket jl kesamben kelurahan calaket	7.96392	112.6319
9	KL 9	jl serayu masuk lewat jl tumenggung suryo	7.96234	112.6405
10	KL 10	depan rumah kosong jl taman slamet	7.97324	112.6227
11	KL 11	parkiran depan RSUD syaiful anwar	7.97202	112.6316
12	KL 12	jl bela negara utara lapangan rampal	7.97113	112.6398
13	KL 13	Dekat rmh P. Djati Jl bareng tenes depan MOG	7.97867	112.6234
14	KL 14	jl kesatrian depan AJENREM 083 depan parkir lapangan tenis	7.9791	112.6422
15	KL 15	Jl kapten piere tendean masuk melalui Jl KH. Tamin samping BRI	7.98724	112.6297
16	KL 16	Jl jodipan wetan no 12 Malang (samping masjid roisiyah malang)	7.98765	112.6392

Table 2. Timing recommendation

f_0 [Hz]	Minimum value for l_w [s]	Minimum number of significant cycles (n_c)	Minimum number of windows	Minimum useful signal duration [s]	Recommended minimum record duration [min]
0.2	50	200	10	1000	30'
0.5	20	200	10	400	20'
1	10	200	10	200	10'
2	5	200	10	100	5'
5	5	200	10	40	3'
10	5	200	10	20	2'

Weather, wind speed and air temperature must be considered because it has a significant influence. It is highly recommended to not perform measurements during heavy rain or wind conditions which are very large. In this study, the average data collection conducted in sunny weather and the wind velocity, is not too large.

Field measurement data is the raw data which is a ground vibration data in function of time. Data is composed of three components, namely the vertical component (up and down), horizontal (North-East), and horizontal (East-West). The received data cannot be processed because it is still hexadecimal format.

The data are first processed using software Datapro to change the format of raw data into ASCII data. The first step is to have raw data we get, then we keep the extention ASR (save as ASR), as shown in Figure 1.

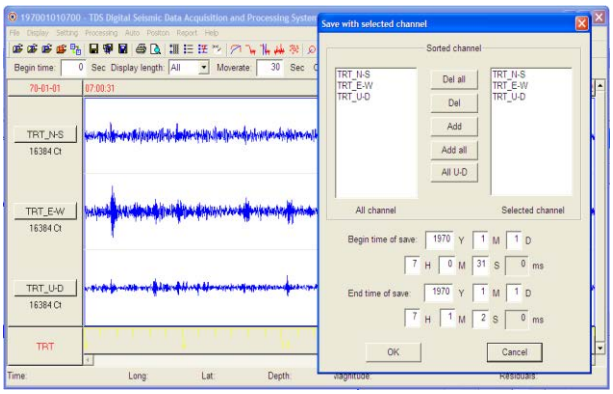

Figure 1. Data Format Conversion process, conversion from ASR data into ASCII data.

This process will generate four files, namely vertical, horizontal (north-south), horizontal (west-east), and the file header. Data in ASCII format also cannot be processed immediately but this data must be modified into SAF format (Sesame ASCII format). SAF format is made with reference to the Sesame standards, such as those found in the manual Sesame HV (2004). This conversion process is done manually by using excel software or Surfer [4].

SAF data in this format is then processed using software GEOPSY. In this processing, data is divided into several windows. For large enough data, it can be done automatically sorting window provided by the software. The selection window is a process of segregation between the tremor signals and transient event (a specific source such as footsteps and vehicles to pass). The function of this process is to avoid the processing of transient events in the analysis.

Detection of transient signals is by comparing the short term average (STA) and long term average (LTA) and also using anti-triggering logarithm. STA is the average value of short-term amplitude (0.5-2.0 seconds), whereas LTA represents an average value of amplitude of long-term (>10 seconds). When the comparison between the STA/LTA exceeds specified thresholds, then the signal can be referred to as "event".

After the transient event is detected, then the data other than transient events are divided into several windows. Window length used in the study was 20.48 s or 2048 data. This is to meet the reliability criteria of processing using the FFT. Based on the Sesame European Research Project, it is suggested that in determining the window length, it has a minimum requirement LW = 10 / fo, where LW is the length of the window and fo is predominant frequency. To get the frequency up to 0.5 Hz, hence the window length must be more than 20 seconds. In this study, the selection window is done automatically because of the large data meets the requirements for the implementation of the FFT process. SLA chosen was 2 seconds with the LTA for 30 seconds following the recommendation of the Sesame project (Figure 3).

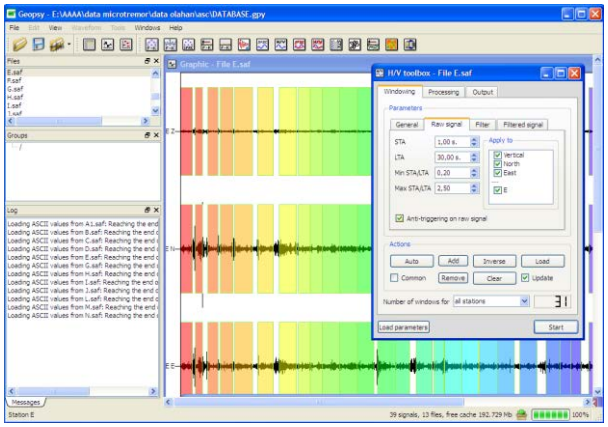

Figure 2. Selection Process of the Window

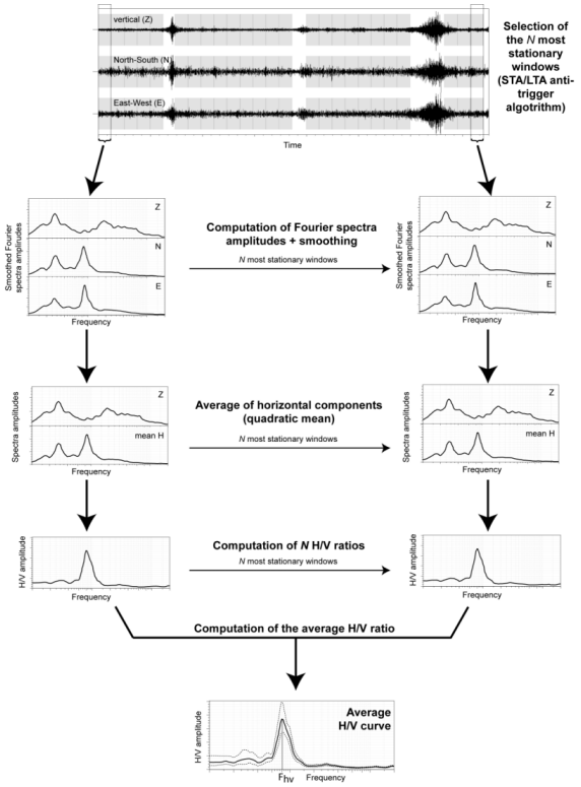

Figure 3.The step of determining the spectrum of H / V

The next step is the processing that is composed of the FFT process, involving the smoothing process. Smoothing process is done by using algorithms Konno and Omachi [5] with bandwidth b coefficient of 40. It is also made the process of cosine taper to minimize the effects of borders or boundaries due to window selection process. Konno-Omachi algorithm is stated in the following equation:

$$\frac{\sin\left(\left(\log_{10}\left(\frac{f}{f_c}\right)\right)^b\right)}{\left(\left(\log_{10}\left(\frac{f}{f_c}\right)\right)^b\right)^4}$$

where:
f = frequency
fc = the central frequency where the smoothing is done
b = bandwidth coefficient

To obtain the spectral ratio of horizontal and vertical components, then the two horizontal components must be one value, using the average of the square, before divided by the horizontal component. This process is performed for every window that is selected. Spectral ratio value of H / V is obtained from the average ratio of H / V of the entire selected window. To obtain a low standard deviation, then the value of H / V must be either a value of more than 0.4 because values below 0.4 will have very high standard deviations.

The end result of data processing is a form of spectral ratio H / V (Figure 5). From this spectrum, we can determine the value of dominant frequency (fo) and peak of HVSR (A) at the measurement location of mikrotremor. Based on the relationship T = 1/fo then we will get the value of the dominant period at the measurement location. To assess the reliability of spectral H / V, according to the recommendations of Sesame, the results obtained should be qualified as follows:

- fo> 10 / lw. Dominant frequency must be greater than 10 divided by window length.
- Value of the significant cycles must be greater than 200, meaning that the value of nc = lw x nw x fo. This value must be greater than 200.

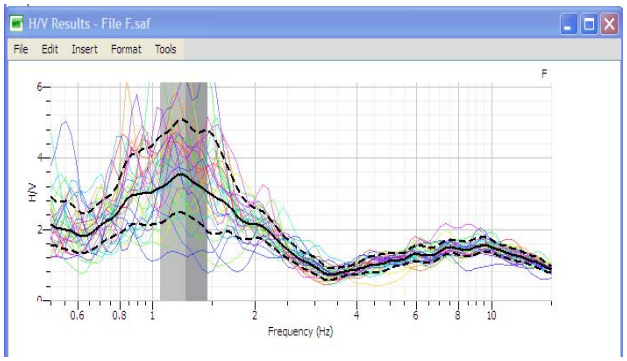

Figure 4. Ratio H/V

Spectral ratio value of H / V (HVSR) obtained will be used to create a contour map showing the peak value HVSR and predominant frequency (fo). This value will be compared with previous results and also results Sesame standards for levels of danger of damage due to earthquakes that occurred. Geological data was not considered in this study due to geological studies for the research area has not been done to the level of detail.

3. Results and Discussions

Research area is administratively located in the region of Malang city. Based on the record of the Karangkates Geophysical Station, on February 19, 1967, Malang has experienced the most destructive earthquake in the area around Sub-district of Dampit and Gondanglegi. In the area around Dampit, there were 1539 buildings damaged, 14 dead and 72 wounded, and in Gondanglegi, there were 119 buildings collapsed, 402 buildings cracked, 9 victims who died, and 49 wounded.

The intensity of the earthquake was recorded at 8-9 MMI with the epicenter in 8.5 south latitude and 113.5 east longitude, or located at 80 km below sea level, south of Malang area. In addition, according to the catalog results and earthquake mitigation projects by SEASEE (Southeast Asia Association of Seismology and Earthquake Engineering), on October 20, 1958, Malang area has experienced an earthquake with magnitude 6.7 on the Richter scale and the scale of MMI was VII-VIII. Victims who died were eight people. Because the earthquakes are likely return

period, then the potential occurrence of earthquakes in the region of Malang is still quite high.

Geologically, the area of the study area is dominated by pumice tuff, tuff breccia, tuff, sandy tuff, lapilli tuff and fine grain. Area study is located on the plateau with an average altitude of about 500 m above sea level. The study area is crossed by the river Brantas, where the flow of the Brantas River is apparently to give value of the seismicity.

Microtremor analysis at University of Brawijaya region, namely HVSR analysis to determine the peak value of HVSR (A) and dominant frequency (fo) has been taking place here. These results are then used to calculate the value of the seismic vulnerability (Kg). Recording the data is shown in Table 3.

Table 3. Recording data

No	Nama	Mulai	Akhir
1	KL 1	15:15:14	15:47:30
2	KL 2	07:53:25	08:25:10
3	KL 3	09:00:12	09:32:00
4	KL 4	10:37:36	11:09:15
5	KL 5	09:53:10	10:25:45
6	KL 6	14:57:40	15:29:05
7	KL 7	14:14:02	14:45:50
8	KL 8	11:21:52	11:53:10
9	KL 9	09:12:42	09:45:05
10	KL 10	13:33:10	14:05:30
11	KL 11	12:50:41	13:13:45
12	KL 12	08:24:38	08:58:15
13	KL 13	14:55:12	15:27:30
14	KL 14	07:45:15	08:18:00
15	KL 15	13:51:40	14:24:10
16	KL 16	12:58:58	13:30:00

Based on 16 data points (Table 3) that have been taken, the raw data were obtained in the form of tremors, mixed with additional waves or transient events. Microtremor data recording techniques are similar to techniques for analyzing seismic data recording. Microtremor recording technique does not need to wait for the event of earthquake, while seismic recording techniques and analysis is conducted when an earthquake occurs. In order to be processed using the software GEOPSY, this data is then combined in a single standard file format based on Sesame SAF. SAF file format includes information on recording time, the number of data, information on types of recorders and other supporting data. This format will be processed using the software GEOPSY, to know the value of HVSR. Results of processing of 16 data points are the obtainment frequency spectrum. Spectrum was then analyzed to obtain peak values of HVSR (A) and predominant frequency (fo) for each point.

Analysis of Spectrum Characteristics HVSR

HVSR spectrum was generated from GEOPSY (Table 3). The dotted lines at the top and bottom end is standard deviation for all values of the ratio of the resulting spectrum, the line without a break in the middle represents the average value generated by the FFT analysis of the entire value of the ratio of H / V. In addition, the colorful line represents the curve of H / V of each window. From the analysis undertaken, the general value of dominant frequency (fo) for UB region ranged from about 0.99 to 8.96 Hz. While the peak value of HVSR (A) is between 1.3 and 5.2. Overall, the spectral shape of H / V gives a clear peak

Table 4. Spectral H / V for each Point Research

No	Spektrum HVSR	Analisis HVSR
KL 1	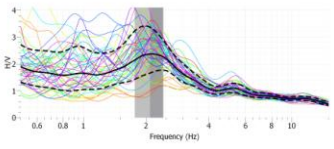	*Windows :46* fo : 2.11654 A : 2.37112
KL 2	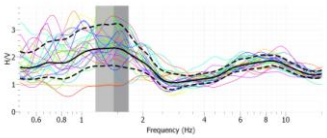	*Windows :27* fo : 1.45045 A : 2.33236
KL 3	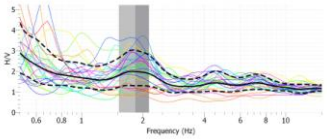	*Windows :28* fo : 1.78248 A : 1.99446
KL 4	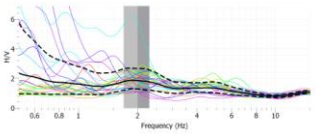	*Windows :27* fo : 1.90927 A : 1.87428
KL 5	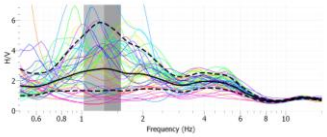	*Windows :45* fo : 1.30840 A : 2.78681
KL 6	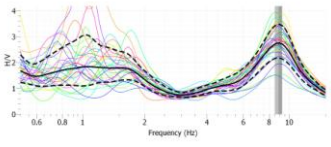	*Windows :31* fo : 8.95953 A : 2.75436
KL 7	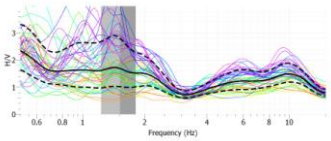	*Windows :45* fo : 1.40147 A : 1.73018
KL 8	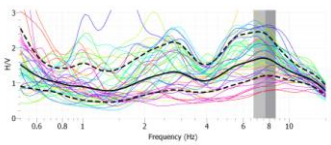	*Windows :44* fo : 7.54541 A : 1.71159
KL 9	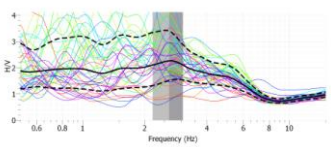	*Windows :43* fo : 2.69197 A : 2.27229

KL 10	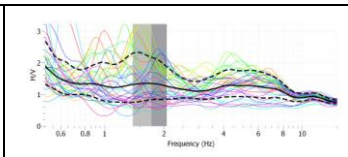	*Windows :36* fo : 1.66412 A : 1.35050
KL 11	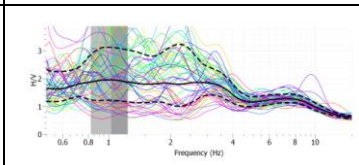	*Windows :61* fo : 0.99398 A : 1.95736
KL 12	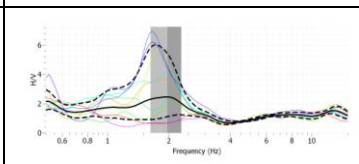	*Windows :09* fo : 1.97600 A : 2.45130
KL 13	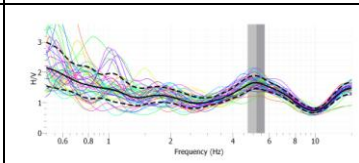	*Windows :44* fo : 5.17081 A : 1.66568
KL 14	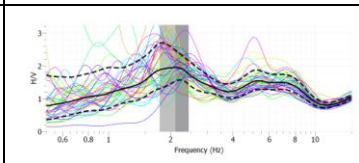	*Windows :43* fo : 2.11654 A : 1.95682
KL 15	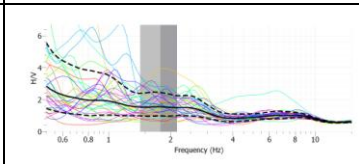	*Windows :35* fo : 1.72228 A : 1.55611
KL 16	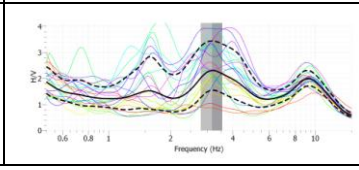	*Windows :22* fo : 3.19648 A : 2.30997

Distribution of Dominant Frequency (fo)

Results of spectral analysis of H / V in the area of research found that the average of Klojen Subdistrict region has a low value of the dominant frequency. For high value of fo, it is found in the KL 6 (7.96204 LS, 7.96204 BT) dan KL 8 (7.96392 LS, 112.63185 BT). For lower values of fo, it is found in the region of KL 11 (7.97202 LS, 112.63158 BT) dan KL 5 (7.95245 LS, 112.64023 BT). Dominant frequency contour maps for UB region is indicated by Figure 5.

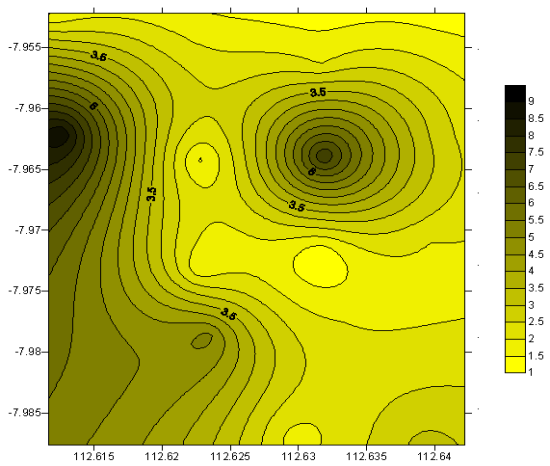

Figure 5. Dominant frequency contour map

The peak value ratio in the study area ranged from 1.4 to 2.8, which means having a low enough value. HVSR peak value ratio can be used in earthquake hazard assessment, but until now there are many pro and contra. Bard states that the peak value HVSR only provides low-level amplification of earthquake vibrations [6]. But other researchers like Mucciarelli *et al.* [7] and Nakamura [8], provides evidence of a clear correlation between the peak value HVSR and earthquake damage.

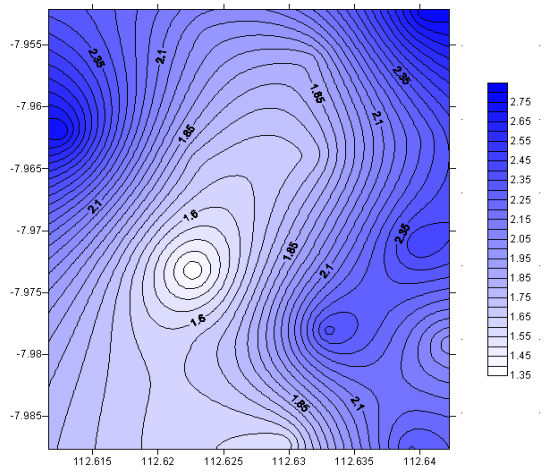

Figure 6. Peak Value Distribution of HVSR

Amplification values affect the level of infrastructure damage in case of earthquakes. Daryono [1] showed that at Yogyakarta earthquake in 2006, over 30% damage occurred in areas with a value of A between 3 and 7. But the most damage distributions, contained in the region with A between 5 and 6. Considering this and also that the high damage will occur in the dominant low-frequency zones with high peak of HVSR spectrum, then we can say that for this research area Klojen Sub-district, the regions with a relatively high level of danger is found in the KL5. In this region, the dominant frequency value is small, whereas the amplification or HVSR peak value is the highest, which are 2.8. This shows that if in the area of the building or other infrastructure development does

not pay attention to earthquake resistant standards, the level of damage that occurs when an earthquake will be higher.

Seismic Vulnerability Index

Seismic vulnerability index (Kg) is an index indicating the level of vulnerability of a layer of soil to deform. Therefore, this index is useful for the detection of areas that are weak zone (unconsolidated sediment) at the time of occurrence of earthquakes. Some studies like Daryono [1] and Nakamura [8] show a good correlation between seismic vulnerability index (Kg) and the distribution of earthquake disaster damage.

This index is obtained from the peak value of HVSR squared, divided by the value of the dominant frequency. For this research area, Kg values are shown in Table 5. It appears that, in general, fairly low index values ranged between 0.2 and 8. But at the point UB 12, Kg values were high, namely 26. From these results we can say that, in general, land surface area of UB is not a weak zone, so it is quite difficult to occur in the event of earthquake deformation. Only the region around Matos has a high value of Kg which means this area will have a higher vulnerability of deformation than in UB.

Table 5. Seismic Vulnerability Index Value

Point	f0 (Hz)	Peak HVSR	Kg
KL 1	2.11654	2.37112	2.656321191
KL 2	1.45045	2.33236	3.750493412
KL 3	1.78248	1.99446	2.231649551
KL 4	1.90927	1.87428	1.83993124
KL 5	1.30840	2.78681	5.935730645
KL 6	8.95953	2.75436	0.846751895
KL 7	1.40147	1.73018	2.135987807
KL 8	7.54541	1.71159	0.388254625
KL 9	2.69197	2.27229	1.918038405
KL 10	1.66412	1.35050	1.095984815
KL 11	0.99398	1.95736	3.854454275
KL 12	1.97600	2.45130	3.040926969
KL 13	5.17081	1.66568	0.536567745
KL 14	2.11654	1.95682	1.809152916
KL 15	1.72228	1.55611	1.405972509
KL 16	3.19648	2.30997	1.669324194

To further ensure this, it must be carried out other research, i.e. research on the acceleration of seismic waves in the basement. Vulnerability index together with the acceleration of seismic waves in the basement was suggested by Nakamura [9] to calculate the value of shear strain (γ) of surface soil layers. Damaging earthquakes will occur when the limits are exceeded due to the shear strain deformation surface layer of soil. Soil is plastic at γ = 1000x10-6, whereas at γ> 10.000x10-6, the ground will deform.

If we look, from the contour map of seismic vulnerability index (Kg) in Figure 7, the results of analysis of the dominant frequency and peak value of HVSR, showed that the area around KL5 is an area that has a dominant low frequency, high amplification values, and the value of the index high seismic vulnerability. This shows that the area is an area that has the highest hazard potential than others, so this is true of development in the area really should follow the standards of earthquake resistant buildings (Figure 7).

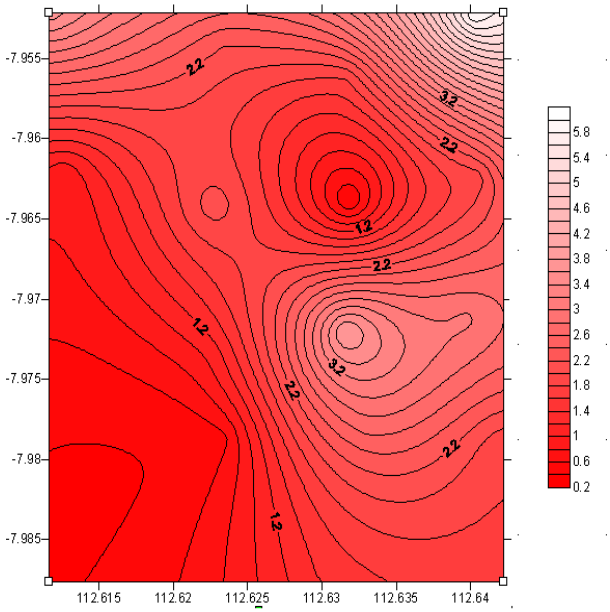

Figure 7. Distribution Maps of Seismic Vulnerability Index

4. Conclusion

Based on the research that has been conducted, several conclusions can be outlined as follows:

1. Values of dominant frequency to Klojen sub-district and the surrounding area is between around 1 and 9 Hz, with an average of less than 3 Hz. The peak value of HVSR or amplification ranged from 1.4 to 2.8.
2. From the analysis of the value of the fo and A, shows that the potential damage from earthquakes is quite low. This is consistent with the seismic vulnerability index value that ranges between 0.4 kg and 6.
3. From the analysis of the three parameters, it was found that a relatively high potential for damage if there are earthquakes in the area around KL5 (7.95245 *LS*, 112.6402 *BT*).

5. Acknowledgements

---

6. References

[1]. Daryono, (2009), Efek Tapak Lokal (Local Site effect) di Graben Bantul Berdasarkan Pengukuran Mikrotremor. International Conference Earth Science and Technology. Yogyakarta.

[2]. Nakamura Y., (1989), A Method for Dynamic Characteristic Estimatimation of Subsurface Using

[3]. Microtremor on The Ground Surface. *Q.R. Of R.T.I.* 30-1, p. 25-33.
[4]. Arai H., (2000). Estimation of Ground Motion Characteristics and Damage Distribution in Golcuk, Turkey, Based on Microtremor Measurements. Earthquake Disaster Mitigation Research Center (EDM), The Institute of Physical and Chemical Research (RIKEN)
[5]. SESAME. (2004). Guidelines for the Implementation of the H/V Spectral Ratio Technique on Ambient Vibrations Measurements, Processing and Interpretation, European Commission – Research General Directorate.
[6]. Konno, K. and Ohmachi, T., (1998), Ground-Motion Characteristics Estimated from Spectral Ratio between Horizontal and Vertical Components of Microtremor. *Bull. Seism. Soc. Am.*, Vol. 88, N. 1, 228-241.
[7]. Bard, P.Y., (1999), Microtremor measurement: a tool for site estimates? States of the art paper, second International Symposium on the Effect of Surface Geology on Seismic Motion, Yokohama, December 1-3, 1998, pp. 1252-1279.
[8]. Mucciarelli, M., Valensise, G., Gallipoli, M.R. and Caputo, R., (1999), Reappraisal of A XVI Century Earthquake Combining Historical, Geological and Instrumental Information, Proceedings of Workshop of E.S.C. Sub-Commision on Historical Seismology, Macerata, Italy.
[9]. Nakamura, Y., (2000). Local Site Effect of Kobe Based on Microtremor Measurement. Proceedings of the 6th International Conference on Seismic Zonation (6ISCZ) EERI, November 12-15, 2000/ Palm Springs. California
[10]. Nakamura, Y., (2008). Clear Identification of Fundamental Idea Of Nakamura's Technique And Its Applications. World Conference of Earthquake Engineering

Zircon Imprinted Polymer: Synthesis, Characterization and Zircon Ion Absorption Properties

Aladin Sianipar [1], Amran M.B. [2], Buchari [3], I Made Arcana [4]

(1) Separation and Speciation Analytical Laboratory, Dept. of Chemistry, ITB, Bandung
(2, 3) Analytical Laboratory, Dept. of Chemistry, ITB, Bandung.
(4) Physical and Inorganic Chemistry Laboratory, Dept. of Chemistry, ITB, Bandung.

Abstract

Ion imprinted polymer (IIP) particles were prepared via bulk polymerization methods by forming binary complex (Zr-Xylenol orange (XO)) in 2-methoxy ethanol (porogen) and copolymerizing in the presence of styrene (functional monomers), divinylbenzene (crosslinking monomers) and benzene peroxide (BPO) as initiator. Zircon ion is ion imprint and is used to form the imprinted polymer. Zircon ion was removed from polymer particles by leaching with 9 M HCl which leaves cavities in the polymer particles followed by filtering, washing, drying in an oven at 50 ^{o}C and grinding process. The polymer particles both prior and after leaching have been characterized by IR, SEM-EDS, Optical photo and TEM. The effect of different mol template complex to the absorption properties of zircon ion also was investigated. Furthermore, their capacity to rebind zircon from dilute aqueous solution was observed. The retention capacity of zircon IIP particles for 1 mmol, 0.01 mmol and 0.001 mmol Zr-XO complex templates was found to be 4.5 mg zircon ion per gram particle in pH 6. 4 and 3, respectively.

***Keywords**: Ion imprinted polymers, zircon ion, solid phase extraction.*

1. Introduction

Zirconium and hafnium co-exist in nature, but they have opposite nuclear characteristics. Thus, they have to be separated prior to their transformation into pure metals. Continuous efforts have been made to develop new extractor for the extraction and possible separation of zirconium and hafnium. Conventional solvent extraction technology use TBP/NHO_3 or MIBK/NaSCN/HNO_3. Previous reports have used other extractors for zirconium/hafnium separation [1-6], among them the most successful was cyanes 925 which successfully extracted 61% zirconium and 4% hafnium giving a separation factor of 37. Taghizadech et al., have been successful to enrich zirconium extraction up to 71% at separation factor of 8.1. They have used Taguchi method to investigate the effect of acid type. The experiment has been applied extraction of zirconium in nitric acid solution [7].

Solid phase extraction (SPE) is replacing liquid-liquid extraction (LLE) due to the following advantages over the former techniques. These include (i) higher enrichment factor, (ii) absence of emulsion, (iii) safety with respect to hazardous samples, (iv) minimal cost due to low consumption of reagents, (v) flexibility and (vi) incorporation into automated analytical techniques. Hence, many current researches focus in selecting the sorbent in SPE i.e. the use of molecular imprinted materials (MIP) due to their low price and stability in different environment. This material also more selective than common solid sorbent such as immobilized naphthalene, cellulose, C18 bonded silica membrane discs, silica gels, glass beads, silica frit, metal hydroxides, active carbon and functionalized polymer support for pre-concentrative separation of metal ion [8-11].

Metal ion-imprinted resin was reported for the first time by Nishide *et al*., which could absorb the guest metal ion from weakly acidic solution. Kabanoc *et al*., also developed adsorbents selective to metal ion by imprinting polymerization and characterized the adsorbents by spectrophotometric analysis [12]. Molecule imprinted polymers are synthesized by polymerization of functional monomers in the presence of template and excess of cross linker. After polymerization, the print is leached out, leaving an imprint of analyte molecule. The imprint of analyte is one active site to improve the sorbent selectiveness.

A survey on the synthesis of metal ion-imprinted polymers shows that these polymers may be roughly classified into the following four approaches based on inclusion of ligand in the polymer matrix, viz. (i) linear chain polymer carrying metal-binding groups being cross-linked

with bifunctional reagent, (ii) chemical immobilization by preparation of binary complexes of metal ions with ligand having vinyl groups, isolation and then polymerization with matrix-forming monomers, (iii) surface imprinting conducted on aqueous-organic interface, (iv) trapping of non-vinylated chelating of metal ions with non-vinylated chelating agent and vinyl ligan [13-15]. Prasada Rao et al. (2006), had reported a comprehensive review of metal ion-imprinted polymers-novel materials for selective recognition of inorganic. Their review attempts to give an accessible summary of field where the trends can be identified in synthetic approach and characterization of ion-imprinted polymers. This review also opens many possibilities for new pre-concentrative separation, sensing and possibly even membrane-based technologies [16].

Here, we report the investigation of particle synthesis for separation and the separation of zirconium from others metals especially from hafnium. The material used was solid phase extraction (SPE), a chelating agent used to extract zirconium. Chelating agent and zirconium formed a molecule complex. In this study, the usage of the xylenol orange (XO) as chelating agent was based on the selectiveness of XO as a chelating agent. Abdul Majeed and Khan M (1987); Grudpan et al. (1998), have used XO for selective agent for the extraction of zirconium by spectrophotometer. Their method has been successful to determine zirconium in NBS steel and eluat from technetium-99m generator samples [13,17].

2. Experimental Details

Instrumentation

ICP-AES (varian) to determine zirconium, single beam spectrophotometer (Hallowpacked) and pH meter (Orion) were used for absorbance and pH measurements respectively. SEM-EDS and TEM (JEOL) was used to scan the micro morphology surface of the material. IR spectroscopy (Shimadzu) was used to scan the spectrum polymer.

Reagents and materials

Xylenol orange and zirconoxichloride from Merck, styren monomer, divenylbenzene (DVB), 2-methoxiethanol and benzene peroxide (BPO) from Sigma Aldrich.

Synthesis of ion imprinted polymer (IIP) particle

The synthesis of IIP materials was carried out in two steps: (1) binary complex formation and (2) copolymerization of binary complex with styrene (monomer), DVB (cross linking monomers).

Formation and stoichiometry of binary complex

The binary complex of zircon ion with xylenol orange was prepare by stirring a mixture of 1 mmol of zircon from zirconoxichloride and 1 mmol xylenol orange in aquademineralization. Absorption spectrum of the complex was confirmed by UV-VIS spectral studies. (Fig.1) It showed an absorption maximum around 550 nm. The stoichiometry of complex was established by Job's plot method.

Copolymerization by bulk

Complex of Zr-XO 1 mmol, styrene 40 mmol, DVB 40 mmol and BPO 0.61 mmol were prepared by stirring the mixture in 10 mL of 2-methoxiethanol as porogen. The polymerization mixture was cooled to 0^oC and purged with N_2 for 10 min, sealed and heated at 80^oC in oil batch with stirring for 12 h. The solid polymer was grounded in mortar and dried in 60^oC for 2 h. The imprint Zircon ion was leached from polymer by stirring with 20 mL HCl 9M for 12 h. The excess amount of HCl was wash with ultrapure water followed by methanol. The complete removal imprint ion was controlled by ICP-AES. Finally the polymer particles were dried in vacuum desiccators and used for determination of capacities retention for zircon ion.

Retention capacity

The retention capacity from aqueous solution was investigated in batch experiment. The polymer particles were suspended in 10 mL solution with zircon ion concentration of 10 mg/L. pH was variated by nitric acid and sodium hidroxyde solution. The concentration of zircon after the treatment was measured by ICP-AES. The extraction and measurement were replicated for each aqueous solution. Retention capacity of zircon was calculated from the following equation:

$$\text{RC (mg Zr/mg IIP)} = \frac{(CA - CB) \text{ x Vol. solution}}{\text{mass of IIP}}$$

3. Result and discussion

Formation and stoichiometry of binary complex

Stoichiometry of complex by job's plot rises from origin as a straight line and breaks at absorbance corresponding to mol fraction of components. The result obtained was shown in Figure 2, from which it is clear that maximum occurs at the mol fraction of Zr/Zr+XO at 0.48.

Job's plot method is based on the principle that the analytical signal due to the complex MLn, formed by the interaction of metal ion M with ligand L according to equilibrium:

$$M + nL \leftrightarrow MLn$$, will attain a maximum at

$$\frac{[M]}{[M]+[L]} = \frac{1}{n} + 1$$

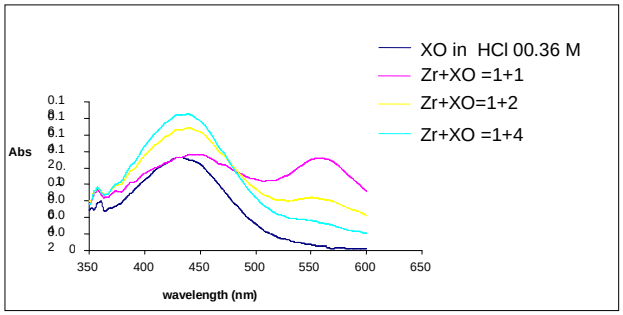

Figure 1. UV-vis absoption spectra of Zr-XO

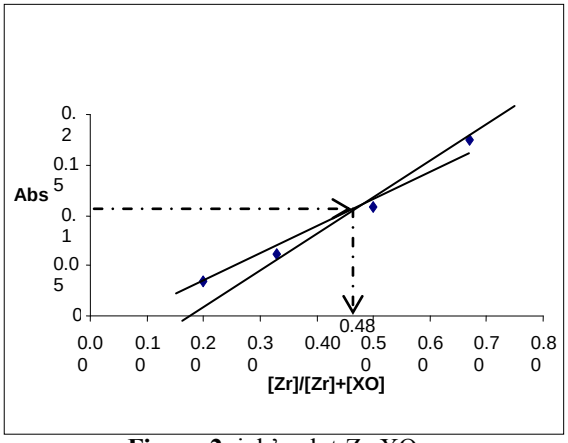

Figure 2. job's plot Zr-XO

Provided the variation of metal and ligand concentration is done by keeping their combined concentration, i.e $[M] + [L]$, constant. Hence, the stoichiometry complex in prepolymerization is 1:0.92 ∞ 1:1 as Zr:OX [8].

Photo optic

The photo optic was shown in Figure 3 (Appendixes) from which clearly shows a significantly different particle colour. Unleached particle colour is violet. This colour is derived from Zr-XO complex and leached particle is red. It indicates that Zr has been removed.

IR spectra

The IR spectra of unleached and leached zircon imprinted polymer were recorded by using KBr pellet method. The IR spectra of unleached and leached IIP materials are given in Figure 4 (Appendixes). All have similar IR spectra which indicate that all the polymers have similar backbone, but have different significant intensity spectra. A band near 1080cm^{-1} present in unleached material is shifted to higher frequency 1089cm^{-1} while leaching. The shift and decrease in strength of vibration can be attributing to bonding between the zircon with xylenol orange. Generally, these observations indicate that the polymer backbone is same in both unleached and leach IIP particle thus suggesting XO is held onto polymer even after leaching.

Scanning electron microscopy (SEM)-Energy disperse spectroscopy (EDS) study

The morphologies of polymers produced by bulk polymerization which was assessed by SEM-EDS with magnitude 2000 are given in Figure 5. The result clearly shows that leached particle morphology is similar as a soaked morphology. It is not smooth if compared to unleached particle. From spectra EDS it can be seen that there is no signal of zircon on particle after leached with HCl 9M for 24 h.

Study of Imprinted Formation of Polymer

Synthesis imprinted polymer by bulk methods has been made with zircon removed from particle and live pore. Zircon has been successfully leached by HCl 9M indicated by SEM-EDS photograph. Finally, the imprint is characterized by transmition electron microscopy (TEM) which the result was shown in Figure 6.

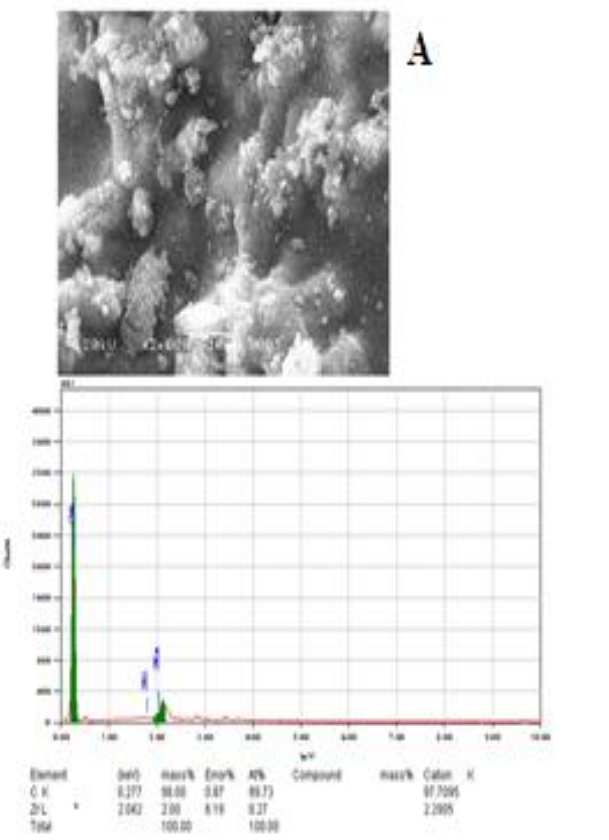

Figure.5. SEM-EDS photograph of unleached (A) and leached (B)

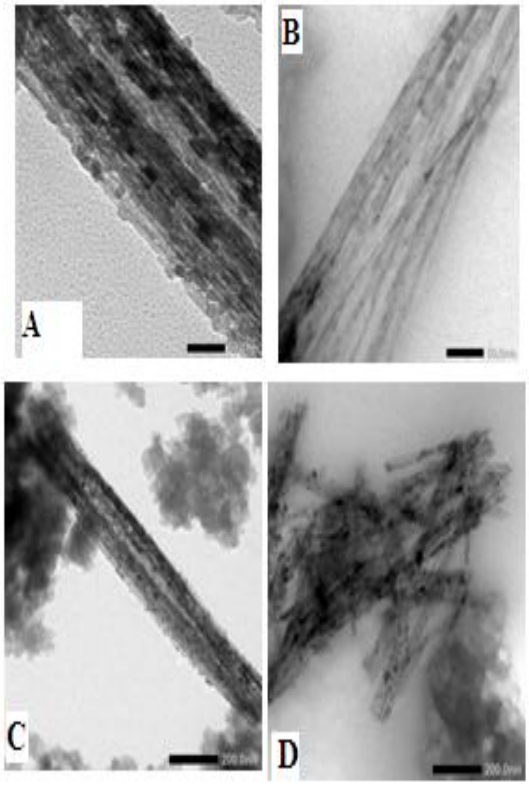

Figure 6. TEM photograph of leached (A and C 50nm, 200 nm particle size respectively), and unleached (B and D 50nm, 200 nm particle size respectively).

Retention capacity study

The retention capacity of IIP materials were determined by 0.05 g of particle suspended with zircon solution 10 mg/L in aqueous. pH was adjusted using nitric acid and sodium hydroxide solution. The retention capacity study was applied in a batch method for 8 hours. The results obtained were shown in Figure.7. IIP suspended with zircon solution is IIP with Zr-XO 1 mmol. Maximum retention capacity is 4.5 mg Zr/g IIP at pH 6.

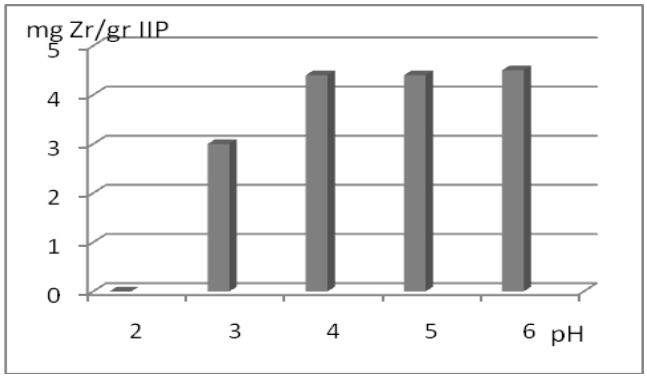

Figure 7. Retention capacity of 1 mmol IIP Zr-XO

In order to investigate the complex concentration effect to the retention capacity, an experiment using several complex concentrations was conducted. The concentration was varied, 0.001, 0.01 and 1 mmol. The results were shown Figure 8.

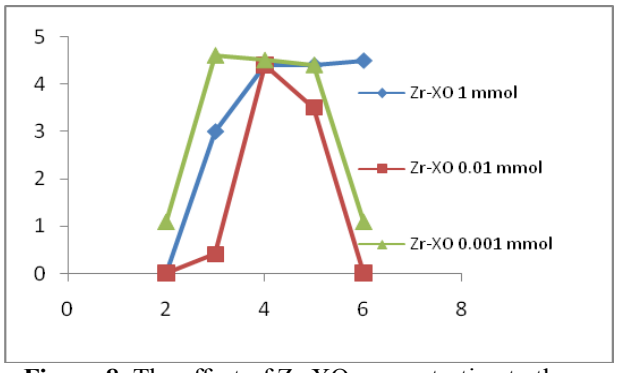

Figure 8. The effect of Zr-XO concentration to the retention capacity.

Degree of complex Zr-XO no effect significant to retention capacity, but it cause pH retention capacity shift to decrease pH on amount Zr-XO decrease. pH shift to decrease of pH from pH 6 to 3 as decrease Zr-XO of IIP particle is indicate that IIP particle can be set pH retention capacity. It is used to improving selectivity of zircon separation from other ion.

4. Conclusion

The investigation synthesis zircon imprinted polymer via bulk polymerization has good potential for selective zircon. Enrichment selectivity can be design by to organize IIP by pH condition and degree of complex template. Further, selectivity factors will be applied to separation zircon from zirconia sand and especially separate from hafnium.

5. Acknowledgements

The authors (Aladin Sianipar and Amran M.B) are thankful to Institute Technology of Bandung in supporting this research.

6. References

[1]. El-yamani and Farrah (1978), …
[2]. Shults and Larsen (1950), …
[3]. Kalyanaraman and Khopkar (1977), …
[4]. Dalsiva *et al*., (2000), …
[5]. Dalsiva and Distin (1998), …
[6]. Poriel *et al.*, (2006), …
[7]. Taghizadeh M., *et. al.*, (2008), *J. Hydrometallurgy*, 90, 115-120.
[8]. Daniel sobhi, Gladis Mary J, Prasada Rao T., (2003), *Ana. chimica acta*, 488, 173-182.
[9]. Kala R., Biju V.M., Prasada Rao T., (2005), *Ana. chimica acta*, 549, 51-58.
[10]. Mostafa Khajeh, *et. al*., (2007), *Ana. chimica acta*, 581, 208-213.
[11]. Biju V.M., Gladis M.J., Prasada Rao T., (2003), *Ana. chimica acta*, 478, 43-51.
[12]. Daniel S., Prabhakara Rao P., Prasada Rao T, Prasada Rao T., (2005), *Ana. chimica acta*, 536, 197-209.
[13]. Kate Grudpan, Mayuree Utamong and Colin G.Taylor, (1998), *Anal. communiction*, 35, 107-108.
[14]. Qun He, Xijun Chang, Qiong Wu, Xinping Huang, zheng Hu, Yunhui Zhai, (2007), *Ana. chimica acta*, 605, 192-197.
[15]. Guo zheng fang, Jin Tan, Xiu-ping Yan, (2005), *Separation Science and Technology*, 40, 1597-1608.
[16]. Prasada Rao T., Kala R., Daniel S., (2006), *Ana. chimica acta*, 578, 105-116.
[17]. Abdul Majeed and Khan M.S., (1987), *Ana. chimica acta*, 192, 125-128.
[18]. Metilda *et.al*, (2007), *Ana. chimica acta*, 582, 147-153.
[19]. Rdivan Say, *et al*, (2003), *Ana. chimica acta*, 480, 251-258
[20]. Prasad K., Kala R., Prasada Rao T., Naidu G.R.K., (2006), *Ana. chimica acta*, 566, 69-74.
[21]. Jingchan zhao, Bing Han, Yanfeng Zhang, Dandan Wang, (2007), *Ana. chimica acta*, 603, 87-92.

.

Appendixes

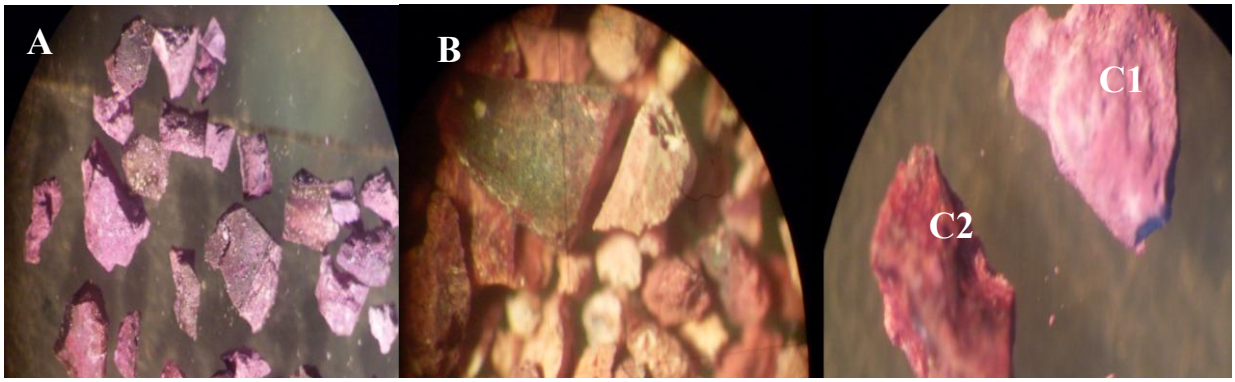

Figure.3. photo optic magnitute 600 polymer particle, unleached (A), leached (B), unleached (C1) and leached (C2) Zr-imprinted polymer with HCl 9 M.

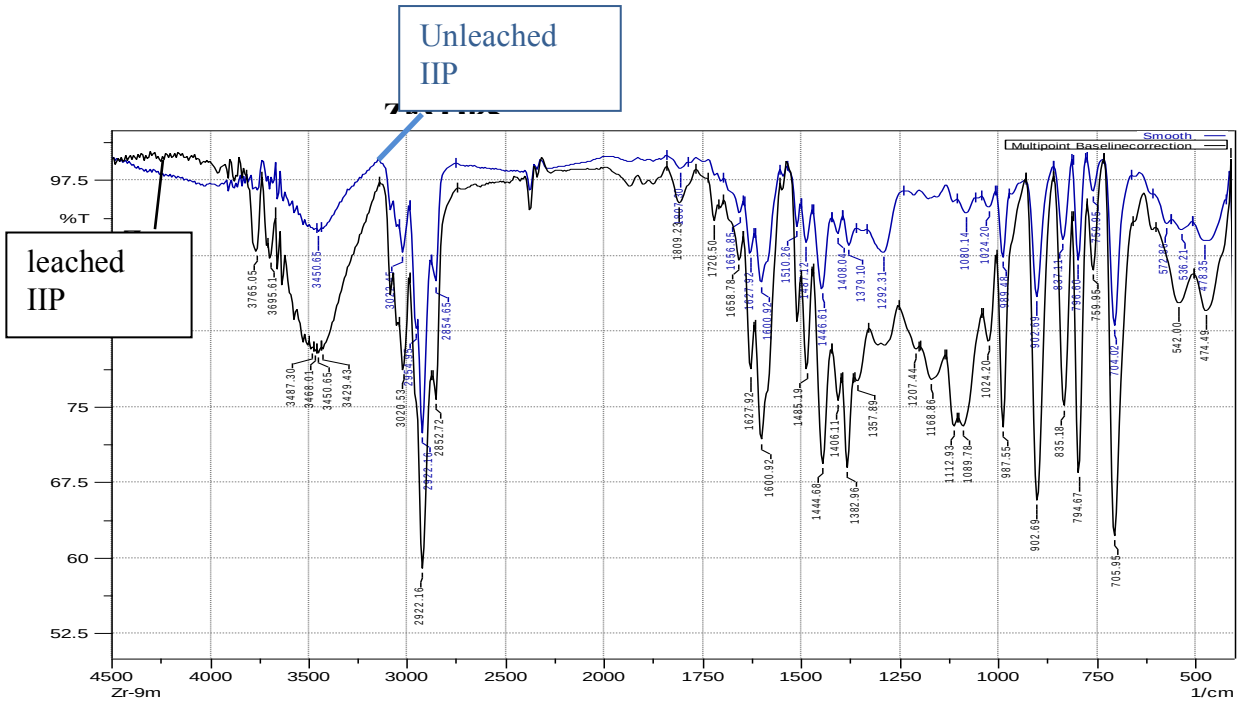

Figure.4. Overlay IR spectra of unleached and leached Zr imprinted polymer

Effect of Pyrrole (Py) Concentration and the Number of Cycles during Electropolymerization of Pyrrole (Py) on Platinum Electrode

Anceu Murniati [1,2], Buchari [3], Suryo Gandasasmita [4], Zeily Nurachman [5]

(1) Chemistry Department, Jenderal Achmad Yani University (UNJANI), Cimahi, Indonesia
(2,3,4,5) Chemistry Department, Bandung Institute of Technology (ITB), Bandung, Indonesia
(an_murniati@yahoo.co.id)

Abstract

Based on the literature, polypyrrole (PPy) is a conducting polymer, with PPy + can combine with anionic species reversible in a solution through a redox process to neutralize the charge. The purpose of this research get the information of PPy coating during the process of electropolymerization of Pyrrole (Py) by cyclic voltametry (CV) methods, based on the number of cycles and variation of monomer concentration. In the optimization studies using 0.05 M Py in 0.1M KCl solution as supporting electrolyte was great of peak current (Ip) on platinum (Pt) electrode versus Ag/AgCl reference electrode and the scan rate was 100 mV/sec. The Voltammogram of PPy based on number of cycles varied are 1; 10; 20;25; 35; and 40 cycles with a certain potential window shows the typical pattern of growth of the polymer during electropolymerization. Thus the cycle that would lead to more risk of trapping the anion which accumulates so that the role of anions has not been maximized, for a modified of PPy coated electrode. In contrast with fewer cycles of anions which are trapped in the polymer are not firmly attached so easily separated during the electropolymerization. Characterization of Py and PPy film was also studied by Infra Red spectroscopy.

Keywords: *platinum electrode, pyrrole (Py), polypyrrole (PPy), electropolymerization.*

1. Introduction

In recent years, polypyrole (PPy) is the most promising conducting polymers that received comprehensive interest due to its excellent characteristics including easy preparation, environmental stability and high conductivity. PPy has convenient operating and attractive prospect of development in the field sensors. These polymers also allow ions to diffuse or migrate within them. An increase in the voltage applied to a polymer electrode leads to removal of electrons and an increasingly positive charge within the volume of polymer. This charge is balance by negative ions that enter the polymer from a neighboring electrolyte phase (or by positive ions that leave) [1]. Cyclic voltametry (CV) is very often used to characterize conducting polymer films [1-2], because the redox can be monitored in the form of a current-potential diagram. Intermediate species of very shot lifetimes can observed with microelectrodes. Since the oxidation of the monomer occurs at higher potential than that of the redox processes of the polymer, side reaction including crosslinking and over oxidation of the polymer could take placed.

Pletcher, *et al.;* Satoh, *et al,* have proposed a mechanism in which cation radical formed by the lost of an electron reacts directly with a neutral molecule giving a cation dimer, then loses a second electron and two protons forming the neutral dimer. This coupling reaction and the resulting polymerization are affected by the monomer concentration [1]. Some research has been reported to use the concentration of Py are 0.5 M Py [3]; 0.25 M Py [4]; 0.3 M Py [5].

According to some authors, a presence of PPy on Pt substrate modifies noticeably its electrochemical behavior [5]. The preparation of PPy/Pt catalyst

composite systems were described for the anodic oxidation of methanol [6].

In this study we reported effect of Py concentration and the number of cycles during electropolymerization of Py on Pt electrode. PPy voltamogram of varying concentrations of Py are 0.001; 0.005; 0.01, and 0.05 M each provide a specific pattern in the potential window of 850 to 1500 mV. In the optimization studies using 0.05 M Py in 0.1 M KCl solution as supporting electrolyte was great of peak current (Ip) versus Ag/AgCl reference electrode and a scan rate was 100 mV/sec. This study shows the voltamogram of PPy film based on number of cycles varied are 1; 10; 20; 25; 35; and 40 cycles with a certain potential window shows the typical pattern of growth of the polymer during electropolymerization. Although up to 40 cycles the voltamogram still showed the formation of a homogeneous PPy films. But with 10 cycles is considered the entire surface of Pt covered with PPy films. Characterization of Py and PPy film was also studied by Fourier Transform Infra Red spectroscopy (FTIR).

2. Experimental Details

Chemicals

Sigma-Aldrich; Pyrrole 98 % was obtained from Sigma Aldrich. KCl was obtained from Merck as supporting electrolyte. $K_3Fe(CN)_6$ was obtained from Sigma Aldrich. All chemicals were dissolved with aquabidest.

Working electrode

Platinum wire with a purity of 99.98%; Φ = 2 mm x 4cm; Pt electrode was prepared by inserting Pt wire on Teflon tube.

Reference electrode

Ag wire Φ = 1 mm x 5cm. Ag/AgCl electrode was prepared by electrolysis of Ag wires using solution 1M KCl solution. Reference electrode is stored in 3 M KCl solution.

Instruments

Potentiostat Basi-Epsilon Version 1.60.70 and Fourier Transformer Infra Red (FTIR) Prestige 21 Shimadzu Japan.

Experimental methods

Electropolymerization was performed in a typical three electrode cell, consisting of minicell of 5 mL volume; platinum rod as working electrode; and platinum counter electrode of 1 mm diam.

Figure 1. Equipment of electropolymeization cell

Electropolimerization of Py on Pt electrode at a potential window of 0 to +1300 mV vs. Ag/AgCl, at a scan rate of 100 mV/s. An electrolysis cell is connected with Epsilon Potentiostat and set of computer programs Basi-Epsilon Version 1.60.70. (Figure 1)

Characterization ofPPy-PPO films

FTIR Prestige 21 Shimadzu Japan was applied to characterize the thickness of Py

and PPy films. The IR data was presented by peak the function of chemical structure of Py and PPy.

3. Results and Discussion

Characterization ofAg /AgCl electrode

There has been much discussion regarding reference electrode Ag wire was calibrated with respect to the redox potential of Fe^{2+}/Fe. The voltametric scan originated -0.5V and was swept positive to 0.8 V, negative to -1.3V, then positive back to 0.5 V vs Ag/AgCl at a scan rate of 20 mV/s has been reported [5].

As the same case, the approach used here was to calibrate the reference electrode was applied to the electrolyte solution $K_3Fe(CN)_6$ To that end, CV was coducted in three electrode cell with a Ag/AgCl as reference electrode; a Pt rod as working elecrode and Pt wire as counter electrode. Top of ForBottom of Form Characterization of Ag/AgCl as reference electrode to give good response when applied as an electrode in electrolytes $K_3Fe(CN)_6$ in one and five cycles of the same operating conditions as follows of the potential window at 0 to 1000; 100 µA at a scan rate of 100 mV/s.

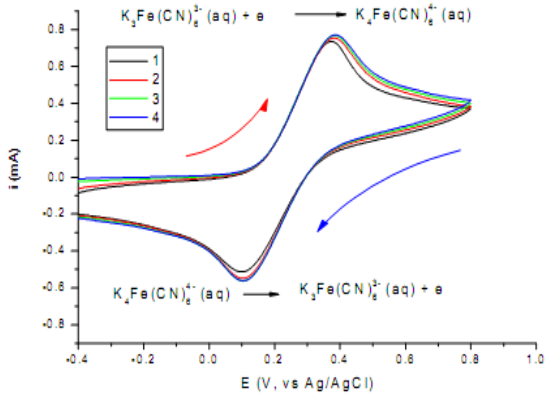

Figure 2. Cyclic voltammogram of $K_3Fe(CN)_6$ with potential window at 0 to 1000 mV, at a scan rate 100 mV/sec and 5 cycles.

Electropolymerization of Py

PPy film obtained by electropolymerization of Py deposited polymer in solution 0.05 M in $KClO_4$ as supporting electrolyte by anodic currents. The direction of scanning electropolymerization potential of Py starting from negative to positive potential at -400 to 1300 mV, and a scan rate 100 mV/sec.

Figure 3. PPy coated Pt electrode

Initially at -800 to 500 mV toward rail is straight and has not happened oxidation of Py. When the potential reached 600 mV oxidation process occurs of Py into PPy on the electrode surface [7]. After passing through the area of potential when the oxidation process took place behind the direction of its potential.

The oxidation of PPy on the electrode surface following the reaction: [8]

$$PPy \rightarrow PPy^{+} + e^{-} \ldots\ldots\ldots\ldots\ldots (1)$$

Oxidation potential maximum peak obtained at 924 mV and peak current of 498 mA, as in voltamogram PPy 1 cycle. (Figure 4 - Appedixes).

The number of cycles affects the homogeneity of the polymer film thickness. The wanted optimum number of cycles of Pt electrode characterized the best voltamogram. The cycle of too little risk of not the entire surface of platinum wire covered with PPy films, while the cycle is too much risk to the thicker polymer film that coats the surface of Pt electrode causes slow diffusion through the

membrane. Although up to 40 cycles the voltamogram still showed the formation of a homogeneous PPy films. But with 10 cycles is considered the entire surface of Pt covered with PPy films. Electropolymerization conditions are in addition affected the number of cycles, need to be studied further of monomer concentration variation.

Variation of Py concentration

PPy voltamogram of varying concentrations of Py are 0.001; 0.005; 0.01, and 0.05 M each provide a specific pattern in the potential window of -850 to 1500 mV. From these voltamogram the peak current (Ip) is indicated by the highest of 0.05 M Py. According to Randles-Sevcik equation stating circuit is proportional to the concentration, diffusion coefficient and the scan rate [8].

FTIR studies

IR spectrum of Py have typical absorption peaks (NH amine at 3402.43; CH aromatic ring at 3103.46; C=C alkene in 1680; C=C aromatic ring, and CN amine. IR spectra data of PPy peak shift occurs, because the formed polymerization (molecules increase in size) so the weaker vibrations, NH amine at 3402 cm^{-1} shifted to 3603 cm^{-1}.

Table 1. Anodic potential (Ep) and peak current (Ip) of PPy on Pt electrode of Py concentration

Py	Pt electrode	
concentration	E p	Ip
0.001 M	878	0.08
0.005M	1471	0.46
0.01 M	990	0.69
0.05 M	947	1.50

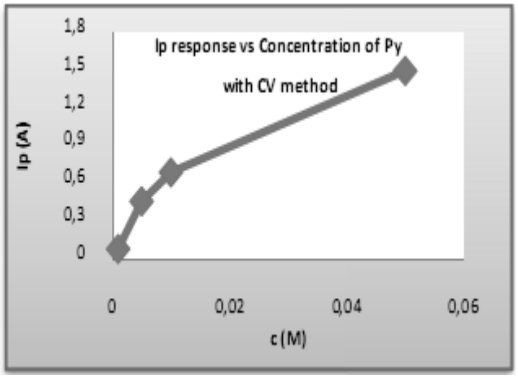

Figure 5. Ip response to concentration of Py, Of the CV method

4. Conclusion

In this report, we have study in the form of thin PPy film onto Pt electrode using electropolymerization by CV methods at the potential windows of -400 to 1300 mv and a scan rate 100 mV/s. This research has been conducted the number of cycles 1; 10; 20; 25; 35; and 40 cycles with a certain potential window shows the typical pattern of growth of the polymer during electropolymerization. The concentration of Py which gives the highest current peak reached at 0.05 M Py.

5. Aknowledgements

This work was realized with the support of "Voucher ITB" and "Hibah Stranas Dikti" fundings.

6. References

[1]. Sadki, Said; Schottland, Philippe; Brodie, Nancy; and Sabouraud, Guillaume (2000), The Mechanism of Py Electropolymeryzation, *Chem.Soc.Rev,* 29, 2 83-293.

[2]. Inzelt (2008), Chapter 4: Chemical and Electrochemical Syntheses of Conducting Polymers, *Conducting Polymers,* Springer.

[3]. Hermelin, E; Petitjean, J; Aeiyach, S; Lacroix, J.C; and Lacaze, P.C (2001), Industrial Polypy Electrodeposition on Zinc-Electroplated Steel, *Journal*

of Applied Electrochemistry, 31, 905- 911.

[4]. Martel, D; Nguyen Cong, H; and Gautier. JR (2008), Induced Effect of Transparent Substrate Composition on Polypyrrole Film, *J.Mater Sci,* 43: 5579-5584.

[5]. Nie, Jun; E, Dennis; Tallman; and Bierwagen, Gordon P (2008), The Electrodeposition of Polypyrrole On Al Alloy From Rom Temperature Ionic Liquid, *J.coat.Technol.Res,* 5 (3), 327-334.

[6]. Juttner, K; Mangold, K-M; Lange, M and Bouzek, K (2004), Preparation and Properties of Composite Polypyrrole/Pt Catalist Systems, *Russian Journal of Electrochemistry,* 40 (3), 359- 368.

[7]. D. Bloor, KM.Cheng and Steven, G.C (1990), The Influence Of Unusual Counterions on The Electrochemistry and Physical Properties of Polypy, *Journal of Material Science,* 25, 38 14- 3837.

[8]. Wang, J. (2000), *Analytical Electrochemistry,* 2nd ed, John Willey and sons, New York.

Appendixes

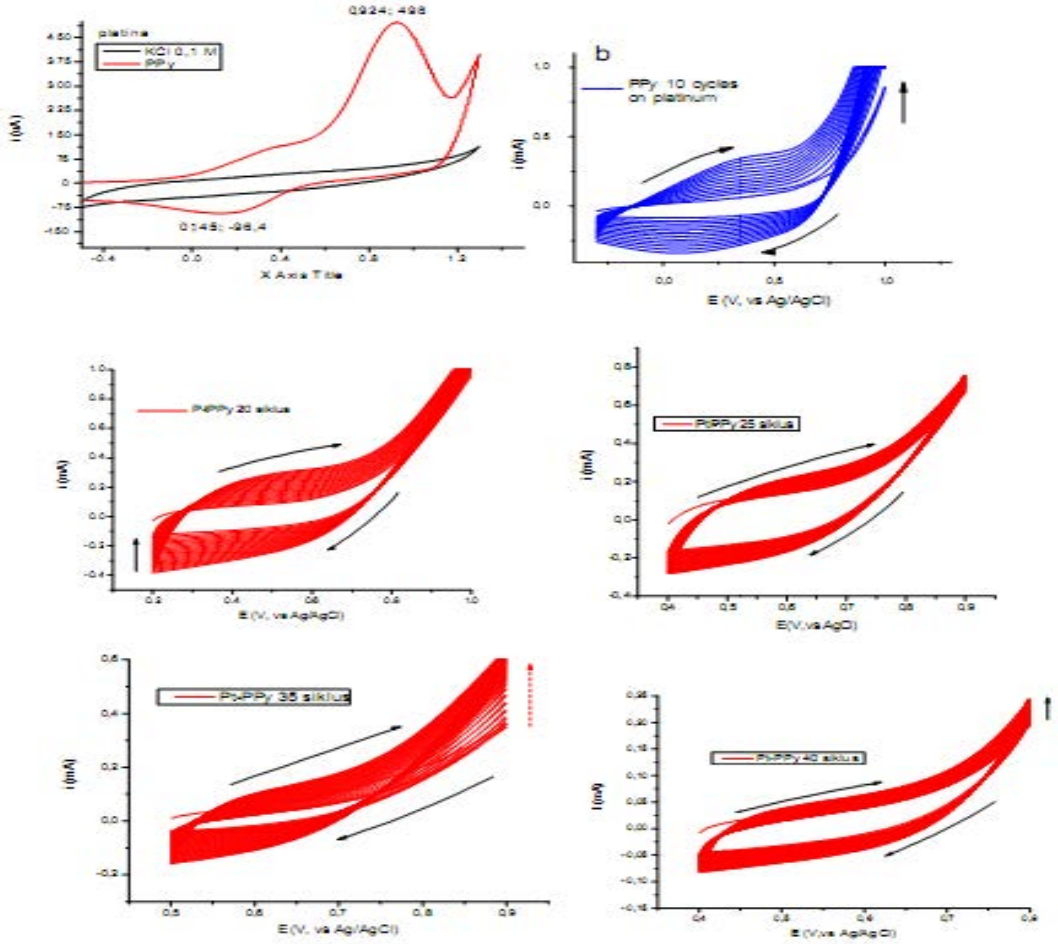

Figure 4. Cyclic voltammogram of PPy on Pt electrode; with potential window at -400 to 1300 mV, at a scan rate 100 mV/sec. The number of cycles are 1; 10; 20; 25; 35; and 40 cycles.

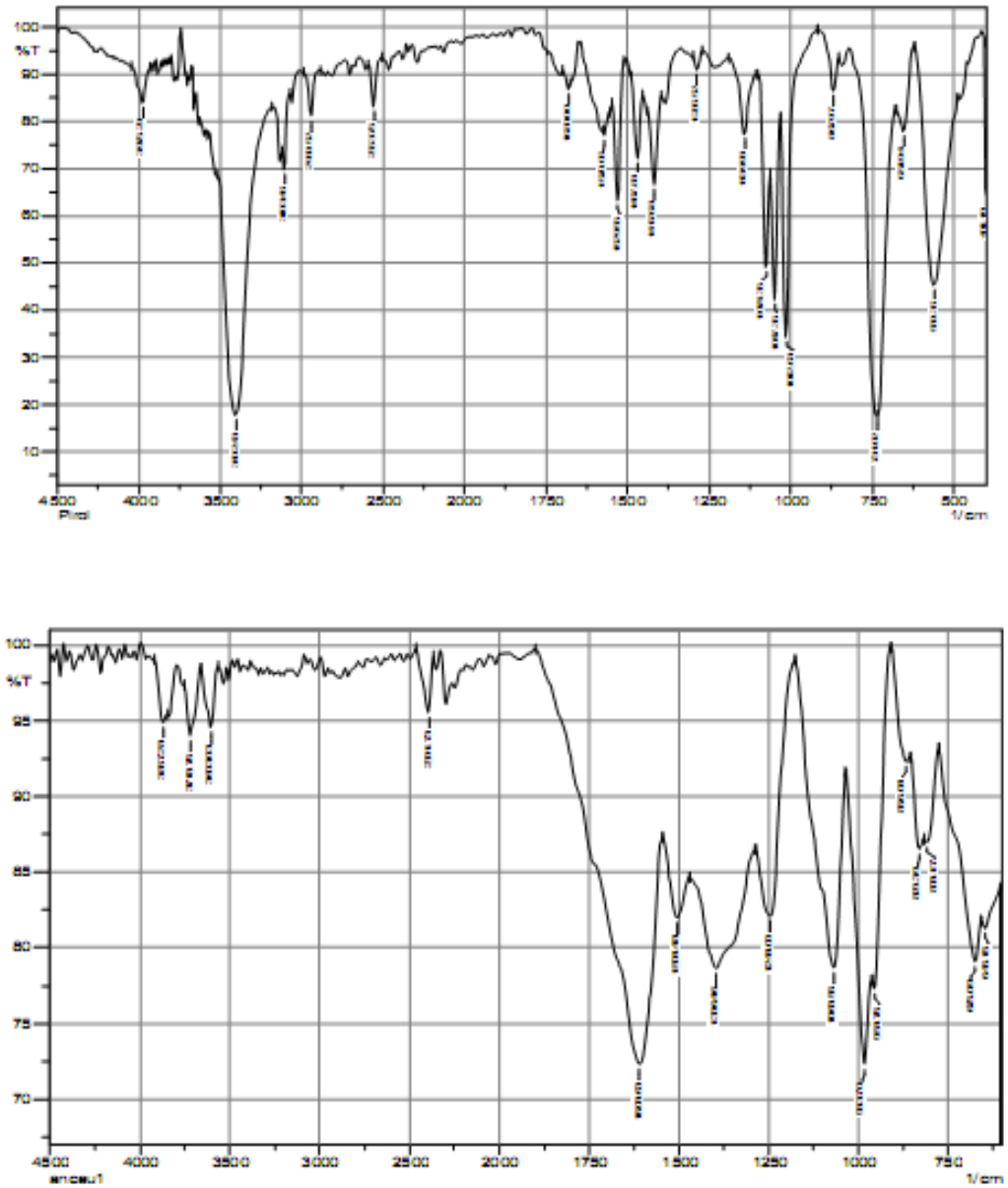

Figure 6. FTIR spectra of Py and PPy film

Development of Biomass Stove by Using Brick Refractory Castable Insulator

Bambang Poerwadi

Department of Chemistry, Faculty of Sciences, University of Brawijaya, Malang, Indonesia
(bpoerwadiub@ gmail.com)

Abstrack

Biomass stove is an alternative source of heat using biomass fuels that can be renewed. To increase the combustion efficiency, the biomass stove is continuously being developed. The main problem in biomass fuel application is the ignition control and supply arrangements in accordance with the required heat. Biomass stoves then are redesigned using simulation design space of primary and secondary air heating and insulation brick refractory applications. Simulation of the air heating chamber based on the comparison of primary and secondary clearance can be optimized for optimum heating differences. The results of optimization were then applied to biomass stoves and the efficiency of heating was tested. The stove was insulated with fireproof brick with low thermal conductivity standard. The redesigned stoves was tested by using coconut shell charcoal with fuel ignition temperature begun at 254 ^{0}C and the highest temperature outside insulator was at 42 ^{0}C. Temperatures in the primary combustion chamber has met the initial combustion of biomass fuel and heating efficiency is relatively good because the insulation refractory bricks was able to maintain the outside temperature at 42 ^{0}C.

Key words: biomass stove, insulator stove, stove redesign

1. Introduction

The available energy in biomass or wood energy resources are always presented in the form of chemical energy imposing reactions for its release and the performance of some actions such as cooking or steam generation. There are a lot of situations where biomass conversion is required. Biomass is basically a solid fuel which must be converted into another more homogeneous or more suitable fuel for its end use form of energy.

Based on that, the employment of several technologies based on some conversion processes is justified. The processes of biomass energy conversion can be classified in three groups: physical, thermo-chemical and biological processes. Figure 1 (Appendix) shows a scheme of these processes indicating the main reagents and products that may be intermediate fuels or energy for end use.

Biomass combustion is a process which takes place in 6 well defined consecutive stages: drying, volatile emission, volatile ignition, volatile flame burning, volatile flame extinction and coke combustion. When biomass is burnt in fixed bed on a gate, the volatile compounds are released and are burnt on the bed. That's why it is convenient to divide the combustion air flow into two parts: the primary air which is used for the coke combustion and the secondary air used for the volatile combustion (Figure 2).

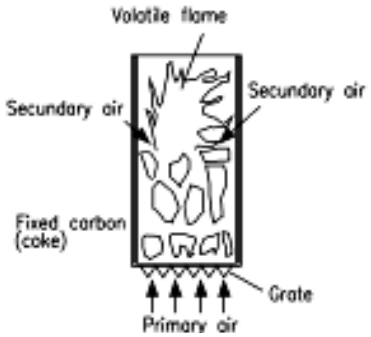

Figure 2: Biomass is burned in the bed scheme

Biomass is an energy source that can be used for cooking in rural communities. Biomass furnace or stove can be used in obtaining the energy from biomass. However, this furnace or stove needs to be developed further to improve the combustion efficiency. Theoretically, the mass of the air needed to burn 1 kg of dry biofuel, standard biomass ($CH_{1.4}O_{0.7}$), is 5.58 kg dry air.

Meanwhile, Indonesia has launched the self sufficient energy village starting in 2007 with criteria as follows [2]:

- Development of power generation facilities from local energy sources (renewable energy)
- Management of energy generation facilities

- Utilization of energy for productive activities
- The purpose of the program aimed at energy independent villages
- Diversification of energy at the rural level
- Improved rural economy

In order to improve the utilization of biomass using the biomass stove, it is necessary to design stoves that have high biomass energy conversion efficiency. Hence, this research is aimed to study the role of insulators to increase the efficiency of the stove. The target of this research is to design high performance stove and also to create biomass stove insulator. Furthermore, a self sufficient energy village can be developed to meet the energy demand in Indonesia.

2. Experimental Details

The experiments were done in 2 stages, including resistance simulation and test phase and divided into some steps as follows:

1. Simulation using the design of space ratio between the primary air heater and secondary air heater
2. The test simulation at optimum condition of heat transfer in which the stove is equipped with insulator using a low conductivity refractory brick.
3. Test using coconut shell charcoal fuel.
4. The analysis of data based on the difference between the inside and the outside temperature of the stove burner.

3. Result and Discussion

The simulation results based on the primary (A1) and secondary (A2) air heater space were compared as shown in Table 1.

Tabel 1. The results of simulation tests with biomass stove insulated with 1 cm thick refractory brick. The biomass burnt was 200 g of coconut shell charcoal.

No	Ratio A1/A2	Temperatures in the central part (^{0}C)	Temperature outside insulator (^{0}C)	Burning time (minutes)
1.	1	242	40	74
2.	1.1	250	40	75
3.	1.2	250	42	74
4.	1.4	254*	42	65

From the experiment results, it was known that the ratio between the theoretical air requirements and the heating fuel ratio is close to the ratio between the primary air heating chamber and secondary air heating space 1-1.4.The test results obtained that the optimum ratio is 1.4 and the temperature reached was 254^0 C. When it is compared to the results obtained [4], the temperature is already a combustion temperature of both the theoretical and real. If this temperature can be maintained continuously while the fuel is being added, the burning fuel happens. This is to overcome the problems arise from the difficulties at the starting of the biomass fuels combustion.

Based on Houck [5] who recommended the usage of shaped fuel pellets which is similar with the form of coconut shell charcoal, biomass fuel have the lowest emission factor in which material used is reduced but it has the highest theoretical efficiency of 78%. The result of this research shows the combustion efficiency of 80% which is close to the results suggested by Houck.

Figure 3 shows part of the space which separates the primary air heater with the secondary air heating chamber. Space heaters are equipped with primary air chamber, where the ash is placed, and the valve of the primary air heater. The temperature outside the stove, 42^0 C, is insulated. This shows that the heating is used mostly for the combustion, while the heat being radiated outside the stove is relatively small. This assumption is according to the level of combustion efficiency obtained theoretically.

Figure 3: Image of biomass stoves with insulator model

Based on the standard EPA (Environmental Protection Agency) and ISO test methods for wood stoves, the model is compliant with biomass stoves model. When compared with similar stove without insulating refractory brick, the combustion efficiency of this stove increases nearly 60%. Even though the price of the stove above is more expensive due to the additional costs of insulators, the safety and the convenience of this stove are better than the already used stove.

Bricks refractory cast able insulator used in this stove has low thermal conductivity which can be used in heating up to 1400^0 C and in accordance to the standard required. Brick

refractory cast able insulator raw material is the local raw materials in Indonesia which is available and easy to get. This research gives contribution to the biomass fuel stove development in order to support the preparation of self sufficient energy village program which has been proclaimed by the Indonesian government in 2007.

4. Conclusion

Biomass stove model that has been designed theoretically meets EPA and ISO standards for wood-fired stove, which has a space ratio between the primary air heater and the secondary air heater chamber 1.4. The temperature in the combustion chamber indeed meets the energy needed for the wood combustion.

5. Acknowledgements

Director General of Higher Education, Indonesia, through science and technology program to the community in 2010

6. References

[1]. Anonim (2008), Insulating Castable, info@ vitcas.com, United Kingdom
[2]. Ariati, R., (2009), Pengembangan Desa Mandiri Energi Berbasis non bahan nabati dan keterkaitannya dengan program elektrifikasi nasional, ESDM, Seminar Nasional peranan EBT dalam mengatasi krisis energy dan menghambat laju pemanasan global, Surakarta.
[3]. Gana, R., (2010), Refractories, PT. Sigma Mitra Sejati, Cilegon, Indonesia
[4]. Harel. P and Baquqnt (1992), Bagasse Combustion, *International Sugar Journal*, Vol.94, No. 1117, pp. 11-18
[5]. Houck. J.E & Paul E.T (1998), Residential Wood Combustion Technology Review, Volume 1, Technicl Report, U.S. Environmental Protection Agency Office of Research and Development, Washington. D.C, Editor: Robert C. McCrillis, 3-14
[6]. Reed. T.B, Aqua Das and Palu S. Anderson (2004), Gasification: A Process Common to All Biomass Stoves. *Proceedins of 2004 ETHOS meeting.*
[7]. Suharno, B., (2008), Type Refractories, Metallurgy and Materail Engineering, Departement University of Indonesia
[8]. Sumarsih Sri (2010), Biobriket
[9]. Widaryanto, E. (2008), Kompor Biji Jarak Pagar UB-16 Untuk Rumah Tangga. Info Tek Jarak Pagar. Pusat Penelitian dan Pengembangan Pertanian. Badan Litbang 3 (3) : 9-12.
[10]. Wirawan, S.S., (2005), Prospek tanaman pertanian sebagai bioenergi BBM masa depan. Prosiding Seminar Nasional, Perhimpunan Agronomi Indonesia, Malang 27-28 September 2005. 21-30.

Appendix

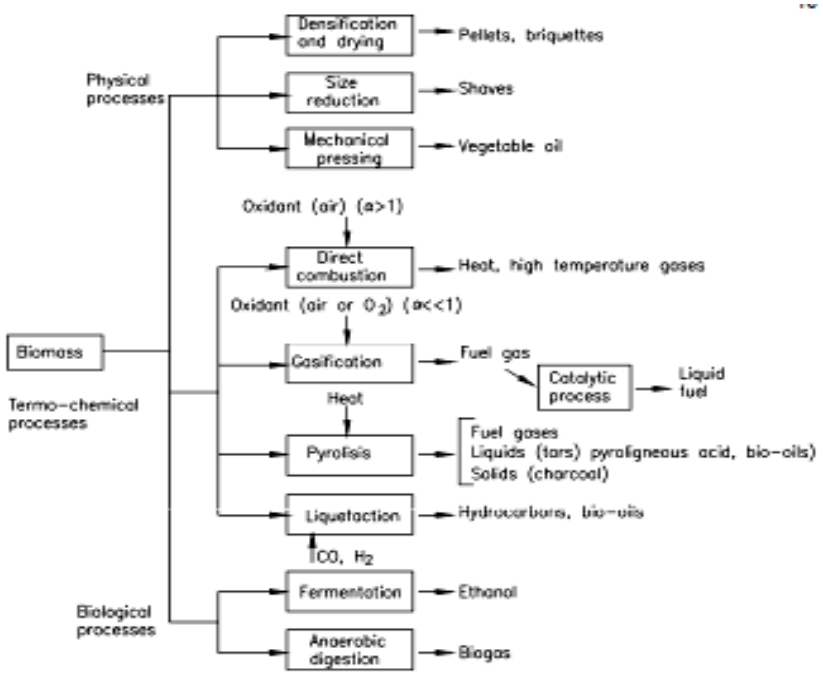

Figure 1: Biomass energy conversion processes

Verification of Absorbed Dose Rate To Water Determination For A Co-60 Gamma Beam Using Farmer Dosemeter and Ptw Unidos in Ulin Hospital, Banjarmasin

C. Tuti Budiantari [1], Nurman Rajagukguk [2]

Center for Technology of Radiation Safety and Metrology, National Nuclear Energy Agency, Jakarta, Indonesia (tuticb@yahoo.com; nurman55@yahoo.com)

Abstract

This paper presents the verification of absorbed dose rate to water determination for a Co-60 teletherapy machine Terragam GIK 9-4/780 belonged to the Ulin Hospital Banjarmasin. Measurement had been carried using a 0.6cc ionization chamber NE 2571 conectted to a Farmer electrometer NE 2570/1B belonged to the National Radiation Metrology Laboratory and an ionization chamber TW 3004 conectted to a PTW Unidos electrometer T10002 belonged to the Ulin Hospital. Measurement had been done at reference condition inside a water phantom at the source to the water phantom surface distance of 80cm, a field size of 10cm x 10cm and a depth of 5cm. The IAEA dosimetry publication in the Technical Report Series (TRS) no. 277 had been used to determine the absorbed dose rate to water of the teletherapy machine. The result obtained showed that the absorbed dose rates at the standard condition were 1846.9 mGy/min and 1865.3 mGy/minute each for ionization chambers NE 2571 and TW 3004. Both results showed a good agreement within 1.0 %. Determination of absorbed dose based on TRS no. 398 and measurement inside a solid phantom were also described.

Keywords*: teletherapy machine, absorbed dose rate to water, ionization chamber, electrometer.*

1. Introduction

The Ulin hospital in Banjarmasin is the only one of hospitals in Kalimantan Island which has a Co-60 teletherapy machine. The machine Terragam GIK 9-4/780 made in the UJP Praha has a Co-60 radioactive source with its acitivity of 348 TBq on 24 May 2006. The machine is completed with three different trays and eight wedges having four different edges of 15°, 30°, 45° and 60° with dimensions of 10 cm x 10 cm and 15 cm x 15 cm [1].

To carry out the quality audit of teletheraphy machine, the radiotherapy unit is completed with radiation measurement instrument such as PTW Unidos electrometer T10002 S/N 20675 connected to 0.6 cc ionization chamber TW 3004 S/N 0262 and TW 30010 S/N 0415 and 0.125 cc ionization chamber TW 31010 S/N 1142 [2-4]. Moreover, it is completed with supporting equipment needed such water and solid phantoms. The quality audit is carried out by medical physicist and technician.

According to the Regulatory Body Decree that every teletherapy machine shall be calibrated after installation and recalibrated every two years [5]. Based on some publications, user is suggested to check routinely the consistency dosimetry parameters of the machine so that radiation treatment to the cancer patient can achieve optimal result. There are two parameters such as mechanical and dosimetry parameters. Mechanical parameters consist of gantry rotation, isocenter, optical distance and field size indicators. Dosimetry parameters consist of homogeneity, radiation beam simetry, penumbra, time error, absorbed dose, etc [6].

For dosimetry parameters, absorbed dose rate to water from radiation beam is the important value because cancer treatment depends on the accuracy of dose given to the patient. To determine absorbed dose rate to water there are some publications that can be used. However, in Indonesia Technical Report Series (TRS) Publications No. 277 and No. 398 published by the IAEA are more used than other publications [7,8].

This paper describes the determination of absorbed dose rate to water of Co-60 beam of teletherapy machine owned by the Ulin hospital. The measurement is carried out by the National Radiation Metrology Laboratory staff and the Ulin hospital medical physicist using his own equipment and dosimetry publication. The aim of this measurement is to know the performance of the instrument and the ability of medical physicist in the hospital if in future this verification is

applied by the Regulatory Body as a calibration substitution.

2. Experimental Detail

Stability Test of the Instrument

First, ionization chamber NE 2571 was connected to Farmer electrometer NE 2570/1B . Then the chamber was inserted to Sr-90 radiation source. The reading for 250 seconds was taken and the chamber was irradiated 5 times. After that the average reading was compared with the reference value. The dosimeter system was stabil and ready to use to measure if the difference between reading of dosimeter at the time of measurement and reference reading was not more than ± 1% [9,10]. This test was carried out at the National Radiation Metrology Laboratory before the dosimeter was brought to the Ulin hospital. The same test was carried out for PTW Unidos by the medical physicist of the Ulin hospital. The instrument used by the LMRN and the Ulin hospital could be seen in Figure 1-2.

Fi

Figure 1. Farmer Electrometer NE 2570/1B S/N 1182 belonged to the LMRN and PTW Unidos electrometer T10002 S/N 20675 belonged to the Ulin hospital

Figure 2. Ionization chamber NE 2571 S/N 2491 and PTW ionization chamber TW 3004 S/N 0262

Ion Recombination Correction Factor Determination

The ionization chamber NE 2571 connected to Farmer dosemeter NE 2570/IB was placed at 5 cm depth inside a water phantom of 30 cm x 30 cm x 30 cm and Source to Surface Distance (SSD) of 80 cm. Field Size (FS) on the phantom surface was set in 10cm x 10cm. Before measurements was done, the chamber was irradiated for 5 minutes to reach thermal equilibrum and for the measuring system to warm up. Then the chamber was iradiated for 1 minute as shown by the machine timer for 5 times. The reading obtained including temperature, pressure, homegeneity was noted. This measurement was done both for V and V/4 voltag by the LMRN Personel (Figure 4).

Then the same measurement was carried out for ionization chamber TW 3004 connected to PTW Unidos T 10002. This measurement was carried out by the medical physicist of the Ulin hospital using its water phantom (Figure 5). The ion recombinatian correction factor was obtained from Figure 13 and the expression 16 in TRS publication No. 277 and no. 398, respectively [7,8].

Polarity Effect Correction Factor Determination

The ionization chamber NE 2571 connected to Farmer dosemeter NE 2570/IB was placed at 5cm depth inside a water phantom of 30cm x 30cm x 30cm and Source to Surface Distance (SSD) of 80 cm . Field Size (FS) on the phantom surface was set in 10cm x 10cm. Then the chamber was iradiated for 1 minute as shown by the machine timer for 5 times. The reading obtained including temperature, pressure, homegeneity was noted. This measurement was carried out both for positive and negative voltages by the LMRN Personel (Figure 4).

Then the same measurement was carried out for ionization chamber TW 3004 connected to PTW Unidos T 10002. This measurement was carried out by the medical physicist of the Ulin hospital using its water phantom (Figure 5). The polarity effect correction factor was obtained by using expression 12 in TRS publication No. 398 [8].

Absorbed dose rate to water of Co-60 beam in a water phantom determination

Measurement of absorbed dose rate to water of Co-60 beam was carried out using the ionization chamber NE 2571 connected to Farmer dosemeter NE 2570/IB. The chamber was put inside water phantom at 5 cm depth, SSD 80 cm and FS on the phantom surface 10 cm x 10 cm. The chamber was irradiated for 1 minute for 5 times using horizontal beam direction and the reading obtained was noted together with temperature and pressure during irradiation. This measurement was carried by the LMRN Personel (Figure 4).

Then the same measurement was carried out for ionization chamber TW 3004 connected to PTW Unidos T 10002 using vertical beam direction. This measurement was carried out by

the medical physicist of Ulin hospital using its water phantom (Figure 5). The absorbed dose rate to water was calculated using the expression 9 and 18 in TRS publication No. 277 and no. 398, respectively [7,8].

Figure 4. Measurement using Farmer dosemeter system belonged to the LMRN

Figure 5. Measurement using PTW Unidos system belonged to the Ulin hospital

Absorbed dose rate to water of Co-60 beam in a solid phantom determination

Figure 6. Absorbed dose to water determination using solid phantom under reference condition: SSD 80 cm, FS on the surface phantom 10 cm x 10 cm and depth 5.66 cm.

Measurement of absorbed dose rate to water of Co-60 beam was carried out using the ionization chamber NE 2571 connected to Farmer dosemeter NE 2570/IB The chamber was put inside solid phantom at 5.66 cm depth [10], SSD 80 cm and FS on the surface phantom 10 cm x 10 cm. The chamber was irradiated for 1 minute for 5 times using vertical beam direction and the reading obtained was noted together with temperature and pressure during irradiation. This measurement was carried by the LMRN Personel (Figure 6).

The absorbed dose rate to water was calculated using the expression 9 and 18 in TRS publication No. 277 and no. 398, respectively [7,8].

3. Result and Discussion

Stability test for 2 dosimeters used for measurement showed that the test result are 0.4 % for Farmer dosemeter and 0.4 % for PTW Unidos. The result of absorbed dose rate determination for Co-60 beam of the teletherapy machine measured by the 2 dosimeters using TRS Publications No. 277 and 398 could be seen in Table 1 and Table 2.

Tabel 1. Calculation result of absorbed dose rate to water of Co-60 beam using TRS No. 277 publication for Farmer Dosimeter dan PTW Unidos

Dosemeter	Farmer	PTW Unidos
Mean Reading (nC)	32.39	28.03
P_{rpl}	0.990	0.990
Multiply factor (mGy/nC)	45.385	52.364
$D_{air(5),}$ mGy/mnt	1455.32	1453.09
PDD_{5cm} (%)	78.8	77.9
D_{max} (mGy/mnt)	1846.9± 5.6	1865.3± 6.1

* Multiply factor = N_D . $S_{w,air}$. $P_{s.}$ P_u

From Table 1 it could be seen that the difference between the absorbed dose rate to water determined by Farmer dosemeter and PTW Unidos using TRS No. 277 publication was 1.0 %. This difference was not significant because of less than 2%. This difference was caused by the Percentage Depth Dose (PDD) used by medical physicist in the Ulin hospital came from manufacture. Meanwhile, the LMRN Personnel used PDD Table from the British Journal of Radiology No. 25 [11]. However, the difference between the absorbed dose to water at 5 cm depth determined by Farmer dosemeter and PTW Unidos was 0.15%. This shows that the performance of PTW Unidos belonged to the Ulin hospital was good enough as well as publication used and the ability of the medical physicists in the Ulin hospital.

The result of absorbed dose to water determination of Co-60 beam using Farmer dosemeter that was calculated based on TRS Publication No. 398 could be seen in Table 2.

Table 2. The result of absorbed dose rate to water determination of Co-60 beam using Farmer dosemeter that was calculated based on Publication TRS No. 398

Mean Reading (nC)	32.39
$N_{D,w}$ (mGy/nC)	45.21
Polarity correction factor	1.003
Recombination correction factor	1.005
$D_{air(5),}$ (mGy/min)	1476.34
PDD_{5cm} (%)	78.8
D_{max} (mGy/min)	1873.5 ± 5.1

The difference between absorbed dose rate that was calculated based on TRS publication no. 277 and no. 398 was 1.4 %. The result of absorbed dose rate to water determination using solid phantom and Farmer dosemeter could be seen in Table 3.

Tabel 3. The result of absorbed dose rate determination of Co-60 beam using Farmer dosemeter based on TRS publication No. 277

Mean Reading (nC)	30.253
$N_{D,w}$ (mGy/nC)	44.867
Recombination correction factor	1.0052
$D_{air(5),}$ (mGy/min)	1364.42
PDD_{5cm} (%)	78.8
D_{max} (mGy/min)	1731.5 ± 5.8

If the absorbed dose rate in Table 3 was compared with data in Tabel 1 and Table 2, the difference was 6.2% and 7.6%. This differences was surely caused by misplace of the chamber inside the solid phantom. The depth of chamber inside the solid phantom should be 4.508 cm, not 5.66 cm [14]. However, for 5.66 cm depth in solid phantom it should be used Percentage Depth Dose of 6.3 cm depth in water that was 72.52%. Hence, maximum absorbed dose rate to water, D_{max}, obtained was 1881.44mGy/minute. Therefore, the differences between solid phantom and water phantom were 1.9% and 0.4% using TRS publication No. 398 and No. 277, respectively.

From the result, it could be stated that at the time being the solid phantom could only be used for relative measurement until a suitable procedure is prepared.

4. Conclusion

Dosimeter performance belonged to the hospital was good enough and dosimetry publication used and the capability of personnel was satisfied. However, it was needed measurement procedure in solid phantom.

5. Acknowledgement

This work was supported by the Department of Radiotherapy of the Ulin Hospital and the National Radiation Metrology Laboratory, The Center for Technology of Radiation Safety and Metrology (PTKMR) - the National Nuclear Energy Agency (BATAN).

6. References

[1]. Manual Pesawat Co-60 Terragam GIK 9-4 / 780
[2]. Anonymous (2010), Sertifikat Kalibrasi Dosimeter Gamma Tingkat Terapi No. LMR-N/Kal/IV-09/10, LMR-N, Laboratorium Metrologi Radiasi Nasional
[3]. Anonymous (2010), Sertifikat Kalibrasi Dosimeter Gamma Tingkat Terapi No. LMR-N/Kal/IV-09/11, LMR-N, Laboratorium Metrologi Radiasi Nasional
[4]. Anonymous (2010), Sertifikat Kalibrasi Dosimeter Gamma Tingkat Terapi No. LMR-N/Kal/IV-09/12, LMR-N, Laboratorium Metrologi Radiasi Nasional
[5]. Anonymous (2007), Peraturan Kepala BAPETEN tentang kalibrasi alat ukur radiasi dan keluaran sumber radiasi, standardisasi radionuklida dan fasilitas kalibrasi, BAPETEN, Jakarta
[6]. Anonymous (1988), International Atomic Energy Agency, Quality Assurance in Radiotherapy, WHO, Geneva
[7]. Anonymous (1987), International Atomic Energy Agency, Technical Report Series No. 277: Absorbed Dose Determination in Photon and Electron Beam, An International Code Practice, IAEA, Vienna
[8]. Anonymous (2000), International Atomic Energy Agency, Absorbed Dose Determination in External Beam Radiotherapy; An International Code of Practice for Dosimetry Based on Standards of Absorbed Dose to Water, Technical Report Series No.398, IAEA, Vienna
[9]. Anonymous (1985), Instruction Manual for 0.6 cc Robust Ionization Chamber, Nuclear Enterprises Limited, Beenham Berkshire, England
[10]. Anonymous (1985), Instruction Manual for Farmer Dosemeter Type 2570/1A & B , Nuclear Enterprises Limited, Beenham Berkshire, England
[11]. Anonymous (1996), Central Axis Depth Dose Data for Use in Radiotherapy, British Journal of Radiology Supplement No. 25, British Institute of Radiology, London.

Assessing Mud Volcano Vulnerable Area Using Fuzzy Approach

Candra Dewi

Computer Science, Faculty of Mathematic and Natural Science, Univ. of Brawijaya (dewi_candra@ub.ac.id)

Abstract

Determining vulnerable area of hot mud volcano is important to provide information on the extent of the area affected by the hazard. Vulnerability analysis for mud volcano deals with uncertainty arises due to the lack of information about system behaviour and inexactness of measurement. Beside, expert knowledge that involved in decision making also includes some vagueness and imprecision to judge the parameters. This paper present the comparison of spatial multi criteria analysis for mud volcano vulnerability within settlement area in Sidoarjo by using three different fuzzy approaches that are Fuzzy-AHP, Fuzzy Simple Additive Weighted (SAW) and Fuzzy Ordered Weighted Averaging (OWA). The first method deals with vagueness that include in expert judgements. While the other methods handle the vagueness that includes in criteria analysis. Base on the spatial analisys can be compared the percentage of vulnerability class for this three method. The analisys showed that different method result different area for each vulnerability class. The order of vulnerability classes also differ for those three methods. However, the percentage of area resulted by using Fuzzy SAW and Fuzzy OWA has the same order although the exact area itself are different.

***Key words**: multi criteria analysis, spatial analysis, fuzzy-AHP, fuzzy SAW, fuzzy OWA*
.

1. Introduction

Identifying vulnerable area of hot mud volcano is important to provide information about the area that is dangerous enough to reduce the impact of the hazards [1-3]. Moreover, this activity also presents information on area which is still effective and potential for further development planning.

Vulnerability assessment requires consideration of a comprehensive set of factors and balancing of multiple objectives in determining the dangerous level of particular area from a defined hazard source. Multi-criteria evaluations techniques can provide tools for analysing the complex trade-offs between choice alternatives with different environmental and socio-economic impacts [4-6].

Vulnerability analysis deals with uncertainty arises due to the lack of information about system behavior (vagueness, ambiguity, fuzziness) and inexactness of measurement (impreciseness, fuzziness) [7]. Expert knowledge that involved in multi criteria decision making will include some vagueness and imprecision to judge the parameters. Using Boolean logic is impossible to model the uncertainties since it only judge the range into crisp value (true or false), which limit the analysis to specific region. Fuzzy logic provides mathematical methods aids in information that are imprecise, incomplete and vague. The value expresses in continuous degrees of belonging to a set, ranging from 0.0 to 1.0.

The study about mud volcano vulnerable analysis using fuzzy approach has been performed before. Vulnerability analysis for mud volcano requires consideration of a comprehensive set of factors that is grouped in certain *range* [8]. Vulnerability analysis for mud volcano hazard involves incorporation of expert knowledge at various levels of decision-making and also for defining the weight of criteria. Expert cannot be sure and certain all the time when deciding this criteria value. The imprecision involved in expert knowledge can be well addressed using fuzzy analysis. To overcome this problem was applied Fuzzy-AHP to handle vagueness and imprecision involved in expert knowledge [8].

Dewi (2008) used the judgment of expert for defining the value of criteria than the value has been obtained from field survey. This research was continued by conducted spatial analysis using the value of criteria obtained from field measurement [9]. The analysis used fuzzy to standardize criteria and used fuzzy additive weighting to aggregate criteria in spatial rule base. However, this research only applied one linguistic variable for each criterion.

Then, in 2010 was continued the research by using fuzzy standardize on criteria. This research applied some linguistic variable at standardize process and used Ordered Weighted Averaging (OWA) method to aggregate the criteria at rule base process [10].

Based on the research that has been conducted, this paper presents the comparison of the vulnerable area which are resulted from applying three different fuzzy approaches have been mentioned above.

2. Experimental Details

Area of Study

The boundary of the study area lies between the latitude of 7°30'35" - 7°32'47" S and longitude 112°41'59" - 112°44'00" E (President Regulation No. 14/2007). The study area is working area of The National Sidoarjo Mudflow Mitigation Team (BPLS), which is located in Sidoarjo Regency, East Java covering three districts i.e. Porong, Jabon and Tanggulangin. The location is shown in

Framework for Vulnerability Analysis

The decision analysis of vulnerability for mud volcano adopts elements from the techniques of multi-criteria evaluation with required modifications. Proposed procedure was conducted in this research is shown in Figure 2.

Firstly, the set of evaluation criteria is specified on the basis of the analysis type. The criteria selected reflect all concerns relevant to the decision problem and contribute toward achieving the objectives. The relationship between the criteria and attributes has hierarchical structure in MCDA [6]. This hierarchy distinguishes the criteria at the highest level and decomposes the attributes at the lower levels. Then, the data is collected accordingly the need analysis to support evaluation criteria. The data collected include spatial data and non spatial data. To obtain the expert judgment regarding the scoring of the criteria, structured questionnaire and interview was used.

The next step is performing multi criteria evaluation using *Fuzzy-AHP* (pada *confidence level* 100%), *Fuzzy Simple Additive Weighed (Fuzzy SAW)* dan *Fuzzy Ordered Weighted Averaging* (OWA). After that, performing GIS Analysis that include the process of generating vulnerability map, conducting sensitivity analysis and comparing vulnerability map with impacted area handled by The National Sidoarjo Mudflow Mitigation Team (BPLS). The last step is conducting recommendation base on the analysis.

The evaluation set considered for mud volcano vulnerability were obtained from studies of some previous research about mud hazard in Sidoarjo, interview and discussion with some experts from BPLS, Environmental Geology and Risk Management expert. The criteria consist of subsidence, bubble gasses, flooded area and water quality. The gases were used consist of H_2S, CH_4 and CO_2.

The alternative for this research is in the context of vulnerability class. The vulnerable class is divided into four groups which is Z1 (High hazardous zone), Z2 (Moderate hazardous zone), Z3 (Low hazardous zone) and Z4 (Not Impacted Zone).

Fuzzy AHP

This paper uses Fuzzy-AHP has been modified by Jeganathan, where the methodology create simple, improved, and sophisticated approach using fuzzy logic Fuzzy.

Fuzzy-AHP uses a range of value to incorporate decision maker's uncertainty. From this range decision maker can select the values that reflect their confidence and also can specify the attitude like optimistic, pessimistic or moderate [8]. Optimistic attitude is represented by the highest value range, moderate attitude is represented by the middle value of range and pessimistic attitude is represented by the lowest value of range.

Triangular or trapezoidal fuzzy number is used to express the decision maker's assessment on alternatives with respect to each criterion. After the criteria are weighted, the overall utilities of alternatives represented by fuzzy number are aggregated by fuzzy arithmetic using Simple Additive Weighting method. To prioritize the alternatives, their fuzzy utilities need to be compared and ranked.

The concept of fuzzy extent analysis is applied to solve the fuzzy reciprocal matrix for determining the criteria importance and alternative performance. To avoid the complex and unreliable process of comparing fuzzy utilities, the alpha-cut concept is used to transform the fuzzy performance matrix representing the overall performance of all alternatives with respect to each criterion into an interval performance matrix.

Fuzzy Simple Additive Weighting (FSAW)

FSAW method uses the weighted average as the aggregation operator and operates on fuzzy data. The entries of decision matrix and weights are specified in term of fuzzy number. The total score is obtained for each alternative by multiplying the importance weight assigned for each attribute by the scale value given to the alternative on that attribute, and summing the product aver all attributes. The utility (attractiveness) of the i^{th} alternative is given by the formula [6]:

$$F_i = \sum_i w_i^- x_{ij}^- \quad (1)$$

Where $\mathbf{x_{ij}}$ = the score of the i^{th} alternative with respect to the j^{th} attribute

$\mathbf{w_i}$ = normaized weight.

Fuzzy Ordered Weighted Averaging (OWA)

OWA is weighted sum with ordered evaluation criteria, where use the order of weight in addition to the criterion weight. A fundamental aspect of this aggregation rule is the reordering step of the weight. Thus, the weighting coefficients are not associated directly with a particular but rather, are assigned to an ordered position of criterion value for a given alternative [6].

3. Result and Discussion

This paper compared the vulnerability classes that are resulted by appliying spatial analisys using *Fuzzy-AHP*, *Fuzzy SAW* and *Fuzzy OWA*. The detail of analisys using those method are explained at previous researchs [8-10]. While the brief comparison of the analysis is displayed at

Table 1.

Table 1. The comparison of percentage of vulnerability class area

Kelas	Percentage of Area		
	Fuzzy-AHP	Fuzzy SAW	Fuzzy OWA
Z1	10.9	4.98	15,33%
Z2	25.0	22.14	28,07%
Z3	49.6	71.11	56,35%
Z4	14.4	1.77	0,24%

Table 1 display the comparison of area percentage for each vulnerability classes using those three methods. The table shows the difference of percentage area and also the order of class resulted on analysis using those methods. However, the percentage of area using *Fuzzy SAW* and *Fuzzy OWA* has the same order although they have difference percentage of area. This occur because this two method beside used the same weighting method that is AHP, also use the same crisp value of evaluation criteria.

Vulnerability class maps resulted using those methods are displayed at

Figure 3. This analysis process used the judgement from some expert from The National Sidoarjo Mudflow Mitigation Team (BPLS) and Centre of Environmental Geology Bandung. But, there are no reference can be used for validation of the vulnerability class till this paper finished. Furthermore, is needed the continued research to obtain this reference. Therefore, the most efective method for this case can be obtained.

4. Conclusion

There are some important points related to this paper:

1. Fuzzy approach can be used at spatial multi criteria analysis for mud volcano to overcome fuzziness that includes both on expert judgement and criteria value. The discussion shows that three mentioned method above result the same largest area that is Z3, than followed by Z2. Furthermore, those three methods have nearly same area for Z2.
2. The analysis divides the class by using the same interval range because there are no reference can be used for validation of the vulnerability class. Furthermore, is needed the continued research to obtain this reference. Therefore, the most efective method for this case can be obtained.

5. Acknowledgments

---

6. References

[1]. Pohl, C. (2007), *Lapindo Brantas and The Mud Volcano Sidoarjo, Indonesia*: *A Background Paper Prepared for Friends of The Earth International And Friends of The Earth Europe*, Friends of the Earth International and Friends of the Earth Europe.

[2]. United Nations Disaster Assessment and Coordination (2006), *Environmental Assessment Hot Mud Flow East Java, Indonesia,* Final Technical Report, UNEP/OCHA Environment Unit, Switzerland, http://ochaonline.un.org/ochaunep, Accesses on January 2009.

[3]. USGS. (*2000)*, *Volcano Hazard-Assessment Techniques*, U.S. Department of the Interior, U.S. Geological Survey, Menlo Park, California, USA. http://volcanoes.usgs.gov/About/What/Asses s/index.html. Accesses at January 2009.

[4]. Rashed, T., and J. Weeks (2003), *Assessing Vulnerability to Earthquake Hazards Through Spatial Multicriteria Analysis Of Urban Areas,* International Journal Geographic Information Science, Tailor & Francis.

[5]. Yalcin, Guler and Z. Akyurek (2002), *Multiple Criteria Analysis for Flood Vulnerable Areas,* Directorate of Land Registry and Cadastre, Ankara, Turkey.
[6]. Malczewski, J., (1999), *GIS and Multicriteria Decision Analysis*, John Wiley & Sons, New York.
[7]. Zischg, A, S. Fuchs and J. Atotter (2005), *Uncertainties And Fuzziness In Analyzing Risk Related To Natural Hazard: A Case Study In The Ortles Alps, South Tyrol, Italy,* Department of Geography, University of Innsbruck, Austria.
[8]. Dewi, C., I W. Astika and G.H. Pamono (2008), *Spatial Multi Criteria Analysis for*
[9]. *Detecting Mud Volcano Vulnerable Area in Sidoarjo Regency, East Java Province*, Master Thesis, SEAMEO-Biotrop, IPB, Bogor.
[10]. Dewi, C. and B. Rahayudi (2009), *Penentuan Kelas Area Bencana Lumpur Lapindo Menggunakan Pendekatan Logika Fuzzy Berbasis Spasial,* Research Report of DPP/SPP Fund, Faculty of Mathematic and Natural Science, University of Brawijaya, Malang.
[11]. Dewi, C., A. B. Astuti and P. P. Adikara (2010), *Aplikasi Fuzzy Rule Base dalam Multi Kriteria Analisis untuk* Penentuan *Kelas Area Bencana Lumpur Lapindo,* Research Report of DPP/SPP Fund, Faculty of Mathematic and Natural Science, University of Brawijaya, Malang.
[12]. Kuswandari (2004), *Assessment of Different Methods for Measuring the Sustainability of Forest management*, MSc Thesis, ITC, The Netherlands.

Appendix

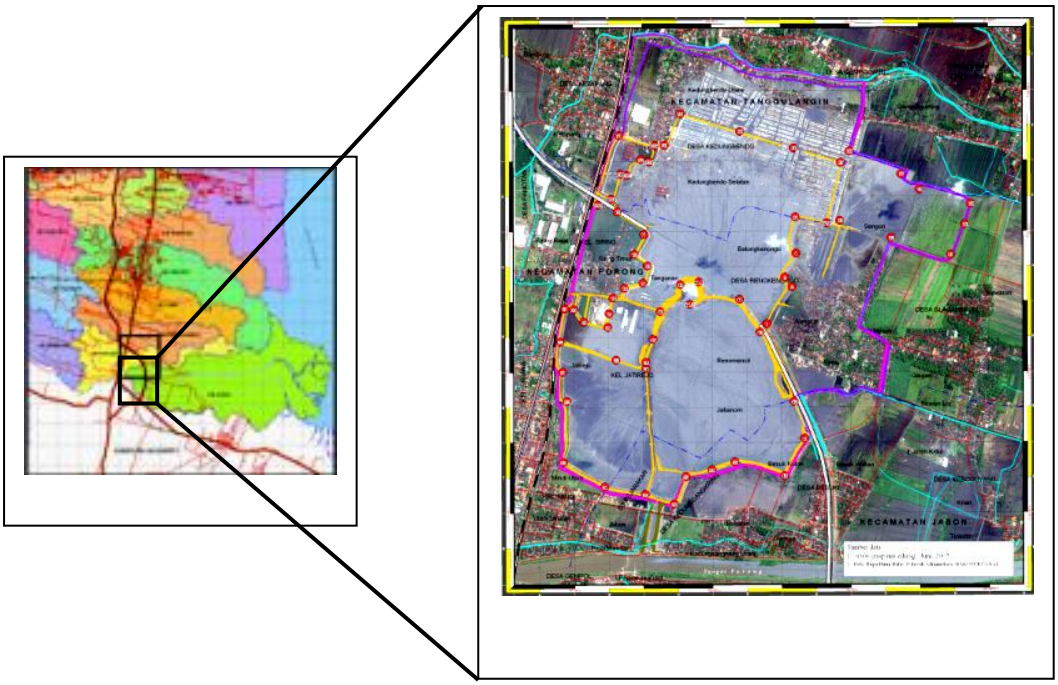

Figure 1. The study areas in Sidoarjo, East Java

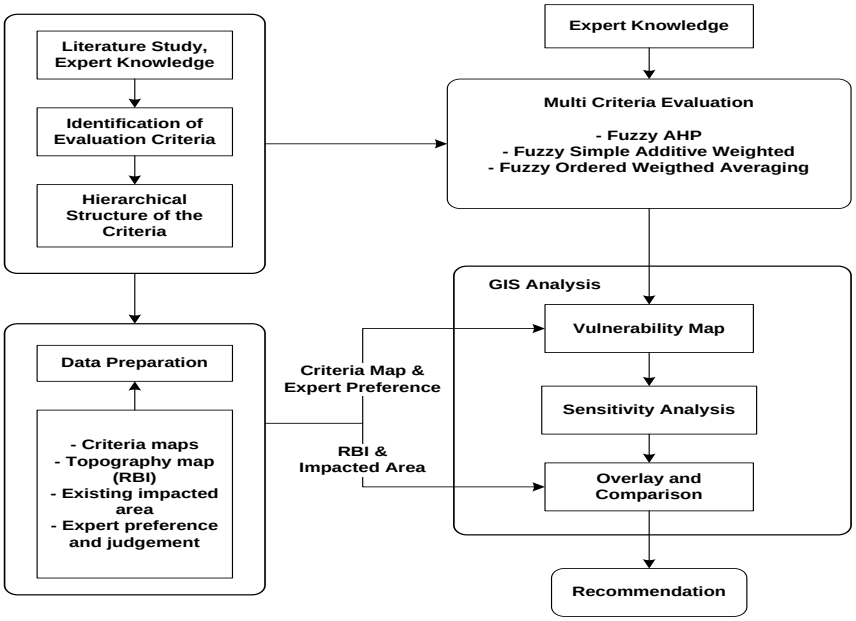

Figure 2. Framework for vulnerability Analysis

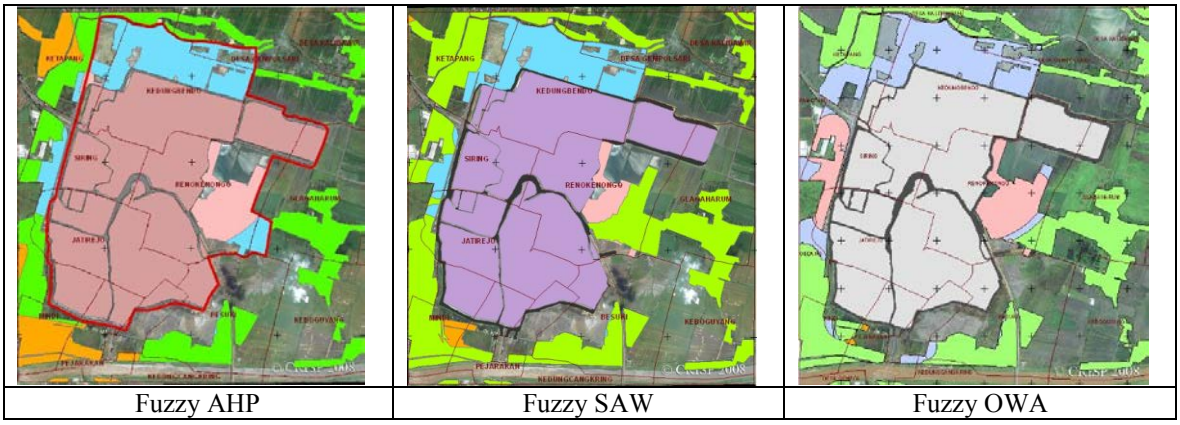

Figure 3. Vulnerability class map using three methods

Sensitivity Enhancement of Enzyme Linked Immunosorbent Assay (ELISA) for *Salmonella* Detection Using Multi Walled Carbon Nanotubes (MWCNTS)

Dyah Kinasih Wuragil [1], Sukunya Oaew [2], Verasak Surareungchai [3]

[1] King Mongkut's University of Technology Thonburi, Bangkok, Thailand (d_kinasih@ub.ac.id)
[2] Biochemical Engineering and Pilot Plant Research Development (BEC)
[3] Biotechnology Division, School of Bioresources and Technology.

Abstract

Salmonella spp. is one of the most frequently occurring foodborne pathogens affecting food safety. Many standard methods to detect Salmonella as food contaminant have been performed. Enzyme linked immunosorbent assay (ELISA) is one type of immunoassay that have been widely used and developed as a tool for detecting Salmonella and other foodborne pathogens. Typical ELISA to detect Salmonella achieved the limit of detection (LOD) of only on 10^6-10^7 CFU/ml. To enhance the sensitivity of ELISA, multi-walled carbon nanotubes (MWCNTs) were applied in the assay by immobilization of biomolecules (antibody and horseradish peroxidase) onto carbon nanotubes. The resulted of Ab-MWCNTs-HRP bioconjugate was made to replace the conventional Ab-HRP complex. The Ab-MWCNTs-HRP was prepared at 1:30 and 1:100 of Ab:HRP ratios, to compare the amount number of HRP carried onto MWCNTs lead to enhance the sensitivity. Direct ELISA is chosen to preliminary test due to the efficiency in time and avoid the cross reactivity between secondary antibody and antigen matrices. This method was found to have a limit of detection (LOD) of 10^4 CFU/ml by using Ab-MWCNTs-HRP at 1:30 of Ab:HRP ratios. It showed 100 times higher sensitive than commercial antibody. Then at 1:100 of Ab: HRP ratios could enhance the sensitivity of ELISA to 10 CFU/ml. The observation using Scanning Probe Electron Microscopy (SPEM) reported that the immobilization of antibody and HRP onto MWCNTs, resulted in the forming of globular shape on the sidewall of MWCNTs. Accordingly, it showed that the immobilization process was successful.

Keywords: *Salmonella, ELISA, MWCNTs, antibody, horseradish peroxidase.*

1. Introduction

Salmonella is a Gram negative foodborne pathogen that originates from a variety of sources. Salmonellosis outbreak has associated with foods because *Salmonella* is commonly found in gastrointestinal track of animals. *Salmonella* is the most disseminator of foodborne pathogen caused the death in United States [1]. Ensuring food safety is important and it is being a responsibility not only for the producers and industry, but also government and consumers. The systematic approach used to prevent foodborne pathogen is hazard analysis critical control point (HACCP) [2].

To detect microbial associated with foodborne pathogen, rapid, reliable, sensitive and specific methods are needed to successfully implement the HACCP program. Conventional methods for detection and identification of *Salmonella* relied on microbiological and biochemical identification is laborious and time consuming. Enzyme linked immunosorbent assay (ELISA) is a type of immunoenzymatic assay that uses solid phase to anchor the antibody-antigen complex. It has been widely used because of the capacity to detect the presence of bacteria antigens without the cells having to be viable [3]. Typical ELISA for detection of *Salmonella* takes one to two days to deliver the result. ELISA methods, available in 96 well formats are the best suited for screening a large number of samples. The ELISA methods for detecting *Salmonella* typically achieved the limit of detection (LOD) of 10^6-10^7 CFU/ml [4,5]. To enhance the sensitivity, nanomaterials were applied to the assay.

Carbon nanotubes (CNTs) represent an important group of nanomaterials that receives great attention as attractive materials in biosensor. CNTs usually have high surface to weight ratio of $300m^2/g$, and most of this surface area is accessible to both electrochemistry and immobilization of biomolecules [6]. CNTs based immunoassay has been applied in electrochemistry to detect protein markers such as haemagglutinins [7], and prostate specific antigen [8]. The other example of this application was

studied by Wang and coworkers [9] who used the CNTs to immobilize alkaline phosphatase to detect DNA and protein. The capacity of CNTs to carry and accumulate the product of enzyme reaction leads to improvement in the sensitivity at 1 pg/ml DNA target and 0.8 ng/ml IgG. Recently, the electrochemical method to detect *Salmonella* had been conducted by using field effect transistor (FET) and could achieve the LOD of 200 CFU/ml [11].

So far, CNTs to detect bacteria have not been applied by using ELISA. This work demonstrated the use of CNTs to detect *Salmonella* by coupling with antibody (Ab) and horseradish peroxidase (HRP).

2. Experimental Details

Materials and reagents

Rabbit anti *Salmonella* with and without horseradish peroxidase conjugate antibodies were purchased from Biodesign International. Peroxidase, *N-hydroxysuccinimide* (NHS), and MES low moisture were from Sigma. Carboxylic multi-walled carbon nanotubes was obtained from Cheaptubes Inc, *N-(-3 Dimethylaminopropyl) – N – ethyl - carbodiimide hydrochloride* (EDAC) was from Fluka, and enzyme substrate of 3,3_,5,5_-tetramethylbenzidine (TMB) was from Zymed, Invitrogen . Buffers used in this study included phosphate buffer saline (PBS) with and without Tween-20 as incubating and washing buffers, and carbonate coating buffer. Distilled and deionized water were used throughout the experiments.

Ab-MWCNTs-HRP bioconjugate preparation

Bioconjugate of Ab-MWCNTs-HRP was prepared according to Yu, *et al* [8] with a slight modification. 1.5 mg multi walled carbon nanotubes carboxylic acid functionalized (MWCNTs-COOH was dispersed in 2 ml PBS pH 7.2 then sonicated for 10 minutes. The dispersion was mixed with 400 mM *N-(-3 Dimethylaminopropyl) – N – ethyl - carbodiimide hydrochloride* or EDAC and 100 mM *N-Hydroxysuccinimiide* (NHS) in 1 ml MES buffer pH 6.0. The mixing solution was then sonicated at room temperature for 2 hours and centrifuge at 14,000 rpm for 5 minutes**.** The supernatant was discharged and pellet was washed twice with PBS. To immobilize the antibody onto CNTs surface, the mixture of MWCNTs was added with 4 µg/ml antibody (rabbit anti *Salmonella* and 120 µg/ml horseradish peroxidase and 4 µg/ml rabbit anti *Salmonella* antibody with 400 µg/ml HRP were used at 1:30 and 1:100, respectively. The reaction mixture was stirred overnight at 4°C, centrifuged at 15,000 rpm, 4°C for 10 minutes, and removed the supernatant. This step was repeated twice to remove any free enzyme and antibody. Then PBST was added to bioconjugate precipitate collected, vortexed and stored in 4 °C

Direct ELISA

The test was performed by coating vary concentrations of *Salmonella* cells in polystyrene microplate (Nunc-immunoplate) and incubated at 4°C overnight followed by washing with PBST 3 times. The step was followed by blocking with 2% BSA in PBST at room temperature for 1 hour and followed by washing step. Incubation in bioconjugate Ab-MWCNTs-HRP or commercial antibody (rabbit anti *Salmonella*-HRP) in 0.5% Tween-PBST was done at room temperature for 1 hour and followed by washing step. The enzyme substrate of 3,3,5,5-tetramethylbenzidine (TMB) was added and incubated for 10 minutes. The stop reaction was done by adding 0.5 M sulphuric acid. Lastly, the reaction was read at 450 nm wavelength (Biotrak II Visible Plate Reader, Amersham Bioscience).

3. Result and Discussion

The resulted Ab-MWCNTs-HRP bioconjugate was made to replace the conventional Ab-HRP complex. Ab-MWCNTs-HRP bioconjugate was resulted from covalent bonding to connect CNTs and proteins (Ab and HRP). There are several reports on the immobilization of protein onto CNTs, and this connection promises capability to control the location of biomolecule, improve stability, accessibility and selectivity, and also reduce leaching [7,8].

In this work, carboxylic functionalized CNTs were activated by adding *N-(-3Dimethylaminopropyl)-N-ethyl-carbodiimide hydrochloride* (EDAC) as a coupling agent. The presence of *N-Hydroxysuccinimiide* forms stable active ester to allow the cross-linked of proteins onto CNTs. The unbound antibody and HRP after immobilization onto CNTs were measured after finishing the coupling process. The differences in the amount of Ab and HRP before and after binding to MWCNTs were calculated, and represent the amount of Ab and HRP linked to MWCNTs. The unbound active antibody was determined by using indirect ELISA. The unbound antibody was calculated as 0.76 µg/ml, which is 19 % of the initial concentration used (4 µg/ml).

Determination of unbound HRP was performed by adding the 3,3_,5,5_-tetramethylbenzidine (TMB) substrate to measure

the active HRP in supernatant after linking Ab-HRP to MWCNTs. The unbound HRP was found to be 21.72µg/ml. It was 18% of the initial concentration that is 120µg/ml. These result showed that the preparation of bioconjugate Ab-MWCNTs-HRP was success to allow immobilization of Ab and HRP onto MWCNTs.

The ELISA was performed as a direct assay. The criteria of ELISA are based on Kumar, *et al* [4] and Karoonuthaisiri, *et al* [5]. A positive ELISA reaction was established when $A_{450\ nm}$ of sample was greater than 2 times the value of negative control.

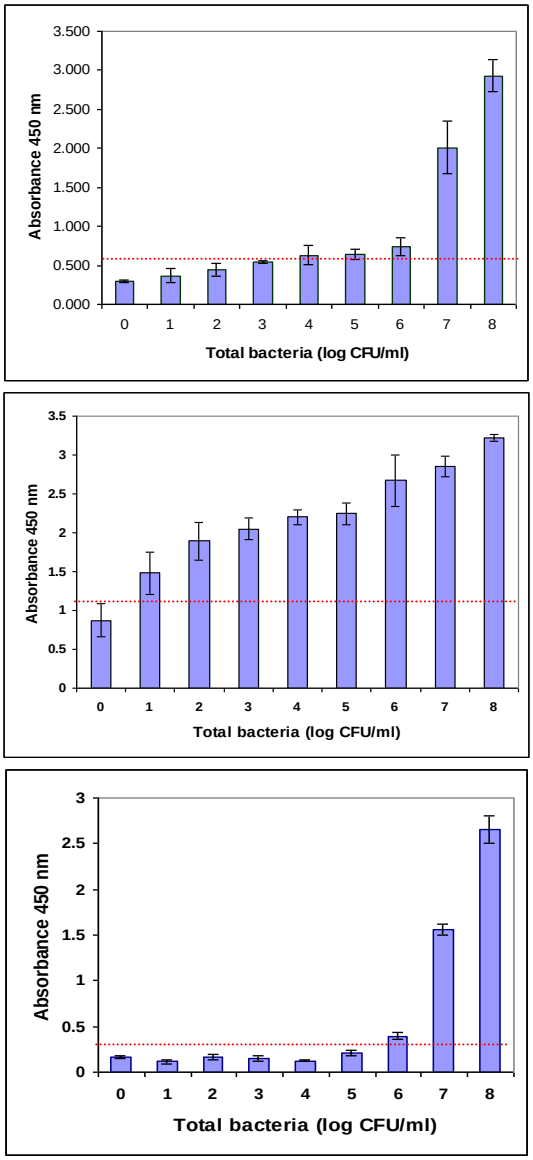

Figure 1 Direct ELISA using bioconjugate Ab-MWCNTs-HRP at (a) 1: 30 ratio, (b) 1:100 ratio, compare to Ab-HRP complex in commercial (c), horizontal lines represent the cutoff value for ELISA.

Figure 1(a) shows that this method was found to have a detection limit of 10^4 CFU/ml. Based on the absorbance values observed in negative control wells (0.300), an absorbance 0.600 was taken as the cutoff value to determine the positive reaction. The limit of detection was 10^4 CFU/ml. Figure 1 (b) shows that the cutoff value of 1.216 was used to determine the positive reaction. The 1:100 ratios of Ab:HRP could enhance the sensitivity of ELISA to 10 CFU/ml.

This Ab-MWCNTs-HRP bioconjugate preparation could achieve 10^3 times more sensitive than Ab-MWCNTs-HRP bioconjugate 1:30 ratio, and 10^5 times more sensitive than commercial antibody (Figure 1c) which reached the sensitivity of 10^6 CFU/ml in direct ELISA.

The high sensitivity of ELISA using the bioconjugate Ab-MWCNTs-HRP relies upon the acts of CNTs to load a large amount of enzymes (HRP) for amplifying the signal in place of conventional Ab-HRP. It is possible that the sensitivity could be improved further by optimizing the Ab-MWCNT-HRP properties and decreasing non specific binding of the assay.

The MWCNTs before immobilization was treated with coupling agents; EDAC and NHS. Images were taken at the same resolution. SPEM images (Figure 2) show that the average diameter of MWCNTs was increased from 41.016 nm to 50.980 nm after the immobilization process. Size analysis of MWCNTs before and after immobilization with antibody and HRP are not shown.

This result agrees with Jiang, *et al.* [14], which was success to immobilize BSA onto MWCNTs. Likewise Yu, *et al.* [8], reported that the immobilization of antibody and HRP onto MWCNTs, resulted in the forming of globular shape on the sidewall of CNTs. Accordingly, our results show that the immobilization process was successful.

4. Conclusions

Bioconjugate of Ab-MWCNTs-HRP was prepared as label to replace common Ab-HRP conjugate in ELISA. Using the Ab-MWCNTs-HRP bioconjugate in direct ELISA, the sensitivity of 10^4 CFU/ml and 10 CFU/ml of 1:30 and 1:100 ratios of Ab:HRP, could be achieved respectively. There were 100 and 10^5 times more sensitive than using commercial antibody.

5. Acknowledgements

DKW acknowledges for the scholarship from The Ministry of National Education, Republic of Indonesia. Technical support for the research has been given by Sensor laboratory, KMUTT and partial financial support has been also given by Betagro Science Center Co.Ltd., Thailand.

6. References

[1]. Maciorowski, K. G., P. Herera., M.M. Kundinger., and S.C. Riecke (2006), *J. Consum. Protec. Food Safety* 1: 197-209.
[2]. Palcheti, M. and M. Mascini (2008), *Anal. Bioanal. Chem.* 391, 455-471.
[3]. Hempen, C. and U. Karst (2006), *Anal.Bioanal. Chem.* 384, 572-583.
[4]. Kumar, S., K. Balakrishna and H.V. Batra (2008), *Biomed. & Environt. Sc.i* 21, 137-143.
[5]. Karoonuthaisiri, N., R. Charlermoj, U. Uawisetwathana, P. Luxananil, K. Kirtikara, and K. Gajanandana (2008), *Biosens. Bioelectron.*
[6]. Veetil, J.V. and K.Ye (2007), *Biotechnol. Prog*. 23, 517-531.
[7]. Takeda, S., A. Sbagyo., Y. Sakoda., A. Ishii., M. Sawamura., K. Sueoka., H. Kida., K. Mukasa., and K. Matsumoto (2005), *Biosens. Bioelectron.* 21,201-205.
[8]. Yu, X., B. Munge., V. Patel., G. Jensen., A. Bhirde., J.D. Gong., S.N.Kim., J.S. Gutkin., F. Papadimitrakopulous., and J.F. Rusling (2006), *J. Am. Chem. Soc.* 128. 11199-11205.
[9]. Wang, J., G. Liu and M.R. Jan (2004), *J.Am.Chem.Soc.* 126. 3010-3011.
[10]. Huang, T.S., Y Tzeng , Y.K. Liu, Y.C. Chen, K.R. Walker, R. Guntupalli, and C. Liu (2004), *Diamond Relat. Mater.* 13. 1098–1102.
[11]. Villamizara, R.A., A.Maroto, F.X. Riusa, I. Inzab and M.J. Figueras (2008), *Biosens. Bioelectron.*24. 279-283.
[12]. Lee, Y., O. Kwon, Y. Yoon, and K. Ryu (2006), *Biotechnol.Lett*. 28, 39–43.
[13]. Jiang, K., L.S. Schadler, R.W. Siegel, X. Zhang, H. Zhang, and M. Terrones (2004), Protein Immobilization on Carbon Nanotubes Via A Two-Step Process of Diimide-Activated Amidation, *Journal of Material Chemistry,* Vol. 14.37-39.

Appendix

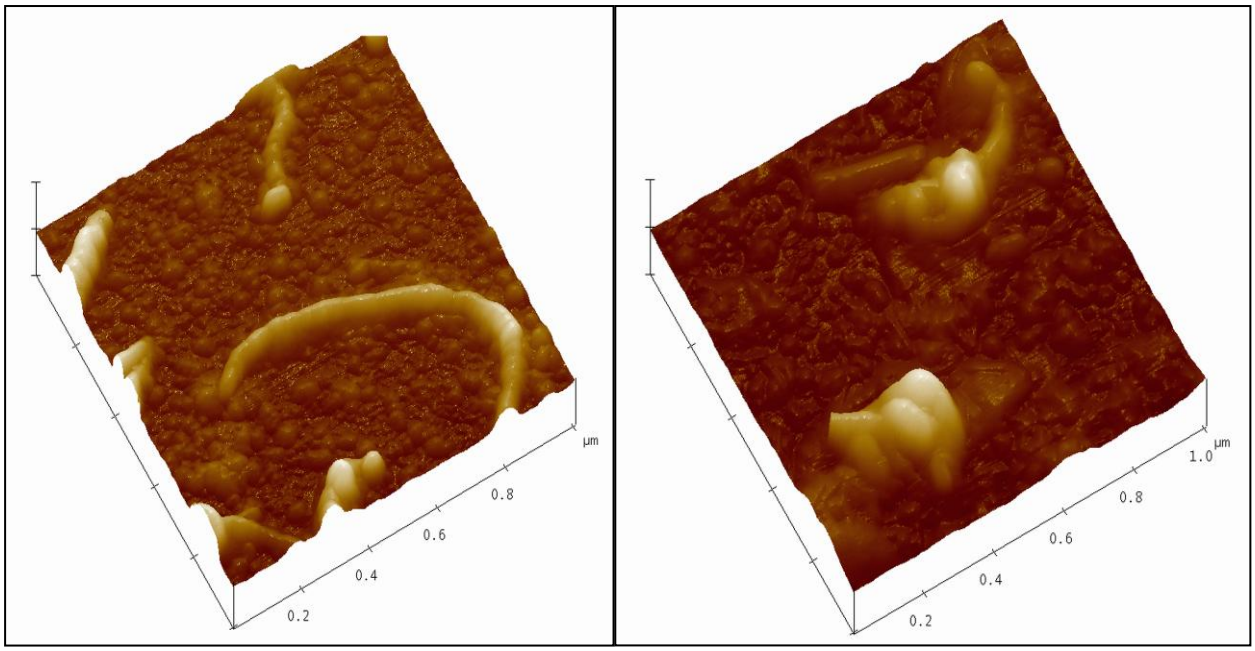

Figure 2. SPEM images of MWCNTs before (a) and after (b) immobilization with antibody and HRP at 1:100 ratios.

Standardization for Gamma Emitting of Co-60 And Cs-137 Mixed Source Using Gamma Spectrometry Method

Gatot Wurdiyanto [1], Hermawan Candra [2], Wijono [3]

[1,2,3] Center for Technology of Radiation Safety and Metrology, National Nuclear Energy Agency of Indonesia (BATAN), Jakarta, Indonesia (Gatot_w@batan.go.id)

Abstract

Standardization has been carried out for gamma emitting of Co-60 and Cs-137 mixed source using gamma spectrometry method in PTKMR - BATAN. Standardization is necessary to improve the quality and effectiveness in measuring radioactivity of the various types of samples. Co-60 and Cs-137 radioisotopes obtained from manufacturer POLATOM - POLAND is the raw material to be processed to become the standard radioactive sources. Preparation method used is gravimetry because it is more accurate. Measurement of radioactivity and impurityy of mixed sources was done using gamma spectrometry method. Standard sources used are Eu-152, Co-60 and Cs-137 which has traceability to the International System. Corrections have been done are dead time, decay, background counting, impurity, and sumpeak. The result of the determination activity of the mix-source is 1,994 Bq for Co-60 and 2,999 Bq for Cs-137, with the 4% of the expanded uncertainty. With the success of this research, the National Radiation Metrology Laboratory, PTKMR-BATAN is capable to make a mixture of standard Co-60 and Cs-137 which has traceability to the International System, so the measurement becomes more accurate and precise that in the end use of nuclear technology in all fields can be accomplished with good safety and security for workers, communities and the environment.

***Keywords**: Standardization, mixed source, gamma spectrometry, and radioactivity.*

1. Introduction

Utilization of nuclear technology in all fields has grown rapidly both in internationally and in Indonesia. Its use requires a standard that meets the technical requirements so that the product has an adequate level of quality. Some laboratories use standards as a calibrator for measuring tool owned, as well as the guarantor of the quality of the product.

Based on the duties and functions as a national reference laboratory in the field of radioactivity measurements, Center for Technology of Radiation Safety and Metrology – National Nuclear Energy Agency be capable of providing a standard source of various kinds and types so that the measurement and testing samples have values that are accurate, precise and traceable to the International System.

In this research, the development of standardized methods for mixed sources Co-60 and Cs-137 in point-shaped has been carried out. How that is done is to standardize the source of a mixture of Co-60 and Cs-137 by gamma spectrometry method. This method was chosen because it is very flexible for measuring radioactive and emits gamma photons can perform qualitative and quantitative analysis. In addition, this method can be used to analyze impurity which is in the source of these standards, so that when detected correction can be performed simultaneously with measurements of radioactivity standard source. Measurement for Co-60 activity is done by analyzing the spectrum at 1173.2 keV and 1332.5 keV gamma energy, for Cs-137 at 661.6 keV energy. Some researcher seperti Hiroshi Miyahara and Chizuo Mori; Y. Kawada and Yoshio Hino standardized mixture Co-60 source and Cs-137 coincidence method $4\pi\beta$-γ [1, 2] for each sample. Standardization Co-60 with this method can be directly carried out because of Co-60 emits beta and gamma simultaneously [3-6]. For Cs-137 method cannot be done directly but use the tracer method, Cs-134 as a tracer.

Co-60 is a radionuclide that has a long half life, which is 5.2711 years, decays by emitting beta particles while emitting gamma photons of 1173.2 keV and 1332.5 keV energies with intensities close to 100%, a stable element of Ni-60 [5]. With these properties, the Co-60 is excellent for a standard source emitting gamma photons at energies above 1000 keV. Cs-137 is a

single gamma emitting radionuclide has very long half life, which is 30.05 years, decays by emitting beta particles then emitted gamma photons at an energy of 661.6 keV with the intensity of 84.99%, to be a stable element of Ba-137 [6]. With properties like this, then the Cs-137 is excellent for a standard source emitting gamma photons in intermediate energy (about 500 keV). If both of these radionuclides are combined, the quality of the measurement will be better because the three energies of the two nuclides have been representing the middle region and the region above 1000 keV.

The purpose of this study was to find the source of the standard mixture of Co-60 and Cs-137 that have traceability to International System, so that the needs of the national mixed radioactive standard source can be held independently. With the standard source of this mixture is expected to result measurement, testing and quality control could be better.

2. Experimental Details

The study begins with preparation, counting activities and impurities, corrections, data analysis and conclusions.

Preparation

Sample preparation begins with preparing the container, tools and support resources in the thin film layer of mylar, then cleaned and sterilized using diluted alcohol from the impurities of other elements. Preparation performed by gravimetric method using a calibrated semi-micro balance device because it is more accurate than other methods. Point sources, prepared as much as three pieces. The source of Co-60 and Cs-137 dropped into a thin layer of mylar and then dried using infra-red rays. After drying the mixture source is covered with a layer of mylar. Furthermore, the source of the mixture is ready to be measured.

Activity measurement

The activity of mixture of point source was measured using gamma spectrometer system as in Figure 1. The detector used is a semiconductor HPGe GC1018 model, serial number 08057902 which has the relative efficiency of 10.3% with an energy resolution of 1.69 keV FWHM (full width at half maximum of full-energy peak) at 1332.5 keV. The detector is equipped with a pre-amplifier model 2002CSL and work on operational voltage 4500 volts with a positive polarity. Amplifiers used were made in Canberra in 2022 while setting type is coarse gain amplifiers at position 100 and fine gain at 0.73. Furthermore, the system is connected to a Multi-Channel Analyzer (MCA) in 2000 which Gennie software in the personal computer. Distance source to detector 25 cm.

Before the measurement, gamma spectrometer system must be calibrated first using the standard sources that have traceability to the international unit system. In this study, the standard source used is multi-gamma Eu-152 point source [7-9]. Measurements were taken three times and measurement time is 60 minutes. Measurement of Eu-152 standard source performed for 10,000 seconds to achieve a higher accuracy value.

Impurities measurement

Impurities were measured using gamma spectrometry device similar to that used when measuring the activity. Measurements were taken several times at different times to see the possibility of having impurities. Sources of measurement standards used in these impurities are Co-60, Cs-137 and Eu-152. The impurity of a standard material should be known and must be corrected to get the value of accurate and presision standards. The instrument used was a gamma spectrometer system can perform qualitative and quantitative analysis. Impurities measurements performed separately for the sum-peak and pile-up effect which took place a minimum. These factors are a major problem when performing quantitative analysis.

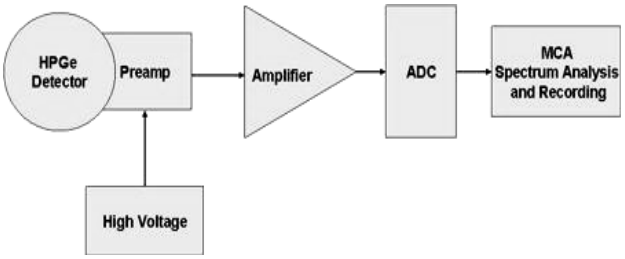

Figure 1. Block diagram of gamma spectrometer system with HPGe detector's

Corrections

In this study, correction is carried out on background counting, dead time, impurity of sample, decay factors, and others. Background correction is done by counting the background for 54,000 seconds. This is done to achieve an accurate measurement value, while the correction of dead time is done directly by setting time on the live-time position.

3. Result and Discussion

Weighing data of mixture Co-60 and Cs-137 source is shown in Table 1. The number of sources that dripped into the buffer adjusted to a diameter which formed less than 0.5 cm and the estimated activity owned does not exceed the maximum limits of the apparatus system used.

The result of the efficiency calibration by using Eu-152 source is shown by the curve in Figure 2. The energy used to make efficiency calibration curve as much as six energies, respectively 244.7, 344.3, 778.9, 964.1, 1112.1 and 1408.0 keV. This is done to minimize the uncertainties in curve fitting. The equation of efficiency calibration curve is $0.1598\ E^{-0.98}$ with correlation coefficient of 0.9997 and the fitting uncertainty of 1.5%. From these curves, obtained value for the efficiency for energy 661.657 keV is 0.000275; for 1173.228 keV is 0.0001569 and for 1332,492 is 0.0001385.

The spectrum of Co-60 and Cs-137 is shown in Figure 3 and obtained using the gamma spectrometer with HPGe semiconductor detector. Spectrum of Cs-137 is located at 661.6 keV, while the energy spectrum of Co-60 at energies 1173.2 and 1332. 5 keV. In this image significant impurities were not found, so corrections to the impurities were not necessary.

Table 1. Weighing data of Co-60 and Cs-137 mix sources

Code number	Weigh (mg)	
	Co-60	Cs-137
Co-Cs 01/2010	8.09	15.91
Co-Cs 02/2010	11.40	10.03
Co-Cs 03/2010	8.02	6.12

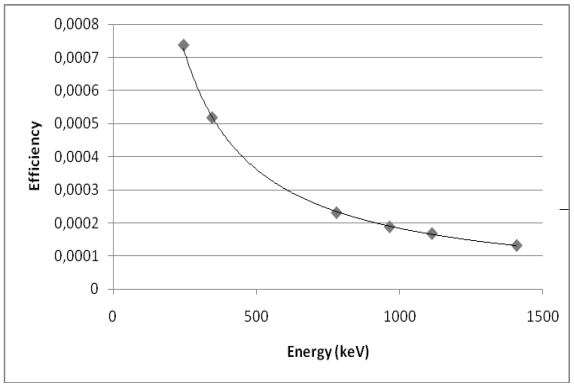

Figure 2. Curve of Efficiency Calibration using Eu-152 Standard Source.

The result of the activity determination of Co-60 and Cs-137 mix source of each standard is shown in Table 2. This result is quite good with the expanded uncertainty of 3.8%. Because the source is taken place from the same solution, specific activity of the master solution can also be calculated. The specific activity value of solution for Co-60 and Cs-137 is determined by dividing to the weight of each source placed on a mylar layer. The result of the specific activity determination of the type are shown in Table 2, with an average value of 249.1 ± 7.3 Bq/mg for Co-60 and 494.3 ± 5.0 Bq/mg for Cs-137. This result is quite good because it has a standard deviation below 3%.

Table 2. Result of the activity measurement of mix source.

Code of mix source	Activity (Bq)		Spec. Activity (Bq/mg)	
	Co-60	Cs-137	Co-60	Cs-137
CoCs 01/10	2076	7951	256.6	499.7
CoCs 02/10	2760	4946	242.1	493.1
CoCs 03/10	1994	2999	248.6	490.0
Mean of spec. Act. (Bq/mg)			249.1	494.3

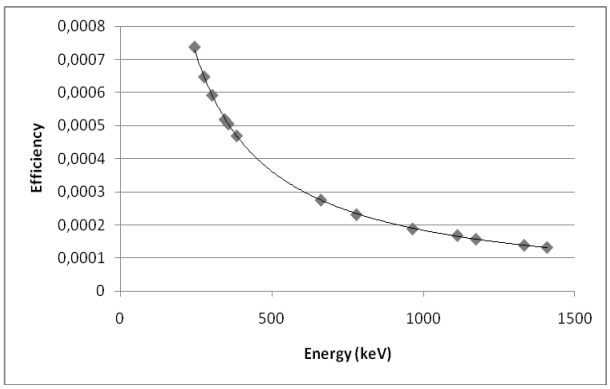

Figure 4. An example of efficiency calibration curve using Eu-152, Co-60 and Cs-137 standard sources.

After the standardization process is completed, the source of these standards are combined with the Eu-152 standard source is used to calibrate the gamma spectrometer system. The result of the efficiency curve is shown in Figure 4. The energy used to make efficiency calibration curve as much as nine of energies: 244.7, 344.3, 661 657, 778.9, 964.1, 1112.1, 1173.228, 1332,492 and 1408.0 keV, respectively. This is done to improve the quality measurements for more accurate, precision and traceable. Efficiency calibration curve is efficiency = $0.1598\ E^{-0.98}$ with correlation coefficient 0.9998 and the fitting uncertainty of 1.5 %.

4. Conclusion

Standardization of a mixture of Co-60 source and Cs-137 form the point of using gamma spectrometry method has been done at the National Radiation Metrology Laboratory. Mixed standard source activity that is created, each to Co-60 and Cs-137 is 2076 Bq and 7951 Bq for CoCs 01/10 code number; 2760 Bq and 4946 Bq for CoCs 02/10 code number; 1994 Bq and 2999 Bq for CoCs 03/10 Code number with the expanded uncertainty of 3.8%.

The specific activity value of the master solution is (249.1 ± 7.3) Bq/mg for Co-60 and (494.3 ± 5.0) Bq/mg for Cs-137. The use of mixed sources Co-60 and Cs-137 as a source standard to calibrate gamma spectrometer system improves the quality of the measurement value.

5. Acknowledgments

Great thanks to Head of Center for Technology of Radiation Safety and Metrology - BATAN and Head of Radiation Metrology Division which provides the opportunity for us to do this research. Hopefully the results of this study are useful so that the proposed use of nuclear technology in all sectors will be work properly, securely and safely.

6. References

[1]. Miyahara H. and C. Mori (1990), Memoirs of the Faculty of Enginnering, Nagoya University, Vol.2, No. 1, Nagoya-Japan.
[2]. Kawada Y. and Yoshio Hino (1972), Report of researches of Electro Technical Laboratory, Tsukuba – Japan.
[3]. International Commission on Radiological Protection (1983), Radionuclide Transformation, ICRP Publication No. 38, 11-13.
[4]. Anonymous (1982), Table de Radionucleides, Laboratoire de Metrologie des Rayonnements Ionisants, Medical Selection, Commissariat a I energie Atomique.
[5]. Ineel, Helmer, R. G. (2010), Table de Radionucleides, LNHB/CEA.
[6]. Ineel, Kri/Helmer, R. G. And V.P. Chechev (2007), Table de Radionucleides, LNHB/CEA.
[7]. Knoll, G. F. (1989), Radiation Detection and Measurement, Second Edition, John Wiley & Sons, Inc.
[8]. Debertin, K And Helmer, R. G. (1988), Gamma and X-ray Spectrometry With Semiconductor Detectors, Elsevier Science Publishers B.V., Amsterdam.
[9]. Susetyo, W. (1988), Spektrometri Gamma dan Penerapannya Dalam Analisis Pengaktifan Neutron, Yogyakarta, Universitas Gajah Mada Press.

Appendix

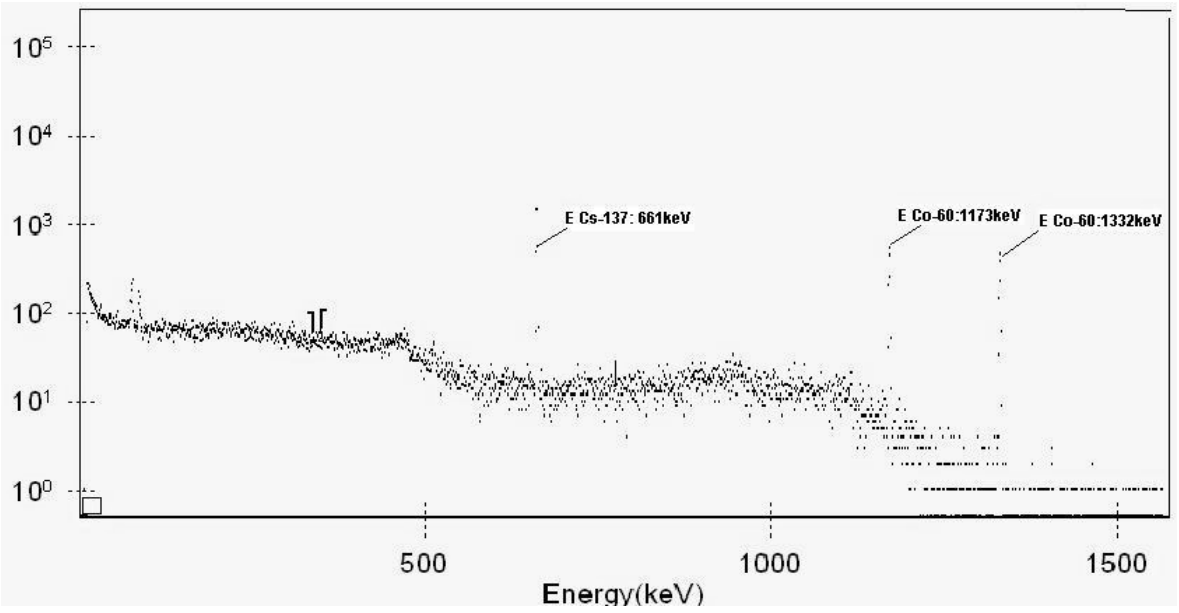

Figure 3. A Gamma-ray spectrum of Co-60 and Cs-137 obtained by HPGe detector.

The Diet Effect Using *Amorphophallus* Sp Raw Flour from East Java on Cholesterol of Rat (*Rattus Novergicus*) Wistar Strain

Harijati N[1], Widyarti S [2], Azrianingsih R [3]

[1,2,3] Department of Biology, Faculty of Science, Brawijaya University, Malang, Indonesia (harijati@ub.ac.id).

Abstract

Obesity is a body condition indicated from the high low-density lipoprotein (LDL) cholesterol presented. This condition should be avoided because it has serious risk to health which can cause heart disease and stroke. Many efforts in reducing obesity such as regular exercises or taking the pill had been done. The first effort is often constrained by the laziness level of patients to exercise, while the second has a significant side effect such as insomnia, increased blood pressure, dry mouth and so forth. Natural effort to provide meal diet from Amorphophallus muelleri, A.variabilis (yam variant: Brongkos 32; Brongkos 5; Wonorejo), Amorphophallus sp (Brangsi yam) to Wistar rats which previously has fattened using diet mix of cholesterol and lard, in addition to PARS (Chicken Feed Race Super-Confeed). As a control, meal from Amorphophallus campanulatus and Amorphophallus konjac (Japan yam) was used. Measurement of LDL-C content was conducted at four different time regime, i.e. 1).before cholesterol diet, 2). 24 days post cholesterol diet, 3) 11 days post yam (+cholesterol) diet, 4). 25 days post yam (+cholesterol) diet. The results show that diet from raw flour of A.variabilis potentially reduce blood cholesterol, 22.98%, 5.85% and 7.37% respectively for consecutive Brongkos 32; Brongkos 5; Wonorejo. Diet from A. Campanulatus and A. Konjac has not been able to reduce cholesterol up to the end of the observation (25 days diet).

Keywords: *cholesterol, obesity, A.variabilis, A.campanulatus, A.konjac.*

1. Introduction

LDL-C is bad cholesterol that tends to attach themselves to blood vessels. Adhesion cholesterol to the artery that went to the heart has risk of cardiovascular disease. Attachment to the artery to the brain has risk of stroke. Therefore, effort is needed to lower LDL-C content. One of the efforts is glucomannan diet. Glucomannan commercially available in the market is a result of refined the *Amorphophallus konjac*, known as konjac-glucomannan (KGM) [1].

Amorphophallus konjac has been found in China and Japan. Based on the data available on the official site of *Amorphophallus* (http://aroid.org), *A.konjac* has not been found in Indonesia. Others *Amophophallus* are found in Indonesia, including the East Java. Possibly endemic *Amorphophallus in* East Java contain high glucomannan and has a potential to reduce LDL-C. Therefore, it is necessary to study diet meal glucomannan from endemic *Amorphophallus* spp in East Java to reduce of LDL-C.

As a soluble fiber, glucomannan can be used to relieve constipation. Glucomanan relieve constipation by decreasing the residence time of fecal material [2]. Glucomanan also can be use to lose weight [3]. In obese patients, consumption of 1 gram of glucomannan and 250 ml of water one hour before meals, three times per day for 8 weeks resulted lowering 2.5 kg body weight [4].

Not only in losing weight, Walsh *et al*. [4] also shows that obese patients succeeded in reducing total cholesterol significantly. In healthy men, consumption of 3.9 grams of glucomannan for 4 weeks lowered total cholesterol (10%), LDL cholesterol (7.2%), triglycerides (23%) and blood pressure cytosolic (2.5%) [5]. In Baboon, glucomannan supplementation lowered liver cholesterol [6]. In mice also showed reduced liver cholesterol diet both glucomannan alone or in combination with chitosan [7].

Glucomannan diet also showed improved lipid profile and decreased levels of fasting blood sugar of type 2 diabetes so Konjac glucomannan can be used as a supplement for type 2 diabetes [8]. And Vuksan *et al*. [9] showed, in addition to improving blood lipid profile also improved glycemic control and blood pressure cytosolic combination with plant sterols, glucomannan can substantially improve the low-density lipoprotein cholesterol (LDL) [10].

2. Experimental Details

Glucomanan source materials were taken from endemic *Amorphophallus* located in East Java: *Amorphophallus campanulatus* (from Selopuro-Selopuro yam), *Amorphophallus muelleri* (from Madiun-Madiun yam), *Amophophallus variabilis* (4 variants: Brangsi yam, Brongkos 32 yam. Brongkos 4 yam, Wonorejo yam). *Amorphophallus konjac* (from Fukoaka, Japan) use as a control. All *Amorphophallus* was made chips, dried (70°C, 3days), and finely powdered. The glucomannan analyzing was conducted according to Chairul and Chairul [11] method.

Fattening Rats

2.5 months old Wistar strain Rat (*Rattus novergicus*), acclimatized in the laboratory with standard feeding (150 g flour PARS/ chicken feed super-Confeed, 50 g wheat flour) as 6 g/rat and provide drink water sufficiently. Fattening occurred after 11 days acclimatization. Fattening is conducted using cholesterol 0.23 mg/kg/BW and lard 4.36 mg/Kg/BW

Treatment

The treatments are organized into eight dietary groups of rats:

A* : Without cholesterol (only PARS and flour diet)
B : Cholesterol diet** + *A.konjac*
C : Cholesterol diet + *A.variabilis* (var.Brangsi)
D : Cholesterol diet + *A.variabilis* (var. Brongkos 32)
E : Cholesterol diet+ *A.variabilis* (var. Brongkos 5)
F : Cholesterol diet + *A.variabilis*(var Wonorejo)
G : Cholesterol diet + *A.muelleri*
H : Cholesterol diet + *A.campanulatus* (var Selopuro)

Notes
*each group: 5 rats
**6g/rat, given after acclimatization (day 12) until day 63. Cholesterol diet consisting of 150 g flour PARS / super chicken feed (Confeed), 50 g wheat flour, 27, 93 g lard, 1.5 g cholesterol and 0.75 g of cholic acid.

Time-point measurement of blood LDL-cholesterol

LDL-cholesterol were measured using blood serum at day 11 (before the cholesterol diet, cholesterol diet start at day 12), 35 (before diet *Amorphophallus*, the diet begins day 38), 49, and 63.

Diet Amorphophallus sp

Diet *Amorphophallus* sp was conducted by direct feeding with dose 60mg/kg /body weigh /day. The flour was dissolved in warm water first then delivered directly into the rat digestive tract through the esophagus using certain tools every day from the day to 38 to day 63.

Fixed parameter

Body weigh were measured every day; LDL-C are measured at four points time as describe above

3. Results and Discussion

The content of glucomannan

The measurement results showed that *A. konjac* has the highest glucomanan content (Table 1). This result was quite reasonable because *A. konjac* is reliable source of glucomannan on world market until now.

In addition of *A.konjac*, *A. variabilis* var. Brongkos 5 (hereafter called Brongkos 5 yam) and Brangsi (hereafter called Brangsi yam) have high glucomanan content as well, followed by *A.muelleri*. *A.campanulatus* gave false high result because the extracted filtrates were dominated by starch. And this fact was reinforced by the structure of the filtrate which can not form a gel when mixed with isopropyl alcohol. Gel form is among glucomannan characters. Based on color of tuber, *A. variabilis* was marketable because buyer prefers flour with white color than other color. Finally, we conclude *A.variablis* as endemic *Amorphophallus* in East Java as potential source of glucomannan and to be considered for cultivation.

Body weigh

The effect diets of cholesterol and glucomanan (yam flour) on body weigh is shown in Figure 1. Weight body indicator is not as expected. Rat body weight continued to rise since acclimatization. Even after giving diets yam flour. Increasing of rat body-weigh both control and treatment indicated that administration of cholesterol and lard do not fatten because treatment rat are not significantly different from negative controls. Diet 'crude extract' flour yam 60 mg/ kg or 10 mg /rat could not give the real effect of weight loss. Therefore considered there is another indicator to see the effect of glucomannan. The indicator is not weight loss, but the decrease in cholesterol. Obesity significantly correlated with cholesterol content [12].

Blood cholesterol content

The result analysis of cholesterol (LDL-C) showed that administration of cholesterol diet for

24 days (day 12-35) led to increased blood cholesterol (from 12 ± 1.2 mg / dL to 37.6 ± 7.7 mg / dL). Blood cholesterol (LDL-C) in the group without dietary cholesterol does not increase relatively to the range of 12 - 12.4 mg / dL. This suggests that cholesterol diet has induced a significant increase in LDL-C (Figure 2). Twenty five days after treatment using glucomannan (Counted from from day 38 until 63), gave varies result between Amorphophallus. Diet of glucomannan from *A. konjac*, Brangsi yam, *A. mulleri*, and Selopuro yam failed to lower blood cholesterol.

However glucomannan from Brongkos 32 yam, var Brongkos 5 yam, and Wonorejo yam can lower blood cholesterol rat respectively by 22.98%, 5.83% and 7:37%. It can be concluded that administration of glucomannan from Brongkos 32 yam, Brongkos 5 yam, and Wonorejo yam gave effect to a decrease in blood cholesterol faster than that of glucomannan from *A. konjac*, Brangsi yam, *A. mulleri*, and selopuro yam (Table 2). In other words *A.variabilis* potentially lowers cholesterol more than *A.konjac*, *A.muelleri* and *A. campanulatus*. And among A.variabilis there is the potential different. When viewed kinds of variants, *A.variabilis* var Brongkos 32 is the most potent than var.Brongkos 5 and var. Wonorejo. However, if the observed days decrease from day 49 to day 63, *A.variabilis* var Brongkos 5 is most potential. And when viewed overall at the point of measurement day 49 to day 63, except controls, all showed showed a tendency lowering LDL-C. It means that this study supports previous research that glucomannan has the potential to reduce LDL-C (1; 3; 5; 15; 10). Associated with the measurement glucomannan (Table 1), *A.konjac* should give decline LDL-C greater than others *Amorphophallus*, because it contains the highest glucomannan. There are two alternatives to address this fact, namely 1). Extend diet yam, for example 4 weeks more. There is a possibility *A.konjac* will be greater lowering of LDL-C or remain consistent with the results of the day to 63, 2). Based on the expression of genes encode synthesis glucomannan, namely glucomannan synthase [13]. Possible gene expression of glucomannan synthase from *A. konjac* is less strong than *A. variabilis*

4. Conclusion

The endemic *Amorphophallus* sp in East Java contain high glucomannan consecutive *A.variabilis* var Brongkos 5, *A.muelleri* and *A.campanulatus*. Meanwhile *Amorphophallus* that greatest lowering of LDL-C for 25 yam flour diet is *A.variabilis* var Brongkos 32.

5. References

[1]. Takigami, S., (2000), Konjac mannan. In: Phillips, G.O., Williams, P.A. (Eds.), Handbook of Hydrocolloids. CRC Press, Florida, pp. 413–424.

[2]. Marzio L, Del Bianco R, Donne MD, Pieramico O, Cuccurullo F. (1989), Mouth-To-Cecum Transit Time In Patients Affected by Chronic Constipation: Effect Of Glucomannan. *Am J Gastroenterol*. 8:888-891.

[3]. Keithley J and Swanson B. (2005), Glucomannan and Obesity: A Critical Review. *Altern Ther Health Med*. 11(6):30-4.

[4]. Walsh DE, Yaghoubian V and Behforooz A. (1984), Effect of Glucomannan on Obese Patients: A Clinical Study. *Int J Obes*. 8: 289-293.

[5]. Arvill A and Bodin L. (1995), Effect of Short-Term Ingestion of Konjac Glucomannan on Serum Cholesterol in Healthy Men. *Am J Clin Nutr*. 61: 585-589

[6]. Venter CS, Vorster HH and Van Ver Nestf DG. (1990), Comparison Between Physiological Effects of Glucomannan and Propionate In Baboons Fed "Western" Diets. *American Institute of Nutrition*. 90:1046-1053.

[7]. Gallaher CM, Munion J, Hesslink Jr R, Wise J and Gal aher DD. (2000), Cholesterol Reduction of Glucomannan and Chitosan is Mediated by Changes in Cholesterol Absorption and Bile Acid and Fat Excretion in Rats. *J. Nutr*. 130: 2753–2759

[8]. Chen HL, Sheu WH, Tai TS, Liaw YP, and Chen YC. (2003), Konjac supplement alleviated hypercholesterolemia and hyperglycemia in type 2 diabetic subjects-a randomized double-blind trial**.** *J Am Coll Nutr*. 22:36-42.

[9]. Vuksan V, Jenkins DJA, Spadafora P, Sievenpiper JI, Owen R, Vidgen E, Brighenti F, Walsh DE, Yaghoubian V and Behforooz A. (1984), Effect of glucomannan on obese patients: a clinical study. *Int J Obes*. 8: 289-293.

[10]. Yoshida M, Vanstone CA, Parsons WD, Zawistowski J and Jones PJH. (2006), Effect of plant sterols and glucomannan on lipids in individuals with and without type II

diabetes. *European Journal of Clinical Nutrition*. 60:529–537.

[11]. Chairul dan Chairul SM. (2006), Isolasi glukomanan dari dua jenis Araceae : Talas (*Colocasia esculenta* (L.) Schot dan Iles-iles (*Amorphophallus campananulatus* Blume). *Berita Biologi* 8(3):171-178

[12]. Njajou OT, Kanaya AM, Holvoet P, Connelly S, Strotmeyer ES, Harris TB, Cummings SR and Hsueh, WC. (2009), Association between oxidized LDL, obesity and type 2 diabetes in a population-based cohort, the Health, Aging and Body Composition Study. *Diabetes/Metabolism Research and Reviews*, 25: 733–739.

[13]. Ramsden L and Northcote DH**.** **(**1987**),** Glucomannan synthase from suspension cultures of *Pinus sylvestris*. *Phytochemistry* 26(10): 2679-2683

Appendixes

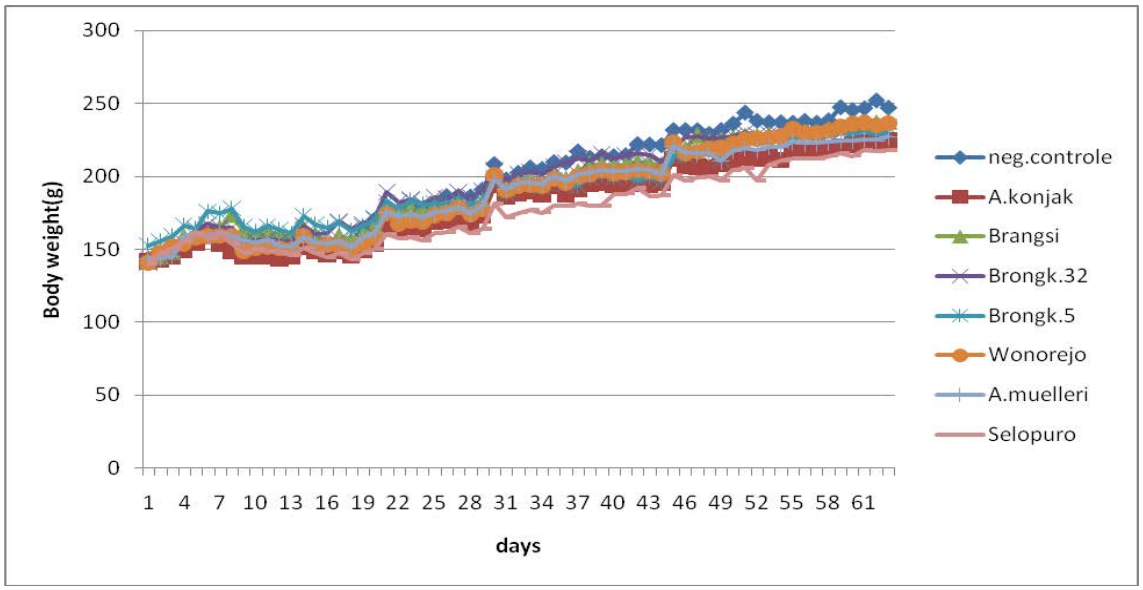

Figure 1. Weight Rats During 63 days of observation. A: control without exposure to dietary cholesterol; B: treatment of *A.konjac* (+ cholesterol diet); C: treatment of Brangsi yam (+ cholesterol diet); D: treatment of Brongkos 32 yam (+ cholesterol diet); E: Brongkos 5 yam (+ cholesterol diet); F: treatment Wonorejo yam (+ cholesterol diet); G: treatment of *A. muelleri* (+ cholesterol diet); H: treatment of *A.campanulatus* (+ cholesterol diet)

.

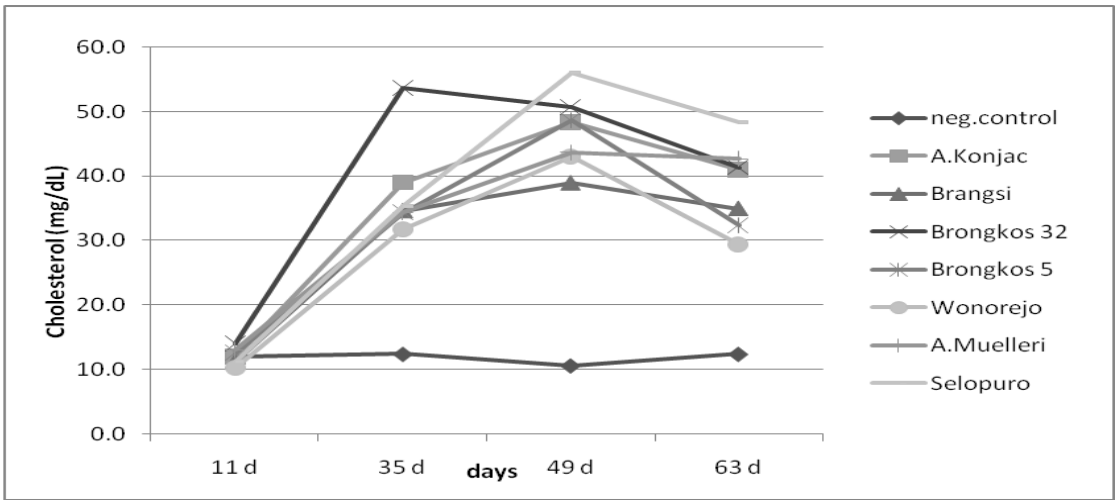

Figure 2. Effect of glucomannan on the reduction of blood cholesterol (LDL-C) in rat received dietary cholesterol. Day 38 starts yam diet (arrows).

Table 1. The measurement results of glucomannan from varies *Amorphophallus* sp

Amorphophallus	Glucomannan content (%)	texture of extraction result	flesh tuber color
A.Konjac	10.34	Gel	white
A.variabilis (var.Brangsi)	4.73	Gel	white
A.variabilis(var.Brongkos 32)	2.97	Gel	white
A.variabilis (var.Brongkos 5)	5.06	Gel	white
A.variabilis (var.Wonorejo)	3.19	Gel	white
A.muelleri	4.40	Gel	yellow
A.campanulatus (var.Selopuro)	4.62 dom.starch	No gelling	yellow

Table 2. Reduced Percentage blood cholesterol after glucomannan administration from varies *Amorphophallus*

Treatment Cholesterol and Glucomana diet	**days**				Reduced Percentage blood cholesterol
	11	**35***	**49**	**63**	
Without Cholesterol diet	12.0	12.4	10.06	12.4	Constant 0%
A.konjac	12.0	39.0	48.3	41.0	Not appear reduced yet
A.variabilis (var.Brangsi)	11.3	34.7	39.0	35.0	Not appear reduced yet
A.variabilis(var.Brongkos 32)	14.0	53.7	50.7	41.3	↓ 22.98%
A.variabilis (var.Brongkos 5)	12.5	34.3	48.7	32.3	↓ 5.83%
A.variabilis (var.Wonorejo)	10.3	31.7	43.0	29.3	↓ 7.37%
A.muelleri	13.0	34.3	43.7	42.7	Not appear reduced yet
A.campanulatus (var.Selopuro)	11.3	35.3	56.0	48.3	Not appear reduced yet

Study on Formation of Fatty Acid Methyl Esters (FAMEs) from Oil Seed Nyamplung (*Calophyllum inophyllum*); The Effect of Homogenous and Heterogenous Catalysts

Hendro Juwono [1], Triyono [2], Sutarno [3], Endang Tri Wahyuni [4]

[(1)] Department of Chemistry, ITS Surabaya, Indonesia
[(2,3,4)] Department of Chemistry, UGM Yogyakarta, Indonesia
Corresponding authors: hjachmad@gmail.com, nehin66@yahoo.com, nehin66@chem.its.ac.id

Abstract

The formation of fatty acid methyl esters compounds (FAMEs) from nyamplung seed oil (Calophyllum inophyllum) have been studied using different catalysts. Namely, metanoic compound as a homogenous catalyst and Al-MCM-41 as a heterogeneous catalyst. Crude oil is treated with degummed nyamplung seed oil, then catalyzed at a temperature of 60^0C in the reactor using air atmosphere. The results was then analyzed using GC-MS. Compounds of homogeneous catalysis has 7 components, which are summarized as lipid acids and fatty acid methyl esters (FAMEs) 6.83 % and 93.17%, while the result of heterogeneous catalysis has 8 components which are organized as lipid acids of 10.26%, 26.29% of heptadecene carbonic acid and 63.35 % of Fatty acid methyl esters (FAMEs).

Keywords: *FAMEs, homogeneous catalysts, heterogeneous catalysts.*

1. Introduction

The catalyst has been used in industry for 100 years, and new catalysis known in 1970 because of the development of environmental protection from industrial waste. Catalysis is a multidisciplinary area of chemistry, especially in the chemical industry. When there is talk about chemical reactions, it is sometimes more inclined to talk about the catalysts and catalysis. As the catalyst Al-MCM-41 were reported Adam (2005) on biomass pyrolysis reaction shows the ability of acid sites is increased in the presence of metallic Al, but Si / Al ratio on the catalyst reactivity is key, catalyst developers are expected to raise rates reactions that occur when compared with no metal [1].

Meanwhile nyamplung plants or *Calophyllum inophyllum* included in the Clusiaceae family originated naturally in the continent of Africa and distributed along the Pacific coast, including along the coast in Indonesia, the shape of the tree and can reach up to 3 meters in diameter, most exploited in timber and crude oil (seed oil). In Indonesia, the plant has not been used especially the potential of oil which contains triglycerides [2,3].

The reaction of triglycerides into FAMEs compounds requires a catalyst to increase the reaction rate. Catalysts used are generally homogeneous and heterogeneous catalysts, homogeneous catalysts used are alkaline methanol, while the heterogeneous catalyst used is Al-MCM41. It is interesting to study how the role of homogeneous or heterogeneous catalyst in the esterification reaction of nyamplung triglycerides of seed oil

(*Calophyllum inophyllum*) and the second compound from the reaction FAMEs.

2. Experimental Details

In general, research activities are divided into three, namely MCM-41 synthesis and modification, structure characterization and properties of catalysts, and catalytic activity test in reaction to the compound of fatty acid methyl ester (FAMEs) from nyamplung plants (*Calophyllum inophyllum*), which usually grow in Indonesia and has not been widely exploited. Product is a very important ingredient in the chemical industry and the availability of alternative energy. Synthesis of fatty acids methyl ester compound was done by the procedure mentioned by Venkanna (2009), Sahoo, (2009), or Vyas (2009) [4-6]. Modified MCM41 catalysts prepared by first synthesizing Al-MCM-41 mesoporous silica from the CTF. Modifications made by impregnation method using Palladium chloride.

Synthesis of Al-MCM-41

Al-MCM-41 synthesized according to the procedures obtained from Adams (2005) [1], namely surfactant tetra decil trimethyl ammonium bromide (TDTMAMB) dissolved in aquadest, then added sodium aluminate and stirred overnight. Establishment of framework Si using Sodium metasilicate, a little sulfuric acid and then stirred until the pH value is achieved. Solution was then stirred and heated at 100 °C for 6 days and washed until neutral and sentrifugated to obtain a white solid. The characterization performed by XRD and N_2 adsorption to determine the catalytic activity and by SEM to see the pores of the catalyst.

Making Fatty acid methyl esters (FAME) from nyamplung seed oil (Calophyllum inophyllum)

This procedure is taken from [4-6]. Seed Nyamplung (*Calophyllum inophyllum*) that have been dried was pressed until the oil obtained. The greenish black oil then filtered and degummed with the addition of 15% phosphoric acid at 70 °C for 20 minutes to obtain clear nyamplung seed oil (*Calophyllum inophyllum*). The making of biodiesel from oil was done by esterification reaction with alcohol and catalyst modification. Products obtained were characterized by GC-MS.

Reaction Catalysis

FAMEs compound formed is taken, weighed and placed in the reactor and then performed catalysis reaction in which catalyzed with some variation made to the catalysis reaction. Products were analyzed by GC-MS.

3. Result and Discussion

Test Results of heterogeneous catalysts

Test results conducted on heterogeneous catalysts, including XRD, SEM, ICP, and nitrogen adsorption. XRD diffractogram obtained are given in Appendixes. Interesting information are learnt from the XRD diffractogram which is the initial catalyst lattice field change when there is metal comes in, as we get compaction of scans that are not directly observe the intensity of the field (100), field (110) and field (200) of MCM-4 1.

SEM test results

Image of SEM micrographs of heterogeneous catalysts is given in Figure 1. SEM micrograph of the picture shows the basic framework of MCM-41 which is hexagonal elongated 3D. Intact in the presence of metallic Al that entered was not damage the field (100) although the intensity was declined.

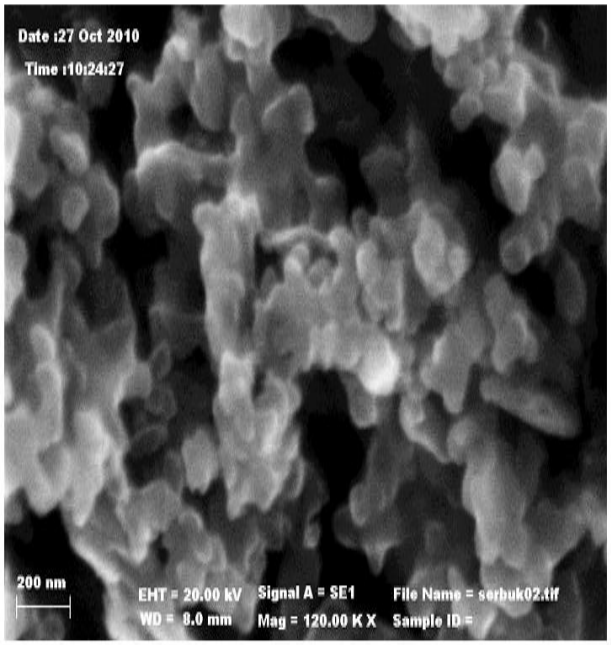

Figure 1. SEM micrograph of heterogeneous catalyst

ICP Test results and nitrogen adsorption

Table 1. ICP Test Results

Catalyst	Aluminum (%)	Silicon (%)
Al-MCM-41	4.81%	81.71%

Table 2. Result of nitrogen adsorption (GSA analysis)

Catalyst	Surface area (m^2/g)	Pore Volume (cc/g)	Pore Radius (Å)
Al-MCM-41	419.934	0.501	15.121

GC-MS test results on the catalysis reaction

Catalysis reaction of triglycerides by homogeneous catalysts and heterogeneous catalysts, providing the products observed by GC-MS is given in Appendixes. Organic fatty acid content is read from the table is 6.83 % and FAMEs (free acid methyl esthers) is 93.17 %.

Table 3. Nyamplung seed oil content from homogenous catalyst

Compound	Concentration (%)	Compound	Concentration (%)
Methyl Palmitate	13.30	Palmitic acid	1.15
Methyl Oleate	62.97	Glycerol	4.53
Methyl Stearate	16.14	Stearic acid	1.15
Methyl Arachidic	0.77		

Table 4. Components of the transesterification of seed oil nyamplung by heterogenous catalyst

Compound	Concentration (%)	Compound	Concentration (%)
Palmitic acid	4.14	Methyl linoleic	15.1995
Linoleic acid	0.95	Methyl stearate	10.35
Carbonic acid	26.29	Methyl oleate	26.49
Stearic acid	6.20	Methyl palmitate	9.96
Methyl hexadecanoat	0	Methyl arachidic	0.63

From the table above, the organic acids as much as 10.34%, 26.29% heptadecene carbonic acid and compounds of FAMEs total of 63.35%. When compared with the compound of FAMEs in Table 3, then there was an increase of 198.67% FAMEs product.

4. Conclusion

From the activity test of homogeneous and heterogeneous catalysts, it can be concluded that the formation of a homogeneous catalyst compound FAMEs of 21.21% while the number of heterogeneous catalysts by 63.35%.

5. Acknowledgements

The first author thanks to chemistry majors ITS, especially PHKI Grant Program that has provided scholarships in Doctoral Program of Chemistry UGM, as well as to DP2M DIKTI Events Calendar which has given the doctoral dissertation research grant in 2010.

6. References

[1]. Adam Judith, *et al*, (2005), Pyrolysis of biomass in the presence of Al-MCM-41 type catalyst, *Fuel*, 84 , 1494 – 1502.

[2]. Sylvie, Crane, *et al*, (2005), Composition of fatty acids triacylglycerols and unsaponifiable matter in Calophyllum calaba oil from guadalope, *Phytochemistry*, 66, 1825 – 1831.

[3]. Hermavathy J, Prabakhar J V, (1990), Lipid composition of Calophyllum inophyllum kernel, *JAOCS*, no 12, 67.

[4]. Venkanna, B. K, Reddy C. V, (2009), Biodiesel production and optimization from Calophyllum inophyllum, *Linn* oil – a three stages method, *Bioresource Technology*, 100, 5122 – 5125.

[5]. Sahoo, P. K, *et al*, (2009), Comparative evaluation of performance and emission characteristic of Jatropha, Karonja and Polanga based biodiesel as fuel in a tractor engine, *Fuel*, 88, 1698 – 1707.

[6]. Vyas, P. Amish, *et al*, (2009), Production of biodisel through transesterification of Jatropha oil using KNO_3/Al_2O_3 solid catalyst, *Fuel* , 88, 625 – 628.

Appendixes

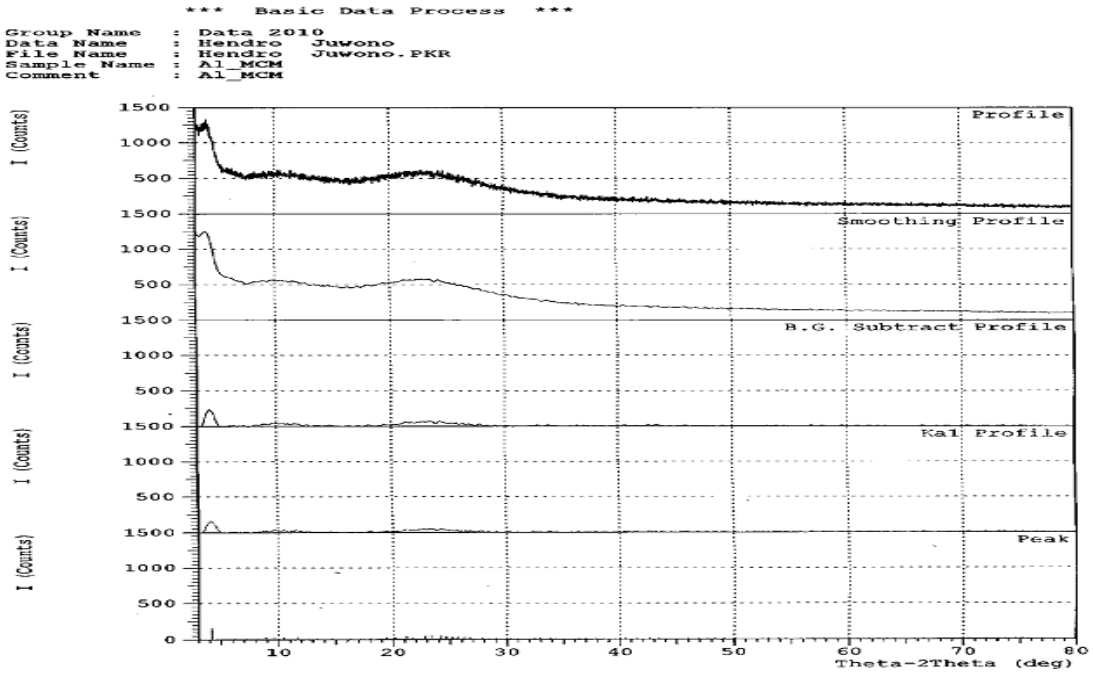

Figure 2. XRD diffractogram of heterogeneous catalyst

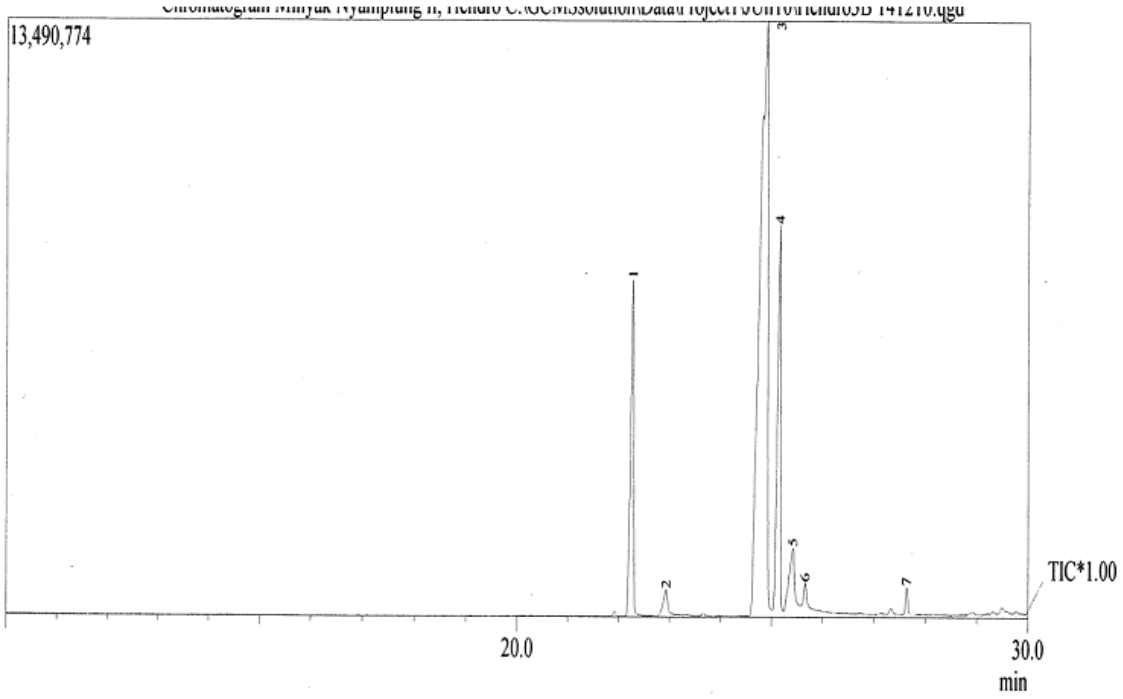

Figure 3. GC – MS of Catalysis reaction of triglycerides by homogeneous catalysts

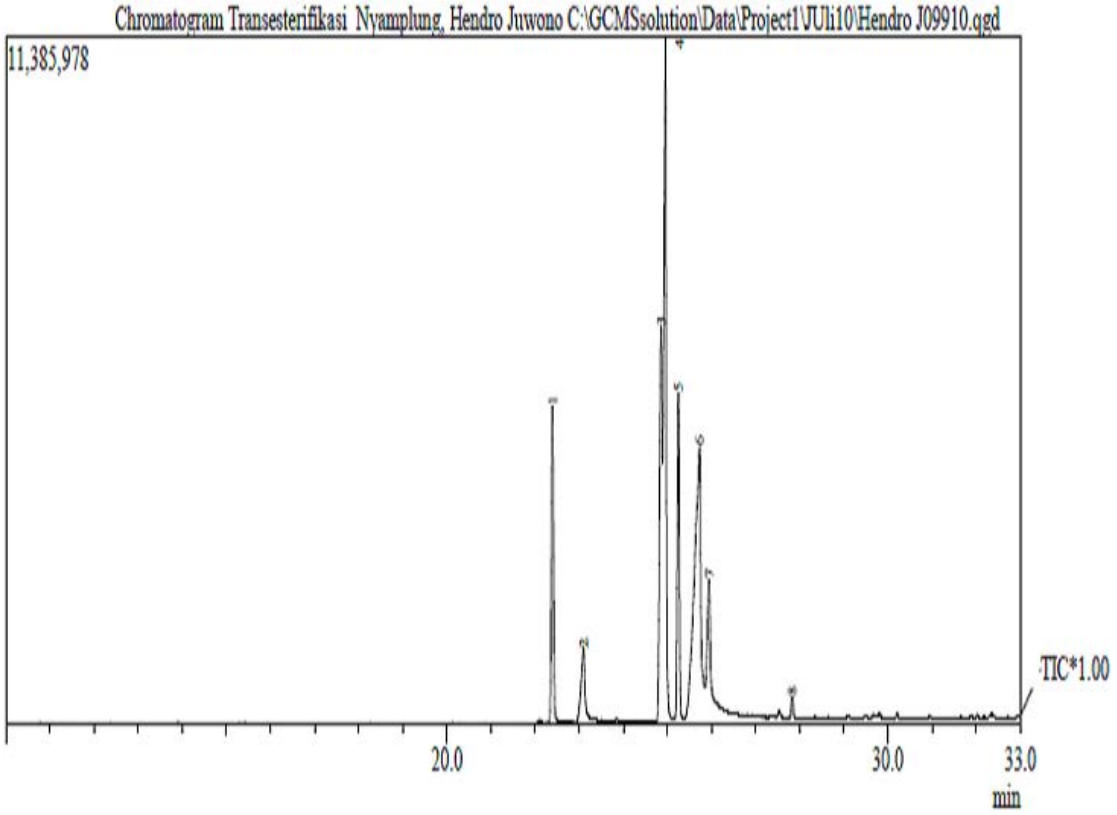

Figure 4. GC – MS of Catalysis reaction of triglycerides by heterogeneous catalysts

Preparation of ^{152}Eu Standard Source in Al_2O_3 Matrix

Hermawan Candra [1], Gatot Wurdiyanto [2], Pujadi [3]

(1,2,3) Center for Technology of Radiation Safety and Metrology, National Nuclear Energy Agency (BATAN), Jakarta, Indonesia (hermawan@batan.go.id)

Abstract

Preparation of ^{152}Eu standard source in Al_2O_3 matrix has been done in PTKMR - BATAN. The variation of weight and density matrix are studied for efficiency calibration curve. The ^{152}Eu standard source powder form was used as a standard measurement of radioactivity of environmental samples which has the form of powder. Standardization of radionuclide solution and samples have been carried out using gamma-spectrometer HPGe detector. The result of activity standard measurement was (7025.26 ±1.58%) kBq/gr. The standardized of ^{152}Eu radionuclide are mixed with the Al_2O_3 powder. Fiver weight variation conducted to test the homogeneity of the source on the matrix, and density variation to study the effect on efficiency calibration curve. The result of homogeneity test show that relative good, with discrepancies about 3.5%. The variation of density matrix affect the efficiency calibration curve, a small matrix density decreased efficienct otherwise at high density increased the efficiency.

***Keywords**: Standard source, ^{152}Eu, homogenity, gamma-spectrometer, density.*

1. Introduction

Radioactivity measurement of environmental samples for the commodity exports of food ingredients are part of radiation monitoring as the technical requirements of export to certain countries. Radionuclide activity measurement of environmental samples is usually done using a gamma spectrometer system. To get accurate results, environmental samples measurement and standards used for calibration is usually arranged to have the physical shape and geometry of the same. However, in practice it is quite difficult to get the same standard sources with the physical form of environmental samples. Therefore it should be used sources of standard physical form and its properties resemble the sample. Examples of environmental samples are usually in the form of volume, matrix solids, powders and liquids have different densities.

Gamma spectrometry systems are typically used for measuring gamma radioactivity of gamma emitter environmental samples. Before the radioactivity measurement is usually through a chemical process. Environmental samples have a small content of radioactivity so that the counting process needs to be done in a long time in terms of geometry and distance between the detector and the sample as possible or detector. Sample preparation process includes the determination of sample density, making the sample geometry and the source must be at or near the same standard, and sample matrix composition.

Radionuclides are often used as a standard is a ^{152}Eu source. Radionuclides can be used as source standards with different variations of the density matrix. ^{152}Eu has a gamma energy range is quite wide, from 121-1408 keV and has a long half -live of 13.52 years, so it is effectively used as a source standards Before being used as a source standard at a mariks, ^{152}Eu radionuclide activity was determined using a gamma spectrometer. With the known specific activity is ^{152}Eu radionuclide activity can be estimated is entered on each sample matrix, the density variations. To determine the homogenity in the spread of ^{152}Eu radionuclide in the matrix-matrix, it is necessary to validate the homogeneity and analysis of the influence of density on radioactivity measurement for each gamma energy in ^{152}Eu.

Homogeneity measurement of a material from the uniformity of distribution in a medium. Uniformity distributing materials to manufacture a benchmark standard sources in various densities. The statistical homogeneity of a standard source at various densities expressed by deviation occurs on these data will provide a resource description of source standard homogeneity.

Gamma spectrometer system is equipment that is often used in the measurement of radionuclide activity and to determine the type impurity contained in a radionuclide. Accuracy analysis of activity measurement depends on the condition of calibration prior to measurement.

One of the factors that affect the calibration is the setting of equipment on the optimum conditions relating of equipment characteristics of used gamma spectrometer.

In gamma spectrometry methods, high pulse generated by the detector and amplifier equivalent of energy gamma rays result from interaction of a radionuclide with a detector. Pulses produced by the detector are recorded in a particular of channel numbers on a multi-channel analyzer (MCA). The relationship between the number of channels in the MCA linear with radionuclide gamma-ray energy obtained from the energy calibration curve. Energy calibration using standard sources of radionuclides that have been known to activity initially, time reference, yield and energy gamma rays. To determine the relationship between the number of gamma ray energy channels with a radionuclide then performed the counting standard sources.

2. Experimental Details

Preparation of Eu-152

The original ^{152}Eu source in the form of Europium Chloride in HCl solution provided by POLATOM – Poladia were prapared in the form of matrix Al_2O_3 and point source. The first step, solution were prepared into solid point source in the form of $EuCl_3$, sucked into a small polyethylene ampoule picnometer (baby botle), and then dropped onto a thin polyester film as source support is about from 5,30 to 20,54 mg. The small polyethylene ampoule picnometer were carefully weighed in each case to determine the mass of the drops. And then, the sources were dried in a chamber with circulating air. After a dry source, the sources were covered with thin polyester film.

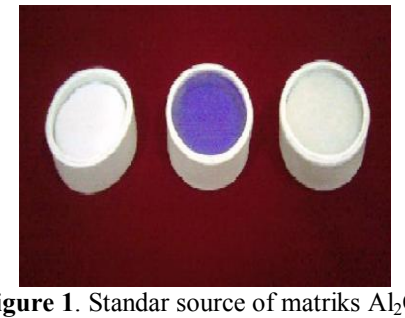

Figure 1. Standar source of matriks Al_2O_3

The second step is preparation of Al_2O_3 matrix. The Al_2O_3 powder of 370.56 grams were made into a concentrated solution by adding H_2O and stirring until smooth, then dropped 155.96 mg of ^{152}Eu into the concentrated solution stirred until homogeneous. After that the mixed of Al_2O_3 and ^{152}Eu are dried until the powder again. The mixed of Al_2O_3 and ^{152}Eu in powder form ware prepared into geometrical source form with varying density from 0.72 to 1.16 gr/cm3 in polyethylene cylidrical container. After that covered the top container with poly ethylene plastic.

Measurement of sample

The first step, activity concentration of Eu-152 solid point source sample were measured twice replicates for each sample. The activity are measured using gamma-spectrometer system HPGe detector, with source and detector distance of 25 cm. Efficiency calibration carried out using Eu-152 standard source of the LMRI – France. Furthermore, activity measurements were taken samples of Al_2O_3 matrix density variation 0.72 to 1.16 gr/cm^3 using gamma spectrometer system enumerator. The distance between detector and sample measurement is 25cm. Activities of each matrix with density variations and weight were used to determine the efficiency at each energy gamma ^{152}Eu By obtaining efficiency in each of energy gamma then calibrate the efficiency curve can be made ^{152}Eu relationship between the efficiency with various densities.

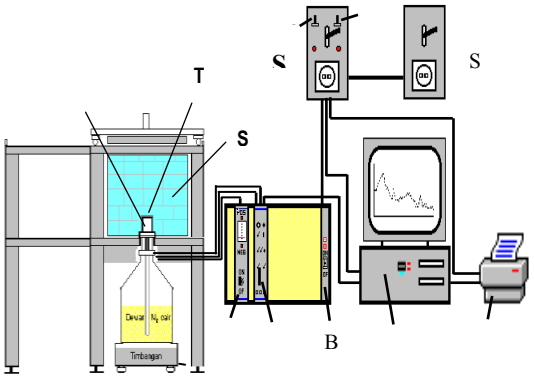

Figure 2. Scheme of the gamma spectrometer system

3. Result And Discussion

This study has been carried out two tests of homogeneity and analysis of the influence of density variations in Eu-152 on each matrix Al_2O_3 from 0.72 to 1.16 gr/cm3 variation. In Table 1 presents the results of measurements of Eu-152 point source, using the gamma counter spectrometer Results Eu-152 activity determination of point source with weight variation showed good results below 2%. The result of this activity is used to determine the specific activity of Al_2O_3 matrix powder that has been incorporated radionuclides Eu-152.

HomogenityTest:

On testing homogeneity of the sample matrix on the variation of density Al_2O_3 0.72 to

1.16 gr/cm^3, activity measured in each matrix. Specific activity of Al_2O_3 matrix value is 3032.6 Bq / gram. While the average activity of each sample matrix density variation is 0.72 to 1.16 gr/cm^3 was 3132.43. Disperancy between the value of specific activity and activity of Al_2O_3 matrix each sample matrix variations in the density of 0.72 to 1.16 gr/cm^3 was 3.1%. This means that the mixing process of Eu-152 radionuclides and Al_2O_3 powder gives good results.

The result of the determination of activity of each sample Al_2O_3 matrix is used to calculate the efficiency of each Eu-152 gamma energy at various densities.

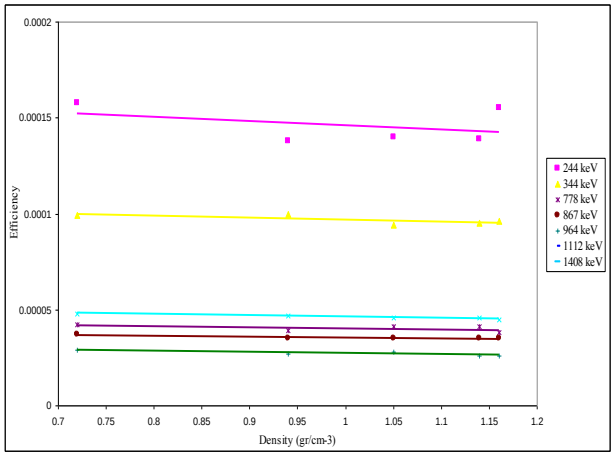

Figure 3. Efficiency Curve Of HPGe Detector on Variety Density

From the picture can be seen that at 244 keV energy linear curve at the top. While higher energy gamma . This can be explained that the efficiency calibration curve using gamma spectrometry, the gamma energy of 244 keV will the result of efiienccyi higher, at energies above 244 keV would be obtained with a small value of the efficiency of light energy increases gamma. This is due to the higher energy gamma the more high also possible escape of the gamma photon detection efficiency of the detector.

In these curves can be observed that the of the difference between the efficiency curves of density in each of energy then seen that the distribution of Eu-152 evenly to each of different density will result in a different count. In addition to the density of a substance , factors also greatly affect the count. So the value of HPGe detector efficiency of each density is different for each energy.

Each density of Eu-152 has a value that is almost the same activity. Small differences of each activity also affects the efficiency curve and density unlinierity. The process of linearity occurs when the relationship of efficiency and density comparable. The greater efficiency of the price density is also greater. unlinierity is not so higher. The closer the condition of a material the greater the gamma radiation absorbed, so that will affect the efficiency of the detector. The spectrum of Eu-152 radionuclides in Al_2O_3 matrix is given in Figure 4.

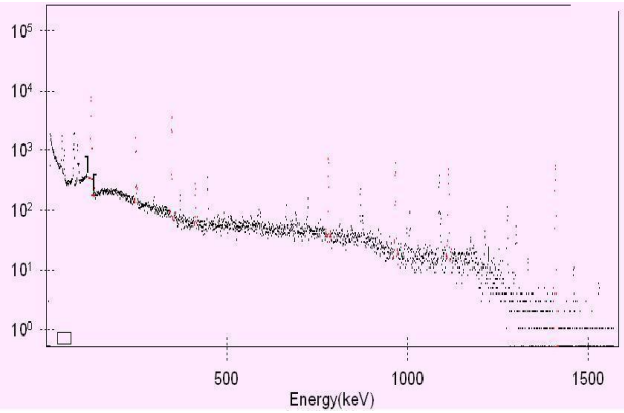

Figure 4. Spectrum Eu-152 dalammatriks Al2O3 with gamma spectrometer

4. Conclusion

BATAN has been able to create a standard source of variety geometry powder form in various matrices. The results showed that homogenity density analysis has given good results using gamma spectrometer with accuracy below 4%.

5. Acknowledgements:

Author thankful to the Research Group of Standardization of Radionuclides, Safety and Technology Center for Radiation Metrology BATAN for the facilities and measurements hence this research can be done.

6. References

[1]. National Council On Radiation Protection And Measurements (1978), A Handbook of Radioactivity Measurements Procedures, NCRP Report No. 58.
[2]. ICRP Publication 38 (…..), Radionuclide Transformation Energy & Intensity of Emissions, Vol. 11-13, Pergamon Press, Oxford.
[3]. K. Debertin and RG. Helmer (1988), Gamma and X-Ray Spectrometry With Semiconductor Detector
[4]. Debertin, Schotzig, K.F. Walz (….), Efficiency Calibration of Semiconductor Spectrometers Techniques and Accurates, PTB Germany

[5]. DEBERTIN (….), International Intercomparison of Gamma-Ray Emision Rate Measurement by Means of Germanium Spectrometers and ^{152}Eu Sources.
[6]. DEBERTIN (1985) A Guide and Instruction for Determining Gammay-ray Emission Rates with Germanium Detector Systems, PTB.
[7]. Wisnu Susetyo (....), Instrumentasi Nuklir II, BATAN.

Appendixes

Table 1. Measurement result of Eu-152 point source activity

Date of Measurement	Code	Source	Activity Bq	Mg	Activity Bq/mg
3-Jan-11	PS15201/2011	Eu-152	49069.023	6.887	7124.645
3-Jan-11	PS15202/2011		149663.29	20.54	7285.88
				Average	7205.26
				Deviation	114.01
				Error (%)	1.5

Tabel 2. Uncertainty component, gamma spectrometer system

UNCERTAINTY BUDGET

Unit measured	:	Activity
Source standardized	:	Eu-152
Standard Source	:	Eu-152
Equipment	:	Spectrometer gamma
Mathematic model	:	Area/(I.eff)
Range of measuring	:	0 - 20 μCi

Componen	Units	Distribution	U (%)	Divider	vi	ui	ci	ui ci	(ui ci)²	(ui ci)4 /vi
1	2	3	4	5	6	7	8	9	10	11
Std Source	Bq	Gaussian	1.5	3	∞	0.5	1	0.5	0.25	0
half life of standard source	Year	Gausian	0.12	1	∞	0.12	1	0.12	0.0144	0
Efficiency	%	normal	3.232	1.73205081	∞	1.86599607	1	1.86599607	3.48194133	0
Intensity of sample	%	Gausian	0.4513	1	∞	0.4513	1	0.4513	0.20367169	0
half life of sample	year	Gausien	0	1	∞	0	1	0	0	0
Area of sample	Cps	normal	0.450069	1	∞	0.450069	1	0.450069	0.2025621	0
Dead time		normal	0.005	1.73205081	∞	0.00288675	1	0.00288675	8.3333E-06	0
SUMs								3.39025182	4.15258346	0
Combine Standard Uncertainty, uc (%)									2.03778887	
Effective freedom of degree									∞	
Coverred factor, k students for veff and CL 95%									1.96	
Expanded uncertainty, U = k uc, (%)									**3.99406618**	

Estimation Parameters of Regression Spasial Lag by Ordinary Least Square Method

Indah Rahmawati [1], Sri Harini [2], Abdul Aziz [3]

[1,2,3] Mathematics Department, Faculty of Science and Technology, UIN of Maulana Malik Ibrahim, Malang, Indonesia (i_r4h34@yahoo.com)

Abstract

Regression analysis is an instrument of analysis which is used for getting relation and mathematic models between dependent variable (y) and one or more independent variable (x). One of important assumptions in regression analysis is there is no error dependence each other (autocorrelation). If one of assumptions happens in regression analysis, we can infer that regression analysis test is unsuitable for making models. One of techniques to solve that problem is by applying regression spatial analysis. Regression spatial is one of methods to solve regression analysis models by affecting local influence. In this paper, will be analyzed estimation parameters $\hat{\sigma}^2$ and $\hat{\beta}$ in regression spatial lag by ordinary least square (OLS) method.

Keywords: *Regression Spatial Lag, Parameter, Ordinary Least Square (OLS).*

1. Introduction

The interpolation of spatial data is a problem relevant to geographical information science, as well as to many order related disciplines, including environmental science, resource management, planning and civil engineering.

Regression analysis is designed for situation where a variable is thought to be related to one or more other measurements made, usually, on the same object. A purpose of the analysis is to use data (observed values of the variables) to estimate the form of this relationship [1].

2. Experimental Details

Spatial Linear Regression Models

The general model of regression spatial is shown as [2]:

$$y = \rho W_1 y + X\beta + u \quad (1)$$

and $u = \lambda W_2 u + \varepsilon$ (2)

$\varepsilon \sim N(0, \sigma^2 I_n)$

where:

- y = constants an $n \times 1$ vector of dependent variables
- ρ = coefficient on the spatiality lagged dependent variable
- W = an $n \times n$ spatial weight matrics
- X = represents an $n \times k$ data matrix containing explanatory variables
- β = vector of coefficient parameter regression
- λ = coefficient on the spatiality error

From the general model (1), we can derive special models by imposing restriction. For example, $\lambda = 0$, produces a spatial lag model shown as

$$y = \rho W_1 y + X\beta + \varepsilon \quad (3)$$

$\varepsilon \sim N(0, \sigma^2 I_n)$

Four Methods of Estimation

In deriving the estimator $\hat{\beta}$, we blithely adopted the least square procedure for doing so. This is well-accepted method of estimation and its rationale will not be discussed here. However, for convenient reference we summarize four common methods of estimation which, although differing in basic concept, all lead to the same estimator under certain frequently-used assumptions. All four procedures are summarized in terms of the full rank model where, in $y = X\beta + \varepsilon$, X has full column rank, $E(y) = X\beta$ and $E(\epsilon) = 0$ [1].

a. Ordinary Least Square (OLS)

This involves choosing $\hat{\beta}$ as the value of b which minimizes the sum of squares of deviations of the observations from their expected values; i.e., choose $\hat{\beta}$ as that β which minimizes $\sum_{i=1}^{N}[y_i - E(y_i)]^2 = (y - X\beta)^T(y - X\beta)$. The resulting estimator is, as we have seen, $\hat{\beta} = (X^T X)^{-1} X^T y$.

b. Generalized Least Square (GLS)

On assuming that the variance-covariance matrix of ε is $var(\varepsilon) = V$, this method involves minimizing $(y - X\beta)^T V^{-1}(y - X\beta)$ with respect

to β. This leads to $\bar{b} = (X^T V^{-1} X)^{-1} X^T V^{-1} y$. Clearly, when $V = \sigma^2 I$, the generalized and the ordinary least square estimators are the same: $\bar{\beta} = \hat{\beta}$.

c. Maximum Likelihood (ML)

With least squares estimation no assumption is made about the form of the distribution of the random error terms in the model, the terms represented by ε. With maximum likelihood estimation, some assumption is made about this distribution (often that it is normal) and the likelihood of the sample of observations represented by the data is then maximized. On assumption that the ε's are normally distributed with zero mean and variance-covariance matrix V, i.e., $\varepsilon \sim N(0, V)$, the likelihood is

$$L = (2\pi)^{-\frac{1}{2}N} |V|^{-1} \exp\{-\tfrac{1}{2}(y - X\beta)^T V^{-1} (y - X\beta)\}$$

.

Maximizing this with respect to β is equivalent to solving $\frac{\partial(\log L)}{\partial \beta} = 0$. The solution is the maximum likelihood estimator of b and turns out to be $\bar{\beta} = (X^T V^{-1} X)^{-1} X^T V^{-1} y$, the same as the generalized least square estimator. As before, when $V = \sigma^2 I$, $\bar{\beta}$ simplifies to $\bar{\beta}$. Only then, in thinking of $\bar{\beta}$ as the maximum likelihood estimator, we do so on the basis of assuming $\varepsilon \sim N(0, f\sigma^2 I)$.

Two well-known points are worth emphasizing about these estimators. First, least squares estimation does not pre-suppose any distributional properties of the ε's other than finite (in our case zero) means and finite variances. Second, maximum likelihood estimation under normality assumptions leads to the same estimator, $\bar{\beta}$, as generalized least squares; and this reduces to the ordinary least squares estimator $\bar{\beta}$ when $V = \sigma^2 I$.

d. The Best Linear Unbiased Estimator (BLUE)

For any row vector t^T conformable with β the scalar $t^T\beta$ is a linear functions of the elements of the parameter vector β. A fourth estimation procedure derives a best, linear, unbiased estimator of $t^T\beta$. The three characteristics of the estimator inherent in its definition lead to its derivation.

i. Linearity: it is to be a linear function of the observations y. Let the estimator be $\lambda^T y$, where λ^T is a row vector of order N, then λ is uniquely determined by the other two characteristics of the definition, as shall be shown.
ii. Unbiasedness: $\lambda^T y$ is to be an unbiased estimator of $t^T\beta$. Therefore $E(\lambda^T y)$ must equal $t^T\beta$; i.e., $\lambda^T X\beta = t^T\beta$. Since this is to be true for all β, $\lambda^T X = t^T$.
iii. A ~~b~~best" estimator: ~~b~~best" means that in the class of *linear*, unbiased estimators of $t^T\beta$, the ~~b~~best" is to be one that has minimum variance. This is the criterion for deriving λ^T.

Consequences of estimation

Properties of $\hat{b} = (X^T X)^{-1} X^T y$ and consequences thereof are now discussed. The topics dealt with in this section are based solely on the two properties so far attributed to e, that $E(e) = 0$ and $var(e) = \sigma^2 I$[1].

a. Unbiasedness

Since $\hat{b}$ is the best linear unbiased estimator of b for $V = \sigma^2 I$, it is unbiased. This can also be shown directly:

$E(\hat{b}) = E(X^T X)^{-1} X^T y = (X^T X)^{-1} X^T X b = b$

. Thus the expected value of $\hat{b}$ is b and so $\hat{b}$ is unbiased, implying, of course, that in $\hat{b}^T = [\hat{b}_0, \hat{b}^T]$ the estimator $\hat{b}$ is also unbiased.

b. Variances

With $\hat{b} = (X^T X)^{-1} X^T y$, it is clear that the variance-covariance matrix of $\hat{b}$ is

$$\begin{aligned} var(\hat{b}) &= E[\hat{b} - E(\hat{b})][\hat{b} - E(\hat{b})]^T \\ &= E[(X^T X)^{-1} X^T y - E((X^T X)^{-1} X^T y) \cdot [(X^T X)^{-1} X^T y - E((X^T X)^{-1} X^T y)]^T \\ &= E(X^T X)^{-1} X^T [y - E(y)][y^T - E(y^T)] X (X^T X)^{-1} \\ &= (X^T X)^{-1} X^T E(ee^T) X (X^T X)^{-1} \\ &= (X^T X)^{-1} \sigma^2 \end{aligned}$$

The in inverse matrix used for obtaining $\hat{b}$ therefore also determines the variances and covariances of the elements of $\hat{b}$.

Properties of point estimators **[3]**

a. Unbiased Estimators

An estimator $\Theta = s(X_1, X_2, \ldots, X_n)$ is said to be an unbiased estimator of the parameter θ if $E(\Theta) = \theta$, for all possible values of θ. If Θ is an unbiased estimator, then its mean square error is given by $E[(\Theta - \theta)^2] = E\{[\Theta - (\Theta)]^2\} = var(\Theta)$. That is, its mean square error equals its variance.

b. Efficient Estimators

An estimators Θ_1 is said to be a more efficient estimator of the parameter θ than the estimator Θ_2 if

i. Θ_1 and Θ_2 are both unbiased estimators of θ.

ii. $Var(\Theta_1) < Var(\Theta_2)$.
The estimator $\Theta_{MV} = s(X_1, X_2, \dots, X_n)$ is said to be a most efficient (or minimum variance) unbiased estimator of the parameter θ if
(i) It is an unbiased estimator of θ.
(ii) $Var(\Theta_{MV}) \leq Var(\Theta)$, for all Θ.

c. Consistent Estimators
The estimator Θ_n of θ based on a random sample of size n is said to be consistent if for any small $\varepsilon > 0$, $\lim_{n\to\infty} P(|\Theta_n - \theta| < \varepsilon) = 1$, or equivalently, $\lim_{n\to\infty} P(|\Theta_n - \theta| \geq \varepsilon) = 0$. The following two conditions are sufficient to define consistency $(\lim_{n\to\infty} P(|\Theta_n - \theta| < \varepsilon) = 1)$:
(i) $\lim_{n\to\infty} E(\Theta_n) = \theta$.
(ii) $Var(\Theta_n) = 0$.

3. Result and Discussion

Process of Spatial Lag

Let the general model of regression spatial lag shown as:

$$y = \rho W_1 y + X\beta + \varepsilon \quad (3)$$
$$y - \rho W_1 y = X\beta + \varepsilon$$
$$[I - \rho W_1]y = X\beta + \varepsilon$$
$$Ay = X\beta + \varepsilon \; ; A = I - \rho W_1$$

Then,

$$Ay = X\beta + \varepsilon \quad (4)$$
$$\varepsilon = Ay - X\beta$$
$$\varepsilon^T\varepsilon = (Ay - X\beta)^T(Ay - X\beta)$$
$$= A^T y^T Ay - X^T\beta^T Ay - A^T y^T X\beta + X^T\beta^T X\beta$$
$$= A^T y^T Ay - X^T\beta^T Ay - X^T\beta^T Ay + X^T\beta^T X\beta$$
$$= A^T y^T Ay - 2X^T\beta^T Ay + X^T\beta^T X\beta \quad (5)$$

Review the differentiation rules [4],
$\frac{\partial \beta^T a}{\partial \beta} = a$ and $\frac{\partial(\beta^T X\beta)}{\partial \beta} = X\beta + X^T\beta$
where β and a are column vector, X is a square matrix, and the derivative $\frac{\partial f}{\partial \beta}$ of a scalar function f with respect to a vector β is defined as the vector of the derivative of f with respect to the elements of β. Then, we minimize (5) by setting its (vector) derivative with respect to β equal to (vector) zero,

$$\frac{\partial}{\partial \beta}\varepsilon^T\varepsilon = 0$$
$$\frac{\partial}{\partial \beta}(A^T y^T Ay - 2X^T\beta^T Ay + X^T\beta^T X\beta) = 0$$
$$\frac{\partial}{\partial \beta}\varepsilon^T\varepsilon = \frac{\partial}{\partial \beta}(A^T y^T Ay - 2X^T\beta^T Ay + X^T\beta^T X\beta)$$
$$= -2X^T Ay + X^T X\beta + (\beta^T X^T X)^T$$
$$= -2X^T Ay + X^T X\beta + X^T X\beta$$
$$= -2X^T Ay + 2X^T X\beta$$
$$-2X^T X\beta = -2X^T Ay$$
$$X^T X\beta = X^T Ay$$
$$\beta = (X^T X)^{-1}X^T Ay \quad (6)$$

The coefficients β and parameter of the error (ε) distribution are generally unknown and are to be estimated. The simplest assumptions of the estimating model in matrix notation are $E[\varepsilon] = 0$ and $E[\varepsilon\varepsilon^T] = \sigma^2 I$[5]. We can write in matrix as:

$$E[\varepsilon\varepsilon^T] = E\left[\begin{bmatrix}\varepsilon_1\\ \vdots \\ \varepsilon_m\end{bmatrix}[\varepsilon_1 \quad \cdots \quad \varepsilon_n]\right]$$

$$= \begin{bmatrix} E[\varepsilon_1{}^2] & E[\varepsilon_1\varepsilon_2] & \cdots & E[\varepsilon_1\varepsilon_n] \\ E[\varepsilon_2\varepsilon_1] & E[\varepsilon_2{}^2] & & E[\varepsilon_2\varepsilon_n] \\ \vdots & & \ddots & \\ E[\varepsilon_m\varepsilon_1] & E[\varepsilon_m\varepsilon_2] & & E[\varepsilon_m\varepsilon_n] \end{bmatrix}$$
$$= \begin{bmatrix} \sigma^2 & 0 & \cdots & 0 \\ 0 & \sigma^2 & & 0 \\ \vdots & & \ddots & \\ 0 & 0 & & \sigma^2 \end{bmatrix}$$

To find the mean vector and the covariance matrix for the sampling distribution of the random vector β, we first substitute $X\beta + \varepsilon$ for y in (6) to obtain [6],

$$\hat{\beta}_{ols} = (X^T X)^{-1}X^T Ay$$
$$= (X^T X)^{-1}X^T(X\beta + \varepsilon)$$
$$= (X^T X)^{-1}X^T X\beta + (X^T X)^{-1}X^T\varepsilon$$
$$= \beta + (X^T X)^{-1}X^T\varepsilon \quad (7)$$
$$\hat{\beta}_{ols} - \beta = (X^T X)^{-1}X^T\varepsilon$$
and, $\hat{\sigma}^2 = \frac{\hat{\varepsilon}^T\hat{\varepsilon}}{n-k}$
$$= \frac{(Ay - X\hat{\beta}_{ols})^T(Ay - X\hat{\beta}_{ols})}{n-k}$$

The mean of β is obtained by taking expectation of (7) giving (by assumption $E(\varepsilon) = 0$),

$$E[\hat{\beta}] = E[\beta + (X^T X)^{-1}X^T\varepsilon]$$
$$= E[\beta] + E[(X^T X)^{-1}] \cdot E[X^T] \cdot E[\varepsilon]$$
$$= \beta + (X^T X)^{-1} \cdot X^T \cdot 0$$
$$= \beta$$

and the vector of residual from the least-squares estimator regression is [4],

$$\varepsilon = Ay - X\beta$$
$$= X\beta + \varepsilon - X((X^T X)^{-1}X^T Ay)$$
$$= X\beta + \varepsilon - X\big((X^T X)^{-1}X^T(X\beta + \varepsilon)\big)$$
$$= X\beta + \varepsilon - X((X^T X)^{-1}X^T X\beta + (X^T X)^{-1}X^T\varepsilon))$$
$$= X\beta + \varepsilon - X(X^T X)^{-1}X^T X\beta - X(X^T X)^{-1}X^T\varepsilon))$$
$$= X\beta + \varepsilon - X\beta - X(X^T X)^{-1}X^T\varepsilon$$
$$= \varepsilon - X(X^T X)^{-1}X^T\varepsilon$$
$$= (I - X(X^T X)^{-1}X^T)\varepsilon \quad (8)$$

An unbiased estimator for $\hat{\sigma}^2$ is $s^2 = \frac{(n-k)^2}{\varepsilon\varepsilon^T}$. To show $\hat{\sigma}^2$, we evaluate the expectation of $\varepsilon\varepsilon^T$ using (8),

$$E[\varepsilon\varepsilon^T] = E\left[\left((I - X(X^TX)^{-1}X^T)\varepsilon\right)\left((I - X(X^TX)^{-1}X^T)\varepsilon\right)^T\right]s^2 = \frac{(n-k)^2}{\varepsilon\varepsilon^T}.$$

$$\begin{aligned}
&= E[\varepsilon(I - X(X^TX)^{-1}X^T)\varepsilon^T] \\
&= E[tr(\varepsilon(I - X(X^TX)^{-1}X^T)\varepsilon^T)] \\
&= E\left[tr\left((I - X(X^TX)^{-1}X^T)\varepsilon\varepsilon^T\right)\right] \\
&= E[tr]\cdot E[I - X(X^TX)^{-1}X^T]\cdot E[\varepsilon\varepsilon^T] \\
&= tr\cdot(I_n - X(X^TX)^{-1}X^T)\cdot\hat{\sigma}^2 \\
&= \hat{\sigma}^2(tr\, I_n - tr\, X(X^TX)^{-1}X^T) \\
&= \hat{\sigma}^2(n-k) \\
\hat{\sigma}^2 &= \frac{E[\varepsilon\varepsilon^T]}{(n-k)} \\
\hat{\sigma}^2 &= E[s^2] \\
s^2 &= E[\hat{\sigma}^2]
\end{aligned}$$

where tr$M$ stands for the trace, or sum of the diagonal elements, of a square matrix M and we have used the fact tr(AB)=tr(BA), A and B not necessarily square.

The covariance matrix of β is, again using (7) by assuming $E(\varepsilon\varepsilon^T) = \sigma^2 I$,

$$\begin{aligned}
Cov(\hat{\beta}) &= E[(\hat{\beta} - E[\hat{\beta}])(\hat{\beta} - E[\hat{\beta}])^T] \\
&= E[(\hat{\beta} - \beta)(\hat{\beta} - \beta)^T] \\
&= E[((X^TX)^{-1}X^T\varepsilon)((X^TX)^{-1}X^T\varepsilon)^T] \\
&= E[(X^TX)^{-1}X^T\varepsilon\varepsilon^TX(X^TX)^{-1}] \\
&= E[(X^TX)^{-1}X^TX\varepsilon\varepsilon^T(X^TX)^{-1}] \\
&= E[(X^TX)^{-1}]\cdot E[X^TX]\cdot E[\varepsilon\varepsilon^T]\cdot E[(X^TX)^{-1}] \\
&= (X^TX)^{-1}\cdot X^TX\cdot\sigma^2 I\cdot(X^TX)^{-1} \\
&= (X^TX)^{-1}\sigma^2
\end{aligned}$$

Properties of Regression Spatial Lag

- Unbiased Estimator β

$$\begin{aligned}
E[\hat{\beta}] &= E[\beta + (X^TX)^{-1}X^T\varepsilon] \\
&= E[\beta] + E[(X^TX)^{-1}]\cdot E[X^T]\cdot E[\varepsilon] \\
&= \beta + (X^TX)^{-1}\cdot X^T\cdot 0 \\
&= \beta
\end{aligned}$$

This proves that $\hat{\beta}$ is unbiased estimator, where X, β are fixed and $E[\varepsilon] = 0$.

- An unbiased estimator for $\hat{\sigma}^2$ is $s^2 = \frac{(n-k)^2}{\varepsilon\varepsilon^T}$.

4. Conclusion

The general model of egression spatial lag is $y = \rho W_1 y + X\beta + \varepsilon$. This paper use ordinary least square (OLS) method to estimate the parameters. The result of that estimation are $\hat{\beta} = (X^TX)^{-1}X^TAy$ and $\hat{\sigma}^2 = \frac{\varepsilon\varepsilon^T}{(n-k)}$.

5. Acknowledgements

The first author thank to Allah swt., her parent, and supervisor (Sri Harini, M.Si and Abdul Aziz, M.Si), thank you very much for the knowledge hence it makes her more knowledgeable about this paper.

6. References

[1]. Searle, S. R., (1971), Linear Models, New York-London-Sydney-Toronto.
[2]. Le Sage, James P. (1999), The Theory and Practice of Spatial Ekonometrics, University of Toledo.
[3]. Hsu, Hwei P., (1996), Schaum's Outline of Theory and Problems of Probability, Random Variables, and Random Processes, The McGraw-Hill Companies, Inc.
[4]. Chow, Gregory C., (1988), Econometrics, International Edition, McGraw-Hill, Inc. Singapore.
[5]. Ghosh, Sukesh K., (1991), Econometrics: Theory and Applications, Pretice Hall, Inc. New York.
[6]. Aziz, Abdul (2010), Ekonometrika: Teori dan Praktik Eksperimen dengan MATLAB, Malang: UIN-Maliki Press.

Estimation Parameters of Regression Spatial Error by *Estimated Generalized Least Square* Method

Lailiatul Mubtadiah [1], Sri Harini [2], Abdul Aziz [3]

[1,2,3] Mathematics Department, Faculty of Science and Technology, UIN of Maulana Malik Ibrahim, Malang, Indonesia (ail4_04_girlz@yahoo.co.id)

Abstract

Regression analysis is a method used to determine the relationship between variables. Influence of these variables can be accepted if the underlying assumptions are met. If one of assumption is not met, the regression analysis test unappropriate is used to make the model. One of cause the unappropriate model of regression analysis is the occurrence of autocorrelation on the error. This can occur because of local influence of regression analysis model. One of way to solve this problem is by spatial regression analysis. Spatial regression analysis is one of method used to analyze the model coused by spatial effects. The Spatial effects can be caused by observation value from observation value in other locations, this characteristic is called the spatial lag. Beside that, the other spatial effect is spatial error, in which error value from a location is influence by the error from other location. Assumption that is used in this model is error in normally distribution and experienced autocorrelation $E(u) \neq 0$*, the mean value is zero and variance covariance which is influenced by autocorrelation on the error. In this researche discusses about the procedures for estimating parameters of spatial error regression model using the Estimated Generalized Least Square (EGLS) method.*

Keywords*:Parameters Estimation, Regression Spatial error, Estimated Generalized Least Square (EGLS), Autocorelation.*

1. Introduction

Analysis Regression is an analysis to determine the relationship of an independent variable Y to dependent variable X. The relationship is then formed in a model that can predict the value of Y to X is given and have a small error. The resulting model is a regression model. In the application of regression analysis, the underlying assumptions must be met which did not contain autocorrelation. But in a study of dependence often occur between errors, the errors of an error location often depend to the error of other locations (nearby). Therefore, another model is needed that takes into account the effect of this spatial dependency. This model is called a spatial regression model.

Spatial regression model is divided into two part, namely spatial lag regression model and spatial error regression model. The research will discuss spatial error regression model that is the error dependence between location. Spatial error regression model is a model that takes into account the spatial error, so the spatial lag coefficient is not considered dependent (ρ = 0). The regression spatial error models are as follows:

$$y = X\beta + u \quad (1)$$

$$u_t = \lambda W u_{t-1} + \varepsilon \quad (2)$$

With ε ~ N (0, Ω) and no autocorrelation. So the general formula of regression spatial error is as follows:

$$\boldsymbol{y = X\beta + \lambda W u + \varepsilon}$$

with:

y = dependent variable vector of size n x 1
X = matrix that contains p independent variables measuring n x p
β = vector of regression coefficient parameters p x 1
λ = coefficient of spatial error autoregression
u = vector error autocorrelation is assumed to contain the size n x 1
W= spatial weight matrix of size nxn error as dependent variables
n = number of observations
p = number of observation parameters
ε= vector of errors that did not experience autocorrelation

thus can be expressed by the following matrix:

$$\begin{bmatrix} Y_1 \\ Y_2 \\ \vdots \\ Y_n \end{bmatrix} = \begin{bmatrix} x_{11} & x_{12} & \cdots & x_{1p} \\ x_{21} & x_{22} & \cdots & x_{2p} \\ \vdots & \vdots & \cdots & \vdots \\ x_{n1} & x_{n2} & \cdots & x_{np} \end{bmatrix} \begin{bmatrix} \beta_1 \\ \beta_2 \\ \vdots \\ \beta_p \end{bmatrix}$$
$$+\lambda \begin{bmatrix} w_{11} & w_{21} & \cdots & w_{1n} \\ w_{21} & w_{22} & \cdots & w_{2n} \\ \vdots & \vdots & \cdots & \vdots \\ w_{n1} & w_{n2} & \cdots & w_{nn} \end{bmatrix} \begin{bmatrix} u_1 \\ u_2 \\ \vdots \\ u_p \end{bmatrix} + \begin{bmatrix} \varepsilon_1 \\ \varepsilon_2 \\ \vdots \\ \varepsilon_n \end{bmatrix}$$

2. Experimental Details

Estimated generalized least squares (EGLS) is a technique for estimating the unknown parameters in a linear regression model. The EGLS is applied when the variances of the observations are unequal (heteroscedasticity), or when there is a certain degree of correlation between the observations. In these cases ordinary least squares can be statistically inefficient, or even give misleading inferences. As for the steps in this research are:

1. Determining the spatial error model regression equation.
2. Define the log-likelihood function for the combined observation vector y, based on the combined standard normal distribution on the error vector ν.
3. Define the parameter estimation errors on spatial regression models estimated using generalized least square (EGLS) by finding the value of the estimated parameters β and σ^2
4. Determining the properties of unbias estimasitor.

3. Result and Discussion

To find the spatial regression model parameter estimation error, first Spatial process as in equation spatial lag become as follows:

$$y = \rho W_1 y + X\beta + u$$
$$y - \rho W_1 y = X\beta + u$$
$$(I - \rho W_1)y = X\beta + u$$
$$Ay = X\beta + u$$
$$\text{with } A = I - \rho W_1 \qquad (3)$$

And equation (2) formed into the equation as follows:

$$u = \lambda W_2 u + \varepsilon$$
$$u - \lambda W_2 u = \varepsilon$$
$$(I - \lambda W_2)u = \varepsilon$$
$$Bu = \varepsilon \quad \text{with } B = I - \lambda W_2 \qquad (4)$$
$$u = (I - \lambda W_2)^{-1}\varepsilon \qquad (5)$$

where the variance covariance matrix of error is $E[\varepsilon \varepsilon^T] = \Omega$, (6)
is the diagonal, there exists a vector of homoskedastic random disturbances *v*, as

$$v = \Omega^{-1/2}\varepsilon \qquad (7)$$

Since ε is an error that is assumed to have zero mean and variance Ω, each valued diagonal elements σ^2. Thus transformed into standard normal form equation ν ∽ N (0,1) with diagonal elements are 1. Random error vector obtained ν ∽ N (0,1), so the error vector u in equation (5) becomes

$$u = B^{-1}\,\Omega^{1/2} v \qquad (8)$$

with the substituting (8) in equation (3) it is obtained

$$Ay = X\beta + B^{-1}\,\Omega^{1/2} v$$

or alternatively,

$$(Ay - X\beta)B\,\Omega^{-1/2} = v \qquad (9)$$

transformation of random variable ν be a random variable y is done through the Jacobian method approach:

$$J = det\left(\frac{\partial v}{\partial y}\right)$$
$$= det\left(\frac{\partial (Ay\,\Omega^{-1/2}B - X\beta\,\Omega^{-1/2}B)}{\partial y}\right)$$
$$= det\left(\frac{\partial (Ay\,\Omega^{-1/2}B - X\beta\,\Omega^{-1/2}B)}{\partial y}\right)$$
$$= det\left(\left(\frac{\partial (Ay\Omega^{-1/2}B}{\partial y}\right) - \left(\frac{\partial (X\beta\Omega^{-1/2}B)}{\partial y}\right)\right)$$
$$= det\,(\Omega^{-\frac{1}{2}}BA) - 0$$
$$= det(\Omega^{-\frac{1}{2}}BA)$$
$$\det\left(\frac{\partial v}{\partial y}\right) = |\Omega^{-1/2}BA| = \Omega^{-1/2}|B||A| \qquad (8)$$

Based on joint standard normal distribution for the error term *v*, and using (8), the log-likelihood function for the joint vector of observation y is obtained as:

$$= -\frac{n}{2}ln(2\pi) - \frac{1}{2}ln\,\Omega + ln|B| + ln|A|$$
$$-\frac{1}{2}(Ay - X\beta)^T B^T \Omega^{-1} B(Ay - X\beta)$$

With,

$$(v^T v) = \left[\left((Ay - X\beta)B\right)^T \Omega^{-1}((A - X\beta))B)\right]$$

This regression model involving spatial error, assuming that A = I and Ω = σ^2 I, so that the square error becomes:

$$= -\frac{n}{2}ln(2\pi) - \frac{1}{2}ln(\sigma^2) + ln|B|$$
$$-\frac{1}{2\sigma^2}(y - X\beta)^T B^T B(y - X\beta) \qquad (10)$$

Estimation Parameter of β with EGLS method

Parameter estimation of β is a minimization of a sum of squared (transformed) errors.

$$\frac{\partial (lnL(\beta,\sigma^2|y))}{\partial (\beta)^T} = \frac{\partial\left[-\frac{n}{2}ln(2\pi) - \frac{n}{2}ln(\sigma^2) + ln|B| - \frac{1}{2\sigma^2}(y - X\beta)^T B^T B(y - X\beta)\right]}{\partial (\beta)^T}$$
$$= 0 + 0 + 0 - \frac{1}{2\sigma^2}\frac{\partial (y - X\beta)^T B^T B(y - X\beta)}{\partial (\beta)^T}$$

$$= -\frac{1}{2\sigma^2}\frac{\partial[(y^T-\beta^T X^T)B^T B(y-X\beta)]}{\partial(\beta)^T}$$
$$= -\frac{1}{2\sigma^2}\left[\frac{\partial(y^T B^T By-\beta^T X^T B^T By-y^T B^T BX\beta+\beta^T X^T B^T BX\beta)}{\partial(\beta)^T}\right]$$
$$= -\frac{1}{2\sigma^2}\left[\frac{\partial(y^T B^T By-\beta^T X^T B^T By-(y^T B^T BX\beta)^T+\beta^T X^T B^T BX\beta)}{\partial(\beta)^T}\right]$$
$$= -\frac{1}{2\sigma^2}\left[\frac{\partial(y^T B^T By-\beta^T X^T B^T By-\beta^T X^T B^T By+\beta^T X^T B^T BX\beta)}{\partial(\beta)^T}\right]$$
$$= -\frac{1}{2\sigma^2}\left[\frac{\partial(y^T B^T By-2\beta^T X^T B^T By+\beta^T X^T B^T BX\beta)}{\partial(\beta)^T}\right]$$
$$= -\frac{1}{2\sigma^2}[-2X^T B^T By+X^T B^T BX\beta+(\beta^T X^T B^T BX)^T]$$
$$= -\frac{1}{2\sigma^2}[-2X^T B^T By+X^T B^T BX\beta+X^T B^T BX\beta]$$
$$= -\frac{1}{2\sigma^2}[-2X^T B^T By+2X^T B^T BX\beta]$$
$$= -\frac{1}{2\sigma^2}[-2(X^T B^T BX)^{-1}X^T B^T By+2(X^T B^T BX)^{-1}X^T B^T BX\beta]$$
$$= -\frac{1}{2\sigma^2}[-2(X^T B^T BX)^{-1}X^T B^T By+2\beta]$$
$$= \frac{1}{2\sigma^2}[(X^T B^T BX)^{-1}X^T B^T By-\beta]$$

by equating the above equation with zero so that

$$\beta = (X^T B^T BX)^{-1}X^T B^T By$$
$$\hat{\beta} = b_{EGLS} = (X^T B^T BX)^{-1}X^T B^T By$$

Substitusing $B = I - \lambda W$ in $\hat{\beta}$, so

$$\beta = (X^T(I-\lambda W_2)^T(I-\lambda W_2)X)^{-1}X^T(I-\lambda W_2)^T(I-\lambda W_2)y$$

The nature of the estimator parameter β Spatial Error Regression

Estimator β is unbias estimator if E (β) = β. Proof:

$$E(\hat{\beta}) = (X^T(I-\lambda W_2)^T(I-\lambda W_2)X)^{-1}X^T(I-\lambda W_2)^T(I-\lambda W_2)y$$
$$= (X^T(I-\lambda W_2)^T(I-\lambda W_2)X)^{-1}X^T(I-\lambda W_2)^T(I-\lambda W_2)E(y)$$
$$= (X^T(I-\lambda W_2)^T(I-\lambda W_2)X)^{-1}X^T(I-\lambda W_2)^T(I-\lambda W_2)X\beta$$
$$= I\beta = \beta$$

So that proved that the estimator β is unbias. After getting unbias nature, then the next will prove efficient nature, an estimator is said to be efficient if the estimator has the smallest variance, the evidence:

$$\hat{\beta}_{EGLS} = (X^T(I-\lambda W_2)^T(I-\lambda W_2)X)^{-1}X^T(I-\lambda W_2)^T(I-\lambda W_2)y$$
$$= (X^T(I-\lambda W_2)^T(I-\lambda W_2)X)^{-1}X^T(I-\lambda W_2)^T(I-\lambda W_2)(X\beta+u)$$
$$= (X^T(I-\lambda W_2)^T(I-\lambda W_2)X)^{-1}X^T(I-\lambda W_2)^T(I-\lambda W_2)(X\beta)+(X^T(I-\lambda W_2)^T(I-\lambda W_2)X)^{-1}X^T(I-\lambda W_2)^T(I-\lambda W_2)u$$
$$= \beta+(X^T(I-\lambda W_2)^T(I-\lambda W_2)X)^{-1}X^T(I-\lambda W_2)^T(I-\lambda W_2)u$$

so

$$cov(\beta_{EGLS}) = E(\beta_{EGLS}-E(\beta_{EGLS}))(\beta_{EGLS}-E(\beta_{EGLS}))$$
$$= E(\hat{\beta}_{EGLS}-\beta)(\hat{\beta}_{EGLS}-\beta)$$
$$= E((X^T(I-\lambda W_2)^T(I-\lambda W_2)X)^{-1}X^T(I-\lambda W_2)^T(I-\lambda W_2)u)x((X^T(I-\lambda W_2)^T(I-\lambda W_2)X)^{-1}X^T(I-\lambda W_2)^T(I-\lambda W_2)u)^T$$
$$= E((X^T(I-\lambda W_2)^T(I-\lambda W_2)X)^{-1}X^T(I-\lambda W_2)^T(I-\lambda W_2)u)x$$
$$(u^T(I-\lambda W_2)^T(I-\lambda W_2)X(X^T(I-\lambda W_2)^T(I-\lambda W_2)X)^{-1})$$
$$= E(X^T(I-\lambda W_2)^T(I-\lambda W_2)X)^{-1}X^T(I-\lambda W_2)^T(I-\lambda W_2)x$$
$$u^T u(I-\lambda W_2)^T(I-\lambda W_2)X(X^T(I-\lambda W_2)^T(I-\lambda W_2)X)^{-1}$$
$$= (X^T(I-\lambda W_2)^T(I-\lambda W_2)X)^{-1}X^T(I-\lambda W_2)^T(I-\lambda W_2)x$$
$$E(u^T u)(I-\lambda W_2)^T(I-\lambda W_2)X(X^T(I-\lambda W_2)^T(I-\lambda W_2)X)^{-1}$$

because

$$E(u^T u) = E\{((I-\lambda W_2)^{-1}\varepsilon)^T(I-\lambda W_2)^{-1}\varepsilon\}$$
$$= (X^T(I-\lambda W_2)^T(I-\lambda W_2)X)^{-1}X^T(I-\lambda W_2)^T(I-\lambda W_2)x$$
$$E\{(I-\lambda W_2)^{-1}\varepsilon((I-\lambda W_2)^{-1}\varepsilon)^T\}(I-\lambda W_2)^T(I-\lambda W_2)x$$
$$= (X^T(I-\lambda W_2)^T(I-\lambda W_2)X)^{-1}X(X^T(I-\lambda W_2)^T(I-\lambda W_2)X)^{-1}X^T(I-\lambda W_2)^T(I-\lambda W_2)x$$
$$E\left\{(I-\lambda W_2)^{-1}\varepsilon\varepsilon^T(I-\lambda W_2)^{-1^T}\right\}(I-\lambda W_2)^T(I-\lambda W_2)x$$
$$= (X^T(I-\lambda W_2)^T(I-\lambda W_2)X)^{-1}X(X^T(I-\lambda W_2)^T(I-\lambda W_2)X)^{-1}X^T(I-\lambda W_2)^T(I-\lambda W_2)x(I-\lambda W_2)^{-1}E(\varepsilon\varepsilon^T)$$
$$s(I-\lambda W_2)^T(I-\lambda W_2)x(I-\lambda W_2)^{-1^T}X(X^T(I-\lambda W_2)^T(I-\lambda W_2)X)^{-1}$$
$$= (X^T(I-\lambda W_2)^T(I-\lambda W_2)X)^{-1}X^T(-\lambda W_2)^T(I-\lambda W_2)x(I-\lambda W_2)^{-1})\sigma^2 I(I-\lambda W_2)^{-1^T}(I-\lambda W_2)^T(I-\lambda W_2)xX(X^T(I-\lambda W_2)^T(I-\lambda W_2)X)^{-1}$$
$$= \sigma^2(X^T(I-\lambda W_2)^T(I-\lambda W_2)X)^{-1}X^T(I-\lambda W_2)^T(I-\lambda W_2)(I-\lambda W_2)^{-1}(I-\lambda W_2)^{T^{-1}}(I-\lambda W_2)^T(I-\lambda W_2)xX(X^T(I-\lambda W_2)^T(I-\lambda W_2)X)^{-1}$$
$$= \sigma^2(X^T(I-\lambda W_2)^T(I-\lambda W_2)X)^{-1}(X^T(I-\lambda W_2)^T(I-\lambda W_2)X)(X^T(I-\lambda W_2)^T(I-\lambda W_2)X)^{-1}$$
$$= \sigma^2(X^T(I-\lambda W_2)^T(I-\lambda W_2)X)^{-1}$$

So far $(\hat{\beta}) = \sigma^2(X^T(I-\lambda W_2)^T(I-\lambda W_2)X)^{-1}$ should be as small as possible so that β efficient.

$$\lim_{n\to\infty} var(\hat{\beta}) = \lim_{n\to\infty}\sigma^2(X^T(I-\lambda W_2)^T(I-\lambda W_2)X)^{-1} = \lim_{n\to\infty}\frac{y-\hat{y}}{n-p}(X^T(I-\lambda W_2)^T(I-\lambda W_2)X)^{-1} = 0.$$

So we can say that β is a consistent estimator.

Estimation Parameter of σ^2 with estimated generalized least square method

$$\frac{\partial(ln\,L(\beta,\sigma^2|y))}{\partial\sigma^2} =$$

$$\frac{\partial\left(-\frac{n}{2}ln(2\pi)-\frac{n}{2}ln(\sigma^2)+\ln|B|-\frac{1}{2\sigma^2}(y-X\beta)^TB^TB(y-X\beta)\right)}{\partial\sigma^2}$$

$$=\frac{\partial\left[-\left(\frac{n}{2}\right)ln\sigma^2-\frac{1}{2\sigma^2}(y-X\beta)^TB^TB(y-X\beta)\right]}{\partial\sigma^2}$$

$$=-\frac{n}{2\sigma^2}+\frac{1}{2(\sigma^2)^2}(y-X\beta)^TB^TB(y-X\beta)$$

$$=\frac{-n\sigma^2+(y-X\beta)^TB^TB(y-X\beta)}{2(\sigma^2)^2}$$

$$\frac{n\sigma^2}{2\sigma^4}=\frac{(y-X\beta)^TB^TB(y-X\beta)}{2\sigma^4}$$

$$\frac{2\sigma^4.n\sigma^2}{2\sigma^4}=(y-X\beta)^TB^TB(y-X\beta)$$

$$\sigma^2=\frac{1}{n}(y-X\beta)^TB^TB(y-X\beta)$$

So, the varians estimator as:

$$\hat{\sigma}^2=\frac{1}{n}(y-X\beta)^TB^TB(y-X\beta)$$

Substitusing $B=I-\lambda W_2$

$$\hat{\sigma}^2=\frac{1}{n}((I-\lambda W_2)(y-X\beta))^T(I-\lambda W_2)(y-X\beta)$$

So, in many ways the ML estimate is similar to the EGLS approach.

4. Conclusion

From the description that has been discussed in chapter three, it can be concluded as follows:

1. Estimator β of spatial regression error with EGLS method is

   $$\hat{\beta}=b_{EGLS}=(X^TB^TBX)^{-1}X^TB^TBy$$

   And the estimator β for each observation location is

   $$\hat{\beta}=(X^T(I-\lambda W_2)^T(I-\lambda W_2)X)^{-1}X^T(I-\lambda W_2)^T(I-\lambda W_2)y$$

   Estimator that is unbias and efficient, so it is a consistent estimator.

2. Variance estimator (σ^2) of the spatial regression error with EGLS method is

   $$\hat{\sigma}^2=\frac{1}{n}(y-X\beta)^TB^TB(y-X\beta)$$

   And the estimator σ^2 for each observation location is

   $$\hat{\sigma}^2=\frac{1}{n}((I-\lambda W_2)(y-X\beta))^T(I-\lambda W_2)(y-X\beta)$$

5. Acknowledgement

The first author thank to Allah swt., parents, friends, and supervisor (Sri Harini, M.Si and Abdul Aziz, M.Si), thank you very much for the knowledge hence it makes her more knowledgeable about this paper. There is also a man who has been a motivator in her life. and hopefully the authors hope this research can provide benefits.

6. References

[1]. Anselin, L., (1988). Spatial Econometrics: Methods and Models. Dordrecht: Kluwer Academics Publishers.
[2]. Azis, A., (2007), Ekonometrika. Malang: Kantor Jaminan Mutu UIN Malang
[3]. Gujarati, D. (2010), Dasar-dasar Ekonometrika. Penaerbit Salemba Empat: Jakarta
[4]. Murray and Larry (2007), Statistik Edisi ke 3. Jakarta: Erlangga
[5]. Sembiring (1995), Analisis Regresi. Bandung: Penerbit ITB
[6]. Walpole, E Ronald dan Myers, Raymond. (1995), Ilmu Peluang dan Statistik untuk Insinyur dan Ilmuwan. Bandung: ITB Bandung

The Determination of Skin Resistance Coefficient of Apples Respect To O_2 and CO_2 Exchange Using SF_6 Gas as a Tracer By a CO_2 Laser Photoacoustic Spectroscopy Method

M.A.J. Wasono

Department of Physics, Faculty of Mathematics and Natural Sciences, Gadjah Mada University Yogyakarta, Indonesia (majwasono@gmail.com)

Abstract

Fruit respiration requires oxygen (O_2) and produces carbon dioxide (CO_2). Gas can diffuse through the fruit skin, therefore the internal gas volume of fruit is continuously exchanging gas with the surrounding air. The internal O_2 concentration in fruit is determined by both the diffusion process and the consumption. Gas exchange rate in fruit which is indicated by diffusion or resistance coefficient is not known accurately for some fruits, for instace apple.Gas exchange using the tracer gas sulphur-hexafluoride (SF_6) which is biologically inert have been studied by a CO_2- laser based photoacoustic (PA) detection system. SF_6 has a very strong absorption band in the infrared wavelength region of the CO_2 laser i.e. absorption coefficient at 10P16 is 560 cm^{-1}atm. Its concentration can be measured on-line, on a time scale of minutes. The lowest concentration which still can be detected by photoacoustic spectrometer according to the absorption spectrum of SF_6 is 74 ± 4 ppt. The spectrometer has been used to measure the resistance coefficient of apple skin (Rome beauty apple). The non-intrusive measurement method was performed by two cases of experiments which are the measurement of skin resistance coefficient from intact apple with an assumption that the pulp did not give contribution to the whole resistance and the measurement of skin resistance coefficient from fruit skin directly. The measurement results for the skin resistance coefficient from the both experiments are ($\rho_s \pm \Delta\rho_s$) = 1.56 ± 0.09 x10^4 s cm^{-1} and ($\rho_s \pm \Delta\ \rho_s$) = 1.4 ± 0.3 x$10^4$ s cm^{-1}, respectively. Comparing the resistances resulting from each of the two cases, the ratio between the skin and the pulp resistance was found. For the investigated apple we found a contribution of the pulp resistance to the total gas exchange resistance of 10%. Hence we can recomend the result to post harvest conservation of fruit.

Keywords: *Photoacoustic, Gas exchange, Apple fruit, Diffusion.*

1. Introduction

Gas exchange by apple is determined by the skin and pulp permeability for gas. A gas like oxygen is required in the metabolic processes of a cell and it diffuses from outside the fruit through the skin into pulp. If the pulp is impenetrable for gas onlycells in the peripheryof the appleare supplied with oxygen while the cell in the core experience anoixc gas conditions. Metabolic processes determine fruit storage because the provide energy to the cells for maintenance. Therefore, metabolic processes are determined by the gas transport properties of the fruit.

Measurements of the gas transport properties of appels were reported in which the internal diffusion was neglected [1-4]. This was justified because the internal gas fraction in apple was 20 – 30% which caused the interval diffusion to be a fast process. The apple could then be assumed to be hollow with only the skin resistance determining the gas exchange.

Instead of measuring the skin resistance we like to know the influence of the internal diffusion resistance to the gas exchange i.e. we like to know the concentration gradient in the apple during gas exchange. A low internal concentration gradient make the metabolic in the fruit uniform. Cameron and Yang [5] and Bank [1] provide methods to measure the skin resistance, but this is insufficient because the combination of skin resistance and internal resistance determine the internal concentraton gradient. Rajapakse et al [6] determined the internal concentration gradient by extracting gas sample from the core and just below the fruit skin for Asian pears. He reported that 15 to 30% of the concentration gradient between the pear core and outside was caused by the pulp but the internal gas volume of the Asian pears was only 1.7 to 2.5% (the pear type were Hosui and Kosui). In this research, the internal concentration gradient of apple (Rome beauty) would be identified by the difference in gas exchange time, when measured at different positions on the fruit (called normalized difference).

The normalized difference is a measure for the internal concentration gradient, the gas exchange time itself measure for the combined skin and pulpresistence of the fruit. During ripening the internal resistence of the apple increases. During ripening the cell membranes in the fruit break down and the inter-cellular space in the fruit are filled with the cell content [6-7]. The gas exchange time is therefore used to following fruit ripening. An additional advantage of using the gas exchange time is that the fruit does not need to be enclosed in a cuvette. Ripening of fruit can therefore be determined in relation to conditions in bulk storage [8]. In this reesearch, the resistance coefficient of apple fruit would be determined by a CO_2 laser- based photoacoustic detection system using SF_6 gas as a tracer.

2.Experimental Details

A diagram of the complete set up is shown in Figure 1.

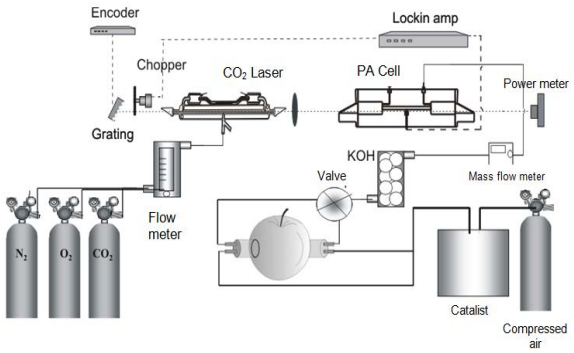

Figure 1. A diagram of photoacoustic spectrometer based on CO_2 Laser coupled with continous flow through system

The wave guide type CO_2 laser emitted approximately 16 lines in the 9 and 11um bands with an output power between 0.1 and 0.4W depending on the emitted laser transition. The step tuning is performed by the adjusment of anguler orientation of the grating which exhibits 150 lines per mm. The CO_2 laser output radiation is intensity modulated by a SRS 540 mechanical chopper operated at the acoustic resonance frequency of the photoacoustic cell. The laser power is measured with an OPHIR 10A power meter.

The apple fruit (Rome beauty species) is from Batu Malang East Java. The fruit was loaded with SF_6 at room temperature in a closed cuvette was 0.5% and the apple was exposed for 24 hours. The SF_6 does not affect the apple, since SF_6 is neither toxic nor bioactive. After taking the apple out of the cuvette, two small collectors, each recording the amount of SF_6 emitted at that point. The collectors were positioned at the apple's widest diameter (Figure 2). The air flowing into the collector came from a bottle with compressed air.

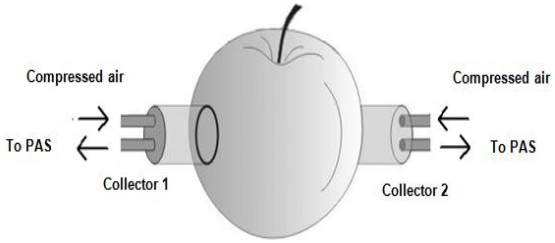

Figure 2. Measuring the gas exchange time using collectors, plays againts the apple skin

An air flow, adjusted with the flow controls, took the tracer gas emitted by the apple, to a PAS. Two collector were used to monitor differences in the two sides of the apple.

The SF_6 emitted from this cuvette diffuse into the apple through the pulp, and was eventually emitted again through the skin. The collectors then detected the local SF_6 emission. The determination of SF_6 concentration is based on the SF_6 absorption at 10P14 and 10P16 laser line.

A rather straight forward alternative measurement of the skin resistance is by measuring the diffusion flux through a piece of skin (Figure 3). This piece was cut with a knife from an apple. This piece of apple skin was sealed at the skin side to a collector using silicon grease. A carrier air flow of 1l/h flow through the collector to the PA detector. To the other side of the skin a calibrated mixture of 0.5% ppm SF_6 in nitrogen was applied.

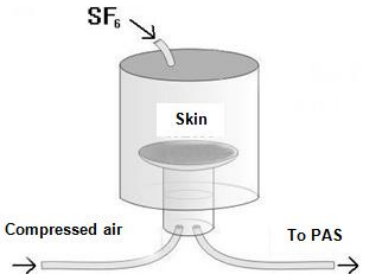

Figure 3. Experimental setup to measure the diffusion resistance through a piece of apple skin

3. Result and Discussion

In order to trace a certain gas amidst an unknown mixture we must be able to recognize the gas. The standart spectrume of the gas, obtained by measuring the absorption as function

of the CO_2 laser wavelength, can be used for that purpose and acts as a fingerprint. SF_6 is known very strong absorption at the 10P16 line. The absoption spectrum of 0.5% SF_6 in nitrogene with respect to CO_2 laser line is shown in Figure 4.

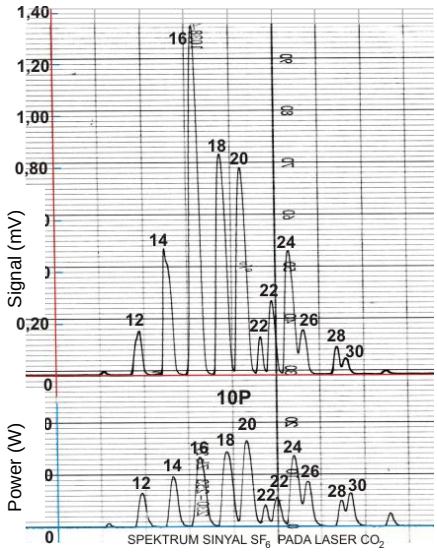

Figure 4. PA signal at 10P group laser lines of 0.5% SF_6 in nitrogen. Strongest absorption occure at 10P16

The PA Spectrometer permits measurement under the lowest detection limit for SF_6 in Nitrogen as low as 74 ± 4 *ppt* (ppt = 10^{-12}) which corresponds to a minimum absortion coefisient of 13 x 10^{-10} cm^{-1} for 1 Hz detection bandwidth. The half response time was found to be 1.2 minute. From the physically results the spectrometer has been applied to monitor SF_6 emmiting by apple fruit.

SF_6 gas emission measurements on intact apples are done by using two collectors installed on the widest diameter on both sides of apples. Observations SF_6 tracer gas emissions at the apple of both collectors over 260 minutes indicated by the Figure 5.

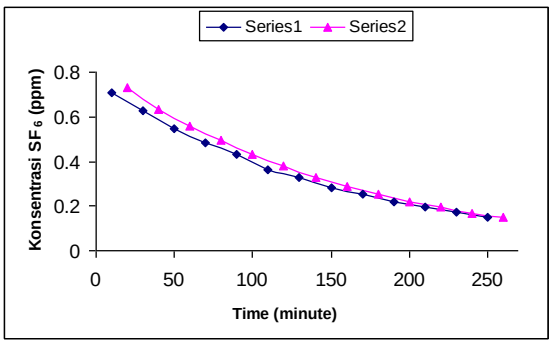

Figure 5. SF_6 emissions in apples from both collectors for 240 minutes

Series 1 shows emissions of SF_6 in the collector 1 while series 2 shows the emission of SF_6 in the collector 2. The time of gas exchange of apple fruit under investigated through two collectors are shown in Figure 6.

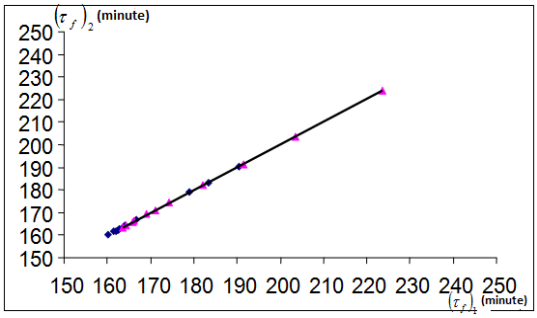

Figure 6. The time of gas exchange for collector 1 vs for collector 2

We can see that the gas exchange time in two relatively equal collectors which is shown by a very small deviation from the line above the curve. It's difference was found normal ($\Delta_{n.g}$) of 0015 or 1.5%. Due to normal differences of small value then it is assumed that the resistance which plays a role in gas exchange is just the skin alone is not the fruit flesh. Retrieved gas exchange time of this experiment was ($\tau_f \pm \Delta \tau_f$) = 153 ± 5 minute.

Rome Beauty apple samples examined in this experiment has a mass 160 ± 5 g, volume 280 ± 5 ml and the largest diameter 26.3 ± 0.1 cm. From the dimensions of the apple samples obtained internal gas fraction value θ_f = 0.46 ± 0.02. From the calculation, it is obtained the skin resistance value ρ_s = 1.56 ± 0.09 x10^4 sec cm^{-1}.

The coefficient of resistance in apple fruit skin can also be determined by investigating the diffusion of gas directly on the skin of apples. SF_6 gas emissions directly through the skin of apple fruit are shown by Figure 7.

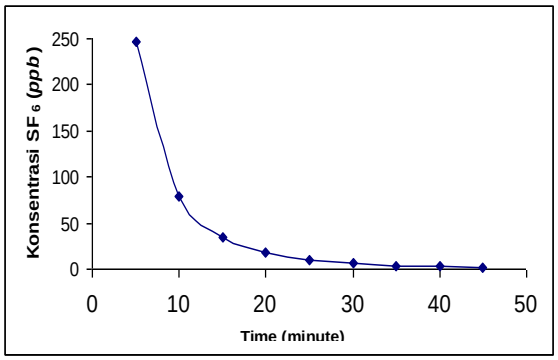

Figure 7. SF_6 emissions in apple skin for 45 minutes

The decrease exponentially concentration of SF_6 gas is used to determine the coefficient of resistance of apple fruit skin. By linearized the curve (Figure 7) the result is shown in Figure 8.

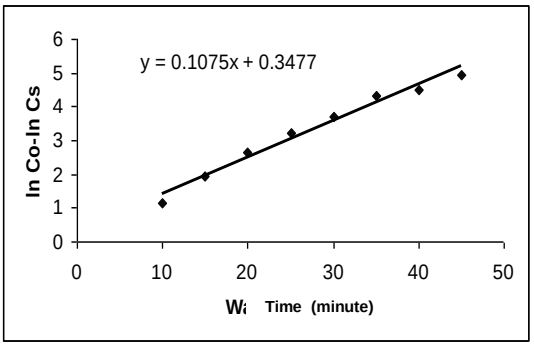

Figure 8. Relationship between $\ln C_0 - \ln C_s$ vs time (t)

Apple skin samples examined in this experiment has a surface area 1.1 ± 0.1 cm^2 and the volume 0.045 ± 0.008 cm^3. The amount of skin resistance Rome Beauty apples kind of SF_6 gas diffusion when calculated on a straight-value ($\rho_s \pm \Delta \rho_s$) = 1.4 ± 0.3 x10^4 sec cm^{-1}. From the two studies performed determining skin resistance is obtained in the form of skin resistance value is almost the same. This shows that the resistance of apple fruit skin can be investigated by using both methods, namely the measurement of whole fruit as well as direct measurements on a piece of skin. Apples used in both experiments should be the same fruit, then the determination of skin resistance of the skin of apple fruit directly used live longer.

4. Conclusion

From the research, it can be concluded that the CO_2 laser photoacoustic detection system can be used to detect gas in a very small order of up to ppt (parts per trillion). This was stated by the lowest detection limit of this system that is equal to 74 ± 4 ppt for SF_6 gas molecules in the nitogen. From the first experiments performed skin resistance coefficient values obtained for ρs = 1.56 ± 0.09 x10^4 sec cm^{-1} and ρs =1.4 ± 0.3 x10^4 sec cm^{-1}.

Comparing the resistances resulting from each of the two cases, the ratio between the skin and the pulp resistance was found. For the investigated apple we found a contribution of the pulp resistance to the total gas exchange resistance of 10%. Hence we can recomend the result to post harvest conservation of fruit.

5. Acknowledgment

---

6. References

[1]. Banks, N.H., (1985), Estimating Skin Resistance to Gas Diffusion in Apples and Potatoes, *Journal of Experimental Botany*, 36, (173), 1842-1850.

[2]. Burg, S.P and Burg, E.A. (1965), Gas Exchange in fruit, *Phsyologia Plantarum* 18,870-884.

[3]. Knee, M., (1991), Rapid measurement of diffusion of gas through the skin of apple fruits, *Hortscience* 26 (7), 885- 887.

[4]. Peppelendbos, H. W. and Jeksrud, W. K., (1998), A Method for the simultaneous measurement of gas exchange and diffusion resistance under various gas condition, *Acta Holtikulturae*, 464, Phostharvest 96, 333-338.

[5]. Chameron, A.C. and Yang, S. F., (1982), A Simple method for the determination of resistance to gas diffusion in plant organs, *Plant Physiology,* 70, 21-23.

[6]. Rajapakse, N., C., Banks, N. H., Hewett, E. W., and Cleland, D. J., (1980), Development of oxygen concentration gradient in flesh tissues of bulky plant organs, *Journal of the American Society for Horticultural Science,* 115 (5), 793-797.

[7]. Kader, A. A., Zagory, D., and Kerbel, E. L., (1989), Modified atmosphere packing of fruits and vegetables, *CRC Critical Reviews in Food Science and Nutrition*, 28, 1 – 30.

[8]. Groot, T., 2002, *Trace Gas Exchange by Rice, Soil and Pears: A Study based on Laser Photoacoustic*, Nijmegen Universiy, Netherland.

Effect of Annealing on the Crystallization and Hysteresis Loop of $Pt/TiO_2/Si(100)/PZT/Au$ Structures

Masruroh

Department of Physics, Faculty of Mathematics and Natural Sciences, Brawijaya University, Malang, Indonesia (rafizen_02@yahoo.com)

Abstract

PZT films were grown on the $Pt/TiO_2/Si(100)$ substrate by low temperature metal-organic chemical vapor deposition (MOCVD), at temperature as low as 380°C. The effects of the annealing treatment by conventional furnace annealing (CFA) on the structural and electrical properties of PZT films were investigated. After the annealing treatment, x-ray diffraction analysis showed that the PZT films were transformed into polycrystalline with partial preferred (100/001) orientation. Moreover, the crystallinity of the (100/001) oriented crystal PZT films were increased by the increases in the temperature of annealing. The ferroelectricity of the PZT films was obviously related to the grain size of the films, such that the remnant polarization ($2Pr$) increased when the grain size is increased. Good ferroelectric properties of PZT were obtained at temperature annealing of 590°C for 20 min. A typical value of remnant polarization ($2Pr$) was 24.80 $\mu C/cm^2$, when the applied voltage was ± 5V, and the leakage current density of the PZT films was 1.697×10^{-5} A/cm^2 at ± 5V.

Keywords: *PZT films, MOCVD, annealing treatment, crystallinity, ferroelectric properties.*

1. Introduction

Ferroelectric thin films based on lead zirconate titanate, $Pb(Zr,Ti)O_3$, have a strong impact for a large number of technological applications, including obviously ferroelectric memory devices [1-3]. These applications are due to the excellent properties of these films, such as high dielectric constants, high remnant polarization and large piezoelectric coefficients. The properties of the PZT films depend on many parameters, including composition, crystal structure, substrate films, film thickness and electrodes. In addition, the composition (Zr/Ti) ratio and crystal orientation, which significantly control the properties of PZT bulk, film thickness and film substrate interface, are also critical for improving the performance of PZT thin films [4].

Many techniques are being investigated for the growth of PZT thin films, including RF-sputtering, laser ablation, sol gel and metal organic chemical vapor deposition (MOCVD). Among these methods, MOCVD is one of the most promising methods because it can achieve low temperature deposition of ferroelectric thin films [5].

Thin film deposition of ferroelectric materials at low temperature is very important in the process integration of FeRAMS, in order to prevent the degradation of ferroelectric thin films and of the ferroelectric/semiconductor interface caused by mutual diffusion and thermal damage [6].

In this study, in order to perform the low-temperature MOCVD of ferroelectric PZT films, we demonstrated the low-MOCVD of PZT at a temperature susceptor of 380°C with applying the low-pressure method using surface reaction. The PZT films were annealed over a temperature range from 550°C to 650°C for 20 min by conventional furnace annealing (CFA) in order to improve the crystallographic and electrical properties. Moreover, the effects of annealing on the structural and electrical properties of the PZT films were also investigated and reported.

2. Experiments

An 80-nm- thick PZT films were grown on the $Pt/TiO_2/Si(100)$ substrate using a liquid delivery metal organic chemical vapor deposition (MOCVD) system named ″Doctor T″ developed by Yamagata University and WACOM R&D Corporation. This MOCVD system features a novel instantaneous vaporizer and has excellent stability for depositing homogeneous films for large wafers. In order to perform the low-temperature MOCVD of ferroelectric PZT films, we demonstrated the low temperature-MOCVD of PZT films at temperature susceptor of 380°C with total pressure of 533 Pa. The source precursors used were $Pb(DMAMP)_2$: 0.232 ccm,

$Zr(MMP)_4$: 0.148 ccm, and $T(MMP)_4$: 0.090 ccm and oxygen (O_2) and argon (Ar) were used as the oxidizing gas and carrier gas, respectively.

For electrical characterization of the thin films, gold top electrodes were applied to the film surfaces using a shadow masking evaporation method. The top electrode structures were patterned with circles using a shadow mask with a diameter of 300 □m. The films were annealed by a CFA from 550°C to 650°C for 20 min in an O_2 atmosphere in order to crystallize the PZT films in the ferroelectric phase. X-ray diffraction (RAD-γ A type, Rigaku denki Co. Ltd.) with CuKα radiation was used to examine the crystal orientation of the PZT films. The polarization as a function of voltage (P-V) was measured as deposited and after performing a thermal annealing process. A ferroelectric test system (Precision LC Radiant Technology) was used to measure their electrical properties by the drive terminal bottom electrode (Pt) was connected to the drive of the precision LC. All measurements were carried out at the room temperature.

3. Result and Discussion

The effects of the different annealing processes on the structure PZT thin film were characterized by x-ray diffraction (XRD). Figure 1 shows the XRD pattern of the PZT films as deposited and after annealing over the temperature range from 550 to 650°C at 20 min. The as-deposited PZT films shows a broad peak of (100) oriented crystal, whereas the (001) oriented crystal was obvious after annealing; both oriented crystal of (100) and (001) were improved by raising the temperature of annealing, and the films annealed at 590°C for 20 min had an obvious larger peak for (100).

Figure 2 shows the ferroelectric hysteresis loops dependence on the crystallization conditions. The P-V hysteresis loops were measured at a frequency of 100 Hz for the sample with an 80-nm PZT thickness and an area of 7.85×10^{-5} cm^2. The P-V hysteresis loops as deposited and annealed at 550°C does not show a ferroelectric hysteresis loops, which is clearly related to the absence of a polycrystalline phase. On the other hand, the P-V hysteresis of the sample annealed from 570°C to 650°C show ferroelectric hysteresis loops. There were considerable changes in the shape of curves and the remnant polarization ($2Pr$) after annealed up to 550°C, where the $2Pr$ of the films increased with increasing annealing temperature, except for the loop at 650°C. The 650°C annealed films became a linear P-V relation (Figure 2d) due to the decreased the peaks of (100) and (001) oriented crystal in the PZT films. However, the hysteresis loops at 570°C (Figure 2a) and 580°C (as shown in Figure 2b) shows paraelectric-like characteristics, but the $2Pr$ and ±Vc indicates improvements with increasing temperature up to 580°C, and the $2Pr$ of each annealed films show 1.128 μC/cm^2 for films annealed at 570°C and 2.386 μC/cm^2 for films annealed at 580°C. The saturated P-V hysteresis is found at a temperature of annealing of 590°C (Figure 2c), and this shows $2Pr$ of about 24.80 μC/cm^2 at an applied voltage of ± 5V.

It is seemed that the ferroelectric properties were dependent on the grain size, thus the $2Pr$ increased when the grain size is increased as listed in Table 1. The grain size (dXRD) was calculated from the FWHM of the (100) and (001) diffraction peak using the Scherrer's equation [5] $d\text{XRD} = K\lambda\beta \cos\theta$ where λ is the X-ray wavelength, β is the FWHM of the diffraction line, θ is the angle of diffraction, and the constant $K = 0.9$. Moreover, the ferroelectric properties are governed by the ferroelectric domain structure, domain nucleation, and domain mobility [7]. The PZT films with larger grain sizes exhibit better ferroelectric properties. Therefore, the film having large grains with a multi-domain-predominated structure can be easily switched leading to large remnant polarization [8].

4. Conclusion

PZT films were deposited on a $Pt/TiO_2/SiO_2/Si(100)$ substrate by low temperature MOCVD, at temperature as low as 380°C, and the effects of annealing treatment by CFA on the structural and electrical properties of PZT films were investigated. The crytallinities of the (100) and (001) oriented crystal PZT films increased with increasing temperature of annealing, except for the PZT films annealed at 650°C. The ferroelectricity of the PZT films was obviously related to the grain size of the films, such that the remnant polarization ($2Pr$) increased when the grain size is increased.

The 590°C annealing temperature for 20 min was an optimal temperature of hot plate annealing conditions for obtaining PZT films of good P-V hysteresis loops and low leakage current density. The $2Pr$ of the PZT thin films obtained under the optimal condition was about 24.80 μC/cm^2, when the applied voltage was ± 5V and the leakage current density of PZT films was about 1.697×10^{-5} A/cm^2 at ± 5V. On the other hand, the 650°C annealed films demonstrated a linear P-V relation

due to the reduction of (100) and (001) PZT oriented crystals.

5. Acknowledgments

The author is grateful to Mr. Fujimoto and Mr. Kosuke OHNO (from Pioneer) for the annealing PZT sample with RTA and XRD measurements, Mr. Yutaka KOJIMA and Mr. M. OHATA from NFT Co., Ltd, and Mr. Scott. P. Chapman and Mr. Joe T. Evans from Radiant Technologies, Inc. for discussion about Radiant Technologies.

6. References

[1]. Antonio Leondino B. J, M. H. Lente, Ricardo G. Mendes, Pedro Iris P. F. and Jose A. E. (2004), *Materials Research*, Vol. 7, No. 2, 363-367,

[2]. Scott, J. F., McMillian, B. M., Araujo, C. A. P. (1998), Ferroelectric Review, V. 1, Gordon and Breach Science Publishers.

[3]. Uchino, K. (2000), Ferroelectrics Devices-Marcels Dekker, Inc

[4]. Chia-Fong CHOU, Han-hang PAN and Chen-Chia CHOU, *Jpn. J. Appl. Phys*. Vol. 41 pp.6679-6681

[5]. Choon-Ho LEE and Sun-II KIM (2002), *Jpn. J. Appl. Phys*. Vol. 41 pp.6701-6704

[6]. Masaru SHIMIZU, Mamoru OKINAWA, Hironori Fujisawa and Hirohiko NIU (2002), *Jpn. J. Appl. Phys*. Vol. 41 pp.6686-6689.

[7]. Hsiu-Yu Chuo, Teng-Ming Chen and Tseung-Yuen Tseng (2003), *Material Chemistry and Physics* Vol. 82 pp. 826-830.

[8]. S.B. Ren, C.J. Lu, J.S. Liu, H.M. Shen, Y.N. Wang (1996), *Phys. Rev*. B 54 R14337.

Appendixes

Table 1. Temperature annealing (TA), grain size (D) and 2 *Pr*

T_A (°C)	D(nm)		$2Pr$
	$I_{(100)}$	$I_{(001)}$	
550	51.496	-	-
570	56.890	27.482	1.128
580	56.792	122.440	2.386
590	56.959	142.986	24.80
650	58.064	81.835	-

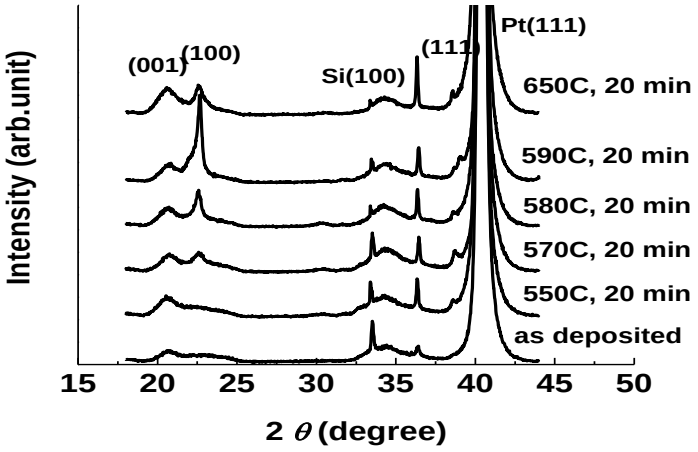

Figure 1. XRD pattern of the PZT films crystallized at different temperature annealing

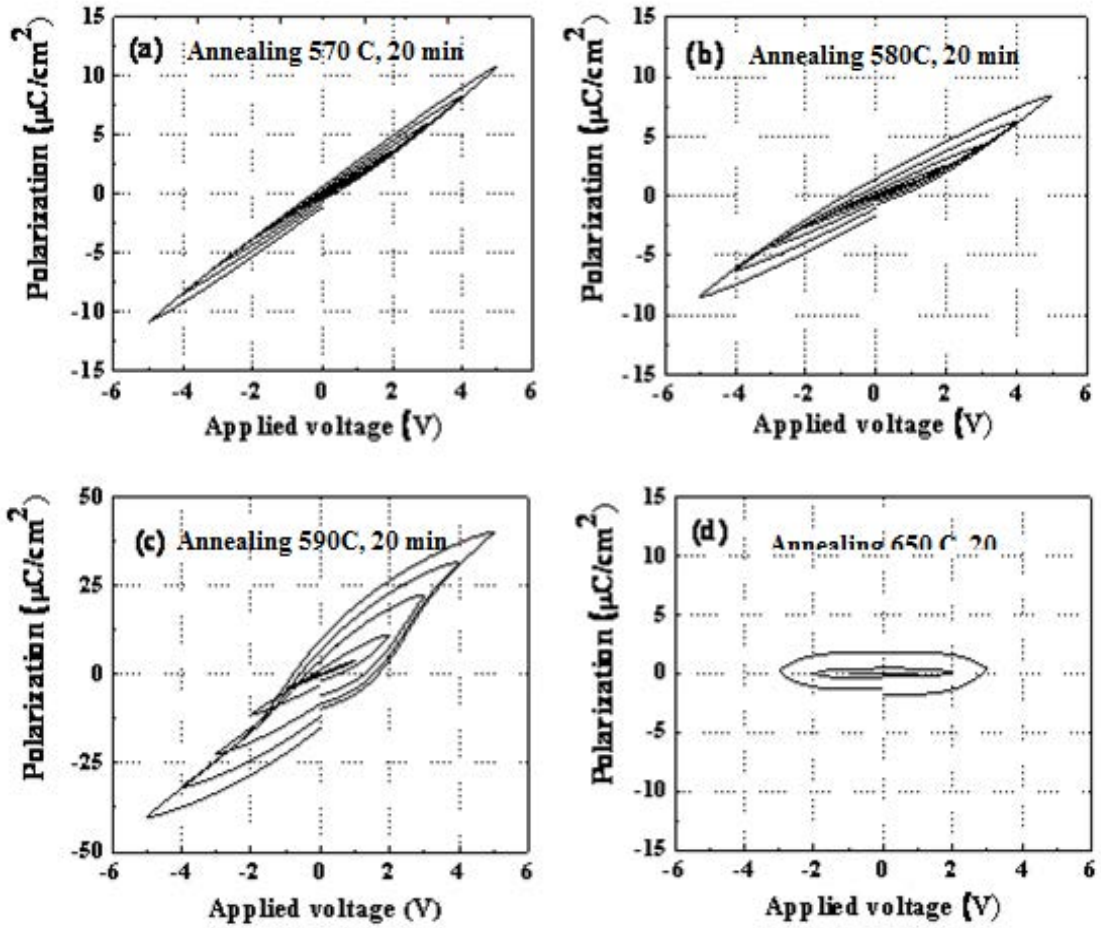

Figure 2. Ferroelectric hysteresis loops dependence on the annealing condition

Resrad Build Code as Supporting Tool to Estimate Radiological Impact from A Concrete Building Material

Moekhamad Alfiyan

Research and Industry Assessment- Nuclear Energy Regulatory Agency (BAPETEN), Jakarta
(m.alfiyan@bapeten.go.id)

Abstract

Building materials is one of natural radiation source because the material from crust earth which is contains naturally radioactive materials with numerous radioactivity levels. Estimation of radiological effect due to concrete building materials to a receptor is described in this paper. This paper relies on the result of RESRAD-BUILD code applying radioactive concentrations in building material from literature. The result shows that received doses by receptor on building center increase in accordance with exposure times. Type of radionuclides which give most contribution to receptor doses is ^{226}Ra, because ^{226}Ra dose effective conversion factor is higher than other. The radiological risk due to ^{226}Ra is $2{,}815.10^{-10}$. It is concluded that radiologic impact to receptor depend on time of exposure to receptor and RESRAD-BUILD code can be used as tool to estimate radiologic effect from building materials.

Keywords: *Radiologic effect, RESRAD – BUILD, receptor.*

1. Introduction

Radiological impact to human is fundamental issue related with nuclear activity, both natural and artificial and the problem is not loss for human live as a reasonable and society consequences. Negative image to nuclear activity has been hampered nuclear application with nuclear accident event to be one of a reason to build public negative.

Basically, radiation has been present in our vicinity as natural radionuclide. It is consist of primordial and cosmic radiation. Primordial radiation is natural radiation occurring together with earth. Based on radiological aspect, essential primordial radionuclide are heavy elements and has a long time decay chain such as uranium series (U-238), actinium series (U-235) and thorium series (Th-232). Cosmic radionuclides are radiounuclides which is derived from reaction between cosmic ray and nucleus in atmosphere, soil and water. In the generally, the radionuclides has low concentration so it need complex procedure for sampling and analyzing. The world wide average, public receive natural radiation exposure and cosmic about 2400 µSv per year. Regarding of assessment results of *United Nations Scientific Committee on the Effects of Atomic Radiation* (UNSCEAR), Public receive external dose from cosmic and land surface is about 840 µSv per year

Therefore, exploitation and resources utilization including building materials for supporting national economic and public prosperity purposes can give add radiation exposure to public, however, public accept it, otherwise nuclear utilization. Resources exploitation including building materials from the earth's crust, dislocation, human action causes the material contains natural radionuclide. Building materials is always present in live us for dwelling place or working place therefore there is radiation exposure in around us.

This paper will explain radiation estimation emanated by building materials by using RESRAD-BUILD code in order to make good opinion to public regarding radiation exposure and to investigate the ability of RESRAD-BUILD code. Another aim of this paper is to complement the previous result of BAPETEN (P2STPFRZR) work, which performed in 2008 on assessment about radioactivity level in drinking water and building material.

Natural Radioactive of Building Materials

Terrestrial radiation exposure, mainly in the form of gamma radiation, is due to so-called primordial radionuclides in the earth crust. Because of their extremely long half-lives, they have existed since the beginning of Earth. Especially potassium 40 and the nuclides of the uranium-radium and thorium series are relevant with respect to radiation exposure of the population. Uranium and thorium disintegrate, via several decay products, to stable lead. One of the

decay products is radon, a naturally occurring radioactive noble gas with a half-life of 3.8 days.

All building materials that originate from minerals always contain a certain amount of radionuclides. These mineral are mainly potassium, uranium, thorium and the radionuclides that are created as their radioactive decay chains. Of these, the most significant is radium (Ra-226). The Ra-226 presence in building materials causes exposure to persons living in dwellings - either by inhalation of radon daughters that decay from radium and release from the building material to indoor air, or by hard gamma radiation that releases from the building material as a consequence of the radioactive decay of the natural radionuclides to be present.

European Union has published activity concentration of some radionuclide in building materials as shown Table 1 (Appendixes). P2STPFRZR-BAPETEN has performed measurement to building materials sample from Indonesia. Activity concentration of radionuclides in the sample is more less than maximum activity concentration in Table 1, concentration activity of Ra-226 and K-40 in cement are about 60.16 Bq/Kg and 120.6, respectively.

Radiation exposure due to building materials can be divided into external and internal exposure. The external exposure is caused by direct gamma radiation. The internal exposure is caused by inhalation of radon (^{222}Rn), thoron (^{220}Th) and their short live decay products. Radon is part of the radioactive decay series of uranium, which is present in building materials. Because radon is an inert gas, it can move rather freely through porous media such as building materials, although usually only a fraction of that produced in the material reaches the surface and enter the indoor air. The most important source of indoor radon is the underlying soil but in some cases and some member state also the building materials may be an important source.

In most cases, the main part of indoor radon on the upper floors of a building originates from building materials. Typical excess indoor radon concentration due to building materials is about 10-20 Bq/m^3, but in some zones and in rare cases it may rise up to greater than 1000 Bq/m^3. Building materials are the most important source of indoor thoron. However, thoron concentrations are usually rather low. Indoor thoron can be an important source of exposure only under some rare conditions where the building materials contain high concentrations of thorium.

Radiation Protection Principles

The purpose of setting controls on the radioactivity of building materials is to limit the radiation exposure due to materials with enhanced or elevated levels of natural radionuclides. The doses to the member of the public should be kept as low as reasonably achievable. However, since small exposure from building materials are ubiquitous. Control should be based on exposure level which is above typical level of exposures and their normal variations. The concentrations of natural radionuclides in building materials vary significantly between and within the member states. Investigations may need to be undertaken of the activities in various building materials where such information is not already available from earlier surveys. All building materials contain some natural radioactivity; small, unavoidable exposures need to be exempted from all possible controls. A uniform exemption level within European Union would allow free movement of most building materials within the EU.

Restriction the use certain building material might have significant economical, environmental or social consequences locally and nationally. Such consequences together with national levels of radioactivity in building materials should be assessed and considered when establishing binding regulations. The amount of radium in building materials should be restricted at least to a level where it is unlikely that it could be a major cause for exceeding the design level for indoor radon is 200 Bq/m^3.

Control on the radioactivity of building materials can be based on radioalogical criteria for exclusion. Controls can be based on a lower dose criterion if it is judged that this is desirable and will not lead to impractical controls. Indonesia regulation will decide 0.3 mSv for upper level of dose constraint therefore the building materials not permitted cause doses more than it.

Separate limitations for radon and thoron exhaling from building materials should be considered where previous evaluations show that building materials may be a significant source of indoor radon or thoron and restrictions put on this source is found to be an efficient and a cost effective way to limit exposure to indoor radon or thoron.

Investigation levels can be derived for practical monitoring purposes. Because more than one radionuclide contribute to the dose, it is practical to prevent investigations levels in the form of an activity concentration index. The activity concentration index should also take into

account typical ways and amounts in which the material is used in a building.

Resrad-Build Code

The RESRAD-BUILD computer code is a pathway analysis model developed to evaluate the potential radiological dose incurred by an individual who works or lives in a building contaminated with radioactive material. The radioactive material in the building structure can be released into the indoor air by mechanisms such as diffusion (radon gas and tritiated water), mechanical removal (decontamination activities), or erosion (removable surface contamination). The transport of radioactive material within the building from one compartment to another is calculated with an indoor air quality model. The air quality model evaluates the transport of radioactive dust particulates and radon progeny due to (1) air exchange between compartments and with outdoor air, (2) the deposition and resuspension of particulates, and (3) radioactive decay and ingrowth. RESRAD-BUILD can model up to three compartments in a building, thereby, for example, making it possible to evaluate situations ranging from a one-room warehouse to a three-story house.

The design of RESRAD-BUILD is similar to that of the RESRAD code: the user can construct the exposure scenario by adjusting the input parameters. Typical building exposure scenarios include long-term occupancy (resident and office worker) and short-term occupancy (renovation worker and visitor). The long-term occupancy scenarios are usually low release scenarios, whereas short-term occupancy scenarios may involve a high release of contaminants in a short time period. Up to 10 receptor locations and 10 distinct source locations can be input into the RESRAD-BUILD code to calculate dose in a single run of the code. The calculated dose can be the total (individual) dose to a single receptor spending time at various locations or the total (collective) dose to a workforce decontaminating the building. If a building is demolished, the RESRAD computer code may be used to evaluate the potential dose from the buried material

The RESRAD-BUILD code considers seven exposure pathways: (1) external exposure directly from the source, (2) external exposure to materials deposited on the floor, (3) external exposure due to air submersion, (4) inhalation of airborne radioactive particulates, (5) inhalation of aerosol indoor radon progeny (in the case of the presence of radon predecessors) and tritiated water vapor, (6) inadvertent ingestion of radioactive material directly from the source, and (7) ingestion of materials deposited on the surfaces of the building compartments.

The radionuclides included in the RESRAD-BUILD code are similar to those included in the RESRAD code. Currently, the RESRAD-BUILD database contains 67 radionuclides, and additional radionuclides are being added. All these radionuclides have a half-life of six months or longer, and they are referred to as principal radionuclides. It is assumed that the short-lived decay products with half-lives of six months or less, referred to as the associated radionuclides, are in secular equilibrium with their parent (principal) radionuclides. For the 67 principal radionuclides in the current RESRAD-BUILD database, there are 53 associated radionuclides. Therefore, a total of 120 radionuclides are available in RESRAD-BUILD Version 3.

2. Experimental Detail

Arranging of this paper was done through review of national and international literatures and RESRAD-BUILD code simulation. The main literature used is international recommendation related with radioactivity into building materials. Aim of the review is to identify type and activity concentrations of radionuclides appropriately into building materials which are used as input parameters of RESRAD-BUILD code to get good result and suit with existing condition. The next step, the simulation result is analyzed to provide radiological determination with the output. The last step of this paper arranging is report composing.

3. Result and Discussion

Simulation of RESRAD-BUILD code take main assumption that a resident of a building are formed by concrete with dimension 6 m x 6 m x 2.5 m. Those concrete walls assumed as contamination source in the simulation. The simulation takes some other assumption as followed:

1. Type of building materials is concrete with activity concentrations level such as maximum activity concentrations in Table 1. The assumption is considered very conservative so worst case can be estimated.
2. Receptor located in centre of the building (3 m, 3 m, 0m)
3. Exposure velocity is 365 days in year
4. Indoor fraction of the receptor is 0,6
5. Receptor does not use shielding
6. Contamination source is square with size 6 m x 2,5m

7. There are no radon and other radionuclides inhalation.
8. Exposure time are designed for 1, 10, dan 20 dan 30 years.

The simulation results indicate that doses is received receptor will increase with add of exposure time, but the increasing is not significant. The result is shown by Table 2 (Appendixes). Dose at t=0 until t<1 year show dose is received by receptor at t=0 until t<1 year. The dose is only from external radiation because the simulation doesn't include radon exposure, inhalation and ingestion.

Dose is received by receptor still below dose constrain, is 0.3 mSv/a, however the dose don't show dose total received by receptor from all natural exposure, but only exposure from designed building materials.

The main radionuclide are simulated include ^{232} Th, ^{226}Ra and ^{40}K while ^{228}Th and ^{228}Ra are ^{232} Th daughters, and ^{210}Pb is ^{226}Ra daughter. In Table 2 can be seen that ^{226}Ra give greatest contribution to receptor total dose. Although initial concentration of ^{226}Ra is simulated less than initial concentration of ^{40}K, however, equivalent effective dose conversion factor for external exposure (DCF) of ^{226}Ra is higher than ^{40}K, equivalent effective dose conversion factor for external exposure (DCF) of ^{226}Ra is 1.94 mRem/a/pCi/cm^2, ^{40}K = 0.171 mRem/a/pCi/cm^2 and ^{232}Th = $6.45.10^{-4}$ mRem/a/pCi/cm^2. Exposure dose is emanated by ^{232} Th and ^{40}K tends to stable, because half live of ^{232} Th and ^{40}K is very long time are 1, 405.10^{10} years for ^{226}Th and $1.28.10^{9}$ years for ^{40}K, respectively.

Risk of receptor in building materials receive dose as in Table 2 will increase in accordance with progressively increasing the residence time. This condition is realistic that the longer a one occupy radioactive contaminant source so the higher risk a one receive exposure from the contaminant source. Risk of receptor resident in the building for 30 years will receive exposure dose 3.30E-02 ± 4.63E-03 is 2.51E-06. Risk level of receptor receive dose total every year is given in Figure 1.

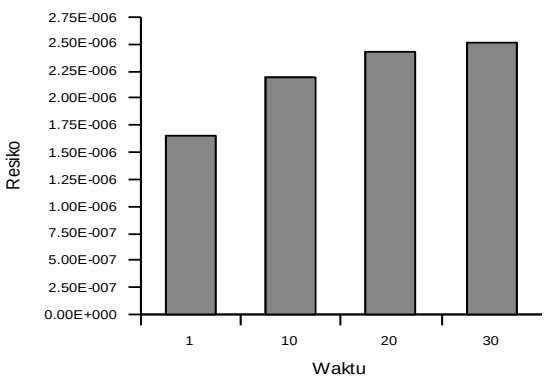

Figure 1. Exposure Risk Levels are received by Receptor

4. Conclusion

1. The result of RESRAD-BUILD code simulation to a receptor in a building with the wall from square concrete contain ^{226}Ra, ^{232} Th, ^{40}K radionuclides will receive dose to receptor below dose criterion so intervention to the building is not needed.
2. ^{226}Ra radionuclide is radionuclide that gives greatest contribution to receptor dose, although initial concentration of radium is more less than ^{40}K due to individual effective dose conversion factor for external radiation of ^{226}Ra is higher than ^{40}K.
3. Receptor risk to receive dose from building is higher in accordance time in building. The risk after exposure during 30 years is 2.51E-06 with the dose is received by receptor is 3.30E-02 ± 4.63E-03.

5. Acknowledgments

---

6. References

[1]. European Commission (1999), Radiological Protection Principles Concerning the Natural Radioactivity of Building Materials, Radiation Protection 112, Directorate-General Environment, Nuclear Safety and Civil Protection

[2]. C-Yu (2008) User's Manual for RESRAD-BUILD Version 3, Argonne National Laboratory.

[3]. P2STPFRZR-BAPETEN (2008), Report of Assessment Result about Radioactivity Level in drinking water and building material

.

Appendix

Table 1. Typical and maximum activity concentrations in common building materials and industrial by-products used for building materials in the EU.

Material	Typical Activity Concentration (Bq/Kg)			Maximum Activity Concentration (Bq/Kg)		
Most common building materials (may include by-product)	^{226}Ra	^{232}Th	^{40}K	^{226}Ra	^{232}Th	^{40}K
Concrete	40	30	400	240	190	1600
Aerated and light-weight concrete	60	40	430	2600	190	1600
Clay (red) bricks	50	50	670	200	200	2000
Sand-lime bricks	10	10	330	25	30	700
Natural Building Stones	60	60	640	500	310	4000
Natural gypsum	10	10	80	70	100	200
Most common industrial by-products used in building materials						
By-product gypsum (Phospogypsum)	390	20	60	1100	160	300
Blast furnace slag	270	70	240	2100	340	1000
Coal fly ash	180	100	650	1100	300	1500

Source: European Commission, 1999

.

Table 2. Total Dose is received by receptor due to building materials exposure and magnitude of each radionuclide contribution to total dose of RESRAD-BUILD simulation results.

Years	Dose (mSv)	Dose Contribution of Each Radionuclides (mSv)					
		^{232}Th	^{228}Th	^{228}Ra	^{226}Ra	^{210}Pb	^{40}K
0	2.09E-02 ± 2.92E-03	4.8 E-06	4.96 E-05	2.96 E-04	1.14 E-02	6.00 E-06	9.12 E-03
1	2.17E-02 ± 3.04E-03	4.8 E-06	3.03 E-04	8.40 E-04	1.14 E-02	1.78 E-05	9.12 E-03
10	2.88E-02 ± 4.04E-03	4.8 E-06	4.48 E-03	3.66 E-03	1.14 E-02	1.78 E-05	9.12 E-03
20	3.20E-02 ± 4.49E-03	4.8 E-06	6.68 E-03	4.68 E-03	1.13 E-02	1.83 E-04	9.12 E-03
30	3.30E-02 ± 4.63E-03	4.8 E-06	7.36 E-03	4.96 E-03	1.13 E-02	2.38 E-04	9.12 E-03

Microparticulated Whey Protein Concentrate (Wpc)-Low Metoxyl Pectin (Lmp) Complexes under Different Acidic Environment: A Rheology and Confocal Laser Scanning Microscopy (Clsm) Studies

Mokhamad Nur [1], Todor Vasiljevic [2], Nicoleta Dragomir [2]

[(1)]) Dept. of Agricultural Product Technology, University of Brawijaya, Malang
[(2)] School of Biomedical and Health Science, Victoria University, Melbourne Email: mnur@ub.ac.id

Abstract

Milk whey protein is liquid waste released during the course of cheese processing and contains valuable components such as β-lactoglobulin (β-lg), α-lactalbumin and bovine serum albumin (which account for the 70% of total whey proteins) (Perez, Carrara, Sánchez, Santiago & Rodríguez Patino, 2009). The microparticulated of whey protein is expected could protect the functional properties of whey juices. However, during the course of WPC manufacturing, the heat treatment given prior to processing may denature the solubility of the protein and other functional properties. The use of low metoxyl pectin to protect this problem is expected. It will avoid the protein denaturation of WPC. However, the implementation of the WPC – LMP complexes in the food formulation may face several problems. The presents of protein and polysaccharide become the main hindrance (Mishra, Mann & Joshi, 2001). Pre-treated WPCs were used in this study: 1) Control (Original pH); 2) pH 3; 3) pH3 and microfluidization and 4) pH3, microfluidization and heat treatment. The objectives of this study were: i) to study the effect of different pre-treatment of WPC, mixture concentration and pH on microstructure properties of biopolymer mixture of pectin and WPC ii) to study the phase separation behavior of two mixtures of biopolymers iii) to investigate the thermal properties of WPC/LM-pectin mixture during different acidic pH (pH 3 and 4) and pre-treatment of WPC. The experiment showed that lowering pH resulted in weaker gels that broke at very low shear rate likely due to incompatibility between two biopolymers. Higher concentrations of these biopolymers resulted in stronger gels. Whey proteins created water in water emulsions with pectin being continuous phase. Whey proteins created fibrilar forms at low pH mainly after microfluidization.

Keywords: *Rheology, Protein-Polysaccharide Interaction, Phase Separation, Whey Protein, Pectin, CLSM.*

Comparison of Three Spatial Analyses in a Randomized Complete Block Design

Mohammad Masjkur

Department of Statistics, Faculty of Sciences, IPB, Bogor, Indonesia (masjkur@ipb.ac.id)

Abstract

Agricultural field trials generally need controlling a soil spatial heterogeneity. The traditional way commonly used for controlling experimental local is a blocking. However, if the soil spatial heterogeneity exists within blocks, the error variation could be inflated and independence assumption of error could be violated. An alternative method for controlling experimental local is a spatial approach. Efficiency of a spatial approach to a randomized complete block design has been widely studied; however it remains difficult to determine which spatial methods that are appropriate for certain experimental conditions. The objective of this study was to compare the efficiency of three spatial analyses, a nearest neighbor approach (NNA), a polynomial trend regression (PTR), and a first-order autoregressive model (AR1) in a randomized complete block design on rice fertilization experiment. The study is expected to support the advancement of experimental design. The research used field trials data of rice fertilization in Karawang and Kebumen region. In Karawang area, fertilizer treatments consist of fourteen levels of fertilizer type, while in Kebumen area consists of twelve levels of fertilizer type with three replications, respectively. In Kebumen region the research was conducted over two growing seasons. The experiment used a randomized complete block design (RCBD). The results showed that the nearest neighbor covariance, polynomial trend and AR1 approaches reduce error variation in average of 70, 53 and 8 percent respectively compared with the randomized complete block design. However, the amount of reduction varied among trials. Use of a spatial nearest neighbor approach increased the level of significance of treatment effects in all trials, while a polynomial trend regression and an AR1 increased the level of significance only in Karawang and Kebumen1, respectively. Therefore, a nearest neighborur approach was more efficient than a polynomial trend regression and an AR1 and also than a RCBD only.

***Keywords**: soil spatial heterogeneity, blocking, nearest neighbor, polynomial trend, AR1.*

1. Introduction

Field trials in agriculture are generally necessary to control the spatial heterogeneity of soil. This is done to reduce error variation and estimate treatment effects more accurate. Soil spatial variability occurs due to influence of natural factors of geological, hydrological or biological and management factors such as fertilization [5, 6].

Common traditional way for local control experiment is a blocking, either one-way or multi-directional. The expectation is that conditions in the experimental area within blocks were relatively homogeneous. The design corresponding to the blocking in one direction is called a randomized block design. The design commonly used in agricultural experiments because of simple implementation. Nevertheless, in recent years use of such methods has been evaluated along with the development of intensive and site-specific farming.

Randomized block design assumes that model errors within blocks distributed independently and identically with the same variance. If spatial variability exists within block, error variation could be inflated and independence assumption of error could be violated [3]. Spatial homogeneity within blocks of more than 8 to 12 plots seldom occurs in field trials. Spatial heterogeneity may persist in small blocks such as a lattice or an α-design [7].

Nowadays, there has been a considerable interest in the use of spatial methods as an alternative methods for local control. The method is based on the assumption that the yield of a plot is closely related to the yields from nearest neighbor plots because of a positive correlation between soil fertility from adjacent plots. Spatial methods commonly used are a nearest neighbor approach, a polynomial trend regression, and a first-order autoregressive model (AR1) [1, 2, 4, 5,7].

Efficiency of spatial methods to a randomized block design has been widely studied. However, it remains difficult to determine which spatial methods that are appropriate for certain experimental conditions. The nearest neighbor approach combined with a randomized block design reduces standard error of treatment means and increases the level of significance of treatment effects [1]. In addition, the nearest neighbor approach more effective than the AR1 approach in reducing residual variation [7]. However, a polynomial trend approach was better than a nearest neighbor approach in controlling soil spatial heterogeneity [4].

This study aimed to compare the efficiency of three spatial analyses, a nearest neighbor approach, a polynomial trend regression and a first-order autoregressive model in a randomized complete block design on rice fertilization experiment.

2. Experimental Details

This study used data of rice fertilization experiment in Karawang and Kebumen region. In Karawang area fertilizer treatments consist of fourteen levels of fertilizer type, while in Kebumen area consist of twelve levels of fertilizer type with three replications, respectively. In Kebumen the research was conducted over two growing seasons. The research used a randomized complete block design (RCBD).

Yield data of each trial were analysed by spatial model as,

$$Y_{ij} = \mu + \eta_{k(ij)} + T_{ij} + \varepsilon_{ij}$$

where Y_{ij} is the rice yield (ku/ha) of the *j*th plot and the *i*th block or plot *ij*, the term $\mu + \eta_{k(ij)}$ represents the mean of *k*th fertilizer effect on plot *ij*, T_{ij} reperesents spatial variability effect on that plot, and ε_{ij} is a random error. The basic model is RCBD variance analysis. In this case, the spatial effect T_{ij} were assumed to be constant for all plot within the same block, that is $T_{ij} = \beta_i$ (the *i*th block effect).

The nearest neighbor covariance analysis (NNA) used papadakis procedure to account spatial effect of neighboring plot, where block effect β_i was preserved. Therefore the term $T_{ij} + \varepsilon_{ij}$ in above equation becomes $\beta_i + bX_{ij} + e_{ij}$ in NNA analysis, where X_{ij} = spatial covariance, b = regression coefficient for X_{ij} and $e_{ij} = Y_{ij} - Y_k$ where Y_k was fertilizer effect mean on plot *ij*. Value $X_{ij} = e_{ij} - (e_{i,j-1(r)} + e_{i,j-1(c)} + e_{i,j+1(r)} + e_{i,j+1(c)}/4)$. Position of four neighboring plot were on the left side, right side, above and below of the plot, respectively.

The polynomial trend regression (PTR) analysis used least square procedure of general linear model. Thus, the term $T_{ij} + \varepsilon_{ij}$ in above equation becomes $\beta_i + \delta_1 x + \delta_2 y + \delta_3 x^2 + \delta_4 y^2 + \delta_5 xy + e_{ij}$, where δ_i was gradient coefficient for Cartesian coordinates (x,y) of observation Y_{ij}. For the first-order autoregressive approach (AR1) analysis used restricted maximum likelihood procedure of mixed linear model.

Criteria for the efficiency of the NNA or PTR to the RCBD were,

1. The coefficient of variation (CV).
2. Coefficient 1- SSEa/SSEu, where SSEa = Sum Squares Error *(adjusted)*, SSEu = Sum Squares Error *(unadjusted)*.

For a measure of the relative efficiency of the AR1 model to the RCBD was calculated as 1-SEDar1/SEDrcbd where SEDar1 = mean standard error differences across all pairs adjusted means for AR(1) and SEDrcbd = mean standard error differences across all pairs adjusted means for RCBD.

3. Result and Discussions

Nearest neighbor approach (NNA)

The use of nearest neighbor approach reduces the coefficient of variability of the model compared with the RCBD. On the location Karawang CV reduction was 0.53 percent, while on the location Kebumen1 and 2 were 20.79 and 14.1 percent respectively (Table 1). The reduction indicates the higher accuracy of the experiment with the use of this covariance and the magnitudes differ between sites.

Covariance analysis showed that the effect of nearest neighbor covariance was significant on rice yield for all trials (P-value < 0.01) (Table 1). In Karawang or Kebumen1 location where the block effect was significant, the covariance effect was also significant (P value = 0.0058 or <0.0001). For the location Kebumen2 which blocks effect was not significant, covariance effect was significant (P value <0.0001). This result indicates that the blocking alone is not effective in controlling the spatial heterogeneity. Thus spatial covariance needs to be taken into account in addition to the blocking in the analysis of the experiment.

Table 1. Coefficient of variation for the NNA, PTA and RCBD

Location	RCBD	NNA	PTA
Karawang	4.22 0.0032 a 0.6728 c	3.69 0.0058b 0.4607c	2.95 0.0898x - <0.0001x^2 - - 0.1541c
Kebumen1	28.32 0.0059a 0.0102c	7.53 <.0001b <.0001c	30.19 0.7710x 0.3696y 0.3061 x^2 0.6874 y^2 0.7141xy 0.0282c
Kebumen2	24.23 0.3543a 0.0006c	10.13 <.0001b <.0001c	22.59 0.5767x 0.2253y 0.0604 x^2 0.5081y^2 0.1844xy 0.0006c

a = P-value for block effect b = P-value for covariance effect c = P-value for fertilizer effect

The use of spatial covariance tends to increase the level of significance of treatment effect. At the location Karawang using a randomized block design has the P-value = 0.6728 for the effect of treatment, but with additional spatial covariance the P-value of treatment effect reduced to 0.4607. In

Kebumen1 location using a randomized block design the treatment effect has P-value = 0.0102, but with additional spatial covariance the treatment effect has smaller P-value (<0.0001). Similarly, for location Kebumen2 using spatial covariance reduced P-value from 0.0006 to <0.0001 compared with RCBD.

Polynomial Trend Approach (PTA)

The use of spatial polynomial trend reduces the coefficient of variation of the model compared with the RCBD for the location Karawang and Kebumen2, while in the location Kebumen1 it increases CV slightly (Table 1). At the location of Karawang and Kebumen2 CV reduction were 1.27 and 1.64 percent respectively, while in the location Kebumen1 CV increase was 1.87 percent. It seems that in the location Kebumen1 spatial polynomial trend is not effective to improve the accuracy of the experiment.

Covariance polynomial trend analysis result showed that in location Karawang x^2 covariance has a significant effect on rice yield (P-value <0.0001), whereas x covariance was not significant (P-value = 0.0898). The coordinates y, y^2 and xy effect is not identified. On location Kebumen1 and 2 the effects of trend polynomial covariance x, y, x^2, y^2 and xy is not significant (P values> 0.05) (Table 1). This result showed that the polynomial trend covariance effectively control the spatial heterogeneity in the location of Karawang, while on location Kebumen was ineffective.

In Karawang site polynomial trend usage increase the level of significance of treatment effect compared with randomized block design. The P-value of treatment effect decreased from 0.6728 to 0.1541. For the location Kebumen1 the use of polynomial trend decreases the level of significance of treatment effect. The P-value of treatment effect increased from 0.0102 to 0.0282, while on location Kebumen2 the P-value of treatment effect remains constant 0.0006.

AR1 Approach

Spatial autoregressive AR1 usage has a smaller value of AIC and BIC from the model compared with the RCBD at Kebumen2 location, while in the location Karawang or Kebumen1 it has a larger value (Table 2). This result shows that in the location Kebumen2 the AR1 model was better than the RCBD. For the location Karawang or Kebumen1 the AR1 model was not better than the RCBD.

Table 2. Value of AIC and BIC for the RCBD and AR1 model

Location		AIC	BIC
Karawang	RCBD	150.2	148.4
	AR1	151.4	148.7
Kebumen1	RCBD	798.9	797.1
	AR1	800.8	798.1
Kebumen2	RCBD	963.7	961.9
	AR1	958.0	956.2

Covariance parameter test results show that spatial correlation of rice yield exist in the location of Kebumen2 (P-value = 0.0093). For the location Kebumen1 and Karawang spatial correlation were not significant (P-value = 0.7327 and 0.3553 respectively) (Table 3).

At the location Kebumen1 the use of spatial autoregressive covariance tends to increase the level of significance of treatment effect compared with randomized block design. The P-value treatment effect decreased from 0.0102 to 0.0081. For the location of Karawang and Kebumen2 spatial autoregressive covariance usage tends to decrease the level of significance of treatment effect. The P-value treatment effect increased from 0.6728 to 0.7288 for Karawang and from 0.0006 to 0.0015 for Kebumen2 (Table 4).

Table 3. Estimation of covariance parameters, standard errors and P-value for the AR1 model

Location	Covariance parameter	Estimate	Standard Error	P>Z
Karawang	AR1	0.20	0.21	0.3553
	Residual	5.62	1.69	0.0004
Kebumen1	AR1	-0.07	0.21	0.7327
	Residual	6.92E12	2.09E12	0.0005
Kebumen2	AR1	0.44	0.17	0.0093
	Residual	7.57E15	2.55E15	0.0015

Table 4. Effect of fertilization and the P-value of AR1 model

Location		F-value	P > F
Karawang	RCBD	0.78	0.6728
	AR1	0.72	0.7288
Kebumen1	RCBD	3.17	0.0102
	AR1	3.31	0.0081
Kebumen2	RCBD	5.10	0.0006
	AR1	4.43	0.0015

Comparison of Spatial Models

There is an interaction between spatial models with a location in terms of increasing accuracy of the experiment. Papadakis nearest neighbor approach reduce the coefficient of variation of the model compared with the RCBD at all locations. Polynomial trend model has a smaller coefficient of variation of the model compared with the RCBD in the location Karawang and Kebumen2, while in the location Kebumen1 has a larger value. Spatial autoregressive AR1 usage has a smaller

value of AIC and BIC from the model compared with the RCBD in Kebumen2 location only, while in the location of Karawang or Kebumen1 has a larger value. The magnitude of CV decrease for nearest neighbor approach in average was larger than PTA and AR1.

The papadakis nearest neighbor has a significant effect on rice yield in all locations. The polynomial trend approach has a significant effect only in the location of Karawang, while on location Kebumen1 and 2 were not significant. The AR1 covariance approach has a significant effect only in the location of Kebumen2, whereas for location Karawang and Kebumen1 were not significant.

The covariance nearest neighbor tends to increase the level of significance of treatment effect in all locations compared with randomized block design. Spatial covariance polynomial trend tends to increase the level of significance of treatment effect only on the location of Karawang, while covariance AR1 increase the level of significance of treatment effect only on the location Kebumen1.

This finding indicates that the covariance nearest neighbor method was appropriate to be used in all locations to improve the accuracy of the experiment. The polynomial trend method was appropriate to be used in the location of Karawang and Kebumen2 only, while in location Kebumen1 was less appropriate. The method of spatial AR1 was suitable for use in location Kebumen2, while in the location of Karawang and Kebumen1 was less suitable.

The NNA, PTA and AR1 spatial model shows higher relative efficiency than the RCBD. The range of residual variation magnitude can be reduced was 3-93 percent (Table 5). In average the magnitude can be reduced for covariance nearest neighbor was larger than spatial covariance polynomial trend and covariance AR1, indicating that covariance nearest neighbor model was better than spatial covariance polynomial trend and covariance AR1.

Table 5. NNA, PTA and AR (1) relative efficiency to RCBD

Location	NNA	PTA	AR(1)
Karawang	27	55	13
Kebumen1	93	12	3
Kebumen2	91	91	8
Average	70	39	8

4. Conclusion

Covariance nearest neighbor approach was more efficient than polynomial trend, AR1 and RCBD. This approach increases the accuracy of experiments and the level of significance of treatment effect.

5. References

[1]. Bermudez, M. and A. P. Mallarino (2004), Yield and Early Growth Responses to Starter Fertilizer in No-Till Corn Assessed with Precision Agriculture Technologies. *Agron. J*. 94:1024–1033.

[2]. Funda T., M. Lstibůrek, J. Klápště, I. Permedlová, J. Kobliha (2007), Addressing Spatial Variability In Provenance Experiments Exemplified In Two Trials With Black Spruce *Journal of Forest Science* 53: 47–56.

[3]. Hong, N., J. G. White, M. L. Gumpertz, R. Weisz (2005), Spatial Analysis of Precision Agriculture Treatments in Randomized Complete Blocks: Guidelines for Covariance Model Selection. *Agron. J*. 97:1082–1096.

[4]. Lambert, D. M., J. L. DeBoer, and R. Bongiovanni (2003), Spatial Regression Models for Yield Monitor Data: A Case Study from Argentina. American Agricultural Economics Association Annual Meeting, Montreal, Canada.

[5]. Parsad, R., and C. Verghese (2010), Nearest Neighborhood Designs. I.A.S.R.I., Library Avenue, New Delhi.

[6]. van Es, H. M., C. P. Gomes, M. Sellman, and C. L. van Es (2007), Spatially-Balanced Complete Block Designs for field experiments. *Geoderma* 140:346-352.

[7]. Yang, Rong-Cai, Terrance Z. Ye, Stanford F. Blade, and Manjula Bandara (2004), Efficiency of Spatial Analyses of Field Pea Variety Trials. *Crop Sci*. 44:49–55.

Laboratory Measurements of Electrokinetic Potential to Determine The Fluid Flow Velocity in Porous Media at Unhas Campus, Tamalanrea, Makassar

Muhammad Hamzah Syahruddin

Geophysics, Physics Departement, University of Hasanuddin, Makassar (hamzah@fmipa.unhas.ac.id)

Abstract

The rate of infiltration or percolation of water into the soil on the campus of Hasanuddin University in Makassar Tamalanrea determined by the permeability or hydraulic conductivity values (K). Results of laboratory experiments of soil samples campus Tamalanrea UNHAS obtained value of K (cm/s) sample-1 is 0.006, sample-2 0.007, sample-3 0.014, and the sample-4 0.022. From the campus soil permeability can be obtained UNHAS Tamalanrea electrohydraulic conductivity value based on the measurement of potential electrokinetic in the laboratory. Conductivity electrohydraulic (C) value states fluid flows in porous media capability to generate electric potential. Results of laboratory experiments showed that the electrohydraulic conductivity in mV/cm for each soil sample from the campus UNHAS Tamalanrea are 0.01402, 0.01664, 0.02843, and 0.03812. Bigger value K measured at the soil surface is the bigger of value C.

Keywords: *potential electrokinetic, permeability, electrohydraulic conductivity.*

1. Introduction

Various potentials are produced in native ground or within the subsurface altered by our actions. Natural potentials occur about dissimilar materials, near varying concentrations of electrolytic solutions, and due to the flow of fluids. Sulfide ore bodies have been sought by the self potential generated by ore bodies acting as batteries. Other occurrences produce spontaneous potentials, which may be mapped to determine the information about the subsurface. Spontaneous potentials can be produced by mineralization differences, electro-chemical action, geothermal activity, and bioelectric generation of vegetation.

Four different electrical potentials are recognized. Electrokinetic, or streaming, potential is due to the flow of a fluid with certain electrical properties passing through a pipe or porous medium with different electrical properties. Liquid-junction, or diffusion, potential is caused by the displacement of ionic solutions of dissimilar concentrations. Mineralization, or electrolytic contact, potential is produced at the surface of a conductor with another medium. Nernst, or shale, potential occurs when similar conductors have a solution of differing concentrations about them. Telford, Geldart and Sheriff (1990) provide equations for differing potentials [1]. Generally, the SP method is qualitative and does not attempt to quantify the anomalous volume size, owing to the unknown volumetric shapes, concentration/density of various masses, and electrical properties of the sought causative media.

2. Experimental Details

The rate of flow of a fluid through any system, porous media, open pipes, etc., is dependent upon two basic properties. First, the fluid potential gradients, and second the resistance to the flow of that fluid along the pathway traversed. The determinable ―constant" integrating the ―resistance" factors for a porous media has been labeled ―permeability". Darcy (1856) performed a series of experiments on the relationship affecting the downward flow of water through sands proposed as filtering material for the water for the town of Dijon, France. His experiments developed the relationship [2]:

$$Q = -KA\left(\frac{h_2 - h_1}{l}\right). \qquad (1)$$

Where Q is volume of water crossing unit area in unit time (L^3t^{-1}), h_1,h_2 is the elevation above a reference level of water in manometers terminated above below a vertical column of sand, respectively (L), K is a factor of proportionality or hydrolic conductivity (Lt^{-1}), l is thickness of the sand (L).

The electrokinetic – potentials were calculated based with the Helmoltz-

Smoluchovsky equation [3] using hydraulic head pressure following as:

$$\nabla V = \frac{\varepsilon_r \varepsilon_0 \zeta \rho g}{\eta \sigma_W} \nabla H \qquad (2)$$

where δ is the zeta-potential, ε_r is the relative dielectric constant of the liquid, ε_0 is the dielectric constant of vacuum, η is the viscosity of the fluid, ρ is the density of the fluid (in kg/m^3), g is the normal gravity value (9.81 m/s^2), H is the hydraulic head, σ is the bulk conductivity of the liquid and ∇V is the potential elektrokinetik gradient normal to the cross section, where C= $\varepsilon_0 \varepsilon_r \delta \rho g / \eta \sigma_w$ define is the electrohydraulic coefficient.

We built an apparatus (Figure 1) to be able to measure the electrokinetic-potential, hydraulic conductivity (K) and the electrohydraulic conductivity (C). To generate fluid flow hydraulic head pressure was used, and to simplify calculations we used four steps with a 40 cm height difference between each step. To measure the electrokinetic potential difference two platinum electrodes were inserted at each end of the column, and were connected to a data logger (voltmeter digital (Sanwa-PC500) resolution 0.01 mV), which was connected to a computer.

To better understand the basic petrophysical properties we used sand as the porous media. This provides the simplicity of standard grain surfaces and can represent all silicate minerals. There are two kinds of samples used in the experiment. First, samples of known grain size of mesh 20, mesh 30 and mesh 40. Second, the sample consisting of several grain sizes. Three different diameters of spherical sands were used, and one with diameters in the range. The different diameters are 595 µm, 420 µm, 297 µm and range 297-595 µm. For the fluids, we used fresh water within the laboratory temperature (20 –25°C).

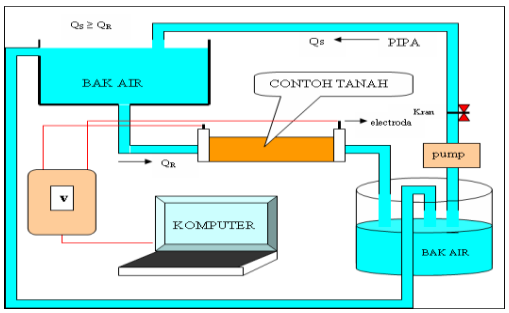

Figure 1. A schematic of the laboratory apparatus

Before the experiment, the sand were washed with fresh water and fully saturated in the fresh water to remove "lempung" and air bubbles. Then, the potential measurements were logged every second by the PC500 and saved directly to flash memory, and were also observed on the computer screen. When the electrokinetic potential values stabilized for a fixed head hydraulic pressure, the hydraulic head pressure was changed to the next step.

3. Result and Discussion

Some results of laboratory studies can be displayed in this paper. These results can be shown in Figure 2 to Figure 5. While the results of experiments for several samples of soil on Campus Tamalanrea Unhas can be shown in Table 1.

Figure 2, as an example for the mesh 10, shows that the change of electrokinetic potential due to the change of hydraulic head pressure. There are four hydraulic head used each 40 cm, 85 cm, 120 cm and 160 cm. For each hydraulic head from 40 cm to 160 cm is obtained recordings electrokinetic potential 6 mV, 9 mV, 10 mV and 14 mV. Therefore, it shows that high hydraulic head pressure generates a large electrokinetic potential.

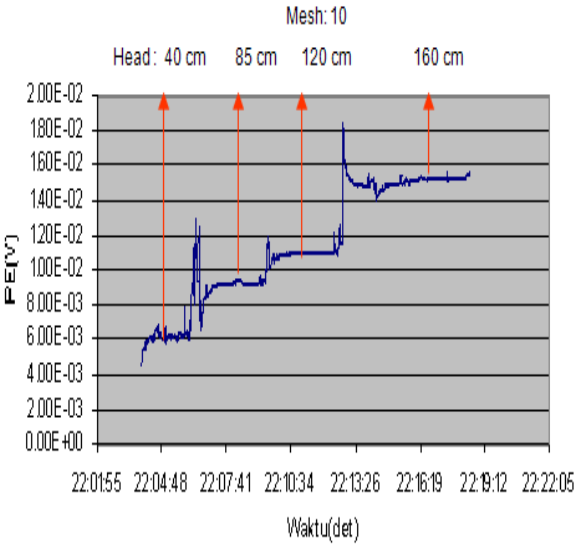

Figure 2. Recorded electrokinetic potential

Figure 3 and Figure 4 shows that the change of hydraulic conductivity due to the change of grain size samples. The figure above shows the relationship between the bigger grain size porous media gives a larger hydraulic conductivity. The same thing happened to C and UB. We can shows that the change of electrohydraulic conductivity due to the change of

grain size samples. The figure above shows the relationship between the bigger grain size porous media gives a larger electrohydraulic conductivity.

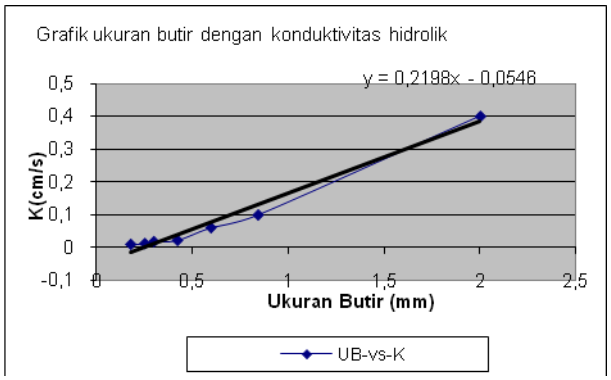

Figure 3. Relationship between K and grain sizes

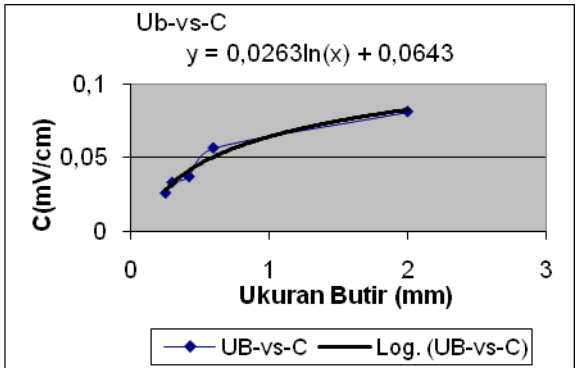

Figure 4. Relationship between C and grain sizes

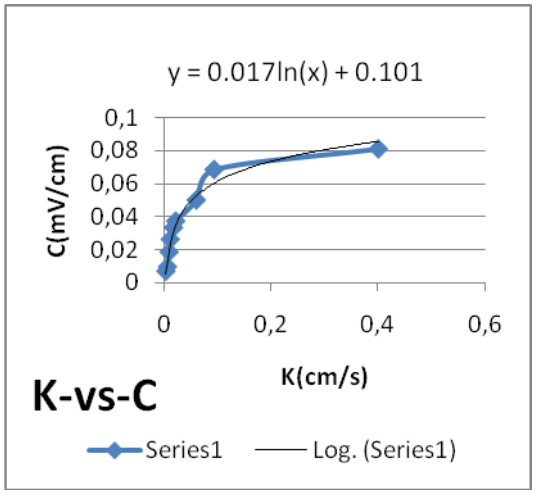

Figure 5. Relationship between K and C

Based on the results of laboratory experiments have been conducted to know the relationship between permeability (K) and conductivity electrohydraulic (C). The relationship between the values of K and C are to be logarithmic. Therefore, the value of K is very large or very small then the value of C is approximately constant as can be seen in Figure 5. The relationship between K and C are very important to know because the soil samples generally have low permeability is difficult to know the value of conductivity electrohydraulic through direct experiments in the laboratory.

The relationship between K and C in Figure 5 is used to determine the electrohydraulic conductivity of soil samples on Unhas campus Tamalanrea Makassar. Of the four soil samples from the S1-S4 are taken from the Unhas campus Tamalanrea already we know the value of K respectively. From the permeability value can be known to the value of C using equations interpolation from the relationship K and C. The value of K and C of the S1, S2, S3 and S4 from Unhas campus can be seen in Table 1.

Tabel 1 K and C values of soil samples Unhas Campus, Tamalanrea

No	Sampel	K (cm/s)	C(mV/cm)
1	Sampel-1	0,006	0,01402
2	Sampel-2	0,007	0,01664
3	Sampel-3	0,014	0,02843
4	Sampel-4	0,022	0,03812

4. Conclusion

Empirical relationship K value and the value of C is the value of K rises exponentially to the value C. Results of laboratory experiments of soil samples obtained from the campus UNHAS Tamalanrea sample K-1 value is 0.006, 0.007-2 sample, the sample and sample-3 0.014 4 0.022. Value of C for each sample S1 to S4 is 0.01402, 0.01664, 0.02843, and 0.03812.

5. Acknowledgements

I would like to thank the support given by Unhas in conducting research and to attend seminars on ICBS. This research was funded by the DIPA UNHAS in 2010

6. References

[1]. Telford, W.M., Geldart, L.P., Sheriff, R.E., dan Keys, D.A. (1990), *Applied Geophysics*, Cambridge University Press.
[2]. Touloukian, Y.S., Ho, C.Y. (1981), *Physical Properties of Rocks and Minerals,* McGraw-Hill Book Company.
[3]. Kim, G., Heinson, G., dan Joseph, J. (2004), Electrokinetic Groundwater Exploration: A New Geophysical Technique, *Regolith 2004*, 181-185.

Polymerization of *β*-Pinene using Zirconium *β*-diketonato Catalysts

Muhammad Yusuf [1], Yessi Permana [2], Ismunandar [3]

[(1,2,3)] Department of Chemistry, Institute Technology of Bandung, Indonesia (Yusuf.6423@students.itb.ac.id)

Abstract

Pine gums contain β-pinene as the major component. Polymerization of β-pinene may alternatively provide an access towards the synthesis of alicyclic hydrocarbon polymers. Petrochemical based β-Pinene has been reported to polymerize via a cationic addition mechanism. The polymerization resulted in low molecular weight polymers with low glass transition temperature (T_g < 100 ºC). Unfortunately, only a limited commercial utilization (coating additives) has been explored from petrochemical based poly(β-pinene). Polymerizations of β-pinene were usually carried out using conventional Lewis acids, for instance $AlCl_3$, $EtAlCl_2$, $Et_3Al_2Cl_3$, $TiCl_4$, $SnCl_4$. Such conventional catalysts suffer from air and moisture giving difficulties in industrial handlings and also have less electronic control towards Lewis acidity. In this offered research, we propose the use of zirconium β-diketonato as active catalysts for the polymerization. Polymerization of β-pinene at 40 ^oC for 24 h min and at room temperature for 24 h showed good catalytic productivity (>99 %) compared to Polymerization of β- pinene at room temperature for 30 minutes (17.56 %). These catalysts are also non corrosive and possess higher stability towards moisture and air,which are of strong benefit for industrial purposes.

Keywords: *Polymerization of β-pinene, Zirconium β-diketonato, Catalytic activity.*

1. Introduction

Bio-based polymer materials from renewable resources have recently been attracting much attention from the viewpoint of environmentally benign and sustainable chemistry [1]. Alicyclic hydrocarbon polymers can be obtained from biomass species among which terpenes, such as limonene, terpinen, phellandrene, and pinene [2]. *β*-Pinene is popular and abundant in nature and find in pine trees up to recent years. One of attractive biomasses to explore is turpentine oil from pine trees. Pine trees are abundantly available and not yet fully explored. Pine trees are also inedible which will not compete with the supply of food stocks [3].

The use of fossil based materials and energy has given negative impact on the environment due to the rise of CO_2 emission as well as the significant decline on Indonesian fossil oil reserves. It is thus of importance for the country to possess technologies in producing bio-based chemicals as substitutes to petroleum-based chemicals to supply local industries in the country with environmentally benign and sustainable materials [1].

Polymerization of *β*-pinene may alternatively provide an access towards the synthesis of alicyclic hydrocarbon polymers. Petrochemical based *β*-Pinene has been reported to polymerize via a cationic addition mechanism. The polymerization resulted in low molecular weight polymers with low glass transition temperature (T_g <100ºC). Unfortunately, only a limited commercial utilization (coating additives) has been explored from petrochemical based poly(β-pinene) [2].

Polymerizations of *β*-pinene are performed by a petrochemical source and is commonly carried out using acid catalysts HCl, HNO_3 ,conventional Lewis acids, for instance $AlCl_3$, $EtAlCl_2$, $Et_3Al_2Cl_3$, $TiCl_4$, $SnCl_4$ or heteropolyacid catalysts (HPA). [2,4,5]. The polymerization of *β*-pinene gave low molecular weight and melting point polymers, called as terpene resins. Unfortunately, only a limited commercial utilization (coating additives and adhesive resins) has been explored from petrochemical based poly(β-pinene). The use of such conventional catalysts suffers from air and moisture giving difficulties in industrial handlings as well as less electronic control towards Lewis acidity.

In this work, we proposed the use of clays-supported zirconium complexes. As preliminary studies we will synthesize metal complexes from *β*-diketonates series. The active catalysts are immobilized into clays, either the synthetic one (e.g. Taeniolite) [6]. By means of such catalysts, we expect to control the Lewis acidity of metal centre through ligands and create a robust system through immobilization of the metal complex into clays. The proposed hybrid catalysts are expected to possess higher stability towards air, higher Lewis acidity,

and re-usability. These properties are expected to give access towards bio-based poly(*β*-pinene) with physical properties suitable and better polymer properties, for toner binders in printing technologies, optoelectronic material and heat resistant material .

2. Experimental Details

Synthesis of zirconium (IV) β-diketone per chlorate

Experiments were carried out with standard Schlenk techniques under nitrogen atmosphere. Contact of the reactants with air and other moistures should be kept to a minimum. Zirconium tetrachloride (1 mmol) was dissolved in freshly dried benzene (10 ml). Treated benzoylacetone / acetylacetone / dibenzoylmethanate (3.4 mmol) in vacuo was dissolved in dry benzene (10 ml) and added to the slurry of zirconium tetrachloride dropwise via cannula and stirred for 3 h at room temperature. After stirring, the solution was refluxed at 85^{o}C for 14 hrs. Solvent was evaporated under vacuum. The product was dissolved in freshly dried methanol (10 ml) and reacted with silver perchlorate (0.9 mmol) in dry methanol (10 ml). The precipitated silver chloride, resulted from the reaction was discarded from the solution by filtration. The solution was boiled under continuous vacuum until crystallization began. It was then allowed to stand under a vacuum, maintained overnight prior to analyses.

Synthesis of zirconium (IV) β-diketone perchlorate/ Clay

Clays (lithium taeniolite from Topy Industry Co., Ltd.) of 0.1 g respectively were swollen by deionized water (20 ml). The synthesized complex, Zr(IV) tris(acetylacetonato) chloride [Zr(acac)3]Cl (2a) (50% of the C.E.C.), was dissolved in deionized water (20 ml) and added into the swollen clay followed by stirring for 48 h and sonication 1.5 h. Lithium taeniolite (CEC of 268.2 meq/100 g) of 0.1 g respectively were swollen by deionized water (10 ml). The synthesized complex, Zr(IV) tris(benzoylacetonato) perchlorate [Zr(bzac)3ClO_4] (2b), Zr(IV) tris(dibenzoylmethanato) perchlorate [Zr(dbzm)$_3ClO_4$] (2c) (50% of the C.E.C.), were dissolved in deionized methanol (30 ml) and added into the swollen clay followed by stirring for 48 h and sonication 1.5 hrs.

Polymerization of β-Pinene

Zirconium *β*-diketonato Catalysts (0.07 mmol) in vacuo was dissolved in dichloromethane (10 ml). *β-Pinene* (1.4 mmol) added to slury Zirconium *β*-diketonato catalysts and stir 30 min to give the product polymers. The reaction was quenched with methanol (1 ml).

3. Results And Discussion

IR Spectroscopy

Coordination of *β*-diketone ligands to zirconium was able to be confirmed from their IR spectra, by the shift of carbonyl stretching frequencies to lower energy levels compared with those in free ligands due to stabilization interaction between filled non-bonding oxygen of a ligand and empty d orbital of zirconium. It was also observed that the growing number of the phenyl ring lowered the carbonyl stretching energy, presumably due to inductive effect of the phenyl ring, which was predominated by resonance effect. Confirmatory evidence about the formation of six-coordinate complexes was from chloride vibrations, observed in the 1531.48 cm^{1} acetylacetonato (acac), 1533.41 cm^{1} benzoylacetonato (Bzac) and 1525.69 cm^{1} dibenzoylmethanato (Dibzm) region, and perchlorate vibrations in the 1529.55 cm ^{1} (Bzac) and 1510 cm ^{1} (Dibzm) which are in a good agreement with reported data on such vibrations . These vibrations indicated the presence of perchlorate as counter anion of the cationic six-coordinate complexes, since perchlorate does not coordinate to a metal center [8].

Table 1. C =O bond due of zirconium (IV) β-diketonate chloride and perchlorate

	vC=O Chloride complex	Perchlorate complex
Acac	1531.48	
Bzac	1533.41	1529.55
Dibzm	1525.69	1510.26

Gas Chromatography Analysis

A series of zirconium *β*-diketonato/ clay catalysts were thus employed for the cationic polymerization of these monomers at various temperatures and various timen in dichloromethane solvents. Polymerization of *β*-pinene catalyzed by ZrdiBzClO_4 catalysts (entry 3) at room temperature for 30 min showed good catalytic activity (17.56 %) compared to ZracacCl (entry 2) (14.7%) and ZrBzClO_4 (entry 1) (9.7%). The increase of reaction temperature to 40°C and time to 24 h increased the catalytic activity to (>99%) using ZrBzClO_4 catalysts (entry 4), ZrBzClO_4 (entry 6) (> 99 %), ZrdiBz/TN (entry 7) (>99 %) and ZracacCl (entry 5) (33.54 %).

Polymerization of *β*-pinene catalyzed by ZrBzClO_4 catalysts (entry 8) at room temperature for 24 h showed good catalytic activity (> 99 %)

compared to ZrdiBz/TN (entry 10) (69.12 %) and ZracacCl (entry 9) (68.67 %).

Table 2. Polymerization of *β*-Pinene Using Zirconium *β*-diketonato/Clay Catalysts

Entry	Catalysts	Time	T	% conv
1	$ZrBzClO_4$	30 min	Room	9.7
2	ZracacCl	30 min	room	14.7
3	$ZrdiBzClO_4$	30 min	room	17.56
4	$ZrBzClO_4$	24 h	40 °C	>99
5	ZracacCl	24 h	40 °C	33.54
6	$ZrdiBzClO_4$	24 h	40 °C	>99
7	ZrdiBz/TN	24 h	40 °C	>99
8	$ZrBzClO_4$	24 h	room	>99
9	ZracacCl	24 h	room	68.67
10	ZrdiBz/TN	24 h	room	69.12

*room temperature = 26-27°C

4. Conclusion

β-pinene were polymerized using Zirconium *β*-diketonato/Clay Catalysts to afford polymers with an alicyclic hydrocarbon structure. Polymerization of *β*-pinene at 40°C for 24 h min and at room temperature for 24 h showed good catalytic productivity (>99 %) compared to Polymerization of *β*-pinene at room temperature for 30 minutes (17.56 %). These catalysts are also non corrosive and possess higher stability towards moisture and air, which are of strong benefit for industrial purposes. Poly (*β*–pinene) have good properties for optoelectronic materials, such as a low dielectric constant, non-hygroscopicity, and good transparency Thus, alicyclic hydrocarbon polymers obtained from a naturally occurring biomass would meet certain requirements in current markets.

5. Acknowledgements

---

6. References

[1]. K, Satoh., S, Saitoh., and Masami Kamigaito (2007), A linear lignin analogue: phenolic alternating copolymers from naturally occurring *α*-methylstyrene via aqueous-controlled cationic copolymerization, *JACS Communication*., 129, 9586-9587.

[2]. K,Satoh., H,Sugiyama., and M, Kamigaito (2006), Biomass-derived heat-resistant alicyclic hydrocarbon polymers: poly(terpenes) and their hydrogenated derivatives, *J. Green. Chem.*, 8, 878 882.

[3]. I.V.Deliy., and I,L.Simakova (2008), Kinetics and thermodinamics of liquid phase isomerization of α and β pinene over Pd/C catalyst, *J. React. Kinet Catal Lett*.,Vol 95,1,161-174.

[4]. A, Corma., M, Renz., and M, Susarte (2009), Transformation of biomass products into fine chemicals catalyzed by solid lewis- and bronsted-acids, *J. Top Catal*., 52,1182–1189.

[5]. H, Zhu., Z, Liu., X, An., and F, Lei (2010), Keggin heteropolyacids as catalyst for the polymerization of β -pinene, *J. Reac Kinet Mech Cat*.,100,355-361

[6]. L, Aldea., Fraile, J, M., H, G, Marín., J, I, García., C. I, Herrerías., J. A, Mayoral, and I, Perez. (2010), Study of the recycling possibilities for azabis(oxazoline)–cobalt complexes as catalysts for enantioselective conjugate reduction**,** *J. Green Chem.*, 12, 435 – 440

[7]. Y, Permana., S, Shimazu., N, Ichikuni., and T, Uematsu (2005), Studies on tris(β-diketonato) zirconium (IV); syntheses,characterization and catalytic activity for ring opening of oxiranes, *J. Catalysis Communications*., 6, 426–430.

[8]. L, Pejov., V. M. Petrusevski (2002), Fourier transform infrared study of perchlorate ($^{35}ClO_4^-$ and $^{37}ClO_4^-$) anions isomorphously isolated in potassium permanganate matrix. Vibrational anharmonicity and pseudo-symmetry effects, *J. Phy Chem. Solid.,* 63, 1873–1881.

Appendixes

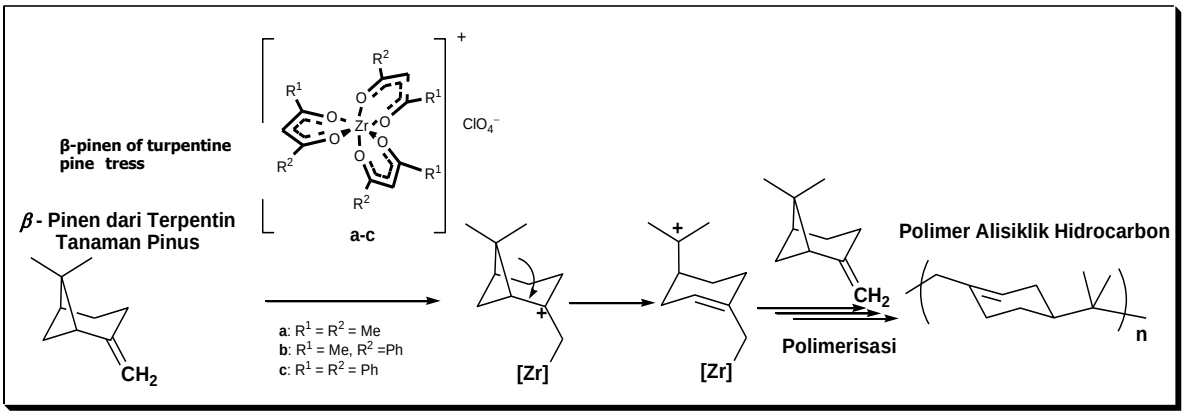

Figure 1. Polymerization of β-pinene using zirconium β-diketonato complexes [2].

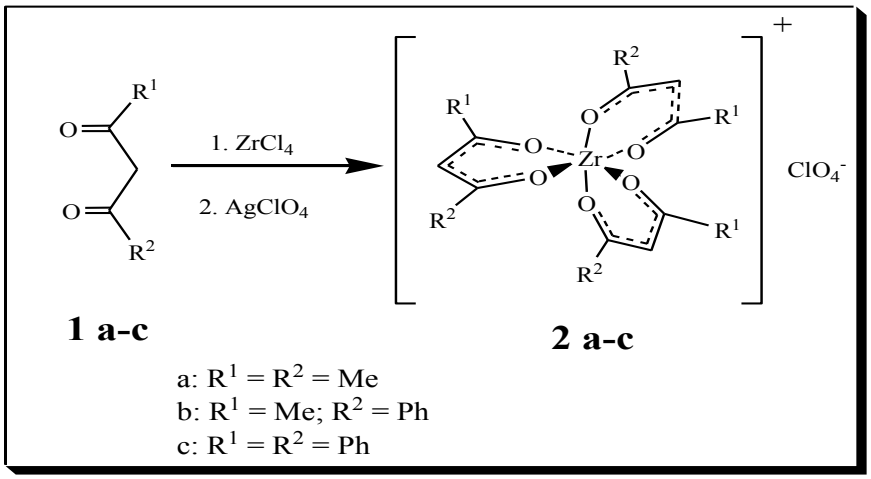

Figure 2. Synthesis of zirconium (IV) β-diketone perchlorate [7].

Standardization of ^{129}I by Photon-Photon Coincidence Method with ^{125}I Tracer

Pujadi M [1], Gatot W [2], Hermawan C [3]

(1,2,3) Center for Technology of Radiation Safety and Metrology, National Nuclear Energy Agency , Jakarta, Indonesia (pujadi@batan.go.id)

Abstract

The standardization of ^{129}I have been carried out by photon-photon coincidence method with ^{125}I tracer in PTKMR-BATAN. Activity standard of ^{129}I is needed for detector calibration in nuclear medicine, surveillance program of the nuclear fuel cycle. Photon radiation emitting of ^{129}I is not simultaneous, so that absolute activity measurement using this method require radionuclide tracer. The radionuclide ^{125}I can be used as a tracer of ^{129}I because both radionuclides have similarities in the chemical properties and emitting photons with similar energies from about 27-40 keV. The sources of ^{125}I and ^{129}I in the form of liquid of potassium iodide (KI) in H_20 solution was prepared individual into solid point source in the form of AgI by adding $AgNO_3$. Two methods of activity measuremnet of ^{125}I were used : the first method with distance of detector and sample source fixed and the second method is movable photon detectors or varying of the sample source and the detector distance from 5 to 120 mm, to obtain varying efficiency. In the first step the activity of a ^{125}I is measured by photon-photon coincidence method. The result of ^{125}I activity measurement as a tracer was 441.34 ± 0.90% Bq/mg, were determined at reference time Juli 15,2010, 12.00 WIB. The second step photons are counted from mixed samples of ^{129}I and of the ^{125}I with the known activity concentration, using the same measuring equipment and same setting is used as for the activity measurement of ^{125}I. The result of ^{129}I activity measurement using ^{125}I tracer was obtained 998,56 ± 1.24% Bq/gr at reference time Juli 15, 2010 ; 12.00 WIB . The both activity value agrees with the results of measurements using calibrated 4πγ ionization chamber, calibration with PTB standard source, with difference about from 0.12 to 0.16 %. The overall result it is concluded that absolute standardization of ^{129}I radionuclide by foton-foton coincidence method with ^{125}I tracer in PTKMR-BATAN has been done well, with good result.

Keywords: *standardization, photon-photon coincidence, tracer, activity, ^{129}I.*

1.Introduction

The radionuclide ^{129}I decays by β- particle to the exited state at 39.6 keV level of ^{129}Xe. The transition to the ground state is strongly converted: only 7.46% γ-rays (^{129}Xe) are emitted, the main part of the radiation consists of conversion electrons followed by K x-rays with energies from 29.5 to 34.5 keV (^{129}Xe) [1,2]. The radionuclide ^{129}I is a volatile fission product with very long half-life ($T_{1/2}$ = 1.61 10^7 years (u = 0.07) [1,2]. The radionuclide ^{129}I standard source is used for calibration of activity measuring equipment in nuclear medicine, such as dose calibrator, and photon detector calibration at the low energy scale and also in surveillance programmes of nuclear fuel cycle [1]. Therefore require an accurate measurement of activity for the reference source.

Accurate activity measurement of ^{129}I can be done using absolut method. Activity measurement of ^{129}I is not easy, because the chemical problems the source a caused by volatility of iodine and high sample masses are necessary because of the long half- life, to obtain a sufficiently large number of counts in a reasonable measuring time [1]. The absolute measurement using 4πβ-γ coincidence counter extremely difficult, because in the sample with high masses β-particle are strongly absorbed, so the efficiency is very small. The absolute activity measurement most suitable using foton-foton coincidence method [5]. The problem is photon radiation emitting of ^{129}I is not simultaneous, so that absolute activity measurement can not directly carried out using photon-photon coincidence method [1,5].

Activity measurement of ^{129}I using photon-photon coincidence method require radionuclide tracer that emits two or more photons simultaneously or cascade without significant delay between each other [1,5]. The radionuclide ^{125}I can be used as a tracer ^{129}I because ^{125}I emits two or more photons radiation simultaneously without significant delay between one and another

and it has similarities in the chemical properties and both radionuclides emitting photons with similar energies from about 27-40 keV [1,5]. Among the widely known standardization methods, the photon-photon coincidence counting using I-125 tracer with efficiency extrapolation method [1,6] was employed.

2. Experiments

Photon-photon coincidence

A photon-photon coincidence system using two NaI(Tl) detectors, crystal size 76x76 mm, 6 mm thick, with Al windows, connected to coincidence unit was constructed in PTKMR – BATAN. Two NaI(Tl) detectors in front of each other were installed, and in the middle between the two detectors installed where to sample source to be measured. The detectors can move simultaneously forwards or backwards in relation to varying distance of source and the detector to obtain the variation of efficiency, accordance with the principles of the method has been described by Schrader and Walz [1,4].

The data collection electronics for the coincidence counting system consist of two amplifiers, two single chanel analizer (SCA), two gate and delay module, a coincidence module, three digital counter and a personal computer. Signal from the detectors are shaped by amplifiers and then fed to SCA, and then fed into gate and delay module for setting signal coincidence of two detector, and then fed into a coincidence module. Each detector has a count of their own, so there is a three channel, two channels of single counts and one count of coincidence. The scheme of the system is presented in Figure 2.

Preparation of sources

Source of ^{125}I were prapared from a solution provided by PRSG-BATAN Serpong and ^{129}I obtained from PTB – Germany. The both solution was in the form of potassium iodide (KI) in H_2O solution. The solution were prepared individual into solid point source in the form of AgI, sucked into a small polyethylene ampoule picnometer (baby bottle), and then dropped onto a thin polyester film as source support is about 10 - 25 mg. After the droplet of ^{125}I were dispensed on the source support, a drop of $AgNO_3$ solution added immediately to convert the volatile I^- into the precipitate of AgI, according to the following reaction :

$$KI + AgNO_3 \longrightarrow Ag_{(s)} + KNO_3$$

The small polyethylene ampoule picnometer were carefully weighed in each case to determine the mass of the drops. Then, the sources were dried in a chamber with circulating air. After a dry source, the sources were then covered with thin polyester film.

Measurement Sample

The first step, the activity concentration of a ^{125}I as a tracer were measured five replicates for each sample. The activity is measured by varying of the sample source and the detector distance from about 5 to 120mm, to obtain varying efficiency.

Measurements were taken at the energy region from 13 to 42 keV. The duration for individual measuring point at a particular distance varied from 100 seconds at low distance to 200 seconds at large distance. The electronics consisted of two counter chains with 5μsec fixed dead time and coincidence circuit with resolution of 5μsec. The all three counting rates were corrected for background, dead time and resolving time for coincidence counting rate. The formula for photon-photon coincidence with fixed detectors described by Taylor [3,6,8] and the formula for photon-photon coincidence with movable detectors and extrapolation method described by Schrader and Walz [1,4].

Impurity measurement

Impurity in the sample was analyzed using a gamma spectrometer. According to data available, the possibility of radionuclides impurities for I-125 is I-126 and for ^{129}I are I-131, I-132, I-133 and I-135. The energy calibration was performed using ^{152}Eu standard source.

3. Result and Discussion

In order to obtain the activity of ^{125}I as a tracer, we measured with two methods, fixed and movable detectors. In addition the activity of ^{125}I were measured also by 4πβ-ionization chamber.

The system arrangement in the tracer measurement on standardization of ^{129}I was the same as for the standardization of ^{125}I by photon-photon coincidence with movable detectors. The electronics consisted of two counter chain with 5μs fixed dead time and the coincidence circuit with a resolution of 5 μs. The lower discriminator levels of the counter chains were adjusted to a photon energy of about 13 keV, with the expectation that completely eliminates the L x-rays of ^{125}Te and ^{129}Xe, so that counted only K x-rays. The calculation activity value of ^{125}I using fixed detectors method calculated using the equations developed by Taylor [3,6,8] and using movable detectors method calculated using Schrader and Walz [1,4]. Adopting values

parameters of ^{125}I from data of TdeR Tabel de Radionuclides [2], the ratio of detection probabilities per disintegration parameter K= 1.086 is calculated. The value of K influence on the calculation using the formula of Taylor, Schrader and KF.Walz. In the Taylor's formula have the constant part : $4K/(1+K)^2$ was obtained 0.9983. In the Schrader and Walz formula have the constant part :$(1+K)^2/ 4K$ was obtained 1.0017, this value is only 0.06% different with the value obtained by Schrader. This difference is due to differences in the parameter values used, but relatively similar with the value obtained by Schrader and Maria Sahagia [8]. However, its influence on the final result is relativelly small, less than 0.1%.

The results of ^{125}I activity measurement are presented in Table 1 (Appendixes). The activity value of ^{125}I using fixed detectors was 440.98 ± 0.70% Bq/mg and using movable detector – extrapolation method was 441.69 ± 0.90%, all results were determined at reference time Juli 15,2010, 12.00 WIB. The both measurement results show the difference only 0.16%, the average result were 441.34 Bq/mg. The relative standar deviation (statistical counting) of the measurement result within several source varied from 0.43 to 0.56 %. The uncertainty value are a combine relative standard uncertainty (quadratic sum). The combine relative standard uncertainty are given in Table 2 (Appendixes). The both activity value agrees with the results of measurements using using calibrated 4πβ- Ionization chamber, calibration with PTB standard source, with difference about 0.08 – 0.24%.

To determine the activity of ^{129}I , the both sample, ^{129}I and ^{125}I as a tracer source, were sandwiched and measured under the same measuring conditions and with the same adjusment as for standardization of ^{125}I. The value of coincidence counting from ^{129}I and ^{125}I mixed sources relatif same with the value of coincidence counting from ^{125}I , considering that coincidences are detected only from the decay of ^{125}I and not from the decay of ^{129}I because photon radiation emitting of ^{129}I is not simultaneous. We varied source and detectors distance from 5 to 120 mm, the result was presented in Table 1.

The activity value of ^{129}I was calculated using the equations developed by Schrader [1]. The first must be calculated ratio of detection probabilities per disintegration parameter k_5 and k_9. Adopting values parameters of ^{125}I and ^{129}I, from data table (Coursol, 1982, 1984), which was quoted by Schrader, the probability of fluorescene escape (f_x) 35,49 keV (^{125}I) = 0.245. The value of ratio of detection probabilities per disintegration ^{125}I (k_5) obtained 1.062, this value is only 0.005% different with the value publication by Schrader (1990).

Using the value of f_x *(from data table Coursol 1982,* 1984), the value of ratio of detection probabilities per disintegration ^{129}I, k_9 obtained 1.038 (Schrader, calculate k_9 = 1.039), this value is only 0.001% different, this small effect on the final result. The activity value of ^{129}I using photon-photon coincidence counting with I-125 tracer was 998.56 ± 1.24% Bq/gram, were determined at reference time Juli 15,2010, 12.00 WIB, are are presented in Table 3. The uncertainty value 1.24 % is a combine relative standard uncertainty (quadratic sum), presented in Tabel 2.

According to H Schrader provided that the chemical stability of the source is guaranteed, the tracer method produces result with good reproducibility and at least low random components uncertainty. The activity value agree with the results of measurements using using calibrated 4πβ- Ionization chamber, calibration with PTB standard source, with difference 0.12%. The radioactive source were checked for contaimination of radionuclides impurities by using β- spectrometer measurement, but no radionuclide impurities were found.

4. Conclusions

The overall result it is concluded that absolute standardization of ^{129}I radionuclide by photon-photon coincidence method with ^{125}I tracer in PTKMR-BATAN has been done well, with good result. The activity value agree with the results of measurement using calibrated 4πβ- ionization chamber, calibration with PTB standard source, with difference 0.12%.

5. Acknowledgements

The authors are thankful to the State Ministry of Research and Technology for the opportunity in –Riset Insentif" program.

6. Reference

[1]. H. Schrader (1990), Standardization of ^{129}I by tracer Method with Photon-photon Coincidences from the Decay of ^{125}I. *Appl.Radiat.Isot*. 41, No.4, pp.417-421.

[2]. Tde R, (2004), Table de Radionuclides. *Atomicand Nuclear Data, Recommended data/tableBNM-LNHB/CEA – Table de Radionuclides – CEA.* http://www.nucleide.org/DDEP_WG/DDEPdata.htm

[3]. S. Pomme, T.Altzitoglou, R. Van Ammel G. Sibbens (2005), *Nuclear Inst. &*

Methods in Physics Research Section A, A 544584-592.
[4]. G. Ratel, J.W. Muller (1988), *Trial comparison of activity measurement of solution of I-125*. BIPM Report-88/2.
[5]. H. Schrader and KF Walz (1987), *Standardization of ^{155}I by photon-photon coincidence counting and efficiency extrapolation. Appl.Radiat.Isot* .41, 417.
[6]. H. Schrader (2006)„ *Photon –photon coincidences for activity determination: I-125 and other radionuclides*. *Appl.Radiat.Isot*. 64. 1179-1185.
[7]. J.G.V. Taylor (1967), *X - ray – X - ray coincidence counting methods for the standardization of ^{125}I and ^{197}Hg,* Proceedings of the Symposium on Standardization of Radionuclides, Vienna, IAEA-Proc.Series SM 78, p.341.
[8]. Maria Sahagia, C. Ivan.E L. Grigorescu, Anamaria R. (2008), *Standardization of ^{125}I by the coincidence method and practical applications. Appl.Radiat.Isot*. 66. 895-899.
[9]. Ratel, G. (1989), *International comparison of activity measurement of a solution of ^{125}I, CCEM-RI(II)/89-2*. BIPM – France.

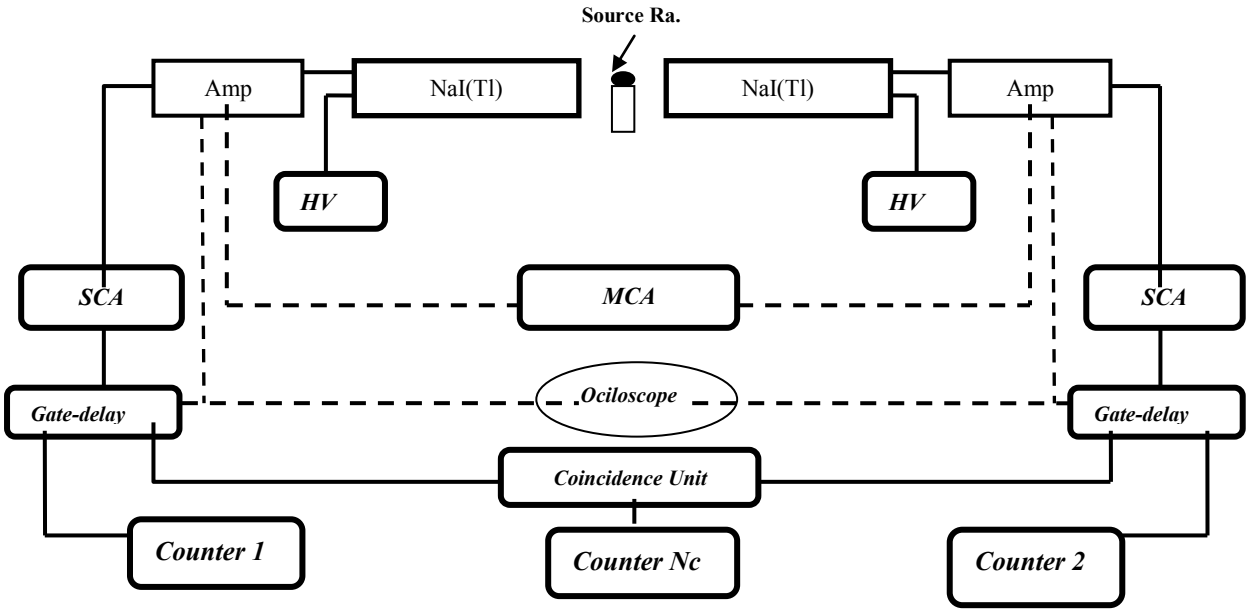

Figure 1. Scheme of the photon-photon coincidence system

Table 1. Measurement result ^{125}I activity as a tracer.

Sample	Massa (mg)	N_0/mg (Bq) Ref. Time : Juli 15, 2010 Fixed detectors	N_0/mg (Bq) Extrapolation Ref. Time : Juli 15, 2010	4πβ- Ionization chamber Ref. Time : Juli 15, 2010
01	12.037	441.62 ± 0.46	439.56± 0.48	The average of 4πx-Ionization chamber measuring result were : 440.61 ± 2.32%.
02	11.963	440.84 ± 0.43	441.31± 0.49	
03	12.162	443.21 ± 0.48	442.90± 042	
04	6.729	440.16 ± 0.43	443.26± 0.52	
05	12.443	439.92 ± 0.46	443.72± 0.54	
06	10.901	439.79 ± 0.47	438.24± 0.56	
07	13.784	437.27 ± 0.49	444.75± 0.43	
08	15.716	442.13 ± 0.45	443.18± 0.48	
09	14.225	442.37 ± 0.44	442.05± 0.46	
10	12.894	441.62 ± 0.46	437.93± 0.47	
Average :		440.98 ± .47%	441.69 ± 0.54%	

Tabel 2. Uncertainty component, in % of the activiy ^{125}I concentration, due to :

Uncertainty Component	**Fixed detectotrs ^{125}I (%)**	**Movable Detectors ^{125}I(%)**	**Movable Detectors ^{129}I(%)**
Statistics counting	0.47	0.54	1.01
Counting time	0.035	0.035	0.035
Wieghing uncertainty	0.05	0.05	0.05
Dead time	0.005	0.005	0.005
Background	0.5	0.5	0.5
Resolution time	0.05	0.05	0.05
Half-life	0.10	0.10	0.10
Impurity	-	-	-
Extrapolation (various distance)	-	0.5	0.5
Combined Uncertaity:	0.70	0.90	1.24

Table 3. Measurement result ^{129}I activity with ^{125}I tracer (Reference Time : Juli 15, 2010 ; 12.00 WIB).

No. Cuplikan	**Variasi jarak (mm)**	**Variasi Nilai : X**	**Aktivitas rerata (N_0) (Bq/gr)**	**N_0 PTB-Jerman**
01	2 – 22	0.042 – 0.058	994.49 ± 1.05%	999.78 Bq/gr.
02	2 – 22	0.046 – 0.056	992.73 ± 1.26%	
03	2 – 22	0.041 – 0.050	1.010.22 ± 1.8%	
04	2 – 22	0.042 – 0.056	998.02 ± 0.98%	
05	2 – 22	0.041 – 0.053	997.32 ± 1.01%	
Rerata :			**998.56± 1.01%**	

MLP Radial Basis Functions for Forecasting of the Chaotic McGlass Time Series

Samingun Handoyo

Dept. of Statistic, Faculty of Science, Brawijaya University, Malang, Indonesia

Abstract

Neural Network (NN), recently was a central topic for research in the field of statistics since NN is no need for strict assumptions as in the conventional statistical methods. MLP with back propagation is an NN architecture and learning algorithms are widely applied to solve problems in the real world, one of which is for time series prediction. This research will implement MLP radial basis function for McGlass Chaotic time series prediction which is a time series that is a solution of delayed differential equations. This chaotic series was often used as a data bencmark by many researchers. There are two types of input format used as input system. Ie: the input format9 and the input format17. From 500 the McGlass data: 350 first data as training data and 150 on the latest data as testing data. The system is built requires two input parameters of the varian and the SSE. The system can also display the optimal parameters of NN weights and displays the value of the target-output numerically and graphs. System performance is evaluated based on the value of MSE, MAPE, the number of epochs and the time required during training process. Results obtained in this study is that the radial basis function NN is able to predict the McGlass data with very high accuracy, faster training time and number of epochs is smaller than compared with back propagation method.

Keywords: *Neural Network*, *Back Propagation, Radial bases function, Time series.*

1. Introduction

Time series is widely observed in many aspects of our lives. Daily temperature, stock market and so forth are examples of time series. Basically, there are two main goals in time series analysis: First, identifying the nature of the phenomenon represented by the sequence of observations and secondly prediction future values [1].

Basically, time series prediction can be considered as a modeling problem. The first step is est ablishing a mapping between input(s) and output(s). Usually, the mapping is nonlinear and chaotic. After such a mapping is set up, then we can use it to predict future values based on past and current observations.

Neural Networks have been widely used as time series forecasters: most often these are feed-forward networks which employ a sliding window over the input sequence. Typical examples of this approach are market predictions, meteorological and network traffic forecasting [1-3].

Two important issues must be addressed in such systems: the frequency with which data should be sampled, and the number of data points which should be used in the input representation. In most applications these issues are settled empirically, but results from work in complex dynamic systems suggest helpful heuristics.

Multi Layer Perceptron (MLP) Radial Basis Functions (RBF) emerged as a variant of ANN in late 80's. However, thier roots are entrenched in much older pattern recognition techniques as for example potential function, clustering, functional approximation, spline interpolation and mixture models [4].

RBF's are embedded in a two layer neural network, where each hidden unit implements a radial activated function. The output units implement a weighted sum of hidden unit outputs. The input into an RBF network is nonlinier while the output is linier. Their excellent approximation capabilities have been studied [5,6]. Due to their nonlinier approximation properties, RBF network are able to model complex mappings, which perceptron neural networks can only model by means of multiple intermediary layers[7].

In order to use a MLP RBF network, we need to specify the hidden unit activation function, the number of processing unit, a creterian for modelling a given task and a training algorithm for finding the parameters of network. Finding the MLP RBF weights is called network training. After training, the MLP RBF network can be used with the data whose underlying statistics is smiliar to that of the training set. MLP RBF networks have been succesfully applied to a large diversity of applications including interpolation [5,6], control engineering

[7], speech recognition [8,9], image restoration [10], etc. The objective of this research is how to design and to implement the MLP RBF network in the McGlass data and also evaluated the network performance using SSE, number of epoch and MAPE.

2. Experimental Details

Formating data training and testing

The McGlass data is a chotic time series data that yeilded from the solution of delayed differential equation as below:

$$\frac{dx(t)}{dt} = \frac{0.2x(t-\tau)}{1+x^{10}(t-\tau)} - 0.1x(t) \qquad (1)$$

where t= time and $\tau =$constan. If $\tau \geq 17$ the series will have chaotic behaviour. Data set consists of 500 items data which devided to become two group. The first group has element of 350 first data item as the data set training and the second group has element of 150 latest data item as the data set testing. Both data set training and testing are built two type of input format ie: input format9 and format17. Each format input is built a matrix input and a vector target.

The first element of input format9 contains the 1st data item until 9th data item, the second element contains the 2th data item until the 10th data item. So this format has input a matrix 341x9 and target a vector 341x1 for training data, while the testing data has input a matrix 141x9 and target a vector 141x1. The first element of input format17 cotains the 1st data item until the 17th data item, the second element contains the 2th data item until the 18th data item. So that format17 has input a matrix 333x17 and target a vector 133x1 for training data, while the testing data has input a matrix 133x17 and target a vector 133x1.

RBF neural network

Radial basis function are embeded into a two layer feed forward neural network. Such a network is characterized by a set of inputs and a set of outputs. In between the inputs and utputs there is a layer of processing units called hidden units. Each of them implements a radial basis function. The way in which the network is used for data modelling is different when approximating time series and in pattern classification. In the first case, the network inputs represent data samples at certain past time laps, while the network has only one output representing a signal value as shown in Figure 1 [7].

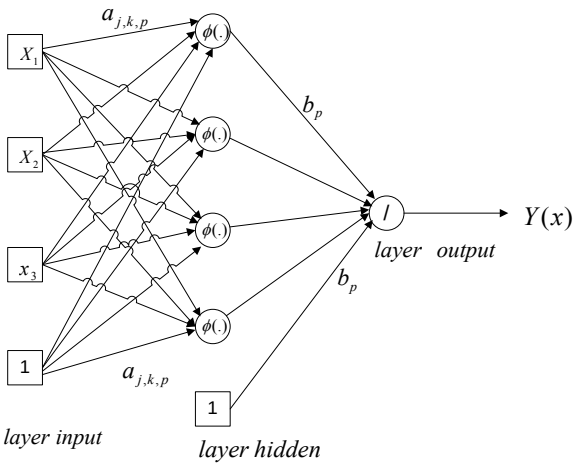

Figure 1. Architecture of RBF network

Various functions have been tested as activation function for RBF networks [6,7]. In time series modelling the most used zctivation function is the thin plate spline [8]. Mixtures of Gaussian have been considered in various scientific fields. The Gaussian activation function for RBF networks is given by:

$$\phi_j(X) = \exp\left[-(X-\mu_j)^T \sum_j^{-1} (X-\mu_j)\right] \qquad (2)$$

for $j = 1,...,L$, where X is the input feature vector, L is the number of hidden units, μ_j and $\sum_j$ are the mean and the covariance matrix of the *j*th aussian function. The mean vector μ_j represent the location, while $\sum_j$ models the shape of activation function. Statistically, an activation function models a probability density function where μ_j and $\sum_j$ represent the first and second order statistics.

The output layer implements a weighted sum of hidden unit outputs:

$$\psi_k(X) = \sum_{j=1}^{L} \lambda_{jk} \varphi_j(X) \qquad (3)$$

For $k = 1,...,M$ where λ_{jk} are the output weights, each corresponding to the connection between a hidden unit and an output unit and M represent the number of output units. The weights λ_{jk} show the contribution of hidden unit to the respective output. The flowchart of computation, as seen in Figure 2 (Appendixes), describes steps

of computation and prediction using RBF network.

3. Result and Dicussion

Determining of system input parameters

At begining the system is excecuted using a parameter by trial and error to some combination value of varian and SSE. This action has goal to get the pair of varian and SSE which has optimum value. The optimum value was reached, if the value of SSE testing has the smallest value. Any value of varian had been tried, and the best performance accurred at varian=0.8. Tabel 1 shows the pairs value of SSE data training and testing at varian=0.8. From Tabel 1, we can know that SSEtest minimun accurs at event 8th. Futhermore, the value of varian=0.8 and the value of SSEtrain=0.0005 are used as input parameters of system. Result of input format9 and input format17 is given in Appendixes.

Tabel 1 Some pairs SSEtrain and SSEtest

Events	SSEtrain	SSETest	MSEtest
1	0,89600	0,35200	0,002496
2	0,46000	0,15900	0,001128
3	0,09800	0,06900	0,000489
4	0,04300	0,05200	0,000369
5	0,01000	0,02700	0,000191
6	0,00500	0,02700	0,000191
7	0,00100	0,01300	9,22E-05
8	0,00050	0,01200	8,51E-05
9	0,00010	0,01400	9,93E-05
10	0,00005	0,01500	0,000106

Two former sections display graphically of the pairs value target and output of training and testing data set. The performance of RBF network and Feed forward network base on 4 charateristic (mape, mse, number of epoch, and time of training in scond) presented in Tabel 2 as below:

Tabel 2. Performance of RBF and FFNN

	Mp	MSE	Epc.	Time
RBF9	0.67	0.000008	166	7.3
FFNN9	0.86	0.000079	931	108.3
RBF17	0.83	0.000107	155	7.1
FFNN17	1.28	0.000299	1238	101.6

In the input format9, RBF has performance better than FFNN. The MSE value of RBF9 is 10 time smaller than FFNN9. The Mape of RBF9 is also smaller than Mape of FFNN. Those results indicate that RBF has more accuracy than FFNN to forecast the McGlass data. The number of epoch and the time needed in training process of RBF method is also smaller than FFNN method. This means that RBF method has more eficient in computation than FFNN method. The semiliar results also can be met in the input format17 but the differences of performance are not as extrime as in input format9.

4. Conclusion

Based on the results form former section, we can conclude some inferences which are:

a. RBF network and FFNN can be used to forecast the McGlass data which yeild high accuracy.
b. RBF network has better performance than FFNN network to forecast McGlass data.
c. The training process in RBF network needs more little time and few epoch than FFNN.

5. Acknowledgement

---

6. References

[1]. Patterson D W, Chan K H, Tan C M. (1993), Time Series Forecasting with neural nets: a comparative study. *Proc. the international conference on neural network applictions to signal processing*. NNASP Singapore pp 269-274.

[2]. Edwards, T., Tansley, D, S.W.,Davey, N.Frank, R. J. (1997), Traffic Trends Analysis using Neural Networks. *Proceedings of the International Workshop on Applications of Neural Networks to Telecommuncations 3*. pp. 157-164.

[3]. Hamilton and James D. (1990), *Time series analysis,* Princeton University Press.

[4]. Bengio, S., Fessant F., Collobert D. A. (1995), Connectionist System for Medium-Term HorizonTime Series Prediction. *In Proc. Intl. Workshop Application Neural Networks to Telecoms* pp. 308-315.

[5]. Moody, J. (1989), ―Fast learning in network of locally-tunned processing unit," *Neural Computing,* vol. 1, pp. 281-294.

[6]. Bors, A. G. And Pitas, I. (1996), ―Median radial basis functions neural network," *IEEE trans. On Neural Network*, vol. 7, no. 6, pp. 1351-1364.

[7]. Broomhead, D.S, and Lowe, D. (1998), " Multivariate functional interpolation and adaptive networks" . *Complex Systems*, vol. 2, pp. 321-355

[8]. Sanner, R. M., and Slotine, J.E. (1994), ―Gaussian networks for direct adaptive control".*IEEE Trans. on Neural Networks*. Vol. 3, no. 6, pp. 873-863.
[9]. Bors, A.G., Gabbouj, G. (1994), ―Minimal topology for a radial basis function neural network for pattren classification." *Digital Signal Processing: a review journal*, vol. 4, no. 3, pp. 173-188.
[10]. Cha, I., and Kassam, S.A. (1996), ―RBFN restoration of nonlinearly degraded image". *IEEE trans. on Image Processing*, vol. 5, no. 6, pp. 964-975.

Appendixes

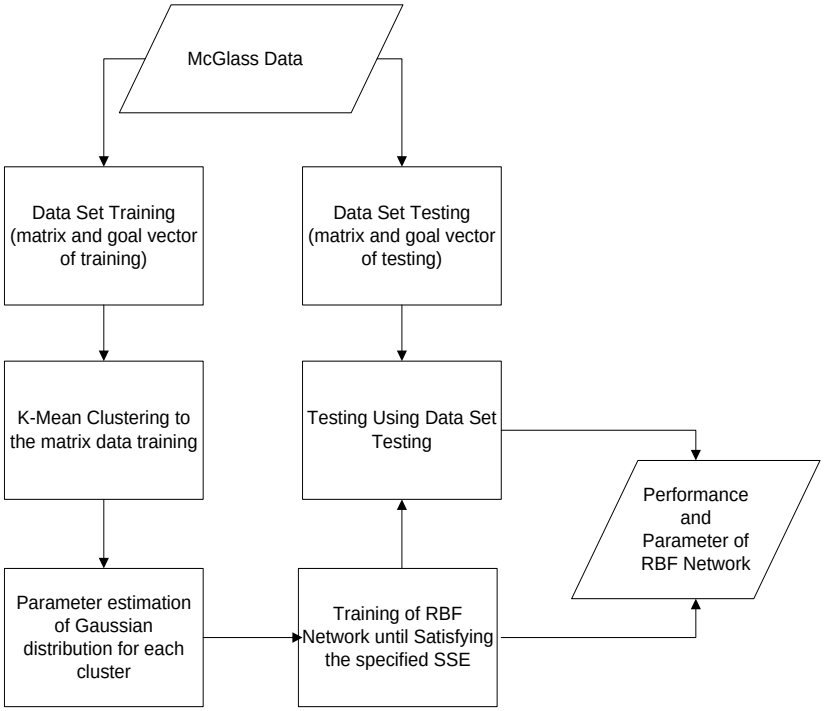

Figure 2. The Steps of computation in system built

Result of input format17

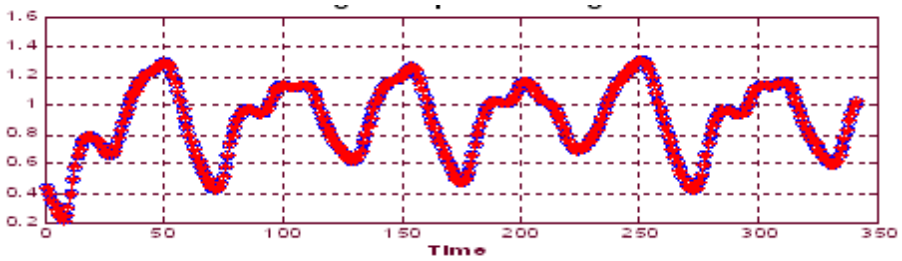

Figure 3. Plot of pairs output and target of training data for RBF

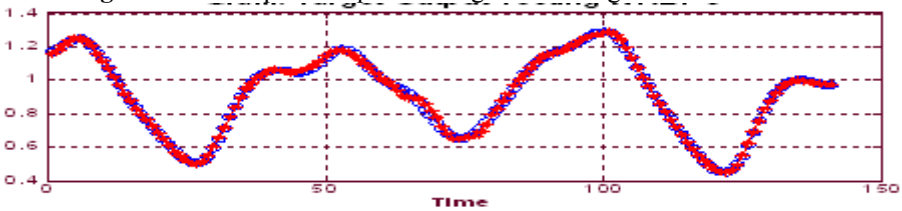

Figure 4. Plot of pairs output and target of testing data for RBF

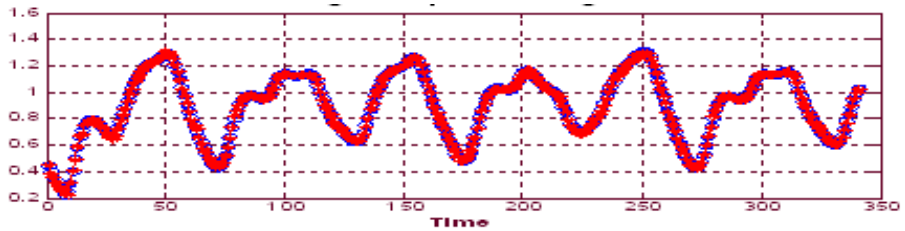

Figure 5. Plot of pairs output and target of training data for feed forward

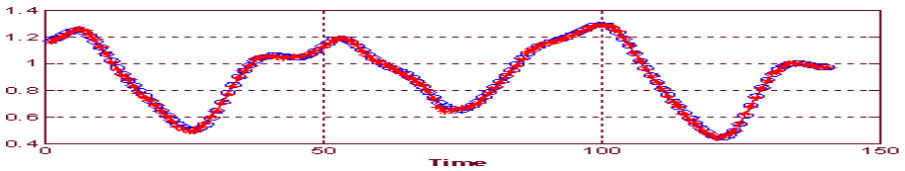

Figure 6. Plot of pairs output and target of testing data for feed forward

Result of input format17

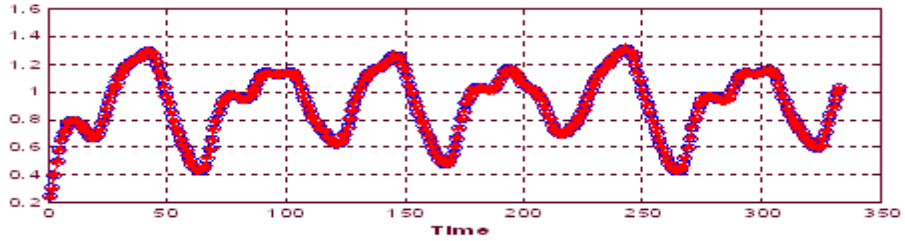

Figure 7. Plot of pairs output and target of training data for RBF

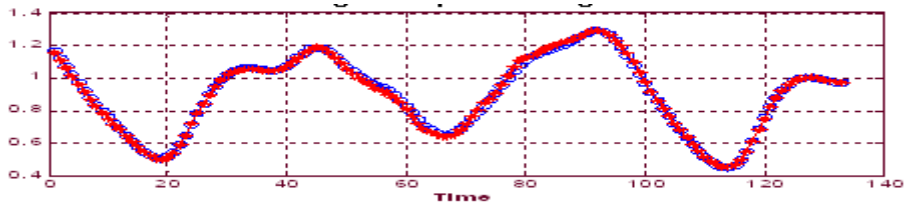

Figure 8. Plot of pairs output and target of testing data for RBF

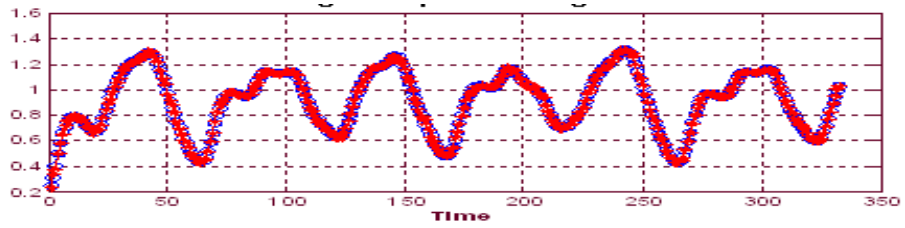

Figure 9. Plot of pairs output and target of training data for feed forward

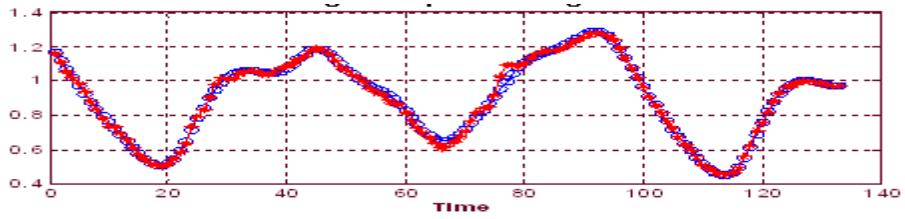

Figure 40. Plot of pairs output and target of testing data for feed forward

Sample Preparation Technique for Total Arsenic in Tuna Fish

Tiny Agustini Koesmawati [1] , Buchari [2], Aminuddin Sulaiman [3], Slamet Ibrahim [4], Kevin A. Francesconi [5]

[1,2,3] Department of Chemistry, FMIPA, Bandung Institute of Technology, Indonesia
(buchari@chem.itb.ac.id)
[4] Department of Pharmacy, FMIPA, Bandung Institute of Technology, Indonesia
[5] Institute of Chemistry–Analytical Chemistry, Karl-Franzens University, Graz, Austria

Abstract

Sample preparation is the most critical part of the analysis as it is responsible for the largest and often hidden source of errors. A conventional microwave oven assisted acid digestion was compared with dry ashing slurry method followed by hydride generator (HG) AAS measurement. The method was validated using DORM-2 certified reference material (dogfish muscle tissue (certified [As] = 18.0±1.1 µg/g found [As] 18.3±0.64 µg/g n=3)). Dry ashing slurry method provided a better result compared to microwave oven assisted acid digestion. This method is simple, economic, effective and reliable and is especially suitable for routine analysis of large amount of samples.

Keywords*: sample preparation, total arsenic*

.1. Introduction

Marine organisms may cause an accumulation of high arsenic concentration, which may be harmful to humans. Hence, arsenic species need to be measured in seafood to discover the potential threat to consumers. It is very well known that arsenic toxicity depends not only on the total concentration but also on the chemical species in which this element occurred [1,2]. Inorganic arsenic species (arsenite (As(III)) and arsenate (As(V))) are more toxic than the methylated arsenicals (monomethylarsonic acid (MMA) and dimethylarsinic acid (DMA)), followed by more complex organic arsenicals (arsenobetain (AB), arsenocholine (AC), tetramethylarsonium ion ($TMAs^+$)), which are considered to be non-toxic to living organisms [3,4,5].

Determination of total arsenic is influenced by a number of factors in these biological animals. The AB molecule is difficult to decompose and may remain intact in situation where most other organic molecules have been decomposed. Generally, available commercial microwave digestion systems seldom exceed temperature greater than 260^0C but AB will remain undigested at temperature less than 300^0C in atmospheric pressure. However, AB digestion can be achieved by using specialized closed vessel with high pressure at 250^0C. Sample preparation plays an important role in the analysis as it is responsible for hidden course of error. This research reported the difference of the results from two digestion methods, conventional microwave oven and dry ashing slurry method for tuna fish sample. The sample was analyzed by HG-AAS for the total arsenic. This method is based on the conversion of inorganic arsenic to $AsCl_3$ by treatment with KI to reduce As(V) to As (III). Total arsenic concentration in dried tuna fish sample from conventional microwave oven digestion was found lower than dry ashing digestion. ICP-MS was used to analyzed the total arsenic in dried tuna fish sample and DORM-2 was used as CRM.

2. Experiment Details

Instrumentation

The hydride Generator Atomic Absorption Spectrophotometer (HG-AAS) used was a Zeeman Hitachi Z-500 with the following condition:

Wavelength	: 193.7 nm
Atomizer	: standard
Flame-type	: air-C_2H_2
Fuel-flow	: 1.7 L/min
Delay time	: 20 sec
Measurement time	: 5 sec

Hydride generator principle

Two peristaltic pumps with twin channels are employed to pump the reagents. Pump-1 is used to pump the reagents Acid (HCl 1.2%) & Boro Hydride (1%), while pump-2 is used to pump the sample. One end of the peristaltic pump tubing is connected to the reservoir & the other

end to the mixing manifold. The mixing manifold has 3 inputs & one output. However, for the analysis on the AAS only three inputs are used, Acid, Boro-Hydride & Sample. This metal hydride is carried into a quartz tube placed above the burner.

Chemicals, Reagents and Standards

Water used throughout the investigation was Milli-Q water (18 MΩ cm). The following chemicals, all of analytical grade, were used in the study: hydrochloric acid, magnesium oxide, magnesium nitrate, sodium borohydride, sodium hydroxide, potassium iodide, and arsenate standard from Merck, Germany.

Determination of total arsenic content

Microwave oven method

A 2 ml HNO_3 p.a. and 0.5 ml H_2O_2 p.a. was added to 500 mg sample of freeze dried tuna fish in Teflon vessel, and left overnight. The vessel was put into microwave oven for 10 minutes at 200^0C, cooled, then added 3 ml HNO_3 p.a, and 1 ml H_2O_2, then put back into the microwave oven for another 10 minutes at 200^0C. After cooling, the sample was transferred from Teflon vessel into conical flash, added 1 ml of H_2SO_4 2.5N, 5 ml $K_2S_2O_8$ 5%, boiled for 30-40 minutes until the solution volume is approximately 10 ml. This solution was transferred to 50 ml volumetric flash, added 5 ml HCl p.a. and 5 ml KI 10%, and HNO_3 0.1N was added to meet the final volume of 50 ml. This solution was ready to be measured by HG-AAS.

Dry ashing method

Slurry, consisting of 50.0 ml water, 3.0 g $Mg(NO_3)_2$ and 5.0 g MgO was added to a sample of freeze dried tuna fish. A 50 mg of sample was weighted and mixed with 1.5 ml slurry in crucible and dried for 16 hours at 80^0C, followed by 1 hour at 200^0C, 1 hour at 300^0C and 8 hours at 500^0C in a muffle furnace. After cooling, the samples were dissolved by adding mixture solution of HCl : KI : ascorbic acid (%:1:1 v/v/v), then warmed for 10 minutes at 40-50^{o}C. Analysis was conducted by hydride generation atomic absorption spectrophotometer (HG-AAS) using Hitachi hydride system HFS-3 coupled to a Hitachi Zeeman Z-500 AAS and arsenic was detected at 193.7 nm. A 1% sodium borohydride ($NaBH_4$) solution was used as the reducing agent. The reaction time was 10 seconds through quartz cell and argon gas was used as a carrier gas. Calibration curve of peak area absorbance versus concentration of arsenic prepared by weighing 0.30, 0.75, 1.20 g As(V) 1 ppm standard to 30 g of 1.5 % HCl in a reaction tube. So that the arsenic was between 10-40 ng/ml. Arsenic concentration in the reaction flask were calculated using linear regression.

ICP-MS with Ultraclave III digestion

Total arsenic content was determined in dried tuna fish sample by ICP-MS (Agilent 7500), followed by an acid mineralization using Ultraclave III. Portion of sample (usually 100 mg of dry mass), HNO_3 (2 ml), and water (2 ml) were transferred to 12 ml quartz tubes. The tubes were placed in a Teflon rack and covered with Teflon caps, and the rack was mounted into microwave system. The holding vessel was filled with 300 g of water and 5 g H_2SO_4, the system was closed and loaded with argon to $4x10^5$Pa and the mixture was heated for 30 minutes at 250^0C. After mineralization, the samples were diluted to 10 ml with water in polypropylene tube before analysis with ICP-MS. The method was validated using the analysis of DORM-2 (dogfish muscle tissue (certified [As] = 18.0±1.1 µg/g found [As] 18.3±0.64 µg/g n=3).

3. Result and Discussion

Major arsenic species found in marine animal is AB [6,7]. AB is not completely transformed into arsenate during digestion; the total arsenic concentration depends on the AB digestion products formed. The variety in total arsenic concentration depends on the digestion procedure used. It is obvious that incomplete digestion of AB to arsenate results a lower of the total arsenic concentration, as shown in Table 1 (Appendixes). ICP-MS was used to check the result of dried tuna fish sample and DORM-2 as certified reference material (CRM).

Figure 1 (Appendixes) showed the calibration curve of arsenic which was measured by ICP-MS. The linear range was found 0-100 ng/g. Figure 2 (Appendixes) showed the calibration curve of As (V) and As (III) which were measured by HG-AAS. The linear range of standard was 0 to 10 ng/g and 0 to 40 ng/g for As (III) and As(V) respectively. All standard solution was prepared by gravimetric method. ICP-MS measurement of total arsenic was carried out in Karl-Franzens University, Graz, Austria, whereas other results were carried out in our laboratory in Indonesia. Dried tuna fish samples used in this study was being prepared in Indonesia.

Table 1 (Appendixes) compared the results for different sample preparations. Pre-reduction using mixing solution of 2M HCl:15% KI:15% ascorbic acid in aqueous (5:1:1 v/v/v) to dry ash digest gave a better result compared to sample

without pre-reduction process. Dry ashing method D-Ash-1 was found unsteady, the RSD was high (RSD = 16.6%) compared to D-Ash-2 with pre-reduction process (RSD = 6.96%). Microwave oven acid digestion method gave a very low results compared to dry ashing method. A true value mean concentration of dried tuna fish sample was found 3.61µg/g.

4. Conclusion

To guarantee the accurate determination of the total arsenic concentration, complete mineralization of arsenic compounds in samples is required. The new and novel procedure has overcome the significant problems associated with the determination of the total Arsenic contained in dried tuna fish. The principal advantages of dry ashing procedure are the possibility of treating large amount of sample and dissolving the resulting ash in a small volume of acid (generally hydrochloric). This procedure allows pre-concentration of trace elements in the final solution which is useful when very low analyte concentrations are used to be determined. Such advantages are not realizable by microwave digestion method. In addition, heterogeneity is a typical property of many biological materials.

The possibility of processing larger amount of sample, which upon mineralization provides a homogeneous solution, helps to minimize sub-sampling errors. The sample matrix is substantially simplified and the resulting ash is completely free of organic matter. This is prerequisite for ensuring accuracy of some analytical techniques wherein analyte response may be influenced by the presence of residual carbon or some undigested organic molecules. The resulting solutions are in very acceptable aspects (clear, colourless and odourless).

It was rarely found when microwave oven digestion methods are used and residual carbon content often attains elevated values. Compared to microwave oven digestion methods, reagent volumes and their handling are reduced in dry ashing procedures. The acidity of the final solutions can efficiently be controlled: the acid is added directly to the ash and only a small fraction is consummated during its dissolution. In microwave oven digestion procedures, the added acids must be sufficient to ensure the destruction of the organic matter and their effective amounts utilized during these chemical reactions which vary quite significantly. Pre-concentration process for dry ashing sample preparation method was found to give a better and steady result compared to microwave oven digestion.

5. Acknowledgements

We would like to thank Ministry of Science and Technology for the financial support to visit Institute of Chemistry, Karl-Franzens University Graz, Austria.

6. References

[1]. P. Fodor, in: L. Ebdon, L. Pitts, R. Cornelis, H. Crews, O.F.X. Donard, Ph. Quevauviller (Eds.), (2001), Trace Element Speciation for Environment, Food and Health, The Royal Society of Chemistry, Cambridge, UK, (Chapter 11).

[2]. R. Eisler (2000), Handbook of Chemical Risk Assessment Health Hazards to Humans, Plants and Animals, Metalloids, Radiation, Cumulative Index to Chemicals and Species, vol. 3, CRC Press, Boca Raton, FL, (Chapter 28).

[3]. S. Garcıa Salgado, M.A. Quijano Nieto, M.M. Bonilla Simo (2006), Optimisation of sample treatment for arsenic speciation in alga samples by focussed sonication and ultrafiltration , *Talanta*, 68, 1522–1527.

[4]. M. Leermakers, W. Baeyens, M. De Gieter, B. Smedts, C. Meert, H.C. De Bisschop, R. Morabito, Ph. Quevauviller (2006), Toxic arsenic compounds in environmental samples: Speciation and validation, *Trends in Analytical Chemistry,* Vol. 25, No. 1.

[5]. K.A. Francesconi, J.S. Edmonds (1994), in: J.O. Nriagu (Ed.), Arsenic in the environment. Part 1. Cycling and Characterization, John Wiley & Sons, New York, pp. 221–263.

[6]. K.A. Francesconi and John S. Edmonds. (1998), Arsenic species in marine samples, *Croatica Chemica Acta* 71 (2), 343-359.

[7]. K. A. Francesconi and Doris Kuehnelt, (2004), Determination of arsenic species: A critical review of methods & applications, 2000–2003, *Analyst*, 12 9 , 373 – 395.

Appendixes

Table 1. Total arsenic concentration in dried tuna fish for different sample preparation

SAMPLE CODE	ICPMS	HG-AAS		
	Ultraclave (µg/g)	MO (µg/g)	D-Ash-1 (µg/g)	D-Ash-2 (µg/g)
T-1	3.36	0.08	1.75	2.80
T-2	3.50	0.09	2.05	3.41
T-3	3.42	0.09	1.36	2.97
T-4	3.58	0.11	1.66	3.23
T-5	3.86	0.08	-	2.98
T-6	3.93	0.08	-	3.07
Mean	3.61	0.09	1.71	3.08
Std. Dev.	0.24	0.01	0.28	0.21
RSD (%)	6.52	14.71	16.57	6.96

DORM-2	19.20
DORM-2	18.20
DORM2	19.40
Mean	18.93
Std. Dev.	0.64
RSD (%)	3.40

D-Ash-1 = without pre-reduction
D-Ash-2 = with pre-reduction
DORM-2 CRM certified value of 18.0 ppm ± 1.1 ppm

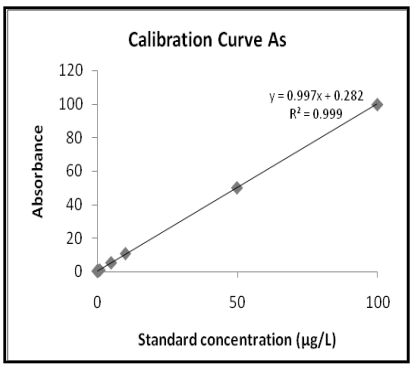

Figure 1. Calibration curve for standard arsenic by ICP-MS

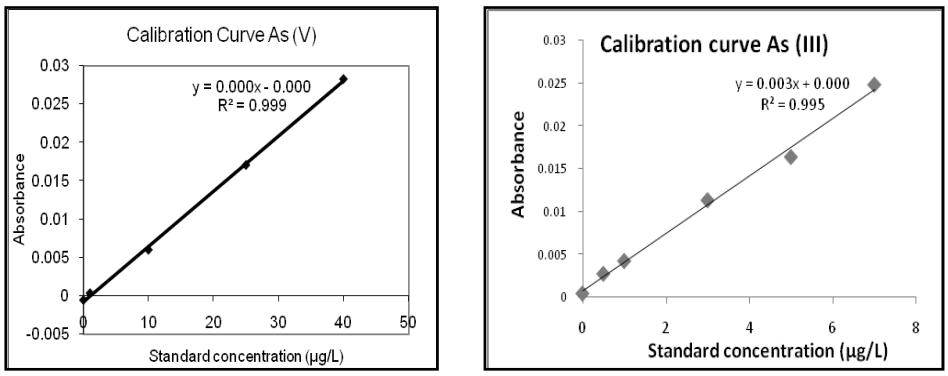

Figure 2. Calibration curve for standard As(V) and As(III)

Test Rate of Evaporation and Oxidation Stability of Synthetic Sex Pheromone Candidate Molecules Engineered Alpha Linolenic Acid (ALA) of Basil Seed Oil (*Ocinum basilicum* L.)

Warsito [1,2], Jumina [3], Chairil Anwar [3]

[1] Student Doctoral Program, Dept. of Chemistry, Faculty of Science, University of Gadjah Mada
[2] Department of Chemistry, Faculty of Science, University of Brawijaya
[3] Department of Chemistry, Faculty of Science, University of Gadjah Mada
Corresponding author: warsitoub88@yahoo.com

Abstract

Evaporation rate test, oxidation stability and test-electroantenogram has been performed of 10,12,14-octadecatrienyl acetate and 10,12,14-octadecatrienal compounds engineered from ALA molecules, each as a candidate synthetic sex pheromone *Glyphodes pyloalis* Walker and *Manduca sexta* Linnaeus. Evaporation rate is determined by processing data measured changes in concentration of sex pheromone candidates (12.5 ppm) in the solvent n-octanol on each interval 0, 1, 2, 3, 4, 5 hours. Oxidation stability is determined by processing the data changes in absorbance at each observation interval of 1, 2, 3, 4, 5 weeks after the sex pheromone candidate solution subjected to UV light for night (6 pm to 6 am) and sunlight for daytime. The results showed that the release of synthetic sex pheromone candidate 10,12,14-octadecatrienyl acetate has a higher evaporation rate compared to synthetic sex pheromone 10,12,14-octadecatrienal with $k\text{-}_{evap.}$ and $t_{1/2}$ respectively (0.029 $hour^{-1}$ and 23.9 hours) and (0.020 $hour^{-1}$ and 34.65 hours). The synthetic sex pheromone candidates both have high stability against oxidation by air and / or UV light.

Keywords: *the rate of evaporation, oxidation stability, EAG, candidate sex pheromone,* $k_{evap.}$ *dan* $t_{1/2}$.

1. Introduction

In an effort to increase the production of plantation crops, such as tobacco (as a producer of large excise > 14 trillion) and mulberry (as a natural feed silkworms) are often constrained by leaf-eating pests. One of the leaf-eating insect pests of tobacco plants is Manduca sexta Linnaeus. Although *M. sexta* L. is not the main insects to tobacco plants in Indonesia, but because the larvae of leaf-eating insects are also others, especially tomatoes, including eggplant, potatoes and cherries [1,2], these insects need to obtain serious attention. Meanwhile, insect larvae attack the leaves of mulberry leaves from young to old leaves by eating all the leaves except leaves bones and can cause the leaves turn to brown transparent is *Glypodes pyloalis* Walker [3,4]. If this insect will have lower production expanded leaves to feed silkworms.

For communication with other insects in the same species, in particular sexual communication, female insects moth *M. sexta* L. and *G. pyloalis* W., secrete sex pheromone consisting of a complex mixture of compounds with unsaturated carbon chains C_{16}. Two major components of the eight constituent pheromone aldehyde compounds *M. sexta* L. who have an attraction to male insects are the two greatest hexadecatrienal isomers, namely E10, E12,E14-16:Ald and E10,E12,Z14-16:Ald [5-7]. While the sex pheromone secreted by female insects G. pyloalis W. has a carbon skeleton analogous to the functional group-acetyl ester, namely isomers E10, E12,E14 and E10,E12,Z14-hexadecatrienil acetate [8-10].

Development of sex pheromone molecules synthesis have been carried out using the basic ingredients of decanediol 1,10-carbon chain extension approach [10C + 6C] to sex pheromone compounds that have a geometry E10,E12,E14, while for the sex pheromone with E10,E12, Z14 geometry uses carbon chain extension [{10C + 4C } + 2C]. The existence of different geometry system, E,E,E and E,E,Z has resulted in differences in the synthesis route and the number of reaction steps that must be passed to obtain their respective sex pheromones. Each line consists of the formation reactions equipped with two double bonds and one double bond stereospesifik through Wittig reaction [5,6].

The use of natural materials as the base material synthesis recently started many

structurally developed and used as a carbon source khiral or geometry of the pheromone molecules. As a source of carbon khiral include R-citronellal compound used as the base material in the synthesis of sex pheromone fly, *Cochliomya hominivorax* [11] and compound R-sitronelol for the synthesis of sex pheromone beetle bucis peas and beans, *Callosobruchus maculus* [12] and soybean lice sex pheromone decay, Euschistus obscures [13]. Compounds (+)-α-pinen can be used to synthesize insect sex pheromone of citrus fruit, *Planococcus citri* and analogues [14]. Meanwhile, as the source geometry, among others, for the synthesis of linolenic acid methyl moth sex pheromone tree sap, *Mnesampela private* [15] and oleic acid for the synthesis of sex pheromone household fly, *Musca domestica* [16].

Based on the above description, the basic framework of the molecular similarity of ALA with sex pheromone molecules from the two insect pests of plants above the ALA molecules have been isolated from basil seed oil (*Ocinum basilicum* L.) and then used as the base material for the synthesis of sex pheromones via three-phase reaction process without going through the extension of carbon chain. The first phase isomerization of unsaturated carbon skeleton and not conjugated from ALA (cis9,cis12,cis15) changed its position and geotrinya into (trans10,trans12,trans14). The second phase change carboxylic functional group (-COOH) of ALA into-acetyl ester (-C(= O)-OCH3, and aldehyde (-CHO), so the geometry and functional groups according to sex pheromone molecules *G. pyloalis* W. and . *M. sexta* L. [17].

Synthetic sex pheromones in integrated pest management, IPM, can be used for the detection and monitoring of insect pests, predict the state of insect larvae populations, to suppress insect populations and reduce operational costs and manpower. To apply as a trap mass or insect mating disruption necessary or media regulator compound release pheromones into the air [18-20] for the amount of synthetic sex pheromone exist in sufficient air, so as to affect the insects that were targeted in accordance with the speed and duration of the planned [21]. Ideally pheromone release rate is relatively constant and are available in the air effectively during the period of flying insects [18]. Besides, many Lepidoptera pheromone component comprising an aliphatic carbon chain with at least membered 10 carbon atoms and one double bond in the molecule, is very susceptible to degradation by UV light and oxidized [18,22]. Thus the evaporation rate test pheromone into the air, the oxidation stability of synthetic sex pheromone is a very important part when candidate sex pheromone will be applied in the field.

2. Experimental Detail

To make solution of candidate synthetic sex pheromone with a concentration of 12.5 ppm using the solvent n-octanol. Synthetic sex pheromone candidate solution is inserted into the vial (4 mL) equipped with a plastic cover to test the rate of evaporation and in the rubber-covered venojec for oxidation stability test.

Test the solution evaporation rate of synthetic pheromone candidates each vial containing a solution of synthetic sex pheromone candidates (each 5 pieces) is placed in the test room. The room measured temperature, pressure and humidity during the experiment. Vials are placed test room open, so space is obtained from the wind outside. The surface of the sex pheromone solution in the vial marked, closed vial is opened and then in turn every hose 0j, 1j, 2 j, 3j, 4j, 5J vial closed. Sex pheromone solution in each vial that has undergone solvent evaporation coupled with n-octanol to mark the beginning of the limit, so the volume of the same sex pheromone solution as before, shaken until homogeneous.

Then each solution of the sex pheromone is made of UV spectrum in the range of 200-400 nm and recorded at a wavelength of maximum absorbance. Absorbance data is converted to the concentration of sex pheromone and made charts the relationship between times with the concentration of pheromone remaining. From the graph defined slope as constant value (k) sex pheromone evaporation and calculated half-life ($t_{1/2}$) process of evaporation.

Oxidation stability test solution of synthetic sex pheromone candidates each test solution sex pheromone (in venojec tube) clamped at a height of 40 cm and at the same height at a distance of 1 m mounted UV lamp. Venojec tube containing a solution of the sex pheromone was placed in a chamber while exposed to UV light (at 6.00 p.m. to 6.00 am) and subjected to sunlight for daytime. Each hose 1, 2, 3, 4, 5 weeks, each solution is made of UV spectrum in the range of 200-400 nm and adde absorbance at maximum wavelength. Furthermore plots the relationship between times versus absorbancei to analyze the oxidation stability of each solution candidate test synthetic sex pheromone.

3. Results and Discussion

The approach used to study the ability of the solvent n-octanol as a regulator of the release candidate of synthetic sex pheromone into the air, in this study carried out by placing a solution of synthetic sex pheromone candidates in small-mouthed glass vial, so that only through surface evaporation vial. Placement test vial near room open space intended for the evaporation of pheromone solution in the vial is influenced by natural air flow velocity, so that the evaporation process is expected to be close to evaporation when a solution of synthetic sex pheromone candidates applied in the field. Changes in concentration can be determined by measuring the absorbance of each solution of the synthetic sex pheromone candidates (12.5 ppm) after evaporation for 0, 1, 2, 3, 4 and 5 hours in experimental space conditions (air temperature 32-30 °C humidity 39 , 9 - 42.9%, the air pressure of 697 mmHg) to synthetic sex pheromone candidate synthetic 10,12,14-octadecatrienyl acetate at 288.5 nm and max experimental conditions (air temperature from 28.5 to 30.5 C, humidity max 280.5 nm.λ49.0 to 54.5%, air pressure 697.5 mmHg) to synthetic sex pheromone candidates 10,12,14-octadecatrienal.

Although some ways of sex pheromone release arrangement can be developed, in this study simulated pheromone discharge arrangements made by dispersing the synthetic sex pheromone candidate compounds into an organic solvent which is less volatile, i.e. n-octanol. Another approach is the solution placed in a small-mouthed glass vial, so that only through surface evaporation vial. In addition vial is placed near open window in the test room that is intended for solution of pheromone evaporation caused by the flow of outside air, so that the evaporation process is expected to be close to evaporation when a solution of synthetic sex pheromone candidates applied in the field.

In line graph Figure 1, it appears that the relationship between ln C_0/C on the evaporation time, both have a relatively high linearity and evaporation followed the order one, like the evaporation of pheromone compounds the other. The release into the air candidate synthetic sex pheromone 10,12,14-octadecatrienyl acetate faster than the release of synthetic sex pheromone 10,12,14-octadecatrienal in n-octanol dispersing media. This means that during the solvent n-octanol surrounding molecules of synthetic sex pheromone candidates 10,12,14-octadecatrienal interaction is stronger than when this solvent molecules surrounding the candidate synthetic sex pheromone 10,12,14-octadecatrienyl acetate. Because of the structural differences in both candidates have a synthetic sex pheromone in functional groups; this means electrons density of oxygen in the aldehyde group is higher than the acetyl group.

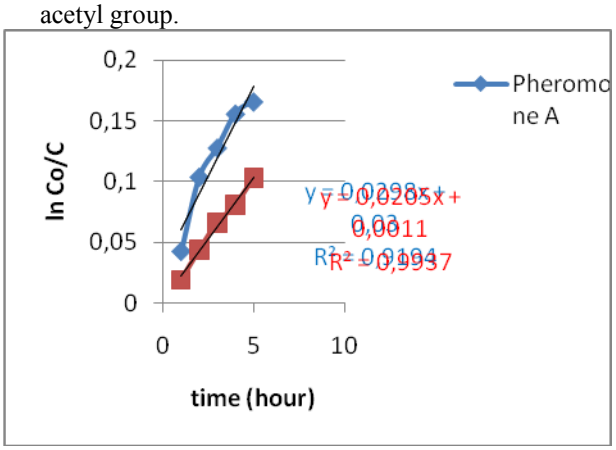

Figure 1. Relation changes of concentration of sex pheromone candidate versus the evaporation time.

Note:
Pheromone A = sex pheromone candidate 10,12,14-octadecatrienyl acetate
Pheromone B = sex pheromone candidate 10,12,14-octadecatrienal

It also seems that the release rate of synthetic pheromone candidates 10,12,14-octadecatrienyl acetate at the beginning of the process of evaporation reaches 3 times faster than the synthetic sex pheromone candidates 10,12,14-heksatrienal (ratio 3: 1), but when the long process of evaporation close to half of each sex pheromone release speed ratio led to a constant value of 1.8: 1. Evaporation constant value (k) and the half-life ($t_{1/2}$) of each candidate synthetic sex pheromone are 0.029 $hour^{-1}$ and 23.9 hours for the synthetic sex pheromone candidates 10,12,14-octadecatrienyl acetate, whereas for the candidate synthetic sex pheromone 10,12,14-octadecatrienal repectively 0.020 $hour^{-1}$ and 34.65 hours.

Oxidation stability testing becomes a very important part studied in this research, because the carbon skeleton of the synthetic sex pheromone candidates contains three double bonds in conjugation system. Besides, the aldehyde functional group in candidate sex pheromone *M. sexta* L. which is prone to oxidation when in contact with air and acetyl functional group (ester) in the synthetic sex pheromone candidate *G. pyloalis* W. very easy to experience the process of hydrolysis when loose in high humidity air.

Study of oxidation stability of synthetic sex pheromone candidates in this study done by

making the solution at a concentration of 12.5 ppm in the solvent n-octanol without added anti-oxidant substances. Experiments carried out by placing a solution of synthetic sex pheromone candidates respectively in venojec tube, and then clamped at statip and subjected to UV light for night (at 06.00 pm to 06.00 am) and with radiation for daytime sun with space conditions (air temperature 32-30 °C, moisture from 39.9 to 42.9%, the air pressure of 697 mmHg). In each time interval 1, 2, 3, 4, 5 weeks was observed solution absorbance at Figure 2 is a graph of the relationship between the absorbance versus irradiation time with UV light.

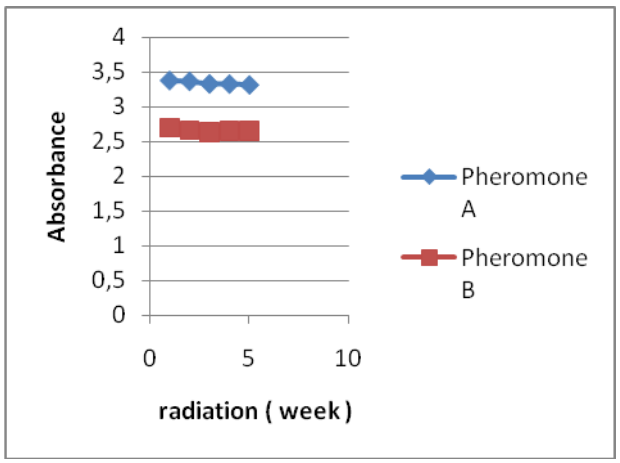

Figure 2. Relation of absorbance versus irradiation time

Note:
Pheromone A = sex pheromone candidate 10,12,14-octadecatrienyl acetate
Pheromone B = sex pheromone candidate 10,12,14-octadecatrienal

The use of UV light that bears directly on a relatively close distance is expected to immediately know the effects on the molecules of pheromone candidates. The absence of a shift λ max and changes in absorbance of each solution candidate synthetic sex pheromone significantly during the experiment (Figure 2) shows that three-carbon unsaturated bond conjugated molecules contained in the synthetic sex pheromone candidates relatively stable. Stability is related to the geometric shape, EEE as the most stable isomer structure than the structure of other isomers. It can also be expressed aldehyde and acetyl groups (esters) in each pheromone are not oxidation or hydrolysis reaction. So, when candidates synthetic sex pheromone was applied in the field is not needed any additional antioxidants.

4. Conclusion

Based on the results described above, can be concluded as follows:

1. The release candidate 10,12,14-octadecatrienyl acetate synthetic sex pheromone for the insect *G. pyloalis* W in n-octanol media have a higher evaporation rate compared to 10,12,14-octadecatrienal synthetic sex pheromones for insect *M. sexta* L. with k-evap. and part-time in a row (0.029 hour^{-1} and 23.9 hours) and (0.020 hour^{-1} and 34.65 hours)
2. Candidates synthetic insect sex pheromone *G. pyloalis* W. and *M. sexta* L., both have high stability against oxidation by air and / or UV light

5. Acknowledgments

Thank to the Directorate General of Higher Education which has funded this research. We also thank to Department of Chemistry, Faculty of Science, University of Gadjah Mada that has been proposed this research.

6. References

[1]. Villanueva, R. (2007), Tobacco Hornworm, *Manduca sexta* (Linnaeus), and Tomato Hornworm, *Manduca quinquemaculata* (Haworth), (Insecta : Lepidoptera : Sphingidae), Entomology and Nematology Department (supported by T.R Fasulo, Featured Creatures Coordinator), Cooperative Extension Sevice, Institute of Food and Agricultural Sciences, University of Florida, Gainesville, FL.32611.

[2]. Mechauber WL, Capaldo CT, Hildebrand J.G. (2002), Behavioral responses of adult female tobacco hornworms, *Manduca sexta,* to hostplant volatiles change with age and mating status. *J. of Insect Sci.*, 2:5, 1-8.

[3]. Yesdani, E., Sendi, J.J., Zibaee, A. and Ghadamyari, M. (2010), Enzymatic properties of a-amylase in the midgut and the salivary glands of mulberry moth, Glyphodes pyloalis Walker (Lepidoptera: Pyralidae), *C.R. Biologies*, 333, 17–22.

[4]. Tashpulatova, B., Mukhamedalieva, S., Dowd, M.K., Talipov, S. and Ibragivo, B.T. (2009), Effect of gossypol and gossypol related compounds on Mulberry Pyralid (Diaphana pyloalis Walker, Lepidoptera : Pyralidae), A Pest of The Mulbery, *Uzbek Biologi Journal*, 2, 1-6.

[5]. Kalinova, B., Hoskovec, M., Liblikas, I., Unelius, C.R., Hansson, B.S. (2001), Detection of Sex Pheromone Components in

Manduca sexta (L.), *Chem. Senses*, 26 : 1175-1186.

[6]. Liblikas, I. (2004), Synthesis and behaviour activity of conjugated polyenic pheromone components, Doctoral Thesis, Stockholm, Institute of Organic Chemistry, Hamburg University, Germany, 1-55.

[7]. Tumlinson, J.H., Brennan, M.M., Dootlittle, R.E., Mitchell, E.R., Brabham, A., Mazomenos, B.E., Baumhover, H.A. and Jackson, D.M. (1989), Identification of pheromone blend attractive to *Manduca sexta* (L.), males in wind tunnel, *Arch. Insect Biochem.Physiol*.10, 255-271.

[8]. Kawazu, K., Honda, H. Nakamura S. and Adati, T. (2007), Identification of Sex Pheromone Components of the Box Tree Pyralid, Glyphodes perspectalis, *J. Chem. Ecol* 33:1978–1985.

[9]. Honda, A. Ando, T., Ogura, Y., Teramine, T. and Ueda, R. (1990), Identification of sex pheromone of the Mulberry pyralid, Glyphodes pyloalis Walker (Lepidoptera : Piralidae), *Appl. Ent. Zool*. 25, 2, 265-272.

[10]. Ando, T. and Ohsawa, H. (1993), Sex Pheromone Candidates with a Conjugated Triene System: Synthesis and chemical characterization, *J. Chem. Ecol*., 19,1, 1-12.

[11]. Mori, K., Ohtaki, T., Ohrui, H., Berkebile, D.R. and Carlson, D.A. (2004), Synthesis of the four stereoisomers of 6-Acetoxy-19-methylnonacosane, the most potent component of the female sex pheromone of the new world screwworm fly, with special emphasis on partial racemization in the course of catalytic hydrogenation, *Eur. J. Org. Chem.,* 1089-1096.

[12]. Nakai, T., Yajima, A., Akasaka, K., Kaihoku, T., Ohtaki, M., Nukada, T., Ohrui, H. And Yabuta G. (2005), Synthesis of the four stereoisomers of 2,6-dimethyloctane-1,8-dioic acid, *Biosci. Biotechnol. Biochem*., 69, 12, 2401-2408.

[13]. Zarbin, P.H.G, Reckziegelb, A., Plassb, E., de Oliveiraa, A.R.M, Simonelli, F. and de A. Marquesa, F. (2000), Synthesis of the Minor Sex Pheromone Component of Two Brazilian Soybean Stink Bugs (Het.: Pentatomidae), and an Analogue Compound, *J. Braz. Chem. Soc.,* Vol. 11, No. 6, 572-577.

[14]. Dunkelblum, E., Zada, A., Gross, S., Fraistat, P. And Mendel, Z. (2002), Sex pheromone and analogs of the citrus mealyburg, Planococcus citri: Synthesis and Biological Activity, *IOBC wprs Bulletin*, 25, 1-9.

[15]. Davies, N.W, Meredith, G., Moleshworth, P.P., Smith, J.A. (2007), Use of the anti-oxidant butylated hydroxytoluene in situ for the synthesis of the moth pheromone (Z,Z,Z)-3,6,9-nonadecatriene, *Aust. J. Chem*., 60, 848-849.

[16]. Zarbin, P.H.G., Villar, J.A.F.P. and Corrêa, A.G. (2007), Insect Pheromone Synthesis in Brazil: an Overview, *J.Braz. Chem. Soc.,* 18, 6, 1100-1124.

[17]. Warsito (2009), Rekayasa molekul asam α-linolenat (ALA) dari minyak biji selasih (*Ocinum basilicum* L.) menjadi kandidat feromon seks. Laporan Penelitian Prioritas Nasional, Direktorat Jenderal Pendidikan Tinggi.

[18]. Zada, A., Falach, L., Byers, A. (2009), Development of sol-gel formulation for low slow release of pheromone, *Chemoecology*, 19, 37-45.

[19]. Hojo, T., Ogawa, K., Alba Noboru, Fakumoto, T., (2006), Sustained releaser comprising sex pheromone substance and pest control method, *United State Patent Application Publication*, Pub. No.: US 2006/0057177 A1.

[20]. Yamamoto, A., Sakurada, T., Saghuci, R., (2001), Method for stabilizing a sex pheromone compound, *United State Patent*, Patent No. : US 6, 252,106 B1.

[21]. Mihou, A.P., Michaelakis, A., Krokos, F.D., Mazomenos, B.E. and Couladouros, E.A., (2007), Prolonged slow release of (z)-11-hexadecenyl acetate employeng polyurea microcapsules, *A.Appl.Entomol*., 13, 2, 128-133.

[22]. Strong, W.B., Millar, J.G., Grant, G.G., Moreira, J.A., Chong, J.M. and Rudolp, C., (2007), Optimazion of pheromone lure and trap design for monitoring the fir coneworm, Dioryctria abietivorella, *Entomol.. Exper. et Appl*., 126, 67-77.

[23]. Park, K.C and Baker, T.C., 2002, Improvement of Signal-to-Noise Ratio in Electroantennogram Responses Using Multiple Insect Antennae, *J. Insect Physiol.*, 48, 1139-1145.

Study of Structure and Magnetic Properties of Complex Compounds of Cu (II) with Nitronil Nytroxide and Dicyanamide Ion Ligands

I Wayan Dasna

Chemistry Department, Faculty of Mathematics and Natural Science, State University of Malang, East Java, Indonesia (idasna@um.ac.id)

Abstract

*The synthesis, X-ray crystal structures and magnetic properties of two new copper(II) complex containing Radical (Rad) (Rad = 2-(4-pyridil)-4,4,5,5-tetramethylimidazoline-1-oxyl-3-oxide) $Cu(Rad)_4Cl_2$ **(1)** and $Cu(Rad)_2[N(CN)_2]_2(H_2O)_2$ (**2**) are reported. The Cu atom in these two complexes are in a distorted octahedral geometry. These two complexes crystalized in triclinic system, space group Pī (#2), with parameters a = 7.138(13) Å, b = 13.283(13) Å, c = 13.900(9) Å, α = 90.94(6)°, β = 93.04(6)°, and γ = 100.65(6)° for complex (**1**); a = 7.210(2) Å, b = 9.996(3)Å, c = 12.931(8) Å, α = 69.61(5) °, β =87.68(4) °, γ = 70.17(2)° for complex (**2**). Magnetic properties of these two complexes show that antiferromagnetic interaction were dominate at low temperature.*

Keywords: *copper(II) complex, magnetic properties.*

1. Introduction

The field of molecular magnet has been an area of increasing interest and remarkable result in the last decade [1,2]. Several different approaches are currently used in order to design and synthesize molecule based magnetic materials exhibiting magnetic properties. One of the most efficient and exciting approaches is the metal-radical pathway where metal ions directly bound to stable organic radical such as nitroxide radical as building block [3].The paramagnetic nitroxide radical NITpPy (Rad), Rad stand for 2-(4-pyridyl)-4,4,5,5-tetramethylimidazoline-1-oxyl 3-oxide, was used as bridging ligand between metal in magnetic materials containing spin residing on *d* orbitals and *p*-orbitals such as $Mn(hfac)_2(NITpPy)$ [4-5] (hfac = hexafluoro-acetylacetonato) or in $[Cu(hfac)_2]_3(NITpPy)_2$ [6].

In the former compound, the Mn sites are μ_2-bridged via the oxygen atoms of the nitroxide groups, while they are linked in the second one via both the nitrogen atom of the p-pyridyl ring and the oxygen atoms of the NO groups. We are investigating such kinds of materials by including paramagnetic nitroxide radicals in the coordination sphere of the metal with the aim of increasing the magnetic moments of the starting complexes. Some paramagnetic nitroxide radicals are known as all – organic ferromagnets at very low temperature. They are also used as bridging ligands between metal ions in magnetic materials.

We are dealing, with the use of the radical and dicyanamide anions $[N(CN)_2]^-$ as ligands between paramagnetic complexes $M^{II}(Rad)_n^{2+}$ ($M=Cu^{II}$, Mn^{II}, Co^{II}). Some complexes were published [7]. This report focused on the compound of $Cu(Rad)_4Cl_2$(1) only containing four radicals and $Cu(Rad)_2[N(CN)_2]_2(H_2O)_2$ that containing radicals and dycianamide anion as ligands. We review here our results of the synthesis, X-ray crystal structure and magnetic properties of these two complexes.

2. Experimental Details

Synthesis

Compound **1** was synthesized by reacting $CuCl_2$ (0.1345 g, 1mmol), Rad (0.9440g, 4 mmol) and $NaN(CN)_2$ (2 mmol) in 10 mL of hot methanol (60°C, reflux). The mixture was stirred for 3 hour and the blue solution was kept overnight at 30°C leading to dark green needle crystals.

Compouns **2** was obtained by disolving 0.651 g (1 mmolof $Cu(Rad)_2(CH_3COO)_2$ in 10 ml of acetonitrile and added to a solution of $NaN(CN)_2$ (0.178 g, 2 mmol) dissolved in a mixture of acetonitrile/water (4 ml/1 ml). The solution was stirred overnight affording green small needle crystals. The product was washed with ethanol and water and recrystallised from acetonitrile.

Crystallographic data and structure determination

Single crystals of the title compounds (**1,2**) were mounted on an Enraf-Nonius four-circle diffractometer equipped with a CCD camera and a graphite monochromated Mo K radiation source (λ = 0.71073 Å). Data collection was performed at room temperature. No absorption corrections were performed and structures were solved with SHELXS-97 and re®ned with the SHELXL-97 program14 by full-matrix least-squares methods on F2. X-ray diffraction was carried out at *Universite de Rennes 1*, Rennes, France with Prof. Lahcene Ouahab and Dr. Stephane Golhen.

Magnetic measurement

Magnetic studies were carried out on a powder sample enclosed in a medical capsule. Magnetic susceptibility measurements were performed at 0.1 T, in the temperature range 2–300 K with a Quantum Design SQUID magnetometer MPMS-5. This work condacted at *Laboratoire des Science Moleculaires,* ICMCB, Pessac, France with Dr. Jean-Pascal Sutter.

3. Result and Discussion

Crystal structure

The crystal data is summarized in Table 1, while the crystal structure of **1** is given in Figure 1. In this strucure, the Cu atom located on inversion center of octahedral geometry. The Cu atom bond to four radicals through the N atom of the pyridyl rings locate in equatorial position while two Chlor atoms are trans coordination in axial position. Study of structure show that in the compund (1), lenght of Cu-N bond for four radicals are not the same lenghth. The distance Cu1-N(1) and Cu1-N(1*i*) are 2,064(3)Å, while the distance of Cu1-N(4) and Cu1-N(4*i*) longer 2,605Å.

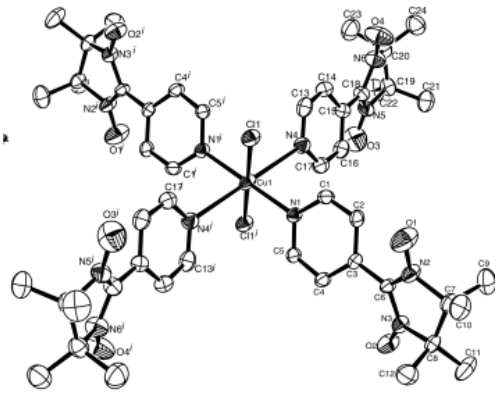

Figure 1. ORTEP representation with 50% ellipsoid probability of compound (**1**)

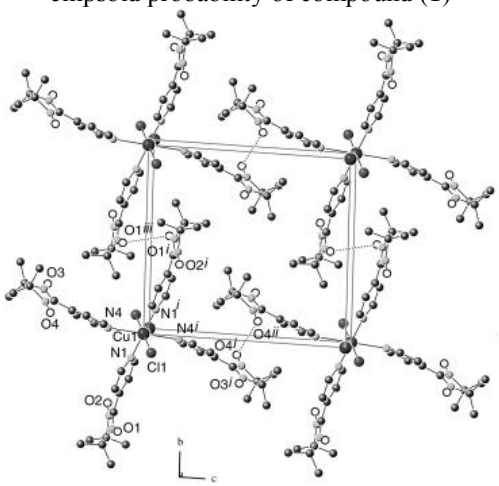

Figure 2. Unit cell content of compound 1

Table 1.Crystal data and structure refinement for (**1**) and (**2**)

Compound	**1**	**2**
Empirical formula	$CuC_{48}H_{64}C_{l2}N_{12}O_8$	$C_{28}H_{36}CuN_{12}O_6$
Formula weight	1071.55	700.23
Crystal system	triclinic	triclinic
space group	Pī (#2)	Pī (#2)
Unit cell		
a/ Å	7.138(13)	7.210(2)
b/ Å	13.283(13)	9.996(3)
c/ Å	13.900(9)	12.931(8)
α (°)	90.94(6)	69.61(5)
β (°)	93.04(6)	87.68(4)
γ (°)	100.65(6)	70.17(2)
Volume/$Å^3$	1293(3)	818.6(6)
Z ; *d* (g.cm^{-3})	1; 1.376	1; 1.420
Indice R final [I >2ζ(I)]		
R1	0.0436	0.0443
wR2	0.1000	0.0946

For complex **1**, N1, N4, N1*i*, N4*i* and Cu1 locate in the same plate. The dihedral angle between this plate and ring of pyridinium N1, C1, C2, C3, C4, C5 is 52,21°. Inclinasion between pyridinium ring and the group O1, N2, C6, N3 et O2 is 31.97°. The angle between plate N1, C1, C2, C3, C4, C5 and plate N4, C13, C14, C15, C16, C17 about 87.10°. Inclination between the last plate and the plate N1, N4, N1i, N4i and Cu1 about 59.82 (16)°. Interaction intermolecular in the unit cell showed in **Figure 2**. The shortest contact observed between $O1^{i}…O1^{iii}$ with distance about 3,6298(78)Å, and the interaction $O4^{i}…O4^{ii}$ about 3,7861 Å in the symmetry *i* = -x,-y, -z, *ii= 1+x, y, 1+z, et iii* = x, 1+y, z.

The compound **2** where contain only two radicals molecules, chour ligands are replaced by two dycianamide anion and two radicals replaced by two aqua moleculs as describe in Figure 3.

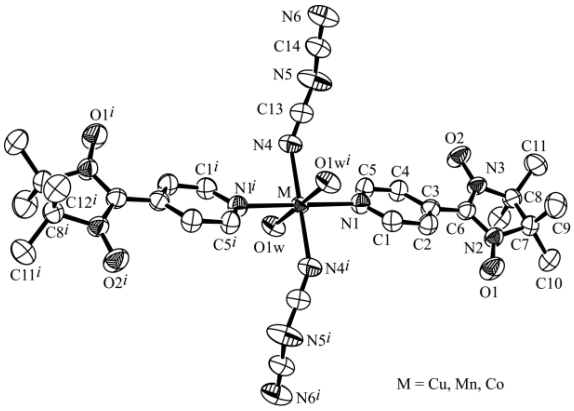

Figure 3. ORTEP structure of 2

This compound have the same structure if Cu(II) replaced by Mn(II) or Co(II). The last two compount are not reported here. The atom Cu adopts a distorted octahedral coordination arrangement with 2 atoms N from pyridine, two atoms N from dycyanamide, and two atom O from water moleculs. The Cu atom bond to radical using N atom of pyridine with bond lenght about 2.026(3)Å. Dicyanamide anion ligand as a terminate (monodentate) ligand (μ1) with distance Cu-N4 about 2.007(3)Å. Interatomic interactiin in compound 2 describe in Tabel 2.

Tabel 2 Interatomic and bond lenght of 2

Interatomic	Bond lenght (Å)
Cu-N1	2.026(3)
Cu-N4	2.007(3)
Cu-O1W	2.332(3)
O1-O1^{i}	3.714(7)
O1-O2^{iii}	3.863(2)

The dihedral angle between the pyridyl ring and the ON-C-NO moieties is 29.6(1)°. N-Cu-N ranging from 89.4(3) to 90.6(3)°. $[N(CN)_2]-$ has average C-N and N≡C bond lengths of 1.297(5) and 1.144(4)Å, respectively. The Cu-N-C fragment deviates from linearity (Cu-N-C 156.0(3)°), while the N-C-N angles (mean value 172.3°) are quite linear. The Cu-N4 ($N(CN)_2$) and Cu-O1w (H_2O) bond lengths are equal to 2.346(3) and 2.024(3) Å. The shortest contact between nitroxide groups is equal to O1···O1=3.714(7) Å (Figure 4).

Intermolecular short contacts are observed between the coordinated water molecule O1w and the non-coordinated N atoms from $N(CN)_2^-$ ligand (O1w···N6 = 2.821(5); O1w···N5 = 2.936(4)Å, indicating the existence of hydrogen bonding.

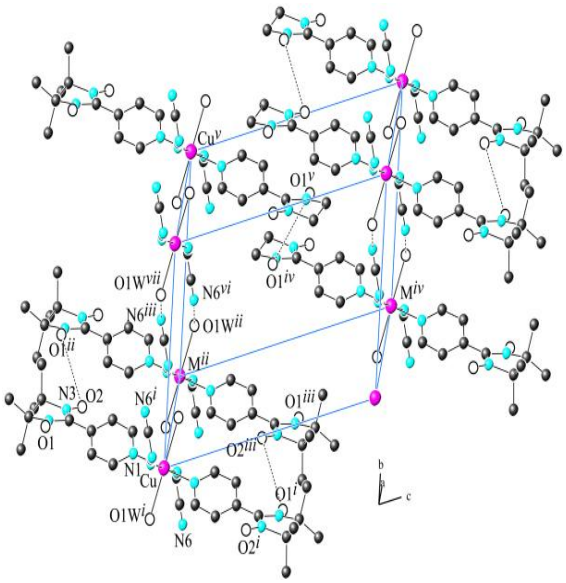

Figure 4. Unit cell content of compound 2 and intermolecular interaction.

Comparing the structure of these two compounds show that replacement of two balk radical ligands with linier ligand as dicyanamide anion and water molecule caused more small interaction in the compound 2. The distance Cu1-N(1) and Cu1-N(1*i*) (2.064(3)Å) and Cu1-N(4) and Cu1-N(4*i*) (2.605Å) in the compound 1 longer than Cu-N1 (2.026(3) Å) and Cu-N4 (2.007(3) Å) in the compound 2. We can not success synthesis $Cu(Rad)_4(N(CN)_2)_2$ up until now. This difficulties due to the use of water to dissolve dicyanamide salt, in which this salt is slightly dissolved in methanol or acetonitril.

Magnetic properties

The temperature dependence of the magnetic susceptibility for the compound **2** was measured in the temperature range 2-300 K, with an applied field of 1000 Oe. We can not measured the magnetic susceptibility for the compound **1** because the sample difficulty. The plots of $\chi_M T$ versus T, where χ_M is the molar magnetic susceptibility corrected for the core diamagnetism and T the temperature, are shown in Figure 5. At 300 K for compound **2** the value of $\chi_M T$ is equal to 1.10 cm^3 K mol^{-1}, a value consistent with non-correlated S_{Cu} = 1/2 and S_{rad}=1/2 spins. The profile of these curves is as anticipated for a three S=1/2 spin system, Rad-Cu(II)-Rad, in antiferromagnetic interaction. Indeed, the

antiferromagnetic correlation of such a linear spin system should lead to a ground state of S=1/2 which is expressed at low temperature by the onset of a plateau in the $\chi_M T$ versus T curve. The subsequent decrease for lower temperatures can be ascribed to the exchange interactions occurring between the $Cu(Rad)_2$ units.

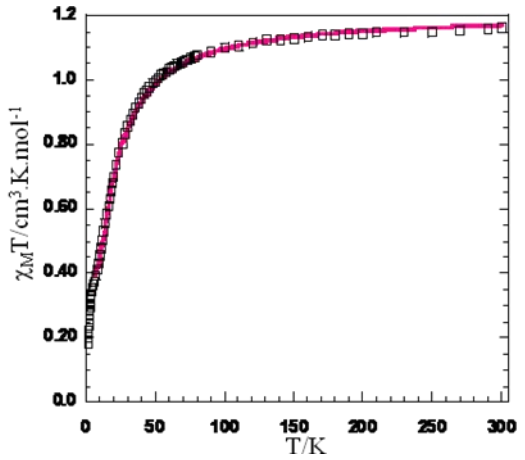

Figure 5. Experimental (χ) and calculated (-) $\chi_M T$ versus T.

4. Conclusion

Two complexes formulated $Cu(Rad)_4Cl_2$ (**1**) and $Cu(Rad)_2[N(CN)_2]_2(H_2O)_2$ (**2**) were obtained and strucurally and magetically characterized. The Cu atoms present a distorted octahedral geometry in wich bond leghts between Cu atom and 6 ligand around Cu are vary. Jahn Teller effect observed in this two compound where ligands in axial position have longer distance and ligands in equatorial position. For compound 2, the magnetic properties revealed intramolecular antiferromagnetif between Rad-Cu-Rad at lower temperature.

5. Acknoledgements

This work is part of our research during doctoral program at the Universite de Rennes 1, France several years ago. Thanks for Monsier le Professor Dr. Lahcene Ouahab, Monsier le Professon Dr. Stephane Golhen, and Monsier le Professor Dr. Jean-Sutter Pascal for all advice and help during my study in Rennes France.

6. References

[1]. Kahn, O. (1993), Molecular Magnetism, VCH, Weinheim, Germany, pp.1-10.

[2]. Gatteschi, D., Kahn,O., Miller, J. S., Palacio, F. (Eds). (1991), Magnetic Molecular Materials, NATO ASI Series E; Kluwer Academic: Dordercht, The Netherland, Vol. 198.

[3]. (a) Caneschi, A., Gatteschi, D., Renard, J.P., Rey, P., Sessoli, R., (1991), *Inorg. Chem*., 28, 331-337. (b) Caneschi A., Gatteschi D., Rey P; Sessoli R., (1988), *Inorg. Chem*, 27, 1756-1761.

[4]. Caneschi A, Gatteschi D., Renard J.P., Rey P., Sessoli R., (1989), *Inorg. Chem*., 28, 1976-1980.

[5]. Caneschi A, Gatteschi D., Sessoli R., Rey P., (1989), *Acc. Chem. Res*. 22, 392-398

[6]. Caneschi A., Ferraro F., Gatteschi D., Rey P., Sessoli R., (1991), *Inorg. Chem*., 30, 3162-3166.

[7]. Dasna, I W., Golhen, S., Ouahab, L., Fettouhi, M., Pena, O., Daro, N. and Sutter, JP. (2001), Sintesis, X-ray Crystal Structures and Magnetic Properties of $Cu(II)(NITpPy)_2[N(CN)_2]_2$.solv (NITpPy = nitronyl nitroxide radical, solv = H_2O or CH_3CN). from Discrete Molecules to 2-D Polymeric Coordination Compounds. *Inorganica Chimica Acta*. 25.

[8]. Dasna, I.W., (2001), Complexes polymeriques de metaux de transition a ligands nitronyl nitroxide et polycyanures: synthese, structure et magnetisme. *These*. Rennes: Universiter de Rennes 1-France.

[9]. Dasna, I W., Golhen, S., Ouahab, L., Fettouhi, M., Pena, O., Daro, N. and Sutter, JP. (2000), A Dimeric Cu(II) Acetate Complex Containing Axially Coordinated p-pyridyl nitronyl nitroxide radical: $[Cu^{II}(CH_3COO)_2(NITpPy)]_2$. *New J. Chem*. 24. 903-906.

[10]. Dasna, I.W. 2010. Kajian struktur dan sifat magnetik senyawa kompleks Cu(I) dan Cu(II) dengan ligan radikal nitronil nitroksida. Proceeding Seminar Nasional Kimia FMIPA Universitas Negeri Malang. 11-13 Oktober 2010.

Characteristics Test and Identification of Radiation Sources from the High Performance Radioisotope Identifier 75023 using Co-60, Cs-137 and Eu-152

Wijono[1], Gatot Wurdiyanto [2], Pujadi[3]

[(1,2,3)] Center for Technology of Radiation Safety and Metrology, National Nuclear Energy Agency, Jakarta, Indonesia (johnrida@batan.go.id)

Abstract

High Performance Radioisotope Identifier is a radioisotope detector and identifier processing technology that uses advanced spectrum of features and algorithms that are able to identify several types and classifications of radioisotopes. Distance factor, the type and activity of radiation sources significantly influence the identification. Result of identification of a single radiation source can be obtained quickly using short sampling method, but for the identification of multiple sources of radiation are some times in compatible with the type and classification of radioisotopes. Therefore it is necesary to make the test characteristics and identification of radiation multiple sources of the High Performance Radioisotope Identifier system using standard of point sources of Co-60, Cs-137 and Eu-152. The identification process begins in the background counting area without using radiation sources that can be determined classification of natural radioisotopes (K-40, Th-232 or the order). The same is done on multiple sources of radiation with 4 kinds of variations, namely Co-60 & Cs-137, Co-60 & Eu-152, Cs-137 & Eu-152 dan Co-60 & Cs-137 & Eu-152. In this process used long and short sampling method for estimating the result of identification in the work area detector sensitive, normal, optimal and over flow. The results showed the detector to function properly as identificators of type and classification of radioisotopes. While the weakness was only able to identify a type of radioisotope which has the largest activity with the 97.7% of high confidence level. Other types of radioisotopes are identified only up to 70% of medium confidence level. The result is expected radioisotope identification process can be done properly and correctly so as to improve radiation protection and safety programs.

Keywords: *multiple sources, detector, long sampling, short sampling.*

1. Introduction

High Performance Radioisotope Identifier (HPRID) is a radioisotope detector and identifier processing technology that uses advanced spectrum of features and algorithms that are able to identify several types and classifications of radioisotopes [1]. The value of dose rate at two specific points from the radiation is inversely proportional to square of the distance. Thus the distance factor will greatly affect the magnitude dose rate at a certain point [2]. It is implemented on method of long and short sampling used to determine the identification on detector HPRID. With this method can also be determined characteristics of the working area of detector HPRID to each classification of radioisotopes which includes background counting area, sensitive, normal, optimal and over flow [1]. Each the radioisotopes classification have energy level and different probabilities so that the values held gamma factor is also different [3]. This has influenced the identification of samples measured.

If the identification process carried out with measuring the dose rate at distances that are less precise with the amount of activity/type of radioisotope, the identification result will have error/does not match the types of radioisotopes to be measured. Therefore it is necesary to make the test characteristics and identification of radiation multiple sources of the High Performance Radioisotope Identifier system using standard of point sources of Co-60, Cs-137 and Eu-152.

2. Experimental Detail

The standards source used to test the characteristics and identification are Co-60, Cs-137 and Eu-152 LMRI. While the radiation measuring device in the form of the detector system HPRID S/n 75023 with a sensitivity of 25 keV until 3 MeV gamma radiation energy. This system is equipped with sodium iodide detector

(NaITl) 2"x2" (gamma spectrometry), moderated He3 tube (neutron) and Geiger-Mueller (gamma). The identification process using a radioisotope detector HPRID begins with the activation system. This is done by pressing and holding down the NAV (↵) approximately 5 seconds until the system start-up screen display active. After a while the image on the screen will appear that will soon turn in to the home screen that provides a quick reference for product information (serial number, model number, date of last calibration, etc.).

On the home screen system takes a few minutes to reach stability, so as to gather background information and configure it self to accommodate information for further data processing. When status has been ready, the system automatically begins measuring the level of dose rate (μRem/hour or μSv/hour) inthe user area (look at the corner of the home screen). Result of detection on the screen provides information to find areas to better detect the maximum signal source in to a real time graph with signal strength shown on the top left corner of the main detection screen.

Background counting is done in the three levels of radioactivity, which is at a low level (conditions in the laboratory), medium level (sampling area TENORM 1) and high level (sampling area TENORM 2). From this counting can be known classification of natural radioisotopes (K-40, Th-232 or the order). The result of reading the identification HPRID include an alarm, the source and the confidence and the provision of risk assessment of the findings reported as innocent, suspect or threat. The same is done on multiple sources of radiation with 4 kinds of variations, namely Co-60 & Cs-137, Co-60 & Eu-152, Cs-137 & Eu-152 dan Co-60 & Cs-137 & Eu-152.

In this process used long and short sampling method for estimating the result of identification in the detector working area of sensitive, normal, optimal and over flow. When reports of low trust (low confidence) in the identification and or suspicious or threat, it is recomended to short sampling (testing the same way with long sampling method but with a distance closer to the sample) to increase the probability of the identification of sources. Before entering the work area HPRD sensitive detector will show the results of the identification of the types of radioisotopes nature or category of NORM (Naturally Occurring Radioactive Material) in accordance with local conditions of background.

Later in the work area sensitive detectors have been able to identify the types of radioisotopes with confidence level of medium (70%) and low (30%). On the identification of this area is still showing one or several types of natural radioisotopes appropriate background conditions. But after entering the normal working area will showing the results of radioisotope identification with a confidence level of high (97.7%) in addition to natural radioisotopes with confidence level of medium and or low.

3. Result and Discussion

The result, such as working area and identification characteristics of HPRID detector system were performed using long sampling and short sampling method for background radioation and several combined of radioisotopes sources. The identification working areas are background, sensitive, normal, optimal and over flow as show in Figure 2.

The identification of a single radioisotope with high confidence level can be achieved at the optimal working area. After reaching a certain distance from the source of the radiation detector is no longer able to detect the types of radioisotopes (over flow working area). The distance depends on the type and magnitude of the resulting dose rate measured radioisotopes. Test scheme characteristics and identification of multiple sources of radiation detectors HPRID showed in Figure1.

Figure 2 showed that Y_0 is the average of equivalent dose rate (μRem/hour) background counting. Average value is not equal among regions background to wards one another. Similiars differences are shown in the results of identification and confidence level of the third stage background counting. At low background counting rate (the conditions in the laboratory) obtained K-40 (NORM) with confidence levels high (97.7%). In the background counting rate is (sampling area TENORM 1) not obtained the result of identification with high confidence level. But the high background counting rate (sampling area TENORM 2) obtained by Th-232 (NORM) with high confidence levels.

In the background counting identification stage to the second and third types of radioisotopes are also obtained non NORM, namely Am-241 and U-232 (Suspicious) with a low confidence level (30%). This proves that HPRID detector sensitivity and identification power are good. The identification results are always shown with indicator light. While the alarm sounds only for the appointment of the identification of suspicious radioisotope such U-232, U-238 and Am-241. To get the identification

with a higher level confidence can be done by changing the position of the long or short sampling method. Measurement with long sampling methods in the work area sensitive detector obtained identification results of Cs-137 (industrial) with 70% confidence level, K-40 (NORM) with a confidence level of 70% and Th-232 (NORM) with a confidence level of 30%, good for the combination with Co-60 and Eu-152. While the results of the identification of the Co-60 and Eu-152 (industrial) began to appear on a normal working area detector with a confidence level respectively 70% and 30%.

In this work area designation identification of Cs-137 has reached the confidence level of 97.7% (Table 1). The result of a single radioisotope identification with 97.7% confidence level is only achieved at optimal detector working area with short sampling method. From all the datas can be viewed classification radioisotopes Cs-137 is the most dominating in addition to Co-60 and Eu-152. This according to the activity of Cs-137 which has the highest activity at the the time of identification of 6.4 μCi.

However different from the results of the identification of Co-60 is more dominant than the Eu-152. This does not fit the standard source activity conditions at the time of measurement. Each with activities 0.3 and 3.2 μCi. This can be happen because the system HPRID detector is more sensitive to radiation energy emitted by Co-60 compared to Eu-152. In addition Co-60 have a gamma ray factor greater than the Eu-152. Co-60 and Eu-152 gamma factor respectively 1.327 and 0.558. Overall the appointment of identification with high levels (97.7%) only for one classification radioisotopes, that is the most dominant value of radioactivity.

In general, such identification can only be achieved using short sampling method. Classification of this radioisotope in the form of NORM or the other category depending on their respective activities. While the appointment of identification with the medium level (70%) and or low (30%) can occur for one or more classifications according to the amount of radioactivity of sample and condition of the natural radioactivity (background).

4. Conclusion

The results showed the detector to function properly as identificators of type and classification of radioisotopes. While the weakness was only able to identify a type of radioisotope which has the largest activity with the 97.7% of high confidence level. Other types of radioisotopes are identified only up to 70% of medium confidence level. The result is expected radioisotope identification process can be done properly and correctly so as to improve radiation protection and safety programs.

5. Acknowledgements

The authors thank to *Dr. Susilo Widodo* as Head of Center for Technology of Radiation Safety and Metrology, National Nuclear Energy Agency; to *Drs. Otto Pribadi Ruslanto, MT* as the Head of Radiation Metrology Division; and to my colleagues: *Hermawan Candra, S.Si*, *Holnisar* and *Rosdiani* who have helped in the implementation of research.

6. References

[1] Operator Manual (2009), *High Performance Radioisotope Identifier*. Part Number 6821684. Revision A. Canada
[2] A. Martin and A. An. Harbison (1986), Introduction *to Radiation Protection*. 3rd edition.
[3] International Commission on Radiological Protection Publication 38 (1983), *Radionuclide Transformations Energy and Intensity of Emissions*. Volumes 11 – 13
[4] International Atomic Energy Agency (1990), *Recommendations for the Safe Use and Regulation of Radiation Sources in Industry. Medicine. Research and Teaching*. Safety Series No. 102. IAEA
[5] Nicholas Tsoulfanidis (1978), *Measurements Procedures*. NCRP Report No.58. 1st edition.

Appendixes

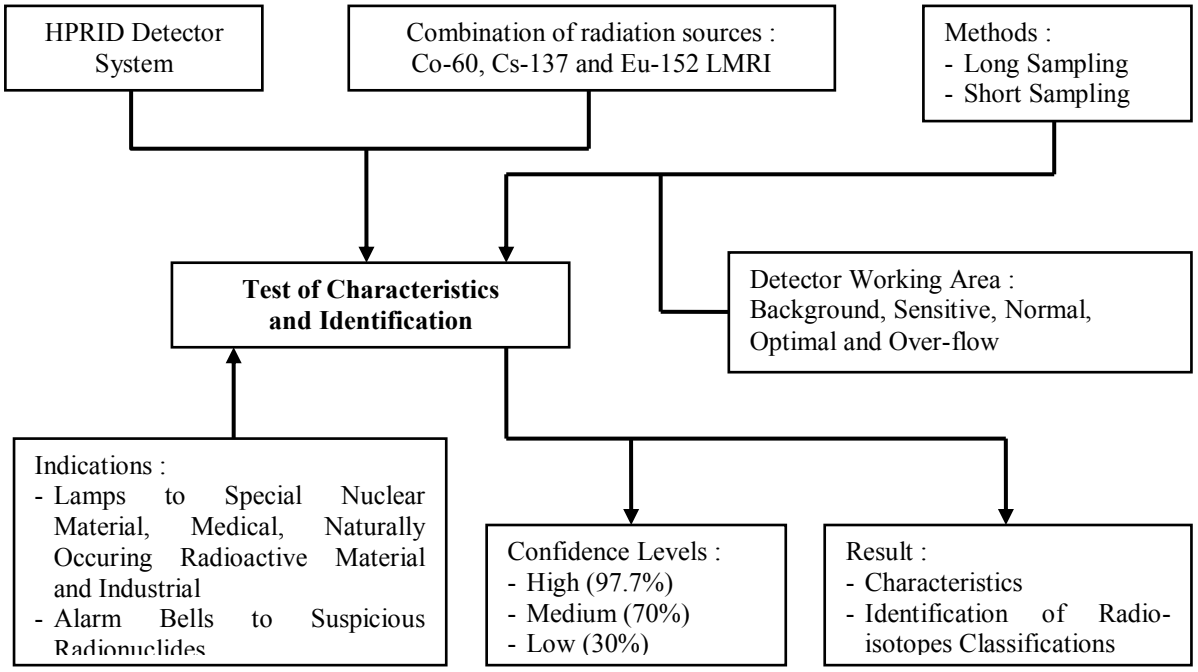

Figure 1. Scheme of Characteristics and Identification Test of HPRID Detector System

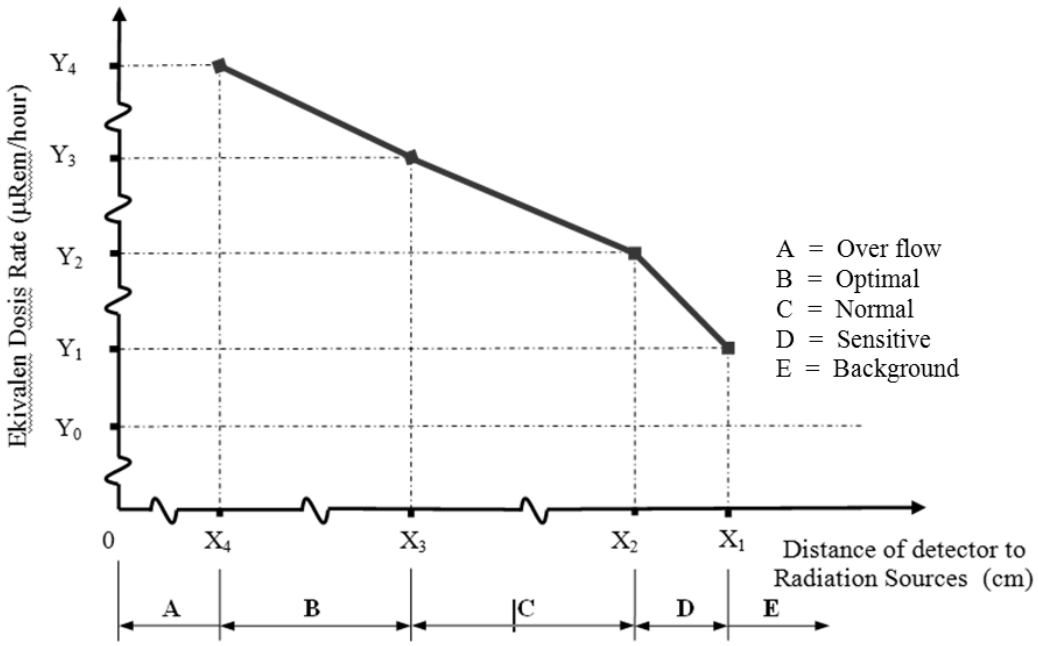

Figure 2. Curve of Identification Working Area of HPRID System

Table 1 The result of radiations sources identification from HPRID system

No	Standard Sources	Long Sampling	Short Sampling	Identification Result	Confidence Level	Indicators
1	Background 1	-	-	- K 40 (NORM) - Th 232 (NORM)	- 97.7% - 30%	- Lamp - Lamp
2	Background 2 (Sampel of Tenorm I)	√	-	K 40 (NORM)	- 97.7%	Lamp
		-	√	- K 40 (NORM) - Ra 226 (NORM) - Am 241 (Suspicious) - U 232 (Suspicious)	- 70% - 70% - 30% - 30%	- Lamp - Lamp - Alarm bell - Alarm bell
3	Background 3 (Sampel of Tenorm II)	√	-	K 40 (NORM)	- 97.7%	Lamp
		√	-	- Th 232 (NORM)	- 97.7%	Lamp
		-	√	- Th 232 (NORM) - U 232 (Suspicious)	- 97.7% - 30%	- Lamp - Alarm bell
4	Co-60 LMRI Code : 5465 and Cs-137 LMRI Code : 6631	√	-	- Cs 137 (Industrial) - K 40 (NORM)	- 97.7% - 30%	- Lamp - Lamp
		√	-	- Cs 137 (Industrial) - Co 60 (Industrial)	- 97.7% - 70%	- Lamp - Lamp
		-	√	Cs 137 (Industrial)	- 97.7%	Lamp
5	Co-60 LMRI Code : 5465 and Eu-152 LMRI Code : 519	√	-	- Co 60 (Industrial) - K 40 (NORM) - Th 232 (NORM)	- 70% - 70% - 30%	- Lamp - Lamp - Lamp
		√	-	- Co 60 (Industrial) - Eu 152 (Industrial) - K 40 (NORM)	- 97.7% - 70% - 70%	- Lamp - Lamp - Lamp
		-	√	- Co 60 (Industrial) - Eu 152 (Industrial)	- 97.7% - 70%	- Lamp - Lamp
6	Cs-137 LMRI Code : 6631 and Eu-152 LMRI Code : 519	√	-	- Cs 137 (Industrial) - K 40 (NORM) - Th 232 (NORM)	- 70% - 70% - 30%	- Lamp - Lamp - Lamp
		√	-	- Cs 137 (Industrial) - K 40 (NORM)	- 97.7% - 70%	- Lamp - Lamp
		√	-	- Cs 137 (Industrial) - Eu 152 (Industrial) - K 40 (NORM)	- 97.7% - 70% - 70%	- Lamp - Lamp - Lamp
		-	√	- Cs 137 (Industrial) - Eu 152 (Industrial)	- 97.7% - 70%	- Lamp - Lamp
7	Co-60 LMRI Code : 5465 and Cs-137 LMRI Code : 6631 and Eu-152 LMRI Code : 5197	√	-	- Cs 137 (Industrial) - K 40 (NORM) - Th 232 (NORM)	- 70% - 70% - 30%	- Lamp - Lamp - Lamp
		√	-	- Cs 137 (Industrial) - K 40 (NORM)	- 97.7% - 70%	- Lamp - Lamp
		√	-	- Cs 137 (Industrial) - Co 60 (Industrial) - Eu 152 (Industrial) - K 40 (NORM)	- 97.7% - 70% - 70% - 30%	- Lamp - Lamp - Lamp - Lamp
		-	√	- Cs 137 (Industrial) - Co 60 (Industrial)	- 97.7% - 70%	- Lamp - Lamp
		-	√	- Cs 137 (Industrial)	- 97.7%	Lamp

Study on Vertex Orders of Almost Moore Digraphs with Self-repeat

Yus Mochamad Cholily

Department of Mathematics, Universitas Muhammadiyah Malang, Indonesia
(yus@umm.ac.id or ymcholily@gmail.com)

Abstract

It is well known that there are no Moore digraphs for $d \geq 2$ and $k \geq 2$. Therefore the study has led to the existence of digraphs which has number of vertices one less than the Moore bound. The digraphs are called almost Moore digraphs and denoted by (d,k)-digraphs. For every vertex u of a (d,k)-digraph there exist exactly one vertex v such that there are two walks of lengths at most k from u to v. The vertex v is called repeat of u denoted by $r(u)$. The smallest positive integer p such that $r^p(u) = r(r^{p-1}(u)) = u$ is called order of u and denoted by $\omega(u)$. For a specific case of $\omega(u) = 1$, u is called self-repeat. This paper studies the structure of (d,k)-digraphs. We present a formula for enumeration of orders of all vertices of almost digraphs which contain self-repeats. In general, we also study several necessary conditions for the existence of almost Moore digraphs.

Keywords: *Moore bound, Moore digraphs, almost Moore digraphs, repeat, order.*

1. Introduction

In this paper we use ordinary notation G as a *directed graph* (*digraph*) which is connected and finite. Notations $V(G)$ and $A(G)$ are used as vertices and arch set. The natural numbers n, d and k are the number of vertices, maximum out-degree and diameter of G.

The *degree/diameter* problem is problem of determining the largest number of vertices n of digraph G, for given maximum number of out-degree d and diameter k. From the spanning tree diagram it is easy to see that the upper bound of n is $M_{d,k} = 1 + d + d^2 + \cdots + d^k$. This bound is called *Moore bound*. A digraph whose attain the upper bound is called a *Moore digraph*.

The non existence of Moore digraphs for $d > 1$ and $k > 1$ was shown in [7, 16]. The study move to the existence of digraphs whose attain to $M_{d,k} - 1$. If such digraphs exist then the digraphs called *almost Moore digraphs* and denoted by (d,k)-digraphs. One of important properties on almost Moore digraphs are the equality of out-degree and in-degree (*diregular*) [15].

Let u be a vertex of a (d,k)-digraph. Since the number of vertices is one less than the Moore bound then there is exactly one vertex v such that there are two walks of length no more than k from u to v. The vertex v is called *repeat* of u and denoted by $r(u)$. In case $r(u)$ the vertex u is called *selfrepeat*. The repeat r is an automorphism on $V(G)$ [4].

Since the repeat function r is an automorphism then we can define a composition of r for integer $p > 1$ as $r^p(u) = r(r^{p-1}(u))$ and $r^0(u) = u$. The smallest number p such that $r^p(u) = u$ is called *order* of u and denoted by $\omega(u)$.

The study of the existence of almost Moore digraphs was done by some authors. For $d \geq 2$, Fiol et.al showed in [9] that $(d,2)$-digraphs are line digraphs of complete digraphs. In case $d = 2$, there are exactly three non isomorphic (2,2)-digraphs [13]. The non existence of digraphs for $d = 2$ can be seen at [13] and for $d = 3$ can be seen at [5].

Necessary conditions for the existence of almost Moore digraphs have been obtained by some researcher ([3],[4],[8],[11]). This paper study on vertex orders of almost Moore digraphs.

2. Study on Vertex Orders

From now on, we define some notations will use in this paper. Let v be a vertex of a (d,k)-digraphs, $d \geq 4, k \geq 3$. For integer Set $N^i(v)$ is a set of vertices whose have distance i from v if $i \geq 0$, and at distance i to v if $i < 0$. Hence, in particular case $i = 0$ is $N^0(v) = \{v\}$, while others for $i = \pm 1$ are out-neighbor and in-neighbor of v. *Least common multiple* of integers m and n will denoted by lcm(m,n).

The two first lemmas below give information about the orders of all vertices between any two vertices whose known the orders.

Lemma 1 [8]
Let u and v be two vertices of a (d,k)-digraph G with $\omega(u) = m$ and $\omega(v) = n$. If W is a walk of length less than k from u to v then all vertices in the walks have orders divisor of lcm(m,n).

Lemma 2 [8]
Let u and v be two vertices of a (d,k)-digraph G with $\omega(u) = m$ and $\omega(v) = n$ and $r(u) \neq v$. If W is a walk of length at most k from u to v the all vertices in the walks have orders divisor of lcm(m,n).

From the two lemmas above we have the following corollary.

Corollary 1 [8]
For any selfrepeat v of a (d,k)-digraph then the permutation r of $N^+(v)$ has the same cycle structure as the permutation r of $N^-(v)$.

The structure of orders $(d,3)$-digraphs was shown in [2]. The following will point out of the structure of (d,k)-digraphs containing self-repeat for any $d \geq 3$ and diameter $k \geq 4$. The some terminologies here are same with in [1]. Let v_0 be a selfrepeat of a (d,k)-digraph and $N^+(v_0)$ has permutation cycles of lengths $1 = s_0, s_1, s_2, \dots, s_t$ with multiplicity $1 = m_0, m_1, m_2, \dots, m_t$. A set S_1 is a set of vertex order of $N^+(v_0)$. A set S_2 is a set of all lcm(s_i, s_j) where s_i, s_j in S_1, lcm(s_i, s_j) not in S_1. The i^{th} element of S_2 will denoted by $s_{2,i}$. Generally, we define the set S_m is set of least common multiple of any m vertices of S_1 where the least common multiple is not including in S_j, $j < m$, $3 \leq m \leq k$. We also use notation $s_{m,i}$ as a i^{th} element of S_m. Besides, $n(p,q)$ is the number of vertices which have order p on $N^q(v_0)$, $q \geq 0$.

Combining the definition and induction, we can see the possibility of vertex order on $N^i(v_0)$ for $2 \leq i \leq k$, as follows.

Theorem 1 [1]
If $u \in N^i(v_0)$ for $2 \leq i \leq k$ then $\omega(u) \in \bigcup_{j=1}^{i} S_j$.

It is easy to see that $V(G) = \bigcup_{i=0}^{k} N^i(v_0)$. Enumeration of vertex order on level 0, 1 and 2 of $N^i(v_0)$ was given in [2]. By enumerating vertex orders on each level of $N^i(v_0)$ we can prove the following theorem. Furthermore, all vertices order of any (d,k)-digraphs which containing selfrepeat can be enumerated.

Theorem 2 [1]
Let G be a (d,k)-digraph containing seflrepeat for $d \geq 4$, $k \geq 3$. Le v be a vertex of G, where $N^+(v)$ consist of permutation cycles with lengths $1 = s_0, s_1, s_2, \dots, s_t$ and multiplicities $1 = m_0, m_1, m_2, \dots, m_t$. Then G consist of exactly k selfrepeats, $\sum_{j=1}^{k} n(s_i, j)$ vertices of order s_i, $i \in \{1,2, \dots, t\}$, and $\sum_{j=l}^{k} n(s_{l,i}, j)$ vertices of orders $s_{l,i} \in S_l$ for $l = 2,3, \dots, k$.

Generally, enumeration of vertex order can be seen in the following formula.

a. $n(1,i) = \begin{cases} 1, & \text{for } i = 1,2, \dots, k-1 \\ 0, & \text{for } i = k. \end{cases}$

b. $n(s_i, 1) = m_i s_i$ for $i = 1,2, \dots, t$.

c. $n(s_i, 2) = m_i s_i + n(s_i, 1) + n(s_i, 1) m_i s_i +$

$$n(s_i, 1) \sum_{s_j | s_i, j \neq i} m_j s_j + m_i s_i \sum_{s_j | s_i, j \neq i} n(s_j, 1) + \sum_{\text{lcm}(s_j, s_l) = s_i} n(s_j, 1)\, m_l s_l$$

d. $n(s_{2,i}, 2) = \sum_{\text{lcm}(s_j, s_l) = s_{2,i}} n(s_j, 1) m_l s_l$

The number of non self-repeats on $N^i(v_0)$ for $i = 3,4, \dots, k$ completely can be seen in [1]. We close the paper by giving the following open problem.

3. Open Problem

Up to now, the existence of almost Moore digraphs is still uncovered. Therefore we propose the two open problems. The first is the existence of almost Moore digraphs containing selfrepeat and second one without selfrepeat.

4. References

[1]. E.T. Baskoro, Y.M. Cholily and M. Miller, (2008), Enumeration of vertex orders of almost Moore digraphs with selfrepeats, Discrete Mathematics 308(1): 123-128.

[2]. E.T. Baskoro, Y.M. Cholily and M. Miller, (2006), Structure of repeat cycles in almost Moore digraphs with selfrepeats and diameter 3, *Bull. Inst. Combin*. Appl. 46, 99-109.

[3]. E. T. Baskoro, M. Miller and J. Plesník, (2000), Further results on almost Moore digraph, *Ars Combin*. 56, 43-63.

[4]. E. T. Baskoro, M. Miller and J. Plesník, (1998), On the structure of digraphs with order close to the Moore bound, *Graphs Combin*. 14, 109-119.

[5]. E.T. Baskoro, M. Miller, J. Sirán and M. Sutton, (2005), Complete characterization of almost Moore digraphs of degree three, *J. Graph Theory*, Vol. 48 (2), 112-126.

[6]. J.C. Bermond, C. Delorme, J.J. Quisquater, (1986), Strategies for interconnection networks: Some methods from graph theory, *J. Parallel Distrib. Comput.* 3, 433-449.

[7]. W. G. Bridges and S. Toueg, (1980), On impossibility of directed Moore graphs, *J. Combin. Theory.* B29, 339-341.

[8]. Y. M. Cholily, E.T. Baskoro and S. Uttunggadewa, (2005), Some conditions for the existence of (*d*,*k*)-digraphs containing selfrepeats, Combinatorial Geometry and Graph Theory, *Lecture Notes in Comput. Sci.* 3330 (J. Akiyama et.al (eds)), 87-93.

[9]. M. A. Fiol, I. Alegre and J. L. A. Yebra, (1983), Line digraph iteration and the (*d*,*k*)-problem for directed graphs, *Proc. 10th Symp. Comp. Architecture*, Stockholn, 174-177.

[10]. M. A. Fiol and J. L. A. Yebra, (1990), Dense bipartite digraphs, *J. Graph Theory* 14, 687-700.

[11]. J. Gimbert, (1999), On the existence of (*d*,*k*)-digraphs, *Discrete Math*. 197/198, 375-391.

[12]. J. Gimbert, (2001), Enumeration of almost Moore digraphs of diameter 2, *Discrete Math*. 231, 177-190.

[13]. M. Miller and I. Fris, (1988), Minimum diameter of diregular digraphs of degree 2, *Comput. J*. 31, 71-75.

[14]. M. Miller and I. Fris, (1992), Maximum order digraphs for diameter 2 or degree 2, *Pullman Volume of Graphs and Matrices, Lecture Note in Pure and Appl. Mathe*. 139, 269-298.

[15]. M. Miller, J. Gimbert, J. Širán and Slamin, (2000), Almost Moore digraphs are diregular, *Discrete Math*. 218, No. 1-3, 265-270.

[16]. J. Plesník, Š. Znám, (1974), Strongly geodetic directed graphs, *Acta F.R.N. Univ. Comen. Mathematica* XXIX, 29-34.

Optimization of Biodiesel Synthesis by Trans-Esterification of *Jatropha Curcas* Oil with High Free Fatty Acid

Aman Santoso

Department of Chemistry, Faculty of Mathematics and Science, State University of Malang, Indonesia
(amansantoso49@yahoo.co.id)

Abstract

Crude Jatropha curcas oil is generally has too high levels of free fatty acid (FFA) for biodiesel raw materials, hence it must be reduced. The purpose of this research was to optimize the esterification conditions of castor oil and transesterification of CJCO. The research stages are as follows: (1) determination of the physical and chemical properties of jatropha oil that covers determination of FFA, saponification number, color, and viscosity; (2) esterification of jatropha oil with methanol that catalyzed by sulfuric acid (3) optimization of mole ratio of oil-methanol and KOH as catalyst on jatropha oil transesterification; and (4) characterization of physical and chemical properties of methilester that produced. Research result were: (1) the jatropha curcas oil characters were brownish yellow color, smell a little bit stung, FFA of 11.27 ± 0.02%, saponification number of 120-125, and viscosity of 29-30 cps; (2) esterification in 1, 2 and 3 hours can reduce the FFA level of CJCO from 12% into 7, 4.5 and 2.5%; (3) the optimum mole ratio of transesterification of oil-methanol is 1:8 at catalyst concentrasion of KOH 0.7% with yield of 97.2%. The character of methylesters (biodiesel) produced from CJCO are light yellow color brownish-yellow, viscosity of 6.0-6.5 cps (decrease to 80% from 29-30 cps), acid number of 0.35 - 0.40, saponification number of 125-128 ± 0,2, density of 0,89 ± 0,2, and cetane number of 46.7.

Keywords: *CJCO, transesterification, FFA, biodiesel.*

1. Introduction

Jatropha curcas oil *(CJCO)* has great potential as raw material of biodiesel, with oil content in the range of 30-40% of dry seeds [1], and can grow on less fertile land or degraded land. *Jatropha curcas* are grow in critical land with the results of 1-15 tons per hectare/year [1] depends on age of the plant, and has productive period to 50 years [2]. Isolation of the mechanical screw pressing is a widely used method in the world to separate the vegetable oils, because it is cheap and easy to operate [3].

Vegetable oil or fat that used as a substitute for petroleum diesel fuel must be converted first into a methyl esters form of fatty acids, which making up the fat / oil with transesterfication reaction to produce biodiesel as a renewable and environmentally friendly fuel [4]. Jatropha oil can be obtained from Jatropha, conventionally, by the press or screw press. In general, conventional processing of castor oil results still contains water hence it has higher percentage of free fatty acid (FFA). The high level of FFA in oil makes it cannot be directly carried out for transesterification of biodiesel, in which FFA levels are reduced first at a certain rate through esterification reaction.

Levels of free fatty acids in *Jatropha curcas* oil that is processed using conventional techniques are very dependent, quality, seeds, and long storage. Stretch of free fatty acids is in the range of 2-22%. *Jatropha curcas* as a source of biodiesel is considered attractive because of high oil content, did not compete for other uses (e.g. when compared with palm oil or sugar cane), and has a very interesting agronomic characteristics [4].

Esther that derived from carboxylic acids is having a general formula-COOR. One way to make the ester compound is by replacing hydrogen atoms on the carboxylic group of carboxylic acid (-COOH) by alkyl (-R) or aryl (for benzene ring / Ar) group. Esterification reaction is generally slow and reversible, with the general reaction as follows:

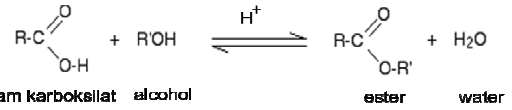

In the esterification reaction as mentined above, a carboxylic acid reacts with one alcohol to produce esters and water molecules.

Transesterification commonly used acid or base catalysts, for example are hydrochloric acid in

methanol, sulfuric acid in methanol and borontrifluorida in methanol. Base catalysts i.e sodium methoxide in methanol and potassium hydroxide in methanol. The mechanism of trans-esterification catalyzed by the base is as follows:

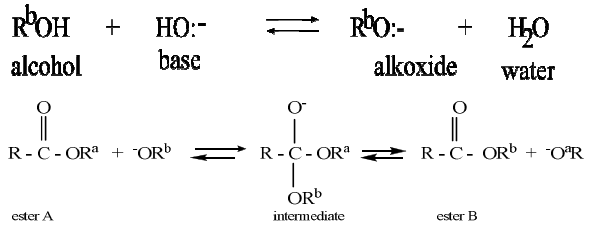

The mechanism of trans-esterification with alkaline catalysts started with the reaction between hydroxide ions (OH^-) with alcohol and form alkoxides. Subsequently, the alkoxide attacks the carbonyl group (with sp^2 carbonyl groups) to form an intermediate tetrahedral (very unstable). Next stage is elimination to produce new esters (B) and a new alcohol (R^aOH).

Vegetable oils have high viscosity, about 10-20 times higher than in diesel oil, hence vegetable oil cannot be used as fuel directly, because it can cause incomplete combustion and lead to crust in the combustion chamber. Thus, vegetable oils for use as fuel must be lowered so close to the viscosity of diesel fuel viscosity.

Viscosity of vegetable oils such as Jatropha oil can be decrease by transesterification reactions that produce methyl esters of fatty acids which are also referred as biodiesel. Transestrification process can reduce the viscosity of vegetable oil to 85% [4]. Transesterification of vegetable oils can be made by reacting oils which are triglycerides with methanol with KOH as base catalyst, resulting methyl esters of fatty acids with glycerol as byproduct. Trnasesterification reaction of vegetable oils in general is as follows:

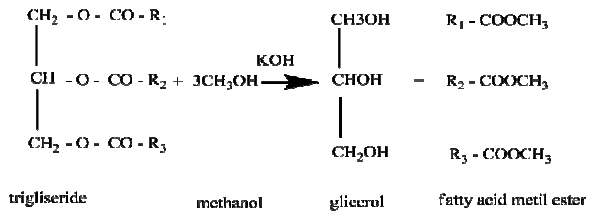

Stoichiometrically, 1 mol triacil glycerol (triglycerides) requires 3 moles of methanol (alcohol) and produced 1 mol of glycerol and 3 moles of fatty acid methyl esters. Conventional synthesis of biodiesel is carried out by transesterification reaction, by reacting vegetable oils with methanol or ethanol with mechanical stirring. This method produces low yields and requires a relatively long time and other constraints i.e difficulty in separating the product. Transesterification in laboratory scale has been done by Alamu (1997) with ethanol 20%, KOH catalyst 1% within 90 minutes with yield of 95.4%.

2. Experimental Details

This study is a laboratory experiment with stages explained as follows

1. Determination of physical and chemical properties of Jatropha oil obtained from Malang BALITTAS, which included the determination of FFA, saponification number, color, and viscosity
2. Esterification of jatropha oil using methanol catalyzed with sulfuric acid in one, two and three stages and time variation of esterification
3. Characterization esterification products of *Jatropha curcas*, particularly level of ALB
4. Transesterification of *Jatropha curcas*, with methanol ratio of (1:7) and catalyzed by KOH 0.7%
5. Characterization of the transesterification of Jatropha oil, include physical and chemical properties as well as determination of fatty acid components by GC-MS.

Castor oil esterification procedure

A total of 100 g of castor oil is inserted into the three neck flask, added with 8 g of methanol and 1 ml of concentrated sulfuric acid. The mixture was then refluxed and stirred at 70° for 2-3 hours. The mixture wass cooled then transferred into a separating funnel. The bottom layer is separated and the upper organic layer was washed with 2x100 ml of warm water, and then evaporated to remove water in oil. The results obtained are weighed to determine yield of esterification and it can be seen by measuring the decrease in levels of FFA. If the FFA levels are still over 3%, then it should be re-esterificated with the same steps as above.

Transesterification of Jatropha curcas oil

Preparation of potassium methoxide: A total of 28 g of methanol (1:7) is poured into Glass Beaker, and then added with 1 g KOH for 1% catalyst. The solution was mixed in electric mixer or stirrer slowly until all the KOH soluble and perfectly formed potassium methoxide.

A total of 100 g *CJCO* is poured in a beaker glass, carefully added with potassium methoxide. Subsequently, the solution was stirred slowly at 200-300 rpm. The mixture is cooled and then transferred into a separating funnel and allowed to stand for 1-2 hours, until there is a clear separation of two layers. Methyl ester located at the upper layer separated from glycerol and washed with water until neutral. Water

remaining in the biodiesel was removed by vacuum distillation, dried by adding anhydrous sodium sulfate, then decantated. The biodiesel finally weighed to determine the yields.

Stages of the above reaction were repeated with the same steps under the influence of the microwave, by changing the catalyst concentration of KOH from 1% to 0.6, 0.7, and 0.8%. Instead of varying the catalyst concentration, variation of alcohol ratio of 1:7 as also conducted for ratio of 1:6 and 1:8.

3. Results and Discussion

The castor oil sample used is provided from BALITTAS Malang, Indonesia with a FFA level approximately 6%, but in about 1 month storage FFA levels rose to around 11-12%.

Table 1. Character jatropha curcas oil

Density	Refractive index	FFA	Saponification	Colour
0.90774 g/mL	1.465	11.27%	123.670	Brownish yellow

This is possible because of the presence of water in oil can cause the hydrolysis reaction produces free fatty acids. Oil hydrolysis reaction is given as follows:

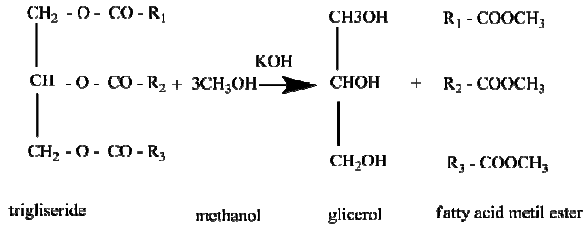

Free fatty acids in oils can be determined by levels of free fatty acid (FFA). The greater the level of FFA means the higher free fatty acids in the oil. As raw material for biodiesel, the presence of free fatty acids would affect the biodiesel reaction process. Transesterification for biodiesel production runs perfect in ALB levels should be reduced to below 3%.

The reduction of Jatropha oil levels of ALB can be performed via esterification with methanol catalyzed reaction of oil with sulfuric acid, with the following reaction:

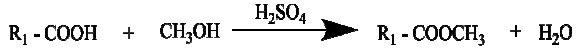

Decreased levels of ALB by esterification influenced the frequency or the number of committed and long esterification reaction. Data on the influence of time and number of stages of esterification of FFA with FFA is given in Table 2.

Table 2 Esterification of *Jatropha curcas*

FFA early (%)	Esterification to	Time (hour)	FFA (%)
11-12	1	1	7.5
11-12	1	2	4.8
11-12	1	1	7.5
	2	1	3.8
	3	1	2.5

The number of additional steps in the esterification reagent has a big influence in lowering levels of ALB castor oil, as in Table 2, esterification stages 1,2,3 with the time of each stage can reduce the ALB 1hr row from 11-12% to 7-8; 4-5 and 2.5 to 3%. ALB levels less than 3% can already be transesterificated. The gradual addition of reagents means very influential in the success of the esterification reaction, especially for materials with high FFA.

Results transesterification of castor oil and methanol mole ratio influenced the concentration of catalyst. Rendement synthesis of biodiesel from jatropha oil at various mole ratios of methanol and catalyst concentration on conventional in reaction time 1 h as in Table 3.

Table 3. Effect of methanol ratio and% KOH on the yield on synthesis of biodiesel from jatropha curcas oil

Methanol ratio	% catalyst KOH	% yield
1: 6	0.6	90.12
	0.7	91.95
	0.8	91.65
1 : 7	0.6	94.37
	0.7	95.69
	0.8	95.52
1 : 8	0.6	94.56
	0.7	95.68
	0.8	95.60

As shown in Table 3 yield experiments on the synthesis of biodiesel from jatropha oil with a mechanical stirrer at different ratios of methanol and the catalyst will also give a different yield, and at ratio of methanol 1:7, catalyst 0.7% KOH obtained the highest yield of 95.69%. To determine the optimization results based on the yield of biodiesel is biodiesel produced can be analyzed by surface response analysis. ANOVA test results in a surface response analysis shows there is a relationship between the factors involved in the reaction. Relations yield, ratio of methanol, the catalyst can be expressed in a mathematical equation that is in the form of a quadratic as in equation 1, as follows:

R = 2019 F + 324 933 K - K2 233 595 - 32 022 ....

description:
R = yield of biodiesel from castor oil
F = ratio of methanol
K = Percent KOH Catalyst

As shown in equation 4, that the yield of biodiesel produced is also percent ratio of methanol and KOH catalyst, where the influence of methanol ratio of order of one and two order of catalyst concentration, with p = 0.0043 is smaller than 0.05 which means that the model equations significant. So the model equations can be used (significant) to determine the relationship yield and percent methanol ratio of catalyst in the synthesis of biodiesel from castor oil conventionally.

Optimization of biodiesel production process with criteria that produced the highest yield can be seen from experimental data and how both can be seen from the analysis of optimization by maximizing yield by surface response analysis RSM). Based on the analysis of maximizing, the yield obtained on the composition of the methanol ratio of 1: 8 with catalyst 0.7% with an estimated yield can reach 97.17%. Yield predictions are still slightly higher than the yield obtained from the experiment that is 95.69%. Comparison of conditions and the optimum yield in the synthesis of biodiesel from the experiment results and the analysis of RSM as shown in the Table 4.

Table 4 Optimum conditions of synthesis of biodiesel from castor oil

	Experiment	RSM result
Maximum yield	95.69	97.17
Methanol ratio	1 : 7	1 : 8
% KOH	0.7	0.7

As shown in Table 4 shows the optimum condition and the results (yield) results of the experiment there is little difference lower than the results of RSM analysis, both in terms of mole ratio and the yield of methanol produced. Correlations among the reagent composition in the production of biodiesel from castor oil conventional and yield predictions generated more clearly seen in Figure 1

As shown in Figure 1 yield relationship exists with the methanol ratio with KOH concentration in the synthesis of biodiesel from castor oil in conventional, where the relationship is in the form of parabola, according to a quadratic equation. Red area in Figure 1 is an area of possible composition of the reactants (ratios of methanol and catalyst) are predicted to obtain the maximum yield (optimal results).

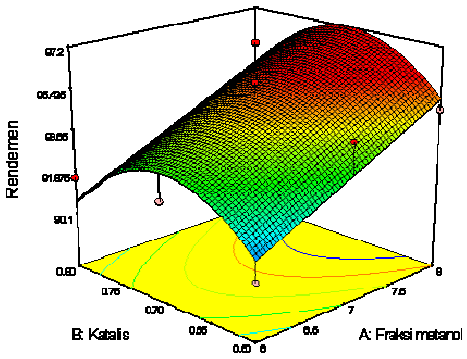

Figure 1. Effect of mole ratio% methanol and a catalyst on the yield biodiesel from castor oil is conventionally processed

The success of conventional trans-esterification of castor oil with a mechanical stirrer, characterized by the formation of dark brown glycerin to settle to the bottom of the layer separating funnel as shown in Figure 2. Furthermore, glycerin is separated and the organic layer was washed with warm water, fatty acid methyl esters as biodiesel. The nature of biodiesel from castor oil shown in Figure 2 has characteristic of pale yellow color with a viscosity between 6.0 to 6.5 cps.

Figure 2 Biodiesel from jatropha curcas

As shown in Figure 2 the results of the synthesis of biodiesel from castor oil with a mechanical stirrer resulting mixture with the top two layers of fatty acid methyl esters and the lower part glycerin. This is consistent conducted by Galardo (2010) on the reaction of biodiesel from vegetable oils by transesterification formed two layers, the top of the bottom of biodiesel and glycerin [6].

The maximum yield of experiments (95.69%) achieved in the methanol ratio of 1:7 with 0.7% KOH concentration. This is consistent conducted Berchmans and Hirata (2008) [7].

Transesterification of castor oil in 1:6 methanol ratio (24%) 1.4% NaOH catalyst biodiesel produced more than 90% in 2 hours, and Chetri et al. (2008) has managed to convert castor oil with two stages with a yield of about 97% fatty acid methyl esters [8].

Based on the analysis of RSM predicted to obtain maximum results on alcohol ratio 1:8 and catalyst concentration of 0.8% KOH in 60 minutes with the highest yield of 97.17%, meaning that based on the analysis of statistical extrapolation can yield obtained is slightly higher than results experiment. The physical properties of castor oil converted into biodiesel viscosity there has been a significant decline of 29-30 cps which fell 80% to just 6.0 to 6.5 cps, it is appropriate that presented by Alamu, et al. (2008) that the trans-esterification of oil viscosity decrease of 80% kernel. While the viscosity of biodiesel is biodiesel according to SNI maximum of 6, meaning that biodiesel from castor oil results of the experiment is still in the range of SNI viscosity of biodiesel.

4. Conclusion

The conclusions of this research are:

1. The jatropha curcas oil characters were brownish yellow color, smell a little bit stung, FFA 11.27 ± 0.02%, saponification number 120-125, and viscosity 29-30 cps;
2. Esterification 1, 2 and 3 hours can reduce level FFA of *CJCO* from 12% became 7, 4.5 and 2.5%.
3. The optimum mole ratio of transesterification of oil-methanol is 1:8 at catalyst concentrasion of KOH 0.7% with yield 97.2%. The character of methylesters (biodiesel) produced from *CJCO* are light yellow color brownish-yellow, viscosity 6.0-6.5 cps (decrease to 80% from 29-30 cps), acid number 0.35 - 0.40, saponification number 125-128 ± 0.2, density 0.89 ± 0.2, and cetane number 46.7.

5.References

[1]. Hariadi, M.S. (2005), Budidaya tanaman jarak (*Jatropha Curcas*) sebagai bahan alternative biofuel, Makalah disampaikan dalam Forum Grup Diskusi (FGD) Prespektif Sumber Daya Lokal Bioenergi Bidang SITEKNAS, Kementrian Riset dan Teknologi, Puspitek Serpong, Tanggal 14-15 September 2005.

[2]. Manurung, R., (2005), Substitute castor oil diesel, (Kompas, 15 March 2005) Margaroni, 1998, Knothe and astanley, 2005 in OJ

[3]. Bargale, P.C. and Sing, J. (2000), Oil Expressin Characteristics of rapeseed for a small capacity screw press, *Journal of Food Science Technology,* V.37: p. 130-134.

[4]. [a] Alamu, O.J., Waheed, M.A. and Jekayinfa, S.O., (2007), Alkali-Catalysed Production and Testing Of Biodiesel from Nigerian Palm Kernel Oil, Agricultural Enginering International: The CIGR *E*journal. Manuscript Number EE 07 009. Vol.IX. July.

[b]. Alamu (2007), Development and evaluation of palm oil fuel biodisesl, The Pacific Journal of Science and Technology, Volume 8 Number 2.

[5]. Hanna, M.A., Isom, L. and Cmaphel, J. (2005), Biodiesel Current perpective and future, *Journal of Science & Industrial Research,* Vol. 64, pp. 854-857

[6]. Gallardo, P.Sp, Rodriguez, A.S.P., Florez, L,D., River, M.A.H., and Torres, R.L. (2010), Synthesis and Characterization of biodiesel from coconut oil using homogenous catalyst. *Journal Material Science Forum,* Vol. 636-637, pages 1410-1411.

[7]. Braechmans, H.J. and Hirata, A. (2008), Biodiesel Production from *Jatropha Curcas* L. Seed Oil with a High Content of Free Acids, *Bioreource Technology* 99 pp. 1716-1721.

[8]. Chetri, A,B., Tango, S.M., Budge, S.M., Watt, K.Cc and Islam, M.R. (2008), Non Edible Plant Oil as Sources for Biodiesel Production, *International Journal of Molecular Sciences* X (8) :422-427

[9]. Akpan, U.G., Jimoh, A. and Mohamed, AD, (…..), Extraction and Modification of castor oil. Department of Chemical Engineering, Federal University Of Technology, PMB Mina Nigeria.

[10]. Grepen. J. Van, B. Shanks, and R. Prushko, (2004), Biodiesel Production Technology, National Renewable Energy Laboratory (NREL), Colorado.

Refinement Optimization of Crude Palm Oil (CPO) using Zeolite or Clay and Its Potential As Biodiesel Raw Materials

Aman Santoso [1], Sri Kumalaningsih [2], Susinggih Wijana [3], Imam Santoso [4]

[(1)] Chemistry Departement, Faculty of Mathematics and Science, State University of Malang, Indonesia
(amansantoso49@yahoo.co.id)
[(2,3,4)] Faculty of Agriculture, Brawijaya University, Malang, Indonesia

Abstract

Crude palm oil of biodiesel raw material can be refined beforehand with local absorbent such as clay or zeolite. The purpose of this study was to determine the optimum conditions of refined palm oil with clay and its potential as a raw material for biodiesel. The stages of research as follow: (1) Determination of physical and chemical properties of palm oil; (2) Optimization of bleaching by activated clay; (3) Optimization of mole ratio of oil-methanol and KOH as catalyst on CPO trans-esterification. Research results showed (1) Palm oil has the character of dark brown color, smell like caramel, free fatty acid content of about 2.5-2.7%, saponification number of 120-125, viscosity of 32-35 cps, and it cannot directly transesterificated; (2) Optimum condition of refining crude palm oil by clay at 1 - 3 % w/w of clay; (3) Optimum condition synthesis biodiesel from CPO at ratio methanol : oil is 1:8 and catalyst concentrasion of KOH of 0.7% with yield 97.7%. Characteristic of biodiesel from palm oil which has rafinated is brownish yellow color, viscosity decreased 81% from 32-35 to 6.5 cps, acid number 0.35 - 0.40, saponification number 120, and cetane number 50.

Keywords: *palm oil, refined, biodiesel, clay, trans-esterification.*

1. Introduction

Exploration of fossil fuel in a sustainable cause oil reserves run out. We must begin optimize to use of alternative renewable energy, for example biodiesel can replace diesel oil. Indonesia is number one producer of palm oil (CPO) in the world with production more than 18 million tons/year, hence potentially become producer of biodiesel. Advantages utilization of biodiesel reduces dependence on fuel, environmentally friendly, and creates jobs. Palm oil has some qualities because it is influenced by, kind, age, duration of seed saving and processing of oil. Therefore, palm oil to be used as a raw material of biodiesel must had some standard of quality, or early treatment is needed so that it can be used as a raw material of biodiesel.

Before processed into biodiesel, crude palm oil refining process requires (degumming), esterification, and decoloration. Degumming aims to eliminate impurities compounds contained in oil, such as gum and fosfatide. Esterification for reduce free fatty acids of palm oil, while decolorizing to absorb color or other impurities. Component of fatty acid composition of palm oil can be seen in Table 1.

Palm oil is easily damaged if left in a certain period as had unpleasant smell (rancid). Rancidity occurred since the outbreak of the bond of triglycerides (oil component) into glycerol and free fatty acids. The colors are affected by the presence of soluble pigment carotene in oil. Melting point of palm oil is in the range of temperature, because the palm oil contains several kinds of fatty acids that have different melting points.

Biodiesel is a fuel that can replace diesel fuel and its renewable energy. Vegetable oil has a very high viscosity can be 10-20 times of diesel oil, vegetable oil and high viscosity can cause incomplete combustion and causing the crust in the combustion chamber. Trans-esterification of fats / oils can be done to reduce the viscosity of vegetable oils to produce fatty acid methyl esters. Trans-esterification can reduce the viscosity of vegetable oil. Trans-esterification of vegetable oils can be performed by mixing the oil, which is triglyseride, with alcohol (methanol / ethanol) in the presence of acid or base catalyst, to produce alkyl esters of fatty acids and glycerol byproduct.

Table 1. Fatty Acid Composition of CPO

Kind of fatty acid	% acid
fatty acid	
$C_{11}H_{23}COOH$ = lauric acid	<1
$C_{13}H_{27}COOH$ = myristic acid	1-6
$C_{15}H_{31}COOH$ = palmitic acid	33-47
$C_{17}H_{35}COOH$ = stearic acid	1-6
$C_{17}H_{33}COOH$ = oleic acid	40-52
$C_{17}H_{31}COOH$ = linoleic acid	2-11

Transformation reactions of oils / fats into glycerin and esters of fatty acids are as follows:

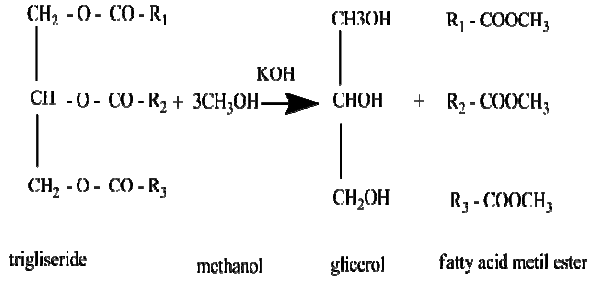

The stoichiometry of 1 mol triglycerides requires 3 mol of ethanol (alcohol) and produced 1 mole of glycerol and 3 moles of fatty acid esters. Based on the review mechanism through which the reaction, trans-esterification of biodiesel through the formation of intermediates form tetrahedral (unstable), the next stage is the formation of methyl esters [1]. The mechanism of trans-esterification catalyzed by the base is shows as follows:

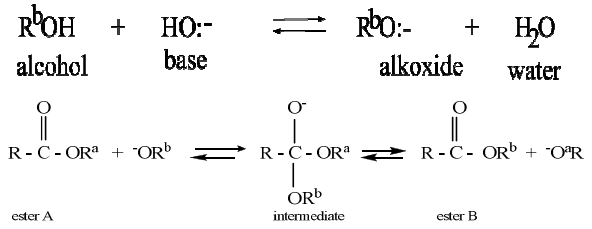

The mechanism of trans-esterification with alkaline catalysts started with the reaction between hydroxide ions (-OH) with alcohol to form alkoxides. Subsequently formed alkoxide attack the carbonyl group (with sp2 carbonyl groups) in A form an intermediate ester tetrahedral (sp^3 C atom) as unstable form, the next stage of elimination to produce esters (B) new and new alcohol (R'OH).

Generally adsorption can be divided into two types namely physical adsorption and chemical adsorption. Physical adsorption is the adsorption caused by interactions between the adsorbent and the adsorbate on the surface because of the style of Van der Waals attraction or hydrogen bonding [2]. Adsorption is a chemical adsorption process involving stronger interactions between adsorbent and adsorbate thus not free to move from one part to another part of the adsorbent surface.

According Djatmiko (1985), factors affecting adsorption include: the nature of adsorbate, contact time, temperature and pH [7]. One of the properties that can affect the adsorption is the solubility and molecular weight compounds adsorbate. Clay derived from nature have been used for various purposes. However, absorption, ion exchange capacity and power of the clay catalyst are not maximized. The activation process of clay will be done in two ways, physically and chemically. Activation of the physical form of heating clay at a temperature of 350-400^{o}C in order to evaporate the water trapped in the porous of the clay so the clay crystal porous and specific surface area increases. In such circumstances allow the occurrence of adsorption on clay.

2. Experimental Details

This was an experiment in laboratory research and outline in this study with the following stages: (1) Determination the physical and chemical properties of palm oil which includes levels of FFA, saponification number, color, and viscosity, (2) Degumming with Phospit Acid, and bleaching with activated clay (through a process of heating), (3) Optimization of mole ratio of oil-methanol and KOH as catalyst on *CPO* trans-esterification, and characterization biodiesel product.

Refined Palm Oil (CPO): Consider 100 g of CPO poured into the Beaker Glass, added 20 g clay (clay 20%) that have been activated by heating 400^{o}C for 30 minutes. Further heated in the temperature range 120-140^{o}C while stirring with a speed of 400-500 rpm for 2 hours. The mixture was cooled, allowed to stand for 3-6 hours, then decantated, and liquid phase was centifugated 20 minutes with a speed of 2000 rpm, decantation taken liquid phase, washed with 2x100 ml of hot water. The oil obtained is evaporated to remove water by heating. The results obtained are weighed to determine yield, and characterization the results wsa obtained: color, free fatty acid levels (FFA) it, saponification number. Performed the same steps as above but with a variation of percent weight change that are used clay from 20% to 7, 5, 3, 2 and 1%.

Trans-esterification of palm oil: Making Potassium methoxide: A total of 28 g of methanol (1:7) is poured into Glass Beaker, and then added carefully 1 g Potassium Hydroxide (KOH) for 1% catalyst. Mix in electric mixer or stir with magnetic stir slowly until all the KOH soluble and perfectly formed potassium methoxide.

A total of 100 g palm oil (CPO) is poured in a Glass Beaker, carefully added a solution of potassium methoxide has been created. Subsequently, the solution was stirred slowly with a speed of 200-300 rpm. The mixture is cooled and then transferred into a separating funnel and allowed to stand for 1-2 hours, until there is complete separation into two layers. Methyl ester located at the upper layer separated from glycerol and washed with water until neutral. Water remaining in the biodiesel removed by vacuum distillation or evaporation, dried by adding anhydrous sodium sulfate, then decantation. The biodiesel was weighed to determine the yield.

Stages of the above reaction were repeated with the same steps under the influence by changing the catalyst concentration of KOH from 1% to 0.6%, 0.7%, 0.8%. Besides varying the catalyst concentration also did variation of the alcohol ratio of the ratio of 1:7 as above replaced with alcohol ratio 1:6 and 1:8.

3. Result and Discusion

Refinement of Crude Palm Oil

Crude palm oil (*CPO*) is obtained which is processed from fresh fruit bunches (FFB), which are generally processed through the pressing of the Palm fruits. Crude Palm Oil (CPO) in the form of a slightly viscous oil brown reddish yellow, CPO generally contain free fatty acids (FFA) about 2-5%, so depending on the treatment process, the longer it is stored FFB caused higher of FFA levels. Palm oil is used in the research was obtained from PT Salim Invomas Pratama in Surabaya. Before being used for biodiesel raw material specified physical and chemical characteristics. Palm oil as raw material for biodiesel as in Figure 1 with the character of reddish brown color and FFA levels from 2.5 to- 2.5%.

Palm oil (CPO) obtained although have not high FFA levels but cannot be directly trans-estherication, this proved the CPO catalyzed trans-esterification with methanolic KOH for 2 hours with the reaction temperature 60 °C showed no formation of glycerol, like as in Figure 2.

Figure 1. CPO

Figure 2. Result directly transeterification CPO

Figure 2 shows the result of direct trans-esterification of palm oil. Making biodiesel from oil or fat is the reaction of triglycerides with alcohols catalyzed base, and the resulting alkyl esters (biodiesel) and glycerol. Glycerol has a higher density than the alkyl esters that will settle to the bottom layer. So the most simple criterion whether trans-esterification process was successful or not can be seen from the form or absence of glycerol layer as in Figure 6. If the reaction produced two-layers and the bottom layer thick reddish-brown color means the form of glycerol and the reaction of biodiesel successfully or has lasted. Based on test results CPO character FFA numbers are not too high, but the color is very dark (reddish brown). Therefore we need techniques to reduce the intensity of color, and this can be done by bleaching. The purpose of bleaching is to eliminate possible metal residues, soaps, products of oxidation of the pigment colors, colors (β karotene the CPO around 800-900ppm). Refined CPO conducted in this study in order to prepare the raw material of biodiesel by bleaching with activated clay by heating 400oC. Colors are very strong CPO therefore required large clay, but the use of absorbent cultivated as little as possible, for further processing easier. Therefore, variation at used were different concentrations (% clay) in this bleaching process. The result of bleaching products CPO at various clay concentrations is shown in Figure 3-5.

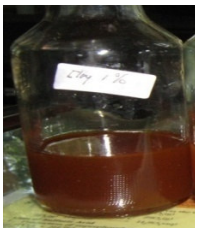

Figure 3. Result (1% clay)

Figure 4. Result (3% clay)

Figure 5. Result (7% clay)

As shown in Figure 3-5, influence weight percent clay used for the bleaching effect on color co produced, where the higher the percent of clay that is used increasingly fading colors or bright CPO. Results bleaching palm oil color from light brown to colorless depending on the amount of clay used the measurement results FFA levels of 1.5 to 2%. Results of CPO in the amount of bleaching clay1-3% are can or successfully trans-esterificaed as in Figure 6, meaning that the results of bleaching with 1-3% clay had to be used as raw material for biodiesel. This is consistent with that proposed by Arumughan et.al (in yellow bk) optimal conditions in 3% bleaching clay containing activated carbon [4].

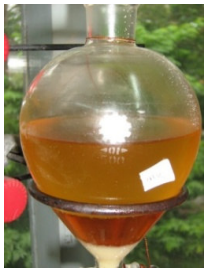

Figure 6. Result trans-esterification of CPO after bleaching

Synthesis of biodiesel in generally with the conventional batch system using a mechanical stirrer, by reacting the oil with alcohol catalyzed base. Maximal results of synthesis biodiesel from palm oil conventionally can be achieved when the trans-esterification reaction carried out at optimum conditions of reaction. Optimization of reaction conditions biodiesel can be made by varying the conditions or the composition of the reactants involved, for example, by varying the mole ratio of alcohol, catalyst concentration, and reaction time. Conventional trans-esterification of palm oil in various ratios of methanol and KOH catalyst results is shown in Table 2.

Table 2. Effect of methanol ratio and % KOH on the yield on synthesis of biodiesel from palm oil conventionally

Methanol ratio	% Catalyst KOH	Yield (%)
1 : 6	0.6	77.20
	0.7	79.60
	0.8	78.80
1 : 7	0.6	80.90
	0.7	81.15
	0.8	81.08
1 : 8	0.6	87.86
	0.7	97.10
	0.8	97.02

Based on experimental data as in Table 2 shows the comparison of methanol and catalysts that differ percent yield a different result, and the highest yield of 97.1% achieved in the methanol ratio of 1:8 with 0.7% KOH concentration. ANOVA results of the response surface shows that there is relationship between the factors involved in the reaction. Relations yield, ratio of methanol, the catalyst can be expressed in a mathematical equation that is in the form of a quadratic as in equation below:

R = 5.195 F2 + 18.9 FK - 78.227 F - K + 361.349 114.067

Description:
R = yield of biodiesel produced
F = ratio of methanol
K = Percent KOH Catalyst

As shown in equation above, the yield of biodiesel is also percent ratio of methanol and KOH catalyst, where the influence of the methanol ratio order of two and the order of a single catalyst, the surface response obtained by ANOVA test of significance of 0.0001 less than 0.05, which means identifying equation model is significant. So the model equations can be used (significant) to determine the relationship yield biodiesel, methanol and catalyst ratios required in the synthesis of biodiesel from palm oil conventionally.

Optimization of biodiesel production process with criteria that produced the highest yield can be seen from experimental data and how both can be seen from the analysis with the maximization of yield optimization with response surface analysis. Based on the analysis of the surface response to the maximization of the yield obtained on the composition of the methanol ratio of 1: 8 with catalyst 0.8%, with an estimated yield can reach 97.7% with the level of desirability (which is cool) 1. Yield predictions are still slightly higher than the yield obtained from the experiment that is 97.12%. Comparison of optimum conditions of synthesis of biodiesel from the results of laboratory experiments and from analysis of RSM as in the Table 3.

As shown in Table 3 yield of biodiesel produced from the extrapolation by RSM analysis gives the possibility of a higher yield than the yield obtained from the experiment. Correlations among the reagent composition in the process of biodiesel production from palm oil yield of the conventional and the resulting predictions can be described as shown in Figure 7.

Table 3. Optimum condition experiment vs RSM

	Experiment	RSM analysis
Yield (%)	97.10	97.70
Methanol Ratio	1 : 8	1 : 8
% KOH	0.7	0.8

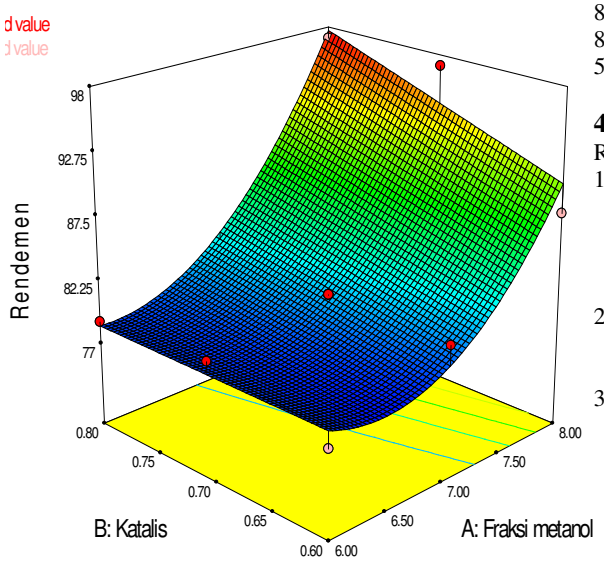

Figure 7. Effect of methanol ratio and % catalyst on the yield of biodiesel from palm oil

As shown in Figure 7, yield relationship exists with the methanol ratio with KOH concentration in the synthesis of biodiesel from palm oil by conventional means, where relationships can be described as parabolic, corresponding to quadratic form of mathematical equations. Red colors in these regions are an area of possible composition of the reactants (ratios of methanol and catalyst) are predicted to obtain the maximum yield.

Conversion of palm oil into biodiesel in conventional has yield of of 97.12%, which is achieved in the methanol ratio of 1:8 with KOH concentration of 0.7. Based on the analysis of RSM predicted to obtain maximum results on alcohol ratio 1:8 and catalyst concentration of 0.8% KOH in 60 minutes with the highest yield of 97.7%, meaning that based on the analysis of statistical extrapolation can yield obtained is slightly higher than results experiment. The physical properties of the conversion of palm oil into biodiesel viscosity there has been a significant decline of 33-34 cps which is down 81% to just 6.5 to 7.0 cps, it's appropriate presented by Alamu, *et al.* that the trans-esterification decrease of 80% palm kernel oil viscosity [4]. While the viscosity of biodiesel is biodiesel according to SNI maximum of 6, meaning that biodiesel from palm oil test results are slightly (0.5 cps) on top of SNI viscosity of biodiesel. So based on the discussions that have been made to conclude the synthesis of biodiesel from palm oil are influenced by methanol ratio and the concentration of the catalyst used, the optimum reaction conditions achieved in the methanol ratio of 1:8 with KOH 0.7% and can reduce the viscosity of oil at 81% from 33-34 to be 6.5 to 7.0 cps, and cetane number 50.

4. Conclusions

Research results showed:

1. Oil palm has the character of dark brown color, somewhat stinging smell like caramel, free fatty acid content of about 2-2.74%, saponification number 120-125, with viscosity of 32-35 cps, and its can't directly trans-esterification.
2. Optimization refining crude palm oil by clay for raw material biodiesel, at consentration 1 until 3 % w/w of clay.
3. Optimum condition synthesis biodiesel from CPO at ratio methanol : oil 1:8 and concentration KOH 0.7% by rendemen maximum 97.7%. Properties of biodiesel from palm oil which has rafinated is brownish yellow color, viscosity decreased to 81% from 32-35 to 6.5 cps, 0.3 to 0.4 acid number, saponification number 120-125.

5. Acknowledgments

---

6. References

[1]. Heyda, C., Tapanes, O. A., Donato, Ananda, G. And Mesquita, J.W. (2008),. Transesterifikasi of jatropha curcas oil gliceride, Experimenta and experimental studies of biodiesel reaction fuel and energy, Abstracts. *Bioresource Technology*, January 14,

[2]. Naik, Malaya. Meher, L.C., Naik, S.N. and Dos, L.M., (2008), Production of biodiesel from high free fatty acids Karanja (pongamita) oli. *Biomassa and Bioenergy*. Volume 32. Issue 4. April 2008. p. 354-357

[3]. Demirbas, A., (2007), Alternative and Renewable Energy Industries; Energy & Fuel, *International Journal of Green Energy*. Volume 4. Issue January. pages 15-26

[4]. Alamu, O.J., Waheed, M.A. and Jekayinfa,S.O., (2007), Alkali-Catalysed Production And Testing of Biodiesel From Nigerian Palm Kernel Oil, Agricultural Enginering International: The CIGR Ejournal. Manuscript Number EE 07 009. Vol.IX. July.

[5]. Grepen. J. Van, B. Shanks, and R. Prushko, (2004), Biodiesel Production Technology, National Renewable Energy Laboratory (NREL), Colorado

[6]. Margaroni (1998), Knothe and Astanley (2005) in O.J. Alamu, Development and evaluation of palm oil biodisel fuel, *The Pacific Journal of Science and Technology*, Volume 8 Number 2. November.

Analysis and Numerical Solution of Saint Venant Equations for the 2D Shallow Water Wave Models with Initial Value Problem and Boundary Value Problems

Ari Kusumastuti [1], Dewi Erla M. [2], Silva Ahmad A. [3]

[1,2,3] Mathematics Department, Faculty of Science and Technology, UIN Maulana Malik Ibrahim, Malang, Indonesia

Abstract

Saint Venant equations are nonlinear partial differential equations that can be applied in the case of fluid flow. In this study, the selected fluid is water. Research in the waters of the question is assumed to waters as shallow water with the boundaries in two dimensions. Solving analytically selected in this study by determining the initial value problem solution and the solution in the limit boundary value problems $0 \leq x \leq L$. *Furthermore, the results of the initial value problem solving and limit values can be applied to the data owned watershed. Numerical solutions are selected by the ADI method in formulating solutions - solutions at each grid point from recktangle object. MATLAB software as a program was built to explain the solutions* u *and* v *which is the propagation of the fluid. New* t *amplitude to the next can be interpreted in 3D graphics can be studied more in-depth.*

Keywords*: Equation 2D Saint Venant, Initial Value Problems, Boundary Value Problems, modeling, non--linear PDE.*

1. Introduction

The problem generally involves the prediction of fluid flow distribution in different quantities, namely the fluid pressure, temperature, density and flow velocity. With this aim, the author involves six basic equations, namely the continuity equation based on the law of conservation of mass, momentum equation along three orthogonal directions (derived from Newton's second law of motion), thermal energy equation derived from the first law of thermodynamics, equation of state, which is the relationship empirically between the fluid, temperature, pressure and density [1].

Channel flow problem does not require the last two equations and hence can be solved with the continuity equation and momentum equation assuming a constant temperature and density. In addition, the assumptions used in the Saint Venant equations are the 2D flow, with uniform velocity, the cross-section and the water level is represented by a horizontal line, the flow of small arches and vertical acceleration are ignored so that the hydrostatic pressure, the influence of shifts and turbulence can be accounted for through the law of analog resistance to the flow channels at rest [1].

From the discussion above, this study becomes important to do because the results of the initial value problem solving and limit values can be implemented on their own data. So, what raised the theme of this research is the analysis of Saint Venant equations for the 2D Shallow Water Wave Models with Initial Value Problem and Boundary Value Problems.

2. Experimental Detail

At the completion of the initial value problem of Saint Venant equations of two-dimensional work with the steps in the Saint Venant equations of momentum and the momentum of the Saint Venant equations y 2D.

Solution of the equations of Saint Venant x momentum carried out by the following procedure. View of the equation of time Saint Venant x

$$(BU_1)_t + (BU_1U_1)_x + (BV_1U_1)_y = -g(B\eta_1)_x + (\nu_1 B(U_1)_x)_x + (\nu_1 B(U_1)_y)_y + \nu U_1$$

Thus, obtained order partial differential equation system of equations is

$$\begin{cases} \left(\frac{\partial U_1}{\partial x} - i\frac{\partial U_1}{\partial y}\right) = w(x,y) \quad (3) \\ B\frac{\partial U_1}{\partial t} + BU_1\frac{\partial U_1}{\partial x} + gB\frac{\partial \eta_1}{\partial x} - \nu U_1 = \\ \qquad \frac{\partial w}{\partial x} + i\frac{\partial w}{\partial y} \quad (4) \end{cases}$$

In initial condition $t=0$, assumed that $U_1(x,0)=f(x)$ and

$$\frac{\partial U_1}{\partial t}(x,0) = g(x)$$

Hence, the equation becomes:

$$Bg(x) + BU_1 f'(x) + gB\frac{\partial \eta_1}{\partial x} - \nu U_1 = \frac{\partial U_1}{\partial t} + U_1\frac{\partial U_1}{\partial x} \quad (5)$$

If the initial conditions of turbulent waves is $\sin\tau$,
then $x_1 = \sin\tau$,
hence $U_1(x_1,0) = U_1(\sin\tau,0) = f(\sin\tau)$.

In equation (5) can be concluded curve tangent partial differential equations, namely:

$$\frac{dt}{ds} = 1, \quad \frac{dx}{ds} = U_1,$$

So that $t=s$, $x=U_1 s$ and

$$U_1 = \int_{s=0}^{s} (Bg(x) + BU_1 f'(x) + gB\frac{\partial \eta_1}{\partial x} - \nu U_1)\, ds$$

Result of the conclusions obtained from the equation with initial condition:

$$x_2 = \sin\tau + U_1 s$$

We get:

$$\begin{aligned} U(x,t) = &\left[\frac{B}{2U_1}G(\sin\tau + 2U_1 t)\right. \\ &+ \frac{3}{2}Bf(\sin\tau + 2U_1 t) \\ &- \frac{\nu}{2U_1}U_1(\sin\tau + 2U_1 t) \\ &\left. + gB\eta_1(\sin\tau + 2U_1 t)\right] \\ &- \left[\frac{B}{2U_1}G(\sin\tau)\right. \\ &+ \frac{B}{2}f(\sin\tau) \\ &- \frac{\nu}{2U_1}U_1(\sin\tau) \\ &\left. + gB\eta_1(\sin\tau)\right] \end{aligned}$$

And

$$\begin{aligned} V(y,t) = &\left[\frac{B}{2V_2}G(\sin\tau + 2V_2 t)\right. \\ &+ \frac{B}{2}f(\sin\tau + 2V_2 t) \\ &- \frac{\nu}{2V_2}U_1(\sin\tau + 2V_2 t) \\ &+ gB\eta_2(\sin\tau + 2V_2 t) \\ &\left. + f(\sin\tau + 2V_2 t)\right] \\ &- \left[\frac{B}{2V_2}G(\sin\tau) + \frac{B}{2}f(\sin\tau)\right. \\ &- \frac{\nu}{2V_2}V_2(\sin\tau) \\ &\left. + gB\eta_2(\sin\tau)\right] \end{aligned}$$

Boundary Value Problems Solution of Saint Venant equations in 2D x momentum carried out as follows:
View from Saint Venant x momentum equation:

$$\begin{aligned} (BU_1)_t + (BU_1U_1)_x + (BV_1U_1)_y &= -g(B\eta_1)_x \\ &+ (\nu_1 B(U_1)_x)_x \\ &+ (\nu_1 B(U_1)_y)_y + \nu U_1 \end{aligned}$$

Introduce stream function:

$$\frac{\partial U}{\partial x} + \frac{\partial V}{\partial y} = 0, \qquad \Delta w = \frac{\partial^2 w}{\partial x^2} + \frac{\partial^2 w}{\partial y^2}$$

Form of the equation can be rewritten in nonlinear partial differential equations of the fourth order as follows:

$$\left[B\frac{\partial}{\partial t}\left(\frac{\partial^2 w}{\partial x^2}+\frac{\partial^2 w}{\partial y^2}\right)\right] + \left[B\frac{\partial w}{\partial y}\frac{\partial}{\partial x}\left(\frac{\partial^2 w}{\partial x^2}+\frac{\partial^2 w}{\partial y^2}\right)\right] + \left[B\left(-\frac{\partial w}{\partial x}\right)\frac{\partial}{\partial y}\left(\frac{\partial^2 w}{\partial x^2} + \frac{\partial^2 w}{\partial y^2}\right)\right] = \left[-gB\frac{\partial \eta_1}{\partial x}\right] + [B\nu_1 \Delta\Delta w] + \left[\nu\frac{\partial w}{\partial y}\right]$$

Using the method of splitting, this equation can be divided into the following form:

$$w = F(y,t)x + G(y,t)$$

So, with the separation solution of Saint Venant x momentum equation for four order can be stated as follows:

$$B\frac{\partial^3 F}{\partial t \partial y^2} + B\frac{\partial^3 G}{\partial t \partial y^2} + B\frac{\partial F}{\partial y}\frac{\partial^2 F}{\partial y^2} + B\frac{\partial G}{\partial y}\frac{\partial^2 F}{\partial y^2} - BF(y,t)\frac{\partial^3 F}{\partial y^3} - BF(y,t)\frac{\partial^3 G}{\partial y^3} = Bi_1\frac{\partial^4 F}{\partial y^4} + Bi_1\frac{\partial^4 G}{\partial y^4} + i_1\frac{\partial F}{\partial y} + i_1\frac{\partial G}{\partial y}$$

so that we obtain separate equations following equation:

$$= \begin{cases} B\dfrac{\partial^3 F}{\partial t \partial y^2} + B\dfrac{\partial F}{\partial y}\dfrac{\partial^2 F}{\partial y^2} - BF(y,t)\dfrac{\partial^3 F}{\partial y^3} = Bi_1\dfrac{\partial^4 F}{\partial y^4} + i_1\dfrac{\partial F}{\partial y} \quad (4) \\ B\dfrac{\partial^3 G}{\partial t \partial y^2} + B\dfrac{\partial G}{\partial y}\dfrac{\partial^2 F}{\partial y^2} - BF(y,t)\dfrac{\partial^3 G}{\partial y^3} = Bi_1\dfrac{\partial^4 G}{\partial y^4} + i_1\dfrac{\partial G}{\partial y} \quad (5) \end{cases}$$

then performed the integration process towards y, so we get

$$B\frac{\partial}{\partial t}\frac{\partial F}{\partial y} + B\left(\frac{\partial F}{\partial y}\right)^2 - BF\frac{\partial}{\partial y}\frac{\partial F}{\partial y} = Bi_1\frac{\partial^2}{\partial y^2}\frac{\partial F}{\partial y} + i_1 F + f_1(t)$$

With separating variable process we get general solution:

$$U_1(y,t) = Y(y)T(t) = a_n \sin\frac{2n\pi}{\sqrt{3}} y b_n e^{\frac{2n\pi}{\sqrt{3}}t}$$

With analog process, for y momentum Saint Venant, we get general solution:

$$V_2(x,t) = X(x)T(t) = a_n \sin\frac{2n\pi}{\sqrt{3}} x b_n e^{\frac{2n\pi}{\sqrt{3}}t}$$

3. Result and Discussion

$$U_1(y,t) = Y(y)T(t) = a_n \sin\frac{2n\pi}{\sqrt{3}} y b_n e^{\frac{2n\pi}{\sqrt{3}}t}$$

and

$$V_2(x,t) = X(x)T(t) = a_n \sin\frac{2n\pi}{\sqrt{3}} x b_n e^{\frac{2n\pi}{\sqrt{3}}t}$$

So, we get

$$W(x,y,t) = U_1(y,t) + V_2(x,t) = 2\left(a_n \sin\frac{2n\pi}{\sqrt{3}} y b_n e^{\frac{2n\pi}{\sqrt{3}}t}\right) + a_n \sin\frac{2n\pi}{\sqrt{3}} x b_n e^{\frac{2n\pi}{\sqrt{3}}t}$$

4. Conclusion

Graphic of the analytical solution of Saint Venant Equations:

```
r = 2:1:5;Cn=0.00001;n=1;t=2;
y = Cn*sin(2*n*pi*r/3^(1/3))*exp(2*n*pi*t/3^(1/3));
plot(r,y)
```

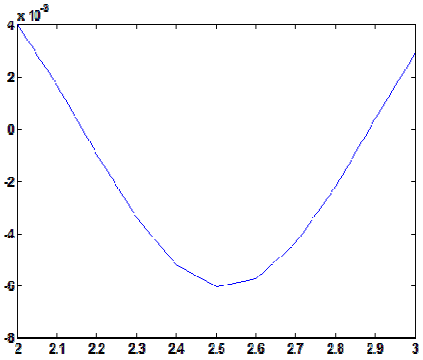

Figure 1. Graphic of the numerical solution of Saint Venant Equations

$$\frac{v_{i,j}^{n+1} - v_{i,j}^{n}}{\Delta t}$$

$$+ \left(u_{i+1,j}^{n} - u_{i,j}^{n}\right)\left[\left(\frac{v_{i+1,j}^{n+1} - 2v_{i,j}^{n+1} + v_{i-1,j}^{n+1}}{B\,\Delta x}\right)\right]$$

$$+ \left(v_{i,j+1}^{n} - v_{i,j}^{n}\right)\left[\left(\frac{v_{i,j+1}^{n+1} - 2v_{i,j}^{n+1} + v_{i,j-1}^{n+1}}{B\Delta y}\right)\right]$$

$$= -g\left(\frac{\eta_{i,j}^{n} - \eta_{i-1,j}^{n}}{\Delta y} + \frac{\eta_{i,j-1}^{n} - \eta_{i-1,j-1}^{n}}{\Delta y}\right)$$

$$+ v_2\left(\frac{v_{i+1,j}^{n+1} - 2v_{i,j}^{n+1} + v_{i-1,j}^{n+1}}{\Delta x^2}\right)$$

$$+ v_2\left(\frac{v_{i,j+1}^{n+1} - 2v_{i,j}^{n+1} + v_{i,j-1}^{n+1}}{\Delta y^2}\right)$$

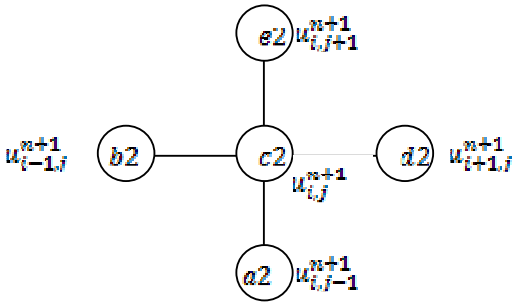

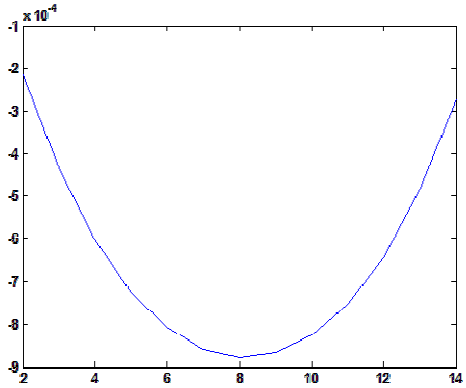

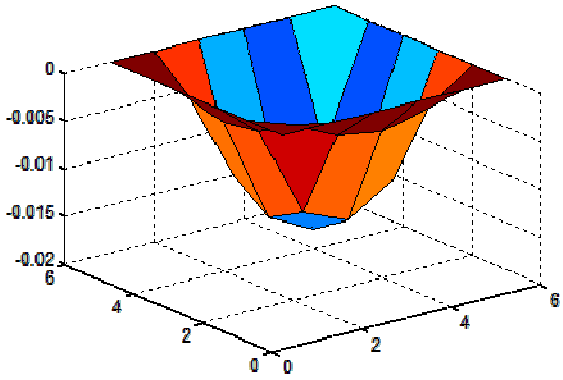

5. Acknowledgement

---

6. References

[1]. Aldrighetti, E. (2007), *Computational Hydraulic Techniques for the Saint Venant Equations in Arbitrarily Shaped Geometry*. Ph.D. Thesis. Department of Mathematics of the University of Trento

[2]. Dake, Jonas M.K. (1985), *Hidrolika Teknik (Edisi Kedua)*.Jakarta: Erlangga

[3]. Pinch, Enid R. (1992), *Optimal Control and the Calculus of Variations*. New York: Oxford University Press

[4]. Zauderer, E. (2006), *Partial Differential Equatios of Applied Mathematics (Third Edition)*. New Jersey: A John Wiley & Sons

[5]. Polyanin, A.D. (2003). Handbook of Nonlinier Partial Differential Equations. Chapman

Spatial Pattern Analysis of Dengue Fever Incident for Early Warning Disaster Information in Surabaya City

Arrowiyah [1], Sutikno [2], Setiawan [3]

[1,2,3] Department of Statistic, Faculty of Mathematics and Natural Science,
Sepuluh Nopember Institute Of Technology, Surabaya, Indonesia
arrowiyah_89@yahoo.co.id; sutikno@statistika.its.ac.id; setiawan@statistika.its.ac.id

Abstract

Surabaya is one of the major cities in East Java Province that the Dengue hemorrhagic fever (DHF)'s incidence is still quite high. Various efforts have been made to overcome the problem of the DHF's incidence in Surabaya, but the number of people with this disease is still not decreasing effectively. This research shows description and map prone spread of the dengue incidence making in period 2006-2009. The number of high incidence of dengue disease tends to occur in the first 6 months (January-June). Spread of dengue incidence was likely to occur in the north, central and east region of Surabaya. The comparison of spatial dependency test results by using the Moran's I index and Geary's C shows that Moran's I index is more sensitive than Geary's C. Some districts that fall into the prone of DBD's spread category are Genteng, Tegalsari, and Gubeng. Districts in the medium category are Pabean Cantikan, Simokerto, Bulak, Mulyorejo, Wonocolo, and T. Mejoyo.

***Keywords**: dengue fever, spread, spatial dependency*

1. Introduction

Dengue Hemorrhagic Fever (DHF) is one of the most dangerous diseases in Surabaya City. All of the efforts that have been done cannot reduce the number of DHF incidents effectively. Lack of information about the place, time and location of the DHF's spread maybe the cause of this problem. Geographical spread mapping is so important in studying the relation between climate and disease or other health's problem.

It is empirical and important for helping the implementation of intervention's planning. Disturbed district spread information that follow the place and time needed to show the district priority of anticipation and tackling program. Therefore, spread's map is needed to show the district priority of anticipation and tackling DHF program in Surabaya City.

Some recent researchs that related with DHF disease are early warning model of dengue fever by using climatic factors such as: Sasmito, Gunaman, and Widiatmoko (2006); and Hidayati (2008). Sasmito et al. (2006) develop an early warning model of dengue in the city of Jakarta. Hidayati (2008) develop a model of DBD in Indramayu district of West Java Province. This research will develop a map of the incident spread of dengue-prone in the city of Surabaya by considering the location (district), time (months), and season with a spatial pattern analysis. This method is quite good in presenting the map at a time of disease susceptibility to identify linkages between location and time [1]. This method is also very effective in detecting variations in geography [2].

2. Experimental Detail

The data that are used in this research are the number of DHF event in Surabaya City that was calculated every month with 31 districts that come from the Health Department in Surabaya City period 2006-2009.

Several methods that was used to analysis DHF with spatial pattern such as Moran's I, Geary's C, and Loca Indicator of Spatial Autocorrelation (LISA). Moran's I index [3] can be defined as,

$$I = \frac{n \sum_{i=1}^{n} \sum_{j=1}^{n} w_{ij}(x_i-\bar{x})(x_j-\bar{x})}{S_0 \sum_{i=1}^{n}(x_i-\bar{x})^2} \quad (1)$$

where n is number of case, x_i is the variable value at a particular location i, x_j is the variable value at a particular location j, $\bar{x}$ is mean of the variable, w_{ij} is a weight index indicating location of I relative to j and S_0 is the sum of w_{ij}. Geary's C [3] can be define as,

$$C = \frac{(n-1) \sum_{i=1}^{n} \sum_{j=1}^{n} w_{ij}(x_i-x_j)^2}{2S_0 \sum_{i=1}^{n}(x_i-\bar{x})^2} \quad (2)$$

where n, x_i, x_j, $\bar{x}$, w_{ij}, and S_0 are same with equation (1). LISA [3] can be define as,

$I_i = z_i \sum_{j=1}^{n} w_{ij} z_j$
(3)

where $z_i = (x_i - \bar{X})/\delta$, $z_j = (x_j - \bar{X})/\delta$, and δ is stansar deviation of the data.

Several steps analysis in this research include: 1). description of the spread of DHF event in each district every month, 2). mapping the DHF disease every month in each year, 3). compare these spread month to month in each year, 4). calculate and test the spatial dependent indeks with Moran's I, Geary's C, and LISA, 5). arrange the moran's scatterplot, and 6). Mapping the proud of DHF.

3. Result and Discussion

DHF event in Surabaya City period 2006-2009 have multiple characteristics. The highest mean of DHF in this period is 17.90 or 18 in Tegalsari district, whereas the lowest mean of DHF in period is 2.38 or 3 in Mulyorejo district. The highest variation of DHF is 399.54 in Tegalsari district, whereas the lowest of DHF is 6.02 in Trenggilis Mejoyo district.

Moreover, the high DHF number in Surabaya City can be shown in North, South, East and Central region of Surabaya. The high number in these regions is because of population density in that district.

The highest density population is located in Simokerto district that is 24,862 people/km^2. While some other districts such as Kenjeran, Tambaksari, Bubutan, Sawahan, and Tegalsari district has a density that are greater than 17,285 people/km^2 (see Figure1)

According to time (month) DHF event in Surabaya City in period 2006-2009, the greatest DHF event in Surabaya City occur in period January-June. This period is rainy season period (December-March) and dry season period (April-June). The spread in 2006-2009 shows that the spread in January-June was mostly happen in Central, South, East, and North region. In contrast, DHF event in July-December was likely to have low number because these months are dry season period (June-September) and transition to rainy season period (October-December). The highest number of DHF surfever in period 2006-2009 was in March 2006 and the lowest number of DHF surfever in period 2006-2009 was in December 2009. As seen in the Figure 2, if the color of the map seems darker, it can be shown that the number of DHF is higher than the bright one.

A comparison between each index's moran's I value and its expectation in period 2006 show that January, February, March, August, September, October, and December have a group pattern in DHF event. It gives information that the number of DHF in each district in these months is similar. April, May, June, July, and November shows indication that the DHF's number have a spread pattern or can inform that the number of DHF in each district in these months is different. More information about these can be found in Table 1.

Table 1. Morans'I Result in period 2006

Month	I	E(I)	Z(I)
January	0.112	-0.033	1.339[a]
February	0.099	-0.033	1.244[b]
March	0.134	-0.033	1.596[a]
April	-0.039	-0.033	-0.057
Mei	-0.057	-0.033	-0.223
June	-0.043	-0.033	-0.088
July	-0.119	-0.033	-0.886[c]
August	0.022	-0.033	0.695
September	0.058	-0.033	0.967[c]
October	-0.013	-0.033	0.188
November	-0.078	-0.033	-0.440
December	-0.016	-0.033	1.670[a]

[a] significant in α=10%, [b] significant in α=15%, [c] significant in α=20%,

Period 2007 show that group pattern occurs in April, July, August, September, October, November, and December. While, January, February, March, May, and June have a spread pattern. On period 2008, January, March, April, May, August, October, and December have a group pattern, while February, June, July, September, and November indicate spread pattern. Next, period 2009 shows that February, March, May, June, July, September, and October indicate group pattern and January, April, August, November, and December indicate spread pattern.

According to test of spatial dependency period 2006 with Moran's I index, January, Maret, and December have significant in α=10%, and February have significant in α=20%. January, February, March, September, and December have positive spatial autocorrelation, while July has negative spatial autocorrelation.

Table 2. Geary's C result in period 2006

Month	C	Z(C)
January	0.978	-0.040
February	1.024	0.029
March	0.909	0.104
April	1.064	0.055
Mei	0.993	0.008
June	1.208	0.256
July	1.291	0.209
August	1.356	0.181
September	1.011	0.007
October	1.106	0.128
November	0.957	-0.037
December	0.940	-0.070

Period 2007 have only two months significant that are June and October. June has positive spatial autocorrelation and October has negative spatial autocorrelation. There are 9 months that have significant in period 2008 such as January, February, April, May, June, July, October, and November. January, April, May, and October have positive spatial autocorrelation, while February, July, and November have negative spatial autocorrelation. According to Geary's C test of spatial dependency, there isn't a significant month. The result of Geary's C test period 2006 can be found in Table 2.

According to Moran's scatter plot in period March 2006, it can be informed that most of the DHF event in Surabaya City happened in the first and second quadrant. The Moran's scatter plot in Figure 3 is the visualization of the DHF's spread. The axis shows standardization observation value and the ordinate shows the standardization observation value according to its neighbor. First and third quadrant shows positive spatial autocorrelation. Whereas, second and fourth quadrant show negative spatial autocorrelation.

The significant test of LISA shows that some districts that have a positive spatial autocorrelation are Tegalsari, Genteng, Gubeng, Sukomanunggal, Tandes, Karang pilang, Wiyung, Lakarsantri, and Sambikerep. Others, such as Trenggilis Mejoyo, Wonocolo, Simokerto, Pabean Cantikan, Bulak, and Mulyorejo have a negative spatial autocorrelation.

An unsafe map of DHF disease that can be made shows in Figure 4. Based on Figure 1 show that Genteng, Tegalsari, and Gubeng have group in high number of DHF and it can be an unsafe district of DHF in Surabaya City, whereas, Wonocolo, Trenggilis Mejoyo, Pabean Cantikan, Simokerto, Bulak, dan Mulyorejo don't have groups. But because of its position around high number of DHF district, it makes these districts come to a medium category. Other district that have green color include in safe category.

The result of spatial dependency test by Moran's I have significant confidence level more than 5%. It means that the district's proximity isn't only overlap between sides or edges, but further. So that, spatial weighted matrix that are match with this is distance continguity. It is caused by mobilization of Surabaya inhabitant it self. Someone can move across more than one district.

4. Conclusion

Most of the DHF disease in Surabaya City happens in rainy season (January-June) and the highest number of DHF disease in Surabaya City happens in North, West, and Central of Surabaya. At the last four years, the highest number of DHF happened in March 2006. Several months that indicate spatial relation in each district are January, March, June, October, and December. Several districts that include in prone category of DHF's spread are Genteng, tegalsari, and Gibeng district. While, Pabean Cantikan, Simokerto, Bulak, Mulyorejo, Wonocolo, and Trenggilis Mejoyo district include in medium category.

5. Acknowledge

This work was supported by ITS grant program 2010.

6. Reference

[1]. Curtis, J. A., and Lee, A. W. (2010), Spatial Pattern of Diabetes Related Health Problems for vulneral Population in Los Angeles, *J. Health*, USA.

[2]. Tottrup C, Tersbol P. B Lindeboom W, and Meyrowitch D. (2009), Putting Child Mortality on Map: Towards an understanding of Inequity in health, *J. Health*, Vol 14 no 6 PP 653-662.

[3]. Lee Jay and Wong S W David (2000), Statistical Analysis eith Arcview GIS, John Willey and Son, INC, USA.

[4]. Indonesian Statistical Agency (2010), Result of Population Census, Aggregat district of Surabaya City, Surabaya.

[5]. Bivand, Roger S, Pebesma, Edzer J, and GR. Virgilio (2008), Applied Spatial Data Analysis with R, Springer Science Bussines Media, USA.

[6]. Kartika Yoli (2007), Pattern of Spatial Spread Dengue Hemorragic Fever in Bogor City in 2005, Bogor Agricultural Institut, Bogor.

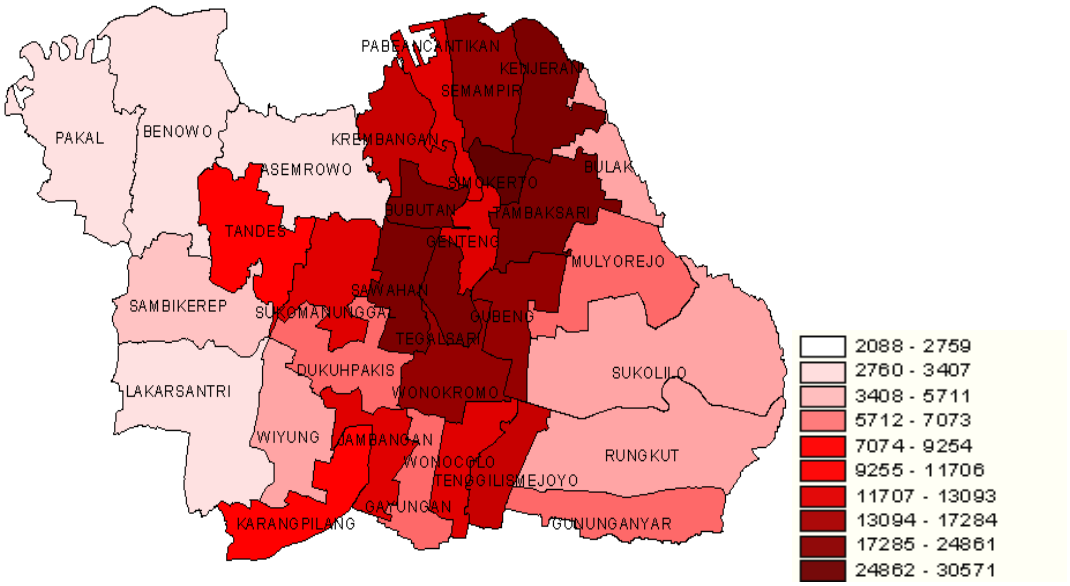

Figure 1. Population Density in Surabaya City According to District in 2009

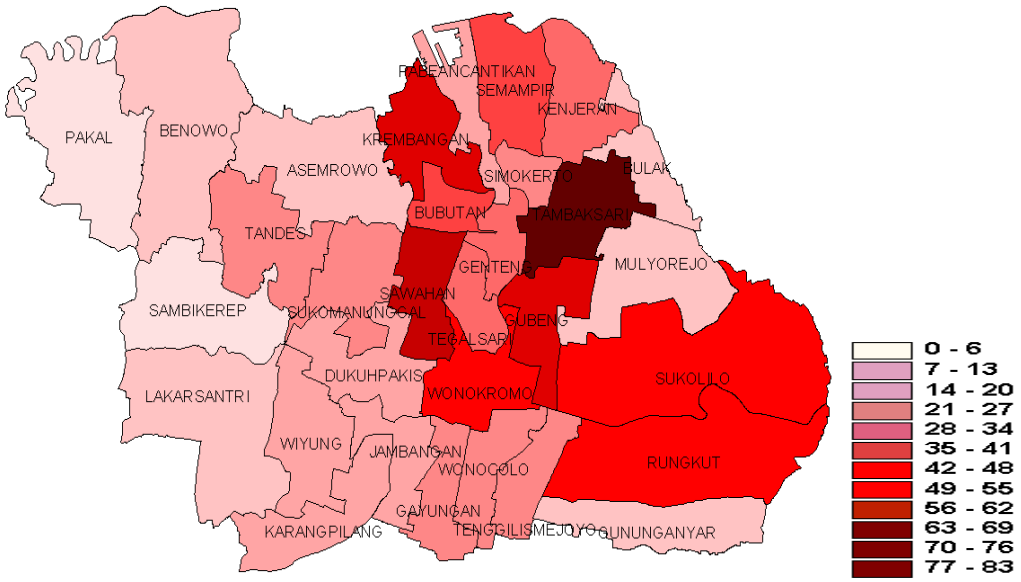

Figure 2. Spread of DHF Event in Surabaya City Every District in Each Month in 2006

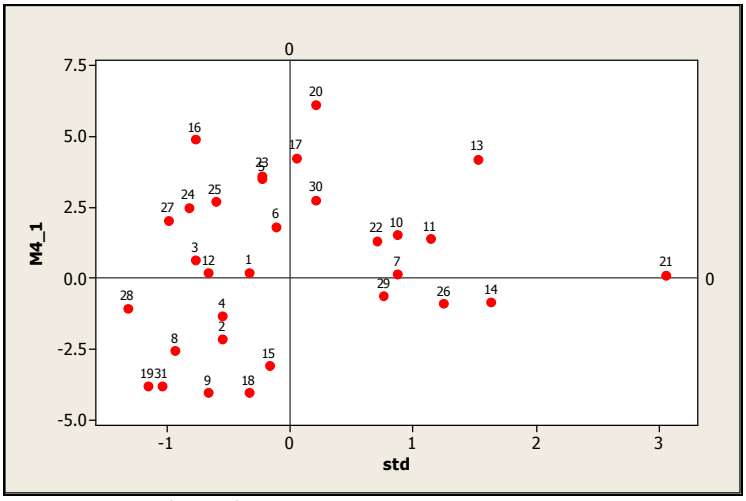

Figure 3. Moran Scatterplot of March 2006

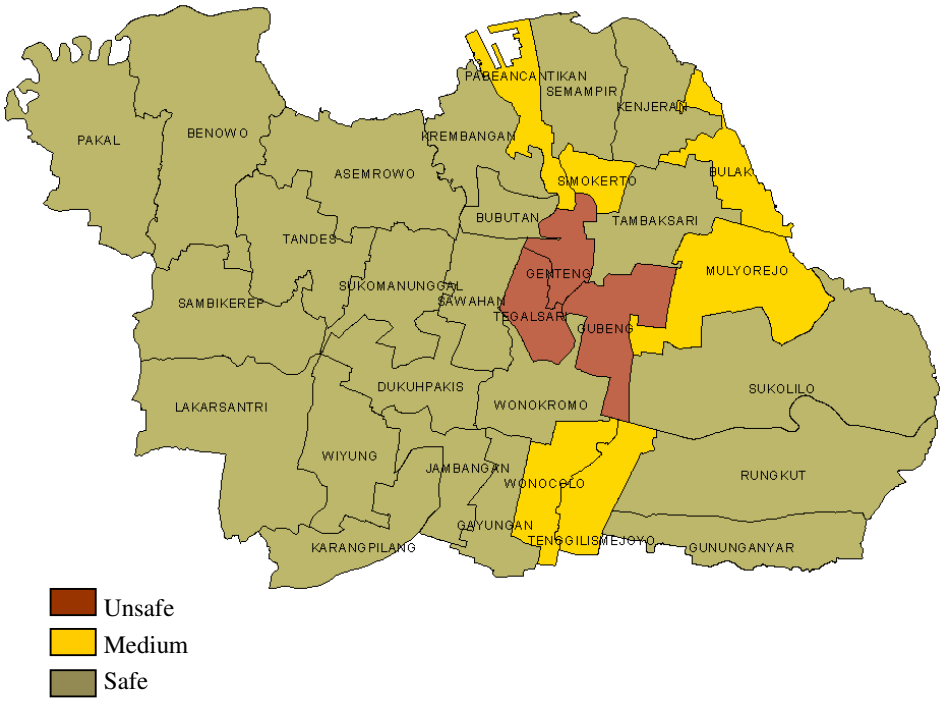

Figure 4. An Unsafe Map of DHF in Surabaya City

Preliminary Study of Traffic Marking Formulation Using Natural Rubber Grafted Modification

Athanasia Amanda Septevani [1], Agus Haryono [2], Dewi Sondari [3], Ahmad Randy [4]

[(1,2,34,)] Polymer Chemistry Group, Research Center for Chemistry, Indonesian Institute of Sciences (LIPI), Tangerang, Indonesia (fani.manda@yahoo.com)

Abstract

The aim of this research is to prepare environmentally friendly waterborne traffic marking using natural rubber grafted modification (NR-G). NR-G will extend its usage. Chemical modification could be done by graft copolymerization of natural rubber. Natural rubber (NR) in this study was chemically modified with methyl methacrylate (MMA) and styrene (S). The expected result of graft copolymerization of MMA and styrene onto natural rubber is obtaining elastomer thermoplastic used as binders on traffic marking. The process of graft copolymerization was carried out by emulsion polymerization of natural rubber and monomer mixture of MMA and styrene with potassium persulphate as an initiator and sodium dodecyl sulphate as an emulsifier. Traffic marking formulation was carried out by mixing of modified natural rubber with filler, pigment, other additive and solvent. Glass beads were added in onto traffic marking formulation to provide retro reflectivity effect so that the marking can be visible at night. Mechanical properties of traffic marking were investigated using tensile strength and modulus of elasticity analyser. Distribution of particle on traffic marking was investigated using particle size analyser. The optimum of traffic marking formulation obtain in this preliminary research have the tensile strength value 3.69 kgf/cm^2 and modulus of elasticity value 3.62 kgf/cm$^{2.}$. Particle size analysis showed the main mode in intermediate range 0.395 – 0.577 μm, with the average size of 0.48 μm.

***Keywords**: Natural rubber, waterborne traffic marking, graft, copolymerization.*

1. Introduction

Natural rubber (NR) is an unsaturated elastomer with some good properties such as high strength, outstanding resilience and high elongation at break. However, its utilization was still limited, particularly in tire industries. Natural rubber modification will extend its usage. Modification of natural rubber could be done physically or chemically. This modification is expected to expand the utilization of NR not only in tire industries. Modification of natural rubber by graft copolymerization had already studied by grafting another polymer chain onto NR particle. Examples of monomer that already studied in this type of modification include styrene, MMA, acrylonitrile, and butyl acrylate [1-5]. The expected result of graft copolymerization MMA and styrene onto natural rubber is obtaining elastomer thermoplastic used as binders on traffic marking.

Traffic marking is lines, symbols and words are often painted on a roadway to help direct drivers and control traffic flow. Traffic marking is a mixture of binders, filler, pigment and other additive at several levels. The most commonly used traffic marking material are preformed tape, paint, thermoplastic and MMA [6]. Traffic marking technology is a continually evolving subject. There are numerous types of materials used in the field today and not limited to paint, epoxy, tape, and thermoplastic.

Solvent-based traffic markings have been widely used in the past because of their convenience and fast-drying properties. But, they have fallen in disfavour because of their release of environment polluting organic solvent into atmosphere. Strict environmental protection laws in 1950s intensified researches on waterborne traffic marking [7]. Water based paints have many merits such as less volatility, safety, especially against fire risk and good hygienic condition during production and application [8-9].

In this research, the water was contained in natural rubber grafted emulsion. The objective of this study was to make formulation of traffic marking using NR-G. In this study we will determine the varied composition effect of NR-G and MMA used.

2. Experimental Details

Material

Natural rubber grafted modification (NR-G) was used as describe by Randy, *et al* [5]. The NR-G product was used directly in the form of emulsion (without drying process). The composition of NR-G which is having highest grafting efficiency was used in this research with the natural rubber and monomer ratio of 60:40 (weight ratio). Filler, pigment, other additive and solvent was used as received.

Method

Natural rubber grafted modification

The process of graft copolymerization was carried out by emulsion polymerization of natural rubber and monomer mixture of MMA and styrene with potassium persulphate as an initiator and sodium dodecyl sulphate as an emulsifier. The natural rubber modification product was used directly in the form of emulsion (without drying process).

Traffic marking formulation

Traffic marking formulation was carried out in the beaker glass equipped with magnetic stirrer. High Impact polystirene (HIPS) was prepared by mixing in methylene chloride until dissolved completely. Dissolved HIPS was slowly poured into NR-G. Then, the mixture was added by filler (pigment, extender, wax & stabilizer), MMA and glass beads. The benzoil peroxide (BPO) was added in just before the formulation was applied to the pavement.

Characterization

Mechanical properties of traffic marking were investigated using tensile strength and modulus of elasticity analyser in Centre for Chemical and Packaging, Ministry of Industry. Distribution of particle on traffic marking was investigated using particle size analyser in Research Centre for Chemistry, Indonesian Institute of Sciences.

3. Result and Discussion

Influence of NR-G onto traffic marking formulation

Table 1 and Figure 1 shows the value and the influence of adding NR-G onto traffic marking formulation to tensile strength and modulus of elasticity value. The 4th sample has smallest value of modulus of elasticity than the other samples. The more number of NR-G, the more elastic its formulation. It was due to natural rubber include elastomer having elasticity properties. Elasticity property is needed for the traffic marking formulation so that the traffic marking would not crack easily. But at the addition of too much NR-G (4th sample), showed the lowest value of tensile strength. This is because of excess content of NR-G that make its composition is not balance with the other binders (HIPS), so that the formulation formed is not compatible and lead to more brittle mixture.

The highest tensile strength of the traffic marking formulation with value was produced by addition of NR-G of 20 g (2nd sample). NR-G have a function as binder filler on traffic marking formulation hence the more adding of NR-G then the stronger of filler bonding on traffic marking. But at the addition of more than 20 g obtain less tensile strength value. Hence, this is the optimum composition of natural rubber needed on traffic marking formulation to obtain optimum value of tensile strength and modulus of elasticity.

Table 1. Value of tensile strength and modulus of elasticity to the adding of NR-G onto traffic marking formulation

Run No	**Composition of NR-G**	**Tensile strength Kgf/cm^2**	**Modulus of elasticity Kgf/cm^2**
1st	17 g	2.17	2.11
2nd	20 g	3.69	3.62
3rd	23 g	2.87	2.84
4th	26 g	1.65	1.6

Influence of adding MMA onto traffic marking formulation

Table 2. Tensile strength and modulus of elasticity of NR-G traffic marking formulation on various concentrations of MMA.

Run No	Composition of MMA	Tensile strength Kgf/cm^2	Modulus of elasticity Kgf/cm^2
2nd	10 g	3.69	3.62
5th	12 g	2.14	2.08
6th	14 g	2.12	2.06
7th	18 g	2.13	2.08

Addition of MMA was found could increase the glass transition of the copolymer, leading to improvement of the cohesive strength [10]. The higher cohesive strength, the higher bonding strength shows between filler particle. The influence of MMA addition onto traffic formulation can be observed on Figure 2 and the value of the tensile strength and modulus of elasticity shown on Table 2. The more MMA adding onto traffic marking formulation, the more elastic traffic marking obtained but addition of

too much MMA do not give significant changes of elasticity property. The optimum condition of tensile strength was obtained at the 1st sample (adding 10g of MMA).

The more MMA addition can reduce the tensile strength which on further addition tends to produce a constant value of tensile strength it was due to adding excess quantity MMA on the formulation can make the formulation becomes more dilute so that traffic marking obtained was brittle. In this preliminary study of traffic marking was selected of 2nd sample as the optimum formulation with the highest tensile strength and modulus of elasticity value. The higher tensile strength, the stronger bonds obtained between filler on the traffic marking formulation. In spite of this formulation is not the most elastic but the modulus of elasticity is not too different from its value.

Particle size distribution

Study of particle size distribution was done to determine the size and distribution of particle filler and binders on traffic marking formulation. Figure 3 showed the particle size distribution of 2nd sample with the main mode in intermediate range 0.395 – 0.577 μm, with the average size of 0.48 μm. Detail of distribution composition per % number could be showed in Table 3.

Table 3. Distribution of filler particle using NR-G on traffic marking formulation

%<	10	25	50	75	90
Size μm	0.395	0.423	0.467	0.521	0.577

Figure 3 was showed that particle distribution of traffic marking formulation tends to uniform and smooth. Correct kinds and quantity of emulsifier needed to make particle distribution of NR-G with the filler tends to more uniform and stable. Emulsifier contained in NR-G is Sodium Dodecyl Sulfate. Quantity of emulsifier should not be excessive due to create foaming formulation and make particle distribution is not stable.

4. Conclusion

Based on the preliminary research of traffic marking formulation using natural rubber grafted obtained in the present study, the optimum of traffic marking formulation have the tensile strength value 3.69 kgf/cm^2 and modulus of elasticity value 3.62 kgf/cm$^{2.}$. Particle size analysis showed the main mode in intermediate range 0.395 – 0.577 μm, with the average size of 0.48 μm.

5. Acknowledgments

This work was supported by Indonesian Government using Thematic Project, Indonesian Institute of Sciences (LIPI).

6. References

[1] N. Pukkate, Y. Yamamoto, S. Kawahara (2008), Mechanism of graft copolymerization of styrene onto deproteinized natural rubber, *Colloid Polym. Sci.*, vol. 286, pp. 411-416.

[2] P. Chumsamrong, O. Monprasit (2007), Preparation, adhesive performance and stability of natural rubber latex grafted with N-butyl acrylate and methyl methacrylate, *Suranaree J. Sci. Technol.*, vol. 14, no. 3, pp. 269-276.

[3] A. Bogner, A. Guimaraes, R.C.O. Guimaraes, A.M. Santos, G. Thollet, P.H. Jouneau, C. Gauthier (2008), Grafting characterization of natural rubber latex particles: wet-STEM imaging contribution, *Colloid Polym. Sci.*, vol. 286, pp. 1049-1059.

[4] K. Charmondusit, S. Kiatkamjornwong, P. Prasassarakich (1998), Grafting of methyl methacrylate and styrene onto natural rubber, *J. Sci. Chula. Univ.*, vol. 23 (2), pp.167-182.

[5] Ahmad Randy, Dewi Sondari, Kuntari A.S., Ariadi B., Surasno (2009), Preparation of Styrene and Methyl Methacrylate Grafted onto Natural Rubber, International Symposium Agricultural Engineering Towards Sustainable Agriculture in Asia, Bogor, Indonesia, November 18-19.

[6] Centre for Transportation Research and Education (2001), Durable, Cost-Effective Pavement markings Phase I: Synthesis of Current Research, Lowa State University, June.

[7] Daoxing Sun and Yiheng Zhang (2010), Preparation of fast drying waterborne nano-complex traffic-marking paint, *Journal of Coating Technology and Research*, February.

[8] S. Fatemi, M.K.Varkani, Z. Ranjbar, S. Bastani (2006), Optimation of the water based road marking paint by experimental design, mixture method, *Prog.Org.Coat*, pp 337-344.

[9] DL. Schmidt (1995), Water-Based Acrylic Coating Composition, US Patent 5,470,908.

[10] Hamada and Ichikawa (2003), ….

Appendixes

Table 4. Composition of traffic marking formulation

Running No	Material Weight (gram)						
	NR-G	MMA	HIPS	MTC	Filler	Glass beads	BPO
1st	17	10	6	50	18.7	6	0.4
2nd	20	10	6	50	18.7	6	0.4
3rd	23	10	6	50	18.7	6	0.4
4th	26	10	6	50	18.7	6	0.4
5th	20	12	6	50	18.7	6	0.4
6th	20	14	6	50	18.7	6	0.4
7th	20	18	6	50	18.7	6	0.4

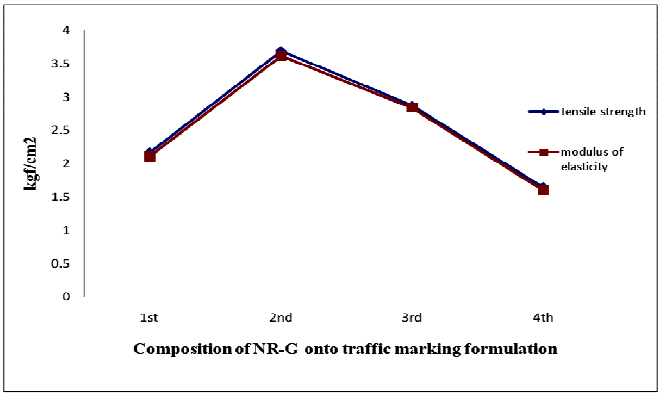

Figure 1. Influence of NR-G adding onto traffic marking formulation

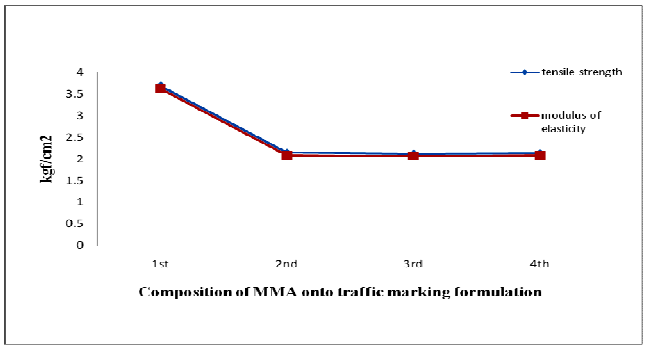

Figure 2. Influence of MMA adding onto traffic marking formulation

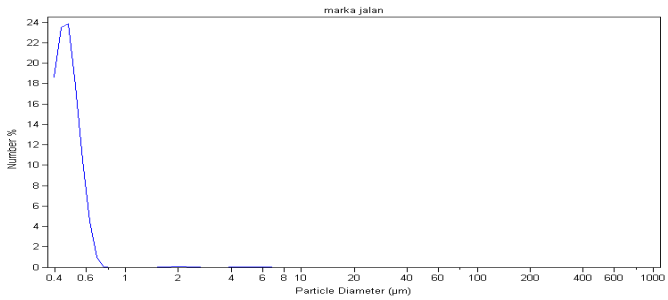

Figure 3. Particle size distribution of 2nd sample traffic marking formulation

Evaluation of Clustering Season Zone in Ngawi – East Java Using Support Vector Machine (SVM)

Bambang Widjanarko Otok [1], Agus Suharsono [2], Elly Nur Shobihah [3]

[1,2,3] Faculty of Mathematics and Natural Science, Sepuluh November Institute of Technology, Surabaya, Indonesia (bambang_wo@statistika.its.ac.id; Agus_s@statistika.ac.id; Alley_sh88@statistika.its.ac.id)

Abstract

Ngawi is the fifth-largest district that contribute 5,74% of the total rice production in East Java Indonesia. Thus, it is needed to find information about weather prediction. First steps to increase the accuration of weather predictions is done by accurately classifying Season Zone (ZOM). Untill now, BMKG [1] still use the complete linkage method to create a grouping of ZOM. While one method of classification which is currently growing rapidly is the non parametric method of Support Vector Machine (SVM) [2]. SVM method One Againts One Strategy is proposed to evaluate the classification accuracy of ZOM, because they have very good perfomance in the process of classification for multiclass SVM. The result of clustering based on rainfall data that has been reduced with factor analysis produced 4 ZOM. The result of clustering evaluation using SVM method provides information that classification accuracy of ZOM after having modification by elevation map is equal to 50%. Meanwhile, the classification accuracy of BMKG's ZOM is equal to 72.2222%. The classification accuracy of ZOM after having modification is lower because clustering results still tend to be subjective, so there is not guarantee to the homogenity.

Key word : *Ngawi, ZOM, Complete linkage, SVM.*

1. Introduction

Indonesia's ability to make accurate model predictions is still likely low. One of the reason why the model is low is because the group lack of precise classification made on the approximate area of climate stations [3]. So far, BMKG still using complete linkage as a method of clustering hierarchy to form ZOM [1], with a commonly used measure of inequality is euclidius distance. Mean while, the classification method to evaluate the accuracy of the classification currently used by BMKG, is discriminant analysis and logistic regression. Because both methods are parametric methods, the use of such methods will have strictly assumptions.

According to BMKG [4], weather, climate, and geosciences have the characteristics of a natural chaotic nonlinear dynamic systems. Therefore, the used of parametric method is insufficient. Several modeling techniques based on machine learning was developed to assist classification by nonparametric methods, such as using Support Vector Machine (SVM) [5]. SVM becomes a popular method because it can provide better generalization ability in the application [6].

SVM can only classify the data into two classes. To overcome this weakness, SVM developed multiclass classification methods, one of them is One Against One Strategy method. SVM is proposed to test the classification accuracy of ZOM in Ngawi district, East Java. Through the development of classification using SVM based on machine learning method, it is expected to increase research papers on the application of statistics in climatology as well as to improve the accuracy of ZOM classification that may upgrade the performance of several locations of certain ZOM that have low-level accuracy.

2. Experimental Details

SVM is one of the machine learning method based on the *structural risk minimization* with induction principle, and has achieved superior performance in a wide range of applications [2,7]. Introduced by Vapnik *et al.* [8], SVM is widely used for pattern recognition and for regression called as Support Vector Regression (SVR) [9]. The aim of SVM is finding the best hyper plane separating two classes in the input space [2]. For classification Season Zone, SVM proposed as non parametric method assessed to give a better accuracy for ZOM classification because it doesn't make any stricly assumtion compulsory.

Data used in this research is secondary data from the monthly Ngawi district's rainfall in

the year 1989 to 2010 is taken from Karangploso second class climatology station in Malang. They were collected from 23 rainfall monitoring stations in the District Ngawi, but after having conversion by choosing the most complete data information, then there just only 18 stations that will be used in the analysis. The eighteen rainfall monitoring stations are namely Mantingan, Ngawi, Ngrambe, Tretes, Kedung urung-urung, Kedunggalar, Walikukun, Jogorogo, Bekoh, Kedung bendo, Ngale, Paron, Mardiasri, Padas, Karangjati, Sambiroto, Begal, Guyung. Before being used, data is proccessed by getting the rainfall average of each month from years (1989 - 2010) on each station. Therefore, we have the 18 rows x 12 columns data set.

Grouping Season Zone means we have to bound some rainfall monitoring stations which have the same characteristics (high homogenity) in one group, and also bound some rainfall monitoring stations which have the very different characteristics (low homogenity) in other groups [10]. Complete linkage as one of the hierarchy clustering method can be efectivelly used when the objects distinctly heterogen. In addition, the euclidius distance is choosen because it measures the rainfall data as objects in same scale. They are said on same scale because scale in a column, called variabel is the same as scale in others column. It means that although we use twelve variables (high dimension data), the fact is we just have one variable (low dimensional data). Because of using euclidius distance, it is urge to reduce the variables before doing clustering analysis, in order to get new independent variables.

For this reduction process, we use factor analysis. Thus, we got factor scores that represented the twelve variables. Here are the 9 steps of this research analysis: Describing the rainfall data in Ngawi district from each station per month in 1989-2010.

a. Performing variables reduction by factor analysis.
b. Identifying members of ZOM's group of complete linkage clustering on rainfall factor score data.
c. Modifying the complete linkage clustering method.
d. Identifying members of ZOM's group of complete linkage clustering with modification.
e. Defining ZOM boundaries based on contour plots modification of rainfall and factor scores.
f. Calculating the value of Sw and Sb to evaluate the homogenity of the grouping.
g. Classifying ZOM using SVM method One Against One Strategy based on complete linkage clustering groups and complete linkage clustering grups with modifications based on elevation maps, latitude, and longitude. In addition, we also classifying ZOM based on ZOM's BMKG 2003, using SVM .
h. Counting the classification accuracy of ZOM using APER table.

Factor Analysis

According to Johnson and Wincern [10], factor analysis is purposed to explain the variance of data to the maximum; to get the new factors that independent to each others; and to get factors that easily interpreted. The orthogonal factor model with m common factors can be written as:

$$\boldsymbol{X}_{(px1)} = \boldsymbol{\mu}_{(px1)} + \boldsymbol{L}_{(pxm)}\boldsymbol{F}_{(mx1)} + \boldsymbol{\varepsilon}_{(px1)} \quad (1)$$

$\boldsymbol{\mu}$ = Vector of mean variable.
$\boldsymbol{F}$ = Vector of *Common factor.*
$\boldsymbol{L}$ = *Loading factor matrice*
$\boldsymbol{\varepsilon}$ = Vector of *Specific factor.*

Complete Linkage Clustering and Euclidius Distance

Complete linkage clustering method ensure all items in a cluster in maximum distance (minimum similiarity) of each other.

$$d_{(UV)W} = \max (d_{UW}, d_{VW}) \quad (2)$$

d_{UW} and d_{VW} = distance between the most distant members of clusters U and W and clusters V and W, respectively.

Similiarity distance means when items or units are clustered, proxymity is usually indicated by some sort of distance. Euclidius distance is often preferred than other distance for the clustering because it do not need prior knowledge of the distinct groups (i.e sample varinces and covariances). Mathematically, it can be write as:

$$d(\boldsymbol{x}_i, \boldsymbol{x}_j) = \sqrt{(\boldsymbol{x}_i - \boldsymbol{x}_j)'(\boldsymbol{x}_i - \boldsymbol{x}_j)} \quad (3)$$

Support Vector Machine with One Againts One Strategy

Support Vector Machine (SVM) apply a simple linear method to the data but in a high-dimensional feature space non-linearly related to the input space [11]. This simplicity combined with state of the art performance on many learning problems (classification, regression, and

novelty detection) has contributed to the popularity of the SVM.

According to Vapnik [8], the elections of maximum margin will give the best generalization ability. And maximizing the margin means equivalent to maximize the distance between the hyper plane and the closest point, $1/\|\vec{w}\|$, provided that:

$$< \vec{w}.\vec{x}_i > +b \geq +1 \; jika \; y_i = +1 \quad (4)$$

$$< \vec{w}.\vec{x}_i > +b < -1 \; jika \; y_i = -1 \quad (5)$$

where the terms of equation (4) and (5) can be used as one condition, namely:

$$y_i(< \vec{w}.\vec{x}_i > +b) \geq 1 \quad , \forall i \quad (6)$$

Thus, the problem becomes Quadratic Programming (QP) problem. To find a minimum solution of equation (7), consider to the constraint equations (8).

Minimize: $\frac{1}{2}\|\vec{w}\|^2$ (7)

Subject to: $y_i(\vec{x}_i.\vec{w}+b)-1 \geq 0, \forall i$ (8)

This issue will be more easily resolved if converted into a Lagrangian formula. Thus the constraint optimization problem can be converted into

$$L(\vec{w}, b, \alpha) = \frac{1}{2}\|\vec{w}\|^2 - \sum_{i=1}^{m} \alpha_i \left(y_i((\vec{x}_i.\vec{w}+b)-1)\right)$$

$$, \; (\alpha_i \geq 0) \quad (9)$$

The optimal value of equation (9) can be calculated by minimizing L by $\vec{w}$ and b, and maximizing L by α_i. By considering that the optimum point of the gradient L = 0, then equation (9) into equation (10) with constraint (11)

Maximize: $\sum_{i=1}^{m} \alpha_i - \frac{1}{2} \sum_{i,j=1}^{N} y_i y_j \alpha_i \alpha_j \vec{x}_i \vec{x}_j$ (10)

Subject to: $\sum_{i=1}^{m} y_i \alpha_i = 0, \forall i : 0 \leq \alpha_i (i = 1,2,\ldots,m)$ (11)

The result of this calculation is obtained α_i mostly positive. The data are correlated with positive α_i is called as a support vector. Thus, support vector is a sub set of data that is located on the margins. Decision function for linear case can be written.

$$f(\vec{x}_j) = \sum_{i=1}^{nsv} \alpha_i y_i \vec{x}_i \vec{x}_j + b \quad (12)$$

Learning method in QP presented above is valid if the learning data are linearly separable. For non-linear separable data we use additional methods called Kernel method [6]. First $\vec{x}_h$ data are mapped by the function $\emptyset(\vec{x}_h)$ to the higher vector space dimension. Kernel methods are formulated as follows:

$$K(\vec{x}_i, \vec{x}_j) = < \emptyset(\vec{x}_i).\emptyset(\vec{x}_j) > \quad (13)$$

One of the kernel functions that can be used is the Gaussian Radial Basis Function (RBF Gaussian).

$$K(\vec{x}_i, \vec{x}_j) = \exp\left(-\frac{\|\vec{x}_i - \vec{x}_j\|^2}{2\sigma^2}\right) \quad (14)$$

In addition, instead of Quadratic Programming (QP), SMO used to overcome the problems of the large size of the kernel matrix (chunking) through solving the global optimization problem into several smaller optimization problem [8]. In this paper we use one against one strategy as multiclass SVM method known as pair wise coupling strategy that works by combining SVM for each pair in each class. Method One Against One is constructed (k(k-1))/2 binary classification model, where k is the number of classes. The object is classified into class by voting method. N-fold cross validation is one evaluation method of the model, so the model can classify as many observation data correctly. Parameter cost (C) and parameter of Kernel function (γ) is set by the user to minimize error.

Season Rainfall Zone (ZOM)

Rainfall has an idea as the height of rain that fell and accumulated in an area where rain water does not soak into the ground, does not flow, and does not evaporate into the atmosphere. Whereas, season zone is area that has clearly distinction between periods of dry season and period of rainy season. According to BMKG 2003, Ngawi district consists of 2 ZOM. Zone 1 includes five stations, ie Jogorogo, Ngrambe, Kedung urung, Tretes, and Mantingan. Zone 2 thirteen stations include Walikulun, Bekoh, Kedunggalar, Guyung, Ngadirejo/ Soko, Madiasri, Ngawi, Paron, Padas, Sambiroto, Karangjati, Ngale.

3. Result and Discussion

Based on the loading factor using varimax rotation, we get 4 factor scores that explain 77.6% of the total diversity. By referring to Anderson [12], the percentage are good enough if the factors entered can explain 60% of the total sample variance. If ZOM BMKG used rainfall data, than ZOM grouping in this research used factor scores. The result of clustering with complete linkage method and distance eucluidius obtained 4 groups observation post, as follows:

Group 1: Mantingan, Ngale, Paron, Mardiasri.
Group 2: Kedung urung-urung, Jogorogo, Karang jati, Guyung.
Group 3: Ngawi, Ngrambe, Kedung galar, Tretes, Walikukun, Bekoh, Padas, Sambiroto, Begal.
Group 4: Kedung Bendo.

After getting the group of rainfall stations, modification need to be done in order to ensure that the stations grouped by considering the location closeness and contour of each station. Thus, the transfer of items is done:

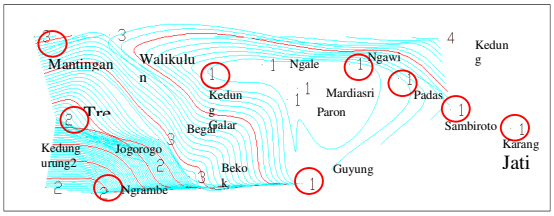

Figure 1. Member of ZOM Group Using Complete Linkage Method with Modification

Based on Figure 1, it shows that for members of the same group will tend to be clustered in certain areas, so it can be made ZOM new design. ZOM design modification based on the elevation map can be determined as follows.
ZOM 1: Ngawi, Kedung galar, Ngale, Paron, Mardiasri, Padas, Karang jati, Sambiroto, Guyung.
ZOM 2: Ngrambe, Tretes, Kedung urung-urung.
ZOM 3: Mantingan, Walikulun, Bekoh, Begal
ZOM 4: Kedung bendo.

Factor analysis needed to avoid dependencies between variables. For ZOM Classification using Complete Linkage Method with modification, the free parameters defined as γ = 0,001 and C =100. The smallest error for this parameter is 35% and the total accuracy of the model is 50%. By this parameter, classification accuracy using SVM based on factor scoring rainfall data is 50%. There are 9 post observations from ZOM 1 appropriate prediction in ZOM 1. There by, the other 9 pos observations have wrong grouping.

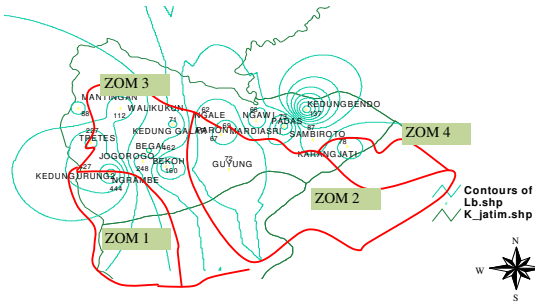

Figure 2. Season Zone Mapping Using Complete Linkage Method Based on Modified Rainfall Contour

On the other side, for ZOM classification based on BMKG, the free parameters defined as γ=0,000001 and C=10. The smallest error for this parameter is 30% and the total accuracy of the model is 72.2222%. By this parameter, classification accuracy using SVM based on factor scoring rainfall data is 72.2222%, there are 13 pos observations from ZOM 2 and appropriate prediction in ZOM 2, but the other 5 post observations have wrong grouping.

4. Conclusion

By using complete linkage and euclidius distance procedure, Ngawi district is grouped into four ZOM. The modification based on the elevation map, longitude, and latitude, obtained that ZOM 1 consists of Ngawi, Kedung galar, Ngale, Paron, Mardiasri, Padas, Karang jati, Sambiroto, dan Guyung. ZOM 2 consists of Ngrambe, Tretes, Kedung urung-urung, dan Jogorogo. ZOM 3 consists of Mantingan, Walikulun, Bekoh, dan Begal. ZOM 4 consists of Kedung bendo.

Evaluation method of ZOM grouping is done by SVM One Against One Strategy provides information that the classification accuracy of ZOM clustered from factor scores using complete linkage method with modification is 50%. Meanwhile, the classification accuracy of ZOM BMKG is 72.2222%. The classification accuracy of ZOM after having modification is lower because clustering results still tend to be subjective, so there is not guarantee to the homogenity.

5. Acknowledgements

We thank to all people who have supported this research including people who work at the Bussiness Laboratory of Department of Statistics Sepuluh November Institute of Technology.

6. References

[1]. Badan Meteorologi dan Geofisika (BMKG) (2003), *Pewilayahan Daerah Tipe Hujan dan Evaluasi Musim Kemarau 2003 serta Prakiraan Sementara Musim Hujan 2003/2004 Kabupaten Indramayu*. BMG, Jakarta.

[2]. Nugroho, A.S., Witarto, A.B., Handoko, D. (2003), *Support Vector Machine –Teori dan Aplikasi dalam Bioinformatika*. [http://www.Ilmukomputer.com], accessed on 24 September 2010.

[3]. Roesmara (2008), *Indonesia Mampu prediksi Iklim*, [http://www.erakomputer.com/content/berita/juli/indonesia-mampu-prediksi-iklim], accessed on 24 September 2010.

[4]. Kadarsah (2007), *Rata-Rata Curah Hujan Bulanan Indonesia (1961-1993)*. [http://www.kadarsah.wordpress.com/2007/06/29], accessed on October 29, 2010.

[5]. Schölkopf B., Smola A. (2002), *Learning With Kernels*. MIT Press.

[6]. Kerami, D., Hendri, M. (2004), *Kajian Kemampuan Generalisasi Support Vector Machine Dalam Pengenalan Jenis Splice Sites Pada Barisan DNA*. MAKARA, SAINS, Vol. 8, No. 3.

[7]. Pontil, M. and Verri, A. (1998), *Support Vector Machines for 3D Object Recognition*, IEEE Trans. On Pattern Analysis and Machine Intelligence, vol. 20, no. 6, pp. 637-646

[8]. Vapnik, V.N. (1999), *The Nature of Statistical Learning Theory*. Springer, New York.

[9]. Lestari, P. (2009). *Aplikasi Metode Support Vector Regression Dalam Pembentukan Model Yield Curve Untuk Government Bonds Indonesia*, ITS, Surabaya.

[10]. Johnson, R. A., and Wichern, D. W. (1992), *Applied Multivariate Statistical Analysis Third Edition*. Prentice Hall, New Jersey.

[11]. Karatzoglou, A., Meyer, D., Hornik, K. (2006), Support Vector Machines in R. *Journal of Statistical Software,* Volume 15, Issue 9.

[12]. Anderson, R.E. and JR, Joseph, F.H. (1984), *Multivariate Data Analysis,* Prentice Hall International. Inc., New Jersey.

[13]. Guo, G.D., Jain, A.K., Ma, W.Y., and Zhang H.J. (2002), "Learning Similarity Measure for Natural Image Retrieval with Relevance Feedback", *IEEE Tran. on Neural Networks*, vol. 13, no. 4, pp. 811-820.

[14]. Hamel, L. (2009), *Knowledge Discovery With Support Vector Machines*, A John Wiley & Sons, Inc., Publication, New Jersey.

[15]. Hearst, M.A., Dumais, S.T. , Osman, E. , Platt, J. ,and Scholkopf, B. (1998), "Support Vector Machines", *IEEE Intelligent Systems*, vol. 13, no. 4, pp. 18-28.

[16]. Hsu, C.W & Lin, C.J. (2002), *A Comparison of Methodes for Multi-class to Binary: A Unifying Approach for Margin Classifier*, Journal of Machine Learning Research 13:415-425.

Performance Genetic Algorithm and Simulated Annealing of Case Studies Flow Shop Scheduling

Dian Ratnawati

Department of Mathematics, Faculty of Science, Brawijaya University
(dian_ilkom@brawijaya.ac.id)

Abstract

Flow shop scheduling is to schedule the production process of each of n jobs that have a definite sequence of production processes, through m the same machine. The objective was to determine the sequence of scheduling jobs that exist in order to deliver optimal performance. Meta-heuristic methods have been used to deal with scheduling problems, especially for optimization. Results obtained nearly optimal or even optimal. Among them will be used in this Research is the Simulated Annealing and Genetic Algorithm. Steps to be done are to solve flow shop scheduling with simulated annealing algorithms and genetic algorithms. Then experiment with both algorithm for various number of jobs.

Keywords: ***Genetic Algorithm, Simulated Annealing Algorithm, Flow shop Scheduling.***

Development of Static Load Sensor Based on PVDF Film Element

Didik R. Santoso

Physics Dept., Fac. of Natural Sciences, Brawijaya University
Email: dieks@ub.ac.id

Abstract

Currently, the application of PVDF film as dynamic loads sensors have been carried out by some researchers, even in the fabrication stage. The principles of piezoelectric sensors, including PVDF material, is to change the mechanical deformation into electrical values (electrical charge) equivalently. Some properties of this material e.g. sensitive, lightweight, strong, and relatively low cost, has made this material as a good choice in the design of the mechanical sensors in the future. But like the piezoelectric materials that others, PVDF is very difficult to use as a static load sensor, with regard to loading effects arising from the wiring on the instruments used. In the contact method measurement system (close circuit), the value of the input impedance of measuring instruments will directly affect the value of the measured variables. Piezoelectric sensors, including PVDF film, require measuring devices that have very high input impedance for loading effects factor can be suppressed. This paper tries to offer some techniques that may be used to make the PVDF film as static load sensors.

Keywords*: static load, sensor, and PVDF film.*

The Profile of the Constituents of White Turmeric Essential Oils (*Curcuma zedoaria* (Berg) Roscoe) in the Variety of Distilate Collection Time

Dore Yulia [1], Rurini Retnowati [2], Moh. Farid Rahman [3]

[(1)] Master Program, Chemistry Dept., Brawijaya University, Malang (dore_yulia@yahoo.com)
[(2,3)] Chemistry Dept., Brawijaya University, Malang (rurini_retnowati@yahoo.com; m_farid@brawijaya.ac.id)

Abstract

The purpose of this research is to identify the components of the essential oils of white turmeric as one of Indonesian traditional medicine and the profile of its constituents in a variety of distillate collection times. The methods used to isolate the essential oils were both steam distillation and water-steam distillation. The C. zedoaria (Berg) Roscoe oils were obtained and collected in 5 hours of distillation and characterized by Gas Chromatography-Mass Spectroscopy (GC-MS) analysis. The essential oils were also obtained by hour from 1 to 5 hours and characterized by GC-MS analysis. The results in the GC-MS analysis showed that the essential oils obtained by 5 hours of steam distillation consisted of camphor (49.51%), isobornyl alcohol (12.66%), borneol (4.23%), furanodiene (3.61%), furanodienone (3.49%), 1,8-cineole (3.42%), camphene (2.28%), β-pinene (1.75%), 2-nonanon (0.76%), and germacrene D (1.19%). The essential oils obtained by 5 hours of steam-water distillation consisted of camphor (28.64 %), isobornyl alcohol (9.70%), furanodienone (4.79%). borneol (3.65%), furanodiene (3.43%), and germacrene D (1.74%). The main component was camphor which was the highest concentration (50.71%) in the third hour of distillate collection obtained by steam distillation.

Keywords: *profile, constituents, distillation, Curcuma zedoaria (Berg) Roscoe, essential oils.*

1. Introduction

White turmeric (*Curcuma zedoaria* (Berg) Roscoe) has been used as traditional medicine by Indonesian people. It belongs to the *Zingiberaceae* family and is used traditionally for the treatment of menstrual disorders, dyspepsia, vomiting, and cancer. The essential oils of the rizhome contain mono and sesquiterpenoids which have antibacterial, antifungal, anti-inflammatory, anticancer, and hepatoprotective activities [1].

The essential oils of the *Zingiberaceae* family, such as ginger (*Zingiber officinale*) and temulawak (*C. xanthorriza*) were isolated using distillation method and sometimes followed by extraction to obtain a higher concentration of the essential oils [5-7]. The solvent that was usually used to extract the essential oils, which has low polarity, is n-hexane [8].

Some constituents isolated from *C. zedoaria* (Berg) Roscoe rhizome has been reported, such as furanodienone, dehidrocurdione, curcumenol, procurcumenol, furanodiene, camphor, and 1,8-cineole. Furanodiene and furanodienone were reported have anti-inflammatory properties; camphor have analgesic, antipyretic and rubifacient properties; and 1,8-cineole was active as antibacterial of *Staphylococcus aureus, Escherichia coli,* and *Pseudomonas aeruginosa* [1-4].

Based on the research so far, the constituents of *C. zedoaria* (Berg) Roscoe had been obtained and identified from an accumulative distillate collection. However the profile of each of the constituents in the variety of distillate collection time has not been reported yet. By observing the profile of the constituents, the essential oils based on one specific constituents or a combination of them will be able to be isolated.

2. Experimental Details

Materials

The sample used was fresh rhizome of *C. zedoaria* (Berg) Roscoe that collected and determined in Balai Materia Medica Batu. The rhizome was dried in room temperature and sliced into 1-2 mm thick. Chemicals used in this research were were n-hexane (pro analysis), while

the chemicals that were technically grade were water and nitrogen gas.

The instruments used in the research were a set of steam distillation and water-steam distillation apparatus with a capacity of 5 kg, 500 mL separating funnel, conical flask 250 mL, a set of GC-MS 2010S Shimadzu QP – Rtx-wax column, balance Mettler PE 3600.

C. zedoaria (Berg) Roscoe Oils Distillation

5000 g of sample was distilled for 5 hours by both types of distillation. Each 250mL of distillate was extracted with 25mL n-hexane. Besides obtaining the oils by collecting the distillate accumulatively, the oil was also collected by distillating the sample from 1 to 5 hours. The *C. zedoaria* oils constituents were identified by GC-MS

Profile Analysis of C. zedoaria (Berg) Roscoe Constituents by Total Ionic Chromatogram (TIC)

The analysis of oil by using GC-MS produced a number of peaks in the TIC data which was used to determine the number of components contained in *C. zedoaria* (Berg) Roscoe oils. The percentage of peak area in TIC was used to determine the composition of the constituents in the oils.

Characterization of the C. zedoaria (Berg) Roscoe Constituents Based on Mass Spectral Analysis by GC-MS

The characterization of the *C. zedoaria* (Berg) Roscoe was determined based on the mass spectra (MS) by GC-MS. The mass spectra data was used to analyze the structure of the composition of essential oils through the analysis of fragmentation patterns.

3. Result and Discussion

The analysis of the essential oils of *C. zedoaria* (Berg) Roscoe in GC-MS produced a Total Ionic Chromatogram (TIC) which used to determine the profile of the essential oils and the constituents structure of the essential oils in each of the distillate collection time. The TIC of the oils obtained by steam distillation in 5 hours of distillate collection time was recorded in Figure 1.

The TIC of the oils obtained by water-steam distillation recorded in Figure 2. Figure 1 and Figure 2 show that the essential oils obtained by steam distillation produce 20 peaks and the oils obtained with water-steam distillation resulting 15 peaks. This indicates that the amount of constituents in the essential oils obtained by steam distillation was higher because the vapor pressure in steam distillation was higher than in water-steam distillation. This higher vapor pressure was able to evaporate more constituents.

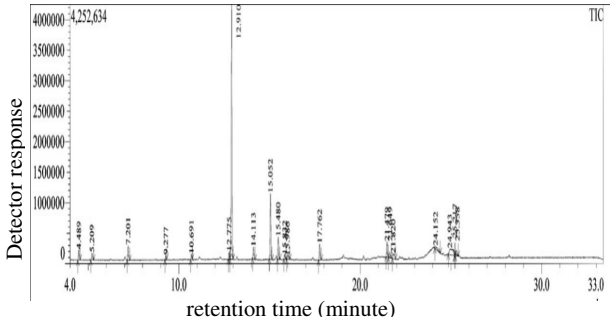

Figure 1. The TIC of the *C. zedoaria* (Berg) Roscoe essential oils obtained by 5 hours of steam distillation by using GC-MS Shimadzu QP-2010S, Rtx-wax column.

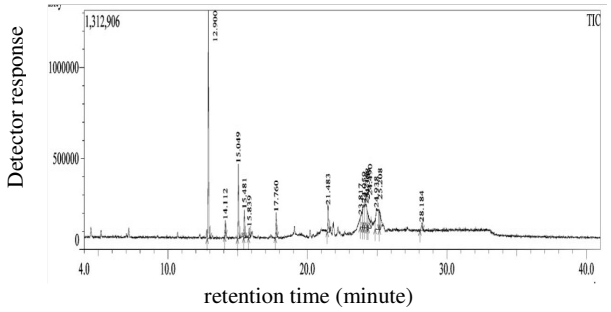

Figure 2. The TIC of the *C. zedoaria* (Berg) Roscoe essential oils obtained by 5 hours of water and steam distillation by using GC-MS Shimadzu QP-2010S, Rtx-wax column.

The MS and fragmentation analysis shows that the constituents of the essential oils of *C. zedoaria* (Berg) Roscoe obtained by 5 hours of steam distillation consisted of camphor (49.51%), isobornyl alcohol (12.66%), borneole (4.23%), furanodiene (3.61%), furanodienone (3.49%), 1,8-cineole (3.42%), camphene (2.28%), β-pinene (1.75%), germacrene D (1.19%), dan 2-nonanone (0.76%). The constituents of the essential oils obtained by 5 hours of water-steam distillation consisted of camphor (28.64%), isobornil alcohol (9.70%), furanodienone (4.79%), borneole (3.65%), furanodiene (3.43%), and germakren D (1.74%).

The profile of the constituents of the essential oils of *C. zedoaria* (Berg) Roscoe in the hours of distillation time was analysed by observing the percentage of peak area in GC-MS data of each constituents obtained hourly from 1 to 5 hours of distillate collection time comparing with the data

of the constituents in the essential oils obtained in 5 hours accumulatively.

The profile of each constituents of the oils obtained by steam distillation has been recorded in Table 1 and the profile of each constituents of the oils obtained by water-steam distillation was has been recorded in Table 2.

The data in Table 1 and Table 2 indicates that the percentage of some compounds was decreasing, such as camphene, camphor, β-pinene, isoborneole, borneole, 2-nonanon, and germacrene-D. Several compounds were increasing in percentage such us furanodiene and furanodienone. This happens due to the vapor pressure of the compounds. The compounds with higher vapor pressure evaporate faster during the distillation process. The vapor pressure of the compounds listed in order of mmHg are camphene (3), camphor (0.15), β-pinene (2.19), 1,8-cineole (100), isoborneole (0.8), borneole (33.5), 2-nonanon (0.2), and germacrene-D (0.00175) [9]. The vapor pressure of furanodiene and furanodienone were unknown but presumed to be lower than the other compounds because the percentage were increasing in the distillate collected from 1 to 5 hours of distillation time.

Camphor was the main constituent in the essential oils obtained both by steam distillation and water-steam distillation based on the data of peak area percentage in Table 1 and Table 2. The percentage of camphor was decreasing in the third hour of distillation presumably because it had already evaporated after three hours. The vapor pressure in steam distillation was able to evaporate camphor more efficiently which resulted in a higher percentage.

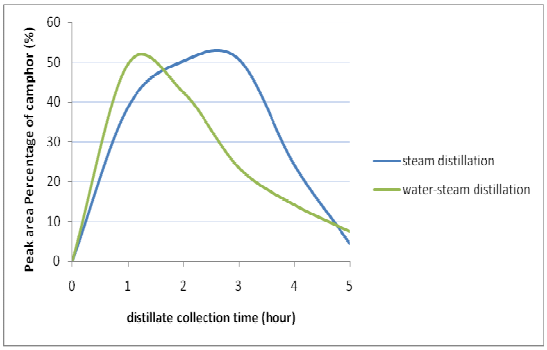

Figure 3. The graph of the percentage of camphor and furanodienone in *C. zedoaria* (Berg) Roscoe oils obtained by steam distillation and water and steam distillation

The percentage of camphor in the essential oils obtained by steam distillation from 1 to 5 hours of distillate collecting time was 38.66%, 50.32%, 50.71%, 24.03%, and 4.37%, respectively. The percentages of camphor in the essential oils obtained by water-steam distillation from 1 to 5 hours of distillate collecting time were 49.49%, 42.28%, 23.49%, 14.18%, and 7.52% respectively. The highest percentage of camphor was in the third hours of distillate collection obtained by steam distillation. The profile of camphor in the essential oils obtained by steam distillation and water-steam distillation was shown in the graph in Figure 3.

Camphor is the compound which has analgesic, antipyretic and rubifacient activity and used for topical medicine. It is used also for decongestant and expectorant [4]. This compound presumed to be the active compound in the *C. zedoaria* (Berg) Roscoe oils. The structure of camphor is shown in Figure 4.

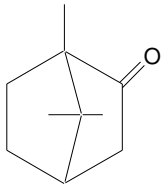

Figure 4. The structure of camphor

4. Conclusion

The characterization results of GC-MS analysis showed that the *C.zedoaria* (Berg) Roscoe oils obtained by 5 hours of steam distillation consisted of camphor (49.51%), isobornyl alcohol (12.66%), borneol (4.23%), furanodiene (3.61%), furanodienone (3.49%), 1,8-cineole (3.42%), camphene (2.28%), β-pinene (1.75%), 2-nonanon (0.76%), and germacrene D (1.19%). The oils obtained by 5 hours of steam-water distillation consisted of camphor (28.64%), isobornyl alcohol (9.70%), furanodienone (4.79%), borneol (3.65%), furanodiene (3.43%), and germacrene D (1.74%). The main component of the essential oils obtained was camphor which was the highest concentration in the third hour collection (50.71%) by using steam distillation method.

5. Acknowledgements

The authors would like to thank Balai Materia Medica-Batu for the supply of the rhizome of *C. zedoaria* (Berg) Roscoe.

6. References

[1]. Lobo, R., K.S. Prabhu, A. Shirwaikar, and A. Shirwaikar (2009), Curcuma zedoaria Rosc. (White turmeric): a review of its chemical, pharmacological and

ethnomedicinal properties, *J. Pharmacy and Pharmaco.*, 61, 13-21.
[2]. Hendry, E. R., T. Worthington, B. R. Conway, and P.A. Lambert (2009), Antimicrobial efficacy of eucalyptus oil and 1,8-cineole alone and in combination with chlorhexidine digluconate against microorganisms grown in planktonic and biofilm cultures, *J. Antimicrob. Chemother.* 64, 6, 1219-1225.
[3]. Saetung, A., A. Itharat, C. Dechsukum, K. Keawpradub, C. Wattanapiromsakul and P. Ratanasuwan (2005), Cytotoxic activity of Thai medicinal plants for cancer treatment, *J. Sci. Technol.*, 27, 469-478.
[4]. Zuccarini, P. and G. Soldani (2009), Camphor: benefits and risks of widely used natural. *acta biologica szegediensis*, 53, 2, 77-82.
[5]. Ma'mun (2006), Karakteristik beberapa minyak atsiri famili zingiberaceae dalam perdagangan. *Bul. Littro*., 17, 2, 91-98.
[6]. Parliament, T.H., (1997), Solvent extraction and distillation techniques in techniques for analyzing food aroma, Marcel Dekker, New York, 13-17.
[7]. Agusta, A., (2000), Minyak atsiri tumbuhan tropika Indonesia, ITB, Bandung.
[8]. Furniss, B.S., A.J. Hannaford, V. Rogers, P.W.G. Smith, and A.R Tutchell (1978), Vogel's textbook of practical organic chemistry. 4th ed., ELBS, London, 143-146.
[9]. Anonymous (2010), Essential oils information, ww.thegoodscentscompany.com. Accessed in June 20th, 2010.

Appendixes

Table 1. Data of the percentage of peak area based on GC-MS analysis of the constituents of *C. zedoaria* (Berg) Roscoe essential oils obtained by steam distillation

Name	First hour	Second hour	Third hour	Forth hour	Fifth hour	Five hour accumulatively
Camphene	-	1.80	1.83	2.10	0.62	2.28
β-pinene	-	1.55	0.71	1.85	0.47	1.75
1,8 cineole	0.96	2.70	1.84	-	-	3.42
2-nonanone	1.07	0.93	0.96	-	-	0.76
Camphor	38.66	50.32	50.71	24.03	4.37	49.51
Isobornyl alcohol	14.8	13.30	14.01	8.96	2.51	12.66
Bornoel	5.89	4.84	5.04	3.30	-	4.23
Germacrene D	1.66	0.88	-	-	-	1.19
Furanodiene	2.69	2.92	3.72	6.35	5.78	3.61
Furanodienone	1.27	1.35	4.19	6.18	10.94	3.49

Table 2. Data of the percentage of peak area based on GC-MS analysis of the constituents of *C. zedoaria* (Berg) Roscoe essential oils obtained by water-steam distillation

Name	First hour	Second hour	Third hour	Fourth hour	Fifth hour	Five hour accumulation
Camphene	4.39	3.11	1.44	0.70	-	-
β-pinene	2.55	2.12	-	-	1.75	-
1,8 cineole	3.88	1.07	1.43	1.21	-	-
Camphor	49.49	42.28	23.49	14.18	7.52	28.64
Isobornyl alcohol	11.96	12.54	9.70	6.31	4.51	9.70
Borneole	3.66	3.83	3.15	1.58	-	3.65
Germacrene D	1.12	1.72	2.10	3.47	-	1.74
Furanodiene	2.64	4.65	6.36	10.85	9.54	3.43
Furanodienone	1.79	4.96	10.18	19.72	16.30	4.79

Nutrient Status Improvement of Ca and Mg in Leaf by Administering Dolomite to Decrease Acidity Levels of Tangerine Fruit (Citrus suhuiensis Tan)

Edi Siswadi [1], Ariffin [2], Syekhfani [3], Sudarmadi Purnomo [4]

[(1)] Post Graduate Program of Agricultural Faculty, Brawijaya University, Malang (edi_sis_83@yahoo.co.id)
[(2,3)] Agricultural Faculty, Brawijaya University, Malang, Indonesia
[(3)] Indonesian Agricultural Department, Malang, Indonesia

Abstract

This study aims to enhance the status of Ca and Mg in leaf tissue by adding dolomite in planting media that will affect the decrease in total acid content in tangerine fruit. The study was conducted using Randomized Completely Block Design, which consists of 7 treatments, each with 3 replications. The treatments were 0.5 kg of dolomite (T1), 1 kg dolomite (T2), 2 kg of dolomite (T3), 3 kg dolomite (T4), and 4 kg of dolomite (T5) per plant. As controls, we used without NPK fertilizer and dolomite treatment (C0), and without NPK fertilizer treatment (C1). Observation parameters were Ca, Mg and K nutrient status of citrus leaf at harvest and the content of citric acid and ascorbic acid of fruit on physiological maturity condition. Data were analyzed using one-way Anova followed by LSD and regression analysis using SPSS program version 16. The results showed that the dolomite improved the status of Ca and Mg and decreased K in citrus leaf tissues. Status of Ca increased from 3.15 ± 0.38% to 4.47 ± 0.45% dry weight of leaves. Status of Mg increased from 0.20 ± 0.03% to 0.40 ± 0.02% dry weight of leaves, and the status of K decreased from 0.41 ± 0.08% to 0.22 ± 0.04% dry weight of leaves. Citric acid content was decreased from 1.15 ± 0.02% to 0.46 ± 0.04% and ascorbic acid content was decreased from 50.66 ± 0.29 mg/100g to 38.77 ± 0.27 mg/100g in citrus fruit.

Keywords*: Citrus suhuiensis Tan., dolomite, TSS.*

1. Introduction

Tangerine fruit productivity in the Indonesia is about 17-25 ton/ha of the potential of 25-40 ton/ha. However, the fruit quality produced is still relatively low and varied [1]. Food stuff quality consists of external quality or physical quality and internal quality or chemical quality. Physical qualities include color, texture, freshness and size, whereas in the internal qualities include sugar level, acid level, protein, vitamins, nitrate, heavy metal content, and pesticide residues [2]. Citrus quality can be divided into physical quality and chemical quality. Physical qualities include fruit weight, fruit size, and skin thickness. Chemical quality consist of the percentage of juice, total soluble solids / TSS, total acid, the ratio of TSS to total acid, and ascorbic acid (vitamin C) [3].

Tangerine citrus quality problems that often found are spongy fruit, not optimally of sweetness (TSS level less than 10^o brix), dull fruit since attacked by mottled disease [4], bitter and pale green color [5]. Good tangerine fruit quality as Directorate of Horticulture (2005) suggestion is total soluble solids (TSS) content 10-12° brix [6]. This TSS is often assumed to reflect the content of total sugars, especially sucrose, 0.5-1% total acid content (citric acid), the TSS:acid ratio with 16.87% acid and 32.50 mg/100 g vitamin C content, and greenish yellow skin color fruit [7]. This means that when a TSS as many as 10-12º brix and acid content as 0.5-1%, so the TSS:acid ratio ranged between 10-24%. The ideal of TSS:acid ratio for citrus production is between 12-15% [2]. The research result showed that the TSS Lumajang tangerine which derived from Jember had 8.5 to 9^o brix TSS and 0.99 to 1.08% acid content, which means having TSS:acid ratio ranged from 0.8 to 9.1%, this means is still below the required quality standard.

Tangerine citrus fruit quality have not been optimal, especially in uniformity of taste, caused not optimally plantation management, especially in relation to fertilization and behavior of farmers when picking fruit is often still not quite right (the fruit harvested prior to physiological maturity) [8]. The quantity and quality of tangerine citrus are determined by the interaction between plant genetic as internal factor and environmental influences as external factor, where these plants

grow. External factors include temperature and humidity, sunlight, water, oxygen, carbon dioxide, and plant nutrients. The environmental is very important to obtain optimum yields [9]. Nutrients are one of environmental factor that can be manipulated easily [10].

In accordance with the nutrient that is required in citrus, nutrients can be grouped into 2, i.e. macro nutrients and micro nutrients. Macro nutrients are required in highly amounts or ≥ 1000 g g-1 plant dry weight, while the micro nutrients only ≤ 100 g g-1 plant dry weight [10]. Elemental macro can also be divided into two, which are primary macro nutrients consisting of N, P, K, and secondary macro nutrients consisting of Ca, Mg and S. While micro-nutrients are B, Fe Mn, Zn, Cu, Mo, Cl, Na, Li, As and F [9]. Macro nutrients in citrus leaf tissue naval and Valencia are regarded optimum when N at 2.4 to 2.6%, P of 0.12 to 0.16%, K at 0.70 to 1.09%, Ca at 3.0 to 5.5% and Mg of 0.26 to 0.6% and S of 0.2 to 0.3% dry weight of leaves [11].

TSS and ascorbic acid levels of tangerine citrus fruit correlated with the elements Ca and Mg in soil [1]. The addition of Ca and Mg fertilizer will be followed by rising levels of TSS, decreasing of citric acid level and ascorbic acid content, also increasing of TSS:acid ratio tangerine citrus fruit [2]. In intertidal zone with a higher Mg will be followed by increasing of better TSS than the soil with less Mg [12]. In contrast, the increasing of 0.3% to 1.7% K in leaf will increase vitamin C, acid percentage in fruit juices, and reduce TSS, the percentage of juice, TSS:acid ratio, and percentage of Mg in the leaves [11].

Mapping of nutritional status of citrus leaves during generative phase in a citrus production center in Jember that have TSS between 8.5 to 9º brix, acid content between 0.99 to 1.08%, and TSS:acid ratio 7.8 to 9.1% positively correlated with the lower Ca and Mg contents in leaf tissue. A 2.97% Ca and 0.15% Mg in dry weight of leaf when the fruit reaches physiological maturity is lower in category when compared to Ca and Mg standard nutrient by Embleton [11]. Therefore, it is needed to decrease the acid content less than 1% and increase the TSS more than 10º brix in order to increase PTT-acid ratio 12-15% or 16% as required by the Directorate of Horticulture [13].

The purpose of this research is to improve Ca and Mg status in leaf tissue by adding dolomite in planting media, so that will be able to improve Ca and Mg status in leaves which resulted in a decrease in both acid content of citric acid in tangerine citrus fruits.

2. Experimental Details

The study was conducted in Sukoreno Village, Umbulsari District, Jember, Indonesia, on the light organic matter association Glei and gray alluvium soil type, with altitude 17m above sea level. Research conducted using randomized complete block design (RCBD) consisting of 63 trees, with 7 treatments, each 3 replications with 3 trees/units. The treatments were without NPK fertilizer and dolomite (C0); NPK fertilization only (C1), NPK+0.5 kg dolomite/plant (T1); NPK+1 kg dolomite/plant (T2); NPK+2 kg dolomite/plant (T3); NPK+3 kg dolomite/plant (T4), and NPK+4 kg dolomite/plant (T5). NPK fertilizer was used Urea 0.75 kg/plant; SP-36 0.60 kg/plant; KCl 0.12 kg / plant, applied 2 times, a half of it was applied in the early rainy season and after harvesting of previous period and the remainder was applied to 4 months later.

Application of dolomite was applied 2 months after the first fertilizer application. Wet ash method using HNO_3 and $HCLO_4$ was applied to measure and determinate the concentration of Ca and Mg in soil and leaves using spectrophotometer. Measurement of vitamin C and citric acid in fruit was done using AOAC standard. The fruit samples were taken according to the criteria of maturity level by matching between fruit color and Munsell color chart, with the following criteria:

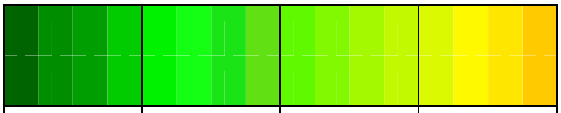

Figure 1. Criteria for Maturity Level According to the Munsell Citrus Fruits Colour Chart (Maturity level of C1: Category I; C2: category II; C3: category III; C4: category IV)

Citric acid content was determined by titration using 0.1 N NaOH with PP indicator. The vitamin C content was determined by Jacobs iodine titration method. The results were analyzed with analysis of variance to examine wether there were any significant result in TSS, sucrose, citric acid, ascorbic acid (vitamin C) levels. The significant result should be followed by HSD 5% (Honestly Significant Difference) [14]. The data was analysed using SPSS program version 16.

3. Result and Discussion

As shown in Figure 2 (appendixes), Results showed that dolomite treatment up to 4 kg/plant increase Ca from 7.98% to 12.06% in

soil and from 3.15% to 4.47% dry weight of leaf as well.

Ca in soil increases Ca in leaf as many as 70%, with the equation Y = 0.51 +0.35 x, R^2 = 0.70. The results also indicate that the dolomite treatment up to 4 kg/plant increase Mg in soil from 2.25% to 6.21%, as given in Figure 3 (appendixes), as well as in leaf from 0.20% to 0.40% dry weight of leaf. With regression analysis, it can be estimated that the increasing of Mg in soil had significant effect on increasing of Mg in leaf as 40% with the equation Y = 0.11 +0.40 x, R^2 = 0.40.

Dolomite treatment up to 4 kg/plant significantly decline vitamin C content in fruit from 50.66 to 38.77 mg/100gr fruit at maturity level category I. At maturity level category IV, vitamin C in fruit decreased from 43.96 to 31.76 mg/100g (Figure 4). Increasing of Ca in leaf also decrease the vitamin C content to 24.7%, as estimated with the equation Y = 59.55-3.89 x, R^2 = 0.247%. Moreover, increasing of Mg in leaf decrease the vitamin C content as many as 42%, as estimated with the equation Y = 51.95-25.66 x, R^2 = 0.42%.

Furthermore, dolomite treatment up to 4 kg/plant can decline fruit citric acid significantly from 1.35% to 1.07% fruit weight at maturity level category I. At maturity level category IV, citric acid in fruit decreased from 1.13% to 0.51% fruit weight (Figure 5). The relationship between increasing of Ca in leaf to the decreasing of citric acid in fruit as 39.9%, can be estimated from equation Y=1.75-0.24 x, R^2 = 0.39%. In addition, the influence of increasing Mg in leaf to the decreasing of citric acid in fruit was 61.4%, as estimated by equation Y=1.26-0.51x, R^2 = 0.61%.

4. Conclusion

The results showed that dolomite treatments improved Ca and Mg status and decreased K status in leaf tissue. Ca status increased from 3.15 ± 0.38% to 4.47 ± 0.45% dry weight of leaf. Mg status increased from 0.20 ± 0.03% to 0.40 ± 0.02% dry weight of leaves, and K status decreased from 0.41 ± 0.08% to 0.22 ± 0.04% dry weight of leaf. Citric acid decreased from 1.15 ± 0.02% to 0.46 ± 0.04% of fruit weight and ascorbic acid decreased from 50.66 ± 0.29 mg/100g to 38.77 ± 0.27 mg/100g fruit weight.

5. Acknowledgements

We thank to the Directorate for Higher Education which has provided BPPS scholarships, so that this research, as part of dissertation, can be finished.

6. References

[1]. Achmadi, W. Annisa, and E. Maf'tuah (2007), Hubungan Sifat Kimia Tanah Terhadap Kualitas Buah Jeruk di lahan Rawa Lebak. Dalam *Prosiding Seminar Nasional Jeruk 2007* Yogyakarta 13-14 Juni 2007.

[2]. Annisa, A and I. Noor (2007), Pengaruh Pemberian Ca dan Mg Terhadap Kualitas Buah Jeruk di Lahan Pasang Surut Tipologi B Trantang, Kalimantan Selatan. Dalam *Prosiding Seminar Nasional Jeruk 2007* Yogyakarta 13-14 Juni 2007.

[3]. Ladaniya, M.S. (2008), *Citrus Fruit Biology: Technology and Evaluation*. Academic Press

[4]. Poerwanto, R. (2004), Program Pengembangan Jeruk Siem di Indonesia. *Prosiding Seminar Jeruk Siem Nasional*. Pusat Penelitian dan Pengembangan Hortikultura Badan Penelitian dan Pengembangan Pertanian.

[5]. Winarno, M. (2004), Keunggulan dan Kelemahan Jeruk Siem di Indonesia. *Prosiding Seminar Jeruk Siem Nasional*. Pusat Penelitian dan Pengembangan Hortikultura Badan Penelitian dan Pengembangan Pertanian.

[6]. Ditjen Bina Produksi Hortikultura (2005), Seri Tanaman Buah. Buku Tahunan Hortikultura 2003. Departemen Pertanian

[7]. Soelarso, B. (2007), *Budidaya Jeruk Bebas Penyakit*. Kanisius. Yogyakarta. 97.

[8]. Suprijanto, A. (2007), Peningkatan Kualitas Buah Jeruk Keprok Siem dengan Teknik Budidaya yang Tepat. *Prosiding Seminar Jeruk Siem Nasional*. Pusat Penelitian dan Pengembangan Hortikultura Badan Penelitian dan Pengembangan Pertanian. Badan Penelitian dan Pengembangan Pertanian.

[9]. Sugito, Y. (1999), Ekologi Tanaman. Fakultas Pertanian Universitas Brawijaya. 127

[10]. Wijaya, K.A. (2008), *Nutrisi Tanaman Sebagai Penentu Kualitas Hasil dan Resistensi Alami Tanaman*. Prestasi Pustaka. Jakarta. 121.

[11]. Embleton, T.W., W.W. Jones, C.K. Labanauskas, and W. Reuther (1973), Leaf Analysis As a Diagnostic Tool and Guide to Fertilization. Dalam *Citrus Industry* Vol III.

[12]. Sumantri (2007), Hubungan kualitas buah jeruk Varietas Siem Banjar (*Citrus suhuiensis* Tan.) dengan Sifat Kimia Tanah dan Air di Lahan Pasang Surut. Dalam *Prosiding Seminar Nasional Jeruk 2007.*

[13]. Ditjen Bina Produksi Hortikultura (2005), Seri Tanaman Buah. Buku Tahunan Hortikultura 2003. Departemen Pertanian
[14]. Steel, R.G.D. and J.H. Torrie (1991), *Prinsip dan Prosedur Statistika*. Gramedia. Jakarta
[15]. Balitbang Departemen Pertanian (2005), Prospek dan Arah Pengembangan Agribisnis Jeruk.

Appendixes

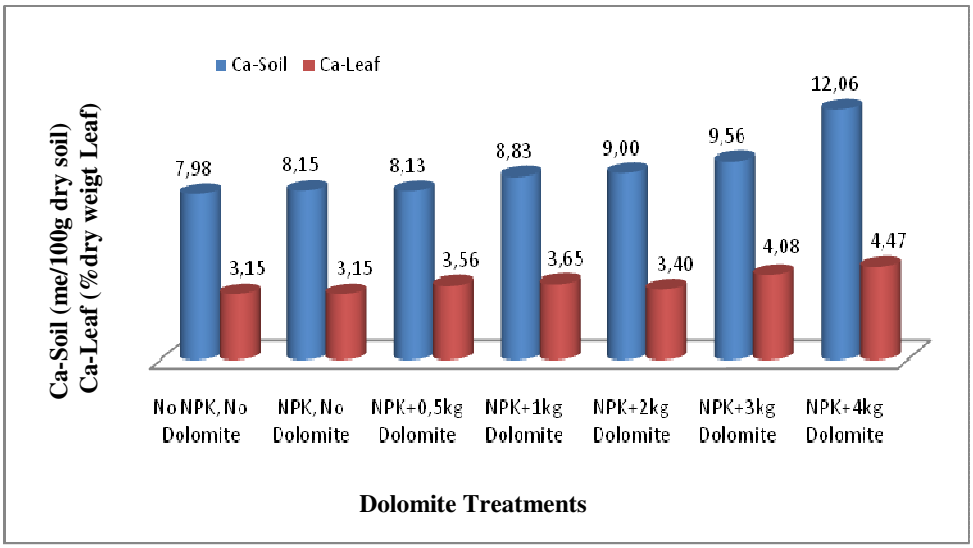

Figure 2. Mean of Ca-Soil and Ca-Leaf Caused Dolomite Treatment

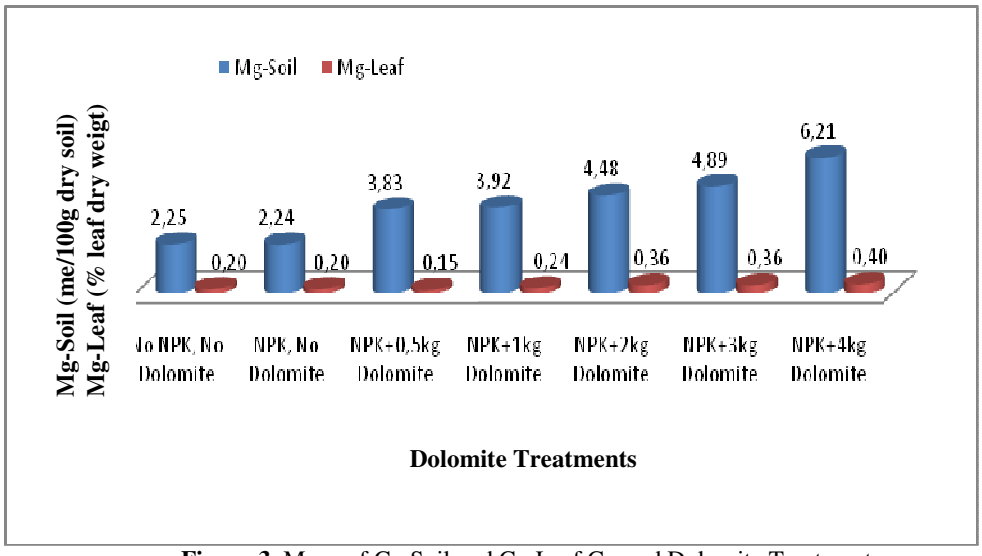

Figure 3. Mean of Ca-Soil and Ca-Leaf Caused Dolomite Treatment

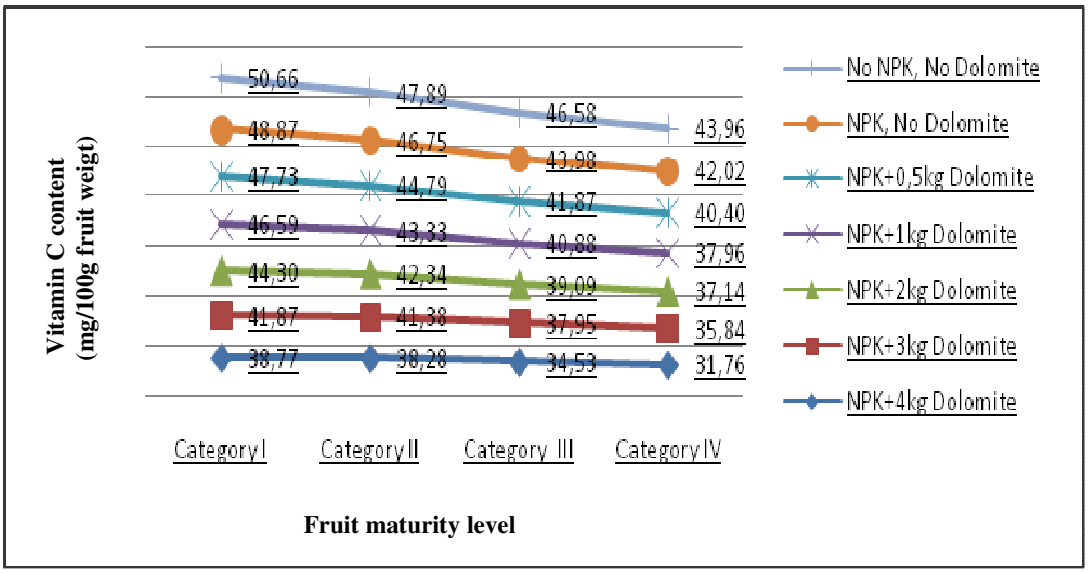

Figure 4. Mean of Vitamin C in Fruit Caused Dolomite Treatment on Some Maturity Level

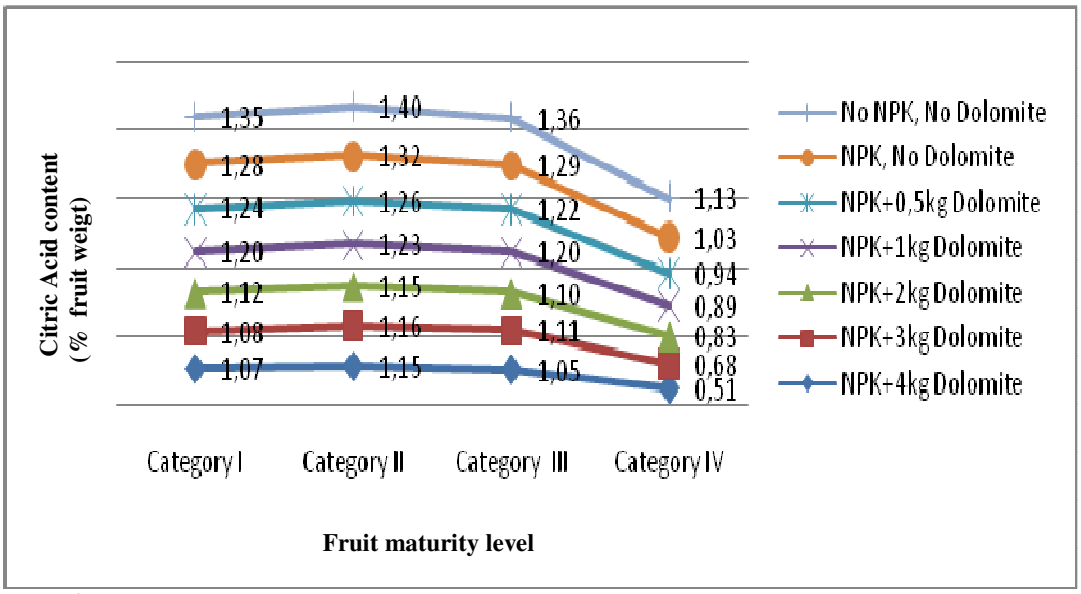

Figure 5. Mean of Citric Acid in Fruit Caused Dolomite Treatment on Some Maturity Level

Developing of Solid Phase Extraction Based on Zeolites: Case Studied Cr(VI)

Eti Rohaeti [1], Betty Marita Soebrata [2], Putri Ratna Furi [3], Irmanida Batubara [4]

[1,2,3,4] Department of Chemistry, Faculty of Mathematics and Natural Sciences, Bogor Agricultural University, Bogor, Indonesia (era4_44@hotmail.com; bettymarita@gmail.com, ime@ipb.ac.id)

Abstract

Chromium especially hexavalent chromium is hazardous to our health, because it is carcinogenic. Therefore, chromium in drinking water should be minimized to less than 50 μg/L. One way to decrease chromium content is using solid phase extraction such as zeolites. Zeolites was modified by cationic surfactant hexadecyltrimethylamonium bromide (HDTMABr) to increase its adsorption capacity. Adsorption capacity of Cr(VI) onto zeolites was 1.90 mg/g, when pH Cr(VI) solutions was 3 and contact time was 18 hours. Adsorption Cr(VI) into zeolites followed Freundlich isotherm equation. The best adsorption capacity of HDTMABr (40.99 mg/g) onto zeolites was achieved when HDTMABr concentration was at 1000 ppm with contact time 30 hours. Adsorption HDTMABr into zeolites followed Langmuir isotherm equation. NaOH 0.5 M dan Na_2CO_3 0.28 M (1:1 v/v) mixture solutions desorped Cr(VI) about 65.67% (by batch extraction) and 3.93% (by fixed-bed extraction). Properties of zeolite after modified with HDTMABr were shown at 2856.33 and 2927.65 cm^{-1} peaks, originated from CH_3 on HDTMABr.

Keywords: *Piper bettle, Piper crocatum, essential oil, tyrosinase activity.*

1. Introduction

The hexavalent chromium is present in nature as CrO_4^{2-}. It is hazardous to our health, because it is toxic and carcinogenic [1]. The present of chromate ion in the environment caused some problems such as how to monitor the chromate level in the environment especially in water or effluent from industrial waste and what is technology to treat or to reduce the risk of negative effect from Cr(VI), especially in drinking water chromium level should be minimized to less than 50 μg/L.

Solid phase extraction had been used to remove or to get the heavy metal residue from component, either in gas, liquid or solid phase. Many solid phases had been used for this purpose, for instance charcoal, resin, and zeolite [2]. Zeolite had been used for treatment of waste. It has pore and rich with cations which can be used as ion exchanged and also as adsorbent.

To increase the ability of zeolite as ion exchanger, modify is needed. On this paper, zeolite was modified with cation surfactant to increase the adsorption capacity. The cation surfactant which used was hexa-decyl-tro-methyl-ammonium (HDTMA) [3]. This research aims were to modify zeolite with HDTMABr and to find the effectiveness of modified zeolite with HDTMABr based on its activity to absorb Cr(VI).

2. Experimental Details

Samples material and preparation

Zeolites washed with water, dried in room temperatue, and the grinded with mortar. The zeolite powders then filter with filter 60 mesh. Then, powder dried at 300°C for 3 hours.

Activation of zeolite

Zeolite was activated chemically with acid. About 100 g zeolite mixed with 250mL HCl 4.0M for 1 hour. The mixture then washed with water till neutral. The zeolit dried on 400°C for 3 hours. Adsorption isotherm of HDTMABr and modification of zeolite with HDTMABr were performed with method of Giachi [4]. Cation exchange capacity was determined using Klute method [5]. Chromium analysis was performed based on Clesceri method [6], while desorption of Cr(VI) was performed based on Zeng method [7].

Chromate adsorption

Zeolite and modified zeolite about 0.5 g each added with Cr(VI) solution in different concentration (2.0 – 60.0 ppm) at pH 3, 4, 5, 6, and 7. The mixtures then shake at 150 rpm for 18, 20, 22, 24, and 26 hours. After that, the mixture separated with centrifuge and filtration method. The filtrate was analyzed for the concentration of

Cr(VI). The adsorption capacity then calculated with equation:

$$Q = \frac{V(C_o - C)}{m}$$

Q is adsorption capacity (mg/g), V is volume (L), C_o id initial concentration of Cr(VI) (ppm), C is final concentration of Cr(VI) (ppm), and m is weight of zeolite (g).

Zeolite characterization

Zeolite was characterized before and after modification, and also for zeolite after desoprtion. Characterization was performed with FT-IR *Spectrum One Perkin Elmer.*

3. Result and Discussion

The adsorption capacity of HDTMA+ increased significantly about 20.99 mg/g from o to 1000 ppm (Figure 1). When HDTMA+ concentration is higher than 1000 ppm, the adsorption capacity increased slowly. HDTMA+ adsorption capacity at concentration 1000 ppm obtain at 30 hours contact time, decreased at 42, 45, and 48 hours.

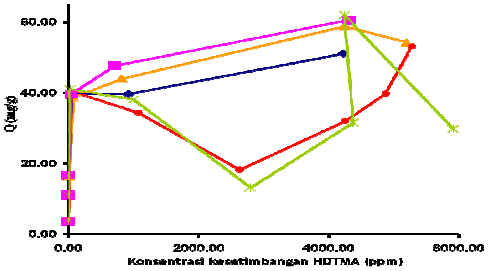

Figure 1. Curve of adsorption capacity of HDTMA on different contact time (●) 24 hours, (×) 30 hours, (♦) 42 hours, (■) 45 hours, and (▲) 48 hours.

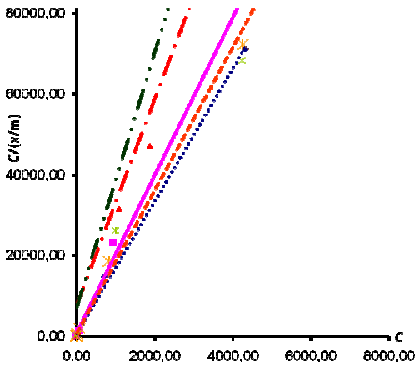

Figure 2. Curve of Isotherm Langmuir of HDTMA on zeolite in different contact time (▬) 24 h, (▬) 30 h, (.....) 42 h, (▬ ▬) 45 h, and (▬) 48 h.

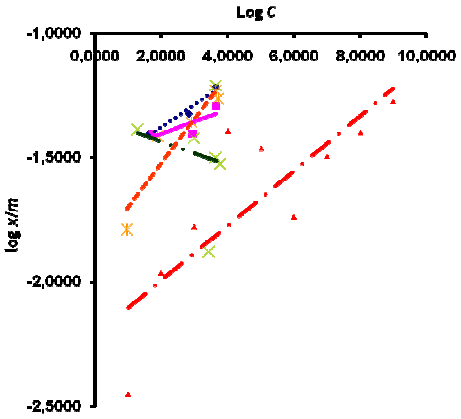

Figure 3. Curve of Isotherm Freundlich adsorption of HDTMA on zeolite at different contact time (▬) 24 h, (▬) 30 h, (.....) 42 h, (▬ ▬) 45 h, and (▬) 48 h.

Isotherm adsorption of HDTMABr on zeolite was analyzed with Langmuir and Freundlich isotherm pattern (Figure 2 and 3, respectively). The five different contact time on isotherm adsorption showed that the high linearity found in Langmuir isotherm (r: 0.7439, 0.6935, 0.998, 0.9964, 0.9959 compared to 0.3062, 0.0403, 0.9614, 0.8704 and 0.5894 on Freundlich isotherm).

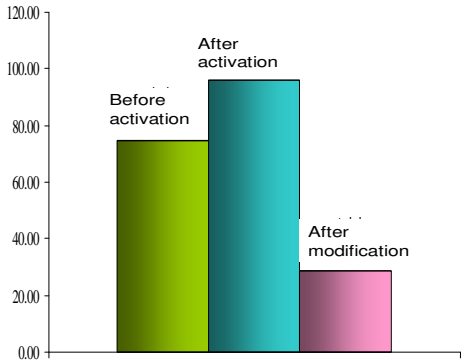

Fig ure 4. Cation Exchange Capacity of Zeolite

Cation exchange capacity (CEC) of initial zeolite is about 74.81 mek/100 g (Figure 4). The CEC was increased up to 96.24 mek/100 g zeolite after activation process with washing with acid. Washing with acid can remove the impurities in the pores of zeolite and turning them into H-

zeolite without changing the position of the framework of silica-alumina.

CEC value decreased after modified zeolite with HDTMABr (20.76 mek/100 g zeolite). The decreasing CEC is happen because a number of HDTMA+ ions formed in to bilayer with each other. This bilayer covered most of zeolite surface through ion exchange mechanism. The smaller CEC value of zeolite showed that this zeolite has ability to absorb ion.

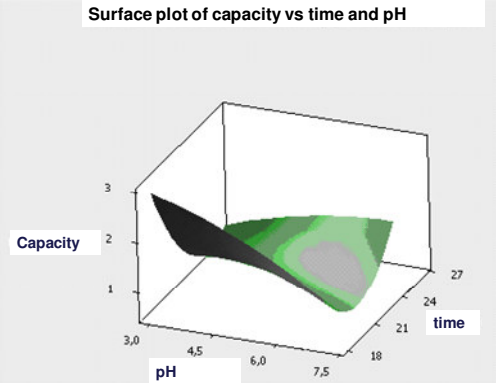

Figure 5. Response surface area interaction curve between capacity, pH, and contact time

Based on Figure 5, adsorption capacity of Cr(VI) is influenced by pH and contact time between Cr(VI) and adsorbent. From response surface data, the composite desirability value was about 1000, it means that the model used has the best accurate prediction. Based on the determination of optimum condition in response surface area the adsorption of Cr(VI) by zeolite modified by HDTMABr 1000 ppm has high capacity at pH 3 with contact time about 18 hours.

Adsorption of Cr(VI) by zeolite strongly influenced by pH of chromate solution used. According to Zeng et al (2009)[7], adsorption capacity of Cr(VI) decreases with increasing pH. The increasing adsorption capacity of Cr(VI) in acid may be due to the equilibrium of chromate and dichromate. Equilibrium reactions which occur are as follows:

$$HCr_2O_7^-(aq) \underset{pH>1}{\overset{pH<1}{\leftrightharpoons}} Cr_2O_7^{2-}(aq) \underset{pH>7}{\overset{pH<7}{\leftrightharpoons}} CrO_4^{2-}(aq)$$

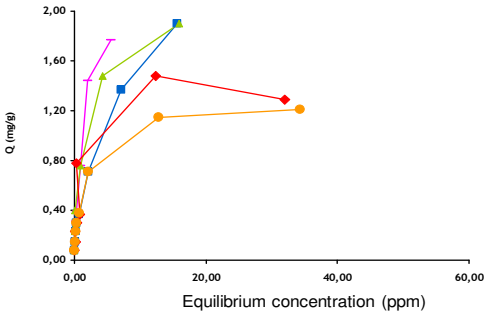

Figure 6. Adsorption capacity of Cr(VI) in 18 hours with variation pH (▮) 3, (▬) 4, (▲) 5, (◆) 6, and (●) 7.

Based on Figure 6, the optimum adsorption capacity produced at pH 3 with capacity about 1.90 mg/g. It means that 1 g of zeolite optimum to absorb Cr(VI) up to 1.9 mg. The comparison between adsorption capacity of Cr(VI) on zeolite with and without modification at Cr(VI) 60 ppm is shown in Figure 7. The highest adsorption on zeolite without modification is about 0.64 mg/g, while for modified zeolite up to 1.9 mg/g (increased about three times).

These results showed a significant increase capacity due to the insertion of cation HDTMA+ which form a bilayer on the surface of zeolite. It in turn alter the originally negative charged zeolite become positive, so that it can absorb the anion Cr(VI) with larger capacity than the unmodified zeolite. The formation of bilayer is formed through hydrophobic interaction between tails of HDTMABr [8 – 11].

Desorption of Cr(VI) were calculated using batch system using the same solution, namely a mixture of NaOH 0.5M and Na_2CO_3 12.28M (1:1 v/v). Desorption with batch system is better than fixed bed method (Figure 7). This is because the batch method will contact strongly and continuously between adsorbent and Cr(VI).

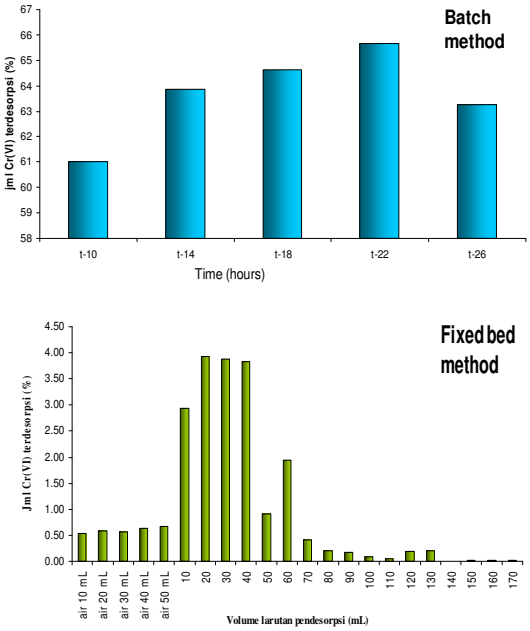

Figure 7. Desorption of zeolite and contact time for batch method and fixed bed method

Figure 7 showed that desorption process in batch method obtained the best contact time for 22 hours with the amount of Cr(VI) about 65.67%. The optimum desorption of Cr(VI) in fixed bed method up to 3.93%.

Characteristics in IR which can distinguish between natural zeolite with modified zeolite was seen in 2927.65 cm^{-1} (area for -N(CH_3)-) which comes from HDTMABr. In addition, the stretch peak 2856.33 cm^{-1} is related to CH_3-R, while in region 3000 – 3500 cm^{-1} is related to CH_3-R asymmetry. According to Li & Gallus (2007), the peak appears on 2860 and 2930 cm^{-1} is generated by themonomers and micelles of $HDTMA^+$ [12].

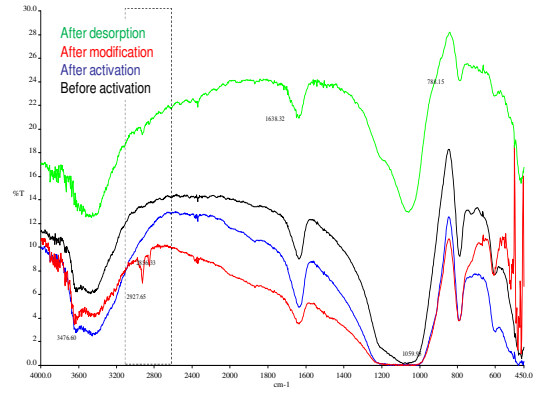

Figure 8. IR Spectrum of zeolit

Based on IR analysis (Figure 8), the zeolite after desorption indicated that leaching solution did not eliminate the HDTMA+ component. Zeolite still shows absorption bands at 2856.33 cm-1, although with very low intensity.

4. Conclusion

Modification of zeolite with HDTMABr could be used as solid phase extraction of Cr(VI) with adsorption capacity about 1.90 mg/g in optimum condition. It gave higher adsorption level than zeolite without modification. NaOH 0.5M mixed with Na_2CO_3 0.28M in ration 1:1 (v/v) is used as solution for desorption of Cr(VI) in batch system with 65.67% of Cr(VI) could be removed from the modified zeolite.

5. References

[1]. Gang D, Banerji S.K., Clevenger T.E., (1999), Chromium (VI) removal by modified PVP-coated silica sel. Proceeding of the 1999 Conference on Hazardous Waste Researche, Missouri, Columbia 64-67.

[2]. Trisunaryanti W, Triwahyuni E, Sudiono S., (2005), Preparasi, modifikasi, dan karakterisasi katalis Ni-Mo/ zeolit alam dan Mo-Ni/ zeolit alam. *Teknoin* 10 (4):269-282.

[3]. Zang P, Avudzega M, Bowman R.S., (2007), Removal of perchlorate from contamined waters using surfactant-modified zeolite. *Journal of Environmental Quality* 1069-1075.

[4]. Ghiaci M, Kia A, Abbaspur Ă, Azad F.S., (2004), Adsorption of chromate by surfactant modified zeolites and MCM-41 molecular sieve. *Separation and Purification Technology* 40:285-295.

[5]. Klute A., (1986), Methods of Soil Analysis Part 1: Physical and Mineralogical Methods. Second Edition. Wisconsin: United States of Agronomy and Soil Science Society of America.

[6]. Clesceri L.S., Greenberg A.E., Eaton A.D., Rice E.W., (2005), Standard Methods for the Examination of Water and Wastewater. 21th Edition. Washington DC: American Public Health Association.

[7]. Zeng Y, Woo Heesoo, Lee Gwanghun, Park Junboum (2009), Adsorption of Cr(VI) on hexadecylpiridinium bromide (HDPB) modified natural zeolites. *Microporous and Mesoporous* …….

[8]. Chutia P, Kato S, Kojima T, Satokawa S., (2009), Adsorption of As(V) on surfactant modified natural zeolites. *Journal of*

Hazardous Material 162: 204-211.

[9]. Cordoves P, Valde´s MG, Fernandez JCT, Luis GP,Calzo JAG, Garcıa MED., (2008), Characterization of the binding site affinity distribution of surfactant modified clinoptilolite. *Microporous and Mesoporous Materials* 109: 38–48.

[10]. Bowman RS, Zhang Pengfei, Xian Tao, Johnson RL, Johnson TL., (2000), Surface-altered zeolites as permeable barriers for *In situ* treatment of contamined groundwater. (Research report). Daytona: National Energy Technology Laboratory.

[11]. Madjan M, Pikus S, Rzaczyn Z, Iwan M, Maryuk O, Kwiatkowski R, Skrzypek H., (2006), Characteristics of chabazite modified by hexadecyltrimethylammonium. *Journal of Molecular Structure* 791: 53–60.

[12]. Li Z, Gallus L., (2007), Adsorption of dodecyltrimethylammonium and hexadecyltrimethylammonium onto kaolinite- competitive adsorption and chain length effect. *Applied Clay Science* 35: 250-257.

Synthesis of Silver (I) Nitrate with Ethylenethiourea and Characterization Using SEM-EDAX

Fariati [1], Markus Diantoro [2], Rokiy Alfanaar [1]

[(1,3)] Chemistry Department, Faculty of Mathematics and Science, State University of Malang, Malang, Indonesia (f4riati@gmail.com; rokiyalfanaar@gmail.com)
[(2)] Physical Department, Faculty of Mathematics and Science, State University of Malang, Malang, Indonesia (m_diantoro@yahoo.com)

Abstract

A complex of silver (I) nitrate and ethylenethiourea has been synthesized in a mixture of 50% hot water and 50% acetonitrile with stoichiometry of 1:1. This complex consists of 31.91% N, 27.30% O, 23.28% S and 17.50% Ag. Scanning Electron Microscopy of the complex showed a fibrous structure. Prediction of molecular formula this complex is $[Ag_2(etu)_2(NO_3)_2]$.

Keywords*: complex silver (I) nitrate, ethylenethiourea, SEM-EDAX.*

1. Introduction

Sulphur donor ligands derivate of thiourea have been utilized in a variety of forms to access coordination complexes, most notably of type B or soft metal. The coordination chemistry of ethylenethiourea with metal ions has been the subject of several recent investigations because their variable binding modes and because of the relevance of their binding sites to those in living system. Crystallographic reports about d^{10} metal complexes of thiourea established that these ligands are coordinated *via* the sulfur atom. Especially the study of coordination and structural chemistry of silver (I) complexes with sulfur containing ligands has been a matter of interest over the last decade due to their wide range of applications in medicine and in analytical chemistry.

Complex of silver (I) nitrate with ethylenethiourea have been synthesized in hot water with stoichiometry 1:3 [1]. $AgNO_3$/etu (1:3) takes the form $[(etu)_2Ag(\mu\text{-S-etu})_2Ag(etu)_2]NO_3$. Synthesis results can be affected by the stoichiometry and the solvent. This research used 1:1 stoichiometry of silver (I) nitrate with ethylenethiourea 1:1. Synthesis of coordination compound was performed in the solvent mixture of 50% hot water and 50% acetonitrile.

Characterization was done using SEM-EDAX. SEM was used to determine the crystal form of coordination compounds of silver (I) nitrate and ethylenethiourea. EDAX was used to compare the elements making up the results of coordination compounds. On the basis of SEM-EDAX data is that the molecular formula of coordination compound can be predicted.

2. Experimental Details

Synthesis

Ethylenethiourea (1 mmol; 0.102 g) was dissolved in 50% hot water and 50% acetonitrile. The ligand solution was then added with a solution of silver (I) nitrate (1 mmol; 0.169 g) in 50% hot water and 50% acetonitrile. Colourless and fibrous mass of product formed upon cooling after 4 days.

3. Result and Discussion

SEM is an instrument that can show the surface appearance of a substance. Reactants were scaned to find out the display surface of the compound. Views surface of silver (I) nitrate is shown in Figure 1, and surface appearance of ethylenethiourea is shown in Figure 2.

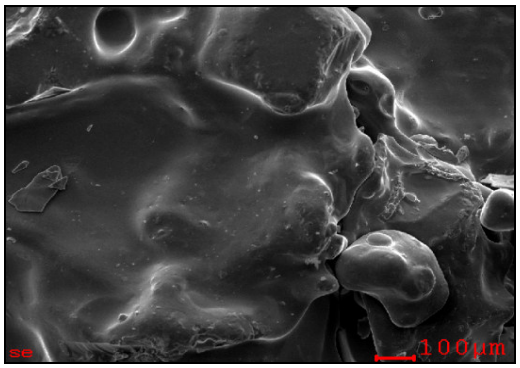

Figure 1. Surface of $AgNO_3$

Figure 2. Surface of ETU

SEM results of the coordination compounds are reported in Figure 3. By compared from SEM data, coordination compound synthesized crystal of silver(I) nitrate and etu had fibrous form.

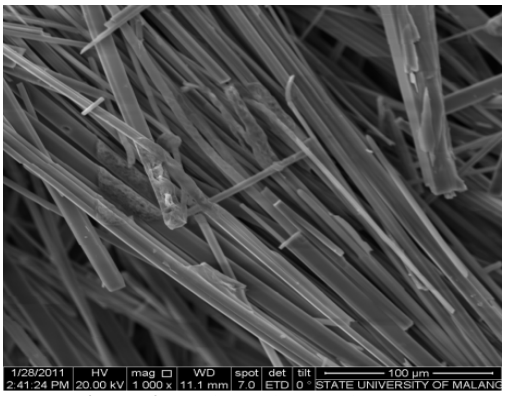

Figure 3. Surface of Crystal Product

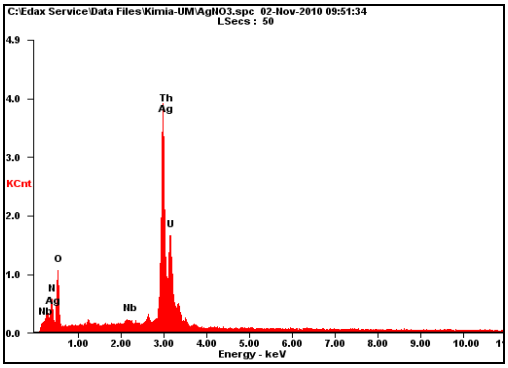

Figure 4. EDAX Diagram of $AgNO_3$

EDAX instrumentation used to determine the elemental content of a substance. Results from EDAX diagram of the energy released is based on an element. EDAX diagram of silver (I) nitrate is shown in Figure 4, and the results of EDAX diagram ethylenethiourea compounds are presented in Figure 5. In the EDAX diagram of silver (I) nitrate, element thorium was appeared. The emergence of thorium is because of the energy of the silver close to energy from thorium.

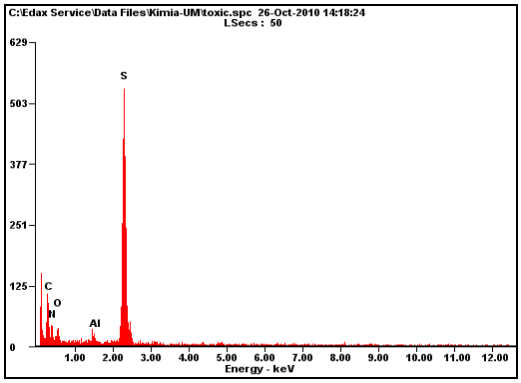

Figure 5. EDAX Diagram of ETU

EDAX results of the coordination compounds of silver (I) nitrate and ethylenethiourea shown in Figure 6. From the diagram can be obtained from data quality and quantity of the constituent elements of coordination compounds. Comparative data elements coordination compounds are shown in Table 1.

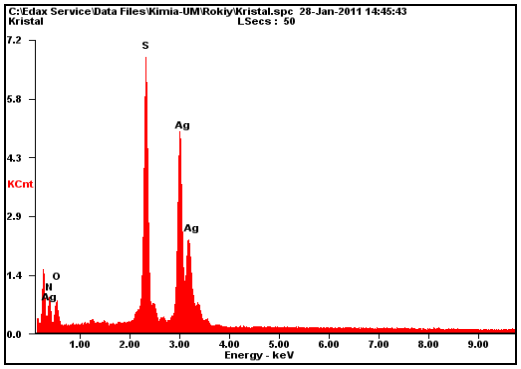

Figure 6. EDAX Diagram of Coordination Compound

Table 1. Comparative Data Element of Coordination Compound

Element	Wt %	At %
N *K*	12.71	31.91
O *K*	12.42	27.3
S *K*	21.22	23.28
Ag *L*	53.66	17.5

Comparison of the Ag atoms and S represents the coordination number of silver coordination compounds (I) nitrate with

ethylenethiourea. Oxygen is shown in the results of EDAX showed the presence of nitrate on the results of coordination compounds. The complex has a predicted molecular formula of $[Ag_2(etu)_2(NO_3)_2]$.

4. Conculsion

Synthesis of coordination compounds of silver (I) nitrate and ethylenethiourea with 1:1 stoichiometric ratio in the solvent mixture of 50% hot water and 50% acetonitrile produce fibrous crystals. The complex has a predicted molecular formula $[Ag_2(etu)_2(NO_3)_2]$ from EDAX result.

5. Acknowledgments

We acknowledge support of this work from Chemistry Department Laboratory FMIPA UM, Physical Department Laboratory FMIPA UM, and Central Laboratory FMIPA UM.

6. References

[1]. Bowmaker, G. A., Chaichit, N., Pakawatchai, C., Skelton, B. W., and White, A. H., (2009), Structural and Spectroscopic Studies of Some Adduct of Silver(I) salt with Ethylenethiourea. *Can. J. Chem*. 87: 161-170.

[2]. Ahmad, S., Isab, A. A. and Penzanowski, H. P. (2002), Silver (I) Complexes of Thiourea. *Transition Metal Chemistry* 27: 782-785.

[3]. Nawas, S., Sadaf, S., Fettoihi, M., Fazal, A., and Ahmad, S., (2010), Dibromidobis (N,N,N,N-tetramethyl-thiourea-κS) cadmium (II). *Acta Cryst*. E66, m950.

[4]. Nawas, S., Sadaf, S., Fettoihi, M., Fazal, A., and Ahmad, S., (2010), Diiodobis(N,N,N,N-tetramethyl-thiourea-κS)cadmium(II). *Acta Cryst*. E66, m951.

[5]. Fettoihi, M., Malik, M. R., Ali, S., Isab, A. A., and Ahmad, S., (2010), Dicyanidobis (thiourea-κS) cadmium (II) monohydrate. *Acta Cryst*. E66, m997.

[6]. Ahmad, S., Saddiqa, A., Monim-ul-Mehboob, M., Altaf, M., and Stoechly-Evans H., (2010), Poly[[μ_3-chlorido-bis(μ_2-thiourea-κS)disilver(I)]nitrate]. *Acta Cryst*. E66, m1072-m1073.

The Structure of Silver (I) Cyanate and Triphenylphosphine, $[AgNCO(PPh_3)]_4$

Fariati [1], Effendy [3], Lilik Sunaria [3]

[(1,2,3)] Chemistry Department, Faculty of Mathematics and Science, State University of Malang, Malang, Indonesia (f4riati@gmail.com; f4riati@um.ac.id; Re_adzkiyah@yahoo.com)

Abstract

The compound $[AgNCO(PPh_3)]_4$ has been synthesized and the structure determined. The compound crystallized in the monoclinic space group $P2_1/C$, a = 24.675(2)Å, b = 12.113(1)Å , c = 25.458(2)Å, β = 114.665(1)°,V= 6914.869(9)Å, z = 4, N = 17707, and was refined to an R value of 0.038 on 3296 F. The structure had a distorted tetrahedral geometry in silver.

Keywords: *Silver (I) cyanate, triphenylphosphine, X-ray crystal structure.*

1. Introduction

Structural studies on complexes formed from the reaction of silver (I) pseudo halide with monodentate tertiary phosphine in 1:1 stoichiometric ratios showed that the majority of the complexes exist as tetrameric 'cubane' clusters of general formula $[AgX(PR_3)]_4$ in which the silver atoms are surrounded by one phosphine ligand and three pseudo halide anions to form a distorted tetrahedral configuration. Exceptions to this include formation of a 'step' tetramer as well as the cubane tetrameric isomer for $[AgI(PPh_3)]_4$ [3], $[AgBr(PPh_3)]_4$ [3], $[AgI(Pcy_3)]_4$ [2], and $[AgNCO(Pcy_3)]_4$ [4] and the adducts of AgCl and AgBr with tris(2,4,6-trimethoxyphenyl)phosphine (tmpp) which form linear two coordinate monomeric complexes, [AgX(tmpp)] [1]. None of dimeric $[\{AgX(PR_3)\}_2]$ complexes with three coordinate silver atoms have been structurally characterized for this system. The basicity and steric profile of triphenylphosphine suggested that the possibility that 2:1 adducts with AgNCO would form such tetramer. In order to explore this we recrystallized 2:1 stoichiometric ratios of AgNCO and $P(C_6H_5)_3$ from acetonitrile. While with other acetonitrile a 'normal' unsolvated cubane $[AgNCO(PPh_3)]_4$[5] tetramer rather than the dimer is formed. We report here this synthetic result together with characterization of the complexes by single crystal X-ray determinations.

2. Experimental Details

Synthesis of AgNCO

The compound $AgNO_3$ 1.000 mg (5.882 mmol) was dissolved in water (5 mL) and KNCO (5.875 mmol) 482 mg was dissolved in water (5 mL). Both solutions were mixed until yellow precipitate is formed, in which the precipitate was then filtered and dried in desiccator.

Synthesis of $[AgNCO(PPh_3)]_4$

Silver (I) cyanate (0.762 mmol) 114.377 mg was dissolved in 5mL acetonitrile and triphenylphosphine ligand ((0.381 mmol) 100 mg in 5 mL acetonitrile) then added. A black precipitate that formed immediately was dissolved by warming ….. and filtered. This filtrate was allowed to cool slowly in dark place to give colorless crystals of the product.

Structure Determination

Was used to determination by unique diffractometer data sets the specified $2\theta_{max}$ limits at room temperature (150 K) (monochromatic Mo Kα radiation, λ 0.7107_3 Å; 2θ/θ scan mode)???. N independent reflections were obtained, N_o with I > 3σ (I) being considered observed and used in the full matrix or large-block least-squares refinement on |F| minimizing. Unless otherwise stated, a Gaussian absorption correction was applied. Anisotropic thermal parameters were refined for the non-hydrogen atoms; $(x, y, z, U_{iso})_H$ were included, constrained at estimated values. Computation used XTAL 3.7 program system implemented by S. R. Hall; neutral atom complex scattering factor were used. Pertinent results are given in the Tables (non-hydrogen atom parameters and geometries) and Figures; the latter show labeling and 20% thermal envelopes for the non-hydrogen atoms. Hydrogen atoms were shown. Have arbitrary radii of 0.1 Å. Material deposited comprise structure factor amplitudes,

thermal and hydrogen atom parameters and full non-hydrogen geometries.

Crystal/ refinement data for [AgNCO(PPh$_3$)]$_4$ = C$_{76}$H$_{60}$Ag$_4$P$_4$N$_4$O$_4$

Monoclinic, space group P2$_1$/*C* (no. 14), *Z* = 4, *M* = 1648.7, *a* = 24.675(2), *b* = 12.113(1), *c* = 25.458(2) Å, β = 114.665(1)°, *U* = 6914.869(9) Å^3, D_c = 1.584 g cm^{-3}, *F(000)* = 3296, μ_{Mo} = 1.261 mm^{-1}, specimen 0.4 x 0.4 x 0.17 mm, λ = 0.7107$_3$, $2\theta_{max}$ = 90°, *N* = 17707, *R* = 0.038, *R'* = 0.044.

3. Results and Discussion

The reaction between silver (I) cyanate with triphenylphosphine ligand in acetonitrile solvent on 2:1 stoichiometric ratio produces cubane colorless crystal form. Structure determination of single crystal with X-ray diffraction method shows that the complex compound recrystallized on monoclinic lattice, space group P2$_1$/*C* 'cubane' tetramer form. (Figure 1). There are 4 asymmetry units in unit cell complex compound in Figure 2.

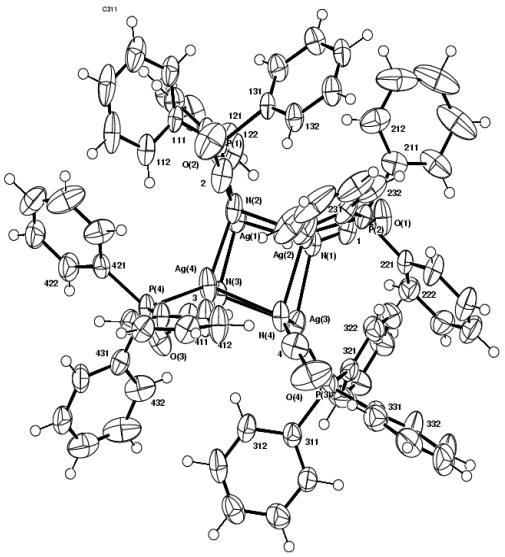

Figure 1. Complex Compound [AgNCO(PPh$_3$)]$_4$

Silver atom on complex compound [AgNCO(PPh$_3$)]$_4$ is four-coordinated with the ligand and forms a distorted tetrahedral. It is bonded to three nitrogen atom from cyanate and one phosphine atom from the ligand. The length of bond and the angle of bond around the silver atom are given in Table 1 and 2.

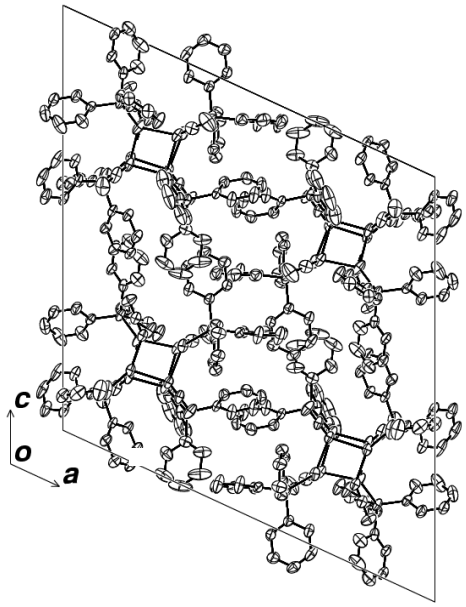

Figure 2. Unit Cell [AgNCO(PPh$_3$)]$_4$

Table 1. Bond Length [AgNCO(PPh$_3$)]$_4$

Distance (Å)	[AgNCO(PPh$_3$)]$_4$
	2.3600(8)
Ag(1)-P(1)	2.359(1)
Ag(2)-P(2)	2.3685(9)
Ag(3)-P(3)	2.362(3)
Ag(4)-P(4)	2.362(4)
<Ag-P>	
	2.422(3)
Ag(1)-N(1)	2.693(3)
Ag(1)-N(2)	2.240(3)
Ag(1)-N(3)	2.436(3)
Ag(2)-N(1)	2.282(3)
Ag(2)-N(2)	2.473(4)
Ag(2)-N(4)	2.363(3)
Ag(3)-N(1)	2.501(3)
Ag(3)-N(3)	2.368(1)
Ag(3)-N(4)	2.332(4)
Ag(4)-N(2)	2.485(3)
Ag(4)-N(3)	2.378(3)
Ag(4)-N(4)	2.414(1)
<Ag-N>	

In Table 2, the angle between N-Ag-P is bigger than regular tetrahedral. This case is due to steric effect of triphenylphosphine ligand and cyanate anion, hence it has bigger angle bond. The length of bond Ag-N is longer than Ag-P. This fact can be explained with the VSEPR theory, in which the atom with more electropositive will occupy bigger space while the atom with more electronegative occupy smaller

space. Followed by the longer of the bond length Ag-N and N-Ag-N angle become smaller.

Table 1.2 Bond Angle $[AgNCO(PPh_3)]_4$

Angle (°)	$[AgNCO(PPh_3)]_4$
P(1)-Ag(1)-N(1)	121.65(9)
P(1)-Ag(1)-N(2)	101.15(6)
P(1)-Ag(1)-N(3)	150.44(9)
P(2)-Ag(2)-N(1)	125.05(9)
P(2)-Ag(2)-N(2)	134.71(8)
P(2)-Ag(2)-N(4)	115.61(8)
P(3)-Ag(3)-N(1)	128.10(8)
P(3)-Ag(3)-N(3)	127.89(8)
P(3)-Ag(3)-N(4)	130.29(7)
P(4)-Ag(4)-N(2)	123.77(7)
P(4)-Ag(4)-N(3)	127.4(1)
P(4)-Ag(4)-N(4)	127.81(8)
<P-Ag-N>	126.122(4)

4. Conclusion

Synthesis silver (I) cyanate with triphenylphosphine ligand produced complex compound tetramer cubic $[AgNCO(PPh_3)]_4$ formed by $P2_1/C$ space group.

5. Acknowledgements

We acknowledge support of this work by Chemistry Laboratory and Central Laboratory of FMIPA UM.

6. References

[1]. Baker, L.J., Bowmaker, G.A., Camp, D., Effendy, Healy, P.C., Schmidbaur, H., Steigelmann, O., and White, A.H., (1992), Structural, Far-IR, and ^{31}P NMR Studies of Two-Coordinate Complexes of Tris(2,4,6-trimethoxyphenyl)phosphine with Silver(I) Halides. *Inorganic Chemistry,* 31(17): 3656-3662.

[2]. Bowmaker, G.A., Effendy, Harvey, P.J., Healy, P.C., Skeleton, B.W., and White, A.H., (1996), Spectroscopic and Structural Studies on 1:1 Adducts of Silver (I) Salts with Tricyclohexilphosphine. *The Journal of Chemical Society, Dalton transaction,* 2459-2465.

[3]. Bowmaker, G.A., Effendy, Hart, R.D., Kildea, J.D., and White, A.H., (1997), Lewis-Base Adducts of Group 11 Metal (I) Compounds. LXXIII Synthesis, Spectroscopy and Structural Systematic of New 1:1 'Cubane' Tetramers of Copper(I) and Silver(I) Halides with Triphenylarsine. *Australian Journal of Chemistry*, 50: 653-670.

[4]. Bowmaker, G.A., Effendy, Harvey, P.J., Healy, P.C., Skeleton, B.W., and White, A.H., (1998), Spectroscopic and Structural Studies on 1:1 Adducts of Silver (I) Salts with Tricyclohexilphosphine. *The Journal of Chemical Society, Dalton transaction,* 2123-2129.

[5]. Cassel, A., (1981), Chlorotris (tri-phenyl-phosphine) silver. *Acta Crystallography,* (B37): 229-231.

[6]. Engelhardt, L. M., Healy, P.C., Patrick, V.A., and White, A.H., (1987), Lewis-Base Adduct of Group 11 Metal (I) Compounds. XXX; 3:1 Complexes of Triphenylphosphine with Silver Halides. *Australian Journal of Chemistry,* 40: 1873-1881.

[7]. Sunaria, L., (2011), Synthesis and Structure Determination of Complex Compound Silver (I) Cyanate with Triphenyilphosphine Ligand by X-ray Diffraction Method. Thesis. Malang: State University of Malang

[8]. Teo, B. K. and Calabrese, J. C., (1976), Stereochemical Systematics of Metal Clusters. 0012 Crystallographic Evidence for a New Cubane Chair Isomerism in Tetrameric Tryphenylphosphine Silver Iodide, $(PPh_3)_4Ag_4I_4$. *Inorganic Chemistry,* 15(10): 2474-2486.

Design,Implementation andAnalysis Performance of XEN Hypervisor Virtual Machine Monitor Based on Linux for Server Technology Solutions in Indonesia

Hendarmawan

Department of Computer Science, Faculty of Science, Brawijaya University
Email: hendarmawan@ub.ac.id

Abstract

The need for server to handle many of the services in the field of technology is very important. On the other hand, the service performance of most of the servers is less than 15%. The researchers try to cope with this problem by trying a new technology. Virtualization of operating system becomes very interesting because it can answer the previous question on what performance of server will be for the next generation. With virtualization technology, this utility will be improved so that servers can increase its performance significantly. One of the virtualization servers is xen virtual machine, which is an open source and using Linuc as its operating platform system. The author chooses this technology due to its hypevisor which allow each server in the xen environment to share the hardware resources without disturbing the other server resources.

Keywords: *Hixen, servers, virtualization, hypervisor technology.*

Study Of Phosphate Coated Wire Electrode Using Chitosan as an Active Material

Hendry Iyabu[1], Hermin Sulistyarti[1], Atikah[1]

[1]Chemistry Department, Faculty of Science, University of Brawijaya, Malang Indonesia

Abstract

Phosphate is one of important environment indicator, as it can stimulate algal bloom which causes the death of organisms. Phosphate coated wire electrode (CWE) with chitosan membrane as an active material and PVC-DOP as a supporting material have been developed as an alternative method of phosphate monitoring. Composition of membrane in this research was optimized. The basic characteristics of CWE tested including Nernst factor, range of concentration, detection limit, respon time, and life time. Besides, the influence of precondition in 0,1 M KH2PO4 solution and foreign ion of NO3- and Cl- were also studied. The resulted CWE membrane made of active material chitosan: PVC: DOP with ratio (% w/w) of 10: 40: 50 followed by dissolving in THF solvent with ratio (w/v) of 1: 3 showed Nernstian character. The produced CWE has basic characteristics of Nernst factor of 59 mV/decade concentration, wide linier working range of concentration from 1 x 10-3 M to 1 x 10-1M or 9.70 x 101 ppm to 9.7 x 103 ppm, low detection limit of 1 x 10-3 M or 9.7 x 101 ppm, fast respond time of 100 seconds, and life time of 10 days. The resulted CWE Phosphate is expected to be used as an alternative method for phosphate monitoring in water samples.

Keywords: ***Phosphate, ISE, CWE, Chitosan*.**

Flow Injection Multichannel Sensor for Nitrate Analysis

Hermin Sulistyarti [1], Atikah [2], Setyawan P. Sakti [3], Spas Kolev [4], R.W. Cattrall [5]

[(1,2)] Chemistry Department, Faculty of Science, University of Brawijaya Malang Indonesia
(sulistyarti@yahoo.com)
[(3)] Faculty of Science, University of Brawijaya Malang Indonesia
[(4,5)] School of Chemistry, The University of Melbourne, Australia

Abstract

It is well known by physician and public health professionals that exposure to high levels of nitrates causes "blue baby syndrome," a condition caused by lack of oxygen in infants. The current EPA standard of 10 ppm does not adequately protect the public health. Therefore, the availability of sensitive method of analysis to monitor the presence of nitrate in water is strongly required. In this work, an on-line nitrate multi sensing cell was developed using active material of Aliquat nitrate. This channel consisted of 8 channels so that 8 replications were obtained in one run of analysis. The system was optimized with regard to flow rate and sample volume to achieve a better sensitivity and fast response. Under the optimum conditions of 2ml/min flow rate and 100 µL sample volume, the system showed linear calibration from 10^{-5} to 10^{-1} M, with Nernst factor of 43mV/decade concentration, detection limit 0.6 ppm, high reproducibility, 30 seconds and gave acceptable results for one week of usage. The sensing membrane is easily recoated for further application; therefore, this system is expected to be an embryo of automated system of potentiometric analysis for environmental samples.

***Keywords**: Nitrate, sensor, aliquat, flow injection.*

1. Introduction

The exposures to high levels of nitrates can causes "blue baby syndrome," a condition caused by lack of oxygen in infants. The current EPA standard of 10 ppm does not adequately protect the public health. Therefore, the availability of sensitive method of analysis to monitor the presence of nitrate in water is strongly required.

Sensor technology, chemical sensors and biosensor has grown rapidly as a fast, accurate, easy, and requires only a few samples and chemical reagents to detect a variety of trace amounts of analytes. Thus, it is well suited for routine analysis. In terms of instrumentation, it is possible to miniaturize and used in flow systems for automation. Various types of solid membrane sensors have been reported, Sulistyarti (2002) has developed a compact sensor AgSCN and AgBr for thiocyanate and bromide [1]. However, a tube solid state sensor is not feasible for the on-line system. Liquid membrane sensors have been introduced by Cattrall and Freiser (1971) for calcium cations [2]. Moreover, Gregorio (1996), showed that various crown ether compound has the ability to act as active compounds for silver cation sensor [3]. Crown ether compounds s,s-dipropylpyridine-2,6-dicarbothiolate showed Nernstian response with a slope of 58 mv/decade change in concentration and linearity (10^{-1}-10^{-5} M). Atikah (2005) has developed a supported liquid membrane sensor coated wire for the determination of nitrate ions which have been improved into a more stable form based on aliquat 336-Nitrate [4,5]. However, no on-line detector based on sensor is currently available in the market.

Flow Injection Analysis (FIA) has been introduced as an analytical technique based on efforts to simplify, miniaturize, and automate analysis. In this technique, the sample solution is injected into the reagent flowing through the capillary tube which is moved by using peristaltic pump, which is forwarded to a detector for quantization. Thus, because all such processes pippetting, dilution, mixing, separation and detection are in a flow system, then these processes which usually time-consuming can be avoided. In addition, the volume of the sample solution may be minimized up to micro litre scale, large consumption of chemicals is reduced, and time of analysis can be shortened dramatically.

Sensor technology has also been modified to be applied at a flow system which is the basis for automation of analytical methods. Shen (1999) has developed a sensor nonactin based in a flow system for determination of ammonia [6] and Gregorio (1996) use a polymer membrane for the determination of silver cations [3]. The flow cells used for both are made of acrylic which is

easily available so that the detection system can be fabricated in house for on-line multi-sensor as part of construction of an automatic analysis system. In this work, an on-line nitrate multi sensing cell was developed using active material of Aliquat nitrate. This channel consisted of 8 channels so that 8 replications were obtained in one run of analysis. The flow cell for on-line multi sensor is completed with the tranducer and interface as well as DAC (data acquisition Card) suits for on-line detector multi sensors.

2. Experimental Details

Chemicals & Reagents

All chemicals and reagents used in this work are in analytical grade unless otherwise stated. Membrane active sensor was composed of Aliquat 336 klorida (metiltrioktilamonium klorida) (Aldrich) as an active material membrane, dibutilftalat (DBP) as *plasticizer* (Sigma), high molecular weight polivinilklorida (PVC) (Sigma), tetrahidrofuran (THF) (E-Merck) as solvent, and KNO_3 (Ajax) as an ionofor exchanger with ocomposition obtained from previous work. All solutions were made up in Millipore deionised water with reagents of analytical grade. The stock solution of 1000 mg L^{-1} nitrate was prepared by dissolving the appropriate amount of the KNO3 (Ajax) and reference solution was 0.1 M KCl.

Flow Injection Procedure

FIA manifold for determining nitrate is shown schematically in Figure 1 (Appendixes). It consisted of a peristaltic pumps (Watson Marlo Alitea, Sweden) furnished with Tygon tubing (TACS Australia), a rotary injection valve (Rheodyne model 5020, USA) with a 100 µl sample loop, a selection valve, Teflon tubing (0.5 mm ID, Supelco, USA), on-line multi sensor with 8 channels as on-line detector [6]. The detector was interfaced to a PC via a PCL-818H data acquisition card (Advantech).

Procedure for on-line nitrate sensor

The top compartment of the constructed flow cell was unscrewed and all of the 8-channel working electrodes as well as the reference and auxiliary electrodes were cleaned up and Coated with Aliquat-nitrate membrane and stand overnight for drying. The reference electrode of Ag/AgCl was prepared by electrolyzing the silver electrode with 0.1 M HCl at 1.5 V for 5 minutes. The flow cell was then reassembled and connected with suitable FIA-system, and ready for the measurement. Potential cell is the difference potential between each of working electrode and reference electrode.

The on-line sensors was then optimized with respect to flow rate and sample volume and the characterized to some standard parameters for sensors, i.e. response time, Nernst factor, linear response range, detection limit, and lifetimes.

3. Result and Discussion

The work was started by monitoring potential difference resulted between each of 8 ISE-nitrate sensors and Ag/AgCl reference electrode for sample nitrate from 10^{-4} up to 10^{-1} M. Ideally, the potential difference of 59.2 mV/decade concentration (Nernstiant). Figure 2 shows that the potential difference obtained per decade concentration is close to 40 mV. This is not surprising as in FI-system most of the measurement is done prior to equilibrium achievement; thus gives less sensitivity, unless otherwise appropriate optimizations are conducted. To achieve high sensitivity and a reasonable sampling rate, the most important operational condition parameters such as flow rates and sample volume were studied for this preliminary work.

Optimization of sample volume

Varying sample volume by changing the sample loop is the simplest method of controlling dispersion. The influence of the sample volume was studied by injecting nitrate samples in the concentration range of 10^{-5} – 10^{-1} M with the sample volume varied from 100 to 250 µL under a fixed flow rate of 1 mL/min. The sensitivity was improved by increasing the sample size as a result of decreasing dispersion rather than by any chemical kinetic effects [7,8] as depicted in Figure 3A. However, it decreased significantly the sampling rate as expected, therefore to assure good reproducibility, acceptable sensitivity and short baseline-to-baseline time (characterized by a narrow peak), a 100 µL sample volume was considered as optimal.

Optimization of flow rate

The flow rates of carrier and reference streams determine the sampling rate and strongly influence the time contact of sample and membrane sensor, thus affecting sensitivity. Theoretically, a decrease in the flow rate of the donor streams will allow longer exposure of the sample zone to the membrane thus enhancing the exchange of nitrate in the membrane interfaces to reach the equilibrium. To achieve better sensitivity the flow rate was varied between 0.5 and 2 ml/min. It should be taken into account that

low flow rates lead to low sampling rates. It was observed that increasing flow rate did not significantly lower the signal, thus the flow rate of 2 ml min^{-1} was chosen to compromise the requirements for high sensitivity and sampling rate (Figure. 3B).

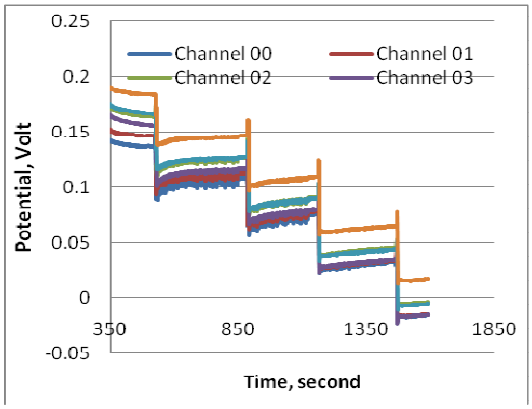

Figure 2: Potential difference of nitrate solutions from 10^{-4} up to 10^{-1} M using 4 channels

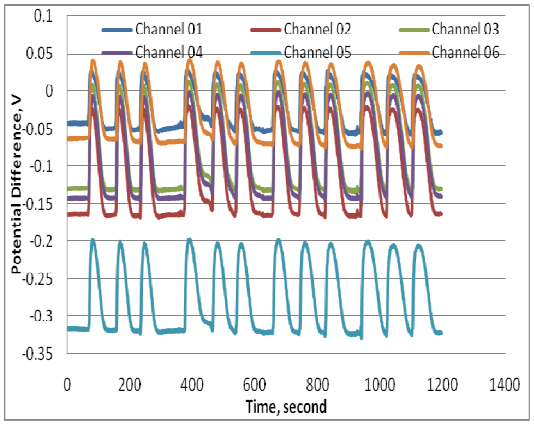

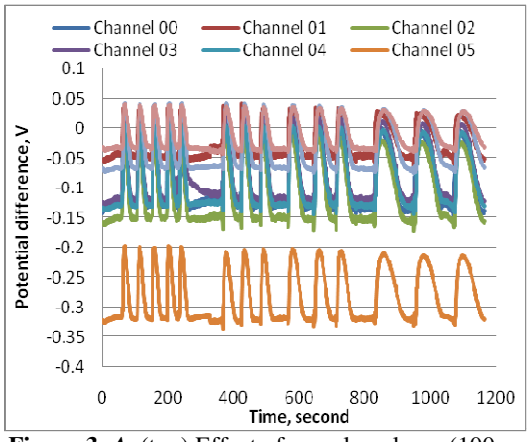

Figure 3: ***A***. (top) Effect of sample volume (100-250 µL) on the potential difference of nitrate solutions of 10^{-1} M using 6 channels; ***B***. (bottom) Effect of flow rate (0.5-2 ml min^{-1}) on the potential difference of nitrate solutions of 10^{-1} M using 6 channels

Method Performance

Under the optimum conditions outlined above (i.e., flow rate 2 mL/min, sample volume 100 µL, coil length 15 cm, donor stream of water, and acceptor stream of reference solution of 0.1M KCl, respectively), the sampling rate was found to be 100-120 samples per hour. The calibration curve was found to be linear (R^2 = 0.999) for concentrations of nitrate in the range of 10^{-5} M up to 10^{-1} M (Figure 4). The Nernst factor was 43 mV/decade concentrations which is understandable as in flow system the potential measurement was not done at the steady state. The sensors gave acceptable results for one week of usage and easily recoated for further applications. Figure 5 shows typical FI-multi sensor responses for nitrate standard solutions and the excellent reproducibility (RSD < 5%, n = 50). The detection limit under the optimum conditions, defined from standard calibration curve, was determined as 10^{-5} M.

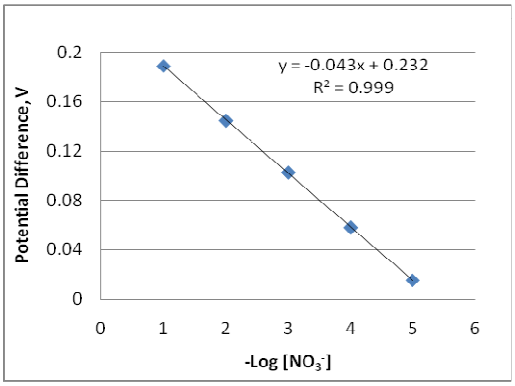

Figure 4: Calibration curve of standard nitrate solutions of one of representative channels

4. Conclusion

The FI-multi sensor system outlined above allows fast, inexpensive, sensitive determination of nitrate which can be easily automated. This method can be used for determining nitrate solution from 10^{-5} M up to 10^{-1} M. The sensing membrane is easily recoated for other membrane sensors for a wide range of applications; therefore, this system is expected to be an embryo of automated system of potentiometric analysis for environmental samples. Further effort is required for improving sensitivity with Nernst factor close to 59.2 mV/decade concentration.

5. Acknowledgments

The authors are grateful to The University of Melbourne, Australia for facilitating research and Directorate General of Higher Education of Indonesia for the financial support

6. References

[1]. Sulistyarti, H., Andayani, U., Anaskah, Y., Fajarini, N., Development of Solid State Sensor for Bromide and Thiocyanate, Natural, Fac. Science University of Brawijaya Malang, publication in progress.

[2]. Cattrall, R.W., Freiser, H., (1971), *Anal Chem*., 43.

[3]. Gregorio, C.G., (1996), A Pyridine Thiol Ester Ionophore As A Neutral Carrier In A Silver Selective Polimer Membrane Sensor, PhD Thesis, La Trobe University, Australia.

[4]. Atikah, (2005), Tranport Phenomena of Nitrate Ion on Coated Wire Electrode Poliviynilchloride Membrane with Aliquat 336-Nitrat, PhD Thesis, ITB Bandung.

[5]. Sulisyarti, H., Atikah, S.P. Sakti, (2007), Development of chemical instrumentation based on sensor and flow injection analysis: An effort for the improvement of monitoring food quality and prevention of instrumentation import dependency, Incentive Report, Ministry of Research and Technology of Indonesia.

[6]. Shen, H., (1999), An Investigation of Application of Ion Selective Electrodes In Flow Injection Analysis and Electrode Arrays in Ion Chromatography, PhD Thesis, La Trobe University, Australia.

[7]. Ruzicka, J., Hansen, E.H., (1981), *Flow Injection Analysis,* John Wiley & Sons, NY.

[8]. Karlberg, B., Pacey, G.E., (1989), *Flow Injection Analysis: A Practical Guide*, Elsevier Amsterdam.

Appendixes

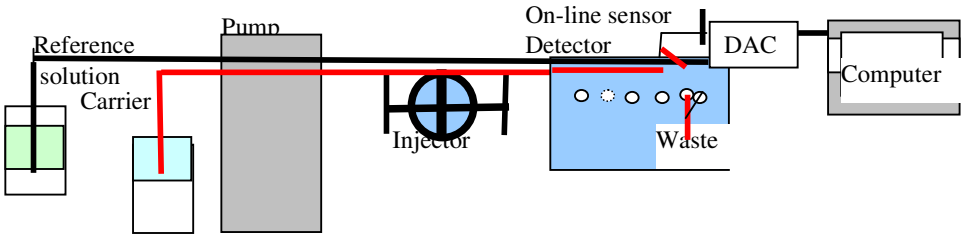

Figure 1: FI-multichannel sensor system for determining nitrate

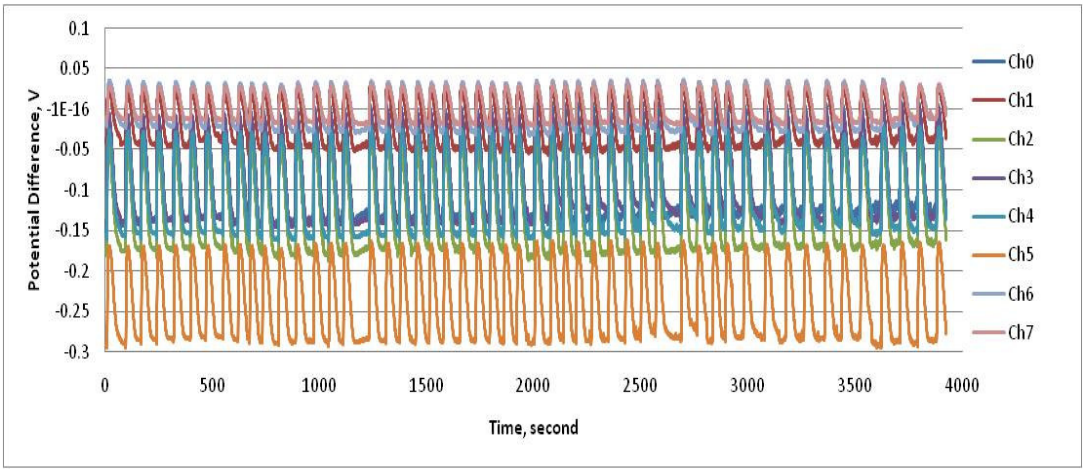

Figure 5. Typical FI-multi sensor responses for nitrate standard solutions from 8 channels

Testing of Radiation Exposure Homogenity of ^{137}Cs Source Spherical Geometry

Holnisar [1], Rosdiani [2], Pujadi [3]

[(1,2,3)] Center for Technology of Radiation Safety and Metrology, National Nuclear Energy Agency, Jakarta
(holnisar@batan.go.id)

Abstract

The spherical geometry radiation source of Cs-137 has been made on the flexy-glass container, with 2.0 cm diameters, for use as a standard source of radiation measuring instrument calibration and intercomparison with measuring tools. The testing of radiation exposure homogeneity carried out by measurement of exposure dose of source, using Ludlum survey meter MICERO R METER MODEL 19, at eight positions circling sphere at the same distance, 30 cm from center of the source, which is expected to represent all positions. The result showed the relative homogeneity of each position is equal with difference from 0.00% to 0.90 %.

Keywords: *Homogenity, Spherical geometry, ^{137}Cs source.*

1. Introduction

Radionuclide standard source has an important role in measuring the activity of radionuclides, especially for calibration of radiation measuring instrument. Radionuclide standard surce must have accurate activity and good homogeneity, especially for the standard source in the form of geometry. The ^{137}Cs standard source in the form spherical geometry was made on the flexy-glass container 2.0 cm diameters and 0.5mm thickness is shown in Figure 1.

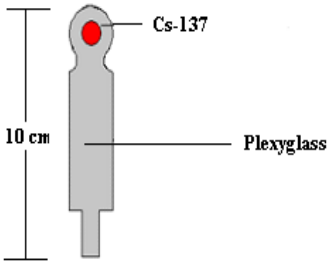

Figure 1. ^{137}Cs source spherical geometry

The purpose of this study is obtain the standard source in the form of spherical geometry so that it can be used for calibrating several instruments at once, because the radiation exposure in all directions, especially in the radiation measuring instrument calibration (survey-meter). Radiation exposure homogenity of the spherical geometry source was test in the various directions around the source. Eight positions around the source with the same distance from the central point source is selected for determine the homogeneity radiation exposure and measurements carried out using LUDLUM MODEL 19 survey-meter. Testing homogenity of radiation exposure will show the feasibility of the standard source for calibration or inter-comparison. Homogenity of radiation exposure for each position is good if the measurement result have difference less than 1% from the average value of all positions [1].

2. Experimental Details

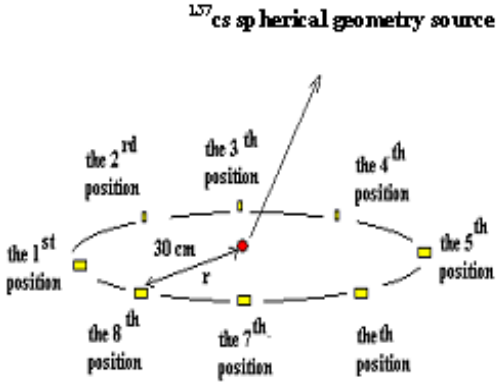

Figure 2. Illustration the testing of radiation exposure homogenity of ^{137}Cs spherical geometry source

Source of ^{137}Cs in the form of Cesium Chloride in H_2O solution were prepared from a solution provided by POLATOM-Polandia. The solution were prepared into solid point souce in

the form of CsCl, sucked into a small polyethylene ampoule picnometer (baby bottle), and then dropped on to the center of plexy-glass as container source. Small polyethylene ampoule picnometer were carefully weighed in each case to determine the mass of the drops. With the dropped mass is known then the source activity can be calculated. The activity source of sperical geometry was calculated 0.32 MBq, and then, the source were dried with a circulation.

Next, the sources were then covered plexy-glass material. The radiation exposures are measured using fixed distance of 30 cm from the central point source. The radiation exposure measurement at eight positions around the source is shown in Figure 2, and was measured fifteen replicated of each position. The all measured were corrected for background.

3. Result and Discussion

The measurement result of radiation exposure at each position have a relative uncertainty ranges from 1.75% to 2.57% (statistical measuring), Table 1. The value of this uncertainty is relatively large due to appointing measurements from the measuring equipment using analog system (needle), so that the subjectivity of the operator influence. The ^{137}Cs source activity of spherical geometry was 0.32 Mbq, theoretically at the distance of 30 cm the radiation exposure equivalent to 28.41μR/H. In Table 2, the mean of measurements are shown the value of radiation exposure by 28.87 μR/ H. The result this measurement have differences with the theoretical 1.6%. The radiation exposure measurement result of each position has different from 0.00 to 0.90 of the average. This result shows that the homogenity of radiation exposure from^{137}Cs in the spherical geometry form is relatively good, the difference in each position less than 1%.

4. Conclusion

Testing of the radiation exposure homogenity measurement of ^{137}Cs source spherical geometry has been done. This source can be used as standard source for calibration and inter-comparison with the measurement of many instruments at once because the radiation exposure at eight positions has differences less than 1%.

5. Acknowledgment

---

6. References

[1]. Holnisar, Hemawan Candra, Gatot Wurdiyanto (2009), *Pengukuran Homogenitas Phantom Pesawat Brakiterapi,* Proceedings of the 6th BSS, Brawijaya University, Indonesia, III 7-11.

[2]. G.F. Knoll (2000), *Radiation Detection and Measurement*, 3rd ed, John Willey & Sons, USA.

[3]. NCRP. (1978), *A handbook of radioactivity measurements prosedur, NCRP report No.58*, Washington DC.

Appendixes

Table 1. The mesuring value of radiation exposure homogeneity from eight position measurements with suvey meter MICERO R METER model 19

No	Position (μR/H)							
	1	**2**	**3**	**4**	**5**	**6**	**7**	**8**
1	29	30	28	29	30	29	29	30
2	29	29	29	28	29	29	29	29
3	30	29	29	29	29	29	28	28
4	29	30	28	28	29	28	28	28
5	28	29	28	28	29	28	29	29
6	29	29	28	29	28	28	28	29
7	29	29	29	28	29	29	29	29
8	28	29	29	29	28	29	30	28
9	28	28	29	29	28	29	28	28
10	29	29	29	29	29	28	30	28
11	29	29	29	29	29	29	30	29
12	30	30	29	30	28	29	29	29
13	30	29	30	29	29	28	28	29
14	29	29	28	29	28	29	29	29
15	29	29	29	29	29	28	29	28
Mean	**29.00**	**29.13**	**28.73**	**28.80**	**28.73**	**29.00**	**28.87**	**28.67**
Rel.dev. (%)	**2.26**	**1.77**	**2.07**	**1.95**	**2.07**	**1.75**	**2.57**	**2.15**

Table 2. The mean measurement of eight positions

NO.	Measuring Position	Result of Measuring (μR/H)
1	1st position	29.00
2	2rdposition	29.13
3	3thposition	28.73
4	4thposition	28.80
5	5thposition	28.73
6	6thposition	29.00
7	7thposition	28.87
8	8thposition	28.67
Average		**28.87**

Comparison of Amobilization Chrome (Cr) in Waste of electroplating with Portland Pozzolan Cement - Kaolin and Portland Pozzolan Cement - Zeolite Use Solidification/Stabilization Technique

Ika Setyorini [1], Lies Wuryanita Adriyani [1]

[(1)] Chemistry Department, Faculty of Science, Brawijaya University
Email : ikaluvmom@gmail.com

Abstract

Industry of electroplating represents the heavy metal waste producer. Solidification/stabilization technique (S/S) have a lot of developed for the processing of waste, contain especially heavy metal. By the process of adsorption, ion of metal Cr will trapped into matrix of solid and ammobilized. Thereby the Cr contamination potency to environment can be reduced. In this research, the comparison effectiveness Portland pozzolan cement - kaolin with the Portland pozzolan cement - zeolite, amobilization of ion of metal Cr use the solidification/stabilization technique. Portland pozzolan cement, kaolin, and zeolite as a binder in solid matrix and also reduce the amount of cement. Comparison of Portland pozzolan cement - kaolin and Portland pozzola cement - zeolite was varied from 1:4 until 4:1 with the factor of water to total solid is 0.65. The results showed that the variation of use portland pozzolan cement – kaolin and portland pozzolan cement – zeolit have an effect in ammobilization of ion metal Cr. Test of compressive strength (UCS) showed increase until 19.2 kN for kaolin and 19.33 kN for zeolite in comparison portland pozzolan cement - kaolin or portland pozzolan cement - zeolite 4:1. Leaching ion of metal Cr use the method of TCLP (Toxicity Characteristics Leaching Procedure) degraded until < 0.0001 mg / g at comparison portland pozzolan cement and kaolin 1:1 and 2:1, and till 0.0073 mg / g at comparison portland pozzolan cement and zeolite 1:2.

Keywords: *Solidification/Stabilization, Ammobilization of ion Cr, Kaolin, Zeolit.*

The Influence of Inoculate Concentration Ratio of Lactic Acid Bacteria *Streptococcus thermophilus, Lactococcus lactis* and *Lactobacillus bulgaricus* toward The Time of pH Decrease and The Weight of Curd in Cheese Production

Marissa Agnestiansyah [1], Chanif Mahdi [2], Anna Roosdiana [3]

[1,2,3] Department of Chemistry, Faculty of Science, Brawijaya University, Malang, Indonesia
(ichaansya@gmail.com; chanifmahdi@gmail.com; aroos@ub.ac.id)

Abstract

Lactic acid bacteria affect the decreasing of milk pH because lactic acid bacteria can deform lactose to lactic acid. This bacterium is also affected the weight of curd that formed in cheese production. The difference of inoculate concentration ratio of lactic acid bacteria will need a different time in decrease milk pH and also the weight of curd. This research was carried out at various concentration of lactic acid bacteria inoculate of Streptococcus thermophilus: Lactococcus lactis: Lactobacillus bulgaricus using five ratios, as followed: 3:1:1; 3:1:2; 3:1:3; 3:1:4 and 3:1:5. Lactic acid bacteria inoculate concentration ratio influenced significantly (P<0.05) of both to the time of pH decrease and the weight of curd. Ratio 3:1:5 indicated the shortest time (72 minutes) to decrease pH until 6.2, whereas ratio of 3:1:2 resulted the maximum weight of curd yielding in 23.1089 gram of curd from 200 mL milk.

Keywords: *lactid acid bacteria, Lactobacillus bulgaricus,cheese.*

1. Introduction

Cheese is one of dairy product that very familiar on the the world community. It has a good taste and high of nutrient. Cheese is made from mammalia's milk like cow that coagulated by enzyme and lactic acid bacteria. The curdling of milk will separate it in two layer, *whey* (the watery part of milk) and *curd* (the solid part of milk). Curd will ripen by lactid acid bacteria to form cheese [1].

Principal factor that influence cheese production are the culture of lactic acid bacteria and enzyme coagulant. Lactid acid bacteria fermented lactose to lactid acid. Lactic acid can accelerate the coagulating process. The coagulating process completed by proteolytic enzyme [6,10].

One of proteolytic enzyme that usually use in making cheese is rennet. Rennet is, by definiton, an extract of the abomasum (the fourth true stomach) young milk-fed calves. Renin is one of enzyme in rennet. The optimum pH of rennet is 6.2 [12].

Lactid acid bacteria that usually use in making cheese are *Streptococcus*, *Leuconostoc* and *Lactobacillus.* The best inoculum for cheese fermentation is mixed cultures of (*Streptococcus thermophilus*, *Lactococcus lactis* and *Leuconostoc mesenteroides* in concentration 10 % at ratio 3:1:2. This mixed culture produce curd in fastest time at 22 hour and pH 4.1 [5].

L. mesenteroides is heterofermentatifve bacteria (produce the other compound beside lactic acid in primary metabolism). It also produces ethanol, acetate and mannitol, whereas lactic acid is more needed in making cheese [3]. *Lactobacillus bulgaricus* is homofermentative lactid acid bacteria. It only produce lactic acid in primary metabolism [8]. Using *L. bulgaricus* as subtituter of *L. mesenteroides* will give more lactid acid in specific ratio, hence, the time of pH decrease will decreased.

Protease activities in *L. bulgaricus* will produce low molecular weight of amino acids and peptides. The amino acid arising from this proteolytic activity has been identified as specific growth stimulants for *S. thermophilus*. Mixed cultures of *S. thermophilus* and *L. bulgaricus* have the higer activity compared single culture [13]. In addition, low molecular weight of peptides can stimulate the growth of *L. lactis* [7]. The association between *L. bulgaricus*, *S. thermophilus* and *L. lactis* can increase its activities to produce lactic acid. The high activity to convert lactose to lactic acid can reduce the time of milk pH deccreasing. The number of acid can influence the rennet activity and coagulating process and will be influence the weight of curd.

The purpose of this research work was to study the influence of inoculate concentration ratio of *S. thermophilus*, *L. lactis* and *L. bulgaricus* toward pH decrease and to find out in what concentration ratio it will gave the highest yield of curd.

2. Experimental Details

Culture

The microorganisms used in this study were from the culture collection of the Biochemistry Laboratory Department of Chemistry and Microbiology Laboratory Departement of Agriculture Engineering at Brawijaya University. Cultures were grown and maintained in sterile reconstituted Man Rogosa Sharpe (MRS) agar. Before quantitatively measuring of bacteria population, it inoculates to Man Rogosa Sharpe (MRS) broth.

Quantitatively measuring of bacteria population

The concentration of bacteria was measured by Neubauer hemacytometer [11].

Determining of The Influence of The Lactic Acid Concentration Ratios to pH Decrease

The inoculate of lactic acid bacteria (*S. thermophilus, L. lactis* and *L. bulgaricus*) was added to 100 mL of pasteurised milk with the ratio respectively 3:1:1; 3:1:2; 3:1:3; 3:1:4; and 3:1:5. Each of the ratio volume is 10 mL. Milk with the bacteria inoculate incubate at 40 ºC. Milk's pH is determining every 15 minute until the pH decrease to 6.2. This starter was then used in cheese production.

The making of cheese

200 mL of cow's milk was pasteurised by heating it at 67°C for 30 minutes. The milk is then cooled to around 40°C. Starter culture of lactic acid bacteria is added at the rate of 4 % (concentration ratio respectively *S. thermophilus*: *L. lactis* : *L. bulgaricus* are 3:1:1; 3:1:2; 3:1:3; 3:1:4; and 3:1:5), left until pH 6.2. The next stage is the addition of $CaCl_2$ 0.02% w/v and rennet 0.25% v/v, left until one hour and rennet will coagulates the milk, separating it into curds and whey (curdling). Following curdling, the curds are cut and heated until 40 ºC. The curd are then drained and pressed. The final stage is ripening in the refrigerator for two weeks by package the curds with alumunium foil.

3. Result and Discussion

The Influence of Inoculate Concentration Ratio of Lactic Acid Bacteria to The Time of pH Decrease

Cheese in one of dairy product that in its production most influence by bacteria culture and enzyme coagulant. Bacteria culture that use is lactic acid bacteria. Lactic acid bacteria have an important purpose to convert lactosa to acid lactic. Acid lactic bacteria will decrease milk pH from 6.7 to 6.2. 6.2 is the optimum pH of rennet.

Lactic acid bacteria use the glucose in fermentation media to growth. Glucose cleavage in the cell of lactic acid bacteria will produce energy to the other compound included lactic acid. *S. thermophilus*, *L. lactis* dan *L. bulgaricus* are homofermentative lactic acid bacteria meaning it only produce acid lactic in their primary metabolism. *S. thermophilus* can produce 1% of lactic acid. As a starter, *S. thermophilus* usually combine with the other *Lactobacillus* that produce aminopeptidase like *L. helveticus, L. bulgaricus,* or *L. lactis.*

In this research, *L. bulgaricus* are used. It produces 4% of lactic acid. The combine of *S. thermophilus* and *L. bulgaricus* will increase their activity to produce acid lactic because of the amino acid from *L. bulgaricus* can stimulate stimulate the growth of *S. thermophilus*. The growth of *L. lactis* will increase wtih the presence of low molecular weight of peptide from the *L. bulgaricus* protease activity. The influence of concentration ratio to the decrease of milk pH is shown in Figure 1.

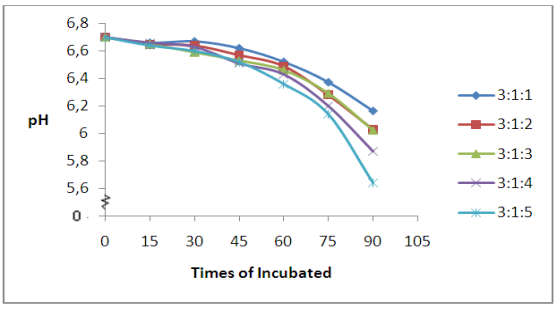

Figure 1 Graphics of the times of incubated and the pH of milk in each of bacteria concentration ratios.

Figure 1 show that the highest number of *L. bulgaricus* will accelerate the decrease of milk pH. Concentration ratio 3:1:5 of *S. thermophilus*: *L. lactis*: *L. bulgaricus* give the fastest time of pH decrease. The ratio and the time that their need to decrease pH until 6.2 repectively 3:1:1; 3:1:2;

3:1:3; 3:1:4; 3:1:5 are 87, 80, 80, 75 and 72 minutes.

The increase number of *L. bulgaricus* will increase the growth of *S. thermophilus* and *L. lactis*. It cause the increase activity of bacteria to deform lactose to lactic acid. It meaning that the producing of lactic acid in one time are increasing. More presence of lactic acid was accelerated the pH decrease.

The Influence of Inoculate Concentration Ratio of Lactic Acid Bacteria to The Weight of Curd

Casein is the major protein of milk. Casein is a phosphoprotein, means that phosphate groups are attached to some of the amino acid side-chains. These are attached mainly to the hydroxyl groups of the serine and threonine moieties. Casein exists in milk as the calcium salt, calsium caseinat. This salt has a complex structure. It is composed of α, β and κ -casein which form a micelle, or a solubilized unit. Neither the α nor the β casein is soluble in milk, and neither is soluble either singly or in combination. If κ-casein is added to either one, or to a combination of the two, however, the result is a casein complex that is soluble owing to the formation of the micelle. The κ casein protein, however, has fewer phosphate groups and a high content of carbohydrate bound to it. It is also thought to have all its serine and threonine residues (which have hydroxyl groups), as well as its bound carbohydrates, on only one side of its outer surfaces. This portion of its outer surface is easily solubilized in water since these polar groups are present. The other portion of its surface binds well to the water-insoluble α and β caseins and solubilizes them by forming a protective colloid or micelle around them that called submicelle (Figure 2). Between the submicelles is connected by calcium phosphat ($Ca_9(P0_4)_6$) to form casein micelle [9].

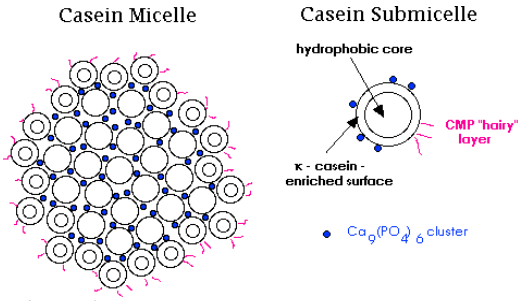

Figure 2. Casein Micelle and Casein Submicelle

Acid from lactic acid bateria solubilized calcium phosphat and the casein getting lose from the micelle. Rennet selectively cleaves the petide chain of κ–casein at phenilalanin 105-methionin 106 into two fragmen: para- κ-casein and glycopeptide. The released glycopeptide is soluble, while para κ–casein precipitates in the presence of Ca^{2+} ions to form curd [4].

Milk coagulation by rennet occurs in two main phases, enzymatic phases and non-enzymatic phase. Enzymatic phase including casein micelle is modificated by enzim. Casein micelle modificated to para κ-kasein micelle by selectively cleaves the peptide chain of κ–casein at phenilalanin 105-methionin 106. Para κ-kasein micelles will agregated in the presence of Ca^{2+}. The agregated of para κ-casein micelle included to non-enzymatic phase. The cleavage occurs at the bond between the phenilalanin 105-methionin 106 amino acid residues causes the release of the charged, glycomacropeptida from the micelle and a reduction in micelle diameter [13]. The loss of this section of the κ-casein protein results in a reduction in the zeta potensial of the micelles and a loss of steric stabilisation taht it provides.

In the second phase of rennet coagulation, the destabilised micelles are aggregated bay a combination of van der Waals', hydrophobic, calcium – mediated and specific ion – pair interactions. At this stage, a protein network forms and traps both fat and moisture. However, the nature of the actual reaction involved in the second phase of rennet coagulation is not fully understood [2].

Acidity is one factor that influences enzymatic coagulation. Rennet coagulation will happen faster in the rennet optimum pH at 6.2. *S. thermophilus*, *L. lactis* dan *L. bulgaricus* are homofermentative lactic acid bacteria that produce lactic acid as their primary metabolite product. The acid fom this bacteria causes pH decreases in milk from 6.7 to 6.2. Utilizing of various concentration ratio of the three bacteria give various result of curd weight (Figure 3).

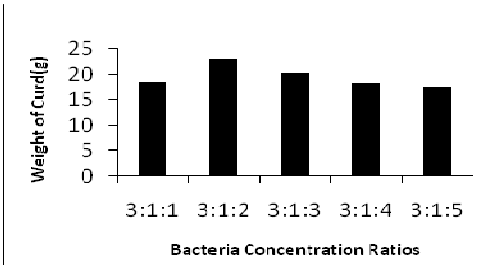

Figure 3 Graphics of bacteria concentration ratios and the weight of curd.

Figure 3 shows that concentration ratio of lactic acid bacteria laktat *S. thermophilus*, *L.*

lactis and *L. bulgaricus* influenced to the weight of curd. The maximum weight of curd resulted at ratio 3:1:2. In this ratio, *L. bulgaricus* was grown so fast, and cause the increase of acid number. The curd was presence because of rennet and acid coagulation. Cheese production processing in two hours causes the decrease of milk pH until 4.6, which is casein isoelectric point. In this pH, casein will coagulated and increase the number of curd. The weight of curd is not in maximum quantity because of the fewer number of *L. bulgaricus* bacteria. At ratio 3:1:3; 3:1:4 and 3:1:5, the weight of curd are decreased because of the decrease of pH cause the rennet cannot work in their optimum pH, hence its activity is decreasing.

4. Conclusion

The conclusions of this research are:

1. Inoculate concentration ratio of lactic acid bacteria *S. thermophilus*, *L. lactis* dan *L. bulgaricus* influence the time of pH decrease. Ratio 3:1:5 indicates the shortest time (72 minutes) to decrease pH until 6.2.
2. Inoculate concentration ratio of lactic acid bacteria *S. thermophilus*, *L. lactis* dan *L. bulgaricus* influence to the weight of curd. Ratio of 3:1:2 resulted the maximum weight of curd yielding in 23.1089 gram curd of 200 mL.

5. Acknowledgements

The contribution made by the following people in preparing this paper is gratefully acknowledged: Dr. Ir. Chanif Mahdi, MS, Dra. Anna Roosdiana, M.App.Sc, Dr. Sasangka Prasetyawan, MS, Ir. Bambang Ismuyanto, MS, Dra. Sri Wardhani, M.Si, M. Farid Rahman, S.Si., M.Si, Qonitah Fardiyah, S.Si., M.Si, the Staff of Departement of Chemistry Faculty of Sciences Brawijaya University, familiy and all of author's friends.

6. References

[1]. Belitz H.D. dan W. Grosch (1999), Food Chemistry, Springer, Germany, pp. 473-482.
[2]. Dalgleish, D. G., (1993), The Enzymatic Coagulation of Milk in Cheese, Chemistry, Physics and Microbiology, Vol. 1: General Aspects, 2nd, editor: Fox P. F., Chapman and Hall, London, pp. 69-100.
[3]. Erten, H., (2000), Fermentation of Glucose and Fructose by *Leuconostoc mesenteroides*, *Turkish Journal of Agriculture Forestry*, 24:527–532.
[4]. Fox, P. F., Guinee T. P., Cogan T. M. and McSweeney P. L. H., (2000), Fundamental of Cheese Science, Aspen Publishers, Maryland, pp. 383-387
[5]. Hariati, I., (2006), Pembuatan Keju Secara Fermentasi oleh Bakteri *Lactococcus lactis, Streptococcus thermophilus dan Leuconostoc mesenteroides*, Tesis, Sekolah Ilmu dan Teknologi Hayati (SITH) – ITB, Bandung.
[6]. Hill, A. R., (2000), Making Cheese at Home, Dairy Science and Technology, University of Guelph, pp. 1-2.
[7]. Juillard,V., Alain Guillot, Dominique Le Bars, dan Jean Claude Gripon, (1998), Specificity of Milk Peptide Utilization by *Lactococcus lactis*, *Applied and Environmental Microbiology*, 64(4): 1230-1236.
[8]. Malaka, R. and Amran L., (2005), Isolasi dan Identifikasi *Lactobacillus bulgaricus* Strain Ropy dari Yoghurt Komersial, *Jurnal Sains & Teknologi*, 5(1): 50-58.
[9]. Minard, R., (2000), Isolation of Casein, Lactose, and Albumin from Milk, Essay Pennsylvania State University, USA pp. 1-8.
[10]. Retno, E., Uki Y. and Ning S. D., (2005), Pembuatan Keju dari Susu Kacang Hijau dengan Bakteri *Lactobacillus bulgaricus*, *Ekuilibrium*, 4(2):58-63.
[11]. Salmah (2004), Analisa Pertumbuhan Mikroba pada Fermentasi, Universitas Sumatra Utara, Digital Library, pp. 1-10.
[12]. Scott, R., (1986), Cheesemaking Practice, Elsevier Applied Science Publishers, London, pp. 109-110.
[13]. Walstra, P., (1993), The Syneresis of Curd in Cheese, Chemistry, Physics and Microbiology, Vol. 1: General Aspects, 2nd, editor: Fox P. F., Chapman and Hall, London, pp. 141-191.
[14]. Nagopal and Sandine (1990), ……

Effect of Carbonization Temperature on Physical Properties of Coconut Shell Carbon

Meytij Jeanne Rampe [1], Bambang Setiaji [2], Wega Trisunaryanti [3], Triyono [4]

[(1)] Department of Chemistry, Faculty of Mathematics and Natural Science, Manado State University, North Sulawesi, Indonesia (meytij_rampe@yahoo.co.id)
[(2,3,4)] Department of Chemistry, Faculty of Mathematics and Natural Sciences, Gadjah Mada University, Yogyakarta, Indonesia

Abstract

The effect of carbonization temperature on physical properties of coconut shell carbon has been examined. The physico-chemistry examination has been done by varying the carbonization temperature of powder carbon and polyvinyl alcohol as raw material. Carbonization was conducted at 1000^{o}C and 1200^{o}C in argon atmosphere. The result showed that increasing of carbonization temperature could change the physical properties of materials carbon.

***Keywords**: coconut shell carbon, physical properties, polyvinyl alcohol.*

1. Introduction

Carbon composites play an important role in brake systems due to their combination of properties [1]. These materials are normally manufactured using a carbon-organic precursor. Carbon materials in the form graphite, glassy carbon, carbon fibers, etc. have been important players in development for several reasons [2]. They are available in a variety of forms and are generally in expensive; the slow kinetics of carbon oxidation lead to a wide useful potential range, particularly in the positive direction, and carbon has a rich surface chemistry, which can be exploited to influence reactivity [3]. In particular, a wide variety of chemical derivatization is possible on graphite and glassy carbon surfaces. Overall, these properties of carbon can be exploited to advantage provided the user is cognizant of the relationships between carbon materials properties, and surface preparation.

Knowledge of the densities of carbon materials phases, particles, processing additives, and bulk systems is important in processing for several reasons [4]. The raw-material storage capacities are directly dependent on the bulk density of the material. We need to know the particle density of raw materials and the phase density of liquids and additives to calculate volumetric proportions from the gravimetric batch composition and to ascertain settling tendencies. A change in a very precisely determined particle density may indicate a change in the phase structure, chemical composition, or porosity of the material [5-7].

The density of a particle is the mass / volume ratio of the particle. In a system of particles, the particle density refers to the mean density of all the different size particles. When the particles are nonporous, the particle density is referred to as the ultimate particle density and is the mean density of the solid phases constituting the particles.

Heating process conducted on coconut shell will produce a gradual change. The first stage is known as carbonization, the carbon samples into coke. The second stage is known as graphitization stage of change, so coke into graphite carbon with irregular structures tend to grow towards the graphite whose structure is irregular [2, 4, 8]. The nature of carbon is very dependent on raw material from which the carbon material is obtained, in addition to the methods and production conditions. The nature of carbon materials is very important in a variety of uses, primarily as an adsorbent, catalyst carrier, molecular sieves, electrode material, carbon structures and so forth.

Charcoal is a porous solid material and is the result of heating of the material containing the element carbon. Most of the pores are still covered with hydrocarbons, tar and other organic compounds and components consist of bonded carbon, ash, water, nitrogen and sulfur [9-12]. Charcoal can be made with direct or indirect heating in the pile and the furnace. In this dissociation process can produce charcoal in addition to other products in the form of distillate

and gas. Products that have commercial value primarily is charcoal.

Graphite is the modification of carbon which is stable under normal conditions. It has a structure consisting of planar layers (Figure 1). In the layer, each C atom is bonded covalently with three other C atoms. Every atom contributes one *p* orbitals and one electron to the delocalized bond system of the layer. This contributes a half-filled band, so we have a two – dimensional metallic state with the corresponding electrical conductivity. Between the layers weak van der Waals forces are the essential attraction forces. The bonds within the layer have a length of 142pm and the distance from layer to layer is 335pm. The high electric conductivity therefore only exists parallel to the layers, but not perpendicular to them. The layers are packed in a staggered manner (Figure 1), half of the atom of one layer is located exactly above atoms of layer below, and the other half are located over the ring centers.

Polyvinyl alcohol (PVA) as an organic adhesive [13] which is inert [14], has been used to obtain products with high density [15]. Further, reported with increasing sintering temperature and polyvinyl alcohol stimulants influence the occurrence of further grain growth with grain size larger. The growth structure of carbon and polyvinyl alcohol with temperature treatment is presented in Figure 2.

Density of a solid can be determined by measuring its mass in air and mass in liquid using a balance. For this purpose, the operations and calculations are also performed.

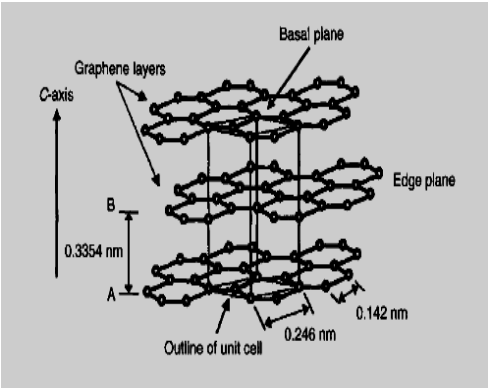

Figure 1. The structure of hexagonal graphite, with trigonal planar bonding within the grapheme layers.

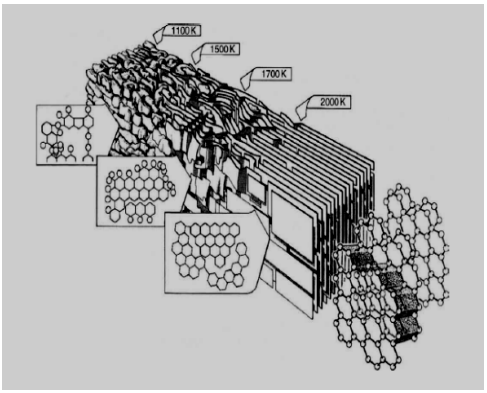

Figure 2. The diagram comprehensively models the structure changes which occur during the heat treatment of graphitizable carbon.

2. Experimental Details

Materials

Raw materials used in this study are charcoals produced by PT Tropica Nucifera Industry Bantul Yogyakarta as a source of carbon and polyvinyl alcohol as a stimulant (p.a. Merck), while Argon gas is used as inert atmosphere to gain the targeted condition.

Instrumentation

Calcination performed uses a tube-Thermolyne Furnaces (Sybron) Type 21100 with a maximum temperature of 1200^{o}C. Raw materials of calcinated charcoal have been done through 100 mesh grinding and sifting. For carbon materials, it is used Tarno compacted Grocki 312 model a maximum of 20 tons. Sintering is carried out using a Carbolite furnace-Edwards Pirani 501 A6D 1600^{o}C maximum temperature with argon gas as the atmosphere. Automatic Densimeter model D-S for automatically measuring density of solid carbon materials.

Procedure

Calcination and Charcoal Preparation

Carbon powder 100 mesh sieves calcined in an inert state through two stages: calcination at 600^{o}C for 3 hours in the condition of nitrogen gas [16, 25]; Concheso et al. 2009; Tae-Hwan et al. 2002), followed by purification charcoal powder by soaking for 24 hours with 1M HCl at room temperature. Carbon was washed with distilled water until the washing water shows a constant pH, and then dried in an oven at 110^{o}C for one night [5,14,16]. Mean while, re-calcinations also carried out at 750^{o}C for 3 hours in a condition of nitrogen gas [17].

The process of pressing and carbonization

Carbon powder that has been calcined was mixed with polyvinyl alcohol (PVA) as much as 0- 1% as stimulants. The next step, homogeneous mixture of polyvinyl alcohol powder calcinated and molded using a cylindrical mold with a diameter of ~15mm. Compaction was performed with pressing on one direction by means of Tarno Grocki 312 model with the thrust of 5 tons. The process of this stage was to produce the sample pellet (green compact).

Samples obtained in this way was dried at room temperature, followed by drying it at 110^{o}C, and then sintered at 1000^{o}C and 1200^{o}C, 5 and 10^{o}C/minute rate of rise of temperature, for 2 hours with the conditions of argon gas in the furnace Carbolite Edwards Pirani 501-A6D, cooling in furnace (annealing). This synthesis process produced dense coke carbon materials [2,8,9].

3. Result and Discussion

Tables 1 and 2 shows data density of carbon materials with stimulant PVA, 1000^{o}C sintering temperature, solvent and powder methods. The relationship between density and concentration of PVA are presented in Figure 3 and 4. Results of density measurements were seen at concentrations of 7.5% PVA powder method with a value of 1.984 g/cm^3. Density values given provide a relationship with the porosity of carbon materials.

Table 1. The Density of Carbon Materials at Sintering Temperature of 1000^{o}C (solvent method)

PVA (wt %)	Average Mass in Air	Average Mass in Water	Density (g/cm^3)
0	4.262	0.430	1.112
2.5	0.687	0.402	0.631
5	2.898	0.193	1.071
7.5	1,601	0.003	1.001

Table 2. The Density of Carbon Materials at Sintering Temperature of 1000^{o}C (powder method)

PVA (wt %)	Average Mass in Air	Average Mass in Water	Density (g/cm^3)
0 %	3.924	0.490	1.145
7.5 %	1.411	0.674	1.984
10 %	0.430	0.876	0.309

Tables 3 and 4 shows data density of carbon materials with stimulant PVA, 1200^{o}C sintering temperature, solvent and powder methods. The relationship between density and concentration of PVA are presented in Figure 5 and 6. Results of density measurements were seen at concentrations of 7.5% PVA with a value of 1.930 g/cm^3. The density of graphite is 2.22 g/cm^3 [18].

Table 3. The Density of Carbon Materials at Sintering Temperature of 1200^{o}C (solvent method)

PVA (wt %)	Average Mass in Air	Average Mass in Water	Density (gr/cm^3)
0	3.512	0.541	1.181
2.5	0.695	1.229	0.367
5	2.127	0.261	0.948
7.5	1.111	0.190	0.829

Table 4. The Density of Carbon Materials at Sintering Temperature of 1200^{o}C (powder method)

PVA (wt %)	Average Mass in Air	Average Mass in Water	Density (g/cm^3)
0	3.924	0.490	1.145
7.5	1.411	0.674	1.984
10	0.430	0.876	0.309

The treatment temperature on the value of the density of carbon material shows the temperature increases the density in general. Increasing the density of C atoms in which the diffusion occurs in the arrangement of the structure and reduced porosity of the carbon amorphous carbon materials developed towards a more regular basis.

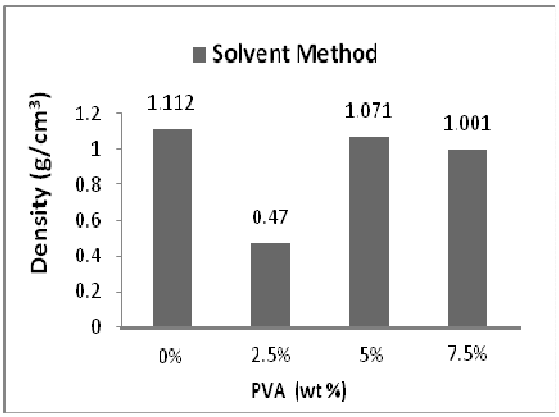

Figure 3. The relationship between concentration of PVA with density on the sintering temperature 1000^{o}C (solvent method)

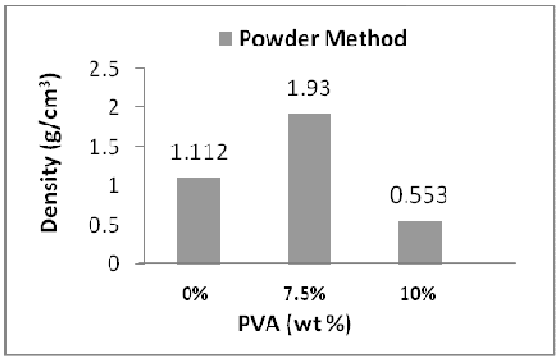

Figure 4. The relationship between concentration of PVA with density on the sintering temperature 1000°C (powder method)

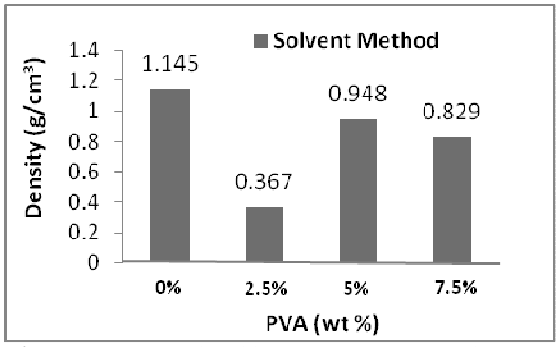

Figure 5. The relationship between concentration of PVA with density on the sintering temperature 1200°C (solvent method)

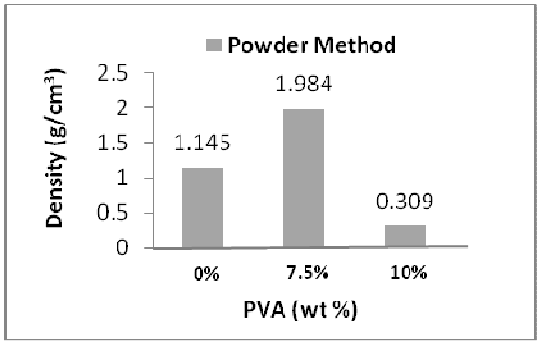

Figure 6. The relationship between concentration of PVA with density on the sintering temperature 1200°C (powder method)

4. Conclusion

The results showed that the concentration of PVA and the method of mixing affect the density of carbon materials. The increasing sintering temperature changes the physical properties of carbon materials.

5. Acknowledgements

The author would like to thank the Department of Chemistry, Faculty of Mathematics and Natural Sciences; and Department of Mechanical and Industrial Engineering, Faculty of Engineering, Gadjah Mada University, Yogyakarta; for the provision of laboratory facilities.

6. References

[1]. Lin C.C. and C.C. Yen (2007), RF Oxygen Plasma Treatment of Activated Carbon Electrodes for Electrochemical Capacitors, *J. Appl. Electrochem.,* 37, 813-817.

[2]. Mendez, S. and R. Santamaria (2008), Structural Changes During Pitch-Based Carbon Granular Composites Carbonization, *J. Mater. Sci.,* 43, 906-921.

[3]. Sahajwalla, V., A.S. Mehta and R. Khanna (2004), Influence of Chemical Compositions of Slag and Graphite on the Phenomena Occurring in the Graphite/Slag Interfacial Region, *Metall. Mat Trans B*., 35B, pp.75-83.

[4]. Kissinger, P.T and W.R. Heineman (1996), Laboratory Techniques in Electroanalytical Chemistry, Marcel Dekker, New York.

[5]. Muller, U (1992), Inorganic Structural Chemistry, Ulrich Muller, John Wiley & Sons, New York.

[6]. Wiratmoko, A. and J. W. Halloran (2009), Fabricated Carbon from Minimally Processed Coke and Coal Tar Pitch as a Carbon-Sequestering Construction Material, *J. Mater. Sci*., 44, 2097-2100.

[7]. Elsayed, M.A., P.J. Hall and M.J. Heslop (2007), Preparation and Structure Characterization of Carbon Prepared from Resorcinol-Formaldehyde Resin by CO_2 Activation, *Adsorption*, 13, 299-306.

[8]. Gupta, S., V. Sahajwalla., J. Burgo., P. Chaubal and T. Youmans (2005), Carbon Structure of Coke at High Temperatures and Its Influence on Coke Fines in Blast Furnace Dust, *Metall and Mat. Trans* B., 36B, 385-394.

[9]. Fraga, M.A *et al.* (2002), Properties of Carbon-Supported Platinum Catalysts: Role of Carbon Surface Sites, *J. Catal*., 209: 355-364.

[10]. Yin, Y., J. Zhang and C. Sheng (2009), Effect of Pyrolysis Temperature on the Characteristic, Micro-Structure and Reactivity of NO Reduction, *Korean J. Chem. Eng*., 26 (3), 895-901.

[11]. Buchman, A. and R.G. Bryant (1999), Molded Carbon-Carbon Composite Based on Microcomposite Technology, *App. Comp. Mat.,* 6, 309-326.

[12]. Souza, B. S., A. P. D. Moreira., A. M. R. F. Teixeira (2009), TG-FTIR Coupling to Monitor the Pyrolysis Products from Agricultural Residues, *J. Therm. Anal. Calorim*., 97, 637-642.

[13]. Miyazaki, K.., N. Maskawa., W. Kobayashi., M. Kaku., N. Yasumaru and J. Kiuchi (2005), Reflectivity in Femtosecond-Laser-Induced Structural Changes of Diamond-like Carbon Film, *Appl. Phys. A*, 80, 17-21.

[14]. Kang, L., J. Zhang., H. Lian, and M. Luo (2007), Co-Pyrolysis Characteristic of Coal and Natural Gas, *Korean J. Chem. Eng.*, 24(3), 508-511.

[15]. Ebner, F., C. Hofer and E.M. Maurer (2004), Conversion of Carbonaceous Material to Graphite Within the Grey Wache Zone of the Eastern Alps, *Int. J. Earth Sci*., 93, 959-973.

[16]. Gonzales, M., A.R.L. Canovas and M.T. Hernandez (2005), Pyrolytic and Graphitic Carbon: Pressure Induced Phases Segregated in Polycrystalline Corundum, *Appl. Phys. A*., 81, 865-869.

[17]. Lalena, J. N., D.A. Cleary., E.E. Carpenter and N.F. Dean (2008), Inorganic Materials Synthesis and Fabrication, Wiley-Interscience, pp. 28-48.

[18]. Klotz, I.M and R.M. Rosenberg (2008), Chemical Thermodynamics: Basic Concepts and Methods, John Wiley & sons, New Jersey.

Analysis of Dinamic Behavior on Chua's Circuit

Moh Anas Kurnia R [1], Erna Apriliani [2]

[1,2] Mathematic, ITS, Surabaya, Indonesia (anaskurnia2009@yahoo.co.id)

Abstract

Chua's circuit is a circuit chaotic system which was constituted by electronic circuits and then often used to predict the state of a dynamic system that gives unexpected result. Chua circuit is a simple circuit, easily observable, universal. This research analyzes the dynamic behavior of Chua's circuit, fixed point, local stability, bifurcation. We analyze in which parameter, the chaos is occurred. We make simulation the behavior dynamical of Chua's circuit. The problems will be solved by finding the history of chaos, chaos theory review, to include some variables that influence, which then enter the parameter range explored further by using a software program MatLab.7.1, exactly ode 45. We have simulated with change R parameter of resistor. Result shows that the simulation does not occur chaotic in Chua's circuit if R > 2035 Ω or R< 2430 Ω.

Keywords: *Chua's circuit, chaos, fixed point, bifurcation.*

1. Introduction

What is chaos? Scientists use the word chaos is to imply that a dynamic system that is predicted to give an unexpected result before [1]. Chaos show uncertainly, chaos, randomness, namely: random movement without goal, without purpose or without a particular principle. The universe of this dynamic seems to be working through a linear system, but many are nonlinear and cannot be understood through linear systems, such as clouds, growth of trees, coastlines, waves, etc., which at first glance seem random and not regularly. This system is called chaotic Chaos associated with chaotic systems, random and not linear arising from small changes in initial conditions and lead to large changes in outcomes or outputs in a system.

Application of chaos theory or random has been widely used in various fields, for example random wave system in a variety of telecommunications equipment at both transmitters and receivers that serves to disguise voice or data that is confidential, in the field of economics to know the fluctuations in prices of many staple commodities, stocks, and forex. In the field of engineering to determine the effect of turbulence on a plane so as to minimize the occurrence of aviation accidents, in the field of biology that is a model of cell growth - cell virus that endanger human life including the HIV virus, H5N1, and others.

To learn about chaos, which is often used is the Chua Circuit, it is because the nature of the Chua circuit which has the simplicity of the circuit, universal in a variety of problems caused, cheap in terms of cost and privileges in terms of controlling chaos [1].

2. Experimental Detail

In this chapter will analyze the fixed point, stability, bifurcation and the value of the parameter range R (resistor) that does not cause the occurrence of chaos in Chua circuits.

Stability Analysis

Step by step analysis of local stability Chua circuit model is as follows:

a. Determining the equilibrium point

In accordance with law of Kirchhoff's I and II, then the differential equations of the Chua circuit as follows [1]:

$$\begin{aligned}\frac{dv_1}{dt} &= \left(\frac{1}{C_1}\right)\left(\frac{1}{R}(v_2 - v_1) - f(v_1)\right)\\ \frac{dv_2}{dt} &= \left(\frac{1}{C_2}\right)\left(\frac{1}{R}(v_1 - v_2) + i_L\right)\\ \frac{di_L}{dt} &= \left(\frac{1}{L}\right)\left(-v_2 - R_0 i_L\right)\end{aligned} \quad (1)$$

where,

C_1 = parameter of capacitor 1 (F = Farad)
C_2 = parameter of capacitor 2 (F = Farad)
R = resistance to change parameters (Ω = ohm)
R_0 = parameter in the coil resistance (Ω = ohm)
L = coil parameters (H = Henry)
N_R = parameter Chua diode
v_1 = parameter voltage through C_1 (V = Volts)

v2 = parameter voltage through C_2 (V = Volts)
i_L = current through the coil (A = Ampere)
With $f(v_1) = G_b v_1 + ½(G_a - G_b)(|v_1 + Bp| - |v_1 - Bp|)$
and can also be written to the following equation

$$f(v_1) = G_b v_1 + (G_a - G_b) f_1(v_1), \quad (2)$$

for

$$f_1(v_1) = \begin{cases} v_1, if \ |v_1| < Bp(v_1) \\ sign(v_1) Bp(v_1), otherwise \end{cases} \quad (3)$$

Fixed point is obtained if,

$$\frac{dv_1}{dt} = 0, \ \frac{dv_2}{dt} = 0, \ \frac{di_L}{dt} = 0$$

From equation (1) can be written as :

$$\begin{aligned} \dot{v}_1 &= f_1(v_1, v_2, i_L) \\ \dot{v}_2 &= f_2(v_1, v_2, i_L) \\ \dot{i}_L &= f_3(v_1, v_2, i_L) \end{aligned} \quad (4)$$

So we obtained fixed point as follows:

$$\begin{aligned} \bar{v}_1 &= -(R_0 + R) i_L \\ \bar{v}_2 &= -R_0 i_L \\ \bar{i}_L &= i_L \end{aligned} \quad (5)$$

For value i_L=0, is obtained $(\bar{v}_1, \bar{v}_2, \bar{i}_L) = (0,0,0)$, which physically means that no electric current flowing in the electrical circuit. But, if the value $i_L \neq 0$, then the fixed point as: $(\bar{v}_1, \bar{v}_2, \bar{i}_L) = (-(R_0 + R) i_L, -R_0 i_L, i_L)$.

b. Linearized system

Therefore equation (1) is a system of nonlinear equations, to solve the equation system must be determining of Jacobinya matrix as follows:

$$A = \begin{bmatrix} \frac{\partial f1}{\partial v1} & \frac{\partial f_1}{\partial v_2} & \frac{\partial f_1}{\partial i_L} \\ \frac{\partial f_2}{\partial v_1} & \frac{\partial f_2}{\partial v_2} & \frac{\partial f_2}{\partial i_L} \\ \frac{\partial f_3}{\partial v_1} & \frac{\partial f_3}{\partial v_2} & \frac{\partial f_3}{\partial i_L} \end{bmatrix},$$

thus obtained from equation (1)

$$A = \begin{bmatrix} -\frac{1}{C_1 R} - f'(v_1) & \frac{1}{C_1 R} & 0 \\ \frac{1}{C_2 R} & -\frac{1}{C_2 R} & \frac{1}{C_2} \\ 0 & -\frac{1}{L} & -\frac{R_0}{L} \end{bmatrix} \quad (6)$$

c. Determining eigenvalue

Eigenvalues obtained by solving the characteristic equation, must be finished the characteristic $|\lambda I - J| = 0$,

$$|A - \lambda I| = \left| \begin{bmatrix} -\frac{1}{C_1 R} - f'(v_1) & \frac{1}{C_1 R} & 0 \\ \frac{1}{C_2 R} & -\frac{1}{C_2 R} & \frac{1}{C_2} \\ 0 & -\frac{1}{L} & -\frac{R_0}{L} \end{bmatrix} - \begin{bmatrix} \lambda & 0 & 0 \\ 0 & \lambda & 0 \\ 0 & 0 & \lambda \end{bmatrix} \right| = 0$$

$$\left| \begin{bmatrix} -\frac{1}{C_1 R} - f'(v_1) - \lambda & \frac{1}{C_1 R} & 0 \\ \frac{1}{C_2 R} & -\frac{1}{C_2 R} - \lambda & \frac{1}{C_2} \\ 0 & -\frac{1}{L} & -\frac{R_0}{L} - \lambda \end{bmatrix} \right| = 0$$

and can be obtained :

$$\begin{aligned} &\lambda^3 + \left(f'(v_1) + \frac{1}{C_1 R} + \frac{R_0}{L} + \frac{1}{C_2 R} \right) \lambda^2 + \\ &\left(\frac{R_0 f'(v_1)}{L} + \frac{f'(v_1)}{C_2 L} + \frac{R_0}{L C_1 R} + \frac{1}{L C_2} + \frac{R_0}{L C_2 R} \right) \lambda + \\ &\left(\frac{1}{L C_1 C_2 R} + \frac{f'(v_1)}{L C_2} + \frac{R_0 f'(v_1)}{L C_2 R} \right) = 0 \end{aligned} \quad (7)$$

Equation (7) can be written as:

$$\lambda^3 + a_1 \lambda^2 + a_2 \lambda + a_3 = 0$$

(8)

Furthermore, Routh-Hurwitz stability criterion can be applied to the equation by defining

$$H_1 = a_1, \ H_2 = \begin{vmatrix} a_1 & 1 \\ a_3 & a_2 \end{vmatrix}, \ H_3 = \begin{vmatrix} a_1 & 1 & 0 \\ a_3 & a_2 & a_1 \\ 0 & 0 & a_3 \end{vmatrix},$$

to be stable, if and only if and $H_1 > 0, H_2 > 0$ and $H_3 > 0$. For $H_1 = a_1$, to obtained

$$H_1 = f'(v_1) + \frac{1}{C_1 R} + \frac{R_0}{L} + \frac{1}{C_2 R}$$

This system will be stable if $H_1 > 0$

$H_1 = f'(v_1) + \frac{1}{C_1 R} + \frac{R_0}{L} + \frac{1}{C_2 R} > 0$, furthermore to $H_2 = \begin{vmatrix} a_1 & 1 \\ a_3 & a_2 \end{vmatrix} = a_1 a_2 - a_3$, next to because $H_2 > 0$, then that be written $a_1 a_2 > a_3$

Next to $H_3 = \begin{vmatrix} a_1 & 1 & 0 \\ a_3 & a_2 & a_1 \\ 0 & 0 & a_3 \end{vmatrix}$, be obtained

$$H_3 = a_1 a_2 a_3 - (a_3)^2$$

This system will be stable if $H_3 > 0$, so

$$a_1 a_2 a_3 - (a_3)^2 > 0$$
$$a_1 a_2 a_3 > (a_3)^2 \qquad (9)$$

For condition $a_3 > 0$, this $a_1 a_2 > a_3$ is obtained in accordance with the requirements $H_2 > 0$ for stability, where $a_1 a_2 > a_3$. Furthermore, if $a_1 > 0$ and $a_3 > 0$, then the result $a_2 > 0$, so that in general equation (8) can be said to be stable if $a_1 > 0$, $a_2 > 0$, $a_3 > 0$, and $a_1 a_2 > a_3$.

To fully this stability requirements as in equation (8), then the values C_1, C_2, R, R_0, L of parameters are substituted, with $f(v_1)$ a function, it must be $f'(v_1)$ determined first. From equation (1) obtained $f(v_1) = G_b v_1 + \frac{1}{2}(G_a - G_b)(|v_1 + B_p| - |v_1 - B_p|)$, obtained the value for $f(v_1)$ as follows :

$f(v_1) = G_b v_1 + (G_a - G_b) Bp$, for $v_1 > Bp$

$f(v_1) = G_b v_1 + (G_a - G_b) v_1$, for $-Bp < v_1 < Bp$

$f(v_1) = G_b v_1 - (G_a - G_b)(-Bp)$, for $v_1 < -Bp$

Next will be determined derived from $f(v_1)$, in particular by :

$$f'(v_1) = \frac{\partial f(v_1)}{\partial v_1} + \frac{\partial f(v_1)}{\partial v_2} + \frac{\partial f(v_1)}{\partial i_L}$$

From equation (1), $f'(v_1)$ can be determined as follows:

$$f'(v_1) = \frac{\partial\left(G_b v_1 + (G_a - G_b) Bp\right)}{\partial v_1} + \frac{\partial\left(G_b v_1 + (G_a - G_b) Bp\right)}{\partial v_2} + \frac{\partial\left(G_b v_1 + (G_a - G_b) Bp\right)}{\partial i_L}$$

$$f'(v_1) = \frac{\partial\left(G_b v_1 + (G_a - G_b) Bp\right)}{\partial v_1} + 0 + 0$$

$$f'(v_1) = G_b \qquad (10)$$

in the same way also obtained

$$f'(v_1) = G_a \qquad (11)$$

for $f(v_1)$ the others with substituting equation (10) is $f'(v_1) = G_b$ ke in equation (7) we obtained :

$$\lambda^3 + (G_b + \frac{1}{C_1 R} + \frac{R_0}{L} + \frac{1}{C_2 R})\lambda^2 + (\frac{R_0 G_b}{L} + \frac{G_b}{C_2 L} + \frac{R_0}{L C_1 R} + \frac{1}{L C_2} + \frac{R_0}{L C_2 R})\lambda + (\frac{1}{L C_1 C_2 R} + \frac{G_b}{L C_2} + \frac{R_0 G_b}{L C_2 R}) = 0$$

3. Result and Discussion

Calculation Results

From the formula that had been predetermined, then the value of each parameter for the Chua electronic circuit inserted by the values $C_1 = 10x10^{-9}$, $C_2 = 100x10^{-9}$, $R_0 = 10$, $L = 22x10^{-3}$, $G_a = -0{,}757x10^{-3}$ $G_b = -0{,}410x10^{-3}$, with the chosen value of R = 2050, from the calculations have been obtained :

$$\lambda^3 + (54.113)\lambda^2 + (478.935.696{,}2)\lambda + 22.172.948.814.944{,}6 = 0 \qquad (12)$$

with respect to equation (8) and (12) then for value a_1, a_2, a_3 as follows :

$a_1 = 54.113 > 0$

$a_2 = 478.935.696{,}2 > 0$

$a_3 = 22.172.948.814.944{,}6 > 0$

So the value of

$a_1 a_2 = (54.113)(478.935.696{,}2)$

$= 25.916.686.427.278,6$

When compared with the value a_1a_2 of a_3, then $a_1a_2 > a_3$, so that requirements the criteria $a_1 > 0$, $a_2 > 0$, $a_3 > 0$, and $a_1a_2 > a_3$ is said to equation (12) can be said requirement of the Routh-Hurwitz stability criterion for a system that can be expressed as a stable system. By using the help of software Mat.Lab.7.1, Eigen value is obtained as follows

$$\left.\begin{aligned}\lambda_1 &= -52.973\\ \lambda_2 &= -570 + 2.045i\\ \lambda_3 &= -570 - 2.045i\end{aligned}\right\} \qquad (13)$$

From acquisition Eigen values obtained to $\lambda_1, \lambda_2, \lambda_3$, all value have negative real part so that it can be said that the fixed point $(\bar{v}_1, \bar{v}_2, \bar{i}_L) = (-2060i_L, -10i_L, i_L)$ is stable. Substituting equation (11) is $f'(v_1) = G_a$ in equation (7) is obtained:

$$\lambda^3 + (G_a + \frac{1}{C_1R} + \frac{R_0}{L} + \frac{1}{C_2R})\lambda^2 + (\frac{R_0G_a}{L} + \frac{G_a}{C_2L} + \frac{R_0}{LC_1R} + \frac{1}{LC_2} + \frac{R_0}{LC_2R})\lambda + (\frac{1}{LC_1C_2R} + \frac{G_a}{LC_2} + \frac{R_0G_a}{LC_2R}) = 0$$

Furthermore, the value of each - each parameter for electronic circuit inserted by the values: $C_1 = 10x10^{-9}$, $C_2 = 100x10^{-9}$, $R_0 = 10$, $L = 22x10^{-3}$, $G_a = -0,757x10^{-3}$, $G_b = -0,410x10^{-3}$, with the chosen value of R = 2050, from the calculations :

$$\lambda^3 + (54.113)\lambda^2 + (478.935.694,67)\lambda + 22.172.948.656.477,9 = 0 \qquad (14)$$

Considering equation (8) and (14) values a_1, a_2, a_3 obtained as follows:

$a_1 = 54.113 > 0$

$a_2 = 478.935.694,67 > 0$

$a_3 = 22.172.948.656.477,9 > 0$

So the value of $a_1a_2 = (54.113)(478.935.694,67)$
$= 25.916.647.209.422$

When compared with the value a_1a_2 of a_3, then $a_1a_2 > a_3$, so that requirements the criteria $a_1 > 0$, $a_2 > 0$, $a_3 > 0$, and $a_1a_2 > a_3$ and is said to equation (14) can be said requirement of the Routh-Hurwitz stability criterion for a system that can be expressed as a stable system. By using the help of software Mat.Lab.7.1, Eigen value is obtained as follows:

$$\left.\begin{aligned}\lambda_1 &= -52.973\\ \lambda_2 &= -570 + 2.045i\\ \lambda_3 &= -570 - 2.045i\end{aligned}\right\} \qquad (15)$$

From acquisition Eigen values obtained $\lambda_1, \lambda_2, \lambda_3$, all value have negative real part so that it can be said that the fixed point $(\bar{v}_1, \bar{v}_2, \bar{i}_L) = (-2060i_L, -10i_L, i_L)$ is stable.

Analysis of bifurcation

In this section will analyze the possibility of bifurcation in dynamical behavior of Chua electronic circuit system of equations (1), one of the requirements of the occurrence of bifurcation is the existence of at least one eigen value is equal to zero [2]. From the fixed point $(\bar{v}_1, \bar{v}_2, \bar{i}_L) = (-2060i_L, -10i_L, i_L)$ bifurcation analysis will happen or not. Suppose equation (8) has one Eigen value = 0, then the characteristic equation can be constructed as follows:

$$(\lambda - a)(\lambda - b)(\lambda - c) = 0$$
$$(\lambda - a)(\lambda^2 - (b + c)\lambda + bc) = 0$$
$$\lambda^3 - (a + b + c)\lambda^2 + (ab + ac + bc)\lambda - abc = 0$$
$$\lambda^3 - (a + b + c)\lambda^2 + (ab + ac + bc)\lambda = abc$$
$$(\lambda^2 - (a + b + c)\lambda + (ab + ac + bc))\lambda = abc$$

If there is Eigen values = 0, for example $(\lambda_1 = 0)$, it is obtained $(\lambda^2 - (a + b + c)\lambda + (ab + ac + bc))(0) = abc$

result $abc = 0$, so that from equation (7) obtained $\frac{1}{LC_1C_2R} + \frac{f'(v_1)}{LC_2} + \frac{R_0f'(v_1)}{LC_2R} = 0$, (16)

from equation (13) and equation (15) that all Eigen values nothing is zero for $(\bar{v}_1, \bar{v}_2, \bar{i}_L) = (-2060i_L, -10i_L, i_L)$ fixed point, it is proving not happen bifurcation.

Next will constructing occurrence of bifurcation, as was previously required that the bifurcation occurs if there is at least one Eigen

value is equal to zero. From equation (16) obtained

$$\frac{1}{LC_1C_2R}+\frac{f'(v_1)}{LC_2}+\frac{R_0f'(v_1)}{LC_2R}=0$$

And can be written

$$\frac{R+C_1R^2f'(v_1)+C_1RR_0f'(v_1)}{LC_1C_2R^2}=0 \qquad (17)$$

Therefore parameter value of $L,C_1,C_2,R\neq 0$, hence equation (17) can be written

$R+C_1R^2f'(v_1)+C_1RR_0f'(v_1)=0$

$R\left(1+C_1Rf'(v_1)+C_1R_0f'(v_1)\right)=0$, because $R\neq 0$, therefore

$$R=\frac{-\frac{1}{C_1}-R_0f'(v_1)}{f'(v_1)} \qquad (18)$$

From equation (18), substituting to equation (10) and (11) then obtained

$$R_a=\frac{-\frac{1}{C_1}-R_0G_a}{G_a}, \text{ for } f'(v_1)=G_a \text{ dan}$$

$$R_b=\frac{-\frac{1}{C_1}-R_0G_b}{G_b}, \text{ for } f'(v_1)=G_b$$

From the calculations have been done with the help of software Mat.Lab. 7.1 and the values obtained are $R_a=2{,}43902x10^{11}$ and $R_b=1{,}321x10^{11}$, both the good and has a large enough value, and not in accordance with the decision R = 2050, so that the construction of the bifurcation in equations (17) with fixed point $(\bar{v}_1,\bar{v}_2,\bar{i}_L)=(-2060i_L,-10i_L,i_L)$, there is no bifurcation.

The simulation results

Next will be seen the simulation results with parameters $C_1=10nF$, $C_2=100nF$, $R_0=10\Omega$, $L=22mH$, $G_a=-0{,}757mS$, $G_b=-0{,}410mS$, $Bp=1{,}70V$, with parameters R = 2050 Ω, using the help of software Mat.Lab. 7.1. image is obtained as given in Figures 1, 2 , 3.

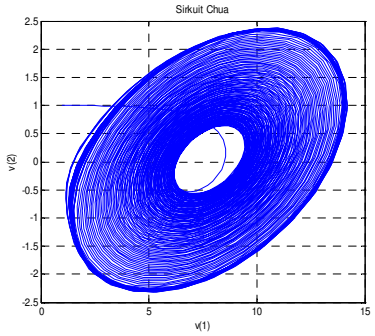

Figure 1

Figure 1 shows v_1,v_2 seen that $(\bar{v}_1,\bar{v}_2,\bar{i}_L)=(-2060i_L,-10i_L,i_L)$ in the stable, does not happen Chaos and bifurcation, in accordance with the analysis that has been done.

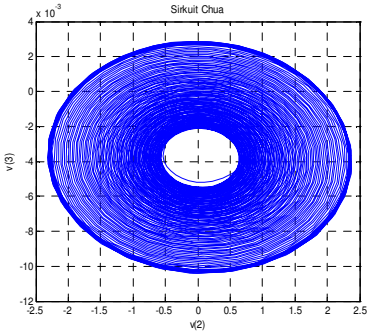

Figure 2

Figure 2 shows v_2,i_L seen that $(\bar{v}_1,\bar{v}_2,\bar{i}_L)=(-2060i_L,-10i_L,i_L)$ the stable fixed point does not occur Chaos and bifurcation does not occur, according to the analysis conducted.

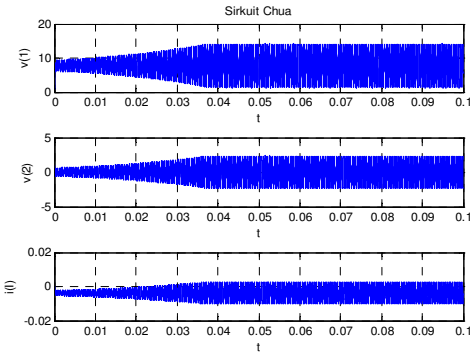

Figure 3

Figure 3.3 shows v_1, v_2, i_L against t, which means the system is stable and there is no chaos at $(\bar{v}_1, \bar{v}_2, \bar{i}_L) = (-2060 i_L, -10 i_L, i_L)$

4. Conclusion

In this paper, it was concluded that a fixed point on the model of Chua circuit is stable if it have $a_1 > 0$, $a_2 > 0$, $a_3 > 0$ and $a_1 a_2 > a_3$ conditions within system, and at the parameter values R = 2050, Chua circuit model has a stable fixed point $(\bar{v}_1, \bar{v}_2, \bar{i}_L) = (-2060 i_L, -10 i_L, i_L)$, there is no chaos and no bifurcation occurs. To obtain a state of chaos can be done by changing the value of the parameter R with another value. This analysis of bifurcation in the Chua circuit model is still very limited in $(\bar{v}_1, \bar{v}_2, \bar{i}_L) = (-2060 i_L, -10 i_L, i_L)$ fixed point and can be developed for fixed point to others. For example changing the others parameter value of capacitor or diode nonlinear.

5. Acknowledgements

The first author wants to express his gratitude to Dr. Erna Apriliani, for inspiration and motivation in this paper. With her enthusiasm, inspiration and great efforts in explaining things clearly and simple, and making mathematics fun for me.

6. References

[1]. Broek, v.d. T.H.A. (2004), Chua's Circuit: Synchronisation, Departement of Electrical Enginering, Eindhoven of Technology.

[2]. S. Wiggins (1990), *Introduction to Applied Nonlinier Dynamical System and Chaos*, 2rd edition, Springer-Verlag, New York.

[3]. Dariel M Maranhao and Carmen P.C. Prado (2005), "Evolution of Chaos in The Matsumoto-chua circuit: A Simbolic Dynamic Approach". *Brazilian Journal of Physics*, Vol 35, no.1, March, 2005.

[4]. Anonymous, *Routh-Hurwizt Stability Criterion,* http://www.personal.rdg.ac.uk/~shshawin/dnb/routhhurwizt.pdf (accessed on 8 June 2010)

Immobilization Lipase from *Mucor miehei* using Silica Gel Matrix

Ninik Afrizatus Sholichah [1], Anna Roosdiana [2], Sutrisno [3]

[(1,2,3)] Department of Chemistry, Faculty of Mathematics and Sciences, Brawijaya University, Malang, Indonesia (afriza.ninik87@gmail.com; aroos@ub.ac.id; tris_mc@ub.ac.id)

Abstract

Lipase immobilization using physical adsorption method in silica gel was applied for lactocyl oleic esterification. Esterification was done in tert-butanol as solvent. The lipase was isolated from Mucor miehei and purified using 20-60% fraction ammonium sulphate. This research was conducted to determine the optimum condition of lipase immobilization using silica gel as the matrix involving the optimum shaking time and lipase concentration, the effect of lipase adsorbed on its specific activity, and the effect of immobilization on immobilized lipase and free lipase specific activity. The lipase activity was calculated based on the number of reacted fatty acid during esterification. The determination of lipase activity was conducted using acid base titrimetry, which was done before and after incubation. The result of this research showed that free lipase with a fraction of 20-60% has a specific activity of 2.073 µg/mg minute, while the immobilized lipase has a specific activity of 3.017 µg/mg minute. The optimum condition of lipase immobilization was achieved at 3 hours of shaking time and at a lipase concentration of 1960 ppm, which resulted in the mass of adsorbed lipase 85.040 mg/g silica gel. The mass of lipase absorbed in silica gel affected its specific activity. At the mass of adsorbed lipase 18.610 – 94.000 mg/g silica gel, a decrease in the specific activity was resulted (3.017 – 1.925 µg/mg minute).

Keywords: *lipase, Mucor miehei , immobilization, silica gel, lactocyl oleic.*

1. Introduction

Lipase is one of the enzymes that are widely used in industry. Lipase can be used as a biocatalyst for the reaction of hydrolysis, esterification, alcoholysis, interesterification, asidolisis, and aminolisis [10]. One role of lipase in esterification is to catalyze the synthesis of sugar esters. Sugar esters are widely used in food industry, cosmetics, pharmaceutical, and biosurfactant [11]. Lactose ester (lactocyl oleic) is one type of sugar esters which is rarely synthesized and studied.

Lipase can be isolated from microbes, plants and animals. Isolation of microbial lipase is more advantageous than lipases isolated from plants and animals, because of the easier isolation process, the fermentation techniques which are relatively inexpensive, and the stable enzyme isolation results in an organic solvent, so it can be used in organic synthesis [7]. Lipase isolated from *Mucor miehei*, *Rhizopus delemar, and Chromabacterium viscosum* are used for esterification of glycerol and fatty acids, forming diglycerides. Esterification reaction produces a high average yield, reaching more than 80%. The biggest yield was generated by the lipase isolated from *M. miehei* reached 85% [2]; therefore *M. meihei* was used for isolation of lipase in this study. Enzyme purification was carried out using ammonium sulfate salts on the fraction of 20-60%, because at this fraction, the activity and specific activity of lipase reached its highest, hence more lipase can be deposited, and thus high purity of the lipase could be obtained [6].

The use of the free enzyme in the esterification process is less efficient, because the enzyme was not stable enough, difficult to separate from the substrate and product, and is difficult to reuse. Therefore, to overcome this problem immobilization was done, so as to minimize the cost of enzyme production [14].

Immobilization is the method used to restrict the movement of certain enzymes in the matrix space. When compared with the enzyme in its free state, the immobilized enzyme has several advantages, such as increased stability, easily recovered, and the resulting product has high purity [13]. Immobilization can be done through the binding on the carriers (matrix support). Lipase immobilization can be influenced by shaking time and lipase concentration. The shaking time and lipase concentration will affect mass of absorbed lipase, therefore contributing to the activity and specific activity of lipase [1]. In

this research, the supporting matrix used was silica gel.

Silica gel is a hydrophilic adsorbent. In general, silica gel is widely used for industrial purposes [4]. In this research, silica gel 60H matrix that has a pore size of 60Å, no binding substance (binder), and a pH of 7 was used.

2. Experimental Details

Rejuvenation of Mucor miehei culture

M. miehei culture was planted in the PDA media using the tip of a needle loop aseptically. Then, the tube was closed with sterile cotton and then placed in an incubator at a temperature of 30º C for 4 days.

Inoculum production

10 mL of sterile distilled water was added to the *M. miehei* cultur which has grown in the slope of the solid media for 4 days. This was then shaken and transferred into 100 ml of liquid media, then incubated on the shaker at 150 rpm at room temperature for up to 24 hours. Spore suspension was served as inoculum.

Production and isolation of lipase

100 mL of sterile liquid medium was added to 12 ml of inoculum aseptically and then incubated at room temperature in a shaker for 96 hours. Isolation of lipase was done by adding 10 mL of 0.2 M phosphate citrate buffer pH 5 into the conical flask containing the mixture of cultures. Then the mixture of cultures and buffer was centrifuged at 3000 rpm at 4°C for 1 hour. The supernatant obtained was crude extract of lipase.

Purification of the crude lipase extracts

Lipase crude extract was purified using ammonium sulfate fraction of 20-60%. Firstly, a fraction 0-20% was made by adding 8.55 g $(NH_4)_2SO_4$ to 75 mL of crude extract lipase, and then stirred until the $(NH_4)_2SO_4$ dissolved. This was then centrifuged at 3000 rpm, temperature of 4°C for 30 minutes. The supernatant obtained was mixed with 19.65g of $(NH_4)_2SO_4$ and centrifuged, resulting a precipitate and supernatant fractions of 20-60%.

The precipitate formed at the 20-60% fraction was purified by dialysis, by adding 10 mL of 0.2 M phosphate citrate buffer pH 5 to the supernatant, inserted in cellophane bag, and then soaked in 100 mL of 0.07 M phosphate citrate buffer pH 5, stirred frequently at 4°C. Then, soaking buffer solution was replaced with a new soaking buffer until all the salt was separated. To make sure that dialysis is completed, testing was done by taking 5 mL of soaking buffer, putting it in a reaction tube and added with 1 mL of 0.1 M HCl solution and 5 drops of $BaCl_2$ solution 0.1 M. If there is no precipitation formed, dialysis was finished.

Preparation of silica gel matrix

Preparation of silica gel matrix was done by heating 5 g of silica gel 60 H size 100-200 mesh in an oven at 100°C for 4 hours. The heating is useful to eliminate water molecules contained in the silica gel.

Lipase immobilization

To determine the optimum shaking time of lipase immobilization, lipase was diluted with 2 ml of citrate-phosphate buffer 0.2 M pH 5 in a total volume of 5mL. The enzyme solution was put in conical flask containing 0.1 g of silica gel. The mixture was then incubated in a shaker at room temperature with a speed of 100 rpm for 1, 2, 3, 4 and 5 hours. The solution was then filtered using Buchner funnel. The filtrate obtained was tested for the remaining protein content, and were plotted on a *Casein* standard curve to show the relationship between shaking time to the mass of absorbed lipase. Determination of optimum lipase concentration used the same procedure but the concentration of lipase used was 0.49, 0.98, 1.47, 1.96, 2.45 mg/mL and the silica gel used was 0.1g. Silica gel was filtered and tested for enzyme activity, while the filtrate is tested for the remaining protein content. The result was then plotted on a *Casein* standard curve to show the relationship between the concentrations of enzyme in solution with the mass of adsorbed lipase.

Determination of protein content

Determination of protein content was done by spectrophotometric method using Biuret reagent. A total of 2 mL of lipase solution plus 8 mL of Biuret reagent and 2 mL of 5000 ppm *Casein* solution was shaken and incubated for 30 minutes at 50°C. Subsequently, absorbance was measured at maximum wavelength of 550 nm casein. By plotting the absorbance value on the *Casein* standard curve regression equation, the protein content was obtained. To determine the remaining protein content after immobilization, the same method was done using 2 mL of filtrate taken from the immobilization. The amount of lipase adsorbed was determined by the following equation:

$$W_{absorbed} = W_{before\ immobilization} - W_{after\ immobilization}$$

Determination immobilized lipase activity

Lactose and oleic acid with mole ratio of 1:10 (0.036 g: 0.282 g) was mixed and put into conical flask. A 5mL of tert-butanol and enzyme (lipase immobilized + silica gel matrix), weight 0.05g, was then added. The mixture was incubated for 24 hours at 50°C. After that, an addition of 3 drops of phenolphtalein indicator was made, then titrated with 0.1767 M KOH until it changes color from colourless to pink and does not disappear for 30 seconds. As a blank titration, the mixture before incubation was used. As for the free lipase activity, determination was done by the same method using 2 mL of purified enzyme. Below is the equation to determine the lipase activity.

$$\text{Lipase activity} = \frac{\text{titration volume (blank - sample)} \times [\text{KOH}]}{\text{enzim volume} \times \text{incubation time}} \times Mr_{(\text{oleic acid})}$$

3. Result and Discussion

Determination of Optimum Conditions of Immobilization Lipase using Silica Gel

The Optimum of shaking time

The mass of adsorbed lipase on silica gel matrix is influenced by the shaking time. Shaking time is the contact time required by the lipase to bind to the silica gel matrix. If lipase is at rest, then diffusion through the surface of silica gel lipase will be slow, therefore shaking will be necessary to accelerate the adsorption.

Determination of optimum shaking time was done by varying shaking time. The variation used was 1, 2, 3, 4, and 5 hours. Immobilization was done using the same lipase concentration and silica gel matrix mass. The concentration of lipase used in the determination of shaking time was 0.98 mg / mL and the mass silica gel 60H used was 0.1 g. Determination of optimum shaking time to mass of absorbed lipase in silica gel matrix is shown in Figure 1.

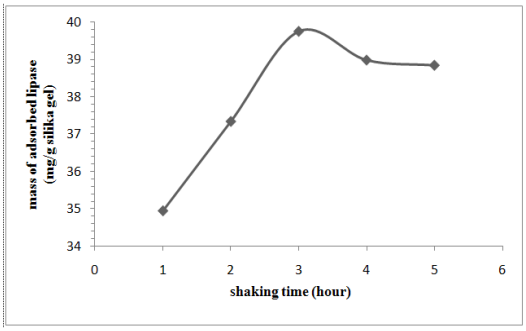

Figure 1. The relationship between shaking time to mass of adsorbed lipase on silica gel

In the shaking time of 1 to 3 hours, the mass of adsorbed lipase increased quite sharply. Increasing contact time will lead to more and more interaction between the lipase with the surface of silica gel, causing the mass of lipase adsorbed on the surface of silica gel to increase. At 3 hours of shaking time, the lipase adsorbed reached the highest mass, showing the optimum shaking time. In the shaking time of 3 hours to 5 hours, the mass of adsorbed lipase does not decrease significantly. This is due to reversible physical adsorption and the weak bonding between the lipase with pore silica gel, resulting in a competition amongst the lipase to bind to the hydrophilic silica gel. The competition allows the substitution of other lipases, resulting in the release of the bond between the lipase with the surface of silica gel (desorption).

Immobilization of lipase using silica gel matrix is a method of immobilization by physical adsorption. The silica gel matrix is an amorphous inorganic polymer containing polar groups, *i.e.*, siloksan (Si–O–Si) and silanol (Si–OH), distributed on the surface. The silica gel matrix is hidrophilic matrix. The enzyme has both hydrophilic and hydrophobic sites. Lipase is an enzyme that has a globular size in three-dimensional form of 35Å x 36Å x 42Å [9], while 60 H silica gel has a pore size of approximately 60 Å.

Silica gel has a pore size larger than the size of lipase, allowing lipase to be adsorbed in porous silica gel. Lipase is a protein that has hydrophilic, amino acid residues *i.e.* tyrosine threonine 29 and 18 [8]. Interactions that can occur between silica gel matrix and lipase are hydrogen bonds. This bonding occurs between the hydrophilic amino acid residues (tyrosine 29 and treonin18) with oxygen atoms from the siloksan group on silica gel. This is could be caused by the presence of interaction between electronegative oxygen atoms in silica gel with hydrogen atoms from the lipase. This hydrogen atom covalently bonds with oxygen atoms in the lipase. Predicted lipase interaction with the surface of silica gel is illustrated in Figure 2.

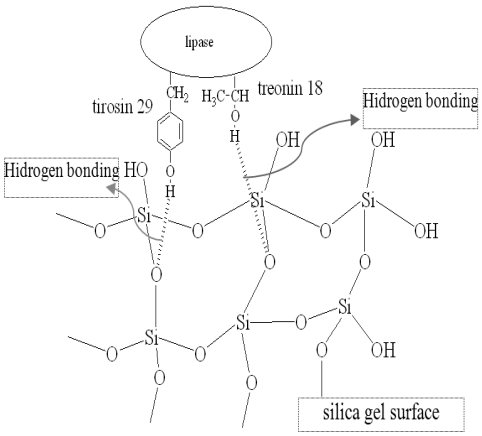

Figure 2. Illustration of interactions between lipase and surface of silica gel

The optimum of lipase concentration

Lipase concentration affects the mass of lipase adsorbed on silica gel. The greater the concentration of lipase, the mass of lipase absorbed tends to increase until it reaches a certain amount. Adsorption is constant if there is a balance between the rates of adsorption and desorption. Determination of optimum lipase concentration was conducted by varying the initial lipase concentration to 490, 980, 1470, 1960, and 2450 ppm by weight of 0.1g of silica gel and the same shaking time for 3 hours. The result is shown in Table 1 and Figure 3.

Table 1. Lipase concentration and mass of absorbed lipase

Initial lipase concentration (ppm)	Lipase concentration remaining (ppm)	Mass of absorbed lipase (mg/g silica gel)
490	170	18.610
980	193	42.300
1470	267	64.030
1960	357	85.040
2450	753	94.000

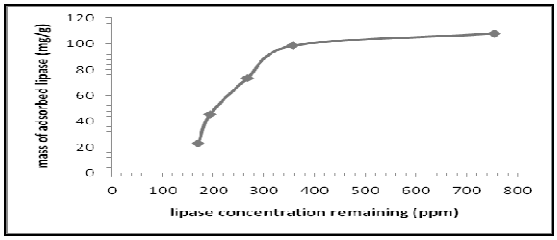

Figure 3. The relationship between the concentrations of remaining lipase to the mass lipase adsorbed on silica gel

In the initial lipase concentration of 490 – 1960ppm, the mass of adsorbed lipase increased sharply. This is caused by a large chemical potential difference between the bulk phases with the surface of silica gel. Consequently, the rate of diffusion of lipase to the surface of silica gel increases, thus increasing the mass of lipase adsorbed. In the initial lipase concentration of 1960ppm, the situation began to balance. Under this circumstance, silica gel pores have been filled by the lipase, thus causing the adsorption rate to slow down. In the initial lipase concentration of 1960-2450ppm, the increase in mass of absorbed lipase is insignificant. Therefore, it can be estimated that the initial lipase concentration of 1960ppm was the optimum concentration that produces an adsorbed lipase mass of 85.040 mg / g of silica gel.

The effect of absorbed lipase mass to specific activity of immobilized lipase

Determination of lipase activity was conducted by enzymatic reacting between lactose with oleic acid by lipase, thus resulting lactocyl oleic ester. In determining the activity, tert-butanol solvent was used. Tert-butanol is a non-polar organic solvent that suitable for esterification catalyzed by lipase. High lipase esterification activity was obtained by using non-polar organic solvents [5]. Because of the hydrophobic solvent, the water will tend to participate in the enzyme molecule, therefore it will increasing the solubility and stability of the enzyme.

Determination of specific activity of immobilized lipase was made on the immobilization of lipase concentration variation. Calculation of specific activities was carried out by calculating the lipase activity compared to the mass of adsorbed lipase. Lipase activity was determined through the oleic lactocyl esterification. Determination of activities was based on the amount of fatty acid oleic acid which reacts during the esterification reaction. Whilst, mass of immobilized lipase was determined by calculating the initial mass minus the mass of lipase unbound to the silica gel matrix. Effect of lipase adsorbed mass on the enzyme specific activity is given in Figure 4.

Table 2. Mass of adsorbed lipase, activity, and specific activity

Mass of adsorbed Lipase (mg/g silica gel)	Activity (µg/g menit)	Specific activity (µg/mg menit)
18.610	69.323	3.017
42.300	115.538	2.540
64.030	127.092	1.727
85.040	161.753	1.636
94.000	207.969	1.925

Based on this research, it is found that increased lipase adsorbed mass tends to lower the specific activity of immobilized lipase. This is caused by the imbalance between the increase in lipase activity and the increase in mass of lipase adsorbed. This imbalance is due to the increasing amount of absorbed lipase mass, which will inhibit the binding of substrate to the active site of lipase. As a result, the enzyme-substrate complex will be difficult to be formed, so that the lipase esterification reaction will be difficult to occur and the specific activity of lipase decreased.

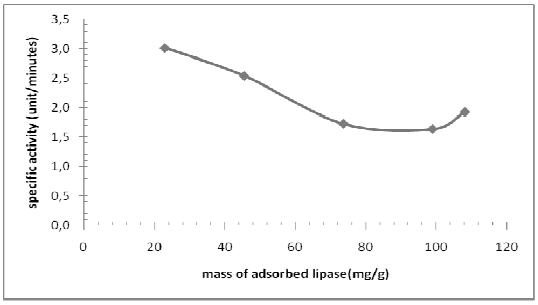

Figure 4. The relation between the mass of adsorbed lipase with the specific activity of immobilized lipase

In the esterification of lactocyl oleic using lipase as a catalyst, lipase does not act as hydrolase. In this reaction, lipase acts as synthetase because that combines two molecules of oleic acid and lactose. Prediction of lactocyl oleic is presented in Figure 5.

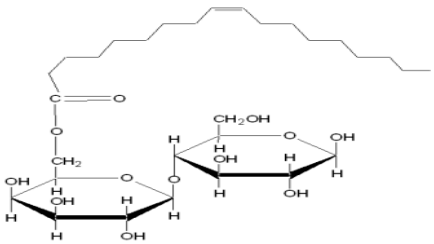

Figure 5. Structure of lactocyl oleic

The effect of immobilization on the specific activity of immobilized lipase

To determine the effect of immobilization, a calculation of the specific activity increase of immobilized lipase to free lipase was done. Based on Table 3, it can be seen that when the mass of the lipase adsorbed is 18.610 – 94.000 mg/g silica gel, there is a lowering of lipase specific activity. This decrease happens because the more lipase adsorbed on the surface of silica gel, it will inhibit the substrate to bind to active site of lipase. As a result, the complex of lipase with the substrate will be difficult to be formed, hence the lipase esterification reaction will be difficult to occur and the specific activity of lipase decreased. Optimal immobilization happens at a mass of adsorbed lipase of 18.610 mg/g silica gel, resulting in an increased of specific activity by 1.455 times.

Table 3. Specific activity of immobilized and free lipase

Mass of adsorbed lipase (mg/g silica gel)	Specific activity (µg/mg minute)	Increase in specific activity(times)
2.450*	2.073	1.000
18.610	3.017	1.455
42.300	2.540	1.225
64.030	1.727	0.833
85.040	1.636	0.789
94.000	1.925	0.929

**) free lipase (mg/mL)*

4. Conclusion

Optimal immobilization was achieved at 3 hours shaking time and at a lipase concentration of 1960ppm, resulting in a lipase adsorbed mass of 85.040 mg / g silica gel.

Increased mass of lipase adsorbed will lower the specific activity of immobilized lipase. At a lipase absorbed mass of 18.610 to 94.000 mg/g silica gel, the specific activity decreased (3.017 – 1.925 g / mg min).

Immobilization using silica gel matrix increases the specific activity of immobilized lipase, which is 1.455 times compared to the specific activity of lipase in its free state.

5. Acknowledgements

The author would like to thank to Dra. Anna Roosdiana, M.App.Sc. and Drs. Sutrisno, MSi. (Laboratory of Biochemistry UB), who provides all facilities of this research

6. References

[1]. Ariesta, R., (2009), Amobilisasi Enzim Lipase dari *Mucor miehei* Menggunakan Matriks Polietilen, Skripsi, Jurusan Kimia Fakultas Matematika dan Ilmu Pengetahuan Alam, Universitas Brawijaya, Malang.

[2]. Berger, M., K. Laumen dan M.P. Schneider (1992), Enzymatic Esterification of Glycerol Lipase – Catalyzed Synthesis of Regioisomerically Pure 1,3-sn-Diacylgliserol**,** J. Am. Oil Chem. Soc*,* 69: 955-960.

[3]. David, A.E., N.S. Wang, V.C. Yang dan A.J. Yang (2006), Chemically Surface Modified Gel (CSMG): An Excellent Enzyme-Immobilization Matrix for Industrial Processes. *J. Biotechnol.* 125: 395–40.

[4]. Khaeruddin, J.M., E. Cathaputra and H.P. Winoto (2007), Produksi Isopropil Alkohol Murni untuk Aditif Bensin yang Ramah Lingkungan sebagai Wujud Pemanfaatan Produk Samping pada Industri Gas Alam, Laporan Penelitian, ITB, pp 11-12.

[5]. Nurhasanah and D. Herasari (2008), Pemurnian Enzim Lipase dari Bakteri Lokal dan Aplikasinya dalam Reaksi Esterifikasi. Seminar Nasional Sains???

[6]. Mahardika (2007), Amobilisasi Enzim Lipase dari *Mucor miehei* dalam Aluminosilikat Mesopori untuk Esterifikasi, Skripsi, Jurusan Kimia Fakultas Matematika dan Ilmu Pengetahuan Alam, Universitas Brawijaya, Malang, 22-23.

[7]. Mohanasrinivasan, P. D., K.P. Dipinsha, C.M. Unnithan, K.M. Viswanath dan C.S. Devi (2009), A Comparative Study of the Lipase Yield by Solid State and Submerged Fermentation Using Fungi Species from Biopharmaceutical Oil Waste, *Afr. J. Biochem,* 8: 73-76.

[8]. Schulz, T., J. Pleiss dan R.D. Schmid (2000), Stereoselectivity of *Pseudomonas cepacia* Lipase toward Secondary Alcohols: A Quantitative Model, *J. Protein Sci*. 9:1053–1062.

[9]. van Pouderoyen, G., T. Eggert, K.E. Jaeger and B.W. Dikjstra (2001), The Crystal Structure of *Bacillus subtilis Lipase*: A Minimal α/β Hydrolase Fold Enzyme, *J. Mol. Bio,* 309: 215-226.

[10]. Wulan, P.P.D.K., M.T. Rejoso and H. Hermansyah (2009), Reaksi Hidrolisis Minyak Zaitun Menggunakan Lipase *Rhizopus oryzae* yang Diimmobilisasi melalui Metode Adsorpsi, Departemen Teknik Kimia Fakultas Teknik, Universitas Indonesia, Jakarta.

[11]. Yoo, I. S., S.J. Park and H.H. Yoon (2007), Enzymatic Synthetis of Sugar Fatty Acid Ester, *J. Ind. Eng. Chem,* 13(1): 1-6.

[12]. Zarcula, C., R. Croitoru, L. Corici, Csunderlick and F. Peter (2009), Improvement of Lipase Catalytic Properties by Immobilization in Hybrid Matrices, *Proceedings of World Acad. Sci. Eng. Technol,* 40:179-180.

[13]. Zubrine, A., S. Budrine, N. Gorochovceva, T. Romaskevic, E. Matullionis and G. Dienys (2003), Immobilization of Hydrolase onto Chitosan Microparticles, *Food Chem. Technol,* 4: 226-230.

[14]. Zuhra, C. F (2002), Penyediaan Asam Eikosapentanoat (EPA) dan Asam Dokosaheksanoat (DHA) melalui Transesterifikasi Minyak Ikan dengan Etanol yang dikatalisis oleh Lipase, Fakultas Matematika Dan Ilmu Pengetahuan Alam, Jurusan Kimia, Universitas Sumatera Utara, Medan.

Existence of Global Solutions to a System of Nonlinear Klein-Gordon Equations

Ratno Bagus Edy Wibowo

Department of Mathematics, Faculty of Mathematics and Natural Science, Brawijaya University, Malang, 65145, Indonesia (rbagus@ub.ac.id)

Abstract

We consider the initial value problem for a system of nonlinear Klein-Gordon equations with quadratic nonlinearities. We prove the existence of scattering states, namely, the asymptotic stability of small solutions in the neighborhood of free solutions for small initial data in the weigthed Sobolev spaces H4,3 (R3)×H3,3 (R3). Our method can be applicable to a system of massive Dirac-massless Klein-Gordon equations in three space dimensions.

We consider a system of semi-linear Klein-Gordon equations (1)

$$\begin{cases} \left(\partial_t^2 - \Delta + m_j^2\right) u_j = \mathcal{N}_j\left(u, \partial u\right), (t,x) \in \mathbf{R} \times \mathbf{R}^n, \\ u_j\left(0,x\right) = u_{1j}^0\left(x\right), \partial_t u_j\left(0,x\right) = u_{2j}^0\left(x\right), x \in \mathbf{R}^n, \end{cases}$$

where $0 \le j \le l$, $m_j > 0$, $u = (u_1, \ldots, u_l)$, the partial derivative $\partial = (\partial_t, \partial_x) = (\partial_t, \partial_1, \ldots, \partial_n)$, the spatial dimension n = 3. We assume that the non- linearity $N_j(y) \in C^{p0}(C^{(2+n)l}; C)$ satisfy the estimates (2)

$$|\mathcal{N}_j(y)| \le C|y|^2, |\partial_y \mathcal{N}_j(y)| \le C|y|,$$
$$|\partial_y^\alpha \mathcal{N}_j(y)| \le C, 2 \le |\alpha| \le p_0.$$

for all |y| ≤ 1. Thus the nonlinearities Nj include quadratic terms, when we restrict our attention to small solutions. Our purpose in the present paper is to prove the global solutions to (1) in the neighborhood of free solutions in the lower order Sobolev spaces comparing with the previous works [1], [2], [3]. We put

$$w_j(t,x) = \begin{pmatrix} w_{1j} \\ w_{2j} \end{pmatrix} \equiv \frac{1}{2}\left(\mathrm{a}u_j + i\mathrm{b}\langle i\nabla\rangle_{m_j}^{-1}\partial_t u_j\right)$$
$$= \frac{1}{2}\begin{pmatrix} u_j + i\langle i\nabla\rangle_{m_j}^{-1}\partial_t u_j \\ u_j - i\langle i\nabla\rangle_{m_j}^{-1}\partial_t u_j \end{pmatrix},$$
$$w_j(0,x) = w_j^0 = \begin{pmatrix} w_{1j}^0 \\ w_{2j}^0 \end{pmatrix} \equiv \frac{1}{2}\left(\mathrm{a}u_{1j}^0 + i\mathrm{b}\langle i\nabla\rangle_{m_j}^{-1}u_{2j}^0\right)$$
$$= \frac{1}{2}\begin{pmatrix} u_{1j}^0 + i\langle i\nabla\rangle_{m_j}^{-1}u_{2j}^0 \\ u_{1j}^0 - i\langle i\nabla\rangle_{m_j}^{-1}u_{2j}^0 \end{pmatrix},$$
$$\mathcal{L}_{m_j} = E\partial_t + iA\langle i\nabla\rangle_{m_j}$$

and

$$F_j(w) = \begin{pmatrix} F_{1j}(w) \\ F_{2j}(w) \end{pmatrix}$$
$$= i\mathrm{b}\mathcal{N}_j\left(w_{1j} + w_{2j}, \langle i\nabla\rangle_{m_j}(w_{1j} - w_{2j}), \nabla(w_{1j} + w_{2j})\right),$$

where

$$\mathrm{a} = \begin{pmatrix} 1 \\ 1 \end{pmatrix}, \mathrm{b} = \begin{pmatrix} 1 \\ -1 \end{pmatrix}, E = \begin{pmatrix} 1 & 0 \\ 0 & 1 \end{pmatrix}, A = \begin{pmatrix} 1 & 0 \\ 0 & -1 \end{pmatrix},$$
$$\langle i\nabla\rangle_{m_j} = \sqrt{m_j^2 - \Delta}, m_j > 0.$$

Then the nonlinear Klein-Gordon equation (1) can be rewritten as a system of equations

$$(3)\quad \begin{cases} \mathcal{L}_{m_j} w_j = \langle i\nabla\rangle_{m_j}^{-1} F_j(w), (t,x) \in \mathbf{R}\times\mathbf{R}^n, \\ w_j(0,x) = w_j^0(x), x \in \mathbf{R}^n, j = 1,\ldots,l., \end{cases}$$

and the solution u_j of (1) can be represented by $u_j = w_{1j} + w_{2j}$. We introduce free evolution groups of (3)

$$\mathcal{U}_{m_j}(t) = \begin{pmatrix} e^{-it\langle i\nabla\rangle_{m_j}} & 0 \\ 0 & e^{it\langle i\nabla\rangle_{m_j}} \end{pmatrix}.$$

The operator

$$\begin{aligned} &\mathcal{J}_{m_j}(t) \\ &= \langle i\nabla\rangle_{m_j} \mathcal{U}_{m_j}(t) x \mathcal{U}_{m_j}(-t) = \langle i\nabla\rangle_{m_j} \left(xE + iA\langle i\nabla\rangle_{m_j}^{-1} t\nabla \right) \\ &= E\langle i\nabla\rangle_{m_j} x + iAt\nabla = xE\langle i\nabla\rangle_{m_j} - E\langle i\nabla\rangle_{m_j}^{-1}\nabla + iAt\nabla \end{aligned}$$

is useful for obtaining the time decay estimates of solutions. We have $[L_{mj}, J_{mj}] = 0$, since $[x, \langle i\nabla\rangle_{mj}] = \langle i\nabla\rangle^{-1}{}_{mj}\nabla$ and the notation

$$\begin{aligned} &\mathcal{J}_{m_j} = \left(\mathcal{J}_{m_j}^{(1)}, \ldots, \mathcal{J}_{m_j}^{(n)} \right) \\ &= \left(\langle i\nabla\rangle_{m_j} \mathcal{U}_{m_j}(t) x_1 \mathcal{U}_{m_j}(-t), \ldots, \langle i\nabla\rangle_{m_j} \mathcal{U}_{m_j}(t) x_n \mathcal{U}_{m_j}(-t) \right). \end{aligned}$$

However it is difficult to calculate the action of J_{mj} on the nonlinearity N_j. Therefore we use the first order differential operator

$$\mathcal{Z} = E(t\nabla + x\partial_t) = \left(\mathcal{Z}^{(1)}, \ldots, \mathcal{Z}^{(n)} \right)$$

which is closely related to J_{mj} by

$$\mathcal{Z}^{(k)} = \mathcal{L}_{m_j} x_k - iA\mathcal{J}_{m_j}^{(k)}$$

and it almost commutes with L_{mj} since

$$\left[\mathcal{L}_{m_j}, \mathcal{Z} \right] = -A\langle i\nabla\rangle_{m_j}^{-1} \nabla \mathcal{L}_{m_j}.$$

Denote the usual Lebesgue space by $L^p(\mathrm{R}^n) = \{ \phi \in S' ; \|\phi\|L^p(\mathrm{R}^n) < \infty\}$, where the norm $\|\phi\|L^p(\mathrm{R}^n) = (\int_{\mathrm{Rn}} |\phi(x)|^p dx)^{1/p}$, if $1 \le p < \infty$ and $\|\phi\|L^\infty(\mathrm{R}^n) = \sup_{x\in \mathrm{R}^n} |\phi(x)|$, if $p = \infty$. Weighted Sobolev space

$$\begin{aligned} H_p^{m,k}(\mathbf{R}^n) = \Big\{ &\phi; \|\phi\|_{H_p^{m,k}(\mathbf{R}^n)} \\ &\equiv \|\langle x\rangle^k (1-\Delta)^{\frac{m}{2}} \phi\|_{L^p(\mathbf{R}^n)} < \infty \Big\}, \end{aligned}$$

where $m, k \in \boldsymbol{R}$, $1 \le p \le \infty$, $\langle x\rangle = \sqrt{(1 + |x|^2)}$, $\Delta = \sum_{i=1}^n \partial_i^2$.

We also write for simplicity $H_2^{m,k}(\mathbf{R}^n), H^m(\mathbf{R}^n) = H_2^{m,0}(\mathbf{R}^n)$, so we usually omit the index 0 if it does not cause confusion. We also use the same notations for the vector functions. We introduce function space of the initial data for the massive Klein-Gordon equations

$$\begin{aligned} \mathbf{X}^{4,3}(\mathbf{R}^n) = \Big\{ &\left(u_{1j}^0, u_{2j}^0\right); \\ &\sum_{j=1}^{l} \left(\|u_{1j}^0\|_{H^{4,3}(\mathbf{R}^n)} + \|u_{2j}^0\|_{H^{3,3}(\mathbf{R}^n)} \right) < \infty \Big\} \end{aligned}$$

.

By the $\mathbf{X}_\delta^{4,3}(\mathbf{R}^n)$ we denote a closed ball of radius $\delta > 0$ with a center at the origin in the space $X^{4,3}(\mathbf{R}^n)$.
Different positive constants we denote by the same letter C. Now we state the main result.

Theorem 1.
Let condition (2) be fulfilled with $p_0 = 4$. Then there exists $\varepsilon > 0$ such that for any initial data $(u_{1j}^0, u_{2j}^0) \in \boldsymbol{X}_{\epsilon_0}^{4,3}(\boldsymbol{R}^3)$ with $\epsilon_0 \in \left(0, \varepsilon^{\frac{4}{3}}\right]$ the Cauchy problem (1) has a unique global solution u such that

$$u_j \in C\left([0,\infty); H^{4,3}(\boldsymbol{R}^3)\right) \cap C^1\left([0,\infty); H^{3,3}(\boldsymbol{R}^3)\right)$$

and

$$\|u_j(t)\|_{L^\infty(\boldsymbol{R}^3)} \leq C\langle t\rangle^{-\frac{3}{2}\left(1-\frac{2}{q}\right)}$$

for all $t \geq 0, 1 \leq j \leq l,$ *where* $2 \leq q < \infty$.

To prove the Theorem 1, we consider the following lemmas to prove time decay estimates through the operator *Jmj*, involving the operators *Z* and *Lmj* for any smooth and decaying functions.

Lemma 2.
Let $m > 0$. Then the estimate is valid

$$\|\phi\|_{L^p(R^n)} \leq C\langle t\rangle^{-\frac{n}{2}\left(1-\frac{2}{p}\right)} \|\phi\|_{H^\nu(R^n)}^{1-\frac{n}{3}\left(1-\frac{2}{p}\right)} \|\mathcal{U}_m(-t)\mathcal{J}_m\phi\|_{H^{\nu-1,\frac{1}{2}}(R^n)}^{\frac{n}{3}\left(1-\frac{2}{p}\right)} + C\langle t\rangle^{-\frac{n}{2}\left(1-\frac{2}{p}\right)} \|\phi\|_{H^\nu(R^n)}^{1-\frac{n}{3}\left(1-\frac{2}{p}\right)} \|\mathcal{U}_m(-t)\phi\|_{H^{\nu-1,\frac{1}{2}}(R^n)}^{\frac{n}{3}\left(1-\frac{2}{p}\right)}$$

and

$$\|\phi\|_{L^p(R^n)} \leq C\langle t\rangle^{-\frac{n}{2}\left(1-\frac{2}{p}\right)} \sum_{|\alpha|\leq 2} \|\mathcal{J}_m^\alpha\phi\|_{H^{\nu-2}(R^n)}^{\frac{n}{6}\left(1-\frac{2}{p}\right)} \|\phi\|_{H^\nu(R^n)}^{1-\frac{n}{3}\left(1-\frac{2}{p}\right)} \times \|\mathcal{J}_m\phi\|_{H^{\nu-1}(R^n)}^{\frac{n}{6}\left(1-\frac{2}{p}\right)} + C\langle t\rangle^{-\frac{n}{2}\left(1-\frac{2}{p}\right)} \|\phi\|_{H^\nu(R^n)}$$

for all $t \geq 0$, *where* $\nu = \left(\frac{n}{2}+1\right)\left(1-\frac{2}{p}\right), 2 \leq p < \frac{2n}{n-3}$ *and* $n \geq 3$, *provided the right-hand sides are finite.*

Lemma 3.
Let $m > 0$. Then the estimate is valid

$$\|\phi\|_{L^p(R^n)} \leq C\langle t\rangle^{-\frac{n}{2}\left(1-\frac{2}{p}\right)} \left(\sum_{|\beta|\leq 2} \|\mathcal{Z}^\beta\phi\|_{H^\nu(R^n)} + \|\mathcal{L}_m\mathcal{Z}\phi\|_{H^{\nu-2,1}(R^n)} + \left(\|\mathcal{L}_m\mathcal{Z}\phi\|_{H^{\nu-1,2}(R^n)} + \langle t\rangle \|\mathcal{L}_m\mathcal{Z}\phi\|_{H^{\nu-1,1}(R^n)}\right)^{\frac{1}{2}} \times \|\mathcal{L}_m\phi\|_{H^{\nu-1,1}(R^n)}^{\frac{1}{2}} \right)$$

for all $t \geq 0$, *where* $\nu = \left(\frac{n}{2}+1\right)\left(1-\frac{2}{p}\right), 2 \leq p < \frac{2n}{n-3}$ *and* $n \geq 3$, *provided the right-hand side is finite.*

Acknowledgement
The author wishes to thank to Prof. Nakao Hayashi for providing nice working conditions during stay in Osaka University and for his continuous encouragements and valuable advices. This is part of a joint work with Prof. N. HAYASHI and Prof. PAVEL. I. NAUMKIN.

References

[1]. Bachelot, Probl`eme de Cauchy global pourdes syst`emes de Dirac-Klein-Gordon, Ann. Inst. Henri Poincar´e, 48(1988), pp. 387-422.
[2]. V. Georgiev, Global solution of the system of wave and Klein-Gordon equations, Math. Z.,203(1990), pp. 683-698.
[3]. S. Klainerman, Global existence of small amplitude solutions to nonlinear Klein-Gordon equations in four space time dimensions, Commun.Pure Appl. Math., 38(1985), pp. 631-641.

Ranked Clusterability Model of Dyad Data in Social Network

R. B. Fajriya Hakim [1], Subanar [2], Edi Winarko [3]

[(1)] Statistics Department, Faculty of Mathematics and Natural Sciences, Indonesia Islamic University (UII), Jogjakarta, Indonesia (hakimf@fmipa.uii.ac.id)
[(2,3)]Mathematics Department, Faculty of Mathematics and Natural Sciences, Gadjah Mada University, Jogjakarta, Indonesia (ewinarko@ugm.ac.id)

Abstract

The dyad as a substantial portion of triads or larger structure formed a ranked clusterability model in social network. Ranked clusterability model of dyads postulates that the hierarchical clustering process starts from the mutual dyads which occur only within clusters then stop until all of the mutual dyads grouped. The hierarchy process continues to cluster the asymmetric dyads which occur between clusters but at different levels. Then the last process is clustering the null dyads, which is clustered at the end of the hierarchy after all of asymmetric dyads grouped and occur only between clusters at the same level of the hierarchy. This paper exploring a ranked clusterability model of dyads from a simple example of social network and representing it to the new sociomatrix that gives better facility to view the whole network than conventional sociomatrix and presents the result in a dendrogram network data. This model gives a new insight to the development of advanced technology and science in a clustering study of emerging social network.

Keywords*: dyad data, ranked clusterability model, social network, network actor.*

1. Introduction

Social networking sites have bombarded the Internet and become one of the most past time trends of all time which have a wide range of people who used them on a daily basis over more than past ten years since the Internet itself. Social Networking sites are a growing phenomenon that have become something more interesting and useful on users' communication. The analysis of social networks, on the other side, become a truly emerging field also. This field has emerged as a key technique in modern sociology, anthropology, geography, social psychology, business, marketing, information science and organisational studies. Social network theory representing a social relationships in terms of nodes and their ties. Nodes are the individual users or actors within the networks, and ties are the relationships or linkages between the actors.

The focus of the analysis lies on the relationships and the ties between actors within the network and there are many opportunities to use a form of analysis that would enable a view of how actors interact with each other. The study about how actors interact with each other will provide new knowledge to the assesment of overall network. The segmentation or clustering about the interaction of actors in the social network has become a focus on marketing science or political sciences. Different in the unit analysis of conventional statistics that use individual as an object of observation, the social network analysis use an entity that consisting of a collection of individuals and the linkages among them.

Network analysis focus on two actors and their ties (dyads), three actors and their ties (triads) or larger systems (subgroups) or entire networks, but in the actual networks, most of the information is at the dyad level and in the real social networks in which the dyad is necessarily embedded, all those other actors intertwine with one or more of its members. A substantial portion of triadic or subgroups or entire networks structure is explained by nodal and dyadic features [1]. Any dyad needs to exist within such groups and is therefore accountable to them to some extent of grouping analysis. In its present form it dates back to Davis and Leinhardt [2] and briefly summarized by Wasserman and Faust [3] that introduced ranked clusterability model for network data and described it as a building that involves a three type of dyad connection.

This paper gives a detailed account of the dyadic approach to ranked clusterability analysis, including how this method considering a level of connection between dyad and differs from the more common individualistic approach when the dyad and not the individual are used as the unit of analysis and presents the result in the dendrogram network data.

2. Studies about dyad

Kenny et al. [7] have explored about dyadic data analysis. They considered that any relation in the social network occur in dyad relationship because the dyad is fundamental unit of interpersonal interaction and interpersonal relations. Most of their methodological and data-analytic approaches used conventional statistical method and do not give more emphasize about three types of dyadic relationship which involves mutual, null and asymmetric relationship that could make dyad grouping. Yablonsky [8] insisted that two actor interaction or dyad is a foundation of both individual and group strength in the social network. His research explored a theory of the dyad and its dimensions and also implications to each member's individual social atom and emphasize the dyad as the nucleus of its own social atom in such sociometric situations.

DeCoster [6] gave the flowchart to examine data from groups and dyads using Anova, he considered about the independene and nonindependence as a relation of an actor in the analysis of variance techniques. Aurifeille and Medlin [9] has applied a study about dyad in business science, especially about segmentation of business partnership. They describe the business partnership as a dyadic structure that influences the firm's performance and using the relationship modes of merging, teaming and sharing. Their dyad segmentation strategies comply the capacity of dyadic relationship to reflect the modes of partnership. Menon and Elkan [10] studied the problem of predicting labels associated with dyad members using new method which learns latent features within a log-linear model in a unsupervised way. They also compare their new approach which maximizing predictive accuracy for both dyad observations and item labels to existing methods for within-network classification.

Mizruchi and Marquis [11] contrasted the dyadic analysis with both individual and system level analysis in their study of corporate political behaviour and suggested that eventhough analysis of individual and system-level are useful but the dyadic analyses are a flexible means to examine the effects of multiple networks at multiple levels. All of the researchers mentioned above emphasize on the analysis of dyad relationship. This paper will use the idea of Davis and Leinhardt [2] that introduced a ranked clusterability model in the study of grouping the two actors in the network and presenting the model in the sociomatrix and dendrogram network data.

3. A Ranked Clusterability Model of Dyadic Data

A simplest form of sociometric choice data.

Conventional data table consists of a rectangular array of measurements. The rows of the array are the objects of observations while the columns consist of attributes or variables (quantitative or qualitative measurements). Each cell of the array then describes the value of some objects on some attribute. Different from conventional data, a pure form of network data consist of a square array of measurements [5].

The rows of the array are the objects of observations and the columns of the array are not attributes or variables that usually used in conventional data, but the same set of objects of observations. The object of observations are commonly mentioned as an actor. Each cell of the array describes a relationship between the actors which is coded zero if the relations being absent and coded one if the ties being present. This binary choice data is the most common approach to look at dyads (sets of two actors) *i.e.* to assigning numbers to relations that indicating the absence or presence of each logically possible relationship between pairs of actors. It is commonly to present the information about social network using graphs, but they become complicated and difficult to see the patterns since there are many actors and kinds of relation. Figure 1 shows a simple directed graph of friendship choices among A, B, C and D.

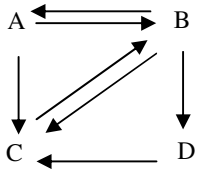

Figure 1. A digraph of friendship choices

Representing information that is derived from that graph into matrices allows the application of mathematical and computer to find the patterns. By converting those directed graph to the matrix, the rows will represent the source of directed ties, and the columns the targets, then the dyadic relationships of each actor shown in Table 1. There are four possible dyadic relationships for directed data: A and B are not connected, A sends to B, B sends to A, or A and B send to each other, meanwhile there are only two possible relationship for undirected data, A and B connected or not connected.

Table 1. Friendship choices

Chooser:	Choice:			
	A	**B**	**C**	**D**
A	0	1	1	0
B	1	0	1	1
C	0	1	0	0
D	0	0	1	0

Using a sociomatrix representation, each cell on the main diagonal (*e.g*. A likes A, B likes B) corresponds to self choice is assumed to be zero [3]. In this matrix, we could see that B chooses A, but A does not choose B. This is an example of an asymmetric matrix that represents directed ties (ties that go from a source to a target). That is, the element *i*, *j*; where *i* and *j* represent the numbers of rows and columns of matrix, does not necessarily equal the element *j*, *i*. If the ties in our matrix representation were undirected, the matrix would necessarily be symmetric; that is, the element *i*, *j* would be equal to element *j*, *i*.

By simple similarity analysis we could treat this data structure using conventional attribute data. We can see similarities between the choices of actors with each other by comparing each row. Meanwhile, by comparing each column we can see the similarities between the selected actors. This method is a simple and useful to see which actors who have a similar position in the network. The study of the position of an actor or an actor embedded among others in a network is a first major emphasis in network analysis. The second major emphasis in network analysis is comparing the cells above and below the main diagonal to check whether there is reciprocity in choices (e.g. A choose C, did C choose A?) and this leads the analyst to see whether the patterns of all individual choices give rises to more overall network pattern [5]. Many studies used by network analysts treat the network data as a conventional data and describing the network data as just a special form of conventional data. This paper is trying to clustering the actors by looking the network data in a different ways.

A New Sociomatrix

In this paper, we present in a different ways of network data matrix. The idea comes up to take the transpose of a directed adjacency matrix or simply means to exchange the rows to the columns so that *i* becomes *j* and vice versa. Usually to measure the degree of reciprocity of ties is using correlation between the adjacency matrix and the transpose matrix that summarizing the degree of symmetry in the pattern of relations among actors. But, we will use a new sociomatrix that combine the adjacency matrix and its transpose to the entries of the top half of the main diagonal matrix. From this matrix we could see the reciprocity of ties and form the hierarchy in a network.

	A	**B**	**C**	**D**
A	0	1	1	0
B	1	0	1	1
C	0	1	0	0
D	0	0	1	0

Figure 2. Sociomatrix of table 1.

For undirected network, the adjacency matrices are symmetrical around their main diagonals; the top half of each matrix is an identical, mirror image of its bottom half, or vice versa. All the relational information in an adjacency matrix for an undirected network is contained in the bottom or top half of the matrix alone; another half is redundant. Analytical procedures in undirected network analysis only require the bottom or top half of the adjacency matrix and not the full matrix. In our example above, the adjacency matrix contains directed data that presents the direction of a relation as running from a row element to a column element. For this reason, a directed matrix is asymmetrical around its main diagonal and therefore, the full matrix must be considered. We are trying to combine the cells in the bottom and the top half of the main diagonal to be the cells in the top half of the main diagonal. For the initial step, we cut all cells in the bottom half of the main diagonal matrix as shown in Figure.3.

	A	**B**	**C**	**D**
A	0	1	1	0
B		0	1	1
C			0	0
D				0

Figure 3. Cut all cells in the bottom half of the main diagonal matrix

Matrix above shows the chooser and their choice, but actor B, C and D not in complete entries of row table, we will complete this table by moving the entries of each cell in the bottom half of main diagonal to the top half of main diagonal, e.g., in the initial table we see that B choose A, so we put this value to the first row and second column behind the value 1 and we also use this way to the other actors (C choose B and D choose C), then our matrix become (Figure 4).

	A	**B**	**C**	**D**
A	0|0	1|1	1|0	0|0
B		0|0	1|1	1|0
C			0|0	0|1

D				0|0

Figure 4. A sociomatrix choices network

In this sociomatrix that contains directed data, the conventions are the first value in the entries (1|0) presents the direction of a relation as running from a row element to a column element and the second value (0|1) presents the direction of a relation as running from a column element to a row element. This matrix helps us to see which actors that connect to each other or reciprocal and which are not. If the entry in the cell is (1|1) then means that the two actors are connected. If the entry in the cell is (1|0), the actor who is on the row chooses the actor who is in the column, but not vice versa. If the entry in the cell is (0|1) then means that the actor who is in the column chooses the actors in a row, but not vice versa. If the entry in cell (0|0) means that the two actors are not connected. The entries contained in any main diagonal is (0|0) for the reason mentioned in [3]. The table also allows us to quickly see whether the network data is symmetric (undirected ties) or asymmetric matrix (directed ties).

A Ranked Clusterability Model of Dyadic Data

Wasserman and Faust [1] and Davis and Leinhardt [2] stated that one need to examine three kinds of dyads when studying ranked clusterability model for complete signed graphs, there are: ++ or (1|1) dyads, in which both actors are connected; -- or (0|0) dyads, in which both actors are not connected and +- or (1|0) or (0|1) dyads, in which one actor chooses his pair but not vice versa. The ranked clusterability model is started by treating a group's ranking structure as a series of ordered levels [2]. The ordered levels was thinked as stories in a building, in the sense that people on a given floor do not differ in level, any two persons on different floors are unambiguously ordered by level, then floors and ceilings mark the levels in a building, and the stories form a complete order. This brings to the three main model: (1|0) or (0|1) are assumed to connect persons in different levels, while (1|1) and (0|0) are assumed to connect persons in the same level.

Within a level, there may be disjoint subsets of people (cliques or subgroups) which is analogous to people in different rooms on a floor of a building. The relations of (1|1) are assumed to connect persons in the same subgroup within a level. The relations (0|0) are assumed to connect persons in different subgroup with a level. Then we can get the model of ranked clusterability as the notion that the relations of (1|0) or (0|1) would divide the members of people in a small groups into levels while the relations of (1|1) and (0|0) would divide the members within levels into subgroup. Wasserman and Faust [1] have explained briefly in which ranked clusterability postulates that (1|1) dyads occur only within clusters and (0|0) dyads occur only between clusters at the same level of the hierarchy or order of clusters. The interesting (0|1) or (1|0) dyads also occur between clusters, but at different levels.

A Level of Connection

We see from the Figure 4 the entry cell in the (A, B) and (B, C) are (1|1) that is, they are reciprocal. For the clustering process, we need to get an additional measure to differentiate between (A, B) and (B, C). Borgatti [12] and Hanneman and Riddle [5] have described about measurement of centrality and flows of networks including geodesic distances, Katz [13], Hubbell, Hoede and Taylor's measurement. In this paper, we will use the ideas of the geodesic distance and the Taylor's measurement. The geodesic distance examines a shortest possible connection between a pair of actors. Taylor's measurement consider the direction of connections, the column marginal of network matrix subtracted from the row marginals that means the balance between each actor's sending connections and their receiving connections [5].

This paper try to combines those two ideas for a level of connection of pair of actors. In any network, if n is the number of actors, there are (n * (n-1)) unique ordered pairs of actors (AB different from BA) and the exclusion of self-ties relationship. We have four actors in our network example. So, in our network of four actors, with directed ties, there are 12 possible relationships. It will be useful to look at each actor in which they are involved to the terms of the kinds of their dyadic relationships. We will see how much the dyadic relationship that occurs with A and B, whether it be as a source or as a target. An actor that both sends and receive ties may be quite different from one who only sends or only receives ties. *First*, the directed ties from A to B. In this case we want to see how much of an actor A sends to the other actors in addition to actor B. This means that the actor A is not just liking an actor B but he did share it with other actors. Actor A not only sends to the actor B but also sends to the actor C. While, actor B was not only choosed by actor A but also choosed by actor C. We ignore the possibility that choices may have different strengths attached to them or may be of different kind of choice types. We could see from the matrix in Figure 5 which is added each row and column marginals.

	A	B	C	D	Total
A	-	1	1	0	2
B	1	-	1	1	3
C	0	1	-	0	1
D	0	0	1	-	1
Total	1	2	3	1	

Figure 5. Matrix for counting a level of connection

Then the value of connections between A and B could be seen from Figure 6, which is the row and column are shaded to show the total choice of A and the total how many actor who choose B.

	A	B	C	D	Total
A	-	1	1	0	**2**
B	1	-	1	1	3
C	0	1	-	0	1
D	0	0	1	-	1
Total	1	**2**	3	1	

Figure 6. Matrix to count the level of connection between actor A and B

We could see the value of A to B from the rows A with total 2 and column B with total 2. Hence, the level of connections of a directed ties from A to B is (2+2)/12 = 4/12. After this point we should see the directed ties from B to A. *Second*, because A and B are reciprocal, then we count the level of connections of a directed ties from B to A, B not only choose A, but he also choose C and D, while, A is the only choosed by B. The calculation showed by the shaded row and column in the Figure 7.

	A	B	C	D	Total
A	-	1	1	0	2
B	1	-	1	1	**3**
C	0	1	-	0	1
D	0	0	1	-	1
Total	**1**	2	3	1	

Figure 7. Matrix to count the level of connection between actor B and A

The value of the connections of a directed ties from B to A is (3+1)/12 = 4/12. Hence, the level of connections a dyadic relationship of A and B is (4/12) + (4/12) = 8/12. We could add this level of connection as an additional measurement to the matrix in the Figure 4 and present it on the Figure 8 for all calculations of dyadic relationships. Ranked clusterability model of dyads postulates that the clustering process starts from the mutual dyads that occur only within clusters until all of the mutual dyads grouped then the hierarchy process continue to cluster the asymmetric dyads that occur between clusters but at different levels and the last process is clustering the null dyads, which is clustered at the end of the hierarchy after all of asymmetric dyads grouped and occur only between clusters at the same level of the hierarchy. The hierarchical process uses the following steps:

Step 1. Form a new sociomatrix from sociomatrix choices network.

	A	B	C	D
A	0|0	1|1 (8/12)	1|0 (5/12)	0|0 (0)
B		0|0	1|1 (9/12)	1|0 (4/12)
C			0|0	0|1 (4/12)
D				0|0

Figure 8. A Sociomatrix with the level of connections

Step 2. Find the maximum value in the matrix using ranked clusterability model

The clustering starts from the mutual dyads and then the asymmetric dyads and finally the null dyads. The table shows that there are mutual dyadic relationships i.e., AB and BC or both of them are a reciprocal relationships. Then the value that we will use to start the clustering is the maximum value of the level of connections between AB or BC. We choose BC because their degree (9/12) is higher than AB (8/12). The hierarchical clustering start from BC.

	BC	A	D
BC	1|1(9/12)	1|1(8/12)	1|0(4/12)
A		0|0	0|0 (0)
D			0|0

Figure 9. First step of clustering

Step 3. Modify the sociomatrix according to step 2

From step 2, BC occupies the first column, next column is occupied by A and D. The value in columns BC and A obtained from the search for maximum value between the BA with CA. The value of BA is (1|1|(8/12)) while the value of CA is (1|0|(5/12)) therefore, we select the value of BA. This was also done for the entries of other cells.

	BCA	D
BCA	1|1(8/12)	1|0(4/12)
D		0|0

Figure 10. Second step of clustering

This clustering process continues until found one large cluster and the last clustering process is

	BCAD
BCAD	1|0(4/12)

Figure 11. The final step of clustering

Step 4. Draw the final dendrogram

Then we can get the dendrogram of actors in the network.

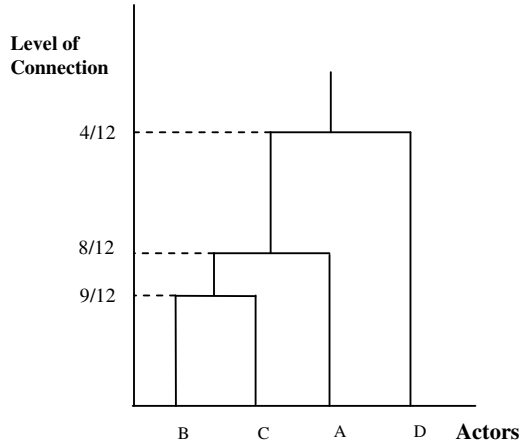

Figure 12.. Dendrogram network data

From the dendrogram we could see that actor B and C as a basis for the friendship choices in the network. Eventhough both of AB and BC are mutual relationship but most of the information is at the both two actor B and C, B chooses all of friends in the network and C has been chosen by all of friends in the network. If we would like to make two cluster based on ranked clusterability of dyadic data from this example of friendship network then the group is (A, B, C) and (D). D has the lowest level of connection of dyad relationship with other friends. This simple example of ranked clusterability gives a new insight in how to view the relationship among actors in the network using sociomatrix, level of connections and dendrogram network data.

4. Conclusion

This paper shows the ranked clusterability model idea from Davis and Leinhardt [2] using new sociomatrix and its level of connection. The new sociomatrix has already help us to understand about ranked clusterability model and could be presented it in a dendrogram network data. In this simple example of choice network data we ignore the possibility that choices may have different strengths attached to them or may be of different kind of choice types. A real network data will be used for this method in the next research and compared to other methods that usually used to cluster the dyads data. Eventhough this research starts from simple example of friendship choices data, the result gives us a new insight in how to view the clustering and relationships among actors in the network.

5. References

[1] Faust, K., (2007), Very local structure in social networks, Sociological Methodology, Volume 37, Issue 1, pages 209-256, December.

[2] Davis, James A., and Leinhardt, S., (1971), The Structure of Positive Interpersonal Relations in Small Groups. In Sociological Theories in Progress. Vol. 2, edited by J. Berger, M. Zelditch, and B. Anderson. Boston: Houghton-Mifflin.

[3] Wasserman, S. and Faust, K., (1994), Social Network Analysis: Methods and Applications. Cambridge: Cambridge University Press.

[4] Holland, Paul W and Leinhardt, Samuel, (1976), Local Structure in Social Networks. Sociological Methodology, Vol. 7., pp. 1-45.

[5] Hanneman, Robert A and Riddle, M., (2005), Introduction to Social Network Methods, University of California, Riverside.

[6] DeCoster, J., (2002), Using ANOVA to Examine Data from Groups and Dyads. Retrieved from the web January, 14, 2011. http://www.stat-help.com/notes.html

[7] Kenny, David A., Deborah A. Kashy, and William L. Cook (2006), Dyadic Data Analysis, Guilford Publications.

[8] Yablonsky, L., (1955), The Sociometry of the Dyad, *Sociometry*, Vol. 18, No. 4, pp. 357-360.

[9] Aurifeille, Jacques-Marie and Christopher J. Medlin (2001), A Dyadic Segmentation Approach toBusiness Partnerships, *European Journal of Economic and Social Systems,* 15 (2), 3-16.

[10] Menon, Aditya K., and Charles E., (2010), Predicting labels for dyadic data, *Data Mining and Knowledge Discovery* 21: 327-343.

[11] Mizruchi, Mark S. and Marquis, Christopher (2006), Egocentric, sociocentric, or dyadic? Identifying the appropriate level of analysis in the study of organizational networks, *Social Networks* Vol 28 (3) pp 187-208.

[12] Borgatti, Stephen P., (2005), Centrality and Network Flow, *Social Networks* 27 pp 55–71.

[13] Katz, L., (1953), A New Status Index Derived from Sociometric Analysis, *Psychometrika*, Vol 18 (1).

Analysis and Numerical Solutions of 2D Navier-Stokes for Model of Shallow Water Flow with Initial Value Problem and Boundary Value Problem

Ririn Kusumawati [1], Ari Kusumastuti [2], Fitriyanti Rumfot [3], Silva Ahmad A. [4]

[(1)] Informatics Department, Faculty of Science and Technology, UIN Maulana Malik Ibrahim, Malang
[(2,3,4)] Mathematics Department, Faculty of Science and Technology, UIN Maulana Malik Ibrahim, Malang

Abstract

The Navier-Stokes equations are equations in non-linear partial differential that can do for fluid of water. This research aims to obtain the solution made in 2D fluid flow initial value problem and boundary value problem. In this case, the d'Alembert solution is a private solution to the initial value problem and the problem of separation of variables of nonlinear partial differential equations is a private solution to the boundary value problem. In this case the limits is define by $0 < x < L$ and $0 < y < W$. ADI method was chosen to formulate the solution for every grid point in rectangle object. MATLAB software was used for constructed model. In this research the numerical solution chosen by the ADI method in formulating solutions- solutions at each grid point of the object rectangle. MATLAB for software programs that are built to explain the v and u solution is the spread of the fluid. New amplitude for the next t which can be interpreted in the 3D graphics can look for more in depth.

Keywords: *Navier-Stokes Equation, Initial Value, Boundary Value, ADI Method.*

1. Introduction

In this research, a mathematical model that can translate Fluid state of water is the Navier-Stokes equation, which is a system of momentum and continuity equations and can apply to laminar or turbulent fluid. The assumption that the fluid is selected in this research is shallow water (shallow water), which shallow waters in question are the waters that have a surface and bottom.

The research emphasizes the analytic and numerical analysis for the wave model in a system that is selected. This is of course that the analysis of this research should be implemented on watershed data encountered, so that the result of this mathematical analysis becomes very factual. Further analytical analysis of wave model results in these waters can be continued in subsequent research in view the level of influence on the sedimentation velocity in the waters and the land around the watershed.

$$\frac{\partial u}{\partial x} - t\frac{\partial u}{\partial y} = w(x,y) \qquad (1)$$

$$\frac{\partial w}{\partial x} + t\frac{\partial w}{\partial y} = \frac{\partial u}{\partial t} + u\frac{\partial u}{\partial x} + v\frac{\partial u}{\partial y} + \frac{\partial p}{\partial x}$$

$$g(x) + uf'(x) + \frac{\partial p}{\partial x} = \frac{\partial u}{\partial t} + u\frac{\partial u}{\partial x} \qquad (3)$$

The general form of 2D Navier-Stokes Equations are:

x momentum:

$$\frac{\partial u}{\partial t} + u\frac{\partial u}{\partial x} + v\frac{\partial u}{\partial y} = -\frac{\partial p}{\partial x} + \frac{1}{Re}\left(\frac{\partial^2 u}{\partial x^2} + \frac{\partial^2 u}{\partial y^2}\right)$$

y momentum:

$$\frac{\partial v}{\partial t} + u\frac{\partial v}{\partial x} + v\frac{\partial v}{\partial y} = -\frac{\partial p}{\partial y} + \frac{1}{Re}\left(\frac{\partial^2 v}{\partial x^2} + \frac{\partial^2 v}{\partial y^2}\right)$$

The objective of this research is to analyzing 2D Navier-Stokes equations to model wave cross section which involves initial value problem and boundary value problem in shallow water.

2. Experimental Details

To solve the initial value problem, the first step of discussion in this research is to determine the initial value problem of a private solution to the 2D Navier-Stokes. Consequently, it can be solved separately with the separation solution can be restated into……???

In the initial conditions (when t = 0), given an initial value $u(x,0) = f(x)$ and $\frac{\partial u}{\partial t}(x,0) = g(x)$ for f(x), g(x) are arbitrary functions. This result in equation (3.5) can be restated as follows:

If the initial condition is assumed turbulent waves in the function sin τ, it can be stated

$$u(x,0) = u(\sin\tau, 0) = f(\sin\tau) \quad (4)$$

In this case vectors tangent direction of the equation is as follows:

$$\frac{dt}{ds} = 1, \quad \frac{dx}{ds} = u,$$
$$\text{and } \frac{du}{ds} = g(x) + uf'(x) + \frac{\partial P}{\partial x} \quad (5)$$

With the above rules can be stated:

$$U(x,t) = \left[\frac{1}{2u_0}G(\sin\tau + 2ut) + \frac{1}{2}f(\sin\tau + 2ut) + P(\sin\tau + 2ut)\right] + \left[-\frac{1}{2u_0}G(\sin\tau) - \frac{1}{2}f(\sin\tau) - P(\sin\tau)\right] \quad (6)$$

with the analog method for the *y* momentum.

Furthermore, a private Solutions Boundary Value Problems Navier-Stokes 2D defined bounded of $0 \prec x \prec L$ and $0 \prec y \prec W$ region in the interval. Defined $\Delta = \frac{\partial^2}{\partial x^2} + \frac{\partial^2}{\partial y^2}$ $\Delta w = \frac{\partial^2 w}{\partial x^2} + \frac{\partial^2 w}{\partial y^2}$ and if $u = \frac{\partial w}{\partial y}$ and $v = -\frac{\partial w}{\partial x}$ called are stream function, the substitution of this function into equation (1) obtained:

$$\frac{\partial}{\partial t}\left(\frac{\partial w}{\partial y}\right) + \left(\frac{\partial w}{\partial y}\right)\frac{\partial}{\partial x}\left(\frac{\partial w}{\partial y}\right) - \frac{\partial w}{\partial x}\frac{\partial}{\partial y}\left(\frac{\partial w}{\partial y}\right) = -\frac{\partial p}{\partial x} + \frac{1}{Re}\left(\frac{\partial^2}{\partial x^2} + \frac{\partial^2}{\partial y^2}\right)\left(\frac{\partial w}{\partial y}\right)$$

Furthermore, by assuming, then the Navier-Stokes equations can be modified in the form of nonlinear partial differential equations of order four:

$$\frac{\partial}{\partial t}(\Delta w) + \left(\frac{\partial w}{\partial y}\right)\frac{\partial}{\partial x}(\Delta w) - \frac{\partial w}{\partial x}\frac{\partial}{\partial y}(\Delta w) = \frac{\partial p}{\partial x} + \frac{1}{Re}\left(\frac{\partial^2}{\partial x^2} + \frac{\partial^2}{\partial y^2}\right)(\Delta w) \quad (7)$$

Furthermore, exact solutions to the Navier-Stokes equations is $w = F(y,t)x + G(y,t)$ so that valid $\frac{\partial w}{\partial x} = F(y,t)$ and $\frac{\partial w}{\partial y} = \frac{\partial F}{\partial y} + \frac{\partial G}{\partial y}$ we can restate that equations with:

$$\frac{\partial^3 F}{\partial t \partial y^2} + \frac{\partial^3 G}{\partial t \partial y^2} + \frac{\partial F}{\partial y}\frac{\partial^2 F}{\partial y^2} + \frac{\partial G}{\partial y}\frac{\partial^2 F}{\partial y^2} - F\left(\frac{\partial^3 F}{\partial y^3} + \frac{\partial^3 G}{\partial y^3}\right) = -\frac{\partial p}{\partial x} + \frac{1}{Re}\left(\frac{\partial^4 F}{\partial y^4} + \frac{\partial^4 G}{\partial y^4}\right) \quad (8)$$

From the form (8) we get

$$\frac{\partial^3 F}{\partial t \partial y^2} + \frac{\partial F}{\partial y}\frac{\partial^2 F}{\partial y^2} - F\frac{\partial^3 F}{\partial y^3} = \frac{1}{Re}\frac{\partial^4 F}{\partial y^4} \quad (9)$$

$$\frac{\partial^3 G}{\partial t \partial y^2} + \frac{\partial G}{\partial y}\frac{\partial^2 F}{\partial y^2} - F\frac{\partial^3 G}{\partial y^3} = \frac{1}{Re}\frac{\partial^4 G}{\partial y^4} \quad (10)$$

Integration of equation (9) of *y*:

$$\int \frac{\partial^3 F}{\partial t \partial y^2} dy + \int \frac{\partial F}{\partial y}\frac{\partial^2 F}{\partial y^2} dy - F\int \frac{\partial^3 F}{\partial y^3} dy = \frac{1}{Re}\int \frac{\partial^4 F}{\partial y^4} dy$$

Thus obtained:

$$\frac{\partial^2 F}{\partial t \partial y} + \left(\frac{\partial F}{\partial y}\right)^2 - F\frac{\partial^2 F}{\partial y^2} = \frac{1}{Re}\frac{\partial^3 F}{\partial y^3} + f_1(t)$$

And integralkan equation (10) of *y*:

$$\int \frac{\partial^3 G}{\partial t \partial y^2} dy + \int \frac{\partial G}{\partial y}\frac{\partial^2 F}{\partial y^2} dy - F\int \frac{\partial^3 G}{\partial y^3} dy = \frac{1}{Re}\int \frac{\partial^4 G}{\partial y^4} dy$$

Thus obtained:

$$\frac{\partial^2 G}{\partial t \partial y} + \frac{\partial G}{\partial y}\frac{\partial F}{\partial y} - F\frac{\partial^2 G}{\partial y^2} = \frac{1}{Re}\frac{\partial^3 G}{\partial y^3} + f_2(t)$$

For any function constant $f_1(t)$ and $f_2(t)$ With the variable separation method: $U(y,t) = Y(y)T(t)$ and $F(y,t) = Y(y)T(t)$

We get:

$$U(y,t) = a_n \sin\left(\frac{n\pi}{\sqrt{2}}\right) b_n e^{\frac{n\pi}{\sqrt{2}}t}$$

and

$$V(x,t) = C_n e^{\frac{n\pi}{\sqrt{2}}t} \sin\left(\frac{n\pi}{\sqrt{2}}\right)$$

3. Result and Discussion

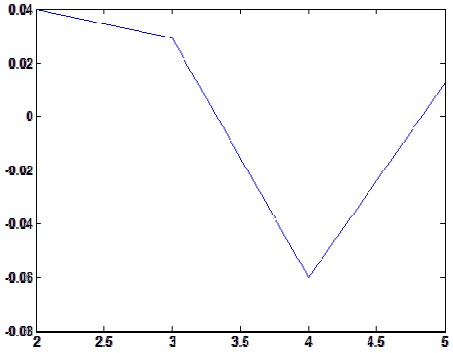

Analytic

$$\left(\frac{v_{i,j}^{n+1} - v_{i,j}^{n}}{\Delta t}\right) + u_{i,j}^{n}\left(\frac{v_{i+1,j}^{n+1} - v_{i-1,j}^{n+1}}{2\Delta x}\right) + v_{i,j}^{n}\left(\frac{v_{i,j+1}^{n+1} - v_{i,j-1}^{n+1}}{2\Delta y}\right) = -\left(\frac{p_{i,j}^{n} - p_{i-1,j}^{n}}{\Delta x} + \frac{p_{i,j-1}^{n} - p_{i-1,j-1}^{n}}{\Delta x}\right) + \frac{1}{Re}\left(\frac{v_{i+1,j}^{n+1} - 2v_{i,j}^{n+1} + v_{i-1,j}^{n+1}}{(\Delta x)^2} + \frac{v_{i,j+1}^{n+1} - 2v_{i,j}^{n+1} + v_{i,j-1}^{n+1}}{(\Delta y)^2}\right)$$

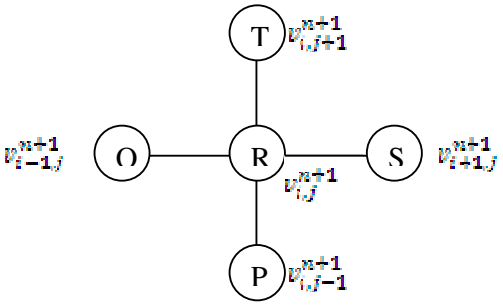

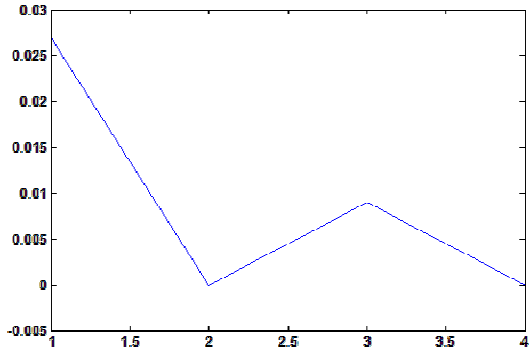

Numeric

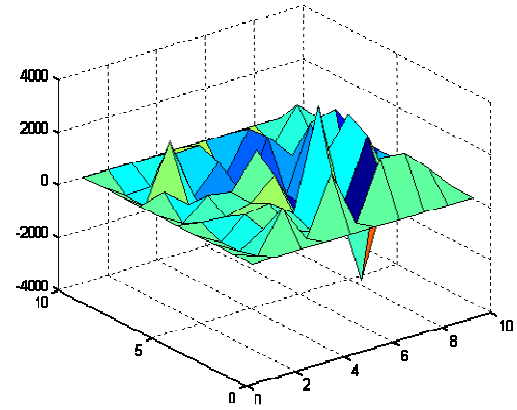

4. References

[1]. Anton, H., (1987), Elementary Linear Algebra. Translation Pantur Silaban ITB.1997. London: Erland

[2]. Finizio, N and Ladaz, G., (1982), Ordinary differential Equations, with Modern Applications. Translated by Widiarti

[3]. Santoso (1988), …...Thesis, Erland: Jakarta

[4]. Furi, S.S.A. (2006), Tafsir Ibn Kathir. Volume 2. Translation Abu al-ihsan Atsari. Bogor: Pustaka Ibnu Kathir

[5]. Godwin, P. B., Dugdale R. H., (1986), Fluid Mechanics Third Edition. London: Erland

[6]. Kaplan, W., (1963), Advanced Calculus: First Edition. Addison-Wesley Publishing Company, Inc.

[7]. Johnson. Lee W. R. Dean Riess. Jimmy T. Arnold (1993), Introduction to Linear Algebra. New York: Addison-Wesley Publishing Company.

[8]. Nagle, K. R and Saff, E.B., (1996), Fundamentals of differential equations and boundary value problems. University of South Florida.

[9]. Munson, Bruce R, *et al.*, (2002), Fundamentals of Fluid Mechanics, Fourth Edition. Volume 1. London: Erland.

[10]. Munson, B.R, *et al*. (2002), Fundamentals of Fluid Mechanics, Fourth Edition. Volume 2. London: Erland.
[11]. Orianto, M and Pratikto (1989), Fluid Mechanics. Yogyakarta: Yogyakarta BPFE
[12]. Polyanin, A. D. and Zaitsev, V. F., (2003), Handbook of Nonlinear Partial Differential Equations, Chapman & Hall / CRC Press
[13]. Soeharjo. (1996), Mathematics IV. Dictates ITS
[14]. Soewarno (1991) Hydrology: Measurement and Data Processing watershed (Hidrometri). New York: Nova Publishers
[15]. Spiegel, M R., (1983), Advanced Mathematics for Engineers and Scientists. Translated by Koko Martono. 1994. London: Erland
[16]. Stewart, J., (2002), Kalkulus vol 1. Translation by I Nyoman Susila, Hendra Gunawan. 2002. London: Erland.
[17]. Stewart, J., (2003), Kalkulus vol 2. Translation by I Nyoman Susila, Hendra Gunawan. 2003. London: Erland.
[18]. Sutrima (2004), Representations Sprektal of Strum-Liouville Operators Berparameter. Journal of Department of Mathematics: FMIPA UNS. 14:17 Mathematics and Science vol. ??
[19]. White F.M. (1988), Fluid Mechanics: Second Edition: Volume 1. London: Erland
[20]. Zauderer, E., (2006), Partial Differential Equations of Applied Mathematics. New Jersey: John Willey & Sons, Inc.

The Optimum Time of Steam Distillation of Wilted Aceh Patchouli Leaves (*Pogostemon cablin* Benth) and The Characterization by Thin Layer Chromatogaphy and Gas Chromatography-Mass Spectra

Rurini Retnowati [1], Sentot Joko Raharjo [2]

[(1)] Chemistry Department, Mathematics and Natural Sciences Faculty, Brawijaya University
(rurini_retnowati@yahoo.com)
[(2)] Master Program, Chemistry Department, Mathematics and Natural Sciences Faculty, Brawijaya University
(sentotjoko@yahoo.co.id)

Abstract

This research aims are to determine the optimum time of steam distillation of wilted drying of Aceh patchouli leaves and the characterization of chemical constituents of the oil by thin layer chromatography (TLC) and gas chromatography-mass spectra (GC-MS). The optimum time was determined by collecting distillate every two hours in 8 hours of steam distillation time and collecting the distillate for 2, 4, 6 and 8 hours of steam distillation time. The TLC analysis was done in silica gel F_{254} as stationary phase and benzene-ethyl acetate (90:10) as an eluent. The mixture of vanillin-sulfuric acid used as visible stain of spot resulted from TLC analysis. The highest yield of patchouli oils was obtained in the second hour of distillate collection (2.7526%) and in the 8^{th} hours of distillate collecting time (6.3831%). The characterization of patchouli oil by TLC method showed six colorful spot, the dark purple color (R_f-1 = 0.87), red hearts color (R_f-2 = 0.68), purple color (R_f-3 = 0.56), pale purple color (R_f-4 = 0.47), purple pink color (R_f-5 = 0.43) and pink color (R_f-6 = 0.25) respectively. The characterization of patchouli oils by GC-MS showed the main component was patchouli alcohol (70.19%) and the highest percentage of the compounds was found at 4 hours of distillate collecting time. The other components of patchouli oils were aromadendrene, seychellene, alpha patchoulene, pogostol and alpha gurjunene.

***Keywords**: patchouli oils, patchouli leaves, wilted drying, steam distillation, distillate collecting time.*

1. Introduction

In general, the extracting of patchouli oil especially of *Pogostemon cablin* Benth is performed by steam distillation process. Before processing, the patchouli leaves was subjected to drying and cutting. The common way of traditional industry in Indonesia was used to dry the leaves under the sun for four hours. So far, the drying of leaves and steam distillation process was only to obtain high yields in such way to accommodate the accumulation of essential oils, regardless of the composition that determines the quality of essential oils.

Time used for distillation and drying process affects the composition of essential oil compounds [1]. Therefore, the use of an effective distillation will reduce the risk of decline in the percentage of components that determine the quality, as well as number of fuel used. One of patchouli oil quality parameters refer to the content of patchouli alcohol and does not refer to the ESO, USA, which uses ISO 3757:2002 standard and requires other components of essential oil of patchouli as a standard parameter [2].

This research was carried out by using the wilted drying method of patchouli leaves for 9 days. Steam distillation is performed with distillation time every 2, 4, 6 and 8 hours. It is also performed by varying the distillate collection time for 2, 4, 6 and 8 hours. Patchouli oil obtained was characterized by using TLC and GC-MS.

2. Experimental Details

Materials and Equipment

The sample used in this study was fresh patchouli leaves from Pujiharjo Village, Tirtoyudo District, Malang Regency. The fresh leaves sample that separated from the stem, then dried in wilted drying by combining its sample dried in 2 hours under the sun and continued of wilted dried for 9 days.

The chemicals used in this research categorized as pro analysis (pa) grade, namely n-

hexane, benzene, ethyl acetate, sulfuric acid, and ethanol, while the technically chemicals grade were vanillin, magnesium sulfate heptahydrate, distilled water, nitrogen gas, and TLC plates silica gel 60 F_{254}.

The eqiupment used in the study include a set of steam distillation apparatus with a capacity of 5 kg, 500 mL separating funnel, 10 mL measuring pipettes, micro pipette, pipette drops, plate evaporator, heater, desiccator, clamps, vessel developer chromatography, peck 25 mL flask, erlenmeyer 250 mL, sprayer gun, a set of tools KG-MS-2010S Shimadzu QP type, balance Mettler PE 3600, pH meters, and sample bottles of 10 mL and 25 mL.

The Patchouli Oils Distillation

The sample of patchouli leaves were dryed by using wilted drying (weighed 0.5 kg for the steam distillation in which the distillate collected every 2 hours from 2 to 8 hours and weighed 0.25 kg for the steam distillation for 2 hours, 4 hours, 6 hours and 8 hours) then distilled by using steam distillation. Each 250 mL distillate was extracted with 3x10 mL of n-hexane. The Patchouli oils obtained was determined its yield and its constituent components.

The Patchouli Oils Profile Analysis by TLC

The patchouli oils obtained from the every 2 hours distillate collection from 2 to 8 hours of steam distillation and the oils obtained by distillation for 2 hours, 4 hours, 6 hours, and 8 hours were spoted using capillary tube (2 µl) at a distance of 1 cm from the bottom plate measuring 1 x 10 cm. The plate was eluated in the developer vessel using the eluent of benzene:ethyl acetate (90:10) and then sprayed with a spot stain solution vanillin-sulfuric acid. Then it was performed with preparative TLC of treatment and wilted drying for 8 hours and analyzed by GC-MS

The Profile Analysis of the Patchouli Oils Components by Total Ionic Chromatogram (TIC) Produced by GC-MS

The patchouli oils were analyzed using GC-MS type Shimadzu QP-2010S. Number of peaks in the TIC data was used to determine the number of components contained in the patchouli oils. The area percentage in the TIC data was used to determine the composition of the patchouli oils.

The Characterization of Each Component of Patchouli Oils Based Mass Spectral Analysis by GC-MS

The characterization of components of patchouli oils was based on mass spectral data in GC-MS analysis. The mass spectra data was used to analyze the structure of the component of essential oils through the analysis of fragmentation patterns. Further data analysis by GC-MS TIC of each composition of patchouli oils components illustrated graph vs the percentage of the peak component of patchouli oils.

3. Result and Discussion

Patchouli Oils Distillation

The patchouli oils obtained have a light yellow color. The yield data were presented in Table 1. Based on Table 1, it can be observed that based on the yield of the essential oils obtained by steam distillation, the effective time for steam distillation was 2 hours because it was decreasing after 2 hours of steam distillation. The decresing value of the yield value presumably because several components had been evaporated after two hours of distillation. This shows that the effective time of the steam distillation based on the yield of the essential oils was 2 hours. On the other hand, the yields of the patchouli oils obtained by steam distillation in 2 hours until 8 hours were increasing. Generally, the highest yield of patchouli oils was found in the distillate obtains by steam distillation for 8 hours (6.3831%).

Table 1. Yield of patchouli oils which dryed by Wilted Drying

Treatment	Code	Yield (%)
Distillate collecting time in every 2 hours from 1 to 8 hours	Ln-S-2	2.7526
	Ln-S-4	1.0272
	Ln-S-6	0.5226
	Ln-S-8	0.4228
Distillate collecting time for 2 hours, 4 hours, 6 hours, and 8 hours of distillation	Ln-L-2	4.8508
	Ln-L-4	5.3858
	Ln-L-6	5.4629
	Ln-L-8	6.3831

The Patchouli Oils Analysis by TLC

The analysis of the essential oils components in TLC were presented in Figure 1. Characterization of patchouli oils by TLC method produces six spots color, the dark purple color (R_f-1 = 0.87), red hearts color (R_f-2 = 0.68), purple color (R_f-3 = 0.56), pale purple color (Rf-4 = 0.47), purple-pink color (R_f-5 = 0.43), and pink color (R_f-6 = 0.25).

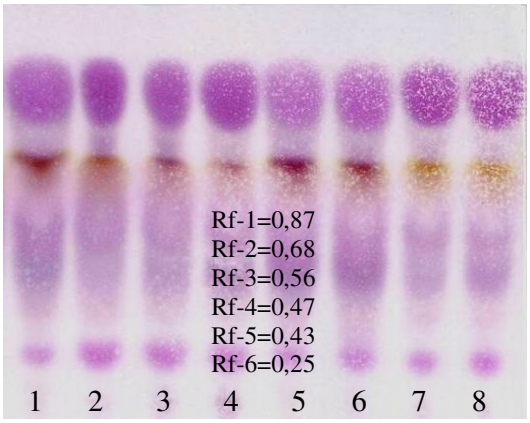

Note : Distilate collecting time :
1 : 2nd hour 5 : For 2 hours
2 : 4th hour 6 : For 4 hours
3 : 6th hour 7 : For 6 hours
4 : 8th hour 8 : For 8 hours

Figure 1. The result of TLC chromatograms of patchouli oils obtained by steam distillation which the distillate were collected in the second, forth, sixth and eight hours of distillation and for 2 hours, 4 hours, 6 hours and 8 hours of distillation

Results of analysis of each patchouli oils of the optimization time of steam distillation with Thin Layer Chromatography method (Figure 1) showed stains of Rf-1 - Rf-6. There was no difference of each patchouli oils of the distillate that collected every 2 hours from 2 to 8 hours and steam distillation for 2 hours, 4 hours, 6 hours 8 hours. The TLC analysis information will help to isolate the main component of patchouli alcohol by using column chromatography for further analysis.

The Patchouli Oils Component Characterization by Using GC-MS Analysis

Analysis of essential oils by using GC-MS gives chromatogram called the Total Ion Chromatogram (TIC). TIC is used to determine the profile and components structure of patchouli oils that obtained by steam distillation which the distillate were collected every 2 hours (from 1 to 8 hours), and the distillate that collected in the distillation of 2 hours, 4 hours, 6 hours and 8 hours.

Based on the TIC data, it was observed that the main component of patchouli oils was patchouli alcohol and the other components were aromadendrene, seychellene, alpha-patchoulene, pogostol, dehydroaromadendrene, and alpha-gurjunene. The structure of components of patchouli oils was presented in Figure 3. The TIC of the components of the patchouli oils obtained by 4 hours of steam distillation, which shows 6 peaks, is presented in Figure 2.

The order of the components in GC-MS analysis related to the polarizability. The data of polarizability in 10-24 cm^3 are alpha-gurjunene (25.66); aromadendrene (25.69); seychellene (25.71); alpha-patchoulene (25.76), patchouli alcohol (26.54); and pogostol (27.13) [3].

The order of the compounds eluated based on the polarizability in GC-MS analysis was also supported by the order of the compounds in TLC analysis in Figure 1.

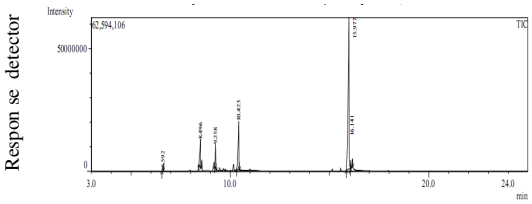

Figure 2. The TIC of the patchouli oils obtained by 4 hours of steam distillation (On-L-4) were analyzed by by using GC-MS Shimadzu QP-2010S, Rtx-Wax column

Table 2. TIC composition of the patchouli oils obtained by steam distillation of wilted patchouli leaves 8 hours (Ln-L-8)

No.	Retention Time	% Area Relatif	Component Name
1	6.600	1.59	Alpha-gurjunene
2	8.514	12.45	Aromadendrene
3	9.273	8.65	Seychellene
4	10.176	2.71	Dehidroaromadendrene
5	15.982	18.89	Alpha-patchoulene
6	16.149	52.27	Patchouli alkohol
7	18.593	3.43	Pogostol

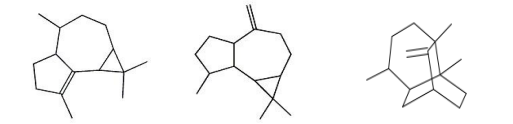
Alpha-gurjunene Aromadendrene Seychellene

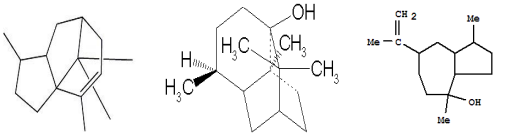

Alpha-patchoulene Patchouli alcohol pogostol

Figure 3. The structure of several components in patchouli oils

The Effect of Distillate Collection Time to The Profile of The Patchouli oils

The effect of the distillate collection time to the patchouli oils component profiles were observed by analyzing the compositions of the

components in the oils obtained by collecting the distillate every 2 hours from 2 to 8 hours (Figure 4A) and collecting the distillate for 2 hours, 4 hours, 6 hours and 8 hours of distillation (Figure 4B) based on GC-MS analysis.

The components with high vapor pressure evaporate first at the steam distillation process. The order of the components vapor pressure data in mmHg were alpha-gurjunene (0.01640), aromadendrene (0.02260), seychellene (0.034000), alpha-patchoulene (0.017700), patchouli alcohol (0.000278), and pogostol (0.000083)

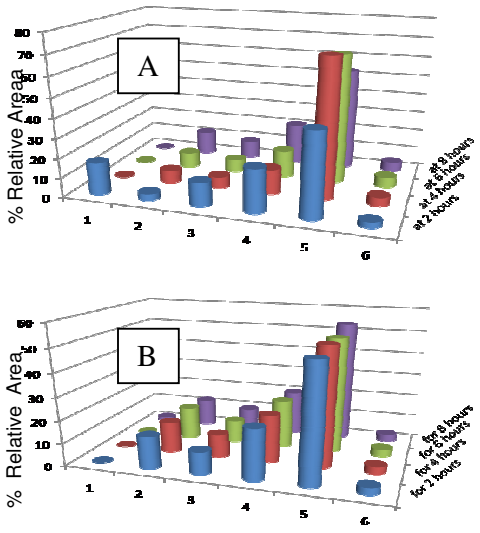

(1)alpha-gurjunene; (2)aromadendrene; (3) seychellene; (4)alpha-patchoulene; (5)patchouli alcohol alkohol; (6)pogostol

Figure 4. The percentage of relative areas of the components of patchouli oils obtained by collecting the distillate every 2 hours from 1 to 8 hours (A) and collecting the distillate for 2 hours, 4 hours, 6 hours, 8 hours (B)

The GC-MS characterization of the patchouli oils showed that the highest patchouli alcohol was obtained from the distillate collecting time at 4 hours. Other component of patchouli oils were alpha-gurjunene, aromadendrene, seychellen, alpha-patchoulene and pogostol. Beside that, the results of GC-MS analysis of each distillate showed that there are the differences in component profile of patchouli oil.

4. Conclusion

1. The highest yields of patchouli oil were obtained at 2 hours of distillation time (2.7526%) and distillate collecting time of 8 hours (6.3831%).
2. TLC analysis showed that there are 6 groups of compounds in patchouli oil and there is no difference component profile in each distillate.
3. The GC-MS characterization of the patchouli oils showed that the highest patchouli alcohol was obtained from the distillate collecting time at 4 hours and indicated that there are the differences in component profile of patchouli oil in each distillate.

5. Acknowledgment

Authors are very thankful to Chemistry Department, Brawijaya University and Pharmacy and Food Analysis Academy "Putra Indonesia Malang" for instrumental support and facilities during the course of work. Authors are also very thankful to Pujiharjo community and Biology Department, Brawijaya University for identification of plant material.

6. References

[1]. Ginting, S., (2004), Pengaruh Lama Distilasi Terhadap Rendemen dan Mutu Minyak atsiri Daun Sereh Wangi, Laporan Peneltian, Fakultas Pertanian, Universitas Sumatra Utara, e-USU Repository, Medan.

[2]. Maryadi, A., (2010), Pembuatan Bahan acuan Minyak Nilam, Pusat Penelitian Sistem Mutu dan Teknologi Pengujian – LIPI

[3]. Thegoodscents, (2010). Essential Oils Information, www.thegoodscentscompany. com. Accessed on 20 Juni 2010

[4]. Ellyta and Elmi, (2005), Upaya Peningkatan Kualitas dan Permasalahan Perdagangan Minyak Nilam di Sumatra Barat, Fakultas Teknologi Industri. Universitas Bung Hatta Padang.

[5]. Erika, (2010), Pengaruh Jenis Metode Terhadap Hasil Isolasi Patchouli Alkohol dalam minyak nilam, Abstrak Skripsi

[6]. Faizal, (2009), Karakterisitk Simplisia dan Isolasi serta Analisis Komponen Minyak Atsiri dari Daun Nilam (Pogostemon cablin Benth.) Asal Aceh Tenggara, Skripsi Fakultas Farmasi, USU, Medan

[7]. Guenther, E., (1947). Essential Oils. Robert E. Krieger Publishing Co., Inc. S. Ketaren (translated). 1987. Minyak Atsiri. Jilid 1. UI-Press. Jakarta.

[8]. Harborne, J.B., (1984). Phytochemical Methods. Chapman and Hall Ltd. K. Padmawinata (translated). 1987. Metode Fitokimia. Penerbit ITB. Bandung.

[9]. Hyung Woo Kim, (2008), *Pogostemon cablin* as ROS Scavenger in Oxidant-

induced Cell Death of Human Neuroglioma Cells, Department of Herbology, College of Oriental Medicine, Dongshin University, Advance Access Publication 7 January 2008

[10]. Ngampong Kongkathip *et al*, (2009), Development of Patchouli with Quality Control and Isolation of Active Coumpound with Antibacterial Activity, Kasetsart *J. Nat Sci.* 43 : 519-525

[11]. Nguyên Xuân D˜ung, (1989), Chemical Composition of Patchouli Oils from Vietnam, Department of Technical Chemistry, University of Hanoi, 19 Le Thanh Tong Street, Hanoi, Vietnam, Patchouli oils, *J. Essent. Oils Res*. (March/April 1989).

Investigation the Mediating Variable: What Necessary?

Solimun

Basic Science Faculty, Brawijaya University, Malang, Indonesia (solimun@ub.ac.id)

Abstract

Students of Management Doctoral Program in Indonesia often analyze mediation variable in their dissertation. Some student (on Management Doctoral Program of Brawijaya University and Airlangga University) investigate this using structural equation modeling (SEM) with only analyze a model that involves a mediation variable. Hair et al. [1] says that for testing of mediation variable is done by comparing the results of analysis of model that involves a mediation variable and the model does not include a mediation variable. Dissertation of 10 students Management Doctoral Program (on Brawijaya University and Airlangga University, in 2009 until 2010, which they were analyzed the mediation variable) was used in this study. SEM was used for data analysis and Hair's rule was used to investigate. The result of study shows that all variables on all model as a mediating variable, if only analyzed with models that involve a mediation variable. However, after was investigated by Hair et al. rule, shows that 3 variable on model is not mediation variables. Investigation the mediating variable use Hair et al. rule is necessary.

Keywords: *investigation, mediation variable, SEM.*

1. Introduction

Research in Management often investigates a system. Where, the system is a relationship among variables, and is called model. They are use structural equation modeling (SEM) to analyze a model. The model is usually has many variables and relationships and a mediating variable is often in the model.

A variable may be called a mediator "to the extent that it accounts for the relation between the predictor and the criterion" [2]. Mediation is the name given to models in which the effect of an antecedent or independent variable (X) on the dependent variable (Y) is transmitted through a third intervening or mediating variables (M). In other words, X affects M, which in turn affects Y [3].

A researcher can determine if mediation exist in several ways. Some student (on Management Doctoral Program of Brawijaya University and Airlangga University) investigate the mediating variable use a structural equation modeling (SEM) analysis. They calculated this analysis use AMOS software. Figure 1 shows a diagram of a single mediator model.

Variable M considered a mediator if (1) X significantly affects M ($\boldsymbol{\alpha} \neq 0$) and M significantly affects Y controlling for X ($\boldsymbol{\beta} \neq 0$). This is called a conventional method. Investigation of the nature and functioning of mediation variables must proceed along two distinct dimensions: (a) the ontological content of the variable and (b) the grounds upon which the scientist is able to justify his introduction of M into the estimation of Y from X [4].

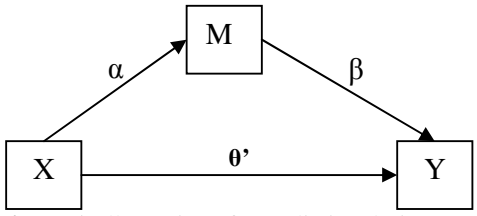

Figure 1. Illustration of a mediation design, X affects Y indirectly through M.

The formal heuristic analysis often used to detect simple mediation effects is straightforward and follows directly from the definition of a mediator provide by Baron and Kenny. Variable M is considered a mediator if (1) X significantly predicts Y (i.e., $\boldsymbol{\theta} \neq 0$ in Figure 2), (2) X significantly predicts M (i.e., $\boldsymbol{\alpha} \neq 0$ in figure 1), and (3) M significantly predicts Y controlling for X (i.e., $\boldsymbol{\beta} \neq 0$ in Figure 1).

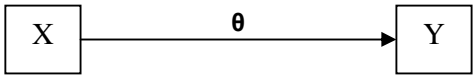

Figure 2. Illustration of direct effect, X affects Y

Baron and Kenny discuss several analyses that should be performed and the results assessed with respect to the criteria just described. These criteria are assessed by estimating the following equations:

$$Y = \delta_1 + \boldsymbol{\theta} X$$

$$M = \delta_2 + \boldsymbol{\alpha} X$$
$$Y = \delta_3 + \boldsymbol{\theta}'X + \boldsymbol{\beta} M$$

where δ_i is an intercept coefficient. When the effect of X on Y is decreasing to zero, with the inclusion of M, a perfect mediation (complete mediation) is said to have occurred. When the effect of X on Y decreases by a nontrivial amount, but not to zero, partial mediation is said to have occurred [2,5].

Test of the intervening variable effect are useful because they examine processes by which variables are related. There are three types test of significance of intervening variables effect, i.e.: causal steps, differences in coefficients, and product of coefficients. Causal steps is consist Judd and Kenny, Baron and Kenny, and Joint Significant of **α** and **β** method**.** Differences in coefficients is consist Freedman and Schatzkin, McGuigan and Langholtz, Clogg *et al.*, and Olkin and Finn method. Product of coefficients consist Sobel first-order solution, Aroian second-order exact solution, and Goodman unbiased solution, MacKinnon *et al.,* and Babko and Riek method [6].

The statistics application not should be complicated and difficult, but must be simple and easy, so that user friendly. The conventional method is more simples and easy rather than the other methods, but how sensitive? This research is conducted to investigate the problem.

2. Experimental Detail

Data was collected from 10 dissertations of Management Doctoral Program students on Brawijaya University and Airlangga University, in 2009 until 2010, which they were analyzed the mediation variable.

A researcher can determine the mediating variable, and whether it is complete or partial, if mediation exists in several ways. Hair *at al.* rule is used in this research. If path labeled **θ'** is expected to be zero due to be mediation (representing complete mediation), a SEM model can represent mediation by including only the path **α** and **β** in the model. But, if **θ'** is does not to be zero, we require to investigate the mediating variable. A series steps can be followed to evaluate mediation, these steps apply using SEM or any other general linear model approach.

1. Establish that the necessary individual relationships have statistically significant relationships:
   a. X is related to Y: Here we are establishing that the direct relationship does exist.
   b. X is related to M: Here we establish that the mediator is related the "input" construct
   c. M is related to Y: Here we establish that the mediator does have relationship with the outcome construct.
2. Estimate an initial model with only the direct effect (**θ**) between X and Y. Then estimate second model adding in the mediating variable (M) and the two path estimates (**α** and **β**)**.** Then asses the extent of mediation as follows:
   a. If the relationship between X and Y (**θ'**) remain significant and unchanged once M is included in the model as an additional predictor (X and M now predict Y), then mediation not supported.
   b. If **θ'** is reduced but remains significant when M is include as an additional predictor, then partial mediation is supported
   c. If **θ'** is reduced to a point where it is not statistically significantly after M is included as a mediating construct, full (complete) mediation is supported [1].

SEM was used for data analysis and Hair *et al.* rule was used to investigate. AMOS software is used for data analysis [7].

3. Result and Discussion

Table 1 (appendix) reports the result of investigation the mediating variable. The table shows the conventional method result that all of model is a mediating variable.

In general, Hair *et al.* rule result that model as a partial mediation. From 10 data (model) which were use in this research, 3 of them was not mediation variable and only 1 as a complete mediation.

The important result is found out that Hair *et al.* rule not have decision, i.e. the fourth model, where **θ** is not statistically significant and **θ'** is increase when M is include as an additional predictor. Moreover, the result is cannot included at the formal heuristic analysis by Baron and Kenny, because **θ** not statistically significantly, that is the model without M is included as a mediating construct.

In author's opinion, the rule to investigate the mediating variables should be completed, namely (1) if **θ** is not statistically significant, (2) **α** is significant, **β** is significant, and (3) **θ'** is significant and increase when M is include as an additional predictor, then partial mediation is supported.

The conventional method is simpler and easier. However, it is less sensitive and insufficient to investigate the mediating variables. In general, the method results a mediation variable, but it is cannot used to determine partial or complete mediation variables. Hence,

investigation by Baron and Kenny methods, Hair *et al.* rule or testing (for example by Sobel test) to determine the mediating variable is necessary.

4. Conclusion

The conventional method to investigate the mediating variable is simple and easy but insufficient. Investigation by Baron and Kenny methods or Hair *et al.* rule to determine the mediating variable is still necessary.

The rule to investigate the mediating variables should be completed, namely (1) if **θ** is not statistically significant, (2) **α** is significant, **β** is significant, and (3) **θ'** is significant and increase when M is include as an additional predictor, then partial mediation is supported.

5. Acknowledgment

I thank to the Head of Mathematics Department, University of Brawijaya, Dr. Abdul Rouf Alghofari, for financial support in the International Conference on Basic Science 2011.

6. References

[1]. Hair Jr., J.F., W.C. Black, B.J. Babin, and R.E Anderson (2010), *Multivariate Data Analysis* 7th Ed. Pearson Prectice Hall (e-books).

[2]. Preacher, K.J. and A.F. Hayes (2004), SPSS and SAS Procedures for Estimating Indirect Effects in Simple Mediation Models. *Behavior Research Methods, Instrument, and Computers.* **36** (4). 717-731.

[3]. Fritz, M.S. and D.P. MacKinnon (2008), A Graphical Representation on the Mediated Effect. *Behavior Research Methods*. **40** (1). 55-60.

[4]. Rozeboom, W.W. (1956), Mediation Variables in Scientific Theory. *Psychological Review*. **63** (4). 249-264.

[5]. Preacher, K.J. and G.J. Leonerdelli (….), *Calculation for the Sobel Test an Interactive Calculation Tool for Mediation Test*.

[6]. MacKinnon, D.P., C.M. Lockwood, J.M. Hoffman, S.G. West, and V. Sheets (2002), A Comparison of Methods to Test Mediation and Other Intervening Variable Effects. *Psychol Methods*. **7** (1), 80-114.

[7]. Arbuckle, J.L. and W. Worthke (1995-1999), *AMOS 4.0 User's Guide*. USA: Small Waters Corporation

Appendix

Table 1. Path coefficient of testing the mediation effect

No	MODEL	Model Without Mediation Variable	Model Include Mediation Variable			Explanation**
			IV -> DP	IV -> MV	MV -> DV	
1	Trust-Commitment-Loyalty	0.523*	0.297*	0.584*	0.419*	Partial Mediation
2	Job Satisfaction- Job Motivation-Performance	0.482*	0.274*	0.475*	0.410*	Partial Mediation
3	Strategic-Organizational Performance-Superiority Competition	0.413*	0.305*	0.366*	0.257*	Partial Mediation
4	Industry Competition- Partnership Strategy-Organizational Performance	-0.164ns	-0.553*	0.433*	0.897*	Partial Mediation
5	Job Behavior-Job Satisfaction-Performance	0.399*	0.357*	0.190*	0.205*	Not Mediation
6	Servqual-Satisfaction-Trust	0.405*	0.342*	0.257*	0.276*	Partial Mediation
7	Customer Value-Relationship Marketing-Customer Satisfaction	0.232*	0.069ns	0.385*	0.406*	Complete Mediation
8	Organizational Culture-Performance-Job Satisfaction	0.290*	0.232*	0.257*	0.236*	Not Mediation
9	Organizational Culture-Entrepreneurship Orientation-Organizational Performance	0.621*	0.414*	0.422*	0.495*	Partial Mediation
10	Information Technology-Competition Strategy-Performance	0.662*	0.612*	0.247*	0.199*	Not Mediation

IV = Independent Variable; DV = Dependent Variable; MV = Mediating Variable
* = Statistically significant at 0.05 level.
ns = Not statistically significant at 0.05 level.
** = The result of the conventional method shows that all of the models as a mediation variable.

Study of Impregnated Co(II) Content in Zeolite-Co(II) Catalyst toward Phenol Oxidation

Sri Wardhani [1], Tutik Setianingsih [2], Agustina Afi Rahman [3]

[1,2,3] Department of Chemistry, Faculty of Science, University of Brawijaya, Malang, Indonesia
(wardhani@ub.ac.id)

Abstract

One of the influence zeolite-CoO preparation is concentration solution of impregnation process, and the purpose research are to know the influences of impregnated Co(II) content toward ability zeolite-CoO in phenol oxidation. The preparation was done by mixing zeolite that activated in acid with $Co(NO_3)_2$ solution on concentration variation from 0.1 to 0.5 M. Co(II) content was measured by atomic absorption spectrophotometer (AAS). Phenol oxidation process was done by mixing phenol, zeolit-Co) catalyst was flew by oxygen. The remain phenol content was analyzed by UV spectrophotometer. The highest phenol oxidation ability condition was found zeolite-CoO 2.34 mmol/g with phenol oxidation percentages 62.95 %. Optimum zeolite-CoO characterized by surface area analyzer.

Keywords *: Zeolite, CoO, phenol, catalyst.*

1. Introduction

Phenol is one of the pollutants in the hazardous waters. phenol concentration in the effluent can be reduced by oxidizing phenol. catalyst needed to increase the rate of chemical reaction. catalyst used in this research is cobalt oxide. cobalt oxide is entrusted with the zeolite to increase the surface area of zeolites and to avoid the effects of sintering. one of the factors that affect the ability of the catalyst is the number of metal impregnated in zeolite.

2. Experimental Details

Preparation of natural zeolite Turen with acid activation [1]

Zeolites was filtered and washed with distilled water and then heated. Next, it was soaked in 0.4M HCl, filtered and washed with distilled water. Zeolite finally dried in an oven until reaches constant weight.

Impregnation of Co ions in zeolites

Zeolites was immersed in a solution of $Co(NO_3)_2$ of various concentrations of 0.1, 0.2, 0.3, 0.4, 0.5 M. The mixture then shaken for 3 hours and then filtered. The filtrate that contains Co^{2+} ions was determined by AAS. Next, zeolites were dried and then calcined at 500^{o}C.

*Phenol oxidation catalyzed by Co (**II)-zeolite***

100 ppm of phenol solution were added with catalyst of zeolite-Co(II), heated to a temperature of 90°C and fed with oxygen gas. Reaction carried out for 30 minutes. Filtrate concentration was then determined by UV spectrophotometer.

3. Result and Discussion

According to Figure 1, concentration of metal ions in zeolite is increasing with the increasing initial concentration of the metal ions. At this stage, there is no information gathered regarding the optimum initial concentration of metal ions used to impregnate zeolite.

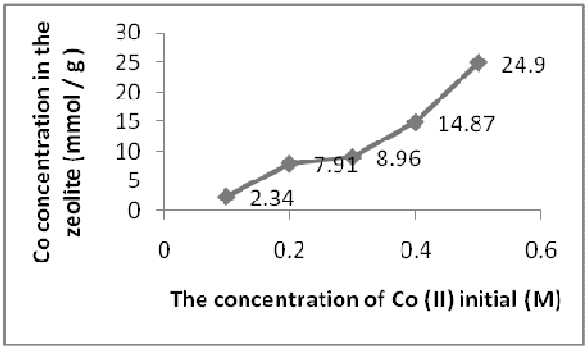

Figure 1. Effect of initial concentration of Co toward the concentration of Co adsorbed in zeolites

Next, as given in Figure 2, is the effect of catalyst type toward the amount of oxidized phenol. The presence of catalyst affects the amount of oxidized phenol. In this case, more than 60% of phenol can be oxidized using zeolite-Co(II) catalyst. This result was nearly four time

higher than using TZ, and about twelve times higher than using ZA.

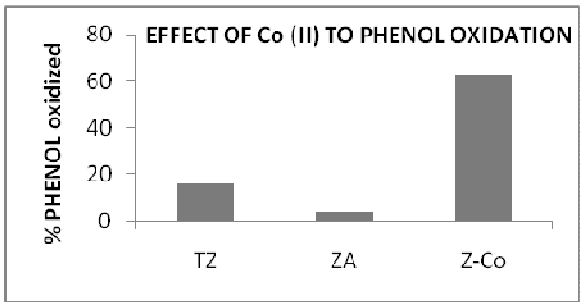

Figure 2. Effect of catalyst type toward phenol oxidation

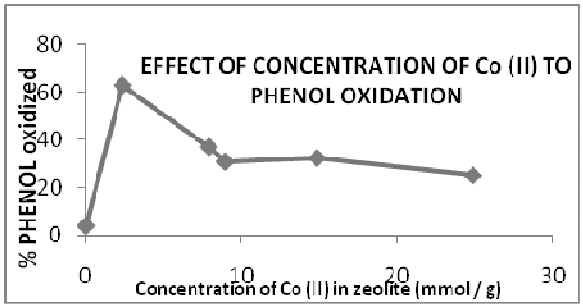

Figure 3. Effect of Co(II) concentrations toward the amount of phenol oxidized

Lastly, metal concentrations effect on the amount of phenol oxidized also investigated. The result, as seen in Figure 3, shows that the greater the Co(II) concentration used, the smaller number of phenol can be oxidized. This result is similar to previous research [2], and might be due to sintering during the oxidation.

4. Conclusion

Concentration of Co (II) impregnated with the zeolite influence the number of oxidized phenol. Catalyst Co (II)-zeolite provides the highest oxidation yields, compared to TZ and ZA, with a concentration of 2.34 mmol/g with a 62.95% of phenol that can be oxidized.

5. Acknowledgements

The authors thank to Dept. of Chemistry, Faculty of Science, University of Brawijaya for financing this paper in ICBS 2011.

6. References

[1]. Nirwana, F.I (2002), studies the influence of the concentration of hydrochloric acid natural zeolite Turen for adsorbent anions, Thesis, Chemistry and Science, UB, Malang

[2]. Agustine, L.R., (1996), Heterogeneous Catalysis for Synthetic Chemist. Marcel Dekker. Inc., New York. pp 153-182

Recent Seismicity at Guntur Volcano Complex, West Java, Indonesia

Sukir Maryanto

Physics Department, Faculty of Science, Brawijaya University, Malang (sukir@ub.ac.id)

Abstract

Guntur is a volcano complex located 35 km South East of Bandung, West Java, Indonesia. Explosive eruptions frequently occurred at Guntur crater during the period from 1690 to the middle of 19th century, however, no eruption has occurred for 167 years after the 1843 eruption. In spite of dormancy of eruptivity, seismicity of the Guntur volcano is high and earthquake swam sometimes occurred. In order to monitor the volcano, Volcanological Survey of Indonesia (present: Center for Volcanology and Geological Hazard Mitigation) and Sakurajima Volcano Research Center, DPRI, Kyoto University installed seismic network composed of 4 stations at the southern flank of the volcano for precise hypocenter determination in 1994. The hypocenters were aligned from SE to NW along the central cones and west of the summit at depth 3-5km. In Kamojang and Darajat geothermal area, the hypocenter aligned from SW to NE along the volcano at depth 3–8 km (Sadikin et al., 2007). The hypocenters at the geothermal area were not well determined due to insufficient coverage of the network. In order to locate the earthquakes more precisely, we use permanent seismic station at volcanoes around Guntur. These are Papandayan, Galunggung, Tangkuban Perahu, Ciremai, Salak and Gede volcanoes. In addition, 4 temporary seismic stations were installed north of Guntur volcano and south off (DAN, WNS, HLM and TRJ stations) to improve coverage of the seismic network. Hypocenters were determined for local tectonic earthquakes with S-P times<4 s during the period from January to October 2009 by using P and S waves, based on velocity structure utilized by BMKG. Hypocenter zone at the geothermal area SW of the Guntur volcano are widely distributed at depths around 3-9 km. The hypocenter zone extends southwestward near Papandayan volcano and westward. Hypocenters were not determined near Cikuray volcano by the previous study. Hypocenters are aligned from north to south at eastern flank of the volcano at depths around 6-12 km. No historic eruptions were recorded at the volcano. We have to examine the hypocenter distribution and focal mechanism in relation with alignment of faults around Guntur volcano.

Keywords*: Guntur volcano, Seismicity, hypocenter, focal mechanism.*

Isolation of α-Linolenic Acid from Fatty Acids of Basil Seed Oil (*Ocimum Basilicum L.*) using Urea Inclusion; Variation of Fatty Acid-Urea Ratio and Temperature Crystallization

Suleman Duengo [1], Rurini Retnowati [2], M. Farid Rahman [2]

[(1)] Postgraduate Program of Chemistry, Brawijaya University, Indonesia (suleman_duengo@yahoo.com)
[(2)] Department of Chemistry, Brawijaya University, Indonesia

Abstract

α-linolenic acid can be isolated from basil seed oil with urea inclusion method. In this method, non-linolenic fatty acids will form inclusions with urea; hence the α-linolenic acid can be separated from non-linolenic component. From this research, it was found that α-linolenic acid can be isolated by using inclusion of urea with the optimum ratio of fatty acid-urea of 1:1.5 and crystallization temperature of 0^0C, and with a percentage of 96.45%.

Keywords*: isolation, Ocimum basilicum L., α-linolenic acid.*

1. Introduction

α-Linolenic acid is an unsaturated fatty acid compound (polyunsaturated fatty acid, PUFA), which is composed of 18 carbon atoms with molecular formula of $C_{18}H_{30}O_2$. α-linolenic acid (ALA) is an omega-3 fatty acids and have pharmacological effects, especially in preventing damage to cell membranes. ALA is also a basic ingredient in the formation of eicosapentaenoic acid (EPA) and docosahexaenoic acid (DHA). EPA and DHA are omega-3 fatty acids found in the human body.

ALA can be obtained from vegetable oils in the basil seed, Armenia, candelnut, flax / linseed, linola, gold of pleasure, hemp, mustard, perilla, soybean, canola, walnuts, chia, crambe, echium, hops, kiwi, pumpkin, black currant and purslane [1]. The percentage ALA in basil seed oil is increase from 43.8 to 64.8%. In addition, basil seed oil contains several other components such as linoleic acid and oleic (17.8 to 31.3% and 8.5 to 13.3%), palmitic acid and stearic acid (6.1 to 11% and 2 to 4%) [1].

ALA can be isolated from basil seed oil using urea inclusion method. In this method, non-linolenic fatty acids will form inclusions with urea; hence ALA can be separated. This method has been used previously to isolate the ALA from linseed oil [2] and soybean seed oils [1,3].

Inclusion is a substance where one component crystallizes with a very hollow structure so that the atoms or small molecules from a second component that is added can be trapped into the cavity. Urea can form inclusions with long chain organic compounds [3]. The ability to form urea inclusion of these can be used in the separation of organic saturated and unsaturated compounds, for example in the isolation of free fatty acids.

Grandgirard (1987) reported the inclusion of urea-fatty acid (1:2) in linseed oil with silenced overnight treatment at 4^0C to produce the separation between α-linolenic acid and the other component (non linolenic acid) [2]. Many non-linolenic component were trapped in the crystal of urea (urea adduct fraction) such as palmitic acid (99.1%), palmitoleic acid (62.5%), stearic acid (99.4%), oleic acid (89.8%), linoleic acid – 18: 2 Z, E and E, Z (83%), and – 18:2 Z, Z (34.9%). Only few ALA (18:3 Z, Z, Z) that are trapped in the amount of 27.1% and the rest still remain in the filtrate [2].

2. Experimental Detail

Material

Fatty acid hydrolysis results of basil seed oil are from the material hall Medica, Batu-Malang. Chemical reagents and solvents were purchased from E-Merck: methanol, n-hexane, hydrochloride acid, and urea.

Urea Inclusion of fatty acids basil seed oil

Urea inclusion method was conducted using two variations, namely the variation ratio of fatty acid-urea and variation of crystallization temperature. The second variation will be the optimum condition of inclusion.

Ratio of fatty acid-urea

Fatty acids was mixed with a hot solution (40^0C) of urea in methanol with variations in the ratio of fatty acid-urea (1:1, 1:1.5, 1:2, 1:2.5, 1:3, 1:3.5). After cooled under nitrogen, the flask was placed at 4^0C overnight. The urea adducts and non-adduct fractions were then separated. The filtrate was transferred into separating funnel, and the fatty acids were extracted with hexane after added with water and HCl 6N.

Crystallization temperature

Fatty acids were mixed with a hot solution (40^0C) of urea in methanol with variations in the ratio optimum of fatty acid-urea. After cooled under nitrogen, the flask was placed at 6, 3, 0, -3, and -6^0C overnight. The urea adducts and non-adduct fractions were then separated. The filtrate was transferred into the separating funnel, and the fatty acids were extracted with hexane after added with water and HCl 6N.

Analysis of α-linolenic acid

0.2 gram of α-linolenic was placed in a round flask and then added with 0.1 mL of 1% H_2SO_4/methanol. The mixture was refluxed for 1 hour at 50^0C. The solution was then cooled and placed in a separating funnel. Next, it was added with $NaHCO_3$ up to neutral and added with 0.05 mL of saturated NaCl. Solution was shaken with great force and left to form two layers of organic layer (top) and water layer (bottom). The organic layer is separated from the water layer and then concentrated under nitrogen. Finally, it was analyzed using GC.

3. Results and Discussion

The ratio of fatty acid-urea

The variation of the ratio fatty acid-urea used are (1:1), (1:1.5), (1:2), (1:2.5), (1:3), (1:3.5) while the temperature used was 4^0C. The result was then esterificated and analyzed by GC (Figure 1). From the GC of α-linolenic acid, the obtained component peaks that appear were based on the retention time.

Figure 1 shows that the 1:1 ratio of fatty acid-urea levels of ALA is small because possibly the amount of urea is insufficient to form inclusion complexes with non-linolenic fatty acids. In contrast, ratio of 1:1.5 increases the ALA levels of 93.79%. Next, it was revealed that ALA levels were decreased with the increasing ratio of fatty acid-urea, which is because some part of ALA crystallized during the process of inclusion. Hence it was concluded that the optimum ratio of fatty acid-urea is 1:1.5.

Crystallization temperature

Gas chromatogram of α-linolenic acid with the inclusion of temperature variations is given in Figure 2. From the GC of ALA, the obtained component peaks that appear based on the retention time, so it can be calculated percentage of ALA as shown in Table 2.

Based on Table 2, it appears that the optimum temperature is 0°C with the inclusion of ALA percentages obtained by 96.45%. This result is better than those conducted by Grandgirard, et.al (1987), which is using urea-fatty acid ratio of 1:2 and the crystallization temperature of 4^0C and only produce ALA by 73%.

Isolation of ALA using urea inclusion method is easier to be done when compared with the freezing point method that requires treatment at extreme temperatures. According to Voet et al. (1999), fatty acids such as lauric acid, myristic acid, palmitic acid, stearic acid, a behenat acid, lignoseric acid and oleic acid which is a monounsaturated fatty acid, has a melting point above 3^0C. While the acid-unsaturated fatty acids such as acid palmitoleat, linoleic acid, and α-linolenic acid has a melting point of $-0{,}5^0$C,-9^0C, and -17^0C [4]. Moreover, ALA as unsaturated fatty acids has double bonds; therefore the molecules are not properly structured. This causes the intermolecular interaction in ALA is lower than those in saturated fatty acids. As a result, a lower melting point makes the acids turn into liquid at room temperature; hence it is hard to be trapped in the cavity of urea crystals.

4. Conclusion

A-linolenic acid can be isolated by using inclusion of urea at optimum crystallization temperature of 0°C and fatty acid-urea ratio of 1:1.5 with percentage of 96.45%.

5. Acknowledgments

Thank to Department of Chemistry, Faculty of Science, Brawijaya University that has been facilitate this reseach

6. References

[1]. Angers.P., Destaillats. F., Galvez. J.M.G. (2006), Conjugated Linolenic Acids Methods for Commercial Preparation and Purification, U.S. Patent Application Publication, Appl. No.10/523,863.

[2]. Grandgirard, A., Julliard, F., Prevost, J., Sebedio, J.L. (1987), Preparation of Geometrical Isomers of Linolenic Acid, *AOCS,* France Vol. 64 No.10.

[3]. Bist, Tao, Mohtar (2007), Method for Preparation, Use and Separation of Fatty Acids Esters, U.S. Patent Application Publication, Appl. No.11/690,540.

[4]. Voet, Donald, Judith G., Pratt, Charlotte W. (1999), Fundamental of Biochemistry, John Willey and Sons. Inc, USA

Appendixes

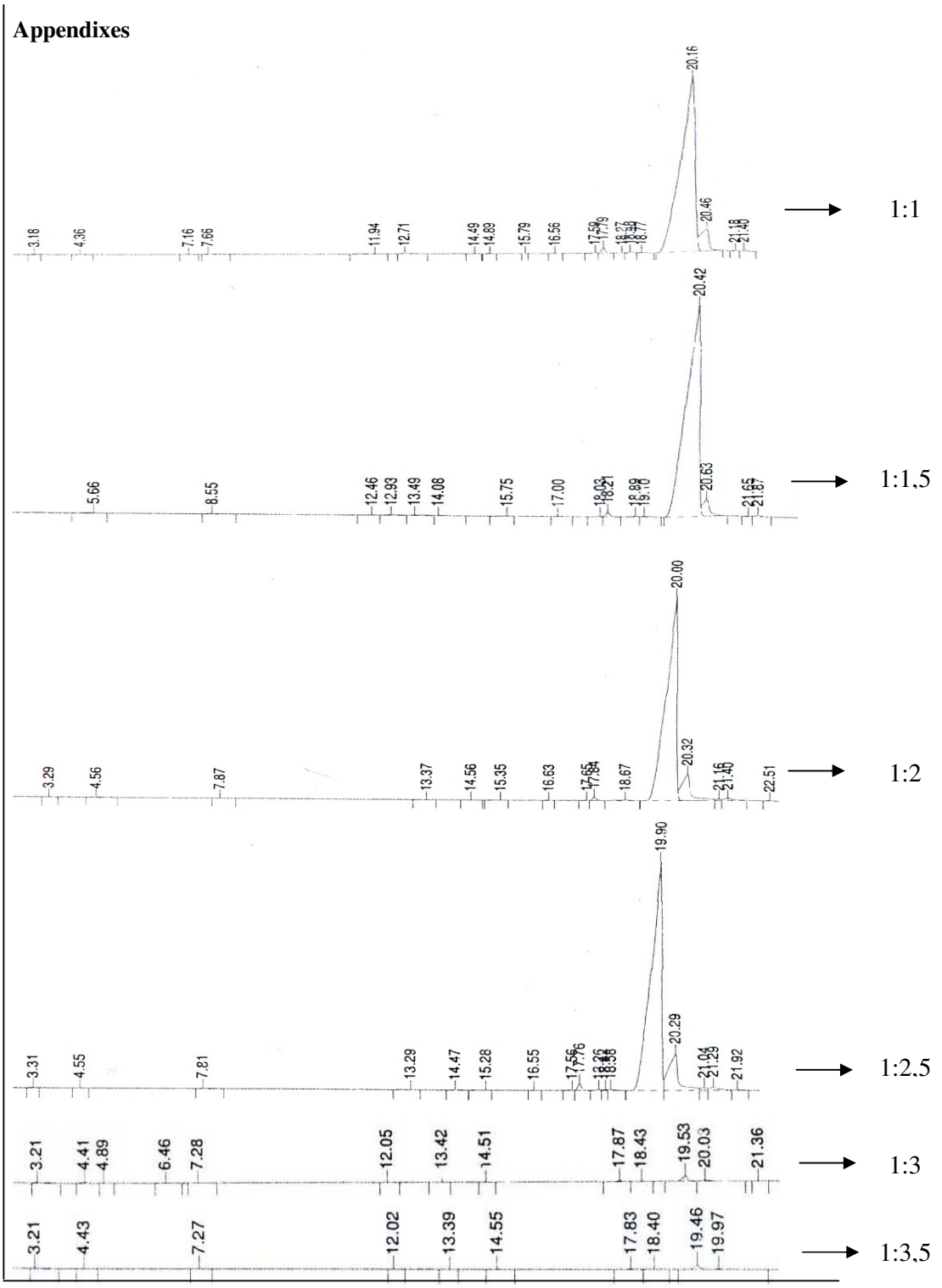

Retention time (minutes)

Figure 1. Gas chromatogram of the ratio fatty acid-urea

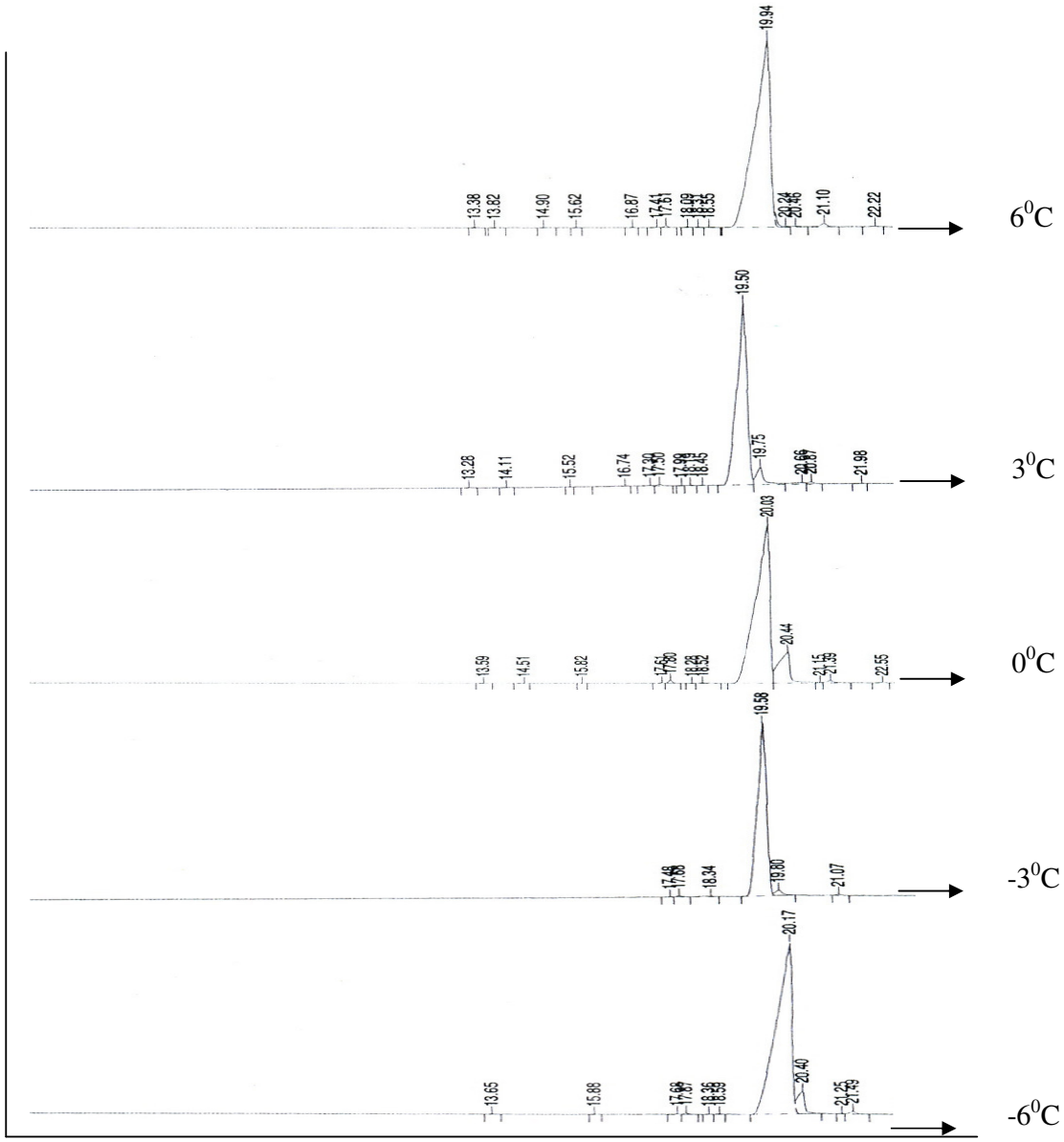

Figure 2. Gas chromatogram of the crystallization temperature.

Table 1.Percentage α-linolenic acid ratio optimization fatty acid-urea

Ratio of FA:urea	1:1	1:1,5	1:2	1:2,5	1;3	1:3,5	1:4	1:4,5
α-linolenic acid (%)	90,73	93,79	87,94	83,63	60,30	64,20	85,81	66,10

Table 2.Percentage α-linolenic acid ratio fatty acid-urea

Temperature (^{0}C)	6	3	0	-3	-6
A-linolenic acid (%)	89,93	83,78	96,45	92,70	92,00

Synthesis and Characterization of Zinc-Soap Based-on Crude Palm Oil

Sutrisno [1], Irma Agustina [2], Ratih Purnamasari [3]

[(1,2,3)] Department of Chemistry, Faculty of Mathematics and Natural Sciences, State University of Malang, Malang, Indonesia (tris_chemum@yahoo.co; tris_chemum@um.ac.id)

Abstract

Zinc stearate (Zn-stearate) and zinc oleate (Zn-oleate) have been synthesized, characterized, and identified from stearic acid and oleic acid and these compounds were called zinc-soap. In the other hand, Al-soap (Al-stearate, Al-oleate, Al-fatty acid from palm oil, and Jathropha curcas oil) have also been synthesized, characterized, and identified. Palm oil is known as a source of fatty acids, and from its saponification reaction by sodium or potassium hydroxide sodium- or potassium soap was obtained. This is known industrially and commercially. Based on the successful result of both Zn-soaps (Zn-stearat and Zn-oleate and Al-soaps and commercially synthesized sodium- or potassium soaps, the synthesis of zinc soap based-on palm oil was carried out. The research was done since palm oil is potentially developed and the diversification products are in the frame of sustainable chemistry in Indonesia and in the world. The research consists of three steps, including (1) saponification reaction of crude palm oil by sodium hydroxide to obtain sodium soap (Na-soap), (2) synthesis of zinc soap (Zn-soap) by trans-saponification of Na-soap with zinc salts, and (3) characterization and identification of Zn-soap. Zinc sulfate and Zinc chloride have been used in the research as the source of aluminum. Aluminum soap can be synthesized from crude palm oil and alcoholic sodium hydroxide by saponification reaction and then reaction of Na-soap and zinc ion by trans-saponification. The physical properties of Zn-soap are yellowis-white powder, m.p. 83–93°C (with Zn-sulfate) and 87–95°C (with Zn-chloride), highly soluble in benzene and vernis, slightly soluble in chloroform, and insoluble in water, ethanol, octanol, petroleum ether, and n-hexane and acetone.

Keywords*: crude palm oil, trans-saponification, Zn-soap.*

1. Introduction

Research of aluminum soap synthesis by saponification reaction and continued by trans-saponification reaction from some fatty acid resources has been carried out by Sutrisno, *et al* since 2003. The generally, well known as soap is sodium or potassium salt from fatty acids, and these soap is called sodium soap or potassium soap. In addition, the soap is salt of fatty acid or long chain carboxylic acid with a metal and by formulated as $(RCOO)_nL$ [1]. R- on acyl group is unsaturated or saturated hydrocarbon, L is a metal cation not only sodium or potassium, but can be calcium, zinc, magnesium, lead, aluminum, or other metal. Based-on define, was known calcium soap, zinc soap, lead soap, or aluminum soap. In addition, the materials as research new object, because multifunction especially in industry. Concept of the soap as carboxylic salt of alkali metal has been developed because research development [2]. The once of the soap is aluminum soap and zinc soap.

Research of aluminum soap synthesis by saponification reaction and continued by trans-saponification reaction from some fatty acid resources has been carried out by Sutrisno, et al since 2003. As fatty acid resources are oleic and stearic acid. Saponification reaction was done by sodium hydroxide, and *trans*-saponification was done by aluminum sulfate and aluminum chloride.

The properties of aluminum oleate synthesis result are white-yellowis powder, decomposition temperature 150^{o}C (melting point is not identified), highly soluble in chloroform and diethyl ether, slightly soluble in benzene, and insoluble in water, alcohol, and acetone [2]. The properties of aluminum stearate synthesis result are white powder, melting point 142–150^{o}C, highly soluble in alkalic, petroleum ether, and turpentene, slightly soluble in benzene, and insoluble in water, alcohol, and ether [3,4]. Aluminum oleate and aluminum stearate was fuctioned as anti water agent, glue agent, lubricant, cosmetics and medicinals, dryng agent for paint and vernis [4]. Accordingly, test to aluminum oleate and

aluminum stearate as aditive lubricant effort was researched by its viscosity measuring. Research of test potention of aluminum soap as aditive of lubricant have been carried out as follow: (1) effect of aluminum oleate to viscosity of gasoline motor lubricant [5], (2) effect of aluminum stearate to viscosity of gasoline motor lubricant [6], (3) effect of aluminium stearate to viscosity of diesel motor lubricant [7], and (4) effect of aluminum oleate to viscosity of gasoline motor lubricant [8]. Result of the research was shown that aluminum oleate and aluminum stearate potentially as aditive of lubricant.

Synthesis aluminum-soap based-on palm oil was carried-out by Sutrisno [9]. The properties of Al-soap based-on are white powder, m.p. 180–218°C (with Al-sulfate) and 203–231°C (with Al-chloride), highly soluble in chloroform, slightly soluble in diethyl ether and *n*-hexane, insoluble in water, ethanol, and acetone.

Succesfully the synthesis of Al-soap will be developed to zinc-soap based-on palm oil. Syntehsis zinc-oleate was carried by Partiwi, 2009 [10] and zinc-stearate by Laili, 2009 [11]. The properties of zinc-oleate are white powder, m.p 64–71ºC, soluble in benzene (0.027 g/mL) dan vernis (0.017 g/mL), insoluble in water, ethanol, aceton, chloroform, *n*-hexane, octanol, and petroleum ether. Properties of zinc-stearate are white powder, m.p 126–130 °C, solubility in benzene 0.030 g/mL and vernis 0.020 g/mL.

Reactions of saponification and trans-saponification to oleic acid and stearic acid with aluminum sulfate and aluminum chloride as bellow:

Step of saponification reaction:

$C_{17}H_{33}COOH_{(l)} + NaOH_{(aq)} \rightarrow C_{17}H_{33}COONa_{(s)} + H_2O_{(l)}$
Oleic acid — Sodium oleate

$C_{17}H_{35}COOH_{(s)} + NaOH_{(aq)} \rightarrow C_{17}H_{35}COONa_{(s)} + H_2O_{(l)}$
Stearic acid — Sodium stearate

Step of trans-saponification reaction:

$2C_{17}H_{33}COONa_{(s)} + Zn^{2+}{}_{(aq)} \rightarrow (C_{17}H_{33}COO)_2Zn_{(s)} + 3Na^{+}{}_{(aq)}$
Sodium oleate — Zn-oleate

$2C_{17}H_{35}COONa_{(s)} + Al^{3+}{}_{(aq)} \rightarrow (C_{17}H_{35}COO)_2Zn_{(s)} + 3Na^{+}{}_{(aq)}$
Sodium stearate — Zn-stearat

Based on accumulated experience and action research, it is argued, that the implementation and development of synthesis aluminum soap generally make used natural product metabolite primer as fatty acid resources, *i.e* palm oil, *Jatropa curcas* oil, and the synthesis of zinc-oleate and zinc-stearate. Theoretically, oleic acid and/or stearic acid can be changed by oil glyceride with vegetable oil as main resources. Research of synthesis aluminium soap by palm oil and/or *Jatropa curcas* oil is effort diversification make-used to these oils and to obtaine new materials potentially in Indonesia, especially farmer products.

2. Experimental Details

Instrumentation

Melting points were measured on melting point apparatus and uncorrected by Shibata Mel-270. AAS and IR spectra were obtained with Shimadzu 1601 and FT-IR JASCO-5300 respectively. AAS was recorded at Chemistry Department, State University of Malang, and IR spectrum was recorded at Chemistry Department, Bandung Institute of Technology.

Materials and chemicals

Samples of crude palm oil were collected at traditional market in Malang. The chemicals that used were sodium hydroxide, ethanol, zinc sulfate, zinc chloride, nitric acid, *n*-hexane, acetone, chloroform, diethyl ether, barium chloride, and silver nitrate.

Procedure

Synthesis sodium soap and aluminum soap

Zinc soap based on palm oil was synthesized by saponification reaction and to be continued with *trans*-saponification reaction. Saponification reaction was carried out by palm oil reacted sodium hydroxide to obtained sodium soap (Na-soap), furthermore sodium soap was reacted with zinc chloride and zinc sulfate *in situ* to obtained zinc soap based on palm oils (Zn-soap).

(1) Saponification reaction

The crude palm oil (10 g) was disolved in alcohol 95%, and then heated in water bath, stirred with magnetic stirrer. Into the mixture added was reacted with 30 mL alcoholic sodium hydroxide 10% (3 g sodium hydroxide was soluble in 30 mL ethanol 95%) in three necks flask, stirred by magnetic stirrer. The addition, 100 mL water was added in this mixture, and then the mixture was heated on 60^{o}C until three hours. The reaction is stopped has been no oil layer on the mixture surface. The mixture is obtained sodium soap (Na-soap).

(2)*Trans*-saponification reaction

Synthesis of sodium soap was carried out as follow: 10 g of crude palm oils was added 30 mL sodium hydroxide alcoholic 10% solution drop by drops. (These of sodium hydroxide solution was prepared of 3 g sodium hydroxide was diluted in 24 mL ethanol absolute) in three necks flask. The mixture was stirred by magnetic stirrer. In the reflux, the mixture diluted in 100 mL water, was

heated on 60°C until ± 3 hours. The reaction is stopped has been no oil layer on the mixture surface. Sodium soap (obtained on saponification step) was reacted with 6,156 g $Al_2(SO_4)_3$ and 50 mL water, heated, and stirred by magnetic stirrer. Result mixture is white suspension and finally precipitated formed.

The next continued, result mixture was refrigerant, decantation, and filtered. Precipitate (residue) result is washed with water until pH laundry water equal to pH water before used to wash. Result mixture synthesis refrigerant in room temperature, and was obtained white solid substance, that is called **palm oil zinc soap (Al-soap).** Qualitatively, water laundries also test by barium chloride and silver nitrate. Its trans-saponification with zinc sulfate, water laundry was tested by $BaCl_2$, and its trans-saponification by zinc chloride was tested by silver nitrate. If no white precipitation, that its water laundry is cleaned and Al-soap synthesis result is pure.

The presence testing of sodium (Na) element as impurity on Al-soap was determinate by atomic absorption spectrometric (AAS). The result of the purification to Al-soap can be found on the Table 1.

Table 1. Testing to water laundry on washing final to Al-soap synthesis

Parameters	Methods	Test Result
pH	pH meter	6 – 7
Sulfate (SO_4^{2-})	Barium precipitation	No precipitation
Chloride (Cl^-)	Silver precipitation	No precipitation
Sodium (Na)	AAS	Not detected

Characterization and identification of zinc soap

Zinc soap that obtained from synthesis is characterized by solubility and melting point tests. Solvents that for used solubility test are water, warm water, absolute ethanol, ethanol 70 and 50%, methanol, chloroform, acetone, and n-hexane. The solubility testing was carried out per 2 mL solvent. Result of solubility can be found in Table 2. Using of Thiele method for melting point to Al-soap, both Al-soap from $ZnSO_4$ and $ZnCl_2$, can be found difference of the melting points, including are 83–93°C (was result by its reaction with zinc sulfate), 87–95°C (was result by its reaction with zinc sulfate). The identification of Zn-soap by infrared (IR) spectrometric can be in Figure 1 and Figure 2.

Table 2. Solubility of Al-soap in some solvents

Solubility	Solvents
Insoluble	water, absolute ethanol, methanol, octanol, acetone, petroleum ether, and *n*-hexane
Highly soluble	benzene, vernis
Slightly soluble	chloroform

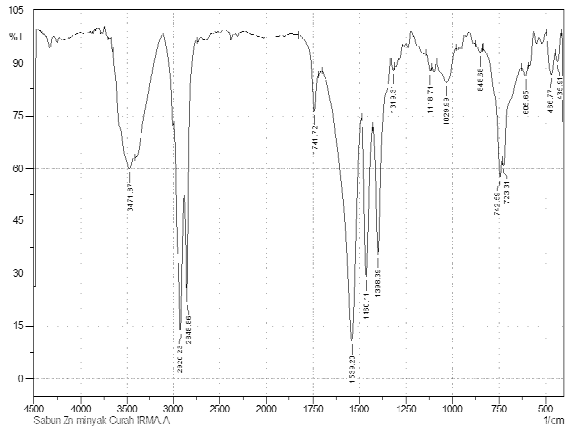

Figure 1. Infrared spectrum of palm oil Zn-soap (palm oil + $ZnSO_4$)

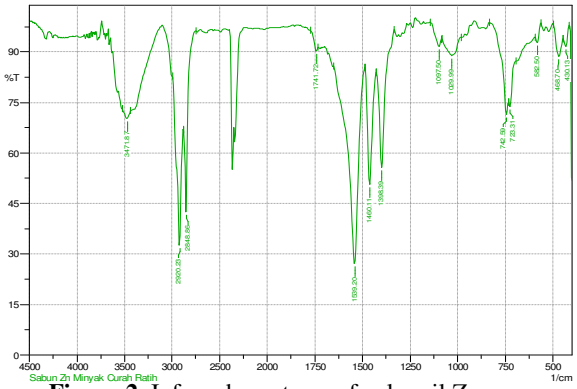

Figure 2. Infrared spectrum of palm oil Zn-soap (palm oil + $ZnCl_2$)

3. Result and Discussion

Saponification reaction principle has been used for synthesized of sodium soap that is react crude palm and sodium hydroxide. The results of reaction of saponification can be found including is change of phase of the palm oil from liquid yellow colored to form of coagulation white colored. The reaction of saponification is given in Figure 3 (Appendixes).

The carboxylic groups ($R_1/R_2/R_3$-COO^-) in the palm oil including are oleic ($C_{17}H_{33}COO^-$),

linoleic ($C_{17}H_{31}COO^-$), palmitic ($C_{15}H_{31}COO^-$), stearic ($C_{17}H_{35}COO^-$), palmitoleic ($C_{15}H_{29}COO^-$), or linolenic ($C_{17}H_{29}COO^-$), that is fatty acids in palm oil. Zinc soap was synthesized by trans-saponification reaction from sodium soap that is produced on stage of saponification reaction *in-situ*. Reaction *trans*-saponification was carried out by zinc sulfate and zinc chloride solution drop by drops. At the time of zinc solution addition emerges white precipitate but then dissolves to return with informer. Addition of zinc on an exess formed more and more white precipatate, up to final form yellowness white precipitate.

In the saponification reaction used sodium hydroxide exess, so that still maked existence of OH^-. If added of zinc ion, so not only Al^{3+} ion was substituted of Na^+ ion, but also can react with OH^- to obtained $Zn(OH)_2$. There is OH^- exess, will be formed tetrahydroxyzincat, $Zn(OH)_4^{2-}$. The $Zn(OH)_4^{2-}$ can be soluble. Thus, precipitate was obtained on the trans-saponification reaction is zinc soap, not zinc hydroxide. Reaction of the process can be formulated as follows:

$$Zn^{2+}_{(aq)} + 3OH^-_{(aq)} \rightarrow Zn(OH)_{2(s)}$$
$$Zn(OH)_{2(s)} + 2OH^-_{(aq)} \rightarrow Zn(OH)_4^{2-}{}_{(aq)}$$
$$Zn(OH)_4^{2-}{}_{(aq)} \rightarrow ZnO_2^{2-}{}_{(aq)} + 2H_2O_{(l)}$$

Based on the principle, the substitution of Na on Na-soap by zinc to zinc soap (Zn-soap) was occurred. Zinc soap of the synthesis produced have properties as bellow: white powdered, melting point 180–218°C (was result by its reaction with zinc sulfate) and 203–231°C (was result by its reaction with zinc sulfate), insoluble in water, warm water, absolute ethanol, ethanol 70%, ethanol 50%, methanol, and acetone; slightly soluble in n-hexane and diethyl ether; and highly soluble in chloroform. Analysis of zinc and sodium to water laundry of Zn-soap (Table 1), have shown that is the Zn-soap pure relatively.

Likewise, spectrometric analysis to two Al-soap (formed by $ZnSO_4$ and $ZnCl_2$) has shown identically. Ideally, *trans*-saponification reaction of Na-soap by zinc ion (from $ZnSO_4$ and/or $ZnCl_2$) becomes zinc soap (Zn-soap) can be formulated and this formulation is presented in Figure 4 (Appendixes).

4. Conclusion

Saponification reaction of crude palm oil with sodium hydroxide was obtained sodium soap. The next step, (1) *trans*-spanofication reaction sodium soap with zinc sulfate was result zinc soap, (2) *trans*-saponification reaction by zinc chloride given zinc soap. The properties zinc soap was white powder solid, melting point 180–218°C (resulted from zinc sulfate), and 203–231°C (resulted from zinc sulfate). The both zinc soap, Zn-soap from $ZnSO_4$ and Zn-soap from ZCl_2 are highly soluble in benzene and vernis, slightly soluble in chloroform, and insoluble in water, ethanol, octanol, petroleum ether, and *n*-hexane and acetone. Based-on these properties, will be studied its properties and potentially as lubricant oil additives.

5. Acknowledgement

I would like to thank The Head of Research Institution State University of Malang (Lembaga Penelitian UM) for support of our research in this area, and also to my students (Agustina and Purnamasari) that has been conducting the laboratory activity in the Department of Chemistry, Faculty of Mathematics and Natural Sciences, State University of Malang, Indonesia.

6. References

[1]. Considine, M. D., (1984), Encyclopedia of Chemistry, 4th ed. New York: Van Nostrand Reinhold Company.

[2]. Kiyokawa (1976), Fatty Acid Aluminium Soap. (Abstract Compilation *Schifinder Scholar*. p. 3. Accessed on 26 November 2001).

[3]. Sutrisno, Dasna, I. W., Parlan, Rachmawati. A, Pangestu, N.P. (2006), Sintesis, karakterisasi, dan identifikasi sabun aluminium oleat. Chemistry National Seminar 4 February 2006. Himpunan Kimia Indonesia (HKI) Jatim – Chemistry Dept FMIPA, State University of Surabaya.

[4]. Hawley, G, G. (1987), Condensed Chemical Dictionary, 8th ed. New York: Van Nostrand Reinhold. p 46-47,49

[5]. Nikmah, L., (2005), Pengaruh Aluminium Oleat terhadap Viskositas Minyak Pelumas Motor Bensin. Skripsi, Jurusan Kimia FMIPA, State University of Malang.

[6]. Harmaningtias, W., (2005). Pengaruh Aluminium Stearat terhadap Viskositas Minyak Pelumas Motor Bensin. Skripsi Jurusan Kimia FMIPA, State University of Malang.

[7]. Yuniarto, E., (2006), Pengaruh Aluminium Stearat terhadap Viskositas Minyak Pelumas Motor Diesel. Skripsi, Jurusan Kimia FMIPA, State University of Malang.

[8]. Kharisuddin, M.A., (2006), Pengaruh Aluminium Oleat terhadap Viskositas Minyak Pelumas Motor Diesel. Skripsi, Jurusan Kimia FMIPA, State University of Malang.

[9]. Sutrisno (2009), Synthesis and Characterization of Aluminium-Soap Based-on Crude Palm Oil, Proceedings International Chemistry Seminar "Palm Oil and Sustainable Chemistry" *Yogyakarta Indonesia,* Editor: Jumina, *et al*, 339 – 345.
[10]. Pratiwi, E. (2009), Sintesis dan Karakterisasi Zink Oleat dari Asam Oleat dengan Zink Sulfat. Skripsi, Jurusan Kimia FMIPA, State University of Malang.
[11]. Nuzula, L., 2009. Sintesis dan Karakterisasi Zink Stearat dari Asam Stearat dengan Zink Klorida. Skripsi, Jurusan Kimia FMIPA, State University of Malang.

Appendixes

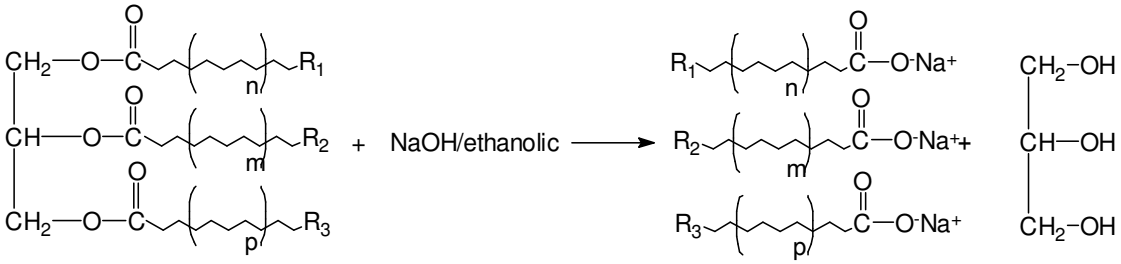

Figure 3. Saponification Reaction

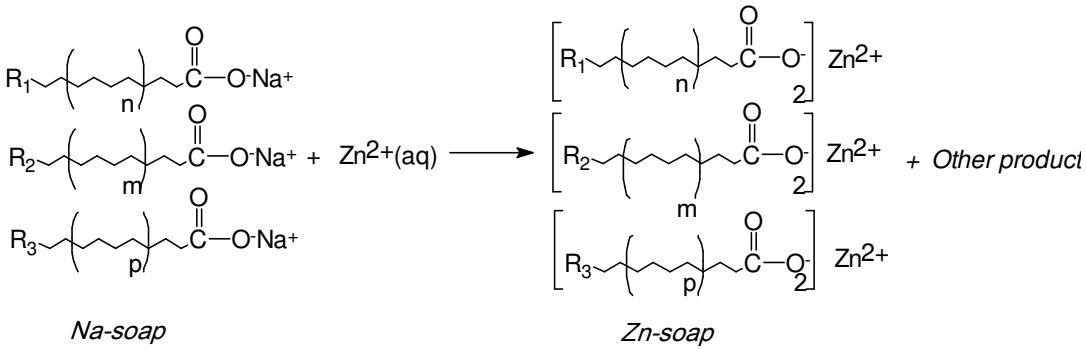

Figure 4. Formulation Reaction of the process

The Effect of Alternative Nitrogen Sources on Xylanase Production from *Trichoderma Viride*

Sutrisno [1], Anna Roosdiana [2], Widyasari S [3]

[1,2,3] Department of Chemistry, Faculty of Sciences, Brawijaya University, Indonesia
(tris_mc@ub.ac.id)

Abstract

Xylanase as extracellular enzyme has been used for hydrolizing xylan to xylose and xylo-oligosaccharide. Xylanase was isolated from Trichoderma viride which was grown on various nitrogen sources, such as peptones, yeast extract, soybean residue, rice bran, and elephant grass. The aims of this research was to investigate the alternative nitrogen sources that used for Trichoderma viride growth medium to produce xylanase with high specific activity, to obtain pure xylanase and to determine the kinetic parameter of enzymatic reaction. Crude xylanase was obtained by growing the Trichoderma viride in liquid medium for 60 hours. Xylanase activity showed by the amount of reducing sugar through hydrolysis reaction at the optimum condition of 60°C, pH 5 and incubation period 55 minutes. Specific activity of xylanase was determined by dividing the xylanase activity to protein content. Xylanase activity enhanced by enzyme purification using ammonium sulphate fraction of precipitation method. The result showed that highest specific activity was resulted on crude xylanase from Trichoderma viride which was grown in peptone nitrogen sources with the value of 4.369 U/µg protein and alternative nitrogen source of rice bran was found of 2.720 U/µg protein. The highest of pure xylanase specific activity was found of 45-60% fraction purification of 13.093 U/µg protein and xylanase specific activity increased 392.53% compared to crude xylanase. The crude enzyme has high substrate affinity than purified enzyme which revealed K_M of 0.06% and 0.09% respectively.

Keywords*: Nitrogen sources, xylanase, specific activity, Trichoderma viride.*

1. Introduction

Xylanase is an extracellular enzyme that can catalyze hydrolysis reaction of xylan into xylose and xilo-oligosaccharides. Xylanase is used in paper bleaching process, a mixture of animal feed, syrup purification, and manufacture of sugar xylose. Xylanase can be produced by some microorganisms such as *Trichoderma viride, Bacillus, Cryptococcus, Aspergillus, Penicillium, Aureo-basidium, Fusarium, Rhizomucor, Humicola* [1].

All microorganisms require a medium containing carbon and nitrogen sources for growth. Xylanase-producing microorganisms require peptone as nitrogen source. Peptone are expensive, so the use of pure compounds directly in media production cost is quite high, therefore it needs to do research to make use of agricultural products or wastes that contain lots of nitrogen to replace these compounds. This research aim is to produce xylanase from the fungus *T. viride* with alternate nitrogen sources peptone, including yeast extract, tofu waste, elephant grass, rice bran and peptone used as a control.

Enzymes produced in media production is usually still mixed with proteins other than enzymes (enzyme crude extract), thus having relatively low specific activity. Therefore, purification is necessary; in order to obtain more pure xylanase which characterized by increased activity of specific enzymes. Purification method is done by adding salt protein precipitation of ammonium sulfate ($(NH_4)_2SO_4$) with various concentrations to a solution of crude extract and stirring at low temperature.

Each enzyme has a Michaelis-Menten constant value specified. Value of K_M can be used to estimate the amount of substrate needed for the enzymatic reaction run efficiently. By knowing the value of K_M and V_m an enzyme it can be done optimizing the use of enzymes such as biocatalisator reaction substrate solution into a product. Specifically, this research will studied the effect of alternative nitrogen sources on production of xylanase from *T. viride* and determination of its kinetics parameters.

2. Experimental Details

Materials

T. viride microbial strains are used for production of xylanase obtained from Microbiology Laboratory of UB. The composition of growth media (g / L) are described as follows: proteous peptone 0.5, urea 0.3, KH_2PO_4 0.2, $CaCl_2$ 0.3, Tween-80 0.2, $(NH_4)_2SO_4$ 1.4; $MgSO_4.7H_2O$ 0.3, and 1% soybean epidermis as carbon source. Medium at pH = 5 sterilized in an autoclave at 121 °C, 15psi for 15 minutes. Trace element solution is then added as much as 0.1%. Repetitions performed for a variety of different nitrogen substrates is replaced by yeast extract peptone, tofu waste, rice bran, and elephant grass. Composition of trace element solution (g/L): $FeSO_4$ 0.05; $ZnSO_4.7H_2O$ 0.014; $CoCl_2$ 0.02; $MnSO_4$ 0.016

Preparation of Inoculum

Preparation of inoculum carried out by taking spores from pure cultures of *Trichoderma viride* that has been aged for 4-6 days from one side, and then suspended in 10mL of sterile distilled water. The suspension was taken of each of 2mL and grown in three pieces, each conical flask containing 13mL of sterile liquid media. These media were then incubated in a shaker for 36 hours and continued with the production of enzymes.

Enzyme Production

Prepared conical flask 250mL 3 pieces, each containing 150mL liquid medium, then sterilized in an autoclave. After it was cool, add 15mL of aseptic inoculum. These media were then incubated in a shaker with a speed of 150rpm at room temperature for 60 hours, after which the enzyme was isolated.

Enzyme Isolation

Xylanase was isolated by centrifugation method. Each of the liquid medium was added with 15mL of acetate buffer pH 5.0 and centrifuged at 3000 rpm for 30 minutes at 4°C. Supernatant obtained a crude extract of xylanase, which were then tested for its activity.

Fractional Precipitation with Ammonium Sulfate

Xylanase crude extract was purified by fractional precipitation method by adding solid ammonium sulfate, with a fraction 0-30%, 30-45%, 45-60% and 60-75%. Sediment fractions were dissolved with 5mL of acetate buffer 0.2 M. Then performed dialysis to separate the ammonium sulfate precipitated protein from the enzyme

Determination of Activity and specific activity of Xylanase Extracts Coarse [2]

Prepared 5 pieces of test tubes and each filled with 1% xylan substrate (w/v) of 1mL. Then the tube was incubated in a water bath at 60 °C for 15 minutes. Then it was added with xylanase crude extract of 1mL, 1 mL of acetate buffer pH 5 and incubated at 60°C for 50 minutes. After that, each tube was incubated in boiling water bath for 15 minutes and cooled in ice water until it reaches room temperature. Then the reducing sugar content was analyzed by spectrophotometry using Nelson-Somogyi reagent.

Xylanase activity was expressed in Units. One unit of enzyme activity is the number of g reducing sugar produced by 1mL of enzyme in each minute. The specific activity of xylanase was defined as the number of units (U) generated by each g protein enzymes. Protein content was determined by spectrophotometry using biuret reagent and used as a standard solution of BSA (Bovin Serum Albumin).

Determination of V_m and K_M

V_m and K_M are determined by enzyme activity assay xylanase with xylan substrate at pH 5, temperature 60 ° C and incubation time of 55 minutes. Xylan substrate concentration variation of (0.1, 0.5, 1.0, 1.5, 2.0)% (w / v). [3].)

3. Results and Discussion

Xylanase produced by *T. viride* grown on media with peptone nitrogen source has the highest specific activity of 4.37 U/g (100%), on the medium with nitrogen source tofu 1.55 U/g protein (35.59%), on media with the source rice bran nitrogen 2.72 U/g protein (62.26%), the medium with nitrogen sources yeast extract 2.09 U/g protein (47.95%) and in the media with elephant grass nitrogen sources 0.9 U/g protein 20.67%.

The highest specific activity of xylanase produced by *T. viride* on alternative nitrogen sources is rice bran. Next step is purification by precipitation method stratified by adding ammonium sulfate precipitation fractions used were 00-30%, 30-45%, 45-60% and 60-75%.

The specific activity of xylanase purified by the addition of ammonium sulfate is higher than the specific activity of crude extracts. The highest specific activity of purified xylanase is in fraction 45-60%

The concentration of substrate is one factor that can affect enzyme activity. Effect of substrate concentration on the xylanase activity before and after purification was done with the variation of substrate concentration (0.1, 0.5, 1.0, 1.5, 2.0) % (w / v), which reacted in optimum condition. V_m and K_M value can be determined by using Lineweaver-Burk equation.

From this equation it can be seen the maximum speed V_M and K_M. The maximum speed V_M xylanase crude extract is at 3.356 g / mL.menit with K_M values of 0.064%, while the maximum speed for pure xylanase is at 0.933 g / mL.menit with K_M values of 0.098%.

4. Conclusion

1. Alternative nitrogen source that is used as a medium for the growth of *T. viride* in producing xylanase with high specific activity of (2.72 ± 0.55) U/µg protein was rice bran.
2. The highest specific activity of purified xylanase fraction at the result of saturation of ammonium sulfate precipitation with 45-60 % was (13.09 ± 1.05) U/µg protein.
3. The specific activity of purified xylanase fraction of 45-60% increase 392.53% compared to the specific activity of crude extracts.
4. V_M and K_M values obtained from *Lineweaver-Burk* equation for crude extract of xylanase was 3.356 µg/mL.min and 0.06% and for purified xylanase was 0.933 µg/mL.min and 0.10 %.

5. Acknowledgement

The authors thank to Dept. of Chemistry, Faculty of Science, University of Brawijaya for financing this paper in ICBS 2011.

6. References

[1]. Haltrich, D., Nidetzky, B., Kulbe, K.D., Steiner, W. and Zupaneie, S. (1996), Production of Fungal Xylanases, http://www2.psu.ac.th/PresidentOffice/EduService/journal/27-2-pdf/10xylanase.pdf, accesed on 15 July 2006

[2]. Isil, S. and N. Aksoz (2005), Investigation of Factors Affecting Xylanase Activity from *Trichoderma harzianum 1073 D3*, *Brazilian Journal of Biology and Technology 48(2):1516-8913*

[3]. Widyasari, S. (2007), Isolasi dan Karakterisasi Ekstrak Kasar Xilanase dari *Trichoderma viride*, Skripsi Program Sarjana Kimia. Universitas Brawijaya, Malang.

Appendixes

Figure 1. Enzyme Production of Xylanase from *T. viride* with different nitrogen sources

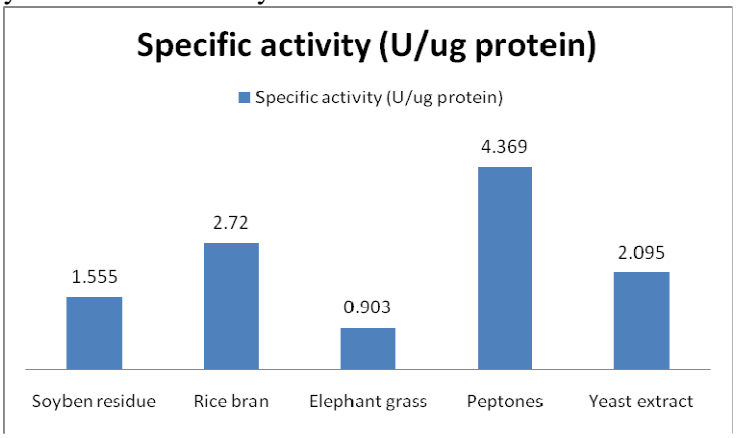

Table 1. Activity and specific activity of xylanase at various fractions of ammonium sulfate precipitation

Fraction	Activity of Enzyme (U/mL)	Protein content (µg/mL)	Specific activity (U/µg protein)	Specific activity increases (%)
0%	2.695	1.016	2.720	0
0-30 %	3.265	0.465	7.016	167.04
30-45 %	2.072	0.258	8.023	201.66
45-60 %	1.463	0.112	13.093	392.53
60-75 %	1.166	0.292	3.910	47.55

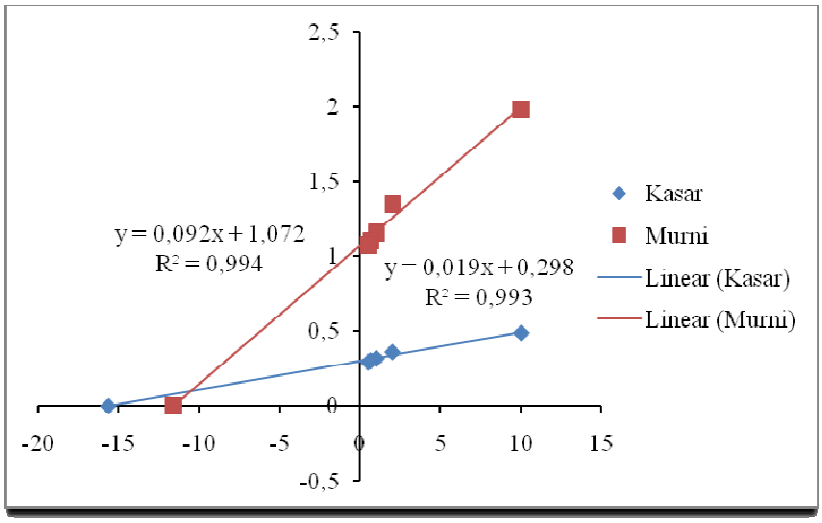

Figure 2. Vo relationship curve with 1 / [S] crude extract and pure xylanase

*Effectivity of Ammonium Iron (III) Hexacyanoferrate Decontaminant in eliminating ^{137}Cs Radionuclides from the Body of Long Tail Monkey (*Macaca fascicularis*)*

Tur Rahardjo

Center for Technology of Radiation Safety and Metrology, National Nuclear Energy Agency, Jakarta
(turahardjo@batan.go.id)

Abstract

The assessment of effectivity of ammonium iron III hexacyanoferrate (AFCF) decontaminant at various doses in eliminating ^{137}Cs radionuclides from the body of long tail monkey had been done. The purpose of this research was to obtain an optimum dose of decontamination in excreting ^{137}Cs from body of long tail monkey (*Macaca fascicularis*). Twelve monkeys were divided into 4 groups of treatment, each was contaminated orally with ^{137}Cs with the activity of 1 µCi/ml and 30 minutes later they were decontaminated with AFCF for 3 days consecutively with total doses of 3000, 4500, and 6000 mg/monkey. Three monkeys without AFCF treatment were used as control. The observation of their effectivity was done by counting the activity of ^{137}Cs in blood, urine**,** feces and organs on days of 1, 2, 3, 4, 5, 6, 7, 14, 21, 28, and 35 post decontamination. The results showed that all three doses of AFCF could increased the elimination of ^{137}Cs through feces and urine up to day 35 as high as 46.32%, 44.20%, 45.39% and 34.27% for 3000, 4500, 6000 mg/monkey and control, respectively. It was known that the orally treatment of AFCF decontaminant was effective in eliminating ^{137}Cs from the body of long tail monkey.

***Keywords**: Decontaminant, ^{137}Cs, and, Ammonium iron III hexacyanoferrate (AFCF).*

1. Introduction

The use of radioactive substances in various industrial activities, medicine, agriculture and other technologies are now widely performed. The processing of nuclear materials has also been implemented as the beginning of the nuclear industry in Indonesia. The rapid advancement of nuclear technology is not free of problems of radiation safety that need to be controlled very well and will bring a serious impact on the risk of release of radioactive elements into the environment and finally deposited in the human body. Some of these contaminants are fission products (^{137}Cs, ^{131}I and ^{90}Sr radionuclides) and contaminants originating from industrial installation that use radioactive substances as a source of radiation such as ^{60}Co0, ^{92}Ir and others [1].

^{137}Cs is a chemical element that is radioactive by emitting gamma rays and is one of fission products of uranium and plutonium fuel in nuclear reactors. ^{137}Cs is a radioisotope that commonly used in industry. Radioisotopes are used in a variety of measurement tools, such as moisture density gauge, measures the thickness of sheet metal, and as a transmitter source of gamma radiation for cancer treatment. Cs is also used for the diagnosis of disease, as a calibration source of radiation equipment and resources in large numbers are used to sterilize medical equipment [2].

^{137}Cs has a physical half-life of 30 years, including radionuclides that are easy to dissolve so that it easily absorbed by body's tissue. The results showed that the average absorption fraction is 0.99 for chloride and 0.82 for oxide. ^{137}Cs also entered the blood will be distributed or absorbed into the body tissue, 10% of Cs issued by the biology of 2 days and 90% slow-release with biological half-life of 110 days and less than 1% of Cs deposited in the body with biological half-life of about 500 days. The high doses of ^{137}Cs will poisonous to the organism while in small doses it can trigger a cancer. Exposure to harmful substances that can enter into human body can be through the inhalation or ingestion, so that the radioactive material will spread in the soft tissues, especially muscle [3].

Ability in dealing with someone who is exposed to radionuclide contamination is needed on a crash nuclear agency. Radionuclides that enter the body should be studied and examined aspects related to health. One of the most important aspects is how to remove them from the

body, because it is harmful when deposited in the body. An important precaution in the handling of victims of nuclear accidents on the state of the decontamination process [4].

Decontamination is a method of cleaning or removal of radionuclides from the body as much as possible (quickly and precisely) as an attempt to minimize the biological effects. This process can be done by the binding of radionuclides by chemical substances and excrete decontamination in complex compounds from the body through urine and feces Thus, the binding process is most effective if the radionuclide is not absorbed into the system and enter the bloodstream. Giving the decontamination immediately after an accident is the most appropriate action [5].

Ammonium Iron (III) Hexacyanoferrate (AFCF) has the chemical formula of NH_4Fe $[Fe(CN)_6]$). AFCF is a material used to bind Cs, which prevents the absorption of radioactive Cs from the digestive tract. AFCF has a molecular weight of 285.87 mol; the maximum absorbance at 685 nm was around 0.84. AFCF contains 30-35% ammonium chloride. Transition metal of hexacyanoferrate has long been recognized in the exchange of ions to bind Cs. AFCF available as food supplements for farm animals in a case of nuclear accidents [6].

AFCF is decontamination that can bind ^{137}Cs in the digestive tract, preventing absorption of ^{137}Cs and accelerate the expenditure of the body. In the case of nuclear accident at Chernobyl, Ukraine in 1986 has been used as decontamination AFCF for ^{137}Cs and ^{134}Cs. Several studies in animals (rats, goats, deer, sheep, chicken broiler) showed that these decontaminants have potential in the binding of Cs so as to minimize the levels of radioactive substances in the body [7].

AFCF binds ^{137}Cs by ion exchange process [8]. AFCF is more effective in binding ^{137}Cs in the digestive tract compared to PB (Prussian Blue). AFCF is a practical and efficient material on the conditions after the Chernobyl accident as it can increase the fiber in ruminant animals and assist in reducing the absorption of ^{137}Cs in the tissue/muscle [9].

AFCF can prevent the absorption of Cs almost completely. This is evidenced in studies using reindeer administered orally AFCF 0.5 g/day and bentonite by 25 g/day. Orally administration of AFCF 5 mg to mouse can eliminate the ^{137}Cs as much as 2.4% to 6.3% and the activity of ^{137}Cs in pig contaminated by Chernobyl accident has been reduced from 360 Bq/kg to 10 to 30 Bq in 27 days [10]. Other research found that as many as 0.2 grams of AFCF in chickens that have been given a mixture of ^{137}Cs in increments of 1 ml of ^{137}Cs at oral administration, within 13 days of ^{137}Cs levels in meat reaches 80-83% lower compared to the control of 89% in liver and 83-84% in kidney [10].

Decontamination process aims to reduce the absorption of radionuclides into the body by increasing the excretion of radionuclides through urine and feces so that minimize their biological effects that might be arise. Each radionuclide has its own decontaminant and each must be tested for its ability. Research by Alatas et al showed that Prussian Blue given orally three hours after oral administration of ^{137}Cs to white mouse can increased the excretion of radionuclides up to 84.80%.

In this study, we used AFCF as decontaminant in long-tailed monkey (M. fascicularis) as experimental animal. When radioactive material entered into the body, it is important to estimate the dose of decontamination. The doses of AFCF used in this study are 3000, 4500 and 6000 mg/monkey. Estimation is done based on the lethal dose (LD50), and it was known that LD50 of AFCF for rats was 2100 mg / kg (Anonymous, 2000).

The purpose of this study was to determine the effectiveness of decontaminant of AFCF in excretion of ^{137}Cs from long-tailed monkey's body Hopefully this can provide information on the effectiveness and effective dose of decontaminant of AFCF ^{137}Cs in the excretion of ^{137}Cs from the body long tail monkeys.

2. Experimental Detail

The object of research

Twelve long-tailed monkeys (*Macaca fascicularis*) of ±5 years old with body weight of ±5.5 kg were obtained from the Primate Section of Bogor Agricultural Institute (IPB), and maintained/quarantined in Biomedical Division Laboratory for 3 months, and determined their body weight, temperature, pulse rate, heart rate, hair loss, and turgor, provided by food and water and their health was monitored by a veterinarian.

Treatment

Macaca fascicularis were divided into 4 groups and each group consists of 3 and then was given orally contaminant (^{137}Cs radionuclide) at 1 µCi/ml of activity (as much as 3 ml/each to all groups of monkeys).

Dose of AFCF was varied into 3.000, 4.500 and 6.000 mg/monkey, and administered orally for 3 consecutive days. Observation of AFCF effectiveness in eliminating the contaminants was carried out by counting ^{137}Cs in stool samples, urine, blood, and organs by using Gamma Spectrometer with germanium semiconductor as detector (NAI-Tl) at 661.607 keV of energy performed on days 1, 2, 3, 4, 5, 6, 7, 14, 21, 28, and 35 post-administration of AFCF.

3. Results and Discussion

Activity of ^{137}Cs accumulated in blood

The results showed that the activity of ^{137}Cs accumulated in the blood of monkeys that were given AFCF was lower than that of controls (Figure 1). ^{137}Cs activity was lowest at doses of 3000 mg (13.15%), whereas 4.500 mg dose was 22.57% and 6.000 mg dose was 25.46% and for control it was 26.85%.

Statistical analysis showed that there was no significant difference on the average ^{137}Cs activity accumulated in the blood at 4 days of treatment, and AFCF did not have a significant influence on the activity of ^{137}Cs excreted through urine and feces. AFCF could suppress the activity of ^{137}Cs in the blood of monkeys compared to control, because AFCF was able to bind ^{137}Cs which prevent the absorption of ^{137}Cs. ^{137}Cs was mostly excreted through feces and urine.

The daily observation of ^{137}Cs activity in the blood showed that there was an increase on day 3, the 7 and 14, and then there was a decrease in the next days. Observation up to 35 days showed that the activity of ^{137}Cs was highly found in blood, where for 3.000 mg dose it was accumulated up to 13.14%, 4.500 mg dose it was 19.33% and the dose of 6000 mg it was 18.19%, while for control it was 26.85%. These increment activity of ^{137}Cs at days 1-35 was caused by the fact that ^{137}Cs that was absorbed in the blood would not removed and only accumulates in the blood, in the organs of the body and be reabsorbed by the body's other organs so that the activity of ^{137}Cs in the blood increases. The results of Alatas et al showed that blood is a media for radionuclide transfer from one organ to another organ.

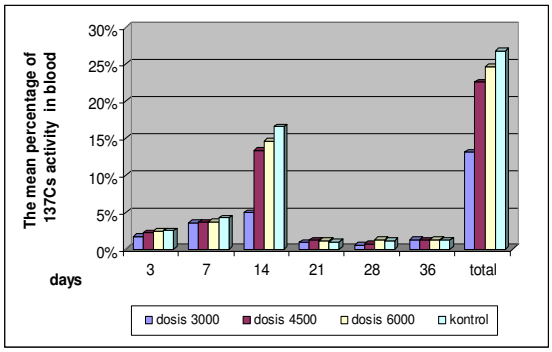

Figure 1. The mean ^{137}Cs activity in blood of monkeys at days post AFCF administration

Activity of ^{137}Cs accumulated in organs

^{137}Cs contaminants that enter the blood circulation will be brought to the whole body and in contact with tissues of body. The observation of ^{137}Cs activity that accumulated in the organs on day-35 post decontamination showed that the activity of ^{137}Cs in monkeys administered with AFCF was lower than the control (Figure 2). The lowest ^{137}Cs activity was observed at a dose of 3000 mg (21%), 4500 mg was 21.52% and 6000 mg was 23.45% and control it was 41.23%. The high activity was found in carcass, kidney, spleen and bone. This indicates that there was a ^{137}Cs transfer from the blood into body fluids (spleen and extra vascular fluids), tissues and other organs. ^{137}Cs activity that accumulated in the carcass for dose of 3.000 mg was 6.16%, 4.500 mg was 6.48%, and 6000 mg was 7.42%, while the control was 24.00%.

The high activity of ^{137}Cs was found in carcass because the carcass is the sum of the residual activity of blood, bone, muscle and organs/tissues of monkeys. Basyarahil stated that very high activity of ^{137}Cs was accumulated in the carcass because the uptake of ^{137}Cs was mainly occurring in muscle as the main component of carcass. The activity in kidney seemingly lower than that of the carcass, i e. 3000 mg dose of 2.63%, 4500 mg dose of 2.44% and 2.74% dose of 6000, while in control of 2.81%. Increased activity of ^{137}Cs in the blood will cause the increased activity of ^{137}Cs in the kidney. Dakk stated that the kidney has a high ability to bind chemicals and collect toxicant than other organs.

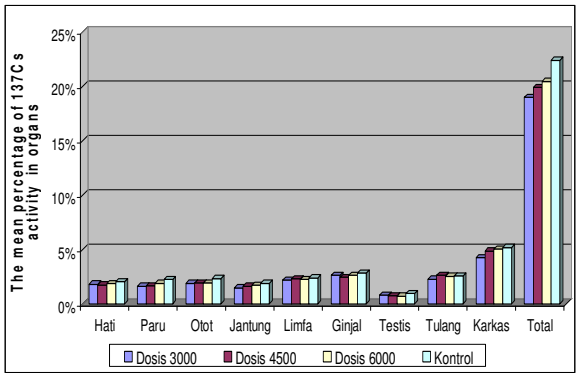

Figure 2. The mean percentage of ^{137}Cs activity in organs at days post AFCF administration

The high activity of ^{137}Cs was also accumulated in bone, the dose of 3000 mg of 2.28%, 4500 mg dose of 2.61%, 6000 mg dose of 2.58% while control was 2.58%. It showed that many ^{137}Cs absorption occurred in the bone. These data were consistent with the research by Alatas et al who found that the high activity of ^{137}Cs was accumulated in bone because the bone is a target organ of ^{137}Cs. The activity of ^{137}Cs accumulated in target organs can be minimized by giving AFCF. Other organs such as cardiac, muscle, liver, lung and testis were quite low. AFCF can suppress the activity of ^{137}Cs in organs compared to control; because of AFCF effectively prevent the absorption of ^{137}Cs by digestion so that the deposition of ^{137}Cs in the organs can be minimized.

The ^{137}Cs excretion through urine

Urine is the main product for the removal of toxic substances/radioactive. Compound in the body that has biotransformation into the form of product will be diluted with water and then issued as urine. The results showed that the higher activity of ^{137}Cs was excreted through urine of monkey given with AFCF compared to control (Figure 3).

Statistical analysis showed that the average ^{137}Cs excreted in urine for all doses was not significant one to each other. AFCF dose did not significantly influence the activity of ^{137}Cs that was excreted through urine. There was a difference in ^{137}Cs activities of daily urine between AFCF at doses of 3000 mg, 4500 mg, 6000 mg, and 0 (control). The highest excretion was occurred on day 1, and then decreased on day 2, until the 35th day (3000 mg excreted 9.36%, 4500 mg 10.97%, 6000 mg 12.01% and 8.74% for controls). This is influenced by monkey's physiology. The results of Rahardjo's showed that the increased activity of ^{137}Cs in urine because monkey consumed lot of water, many radionuclides were come out of urine and caused more quickly dissolution process in the body.

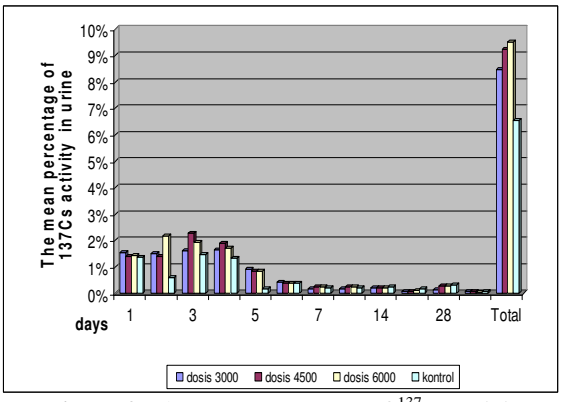

Figure 3. The mean percentage of ^{137}Cs activity that in excretion through urine after administration decontamination AFCF

Observations on the 2nd until 35th day shows a decline of the activity of ^{137}Cs was occurred in urine, except on day 14 and day 28 that was increased. On day 14, an increase was found for dose of 3000 mg, i.e. 0.20% and 0.24% of control. On the 35th day, a decline in the activity of ^{137}Cs was observed through urine. Dose of 3.000 mg was able to excrete ^{137}Cs through urine up to 0.07%, 4.500 mg was 0.05%, 6000 mg was 0.05% while 0.06% for control. The occurrence of decreased activity on day 35, presumably because until day 35, ^{137}Cs activity has been accumulated in many organs/carcass and already absorbed by body tissues, hence the ^{137}Cs excreted through the urine was quite low. Dakk explained that the transfer of chemical compounds from the blood into the fluid or organ for excretory (eg urine, lung or kidney), leading to reduced toxicity in the body.

The ^{137}Cs activity is excreted through feces

^{137}Cs activity excreted through the feces was very high in the group of monkey treated with AFCF compared to control. The activity of ^{137}Cs for dose of 3.000 mg was 28.69%, 4.500 mg was 26.50% and dose of 6.000 mg was 24.89% and all was higher than that of control (19.32%) (Figure 4).

Statistical analysis showed that there was no significant difference between the average of ^{137}Cs excreted via feces for all doses of AFCF. This indicated that each treatment was able to excrete the ^{137}Cs in equal amount. However, it was known that dose of 3.000 mg was most effective in excreting the ^{137}Cs from the body

compared to other doses. An increased activity of ^{137}Cs in feces at day 1 for dose of 4.500 mg was 2.39% and for control was 1.21%, whereas dose of 3.000 mg and 6.000 mg did not show any increment. Because there was a high enough of radionuclide excreted through feces, so its excretion through urine was very low. Dose of 4.500 mg showed an increased excretion compared to 3.000 mg, 6.000 mg, and 0 (control). This increased activity of ^{137}Cs for 4500 mg because AFCF was not directly digested by the body system, and AFCF bound ^{137}Cs directly in the digestive tract and immediately excreted on the first day. ^{137}Cs was excreted in highest amount until day 3. Dose 3.000 mg excreted up to 7.48%, 4.500 mg excreted 5.31%, 6.000 mg excreted 3.11% and control excreted 5.36%. These showed that 3.000 mg was the most effective dose where ^{137}Cs was bounded by AFCF in the digestive tract and then excreted through feces in relatively high amount. This increase was also influenced by the activity in the blood and excretion of ^{137}Cs through urine. At day 3, a low ^{137}Cs activity was seen in blood and urine, because mostly ^{137}Cs was excreted through feces. The most effective dose was 3.000 mg compared to 4.500, 6000 mg, and 0 (control). This high activity of ^{137}Cs in feces resulted in low activity in blood and organs, so that there was no precipitation of radionuclide in a long time in the body.

The total activity of ^{137}Cs which was excreted through feces and urine was quite high in the group of AFCF compared to control. ^{137}Cs excretion was highest for 3.000 mg of dose (46 332%), followed by 44.20% for 4.500 mg, 6.000 mg excreted 45.39% and control was 34.37%. ^{137}Cs was excreted through feces than urine. This result was in accordance with research conducted by Sanusi, where the ^{137}Cs was excreted in higher amount in feces than in urine. This is because ^{137}Cs was given orally. The duration of excretion process through kidney also caused low ^{137}Cs activity in urine. ^{137}Cs excreted through urine and feces is associated with its biological half-life.

In Pharmacology, it was stated that the important parameters that associated with the excretion of chemical substances from the body is a half-life. ^{137}Cs excreted through urine and feces until the day 35th was not reached its half life (50%). Up to day 35th the activity of ^{137}Cs was 54% for 3.000 mg, 56% for 4.500 mg, 55% for 6.000 mg, 66% for control. These data indicate that the biological half-life (t1/2) of Cs-137 is more than 35 days. However, AFCF was able to reduce the activity of ^{137}Cs from the body in higher amount than that of without AFCF (control).

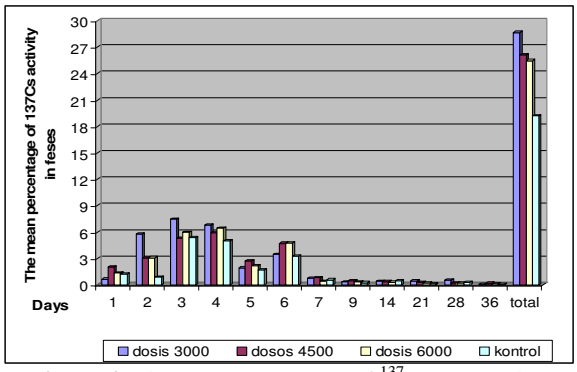

Figure 4. The mean percentage of ^{137}Cs excreted through feces of monkey at day 1 to 35 post-administration of AFCF.

4. Conclusion

1. Decontamination of ^{137}Cs with AFCF at doses of 3.000, 4.500 mg and 6.000 mg were known effective in excreting ^{137}Cs from long-tailed monkeys and the excretion was represented by two phases, the first was rapid excretion (day 1 to 7) followed by a second slower phase (day 9 to 35-th)
2. Decontamination of ^{137}Cs with AFCF was most effective at dose of 3.000 mg (excreting up to 46.32% of ^{137}Cs compared to doses of 4.500 mg (44.20%), 6.000 mg (45.39%) and controls (34.27%). The lowest ^{137}Cs activity that accumulates in blood and organs was observed at 3.000 mg, so that AFCF at dose of 3.000 mg was more effective than that of doses of 4.500 mg, 6.000 mg and control.

5. Acknowledgement

---

6. References

[1]. NCRP Report No. 65 (1979), Management of Persons Contaminated with Radionuclides accidentally, National Council on Radiation Protection and Measurements, Bethesda, Maryland, USA.

[2]. United Nations Scientific Committee on the Effects of Atomic Radiation (1982), Ionizing radiation: Sources and Biological Effects, 1982 Report to the General Assembly, United Nations, New York.

[3]. Ward, W.A. (2006), Nuclear Technology: Radiation Protection and Its Application. Publishers. Andi Offset. Yogyakarta.

[4]. Rahardjo, T., M. Sanusi and D. Tetriana (2007), The effectiveness of Prussian Blue in the elimination of Cs-137 from the body post orally contamination of long tail

Monkeys with Cs-137, Proceedings of the Presentation of Scientific and Environmental Radiation Safety XIIII, BATAN Jakarta.

[5]. Alatas, Z., M. Syaifudin and S. Nurhayati (1996), The effectiveness of Prussian Blue for decontamination Cesium-137 in white rats. Proceedings of Scientific Presentations Radiation and Environmental Safety, BATAN, pp. 210-218.

[6]. Basyarahil, J.G. (1997), Decontamination mixed radionuclides of Cs-137 and Am-241 in the white rat body (*Ratus norvegicus var wistar*) Thesis: Physics Studies Program of Faculty of Mathematics and Natural Sciences (MIPA). Airlangga University, Surabaya.

[7]. Kaikkonen, M and J. Lehto (2000), Coprecipitating Ammonium (III) hexacyanoferrate from aqueous dispersion with albumin and trichloroacetic acid, *Radiochemistry Laboratory*, University of Helsinki. Firlandia.

[8]. Schimansky, K. (1997), The stability and cesium binding properties of ammonium iron and copper ammonium hexacyanoferrate on a polystyrene carrier for the decontamination of Cs-contaminated whey powder under various test conditions, *Journal of Environmental*.

[9]. Cort, M.D. (2002), Environmental monitoring. A European Manual for Off-site Emergency Planning and Response To the nuclear Accidents, Institute for Environment and Sustainability.

[10]. Dotzel, M.M. (2003), Guidance for industry on Prussian Blue for treatment of internal contamination with Thalium or radioactive Cesium avaibility Food and Drug Administration. *Journal of the Department of Health and Human Services*.

[11]. Mitrovic, B., G. Vitorovic, D. Vitorovic, H. Dakovic and M. Stojanovic (2007), AFCF and clinoptilolite use in reduction of 137 Cs depositions in several days contaminated broiler chicks, *Journal of Environmental*, **95**, 171-177.

[12]. Le Gall, B.F. Taran, D. Renault, J.C. Wilk and E. Ansoborlo (2006), Comparison of Prussian Blue and apple pectin efficacy on Cs-137 decorporation in rat, *Biochimie*, **88**(11), 1837-1841.

[13]. Laboratory of Pharmacology (1991). Lecture Notes Pharmacology. Publisher: Book of Medicine, Sriwijaya University EGC. Jakarta.

Preparation of Lead(II) Coated Wire Electrode Using Chitosan Membrane for Monitoring Lead(II) in Water Samples

Wiwin Rewini Kunusa [1], Atikah [2], Hermin Sulistyarti [2]

[(1)]Master Program (Analytical Chemistry), Faculty of Science, Brawijaya University, Malang
[(2)]*Chemistry Department, Faculty of Science, Brawijaya University, Malang*

Abstract

Ion selective electrode (ESI) is an innovation in potentiometric electrochemical sensors which has high selectivity, high sensitivity, and fast analysis. In this work, ISE of Lead(II) was developed by coating platinum with active membrane made of mixture with composition of 10% chitosan: 40% PVC: 50% plasticizer DOP and DBP in THF solvent. The resulted ISE-Lead(II) was characterized and applied for synthetic and real samples. The results showed that the ISE-Lead(II) gave Nernst factor of 29.1 mV/concentration with correlation coefficient, R2, 0.9661, linear concentration range from 1x10-4 to 1x10-1M, detection limit 1, 9952x10-5M or 4.13 ppm, response time of 30 seconds and life time of 65 days. Lead(II) ISE showed good performance between temperature of 25-350C and pH of 4-6. Foreign ions, such as Hg2+, Cu2+, Cd2+ concentration of 10-3M did not interfere Lead(II) ESI, with selectivity coefficient, Kij, in order of Cu2+ < Cd2+ < Hg2+ < Pb2+. This method showed good agreement with the resutls obatined from AAS standard method, and therefore, the Lead(II) ISE potentiometric method can be used as an alternative method for determining Lead(II) in water samples.

Keywords: *Lead(II), potentiometric, sensors, ISE, chitosan.*

ERRATUM

Testosterone Level of Male Cattle at Regional Artificial Insemination Center in Airlangga University, Faculty of Veterinary Medicine

Sri Pantja Madyawati [1], Pudji Srianto [2], Trilas Sardjito [3]

[(1,2,3)] Department of Veterinary Reproduction, Airlangga University, Faculty of Veterinary Medicine

Abstract

The objective of this study was to investigate whether testosterone level of the cattle influences spermatozoa quality thus it is eligible for processing into frozen semen. The results of this study showed that the mean testosterone level examined by solid phase RIA method in Friesian Holstein (FH) dairy cattle 1 was 1.545 ± 1.232 ng/ml and FH dairy cattle 2 amounted to 1.213 ± 0.537 ng/ml. From this research we can conclude that there is no significant difference in testosterone level in the blood of FH dairy cattle 1 and 2 whose semen will be processed into frozen semen.

Keywords*: testosterone, Friesian Holstein dairy cattle.*

1. Introduction

Government efforts in increasing the livestock population are done through livestock breeding and the application of reproductive biotechnology [1]. Artificial insemination biotechnology is one of the reproductive biotechnologies that serve to improve the genetic quality of cattle livestock by producing frozen semen from superior bulls [2].

Regarding the decree of the Directorate General of Animal Husbandry in 2007, the Animal Teaching Center (TTP) of Airlangga University Faculty of Veterinary Medicine officially has become the Regional Artificial Insemination Center (BIBD), which can produce and distribute frozen semen.

Significant problem in the semen production process is the semen quality, origin of the male cattle, animal health test and recording [3]. Our Animal Teaching Center has Frisian Holstein (FH), Simental and Limousin cattle that have been certified. They derive from the Animal Embryo Center Cipalang and their semen is already to collect. However, there are no studies on some factors occurring in male cattle, including testosterone level that might have effect on semen quality.

The objective of this study was to investigate whether testosterone level of the male cattle influences spermatozoa quality thus it is eligible for processing into frozen semen.

2. Experimental Details

Testosterone level is measured using two male FH dairy cattle by taking their blood via the jugular vein which was collected in vacumtainer at 10 ml. Blood collection was performed at intervals of ten days.

Next, tubes containing blood sample were allowed to stand in refrigerator for 60 minutes, then centrifuged at 3000 rpm for 30 minutes to obtain serum. Further, serum was put into the Ependorf tube and stored in the freezer at -18˚C until testing.

Testosterone levels of the blood serum were measured using solid-phase RIA method with the following stages:

- Label 4 of the polypropylene tubes was not coated with antibodies (uncoated tubes) for TC and NSB
- Label 12 of tubes was coated with antibodies (total testosterone Ab-coated tubes) for Standard A to F.
- Other label of the tubes was coated with antibodies (total testosterone Ab-coated tubes) for control. All samples were duplicated.
- Add 50 µl standard, control and sample to the tubes already coated with antibodies according to their codes and then vortexed.
- Then add 1 ml ^{125}I Total Testosterone (tracer) to all tubes and then vortexed.
- Incubated for 3 hour at temperature 37˚C. Afterwards, fill all tubes except for TC tubes by turning the tubes on the shelves where radioactive waste is stored.
- Keep these tubes remain upside down on the shelf on the absorbent papers for 5-10 minutes, and then read with Gamma counter for 1 minute [4].

3. Results and Discussion

Blood serum of two male FH dairy cattle whose testosterone levels are measured using solid-phase RIA method can be seen in Table 1.

Table 1. Testosterone levels of FH dairy cattle with solid-phase RIA Method

Serum Collection	Type of Cattle	
	FH 1 (ng/ml)	FH 2 (ng/ml)
1	3.7	0.76
2	0.95	1.6
3	1.1	0.72
4	0.12	1.8
5	1.3	1.7
Mean	1.545	1.213
SD	1.232	0.537

Statistical analysis is carried out using *t* test, suggesting that there is no significant difference in testosterone levels between FH dairy cattle 1 and FH dairy cattle 2 ($p > 0.05$).

Testosterone is a steroid hormone produced by Leydig cells in testes due to hormonal stimulation of interstitial cell stimulating hormone (ICSH) generated by the anterior pituitary. This hormone is a male hormone that is released in a diurnal way so that hormone levels in blood testosterone levels are highly varying [2].

Testosterone plays significant role in an activation of spermatozoa formation. This is consistent with opinion of Thomaszewka Wodzicka (1991) saying that some hormones essential for spermatogenesis are including FSH, LH and testosterone [5]. These hormones work together in a very complex way that is not known completely. The hormone greatly influences the spermatogonia in the seminiferous tubules that causes the occurrence of spermatogenesis, a continuous process throughout life and begins with the division of spermatogonia into spermatocytes and spermatids which then become spermatozoa. Additionally, Partodihardjo (1992) states that testosterone is the most potent hormone from androgen group and serves to stimulate maturation of spermatozoa formed in the body of seminiferous tubules, also stimulate the growth of accessory glands (prostate, vesicular gland and bulbourethralis) and stimulate the male sex characteristics [6].

Testosterone level is frequently associated with high or low libido in male animals. This is consistent with opinions of Hardjopranjoto (1995) saying that male animal experiencing atrophy of the testicular gland will show symptoms of decreased sexual libido and lower semen production so that the males would be fertile [7]. Administration of testosterone can restore libido to normal.

Observations while collecting semen for processing into frozen semen showed that there is no significant difference in testosterone level between Limousin and Simental cattle. This was indeed shown that when collecting semen from Bos Taurus at the late afternoon, we always got an adequate number of spermatozoa for processing into frozen semen.

The quality of semen that deserves to be produced into frozen semen must meet some criteria specified in the standard of quality for all of Artificial Insemination Centers in Indonesia.

4. Conclusion

From the results and discussion above we can conclude that there is no significant difference in testosterone level between FH dairy cattle 1 and FH dairy cattle 2.

5. Acknowledgements

---

6. References

[1]. Direktorat Jenderal Peternakan, (2005). Panduan Lomba dan Kontes Ternak Nasional dalam Rangka Pekan Peternakan Unggulan Nasional 2005. Direktorat Jenderal Peternakan Departemen Pertanian.

[2]. Hafez, E.S.E, (2000). Reproduction inFarm Animal. 7th Ed. Lippicot William and Wilkins, Philadelphia USA 437-441

[3]. Sarastina, (2002). Penanganan Mutu Semen Beku.Makalah Pelatihan Inseminasi Buatan Sapi/Kerbau Angkatan I. Departemen Pertanian Direktorat Jenderal Bina Produksi Peternakan.

[4]. Mahaputra, L., (1990). Pengukuran Kadar Progesteron Air Susu dan LH Serum Untuk Menentukan Status Reproduksi dan Upaya Penanggulangan Infertilitas pada Sapi Perah Pasca Lahir. Disertasi. Universitas Airlangga, Surabaya

[5]. Wodzicka-Thomaszewka, M., I. K. Sutama, I. G. Putu dan T. D. Chaniago. (1991). Reproduksi, Tingkah Laku dan Produksi Ternak di Indonesia. PT. Gramedia Pustaka Utama, Jakarta

[6]. Partodihardjo, S., (1992). Ilmu Reproduksi Hewan. Mutiara Sumber Widya, Jakarta

[7]. Hardjopranjoto, S. (1995). Ilmu Kemajiran pada Ternak. Cetakan I Airlangga University Press, 181-182.

[8]. Direktorat Jenderal Peternakan, 2007. Petunjuk teknis Produksi dan Distribusi Semen Beku. Departemen Pertanian Direktorat Jenderal Peternakan, Jakarta.

Normative Law Dimension Introduction of Variety Description for Pests and Plant Disease in Sustainable Food Crop Cultivation

Bambang Sudjito

Faculty of Law, Brawijaya University, Malang, Indonesia (b_jito@ub.ac.id)

Abstract

Within the framework of sustainable food crop cultivation need to be considered seed crop, crop protection, and food crop cultivation that to be good and right, as the legal provisions in the Act 12 – 1992, Government Regulation 44 - 1995, Government Regulation 6 - 1995, and Regulation of the Minister of Agriculture. 48/Permentan/140.OT/8/2006. Henceforth, within the framework of sustainable food crop cultivation has been made possible threat germ and plant diseases, that has not been early prevented through superior variety with its each descriptions and developed in the form of "bina" seed. Similarly, the existence of regulations related to sustainable food crop cultivation is possible there have been inconsistent, unclearness, and inclarity, beside vacuum of law substance. With a through normative law study was expected to be able give the inputs related with sustainable food crop cultivation to scientists or academics beside practitioner or bureaucrat.

Keywords: *Normative law, Variety description, germ and plant disease prevention, and sustainable food crop cultivation.*

1. Introduction

Within the framework of crop cultivation known various kinds of food crops, including rice or *Oryza sativa*, corn or *Zea mays*, and soybean or *Glycine max Merr*, similarly, various types of pests / diseases of plants in cultivation of food crops. Against many pests / plant diseases in the cultivation of food crops, which includes data for plant pests for food crops with the potential loss resulting from it in addition to endemic areas the main plant pests, as a description in Table 2.

Similarly, attacks a variety of pests/plant diseases in the cultivation of food crops, as contained in the following print media [1]:

a. Articles "Corn caterpillar epidemic", published in the daily Kompas, August 11, 2008;
b. Article "Soybean green caterpillar pests and locusts", as published in the daily Surya, September 28, 2008;
c. Articles "corn downy mildew threatens farmers back", published in the daily Kompas, May 18, 2009;
d. Article "Pests of paddy spread can be explosive in East Java because of changes in the weather", as published in the daily Kompas, January 17, 2011;
e. Articles "pest dominates, in some areas began to harvest rice," which appeared in Kompas daily, dated January 18, 2011
f. Articles "chocolate bar hopper, the feared pests and how to eradicate", published in Kompas daily, dated February 9, 2011.

The existence of legal substance of the laws and regulations related to the introduction of variety descriptions for the prevention of pests and plant diseases in a sustainable food crop cultivation possible inconsistent, unclearness, and inclarity, beside vacuum of law substance. Thus, the objectives to be achieved in this research are:

1. knowing and understanding the reality of inconsisten, inclearness, and inclarity beside vacuum of law and regulations substance related to the introduction of variety descriptions for the prevention of pests and plant diseases in the sustainable cultivation of food crops;
2. Knowing, understanding, and implementing various legal efforts should be made in the face of the reality of inconsistent, unclearness, and inclarity beside vacuum of law and regulations substance related to the introduction of variety descriptions for the prevention of pests and plant diseases in the sustainable cultivation of food crops.

The benefits expected from this research are:

1. Benefits for academics and researchers associated with the development of science and technology. In this sense, legal science, agricultural science, and related area, including taxonomy, morphology, and physiology of plants within the framework of sustainable crop cultivation
2. The benefits for bureaucrats within the scope of agriculture/farm outside the scope of the description associated with the introduction of varieties for the prevention of pests and plant diseases in the sustainable cultivation of food crops in addition to law enforcement.

2. Experimental Detail

This type of research within the scope of judicial normative, while the method of approach through statute approach [2]. Therefore, the type of data in this study, which includes primary legal materials, secondary, and tertiary [3], while the source of the data in this study, which covers the laws and regulations in addition to the writings of experts through results of research, journals, and articles. Henceforth, data collection techniques used through the identification and classification of legal substance of the laws and regulations related to the introduction of variety descriptions for the prevention of pests and plant diseases in the sustainable cultivation of food crops, while the data analysis techniques through

descriptive analytical through the legal principle and legal policy in the regulation the laws [4].

3. Result and Discussion

The existence of legal systems in public life [5] mechanism that functions as an integrator with adaptive systems procurement facilities instrumental to overcome obstacles be side adaptive structures, which include science and technology. In this case, science and technology, as the science of humanities, social, and natural sciences, including scientific knowledge related to pests and plant diseases and control.

Crop protection, which includes prevention of loss of crops caused by plant pests and outside plant pests [6]. Therefore, crop protection policy, in addition to do with technical policy of plant protection, which includes prevention of loss of crops caused by plant pests and outside plant pests; also performed with the policy of plant protection law, which includes preparation/renewal of law, correctional/law enforcement, and law enforcement related to crop protection, as well as pest and disease control with respect to the description of varieties of crops to prevent pests/plant diseases within the framework of sustainable cultivation.

The various steps that need to be known and understood within the framework of sustainable food crop cultivation, including cultivation of food crops is good and right, which includes the experimental stage, valuation, disposition, and the withdrawal of crop varieties, production, certification, and circulation building next to the entry of seed and expenditure of seeds, and cultivation of food crops is good and right. Furthermore, the existence of Sutau that resistance to pests/plant diseases can only be known and understood through the description of the variety in the stages of testing, evaluation, disposition, and the withdrawal of varieties of a crop. In this case, descriptions of different varieties of food crops with the advantages and disadvantages to pests/plant diseases through various decisions of the Minister of Agriculture relating to the release of varieties to be developed in plant cultivation as "bina" seed, which is certified and labeled. Therefore, within the framework of food crop is good and right, from the beginning has been known and understood the advantages and disadvantages to pests and plant diseases through the description of varieties, so that will facilitate the prevention and control of pests/plant diseases within the framework of sustainable cultivation of food crops .

Various legal provisions in the laws and regulations related to the cultivation of food crops are good and right, which includes:

1. Legal provisions in the Act 12 - 1992 on Plant Cultivation System, among others, Article 12 paragraph (1), and paragraph (2), article 13 paragraph (2) and paragraph (3), and Article 17 paragraph (2), and paragraph (3);
2. Legal provisions in the Act 16 - 1992 concerning Animal, Fish, and Plants, among others, Article 5 and Article 10;
3. Legal provisions in Government Regulation 44 - 1995 on the Seed Plants, among others, Article 18 paragraph (2) and paragraph (3), chapter 20, article 21, article 24, article 25 paragraph (2), article 32, article 33 paragraph (1), article 34 paragraph (1) and (2), and article 38;
4. Legal provisions in Government Regulation 6 - 1995 on Plant Protection, among others, Article 5 paragraph (2) and Article 6 paragraph (1);
5. Legal provisions in Government Regulation 14 - 2002 on Plant Quarantine, among others, article 2 and article 7;
6. Legal provisions in the Regulation of the Minister of Agriculture No 48/Permentan/140.OT/8/2006 on Food Crop Cultivation of Good and True, as the seed and crop protection in the annex to Regulation of Minister of Agriculture 48 / Permentan / 140.OT / 8 / 2006;
7. Legal provisions in the Regulation of the Minister of Agriculture No 37/Permentan/140.OT/8/2006 of Testing, Assessment, Disposal, and Withdrawal Variety, among others, Article 4 paragraph (1), article 10 paragraph (2), article 11 paragraph (3), and Article 19 paragraph (2);
8. Legal provisions in the Regulation of the Minister of Agriculture No 39/Permentan/140.OT/8/2006 of Production, Certification, and Distribution of Seed Development, among others, Article 5 paragraph (1) and paragraph (2), article 11 paragraph (1) and paragraph (2), article 13 paragraph (2) and paragraph (3), article 14 paragraph (2), paragraph (3), and paragraph (4), and article 24;
9. Legal provisions in the Regulation of the Minister of Agriculture No. 38 / Permentan/140.OT/8/2006 of Revenue and Expenditure Seeds, among others, Article 11, Article 16 paragraph (1), and paragraph (2), article 29 paragraph (1), and Article 30 paragraph (1);

Furthermore, the existence of legal substance in the Minister of Agriculture No. 37 / Permentan / 140.OT / 8 / 2006, which is implemented in a variety of Decree of the Minister of Agriculture relating to the release of varieties. In this case, the description of rice plants (***Oryza sativa***), maize (***Zea mays***) and soybean (***Glysine max Merr***) with various advantages and disadvantages of each, among others:

By considering the findings of the data with testing, evaluation, disposition, and the withdrawal of varieties of plants can be analyzed, that law substance related to test adaptation and / or observation to test new varieties, beside e legal provisions of article 18 paragraph (2) and (3) Government Regulation 44 - 1995 also legal provisions of Article 4 paragraph (1), article 10 paragraph (2), and article 11 (3) Regulation of the Minister of Agriculture No 37 / Permentan / 140.OT / 8 / 2006 have found any inconsistent, unclearness, and inclarity. Therefore, it can be seen and understood that the purpose of the laws and regulations to be inconsistent, unclearness, and inclarity, because only follow mere consumer tastes.

By considering the findings of the data with the production, certification, and "bina" seed distribution it can be analyzed, that substance of law related to the production, certification, and distribution of "bina" seed as the legal provisions of article 13 paragraph (2) and paragraph (3) the Act 12 - 1992, Article 33 paragraph (1) government regulation 44 - 1995, and

article 11 paragraph (2), article 13 paragraph (2), article 14 paragraph (2), and article 24 Regulation of the Minister of Agriculture No 39/Permentan/140 .OT/8/2006 in addition to income and expediture of seed, as the legal provisions of article 17 paragraph (3) the Act 12 - 1992, article 34 paragraph (1) and (2) Government Regulation 44 - 1995, and article 16 paragraph (1) and paragraph (2) Regulation of the Minister of Agriculture No. 38 / Permentan / 140.OT / 8 / 2006 have found any inconsistent, unclearness, and inclarity, so the goal rather than the laws and regulations to be inconsistent, unclearness, and inclarity beside vacuum. In this case, certification can be interpreted with certification through field inspection, laboratory testing, and installation of labels, seed certification, quality management system certification, or certification of products. In the future, "stipulation of certain seeds from the outside does not need to check the truth of the seed source ...." Therefore, it can be seen and understood the objectives of the laws and regulations are inconsistent, unclearness, and inclarity beside vacuum, especially during the process of seed health certification that the indicator only in the purity of seeds, a mixture of other varieties, growing power, and water content.

Thus, based on data findings related to cultivation of food crops is good and right can be analyzed, that linkage legal substance testing, evaluation, disposition, and the withdrawal of varieties that were followed by Ministerial Decree on the release of varieties by a description of variety, production, certification, and circulatory "bina" seed in addition to the income and expenditure of seeds, and cultivation of food crops is good and right, as the legal provisions in the Act 12 - 1992, the Act 16 - 1992, Government Regulation 44 - 1995, Government Regulation 6 - 1995, and Government Regulation 14 - 2002 in addition to the legal provisions in the Regulation of the Minister of Agriculture No. 37 / Permentan / 140.OT / 8 / 2006, Regulation of the Minister of Agriculture No. 39 / Permentan / 140.OT / 8 / 2006, Regulation of the Minister of Agriculture No 38 / Permentan / 140.OT / 8 / 2006, and Regulation of the Minister of Agriculture No 48 / Permentan / 140.OT / 8 / 2006 had found inconsistent, unclearness, and inclarity beside vacuum, in addition to descriptions of superior variety and / or weakness that has not / is not loaded in containers and / or label products, as well as certification that the term can be interpreted with certification through field inspection, laboratory testing, and installation of labels, seed certification, quality management system certification, or certification of products, so that the objectives of the legislation invitation to be inconsistent, unclearness, and inclarity beside vacuum.

4. Conclusion

The conclusions that can be obtained in the study of this law are:

1. The laws and regulations related to the introduction of the description of varieties to prevent pests / plant diseases within the framework of sustainable food crop cultivation in the implementation is still found any inconsistent, unclearness, and inclarity beside vacuum.
2. Remedies associated with the introduction of the description of varieties to prevent pests / plant diseases within the framework of sustainable cultivation of food crops through the preparation / renewal of the law based on the principle of legal principle and legal policy in the laws and regulations, especially the description of the variety of advantages and/or weaknesses that have not / not loaded in packaging and/or label products in addition to seed health indicators in the process of seed certification.

5. Acknowledgements

---

6. References

[1]. Anonymous, Kompas 11 August 2008; 28 September 2008; 18 May 2009; 17 January 2011; 18 January 2011; 9 February 2011; 19 August 2005; 28 January 2011.
[2]. Marzuki, Peter Mahmud (2008), Penelitian Hukum, Kencana Prenada Media Group, Jakarta.
[3]. Sukanto, S dan Mamudji, S, 1985, Penelitian Hukum Normatif, Rajawali Pers, Jakarta
[4]. Lembaga Administrasi Negara, 1995, Sistem Administrasi Negara Republik Indonesia, Hajimasagung, Jakarta
[5]. Vihelm, Aubert, 1973, Sociology of Law, Penguin Books – Middlesex
[6]. Untung, K, 2007, Kebijakan Perlindungan Tanaman, Gajah Mada University pers, Yogyakarta
[7]. Anonymous (1992), UU No 12, RI
[8]. Anonymous (1992), UU No 16, RI
[9]. Anonymous (1995), PP No 44, RI
[10]. Anonymous (1995), PP No 6, RI
[11]. Anonymous (1995), PP No 14, RI
[12]. Anonymous (2006), PP No 37 / Permentan / 140.OT / 8 / 2006.
[13]. Anonymous (2006), PP No 38 / Permentan / 140.OT / 8 / 2006.
[14]. Anonymous (2006), PP No 39 / Permentan / 140.OT / 8 / 2006.
[15]. Anonymous (2006), PP No 48 / Permentan / 140.OT / 8 / 2006.

Appendixes

Figure 1.Example (Ind: Wereng batang coklat) (Kompas, 19 August 2005)

Figure 2.Example (Ind: Wereng batang coklat) (Kompas, 28 January 2011)

Table 1. Potential loss result to attacks superior plants disturber organism of food crops in East Java

No	Commodity	Plant pests	Year		
			2004 (ton)	2005 (ton)	2006 (ton)
1	Paddy	1. Rat	4749.69	5721.68	4866.60
		2. Stem borer	4008.29	4775.91	6606.85
		3. Stem brown Planthopper	1289.94	1275.33	3552.19
		4. Bacterial leaf Blight	8048.74	8380.63	26811.12
		5. Tungro	1207.12	1391.11	1718.05
		6. Blas	522.47	4797.27	2243.44
2	Corn	1. Rat	321.07	207.02	382.55
		2. Stem borer	61.35	132.32	669.46
		3. Cob borers	192.72	115.53	762.90
		4. Grasshopper	521.79	272.87	2709.10
		5. Leaf rust	479.84	717.37	2093.03
		6. Albino	255.65	742.03	3422.64
3	Soybean	1. Silkworm span	73.93	126.41	23.82
		2. Armyworm	28.18	146.96	52.77
		3. Soybean beetle	22.80	72.48	23.50
		4. Pod borer	22.80	16.38	19.23
		5. Caterpillar pod	16.95	30.80	5.17
		6. Leaf rust	53.51	36.02	46.29

Data source: Department of Agriculture Province of East Java, Annual Report 2004 to 2006 (recycled).

Table 2. Regional endemic plant pests attack main food crops in East Java (Season Planting 2006)

No	Commodity	Plant pests	Regional (District)	Amount
1	Paddy	1. Rat	Tuban, Bojonegoro, Lamongan, Sidoarjo, Madiun, Malang, Lumajang, Jember, Banyuwangi	9
		2. Stem borer	Tuban, Bojonegoro, Lamongan, Ngawi, Lumajang, Jember, Bondowoso, Banyuwangi	8
		3. Stem brown	Madiun, Jember	2
		4. Planthopper	Tuban, Bojonegoro, Lamongan, Magetan, Madiun, Trenggalek, Jember	7
		5. Bacterial leaf Blight	Pasuruan, Probolinggo, Lumajang, Jember, Bondowoso, Situbondo, Banyuwangi	7
		6. Tungro	Pacitan	1
		7. Blas	Tuban, Bojonegoro, Lamongan, Malang, Lumajang, Jember	6
2	Corn	1. Rat	Probolinggo	1
		2. Stem borer	Probolinggo	1
		3. Cob borers	Bojonegoro	1
		4. Grasshopper	Tuban, Bojonegoro, Jombang, Tulungagung	4
		5. Leaf rust	Kediri	1
		6. Albino	Kediri Situbondo	2
3	Soybean	1. span caterpillar	Tulungagung, Jember	2
		2. "grayak" caterpillar	Bojonegoro, Lamongan, Pasuruan, Banyuwangi	4
		3. Soybean bumble	Ponorogo	1

Data source: Department of Agriculture Province of East Java, Annual Report 2004 to 2006 (recycled).

Table 3. Description superior varieties of rice (*Oryza sativa*) with resistance against pests / diseases

No	Variety	Variety released		Desecription pests / disease endurence	
		Kep.Mentan	Date	Superior	Weakness
1	Ciherang	60/Kpts/TP.240/2/2000	25-02-2000	Hold brown planthopper biotype 2 and 3	
2	Cibogo	393/Kpts/SR.120/8/2003	05-08-2003	Hold brown planthopper biotype 2, moderately resistant strains HDB IV, and brown planthopper biotype 3	"tungro" virus susceptible
3	Yuwono	573/Kpts/SR.120/10/2004	12-10-2004	Hold brown planthopper biotypes 1 and 2, moderately resistant biotype 3, resistant bacterial leaf blight strains III, and moderately resistant strains IV	
4	Rojolele	126/Kpts/TP.240/2/2003	14-02-2003		Brown rice pests sensitive
5	Pandanwangi	163/Kpts/LB.240/3/2004	17-03-2004		Biotype 2 and 3 brown rice pests, Rise pests susceptible, Strain 4 leaf blight bactaeria, Tungro
6	Way Apo Buru	21/Kpts/TP.240/1/98	13-01-1998	Hold brown planthopper biotype 2 and 3, leaf blight-resistant strains III and IV	Peka brown planthopper Vulnerable brown planthopper biotype 2 and 3,
7	Memberamo	584/Kpts/TP.240/9/95	04-09-1995	Blight-resistant strains III, moderately resistant " tungro"	bacterial leaf blight strains 4, tungro
8	IR 64	449/Kpts/TP.240/7/1986	17-07- 1986	Hold brown planthopper biotype 1, 2 and green leafhoppers, hold dwarf grass, moderately resistant leaf blight	
9	Intani 2	644/Kpts/TP.240/12/2001	03-12-2001		Somewhat sensitive to brown planthopper biotype SU (scale 4.3), somewhat sensitive strain BLB VIII
10	Mira 1	134/Kpts/SR.120/3/2006	06-03-2006	Moderately resistant brown planthopper biotype 3 (scale 3.67), moderately resistant	

				strains III and IV BLB Hold brown planthopper biotype 2, moderately resistant biotype 3, resistant bacterial leaf blight strains III, and IV moderately resistant strains	

Data source: The decisions set of Agriculture Minister beside superior variety description Rice 1943 - 2009, Center for Agricultural Crops-Food Research and Development, Bogor, 2009 (recycled).

Table 4. Description superior varieties of maize (*Zea mays*) with resistance against pests / diseases

No	Variety	Variety released		Desecription pests / disease endurence	
		Kep. Mentan	Date	Superior	Weakness
1	Semar 9	172/Kpts/TP.240/6/99	22-06-1999	Hold downy mildew, leaf spot and rust	
2	Bisma	585/Kpts/TP.240/9/95	04-09-1995	Leaf spot and rust resistant	
3	Jaya 3	304/Kpts/TP.240/4/2002	25-04-2002	Downy mildew resistant	
4	SHS 11	375/Kpts/SR.120/6/2004	04-06-2004	Downy mildew resistant	
5	Bisi 2	589/Kpts/TP.240/9/95	04-09-1995		Tolerant of downy mildew and leaf rust
6	P 21	388/Kpts/SR.120/7/2003	29-07-2003	Leaf rust resistance, gray leaf spot Cercuspora zeaemaydis, moderately resistant Diplodia cob rot, viruses, and the germination of cob,	Somewhat susceptible stem rot bacteria, and downy mildew
7	NK 33	129/Kpts/TP.240/2/2003	14-02-2003	Moderately resistant downy mildew, leaf blight, and rust Stainless	
8	DK 3	162/Kpts/LB.240/3/2004	17-03-2004	Rust Tolerant	Tolerant of downy mildew

Data source: The decisions set of Agriculture Minister beside superior variety description Rice 1943 - 2009, Center for Agricultural Crops-Food Research and Development, Bogor, 2009 (recycled).

Table 5. ***Description superior soybean plant varieties (Glysine max Merr) with resistance against pests / diseases***

No	Variety	Variety released		Desecription pests / disease endurence	
		Kep. Mentan	Tanggal	Kunggulan	Kelemahan
1	Anjasmoro	537/Kpts/TP.240/10/2001	22-10- 2001	Hold split peas,	Medium leaf rust
2	Argopuro	204/Kpts/SR.120/4/2005	11-04-2005	Moderately resistant bean fly, armyworm, the suction pods	Sensitive leaf virus (CMMV
3	Baluran	275/Kpts/TP.240/4/2002	15-04-. 2002		Rust tolerant
4	Gepak Kuning	240/Kpts/SR.120/3/2008	06-03- 2008	Moderately resistant armyworm and leaf rollers	

Data source: The decisions set of Agriculture Minister beside superior variety description Rice 1943 - 2009, Center for Agricultural Crops-Food Research and Development, Bogor, 2009 (recycled).

Identification of Clay Minerals by Using Differential Thermal Analysis (DTA) and Fourier Transform Infrared (FTIR)

Rachmat Slamet Santoso

Department of Chemistry, Faculty of Mathematics and Natural Science, Manado State University, Indonesia
(santoso.3571@gmail.com)

Abstract

Identification of clay minerals by using DTA and FTIR have been performed. DTA spectrum pattern of the thermochemical reaction and studied the infrared absorption bands of clay. The results indicate that DTA analysis for the suspension and clay tailings showed endothermic reaction in a row at a temperature of 527.41°C and 516.71°C while the exothermic reaction at a temperature of 949.82°C and 950.90°C is a mineral haloysite. Analysis by FTIR provides a characteristic absorption spectrum of kaolin minerals (haloysite), silica (trydimite / cristobalite), mica, and feldspar.

Keywords: *clay minerals, DTA, thermal reaction, FTIR, spectral.*

1. Introduction

Differential Thermal Analysis (DTA) is a technique that is widely used and very useful especially in the identification of amorphous material when X-ray diffraction analysis yields only curves without a pattern. The use of time is mainly in the fields of geology, and later developed for the study and analysis of ceramics, glass polymers, cement industry, adhesives and so forth. Clay is an alumina silicate compounds are used as basic material for the manufacture of ceramics [1].

Clay is very beneficial for humans because the material is easily shaped when mixed with water in a certain ratio. This means that the addition of certain water on the clay would be enough plastic to be formed without cracks. If the object has been formed it is dried, the object is strong enough in the next execution. For example, at the time appointed for the dried, decorated and arranged in the furnace, the object will not be broken / damaged. We have clay everywhere around the world, but from one region to other regions have different properties. Some areas may simply be used for the manufacture of ceramic goods are another area if you want to use, previously purified in advance or be mixed with other ingredients to be easily done [2].

Ceramic industry is very broad, not limited to roof tiles, bricks and pottery items only. Now look in the form of electrical devices, laboratory equipment, motor vehicles, aircraft up to the spacecraft, places metal casting and more all have parts made of ceramics. Ceramic industry should have a basic knowledge of the appropriate type of clay ceramic products, in order to choose and work, preparing the composition of the materials used to obtain better results as expected. To get the raw material quality and stable prior to use such material must be processed first through the process of mineral processing (beneficiation). Some of the methods used for material processing is the separation of the solutions, how to vote, how to wash and how classification. The method used for identification of clay minerals, among others, is the method of differential thermal analysis (DTA) and Fourier Transform Infrared (FTIR) [3,4].

2. Experimental Section

Materials

Raw materials used in this study are clay from the village Pulutan, Remboken, Minahasa, Sulawesi as a sample and Hydrocloric Acid pa merck, filter papers Whatman (ashless, circles 125 mm Ø).

Instrumentation

Drying performed uses a tube-Thermolyne Furnaces (Sybron) Type 21100 with a maximum temperature 1200°C. Raw materials clay that has been done through 100 mesh grinding and sifting. Differential Thermal Analysis (DTA) model 1600 TA Instrument with thermal analyst 2000, FTIR Shimadzu model DR-8011 for identification the functional group for clay materials, sintering is carried out using a Carbolite furnace-Edwards Pirani 501 A6D 1600°C maximum temperature with argon gas as the atmosphere.

Procedure

Clay from the village Pulutan Minahasa district of North Sulawesi province was used as raw materials for traditional ceramics. HCl, DTA TA 1600 model instrument with Therrnal software analyst in 2000 to study the thermal reactions in clay minerals, FTIR Shimadzu DR-8011 model to determine the functional group in the structure of clay minerals. This research was conducted through three stages of research. The steps undertaken were as follows:

Phase preparation

Clay material from the village Pulutan, Minahasa, North Sulawesi province taken at a depth of 50-250 cm, dried in the sun for 6 days, dried clay is crushed and then sieved with 100 mesh sieve.

Phase beneficiation

Clay powder 200 mesh was suspended in 1000 mL distilled water, beaten repeatedly. The suspension is left up to the separation of granular particles of clay based on the particle size fraction, where at the top of suspense at the bottom of the clay and loam in the form of tailings. Clay suspension was separated from the tailings and each is inserted in a different beaker. Clay suspension was mixed again with distilled water to 1000 mL, beaten and left in place until the separation of clay particles. Clay suspension was separated again from the tailings and put in a different beaker. The resulting suspension was centrifuged; the centrifuge is dried in an oven with a temperature of 120^{o}C. The samples were then dried in furnaces at the temperatures of 1200^{o}C [5,6].

Analysis of clay minerals

Analysis of clay minerals was conducted using Fourier Transform Infrared (FTIR) - KBr pellets and Differential Thermal Analysis (DTA) [7].

3. Result and Discussion

Analysis of DTA curve of suspense, tailings and finished ceramic products is given in Figure 1. Spectrum of Differential Thermal Analysis (DTA) of clay suspension that has been through treatment of separation beneficiation in the form of clay particle fraction was dried at a temperature of 120^{o}C.

Figure 1(1) shows the DTA spectrum suspense clay following endothermic reaction at 527.41°C peak temperature with strong intensity and reaction temperature of 949.82°C exothermic peak with moderate intensity. Endothermic peak was due to the dehydration reaction in which loss of hidroxyl groups or absorbed water molecules in the crystal lattice of clay minerals characteristics halloysite of kaolin mineral. It is known from previous studies, mineral DTA spectrum provides 2 standard halloysite endothermic peak at 130^{o}C temperature as a result of the loss of absorbed water molecules between the crystal lattice, and the temperature of 530^{o}C, which is dehydration reaction and exothermic reaction at a temperature of 900-1000^{o}C [7-9].

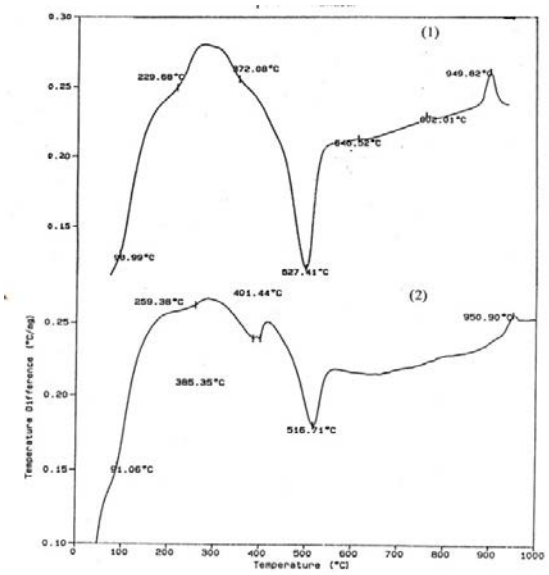

Figure 1. DTA curves of clay suspension (1) and clay tailing (2)

The peak temperature of 949.82°C is due to the formation of γ-alumina and mulit. Temperature 229.68°and 372.08°C indicates the inversion temperature of tridymite from α to β form, and the β1 to β2 where the rearrangement occurred in the presence of crystal heating. Temperature 646.52 and 802.01^{o}C can be a conversion of tridymite to cristobalite form that includes the rearrangement of tetrahedral SiO_4. The temperature can be inverse temperature cristobalite α to β and inverse tridymite [3].

Figure 1(2) shows the DTA spectrum of the suspension. The spectrum is visible only endothermic peaks are weak, there is no typical sharp peaks indicating the existence of a particular mineral. Weak endothermic peak at 511.47; 645.86; 795.65 ^{o}C and which at 511.47°C can be caused by a phase change of quartz (αQ - βQ) which is about (520-578^{o}C), temperature 645.86°C may be caused transition of quartz (Q) (650^{o}C) which is described as: αQ irregular situation > βQ. Temperature 645.86°C may also show Curie temperature magnetite (γ-Fe_2O_3) contained in the clay. While at 795.65°C, transformation of

feldspar group in accordance with the temperature 780-820^{o}C, the transformation of the form in accordance with the form of feldspar feldspar lower to higher forms involving Al-Si distribution is irregular to Al-Si distribution irregular. No clear peaks are caused by the addition of alumina, Al_2O_3 which can cause high content of oxides. This is due to two factors: the chemical effect of the nature of solid solutions and physical effects of the effects of glass formation in the presence of impurities.

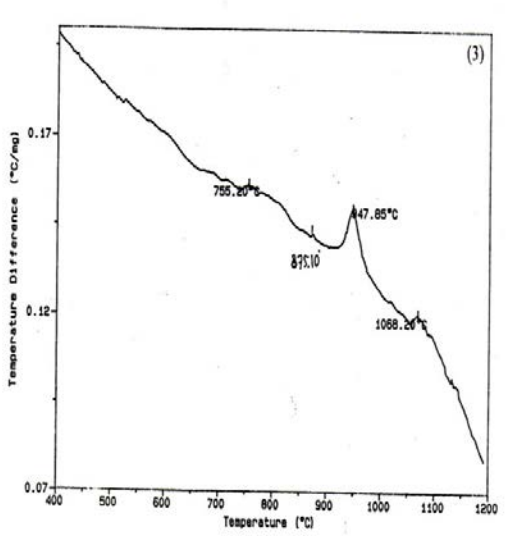

Figure 2. DTA curves of ceramic product.

Figure 2 shows the DTA spectrum of clay tailings. The spectrum shows the endothermic reaction at 516.71°C peak temperature with moderate intensity and exothermic reaction at 950oC temperature peak with weak intensity. Endothermic peak was due to the dehydration reaction, in which loss of the absorbed water molecules in the crystal lattice of from kaolin clay minerals. Exothermic peak at 950.90°C was caused by the formation of γ-alumina and silica mullite and minerals. Temperature 259.38^{o}C characterize inverse of α-cristobalite. Temperature of 385.35°C and 401.44°C is the structural decomposition reaction of organic compounds contained in the clay.

DTA curve of ceramics products is given in Figure 2. FTIR analysis of the clay prior to beneficiation, tailings, ceramic products and ceramic products so that sintering at temperatures 1000^{o}C. Infrared spectra of clay with no beneficiation are given in Figure 3, while wave number data and the intensity of absorption are presented in Table 1.

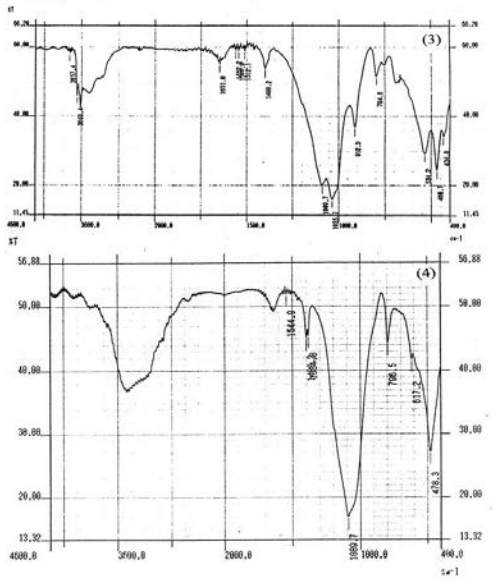

Figure 3. FTIR curves without beneficiation of clay (3) and suspension clay (4).

Table 1. Infrared absorption of clay from village Pulutan, Minahasa

Wave number (cm^{-1})			Attribution from
Clay raw material	**Clay suspension**	**Clay tailing**	
3693.4 m	3693.4 m	3693.4 m	Halloysite
3624.0 m	3624.0 m	3624.0 m	
1031.8 vs	1035.7 vs	1035.7 vs	
910.3 s	910.7 s	912.3 s	
754.1 w	752.2 w	752.2 w	
690.5 w	688.5 w	688.5 w	
540.0 s	534.2 s	534.2 s	
470.6 vs	468.7 vs	468.7 vs	
434.0 s	434.0 s	434.0 s	
1093.6 vs	1089.7 vs	1089.7 vs	Tridymite/ Cristobalite
794.6 v	794.6 s	794.6 s	
470.6 vs	468.7 vs	468.7 vs	
1093.6 s	1089.7 vs	1089.7 vs	Mica (illite)
910.3 s	910.7 s	912.3	
754.1 w	752.2 w	752.2 w	
690.5 w	688.5 w	688.5 w	
470.6 vs	468.7 vs	468.7 vs	
540.0 s	534.2 s	534.2 s	Feldspar
470.6 vs	468.7 vs	468.7 vs	

Description:
vs = very strong, s = strong, m = medium, w = weak

Figure 3 show that the three curves between tanpe clay beneficiation, suspense-clay tailings that have been dried at a temperature of 120^{o}C, there was no significant difference (mean). All three give the peak absorption band that basically has

the same pattern of IR spectra. Peak absorption bands that always existed continuously on the wave number as barikut: absorption bands 3693.4 and 3624.0 cm^{-1} sharp and medium wave numbers shows stretching vibration of OH groups on the surface of the outer and inner bound to Al or Mg elements contained in clay minerals (such as kaolinite and halloysite) or can be water that is absorbed on the clay [10].

Furthermore, only pattern without beneficiation spectra in the band spectra at wave number is followed by a broad band, this absorption band most likely from the water. Ribbon 1400.2 cm^{-1} absorption band is weak, 1093.6 and 1089.7 cm^{-1} sharp and very strong characterizes the stretching vibration of Si-O-Si contained in the structure of kaolin minerals (haloisit), the mineral silica (such as tridymite and cristobalite), and mica (illite typical) [4,10], 1031.8 and 1035.7 cm^{-1} sharp and very strong due to the existence of Si-O stretching vibration -Si contained in kaolin minerals (kaolinite and halloysite typical). Absorption at 910.3 and 912.3 cm^{-1} characterizes the existence of a sharp and strong Al-OH bending vibration that may be contained in the kaolin and mica minerals (eg illite), 794.6 cm^{-1} band is strong Si-O bending vibrations in kaolin and silica minerals (such as tridymite and cristobalite), 754.1 and 752.2 cm^{-1} band shows weak vibrational Si-O-Al from kaolin and mica minerals (typical illite), 690.0 and 688.5 cm^{-1} band showed weak vibration of Si-O-Al minerals such as kaolin (typical halloysite) and mica, 540.0 cm^{-1} and 534.2 cm^{-1} showed strong and sharp vibration of Si-O-Al contained in the structure of kaolin minerals (halloysit), mica and feldspar [10,11]. Moreover, adsorbtion at 470.6 and 467.7 cm^{-1} which were sharp and very strong show of Si-O bending vibration in the mineral kaolin and feldspar, and the last gives absorption bands at 434.0 cm^{-1} band is weak, which is caused by the vibration of Si-O in the structure of kaolin minerals.

FTIR curves of clay tailings (4) and product is given in Figure 3 and 4. With the treatment of materials processing (beneficiation) of clay materials can reduce the materials contained impurities in the clay. This can be seen clearly in the infrared spectrum of the clay prior to beneficiation process (absorption band 540.0 cm^{-1}), absorption band at 540.0 cm^{-1} characteristic of hematite (Fe_2O_3) show strong absorption and infrared spectra of the clay after the beneficiation process is on absorption band 553.0 cm^{-1} characteristic (Fe_2O_3) which has undergone a shift shows weak absorption [4]. Hence, the beneficiation process reduces contents of impurities such as chemical composition of hematite which contains elements of iron (Fe), which is not desirable in ceramic products. The quality of ceramics is determined by the Fe content in the clay which is the main pollutant of ceramic products, where no element Fe or Fe element content <0.5% of white ceramic products [2,8].

Clay minerals contain water, where mineral water structurally bound in the clay. When the temperature raises prograsively, these minerals will decompose at specific temperatures by releasing water (H_2O).

Ferrous compounds oxidized to the corresponding compound ferry or a ferry oxide red [5,6]. At temperatures of 900^oC is usually required for rapid oxidation, but if the temperature is too high, iron oxide (Fe_2O_3) will decompose and produce magnetic Fe_3O_4. Hydrate of iron oxide compounds in the form of ferro will easily oxidized and releases water vapor. Kaolinite ($Al_2O_3.2SiO_2.2H_2O$) was decomposed completely at temperatures below 559^oC into amorphous alumina (Al_2O_3) and amorphous silica (SiO_2) and this form will stay fixed until the temperature reached 980^oC. Amorphous form of alumina crystallized at temperatures between 500 - 1000^oC and at a higher temperature it will be changed to α-Al_2O_3 in the form of corrondum [5,12]. Other minerals contained in the arch decompose at temperatures <900^oC.

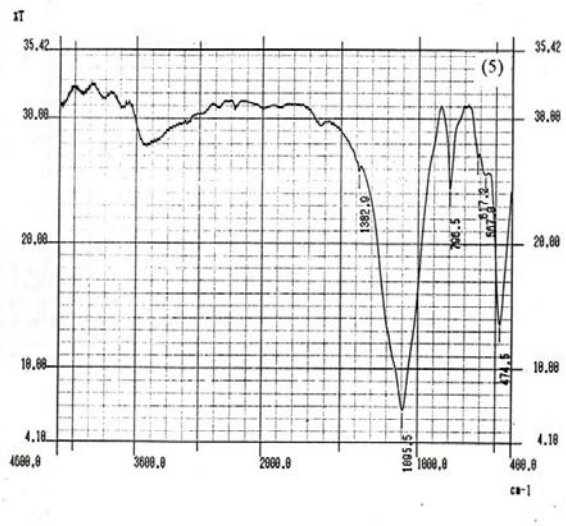

Figure 4. FTIR curves of ceramic product.

4. Conclusion

Beneficiation process reduces content of iron (Fe) in the ceramic products as indicated by the decrease at the intensity of absorption bands of compounds hematite (Fe_2O_3). Thermochemical reaction of clay minerals shows halloysite mineral characteristics and patterns of the infrared

spectrum to provide the main clay minerals halloysite.

5. Acknowledgement

The author would like to thank the Department of Chemistry, Faculty of Mathematics and Natural Sciences, Manado State University, Manado; for the provision of laboratory facilities.

6. References

[1]. Askeland, D.R., (1999), The Science and Enginering of Materials, Brodes/Cole Enginering Devision, New York.
[2]. Callister, W.D., (2008), Materials Science and Enginering, John Wiley & Sons, New York.
[3]. Deer, W.A., Howie, R.A. and Zussman, J, (2000), Rock Forming Minerals, Vol.3 Sheet Silicates, Longman, London.
[4]. Hann, R, (2006), Infrared Absorption Spectrum of Silicon Dioxide, *J. Am. Ceram. Soc*., 8, 595-599.
[5]. Kruglitsky, N.N and Datsenko, B.M., (2005), The Influence of Raw Materials Composition on the Properties of Fired Clay Product, *J. Ceram. Inter,* 10, 78-80.
[6]. Lewis, J.A; Blackman, K.A and Ogden, A.L, (2006), Rheologhical Properties and Stress Development during Drying of Tape-Cast Ceramis Layers, *J. Am. Ceram. Soc.* 79. 3225-3234.
[7]. Mackenzie, R.C., (1990), Differential Thermal Analysis, Academic Press, New York.
[8]. Reed, J.S., (1989), Introduction to the Principles of Ceramic Processing, John Wiley and Sons, Singapore.
[9]. Stone, R.L., (2002), Differential Thermal DTA of Kaolin Group Minerals under Controlled partial Pressure of H_2O, *J. Am. Ceram. Soc.*, 35, 90-99.
[10]. Van der Marel, H.W and Beutelspacher, H., (1972), Atlas of Infrared Spectroscopy of Clay Minerals and Their Admistures, Elsevier, New York.
[11]. Van Olphen, (1977), Clay Colloid Chemistry, John Wiley & Sons, New York.
[12]. Worall, W.E., (1975), Clay and Ceramic Raw Material, Applied Science Publisher, LTD, London.

Face Detection Image Based RGB Color Using Cube Form

Muh. Arif Rahman

Computer Science Department, Mathematics and Natural Science Faculty, Brawijaya University (m_arif@ub.ac.id)

Abstract

We proposed face detection algorithm that work for color image. Our algorithm has two steps to identify face on image. First we develop a skin-based classification of RGB skin human face image using HSV, YbYr and threshold-based method. Second we calculate each region to detect if it represents human face or not using edge detection to perform face feature from the edge of image. The result of our experiment show that 86% of the image to detect the presence of his face, 9% error detection occurred and 5% were not able to detect the presence of faces and the rate of computation depend of method we chosen.

Keywords: ---

1. Introduction

The scope of human and computer interaction is facial recognition which is contained in the image and video. One step before the existence of face recognition is face detection. There are number of factors to face detection such as difficulty in detection of facial age, geometry face, position face in image, lighting influence, differences of gender, similarity of background color and so forth that cause face detection is not easy to do. That why research on face detection research is interesting. Many methods have been developed to detect the presence of faces in the last 20 years. One of face detection that is easy and quick is distinguish skin color and objects around them [1].

In general there are 3 categories of face detection method that is low-level analysis, feature analysis and model of the active area. Face detection based on segmentation and color is a method that includes the category of low-level analysis [2]. Those two methods do not require complex computations and so quickly able to detect the presence of faces in an image with accuracy up to 90-100%. However, some training data has difference color of face and background [3], whereas for face color and background color is almost the same there has been no report result.

Another approach for face detection is to use the merging feature analysis and methods of hair color. From the experimental results it is difficult to detect face on person that has no hair, and then the object is not able to recognize faces. The difficulty of detect face if the background color of image nearly the same with color skin [4].

Other research was using hair analysis in addition to characteristics of the eye. The presence of eye position determines the position of the face. The result of such research produces 87-90% level of truth with computational time less than 1 sec [5].

.This research uses a different approach to determining the existence of the face. The proposed method is to perform edge detection on the Origin of image and then extract face object based on skin color. Both results will be combined and find area that has left-right edge candidate of the face and chin-head using the line shift. The existence of the object candidate's face will be stored and then recursively to find exact face area. Areas that are not detected as a face will be white. While the detected faces will be colored black. Face candidate areas are then tested to determine the actual face area.

Digital Image

Digital image can be expressed as a function of two variables: f (x, y). where x and y are spatial coordinates, while the value of f (x, y) is the intensity of light at these coordinates. In discrete space, the value of x, y and f (x, y) is limited. Value of x stated number of pixels each row, y values stated number of pixels each column. The number of pixels is multiply the value of x and y. Value of f (x, y) between 0 to 255. Values are expressed degrees of gray a color [6]. A value of 0 states the pixel is very dark (black), while the value of 255 state pixel colors is very bright (white).

Digital image is represented in the form of an array. Each element contain intensity values which is called pixel. Figure 1 shows the value of the pixels element [i, j].

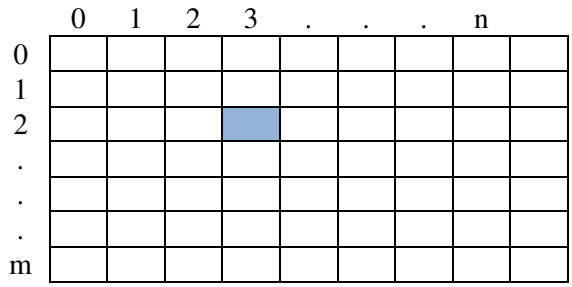

Figure 1. Pixel at [3,2]

Each pixel has 3 colors known as RGB color that is Red, Green and Blue. Consider Figure 2 below:

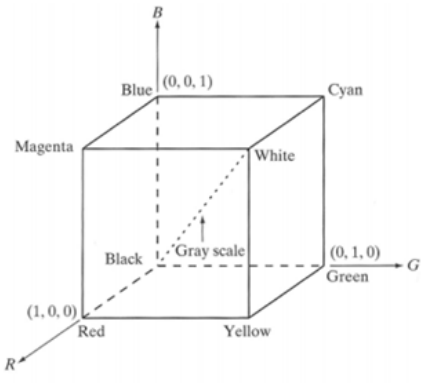

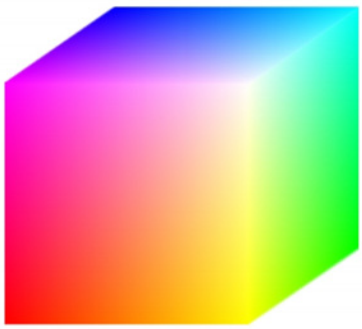

Figure 2: RGB Color Space

Normalized RGB

Normalized RGB is an extension of the RGB color where each color pixel is percentage of RGB value of pixel and sum of value R, G and B color [7]. This is to overcome the differences in intensity on the same objects that were photographed in different lighting. Formulation NRGB stated as follows:

$$r = \frac{R}{(R+G+B\}} \qquad (1)$$

$$g = \frac{G}{(R+G+B)}$$

$$b = \frac{B}{(R+G+B)}$$

Components r, g and b is an element of normalization of R, G and B. The value of normalization r, g and b lead to differences of illumination each pixel that are not dependent of light on image.

HSV Color Space

HSV stands for Hue, Saturation and Value. HSV is a perspective view of the approaching color color viewable by the human eye [7]. Figure 3 is a color model HSV.

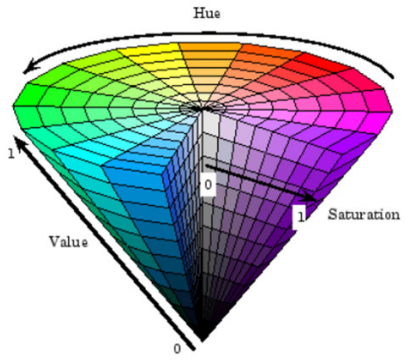

Figure 3. HSV Color Space

Hue is an angle which is has 0 s / d 360o. Saturation and intensity has value [0, 1]. Here is the formulation of RGB to HSV conversion.

Color r, g, br, g, b ∈ [0,1] is the component colors red, green and blue of RGB
M is the max (r, g, b) and m = min (r, g, b) then

$$H_o = \begin{cases} 0 & \text{if } M = m \\ \left(\frac{6+g-b}{6\cdot(M-m)}\right) \bmod 1 & \text{if } M = r \\ \frac{2+b-r}{6\cdot(M-m)} & \text{if } M = g \\ \frac{4+r-g}{6\cdot(M-m)} & \text{if } M = b \end{cases} \qquad (2)$$

$$S_o = \begin{cases} 0 & \text{if} \quad M = m \\ \dfrac{M-m}{M+m} & \text{if} \quad M \le 1-m \\ \dfrac{M-m}{2-(M+m)} & \text{if} \quad M > 1-m \end{cases}$$

$$V_o = M$$

2. Experimental Details

Color Skin Model

Skin color model is defined Yanjiang & Baozong [8] after a series of tests on facial images. The formulation is as follows:

$$0.36 \leqslant r \leqslant 0.465, \quad 0.28 \leqslant g \leqslant 0.363, \\ 0 \leqslant H \leqslant 50, \quad 0.20 \leqslant S \leqslant 0.68, \quad 0.35 \leqslant V \leqslant 1.0, \qquad (3)$$

Canni Edge Detection

There are a number of edge detection methods such as Canny method. Prewit and Sobel. Edge detection sought by performing differentiation horizontally and vertically at each pixel [6]. If the value is greater then absulutenya occur significant differences in the pixels of one another. Canny operator for edge detection is defined as follows:

-1	0	+1
-2	0	+2
-1	0	+1

Gx

+1	+2	+1
0	0	0
-1	-2	-1

Gy

Figure 4: Canni Operator

While the value of edge detection is defined as follows:

$$|G| = |G_x| + |G_y| \qquad (4)$$

Data

Data is taken from http://cswww.essex.ac.uk/mv/allfaces/index.html containing 395 faces where each face has 20 different scene so that the total image that there is 7900. Image format used is JPEG 24bit. Figure 5 is an example of the images in the folder asamma consists of 20 images.

Proposed Algorithm

1. Read the image and save in array A
2. Perform edge detection using the formula (4) and store in array B
3. Perform image classification which has a skin color using formula (3) and store in array C.
4. In the object A remove / ignore the pixels that are not considered skin color
5. Perform a search in the image using 4x15 rectangular box and the detection of the presence of the greatest value of Gh in Horizontal
6. Find a pair of Gh.
7. Perform the same process for the GV is in a vertical differentiation value to finding pairs
8. Gh and GV pairs form so that a box size s. rx
9. Perform 5-8 process until no more candidate objects found face
10. Based on the results of 5-9, remove / ignore the pixels that are not the candidate's face.
11. Do it over and over in the box to the candidate's face to detect the presence of faces.
12. Do coloring box on an array of facial images A and evaluate whether the true object of his face had been found.

3. Result and Discussion

After conducting a series of experiments on the 7900 picture it was found that 86% of the image to detect the presence of his face, 9% error detection occurred and 5% were not able to detect the presence of faces. All experiment of each image consumes time less than 1 second. Image with significance difference color between skin face and background is difficult to identify the presence of face.

4. Conclusion

In this paper, we have presented a new approach to detect face in color image. The result is good when image has significance difference color skin face and the background. This algorithm is combining 2 method i.e. edge detection and color skin classifier.

5. Acknowledgement

---

6. References

[1]. Campadelli, P., Cusmai, F., and Lanzarotti, R., (2003), A color based method for face detection, Proceedings of the International Symposium on Telecommunications.

[2]. Hjelmas, E., (2001), Face Detection: A Survey, Computer Vision and Image Understanding.

[3]. Goyani, M., *et. al*. (2010), Acceptance / Rejection Rule Based Algorithm for Multiple Face Detection in Color Images, *International Journal of Engineering Science and Technology* Vol. 2(6).

[4]. Data, M., Rahman, M. A., (2010), Pendeteksian Wajah Secara Cepat Menggunakan Teknik Windowing Dengan Ciri Rambut dan Kulit, Honour Thesis, Computer Science Dept, Brawijaya University, Malang

[5]. Wang, Y., and Yuan, B., (2001), A novel approach for human face detection from color images under complex background, *The Journal of the Pattern Recognition Society*.

[6]. Gonzalez, R. and Woods, (2002), Digital Image Processing, 2 ed., Addison-Wesley Longman Publishing Co., Inc.

[7]. Ming-Hsuan, Y., and Narendra, A., (1998) Detecting Human Faces in Color Images, Proceedings of the International Conference on Image Processing, vol. 1, Oct. 4-7, pp. 127-130.

Airborne Measurements of Particle Concentration from Biomass Burning in Nothern Territory

Arinto Yudi Ponco Wardoyo

Physics Deparment, Faculty of Science, Brawijaya University, Malang (a.wardoyo@ub.ac.id)

Abstract

Airborne measurements of particle number concentrations from biomass burning were conducted in the Northern Territory, Australia, during June and September campaigns in 2003, which is the early and the late dry season in that region. The airborne measurements were performed along horizontal !ight tracks, at several heights using an aircraft Beech Super King B200 in order to gain insight into the particle concentration levels and their variation with height within the lower boundary layer (LBL), upper boundary layer (UBL), and also in the free troposphere (FT). The particle measurements were conducted using a TSI Scanning Mobility Particle Sizer (SMPS) that was mounted in a single, two levels, 19-inch rack, with anti-vibration mounts, and was located on the left hand side of the aircraft. The measurements found that the concentration of particles during the early dry season was lower than that for the late dry season. For the June campaign, the concentration of particles in LBL, UBL, and FT were (685±245) particles/cm^3, (365±183) particles/cm^3, and (495±45) particles/cm^3 respectively. For the September campaign, the concentrations of particles were found to be (1233±274) particles/cm^3 in the LBL, (651±68) particles/cm^3 in the UBL, and (568±70) particles/cm^3 in the FT.
Keywords: *Airborne measurement, particle concentration, biomass burning.*

1. Introduction

Biomass burnings including forest fires, agriculture burning, prescribed wild land, agricultural waste burning, logging slash, land clearing slash, burning for cooking and heating have been identified as a major contributor of particles and gaseous in the atmosphere [1,2]. Their emissions have played a role in influence of atmospheric process changes [3]; acidification of clouds, rain, and fog [4]; radiation transport that includes in a small scale even in a mesoscale [5].

Forest fires occur regularly along year in almost all the part of the world, such as: Africa, South East Asia, South America, Mediterranean region, USA, Canada, Russia, and Australia. The fires have significantly consumed huge areas of the world. The data show forest fires consuming million hectares of the burnt areas. More than 1.3 million hectares of forest was burnt in China in 1987. At the same year, forest fire in Eastern Asia consumed approximately 14 million hectares [6]. In 1994 and 1997, forest burning destroyed more than 50,000 km^2 and 20.000 km^2 in Indonesia [4]. Other data show that 100,000 km^2 of forest in northern latitudes, 400,000 km^2 of tropic and sub tropic forest, 5 to 10 million km^2 of open forest and Savannas are burnt every year [2].

In Australia, biomass burning occurs all times since millions of years ago. Natural ecosystem, weather condition, landscape, and even biological diversity of Australia sustain Australia to the fires. Climate change is as a factor to increase the frequency, intensity and size of forest fires in much of Australia [7]. Variation of climate around Australia affects the different frequency of forest fires that mostly happen in the zone dominated by dry eucalypt forests. The burnt areas of Australia are estimated about 6.5 percent per year, except the forest fires in 1974 – 1975 burned 15.2 percent of the continent [8]. In the years, a massive 33.5 percent of the northern territory was burned (Luke and McArthur 1978). According to the Australia fire report, about 115000 to 230000 fires per year have been portrayed by a satellite remote sensing during the fire seasons 1998-1999 and 1999-2000, burning the area of 31 and 71 million hectares respectively [9].

The Western Australian Department of Land Information reported that forest fires across Australia a 1997 to 2003 affected the area from 26.3 million hectare to 80.1 million hectares. The greatest extent of forest fires was in the savannas of northern Australia. Australian Bureau Statistic also reported that there were 5999 forest fires consuming 21 million hectare areas across Australia in which was most area in northern territory Australia of 15 million hectare areas happening from July 2002 and February 2003 [10]. Kakadu National Park located at the northern Australia suffers with forest fires from year to year. The data from 1980 to 1995, more than one million areas were destroyed by forest fires in the areas [11].

Northern territory Australia which is a large savannah region has a wet-dry season. Wet season occurs from November to April with the average annual precipitation of over 1000 mm falls and dry season extends from May to October. Forest fires mostly happen in every dry season [11], in which the fires are mild intensity in the early dry season (EDS) and are often of high intensity in the late dry

season (LDS) [12]. The fires release significant amount of gaseous and particles every year. Knowing a profile of particles emitted by the fires is an important issue for the impact assessments. This study which was a part of large project for aerosol measurements in the Northern Territory Australia aimed for obtaining a concentration profile of biomass burning particles along determined flight areas. The airborne measurements were conducted in early dry season in a four day airborne measurement campaign.

2. Experimental Details

Study Area

The study was conducted over the large areas of tropical savannas of the Northern Territory, Australia. This is a sparsely populated area with no major cities or industrial complexes that would add additional anthropogenic sources to the background aerosol loading. The dominant vegetation type of these savannas is a mixture of annual grasses, such as *Sorghum* species and perennial grasses, and tropical savanna woodland, made up of sporadic trees, predominantly the *Eucalyptus miniatia* [13,14]. A large fraction of the vegetation is burnt annually by naturally occurring fires [15].

Measurement Times and Locations

The airborne measurements of particle number concentration and particle size distribution were conducted during two campaigns, in June and September 2003, which were in the EDS and the LDS, respectively. The measurements were performed both in the morning and in the afternoons with the duration of each flight leg from 20 to 30 minutes. The total time spent for each measurement for every flight was approximately four hours. This included transit from Darwin to on station, a vertical stack of horizontal flight legs and return transit to Darwin. In June the flights were on the Monday, Tuesday and Thursday afternoons with the final flight on the Friday morning. In September campaign, the fights were conducted two times in the morning (Tuesday and Thursday) and two in the afternoon (Monday and Friday).

The airborne measurements were carried out along a predetermined horizontal path, that extended from a point South West (SW) of Jabiru (13.08 South (S) 132.32 East (E)) to a point North East of Jabiru (12.11 S 133.15 E), in Kakadu National Park, Northern Territory. The dot spots are accumulative fires detected between 22-28 June and 21-27 September 2003. The satellite data shows that there were 39, 28, 72 and 41 hotspots detected on the 23rd, 24th, 26th and 27th of June 2003 and 3, 11, 11, and 6 hotspots on the 22nd, 23rd, 25th and 26th of September 2003, respectively. Although there were fewer fires in September 2003, the intensity of the fires in September was higher than those occurring in June 2003. Further the majority of the fires were located in the proximity to the flight tracks.

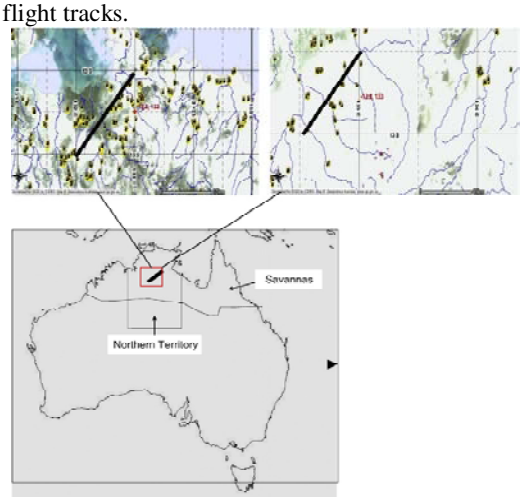

Figure 1. Location of the !ight tracks.

The two maps zoomed in over the !ight path (indicated by the black line) at the Northern end of the Northern Territory, show satellite "re spot data for 22–28 June 2003 (left) and 21–27 September 2003 (right) [16].

Instrumentation Set Up

A range of scientific instrumentation was fitted to an aircraft (Beech Super King Air B200T) that has been configured for scientific research. This equipment was either purpose built for aircraft sampling or was modified to be applicable for this purpose. An isokinetic inlet was fitted externally to the fuselage of the aircraft, which was fed into the cabin of the aircraft to provide suitable sampling lines for a range of aerosol measuring instruments. The particle measurements were conducted using a TSI Scanning Mobility Particle Sizer (SMPS) consisting of a TSI 3010 Condensation Particle Counter (CPC) and a TSI 3080 Electrostatic Classifier (EC). The SMPS was mounted in a single, two levels, 19 inch rack, with anti-vibration mounts, and was located on the left hand side of the aircraft.

The SMPS was operated with a sheath air flow of 3 L/m and a sample flow of 0.3 L/m. The scanning time and retrace time were set 120 and 30 seconds, respectively. The multiple charge correction algorithms were also employed. The SMPS was calibrated daily using 100 nm size PSL before each flight. The measurement range of the SMPS was set up depending on the atmospheric pressure at which the measurements were conducted, such that when the pressure was lower the bottom cut point became higher. The bottom cut points were calculated at the beginning of each

path and the values were entered manually into the software.

3. Results and Discussion

The particle concentrations measured as a function of height during the June campaign are presented in Figure 2. Each point on the graph represents the average particle concentration, as well as the standard deviation, calculated at each height.

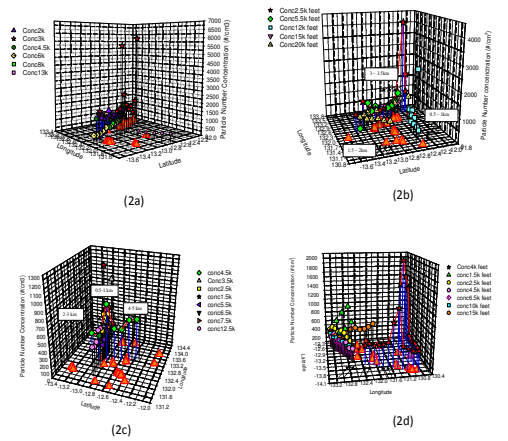

Figure 2. The measured concentrations during the June campaign.

In general, the particle concentrations measured on each day during the June campaign showed similar trends, with the particle concentrations being relatively high below 1800m and decreasing as the height increased above 1800m. At the height below 1800m, the average concentration was around 900 particles/cm^3 for the 23rd and 24th of June, and 580 and 500 particles/cm^3 for the 26th and 27th of June, respectively. On most days the decrease in concentrations to approximately 350 particles/cm^3, occurred at a height of around 2000m. The drop in particle concentration appears above the boundary layer height, that varied between 1700 and 2000m. The average concentrations of particles measured above 3900m (in the free troposphere) in June were around 400 particles/cm^3. The only exception was on the 24th of June, when the concentration in the FT was larger and decreased to approximately 550 particles/cm^3 and remained fairly constant even up to height of 6500m. It can be seen that the standard deviation of the concentrations is high below 1800m, which implies that the variation in the concentrations of particles up to this height is relatively large over the flight paths. This is likely to be a result of the fire locations close to the flight paths with not enough mixing.

The measurements carried out on the 26th and 27th of June found similar concentrations for all the measured heights, with the concentrations below the boundary layer being lower than those measured on the previous days. This is most likely due to the fact that the location of the fires and the wind direction on these two days caused the smoke to be blown away from the flight paths.

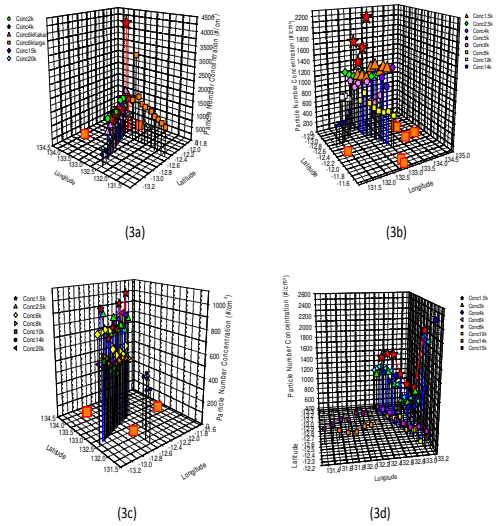

Figure 3. The measured concentrations of particles during the September campaign.

In general, the concentrations of particles measured during the September campaign were higher than those measured during the June campaign, despite the smaller number of fires during the September campaign. Figure 3 shows the concentration of particles measured for different heights during the September campaign.

Similar trends as in the June campaign were also observed with the vertical distribution of the particle concentrations significantly dropping above the boundary layer. A particle concentration of around 500 particles/cm^3, similar to the June flights, was observed for larger heights in the FT. Another interesting thing to note is that during 3 out of 4 September flights there were an increase in the particle concentration just below the inversion layer.

In order to compare the particle concentrations for the two campaigns, across all of the altitudes measured, particle concentration was averaged over each height within each campaign. This is presented in Figure 4. The altitudes were divided into 3 regions: Region I - lower boundary layer (LBL), for heights below 1800 m for the June campaign and below 1950 m for the September campaign; Region II - upper boundary layer (UBL), for heights between 2000-3900 m; and Region III - free troposphere (FT), for heights above 3900 m.

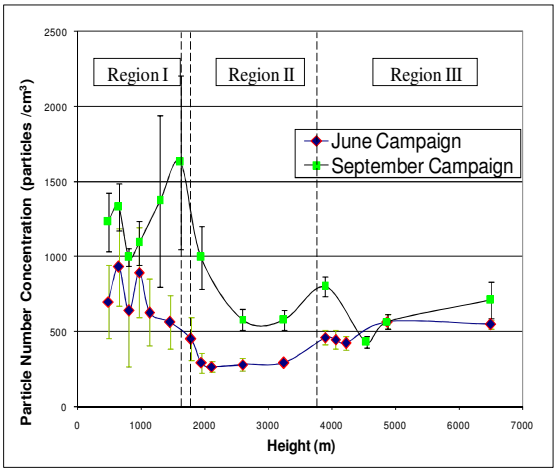

Figure 4. Average particle concentrations measured during June and September campaigns.

The average and standard deviation of the particle concentration in Region I presented in Figure 4 was (685 ± 245) particles/cm^3 for the June campaign and (1233 ± 274) particles/cm^3 for the September campaign. The concentration decreased in Region II to (365 ± 183) particles/cm^3 and (651 ± 68) particles/cm^3 for June and September campaigns, respectively. The concentration of particles in Region III was (495 ± 45) particle/cm^3 for June campaign and (568 ± 70) particles/cm^3 for September campaign.

4. Conclusions

- The average concentration of particles during the June campaign was smaller than in September, for all altitudes in the first two regions.
- The June flights show a decrease in particle concentration with an increase altitude whilst the September measurements show an increase up to the boundary layer.
- Biomass burning particles did not penetratee into the FT for both campaigns.

5. Acknowledgements

The author would like to greatfully thank to Lidia Morawska and Zoran Ristovksi (Queensland University of Technology, Brisbame, Australia) for involving me in this project. I gratefully acknowledge of Milan Jamriska and Steve Carr (Defence Science and Technology Organisation (DSTO), Australia) with suppying September Campaigne data.

6. References

[1]. Dennis, A., M. Fraser, et al. (2002). "Air pollutant emissions associated with forest, grassland, and agricultural burning in Texas." Atmospheric Environment **36**(23): 3779-3792.

[2]. Uherek, E. (2004). "Vegetation fire." Accessed Mei 2004, from http://www.atmosphere.mpg.de.

[3]. Shaw, R. W. (1987). "Air pollution by particles." Science Environment **255**: 96 - 103.

[4]. Nichol, J. (1997). "Bioclimatic impacts of the 1994 smoke haze event in southeast Asia."

[5]. Wurzler, S. and M. Simmel. (2005). "Impact of vegetation fires on composition and circulation of the atmosphere." Accessed March 2005, http://projects.tropos.de:8088/afo200g3/.

[6]. Cahoon, D. R., B. J. Stock, J. S. Levine, W. R. Cofer III and C. C. Chung,(1992), Evaluation of a technique for satellite-derived estimation of biomass burning. Journal of Geophysical Research, 97(D4), 3805-3814.

[7]. Campbell (2003)

[8]. Luke, R. H. and A. G. McArthur,(1978), Bushfires in Australia. Australian Government Publishing Service, Canberra.

[9]. Gill, M. and P. H. R. Moore,(2005). Fire Situation in Australia, March 2005, http://www.fao.org/docrep.

[10]. ABS, (2004). Environment bushfires, Australian Bureau of Statistics, Accessed March 2005, http://www.abs.gov.au/ausstats.

[11]. Gill, A. M., P. G. Ryan, et al. (2000). "Fire regimes of world heritage Kakadu National Park Australia." Australia Ecology **25**: 616-625.

[12]. Williams, R. J., A. M. Gill, et al. (1998). "Seasonal changes in fire behavior in a tropical savanna in northern Australia." International Journal of Wildland Fire **8**: 227-239.

[13]. Wilson, B. A., P. S. Brocklehurst, et al. (1990). "Vegetation survey of the Northern Territory Australia." Technical Report no: 49, Conservation Commission of the Northern Territory, Darwin.

[14]. Williams, R. J., G. D. Cook, et al. (1999). "Fire regime, fire intensity and tree survival in a tropical savanna in northern Australia." Australian Journal of Ecology **24**: 50-59.

[15]. Russell-Smith, J., P. B. Ryan, et al. (1997). "A LANDSAT MSS-derived fire history of Kakadu National park, monsoonal Australia, 1980-94: seasonal effect, frequency and patchiness." Journal of Applied Ecology **34279-87**.

[16]. Ristovski, Z.D., Wardoyo, A.Y.P, Morawska. L, Jamriska, M., Carr, S, and Johnson, G. (2009).Biomass burning in!uenced particle characteristics in Northern Territory Australia based on airborne measurements, Atmos. Res.doi:10.1016/j.atmosres.2009.12.002.

BIBLIOGRAPHY OF FIRST AUTHOR

Name	Affiliation	email
A.Ghanaim Fasya	Department of Chemistry, Faculty of Sciences, University of Brawijaya	fasya_46@yahoo.co.id
Abdurrouf	Departement of Physics, University of Brawijaya	a.abdurrouf@ub.ac.id.com
Adeodatus Yuda Handaya	Surgery Division of RSUD Kepanjen Malang	yudahandaya@yahoo.com
Adi Susilo	Geophysics, Dept of Physics, University of Brawijaya, Malang	adisusilo@ub.ac.id
Afnidar	Department of Chemistry, Open University of Jakarta, Indonesia	
Agnisa Bhakti Persada	Business Laboratory, Statistics, FMIPA ITS, Surabaya	agnisa_persada@yahoo.com
Agus Haryono	Polymer Chemistry Group, Research Center for Chemistry Indonesian Institute of Sciences (LIPI), Jakarta	haryonolipi@yahoo.com
Ahmad Husni	Environmental Chemistry, Department of Chemistry, Faculty of Mathematics and Natural Sciences, Brawijaya University	solonese2002@yahoo.com
Aladin Sianipar	Separation and Speciation Analytical Lab, Chemistry, ITB, Bandung	aladin_ssi@yahoo.com
Aman Santoso	Posrgraduate Program, Faculty of Agriculture, University of Brawijaya	amansantoso49@yahoo.co.id
Ari Kusumastuti	Mathematics Department, Faculty of Science and Technology, State Islamic University Maulana Malik Ibrahim of Malang	saad3108@gmail.com
Arinto Yudi Ponco Wardoyo	Physics Deparment, Faculty of Science, Brawijaya University	a.wardoyo@ub.ac.id
Arrowiyah Binti Qomari	Dept. of Statistics ITS, Surabaya	arrowiyah_89@yahoo.co.id
Asep Awaludin Prihanto	Faculty of Fisheries and Marine Science, Brawijaya University	asep_awa@yahoo.com
Asyik Nur Allifah AF	Magister Program, Faculty of Sciences, Brawijaya University	
Athanasia Amanda Septevani	Polymer Chemistry Group, Research Center for Chemistry Indonesian Institute of Sciences, Jakarta	fani.manda@yahoo.com
Atikah	Chemistry, Faculty of Science, University of Brawijaya	atikadhikara@yahoo.com

Name	Affiliation	email
Aulanni'am	Biochemistry Laboratory, Chemistry Department Faculty of Sciences, Brawijaya University	aulanibiochem@yahoo.com, aulani@ub.ac.id
Ayik Rosita P	Faculty of Pharmacy, University of Jember, Indonesia	aixrose_pee@yahoo.co.id
Bambang Poerwadi	Dept. of Chemistry, faculty of Science, Brawijaya University	bpoerwadiub@ gmail.com
Bambang Sudjito	Law Faculty Brawijaya University	b_jito@ub.ac.id
Bambang W.O.	Bussiness laboratory of Department of Statistics, Sepuluh November Institute of Technology, Surabaya	Alley_sohib@yahoo.co.id
Barlah Rumhayati	Chemistry Department, Faculty of Science, Brawijaya University, Malang	
C. Tuti Budiantari	Center for Technology of Radiation Safety and Metrology, National Nuclear Energy Agency, Jakarta, Indonesia	tuticb@yahoo.com
Candra Dewi	Computer Science, Faculty of Science, Brawijaya University	dewi_candra@ub.ac.id
Danar Puwonugroho	Department of Cemistry, Faculty of Science, Brawijaya University, Indonesia	danar@ub.ac.id
Dedy Kurniawan	Biology Department, Faculty Sciences, Brawijaya University	rudededy@gmail.com
Dewi Ayu Lestari	Purwodadi Botanical Garden – LIPI, East Java	chunyang_dee@yahoo.co.id
Dore Yulia	Department of Chemistry, Faculty of Science, Brawijaya University	dore_yulia@yahoo.com
Dwi Ningsih	Faculty of Pharmacy, Setia Budi University, Surakarta	dwiee_nink@yahoo.co.id
Dwi Rasy Mujiyanti	Department of Chemistry, Lambung Mangkurat University, Banjarbaru, South Borneo, 70714, Indonesia	dwi_rasy@yahoo.com
Dyah Kinasih ti Wuragil	Veterinary Medicine School, University of Brawijaya, Malang, Indonesia	d_kinasih@ub.ac.id
Eddy Heraldy	Department of Chemistry, Faculty of Mathematics and Natural Sciences, Sebelas Maret University, Surakarta, Indonesia	eheraldy@gmail.com
Edi Siswadi	Post Graduate Program of Agricultural Faculty, Brawijaya University	edi_sis_83@yahoo.co.id
Eti Rohaeti	Department of Chemistry, Faculty of Mathematics and Natural Sciences, Bogor Agricultural University, Indonesia	er_a444@hotmail.com

Name	Affiliation	email
Evi Hanizar	IKIP PGRI Jember, Indonesia	ev_ha@yahoo.co.id
Evi Susanti	Department of Biochemistry, Faculty of Science, State University of Malang	esusanti.kim@gmail.com
Fariati	Chemistry Department, Faculty of Mathematics and Science, State University of Malang, Malang	f4riati@gmail.com
Gatot Ciptadi	Faculty of Animal Husbandry, Brawijaya University	ciptadi@yahoo.com
Gatot Wurdiyanto	Center for Technology of Radiation Safety and Metrology, National Nuclear Energy Agency (PTKMR-BATAN), Jakarta, Indonesia	gatot_w@batan.go.id
Gunandjar	Radioctive Waste Technology Center, National Nuclear Energy Agency of Indonesia (BATAN), Jakarta	gunand-m@batan.go.id
Hayyu Febriani	University of Brawijaya, Malang	ayie.redluph@gmail.com
Harijati N.	Department of Biologi, Faculty Science, Brawijaya University	harijati@ub.ac.id
Herawati	Veterinary Medicine School, University of Brawijaya, Malang	herawati58@ub.ac.id
Hermawan Candra	National Nuclear Energy Agency, Jakarta, Indonesia	hermawan@batan.go.id
Hermin Sulistyarti	Chemistry Department, Faculty of Science, University of Brawijaya, Malang	sulistyarti@yahoo.com
Holnisar	Center for Technology of Radiation Safety and Metrology, National Nuclear Energy Agency (PTKMR-BATAN), Jakarta, Indonesia	holnisar@batan.go.id
I Nengah Kundera	Biology, Tadulako University , Palu, Central Sulawesi	
I Wayan Dasna	Chemistry Dept, Faculty of Science, State University of Malang	idasna@um.ac.id
Icuk Setiyawati	Department of Physics, Faculty of Science, Brawijaya University	icunk_ube@yahoo.com
Iin Kurnia	Department of Biomedical, Center for Technology of Radiation Safety and Metrology National Nuclear Energy Agency, Jakarta	ime@ipb.ac.id
Indah Rahmawati	Mathematics Department, Faculty of Science and Technology, UIN Maulana Malik Ibrahim, Malang	i_r4h34@yahoo.com
Irmanida Batubara	Department of Chemistry, Faculty of	imebatubara@gmail.com

Name	Affiliation	email
	Mathematics and Natural Sciences, Bogor Agricultural University, Indonesia	
Ismail	Forest Management, Faculty of Agriculture, University of 17 Agustus 1945, Samarinda,East Kalimantan, Indonesia	pinaringan_b@yahoo.co.id
Khothibul Umam Al Awwaly	Animal Product Technology Department, Faculty of Animal Husbandry University of Brawijaya	aak_umam@ub.ac.id
Lailiatul Mubtadiah	Dept. of Mathematics, Faculty of Science and Technology, UIN Maulana Malik Ibrahim, Malang	ail4_04_girlz@yahoo.co.id
Lilibeth de la Cruz Coo	University of the Philippines, Phillipines	ldlccoo@yahoo.com, christian_11_lr@yahoo.com, azrasco@yahoo.com
Lilik Sunaria	Chemistry Department, Faculty of Mathematics and Sciences, State Univercity of Malang	Re_adzkiyah@yahoo.com
M.A.J Wasono	Department of Physics, Faculty of Mathematics and Natural Sciences, Gadjah Mada University Yogyakarta, Indonesia	majwasono@gmail.com
M. Lathifurrijal	Department of Chemistry, Faculty of Science and Technology, State Islamic University of Maulana Malik Ibrahim, Malang	iejang@yahoo.com
Marissa Agnestiansyah	Department of chemistry, Faculty of Science, brawijaya University	rissa_ansya@yahoo.com
Masruroh	Department of Physics, Faculty of Science, Brawijaya University	rafizen_02@yahoo.com
Meytij Jeanne Rampe	Department of Chemistry, Faculty of Mathematics and Natural Science, Manado State University, Indonesia	meytij_rampe@yahoo.co.id
Moekhamad Alfiyan	BAPETEN, Jakarta, Indonesia	m.alfiyan@bapeten.go.id
Mokhamad Nur	Dept. of Agricultural Product Technology, University of Brawijaya, Malang	mnur@ub.ac.id
Moh. Anas Kurnia R	Student of Mathematic (Double Degree), ITS, Surabaya	anaskurnia2009@yahoo.co.id
Muhamad Agus Wibowo	Chemistry, FMIPA, Tanjungpura University, Pontianak	aguso2@yahoo.com
Muhamad Firdaus	Faculty of Fisheries and Marine Science, Brawijaya University	muhamadfir@yahoo.com
Muhammad Hamzah Syahruddin	Geophysics, Department of Physics, Universitas of Hasanuddin, Makasar	hamzah@fmipa.unhas.ac.id
Muhammad Hilman	Department of Biology, Faculty of Sciences,	muhammadhilman87@gmail.com

Name	Affiliation	email
F. Amin	Brawijaya University	
Muhammad Yusuf	Department of Chemistry, Institute Technology of Bandung, Indonesia	Yusuf.6423@students.itb.ac.id
Mukh Syaifudin	Center for Technology of Radiation Safety and Metrology	mukh_syaifudin@batan.go.id
Ni Made Suaniti	Chemistry, Faculty of Science, Universitas of Udayana, Bali	suanitisr@yahoo.com
Ni Wayan S. Wardhani	Dept. of Mathematics, Faculty of Sciences, University of Brawijaya, Indonesia	wsardhani@yahoo.com
Ninik Afrizatus	Department of Chemistry, Faculty of Science, University of Brawijaya	afriza.ninik87@gmail.com
Noer Komari	Chemistry, Faculty of Mathematical and Natural Science, University of Lambung Mangkurat, Banjarmasin	noerkomari@yahoo.com
Nur Alim Natsir	State Islamic Institute of Ambon, Indonesia	allif_af@yahoo.com
Nur Faizah	Department of Statistics, FMIPA-ITS	nur_faizah39@yahoo.com, bambang_wo@statistika.its.ac.id
Nur Lailatul Rahmah	Department of Chemistry, Faculty of Sciences, Brawijaya University	cahya_leyla@yahoo.com
Parawita Dewanti	Agriculture Department University of Jember	parawita@yahoo.co.id
Pujadi M	for Technology of Radiation Safety and Metrology, National Nuclear Energy Agency, Jakarta, Indonesia	pujadi@batan.go.id
Qonita Fardiyah	Department of Chemistry, Faculty of Science, Brawijaya University	qfardiyah@yahoo.com
R Bagus Fajriya Hakim	Statistics Department, Faculty of Mathematics and Natural Sciences	hakimf@fmipa.uii.ac.id
R. Priyadarshini	UPN “Veteran” Surabay, East Java	rssyd_priyadarshini@yahoo.com
Rahmi Nurdiani	Faculty of Fisheries and Marine Science, Brawijaya University	rahminurdiani@yahoo.com
Raja B.D. Sormin	Faculty of Fisheries and Marine Science, University of Pattimura, Ambon	rbd.sormin@yahoo.com
Ratno Bagus Edy Wibowo	Department of Mathematics, Faculty of Mathematics and Natural Science, University of Brawijaya	rbagus@ub.ac.id
Reni Ambarwati	Department of Biology, Faculty of Mathematics and Natural Science, Surabaya State University	renibio95@yahoo.co.id
Ririn Kusumawati	Department of Mathematics Faculty of Science and Technology, State Islamic	saad3108@gmail.com

Name	Affiliation	email
	University Maulana Malik Ibrahim of Malang	
Rosalina A. L.	Department of Chemistry, Faculty of Sciences, Brawijaya University	deeochalina@yahoo.com
Rurini Retnowati	Chemistry Department, Mathematics and Natural Sciences Faculty, University of Brawijaya, Malang	rurini_retnowati@yahoo.com
Samingun Handoyo	Department of Statistic, Faculty of Science, Brawijaya University	bujur83@yahoo.co.id
Sentot Joko Raharjo	Dept. of Chemistry, University of Brawijaya	sentotjoko@yahoo.co.id
Siti Nurhayati	Department of Biomedical, Center for Technology of Radiation Safety and Metrology, National Nuclear Energy Agency, Jakarta	Nurhayati_s@batan.go.id
Yanti Lusiyanti	Department of Biomedical, Center for Technology of Radiation Safety and Metrology National Nuclear Energy Agency, Jakarta	k_lusiyanti@batan.go.id
Solimun	Statistics Departement, Basic Science Faculty, Brawijaya University	solimun@ub.ac.id
Sri Rahayu	Departement of Biology, Faculty of Mathematics and Natural Sciences, Brawijaya University, Indonesia	srahayu@ub.ac.id
Sri wardhani	Chemistry, Faculty of Science, University of Brawijaya	wardhani@ub.ac.id
Suharti	Chemistry Department, State University of Malang, Indonesia	s.suharti@um.ac.id
Suleman Duengo	Department of Chemistry, Faculty of Science, University of Brawijaya	suleman_duengo@yahoo.com
Sulistyo Saputro	Chemistry Study Program, Department of Mathematics and Natural Science Education, Faculty of Teacher Training and Education, Sebelas Maret University, Surakarta, Indonesia	sulistyo68@yahoo.com
Sunaryo	Division of Geophysics, Physics Department of Science Faculty, Brawijaya University	sunaryo@ub.ac.id
Susilo Widodo	Center for Technology of Radiation Safety and Metrology, National Nuclear Energy Agency (PTKMR-BATAN), Jakarta, Indonesia	swidodo@batan.go.id
Sutrisno	Department of Chemistry, Faculty of Mathematics and Natural Sciences Universitas Negeri Malang	tris_chemum@yahoo.com; tris_shanta@telkom.net

Name	Affiliation	email
Sutrisno	Department of Chemistry Faculty of Sciences Brawijaya University, Indonesia	tris_mc@ub.ac.id
Tagor Siregar	Department of Food Technology, Universitas Pelita Harapan	tagor_siregar@uph.edu
Tati Herlina	Department of Chemistry, Faculty of Mathematics and Natural Sciences, Universitas Padjadjaran, Sumedang, Indonesia	tatat_04her@yahoo.com
Tiny Agustini Koesmawati	Department of Chemistry, Bandung Institute of Technology	buchari@chem.itb.ac.id
Titut Yulistyarini	Purwodadi Botanical Garden, Indonesian Institute of Sciences (LIPI), Pasuruan Regency, East Java, Indonesia	tyulistyarini@yahoo.com
Tur Rahardjo	Center for Technology of Radiation Safety and Metrology, National Nuclear Energy Agency, Jakarta	turahardjo@batan.go.id
Usman Pagalay	Doctoral Program, Faculty of Medical Science, University of Brawijaya	usmanpagalay@yahoo.co.id
Valentina Adimurti Kusumaningtyas	Dept. of Chemistry, Faculty of Mathematics and Natural Sciences, University of Jenderal Achmad Yani	valentina_adimurti@yahoo.com
Warsito	Students Doctoral Program of Chemistry, Faculty of Science, University of Gadjah Mada	warsitoub88@yahoo.com
Wijono	Center for Technology of Radiation Safety and Metrology, National Nuclear Energy Agency (PTKMR-BATAN), Jakarta, Indonesia	johnrida@batan.go.id
Wike Herawaty	Student of Biomedic Doctoral Program of Brawijaya University, Malang, Indonesia	drg_wike@yahoo.co.id
Wiwin Maisyaroh	Graduate School of Biology, Faculty of Science, UB, Malang	may_nis@yahoo.co.id
Yoga Dwi Jatmiko	Department of Biology, Faculty of Sciences, University of Brawijaya	jatmiko_yd@ub.ac.id
Yus Mochamad Cholily	Department of Mathematics, Universitas Muhammadiyah Malang	yus@umm.ac.id, ymcholily@gmail.com
Zainus Salimin	Radioactive Waste Technology Center, BATAN, Jakarta	zainus_s@batan.go.id
Zubaidah Alatas	Centrer for Technology of Radiation Safety and Metrology, National Nuclear Energy Agency (BATAN), Jakarta	zalatas@batan.go.id

SPONSORSHIPS

PT ARFINDO BERSINAR
Bruker Distributor In Indonesia
Jl Raya Alternatif Cibubur Ruko Kranggan Permai
Bl RT-16/26,Jati Sampurna, Jakarta 17433
Tel : +62 21 845 6737
Fax : +62 21 845 98037
Sales : arfina@arfindo.com
Service : andi.faizal@arfindo.com
Application: Reza@arfindo.com
Website : http://www.arfindo.com/

PERUM PERHUTANI UNIT II JAWA TIMUR
Jalan Gentengkali 49 Surabaya, East Java, Indonesia
Email : humas_unit2@yahoo.com
Tel : +62315342851
Fax : +62315474713
Website:
http://www.unit2.perumperhutani.com

TUGU HOTEL MALANG
Jalan Tugu No. 3 Malang, East Java, Indonesia
Tel. :+62 341 363 891
Fax. :+62 341 362 747, 362 765
Email : malang@tuguhotels.com
Website: www.tuguhotels.com

Supported by:

CV. MAKMUR SEJATI
Perum Griyashanta L 238 Malang, East Java, Indonesia
Phone/Fax: +62 341 4345654 - 90 57 100
E- mail : makmur_sejati@yahoo.com
Website : www.makmur-sejati.co.nr

PT. OTSUKA INDONESIA FACTORY LAWANG
Jl. Sumber Waras No. 25, Lawang,Malang, East Java 65216 Indonesia.
Phone :(62-341) 426-244
Fax. :(62-341) 426-644

CV. KRISTALINDO BIOLAB
JL. Arief Rachman Hakim No 61-63 Blok M 60117 Surabaya
Phone: +62 31 5998 626
Fax : +62 31 5998 627

PT. AMERTA INDAH OTSUKA PASURUAN
Jl. Raya Pasuruan - Malang Km. 11, Desa Pacarkeling, Kecamatan Kejayan, Kabupaten Pasuruan, East Java, 67172

PT. SUARA MUDA SAKTI ELFARA 93 FM MALANG
Jln. Tidar Barat No.1 Malang. 65146.
On Air : +62341-577001,
Office : +62341-577002

PEMERINTAH KOTA MALANG
Jl. Tugu Nomor 1 Malang, East Java, Indonesia
Phone : 0341 362 704
Website: http://www.malangkota.go.id/